

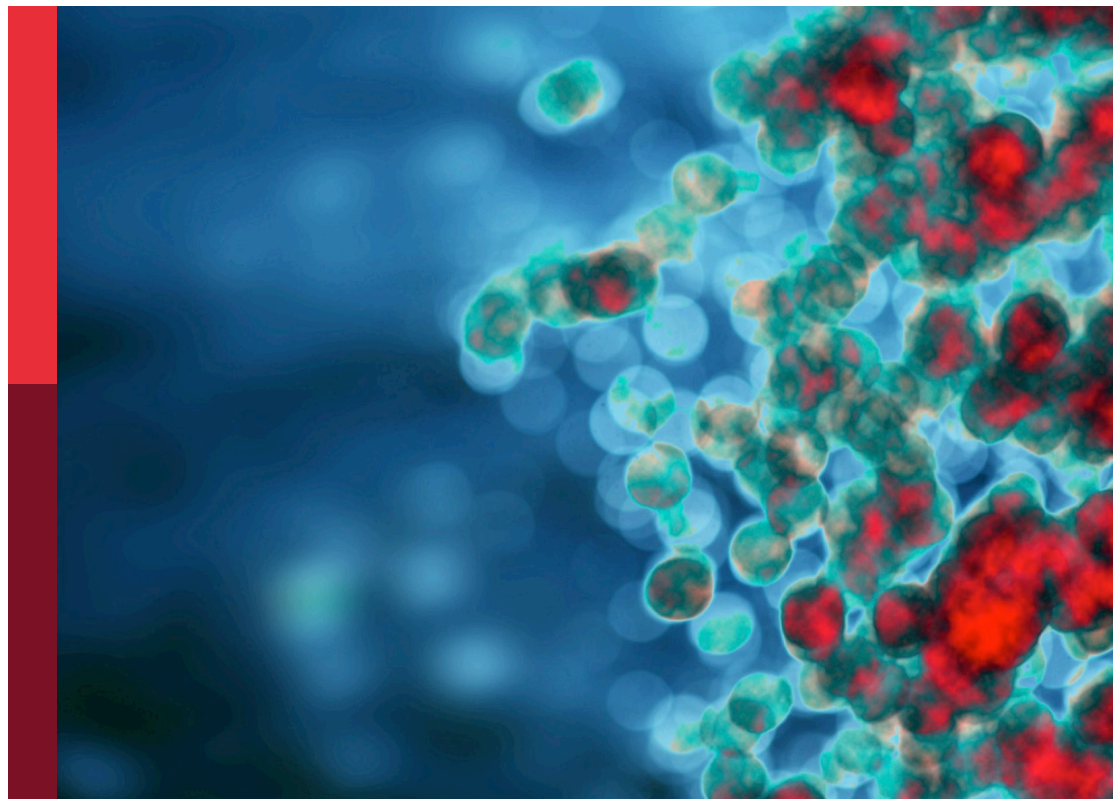
# Antiviral innate immune sensing, regulation, and viral immune evasion

**Edited by**

Chenhe Su, Rongtuan Lin, Junji Xing and  
Hongjuan You

**Published in**

Frontiers in Immunology



#### FRONTIERS EBOOK COPYRIGHT STATEMENT

The copyright in the text of individual articles in this ebook is the property of their respective authors or their respective institutions or funders. The copyright in graphics and images within each article may be subject to copyright of other parties. In both cases this is subject to a license granted to Frontiers.

The compilation of articles constituting this ebook is the property of Frontiers.

Each article within this ebook, and the ebook itself, are published under the most recent version of the Creative Commons CC-BY licence. The version current at the date of publication of this ebook is CC-BY 4.0. If the CC-BY licence is updated, the licence granted by Frontiers is automatically updated to the new version.

When exercising any right under the CC-BY licence, Frontiers must be attributed as the original publisher of the article or ebook, as applicable.

Authors have the responsibility of ensuring that any graphics or other materials which are the property of others may be included in the CC-BY licence, but this should be checked before relying on the CC-BY licence to reproduce those materials. Any copyright notices relating to those materials must be complied with.

Copyright and source acknowledgement notices may not be removed and must be displayed in any copy, derivative work or partial copy which includes the elements in question.

All copyright, and all rights therein, are protected by national and international copyright laws. The above represents a summary only. For further information please read Frontiers' Conditions for Website Use and Copyright Statement, and the applicable CC-BY licence.

ISSN 1664-8714  
ISBN 978-2-8325-5178-3  
DOI 10.3389/978-2-8325-5178-3

## About Frontiers

Frontiers is more than just an open access publisher of scholarly articles: it is a pioneering approach to the world of academia, radically improving the way scholarly research is managed. The grand vision of Frontiers is a world where all people have an equal opportunity to seek, share and generate knowledge. Frontiers provides immediate and permanent online open access to all its publications, but this alone is not enough to realize our grand goals.

## Frontiers journal series

The Frontiers journal series is a multi-tier and interdisciplinary set of open-access, online journals, promising a paradigm shift from the current review, selection and dissemination processes in academic publishing. All Frontiers journals are driven by researchers for researchers; therefore, they constitute a service to the scholarly community. At the same time, the *Frontiers journal series* operates on a revolutionary invention, the tiered publishing system, initially addressing specific communities of scholars, and gradually climbing up to broader public understanding, thus serving the interests of the lay society, too.

## Dedication to quality

Each Frontiers article is a landmark of the highest quality, thanks to genuinely collaborative interactions between authors and review editors, who include some of the world's best academicians. Research must be certified by peers before entering a stream of knowledge that may eventually reach the public - and shape society; therefore, Frontiers only applies the most rigorous and unbiased reviews. Frontiers revolutionizes research publishing by freely delivering the most outstanding research, evaluated with no bias from both the academic and social point of view. By applying the most advanced information technologies, Frontiers is catapulting scholarly publishing into a new generation.

## What are Frontiers Research Topics?

Frontiers Research Topics are very popular trademarks of the *Frontiers journals series*: they are collections of at least ten articles, all centered on a particular subject. With their unique mix of varied contributions from Original Research to Review Articles, Frontiers Research Topics unify the most influential researchers, the latest key findings and historical advances in a hot research area.

Find out more on how to host your own Frontiers Research Topic or contribute to one as an author by contacting the Frontiers editorial office: [frontiersin.org/about/contact](https://frontiersin.org/about/contact)

# Antiviral innate immune sensing, regulation, and viral immune evasion

This ebook is split into several files; this is part one of the ebook, please see the overview text of the Research Topic page to access the second part of the ebook.

## Topic editors

Chenhe Su — Henan Normal University, China

Rongtuan Lin — McGill University, Canada

Junji Xing — Houston Methodist Research Institute, United States

Hongjuan You — Xuzhou Medical University, China

## Citation

Su, C., Lin, R., Xing, J., You, H., eds. (2024). *Antiviral innate immune sensing, regulation, and viral immune evasion*. Lausanne: Frontiers Media SA.  
doi: 10.3389/978-2-8325-5178-3

## Table of contents

- 06 **Editorial: Antiviral innate immune sensing, regulation, and viral immune evasion**  
Wenting Lu, Ling Wang and Junji Xing
- 11 **Th2-Oriented Immune Serum After SARS-CoV-2 Vaccination Does Not Enhance Infection *In Vitro***  
Ning Luan, Tao Li, Yunfei Wang, Han Cao, Xingxiao Yin, Kangyang Lin and Cunbao Liu
- 21 **Evaluation of the Safety and Immunogenicity of Duck-Plague Virus *gE* Mutants**  
Yaru Ning, Yalin Huang, Mingshu Wang, Anchun Cheng, Renyong Jia, Mafeng Liu, Dekang Zhu, Shun Chen, Xinxin Zhao, Shaqiu Zhang, Qiao Yang, Ying Wu, Juan Huang, Bin Tian, Xumin Ou, Sai Mao, Qun Gao, Di Sun, Yanlin Yu and Ling Zhang
- 34 **cGAS Restricts PRRSV Replication by Sensing the mtDNA to Increase the cGAMP Activity**  
Xiao-Na Liu, Li-Wei Li, Fei Gao, Yi-Feng Jiang, Wan-Zhe Yuan, Guo-Xin Li, Ling-Xue Yu, Yan-Jun Zhou, Guang-Zhi Tong and Kuan Zhao
- 44 **Host Restrictive Factors Are the Emerging Storm Troopers Against Enterovirus: A Mini-Review**  
Chen Huan, Xinglong Qu and Zhaolong Li
- 51 **Antiviral Activities of Interleukin-27: A Partner for Interferons?**  
Heather Amsden, Olena Kourko, Madison Roth and Katrina Gee
- 62 **The Integrated Analysis Identifies Three Critical Genes as Novel Diagnostic Biomarkers Involved in Immune Infiltration in Atherosclerosis**  
Zhen Ye, Xiao-kang Wang, Yun-hui Lv, Xin Wang and Yong-chun Cui
- 72 **Advances in Vaccine Development of the Emerging Novel Genotype Fowl Adenovirus 4**  
Aijing Liu, Yu Zhang, Hongyu Cui, Xiaomei Wang, Yulong Gao and Qing Pan
- 79 **Bat Employs a Conserved MDA5 Gene to Trigger Antiviral Innate Immune Responses**  
Jie Wang, Zhenyu Lin, Qiuju Liu, Feiyu Fu, Zhaofei Wang, Jingjiao Ma, Hengan Wang, Yaxian Yan, Yuqiang Cheng and Jianhe Sun
- 90 **Paeonol Interferes With Quorum-Sensing in *Pseudomonas aeruginosa* and Modulates Inflammatory Responses *In Vitro* and *In Vivo***  
Huaqiao Tang, Dan Yang, Ling Zhu, Fei Shi, Gang Ye, Hongrui Guo, Huidan Deng, Ling Zhao, Zhiwen Xu and Yinglun Li
- 104 **The Investigation of Hepatitis B Vaccine Immune Responses in Occult Hepatitis B Virus-Infected Patients**  
Jing Peng, Xueying Yao, Chunyan Yuan, Xiaoli Liu, Renxiang Xia, Jian He, Rui Li and Yunqing Yao

- 112 **The Correlation Between Immune Invasion and SARS-COV-2 Entry Protein ADAM17 in Cancer Patients by Bioinformatic Analysis**  
Kai Wang, Haoyue Deng, Binghui Song, Jiayue He, Shuguang Liu, Jiewen Fu, Lianmei Zhang, Dabing Li, Kyathegowdanadoddi Srinivasa Balaji, Zhiqiang Mei, Jingliang Cheng and Junjiang Fu
- 125 **Duck LGP2 Downregulates RIG-I Signaling Pathway-Mediated Innate Immunity Against Tembusu Virus**  
Tianxu Li, Yanyan Ren, Tingting Zhang, Xinyu Zhai, Xiuyuan Wang, Jinchao Wang, Bin Xing, Runchun Miao, Ning Li and Liangmeng Wei
- 137 **Viral Circular RNAs and Their Possible Roles in Virus-Host Interaction**  
Xing Zhang, Zi Liang, Chonglong Wang, Zeen Shen, Sufei Sun, Chengliang Gong and Xiaolong Hu
- 148 **Investigation of Antibody Levels During Three Doses of Sinopharm/BBIBP Vaccine Inoculation**  
Jing Ma, Zhangkai J. Cheng, Mingshan Xue, Huimin Huang, Shiyun Li, Yanting Fang, Yifeng Zeng, Runpei Lin, Zhiman Liang, Huan Liang, Yijun Deng, Yuanyi Cheng, Shuangshuang Huang, Qian Wang, Xuefeng Niu, Siping Li, Peiyan Zheng and Baoqing Sun
- 157 **Duck Plague Virus Negatively Regulates IFN Signaling to Promote Virus Proliferation via JNK Signaling Pathway**  
Liping Wu, Bin Tian, Mingshu Wang, Anchun Cheng, Renyong Jia, Dekang Zhu, Mafeng Liu, Qiao Yang, Ying Wu, Juan Huang, XinXin Zhao, Shun Chen, Shaqiu Zhang, Xumin Ou, Sai Mao, Qun Gao, Di Sun, Yanling Yu, Ling Zhang and LeiCHang Pan
- 170 **Identification of Critical Biomarkers and Immune Infiltration in Rheumatoid Arthritis Based on WGCNA and LASSO Algorithm**  
Fan Jiang, Hongyi Zhou and Haili Shen
- 181 **SARS-CoV-2 Achieves Immune Escape by Destroying Mitochondrial Quality: Comprehensive Analysis of the Cellular Landscapes of Lung and Blood Specimens From Patients With COVID-19**  
Chenyang Duan, Ruiyan Ma, Xue Zeng, Bing Chen, Dongyao Hou, Ruixue Liu, Xuehan Li, Liangming Liu, Tao Li and He Huang
- 195 **Insights on the cGAS-STING Signaling Pathway During Herpesvirus Infections**  
Lishuang Deng, Zhiwen Xu, Fengqin Li, Jun Zhao, Zhijie Jian, Huidan Deng, Siyuan Lai, Xiangang Sun, Yi Geng and Ling Zhu
- 205 **Characterization of the Immunologic Phenotype of Dendritic Cells Infected With Herpes Simplex Virus 1**  
Jingjing Zhang, Xingli Xu, Suqin Duan, Yang Gao, Danjing Ma, Rong Yue, Fengyuan Zeng, Xueqi Li, Ziyang Meng, Xinghang Li, Zhenye Niu, Guorun Jiang, Li Yu, Yun Liao, Dandan Li, Lichun Wang, Heng Zhao, Ying Zhang and Qihan Li

- 218 **The Essential Role of Sorting Nexin 5 in Virus-Induced Autophagy**  
Dong-Yi Li, Jun-Hao Wen, Shan Liang and Ji-Xin Tang
- 222 **2B and 3C Proteins of Senecavirus A Antagonize the Antiviral Activity of DDX21 *via* the Caspase-Dependent Degradation of DDX21**  
Kuan Zhao, Xiao-Ran Guo, Shuai-Feng Liu, Xiao-Na Liu, Ying Han, Lu-Lu Wang, Bai-Shi Lei, Wu-Chao Zhang, Li-Min Li and Wan-Zhe Yuan
- 233 **Porcine epidemic diarrhea virus strain FJzz1 infection induces type I/III IFNs production through RLRs and TLRs-mediated signaling**  
Pengfei Chen, Junrui Zhu, Jiarong Yu, Ruilin Liu, Mengqin Lao, Lingxue Yu, Fei Gao, Yifeng Jiang, Changlong Liu, Wu Tong, Huili Liu, Guangzhi Tong and Yanjun Zhou
- 247 **Mfn2 is responsible for inhibition of the RIG-I/IRF7 pathway and activation of NLRP3 inflammasome in Seneca Valley virus-infected PK-15 cells to promote viral replication**  
HuiDan Deng, Song Zhu, Ling Zhu, Jing Sun, YuChun Ding, FengQin Li, ZhiJie Jian, Jun Zhao, LiShuang Deng, JunLiang Deng, YouTian Deng, HongRui Guo, XianGang Sun, Si Yuan Lai, HuaQiao Tang, HengMin Cui, Liang Peng Ge and ZhiWen Xu
- 259 **Goose STING mediates IFN signaling activation against RNA viruses**  
Feiyu Fu, Zhenyu Lin, Yanlin Li, Jie Wang, Yawen Li, Pengcheng Liu, Zhaofei Wang, Jingjiao Ma, Yaxian Yan, Jianhe Sun and Yuqiang Cheng
- 271 **Genomic analysis quantifies pyroptosis in the immune microenvironment of HBV-related hepatocellular carcinoma**  
Jiarui Li, Jinghui Yu, Ting Zhang, Xingyu Pu, Yilan Li and Zhongjun Wu
- 287 **When liquid-liquid phase separation meets viral infections**  
Wenqiang Wei, Lu Bai, Bing Yan, Weiquan Meng, Hongju Wang, Jingbo Zhai, Fusheng Si and Chunfu Zheng
- 297 **DEAD-box RNA helicase 21 negatively regulates cytosolic RNA-mediated innate immune signaling**  
Jia Li, Puxian Fang, Yanrong Zhou, Dang Wang, Liurong Fang and Shaobo Xiao
- 310 **BAG6 negatively regulates the RLR signaling pathway by targeting VISA/MAVS**  
Jing-Ping Huang, Jing Li, Yan-Ping Xiao and Liang-Guo Xu
- 323 **Human metapneumovirus M2-2 protein inhibits RIG-I signaling by preventing TRIM25-mediated RIG-I ubiquitination**  
Yukie Tanaka, Naoko Morita, Yoshinori Kitagawa, Bin Gotoh and Takayuki Komatsu



## OPEN ACCESS

EDITED AND REVIEWED BY  
Pei-Hui Wang,  
Shandong University, China

\*CORRESPONDENCE  
Junji Xing  
✉ [jxing@houstonmethodist.org](mailto:jxing@houstonmethodist.org)

†These authors have contributed equally to this work

RECEIVED 19 December 2023  
ACCEPTED 26 December 2023  
PUBLISHED 04 January 2024

CITATION  
Lu W, Wang L and Xing J (2024) Editorial:  
Antiviral innate immune sensing, regulation,  
and viral immune evasion.  
*Front. Immunol.* 14:1358542.  
doi: 10.3389/fimmu.2023.1358542

COPYRIGHT  
© 2024 Lu, Wang and Xing. This is an open-  
access article distributed under the terms of  
the [Creative Commons Attribution License  
\(CC BY\)](https://creativecommons.org/licenses/by/4.0/). The use, distribution or reproduction  
in other forums is permitted, provided the  
original author(s) and the copyright owner(s)  
are credited and that the original publication  
in this journal is cited, in accordance with  
accepted academic practice. No use,  
distribution or reproduction is permitted  
which does not comply with these terms.

# Editorial: Antiviral innate immune sensing, regulation, and viral immune evasion

Wenting Lu<sup>1†</sup>, Ling Wang<sup>1,2†</sup> and Junji Xing<sup>1,3\*</sup>

<sup>1</sup>Department of Surgery and Immunobiology and Transplant Science Center, Houston Methodist Research Institute, Houston Methodist, Houston, TX, United States, <sup>2</sup>Department of Obstetrics and Gynecology, The Second Hospital of Jilin University, Changchun, China, <sup>3</sup>Department of Cardiovascular Sciences, Houston Methodist Research Institute, Houston Methodist, Houston, TX, United States

## KEYWORDS

innate immunity, antiviral immunity, innate immune sensing, immune regulation, viral immune evasion, pattern recognition receptor

## Editorial on the Research Topic

### Antiviral innate immune sensing, regulation, and viral immune evasion

Antiviral innate immune response represents a critical line of defense against viral infections, encompassing sensing and responding to viruses (1, 2). Central to this defense are host pattern recognition receptors (PRRs) which play a crucial role in recognizing pathogen-associated molecular patterns (PAMPs) on the surface of viruses, mainly including Toll-like receptors (TLRs), RIG-I-like receptors (RLRs), and NOD-like receptors (NLRs) (3–6). Activation of these PRRs triggers a cascade of events, leading to the induction of cytokines, chemokines, and type I interferons (IFNs) that collectively contribute to viral clearance (7–10). Despite these formidable defense mechanisms, viruses have evolved sophisticated strategies to evade and subvert these defenses, employing a variety of mechanisms to disrupt or manipulate the host's innate immune signaling pathways (11–13). Therefore, understanding the dynamic interplay between antiviral innate immune sensing, regulatory mechanisms, and the strategies employed by viruses for immune evasion is paramount for unraveling the complexities of host-pathogen interactions and devising innovative approaches for antiviral therapeutics.

This Research Topic “*Antiviral Innate Immune Sensing, Regulation, and Viral Immune Evasion*” highlights 47 recent studies that investigate the mechanisms about antiviral innate immune sensing and regulation in the host, and summarize the innate immune evasion strategies employed by viruses.

After a virus successfully infiltrates the host, PRRs play a crucial role in sensing the presence of viral DNAs and RNAs. Subsequently, they initiate a cascade of signal transduction events to regulate the antiviral response. Deng et al. reviewed the intricate interplay between herpesviruses and the cGAS-STING signaling pathway, a critical component of the host's innate immunity. They discussed how herpesviruses activate or target this pathway to modulate host antiviral responses and explored potential immunotherapy strategies to boost the cGAS-STING signaling pathway. Fu et al. found that goose STING (GoSTING) played a crucial role in regulating the type I interferon pathway and contributes to the innate immune defense against RNA viruses in geese, as it induced the expression of interferons, interferon-stimulated genes, and proinflammatory

cytokines while inhibiting virus replication. **Li et al.** investigated the regulatory role of duck laboratory of genetics and physiology 2 (duLGP2) in the duck RIG-I (duRIG-I)-mediated antiviral innate immune signaling system. They showed that duLGP2 could both suppress and enhance duRIG-I-mediated signaling pathways in response to duck Tembusu virus (DTMUV) infection, shedding light on the regulatory networks of the antiviral innate immune system in ducks. **Chen et al.** highlighted the involvement of RIG-I-like receptors (RLRs) and Toll-like receptors (TLRs) in the induction of type I/III interferons and ISGs, contributing to the antiviral effects of innate immunity against PEDV. The formation mechanism of membranellar organelles, known as liquid-liquid phase separation (LLPS), is not well understood in eukaryotic cells. **Ye et al.** examined the proteome response in Muscovy duck lung tissue during infection with highly virulent H5N1 HPAI virus (DK383) and avirulent H5N1 HPAI virus (DK212). They revealed distinct proteomic responses between the two strains, with DK383 inducing a stronger response associated with severe disease, while DK212 triggered responses related to dendritic cell maturation, phagocyte adhesion, and macrophage immune response, suggesting that these different proteome profiles, along with insights into the Akt/mTOR/p70S6K pathway, may contribute to understanding the pathogenesis of H5N1 viruses. **Huang et al.** identified BAG6 as a crucial negative regulator in the RIG-I-like receptor (RLR) signaling pathway. BAG6 was shown to inhibit the aggregation of the virus-induced signaling adaptor protein VISA, thereby attenuating downstream signaling by promoting K48-linked ubiquitination and inhibiting the recruitment of TRAF2, highlighting its critical role in the innate immune response to RNA virus infection. **Zhang et al.** examined the role of C-reactive protein (CRP) in influenza A virus infection by comparing the responses in CRP knockout mice (KO), human CRP transgenic mice (KI), and wild-type mice (WT) infected with influenza A H1N1. They showed that the absence of CRP or the presence of human CRP worsened influenza infection in mice, and CRP appeared to play a complex role in immune regulation during influenza infection. The sensing of COVID-19 virus also involves PRR activation, prompting signaling pathways to produce interferons and antiviral molecules, crucial for limiting virus replication and spread. **Li et al.** revealed that the SARS-CoV-2 Nsp14 protein played a role in activating NF- $\kappa$ B signaling, leading to the upregulation of pro-inflammatory cytokines such as IL-6 and IL-8. The interaction between Nsp14 and host Inosine-5'-monophosphate dehydrogenase 2 (IMPDH2) was identified as a crucial mechanism, and inhibiting IMPDH2 or NF- $\kappa$ B restricted SARS-CoV-2 infection, highlighting a potential target for therapeutic intervention. **Zhaoyang et al.** evaluated host DNA-removed metagenomic next-generation sequencing (mNGS) technology for detecting SARS-CoV-2 in 46 swab specimens from COVID-19 patients. The host DNA-removed mNGS demonstrated high sensitivity for detecting SARS-CoV-2, providing potential utility for comprehensive identification of the virus. **Hoque et al.** employed machine learning approaches to analyze RNA-seq data from COVID-19 patients, recovered individuals, and healthy individuals to identify differentially expressed genes (DEGs) and associated pathways. They found DEG signatures in both COVID-19 patients and recovered individuals,

highlighting potential molecular factors and pathways connected to COVID-19 comorbidities, providing insights into the interplay between COVID-19 progression and recovery stages. **Wang et al.** investigated the expression of ADAM17 in normal and tumor tissues. They showed that ADAM17 expression was significantly associated with immunomodulators and immune cell infiltration, suggesting potential implications for cancer patients infected with COVID-19 and providing insights into anti-COVID-19 development strategies. **Cheng et al.** investigated ISG20 expression and its potential role in cancer susceptibility to SARS-CoV-2 infection. They found that ISG20 expression was elevated in various cancer types, potentially reducing vulnerability to SARS-CoV-2, and higher ISG20 expression was associated with longer overall survival in specific cancers. The signal transduction cascade culminates in the production of interferons, pivotal for orchestrating antiviral responses. Consequently, the regulation of each molecule within the signaling pathway profoundly influences the effectiveness of the antiviral response. **Liu et al.** investigated the role of Heat Shock Protein 90 kDa alpha class A member 1 (HSP90AA1) in classical swine fever virus (CSFV) infection. They found that overexpression of HSP90AA1 inhibited CSFV replication by interacting with the viral NS5A protein and activating JAK/STAT and NF- $\kappa$ B signaling pathways, providing valuable insights for potential anti-CSFV strategies. **Ning et al.** investigated the role of gE, a protein in the duck plague virus (DPV), by creating mutant viruses with specific gE domain deletions. They found that DPV CHV-gE $\Delta$ ET, a mutant with the extracellular domain of gE deleted, showed reduced virulence and could potentially be a candidate for a vaccine against duck plague. **Tang et al.** demonstrated that paeonol exhibited anti-virulence activity against *Pseudomonas aeruginosa* infection by reducing bacterial adhesion, invasion, and virulence factor expression through inhibition of quorum sensing (QS). Paeonol was also shown to enhance macrophage clearance of *P. aeruginosa* by modulating cytokine expression and inhibiting the TLR4/MyD88/NF- $\kappa$ B signaling pathway, supporting its potential as a promising anti-infective drug targeting QS and virulence factors. **Ye et al.** identified diagnostic markers for atherosclerosis (AS) and found 17 differentially expressed genes (DEGs) associated with AS, with FHL5, IBSP, and SCRG1 identified as potential diagnostic markers. These genes were found to be associated with various immune cells, suggesting their potential role in the development and progression of AS. Fowl adenovirus (FAdV), also known as "Angara disease," has caused significant economic losses in the global poultry industry. **Jiang et al.** identified biomarkers related to rheumatoid arthritis (RA) and their connection to immune cell infiltration. Through gene analysis, they identified six hub genes, including CKS2, CSTA, and LY96, which had high diagnostic value and were associated with the concentrations of several immune cells. These findings suggested that these genes, particularly CKS2, CSTA, and LY96, could be valuable for diagnosing and treating RA. **Li et al.** provided opinion about the essential role of sorting nexin 5 (SNX5) in virus-induced autophagy. **Ren et al.** investigated the optimal concentration of Selenium Nanoparticles (SeNPs) and their mechanism in combating Porcine Delta coronavirus (PDCoV) in swine testis (ST) cells. They demonstrated that 4  $\mu$ g/mL SeNPs significantly reduced PDCoV replication, alleviated PDCoV-induced mitochondrial division, and



antagonized PDCoV-induced apoptosis, offering potential insights for anti-PDCoV drug development. In response to porcine epidemic diarrhea virus (PEDV) infection, LLC-PK1 cells exhibit a time- and dose-dependent upregulation of interferon-stimulated genes (ISGs), with significant activation of the JAK-STAT signaling pathway. [Wei et al.](#) reviewed the significance of LLPS in understanding viral infections and immune regulation, offering insights into potential antiviral therapeutic strategies. The heterogeneous nuclear ribonucleoproteins (hnRNPs) constitute a diverse family of RNA binding proteins with various functions in RNA metabolism, including alternative splicing, mRNA stabilization, and translational regulation. [Wang et al.](#) reviewed the roles of hnRNPs in the life cycle of positive single-stranded RNA viruses, emphasizing their interactions with viral RNA or proteins, and their regulatory effects on processes such as viral translation, genome replication, and virion release. [Hu et al.](#) investigated the effects of Tai Chi intervention on NLRP3 inflammasome and related inflammatory factors in middle-aged and older individuals with pre-diabetes mellitus (PDM). They showed that 12 weeks of Tai Chi intervention led to improvements in blood glucose, lipid levels, and insulin resistance, possibly by reducing the levels of NLRP3 inflammasome and its associated inflammatory factors in the serum of pre-diabetic patients. [Lu et al.](#) conducted whole-transcriptome sequencing on sheep embryonic testicular cells infected with Bluetongue Virus (BTV) serotype 1, and revealed 1504 differentially expressed mRNAs, 78 microRNAs, 872 long non-coding RNAs, and 59 circular RNAs, providing a more comprehensive understanding of BTV-host interactions and pathogenic mechanisms. [Wang et al.](#) established two molecular patterns of virus-related genes (VRGs) in burn patients using consensus clustering and weighted gene co-expression network analysis (WGCNA). A 2-gene signature (CD69 and SATB1) was identified as an independent prognostic factor, providing a potential biomarker for predicting survival and guiding immunotherapy strategies in burns with viral infections. [Huan et al.](#) discussed the mechanisms by which host restrictive factors inhibit enterovirus infections and highlighted the potential of those factors as targets for antiviral drug development. In sight of virus sensing and regulation, extensive vaccine development, including for COVID-19, underscores the critical need for a comprehensive understanding of host-pathogen interactions. [Yuan et al.](#) discussed the factors contributing to the low vaccine protection rate against COVID-19 and suggested that immunosuppressive parasite infections, particularly *Toxoplasma gondii* (*T. gondii*), might play a significant role in vaccine failure. [Luan et al.](#) examined the risk of antibody-dependent enhancement (ADE) in immune cell lines using immune serum from mice and humans vaccinated with alum-adsorbed inactivated SARS-CoV-2 vaccines. These results suggested that ADE did not occur, and the lower protection rate of these vaccines might be due to lower neutralizing antibody levels or pulmonary eosinophilic immunopathology, emphasizing the need for adjustments in vaccination strategies to enhance efficacy. [Ma et al.](#) evaluated the performance of a chemiluminescent immunoassay (CLIA) for detecting specific antibodies against SARS-CoV-2 in individuals vaccinated with the Sinopharm/BBIBP vaccine. They demonstrated that high levels of neutralizing antibodies, receptor-binding-domain antibodies, and IgG persisted for over three months

after the booster injection, and CLIA was consistently reliable in detecting vaccination-induced immunity. [Liu et al.](#) discussed the development of vaccines against fowl adenovirus 4 (FAdV-4) and their importance in controlling hydropericardium hepatitis syndrome (HHS), emphasizing the need for further research on cross-protection and vaccine immunogenicity. [Peng et al.](#) investigated the therapeutic potential of hepatitis B vaccine immunotherapy for occult hepatitis B virus infection (OBI) patients. They showed that hepatitis B vaccine treatment significantly increased serum hepatitis B surface antibodies, along with peripheral blood B and CD8<sup>+</sup> T lymphocytes, suggesting a potential immunotherapeutic approach for OBI patients. The global health challenge posed by enterovirus infections, coupled with the lack of specific drugs and broad-spectrum vaccines, necessitates the development of effective strategies.

Despite the existence of a comprehensive and precise innate immune system designed to avoid virus infections, viruses have evolved numerous strategies to evade immune responses. [Duan et al.](#) analyzed RNA-sequencing data from COVID-19 patients and found significant changes in mitochondrion-related gene expression and functions, along with alterations in metabolic pathways. They proposed a detailed mechanism involving mitochondrial damage in COVID-19, including excessive mitochondrial fission, impaired mitochondrial degradation, and disruptions in cellular processes that contribute to immune escape and inflammation in patients. [Zheng et al.](#) utilized bioinformatics analysis on datasets related to rheumatoid arthritis (RA), *Staphylococcus aureus* bacteremia (SAB), and severe acute respiratory syndrome coronavirus 2 (SARS-CoV-2) to identify shared biomarkers and disease targets. The hub gene IFI44 was identified as a common factor in RA, COVID-19, and SAB, suggesting its role in immune escape mechanisms. IFI44 was shown to negatively regulate the interferon signaling pathway, promoting viral replication and bacterial proliferation, making it a potential molecular target for SARS-CoV-2 and *S. aureus* immune escape in RA. [Jian et al.](#) reviewed how Arter viruses employ various strategies, involving both structural and nonstructural proteins, to counteract the host's interferon (IFN) production and impede the IFN-activated antiviral signaling pathways. Herpes simplex virus type 2 (HSV-2) can establish lifelong latency within dorsal root ganglia by evading the host's innate immunity. [Hu et al.](#) identified the immediate early protein ICP22 of HSV-2 as a crucial viral element that inhibits NF- $\kappa$ B activation, demonstrating its role in suppressing host antiviral responses and providing insights into the mechanism of HSV-2 immune evasion. [Liu et al.](#) discussed the strategies employed by alphaviruses, such as CHIKV, SINV, and VEEV, to evade various components of the host antiviral innate immune response, including cGAS-STING, IFN, transcriptional host shutoff, translational host shutoff, and RNA interference (RNAi). [Liu et al.](#) found that cGAS, an innate immune DNA sensor, played a role in inhibiting porcine reproductive and respiratory syndrome virus (PRRSV) infection by sensing mitochondrial DNA (mtDNA) released into the cytoplasm during PRRSV infection. [Wang et al.](#) focused on the innate immune system of bats and identified the *Tadarida brasiliensis* MDA5 gene (batMDA5), which plays a major role in sensing and responding

to RNA viral infections. BatMDA5 was found to activate the production of IFN $\beta$  and inhibit the replication of vesicular stomatitis virus (VSV-GFP) in bat cells, highlighting the important role of this gene in the bat's innate immune response against RNA viruses. Zhang et al. found that both the wild-type and attenuated M6 strains of HSV-1 could infect dendritic cells and induce changes in transcriptional profiles related to innate immune and inflammatory responses. They showed that HSV-1, particularly the wild-type strain, interfered with antiviral immunity by modifying the immunological phenotype of dendritic cells, leading to deficient immune responses in infected individuals. Circular RNAs (circRNAs) as novel regulatory molecules have been recognized in diverse species, including viruses. The virus-derived circRNAs play various roles in the host biological process and the life cycle of the viruses. Zhang et al. summarized the role of circular RNAs (circRNAs) derived from both DNA and RNA viruses in host biological processes and viral life cycles. Influenza virus infection often triggers a cytokine storm, contributing to severe outcomes. Zhang et al. examined the impact of influenza infection on PPAR $\gamma$  expression and activity in human alveolar macrophages (AMs) and a mouse model. They demonstrated that influenza virus reduced PPAR $\gamma$  expression and transcriptional activity in AMs, contributing to the proinflammatory response and lung pathology associated with the infection, but PPAR $\gamma$  agonist treatment could mitigate these effects. Li et al. investigated the relationship between pyroptosis, a pro-inflammatory cell death process, and tumor immunity in hepatitis B virus-related hepatocellular carcinoma (HBV-HCC). They developed a pyroptosis-score (PYS) and found that higher PYS was associated with poor prognosis but increased susceptibility to anti-PD-L1 treatment in HBV-HCC patients, suggesting the potential of targeting pyroptosis as a strategy in inflammation-driven cancers. Amsden et al. summarized the IFN-dependent and IFN-independent antiviral mechanisms of IL-27 and highlighted the potential of IL-27 as a therapeutic cytokine for viral infection. Wu et al. used a duck monocyte/macrophages cell model to investigate the transcriptome associated with duck plague virus (DPV) infection. They found that DPV differentially regulated various signaling pathways, including MAPK, NF- $\kappa$ B, and IFN pathways, and discovered that the JNK pathway negatively regulates the IFN pathway and promotes virus proliferation. Seneca Valley virus (SVV), known for causing vesicular disease in swine, was found to inhibit the expression of Mitofusin-2 (MFN2), a protein involved in mitochondrial dynamics. Deng et al. explored the interactions between Seneca Valley virus (SVV) and host cells. They found that SVV inhibited the host protein Mitofusin-2 (MFN2), which leads to the activation of the RIG-I/IRF7 signaling pathway and increased expression of IFN- $\lambda$ 3, contributing to SVV's ability to evade the host immune response and replicate. DEAD-box RNA helicase 21 (DDX21) serves as an ATP-dependent RNA helicase involved in various cellular processes, including RNA splicing, transcription, and translation. Li et al. investigated the role of DEAD-box RNA helicase 21

(DDX21) in regulating interferon production. They found that DDX21 functioned as a negative regulator of interferon-beta (IFN- $\beta$ ) production by competing with retinoic acid-inducible gene I (RIG-I) for binding to double-stranded RNA (dsRNA), thus helping to maintain immune homeostasis. Senecavirus A (SVA) poses a significant threat to the swine industry, causing swine vesicular disease, and its replication mechanism is not well understood. Zhao et al. found that the host protein DDX21 played a role in inhibiting Senecavirus A (SVA) replication, but SVA counteracted this antiviral effect by inducing the degradation of DDX21 through the actions of its 2B and 3C proteins, involving the caspase pathway. Tanaka et al. investigated how human metapneumovirus (HMPV) interferes with the RIG-I/TRIM25-mediated antiviral response. They found that HMPV M2-2 inhibited RIG-I signaling by forming a complex with RIG-I CARD and TRIM25, similar to the immune evasion mechanisms employed by other viruses in the Paramyxoviridae and Pneumoviridae families.

In conclusion, our gratitude goes out to all the authors who have placed their discoveries in our hands, as well as to the referees for their meticulous and perceptive evaluations. We believe that the compilation of articles in this subject area will engage researchers specializing in antiviral innate immunity and the evasion strategies employed by viruses. Understanding the intricacies of antiviral immune detection and evasion is anticipated to contribute valuable knowledge for the development of vaccines and antiviral treatments, potentially influencing the approach to the ongoing COVID-19 pandemic and other future infectious diseases.

## Author contributions

WL: Writing – original draft. LW: Writing – original draft. JX: Conceptualization, Funding acquisition, Writing – review & editing.

## Funding

The author(s) declare financial support was received for the research, authorship, and/or publication of this article. This work was supported by the American Heart Association Career Development Award 20CDA35260116 and Transformational Project Award 23TPA1055437 (<https://doi.org/10.58275/AHA.23TPA1055437.pc.gr.172259>) (JX).

## Acknowledgments

We would like to thank the authors, reviewers, and editors for their essential contribution to this exciting and unexplored Research Topic, as well as of the members of the Frontiers in Immunology Editorial Office.

## Conflict of interest

The authors declare that the research was conducted in the absence of any commercial or financial relationships that could be construed as a potential conflict of interest.

The author(s) declared that they were an editorial board member of Frontiers, at the time of submission. This had no impact on the peer review process and the final decision.

## Publisher's note

All claims expressed in this article are solely those of the authors and do not necessarily represent those of their affiliated organizations, or those of the publisher, the editors and the reviewers. Any product that may be evaluated in this article, or claim that may be made by its manufacturer, is not guaranteed or endorsed by the publisher.

## References

1. Akira S, Uematsu S, Takeuchi O. Pathogen recognition and innate immunity. *Cell* (2006) 124:783–801. doi: 10.1016/j.cell.2006.02.015
2. Lin R, Xing J, Zheng C. Editorial: sensing DNA in antiviral innate immunity. *Front Immunol* (2021) 12:644310. doi: 10.3389/fimmu.2021.644310
3. Li D, Wu M. Pattern recognition receptors in health and diseases. *Signal Transduct Target Ther* (2021) 6:291. doi: 10.1038/s41392-021-00687-0
4. Zhang E, Fang M, Jones C, Minze LJ, Xing J, Zhang Z. Mechanisms involved in controlling RNA virus-induced intestinal inflammation. *Cell Mol Life Sci* (2022) 79:313. doi: 10.1007/s00018-022-04332-z
5. Xing J, Zhang A, Du Y, Fang M, Minze LJ, Liu YJ, et al. Identification of poly (ADP-ribose) polymerase 9 (PARP9) as a noncanonical sensor for RNA virus in dendritic cells. *Nat Commun* (2021) 12:2681. doi: 10.1038/s41467-021-23003-4
6. Xing J, Zhou X, Fang M, Zhang E, Minze LJ, Zhang Z. DHX15 is required to control RNA virus-induced intestinal inflammation. *Cell Rep* (2021) 35:109205. doi: 10.1016/j.celrep.2021.109205
7. McNab F, Mayer-Barber K, Sher A, Wack A, O'Garra A. Type I interferons in infectious disease. *Nat Rev Immunol* (2015) 15:87–103. doi: 10.1038/nri3787
8. Xing J, Weng L, Yuan B, Wang Z, Jia L, Jin R, et al. Identification of a role for TRIM29 in the control of innate immunity in the respiratory tract. *Nat Immunol* (2016) 17:1373–80. doi: 10.1038/ni.3580
9. Xing J, Zhang A, Zhang H, Wang J, Li XC, Zeng MS, et al. TRIM29 promotes DNA virus infections by inhibiting innate immune response. *Nat Commun* (2017) 8:945. doi: 10.1038/s41467-017-00101-w
10. Fang M, Zhang A, Du Y, Lu W, Wang J, Minze LJ, et al. TRIM18 is a critical regulator of viral myocarditis and organ inflammation. *J BioMed Sci* (2022) 29:55. doi: 10.1186/s12929-022-00840-z
11. Minkoff JM, tenOever B. Innate immune evasion strategies of SARS-CoV-2. *Nat Rev Microbiol* (2023) 21:178–94. doi: 10.1038/s41579-022-00839-1
12. Hilleman MR. Strategies and mechanisms for host and pathogen survival in acute and persistent viral infections. *Proc Natl Acad Sci U.S.A.* (2004) 101 Suppl 2:14560–6. doi: 10.1073/pnas.0404758101
13. Wang L, Xing J. Editorial: Community series in antiviral innate immune sensing, regulation, and viral immune evasion: volume II. *Front Immunol* (2023) 14:1341193. doi: 10.3389/fimmu.2023.1341193



# Th2-Oriented Immune Serum After SARS-CoV-2 Vaccination Does Not Enhance Infection *In Vitro*

Ning Luan<sup>1†</sup>, Tao Li<sup>2†</sup>, Yunfei Wang<sup>1</sup>, Han Cao<sup>1</sup>, Xingxiao Yin<sup>1</sup>, Kangyang Lin<sup>1</sup> and Cunbao Liu<sup>1\*</sup>

<sup>1</sup> Institute of Medical Biology, Chinese Academy of Medical Sciences and Peking Union Medical College, Kunming, China, <sup>2</sup> Institute for Biological Product Control, National Institutes for Food and Drug Control and WHO Collaborating Center for Standardization and Evaluation of Biologicals, Beijing, China

## OPEN ACCESS

### Edited by:

Chunfu Zheng,  
University of Calgary, Canada

### Reviewed by:

Chuanbin Shen,  
St. Michael's Hospital, Canada  
Zizhang Sheng,  
Columbia University Irving Medical  
Center, United States

### \*Correspondence:

Cunbao Liu  
cunbao\_liu@163.com

<sup>†</sup>These authors have contributed  
equally to this work

### Specialty section:

This article was submitted to  
Viral Immunology,  
a section of the journal  
Frontiers in Immunology

Received: 24 February 2022

Accepted: 17 March 2022

Published: 08 April 2022

### Citation:

Luan N, Li T, Wang Y, Cao H,  
Yin X, Lin K and Liu C (2022)  
Th2-Oriented Immune Serum  
After SARS-CoV-2 Vaccination Does  
Not Enhance Infection *In Vitro*.  
*Front. Immunol.* 13:882856.  
doi: 10.3389/fimmu.2022.882856

The relatively lower protection rate of the alum-adjuvanted inactivated severe acute respiratory syndrome coronavirus 2 (SARS-CoV-2) vaccines reminds us of the antibody-dependent enhancement (ADE) phenomenon observed in preclinical studies during the development of vaccines for Middle East respiratory syndrome coronavirus (MERS-CoV) and severe acute respiratory syndrome coronavirus 1 (SARS-CoV-1). In this study, using the S1 segment of the SARS-CoV-2 spike protein or inactivated whole SARS-CoV-2 virus as an antigen and aluminum as an adjuvant, the risk of ADE of infection with T helper 2 (Th2)-oriented immune serum from mice (N=6) and humans (N=5) was examined in immune cell lines, which show different expression patterns of Fc receptors. Neither the immune serum from alum-adjuvanted S1 subunit vaccines nor inactivated SARS-CoV-2 vaccination enhanced SARS-CoV-2 S pseudotyped virus infection in any of the tested cell lines *in vitro*. Because both of these Th2-oriented immune sera could block SARS-CoV-2 infection without ADE of infection, we speculate that the lower protection rate of the inactivated SARS-CoV-2 vaccine may be attributed to the lower neutralizing antibody titers induced or the pulmonary eosinophilic immunopathology accompanied by eosinophilic infiltration in the lungs upon virus exposure. Adjustment of the immunization schedule to elevate the neutralizing antibody levels and skew adjuvants toward Th1-oriented responses may be considered to increase the efficacies of both inactivated and spike protein-based subunit SARS-CoV-2 vaccines.

**Keywords:** inactivated SARS-CoV-2 vaccine, spike protein subunit vaccine, aluminum adjuvant, Th2, antibody-dependent enhancement of infection

## INTRODUCTION

Previous experience on the development of coronavirus vaccines for severe acute respiratory syndrome coronavirus 1 (SARS-CoV-1) and Middle East respiratory syndrome virus (MERS-CoV) has revealed that the T helper 2 (Th2) response bias of these vaccines is accompanied by a pulmonary immune pathology characterized by eosinophil infiltration upon virus challenge, although the subunit vaccines based on either the spike protein or the inactivated vaccine

combined with aluminum adjuvant exert certain protective effects on reducing the viral loads in animal models during a subsequent challenge (1–4). *In vitro* analyses show that serum obtained after the administration of these vaccines could enhance viral infection, mainly through the Fc receptors (FcRs) of immune cells (5, 6). Although these infections have been proven to be abortive, viral elimination is reportedly associated with the production of multiple antiviral and proinflammatory cytokines, which may result in vaccine-associated enhanced respiratory disease (VAERD) (5, 7–11). Correspondingly, adjuvants that promote Th1 response bias have been adopted to avoid or reduce the risk of VAERD and improve the protective effect of these vaccines in preclinical studies (12–14).

Coincidentally, all successful SARS-CoV-2 vaccines with a protection rate greater than 90% have exhibited Th1-cell-skewed responses of their spike protein antigens during preclinical and clinical studies (15–19). These vaccines include the mRNA vaccine BNT162b2 developed by BioNTech (Germany), mRNA-1273 developed by Moderna (USA), and the subunit vaccine NVX-CoV2373 developed by NOVAVAX (USA). While Th1-oriented responses are induced by the intracellular translation of spike proteins and the innate immunity mobilization ability for mRNA vaccines, NVX-CoV2373 relies on its Th1-cell-biasing adjuvant Matrix-M (20–22).

Aluminum, which induces typical Th2 response bias for subunit and inactivated vaccines, has recently been the only adjuvant in vaccines licensed worldwide for human use (23). Aluminum has been applied as the adjuvant in inactivated SARS-CoV-2 vaccines, which show a protection rate ranging from 50.7% to 83.5% according to recently published clinical phase III data (Clinical trials registration numbers: NCT04510207, NCT04456595, NCT04582344, and NCT04651790) (24–27). No enhanced respiratory disease (ERD) typical of an increased eosinophilic proinflammatory pulmonary response upon challenge has been detected in preclinical studies of these inactivated SARS-CoV-2 vaccines in either murine or nonhuman primate (NHP) pneumonia models (28–32). However, whether the relatively lower vaccine efficacy originates from lower induction of neutralization antibody production or the possibility of antibody-dependent enhancement (ADE) of infection caused by Th2-oriented serum and a subsequent pulmonary immune pathology remains to be determined (28–30).

S1 is the coronavirus spike protein segment that contains the N-terminal segment and the receptor-binding domain (RBD) responsible for viral attachment to host cells and is thus widely considered a potential coronavirus vaccine target (4, 33–35). When adjuvanted with alum, serum obtained after SARS-CoV-1 S1 subunit vaccination reportedly induces ADE of infection similar to that observed with serum obtained after vaccination with inactivated whole SARS-CoV-1 viruses (5). Considering several IgG1 subtype monoclonal antibodies targeting SARS-CoV-2 spike protein have been reported to induced ADE of infection *in vitro* recently, the risk of Th-2 oriented immune serum after SARS-CoV-2 vaccination that containing polyclonal antibodies targeting the spike protein to enhance virus infection is to be assessed (36–38). In this study, using the S1 segment of SARS-CoV-2 and inactivated whole SARS-CoV-2 virus as

antigen and aluminum as an adjuvant, we studied the risk of ADE of infection with Th2-oriented immune serum from mice and humans in immune cell lines expressing different patterns of FcRs. We aimed to provide helpful clues regarding adjusting immunization schedules or using new adjuvants to develop more effective subunit/inactivated SARS-CoV-2 vaccines.

## MATERIALS AND METHODS

### Cells and Human Serum Samples

Raji (Burkitt's lymphoma/B lymphoblasts), THP-1 (human acute monocytic leukemia cells), and K562 (human chronic myelogenous leukemia cells) cells were cultured in Roswell Park Memorial Institute (RPMI) 1640 medium (BD, USA) supplemented with 10% v/v fetal bovine serum (FBS, Biological Industries, Israel) and 100 U/mL penicillin-streptomycin (Thermo Fisher, USA). Vero (African green monkey kidney epithelial cells) and KMB17 (human embryonic lung fibroblast-like cells) cells were cultured in Dulbecco's modified Eagle's medium (DMEM, BD, USA) supplemented with 10% v/v FBS and 100 U/mL penicillin-streptomycin. All cells were obtained from the Conservation Genetics Chinese Academy of Sciences Kunming Cell Bank and maintained at 37°C in an environment with 5% CO<sub>2</sub> before use.

Human sera from a phase II clinical trial (Clinical trials registration number: NCT04412538) of an inactivated SARS-CoV-2 vaccine adjuvant with aluminum and SARS-CoV-2-infected human convalescent serum (HCS) were supplied by Professor Qihan Li from the Institute of Medical Biology, Chinese Academy of Medical Sciences (IMB, CAMS) (39). Specifically, healthy volunteers aged 18–59 years were intramuscularly inoculated twice with the KMS-1 SARS-CoV-2 strain (GenBank accession number MT226610.1) that was double inactivated by formaldehyde plus  $\beta$ -propiolactone and adjuvanted with aluminum hydroxide at medium doses (containing 100 enzyme-linked immunosorbent assay units (EUs) of viral antigen) or high doses (containing 150 EUs of viral antigen). Fourteen or 28 days after boost immunization, immune serum was collected to determine the authentic SARS-CoV-2 neutralization titers. Briefly, diluted serum samples (1:4, 1:8, 1:16, 1:32, 1:64, 1:128, and 1:256) were incubated at 37°C for 2 h with a virus at a titer 100 times higher than the 50% cell culture infectious dose (CCID<sub>50</sub>). The mixture was then added to Vero cells in 96-well plates and incubated at 37°C. After 1 week, the viral cytopathic effect (CPE) was observed and assessed with an inverted microscope (Nikon, Tokyo, Japan). The neutralization titers were defined as the highest dilution at which no CPE was observed, and neutralization titers under 4 were defined as 1 for calculation. Typical serum (N=5) with positive seroconversion, including neutralization titers equal to 4, 8, 32, 128, and 256, was collected randomly for this study.

### Immunization of Mice

Specific pathogen-free (SPF) female BALB/c mice at 6 weeks of age (14–17 g) were supplied and maintained by the Central

Services of the IMB, CAMS. The animals were randomly divided into 3 groups, and each group consisted of 6 mice ( $N=6$ ). SARS-CoV-2 S1 proteins expressed by HEK293 cells were purchased from Sino Biological Inc. (China). The purity of S1 was  $>90\%$  as determined by SDS-PAGE and  $>95\%$  as determined by size-exclusion chromatography high-performance liquid chromatography. S1 was diluted to  $5 \mu\text{g}/\text{mouse}/\text{dose}$  in  $25 \mu\text{L}$  of phosphate-buffered saline (PBS, pH 7.40) and mixed with the same volume of aluminum (Thermo Fisher, USA) to induce a typical Th2 response or nucleic acid immunostimulant mixtures that have been proven to induce a typical Th1 response (40). The nucleic acid immunostimulant mixtures contained  $20 \mu\text{g}/\text{mouse}/\text{dose}$  oligodeoxynucleotide containing CpG motifs (CpG ODN 2395, from *In vivo*Gen, USA) and  $25 \mu\text{g}/\text{mouse}/\text{dose}$  low-molecular-weight polyinosinic-polycytidylic acid (poly(I:C), from *In vivo*Gen, USA). Fifty microliters of immunogens or PBS (sham group) were administered intramuscularly to the thigh muscle three times at 2-week intervals.

### Enzyme-Linked Immunosorbent Assay (ELISA) of Antibody Titers

Two weeks after the final immunization, mice were anesthetized by an intraperitoneal injection of tribromoethanol, and blood was collected *via* cardiac puncture. After overnight clotting at  $4^\circ\text{C}$ , serum was collected by centrifugation at  $1000 \text{ g}$  for 10 min and pooled for further analysis. S1-specific IgG/IgG1/IgG2a titers were detected by ELISA (41, 42), and the IgG1-to-IgG2a titer ratio was calculated to evaluate the Th1-Th2 balance described previously (43, 44). Specifically, HEK293 cells expressing SARS-CoV-2 S1 protein (Sino Biological Inc., China) at  $2 \mu\text{g}/\text{mL}$  were coated on 96-well plates overnight at  $4^\circ\text{C}$ . The plates were washed with wash buffer ( $0.05\%$  (v/v) polysorbate 20 in PBS) once and then blocked with  $5\%$  (v/v) skim milk dissolved in wash buffer for 1 h at  $37^\circ\text{C}$ . The plates were washed four times and incubated with serially diluted mouse sera for 1 h at  $37^\circ\text{C}$ . After five washes, the plates were incubated with goat anti-mouse IgG/IgG1/IgG2a HRP-conjugated secondary antibodies (Thermo Fisher Scientific, USA) for 1 h at  $37^\circ\text{C}$ . After five washes,  $3,3',5,5'$ -tetramethylbenzidine (TMB, BD Bioscience, USA) substrate was added, the plates were incubated in the dark at room temperature for 10 min. The reactions were stopped by adding 2 M sulfuric acid, and the absorbance at 450 nm was detected using a microplate reader (Bio-Tek Instruments, Inc., USA). The antibody titers were defined by end-point dilution with a cutoff signal of  $\text{OD}_{450} = 0.1$ .

### Western Blot

Cells were cultured in 6-well plates until the concentration reached  $1 \times 10^6$  cells/mL for protein expression analysis. After three washes with PBS, radioimmunoprecipitation (RIPA) lysis buffer (Sigma, USA) supplemented with  $1\%$  protease inhibitor cocktail (MedChemExpress, USA) was added for the extraction of cellular protein. After quantification with a bicinchoninic acid (BCA) protein assay kit (Beyotime, China),  $10 \mu\text{g}$  of total protein was subjected to sodium dodecyl sulfate-polyacrylamide gel electrophoresis (SDS-PAGE) and transferred to a polyvinylidene fluoride (PVDF) membrane. After blocking with  $5\%$  milk,

antibodies (Abcam, USA) against angiotensin-converting enzyme 2 (anti-ACE2, 1:5 000), Fc $\gamma$ R1 (anti-CD64, 1:10 000) and Fc $\gamma$ R2 (anti-CD32A+CD32B+CD32C, 1:10 000) were used for assessing the protein expression of cells. A mouse monoclonal antibody against  $\beta$ -actin (Multi Sciences Biotech, China) was used to identify the quality of the protein extracted. Detection was performed using the enhanced chemiluminescence (ECL) reagent (Multi Sciences Biotech, China).

### Reverse Transcriptase PCR (RT-PCR)

Cells were cultured in 6-well plates at a concentration of  $1 \times 10^6$  cells/mL for gene transcription analysis. Total RNA of cells was isolated with TRIzol™ Reagent (Thermo Fisher Scientific, USA) and stored at  $-80^\circ\text{C}$  until use. According to the manufacturer's instructions, cDNAs were constructed with a PrimeScript™ RT Reagent Kit with gDNA Eraser (Takara, China). Briefly,  $2 \mu\text{L}$  of  $5 \times \text{gDNA}$  Eraser Buffer,  $1 \mu\text{L}$  of gDNA Eraser, and  $7 \mu\text{L}$  of RNA dissolved in RNase-free water were mixed to obtain a total volume of  $10 \mu\text{L}$ . After incubation at  $42^\circ\text{C}$  for 2 min, the mixture was then added to the reaction solution, which contained  $1 \mu\text{L}$  of PrimeScript RT Enzyme Mix I,  $1 \mu\text{L}$  of RT Primer Mix,  $4 \mu\text{L}$  of  $5 \times$  PrimeScript Buffer, and  $4 \mu\text{L}$  of RNase-free water. cDNAs were synthesized using the following PCR procedure:  $37^\circ\text{C}$  for 15 min,  $85^\circ\text{C}$  for 5 s, and maintained at  $4^\circ\text{C}$ .

RT-PCR was performed using previously described primer pairs to examine the expression of the genes encoding human ACE2, human Fc $\gamma$ R1A, human Fc $\gamma$ R2A, human Fc $\gamma$ R2B, and human glyceraldehyde-3-phosphate dehydrogenase (GAPDH) (5). The PCRs were initialized using a general procedure of  $94^\circ\text{C}$  for 5 min, 30 cycles of denaturation at  $94^\circ\text{C}$  for 45 s, annealing at  $60^\circ\text{C}$  for 45 s, and extension at  $72^\circ\text{C}$  for 45 s, and a final extension step of  $72^\circ\text{C}$  for 7 min. The PCR products were verified by  $2\%$  agarose gel electrophoresis.

### Pseudovirus-Based Neutralization Assay

SARS-CoV-2 S pseudotyped virus was used for neutralization assays in biosafety level 2 facilities. This pseudovirus was based on vesicular stomatitis virus (VSV) with the G gene replaced by the firefly luciferase reporter gene and the spike protein from SARS-CoV-2 incorporated as the membrane protein (45). Specifically, the pseudoviruses were diluted to  $1.3 \times 10^4$  50% tissue culture infectious dose (TCID $_{50}$ )/mL with complete DMEM before use. Fifty microliters of diluted SARS-CoV-2 S pseudovirus and  $50 \mu\text{L}$  of immune serum in serial dilutions were coinoculated at  $37^\circ\text{C}$  in an environment with  $5\%$   $\text{CO}_2$  for 60 min. Subsequently,  $100 \mu\text{L}$  of Vero-E6 cells ( $2 \times 10^5$  cells/mL) was seeded in each mixture for another 24 h at  $37^\circ\text{C}$  in an atmosphere with  $5\%$   $\text{CO}_2$ . Finally,  $100 \mu\text{L}$  of supernatant was discarded before testing. A cell control (CC), in which only cells with culture medium were added, and a virus control (VC), in which only pseudovirus and cells but no serum were added, were established separately. According to the manual protocol, the luciferase activity was assayed using a Britelite Plus Ultra-High Sensitivity Luminescence Reporter Gene Assay System (PerkinElmer, USA) and monitored using an EnSight™ Multimode Plate Reader (PerkinElmer, USA) (45).

## Pseudovirus-Based Antibody-Dependent Enhancement (ADE) of Infection *In Vitro*

The ADE of infection was evaluated *in vitro* using immune cell lines with different FcR expression patterns. Briefly, 25  $\mu$ L of serially diluted serum and 25  $\mu$ L of SARS-CoV-2 S pseudovirus (containing 250 TCID<sub>50</sub> pseudoviruses) were incubated at 37°C in an atmosphere with 5% CO<sub>2</sub> for 60 min. Then, 100  $\mu$ L of cells (2 $\times$ 10<sup>5</sup> cells/mL) was added to the mixtures for an additional 24 h of incubation. Afterward, the plates were centrifuged for 10 min at 300  $\times$ g, and 50  $\mu$ L of cell supernatant was discarded before testing. Cell control (CC), virus control (VC), and luciferase activity assays were performed as described above (37).

## Data Analysis

The data were processed with GraphPad Prism 7.0 (San Diego, CA, USA) and are shown as the means and standard deviations.

## RESULTS

### In SARS-CoV-2 S1 Subunit Vaccine-Immunized Mice, Aluminum Induces Th2 Responses, and Nucleic Acid Adjuvants Induce Th1 Responses

Two weeks after the third immunization (Figure 1A), vaccines with nucleic acid adjuvants (i.e., 20  $\mu$ g of CpG ODN 2395 + 25  $\mu$ g of poly(I:C)/mouse/dose) induced total S1-specific IgG antibody titers that were twofold higher (32,000 compared with 16,000) than those obtained with alum adjuvants (Figure 1B) and substantially higher production of S1-specific IgG2a subtype antibody (64,000 versus 500) (Figure 1C).

Although the S1-specific IgG1/IgG2a ratio in nucleic acid-adjuvanted immunized serum was 0.25, the IgG1/IgG2a ratio in alum-adjuvanted immunized serum was as high as 64, which is a typical Th2-oriented immune response (Figure 1D).

### Certification of Receptor Expression

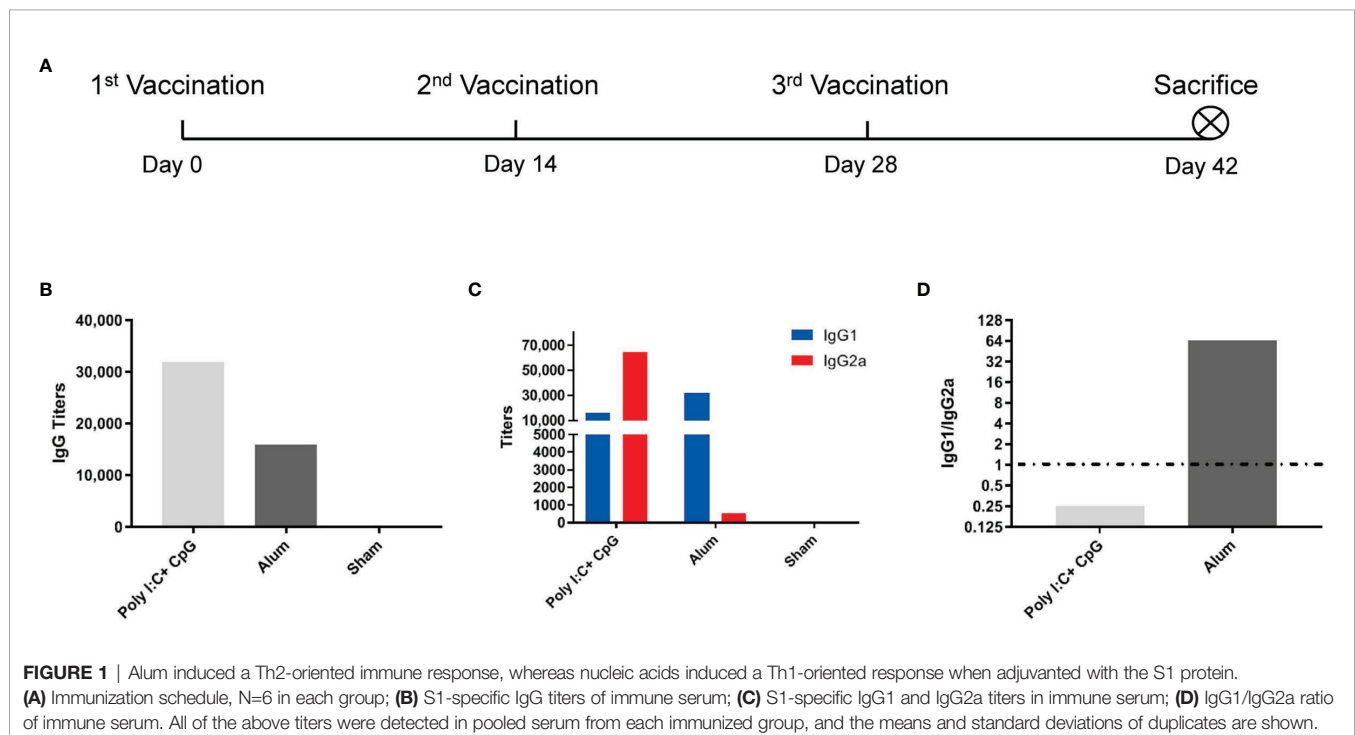
Both expressed proteins (Figure 2A) and transcribed genes (Figure 2B) of ACE2 (the main receptor for SARS-CoV-2 infection) but not any type of Fc $\gamma$ R were detected in Vero cells that were used for the proliferation of SARS-CoV-2 for inactivated vaccines, which makes Vero cells suitable for detection of the Fc $\gamma$ R-independent enhancement of infection by serum (4, 46).

The protein level of Fc $\gamma$ R1 in THP-1 and KMB17 cells was detected (Figure 2A). According to a detailed subtype analysis at the gene transcription level (Figure 2B), Fc $\gamma$ R1A was expressed in THP-1 cells, and the other type of Fc $\gamma$ R1, i.e., Fc $\gamma$ R1B, was expressed in KMB17 cells, possibly as a pseudogene.

Fc $\gamma$ R2 was detected at the protein level in Raji and THP-1 cells (Figure 2A). According to a detailed subtype analysis at the transcribed gene level (Figure 2B), Fc $\gamma$ R2B was expressed in Raji cells, and Fc $\gamma$ R2A was expressed in THP-1 cells. Although the gene transcription of Fc $\gamma$ R2A was also detected in K562 cells, a Western blot assay indicated that the corresponding protein was not expressed (Figure 2A).

### Th2-Oriented Immune Serum From S1-Based Subunit Vaccines Does Not Enhance Infection *In Vitro*

For the pseudovirus-based neutralization assay, although no luminescence was detected in the Vero cell control (CC), the luminescence of the virus control (VC) group was as high as 6 $\times$ 10<sup>5</sup>,



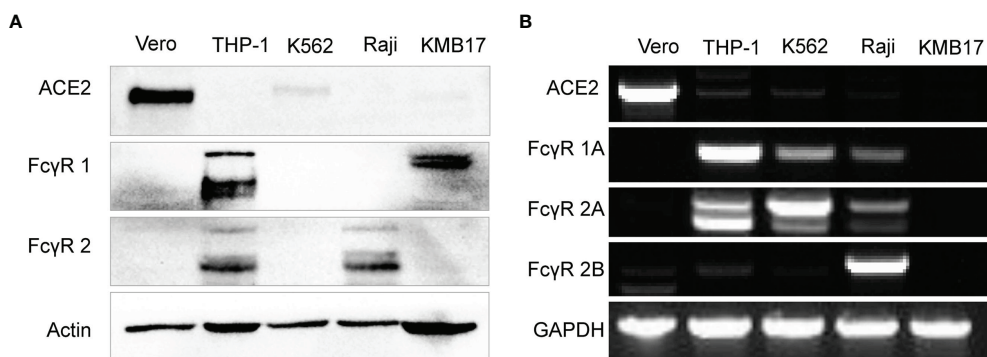


**FIGURE 2** | Fc receptor expression patterns in immune cell lines. **(A)** The protein expression levels of ACE2, FcγR1 and FcγR2 were detected by Western blot. **(B)** The gene expression of ACE2 and more specific FcγR subtypes, including FcγR1A, FcγR2A, and FcγR2B, was detected by RT-PCR.

which implied successful infection of Vero cells by SARS-CoV-2 S pseudotyped virus. Although the serum of PBS-administered mice (Sham in **Figure 3A**) showed no influence on pseudovirus infection, serum from S1-immunized mice blocked pseudovirus entry. If a luminescence of  $1 \times 10^5$  was taken as the cutoff value (which represents a more than 80% reduction in luminescence compared with that of the VC control), the virus neutralization titer (VNT) for serum from the nucleic acid-adjuncted S1 subunit vaccine group was approximately 1150, which was higher than that for serum from the alum-adjuncted S1 subunit vaccine group (VNT=700).

In the *in vitro* assays of the pseudovirus-based ADE of infection, even luminescence as low as  $1 \times 10^4$  (1/10 of that in the pseudovirus-based neutralization assay in **Figure 3A**, and background values around those detected in the VC control groups for each of the four cells) was taken as the cutoff value, and serum from neither the nucleic acid-adjuncted S1 subunit vaccine group nor the alum-adjuncted S1 subunit vaccine group showed ADE of infection in any of the four tested cell lines (**Figures 3B–E**). These cell lines included Raji cells that were confirmed to exhibit FcγR2B expression, which contributes to the enhancement of SARS-CoV-2 infection (37, 46), and THP-1 cells were confirmed to exhibit FcγR2A expression, which contributes to enhancement of MERS-CoV (47) and SARS-CoV-1 (5, 48) infection.

### Th2-Oriented Immune Serum After SARS-CoV-2 Inactivated Vaccine Administration Does Not Enhance Infection *In Vitro*

Considering that differences exist between the Fc fragment of mouse IgG and human IgG and that antibodies targeting other parts of the SARS-CoV-2 antigen except for the S1 segment may also show potential to promote infection, human sera after an inactivated SARS-CoV-2 vaccine adjuvant with alum were also tested in the abovementioned cell lines.

For the pseudovirus-based neutralization assay (**Figure 4A**), none of the five sera from the SARS-CoV-2 inactivated vaccine groups, nor the six HCSs efficiently blocked the entrance of pseudovirus at a dilution of 1:1000, as reflected by corresponding luminescence reads that were higher than the cutoff value of  $1 \times 10^5$  established in the previous section (**Figure 3A**).

In the *in vitro* assay of the pseudovirus-based ADE of infection, none of the five sera from the SARS-CoV-2 inactivated vaccine groups, nor the six HCSs showed ADE of infection (shown as luminescence lower than  $1 \times 10^4$ , the cutoff value for ADE discussed in the above subsection) in all four cell lines with serum dilutions from 1:1000 to 1:4000 (**Figures 4B–E**), as previously reported for the dilutions to detect ADE of infection with the SARS-CoV-1 subunit and inactivated vaccines adjuvanted with alum (5).

## DISCUSSION

According to preclinical studies of MERS-CoV and SARS-CoV-1 vaccines, both alum-adjuncted spike-protein-based subunits and inactivated vaccines provide partial protection upon challenge, which means that although the viral loads are lower than those in infected control animals, pulmonary immunopathology has been observed in both murine and NHP models (1–4). Notably, these immunopathologies were exacerbated compared with those of the infected control animals and were thus designated VAERD. An *in vitro* analysis showed that sera from these vaccines could enhance the infection of viruses in immune cell lines with different patterns of FcRs (5, 6). Concurrent with the reduced viral loads observed *in vivo*, these *in vitro* infections are abortive, but eliminating the virus is associated with releasing multiple proinflammatory cytokines that may cause a pulmonary immune pathology *in vivo* (5, 7–10).

Mouse serum resulting from three administrations of S1 protein adjuvanted with nucleic acid adjuvants induced higher SARS-CoV-2 neutralization titers than those in human serum after two administrations of inactivated SARS-CoV-2 vaccines, as reflected by the results showing that mouse serum resulting from the administration of S1 protein adjuvanted with nucleic acid adjuvants could still efficiently block the entrance of pseudovirus at a dilution of 1:1150 (**Figure 3A**), whereas none of the sera from alum-adjuncted inactivated SARS-CoV-2 vaccines could block the entrance of pseudovirus at a dilution of 1:1000 (**Figure 4A**). The extent to which formaldehyde treatment alters the native conformations of viral immunogens and may therefore affect the



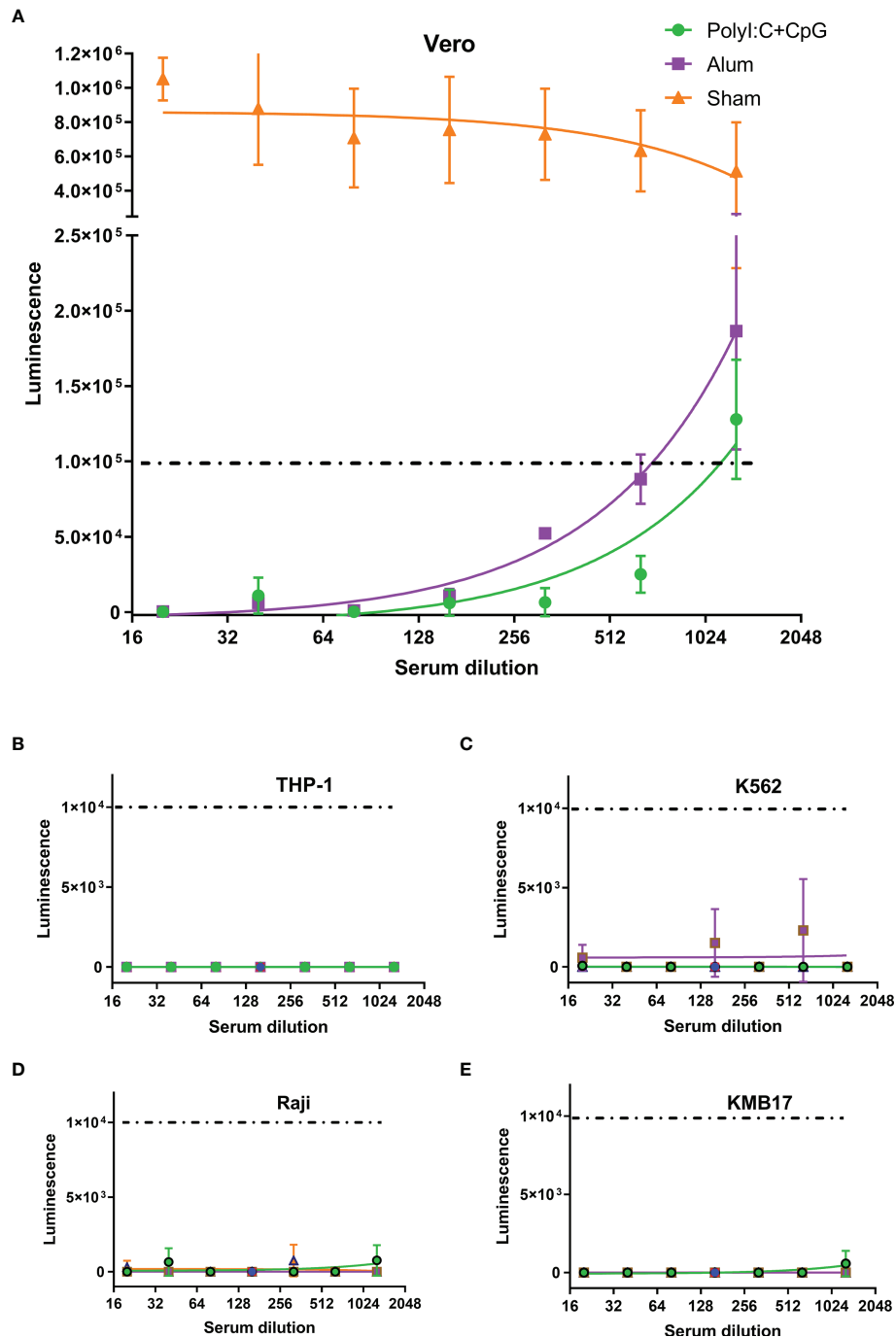


**FIGURE 3** | Th2-oriented immune serum after S1-based subunit vaccine administration does not enhance infection *in vitro*. **(A)** Pseudovirus-based neutralization assay of immune serum in Vero cells that express ACE2. **(B–E)** Assay of pseudovirus-based antibody-dependent enhancement of infection with immune serum in different FcγR-expressing cells. PolyI:C+CpG, nucleic acid-adjuvanted plus S1-purified protein immune serum; Alum, alum-adjuvanted plus S1-purified protein immune serum; Sham, serum from mice intramuscularly administered PBS instead of immunogens. All of the above analyses were performed using pooled serum from each immunized group. The means and standard deviations of duplicates are shown.

humoral immune responses elicited by inactivated vaccines remains to be further investigated.

Consistent with previous reports on anti-SARS-CoV-1 antibodies in which none of the sera-inducing ADE of

infection contain IgG2a antibodies (5), recent reports suggest that the SARS-CoV-2-targeting antibodies inducing ADE of infection are all IgG1 subtype monoclonal antibodies (36–38). Compared with immune sera from SARS-CoV-1 and MERS,

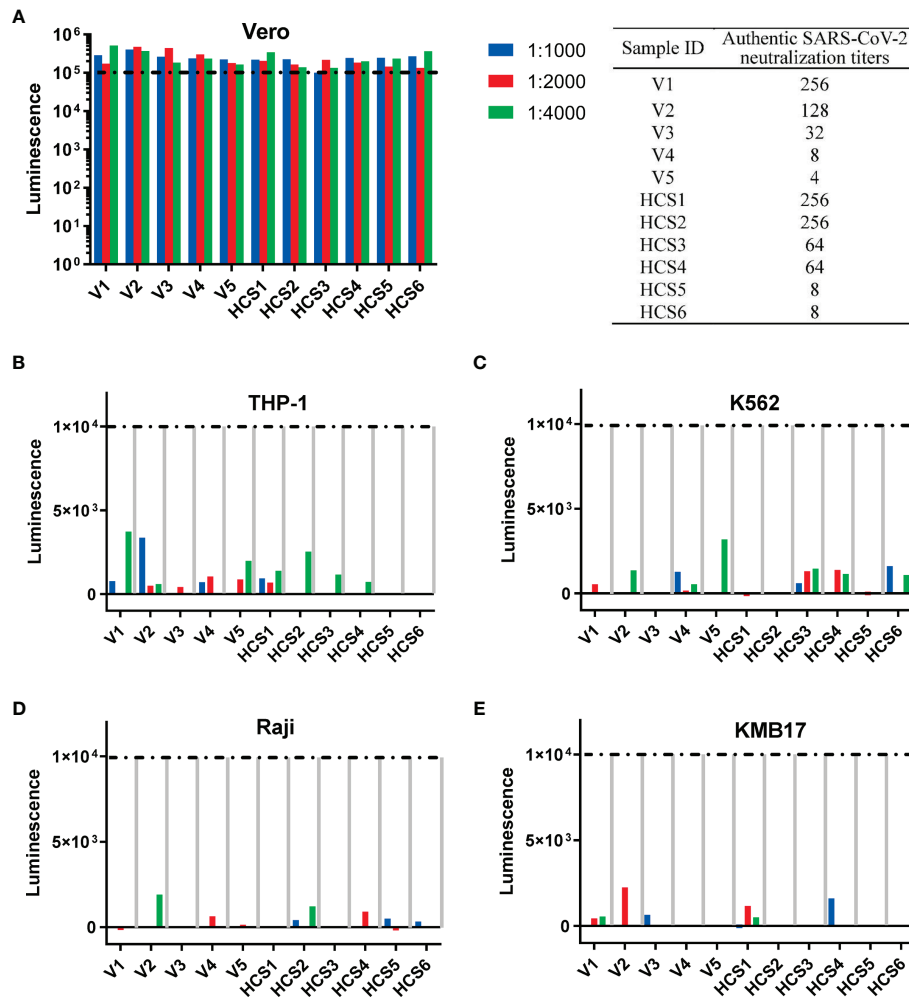


**FIGURE 4** | Th2-oriented immune serum after SARS-CoV-2 inactivated vaccine administration does not enhance infection *in vitro*. **(A)** Pseudovirus-based neutralization assay of human serum with low to high authentic SARS-CoV-2 neutralization titers (from 4 to 256) in Vero cells that express ACE2. The sample ID and authentic SARS-CoV-2 neutralization titer are shown in the table on the right. **(B–E)** Assay of pseudovirus-based antibody-dependent enhancement of infection with human serum in cells with different FcγR expression patterns. V1–V5, human sera after inactivated SARS-CoV-2 vaccination; HCS1–6: human convalescent serum. Each sample is shown separately.

which mainly depend on FcγR1 and FcγR2a for ADE of infection, ADE of infection by monoclonal antibodies against SARS-CoV-2 could be independent of FcγR (i.e., ACE2-dependent) or dependent on FcγR2b or FcγR1 (5, 37, 46). Nonetheless, after administering either alum- or nucleic acid-adjuvanted spike protein, immune serum contained polyclonal antibodies of both the IgG1 and IgG2a subtypes, although at different proportions (**Figure 1**). None of these polyclonal antibodies induced either ACE2-dependent or FcγR-dependent enhancement of infection, even at subneutralizing or non-neutralizing concentrations (**Figure 3**). A similar conclusion could also be drawn for human serum after inactivated SARS-CoV-2 vaccines that contain full-length spike proteins and other antigens, e.g., nucleocapsid proteins (5, 49) (**Figure 4**).

These results again turned our attention to Th2-type immunopathology. Previous preclinical research on both spike

protein-based SARS-CoV-1 subunit vaccines and inactivated vaccines have shown that formulations with Th1-oriented adjuvants, including delta inulin and Toll-like receptor agonists, could prevent or reduce excess eosinophilic infiltration in the lungs, alleviate pulmonary eosinophilic immunopathology and enhance vaccine protection in mouse models (12, 13). These SARS-CoV-1 vaccine preclinical studies are consistent with SARS-CoV-2 phase III clinical trials due to the higher protection rate of Th1-oriented mRNA vaccines and M-matrix-adjuvanted spike protein-based subunit vaccines (50–52). Indeed, trace amounts of virus that vaccinated people primarily encounter could be eliminated more easily than the high dose of viruses administered to animal models, and this finding stresses the influence of the immune pathology on the comparably lower protection rate of inactivated SARS-CoV-2 vaccines adjuvanted with alum, which induced typical Th2-oriented immune responses (24–27, 53). Although no ERD typical of an

increased eosinophilic proinflammatory pulmonary response upon challenge has been detected in preclinical studies of these inactivated SARS-CoV-2 vaccines in both murine and NHP pneumonia models (28–30), a recent parallel preclinical study of a SARS-CoV-2 mRNA vaccine and a full-length spike protein subunit vaccine adjuvanted with alum showed VAERD in mouse pneumonia models for the later (54). This result appears to be more reasonable and consistent with the conclusions from previous SARS-CoV-1 and MERS-CoV studies.

In conclusion, our studies demonstrated that Th2-oriented immune serum after SARS-CoV-2 vaccination does not enhance infection *in vitro*. We infer that the lower protection rate of inactivated SARS-CoV-2 vaccines may result from lower or waning induction of neutralization antibody production or a pulmonary eosinophilic immunopathology accompanied by eosinophilic infiltration in the lungs upon virus exposure. The immunization schedule and new adjuvants that can elevate neutralizing antibody levels and induce Th1-oriented responses to avoid a potential pulmonary eosinophilic immunopathology may be considered to elevate the protection rate of both inactivated and spike protein-based subunit SARS-CoV-2 vaccines (55–58).

## DATA AVAILABILITY STATEMENT

The raw data supporting the conclusions of this article will be made available by the authors, without undue reservation.

## ETHICS STATEMENT

The studies involving human participants were reviewed and approved by the Experimental Management Association of the IMB, CAMS. The patients/participants provided their written

informed consent to participate in this study. The animal study was reviewed and approved by the Ethics Committee of Animal Care and Welfare of IMB, CAMS, and the Yunnan Provincial Experimental Animal Management Association.

## AUTHOR CONTRIBUTIONS

Conceptualization, CL. Data curation, NL and TL. Investigation, NL, TL, YW, HC, XY, and KL. Project administration, CL. Supervision, CL. All the authors have read and agreed to the published version of the manuscript.

## FUNDING

This work was supported by the National Key R&D Program of China (grant numbers 2020YFC0849700 and 2020YFC0860600), the Major Science and Technology Special Projects of Yunnan Province (grant numbers 202003AC100009 and 202002AA100009), the CAMS Innovation Fund for Medical Sciences (CIFMS) (grant number 2021-12M-1-043), the Nonprofit Central Research Institute Fund of the Chinese Academy of Medical Sciences (2021-JKCS-012), the Special Biomedicine Projects of Yunnan Province (202102AA310035), the National Natural Science Foundation of China (82104130), the Fundamental Research Funds for the Central Universities (3332021072), the Basic Research Projects of Yunnan Province (202101AU070176 and 202101AT070286), the Funds for the Training of High-Level Health Technical Personnel in Yunnan Province (grant number H-2019063) and the Funds for High-level Scientific and Technological Talents Selection Special Project of Yunnan Province.

## REFERENCES

- Agrawal AS, Tao X, Algaissi A, Garron T, Narayanan K, Peng B, et al. Immunization With Inactivated Middle East Respiratory Syndrome Coronavirus Vaccine Leads to Lung Immunopathology on Challenge With Live Virus. *Hum Vaccin Immunother* (2016) 12(9):2351–6. doi: 10.1080/21645515.2016.1177688
- Tseng CT, Sbrana E, Iwata-Yoshikawa N, Newman PC, Garron T, Atmar RL, et al. Immunization With SARS Coronavirus Vaccines Leads to Pulmonary Immunopathology on Challenge With the SARS Virus. *PLoS One* (2012) 7(4): e35421. doi: 10.1371/journal.pone.0035421
- Bolles M, Deming D, Long K, Agnihothram S, Whitmore A, Ferris M, et al. A Double-Inactivated Severe Acute Respiratory Syndrome Coronavirus Vaccine Provides Incomplete Protection in Mice and Induces Increased Eosinophilic Proinflammatory Pulmonary Response Upon Challenge. *J Virol* (2011) 85(23):12201–15. doi: 10.1128/JVI.06048-11
- Wang Q, Zhang L, Kuwahara K, Li L, Liu Z, Li T, et al. Immunodominant SARS Coronavirus Epitopes in Humans Elicited Both Enhancing and Neutralizing Effects on Infection in Non-Human Primates. *ACS Infect Dis* (2016) 2(5):361–76. doi: 10.1021/acsinfecdis.6b00006
- Jaume M, Yip MS, Cheung CY, Leung HL, Li PH, Kien F, et al. Anti-Severe Acute Respiratory Syndrome Coronavirus Spike Antibodies Trigger Infection of Human Immune Cells *via* a pH- and Cysteine Protease-Independent Fcγ<sub>2</sub> Pathway. *J Virol* (2011) 85(20):10582–97. doi: 10.1128/JVI.00671-11
- Wang SF, Tseng SP, Yen CH, Yang JY, Tsao CH, Shen CW, et al. Antibody-Dependent SARS Coronavirus Infection Is Mediated by Antibodies Against Spike Proteins. *Biochem Biophys Res Commun* (2014) 451(2):208–14. doi: 10.1016/j.bbrc.2014.07.090
- Lee WS, Wheatley AK, Kent SJ, DeKosky BJ. Antibody-Dependent Enhancement and SARS-CoV-2 Vaccines and Therapies. *Nat Microbiol* (2020) 5(10):1185–91. doi: 10.1038/s41564-020-00789-5
- Zheng J, Wang Y, Li K, Meyerholz DK, Allamargot C, Perlman S. Severe Acute Respiratory Syndrome Coronavirus 2-Induced Immune Activation and Death of Monocyte-Derived Human Macrophages and Dendritic Cells. *J Infect Dis* (2021) 223(5):785–95. doi: 10.1093/infdis/jiaa753
- Liu L, Wei Q, Lin Q, Fang J, Wang H, Kwok H, et al. Anti-Spike IgG Causes Severe Acute Lung Injury by Skewing Macrophage Responses During Acute SARS-CoV Infection. *JCI Insight* (2019) 4(4):e123158. doi: 10.1172/jci.insight.123158
- Zhou J, Chu H, Li C, Wong BH, Cheng ZS, Poon VK, et al. Active Replication of Middle East Respiratory Syndrome Coronavirus and Aberrant Induction of Inflammatory Cytokines and Chemokines in Human Macrophages: Implications for Pathogenesis. *J Infect Dis* (2014) 209(9):1331–42. doi: 10.1093/infdis/jit504
- Rotondo JC, Martini F, Maritati M, Mazziotta C, Mauro GD, Lanzillotti C, et al. SARS-CoV-2 Infection: New Molecular, Phylogenetic, and Pathogenetic Insights. Efficacy of Current Vaccines and the Potential Risk of Variants. *Viruses* (2021) 13(9):1687. doi: 10.3390/v13091687

12. Iwata-Yoshikawa N, Uda A, Suzuki T, Tsunetsugu-Yokota Y, Sato Y, Morikawa S, et al. Effects of Toll-Like Receptor Stimulation on Eosinophilic Infiltration in Lungs of BALB/c Mice Immunized With UV-Inactivated Severe Acute Respiratory Syndrome-Related Coronavirus Vaccine. *J Virol* (2014) 88 (15):8597–614. doi: 10.1128/JVI.00983-14
13. Honda-Okubo Y, Barnard D, Ong CH, Peng BH, Tseng CT, Petrovsky N. Severe Acute Respiratory Syndrome-Associated Coronavirus Vaccines Formulated With Delta Inulin Adjuvants Provide Enhanced Protection While Ameliorating Lung Eosinophilic Immunopathology. *J Virol* (2015) 89 (6):2995–3007. doi: 10.1128/JVI.02980-14
14. Roberts A, Lamirande EW, Vogel L, Baras B, Goossens G, Knott I, et al. Immunogenicity and Protective Efficacy in Mice and Hamsters of a Beta-Propiolactone Inactivated Whole Virus SARS-CoV Vaccine. *Viral Immunol* (2010) 23(5):509–19. doi: 10.1089/vim.2010.0028
15. Corbett KS, Edwards DK, Leist SR, Abiona OM, Boyoglu-Barnum S, Gillespie RA, et al. SARS-CoV-2 mRNA Vaccine Design Enabled by Prototype Pathogen Preparedness. *Nature* (2020) 586(7830):567–71. doi: 10.1038/s41586-020-2622-0
16. Corbett KS, Flynn B, Foulds KE, Francica JR, Boyoglu-Barnum S, Werner AP, et al. Evaluation of the mRNA-1273 Vaccine Against SARS-CoV-2 in Nonhuman Primates. *N Engl J Med* (2020) 383(16):1544–55. doi: 10.1056/NEJMoa2024671
17. Laczko D, Hogan MJ, Toulmin SA, Hicks P, Lederer K, Gaudette BT, et al. A Single Immunization With Nucleoside-Modified mRNA Vaccines Elicits Strong Cellular and Humoral Immune Responses Against SARS-CoV-2 in Mice. *Immunity* (2020) 53(4):724–32.e727. doi: 10.1016/j.immuni.2020.07.019
18. Jackson LA, Anderson EJ, Roupael NG, Roberts PC, Makhene M, Coler RN, et al. An mRNA Vaccine Against SARS-CoV-2 - Preliminary Report. *N Engl J Med* (2020) 383(20):1920–31. doi: 10.1056/NEJMoa2022483
19. Walsh EE, Frenck RW Jr, Falsey AR, Kitchin N, Absalon J, Gurtman A, et al. Safety and Immunogenicity of Two RNA-Based Covid-19 Vaccine Candidates. *N Engl J Med* (2020) 383(25):2439–50. doi: 10.1056/NEJMoa2027906
20. Guebre-Xabier M, Patel N, Tian JH, Zhou B, Maciejewski S, Lam K, et al. NVX-CoV2373 Vaccine Protects Cynomolgus Macaque Upper and Lower Airways Against SARS-CoV-2 Challenge. *Vaccine* (2020) 38(50):7892–6. doi: 10.1016/j.vaccine.2020.10.064
21. Keech C, Albert G, Cho I, Robertson A, Reed P, Neal S, et al. Phase 1-2 Trial of a SARS-CoV-2 Recombinant Spike Protein Nanoparticle Vaccine. *N Engl J Med* (2020) 383(24):2320–32. doi: 10.1056/NEJMoa2026920
22. Tian JH, Patel N, Haupt R, Zhou H, Weston S, Hammond H, et al. SARS-CoV-2 Spike Glycoprotein Vaccine Candidate NVX-CoV2373 Immunogenicity in Baboons and Protection in Mice. *Nat Commun* (2021) 12(1):372. doi: 10.1038/s41467-020-20653-8
23. HogenEsch H, O'Hagan DT, Fox CB. Optimizing the Utilization of Aluminum Adjuvants in Vaccines: You Might Just Get What You Want. *NPJ Vaccines* (2018) 3:51. doi: 10.1038/s41541-018-0089-x
24. Palacios R, Batista AP, Albuquerque CSN, Patio EG, Santos JDP, Mnica TRPC, et al. Efficacy and Safety of a COVID-19 Inactivated Vaccine in Healthcare Professionals in Brazil: The PROFISCOV Study. *Soc Sci Res Net* (2021). doi: 10.2139/ssrn.3822780.
25. Al Kaabi N, Zhang Y, Xia S, Yang Y, Al Qahtani MM, Abdulrazzaq N, et al. Effect of 2 Inactivated SARS-CoV-2 Vaccines on Symptomatic COVID-19 Infection in Adults: A Randomized Clinical Trial. *JAMA* (2021) 326(1):35–45. doi: 10.1001/jama.2021.8565
26. Tanriover MD, Doganay HL, Akova M, Guner HR, Azap A, Akhan S, et al. Efficacy and Safety of an Inactivated Whole-Virion SARS-CoV-2 Vaccine (CoronaVac): Interim Results of a Double-Blind, Randomised, Placebo-Controlled, Phase 3 Trial in Turkey. *Lancet* (2021) 398(10296):213–22. doi: 10.1016/S0140-6736(21)01429-X
27. Jara A, Undurraga EA, Gonzalez C, Paredes F, Fontecilla T, Jara G, et al. Effectiveness of an Inactivated SARS-CoV-2 Vaccine in Chile. *N Engl J Med* (2021) 385(10):875–84. doi: 10.1056/NEJMoa2107715
28. Gao Q, Bao L, Mao H, Wang L, Xu K, Yang M, et al. Development of an Inactivated Vaccine Candidate for SARS-CoV-2. *Science* (2020) 369 (6499):77–81. doi: 10.1126/science.abc1932
29. Wang H, Zhang Y, Huang B, Deng W, Quan Y, Wang W, et al. Development of an Inactivated Vaccine Candidate, BBIBP-CorV, With Potent Protection Against SARS-CoV-2. *Cell* (2020) 182(3):713–21.e719. doi: 10.1016/j.cell.2020.06.008
30. Wang ZJ, Zhang HJ, Lu J, Xu KW, Peng C, Huo J, et al. Low Toxicity and High Immunogenicity of an Inactivated Vaccine Candidate Against COVID-19 in Different Animal Models. *Emerg Microbes Infect* (2020) 9(1):2606–18. doi: 10.1080/22221751.2020.1852059
31. Bewley KR, Gooch K, Thomas KM, Longet S, Wiblin N, Hunter L, et al. Immunological and Pathological Outcomes of SARS-CoV-2 Challenge Following Formalin-Inactivated Vaccine in Ferrets and Rhesus Macaques. *Sci Adv* (2021) 7(37):eabg7996. doi: 10.1126/sciadv.abg7996
32. Yuan L, Tang Q, Zhu H, Guan Y, Cheng T, Xia N. SARS-CoV-2 Infection and Disease Outcomes in Non-Human Primate Models: Advances and Implications. *Emerg Microbes Infect* (2021) 10(1):1881–9. doi: 10.1080/22221751.2021.1976598
33. He Y, Li J, Heck S, Lustigman S, Jiang S. Antigenic and Immunogenic Characterization of Recombinant Baculovirus-Expressed Severe Acute Respiratory Syndrome Coronavirus Spike Protein: Implication for Vaccine Design. *J Virol* (2006) 80(12):5757–67. doi: 10.1128/JVI.00083-06
34. Ren W, Sun H, Gao GF, Chen J, Sun S, Zhao R, et al. Recombinant SARS-CoV-2 Spike S1-Fc Fusion Protein Induced High Levels of Neutralizing Responses in Nonhuman Primates. *Vaccine* (2020) 38(35):5653–8. doi: 10.1016/j.vaccine.2020.06.066
35. Wang N, Shang J, Jiang S, Du L. Subunit Vaccines Against Emerging Pathogenic Human Coronaviruses. *Front Microbiol* (2020) 11:298. doi: 10.3389/fmicb.2020.00298
36. Liu Y, Soh WT, Kishikawa JI, Hirose M, Nakayama EE, Li S, et al. An Infectivity-Enhancing Site on the SARS-CoV-2 Spike Protein Targeted by Antibodies. *Cell* (2021) 184(13):3452–66.e3418. doi: 10.1016/j.cell.2021.05.032
37. Wang S, Peng Y, Wang R, Jiao S, Wang M, Huang W, et al. Characterization of Neutralizing Antibody With Prophylactic and Therapeutic Efficacy Against SARS-CoV-2 in Rhesus Monkeys. *Nat Commun* (2020) 11(1):5752. doi: 10.1038/s41467-020-19568-1
38. Zhou Y, Liu Z, Li S, Xu W, Zhang Q, Silva IT, et al. Enhancement Versus Neutralization by SARS-CoV-2 Antibodies From a Convalescent Donor Associates With Distinct Epitopes on the RBD. *Cell Rep* (2021) 34 (5):108699. doi: 10.1016/j.celrep.2021.108699
39. Che Y, Liu X, Pu Y, Zhou M, Zhao Z, Jiang R, et al. Randomized, Double-Blinded and Placebo-Controlled Phase II Trial of an Inactivated SARS-CoV-2 Vaccine in Healthy Adults. *Clin Infect Dis* (2021) 73(11):e3949–55. doi: 10.1093/cid/ciaa1703
40. Cao H, Yang S, Wang Y, Luan N, Yin X, Lin K, et al. An Established Th2-Oriented Response to an Alum-Adjuvanted SARS-CoV-2 Subunit Vaccine Is Not Reversible by Sequential Immunization With Nucleic Acid-Adjuvanted Th1-Oriented Subunit Vaccines. *Vaccines (Basel)* (2021) 9(11):1261. doi: 10.3390/vaccines9111261
41. Cao H, Wang Y, Luan N, Liu C. Immunogenicity of Varicella-Zoster Virus Glycoprotein E Formulated With Lipid Nanoparticles and Nucleic Immunostimulators in Mice. *Vaccines (Basel)* (2021) 9(4):310. doi: 10.3390/vaccines9040310
42. Wang P. Natural and Synthetic Saponins as Vaccine Adjuvants. *Vaccines (Basel)* (2021) 9(3):222. doi: 10.3390/vaccines9030222
43. Lefebvre DJ, Benaissa-Trouw B, Vliegthart JF, Kamerling JP, Jansen WTM, Kraaijeveld K, et al. Th1-Directing Adjuvants Increase the Immunogenicity of Oligosaccharide-Protein Conjugate Vaccines Related to Streptococcus Pneumoniae Type 3. *Infect Immun* (2003) 71(12):6915–20. doi: 10.1128/IAI.71.12.6915-6920.2003
44. Mountford AP, Fisher A, Wilson RA. The Profile of IgG1 and IgG2a Antibody Responses in Mice Exposed to *Schistosoma mansoni*. *Parasite Immunol* (1994) 16(10):521–7. doi: 10.1111/j.1365-3024.1994.tb00306.x
45. Nie J, Li Q, Wu J, Zhao C, Hao H, Liu H, et al. Quantification of SARS-CoV-2 Neutralizing Antibody by a Pseudotyped Virus-Based Assay. *Nat Protoc* (2020) 15(11):3699–715. doi: 10.1038/s41596-020-0394-5
46. Li D, Edwards RJ, Manne K, Martinez DR, Schafer A, Alam SM, et al. *In Vitro* and *In Vivo* Functions of SARS-CoV-2 Infection-Enhancing and Neutralizing Antibodies. *Cell* (2021) 184(16):4203–19.e4232. doi: 10.1016/j.cell.2021.06.021

47. Wan Y, Shang J, Sun S, Tai W, Chen J, Geng Q, et al. Molecular Mechanism for Antibody-Dependent Enhancement of Coronavirus Entry. *J Virol* (2020) 94(5):e02015–19. doi: 10.1128/JVI.02015-19
48. Yip MS, Leung HL, Li PH, Cheung CY, Dutry I, Li D, et al. Antibody-Dependent Enhancement of SARS Coronavirus Infection and Its Role in the Pathogenesis of SARS. *Hong Kong Med J* (2016) 22(3 Suppl 4):25–31.
49. Zhang Y, Li D, Zhao H, Wang L, Liao Y, Li X, et al. The Role of Multiple SARS-CoV-2 Viral Antigens in a Vaccine-Induced Integrated Immune Response. *Vaccine* (2021) 39(18):2500–3. doi: 10.1016/j.vaccine.2021.03.067
50. Baden LR, El Sahly HM, Essink B, Kotloff K, Frey S, Novak R, et al. Efficacy and Safety of the mRNA-1273 SARS-CoV-2 Vaccine. *N Engl J Med* (2021) 384(5):403–16. doi: 10.1056/NEJMoa2035389
51. Heath PT, Galiza EP, Baxter DN, Boffito M, Browne D, Burns F, et al. Safety and Efficacy of NVX-CoV2373 Covid-19 Vaccine. *N Engl J Med* (2021) 385(13):1172–83. doi: 10.1056/NEJMoa2107659
52. Polack FP, Thomas SJ, Kitchin N, Absalon J, Gurtman A, Lockhart S, et al. Safety and Efficacy of the BNT162b2 mRNA Covid-19 Vaccine. *N Engl J Med* (2020) 383(27):2603–15. doi: 10.1056/NEJMoa2034577
53. Li D, Luan N, Li J, Zhao H, Zhang Y, Long R, et al. Waning Antibodies From Inactivated SARS-CoV-2 Vaccination Offer Protection Against Infection Without Antibody-Enhanced Immunopathology in Rhesus Macaque Pneumonia Models. *Emerg Microbes Infect* (2021) 10(1):2194–8. doi: 10.1080/22221751.2021.2002670
54. DiPiazza AT, Leist SR, Abiona OM, Moliva JJ, Werner A, Minai M, et al. COVID-19 Vaccine mRNA-1273 Elicits a Protective Immune Profile in Mice That is Not Associated With Vaccine-Enhanced Disease Upon SARS-CoV-2 Challenge. *Immunity* (2021) 54(8):1869–82.e1866. doi: 10.1016/j.immuni.2021.06.018
55. Ella R, Reddy S, Jogdand H, Sarangi H, Ganneru H, Prasad H, et al. Safety and Immunogenicity of an Inactivated SARS-CoV-2 Vaccine, BBV152: Interim Results From a Double-Blind, Randomised, Multicentre, Phase 2 Trial, and 3-Month Follow-Up of a Double-Blind, Randomised Phase 1 Trial. *Lancet Infect Dis* (2021) 21(7):950–61. doi: 10.1016/S1473-3099(21)00070-0
56. Ganneru B, Jogdand H, Daram VK, Das D, Molugu NR, Prasad SD, et al. Th1 Skewed Immune Response of Whole Virion Inactivated SARS CoV 2 Vaccine and its Safety Evaluation. *iScience* (2021) 24(4):102298. doi: 10.1016/j.isci.2021.102298
57. Liang JG, Su D, Song TZ, Zeng Y, Huang W, Wu J, et al. S-Trimer, a COVID-19 Subunit Vaccine Candidate, Induces Protective Immunity in Nonhuman Primates. *Nat Commun* (2021) 12(1):1346. doi: 10.1038/s41467-021-21634-1
58. Richmond P, Hatchuel L, Dong M, Ma B, Hu B, Smolenov I, et al. Safety and Immunogenicity of S-Trimer (SCB-2019), a Protein Subunit Vaccine Candidate for COVID-19 in Healthy Adults: A Phase 1, Randomised, Double-Blind, Placebo-Controlled Trial. *Lancet* (2021) 397(10275):682–94. doi: 10.1016/S0140-6736(21)00241-5

**Conflict of Interest:** The authors declare that the research was conducted in the absence of any commercial or financial relationships that could be construed as a potential conflict of interest.

**Publisher's Note:** All claims expressed in this article are solely those of the authors and do not necessarily represent those of their affiliated organizations, or those of the publisher, the editors and the reviewers. Any product that may be evaluated in this article, or claim that may be made by its manufacturer, is not guaranteed or endorsed by the publisher.

Copyright © 2022 Luan, Li, Wang, Cao, Yin, Lin and Liu. This is an open-access article distributed under the terms of the Creative Commons Attribution License (CC BY). The use, distribution or reproduction in other forums is permitted, provided the original author(s) and the copyright owner(s) are credited and that the original publication in this journal is cited, in accordance with accepted academic practice. No use, distribution or reproduction is permitted which does not comply with these terms.



# Evaluation of the Safety and Immunogenicity of Duck-Plague Virus gE Mutants

Yaru Ning<sup>1,2,3†</sup>, Yalin Huang<sup>1,2,3†</sup>, Mingshu Wang<sup>1,2,3†</sup>, Anchun Cheng<sup>1,2,3\*</sup>, Renyong Jia<sup>1,2,3</sup>, Mafeng Liu<sup>1,2,3</sup>, Dekang Zhu<sup>2,3</sup>, Shun Chen<sup>1,2,3</sup>, Xinxin Zhao<sup>1,2,3</sup>, Shaqiu Zhang<sup>1,2,3</sup>, Qiao Yang<sup>1,2,3</sup>, Ying Wu<sup>1,2,3</sup>, Juan Huang<sup>1,2,3</sup>, Bin Tian<sup>1,3</sup>, Xumin Ou<sup>1,2,3</sup>, Sai Mao<sup>1,2,3</sup>, Qun Gao<sup>1,2,3</sup>, Di Sun<sup>1,2,3</sup>, Yanlin Yu<sup>1,2,3</sup> and Ling Zhang<sup>1,2,3</sup>

## OPEN ACCESS

### Edited by:

Chunfu Zheng,  
University of Calgary, Canada

### Reviewed by:

Xiaochuan Liu,  
University of California, Riverside,  
United States  
Hong-Yi Xin,  
National University of Singapore,  
Singapore

### \*Correspondence:

Anchun Cheng  
chenganchun@vip.163.com

<sup>†</sup>These authors have contributed  
equally to this work

### Specialty section:

This article was submitted to  
Viral Immunology,  
a section of the journal  
Frontiers in Immunology

Received: 24 February 2022

Accepted: 28 March 2022

Published: 20 April 2022

### Citation:

Ning Y, Huang Y, Wang M, Cheng A, Jia R, Liu M, Zhu D, Chen S, Zhao X, Zhang S, Yang Q, Wu Y, Huang J, Tian B, Ou X, Mao S, Gao Q, Sun D, Yu Y and Zhang L (2022) Evaluation of the Safety and Immunogenicity of Duck-Plague Virus gE Mutants. *Front. Immunol.* 13:882796. doi: 10.3389/fimmu.2022.882796

<sup>1</sup> Research Center of Avian Disease, College of Veterinary Medicine, Sichuan Agricultural University, Chengdu, China, <sup>2</sup> Institute of Preventive Veterinary Medicine, Sichuan Agricultural University, Chengdu, China, <sup>3</sup> Key Laboratory of Animal Disease and Human Health of Sichuan Province, College of Veterinary Medicine, Sichuan Agricultural University, Chengdu, China

Duck plague (DP) is an acute infectious disease in the duck industry. The duck plague virus (DPV) is the pathogen, a subfamily of *alphaherpesvirinae*. gE is a type I membrane protein that contains three parts: an extracellular domain, a transmembrane domain, and a cytoplasmic domain. gE is the major virulence determinant of  $\alpha$ -herpesvirus. However, the functions of the gE extracellular and cytoplasmic domains have not been reported in DPV. In this study, a gE extracellular domain deletion mutant and a gE cytoplasmic domain deletion mutant were constructed from DPV. Virus replication kinetics showed that the growth titers of both the gE ectodomain-deleted mutant virus and the gE cytoplasmic domain-deleted virus in DEFs were lower than that of the parental virus CHv-50. DPV CHv-gE $\Delta$ ET and DPV CHv-gE $\Delta$ CT were continuously passed to the 20th passage in DEFs and the 10th in ducklings. The mutant virus DNA after passage was extracted for identification. The results showed that the gE ectodomain and gE cytoplasmic domain deletion mutant viruses have good genetic stability. The ducklings in each group (n=10) were inoculated with the same titers of DPV CHv-gE $\Delta$ ET, DPV CHv-gE $\Delta$ CT, DPV CHv- $\Delta$ gE, and parental CHv-50, respectively. Clinical symptoms and serum antibody levels were detected after inoculation. The results showed that the virulence of DPV CHv-gE $\Delta$ CT to ducklings was reduced compared with parental CHv-50, while the virulence of DPV CHv-gE $\Delta$ ET to ducklings was significantly reduced.  $10^5$  TCID<sub>50</sub> DPV CHv-gE $\Delta$ ET or DPV CHv- $\Delta$ gE can induce ducklings to produce DPV-specific antibodies, protect the ducklings from virulent CHv challenge. Therefore, DPV CHv-gE $\Delta$ ET may serve as a promising vaccine candidate to prevent and control duck plague.

**Keywords:** duck plague virus, gE, extracellular domain, genetic stability, pathogenicity, vaccine

## INTRODUCTION

Duck plague (DP) is an acute disease with a high fatality rate caused by DPV, which has caused significant economic losses to the duck industry around the world and has shown a trend of younger age in recent years (1–3). Studies have shown that duck herd immunization with the attenuated vaccine can prevent the occurrence of duck plague, but after immunization, it is impossible to distinguish whether it is wild virus infection or vaccine immunization produces antibodies, resulting in the lack of strong physicochemical technical support for the technical plan to purify DPV infection through immunization (4). Therefore, there is an urgent need to develop a more effective vaccine to eradicate DPV. It has been reported that many countries have successfully eradicated pseudorabies through the gene deletion DIVA (differentiating infected from vaccinated animals) vaccine. Like PRV, DPV is also a member of the *alphaherpesviruses* (5–7). Therefore, the emerging DPV gene-deleted attenuated mutant virus is promising as a candidate vaccine for the control and eradication of duck plague.

DPV is a member of the *alphaherpesvirus* subfamily, with a double-stranded DNA genome of approximately 162 kb and a capsid, tegument, and envelope. The gE protein in DPV is encoded by the *US8* gene and has the characteristics of a typical type I membrane protein. The polypeptide chain transmembrane once, the N-terminus is outside the cell membrane, and the C-terminus is inside the cell membrane. Therefore, according to the transmembrane structure of gE protein, we divided it into three parts: extracellular domain, transmembrane domain and intracellular domain. gE is a non-essential structural protein that facilitates the spread of viruses from cell to cell, under certain circumstances, promotes anterograde transport of latent virions after reactivation, and is neurotoxic (8). The viral plaques of the mutant virus BAC-CHv-ΔgE on DEFs were about 60% smaller than that of the wild virus BAC-CHv (9). Electron microscopy results showed that the deletion of DPV gE caused a large number of capsids to accumulate around the vesicles, and only a few were able to bud into vesicles, which is consistent with reports in other herpesviruses such as HSV-1, HSV-2, VZV, PRV, suggesting that gE plays an important role in virion morphogenesis prior to final cytoplasmic nucleocapsid wrapping (10, 11). The gE CT is involved in the second coating of the nucleocapsid in specific parts of the Golgi apparatus, selectively distributing nascent virions to cell junctions and promoting the spread of viruses between cells. Viruses with deletions in different regions of gE CT were constructed on HSV-1 gD gene deletion strains, and it was found that after deletion of amino acids 470–495, a large number of nucleocapsids accumulated in the cytoplasm (12). DPV gE CT interacts with UL11. In the absence of gE CT, the amount of UL11 packaged into virions is reduced by 58.1 ~ 80%, and the nucleocapsid cannot complete the secondary coating to form complete virions, which inhibits the release of the virus (13, 14). gE ET mainly plays a role in the intercellular propagation between epithelial cells and polar cells such as neural tissue. Through the receptor mechanism, gE ET localizes the gE/gI complex at the extracellular junction and binds to the adjacent cell receptor, promoting the fusion of infected cells and adjacent non-infected

cells. The amino acids 277, 291, and 348 of HSV gE ET were mutated to construct three mutant strains. Small plaques were formed after infecting cells, similar to the gE gene deletion strain, and the transmission of the virus from the cornea to the epithelial tissue was restricted (15). The deletion of amino acids 208–236 in the cysteine region of VZV gE ET changed the distribution of gE on the cell membrane and affected the spread of the virus between cells (16).

Notably, DPV can replicate and persist at high levels in duck tissues (17), which is associated with the ability of the virus to evade host immune defenses. gE forms a dimer with gI and participates in the immune evasion function of the virus to enhance the virulence of the virus. It is a good vaccine target protein. PRV gE has been reported to inhibit cGAS/STING-mediated IFN-β production by degrading CBP to disrupt the enhanced assembly of IRF3 and CBP (18). HSV gE binds to the Fc segment of IgG, which spatially prevents IgG or Fc-dependent effector cells from approaching the virus or virus-infected cells. Complement C1q cannot bind to the IgG Fc site, blocking the classical pathway of complement (19, 20). Protects viruses from immune processes such as antibody-dependent cytotoxicity and antibody-dependent cell-mediated phagocytosis (21–23). gE can also interact with prohibitin-1, which is conserved in all herpesviruses, for cell-to-cell transmission through the MAPK/ERK pathway (24). However, the molecular mechanism by which DPV gE plays a role in cell-to-cell transmission, evading the immune responses, and enhancing viral virulence has not been fully elucidated. The reported virulence genes mainly express non-essential envelope glycoproteins or nonstructural proteins. For example, the main virulence genes of PRV include gB, gC, TK, US3 (25–27). Therefore, studying the function of DPV gE from histopathology and *in vivo* colonization is crucial for the prevention and treatment of DPV infection, and there is no report on the key regions of gE virulence genes in DPV.

This study constructed CHv-gEΔET and CHv-gEΔCT deletion mutant viruses using bacterial artificial chromosome cloning of the DPV CHv-BAC-G strain. The efficacy of the mutant virus as a candidate vaccine for the control or eradication of duck plague in duck flocks was evaluated, and the safety and immunogenicity of the mutant virus were evaluated.

## MATERIALS AND METHODS

### Animals and Ethics Statement

9-day-old Cherry Valley duck embryos and 7-day-old healthy Cherry Valley ducks were purchased from a farm operated by Sichuan Agricultural University (Sichuan, China). All experimental ducks did not contain DPV and were negative for DPV antibodies (28). The experimental animal protocol was approved by the Ethics and Animal Welfare Committee of Sichuan Agricultural University and carried out following the Chinese version of the Guide for the Care and Use of Laboratory Animals.

### Viruses and Cells

Parent virus CHv-50 (GenBank: JQ647509.1) (3) and DPV CHv-ΔgE deletion mutant virus were provided by our laboratory.

DEFs were prepared from 9-day-old Cherry Valley duck embryos in Modified Eagle’s Medium (MEM, Gibco, Rockford, USA) supplemented with 10% neonatal bovine serum (NBS, Gibco, Rockford, USA) and 1% antibiotics (penicillin and streptavidin), cultured at 37°C in a 5% CO<sub>2</sub> incubator.

### Generation of Mutant Viruses DPV CHv-gEΔET and DPV CHv-gEACT

The DPV CHv-BAC-GS1783 (29) strain is stocked in our lab, in which the entire DPV CHv genome tagged with an enhanced green fluorescent protein (EGFP) is inserted BAC for stable propagation in *E. coli* strain GS1783. The construction of DPV CHv-gEΔET was based on two markerless two-steps Red recombination (30). Briefly, the linear PCR product, ‘a-*I-Sce I*-Kan-a-b’ was amplified and electroporated into DPV CHv-BAC-GS1783 to induce the first step of Red recombination, thereby replacing the *gE-ET* gene with Kan, a and b are the 40 bp homology arms on the left and right sides of the *gE-ET* gene, respectively. Subsequently, the *I-Sce I* site is cleaved by the *I-Sce I* endonuclease, and the Kan is removed in the second step by Red recombination. Amplify the linear PCR product again, ‘a’-UL23-a’-UL23-b’-b-*I-Sce I*-Kan-b-c’, electroporate it into DPV CHv-BAC-gEΔET-GS1783, induce the first step of Red recombination, a, b and c are successive homology arms downstream of the miniF sequence. Subsequently, the *I-Sce I* site is cleaved by the *I-Sce I* endonuclease, and the Kan is removed in the second step by Red recombination. The deletion of *gE-ET* was confirmed by identifying primers and sequencing. The plasmid DPV CHv-gEΔET-GS1783 was transfected into DEFs, and purified by spotting to obtain the DPV CHv-gEΔET deletion mutant virus. The same procedure was performed to construct and obtain DPV CHv-gEACT deletion mutant virus. All primers used in this study are listed in Table 1.

### Identification of Deletion Mutant Virus by PCR and Western Blot

After DPV CHv-ΔgE, DPV CHv-gEΔET, and DPV CHv-gEACT deletion mutant viruses infected DEFs to produce 80% lesions, the samples were frozen and thawed three times, and the obtained viruses were identified by PCR and Western blot. In PCR identification, primer UL30-F/R is used to identify whether the DPV UL30 gene is contained. Primers BAC-F/R are used to identify whether it contains miniF element, primer UL23-F/R is used to identify whether continuous *UL23* gene is contained, Primers *gE-F/R* were used to identify deletions of the *gE* gene. DEFs were infected with DPV CHv-ΔgE, DPV CHv-gEΔET, and DPV CHv-gEACT deletion mutant viruses with an MOI of 0.1 to analyze the *gE* expression in deletion mutant viruses, and 48 h later, cells were lysed with RIPA lysate, and the protein lysate was collected. Add 1% PMSF to the lysis buffer. Western blot analysis was performed with rabbit anti-*gE* and goat anti-rabbit IgG antibodies.

### Viral Growth Curves

Multistep growth kinetics of the parental strain CHv-50, DPV CHv-gEΔET, and DPV CHv-gEACT deletion mutant viruses were performed as previously described with minor modifications (31, 32). Briefly, DEFs cultured in 24-well cell

TABLE 1 | The primers used to construct and identify deletion-mutant virus CHv-gEΔET and CHv-gEACT.

Primer name	Sequence (5’-3’)	Purpose
ΔET-Kan-F	CTGCCGGCCAGACTAGGGAACCTCAACAATTGGTAGCATGTAGGGATAACAGGGTAATCGATT	Replacement of the <i>gE-ET</i> gene by the kan cassette
ΔET-Kan-R	TAATAGTCAGACCCCTAGTACTCCGAGACCGACTACAAACATCGTACCAATTTGTTGAGTTCGGTAGTCTGGCCGGCAGGCCAGTGTACAAACCAAT	
ΔCT-Kan-F	CGTGACTATTATAATCTCGCTGTTTCATCCATCTTTTATAGGGATAACAGGGTAATCGATT	Replacement of the <i>gE-CT</i> gene by the kan cassette
ΔCT-Kan-R	CTATTTCACTAGTGAGTCATTAGTTCAACATCCCATGATCATAAAAAAGATGGATGAACAGCCAGGATTAATAATAGTCAAGCCAGTGTACAAACCAAT	
<i>gE-F</i>	TCTCAAGACGCTCTGGAATC	Identification of the <i>gE</i> gene deletion
<i>gE-R</i>	AGCGAGTACTTCTCTGCGTC	
BAC-Kan-F	TTATTAATCTCAGGAGCCTGTAGCGTTTATAGGAAGTAGTGTTCCTGTCATGATGCCTGAAGCGGTAAACGAAAAACGATTGTTACAAACCAATTTAACC	Delete BAC miniF sequence and EGFP selection marker
BAC-Kan-R	ATCGTTTTGTTTACCGCTTGAGGCATCATGACAGACACTACTCTCCTATTAGGGATAACAGGGTAATCGAT	
BAC-UL23-F	GCCTGCAAGCGGTAACGAAACCGATTCAATTAATTTGTCATCTCGG	Delete BAC miniF sequence and EGFP selection marker
BAC-UL23-R	CGGCTCCACTTCAACGTAACACCGCAGGAGATTCTATTGTTTCCTGAAGGCATATTCAACGGGACATATTAAAAATTGA	
UL30-F	GGACAGCGTACACAGATAA	Identification of the DPV <i>UL30</i> gene
UL30-R	ACAAATCCCAAGCGTAG	
UL23-F	GCCTGCAAGCGGTAACGAAACCGATTCAATTAATTTGTCATCTCGG	Identification of the <i>UL23</i> gene deletion
UL23-R	CGGCTCCACTTCAACGTAACACCGCAGGAGATTCTATTGTTTCCTGAAGGCATATTCAACGGGACATATTAAAAATTGA	
BAC-F	GTTATCCACTGAGAAGCGAACG	Identification of the BAC miniF sequence deletion
BAC-R	GGCTGTAAAAAGGACAGACCACA	



culture plates were infected with a virus at an MOI of 0.01. After the virus was adsorbed for 2 h at 37°C and 5% CO<sub>2</sub>, the medium was discarded, the cells were washed with PBS (pH 7.4), and then the culture medium was replaced with MEM containing 2% NBS. The infected cells were collected at 12, 24, 48, and 72 h after infection, the volume of each sample was increased to 500 µL with MEM, the samples were freeze-thawed three times, and virus titers were determined by TCID<sub>50</sub> on DEFs. All experiments were repeated 3 times.

## Evaluation of Genetic Stability of Deletion Mutant Viruses

DEFs were separately infected with the DPV CHv-ΔgE, DPV CHv-gEΔET and DPV CHv-gEΔCT deletion mutant viruses. After the cells appeared 80% lesions, the samples were frozen and thawed 3 times, and the first-generation viruses were collected. The virus was re-infected with DEFs to prepare the next generation of the virus, and the deletion mutant virus was uploaded to the 20th passage in DEFs according to this method. DNA was extracted from the 10th and 20th passages of each virus according to the instructions of the Magen kit, and PCR identification was performed. The primers used are listed in **Table 1**. Virus titers at passages 1, 5, 10, 15, and 20 for each virus were determined by TCID<sub>50</sub> on DEFs. All experiments were repeated 3 times.

Forty 14-day-old ducklings were divided into 4 groups, the first 3 groups were inoculated with DPV CHv-ΔgE, DPV CHv-gEΔET, DPV CHv-gEΔCT deletion mutant virus by intramuscular injection at a dose of 10<sup>6</sup> TCID<sub>50</sub>/dose, and the last group was intramuscularly inoculated with the same volume of MEM. Seven days after inoculation, 5 ducklings in each group were randomly selected for culling, and the pathological changes of liver, spleen, and duodenum were observed. Take 1 g of liver tissue from each group for grinding, add normal saline at a ratio of 1:9 to make a homogenate, and inoculate new 14-day-old ducklings again. In this way, the mutant virus is transmitted to the 10th generation in ducklings. DNA was extracted from the 1st, 5th, and 10th passages of each virus according to the instructions of the Magen kit, and PCR identification was performed. The primers used are listed in **Table 1**. TaqMan-MGB probe fluorescence real-time quantitative PCR method (33) was used to detect the viral copies in liver tissue at passages 1, 5, and 10 of each virus.

## Safety Evaluation of Deletion Mutant Viruses

130 14-day-old ducklings were divided into 13 groups. Groups 1, 2, and 3 were inoculated with CHv-50 by intramuscular injection at 10<sup>4</sup> TCID<sub>50</sub>/dose, 10<sup>5</sup> TCID<sub>50</sub>/dose, and 10<sup>6</sup> TCID<sub>50</sub>/dose, respectively. Groups 4, 5, and 6 were inoculated with DPV CHv-ΔgE by intramuscular injection at 10<sup>4</sup> TCID<sub>50</sub>/dose, 10<sup>5</sup> TCID<sub>50</sub>/dose, and 10<sup>6</sup> TCID<sub>50</sub>/dose, respectively. Groups 7, 8, and 9 were inoculated with DPV CHv-gEΔET by intramuscular injection at 10<sup>4</sup> TCID<sub>50</sub>/dose, 10<sup>5</sup> TCID<sub>50</sub>/dose, and 10<sup>6</sup> TCID<sub>50</sub>/dose, respectively. Groups 10, 11, and 12 were inoculated with DPV CHv-gEΔCT by intramuscular injection of 10<sup>4</sup> TCID<sub>50</sub>/dose, 10<sup>5</sup> TCID<sub>50</sub>/dose, and 10<sup>6</sup> TCID<sub>50</sub>/dose, respectively. The control group was intramuscularly inoculated with the same volume of

MEM. Five ducks were randomly selected from each group to measure the rectal body temperature every day, and the death of each group of ducks was recorded for 10 days.

## Evaluation of Immune Efficacy of Deletion Mutant Viruses

40 14-day-old ducklings were divided into 4 groups, the first group was inoculated with a dose (10<sup>7.7</sup> copies)/dose of live duck plague vaccine CVCC AV1222, and the second and third groups were inoculated with the same number of copies/dose of DPV CHv-ΔgE and DPV CHv-gEΔET deletion mutant virus, the fourth group was the control group, each inoculated with 1 mL of MEM. On the 14th day after immunization, the ducklings were injected with 100 LD<sub>50</sub>/duck virulent Chinese strains of duck plague virus (CHv) and were continuously observed for 10 days after the challenge, and the clinical symptoms and death were recorded every day.

Similar to the above grouping and inoculation, blood was collected from each group of ducklings on the 7th, 14th, 21th, and 28th days after immunization, and serum was collected for neutralizing antibody detection. The serum to be tested was filtered with a 0.22 filter and inactivated at 56°C for 30 min. The treated serum to be tested was diluted 2<sup>1</sup> ~ 2<sup>8</sup> times, and 50 µL per well was added to a 96-well plate with DEFs. Add 50 µL of 1000 TCID<sub>50</sub> of CHv to each well, incubate at 37°C for 2 h, discard the supernatant and add 100 µL of MEM with 2% NBS. Continue to culture to observe cytopathic changes and calculate the neutralization index according to the Read-Muench method. All experiments were repeated 3 times.

## Statistical Analysis

The data are expressed as the means ± S.D. Statistical analysis was performed with Student's *t*-test (GraphPad Prism 6); \**P*<0.05, \*\**P*<0.01, \*\*\**P*<0.001 and \*\*\*\**P*<0.0001 indicate statistical significance compared with the control.

## RESULTS

### Construction and Rescue of CHv-gEΔET and CHv-gEΔCT Deletion Mutant Viruses

To explore the virulence gene functions of the ET and CT of gE, in DPV CHv-BAC-GS1783, we used two-step homologous recombination, the first homologous recombination first deleted gE-ET (**Figure 1A**), and constructed a DPV CHv-BAC-gEΔET-GS1783, the miniF was deleted by the second homologous recombination to construct DPV CHv-gEΔET-GS1783 (**Figure 1B**). DPV CHv-gEΔCT-GS1783 was constructed in the same way as described in Materials and methods. The plasmids of DPV CHv-gEΔET-GS1783 and DPV CHv-gEΔCT-GS1783 were respectively extracted and transfected into DEFs. At 48 h after transfection, small green fluorescent spots were observed in DEFs. After 144 h, green fluorescent spots were distributed in the entire field of view, and the cells produced lesions (**Figure 2A**). After collecting the virus solution to infect DEFs, pick the virus solution with cytopathic but no fluorescence

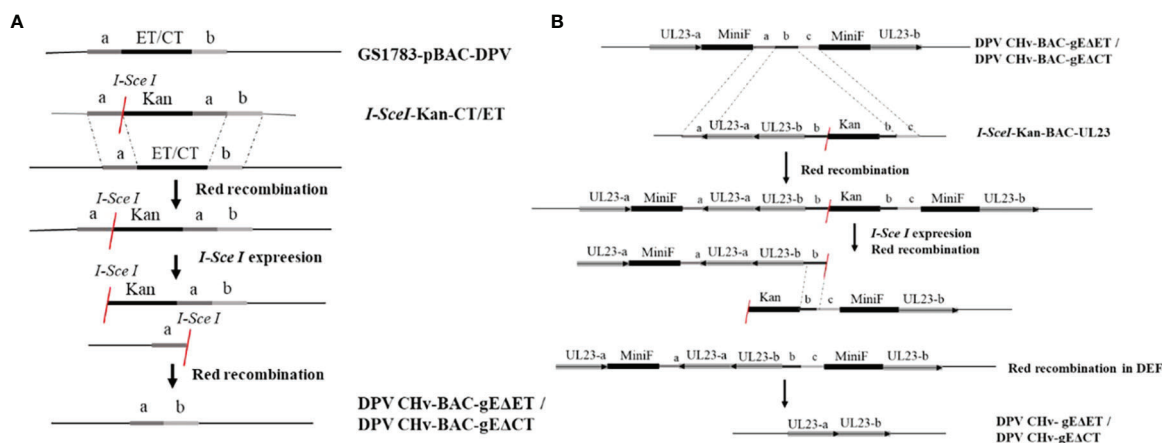


**FIGURE 1** | Homologous recombination diagram. Schematic diagram of the construction of the deletion mutant virus CHv-gE $\Delta$ ET and CHv-gE $\Delta$ CT using the Red recombination system. **(A)** Schematic diagram of the construction of the deletion mutant virus CHv-BAC-gE $\Delta$ ET and CHv-BAC-gE $\Delta$ CT using the Red recombination system. **(B)** Schematic diagram of the construction of the deletion mutant virus CHv-gE $\Delta$ ET and CHv-gE $\Delta$ CT using the Red recombination system again.

to re-infect DEFs, resulting in stable DPV CHv-gE $\Delta$ ET and DPV CHv-gE $\Delta$ CT deletion mutations with cytopathic and no fluorescence virus (**Figure 2B**).

### Identification of DPV CHv-gE $\Delta$ ET and DPV CHv-gE $\Delta$ CT Deletion Mutant Viruses

To identify the non-fluorescent deletion mutant virus after purification, viral DNA was extracted from DEFs infected with DPV CHv-gE $\Delta$ ET, DPV CHv-gE $\Delta$ CT, DPV CHv- $\Delta$ gE, and CHv-50 viruses, and PCR identification analysis were performed. Using the *UL30* gene identification primers can amplify the *UL30* gene fragment from the above DNA, indicating that the purified deletion mutant virus is duck plague virus, using the BAC identification primers cannot amplify the miniF element from the above DNA, indicating that all the purified deletion mutant virus has completely removed the miniF element, the *UL23* gene fragment can be amplified from the above DNA using the *UL23* gene identification primer, indicating that the purified deletion mutant virus *UL23* gene has been restored, amplification fragment of 884 bp, 1859 bp, 599 bp and 2072 bp from DNA infected with DPV CHv-gE $\Delta$ ET, DPV CHv-gE $\Delta$ CT, DPV CHv- $\Delta$ gE and CHv-50 using *gE* gene deletion identification primers, respectively, indicating that the ET segment and CT segment of the *gE* gene have been correctly deleted, the sizes of the above target fragments were in line with expectations. DPV CHv- $\Delta$ gE and CHv-50 were used as negative and positive controls, respectively, and the Mock group was used as a control to demonstrate the specificity of the primers (**Figure 2C**).

The expression of gE protein in the deleted mutant virus was further analyzed by Western blot. As shown in **Figure 2D**, only CHv-50 can express the complete gE protein, about 20 kDa of gE protein in DPV CHv-gE $\Delta$ ET, DPV CHv-gE $\Delta$ CT of gE protein is about 70 kDa, DPV CHv- $\Delta$ gE does not express gE protein, the results are in line with expectations, indicating that both DPV

CHv-gE $\Delta$ ET and DPV CHv-gE $\Delta$ CT recombinant viruses can be used in subsequent experiments.

### Growth Curves of Deletion Mutant Viruses

The multi-step growth kinetics of DPV CHv-gE $\Delta$ ET and DPV CHv-gE $\Delta$ CT deletion mutant viruses were evaluated after infecting DEFs with the same MOI = 0.01, collecting virus fluids at different time points, and detecting virus titers. As shown in **Figure 3**, the incubated virus entered the cell and started virus replication. At the initial 12 h of infection, the intracellular virus titers of the two deletion mutant viruses and the parental virus were not detected, indicating that the infectivity virus particles had not yet formed at this time. At 24 h after infection, infectious virions could be detected, indicating that a new generation of virions had been replicated in the cells. Then the virus titer gradually increased and reached a peak at 72 h, during which time the three virus strains were in the stage of replication and release. At 72 ~ 96 h after infection, the virus titers of the three virus strains all showed a downward trend. At this time, the virus titers decreased due to severe cytopathic changes. Compared with the parental virus, the viral titers of DPV CHv-gE $\Delta$ ET and DPV CHv-gE $\Delta$ CT decreased by approximately 80 and 25 fold, respectively, at 72 h of infection. These results suggest that deletion of both gE-ET and gE-CT affects the proliferative capacity of the virus.

### Genetic Stability of DPV CHv-gE $\Delta$ ET and DPV CHv-gE $\Delta$ CT

To evaluate the genetic stability of deletion mutant viruses *in vitro*, the viral titers of DPV CHv-gE $\Delta$ ET and DPV CHv-gE $\Delta$ CT deletion mutant viruses at passages 1, 5, 10, 15, and 20 after infection in DEFs were detected. As shown in **Figure 4A**, the titers of deletion mutant viruses at different passages were all around  $10^5$  TCID<sub>50</sub>/0.1 mL, with no significant difference ( $P > 0.05$ ). The virus titers of deletion mutant viruses were

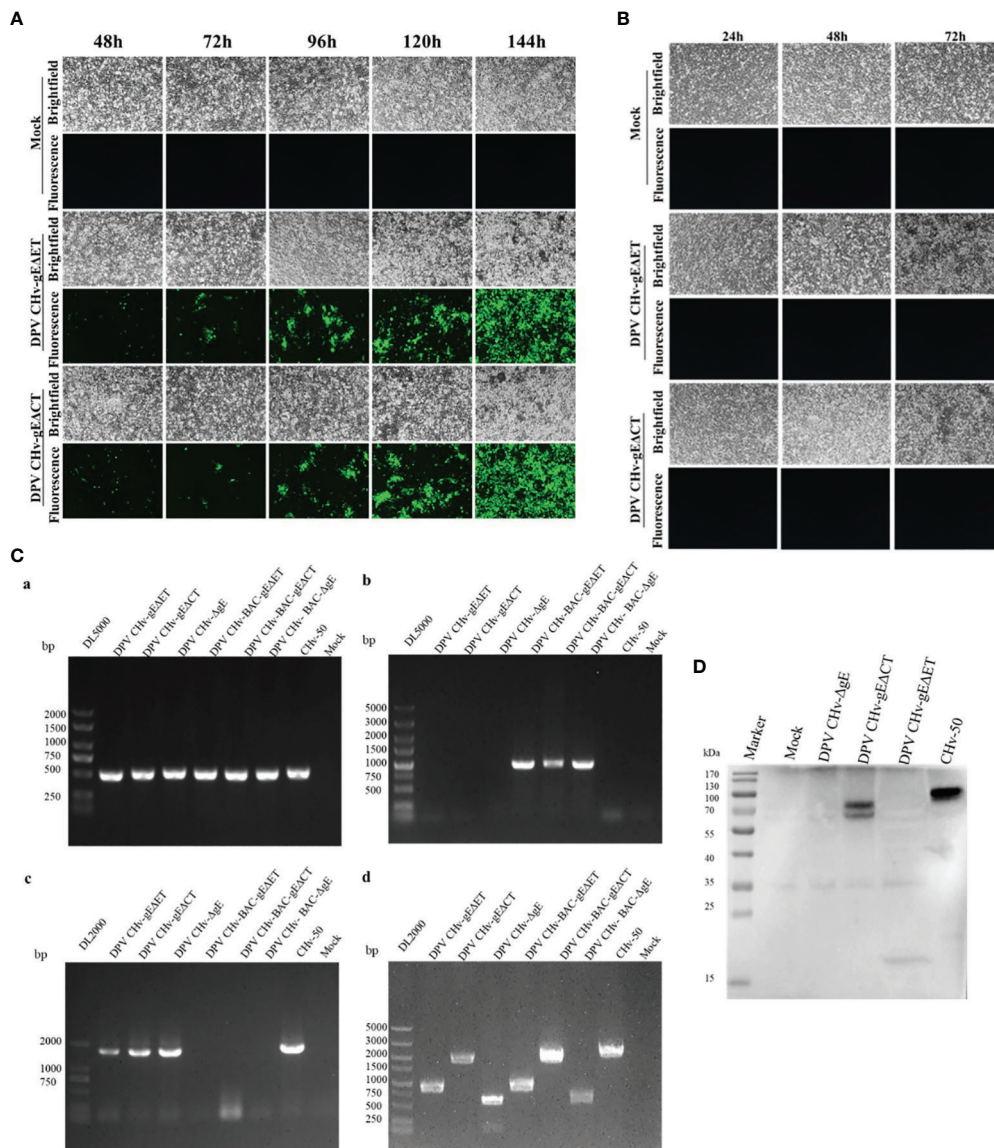
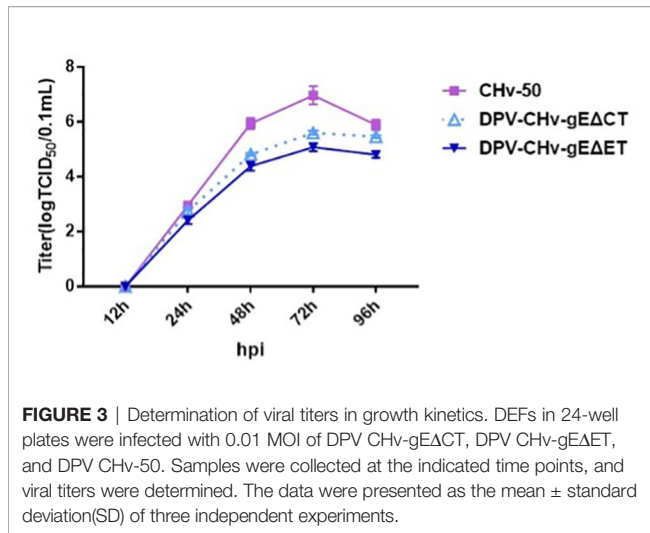


**FIGURE 2 |** Generation and identification of mutant viruses for DPV CHv-gEΔET and DPV CHv-gEΔCT. **(A)** Transfection of the plasmids DPV CHv-gEΔET-GS1783/DPV CHv-gEΔCT-GS1783 into DEFs resulted in numerous fluorescent spots and cytopathies, the mutant virus DPV CHv-gEΔET/DPV CHv-gEΔCT were rescued. **(B)** Cells with cytopathic but no fluorescent spots were picked into new DEFs, resulting in the non-fluorescent mutant virus. **(C)** PCR identification of mutant viruses: **(a)** *UL30* gene identification primer, **(b)** BAC identification primer, **(c)** *UL23* gene identification primer, **(d)** *gE* gene deletion identification primer. **(D)** DEFs were infected with DPV CHv-ΔgE, DPV CHv-gEΔCT, DPV CHv-gEΔET, and DPV CHv-50, and an anti-gE polyclonal antibody was used for WB.

stable after serial passage on DEFs. DNA of passage 10 and 20 deletion mutant viruses were extracted and identified by PCR as described in Methods. As shown in **Figure 4B**, the *UL30* gene fragments from the DPV CHv-gEΔET and DPV CHv-gEΔCT mutant viral DNAs after serial passages were identified by the *UL30* primers. The target gene fragments amplified from the DPV CHv-gEΔET and DPV CHv-gEΔCT mutant viral DNAs after *gE* deletion primers identified serial passages, and the sizes were in line with expectations. The above results show that after the serial passage of DPV CHv-gEΔET and DPV CHv-gEΔCT

mutant viruses in DEFs, the deleted genes in the viral genome will not undergo reverse mutation and stably inherited *in vitro*.

To assess the genetic stability of deletion mutant viruses *in vivo*, the mortality of DPV CHv-gEΔET and DPV CHv-gEΔCT deletion mutant virus in ducklings after serial passage was detected, and the disease and virus infection in different organs were detected. As shown in **Table 2**, after the DPV CHv-gEΔCT group was infected with ducklings, only a small number of deaths occurred in the 2nd, 5th, and 6th generations, while the DPV CHv-gEΔET group and DPV CHv-ΔgE group were the same as the Mock group, no deaths



occurred. The liver, spleen, and duodenum of ducklings infected with different generations of mutant deletion virus were necropsied to observe the lesions. After the ducklings were infected with DPV CHv-gEΔCT, only the duodenal mucosa showed slight hemorrhage, and other organs showed slight hemorrhage. No lesions were

observed in all organs in the DPV CHv-gEΔET group and the DPV CHv-ΔgE group, as in the Mock group (**Figure 5**). The viral DNA in the liver of ducks infected with 1, 5, and 10 generations of deletion mutant virus was extracted, and PCR identification and quantitative detection of the virus content were carried out. As with the *in vitro* detection, all the target bands were in line with expectations, and the virus in the liver of different generations mutant virus loads was stable between  $10^7 \sim 10^8$  copies/g (**Figures 4C, D**). The above results show that after the DPV CHv-gEΔET and DPV CHv-gEΔCT mutant viruses are serially passaged in ducklings, the deleted genes in the viral genome will not undergo reverse mutation and can be stably inherited *in vivo*.

### Safety of DPV CHv-gEΔET and DPV CHv-gEΔCT

The body temperature of most ducklings inoculated with parental virus CHv-50 will rise to above 43°C. The body temperature of ducklings in the  $10^4$  TCID<sub>50</sub> groups reached the peak on the 5th day, and the body temperature of the ducklings in the  $10^5$  TCID<sub>50</sub> and  $10^6$  TCID<sub>50</sub> groups both reached the peak on the 4th day. After reaching the peak, it will drop to the normal body temperature range of 40.5 ~ 42.5°C (**Figure 6**). 6 ~ 7 days is the peak period of death, and the mortality of different inoculation dose groups is distributed in a

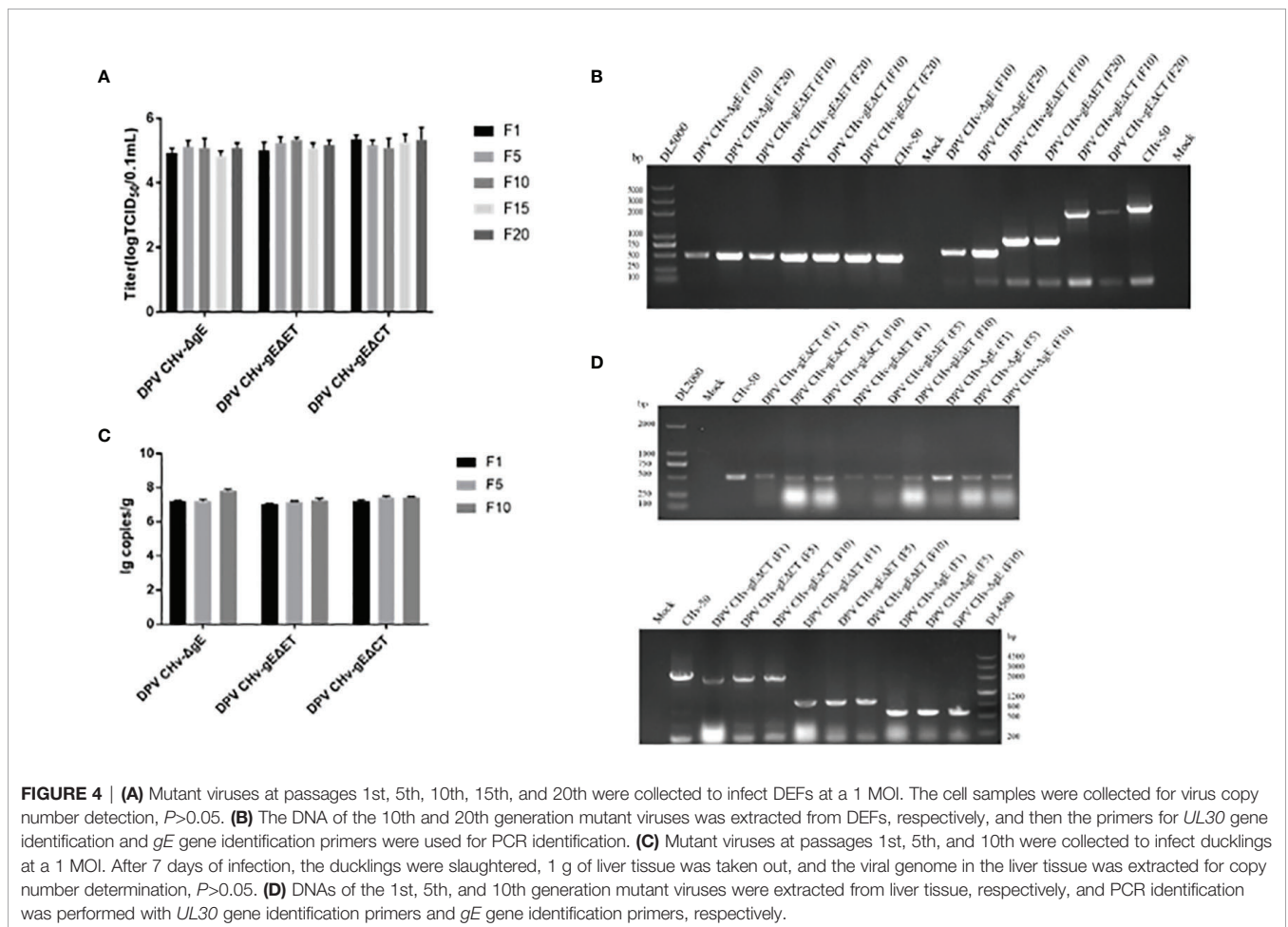


**TABLE 2** | The number of death ducklings for each group.

Group	F1	F2	F3	F4	F5	F6	F7	F8	F9	F10
DPV CHv-gEΔET	0/5	0/5	0/5	0/5	0/5	0/5	0/5	0/5	0/5	0/5
DPV CHv-gEΔCT	0/5	1/5	0/5	0/5	1/5	2/5	0/5	0/5	0/5	0/5
DPV CHv-ΔgE	0/5	0/5	0/5	0/5	0/5	0/5	0/5	0/5	0/5	0/5
Control	0/5	0/5	0/5	0/5	0/5	0/5	0/5	0/5	0/5	0/5

The numerator is the mortality numbers, and the denominator is the number of ducks challenged with viruses.

gradient. The ducklings in the  $10^4$  TCID<sub>50</sub> group did not die, and the ducklings in the  $10^5$  TCID<sub>50</sub> group had a mortality rate of 50%, and 1, 2, 2, died on days 5, 6, and 7, respectively. Ducklings in the  $10^6$  TCID<sub>50</sub> group had a mortality rate of 60%, 1, 1, 2, and 2 died on days 4, 5, 6, and 7, respectively (**Figure 6**). The DPV CHv-gEΔET group, DPV CHv-gEΔCT group, DPV CHv-ΔgE group were the same as the MEM group, the body temperature of the different dose groups after inoculation of the ducklings always fluctuated within the normal range within 10 days. Only DPV CHv-gEΔCT group died at  $10^5$  TCID<sub>50</sub> and  $10^6$  TCID<sub>50</sub> doses, and the mortality rate was 20% (**Table 3**). No deaths occurred within 10 days in the DPV CHv-gEΔET group, DPV CHv-gEΔCT group, DPV CHv-ΔgE group, and MEM group. The above results indicated that both ET and CT lacking gE would reduce the pathogenicity of the virus to ducklings, while the pathogenicity of the ET virus lacking gE was more significantly reduced to ducklings.

### Immunogenicity of DPV CHv-gEΔET

The clinical symptoms of the ducklings in different immunization groups after the challenge were observed. Only the ducklings in the control group began to be lethargic, poor in appetite, tearing, and

the feathers around the eyelids formed eye circles on the 4th day after the challenge. As shown in **Figure 7**, the body temperature of the ducklings in different immunization groups was measured after the challenge, the body temperature of the control group increased, and the body temperature exceeded 42.5°C on the 4th day after the challenge, and then the body temperature continued to be high until all died. The body temperature of the DPV CHv-ΔgE group and DPV CHv-gEΔET group was slightly higher than that of the vaccine group, but both fluctuated within the normal range. Statistics on the death of ducklings in different immunization groups after challenge, the control group began to die on the 5th day, and the 7th day was the peak period of death, and all died within 7 days, while the DPV CHv-ΔgE group, DPV CHv-gEΔET group like the vaccine group, all the ducklings were survived, indicating that the ducklings immunized with DPV CHv-ΔgE and DPV CHv-gEΔET could resist the challenge of virulent DPV CHv by 100%.

Neutralizing antibodies were detected in the sera of ducklings in different immunization groups. Neutralizing antibodies could be detected in the DPV CHv-ΔgE group, DPV CHv-gEΔET group, and vaccine group on the 7th day after immunization, and then the antibody levels gradually increased. On the 28th day after immunization, the neutralizing titers in the sera of ducklings in

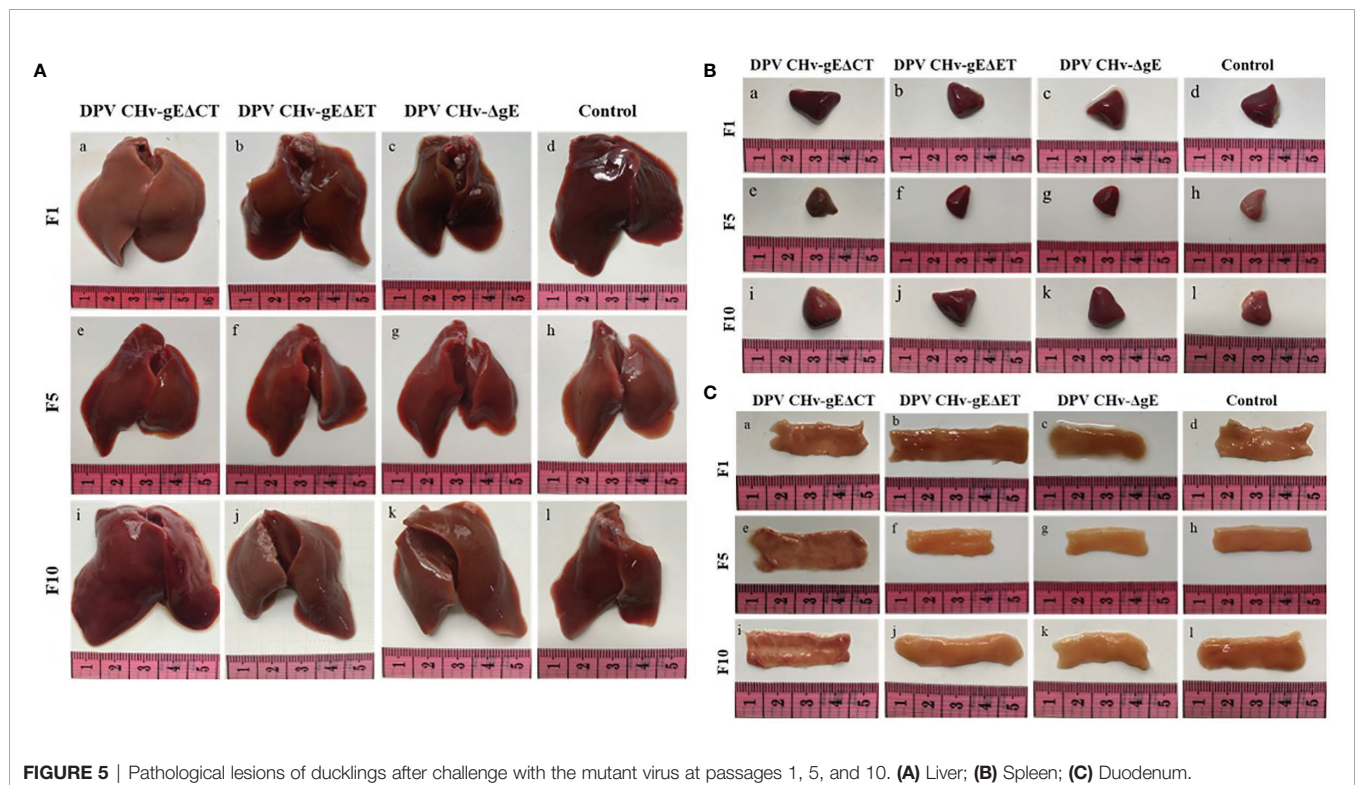


**FIGURE 5** | Pathological lesions of ducklings after challenge with the mutant virus at passages 1, 5, and 10. (A) Liver; (B) Spleen; (C) Duodenum.

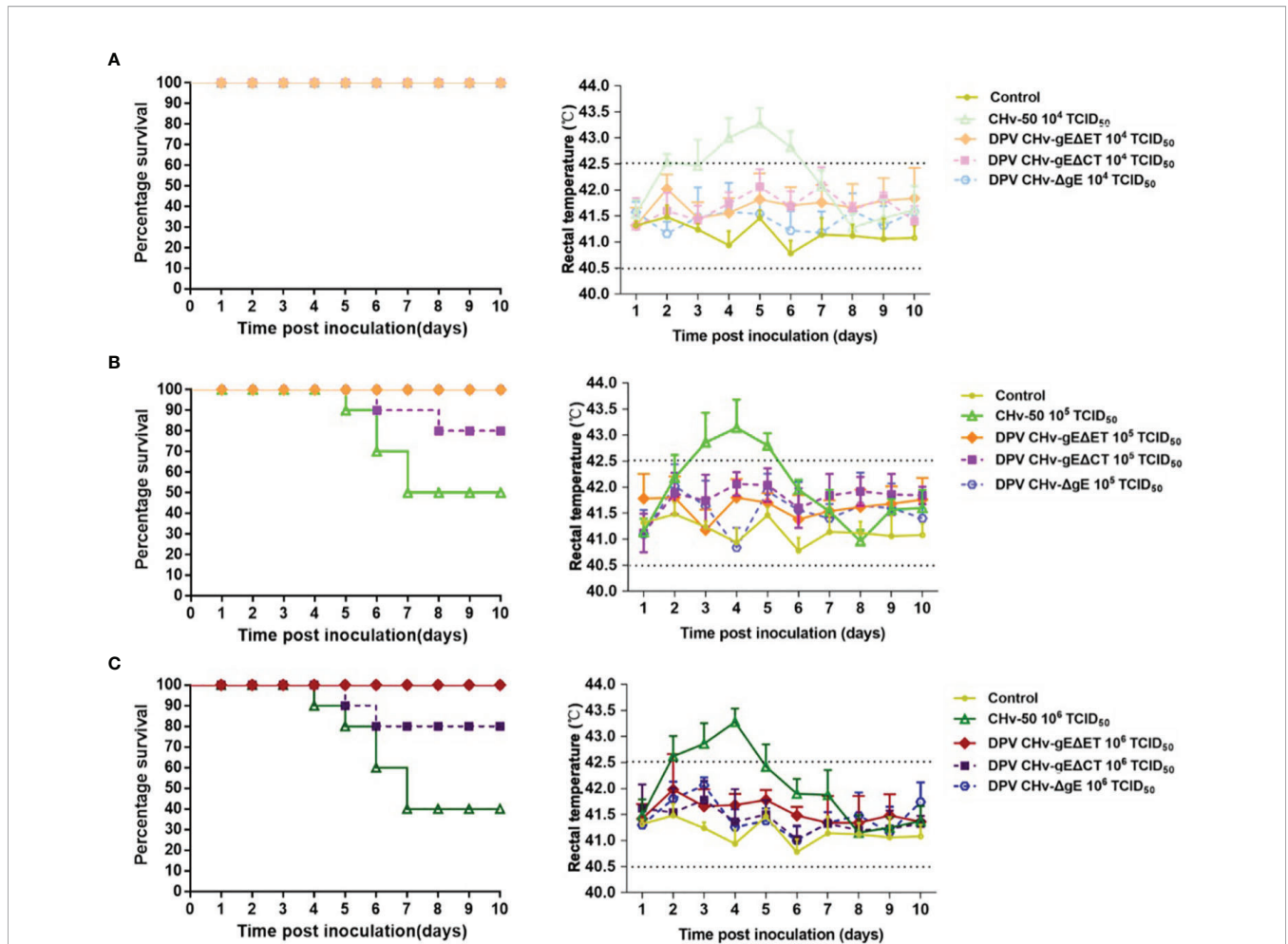


**FIGURE 6** | Survival percentage (left) and rectal temperatures (right) of ducklings. **(A)** Inoculated with a dose of  $10^4$  TCID<sub>50</sub> of mutant viruses; **(B)** Inoculated with a dose of  $10^5$  TCID<sub>50</sub> of mutant viruses; **(C)** Inoculated with a dose of  $10^6$  TCID<sub>50</sub> of mutant viruses.

different immunization groups DPV CHv-ΔgE group, DPV CHv-gEΔET group, and vaccine group reached  $2^{4.8}$ ,  $2^{4.4}$ , and  $2^{5.6}$  (Figure 8), respectively, there was no significant difference in valence ( $P>0.05$ ), but both were extremely significantly higher than those in the control group ( $P<0.001$ ,  $P<0.0001$ ), indicating that DPV CHv-ΔgE and DPV CHv-gEΔET could stimulate ducklings to produce significant neutralizing antibodies.

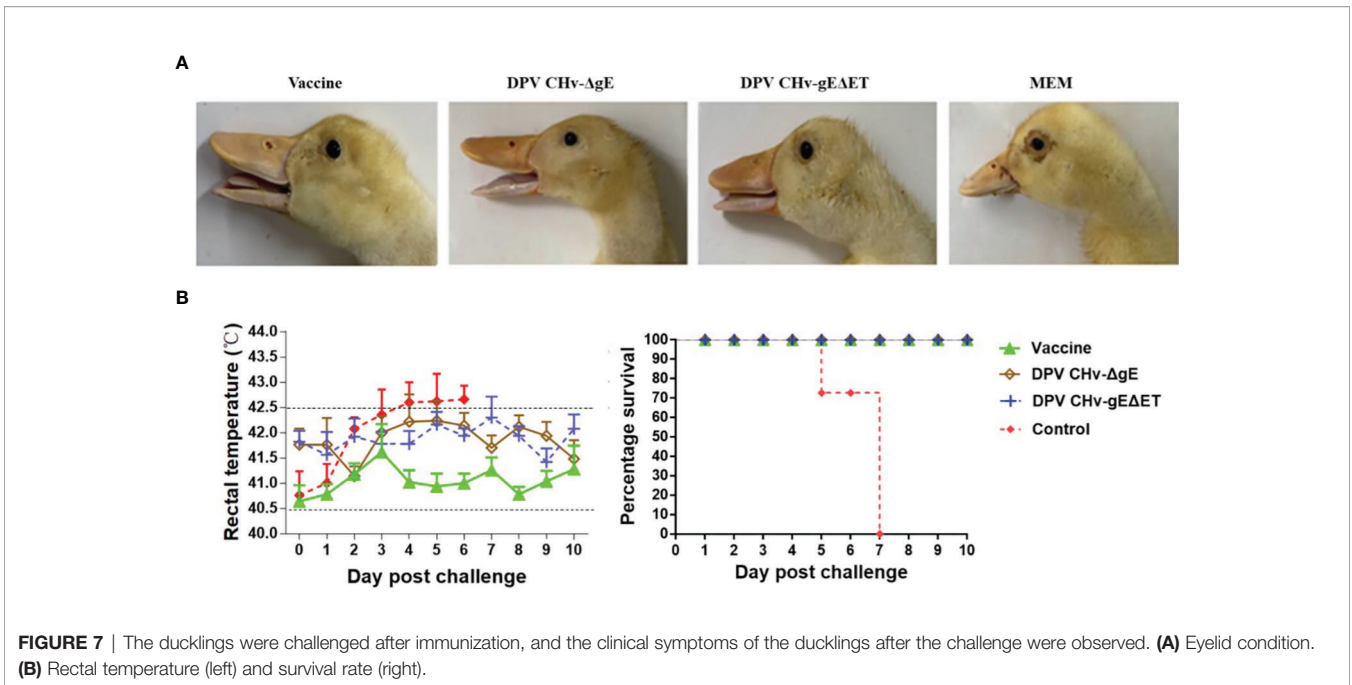
## DISCUSSION

In *alphaherpesviruses*, *gE* is an important virulence gene that affects the virus’s virulence. Selecting the deletion of the *gE* gene can reduce the virulence of the virus without affecting the immunogenicity and growth ability of the virus (34, 35). Virulence genes such as *gE* and *gI* have various degrees of insertion, deletion, and base substitution

**TABLE 3** | Mortality statistics of ducks.

Group	Challenge dose (TCID <sub>50</sub> )		
	10 <sup>4</sup>	10 <sup>5</sup>	10 <sup>6</sup>
CHv-50	0/10	5/10	6/10
DPV CHv-gEΔET	0/10	0/10	0/10
DPV CHv-gEΔCT	0/10	2/10	2/10
DPV CHv-ΔgE	0/10	0/10	0/10
MEM	0/10	0/10	0/10

The numerator is the mortality numbers, and the denominator is the number of ducks challenged with viruses.

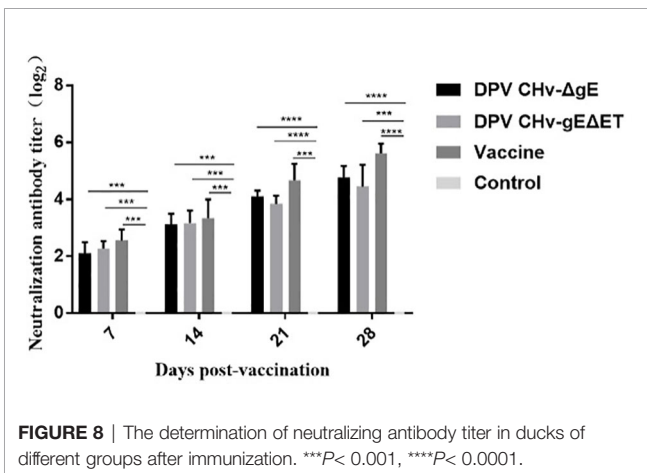


mutations, resulting in the emergence of highly toxic and lethal PRV mutant strains (36–39). The PRV mutant strain ZJ01, with 2 amino acid insertions in its *gE* sequence, caused all 14/80-day-old pigs to die (40). Two recombinant viruses, rZJ01-LA/*gEI* and rLA-ZJ01/*gEI*, were generated by exchanging the *gE* and *gI* genes of the LA strain and the ZJ01 strain. It was found that rLA-ZJ01/*gEI* exhibited higher virulence than its parental virus rLA, indicating that changes in the *gE* gene were part of the reason for the increased virulence of PRV strains in recent years (41). The bacterial artificial chromosome (BAC) of DPV is an effective tool for the study of duck plague virus, an infectious clone of a virulent strain of DPV CHv (DPV CHv-BAC-GS1783) was previously constructed in our laboratory and used in this study to generate mutant virus DPV CHv- $\Delta$ *gE*, DPV CHv-*gE* $\Delta$ ET and DPV CHv-*gE* $\Delta$ CT (29, 30, 42, 43). It should be further mentioned that the above mutant virus lacks *gE* and different functional regions of *gE* and lacks miniF on its basis. Otherwise,

the deletion-mutant virus cannot infect ducks or be used as a live vaccine. The *gE* gene of DPV has been confirmed to play an important role in the assembly of virions, with only minor damage to virus replication. In this study, the dynamic growth curve of the mutant virus after *gE* deletion in different regions was determined, which also confirmed this conclusion. By measuring the *in vitro* proliferation of DPV CHv-*gE* $\Delta$ ET and DPV CHv-*gE* $\Delta$ CT mutant viruses on DEFs, both mutant viruses were found to reduce virus titers on host cells, but to a lesser extent. However, further research is needed on the specific functions of *gE* ET and *gE* CT.

Vaccine immunization is an important means of preventing and controlling viral diseases. Recombinant vector vaccines have become one of the hotspots in vaccine research due to their unique advantages. There are many non-essential regions in the DPV genome (1, 3), such as the *gE/gI* genes (44, 45), which can be used as insertion sites for foreign genes. Therefore, DPV attenuated/attenuated strains have the advantage of being used as multiplex recombinant live vaccine carriers in addition to being used as DPV vaccines. Many researchers have expressed the immunogenic genes of Avian Influenza virus, duck Tembusu virus, duck hepatitis virus, chicken infectious bronchitis virus, and Newcastle disease virus using traditional attenuated vaccine strains (46–52). DPV immunized ducks with recombinant Avian Influenza virus can produce better protective effects. Immunized chickens can also quickly produce immune protection. The virus cannot replicate efficiently in chickens, so the safety is high. Therefore, the analysis of DPV-related genes, especially the functions of virulence-related genes similar to *gE*, is of great significance for the prevention and control of DPV and immune purification and promoting the application of DPV in avian multivalent live vector vaccine vectors.

The genetic stability of mutant virus is one of the important contents of mutant virus research. The stability of the mutant virus is evaluated mainly through the continuous passage of the mutant



virus *in vitro* and *in vivo*. We serially passaged the mutant viruses DPV CHv-gEΔET and DPV CHv-gEΔCT on DEFs and in ducklings, respectively, and measured the virus titer, whether the deleted gene was restored, and the pathogenic changes in susceptible animals. Found that the missing gene sequence of the mutant virus has not recovered, nor has the virulence returned, indicating that the mutant virus has good genetic stability, which is the premise for subsequent studies of mutant viruses as multivalent live vector vaccines or attenuated vaccine vectors. We grouped the mutant viruses DPV CHv-gEΔET and DPV CHv-gEΔCT according to the challenge dose gradient setting and conducted a pathogenicity study in 14-day-old ducklings, and preliminary analysis was made from body temperature, death, and antibody production after challenge. The results showed that the body temperature of the ducklings in the parental virus CHV-50  $10^5$  TCID<sub>50</sub>,  $10^6$  TCID<sub>50</sub> groups increased and exceeded the normal body temperature range 3 to 4 days after the challenge, and the mortality rate showed a gradient difference according to the challenge dose. The body temperature of DPV CHv-gEΔCT fluctuated within the normal range, and the mortality rates were 20% ( $10^6$  TCID<sub>50</sub>), 20% ( $10^5$  TCID<sub>50</sub>), and 0% ( $10^4$  TCID<sub>50</sub>), respectively. The body temperature of DPV CHv-gEΔET and DPV CHv-ΔgE in each dose group, fluctuated within the normal range, and no death occurred. DPV-specific serum antibodies could be detected in the ducklings on the 10th day after inoculation (data not shown). The above data show that gE deletion of ET or CT will reduce the pathogenicity of the virus. The pathogenicity of the mutant virus to ducklings after gE deletion of ET is significantly reduced, and the ducklings can be induced to produce specific serum antibodies. It further shows that DPV *gE* is also an important virulence gene, and the gE ET is an important region associated with virulence.

On the basis that the DPV CHv-gEΔET mutant virus has been proved to have stable inheritance, significantly reduce virus virulence, and induce DPV-specific serum antibodies in ducklings, further research on subsequent vaccines was carried out. In this study, the DPV CHv-gEΔET mutant virus was used to study the immune efficacy of the DPV CHv-gEΔET mutant virus by selecting the live duck plague vaccine that is widely used in China as a comparison. In the challenge protection trial, a lethal dose of CHV was administered after immunization, and no death and clinical symptoms were found in the DPV CHv-gEΔET, DPV CHv-ΔgE, and vaccine groups, and the challenge protection rate was 100%, the control group all died. In addition, judging whether the potential to develop into a vaccine is related to the challenge protection rate and observing the changes in antibody levels after immunization. Whether the body can produce high antibodies for a long time after vaccination is very important to fight viral infection. It is also one of the criteria for evaluating the quality of vaccines. Through neutralizing antibody detection, it was found that ducklings could produce certain neutralizing antibodies on the 7th day after immunizing with DPV CHv-ΔgE or DPV CHv-gEΔET mutant virus, and the antibody level on the 7th to 28th day after immunization rising. The levels of neutralizing antibodies produced after immunizing ducklings with the two mutant viruses were similar, significantly higher than those in the Mock group but slightly lower than

those in the vaccine group. The above shows that the deletion of the *gE* gene or the deletion of gE ET in DPV reduces the virus's virulence and stimulates the ducklings to produce a similar level of the humoral immune response, which can provide the same protection to the immunized animals. In this study, we lacked the detection of cellular immunity, and perhaps the reason for the immune protection of the DPV CHv-gEΔET mutant virus could be further explained by the study of cellular immunity.

It is well known that gE and gI function as dimers in *alphaherpesviruses* (10, 53). Previous studies in our laboratory have also demonstrated that gE and gI in DPV can form dimers, and amino acids 1-279 of gI can locate gE from the endoplasmic reticulum to the Golgi O-glycosylation modification (data unpublished). However, whether the complex position between gE and gI in DPV is also in the gE ET region, and the specific amino acid sites in gE that affect the complex formation with gI are currently being screened. The current research results and subsequent related research will provide a corresponding theoretical basis for the prevention and control of DPV and duck plague purification and promote the application of DPV in avian multivalent live vector vaccine vectors.

## DATA AVAILABILITY STATEMENT

The datasets presented in this study can be found in online repositories. The names of the repository/repositories and accession number(s) can be found in the article/supplementary material.

## ETHICS STATEMENT

The experimental animal protocol was approved by the Ethics and Animal Welfare Committee of Sichuan Agricultural University and carried out following the Chinese version of the Guide for the Care and Use of Laboratory Animals.

## AUTHOR CONTRIBUTIONS

Conceptualization, YN and AC. Methodology, YN and YH. Software, YN and QY. Validation, MW. Formal analysis, YN. Investigation, YN. Resources, AC, MW, SC, DZ, ML, QY, YW, XZ, SZ, JH, BT, RJ, XO, SM, QG, DS, YY, and LZ. Data curation, YN. Writing-original draft preparation, YN. Writing-review and editing, AC. Visualization, BT, RJ, ML, QY, and DS. Supervision, YN and AC. Project administration, MW and AC. Funding acquisition, MW, AC, RJ, SC, DZ, and ML. All authors have read and agreed to the published version of the manuscript.

## FUNDING

This work was supported by the National Natural Science Foundation of China (32072894), the China Agriculture



Research System of MOF and MARA, and the Sichuan Veterinary Medicine and Drug Innovation Group of China Agricultural Research System (SCCXTD-2020-18).

## REFERENCES

- Cheng AC. *Duck Plague*. Beijing: China Agricultural Press. (2015).
- Qi X, Yang X, Cheng A, Wang M, Zhu D, Jia R, et al. Intestinal Mucosal Immune Response Against Virulent Duck Enteritis Virus Infection in Ducklings. *Res Vet Sci* (2009) 87(2):218–25. doi: 10.1016/j.rvsc.2009.02.009
- Wu Y, Cheng A, Wang M, Yang Q, Zhu D, Jia R, et al. Complete Genomic Sequence of Chinese Virulent Duck Enteritis Virus. *J Virol* (2012) 86(10):5965. doi: 10.1128/JVI.00529-12
- Dhama K, Kumar N, Saminathan M, Tiwari R, Karthik K, Kumar MA, et al. Duck Virus Enteritis (Duck Plague) - A Comprehensive Update. *Vet Q* (2017) 37(1):57–80. doi: 10.1080/01652176.2017.1298885
- Koyanagi N, Kawaguchi Y. Evasion of the Cell-Mediated Immune Response by Alphaherpesviruses. *Viruses* (2020) 12(12):1354. doi: 10.3390/v12121354
- Wang J, Song Z, Ge A, Guo R, Qiao Y, Xu M, et al. Safety and Immunogenicity of an Attenuated Chinese Pseudorabies Variant by Dual Deletion of TK&gE Genes. *BMC Vet Res* (2018) 14(1):287. doi: 10.1186/s12917-018-1536-7
- Yu X, Jia R, Huang J, Shu B, Zhu D, Liu Q, et al. Attenuated Salmonella Typhimurium Delivering DNA Vaccine Encoding Duck Enteritis Virus UL24 Induced Systemic and Mucosal Immune Responses and Conferred Good Protection Against Challenge. *Vet Res* (2012) 43(1):56. doi: 10.1186/1297-9716-43-56
- Dogrammatzis C, Waisner H, Kalamvoki M. "Non-Essential" Proteins of HSV-1 With Essential Roles *In Vivo*: A Comprehensive Review. *Viruses* (2020) 13(1):17. doi: 10.3390/v13010017
- Liu T, Wang M, Cheng A, Jia R, Yang Q, Wu Y, et al. Duck Plague Virus gE Serves Essential Functions During the Virion Final Envelopment Through Influence Capsids Budding Into the Cytoplasmic Vesicles. *Sci Rep* (2020) 10(1):5658. doi: 10.1038/s41598-020-62604-9
- Farnsworth A, Johnson DC. Herpes Simplex Virus Ge/gI Must Accumulate in the Trans-Golgi Network at Early Times and Then Redistribute to Cell Junctions to Promote Cell-Cell Spread. *J Virol* (2006) 80(7):3167–79. doi: 10.1128/JVI.80.7.3167-3179.2006
- Brack AR, Dijkstra JM, Granzow H, Klupp BG, Mettenleiter TC. Inhibition of Virion Maturation by Simultaneous Deletion of Glycoproteins E, I, and M of Pseudorabies Virus. *J Virol* (1999) 73(7):5364–72. doi: 10.1128/JVI.73.7.5364-5372.1999
- Farnsworth A, Wisner TW, Johnson DC. Cytoplasmic Residues of Herpes Simplex Virus Glycoprotein gE Required for Secondary Envelopment and Binding of Tegument Proteins VP22 and UL11 to gE and gD. *J Virol* (2007) 81(1):319–31. doi: 10.1128/JVI.01842-06
- Yang L, Shen B, Wang M, Cheng A, Yang Q, Wu Y, et al. The Intracellular Domain of Duck Plague Virus Glycoprotein E Affects UL11 Protein Incorporation Into Viral Particles. *Vet Microbiol* (2021) 257:109078. doi: 10.1016/j.vetmic.2021.109078
- Han J, Chadha P, Meckes DG Jr, Baird NL, Wills JW. Interaction and Interdependent Packaging of Tegument Protein UL11 and Glycoprotein E of Herpes Simplex Virus. *J Virol* (2011) 85(18):9437–46. doi: 10.1128/JVI.05207-11
- Polcivova K, Goldsmith K, Rainish BL, Wisner TW, Johnson DC. The Extracellular Domain of Herpes Simplex Virus gE is Indispensable for Efficient Cell-to-Cell Spread: Evidence for Ge/gI Receptors. *J Virol* (2005) 79(18):11990–2001. doi: 10.1128/JVI.79.18.11990-12001.2005
- Berarducci B, Rajamani J, Reichelt M, Sommer M, Zerboni L, Arvin AM. Deletion of the First Cysteine-Rich Region of the Varicella-Zoster Virus Glycoprotein E Ectodomain Abolishes the gE and gI Interaction and Differentially Affects Cell-Cell Spread and Viral Entry. *J Virol* (2009) 83(1):228–40. doi: 10.1128/JVI.00913-08
- Chang H, Cheng A, Wang M, Jia R, Zhu D, Lou Q, et al. Immunofluorescence Analysis of Duck Plague Virus gE Protein on DPV-Infected Ducks. *Virol J* (2011) 8:19. doi: 10.1186/1743-422X-8-19
- Lu M, Qiu S, Zhang L, Sun Y, Bao E, Lv Y. Pseudorabies Virus Glycoprotein gE Suppresses Interferon- $\beta$  Production *via* CREB-Binding Protein Degradation. *Virus Res* (2021) 291:198220. doi: 10.1016/j.virusres.2020.198220
- Quast I, Keller CW, Maurer MA, Giddens JP, Tackenberg B, Wang LX, et al. Sialylation of IgG Fc Domain Impairs Complement-Dependent Cytotoxicity. *J Clin Invest* (2015) 125(11):4160–70. doi: 10.1172/JCI82695
- Sun H, Olsen HS, Mérigeon EY, So E, Burch E, Kinsey S, et al. Recombinant Human IgG1 Based Fc Multimers, With Limited FcR Binding Capacity, can Effectively Inhibit Complement-Mediated Disease. *J Autoimmun* (2017) 84:97–108. doi: 10.1016/j.jaut.2017.08.004
- Lubinski JM, Lazear HM, Awasthi S, Wang F, Friedman HM. The Herpes Simplex Virus 1 IgG Fc Receptor Blocks Antibody-Mediated Complement Activation and Antibody-Dependent Cellular Cytotoxicity *In Vivo*. *J Virol* (2011) 85(7):3239–49. doi: 10.1128/JVI.02509-10
- Jenks JA, Goodwin ML, Permar SR. The Roles of Host and Viral Antibody Fc Receptors in Herpes Simplex Virus (HSV) and Human Cytomegalovirus (HCMV) Infections and Immunity. *Front Immunol* (2019) 10:2110. doi: 10.3389/fimmu.2019.02110
- Bournazos S, DiLillo DJ, Ravetch JV. The Role of Fc-Fc $\gamma$ R Interactions in IgG-Mediated Microbial Neutralization. *J Exp Med* (2015) 212(9):1361–9. doi: 10.1084/jem.20151267
- Watanabe M, Arai J, Takeshima K, Fukui A, Shimojima M, Kozuka-Hata H, et al. Prohibitin-1 Contributes to Cell-To-Cell Transmission of Herpes Simplex Virus 1 *via* the MAPK/ERK Signaling Pathway. *J Virol* (2021) 95(3):e01413–20. doi: 10.1128/JVI.01413-20
- Tang YD, Liu JT, Wang TY, Sun MX, Tian ZJ, Cai XH. Comparison of Pathogenicity-Related Genes in the Current Pseudorabies Virus Outbreak in China. *Sci Rep* (2017) 7(1):7783. doi: 10.1038/s41598-017-08269-3
- Zhou J, Li S, Wang X, Zou M, Gao S. Bartha-K61 Vaccine Protects Growing Pigs Against Challenge With an Emerging Variant Pseudorabies Virus. *Vaccine* (2017) 35(8):1161–6. doi: 10.1016/j.vaccine.2017.01.003
- Wang J, Cui X, Wang X, Wang W, Gao S, Liu X, et al. Efficacy of the Bartha-K61 Vaccine and A Ge/GI/TK Prototype Vaccine Against Variant Porcine Pseudorabies Virus (vPRV) in Piglets With Sublethal Challenge of vPRV. *Res Vet Sci* (2020) 128:16–23. doi: 10.1016/j.rvsc.2019.10.005
- Wu Y, Cheng A, Wang M, Zhang S, Zhu D, Jia AB, et al. Serologic Detection of Duck Enteritis Virus Using an Indirect ELISA Based on Recombinant UL55 Protein. *Avian Dis* (2011) 55(4):626–32. doi: 10.1637/9766-042111-Reg.1
- Wu Y, Li Y, Wang M, Sun K, Jia R, Chen S, et al. Preliminary Study of the UL55 Gene Based on Infectious Chinese Virulent Duck Enteritis Virus Bacterial Artificial Chromosome Clone. *Virol J* (2017) 14(1):78. doi: 10.1186/s12985-017-0748-y
- Tischer BK, Smith GA, Osterrieder N. En Passant Mutagenesis: A Two Step Markerless Red Recombination System. *Methods Mol Biol (Clifton NJ)* (2010) 634:421–30. doi: 10.1007/978-1-60761-652-8\_30
- You Y, Liu T, Wang M, Cheng A, Jia R, Yang Q, et al. Duck Plague Virus Glycoprotein J Is Functional But Slightly Impaired in Viral Replication and Cell-to-Cell Spread. *Sci Rep* (2018) 8(1):4069. doi: 10.1038/s41598-018-22447-x
- Deng L, Wang M, Cheng A, Yang Q, Wu W, Jia R, et al. The Pivotal Roles of US3 Protein in Cell-To-Cell Spread and Virion Nuclear Egress of Duck Plague Virus. *Sci Rep* (2020) 10(1):7181. doi: 10.1038/s41598-020-64190-2
- Guo Y, Cheng A, Wang M, Shen C, Jia R, Chen S, et al. Development of TaqMan MGB Fluorescent Real-Time PCR Assay for the Detection of Anatid Herpesvirus 1. *Virol J* (2009) 6:71. doi: 10.1186/1743-422X-6-71
- Bouma A. Determination of the Effectiveness of Pseudorabies Marker Vaccines in Experiments and Field Trials. *Biologicals J Int Assoc Biol Standard* (2005) 33(4):241–5. doi: 10.1016/j.biologicals.2005.08.011
- Casal J, Planasdemunt L, Varo JA, Martín M. The Use of Different Vaccination Schedules for Sows to Protect Piglets Against Aujeszky's Disease. *J Vet Med B Infect Dis Vet Public Health* (2004) 51(1):8–11. doi: 10.1046/j.1439-0450.2003.00721.x

## ACKNOWLEDGMENTS

We apologize to the authors of articles reporting relevant research not cited in this manuscript due to limited space.

36. Sun Y, Liang W, Liu Q, Zhao T, Zhu H, Hua L, et al. Epidemiological and Genetic Characteristics of Swine Pseudorabies Virus in Mainland China Between 2012 and 2017. *PeerJ* (2018) 6:e5785. doi: 10.7717/peerj.5785
37. Wang Y, Qiao S, Li X, Xie W, Guo J, Li Q, et al. Molecular Epidemiology of Outbreak-Associated Pseudorabies Virus (PRV) Strains in Central China. *Virus Genes* (2015) 50(3):401–9. doi: 10.1007/s11262-015-1190-0
38. Tong W, Liu F, Zheng H, Liang C, Zhou YJ, Jiang YF, et al. Emergence of a Pseudorabies Virus Variant With Increased Virulence to Piglets. *Vet Microbiol* (2015) 181(3-4):236–40. doi: 10.1016/j.vetmic.2015.09.021
39. Wu X-M, Chen QY, Chen RJ, Che YL, Wang LB, Wang CY, et al. Pathogenicity and Whole Genome Sequence Analysis of a Pseudorabies Virus Strain FJ-2012 Isolated From Fujian, Southern China. *Can J Infect Dis Med Microbiol = J Canadien Des Maladies Infectieuses la Microbiologie Medicale* (2017) p:9073172. doi: 10.1155/2017/9073172
40. Gu Z, Hou C, Sun H, Yang W, Dong J, Bai J, et al. Emergence of Highly Virulent Pseudorabies Virus in Southern China. *Can J Vet Res = Rev Can Recherche Veterinaire* (2015) 79(3):221–8.
41. Dong J, Gu Z, Jin L, Lv L, Wang J, Sun T, et al. Polymorphisms Affecting the gE and gI Proteins Partly Contribute to the Virulence of a Newly-Emergent Highly Virulent Chinese Pseudorabies Virus. *Virology* (2018) 519:42–52. doi: 10.1016/j.virol.2018.03.024
42. Chai Y, Shan S, Weissman KJ, Hu S, Zhang Y, et al. Heterologous Expression and Genetic Engineering of the Tubulysin Biosynthetic Gene Cluster Using Red/ET Recombineering and Inactivation Mutagenesis. *Chem Biol* (2012) 19(3):361–71. doi: 10.1016/j.chembiol.2012.01.007
43. Bian X, Huang F, Stewart FA, Xia L, Zhang Y, Müller R. Direct Cloning, Genetic Engineering, and Heterologous Expression of the Syringolin Biosynthetic Gene Cluster in *E. Coli* Through Red/ET Recombineering. *Chembiochem Eur J Chem Biol* (2012) 13(13):1946–52. doi: 10.1002/cbic.201200310
44. Chang H, Cheng A, Wang M, Zhu D, Jia R, Liu F, et al. Cloning, Expression and Characterization of gE Protein of Duck Plague Virus. *Viol J* (2010) 7:120. doi: 10.1186/1743-422X-7-120
45. Zhou X, Wang M, Cheng A, Yang Q, Wu Y, Jia R, et al. Development of a Simple and Rapid Immunochromatographic Strip Test for Detecting Duck Plague Virus Antibodies Based on gI Protein. *J Virol Methods* (2020) 277:113803. doi: 10.1016/j.jviromet.2019.113803
46. Liu J, Chen P, Jiang Y, Deng G, Shi J, Wu L, et al. Recombinant Duck Enteritis Virus Works as a Single-Dose Vaccine in Broilers Providing Rapid Protection Against H5N1 Influenza Infection. *Antiviral Res* (2013) 97(3):329–33. doi: 10.1016/j.antiviral.2012.12.015
47. Zou Z, Hu Y, Liu Z, Zhong W, Cao H, Chen H, et al. Efficient Strategy for Constructing Duck Enteritis Virus-Based Live Attenuated Vaccine Against Homologous and Heterologous H5N1 Avian Influenza Virus and Duck Enteritis Virus Infection. *Vet Res* (2015) 46(1):42. doi: 10.1186/s13567-015-0174-3
48. Zou Z, Liu Z, Jin M. Efficient Strategy to Generate a Vectored Duck Enteritis Virus Delivering Envelope of Duck Tembusu Virus. *Viruses* (2014) 6(6):2428–43. doi: 10.3390/v6062428
49. He D, Zhang X, Chen L, Tang Y, Diao Y. Development of an Attenuated Live Vaccine Candidate of Duck Tembusu Virus Strain. *Vet Microbiol* (2019) 231:218–25. doi: 10.1016/j.vetmic.2019.03.022
50. Kang M, Roh J-H, Jang H-K. Protective Efficacy of a Bivalent Live Attenuated Vaccine Against Duck Hepatitis A Virus Types 1 and 3 in Ducklings. *Vet Microbiol* (2018) 214:108–12. doi: 10.1016/j.vetmic.2017.12.018
51. Li H, Wang Y, Han Z, Wang Y, Liang S, Jiang L, et al. Recombinant Duck Enteritis Viruses Expressing Major Structural Proteins of the Infectious Bronchitis Virus Provide Protection Against Infectious Bronchitis in Chickens. *Antiviral Res* (2016) 130:19–26. doi: 10.1016/j.antiviral.2016.03.003
52. Ding L, Chen P, Bao X, Li A, Jiang Y, Hu Y, et al. Recombinant Duck Enteritis Viruses Expressing the Newcastle Disease Virus (NDV) F Gene Protects Chickens From Lethal NDV Challenge. *Vet Microbiol* (2019) 232:146–50. doi: 10.1016/j.vetmic.2019.04.022
53. Husak PJ, Kuo T, Enquist LW. Pseudorabies Virus Membrane Proteins gI and gE Facilitate Anterograde Spread of Infection in Projection-Specific Neurons in the Rat. *J Virol* (2000) 74(23):10975–83. doi: 10.1128/JVI.74.23.10975-10983.2000

**Conflict of Interest:** The authors declare that the research was conducted in the absence of any commercial or financial relationships that could be construed as a potential conflict of interest.

**Publisher's Note:** All claims expressed in this article are solely those of the authors and do not necessarily represent those of their affiliated organizations, or those of the publisher, the editors and the reviewers. Any product that may be evaluated in this article, or claim that may be made by its manufacturer, is not guaranteed or endorsed by the publisher.

Copyright © 2022 Ning, Huang, Wang, Cheng, Jia, Liu, Zhu, Chen, Zhao, Zhang, Yang, Wu, Huang, Tian, Ou, Mao, Gao, Sun, Yu and Zhang. This is an open-access article distributed under the terms of the Creative Commons Attribution License (CC BY). The use, distribution or reproduction in other forums is permitted, provided the original author(s) and the copyright owner(s) are credited and that the original publication in this journal is cited, in accordance with accepted academic practice. No use, distribution or reproduction is permitted which does not comply with these terms.



# cGAS Restricts PRRSV Replication by Sensing the mtDNA to Increase the cGAMP Activity

Xiao-Na Liu<sup>1†</sup>, Li-Wei Li<sup>2†</sup>, Fei Gao<sup>2</sup>, Yi-Feng Jiang<sup>2</sup>, Wan-Zhe Yuan<sup>1,3</sup>, Guo-Xin Li<sup>2</sup>, Ling-Xue Yu<sup>2</sup>, Yan-Jun Zhou<sup>2</sup>, Guang-Zhi Tong<sup>2</sup> and Kuan Zhao<sup>1,3\*</sup>

<sup>1</sup> College of Veterinary Medicine, Hebei Agricultural University, Baoding, China, <sup>2</sup> Shanghai Veterinary Research Institute, Chinese Academy of Agricultural Sciences, Shanghai, China, <sup>3</sup> Hebei Veterinary Biotechnology Innovation Center, Hebei Agricultural University, Baoding, China

## OPEN ACCESS

### Edited by:

Chunfu Zheng,  
University of Calgary, Canada

### Reviewed by:

Shen Yang,  
University of California, San Diego,  
United States  
Junhua Huang,  
Wuhan Polytechnic University, China

### \*Correspondence:

Kuan Zhao  
zhaokuan519@126.com

<sup>†</sup>These authors have contributed  
equally to this work

### Specialty section:

This article was submitted to  
Viral Immunology,  
a section of the journal  
Frontiers in Immunology

Received: 01 March 2022

Accepted: 28 March 2022

Published: 26 April 2022

### Citation:

Liu X-N, Li L-W, Gao F, Jiang Y-F,  
Yuan W-Z, Li G-X, Yu L-X, Zhou Y-J,  
Tong G-Z and Zhao K (2022)  
cGAS Restricts PRRSV Replication  
by Sensing the mtDNA to  
Increase the cGAMP Activity.  
*Front. Immunol.* 13:887054.  
doi: 10.3389/fimmu.2022.887054

Porcine reproductive and respiratory syndrome virus (PRRSV) is an RNA virus that causes great economic losses globally to the swine industry. Innate immune RNA receptors mainly sense it during infection. As a DNA sensor, cyclic GMP-AMP synthase (cGAS) plays an important role in sensing cytosolic DNA and activating innate immunity to induce IFN-I and establish an antiviral cellular state. In contrast, the role of innate immune DNA sensors during PRRSV infection has not been elucidated. In this study, we found that cGAS facilitates the production of IFN- $\beta$  during PRRSV infection. Western blot and virus titer assays suggested that cGAS overexpression suppressed the replication of multiple PRRSV strains, while knockout of cGAS increased viral titer and nucleocapsid protein expression. Besides, our results indicated that the mitochondria were damaged during PRRSV infection and leaked mitochondrial DNA (mtDNA) into the cytoplasm. The mtDNA in the cytoplasm co-localizes with the cGAS, and the cGAMP activity was increased when the cGAS was overexpressed during PRRSV infection. Furthermore, the cGAMP also possesses an anti-PRRSV effect. These results indicate for the first time that cGAS restricts PRRSV replication by sensing the mtDNA in the cytoplasm to increase cGAMP activity, which not only explains the molecular mechanism by which cGAS inhibits PRRSV replication but also provides research ideas for studying the role of the cGAS-STING signaling pathway in the process of RNA virus infection.

**Keywords:** PRRSV, cGAS, mtDNA, cGAMP, replication, antiviral activity

## INTRODUCTION

Porcine reproductive and respiratory syndrome (PRRS), characterized by manifest reproductive problems in sows and respiratory problems in piglets, is one of the most problematic infectious diseases for the swine industry worldwide (1). Since 2006, a highly-pathogenic form of the PRRS virus (HP-PRRSV) has circulated in China, resulting in considerable economic loss (2).

PRRSV, the causative agent of PRRS, is in the family *Arteriviridae* of the order *Nidovirales* (3). PRRSV is an enveloped, single-stranded, positive-sense RNA virus. Its genome RNA is

approximately 15.4 kb consisting of at least 10 open reading frames (ORFs), a 5'-untranslated region (UTR), and a 3'-UTR (4). PRRSV was found to suppress interferon (IFN) production activated by double-stranded RNA (dsRNA). PRRSV proteins, namely, Nsp1, Nsp2, Nsp4, Nsp11, and N, have been identified and characterized as IFN antagonists (5, 6). To further ensure the normal physiological state of the host, the host has evolved a series of strategies to resist the virus. Immediately after PRRSV infection, the main host pattern recognition receptors (PRRs) are retinoic acid-inducible gene I (RIG-I), which can directly recognize and bind viral 5'-PPP RNA and short double-stranded RNA and then activate innate immunity against viral infections (7). So far, many interferon-stimulated genes (ISGs) that result in PRRSV resistance have been identified (8, 9).

Cyclic GMP-AMP (cGAMP) synthase (cGAS) is a newly identified DNA sensor that triggers IFN-I production. It plays an important role in sensing cytosolic DNA and triggering a stimulator of IFN genes (STING) dependent signaling to induce IFN-I (10). Additionally, PRR ligands, namely, bacteria, DNA viruses, and retroviruses, induce the expression of cGAS in an IFN-I-dependent manner. Besides, cGAS can positively regulate the production of IFN, so cGAS was considered a new ISG (11). During DNA virus infection, the virus genome is directly recognized and bound to cGAS to activate the cGAMP activity, which induces the production of IFN. Numerous DNA viruses activate the cGAS-STING pathway, and cGAS-deficient mice are more susceptible to lethal infection after exposure to many DNA viruses, namely, herpes simplex virus 1 (HSV-1), vaccinia virus (VACV), and murine gammaherpesvirus 68 (MHV68) (12). However, emerging evidence indicates that, in addition to its well-established role in sensing cytosolic DNA, the cGAS is also involved in restricting RNA virus infection, suggesting crosstalk exists between the innate sensing of cytosolic DNA and RNA (13). Several studies reveal that the replication of RNA viruses, namely, equine arterivirus (EAV), dengue virus (DENV), West Nile virus (WNV), influenza A virus (IAV), and chikungunya virus (CHIKV), is greatly facilitated in cells and mice with a deficiency of cGAS (14–16). Interestingly, we found that overexpressing cGAS inhibits PRRSV replication and knockout of cGAS increases PRRSV replication. However, PRRSV and other RNA viruses do not form dsDNA or DNA:RNA complexes during infection, so cGAS must be activated by other means during the infection of these RNA viruses, but the mechanism is unclear.

Here, we show that cGAS plays an important role in inhibiting PRRSV replication. PRRSV infection causes mitochondrial damage, resulting in mitochondrial DNA (mtDNA) leaking into the cytoplasm. cGAS is activated by binding to mtDNA in the cytoplasm, increasing cGAMP activity, promoting IFN production, and inhibiting PRRSV replication. Together, this study elucidates for the first time the molecular mechanism by which cGAS inhibits PRRSV replication and will provide research ideas for studying the role of the cGAS-STING signaling pathway in the process of RNA virus infection.

## MATERIALS AND METHODS

### Cells and Virus

African green monkey kidney (Marc-145) cells were maintained in Dulbecco's modified Eagle's medium (DMEM) containing 10% fetal bovine serum (FBS; Gibco, Thermo Fisher Scientific, Waltham, MA, USA) at 37°C and under 5% CO<sub>2</sub>. The HP-PRRSV strain HuN4 (GenBank accession No. EF635006), a classic type 2 strain (vAPRRS; GenBank accession No. GQ330474), and a classic type 1 strain (vSHE; GenBank accession No. GQ461593). All the viruses, cells and vectors used in our experiment are stored in our lab.

### Construction of Plasmids

To create p3xFlag-cGAS, the porcine cGAS (MB21D1) gene (GenBank accession no. XM\_013985148.2) was amplified from the porcine alveolar macrophages (PAMs) and cloned into p3xFlag. According to the instructions of the manufacturer, the plasmids were constructed by homologous recombination with the NEBuilder<sup>®</sup> HiFi DNA Assembly Master Mix (New England Biolabs; Ipswich, MA). The primers used for gene amplification are listed in **Table 1**.

### Plasmid Transfection and Virus Challenge

Marc-145 cells cultured in 6-well plates were transfected with 1 µg of p3xFlag-cGAS using X-treme GENE HP DNA reagent (Roche Applied Science, Penzberg, Germany), to investigate the effect of cGAS on IFN-β production and PRRSV replication. Next, 24 h post-transfection (hpt), the cells were infected with PRRSV HuN4 (a multiplicity of infection, MOI, of 0.1). After inoculation for 1 h at 37°C, the supernatants were discarded, and the cells were washed three times with phosphate-buffered saline (PBS). The supernatant was harvested at 12, 24, 36, and 48 h post-infection (hpi), and the cells were lysed using RIPA lysis buffer (Thermo Fisher Scientific). IFN-β was assessed by quantitative real-time reverse-transcription polymerase chain reaction (qRT-PCR) and ELISA with the Monkey IFN-β ELISA Kit (Cusabio) according to the instructions of the manufacturer. Viral titers in the supernatants were determined

**TABLE 1** | Sequences of primers and gRNAs used in this study.

Primer	Sequence (5'–3')
Monkey-IFN-β-F	GCAATTGAATGGAAGGCTTGA
Monkey-IFN-β-R	CAGCGTCCTCCTTCTGGAACT
β-actin-F	CGGGAAATCGTGCCTGAC
β-actin-F	ATGCCAGGAAGGAAGGTTG
p3xFlag-cGAS-F	AAGCTTGCGGCCGCGATGGCCGCCGCGGGGAAAG
p3xFlag-cGAS-R	AGATCTATCGATGAATTTACCAAAAAAATCGGAAATCCA
cGAS-Exon1-gRNA-F	CACCGAGACTCGTTCGCGTCGGTCTC
cGAS-Exon1-gRNA-R	AAACGACCGACCGCAACGAGTCTC
cGAS-Exon2-gRNA-F	CACCGCTAGAAGAATATTCTGACAC
cGAS-Exon2-gRNA-F	AAACGTGTCAGAATATTCTTCTAGC

using a microtitration assay according to the method of Reed and Muench (17). The amount of N protein was then detected in cell lysates by western blot (WB) using a mouse anti-N polyclonal antibody (1:1,000) produced by the authors.

### qRT-PCR

Total RNA was extracted using an RNeasy mini kit (Qiagen, Hilden, Germany), following the instructions of the manufacturer. Reverse transcription reactions were performed at 25°C for 5 min and 42°C for 1 h using the M-MLV reverse transcription-polymerase system (TaKaRa, Dalian, China). SYBR Premix Ex Taq™ (Takara) was used to quantify the levels of IFN- $\beta$ . Relative expression levels were analyzed using the  $\Delta\Delta C_t$  method (18), with  $\beta$ -actin mRNA as a control. Primers are listed in **Table 1**. qPCR detected the mtDNA in the cytoplasm of Marc-145 cells after being infected with PRRSV (refer to 19).

### WB

Cell lysates were by incubating cells in RIPA for 15 min at 4°C with 1 mM phenylmethylsulfonyl fluoride and 1 mg/ml of protease inhibitor cocktail (Roche). After centrifuging at 12,000 $\times g$  for 10 min, the supernatants of cell lysates were mixed with 5 $\times$  sodium dodecyl sulfate-polyacrylamide gel electrophoresis (SDS-PAGE) sample loading buffer (Beyotime) and placed in boiling water for 5 min. The proteins were separated by SDS-PAGE and transferred onto a nitrocellulose membrane. The membrane was blocked in 5% skim milk for 2 h at room temperature before incubating with the indicated antibody for 1 h at room temperature. After 3 washes with Tris-buffered saline with 0.1% Tween 20, the membrane was incubated for 1 h at room temperature with horseradish peroxidase-conjugated goat anti-mouse/rabbit IgG (H + L) (1:5,000). The membranes were visualized by treating them with Pierce ECL WB substrate (Thermo Fisher Scientific). For the quantification of target proteins, their levels were normalized to the levels of  $\beta$ -actin.

### Cytoplasmic Mitochondrial DNA Extraction

Marc-145 cells were seeded in a 10-cm dish and infected with PRRSV at different MOIs (0.5, 1, and 1.5). The uninfected cells act as a control. At 24 hpi, the culture medium was discarded, and the cells were washed twice with PBS. The cells were scraped off with the scraper and then sent to separate the cytoplasm without mitochondria with the Mitochondria Isolation Kit for Cultured Cells kit (Thermo Fisher). The cytoplasm DNA was extracted with a QIAamp DNA Mini Kit (QIAGEN) and quantified with qPCR.

### Establishment of the cGAS Knockout (cGAS-KO) Marc-145 Cells

The cGAS-KO Marc-145 cells were generated using the CRISPR/Cas9 system and then used to evaluate the effect of cGAS deletion on PRRSV replication. Two guide RNAs, RNA1 and RNA2, were designed by the online-Optimized CRISPR Design tool (<http://crispr.mit.edu/>) (**Table 1**) and constructed into the PX459M and EZ-guide plasmid with *Bbs* I. Then, the gRNA2 was subcloned into PX459M-gRNA1 by *Xho* I and *Hind* III. The plasmid with

two gRNA named PX459-gRNA1/2 was used to transfect Marc-145 cells. At 36 hpt, the cells were passaged and diluted into a six-well plate with the media to which puromycin (15  $\mu g/ml$ ) was added. The cells were maintained in selective media for 48 h. Then, the clones were separated into a 96-well plate with single or double cells in each hole. The media was refreshed the following day, and clones were isolated after single-cell plating. Following PCR amplification of a 500-bp region centered on the CRISPR guide, indels were analyzed by sequencing. A WB using a specific cGAS antibody (HPA031700; Sigma, USA) was performed to confirm the absence of the target protein.

### Confocal Fluorescence Microscopy

Marc-145 cells were infected or uninfected with PRRSV at MOI = 0.5. Then, 24 hpt, the cells were fixed in 4% paraformaldehyde for 30 min, blocked with 3% bovine serum albumin for 1 h and permeabilized with 0.1% Triton X-100 for 15 min. The transfected cells were incubated with the indicated antibodies for 1 h at 37°C and washed thrice with PBS. The cells were then incubated at 37°C for 1 h with secondary antibodies, then stained with 1 g/ml of 4, 6-diamidino-2-phenylindole (DAPI) for 10 min, and examined using a Zeiss confocal system.

### Electron Microscopy

Marc-145 cells were seeded into a 5-cm dish and infected with PRRSV. At 36 hpi, the supernatant was discarded and washed thrice with PBS. The cells were fixed at 2% glutaraldehyde. Cell pellets were embedded in 2% agarose, postfixed with 1% osmium tetroxide, and dehydrated with an ethanol series. Samples were infiltrated, embedded, and polymerized for 48 h at 60°C. Ultrathin sections were prepared and examined using a transmission electron microscope (20). The uninfected Marc-145 cells act as the negative control.

### cGAMP Activity Assay

Marc-145 cells were transfected for 30 h with p3xFlag-cGAS or control plasmid before being infected with or without PRRSV at an MOI of 0.5 for 36 h. To test for cGAMP activity, cells were lysed with hypotonic buffer (10 mM Tris-HCl, pH 7.4, 10 mM KCl, 1.5 mM MgCl<sub>2</sub>) and centrifuged at 100,000 $\times g$  for 20 min. The supernatants were incubated at 95°C for 5 min before being centrifuged at 12,000 $\times g$  for 5 min. Supernatants were recovered and treated or 30 min at 37°C with 1 U/ $\mu l$  of benzonase (EMD Millipore), followed by 60 min at 50°C with 100  $\mu g/ml$  of Proteinase K (Thermo Fisher Scientific). The supernatant was incubated for 5 min at 95°C before being cooled to 25°C. The supernatant was treated with 1 $\times$  digitonin permeabilization solution. The buffer was incubated with Marc-145 cells for 20 min at 37°C. The digitonin permeabilization solution was aspirated from the cells and replaced with normal growth media. RNA was isolated from the Marc-145 cells 12 h later, and the IFN transcript was analyzed (21).

### Statistical Analysis

All the experiments mentioned above were performed using three independent experiments. Statistical significance was analyzed using t-tests. The data shown are the means  $\pm$

standard variations (SD) of three independent experiments. P-values of less than 0.05 were considered statistically significant.

## RESULTS

### Overexpression of cGAS Induces the Production of IFN- $\beta$ During PRRSV Infection

As a DNA sensor, cGAS can be activated to induce the production of IFN- $\beta$  and ISGs during DNA virus infection. However, our findings showed that an RNA virus overexpressing the cGAS during PRRSV infection could also promote IFN- $\beta$  production at the transcription and protein levels. As shown in **Figure 1A**, overexpression of cGAS significantly increases the IFN- $\beta$  at the mRNA level during PRRSV infection. Furthermore, at 12 hpi, the content of IFN- $\beta$  in the supernatant of the Marc-145 transfected with cGAS was significantly higher than that of untransfected cGAS ( $p < 0.05$ ) (**Figure 1B**). cGAS induces the production of IFN- $\beta$  during PRRSV infection, according to all of these studies.

### cGAS Exhibits Anti-PRRSV Activity

To examine the effects of cGAS on PRRSV replication, cGAS was overexpressed in the Marc-145 cells by transfection with p3xFlag-cGAS. As shown in **Figure 2A**, when cGAS was overexpressed, the N protein levels of PRRSV were lower than those in the control cells, especially at 12–36 hpi. Furthermore, there was a significant difference in viral titers between cells transfected with p3xFlag-cGAS or p3xFlag, with an approximate 1.0–2.0 log decrease in virus titers from 12 to 36 hpi ( $p < 0.05$ ,  $p < 0.01$ ) (**Figure 2B**). In contrast, when the cGAS gene was knocked out in the Marc-145 cells, the N protein levels of PRRSV were higher than those in wild-type Marc-145 cells (**Figure 2C**). The virus titers were increased during PRRSV infection at different times and were significantly different in the cGAS knockout Marc-145 cells at 36 hpi ( $p < 0.01$ ). These observations suggest that cGAS is a cellular antiviral factor that represses PRRSV infection.

### Mitochondria Were Damaged During PRRSV Infection

Mitochondria are key participants in innate immune pathways, functioning as both signaling platforms and contributing to effector responses. mtDNA, engaging PRRs and triggering type I IFNs and ISG expression, may leak into the cytoplasm when mitochondria are damaged. To investigate the morphological alteration of mitochondria after PRRSV infection, Marc-145 cells were infected with PRRSV at an MOI of 0.5 and were subjected to IFA and transmission electron microscopy analysis. The results showed that TOM20, the mitochondrial protein, was typically tubular in uninfected cells and fragmented in PRRSV infected cells (**Figure 3A**). Besides, transmission electron microscopy results showed that the mitochondria were fragmented, and the number of mitochondrial ridges was significantly reduced. Furthermore, the mitochondrial morphology appears vacuolar when infected with PRRSV (**Figure 3B**). Together, these results demonstrate that PRRSV infection induces mitochondrial damage.

### mtDNA Leak to the Cytoplasm During PRRSV Infection

As PRRSV infection induces mitochondrial damage, we hypothesize the mtDNA is leaked to the cytoplasm when there is a PRRSV infection. To further verify this hypothesis, the Marc-145 cells infected with or without PRRSV were subjected to IFA and qPCR to detect the mtDNA in the cytoplasm. As shown in **Figure 4A**, there is a large amount of double-stranded DNA (dsDNA) in the cytoplasm of PRRSV-infected cells, but there is no double-stranded DNA in the cytoplasm of uninfected cells. Besides, qPCR results showed that the amount of mtDNA was significantly increased when PRRSV infection was detected (**Figure 4B**;  $p < 0.05$ ,  $p < 0.01$ ,  $p < 0.001$ ). Moreover, as the dose of infection increases, the amount of mtDNA in the cytoplasm also increases. These results suggest that mtDNA is leaked into the cytoplasm when there is a PRRSV infection.

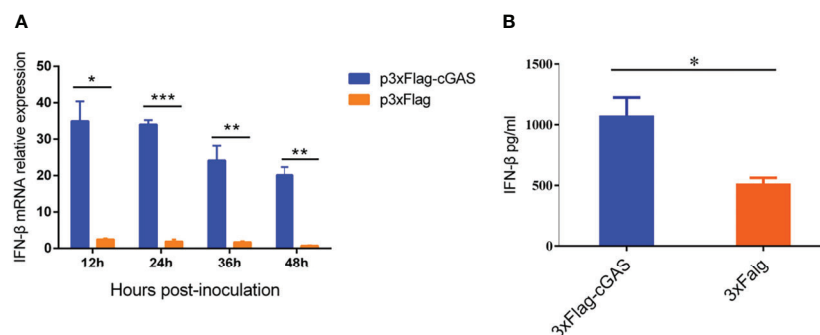


**FIGURE 1** | cGAS increases IFN- $\beta$  expression during PRRSV infection. **(A)** IFN- $\beta$  relative mRNA level in Marc-145 cells transfected with p3XFLAG or p3XFLAG-cGAS after being infected with PRRSV. **(B)** The Marc-145 cells were transfected with p3XFLAG or p3XFLAG-cGAS for 36 h and then infected with PRRSV, the IFN- $\beta$  production was detected by Monkey Interferon  $\beta$  ELISA Kit. The statistical significance of differences was determined using Student's *t*-test (\* $p < 0.05$ ; \*\* $p < 0.01$ ; \*\*\* $p < 0.001$ ).

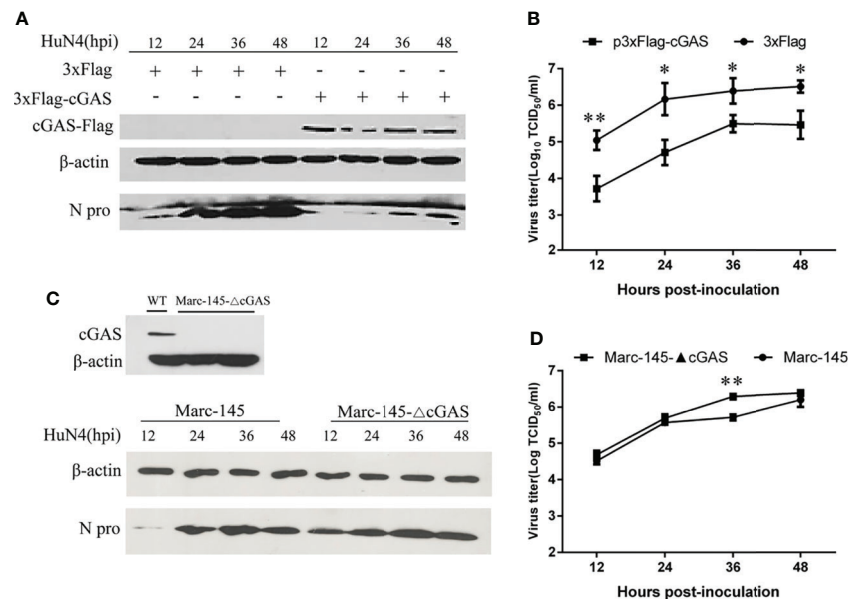


**FIGURE 2** | cGAS affects the replication of PRRSV. Marc-145 cells transfected with p3xFlag-cGAS (2 μg) or p3xFlag (2 μg) were inoculated with the PRRSV HuN4 strain at an MOI of 0.1. The cells and supernatant were harvested at the indicated times. **(A)** The replication of PRRSV was evaluated by WB with an anti-N polyclonal antibody. **(B)** The infectious viral titer in the supernatant was determined by a microtitration assay and calculated as log<sub>10</sub> TCID<sub>50</sub> per ml. **(C)** WB analysis of endogenous cGAS levels in cGAS-KO Marc-145 cells and wild-type Marc-145 cells were infected with PRRSV at an MOI of 0.1. The replication of PRRSV was evaluated by WB with an anti-N polyclonal antibody. **(D)** The viral titer in the supernatant was determined by TCID<sub>50</sub>. β-actin expression was used as a loading control. The data are presented as the mean ± SD from three experiments. The statistical significance of differences was determined using the Student's *t*-test (\**p* < 0.05; \*\**p* < 0.01).

## mtDNA Co-Location With cGAS During PRRSV Infection

To confirm whether the cytoplasmic mtDNA induced by PRRSV infection can bind to cGAS, the Marc-145 cells infected with PRRSV were fixed to verify co-localization between cGAS and mtDNA. The results showed that PRRSV infection could induce mtDNA into the cytoplasm and co-localize with cGAS (Figure 5).

## cGAS Activates cGAMP Activity During PRRSV Infection

We have demonstrated that PRRSV replication can be inhibited by cGAS. Besides, the cGAS, acting as the viral sensor, can activate the cGAMP. So, we detected cGAMP activity during PRRSV infection. The findings show that cGAS overexpressing alone cannot increase cGAMP activity, and PRRSV infection alone can only increase cGAMP activity to a certain extent. The cGAMP activity was significantly increased when overexpressing cGAS during PRRSV infection (Figure 6A). This phenomenon may be because PRRSV infection causes mtDNA to leak into the cytoplasm, which binds to cGAS and then activates cGAMP activity. While overexpressing cGAS alone does not increase cGAMP activity because there is no mtDNA as an activator.

## PRRSV Was Restricted by cGAMP

cGAS inhibits PRRSV replication, and cGAS can activate the activity of cGAMP. To test whether the PRRSV was restricted by

cGAMP, Marc-145 cells were treated with cGAMP at 10 μg/ml. The N protein level of PRRSV was significantly decreased at different times (Figure 6B). Additionally, the Marc-145 cells were treated with different concentrations of cGAMP and then infected with PRRSV. The results indicated that the expression level of N protein was decreased with increasing cGAMP concentration (Figure 6C). The results demonstrated that PRRSV was dose-dependently restricted by cGAMP.

## cGAS Suppresses Different Genotypes of PRRSV

To verify the inhibition of cGAS on classic type 2 (vAPRRS) and classic type 1 strains (vSHE), the Marc-145 cells were transfected with cGAS and then infected with the vAPRRS and vSHE strains. The results showed that the viral titer and the N protein level of the virus were significantly decreased compared with the untransfected with the cGAS. The results indicated that cGAS could restrict multiple PRRSV strains.

## DISCUSSION

PRRSV has been a major threat to global industrial pig farming since its discovery in the late 1980s (22), particularly during the HP-PRRSV outbreak in 2006 (23). Vaccination has been used to control PRRSV. However, commercially available vaccines fail to

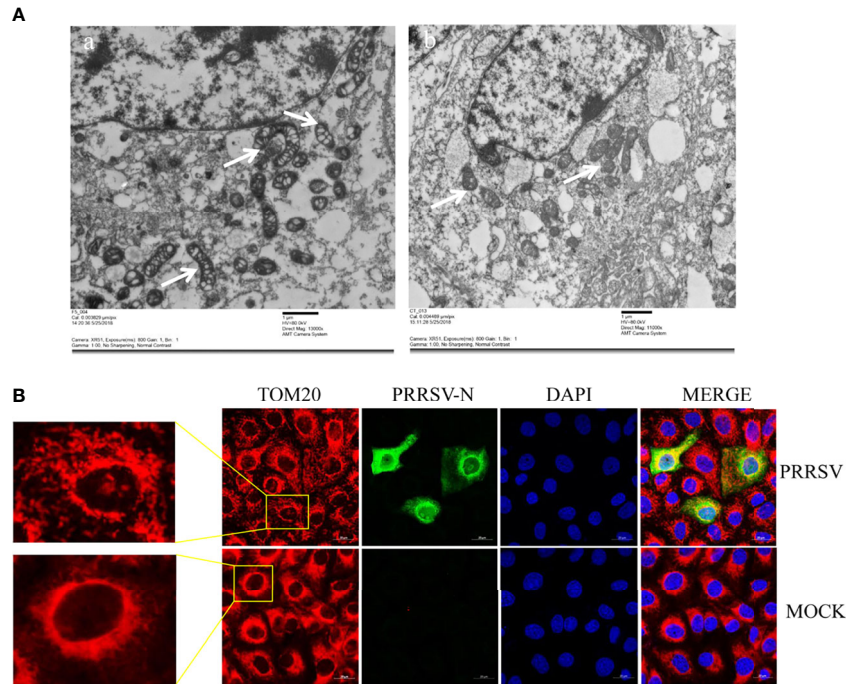


**FIGURE 3 |** PRRSV infection induces mitochondrial damage. **(A)** Electron microscopy analysis showing mitochondrial fission and defects in PRRSV-infected cells (Left). At 24 h post-infection, PRRSV infected Marc-145 cells, and uninfected cells were examined by electron microscope. The images show elongated mitochondria in uninfected cells and fragmented mitochondria with defective cristae in infected cells (White Arrow). **(B)** At 24 h post-infection, Marc-145 cells were immunostained with antibodies specific to TOM20 (red), N (green). The zoomed images show typical tubular mitochondria in uninfected cells and fragmented mitochondria in PRRSV infected cells.

provide sustainable protection against PRRSV due to its rapid evolution. Antiviral therapies provide creative insights to guide future PRRSV control and prevention efforts, especially in cases where existing vaccines fail to match the circulating virus (24). Our study found that overexpression of cGAS inhibits PRRSV

replication, while knockout cGAS facilitates PRRSV replication in Marc-145 cells (Figure 2). During PRRSV infection, cGAS can activate cGAMP activity and then induce the production of IFN to inhibit PRRSV replication (Figures 1, 6). Our results showed that cGAS, as a newly discovered ISG, might have potential use

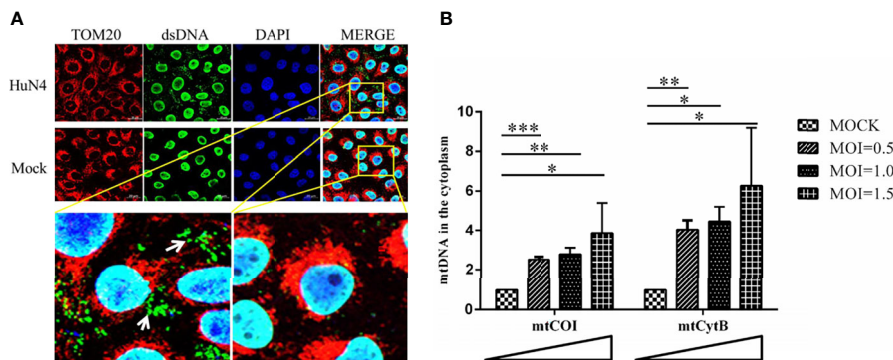


**FIGURE 4 |** PRRSV infection induces mtDNA leaking into the cytoplasm. **(A)** At 24 h post-infection, Marc-145 cells were immunostained with antibodies specific to TOM20 (red), dsDNA (green). The nucleus is stained with DAPI (blue) in the merged images. The zoomed images show that large amounts of dsDNA (green) accumulate in the cytoplasm of the PRRSV infected cells. **(B)** Fold induction of levels of mitochondria-specific DNA sequences mtCOI and mtCytB present in the cytosol of Marc-145 cells infected with PRRSV at MOI 0.5, 1 and MOI 1.5. The statistical significance of differences was determined using the Student's *t*-test (\**p* < 0.05; \*\**p* < 0.01; \*\*\**p* < 0.001).



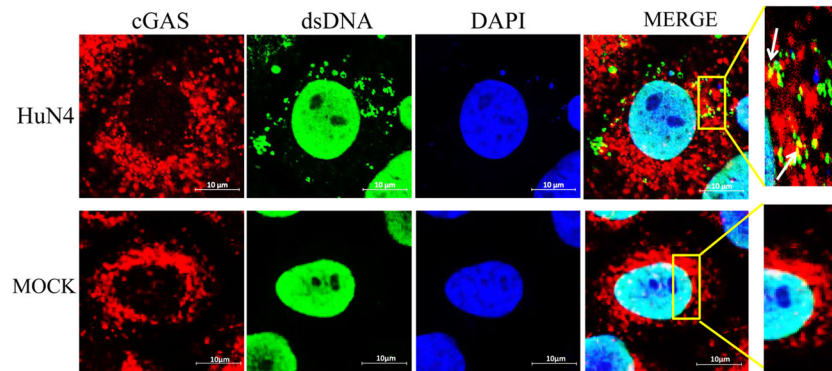


**FIGURE 5** | mtDNA co-located with cGAS during PRRSV infection. Marc-145 cells were infected with the PRRSV HuN4 strain and the uninfected served as the negative control. The cells were fixed 24 h after infection and then subjected to indirect immunofluorescence to detect cGAS protein (red) and mtDNA (green). The nucleus is stained with DAPI (blue). The zoomed images show that mtDNA co-located with cGAS in the infected Marc-145 cells (yellow).

as a novel approach to control PRRSV infection. Therefore, understanding the mechanism of cGAS restriction of PRRSV will be beneficial for developing effective therapies to control outbreaks of this disease in the future.

As the first line of host defense, the innate immune system uses PRRs to detect invading pathogens. cGAS is a conserved component of the innate system in DNA virus infection. It binds to cytosolic double-stranded DNA (dsDNA) from various sources, including bacteria, DNA viruses, and retroviruses. Following the binding of dsDNA, cGAS catalyzes the production of a second messenger known as cGAMP, which subsequently binds to the adaptor protein STING on the endoplasmic reticulum (ER) membrane (25). STING recruits

TANK binding kinase 1 (TBK1) and activates transcription factors interferon regulatory factor 3 (IRF3) and nuclear factor- $\kappa$ B (NF- $\kappa$ B), which then translocate into the nucleus to induce the production of IFN and other inflammatory cytokines, establishing an antiviral state in infected and uninfected neighboring host cells (26). cGAS inhibited the replication of many DNA viruses, including HSV-1, MHV68, and vaccinia virus. Currently, this is considered the classical pathway by which cGAS exerts its antiviral effect (13). Several studies have revealed that cGAS is also engaged in antiviral responses to RNA viruses, namely, EAV, DENV, WNV, IAV, and CHIKV (14–16). However, how cGAS is involved in RNA virus-induced immune responses is largely unknown. Although cGAS was reported to

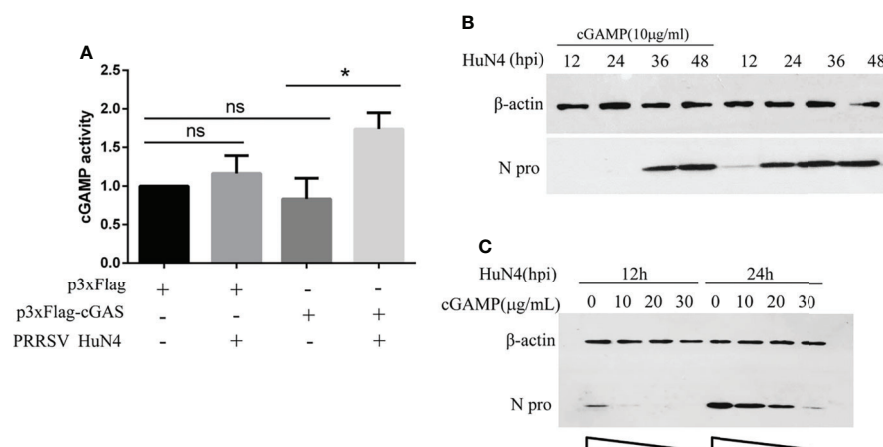


**FIGURE 6** | cGAS activates cGAMP activity during PRRSV infection, and cGAMP inhibits PRRSV replication. **(A)** Marc-145 cells were transfected with p3xFlag, p3xFlag-cGAS, and infected with or without PRRSV. The cGAMP activity was measured by qRT-PCR to detect the transcript levels of IFN $\beta$ 1. The statistical significance of differences was determined using the Student's *t*-test ( $p < 0.05$ ; ns, not significant). **(B)** The Marc-145 cells were treated with cGAMP for 12 h at different concentrations and then infected with PRRSV at 0.5 MOI. The cells were harvested at 12 and 24 hpi. The N protein level was detected by WB with anti-N pAb. **(C)** The Marc-145 cells were treated with cGAMP of 10  $\mu$ g/ml for 12 h, and the cells were infected with PRRSV at 0.5 MOI. The cells were harvested at a different time, and the N protein was detected by WB with the anti-N pAb.

bind dsRNA, this interaction did not lead to the production of cGAMP (27). Therefore, cGAS may play its role in antiviral responses to RNA viruses differently from the classical pathway.

Our study demonstrated that the cGAS is important in inhibiting PRRSV replication, consistent with previous studies (28). Their study suggested that cGAS and STING possess the anti-PRRSV effect. Nevertheless, the mechanism is unclear (28). Our findings show that cGAS overexpression promotes IFN- $\beta$  production during PRRSV infection at both the transcription and translation levels (Figure 1). Additionally, overexpression of cGAS decreased the N protein level of PRRSV and the viral titer.

In contrast, knockout cGAS facilitates the replication of PRRSV (Figures 2C, D). While PRRSV has been identified and characterized as an IFN- $\beta$  antagonist virus, the Nsp1, Nsp2, Nsp4, Nsp11, and N protein of PRRSV play an important role in its innate immunity antagonism (29). Besides, during PRRSV infection, the virus genome was released into the cytoplasm, ORF1a and ORF1b were translated to produce two large polyproteins and autocatalytic processing to generate at least 14 Nsps. Some Nsps assemble into a replication and transcription complex (RTC) to direct genome amplification and subgenomic mRNA synthesis to produce a nested set of six major subgenomic mRNAs that are both 5'- and 3'-coterminal with the genomic RNA (30). No DNA or DNA intermediate exists in the life cycle of PRRSV. Even so, cGAS can still activate innate immunity and exert anti-PRRSV effects, so we hypothesized that cGAS exerts antiviral effects through a non-canonical pathway.

To further elucidate the molecular mechanism by which cGAS activates innate immunity to suppress PRRSV replication, we

examine the effects of PRRSV infection on mitochondria. The results suggest that PRRSV infection-induced mitochondrion damage and leaked mtDNA into the cytoplasm are dose-dependent (Figure 4B). When mtDNA is released into the cytoplasm, it can act as a danger-associated molecular pattern (DAMP) to stimulate IFN- $\beta$  production *via* the cGAS-STING pathway (31). cGAS catalyzes the production of a second messenger known as cGAMP, which subsequently binds to the adaptor protein STING on the endoplasmic reticulum (ER) membrane to activate innate immunity (25). Our findings show that cGAS overexpression alone cannot increase cGAMP activity and PRRSV infection alone can only increase cGAMP activity to a certain extent.

In contrast, the cGAMP activity was significantly increased upon cGAS being overexpressed during PRRSV infection. Therefore, the increase in cGAMP activity depends on two necessary conditions, PRRSV infection and cGAS (Figure 6A). Only during PRRSV infection can mtDNA be released into the cytoplasm to activate cGAS and then catalyze the production of cGAMP. cGAMP can bind to the adaptor protein STING and then coordinate the activation of inflammatory transcription factors to induce IFN expression and establish an antiviral cellular state (32). Besides, laser confocal results confirmed that cGAS can co-localize with mtDNA in the cytoplasm during PRRSV infection. Furthermore, Marc-145 cells treated with cGAMP alone can inhibit the PRRSV (Figures 6B, C). Moreover, besides HP-PRRSV, cGAS suppresses the classic type 1 strain (vSHE) (Figures 7A, B) and the classic type 2 strain (vAPRRS) (Figures 7C, D). Compared with the type 2 PRRSV virus, cGAS had a stronger inhibitory effect on type 1

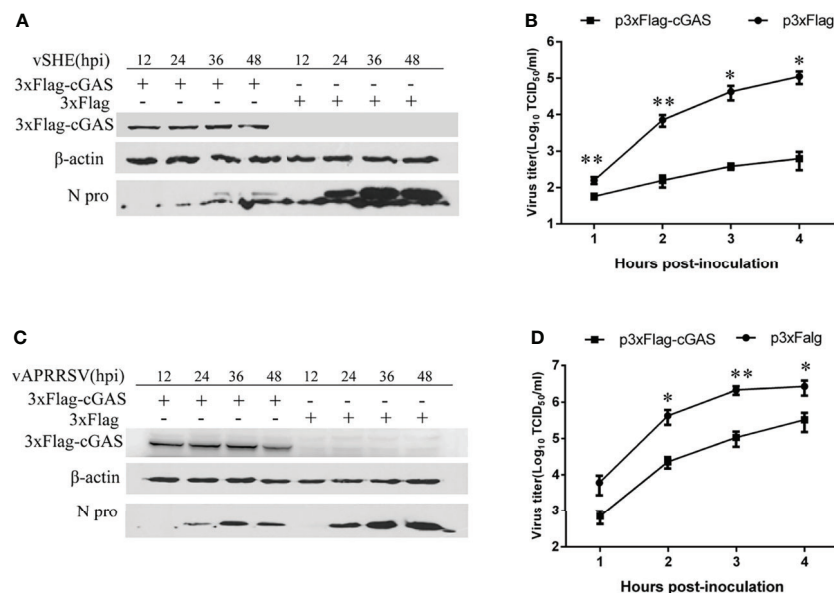


**FIGURE 7** | cGAS overexpression inhibits classical Europe-type (genotype I) and North America-type (genotype II) PRRSV replication. (A, B) PRRSV vSHE strain (genotype I) and (C, D) vAPRRSV (genotype II) strain proliferation in MARC-145 cells transfected with p3xFlag-cGAS or control plasmids. The N protein expression levels of PRRSV were analyzed by WB. Viral titers from Marc-145 cells transfected with p3xFlag-cGAS or control plasmids were determined by a microtitration assay and calculated as log<sub>10</sub> TCID<sub>50</sub> per ml. Data represent the mean  $\pm$  standard deviation of three independent experiments. Statistical significance was analyzed using Student's t-test (\* $p$  < 0.05; \*\* $p$  < 0.01).

PRRSV, which may be more sensitive to cGMAP. These results elucidate that cGAS inhibits multiple PRRSV replication. Besides PRRSV, DENV was also restricted by cGAS with a similar method (19, 33, 34). Certainly, RNA viruses have evolved effective strategies to antagonize the function of cGAS to facilitate their replication in host cells. DENV NS2B protease cofactor targets the cGAS for lysosomal degradation to avoid the detection of mtDNA during infection (34). CHIKV inhibits type-I interferon responses mediated by cGAS-STING by degrading cGAS (16). Virus and cGAS are always in a state of mutual antagonism, but how PRRSV antagonizes the antiviral effect of cGAS in natural infection remains to be further studied.

Overall, this study demonstrated that PRRSV infection induces mitochondrial damage and leaks mtDNA into the cytoplasm. cGAS restricts PRRSV replication by detecting the mtDNA in the cytoplasm, activating the cGAMP activity, and inducing the production of IFN- $\beta$ . These results establish a foundation for further exploration of cGAS involved in resistance to PRRSV transmission. Our study highlights the importance of cGAS in PRRSV replication and suggests potential antiviral therapies.

## DATA AVAILABILITY STATEMENT

The original contributions presented in the study are included in the article/supplementary material. Further inquiries can be directed to the corresponding author.

## REFERENCES

- Chand RJ, Tribble BR, Rowland RR. Pathogenesis of Porcine Reproductive and Respiratory Syndrome Virus. *Curr Opin Virol* (2012) 2:256–63. doi: 10.1016/j.coviro.2012.02.002
- Tian K, Yu X, Zhao T, Feng Y, Cao Z, Wang C, et al. Emergence of Fatal PRRSV Variants: Unparalleled Outbreaks of Atypical PRRS in China and Molecular Dissection of the Unique Hallmark. *PLoS One* (2007) 2:e526. doi: 10.1371/journal.pone.0000526
- Han J, Zhou L, Ge X, Guo X, Yang H. Pathogenesis and Control of the Chinese Highly Pathogenic Porcine Reproductive and Respiratory Syndrome Virus. *Vet Microbiol* (2017) 209:30–47. doi: 10.1016/j.vetmic.2017.02.020
- Han M, Yoo D. Engineering the PRRS Virus Genome: Updates and Perspectives. *Vet Microbiol* (2014) 174:279–95. doi: 10.1016/j.vetmic.2014.10.007
- Huang C, Zhang Q, Guo XK, Yu ZB, Xu AT, Tang J, et al. Porcine Reproductive and Respiratory Syndrome Virus Nonstructural Protein 4 Antagonizes Beta Interferon Expression by Targeting the NF- $\kappa$ B Essential Modulator. *J Virol* (2014) 88:10934–45. doi: 10.1128/JVI.01396-14
- Yoo D, Song C, Sun Y, Du Y, Kim O, Liu HC. Modulation of Host Cell Responses and Evasion Strategies for Porcine Reproductive and Respiratory Syndrome Virus. *Virus Res* (2010) 154:48–60. doi: 10.1016/j.virusres.2010.07.019
- Chan YK, Gack MU. Viral Evasion of Intracellular DNA and RNA Sensing. *Nat Rev Microbiol* (2016) 14:360. doi: 10.1038/nrmicro.2016.45
- Wang H, Bai J, Fan B, Li Y, Zhang Q, Jiang P. The Interferon-Induced Mx2 Inhibits Porcine Reproductive and Respiratory Syndrome Virus Replication. *J Interferon Cytokine Res Off J Int Soc Interferon Cytokine Res* (2016) 36:129–39. doi: 10.1089/jir.2015.0077
- Zhao M, Wan B, Li H, He J, Chen X, Wang L, et al. Porcine 2', 5'-Oligoadenylate Synthetase 2 Inhibits Porcine Reproductive and Respiratory Syndrome Virus Replication *In Vitro*. *Microb Pathogen* (2017) 111:14–21. doi: 10.1016/j.micpath.2017.08.011

## AUTHOR CONTRIBUTIONS

KZ designed the experiments. KZ, XL, LL, FG, YJ, GL, and LY performed the experiments. KZ and LL analyzed the data and wrote the manuscript. WY, YZ, and GT made constructive comments on the experiments. All authors listed have made a substantial, direct, and intellectual contribution to the work and approved it for publication.

## FUNDING

This work was supported by the National Natural Science Foundation of China (Grant No. 32102644); the Talents Introduction Projects of Hebei Agricultural University (Grant No. YJ201945); the Key Research and Development Projects of Hebei (Grant No. 20326625D); the State Key Laboratory of Veterinary Etiological Biology, Lanzhou Veterinary Research Institute, Chinese Academy of Agricultural Sciences (Grant No. SKLVEB2020KFKT016); Basic Scientific Research Funds of Provincial Universities in Hebei Province (KY202017).

## ACKNOWLEDGMENTS

We thank all Dr. Tong's lab members for their suggestions and excellent technical assistance.

- Ablasser A, Goldeck M, Cavlar T, Deimling T, Witte G, Röhl I, et al. cGAS Produces a 2'-5'-Linked Cyclic Dinucleotide Second Messenger That Activates STING. *Nature* (2013) 498:380. doi: 10.1038/nature12306
- Ma F, Li B, Liu SY, Iyer SS, Yu Y, Wu A, et al. Positive Feedback Regulation of Type I IFN Production by the IFN-Inducible DNA Sensor cGAS. *J Immunol* (2015) 194:1545–54. doi: 10.4049/jimmunol.1402066
- Ma Z, Damania B. The cGAS-STING Defense Pathway and Its Counteraction by Viruses. *Cell Host Microbe* (2016) 19:150–8. doi: 10.1016/j.chom.2016.01.010
- Ni G, Ma Z, Damania B. cGAS and STING: At the Intersection of DNA and RNA Virus-Sensing Networks. *PLoS Pathog* (2018) 14:e1007148. doi: 10.1371/journal.ppat.1007148
- Holm CK, Rahbek SH, Gad HH, Bak RO, Jakobsen MR, Jiang Z, et al. Influenza A Virus Targets a cGAS-Independent STING Pathway That Controls Enveloped RNA Viruses. *Nat Commun* (2016) 7:1–9. doi: 10.1038/ncomms10680
- Schoggins JW, MacDuff DA, Imanaka N, Gainey MD, Shrestha B, Eitson JL, et al. Pan-Viral Specificity of IFN-Induced Genes Reveals New Roles for cGAS in Innate Immunity. *Nature* (2014) 505:691. doi: 10.1038/nature12862
- Webb L, Veloz J, Pintado-Silva J, Zhu T, Rangel M, Mutetwa T, et al. Chikungunya Virus Antagonizes cGAS-STING Mediated Type-I Interferon Responses by Degrading cGAS. *PLoS Pathog* (2020) 16:e1008999. doi: 10.1371/journal.ppat.1008999
- Reed LJ, Muench H. A Simple Method of Estimating Fifty Per Cent Endpoints. *Am J Epidemiol* (1938) 27:493–7. doi: 10.1093/oxfordjournals.aje.a118408
- Bookout AL, Cummins CL, Mangelsdorf DJ, Pesola JM, Kramer MF. High-Throughput Real-Time Quantitative Reverse Transcription PCR. *Curr Protoc Mol Biol* (2006) 73(1):15.8.1–28. doi: 10.1002/0471142727.mb1508s73
- Sun B, Sundström KB, Chew JJ, Bist P, Gan ES, Tan HC, et al. Dengue Virus Activates cGAS Through the Release of Mitochondrial DNA. *Sci Rep* (2017) 7:1–8. doi: 10.1038/s41598-017-03932-1
- Li S, Wang J, Zhou A, Khan FA, Hu L, Zhang S. Porcine Reproductive and Respiratory Syndrome Virus Triggers Mitochondrial Fission and

- Mitophagy to Attenuate Apoptosis. *Oncotarget* (2016) 7:56002. doi: 10.18632/oncotarget.10817
21. Wu J, Sun L, Chen X, Du F, Shi H, Chen C, et al. Cyclic GMP-AMP is an Endogenous Second Messenger in Innate Immune Signaling by Cytosolic DNA. *Science* (2013) 339:826–30. doi: 10.1126/science.1229963
  22. Shi M, Lam TT, Hon CC, Hui RK, Faaberg KS, Wennblom T, et al. Molecular Epidemiology of PRRSV: A Phylogenetic Perspective. *Virus Res* (2010) 154:7–17. doi: 10.1016/j.virusres.2010.08.014
  23. Tong GZ, Zhou YJ, Hao XF, Tian ZJ, An TQ, Qiu HJ. Highly Pathogenic Porcine Reproductive and Respiratory Syndrome, China. *Emerg Infect Dis* (2007) 13:1434. doi: 10.3201/eid1309.070399
  24. Li L, Zhao K, Gao F, Jiang Y, Shan T, Tong W, et al. Restriction of Porcine Reproductive and Respiratory Syndrome Virus Replication by Galectin-1. *Vet Microbiol* (2019) 235:310–8. doi: 10.1016/j.vetmic.2019.07.024
  25. Wu J, Chen ZJ. Innate Immune Sensing and Signaling of Cytosolic Nucleic Acids. *Annu Rev Immunol* (2014) 32:461–88. doi: 10.1146/annurev-immunol-032713-120156
  26. Barber GN. STING: Infection, Inflammation and Cancer. *Nat Rev Immunol* (2015) 15:760–70. doi: 10.1038/nri3921
  27. Civril F, Deimling T, de Oliveira Mann CC, Ablasser A, Moldt M, Witte G, et al. Structural Mechanism of Cytosolic DNA Sensing by cGAS. *Nature* (2013) 498:332–7. doi: 10.1038/nature12305
  28. Xu Y, Zhang Y, Sun S, Luo J, Jiang S, Zhang J, et al. The Innate Immune DNA Sensing cGAS-STING Signaling Pathway Mediates Anti-PRRSV Function. *Viruses* (2021) 13:1829. doi: 10.3390/v13091829
  29. Lunney JK, Fang Y, Ladinig A, Chen N, Li Y, Rowland B, et al. Porcine Reproductive and Respiratory Syndrome Virus (PRRSV): Pathogenesis and Interaction With the Immune System. *Annu Rev Anim Biosci* (2016) 4:129–54. doi: 10.1146/annurev-animal-022114-111025
  30. Yun S-I, Lee Y-M. Overview: Replication of Porcine Reproductive and Respiratory Syndrome Virus. *J Microbiol* (2013) 51:711–23. doi: 10.1007/s12275-013-3431-z
  31. Aguirre S, Luthra P, Sanchez-Aparicio MT, Maestre AM, Patel J, Lamothe F, et al. Dengue Virus NS2B Protein Targets cGAS for Degradation and Prevents Mitochondrial DNA Sensing During Infection. *Nat Microbiol* (2017) 2:17037. doi: 10.1038/nmicrobiol.2017.37
  32. Franz KM, Neidermyer WJ, Tan YJ, Whelan SP, Kagan JC. STING-Dependent Translation Inhibition Restricts RNA Virus Replication. *Proc Natl Acad Sci* (2018) 115:E2058–67. doi: 10.1073/pnas.1716937115
  33. Aguirre S, Fernandez-Sesma A. Collateral Damage During Dengue Virus Infection: Making Sense of DNA by cGAS. *J Virol* (2017) 91:e01081–01016. doi: 10.1128/JVI.01081-16
  34. Aguirre S, Luthra P, Sanchez-Aparicio MT, Maestre AM, Patel J, Lamothe F, et al. Dengue Virus NS2B Protein Targets cGAS for Degradation and Prevents Mitochondrial DNA Sensing During Infection. *Nat Microbiol* (2017) 2:1–11. doi: 10.1038/nmicrobiol.2017.37

**Conflict of Interest:** The authors declare that the research was conducted in the absence of any commercial or financial relationships that could be construed as a potential conflict of interest.

**Publisher's Note:** All claims expressed in this article are solely those of the authors and do not necessarily represent those of their affiliated organizations, or those of the publisher, the editors and the reviewers. Any product that may be evaluated in this article, or claim that may be made by its manufacturer, is not guaranteed or endorsed by the publisher.

Copyright © 2022 Liu, Li, Gao, Jiang, Yuan, Li, Yu, Zhou, Tong and Zhao. This is an open-access article distributed under the terms of the Creative Commons Attribution License (CC BY). The use, distribution or reproduction in other forums is permitted, provided the original author(s) and the copyright owner(s) are credited and that the original publication in this journal is cited, in accordance with accepted academic practice. No use, distribution or reproduction is permitted which does not comply with these terms.



# Host Restrictive Factors Are the Emerging Storm Troopers Against Enterovirus: A Mini-Review

Chen Huan<sup>1</sup>, Xinglong Qu<sup>2</sup> and Zhaolong Li<sup>1\*</sup>

<sup>1</sup> Center of Infectious Diseases and Pathogen Biology, Institute of Virology and AIDS Research, Key Laboratory of Organ Regeneration and Transplantation of The Ministry of Education, The First Hospital of Jilin University, Changchun, China,

<sup>2</sup> Respiratory Department of the First Hospital of Jilin University, Changchun, China

Enterovirus infection continues to be a global health problem. The lack of specific drugs and broad-spectrum vaccines means an urgent need to develop effective strategies against enteroviruses. Host restrictive factors are a class of intrinsic host antiviral factors that have been broadly defined and investigated during HIV infections and have great significance for drug development and treatment design. In recent years, the essential role of host restrictive factors in regulating enteroviral infections has been gradually recognized and investigated. An increasing number of studies have shown that host-restrictive factors regulate multiple steps in the life cycle of enteroviruses. This mini-review discusses the restrictive factors against enteroviruses, their antiviral mechanism, and the arms race between them and enteroviruses. We also summarise the pathways that enteroviruses use to impair host antiviral signals. This mini-review characterizes the essential role of host restriction factors in enterovirus infections, which provides ideas and potential targets for antiviral drug design by regulating host restrictive factors. It also reveals potential future research on the interplay between host restrictive factors and enteroviruses.

**Keywords:** host restrictive factors, enteroviruses, virus-host interplay, antiviral, arms race

## OPEN ACCESS

### Edited by:

Junji Xing,  
Houston Methodist Research Institute,  
United States

### Reviewed by:

Longhuan Ma,  
University of Florida, United States

### \*Correspondence:

Zhaolong Li  
lizhaolong@jlu.edu.cn

### Specialty section:

This article was submitted to  
Viral Immunology,  
a section of the journal  
Frontiers in Immunology

**Received:** 01 April 2022

**Accepted:** 12 April 2022

**Published:** 04 May 2022

### Citation:

Huan C, Qu X and Li Z (2022)  
Host Restrictive Factors Are the  
Emerging Storm Troopers Against  
Enterovirus: A Mini-Review.  
*Front. Immunol.* 13:910780.  
doi: 10.3389/fimmu.2022.910780

## INTRODUCTION

There are more than 100 subtypes of enteroviruses that infect humans, including the well-known enterovirus 71 (EV71), enterovirus D68 (EVD68), coxsackieviruses A and B, and poliovirus (PV) (1), and several subtypes of these induce hand-foot-and-mouth disease (HFMD) epidemics every year (2–5). Moreover, EVD68 has been the cause of an unprecedented epidemic of respiratory disease, whose symptoms are unlike its common symptoms and have been temporally associated with acute flaccid myelitis (AFM) (6–8). However, the lack of effective drugs and broad-spectrum vaccines has exacerbated severe health problems.

A series of studies have investigated the interactions between host innate immunity and enteroviruses. Host restriction factors are expressed and/or induced in response to virus infection and include proteins from interferon-stimulated genes (ISGs) (9–19). APOBEC3G (A3G), SAMHD1, and BST2 have been extensively investigated in HIV infection (13). Since the antiviral effects of restrictive factors tend to have a broad spectrum, the regulatory function of host restriction factors during enterovirus infection has been investigated in recent years and has become a rising

focus of enterovirus research. For example, we identified A3G and SAMHD1 restricted multiple enteroviruses and revealed a novel antiviral mechanism (20–23). IFNs and NF- $\kappa$ B signals are activated by viral infection (24–30), which induces the expression of downstream host-restrictive factors to fight against viruses *via* their pathways. However, viruses can impair restriction through multiple strategies. Here, we discuss the host restriction factors that play essential roles in regulating enteroviruses, the underlying mechanism they suppress, and how enteroviruses break host restrictions. This mini-review provides new information that can be used to select potential drug targets against enteroviruses and enlighten the direction of future studies in antiviral research.

## HOST RESTRICTIVE FACTORS PLAY ANTIVIRAL ROLES DURING ENTEROVIRUSES INFECTION

Many in-depth studies on the interaction between enteroviruses and host factors have shown that host-restrictive factors play

regulatory roles in different stages of the viral life cycle. We have summarised these studies based on the lifecycles of enterovirus infections (Figure 1 and Table 1).

## VIRAL ENTRY

Enteroviruses invade host cells by first interacting with specific receptors on the cell surface, where virions are endocytosed, or viral nucleic acids are released into the cells. For instance, scavenger receptor class B member 2 (SCARB2) was identified as a receptor for EV71 by Yamayoshi et al. (41). On this basis, Nakata et al. reported that acid beta-glucosidase 1 (GAB1) restricts EV71 infections by interacting with SCARB2 and reducing the expression of SCARB2 on the cell surface which interferes with the interactions between EV71 and SCARB2 (42). Further investigations showed that recombinant human GBA1, a molecular drug originally used to treat Gaucher's disease (33, 40, 43), protected against EV71 infection (42), hinting that researchers could design anti-enterovirus drugs based on host restrictive factors.

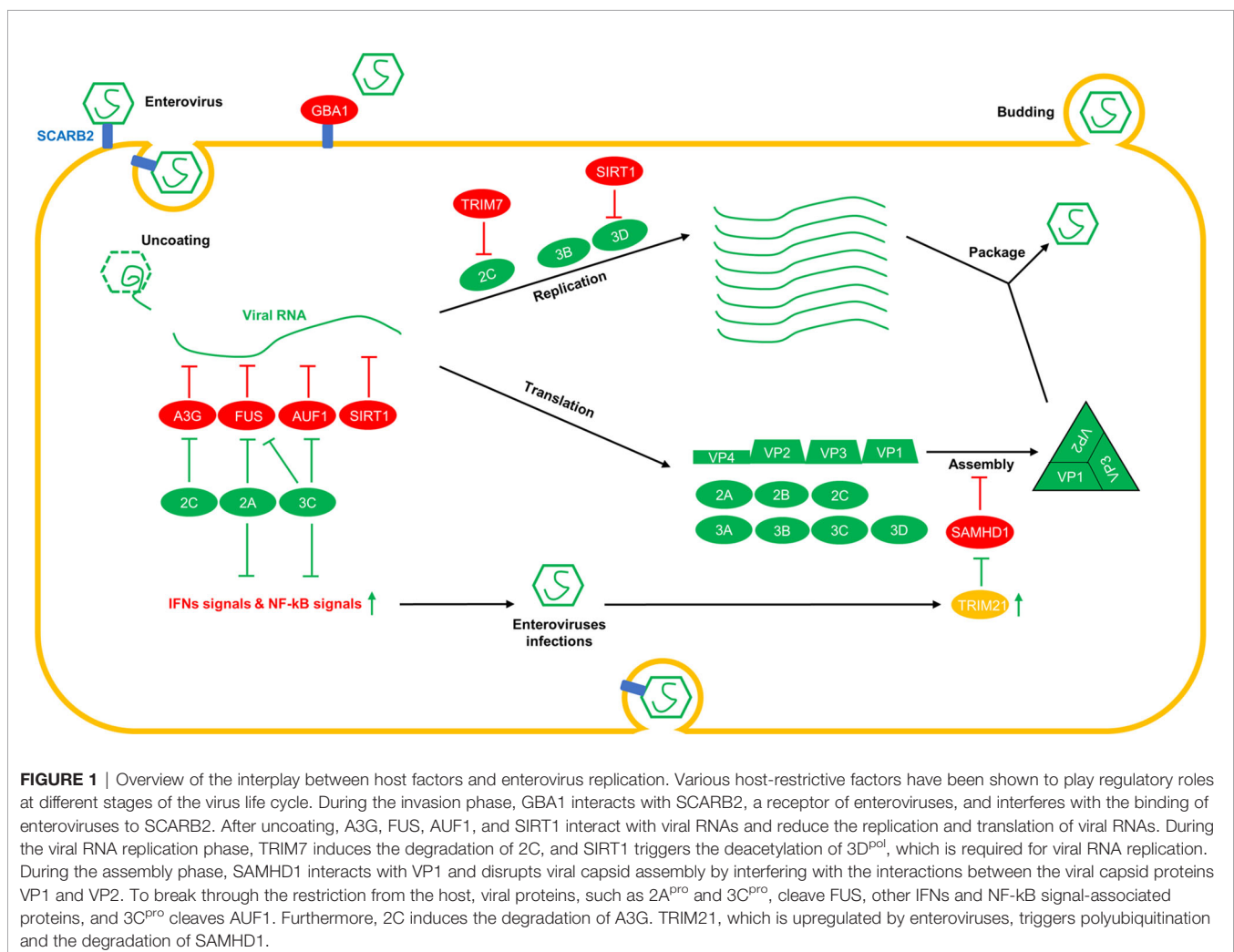


**TABLE 1 |** Host restrictive factors identified in this review.

Gene names	Viral type	Antiviral mechanism	References
A3G	EV71, CA16, EVD68	1. Competitively binds to 5'UTR along with PCBP1. 2. Interacts with 3D <sup>pol</sup> and is packaged into progeny virions.	(26, 31) (32)
AUF1	PV, CVB3	1. Interacts with viral IRES.	(33–35)
FUS/TLS	CVB3	1. Interacts with viral RNA. 2. Formation of stress granules and regulates innate immunity.	(36)
GBA1	EV71	1. Reduces the expression of SCARB2 on the cell surface. 2. Interferes with EV71 binding to SCARB2.	(17)
SAMHD1	EV71, CA16, EVD68	1. Interferes with the interactions between VP1 and VP2.	(37, 38)
SIRT1	EV71	1. Interacts with viral 5'UTR. 2. Reduces the acetylation of 3D <sup>pol</sup> .	(39)
TRIM7	EV71, CVB3, E11, EVD68, PV	1. Degrades viral 2BC protein.	(40)

Host restrictive factors are listed in alphabetical order.

## VIRAL RNA REPLICATION AND THE PROTEIN TRANSLATION PHASES

After entering host cells, RNAs from enteroviruses are replicated and translated into viral proteins under the regulation of host factors (22, 34–36, 39, 44) and viral proteins, including 2BC, 3AB, and 3D (31, 32, 45–49). During this phase, many restrictive factors are involved in inhibiting virus replication. TRIM7, an E3 ligase, has been reported to restrict the replication of multiple enteroviruses by triggering polyubiquitination of their 2BC proteins and inducing the degradation of 2BC proteins *via* the proteasomal pathway (50).

AU-rich element degradation factor 1 (AUF1) binds to the internal ribosome entry site (IRES) of viral RNA and restricts the replication of poliovirus and CVB3 (51–53). However, the 3C<sup>pro</sup> component of enteroviruses can cleave AUF1 to break through the restriction (53).

Like AUF1, fused sarcoma/translocated in liposarcoma (FUS/TLS) is a novel host antiviral factor that restricts CVB3 replication by directly inhibiting viral RNA transcription and protein translation. Moreover, FUS, which binds to viral RNA, triggers the formation of stress granules and regulates the activity of host antiviral innate immunity (54). CVB3 infection induces cytoplasmic mislocalization and cleavage of FUS through the enzymatic activity of viral proteases to evade the FUS-mediated antiviral response and innate immunity (54). In addition, as a class III NAD<sup>+</sup>-dependent histone, the deacetylase (HDAC), SIRT1, suppresses EV71 replication by repressing viral RNA transcription and attenuating viral RNA translation (55). Mechanistically, Han et al. identified the interactions between SIRT1 and viral 3D<sup>pol</sup>, and revealed that SIRT1 inhibits 3D<sup>pol</sup> activity by reducing the acetylation of 3D<sup>pol</sup>. They also found that SIRT1 was able to interact with the viral 5'-UTR and interfere with viral RNA transcription and translation. Additionally, the expression of SIRT1 is upregulated by EV71 infection (55). However, Li et al. observed that EV71 infections could reduce the expression of SIRT1, and administration of the ROS inhibitor N-acetyl-L-cysteine (NAC) reduced apoptosis levels and inflammation, downregulated EV71 propagation, and increased SIRT1 expression in EV71-infected cells (56). Nevertheless, the mechanism underlying the regulation of SIRT1 expression induced by EV71 infection remains unclear.

A3G has been identified as a host-restrictive factor that suppresses HIV replication *via* cytosine deaminase activity (37, 38). In recent years, A3G has been shown to restrict the replication of enteroviruses, such as EV71, CA16, and EVD68, but not CA6 (20, 22, 57). These reports propose novel antiviral mechanisms independent of the cytosine deaminase activity shown by A3G. Li et al. suggested that while suppressing multiple enteroviruses, A3G competitively binds to the viral 5'UTR together with PCBP1, which is required for the transcription and translation of viral RNAs (22, 57). Further investigation showed that PCBP2, but not PCBP1, was required for CA6 replication, which would explain why A3G failed to restrict CA6 replication (22). In addition, Wang et al. suggested that A3G interacts with the 3D<sup>pol</sup> of EV71 and packages it into progeny virions to reduce its infectivity (20). They also found that an inhibitor named IMB-Z inhibited EV71 replication by upregulating the expression of A3G (20). These studies confirmed that A3G inhibits enterovirus and that the mechanism was independent of its cytosine deaminase activity. In addition, other members of the APOBEC3 family, including A3A, A3D, and A3F, were found to possess antiviral activity against EV71 (57).

In contrast, Li et al. reported that A3G is degraded by the 2C proteins in enteroviruses, including EV71, CA6, CA16, CVB3, and EVD68 (57). In their study, viral 2C proteins triggered the polyubiquitination of A3G. Then the polyubiquitinated A3G was recognized by P62 and degraded by autolysosomes.

## VIRAL ASSEMBLY PHASE

Like A3G, SAMHD1, another anti-HIV-restrictive factor, has been extensively investigated (14, 58, 59). SAMHD1 inhibits multiple retroviruses and DNA viruses (60–62), but its antiviral mechanism is unclear. Several studies have suggested that SAMHD1 restricts viruses through its dNTPase activity (14, 60, 63–65), and other studies have argued that its nuclease activity also contributes to its antiviral activity (66–68). For enteroviruses, Li et al. reported that SAMHD1 restricted EV71 replication independently of the dNTPase and nuclease activity of SAMHD1 (21). Furthermore, Zhao et al. reported that SAMHD1 restricted the replication of enteroviruses, including

EV71, EVD68, and CA16, but not CA6, by interfering with the interactions between the viral capsid proteins VP1 and VP2 (23). Zhao et al. showed that SAMHD1 interacts with the EV71-VP1 domain, which is essential for the interaction between EV71-VP1 and EV71-VP2 and attenuates the interaction between EV71-VP1 and VP2. However, the interaction between SAMHD1 and CA6-VP1 did not disrupt the interaction between VP1 and VP2 of CA6, which may explain why SAMHD1 failed to inhibit CA6 (23).

In response to the inhibition of SAMHD1, EV71 has evolved a strategy to overcome this restriction and ensure the survival of its progeny. In a study by Li et al., EV71 infection induced proteasome-associated degradation of SAMHD1 by upregulating the expression of E3 ligase TRIM21, which triggers the polyubiquitination SAMHD1. TRIM21 upregulation is interferon receptor-dependent (21). Li et al. also identified the interaction domains between SAMHD1 and TRIM21 and the ubiquitination site on SAMHD1, which may provide clues for further drug target screening and design.

Several host restrictive factors play essential regulatory roles in various stages of the enterovirus life cycle, and exploring the mechanism underlying the interplay between host restrictive factors and enteroviruses will provide an important scientific basis for strategies against strategies for enterovirus infection.

## ENTEROVIRUSES BREAK OUT OF HOST RESTRICTION BY BLOCKING ANTIVIRAL PATHWAYS

During the long-term arms race, viruses evolve strategies to impair restriction from the host. In addition to the antagonistic strategies against the host restrictive factors mentioned above, enteroviruses also can disrupt other antiviral pathways to ensure their life cycle within the host (**Figure 1**). EV71 3C<sup>Pro</sup> has been reported to cleave multiple innate immune pathway-related proteins, including TRIF (26, 69), TRIM25 (70), TAK1, TAB1, TAB2, TAB3 (71), NLRP3 (72), IRF3 (73), IRF7 (74), IRF9 (75) and PMLIII and IV (76), and reduce IFN and NF- $\kappa$ B signals (77). As this type of research expands, the 3C<sup>Pro</sup> in EVD68 has also been reported to cleave IRF7 and affect IFN signaling (78, 79). Furthermore, the 2A<sup>Pro</sup> in EV71 has been reported to cleave MAVS, MDA5, and NLPR3 (72, 80, 81) and downregulate IFN and NF- $\kappa$ B signaling. In addition to these viral proteases, the 2C proteins in multiple enteroviruses have been reported to suppress NF- $\kappa$ B and IFN signals by binding to IKK $\beta$ , P65, and MDA5 (82–86). After that, reducing the antiviral signal levels will decrease the expression of antiviral factors, which contain many host restrictive factors and are beneficial to the unscrupulous replication of viruses.

## DISCUSSION

Enterovirus infections are prevalent worldwide. However, the lack of specific drugs and broad-spectrum multivalent vaccines

poses an urgent health threat. So, considerable studies on drug design targeting viral proteins have been conducted but unsuccessful (87). The high mutagenicity of RNA viruses and the similarity between the virus enzyme active domain and the host protein present considerable obstacles to selecting drug targets (88–92). The discovery of host restriction factors against enteroviruses and their interactions with viruses has attracted attention as a new antiviral strategy. Under this strategy, we could regulate the expression of host restrictive factors and effectively inhibit viral infections. Furthermore, we have identified the ‘Achilles heel’ of enteroviruses based on studies of hosting restrictive factors against enteroviruses. For instance, Zhao et al. reported that 119–223aa in VP1 were essential for the interactions between VP1 and VP2 (23). Based on this assumption, the inhibitors targeting 119–223aa in VP1 would possess a space-occupying effect and restrict the replication of enteroviruses, which may be a promising drug against EV71 infection.

On the other hand, viruses have evolved various methods to overcome the restriction of host restrictive factors, and treatment design against enteroviruses from this perspective will kill two birds with one stone. As reported by Li et al., the 2C protein of enteroviruses interacts with A3G and triggers the degradation of A3G (22, 57). Thus, inhibitors targeting the 2C domain that binds A3G can interfere with the interaction between the 2C protein and A3G and prevent the escape of the enteroviruses from A3G. At the same time, even if the target domain of the 2C protein mutates and causes the effects of inhibitors to be off-target, the mutant 2C protein will fail to bind to A3G and break out the restriction from A3G, indicating that A3G could exert its antiviral activity and that the inhibitors targeting this domain will stably inhibit enteroviruses by inducing virus mutation to a greater extent.

Third, as the endogenous component of host cells, it is important to note that antiviral strategies that regulate the expression of host restrictive factors will greatly reduce any side effects, which will be milder and safer than those experienced after using drugs. As Wang et al. showed in their study, IMB-Z inhibits EV71 replication by upregulating the expression of A3G (20). Moreover, 80  $\mu$ M IMB-Z induced adequate A3G expression and greatly inhibited the replication of EV71 in a variety of cells. At the same time, 200  $\mu$ M IMB-Z did not affect cell activity in cell lines, including Vero, HeLa, HCT-8, HEK293T, and SK-N-SH. Therefore, these findings have implications for the safety of antiviral strategies against enteroviruses by regulating the expression of host-restrictive factors.

In recent years, antimicrobial peptides (93) and mRNA drugs (94) have attracted increased interest among scientists, health professionals, and pharmaceutical companies because of their therapeutic potential. With the development of polypeptide and mRNA drugs, the functional domains of host restrictive factors will rapidly develop into antiviral drugs and become the mainstay of novel antiviral therapies. Therefore, identifying human host restrictive factors and exploring the interaction mechanism between a virus and host restrictive factors will



become the premise and basis for us to master important antivirus strategies in the future.

In conclusion, studies on the interactions between host restrictive factors and enteroviruses will deepen understanding of virus-host interactions, provide a theoretical basis, and reveal potential targets that are not prone to off-target effects. This information can then be used to develop anti-enterovirus drugs.

## AUTHOR CONTRIBUTIONS

ZL conceptualized the ideas. XQ performed the literature search, drafted the original manuscript, and drew the figures. CH revised

the manuscript. All the authors approved the final version of the manuscript.

## FUNDING

This work was supported in part by funding from the National Natural Science Foundation of China (81701987 to ZL and 81801994 to CH), the Science and Technology Department of Jilin Province (20210101300JC), China Postdoctoral Science Foundation (2020M670826), and the Education Department of Jilin Province (JJKH20211141KJ).

## REFERENCES

- Baggen J, Thibaut HJ, Strating J, van Kuppeveld FJM. The Life Cycle of Non-Polio Enteroviruses and How to Target It. *Nat Rev Microbiol* (2018) 16 (6):368–81. doi: 10.1038/s41579-018-0005-4
- Bian L, Wang Y, Yao X, Mao Q, Xu M, Liang Z. Coxsackievirus A6: A New Emerging Pathogen Causing Hand, Foot and Mouth Disease Outbreaks Worldwide. *Expert Rev Anti Infect Ther* (2015) 13(9):1061–71. doi: 10.1586/14787210.2015.1058156
- Fu X, Wan Z, Li Y, Hu Y, Jin X, Zhang C. National Epidemiology and Evolutionary History of Four Hand, Foot and Mouth Disease-Related Enteroviruses in China From 2008 to 2016. *Viol Sin* (2020) 35(1):21–33. doi: 10.1007/s12250-019-00169-2
- Zhang C, Zhu R, Yang Y, Chi Y, Yin J, Tang X, et al. Phylogenetic Analysis of the Major Causative Agents of Hand, Foot and Mouth Disease in Suzhou City, Jiangsu Province, China, in 2012–2013. *Emerg Microbes Infect* (2015) 4(2):e12. doi: 10.1038/emi.2015.12
- Zhao TS, Du J, Sun DP, Zhu QR, Chen LY, Ye C, et al. A Review and Meta-Analysis of the Epidemiology and Clinical Presentation of Coxsackievirus A6 Causing Hand-Foot-Mouth Disease in China and Global Implications. *Rev Med Virol* (2020) 30(2):e2087. doi: 10.1002/rmv.2087
- Dyda A, Stelzer-Braid S, Adam D, Chughtai AA, MacIntyre CR. The Association Between Acute Flaccid Myelitis (AFM) and Enterovirus D68 (EV-D68) - What Is the Evidence for Causation? *Euro Surveill* (2018) 23 (3):17–00310. doi: 10.2807/1560-7917.ES.2018.23.3.17-00310
- Holm-Hansen CC, Midgley SE, Fischer TK. Global Emergence of Enterovirus D68: A Systematic Review. *Lancet Infect Dis* (2016) 16(5):e64–75. doi: 10.1016/S1473-3099(15)00543-5
- Hixon AM, Frost J, Rudy MJ, Messacar K, Clarke P, Tyler KL. Understanding Enterovirus D68-Induced Neurologic Disease: A Basic Science Review. *Viruses* (2019) 11(9):821. doi: 10.3390/v11090821
- Bonvin M, Achermann F, Greeve I, Stroka D, Keogh A, Inderbitzin D, et al. Interferon-Inducible Expression of APOBEC3 Editing Enzymes in Human Hepatocytes and Inhibition of Hepatitis B Virus Replication. *Hepatology* (2006) 43(6):1364–74. doi: 10.1002/hep.21187
- Sarkis PT, Ying S, Xu R, Yu XF. STAT1-Independent Cell Type-Specific Regulation of Antiviral APOBEC3G by IFN-Alpha. *J Immunol* (2006) 177 (7):4530–40. doi: 10.4049/jimmunol.177.7.4530
- Ying S, Zhang X, Sarkis PT, Xu R, Yu X. Cell-Specific Regulation of APOBEC3F by Interferons. *Acta Biochim Biophys Sin (Shanghai)* (2007) 39 (4):297–304. doi: 10.1111/j.1745-7270.2007.00275.x
- Mohanram V, Skold AE, Bachle SM, Pathak SK, Spetz AL. IFN-Alpha Induces APOBEC3G, F, and A in Immature Dendritic Cells and Limits HIV-1 Spread to CD4+ T Cells. *J Immunol* (2013) 190(7):3346–53. doi: 10.4049/jimmunol.1201184
- Simon V, Bloch N, Landau NR. Intrinsic Host Restrictions to HIV-1 and Mechanisms of Viral Escape. *Nat Immunol* (2015) 16(6):546–53. doi: 10.1038/ni.3156
- Goldstone DC, Ennis-Adeniran V, Hedden JJ, Groom HC, Rice GI, Christodoulou E, et al. HIV-1 Restriction Factor SAMHD1 Is a Deoxynucleoside Triphosphate Triphosphohydrolase. *Nature* (2011) 480 (7377):379–82. doi: 10.1038/nature10623
- Cobos Jimenez V, Booiman T, de Taeye SW, van Dort KA, Rits MA, Hamann J, et al. Differential Expression of HIV-1 Interfering Factors in Monocyte-Derived Macrophages Stimulated With Polarizing Cytokines or Interferons. *Sci Rep* (2012) 2:763. doi: 10.1038/srep00763
- Nguyen TT, Hu Y, Widney DP, Mar RA, Smith JB. Murine GBP-5, a New Member of the Murine Guanylate-Binding Protein Family, Is Coordinately Regulated With Other GBPs *In Vivo* and *In Vitro*. *J Interferon Cytokine Res* (2002) 22(8):899–909. doi: 10.1089/107999002760274926
- Aebi M, Fah J, Hurt N, Samuel CE, Thomis D, Bazzigher L, et al. cDNA Structures and Regulation of Two Interferon-Induced Human Mx Proteins. *Mol Cell Biol* (1989) 9(11):5062–72. doi: 10.1128/mcb.9.11.5062-5072.1989
- Passos V, Zillinger T, Casartelli N, Wachs AS, Xu S, Malassa A, et al. Characterization of Endogenous SERINC5 Protein as Anti-HIV-1 Factor. *J Virol* (2019) 93(24):e01221-19. doi: 10.1128/JVI.01221-19
- D'Urbano V, Bertoldi A, Re MC, De Crignis E, Tamburello M, Primavera A, et al. Restriction Factors Expression Decreases in HIV-1 Patients After cART. *New Microbiol* (2021) 44(2):95–103.
- Wang H, Zhong M, Li Y, Li K, Wu S, Guo T, et al. APOBEC3G Is a Restriction Factor of EV71 and Mediator of IMB-Z Antiviral Activity. *Antiviral Res* (2019) 165:23–33. doi: 10.1016/j.antiviral.2019.03.005
- Li Z, Huan C, Wang H, Liu Y, Liu X, Su X, et al. TRIM21-Mediated Proteasomal Degradation of SAMHD1 Regulates Its Antiviral Activity. *EMBO Rep* (2020) 21(1):e47528. doi: 10.15252/embr.201847528
- Li Z, Yang X, Zhao Z, Liu X, Zhang W. Host Restriction Factor A3G Inhibits the Replication of Enterovirus D68 Through Competitively Binding 5' UTR With PCBP1. *J Virol* (2022) 96(2):e0170821. doi: 10.1128/JVI.01708-21
- Zhao Z, Li Z, Huan C, Liu X, Zhang W. SAMHD1 Inhibits Multiple Enteroviruses by Interfering With the Interaction Between VP1 and VP2 Proteins. *J Virol* (2021) 95(13):e0062021. doi: 10.1128/JVI.00620-21
- Takaoka A, Yanai H. Interferon Signalling Network in Innate Defence. *Cell Microbiol* (2006) 8(6):907–22. doi: 10.1111/j.1462-5822.2006.00716.x
- Sheppard P, Kindsvogel W, Xu W, Henderson K, Schlutsmeyer S, Whitmore TE, et al. IL-28, IL-29 and Their Class II Cytokine Receptor IL-28R. *Nat Immunol* (2003) 4(1):63–8. doi: 10.1038/ni873
- Wang C, Ji L, Yuan X, Jin Y, Cardona CJ, Xing Z. Differential Regulation of TLR Signaling on the Induction of Antiviral Interferons in Human Intestinal Epithelial Cells Infected With Enterovirus 71. *PLoS One* (2016) 11(3):e0152177. doi: 10.1371/journal.pone.0152177
- Kawai T, Akira S. TLR Signaling. *Cell Death Differ* (2006) 13(5):816–25. doi: 10.1038/sj.cdd.4401850
- Rothenfusser S, Goutagny N, DiPerna G, Gong M, Monks BG, Schoenemeyer A, et al. The RNA Helicase Igp2 Inhibits TLR-Independent Sensing of Viral Replication by Retinoic Acid-Inducible Gene-I. *J Immunol* (2005) 175 (8):5260–8. doi: 10.4049/jimmunol.175.8.5260
- Yoneyama M, Kikuchi M, Matsumoto K, Imaizumi T, Miyagishi M, Taira K, et al. Shared and Unique Functions of the DEXD/H-Box Helicases RIG-I,

- MDA5, and LGP2 in Antiviral Innate Immunity. *J Immunol* (2005) 175(5):2851–8. doi: 10.4049/jimmunol.175.5.2851
30. Ho HY, Cheng ML, Weng SF, Chang L, Yeh TT, Shih SR, et al. Glucose-6-Phosphate Dehydrogenase Deficiency Enhances Enterovirus 71 Infection. *J Gen Virol* (2008) 89(Pt 9):2080–9. doi: 10.1099/vir.0.2008/001404-0
  31. Schein CH, Oezguen N, Volk DE, Garimella R, Paul A, Braun W. NMR Structure of the Viral Peptide Linked to the Genome (VPg) of Poliovirus. *Peptides* (2006) 27(7):1676–84. doi: 10.1016/j.peptides.2006.01.018
  32. Pfister T, Jones KW, Wimmer E. A Cysteine-Rich Motif in Poliovirus Protein 2C(ATPase) Is Involved in RNA Replication and Binds Zinc *In Vitro*. *J Virol* (2000) 74(1):334–43. doi: 10.1128/JVI.74.1.334-343.2000
  33. Davies EH, Erikson A, Collin-Histed T, Mengel E, Tylki-Szymanska A, Vellodi A. Outcome of Type III Gaucher Disease on Enzyme Replacement Therapy: Review of 55 Cases. *J Inherit Metab Dis* (2007) 30(6):935–42. doi: 10.1007/s10545-007-0577-z
  34. Lin JY, Li ML, Huang PN, Chien KY, Horng JT, Shih SR. Heterogeneous Nuclear Ribonuclear Protein K Interacts With the Enterovirus 71 5' Untranslated Region and Participates in Virus Replication. *J Gen Virol* (2008) 89(Pt 10):2540–9. doi: 10.1099/vir.0.2008/003673-0
  35. Lin JY, Shih SR, Pan M, Li C, Lue CF, Stollar V, et al. hnRNP A1 Interacts With the 5' Untranslated Regions of Enterovirus 71 and Sindbis Virus RNA and Is Required for Viral Replication. *J Virol* (2009) 83(12):6106–14. doi: 10.1128/JVI.02476-08
  36. Luo Z, Dong X, Li Y, Zhang Q, Kim C, Song Y, et al. PolyC-Binding Protein 1 Interacts With 5'-Untranslated Region of Enterovirus 71 RNA in Membrane-Associated Complex to Facilitate Viral Replication. *PLoS One* (2014) 9(1):e87491. doi: 10.1371/journal.pone.0087491
  37. Sheehy AM, Gaddis NC, Choi JD, Malim MH. Isolation of a Human Gene That Inhibits HIV-1 Infection and Is Suppressed by the Viral Vif Protein. *Nature* (2002) 418(6898):646–50. doi: 10.1038/nature00939
  38. Vartanian JP, Guetard D, Henry M, Wain-Hobson S. Evidence for Editing of Human Papillomavirus DNA by APOBEC3 in Benign and Precancerous Lesions. *Science* (2008) 320(5873):230–3. doi: 10.1126/science.1153201
  39. Lin JY, Brewer G, Li ML. HuR and Ago2 Bind the Internal Ribosome Entry Site of Enterovirus 71 and Promote Virus Translation and Replication. *PLoS One* (2015) 10(10):e0140291. doi: 10.1371/journal.pone.0140291
  40. Weinreb NJ, Barranger JA, Charrow J, Grabowski GA, Mankin HJ, Mistry P. Guidance on the Use of Miglustat for Treating Patients With Type 1 Gaucher Disease. *Am J Hematol* (2005) 80(3):223–9. doi: 10.1002/ajh.20504
  41. Yamayoshi S, Yamashita Y, Li J, Hanagata N, Minowa T, Takemura T, et al. Scavenger Receptor B2 Is a Cellular Receptor for Enterovirus 71. *Nat Med* (2009) 15(7):798–801. doi: 10.1038/nm.1992
  42. Nakata K, Takeda S, Tanaka A, Kwang J, Komano J. Antiviral Activity of Acid Beta-Glucosidase 1 on Enterovirus 71, a Causative Agent of Hand, Foot and Mouth Disease. *J Gen Virol* (2017) 98(4):643–51. doi: 10.1099/jgv.0.000723
  43. Charrow J, Andersson HC, Kaplan P, Kolodny EH, Mistry P, Pastores G, et al. Enzyme Replacement Therapy and Monitoring for Children With Type 1 Gaucher Disease: Consensus Recommendations. *J Pediatr* (2004) 144(1):112–20. doi: 10.1016/j.jpeds.2003.10.067
  44. Li Z, Liu X, Wang S, Li J, Hou M, Liu G, et al. Identification of a Nucleotide in 5' Untranslated Region Contributing to Virus Replication and Virulence of Coxsackievirus A16. *Sci Rep* (2016) 6:20839. doi: 10.1038/srep20839
  45. Sun Y, Wang Y, Shan C, Chen C, Xu P, Song M, et al. Enterovirus 71 VPg Uridylation Uses a Two-Molecular Mechanism of 3D Polymerase. *J Virol* (2012) 86(24):13662–71. doi: 10.1128/JVI.01712-12
  46. Liu Y, Franco D, Paul AV, Wimmer E. Tyrosine 3 of Poliovirus Terminal Peptide VPg(3B) has an Essential Function in RNA Replication in the Context of Its Precursor Protein, 3AB. *J Virol* (2007) 81(11):5669–84. doi: 10.1128/JVI.02350-06
  47. Morasco BJ, Sharma N, Parilla J, Flanagan JB. Poliovirus Cre(2C)-Dependent Synthesis of VPgpUpU Is Required for Positive- But Not Negative-Strand RNA Synthesis. *J Virol* (2003) 77(9):5136–44. doi: 10.1128/JVI.77.9.5136-5144.2003
  48. Tang WF, Yang SY, Wu BW, Jheng JR, Chen YL, Shih CH, et al. Reticulon 3 Binds the 2C Protein of Enterovirus 71 and Is Required for Viral Replication. *J Biol Chem* (2007) 282(8):5888–98. doi: 10.1074/jbc.M611145200
  49. Xia H, Wang P, Wang GC, Yang J, Sun X, Wu W, et al. Human Enterovirus Nonstructural Protein 2catpase Functions as Both an RNA Helicase and ATP-Independent RNA Chaperone. *PLoS Pathog* (2015) 11(7):e1005067. doi: 10.1371/journal.ppat.1005067
  50. Fan W, Mar KB, Sari L, Gaszek IK, Cheng Q, Evers BM, et al. TRIM7 Inhibits Enterovirus Replication and Promotes Emergence of a Viral Variant With Increased Pathogenicity. *Cell* (2021) 184(13):3410–25.e17. doi: 10.1016/j.cell.2021.04.047
  51. Lin JY, Li ML, Brewer G. mRNA Decay Factor AUF1 Binds the Internal Ribosomal Entry Site of Enterovirus 71 and Inhibits Virus Replication. *PLoS One* (2014) 9(7):e103827. doi: 10.1371/journal.pone.0103827
  52. Wu S, Lin L, Zhao W, Li X, Wang Y, Si X, et al. AUF1 Is Recruited to the Stress Granules Induced by Coxsackievirus B3. *Virus Res* (2014) 192:52–61. doi: 10.1016/j.virusres.2014.08.003
  53. Ullmer W, Semler BL. Direct and Indirect Effects on Viral Translation and RNA Replication Are Required for AUF1 Restriction of Enterovirus Infections in Human Cells. *mBio* (2018) 9(5):e01669-18. doi: 10.1128/mBio.01669-18
  54. Xue YC, Ng CS, Mohamud Y, Fung G, Liu H, Bahreyni A, et al. FUS/TLS Suppresses Enterovirus Replication and Promotes Antiviral Innate Immune Responses. *J Virol* (2021) 95(12):e00304-21. doi: 10.1128/JVI.00304-21
  55. Han Y, Wang L, Cui J, Song Y, Luo Z, Chen J, et al. SIRT1 Inhibits EV71 Genome Replication and RNA Translation by Interfering With the Viral Polymerase and 5'UTR RNA. *J Cell Sci* (2016) 129(24):4534–47. doi: 10.1242/jcs.193698
  56. Li H, Bai Z, Li C, Sheng C, Zhao X. EV71 Infection Induces Cell Apoptosis Through ROS Generation and SIRT1 Activation. *J Cell Biochem* (2020) 121(10):4321–31. doi: 10.1002/jcb.29628
  57. Li Z, Ning S, Su X, Liu X, Wang H, Liu Y, et al. Enterovirus 71 Antagonizes the Inhibition of the Host Intrinsic Antiviral Factor A3G. *Nucleic Acids Res* (2018) 46(21):11514–27. doi: 10.1093/nar/gky840
  58. Hrecka K, Hao C, Gierszewska M, Swanson SK, Kesik-Brodacka M, Srivastava S, et al. Vpx Relieves Inhibition of HIV-1 Infection of Macrophages Mediated by the SAMHD1 Protein. *Nature* (2011) 474(7353):658–61. doi: 10.1038/nature10195
  59. Laguette N, Sobhian B, Casartelli N, Ringeard M, Chable-Bessia C, Segéral E, et al. SAMHD1 is the Dendritic- and Myeloid-Cell-Specific HIV-1 Restriction Factor Counteracted by Vpx. *Nature* (2011) 474(7353):654–7. doi: 10.1038/nature10117
  60. Ballana E, Este JA. SAMHD1: At the Crossroads of Cell Proliferation, Immune Responses, and Virus Restriction. *Trends Microbiol* (2015) 23(11):680–92. doi: 10.1016/j.timm.2015.08.002
  61. Hollenbaugh JA, Gee P, Baker J, Daly MB, Amie SM, Tate J, et al. Host Factor SAMHD1 Restricts DNA Viruses In non-Dividing Myeloid Cells. *PLoS Pathog* (2013) 9(6):e1003481. doi: 10.1371/journal.ppat.1003481
  62. Chen Z, Zhu M, Pan X, Zhu Y, Yan H, Jiang T, et al. Inhibition of Hepatitis B Virus Replication by SAMHD1. *Biochem Biophys Res Commun* (2014) 450(4):1462–8. doi: 10.1016/j.bbrc.2014.07.023
  63. Powell RD, Holland PJ, Hollis T, Perrino FW. Aicardi-Goutieres Syndrome Gene and HIV-1 Restriction Factor SAMHD1 Is a dGTP-Regulated Deoxynucleotide Triphosphohydrolase. *J Biol Chem* (2011) 286(51):43596–600. doi: 10.1074/jbc.C111.317628
  64. Lahouassa H, Daddacha W, Hofmann H, Ayinde D, Logue EC, Dragin L, et al. SAMHD1 Restricts the Replication of Human Immunodeficiency Virus Type 1 by Depleting the Intracellular Pool of Deoxynucleoside Triphosphates. *Nat Immunol* (2012) 13(3):223–8. doi: 10.1038/ni.2236
  65. Antonucci JM, St Gelais C, de Silva S, Yount JS, Tang C, Ji X, et al. SAMHD1-Mediated HIV-1 Restriction in Cells Does Not Involve Ribonuclease Activity. *Nat Med* (2016) 22(10):1072–4. doi: 10.1038/nm.4163
  66. Beloglazova N, Flick R, Tchigvintsev A, Brown G, Popovic A, Nocek B, et al. Nucleic Acid Activity of the Human SAMHD1 Protein Implicated in the Aicardi-Goutieres Syndrome and HIV-1 Restriction. *J Biol Chem* (2013) 288(12):8101–10. doi: 10.1074/jbc.M112.431148
  67. Choi J, Ryoo J, Oh C, Hwang S, Ahn K. SAMHD1 Specifically Restricts Retroviruses Through its RNase Activity. *Retrovirology* (2015) 12:46. doi: 10.1186/s12977-015-0174-4
  68. Ryoo J, Choi J, Oh C, Kim S, Seo M, Kim SY, et al. The Ribonuclease Activity of SAMHD1 Is Required for HIV-1 Restriction. *Nat Med* (2014) 20(8):936–41. doi: 10.1038/nm.3626
  69. Lei X, Sun Z, Liu X, Jin Q, He B, Wang J. Cleavage of the Adaptor Protein TRIF by Enterovirus 71 3C Inhibits Antiviral Responses Mediated by Toll-Like Receptor 3. *J Virol* (2011) 85(17):8811–8. doi: 10.1128/JVI.00447-11

70. Xiao H, Li J, Yang X, Li Z, Wang Y, Rui Y, et al. Ectopic Expression of TRIM25 Restores RIG-I Expression and IFN Production Reduced by Multiple Enteroviruses 3C(Pro). *Virol Sin* (2021) 36(6):1363–74. doi: 10.1007/s12250-021-00410-x
71. Lei X, Han N, Xiao X, Jin Q, He B, Wang J. Enterovirus 71 3C Inhibits Cytokine Expression Through Cleavage of the TAK1/TAB1/TAB2/TAB3 Complex. *J Virol* (2014) 88(17):9830–41. doi: 10.1128/JVI.01425-14
72. Wang H, Lei X, Xiao X, Yang C, Lu W, Huang Z, et al. Reciprocal Regulation Between Enterovirus 71 and the NLRP3 Inflammasome. *Cell Rep* (2015) 12(1):42–8. doi: 10.1016/j.celrep.2015.05.047
73. Lei X, Liu X, Ma Y, Sun Z, Yang Y, Jin Q, et al. The 3C Protein of Enterovirus 71 Inhibits Retinoid Acid-Inducible Gene I-Mediated Interferon Regulatory Factor 3 Activation and Type I Interferon Responses. *J Virol* (2010) 84(16):8051–61. doi: 10.1128/JVI.02491-09
74. Lei X, Xiao X, Xue Q, Jin Q, He B, Wang J. Cleavage of Interferon Regulatory Factor 7 by Enterovirus 71 3C Suppresses Cellular Responses. *J Virol* (2013) 87(3):1690–8. doi: 10.1128/JVI.01855-12
75. Hung HC, Wang HC, Shih SR, Teng IF, Tseng CP, Hsu JT. Synergistic Inhibition of Enterovirus 71 Replication by Interferon and Rupintrivir. *J Infect Dis* (2011) 203(12):1784–90. doi: 10.1093/infdis/jir174
76. Li Z, Wu Y, Li H, Li W, Tan J, Qiao W. 3C Protease of Enterovirus 71 Cleaves Promyelocytic Leukemia Protein and Impairs PML-NBs Production. *Virol J* (2021) 18(1):255. doi: 10.1186/s12985-021-01725-7
77. Wen W, Qi Z, Wang J. The Function and Mechanism of Enterovirus 71 (EV71) 3c Protease. *Curr Microbiol* (2020) 77(9):1968–75. doi: 10.1007/s00284-020-02082-4
78. Tan J, George S, Kusov Y, Perbandt M, Anemuller S, Mesters JR, et al. 3C Protease of Enterovirus 68: Structure-Based Design of Michael Acceptor Inhibitors and Their Broad-Spectrum Antiviral Effects Against Picornaviruses. *J Virol* (2013) 87(8):4339–51. doi: 10.1128/JVI.01123-12
79. Xiang Z, Liu L, Lei X, Zhou Z, He B, Wang J. 3c Protease of Enterovirus D68 Inhibits Cellular Defense Mediated by Interferon Regulatory Factor 7. *J Virol* (2016) 90(3):1613–21. doi: 10.1128/JVI.02395-15
80. Wang B, Xi X, Lei X, Zhang X, Cui S, Wang J, et al. Enterovirus 71 Protease 2Apro Targets MAVS to Inhibit Anti-Viral Type I Interferon Responses. *PLoS Pathog* (2013) 9(3):e1003231. doi: 10.1371/journal.ppat.1003231
81. Feng Q, Langereis MA, Lork M, Nguyen M, Hato SV, Lanke K, et al. Enterovirus 2Apro Targets MDA5 and MAVS in Infected Cells. *J Virol* (2014) 88(6):3369–78. doi: 10.1128/JVI.02712-13
82. Wang SH, Wang K, Zhao K, Hua SC, Du J. The Structure, Function, and Mechanisms of Action of Enterovirus Non-Structural Protein 2c. *Front Microbiol* (2020) 11:615965. doi: 10.3389/fmicb.2020.615965
83. Zheng Z, Li H, Zhang Z, Meng J, Mao D, Bai B, et al. Enterovirus 71 2C Protein Inhibits TNF-Alpha-Mediated Activation of NF-kappaB by Suppressing IkkappaB Kinase Beta Phosphorylation. *J Immunol* (2011) 187(5):2202–12. doi: 10.4049/jimmunol.1100285
84. Li Q, Zheng Z, Liu Y, Zhang Z, Liu Q, Meng J, et al. 2c Proteins of Enteroviruses Suppress IKKbeta Phosphorylation by Recruiting Protein Phosphatase 1. *J Virol* (2016) 90(10):5141–51. doi: 10.1128/JVI.03021-15
85. Du H, Yin P, Yang X, Zhang L, Jin Q, Zhu G. Enterovirus 71 2c Protein Inhibits NF-KappaB Activation by Binding to RelA(P65). *Sci Rep* (2015) 5:14302. doi: 10.1038/srep14302
86. Li L, Fan H, Song Z, Liu X, Bai J, Jiang P. Encephalomyocarditis Virus 2C Protein Antagonizes Interferon-Beta Signaling Pathway Through Interaction With MDA5. *Antiviral Res* (2019) 161:70–84. doi: 10.1016/j.antiviral.2018.10.010
87. Wang L, Wang J, Wang L, Ma S, Liu Y. Anti-Enterovirus 71 Agents of Natural Products. *Molecules* (2015) 20(9):16320–33. doi: 10.3390/molecules200916320
88. Caligiuri P, Cerruti R, Icardi G, Bruzzone B. Overview of Hepatitis B Virus Mutations and Their Implications in the Management of Infection. *World J Gastroenterol* (2016) 22(1):145–54. doi: 10.3748/wjg.v22.i1.145
89. Liang B, Jiang J, Pan P, Chen R, Zhuang D, Zhao F, et al. Morphine Increases Lamivudine- and Nevirapine-Induced Human Immunodeficiency Virus-1 Drug-Resistant Mutations *In Vitro*. *Microb Drug Resist* (2017) 23(3):285–93. doi: 10.1089/mdr.2015.0347
90. Ma J, Zhang Y, Chen X, Jin Y, Chen D, Wu Y, et al. Association of Preexisting Drug-Resistance Mutations and Treatment Failure in Hepatitis B Patients. *PLoS One* (2013) 8(7):e67606. doi: 10.1371/journal.pone.0067606
91. Razonable RR. Drug-Resistant Cytomegalovirus: Clinical Implications of Specific Mutations. *Curr Opin Organ Transplant* (2018) 23(4):388–94. doi: 10.1097/MOT.0000000000000541
92. Yin F, Wu Z, Fang W, Wu C, Rayner S, Han M, et al. Resistant Mutations and Quasispecies Complexity of Hepatitis B Virus During Telbivudine Treatment. *J Gen Virol* (2015) 96(11):3302–12. doi: 10.1099/jgv.0.000285
93. Boparai JK, Sharma PK. Mini Review on Antimicrobial Peptides, Sources, Mechanism and Recent Applications. *Protein Pept Lett* (2020) 27(1):4–16. doi: 10.2174/0929866526666190822165812
94. Yu AM, Choi YH, Tu MJ. RNA Drugs and RNA Targets for Small Molecules: Principles, Progress, and Challenges. *Pharmacol Rev* (2020) 72(4):86298. doi: 1124/pr.120.019554

**Conflict of Interest:** The authors declare that the research was conducted in the absence of any commercial or financial relationships that could be construed as a potential conflict of interest.

**Publisher's Note:** All claims expressed in this article are solely those of the authors and do not necessarily represent those of their affiliated organizations, or those of the publisher, the editors and the reviewers. Any product that may be evaluated in this article, or claim that may be made by its manufacturer, is not guaranteed or endorsed by the publisher.

Copyright © 2022 Huan, Qu and Li. This is an open-access article distributed under the terms of the Creative Commons Attribution License (CC BY). The use, distribution or reproduction in other forums is permitted, provided the original author(s) and the copyright owner(s) are credited and that the original publication in this journal is cited, in accordance with accepted academic practice. No use, distribution or reproduction is permitted which does not comply with these terms.



# Antiviral Activities of Interleukin-27: A Partner for Interferons?

Heather Amsden, Olena Kourko<sup>†</sup>, Madison Roth<sup>†</sup> and Katrina Gee<sup>\*</sup>

Department of Biomedical and Molecular Sciences, Queen's University, Kingston, ON, Canada

## OPEN ACCESS

### Edited by:

Junji Xing,  
Houston Methodist Research Institute,  
United States

### Reviewed by:

Xiaochuan Liu,  
University of California, Riverside,  
United States  
Junhua Huang,  
Wuhan Polytechnic University, China  
Longhuan Ma,  
University of Florida, United States

### \*Correspondence:

Katrina Gee  
kgee@queensu.ca

<sup>†</sup>These authors have contributed  
equally to this work

### Specialty section:

This article was submitted to  
Viral Immunology,  
a section of the journal  
Frontiers in Immunology

Received: 23 March 2022

Accepted: 14 April 2022

Published: 10 May 2022

### Citation:

Amsden H, Kourko O, Roth M and  
Gee K (2022) Antiviral Activities of  
Interleukin-27: A Partner  
for Interferons?  
*Front. Immunol.* 13:902853.  
doi: 10.3389/fimmu.2022.902853

Emergence of new, pandemic-level viral threats has brought to the forefront the importance of viral immunology and continued improvement of antiviral therapies. Interleukin-27 (IL-27) is a pleiotropic cytokine that regulates both innate and adaptive immune responses. Accumulating evidence has revealed potent antiviral activities of IL-27 against numerous viruses, including HIV, influenza, HBV and more. IL-27 contributes to the immune response against viruses indirectly by increasing production of interferons (IFNs) which have various antiviral effects. Additionally, IL-27 can directly interfere with viral infection both by acting similarly to an IFN itself and by modulating the differentiation and function of various immune cells. This review discusses the IFN-dependent and IFN-independent antiviral mechanisms of IL-27 and highlights the potential of IL-27 as a therapeutic cytokine for viral infection.

**Keywords:** interleukin-27, interferons, virus, viral immunology, infection, antiviral immunity

## INTRODUCTION

The emergence of novel viral threats, such as the current COVID-19 pandemic, has highlighted the importance of viral immunology. Understanding of the immune response during viral infection sheds light on aspects that can be manipulated with vaccines and therapies to enhance antiviral activities. Within the immune defenses, Toll-like receptors (TLRs) are among the four major sub-families of pattern recognition receptors (PRRs) capable of recognizing pathogen-associated molecular patterns (PAMPs) (1). Viral PAMPs activate TLRs expressed by antigen presenting cells (APCs) to produce soluble mediators, such as cytokines (2). Cytokines influence how antiviral responses are initiated by innate immune cells and maintained by adaptive immune cells, orchestrating immune responses that lead to favourable or detrimental outcomes. For instance, sufficient cytokine-induced inflammation and immune cell recruitment is crucial for viral clearance, however, overproduction of cytokines can lead to excessive inflammation and tissue damage, characteristic of a cytokine storm (3). Therefore, understanding the complex regulations and actions of cytokines is crucial in further understanding antiviral responses and developing antiviral therapies.

Produced in response to TLR activation, interleukin-27 (IL-27) is a cytokine of interest for its activity against viral infection. IL-27 is composed of two subunits, IL-27p28 and Epstein-Barr virus-induced gene 3 (EBI3) (4), and signals *via* a heterodimeric receptor consisting of WSX-1 and glycoprotein (gp130) (5). IL-27 belongs to both the IL-6 and IL-12 superfamilies of cytokines as it shares the gp130 subunit (IL-6 family) and is heterodimeric in nature (IL-12 family) (6). Binding to its receptor predominantly activates Janus kinase 1 and 2 (JAK1 and JAK 2), which then phosphorylates signal transducer and activator of transcription (STAT) 1 and 3 (5). Tyrosine-phosphorylated STAT1

and STAT3 dimerize and translocate to the nucleus to activate transcription of various genes. Due to the similarities in structure of cytokine and receptor subunits of IL-27 with IL-6 and IL-12, this cytokine was expected to be pro-inflammatory, which was emphasized by early studies demonstrating the ability of IL-27 to promote NK and T cell proliferation and production of IFN $\gamma$  (4, 7). Later studies highlighted additional mechanisms governed by this cytokine, including, inhibiting Th2 and Th17 cell activities, and anti-inflammatory functions such as stimulating the production of IL-10 by T cells (8, 9). Within innate immunity, IL-27 can upregulate TLR expression and function in myeloid cells (10–15).

The vast immunomodulatory properties of IL-27 link innate and adaptive immune responses, and have made it a cytokine of interest for developing novel antiviral therapies and adjuvants for vaccines (16, 17). Evidence of the potency of IL-27 as an antiviral cytokine has been accumulating over the past decade and demonstrates that IL-27 can inhibit a wide range of viral infections including human immunodeficiency virus (HIV),

hepatitis B virus (HBV), hepatitis C virus (HCV), herpes simplex virus (HSV), influenza, zika virus (ZIKV) *in vitro* and *in vivo* (18–30) (**Table 1**). Interestingly, the antiviral functions of IL-27 also parallel those of IFNs, and with evidence that IL-27 and IFN each possess the ability to induce expression of the other (18, 20, 28, 29, 36, 39, 40, 43, 44) it is important to consider how these cytokines may act synchronously or asynchronously with one another. In this review, we discuss the antiviral effects of IL-27 by broadly grouping these effects into IFN-dependent and IFN-independent mechanisms.

## INTERFERON-DEPENDENT MECHANISMS

Interferons (IFNs) are a class of antiviral cytokines produced by a variety of cell types, such as macrophages and dendritic cells (DCs), in response to PRR stimulation. Three families of IFNs have been characterized: type I IFNs (IFN $\alpha/\beta$ ), type II IFNs

**TABLE 1** | Evidence of IL-27 inhibition of viral infection.

Virus	Model	Mode of inhibition by IL-27	Reference
ZIKV	Primary human keratinocytes	Activation of STAT1 leads to <i>OAS2</i> transcription independent of type I and type II IFNs	Kwock et al. (19)
HBV	Human hepatocyte cell lines (HepG2, Huh7)	Increases type I and III IFN production leading to <i>OAS1</i> , <i>PKR</i> , and <i>MX1</i> transcription	Cao et al. (20)
	Human kidney cell line (HEK 293), human hepatocyte cell line (HepG2)	Complexes with IL-6R to inhibit infection Type I IFN-mediated IL-27 production induces TRIM25 expression	Yang et al. (31) Tan et al. (21)
HIV	Primary human MDMs	Increases IFN $\alpha$ production leading to enhanced APOBEC cytidine deaminase expression Reduces SPTBN1 expression independently of IFN $\alpha$	Greenwell-Wild et al. (23) Dai et al. (24)
	Primary human monocyte-derived DCs	Increases transcription of ISGs such as <i>MX1</i> and <i>OAS2</i> independently of type I IFNs	Imamichi et al. (32) Chen et al. (25)
HCV	Human hepatocyte cell line (Huh7.5)	Inhibition partially dependent on IFN $\alpha$	Frank et al. (26)
	Mice	Increases HCV-specific IFN $\gamma$ -producing CD8+ T cells synergistically with IL-12	Matsui et al. (17)
IAV	Human hepatocyte cell line (HepG2)	Increases transcription of <i>MX1</i> independently of IFN $\alpha$ and IFN $\gamma$	Bender et al. (27)
	Primary human PBMCs and lung epithelial cell line (A549)	Induces IFN $\alpha$ production which leads to expression and activation of PKR	Liu et al. (29)
	Human lung epithelial cell line (A549)	Complexes with IL-6R to induce type I and III IFNs which leads to increased ISG transcription	Zuo et al. (33) Yang et al. (31) Wang et al. (34)
Mice		Augments NK cell cytokine production and effector functions	Kumar et al. (28)
		Increases IAV-specific IFN $\gamma$ -producing CD8+ T cells	Mayer et al. (35)
		Mediates immunopathology by promoting T-cell production of IL-10	Liu et al. (18) Jiang et al. (36) Sun et al. (37)
CHIKV	Primary human MDMs	Inhibits infection in the absence of IFNs	Valdés-López et al. (38)
LCMV	Mice	Promotes pDC differentiation and NK cell effector functions	Harker et al. (39)
HSV-1	Primary human macrophages and DCs, human epithelial and glioma cell lines (HeLa, U373MG, and T98G)	Enhances proinflammatory cytokine IL-6, IP-10 and MIG production	Heikkilä et al. (40)
	African green monkey kidney epithelial cell line (Vero cells)	Complexes with IL-6R to inhibit infection	Zuo et al. (33)
SeV	Primary human keratinocytes	Activation of STAT1 leads to <i>OAS2</i> transcription independent of type I and type II IFNs	Kwock et al. (19)
	Mice	Mediates immunopathology by promoting T-cell production of IL-10	Muallem et al. (41)
DENV	Primary human cell co-cultures	Production by DCs promotes T <sub>FH</sub> cell differentiation, supporting B-cell antibody production	Sprockholt et al. (42)

(IFN $\gamma$ ) and type III IFNs (IFN $\lambda$ 1, 2, 3, and 4). Signaling by type I and III IFNs induces STAT1 and STAT2 phosphorylation and dimerization, with the resulting STAT1/STAT2 complex interacting with IFN regulatory factor-9 (IRF9) to form ISGF3 (ISGF3) (45). ISGF3 translocates to the nucleus and binds to IFN-stimulated response elements (ISRE) to activate transcription of antiviral genes known as interferon stimulated genes (ISGs). Similarly, type II IFNs induce several ISGs through homodimerization of phosphorylated STAT1 which binds gamma activated sequence (GAS) elements in the nucleus (45). ISGs encompass a broad range of genes whose products inhibit some stage of the viral life cycle. For instance, bone marrow stromal cell antigen 2 (BST-2) inhibits budding of several enveloped viruses (46), whereas myxovirus resistance protein 1 (MX1) inhibits viral transcription (47). A detailed review of ISG production and function is beyond the scope of this paper and can be reviewed in greater detail here (45, 48, 49).

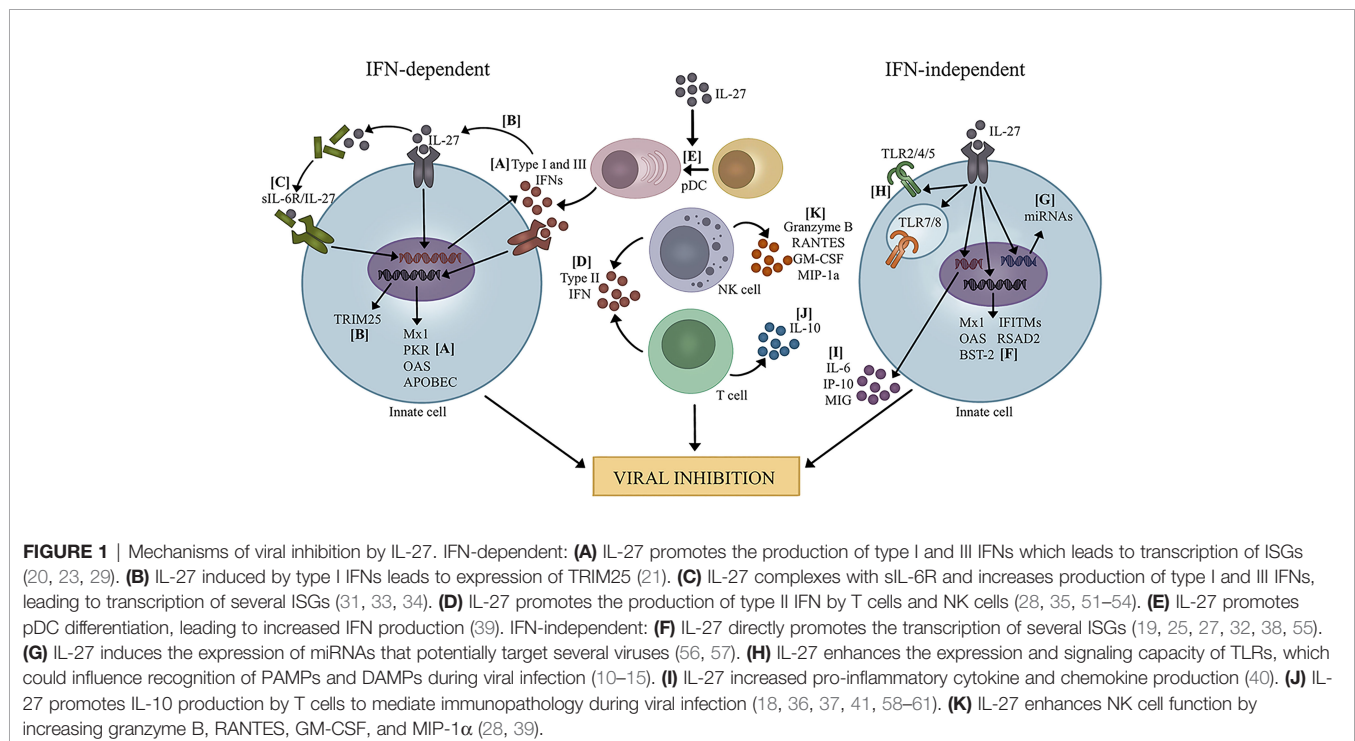
Activation and production of IFNs and IL-27 appear connected. Clinical studies demonstrate that IL-27 and IFN levels are tightly correlated during viral infection (20, 50). Additionally, *in vitro* and *in vivo* studies confirm that IL-27 directly induces IFN production and vice versa by various cell types, such as DCs, macrophages, NK cells, hepatocytes, and lung epithelial cells (18, 20, 28, 29, 36, 39, 40, 43, 44). As such, much of the antiviral activity associated with IL-27 has been attributed to its augmentation of IFN production (Figure 1).

## IL-27 Induction of IFNs Enhances ISG Transcription

Accumulating evidence supports the proposal that IL-27 enhances ISG transcription during viral infection by augmenting the

production of IFNs. For instance, IL-27 enhances IFN $\alpha$  and IFN $\lambda$ 1 production by human hepatocytes during HBV infection, leading to increased expression of ISGs, such as 2'-5'-oligoadenylate synthetase 1 (OAS1), MX1 and protein kinase R (PKR), and inhibition of HBV replication (20). Promotion of extracellular signal-regulated kinase 1 (ERK1)/ERK2 signaling as well as nuclear factor kappa B (NF $\kappa$ B) nuclear translocation by IL-27 was found to regulate IFN- $\lambda$ 1 expression (20). Inhibition of these IFNs using an RNA interference approach ablated this effect, suggesting that the antiviral effects of IL-27 were mediated by the enhanced production of IFN $\alpha$  and IFN $\lambda$ 1 (20). The addition of type I IFN neutralizing antibodies similarly reduced the ability of IL-27 to inhibit influenza A virus (IAV) infection in human peripheral blood mononuclear cells (PBMCs) (29). Neutralizing IFN $\alpha$ / $\beta$  reduced phosphorylation of STAT1 and STAT2, along with reduced phosphorylation of the ISG PKR, demonstrating that the type I IFNs induced by IL-27 activated PKR to limit IAV infection in this model (29). One study compared the effects of adding IL-27 or IFN $\alpha$  to HIV-infected primary human monocyte-derived macrophages (MDMs) (23). Addition of IL-27 or IFN $\alpha$  separately inhibited HIV through induction of host restriction factors apolipoprotein B mRNA editing enzyme catalytic polypeptide (APOBEC) cytidine deaminases. However, the kinetics of this induction differed, with a delayed synthesis of APOBEC cytidine deaminases observed with IL-27 compared to IFN $\alpha$ . Interestingly, IL-27 was found to induce IFN $\alpha$  and use of IFN $\alpha$ / $\beta$ -receptor neutralizing antibodies revealed that intermediate IFN $\alpha$  was required to inhibit HIV replication (23).

*In vitro* and clinical studies show that IL-27 can interact with IL-6 to form a complex during viral infection (33). IL-6 is a



pleiotropic cytokine produced in response to infection and tissue damage that modulates numerous antiviral responses such as T cell and macrophage activity [reviewed here (62)]. The IL-27p28 subunit of IL-27 has been demonstrated to form a complex with soluble IL-6 receptor (sIL-6R) and induce STAT1 and STAT3 signaling in IL-27 responsive cells (63). This IL-6/IL-27 complex exerts antiviral effects against a number of viruses, including influenza, Sendai virus (SeV), vesicular stomatitis virus (VSV), HSV-1, enterovirus 71 (EV71), and HBV (31, 33, 34). Mechanistically, the IL-6/IL-27 complex inhibited viral infection by promoting type I and III IFN production which led to downstream activation of ISGs such as *OAS1*, *PKR*, and *MX1* (31, 33, 34). Induction of IFNs was due to IL-6/IL-27 complex interaction with the mitochondrial antiviral signaling protein (MAVS)/TNF receptor-associated factor 3 (TRAF3)/TRAF6 pathway, leading to subsequent nuclear translocation of NF $\kappa$ B (31, 33). Of the two IL-27 subunits, IL-27p28 was found to mediate much of the antiviral response, as significant reductions in viral inhibition and IFN and ISG expression were reported when IL-27p28 was silenced using RNA interference (33, 34). Similar reductions in IFN and ISG expression were observed when EBI3 was silenced, however, this decrease was not as robust as in the absence of IL-27p28 (33). Nonetheless, increased viral inhibition was observed upon treatment with the IL-6/IL-27 complex compared to the individual subunits of the complex (31, 33), suggesting that the sIL-6R subunit contributes to the antiviral effects as well. Moreover, the IL-27p28 subunit (also known as IL-30) can act independently from EBI3 (6) and IL-27p28 bound to sIL-6R without EBI3 does exert antiviral effects (31). However, addition of an IL-27p28 expressing plasmid had no effect on the viral replication of IAV, EV71, or HBV (31), suggesting that the interaction of IL-27p28 with sIL-6R and/or EBI3 promotes the antiviral activities of IL-27p28. Further investigation into the mechanism behind the antiviral functions of the IL-6/IL-27 complex is therefore warranted.

Increased ISG transcription as a consequence of IL-27-induced IFNs can contribute to effective viral clearance. However, this antiviral defense does not counteract the numerous anti-IFN mechanisms that viruses have developed to interfere with ISG production, such as inhibiting IFN signaling (64). This strategy may therefore be most beneficial to uninfected bystander cells where IFNs can signal unimpeded by viral inhibitory mechanisms to promote antiviral states. Alternatively, IL-27 induction of IFNs by infected cells could be enough to overcome viral inhibition of IFNs and could then result in robust ISG transcription.

## IL-27 Promotes IFN $\gamma$ Production

IFN $\gamma$  is a pleiotropic cytokine produced predominantly by activated NK cells and T cells. Beyond promoting ISG transcription, IFN $\gamma$ -mediated augmentation of innate immune responses, including antigen presentation, makes it a key link between innate and adaptive responses during infection (65). A growing body of evidence demonstrates that IL-27 signaling promotes IFN $\gamma$  production by CD8 $^{+}$  T cells during viral infection. *In vitro* data demonstrates that STAT1 and T-bet

activation induced by IL-27 treatment concurrently with IL-12 augments IFN $\gamma$  production by CD8 $^{+}$  T cells (51–53). CD8 $^{+}$  T cell effector functions, such as granzyme B and perforin production, are also increased by IL-27 (51, 52). Consistent with these data, IL-27 receptor (IL-27R) and T-bet signaling were found to be critical for IFN $\gamma$  production *in vivo* during viral infection (35, 54). A lack of IL-27 signaling resulted in reduced expression of IFN $\gamma$  and T-bet in the lungs of respiratory syncytial virus (RSV) infected *il27ra* $^{-/-}$  mice compared to infected WT controls (54). In mixed bone marrow (BM) chimera mice generated from *il-27ra* $^{-/-}$  and WT donors, a reduced frequency of IFN $\gamma$  producing IAV antigen-specific *il-27ra* $^{-/-}$  CD8 $^{+}$  T cells compared to internal WT controls were isolated from spleens and lymph nodes following IAV infection (35). The production of IFN $\gamma$ -producing, HCV-specific CD8 $^{+}$  T cells in the spleens of mice was similarly enhanced by coadministration of either an IL-23 or IL-27 and an IL-12 expression plasmid following immunization (17). The promotion of IFN $\gamma$ -producing antigen-specific CD8 $^{+}$  T cells by IL-27 highlights the adjuvant potential of this cytokine for prophylactic measures against viral infection.

*In vitro* studies with primary human NK cells demonstrated that IL-27 can work synergistically with IL-15 and/or IL-18 to promote IFN $\gamma$  secretion by NK cells (66, 67). In a mechanism similar to CD8 $^{+}$  T cells, IL-27 induction of STAT1 and T-bet activity have been shown to be involved in this process (67). In the context of viral infection, NK cells from *ebi3* $^{-/-}$  and *il27Ra* $^{-/-}$  mice exhibited significant reductions in IFN $\gamma$  production during the early phase of IAV infection compared to WT controls (28). In this study, stimulation of NK cells *in vitro* with IL-27 alone had no effect on IFN $\gamma$  production. However, IL-27 significantly augmented NKG2D activation of NK cells and subsequent IFN $\gamma$  production, suggesting that IL-27 may act as an additional signal alongside IL-15 or IL-18 to enhance NK cell activation at the site of viral infection (28).

A clinical study aligns with these data, as a positive correlation between IL-27 and IFN $\gamma$  plasma levels in CMV-infected patients has been observed (50). However, contradictory findings of whether IL-27 promotes IFN $\gamma$  production by T cells and NK cells have been reported. Increased IFN $\gamma$ -producing T cells and NK cells in virally infected *il27ra* $^{-/-}$  mice have been observed compared to their WT counterparts (18, 39). The timing of IL-27 activity may be critical as to whether it increases or decreases IFN $\gamma$  production systemically during viral infection. Early IL-27 signaling may promote IFN $\gamma$  production to increase viral clearance. However, IL-27 also promotes IL-10 production, (reviewed in a later section) which could downregulate IFN $\gamma$  production later during infection to mediate immunopathology.

## IL-27 Supports pDC Differentiation

Plasmacytoid DCs (pDCs) are a subset of DCs that specialize in sensing viral DNA and RNA, upon which IFNs are rapidly produced (68). Following production of IFNs, pDCs help shape the adaptive immune response by stimulating T cells (68). IL-27 was shown to support the development of pDCs in mice during viral infection (39). In *il27ra* $^{-/-}$  mice, a lack of pDC expansion was observed during chronic LCMV infection, and this was associated with reduced type I IFN levels and increased

viremia compared to WT controls (39). As a result, LCMV infected *il27ra*<sup>-/-</sup> mice suffer from higher viral load compared to their WT counterparts. Moreover, a significant reduction in CD86, a key costimulatory molecule for T cell activation, was found in pDCs and other DC subsets from chronically LCMV infected *il27ra*<sup>-/-</sup> mice (39). Together, these data suggest that IL-27 promotes pDC differentiation and in the absence of IL-27 signaling, pDC numbers and function are reduced, which potentially leads to inefficient IFN production and T cell activation. The factors that regulate pDC specification are complex and the way in which IL-27 promotes this differentiation is unknown. However, there is evidence that IL-27 can promote the expression of the transcription factor interferon regulatory factor 8 (IRF8) (69), which has been suggested as one of the initiators of pDC differentiation (68).

### Type I IFNs Promote IL-27

The axis between IL-27 and type I IFNs is bidirectional, with type I IFN-induced IL-27 also promoting antiviral activities. Type I IFNs directly augment IL-27 production *via* IRF-1 initiation of IL-27p28 subunit transcription (44, 70). During HBV infection, type I IFN-mediated gene and protein production of the ISG tripartite motif containing 25 (TRIM25) was found to be dependent upon intermediate IL-27 signaling (21). IFN $\alpha$  conditioned DCs were highly efficient at cross-priming CD8<sup>+</sup> T cells with viral antigen, and this was associated with an increased potential to express IL-23 and IL-27 (43). IL-27 enhances HLA-ABC and HLA-DR expression in DCs (25), therefore, IFN $\alpha$ -induced IL-27 may result in augmented antigen presentation in DCs. IL-27 produced as a consequence of type I IFN signaling has also been shown to influence T cell responses during viral infection (36, 37, 42, 58). For instance, type I IFN-induced IL-27 production by primary human DCs in response to dengue virus (DENV) infection was critical for T follicular helper (T<sub>FH</sub>) cell differentiation, consequently supporting secretion of antibodies by activated B cells (42). Further discussion of T cell function influenced by type I IFN-mediated IL-27 will be done below (see section 4.3).

## INTERFERON-INDEPENDENT MECHANISMS

Studies have shown that inhibition of IFNs using neutralizing antibodies does not fully ablate viral inhibition upon IL-27 treatment (20, 26, 29), which suggests that IL-27 has other IFN-independent mechanisms of viral control. For example, mice knock-out (KO) experiments support this idea, as subcutaneous infection with ZIKV causes 50% mortality in *ifnar1*<sup>-/-</sup> mice but 100% mortality in *ifnar1*<sup>-/-</sup>*il27ra*<sup>-/-</sup> mice, demonstrating additional antiviral activities of IL-27 beyond IFN modulation (19).

### Direct Induction of ISGs by IL-27

Induction of ISG transcription is not exclusive to IFNs and can be done by any substrate that activates interferon regulatory

factors (IRFs) (45). Accumulating evidence suggests that along with inducing IFNs, which signal to promote ISG transcription, IL-27 can also directly induce ISG production (**Figure 1**). For instance, IL-27 inhibited HIV infection in primary human monocyte-derived DCs and macrophages through induction of several ISGs including *MX1*, *OAS2*, *OAS3*, interferon-induced transmembrane protein 1 (*IFITM1*), *IFITM3*, radical S-adenosyl methionine domain containing 2 (*RSAD2*), and *PKR*, even in the presence of type I IFN neutralizing antibodies (25, 32). BST-2, a key inhibitor of HIV infection, was upregulated in primary human monocytes and T cells at both the gene and protein level in response to IL-27 treatment (55, 71). Addition of the vaccinia virus-encoded type I IFN decoy receptor B18R abrogated IFN-mediated induction of BST-2, but had no effect on IL-27-mediated BST-2 expression, demonstrating that BST-2 induction by IL-27 is independent of intermediate type I IFN production (55). Knockdown of IFN receptors IFNAR1 and IFNGR1 in primary human keratinocytes similarly had no effect on IL-27-induced upregulation of *OAS2* expression during ZIKV and Sendai virus infection (19). Moreover, HepG2 cells infected with avian and human influenza upregulate *MX1* to a greater extent following IL-27 treatment, and this was unaffected by the presence of IFN $\alpha$  and IFN $\gamma$  neutralizing antibodies (27). In a model of chikungunya virus (CHIKV) infection of primary human MDMs, there is a lack of expression of all three IFN types, despite a robust antiviral response being observed (38). Expression of IL-27 on the other hand, is significantly increased, and IL-27 treatment dose-dependently inhibited CHIKV replication. Investigation of THP-1 derived macrophages revealed that IL-27 promoted ISG production, such as *IFITMs*, *MX1*, *MX2*, *PKR*, and *RSAD2*. Therefore, IL-27 might be responsible for the anti-CHIKV response in the absence of IFNs (38). The direct induction of ISGs by IL-27 may be a mechanism to prevail over virus-mediated inhibition of IFN signaling and ISG transcription. In other words, IL-27 may serve as a backup antiviral response in the absence of efficient IFN function.

Similar to IFNs, IL-27 relies on JAK-STAT signaling for ISG production. Phosphorylation of STATs 1, 2, and 3 is frequently reported in the context of viral infection (19, 20, 25, 27, 29, 72). STAT1/STAT3 heterodimerization is favoured by IL-27 during viral infections such as HBV and HSV (21, 40, 73), and may represent an alternative pathway to ISG production, as the STAT1/STAT3 heterodimer is not typically associated with IFN signaling. There is limited evidence that IL-27 signals through STAT1/STAT2, thus increased production of this heterodimer is likely due to IL-27-induced type I and III IFN production. Indeed, in the absence of type I IFNs, IL-27-mediated STAT1/STAT2 phosphorylation was significantly reduced, suggesting that enhanced phosphorylation of this heterodimer was due to IL-27-induced type I IFN production (29). Significant STAT1 phosphorylation and STAT1/STAT1 homodimerization during viral infection has also been reported (19, 27). There is evidence that, IL-27 signals *via* STAT1/STAT1 dimers (74) and therefore may do so to directly induce ISG transcription. Notably, type II IFNs also signaling



through STAT1 homodimers, thus the potential of type II IFNs being involved in IL-27-induced STAT1 homodimerization cannot be completely ruled out. The redundancy in signaling by IL-27 and type II IFNs helps explain the overlapping profiles of ISGs induced by IL-27 and IFNs (32, 53, 75). However, the similarity in IFN and IL-27 signaling also raises the question as to whether viral mechanisms developed to interfere with IFN signaling may affect IL-27 signaling as well. Clinical studies support this notion, as a negative correlation between IL-27 serum and plasma expression and viral load was reported in HIV-positive and HIV-HCV co-infected patients (76, 77). *In vitro*, HIV infection and the HIV protein Tat inhibited LPS-induced IL-27 production in primary human MDMs (78). These studies suggest that HIV inhibits IL-27 as a mechanism of immune suppression. However, contradictory findings from clinical studies have been observed, with one study reporting a positive correlation (79) and another reporting no relationship between IL-27 and HIV viral load (80). Differences in severity of infection regardless of viral load could account for these contradictions, however, further investigation into whether HIV impedes IL-27 production is needed. Nonetheless, HIV could interfere with IL-27 function rather than production. For instance, PBMCs isolated from HIV patients had impaired responses to IL-27, with downregulation of IL-27-induced IL-6, TNF $\alpha$ , and IL-10 compared to PBMCs from healthy controls (81). Whether other viruses have the capacity to interfere with IL-27 production and signaling remains to be determined.

## IL-27 Modulates the Antiviral Innate Response

Beyond IFN and ISG induction, IL-27 has been shown to promote antiviral responses by influencing the effector functions of innate immune cells (**Figure 1**). For instance, primary human monocytes differentiated into macrophages in the presence of IL-27 (referred to as I-Macs) produced several microRNA (miRNAs) demonstrated to target the open-reading frames of viruses such as HSV-1, HSV-2, and HHV-8 (56). Similar miRNAs with antiviral potential were observed in primary human DCs in response to IL-27 treatment (57). I-Macs also displayed an HIV-resistant phenotype characterized by reduced levels of the HIV-supportive host factor spectrin B nonerythrocyte 1 (SPTBN1) (24). Blocking IFN $\alpha$  with neutralizing antibodies had no effect on I-Macs resistance to HIV, suggesting that IL-27 rather than intermediate IFN $\alpha$  production was responsible for the HIV-resistant phenotype. Resistance to other viruses, such as influenza, SIV, and KSHV, was also observed by I-Macs compared to primary human monocytes differentiated into macrophages without IL-27 (24). Moreover, IL-27 treatment influences cytokine production. Following IL-27 treatment, enhanced secretion of cytokines IL-6, IP-10 (CXCL10), and MIG by macrophages, DCs, and human epithelial cell lines was observed along with restricted HSV-1 replication (40). Augmentation of proinflammatory cytokine production by IL-27 may help promote inflammation and immune cell recruitment needed for viral clearance. However, a balance in proinflammatory cytokine production is needed in

order to mitigate the risk of unregulated inflammation and detrimental cytokine storm.

Going hand in hand with macrophage differentiation, IL-27 may also influence macrophage polarization, which could have implications for viral inhibition. Briefly, environmental stimuli induce different polarization states in macrophages. In general, M1 macrophages display pro-inflammatory and antiviral properties and have been shown to be more resistant to viral infection, whereas M2 macrophages display anti-inflammatory properties and are more permissive to infection but important for mediating immunopathology (82, 83). There is evidence to suggest that IL-27 skews macrophage polarization to the M1 phenotype (69, 84, 85); therefore, IL-27 may reduce the ability of viruses to infect macrophages by promoting M1 polarization. Genetic analysis of HIV-resistant I-Macs (monocytes treated with IL-27 during differentiation to macrophages) revealed an upregulation of M1 markers CD80 and TNF (24). Further, primary human M1-like macrophages were found to be potent producers of type I and III IFNs during rhinovirus infection *in vitro* (86), therefore, by promoting M1 polarization, IL-27 may increase IFN production as well. However, a direct connection between IL-27, macrophage polarization, IFN production, and viral infection has not yet been studied in detail.

Recent insights demonstrate that IL-27 can modulate the function of TLRs, an important class of PRRs involved in recognizing viral components. Augmented signaling capacity and resulting cytokine production by cell surface TLR2, 4, and 5 on human monocytes and macrophages (primary and cell lines) has been observed as a result of IL-27 treatment (10–14). Intracellular TLR7 and 8 are similarly affected by IL-27, with enhanced TLR7 expression and TLR8-mediated cytokine production observed upon treatment with IL-27 in THP-1 monocytes and THP-1-derived macrophages (15). Recognition of viral PAMPs, such as viral DNA and RNA, and damage-associated molecular patterns (DAMPs) from dead or dying cells by these TLRs is essential for activating innate immunity against a variety of viruses (87). Therefore, IL-27-mediated increase of TLR expression and signaling may enhance recognition of viruses and induce a more robust antiviral response. Moreover, several viruses, such as HCV, human cytomegalovirus (HCMV), HSV, Kaposi's sarcoma-associated herpes virus (KSHV), and vaccinia virus have evolved mechanisms of inhibiting TLR function (88–96). The increase in TLR expression and function by IL-27 could help counteract these inhibitory mechanisms. Currently, the potential relationship between IL-27 modulation of TLRs and viral immune responses has not been elucidated.

Another way that IL-27 promotes innate immune responses during viral infection is by augmenting NK cell function. Beyond promoting IFN $\gamma$  production, IL-27 also enhances the production of GM-CSF, RANTES, and MIP-1 $\alpha$  by NK cells following NKG2D-mediated activation (28). The chemoattractant properties of RANTES and MIP-1 $\alpha$  promote the migration of immune cells to the site of infection, including memory and effector T cells, granulocytes, and macrophages (97, 98). GM-CSF is a growth factor responsible for the survival, proliferation and activation of immune cells such as macrophages and DCs (99). Increased

infiltration and activation of immune cells at the site of infection in response to these cytokine and chemokines could support viral clearance. However, enhanced immune cell infiltration has been linked to cytokine storm and worse outcomes during infections such as IAV (100), therefore, a balance is needed to ensure effective viral clearance without causing severe immunopathology. Additionally, NK cell production of granzyme B, a protease that kills virus-infected cells, was diminished in *il27ra*<sup>-/-</sup> mice and associated with reduced viral clearance, suggesting a role of IL-27 in mediating NK cell effector functions during virus infection (28, 39).

## IL-27 Promotes IL-10 Production to Mediate Immunopathology During Virus Infection

Much of the morbidity and mortality caused by viral infections can be attributed to overactive immune responses including overproduction of cytokines, infiltration of immune cells and excessive inflammation that damages the body. As such, balancing these strong effector responses is critical to limiting immunopathology. IL-10 is an important immunoregulatory cytokine that mediates this balance in the immune response, as it can suppress both innate and adaptive immune responses to viral infections (101). However, certain viruses can also exploit the immunomodulatory functions of IL-10 to establish chronic infection (102–104). While various innate and adaptive immune cell types have been identified as IL-10 producers, CD4<sup>+</sup> and CD8<sup>+</sup> T cells are important sources of IL-10 during viral infections (105, 106).

There is increasing evidence that IL-27 is a potent inducer of IL-10 production from CD4<sup>+</sup> and CD8<sup>+</sup> T cells in a variety of viral infections, thereby having implications on antiviral immune responses and viral clearance (**Figure 1**). Significant reductions in IL-10-producing CD4<sup>+</sup> and CD8<sup>+</sup> T cells are observed during viral infection in *il27ra*<sup>-/-</sup> and *ebi3*<sup>-/-</sup> mice compared to their WT counterparts (18, 37, 41, 58, 59). Indeed, a study by Perona-Wright and colleagues (60) demonstrated that direct IL-27 signaling was critical for IL-10 production by CD8<sup>+</sup> T cells. When mice with mixed bone marrow from WT and IL27Ra<sup>-/-</sup> congenic bone marrow were infected with Sendai virus, WT but not the IL-27R-deficient CD8<sup>+</sup> T cells produced IL-10 (60). Mechanistically, influenza infection models have demonstrated that IL-27 augments IL-10 production by CD8<sup>+</sup> T cells synergistically with IL-2 by promoting and sustaining expression of IRF4 and B-lymphocyte maturation protein-1 (Blimp-1) (36, 37). On the other hand, IL-27 activation of STAT4 was found to partially mediate IL-10 production by murine CD4<sup>+</sup> T cells (18). The increases in IL-10 by IL-27 appears to be partially reliant on type I IFNs. Type I IFN signaling was reported to enhance IL-27 secretion by myeloid cell populations during MCMV and IAV viral infections, which in turn promoted IL-10 production by T cells *in vivo* (36, 37, 58). *In vitro* data demonstrate a more direct role of type I IFNs, as the addition of IFN $\alpha$  greatly enhanced IL-10 secretion by CD8<sup>+</sup> T cells in conjunction with IL-27 and IL-2 treatment (36). Thus, the increase in IL-10 expression by IL-27 may not be an entirely IFN-independent mechanism. However, other cytokines can also

promote IL-27-mediated IL-10. For instance, IL-6 has been reported to be involved in inducing IL-10, as IL-6 enhanced IL-27 production by murine macrophages and monocytes during RSV infection which in turn promoted T-regulatory cell (Treg)-derived IL-10 (61).

There are mixed reports as to whether IL-27-induced IL-10 increases or decreases survival following viral infection. Increased IL-10-producing T cells due to IL-27 was found to enhance survival during infection with viruses such as IAV, RSV, and SeV by attenuating immune cell infiltration, cytokine production, and inflammation (18, 41, 61). However, IL-27-induced IL-10-producing T cells have also been reported to promote viral persistence during murine cytomegalovirus (MCMV), mouse hepatitis virus (MHV) strain murine hepatitis virus (JHMV), and IAV infection by over suppression of the immune responses leading to ineffective viral clearance (18, 58, 59). The aspect that appears critical to whether the IL-27-induced IL-10 response attenuates or augments viral infection is timing. Early IL-27 signaling induces IL-10 which downregulates the immune response too quickly, leading to viral spread (18, 58, 59). However, if IL-27 induces IL-10 at a later time during infection, immunopathology is reduced while preserving the antiviral immune response (18, 41, 61). The timing of IL-27 function during virus infection appears paradoxical, as early IL-27 signaling is important for enhancing innate antiviral responses and potentially regulating IFN $\gamma$  production, but also may attenuate these very responses by increasing IL-10. The availability of IL-27, the cell types responding and the kinetics of virus infection all may come into play to determine whether IL-27 signaling enhances or attenuates antiviral immune responses.

## DISCUSSION

The importance of IFNs in establishing a successful antiviral response is indisputable. However, strong selective pressure from IFNs has led to the evolution of a variety of viral IFN-inhibitory mechanisms that allow viruses to effectively establish infection (64, 107). Alternative pathways have developed in order to keep up with this virus-immune response evolutionary arms race. IL-27 may represent one of these alternative pathways. As an inducer of type I, type II, and type III IFNs (17, 20, 23, 28, 29, 35, 51, 52, 54), IL-27 may augment IFN production such that a robust antiviral response still occurs despite viral IFN-inhibitory mechanisms. It is interesting to speculate whether IL-27 has a dominant role in the induction of IFNs in general during viral infection. There is evidence for mutual direct induction between IL-27 by IFNs (20, 44, 70). However, as numerous stimulants promote IFN and IL-27 production during viral infection, such as viral PAMPs, DAMPs, and other cytokines, the role of IL-27 in promoting IFN production may be supportive, rather than dominant. Further, IL-27 has overlapping functions with IFNs, and can directly promote ISG transcription (19, 25, 27, 32, 55, 71). Being independent of IFNs, IL-27 signaling may be able to bypass the IFN-inhibitory mechanisms of viruses and successfully induce ISG transcription. However, IL-27 signaling pathways are similar

to that of IFNs, making it plausible that viral mechanisms developed to interfere with IFN signaling may be effective at hindering IL-27 signaling as well.

Overall, the interwoven relationship between IFNs and IL-27 makes it difficult to delineate their antiviral mechanisms as entirely separate. The most compelling evidence that IL-27 also acts independently of IFNs is that in IFN-deficient models, inhibition of viral replication still occurs upon IL-27 treatment (25, 26, 29). Indeed, these IFN-independent mechanisms include acting as a IFN itself and directly inducing ISGs, but also modulating other immune responses such as proinflammatory cytokine and chemokine production (28, 40), macrophage and DC differentiation (24, 39), and IL-10 anti-inflammatory function (18, 36, 37, 41, 58–61). The vast array of responses influenced by IL-27 relates to its ability to inhibit a variety of viral infections and makes it a promising therapeutic and vaccine adjuvant for existing and emerging viral threats.

## AUTHOR CONTRIBUTIONS

HA and KG conceptualized this review; HA led the writing of this review with OK and MR contributing equally to

information on the biology of IL-27 and on IL-27 and T cell responses respectively. HA designed the figure and table. OK was responsible for the initial editing of the review and HA was responsible for combining edits from all authors. KG oversaw all aspects or writing editing and submitting the review. All authors contributed to the article and approved the submitted version.

## FUNDING

This work was supported by funding from the Natural Sciences and Engineering Research Council of Canada (NSERC), grant number: RGPIN-2017-04526.

## ACKNOWLEDGMENTS

HA was supported by a Franklin Bracken award from Queen's University. OK was supported by an Alexander Graham Bell Canada Graduate Scholarship (NSERC-CGS-D).

## REFERENCES

- Amarante-Mendes GP, Adjemian S, Branco LM, Zanetti LC, Weinlich R, Bortoluci KR. Pattern Recognition Receptors and the Host Cell Death Molecular Machinery. *Front Immunol* (2018) 9:2379. doi: 10.3389/fimmu.2018.02379
- Thompson MR, Kaminski JJ, Kurt-Jones EA, Fitzgerald KA. Pattern Recognition Receptors and the Innate Immune Response to Viral Infection. *Viruses* (2011) 3(6):920–40. doi: 10.3390/v3060920
- Tisoncik JR, Korth MJ, Simmons CP, Farrar J, Martin TR, Katze MG. Into the Eye of the Cytokine Storm. *Microbiol Mol Biol Rev* (2012) 76(1):16–32. doi: 10.1128/mmb.05015-11
- Pflanz S, Timans JC, Cheung J, Rosales R, Kanzler H, Gilbert J, et al. IL-27, A Heterodimeric Cytokine Composed of Ebi3 and P28 Protein, Induces Proliferation of Naive CD4+ T Cells. *Immunity* (2002) 16(6):779–90. doi: 10.1016/s1074-7613(02)00324-2
- Pflanz S, Hibbert L, Mattson J, Rosales R, Vaisberg E, Bazan JF, et al. Wsx-1 and Glycoprotein 130 Constitute a Signal-Transducing Receptor for IL-27. *J Immunol* (2004) 172(4):2225–31. doi: 10.4049/jimmunol.172.4.2225
- Kourko O, Seaver K, Odoardi N, Basta S, Gee K. IL-27, IL-30, and IL-35: A Cytokine Triumvirate in Cancer. *Front Oncol* (2019) 9:969. doi: 10.3389/fonc.2019.00969
- Chen Q, Ghilardi N, Wang H, Baker T, Xie MH, Gurney A, et al. Development of Th1-Type Immune Responses Requires the Type I Cytokine Receptor TCCR. *Nature* (2000) 407(6806):916–20. doi: 10.1038/35038103
- Lucas S, Ghilardi N, Li J, de Sauvage FJ. IL-27 Regulates IL-12 Responsiveness of Naive CD4+ T Cells Through Stat1-Dependent and -Independent Mechanisms. *Proc Natl Acad Sci USA* (2003) 100(25):15047–52. doi: 10.1073/pnas.2536517100
- Diveu C, McGeachy MJ, Boniface K, Stumhofer JS, Sathe M, Joyce-Shaikh B, et al. IL-27 Blocks Rorc Expression to Inhibit Lineage Commitment of Th17 Cells. *J Immunol* (2009) 182(9):5748–56. doi: 10.4049/jimmunol.0801162
- Kalliolias GD, Ivashkiv LB. IL-27 Activates Human Monocytes Via Stat1 and Suppresses IL-10 Production But the Inflammatory Functions of IL-27 Are Abrogated by TLRs and P38. *J Immunol* (2008) 180(9):6325–33. doi: 10.4049/jimmunol.180.9.6325
- Guzzo C, Ayer A, Basta S, Banfield BW, Gee K. IL-27 Enhances LPS-Induced Proinflammatory Cytokine Production Via Upregulation of TLR4 Expression and Signaling in Human Monocytes. *J Immunol* (2012) 188(2):864–73. doi: 10.4049/jimmunol.1101912
- Petes C, Mintsopoulos V, Finnen RL, Banfield BW, Gee K. The Effects of CD14 and IL-27 on Induction of Endotoxin Tolerance in Human Monocytes and Macrophages. *J Biol Chem* (2018) 293(45):17631–45. doi: 10.1074/jbc.RA118.003501
- Petes C, Odoardi N, Plater SM, Martin NL, Gee K. IL-27 Amplifies Cytokine Responses to Gram-Negative Bacterial Products and Salmonella Typhimurium Infection. *Sci Rep* (2018) 8(1):13704. doi: 10.1038/s41598-018-32007-y
- Petes C, Wynick C, Guzzo C, Mehta D, Logan S, Banfield BW, et al. IL-27 Enhances LPS-Induced IL-1 $\beta$  in Human Monocytes and Murine Macrophages. *J Leukoc Biol* (2017) 102(1):83–94. doi: 10.1189/jlb.3A0316-098R
- Odoardi N, Kourko O, Petes C, Basta S, Gee K. TLR7 Ligation Inhibits TLR8 Responsiveness in IL-27-Primed Human THP-1 Monocytes and Macrophages. *J Innate Immun* (2021) 6:1–14. doi: 10.1159/000515738
- Swaminathan S, Dai L, Lane HC, Imamichi T. Evaluating the Potential of IL-27 as a Novel Therapeutic Agent in HIV-1 Infection. *Cytokine Growth Factor Rev* (2013) 24(6):571–7. doi: 10.1016/j.cytogfr.2013.07.001
- Matsui M, Moriya O, Belladonna ML, Kamiya S, Lemonnier FA, Yoshimoto T, et al. Adjuvant Activities of Novel Cytokines, Interleukin-23 (IL-23) and IL-27, for Induction of Hepatitis C Virus-Specific Cytotoxic T Lymphocytes in HLA-A\*0201 Transgenic Mice. *J Virol* (2004) 78(17):9093–104. doi: 10.1128/JVI.78.17.9093-9104.2004
- Liu FD, Kenngott EE, Schroter MF, Kuhl A, Jennrich S, Watzlawick R, et al. Timed Action of IL-27 Protects From Immunopathology While Preserving Defense in Influenza. *PLoS Pathog* (2014) 10(5):e1004110. doi: 10.1371/journal.ppat.1004110
- Kwock JT, Handfield C, Suwanpradit J, Hoang P, McFadden MJ, Labagnara KF, et al. IL-27 Signaling Activates Skin Cells to Induce Innate Antiviral Proteins and Protects Against Zika Virus Infection. *Sci Adv* (2020) 6(14):eaay3245. doi: 10.1126/sciadv.aay3245
- Cao Y, Zhang R, Zhang W, Zhu C, Yu Y, Song Y, et al. IL-27, A Cytokine, and IFN- $\lambda$ 1, A Type III IFN, Are Coordinated to Regulate Virus Replication Through Type I IFN. *J Immunol* (2014) 192(2):691–703. doi: 10.4049/jimmunol.1300252
- Tan G, Xiao Q, Song H, Ma F, Xu F, Peng D, et al. Type I IFN Augments IL-27-Dependent Trim25 Expression to Inhibit Hbv Replication. *Cell Mol Immunol* (2018) 15(3):272–81. doi: 10.1038/cmi.2016.67

22. Fakruddin JM, Lempicki RA, Gorelick RJ, Yang J, Adelsberger JW, Garcia-Pineres AJ, et al. Noninfectious Papilloma Virus-Like Particles Inhibit HIV-1 Replication: Implications for Immune Control of HIV-1 Infection by IL-27. *Blood* (2007) 109(5):1841–9. doi: 10.1182/blood-2006-02-001578
23. Greenwell-Wild T, Vázquez N, Jin W, Rangel Z, Munson PJ, Wahl SM. Interleukin-27 Inhibition of HIV-1 Involves an Intermediate Induction of Type I Interferon. *Blood* (2009) 114(9):1864–74. doi: 10.1182/blood-2009-03-211540
24. Dai L, Lidie KB, Chen Q, Adelsberger JW, Zheng X, Huang D, et al. IL-27 Inhibits HIV-1 Infection in Human Macrophages by Down-Regulating Host Factor Sptbn1 During Monocyte to Macrophage Differentiation. *J Exp Med* (2013) 210(3):517–34. doi: 10.1084/jem.20120572
25. Chen Q, Swaminathan S, Yang D, Dai L, Sui H, Yang J, et al. Interleukin-27 Is a Potent Inhibitor of Cis HIV-1 Replication in Monocyte-Derived Dendritic Cells Via a Type I Interferon-Independent Pathway. *PLoS One* (2013) 8(3):e59194. doi: 10.1371/journal.pone.0059194
26. Frank AC, Zhang X, Katsounas A, Bharucha JP, Kotttilil S, Imamichi T. Interleukin-27, an Anti-HIV-1 Cytokine, Inhibits Replication of Hepatitis C Virus. *J Interferon Cytokine Res* (2010) 30(6):427–31. doi: 10.1089/jir.2009.0093
27. Bender H, Wiesinger MY, Nordhoff C, Schoenherr C, Haan C, Ludwig S, et al. Interleukin-27 Displays Interferon-Gamma-Like Functions in Human Hepatoma Cells and Hepatocytes. *Hepatology* (2009) 50(2):585–91. doi: 10.1002/hep.22988
28. Kumar P, Rajasekaran K, Nanbakhsh A, Gorski J, Thakar MS, Malarkannan S. IL-27 Promotes NK Cell Effector Functions via MAF-NRF2 Pathway During Influenza Infection. *Sci Rep* (2019) 9(1):4984. doi: 10.1038/s41598-019-41478-6
29. Liu L, Cao Z, Chen J, Li R, Cao Y, Zhu C, et al. Influenza A Virus Induces Interleukin-27 Through Cyclooxygenase-2 and Protein Kinase A Signaling. *J Biol Chem* (2012) 287(15):11899–910. doi: 10.1074/jbc.M111.308064
30. Poudyal D, Yang J, Chen Q, Goswami S, Adelsberger JW, Das S, et al. IL-27 Posttranslationally Regulates Y-Box Binding Protein-1 to Inhibit HIV-1 Replication in Human CD4+ T Cells. *AIDS* (2019) 33(12):1819–30. doi: 10.1097/QAD.0000000000002288
31. Yang XD, Hao H, Xia ZC, Xu G, Cao ZY, Chen XY, et al. Soluble IL-6 Receptor and IL-27 Subunit p28 Protein Complex Mediate the Antiviral Response Through the Type III IFN Pathway. *J Immunol* (2016) 197(6):2369–81. doi: 10.4049/jimmunol.1600627
32. Imamichi T, Yang J, Huang DW, Brann TW, Fullmer BA, Adelsberger JW, et al. IL-27, A Novel Anti-HIV Cytokine, Activates Multiple Interferon-Inducible Genes in Macrophages. *AIDS* (2008) 22(1):39–45. doi: 10.1097/QAD.0b013e3282f3356c
33. Zuo Q, Cheng Z, Zhang G, Xia Y, Xu G, Cao W, et al. Role of IL-6-IL-27 Complex in Host Antiviral Immune Response. *J Immunol* (2021) 207:577–89. doi: 10.4049/jimmunol.2100179
34. Wang Q, Chen XY, Feng J, Cao YH, Song Y, Wang H, et al. Soluble Interleukin-6 Receptor-Mediated Innate Immune Response to DNA and RNA Viruses. *J Virol* (2013) 87(20):11244–54. doi: 10.1128/JVI.01248-13
35. Mayer KD, Mohrs K, Reiley W, Wittmer S, Kohlmeier JE, Pearl JE, et al. Cutting Edge: T-Bet and IL-27R Are Critical for *in Vivo* IFN-Gamma Production by CD8 T Cells During Infection. *J Immunol* (2008) 180(2):693–7. doi: 10.4049/jimmunol.180.2.693
36. Jiang L, Yao S, Huang S, Wright J, Braciale TJ, Sun J. Type I IFN Signaling Facilitates the Development of IL-10-Producing Effector CD8(+) T Cells During Murine Influenza Virus Infection. *Eur J Immunol* (2016) 46(12):2778–88. doi: 10.1002/eji.201646548
37. Sun J, Dodd H, Moser EK, Sharma R, Braciale TJ. CD4+ T Cell Help and Innate-Derived IL-27 Induce Blimp-1-Dependent IL-10 Production by Antiviral CTLs. *Nat Immunol* (2011) 12(4):327–34. doi: 10.1038/ni.1996
38. Valdés-López JF, Fernandez GJ, Urcuqui-Inchima S. Interleukin 27 as an Inducer of Antiviral Response Against Chikungunya Virus Infection in Human Macrophages. *Cell Immunol* (2021) 367:104411. doi: 10.1016/j.cellimm.2021.104411
39. Harker JA, Wong KA, Dallari S, Bao P, Dolgote A, Jo Y, et al. Interleukin-27R Signaling Mediates Early Viral Containment and Impacts Innate and Adaptive Immunity After Chronic Lymphocytic Choriomeningitis Virus Infection. *J Virol* (2018) 92(12):e02196-17. doi: 10.1128/JVI.02196-17
40. Heikkilä O, Nygårdas M, Paavilainen H, Ryödi E, Hukkanen V. Interleukin-27 Inhibits Herpes Simplex Virus Type 1 Infection by Activating Stat1 and 3, Interleukin-6, and Chemokines IP-10 and MIG. *J Interferon Cytokine Res* (2016) 36(11):617–29. doi: 10.1089/jir.2016.0015
41. Muallem G, Wagage S, Sun Y, DeLong JH, Valenzuela A, Christian DA, et al. IL-27 Limits Type 2 Immunopathology Following Parainfluenza Virus Infection. *PLoS Pathog* (2017) 13(1):e1006173. doi: 10.1371/journal.ppat.1006173
42. Sprockholt JK, Kaptein TM, van Hamme JL, Overmars RJ, Gringhuis SI, Geijtenbeek TBH. Rig-I-Like Receptor Activation by Dengue Virus Drives Follicular T Helper Cell Formation and Antibody Production. *PLoS Pathog* (2017) 13(11):e1006738. doi: 10.1371/journal.ppat.1006738
43. Lapenta C, Santini SM, Spada M, Donati S, Urbani F, Accapezzato D, et al. IFN-Alpha-Conditioned Dendritic Cells Are Highly Efficient in Inducing Cross-Priming CD8(+) T Cells Against Exogenous Viral Antigens. *Eur J Immunol* (2006) 36(8):2046–60. doi: 10.1002/eji.200535579
44. Pirhonen J, Siren J, Julkunen I, Matikainen S. IFN-Alpha Regulates Toll-Like Receptor-Mediated IL-27 Gene Expression in Human Macrophages. *J Leukoc Biol* (2007) 82(5):1185–92. doi: 10.1189/jlb.0307157
45. Goraya MU, Zaighum F, Sajjad N, Anjum FR, Sakhawat I, Rahman SU. Web of Interferon Stimulated Antiviral Factors to Control the Influenza A Viruses Replication. *Microb Pathog* (2020) 139:103919. doi: 10.1016/j.micpath.2019.103919
46. Yi E, Oh J, Gao NQ, Oh S, Park SH. Enhanced Production of Enveloped Viruses in BST-2-Deficient Cell Lines. *Biotechnol Bioeng* (2017) 114(10):2289–97. doi: 10.1002/bit.26338
47. Haller O, Kochs G. Interferon-Induced Mx Proteins: Dynamins-Like GTPases With Antiviral Activity. *Traffic* (2002) 3(10):710–7. doi: 10.1034/j.1600-0854.2002.31003.x
48. Schoggins JW. Interferon-Stimulated Genes: What Do They All Do? *Annu Rev Virol* (2019) 6(1):567–84. doi: 10.1146/annurev-virology-092818-015756
49. Schoggins JW, Rice CM. Interferon-Stimulated Genes and Their Antiviral Effector Functions. *Curr Opin Virol* (2011) 1(6):519–25. doi: 10.1016/j.coviro.2011.10.008
50. Shin MS, Lee JS, Lee N, Lee WW, Kim SH, Kang I. Maintenance of Cmv-Specific CD8+ T Cell Responses and the Relationship of IL-27 to IFN-Gamma Levels With Aging. *Cytokine* (2013) 61(2):485–90. doi: 10.1016/j.cyto.2012.11.024
51. Morishima N, Owaki T, Asakawa M, Kamiya S, Mizuguchi J, Yoshimoto T. Augmentation of Effector CD8+ T Cell Generation With Enhanced Granzyme B Expression by IL-27. *J Immunol* (2005) 175(3):1686–93. doi: 10.4049/jimmunol.175.3.1686
52. Schneider R, Yaneva T, Beauseigle D, El-Khoury L, Arbour N. IL-27 Increases the Proliferation and Effector Functions of Human Naïve CD8+ T Lymphocytes and Promotes Their Development Into Tc1 Cells. *Eur J Immunol* (2011) 41(1):47–59. doi: 10.1002/eji.201040804
53. Cheng J, Myers TG, Levinger C, Kumar P, Kumar J, Goshu BA, et al. IL-27 Induces IFN/Stat1-Dependent Genes and Enhances Function of TIGIT(+) HIVgag-Specific T Cells. *iScience* (2022) 25(1):103588. doi: 10.1016/j.isci.2021.103588
54. de Almeida Nagata DE, Demoor T, Ptaschinski C, Ting HA, Jang S, Reed M, et al. IL-27R-Mediated Regulation of IL-17 Controls the Development of Respiratory Syncytial Virus-Associated Pathogenesis. *Am J Pathol* (2014) 184(6):1807–18. doi: 10.1016/j.ajpath.2014.02.004
55. Guzzo C, Jung M, Graveline A, Banfield BW, Gee K. IL-27 Increases BST-2 Expression in Human Monocytes and T Cells Independently of Type I IFN. *Sci Rep* (2012) 2:974. doi: 10.1038/srep00974
56. Swaminathan S, Hu X, Zheng X, Kriga Y, Shetty J, Zhao Y, et al. Interleukin-27 Treated Human Macrophages Induce the Expression of Novel MicroRNAs Which May Mediate Anti-Viral Properties. *Biochem Biophys Res Commun* (2013) 434(2):228–34. doi: 10.1016/j.bbrc.2013.03.046
57. Hu X, Chen Q, Sowrirajan B, Bosche M, Imamichi T, Sherman BT. Genome-Wide Analyses of MicroRNA Profiling in Interleukin-27 Treated Monocyte-Derived Human Dendritic Cells Using Deep Sequencing: A Pilot Study. *Int J Mol Sci* (2017) 18(5):925. doi: 10.3390/ijms18050925
58. Clement M, Marsden M, Stacey MA, Abdul-Karim J, Gimeno Brias S, Costa Bento D, et al. Cytomegalovirus-Specific IL-10-Producing Cd4+ T Cells Are

- Governed by Type-I IFN-Induced IL-27 and Promote Virus Persistence. *PLoS Pathog* (2016) 12(12):e1006050. doi: 10.1371/journal.ppat.1006050
59. de Aquino MT, Kapil P, Hinton DR, Phares TW, Puntambekar SS, Savarin C, et al. IL-27 Limits Central Nervous System Viral Clearance by Promoting IL-10 and Enhances Demyelination. *J Immunol* (2014) 193(1):285–94. doi: 10.4049/jimmunol.1400058
  60. Perona-Wright G, Kohlmeier JE, Bassity E, Freitas TC, Mohrs K, Cookenham T, et al. Persistent Loss of IL-27 Responsiveness in CD8+ Memory T Cells Abrogates IL-10 Expression in a Recall Response. *Proc Natl Acad Sci USA* (2012) 109(45):18535–40. doi: 10.1073/pnas.1119133109
  61. Pyle CJ, Uwadiae FI, Swieboda DP, Harker JA. Early IL-6 Signaling Promotes IL-27 Dependent Maturation of Regulatory T Cells in the Lungs and Resolution of Viral Immunopathology. *PLoS Pathog* (2017) 13(9):e1006640. doi: 10.1371/journal.ppat.1006640
  62. Velazquez-Salinas L, Verdugo-Rodriguez A, Rodriguez LL, Borca MV. The Role of Interleukin 6 During Viral Infections. *Front Microbiol* (2019) 10:1057. doi: 10.3389/fmicb.2019.01057
  63. Crabe S, Guay-Giroux A, Tormo AJ, Duluc D, Lissilaa R, Guillot F, et al. The IL-27 P28 Subunit Binds Cytokine-Like Factor 1 to Form a Cytokine Regulating NK and T Cell Activities Requiring IL-6R for Signaling. *J Immunol* (2009) 183(12):7692–702. doi: 10.4049/jimmunol.0901464
  64. Schulz KS, Mossman KL. Viral Evasion Strategies in Type I IFN Signaling - A Summary of Recent Developments. *Front Immunol* (2016) 7:498. doi: 10.3389/fimmu.2016.00498
  65. Lee AJ, Ashkar AA. The Dual Nature of Type I and Type II Interferons. *Front Immunol* (2018) 9:2061. doi: 10.3389/fimmu.2018.02061
  66. Choi YH, Lim EJ, Kim SW, Moon YW, Park KS, An HJ. IL-27 Enhances IL-15/IL-18-Mediated Activation of Human Natural Killer Cells. *J Immunother Cancer* (2019) 7(1):168. doi: 10.1186/s40425-019-0652-7
  67. Ziblat A, Domaica CI, Spallanzani RG, Iraolagoitia XL, Rossi LE, Avila DE, et al. IL-27 Stimulates Human NK-Cell Effector Functions and Primes NK Cells for IL-18 Responsiveness. *Eur J Immunol* (2015) 45(1):192–202. doi: 10.1002/eji.201444699
  68. Reizis B. Plasmacytoid Dendritic Cells: Development, Regulation, and Function. *Immunity* (2019) 50(1):37–50. doi: 10.1016/j.immuni.2018.12.027
  69. Chiba Y, Mizoguchi I, Furusawa J, Hasegawa H, Ohashi M, Xu M, et al. Interleukin-27 Exerts Its Antitumor Effects by Promoting Differentiation of Hematopoietic Stem Cells to M1 Macrophages. *Cancer Res* (2018) 78(1):182–94. doi: 10.1158/0008-5472.CAN-17-0960
  70. Remoli ME, Gafa V, Giacomini E, Severa M, Lande R, Coccia EM. IFN- $\beta$  Modulates the Response to TLR Stimulation in Human Dc: Involvement of IFN Regulatory Factor-1 (IRF-1) in IL-27 Gene Expression. *Eur J Immunol* (2007) 37(12):3499–508. doi: 10.1002/eji.200737566
  71. Richard J, Prevost J, von Bredow B, Ding S, Brassard N, Medjahed H, et al. BST-2 Expression Modulates Small Cd4-Mimetic Sensitization of HIV-1 Infected Cells to Antibody-Dependent Cellular Cytotoxicity. *J Virol* (2017) 91(11):e00219–17. doi: 10.1128/JVI.00219-17
  72. Harker JA, Dolgoter A, Zuniga EI. Cell-Intrinsic IL-27 and gp130 Cytokine Receptor Signaling Regulates Virus-Specific CD4(+) T Cell Responses and Viral Control During Chronic Infection. *Immunity* (2013) 39(3):548–59. doi: 10.1016/j.immuni.2013.08.010
  73. Guo Y, Cao W, Zhu Y. Immunoregulatory Functions of the IL-12 Family of Cytokines in Antiviral Systems. *Viruses* (2019) 11(9):772. doi: 10.3390/v11090772
  74. Hirahara K, Onodera A, Villarino AV, Bonelli M, Sciume G, Laurence A, et al. Asymmetric Action of Stat Transcription Factors Drives Transcriptional Outputs and Cytokine Specificity. *Immunity* (2015) 42(5):877–89. doi: 10.1016/j.immuni.2015.04.014
  75. Rolvering C, Zimmer AD, Kozar I, Hermanns HM, Letellier E, Vallar L, et al. Crosstalk Between Different Family Members: IL27 Recapitulates IFN $\gamma$  Responses in Hcc Cells, But Is Inhibited by IL6-Type Cytokines. *Biochim Biophys Acta Mol Cell Res* (2017) 1864(3):516–26. doi: 10.1016/j.bbamcr.2016.12.006
  76. Guzzo C, Hopman WM, Che Mat NF, Wobeser W, Gee K. Impact of HIV Infection, Highly Active Antiretroviral Therapy, and Hepatitis C Coinfection on Serum Interleukin-27. *AIDS* (2010) 24(9):1371–4. doi: 10.1097/QAD.0b013e3283391d2b
  77. Zheng YH, Xiao SL, He B, He Y, Zhou HY, Chen Z, et al. The Role of IL-27 and Its Receptor in the Pathogenesis of HIV/AIDS and Anti-Viral Immune Response. *Curr HIV Res* (2017) 15(4):279–84. doi: 10.2174/1570162x15666170517130339
  78. Gajanayaka N, O'Hara S, Konarski Y, Fernandes J, Muthumani K, Kozlowski M, et al. HIV and HIV-Tat Inhibit LPS-Induced IL-27 Production in Human Macrophages by Distinct Intracellular Signaling Pathways. *J Leukoc Biol* (2017) 102(3):925–39. doi: 10.1189/jlb.4A0716-332RR
  79. Ruiz-Riol M, Berdnik D, Llano A, Mothe B, Gálvez C, Pérez-Álvarez S, et al. Identification of Interleukin-27 (IL-27)/IL-27 Receptor Subunit Alpha as a Critical Immune Axis for *in Vivo* HIV Control. *J Virol* (2017) 91(16):e00441–17. doi: 10.1128/jvi.00441-17
  80. Swaminathan S, Hu Z, Rupert AW, Higgins JM, Dewar RL, Stevens R, et al. Plasma Interleukin-27 (IL-27) Levels Are Not Modulated in Patients With Chronic HIV-1 Infection. *PLoS One* (2014) 9(6):e98989. doi: 10.1371/journal.pone.0098989
  81. Guzzo C, Hopman WM, Che Mat NF, Wobeser W, Gee K. IL-27-Induced Gene Expression Is Downregulated in HIV-Infected Subjects. *PLoS One* (2012) 7(9):e45706. doi: 10.1371/journal.pone.0045706
  82. Sang Y, Miller LC, Blecha F. Macrophage Polarization in Virus-Host Interactions. *J Clin Cell Immunol* (2015) 6(2):311. doi: 10.4172/2155-9899.1000311
  83. Labonte AC, Tosello-Trampont AC, Hahn YS. The Role of Macrophage Polarization in Infectious and Inflammatory Diseases. *Mol Cells* (2014) 37(4):275–85. doi: 10.14348/molcells.2014.2374
  84. Yao L, Wang M, Niu Z, Liu Q, Gao X, Zhou L, et al. Interleukin-27 Inhibits Malignant Behaviors of Pancreatic Cancer Cells by Targeting M2 Polarized Tumor Associated Macrophages. *Cytokine* (2017) 89:194–200. doi: 10.1016/j.cyto.2015.12.003
  85. Shimizu M, Ogura K, Mizoguchi I, Chiba Y, Higuchi K, Ohtsuka H, et al. IL-27 Promotes Nitric Oxide Production Induced by LPS Through Stat1, NF- $\kappa$ B and MAPKs. *Immunobiology* (2013) 218(4):628–34. doi: 10.1016/j.imbio.2012.07.028
  86. Nikonova A, Khaitov M, Jackson DJ, Traub S, Trujillo-Torralbo MB, Kudlay DA, et al. M1-Like Macrophages Are Potent Producers of Anti-Viral Interferons and M1-Associated Marker-Positive Lung Macrophages Are Decreased During Rhinovirus-Induced Asthma Exacerbations. *EBioMedicine* (2020) 54:102734. doi: 10.1016/j.ebiom.2020.102734
  87. Carty M, Bowie AG. Recent Insights Into the Role of Toll-Like Receptors in Viral Infection. *Clin Exp Immunol* (2010) 161(3):397–406. doi: 10.1111/j.1365-2249.2010.04196.x
  88. Park A, Ra EA, Lee TA, Choi HJ, Lee E, Kang S, et al. HCMV-Encoded US7 and US8 Act as Antagonists of Innate Immunity by Distinctly Targeting TLR-Signaling Pathways. *Nat Commun* (2019) 10(1):4670. doi: 10.1038/s41467-019-12641-4
  89. Li K, Foy E, Ferreon JC, Nakamura M, Ferreon AC, Ikeda M, et al. Immune Evasion by Hepatitis C Virus NS3/4a Protease-Mediated Cleavage of the Toll-Like Receptor 3 Adaptor Protein Trif. *Proc Natl Acad Sci USA* (2005) 102(8):2992–7. doi: 10.1073/pnas.0408824102
  90. Abe T, Kaname Y, Hamamoto I, Tsuda Y, Wen X, Taguwa S, et al. Hepatitis C Virus Nonstructural Protein 5a Modulates the Toll-Like Receptor-Myd88-Dependent Signaling Pathway in Macrophage Cell Lines. *J Virol* (2007) 81(17):8953–66. doi: 10.1128/jvi.00649-07
  91. Stack J, Haga IR, Schröder M, Bartlett NW, Maloney G, Reading PC, et al. Vaccinia Virus Protein A46r Targets Multiple Toll-Like-Interleukin-1 Receptor Adaptors and Contributes to Virulence. *J Exp Med* (2005) 201(6):1007–18. doi: 10.1084/jem.20041442
  92. Maloney G, Schröder M, Bowie AG. Vaccinia Virus Protein A52r Activates p38 Mitogen-Activated Protein Kinase and Potentiates Lipopolysaccharide-Induced Interleukin-10. *J Biol Chem* (2005) 280(35):30838–44. doi: 10.1074/jbc.M501917200
  93. Bussey KA, Reimer E, Todt H, Denker B, Gallo A, Konrad A, et al. The Gammaherpesviruses Kaposi's Sarcoma-Associated Herpesvirus and Murine Gammaherpesvirus 68 Modulate the Toll-Like Receptor-Induced Proinflammatory Cytokine Response. *J Virol* (2014) 88(16):9245–59. doi: 10.1128/jvi.00841-14

94. Lagos D, Vart RJ, Gratrix F, Westrop SJ, Emuss V, Wong PP, et al. Toll-Like Receptor 4 Mediates Innate Immunity to Kaposi Sarcoma Herpesvirus. *Cell Host Microbe* (2008) 4(5):470–83. doi: 10.1016/j.chom.2008.09.012
95. van Lint AL, Murawski MR, Goodbody RE, Severa M, Fitzgerald KA, Finberg RW, et al. Herpes Simplex Virus Immediate-Early ICP0 Protein Inhibits Toll-Like Receptor 2-Dependent Inflammatory Responses and Nf-Kappab Signaling. *J Virol* (2010) 84(20):10802–11. doi: 10.1128/jvi.00063-10
96. Landais I, Pelton C, Streblov D, DeFilippis V, McWeeney S, Nelson JA. Human Cytomegalovirus Mir-UI112-3p Targets TLR2 and Modulates the TLR2/IRAK1/Nf- $\kappa$ b Signaling Pathway. *PLoS Pathog* (2015) 11(5):e1004881. doi: 10.1371/journal.ppat.1004881
97. Schall TJ, Bacon K, Toy KJ, Goeddel DV. Selective Attraction of Monocytes and T Lymphocytes of the Memory Phenotype by Cytokine Rantes. *Nature* (1990) 347(6294):669–71. doi: 10.1038/347669a0
98. Taub DD, Conlon K, Lloyd AR, Oppenheim JJ, Kelvin DJ. Preferential Migration of Activated CD4+ and CD8+ T Cells in Response to MIP-1 Alpha and Mip-1 Beta. *Science* (1993) 260(5106):355–8. doi: 10.1126/science.7682337
99. Hamilton JA, Achuthan A. Colony Stimulating Factors and Myeloid Cell Biology in Health and Disease. *Trends Immunol* (2013) 34(2):81–9. doi: 10.1016/j.it.2012.08.006
100. Liu Q, Zhou YH, Yang ZQ. The Cytokine Storm of Severe Influenza and Development of Immunomodulatory Therapy. *Cell Mol Immunol* (2016) 13(1):3–10. doi: 10.1038/cmi.2015.74
101. Rojas JM, Avia M, Martin V, Sevilla N. IL-10: A Multifunctional Cytokine in Viral Infections. *J Immunol Res* (2017) 2017:6104054. doi: 10.1155/2017/6104054
102. Flynn JK, Dore GJ, Hellard M, Yeung B, Rawlinson WD, White PA, et al. Early IL-10 Predominant Responses Are Associated With Progression to Chronic Hepatitis C Virus Infection in Injecting Drug Users. *J Viral Hepat* (2011) 18(8):549–61. doi: 10.1111/j.1365-2893.2010.01335.x
103. Richter K, Perriard G, Behrendt R, Schwendener RA, Sexl V, Dunn R, et al. Macrophage and T Cell Produced IL-10 Promotes Viral Chronicity. *PLoS Pathog* (2013) 9(11):e1003735. doi: 10.1371/journal.ppat.1003735
104. Blackburn SD, Wherry EJ. IL-10, T Cell Exhaustion and Viral Persistence. *Trends Microbiol* (2007) 15(4):143–6. doi: 10.1016/j.tim.2007.02.006
105. Weiss KA, Christiaansen AF, Fulton RB, Meyerholz DK, Varga SM. Multiple CD4+ T Cell Subsets Produce Immunomodulatory IL-10 During Respiratory Syncytial Virus Infection. *J Immunol* (2011) 187(6):3145–54. doi: 10.4049/jimmunol.1100764
106. Sun J, Madan R, Karp CL, Braciale TJ. Effector T Cells Control Lung Inflammation During Acute Influenza Virus Infection by Producing IL-10. *Nat Med* (2009) 15(3):277–84. doi: 10.1038/nm.1929
107. Katze MG, He Y, Gale MJr. Viruses and Interferon: A Fight for Supremacy. *Nat Rev Immunol* (2002) 2(9):675–87. doi: 10.1038/nri888

**Conflict of Interest:** The authors declare that the research was conducted in the absence of any commercial or financial relationships that could be construed as a potential conflict of interest.

**Publisher's Note:** All claims expressed in this article are solely those of the authors and do not necessarily represent those of their affiliated organizations, or those of the publisher, the editors and the reviewers. Any product that may be evaluated in this article, or claim that may be made by its manufacturer, is not guaranteed or endorsed by the publisher.

Copyright © 2022 Amsden, Kourko, Roth and Gee. This is an open-access article distributed under the terms of the Creative Commons Attribution License (CC BY). The use, distribution or reproduction in other forums is permitted, provided the original author(s) and the copyright owner(s) are credited and that the original publication in this journal is cited, in accordance with accepted academic practice. No use, distribution or reproduction is permitted which does not comply with these terms.



# The Integrated Analysis Identifies Three Critical Genes as Novel Diagnostic Biomarkers Involved in Immune Infiltration in Atherosclerosis

Zhen Ye<sup>1,2†</sup>, Xiao-kang Wang<sup>1†</sup>, Yun-hui Lv<sup>1†</sup>, Xin Wang<sup>1\*</sup> and Yong-chun Cui<sup>1\*</sup>

<sup>1</sup> Center for Cardiovascular Experimental Study and Evaluation, Fuwai Hospital, Chinese Academy of Medical Sciences and Peking Union Medical College, State Key Laboratory of Cardiovascular Disease, National Center for Cardiovascular Diseases, Beijing Key Laboratory of Pre-clinical Research and Evaluation for Cardiovascular Implant Materials, Beijing, China, <sup>2</sup> Department of Pharmacy, Suqian First Hospital, Suqian, China

## OPEN ACCESS

### Edited by:

Rongtuan Lin,  
McGill University, Canada

### Reviewed by:

Zhongjie Shi,  
Wayne State University, United States  
Wu Zhenghao,  
I.M. Sechenov First Moscow State  
Medical University, Russia

### \*Correspondence:

Yong-chun Cui  
cuiyongchun@fuwai.com  
Xin Wang  
wangxinfuwai@188.com

<sup>†</sup>These authors contributed  
equally to this work

### Specialty section:

This article was submitted to  
Viral Immunology,  
a section of the journal  
Frontiers in Immunology

Received: 28 March 2022

Accepted: 13 April 2022

Published: 18 May 2022

### Citation:

Ye Z, Wang X-k, Lv Y-h, Wang X and  
Cui Y-c (2022) The Integrated Analysis  
Identifies Three Critical Genes as Novel  
Diagnostic Biomarkers Involved in  
Immune Infiltration in Atherosclerosis.  
*Front. Immunol.* 13:905921.  
doi: 10.3389/fimmu.2022.905921

Atherosclerosis (AS), a chronic inflammatory disease of the blood vessels, is the primary cause of cardiovascular disease, the leading cause of death worldwide. This study aimed to identify possible diagnostic markers for AS and determine their correlation with the infiltration of immune cells in AS. In total, 10 serum samples from AS patients and 10 samples from healthy subjects were collected. The original gene expression profiles of GSE43292 and GSE57691 were downloaded from the Gene Expression Omnibus database. Least absolute shrinkage and selection operator regression model and support vector machine recursive feature elimination analyses were carried out to identify candidate markers. The diagnostic values of the identified biomarkers were determined using receiver operating characteristic assays. The compositional patterns of the 22 types of immune cell fraction in AS were estimated using CIBERSORT. RT-PCR was performed to further determine the expression of the critical genes. This study identified 17 differentially expressed genes (DEGs) in AS samples. The identified DEGs were mainly involved in non-small cell lung carcinoma, pulmonary fibrosis, polycystic ovary syndrome, glucose intolerance, and T-cell leukemia. FHL5, IBSP, and SCRG1 have been identified as the diagnostic genes in AS. The expression of SCRG1 and FHL5 was distinctly downregulated in AS samples, and the expression of IBSP was distinctly upregulated in AS samples, which was further confirmed using our cohort by RT-PCR. Moreover, immune assays revealed that FHL5, IBSP, and SCRG1 were associated with several immune cells, such as CD8 T cells, naïve B cells, macrophage M0, activated memory CD4 T cells, and activated NK cells. Overall, future investigations into the occurrence and molecular mechanisms of AS may benefit from using the genes FHL5, IBSP, and SCRG1 as diagnostic markers for the condition.

**Keywords:** atherosclerosis, immune infiltration, diagnosis, biomarker, GEO datasets, machine learning

## INTRODUCTION

Atherosclerosis (AS) is a cardiovascular disease caused by the thickening and hardening of arterial walls due to the accumulation of cells, cholesterol, and extracellular matrix (1, 2). Epidemiological research has indicated that hypertension, smoking, diabetes mellitus, and hypercholesterolemia are the main dangerous elements for AS and associated illness processes (3, 4). Besides this, according to laboratory and clinical data results, the combined impacts of aging and inflammation result in a high occurrence rate of AS (5). Though a great improvement in its treatment has been made, the danger of co-morbidities in AS is still serious (6, 7). AS is a chronic and complicated course involving many cells and molecular alterations. Furthermore, it is estimated that approximately 50% of the risk for atherosclerosis is genetically determined (8, 9). Therefore, the diagnosis of AS requires more novel biomarkers and forecasting models to be authenticated.

Data mining has been applied in many fields, containing sequence analysis, microarray gene expression, single-nucleotide polymorphism inspection as well as the analysis of genomic loss and amplification (copy number variation) (10, 11). With the help of microarrays, integration bioinformatics makes scholars confirm distinctively expressed targeted genes soon between AS specimens in one test (12, 13). AS diagnostic markers could be derived from aberrantly expressed genes. TP53, MAPK1, STAT3, HMOX1, and PTGS2 have been identified to be the underlying diagnostic biomarkers for AS according to the identification of a gene expression profile analysis (14, 15). Preclinical AS may be diagnosed using intercellular adhesion molecule-1 (16, 17). At the same time, diagnostic values will be increased by a large margin if many biomarkers are combined in one model.

In this study, the GSE43292 and GSE57691 datasets published by Bricca et al. and Erik et al. were reanalyzed (18, 19). We screened the abnormally expressed genes in AS samples from big data analysis. Machine learning algorithms were applied to screen and confirm the diagnostic biomarkers for AS. In this paper, CIBERSORT was first applied to quantify the immune cells of specimens of AS and normal tissues based on the gene expression profile. We also looked into the interaction between the detected biomarkers and the infiltrating immune cells to provide the groundwork for future studies.

## MATERIALS AND METHODS

### Microarray Datasets

The study downloaded the original gene expression profiles GSE43292 and GSE57691 from the Gene Expression Omnibus (GEO) database (<https://www.ncbi.nlm.nih.gov/geo/>). In total, 32 non-AS and 32 AS arterial samples were included in the GSE43292 dataset. The GSE57691 dataset included 10 non-AS and 9 AS arterial specimens.

### Patients and Samples

A total of 20 patients from the Suqian First Hospital, with admission dates from 2020 to 2022 were registered and separated into the AS

group ( $n = 10$ ) and the control group ( $n = 10$ ). Blood specimens from the two groups were gathered through venipuncture, and the serum was obtained through centrifugation at 1,500g under 4°C and then reserved under -80°C for further use. The study protocol was authorized by the clinical study ethics committee of the Suqian First Hospital. Every method used was according to the related guidelines and regulations. Every participant has signed an informed consent form.

### Data Processing and Screening of Differentially Expressed Genes

Using the combat function of the SVA package, GSE43292 and GSE57691 were combined into a metadata cohort, and batch effects were removed. Comparing the AS arterial samples with the non-AS arterial samples, the “limma” package was applied for the identification of differentially expressed genes (DEGs) with threshold of  $|\text{fold change (FC)}| > 1.2$  and  $P\text{-value} < 0.01$ .

### Functional Enrichment Analysis

The “ClusterProfiler” package of R software was applied in function gathering analysis, and there were significant ( $q$ -values less than 0.01) biological processes and Kyoto Encyclopedia of Genes and Genomes (KEGG) pathways used in this study (20). Disease Ontology (DO) gathering analysis was operated on DEGs with the “clusterProfiler” and DOSE packages of R.

### Candidate Diagnostic Biomarkers

Support vector machine recursive feature elimination (SVM-RFE) and least absolute shrinkage and selection operator (LASSO) were employed to classify the diagnostic indicators of AS. The “Glmnet” package was employed to analyze the binomial response type and 1 alpha value. In addition, as a supervised machine learning means to support vectors, the SVM explores the optimal variables by clearing the character vectors produced by the SVM. The SVM sorter of R package e1071 was used in the classification analysis of the selective markers for AS diagnosis;  $k = 5$  was set for  $k$ -fold cross-validation. The halving parameter mentioned above was set as 100.

### Evaluation of Immune Cell Infiltration

Gene expression matrix information was uploaded to CIBERSORT (<https://cibersort.stanford.edu/>) to assess the enrichment of immune invasions, and we got the immune cell infiltrate matrix. Next, the “corrplot” package was used to make a correlation heat map to see the pertinence of 22 kinds of infiltrated immune cells.

### Association Between Critical Genes and Infiltrating Immune Cells

The relationship of the confirmed genes to the standards of infiltrated immune cells was found with Spearman’s rank analysis using R software. The consequent relationships were seen by chart technology using the “ggplot2” package (21).

### Quantitative Real-Time PCR Assay

Total RNA was separated with TRIZOL reagent based on the protocol from the manufacturer (Invitrogen). The RNA was reverse-transcribed with SuperScript First Strand cDNA System



(Invitrogen) based on the instructions from the manufacturer. SYBR Green RT-PCR Master Mix and 1.0  $\mu$ l of cDNA were used in the PCR amplification using Applied Biosystems 7900HT (Applied Biosystems, Takara). The results were gathered and studied by SDS2.3 Software (Applied Biosystems). The expression standard of every candidate gene was the internal standard compared with that of GAPDH. This relative quantitative data was conveyed using the  $2^{-\Delta\Delta Ct}$  method. Every test was repeated 3 times. The primers are shown in **Supplementary Table S1**.

## Statistical Analysis

Statistical analyses were performed with R software v3.5.0 (R Core Team, MA, USA) and GraphPad Prism v7.00 (GraphPad Software Inc., La Jolla, CA, USA). R "glmnet" package was used to finish the LASSO regression analysis, while the e1071 package ran the SVM algorithm. The significance of distinction in the two groups was calculated with Student's *t*-test. All  $P < 0.05$  were regarded as statistically evident.

## RESULTS

### Identification of the Dysregulated Genes in AS Patients

To screen the dysregulated genes in AS, we analyzed the GSE43292 and GSE57691 datasets using the "limma" package in R software. Through a volcano plot and a hierarchical cluster, we identified a total of 17 DEGs (fold change  $> 1.2$ ), among which 7 (FHL5, CASQ2, SCRG1, CNTN1, TPH1, CNTN4, and CNN1) were downregulated and 10 (TM4SF19, IGJ, CD36, DPP4, HMOX1, FABP4, IBSP, MMP7, MMP9, and MMP12) were upregulated (**Figures 1A, B**).

## Functional Correlation Analysis

We performed a functional correlation analysis to determine the features of the above-mentioned 17 DEGs in life activity. The consequences of the GO analysis showed that the 17 DEGs might be mainly abundant in the extracellular matrix organization, extracellular structure organization, external encapsulating structural organization, membrane raft, membrane microdomain, caveola, endopeptidase activity, serine-type endopeptidase as well as metalloendopeptidase activity (**Figure 2A**). The KEGG assays indicated that the 17 DEGs were mainly enriched in the PPAR signaling pathway (**Figure 2B**). The DO pathway enrichment analyses showed that diseases enriched by DEGs were mainly associated with non-small cell lung carcinoma, pulmonary fibrosis, polycystic ovary syndrome, glucose intolerance, and T-cell leukemia (**Figure 2C**).

### Identification and Validation of Diagnostic Genes

Two distinct algorithms were applied to filter underlying markers. The DEGs were decreased with the LASSO regression algorithm, which confirmed five genes to be diagnostic biomarkers of AS (**Figure 3A**). Apart from the five characters in the DEGs that were decided with the SVM-RFE algorithm (**Figure 3B**), 3 overlapping characters (FHL5, IBSP, and SCRG1) in the 2 algorithms were finally chosen (**Figure 3C**).

### Expression and Diagnostic Value of FHL5, IBSP, and SCRG1 in AS

We observed that SCRG1 and FHL5 decreased in AS samples compared with those in control samples (**Figures 4A, B**), while IBSP expression was distinctly increased in AS samples (**Figure 4C**). In addition, according to the ROC assays, the low SCRG1 conveyed had an AUC result of 0.870 (95% CI: 0.789 to 0.940) in AS

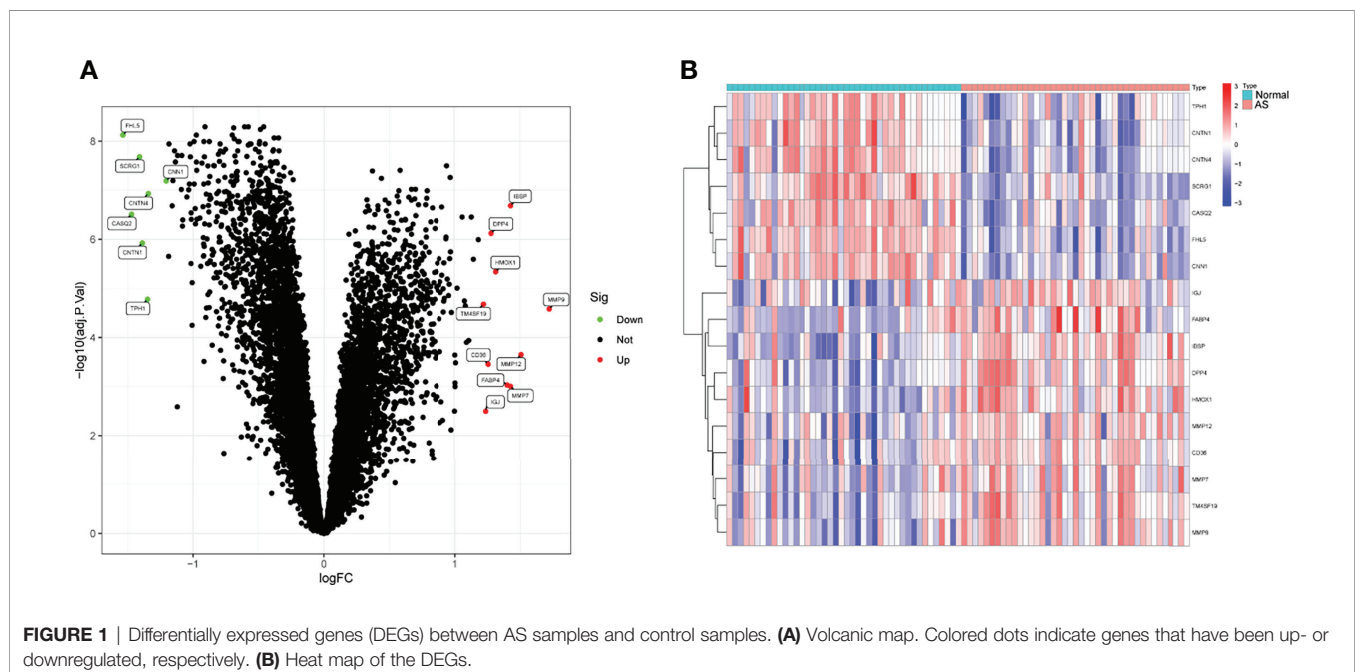


**FIGURE 1** | Differentially expressed genes (DEGs) between AS samples and control samples. **(A)** Volcanic map. Colored dots indicate genes that have been up- or downregulated, respectively. **(B)** Heat map of the DEGs.

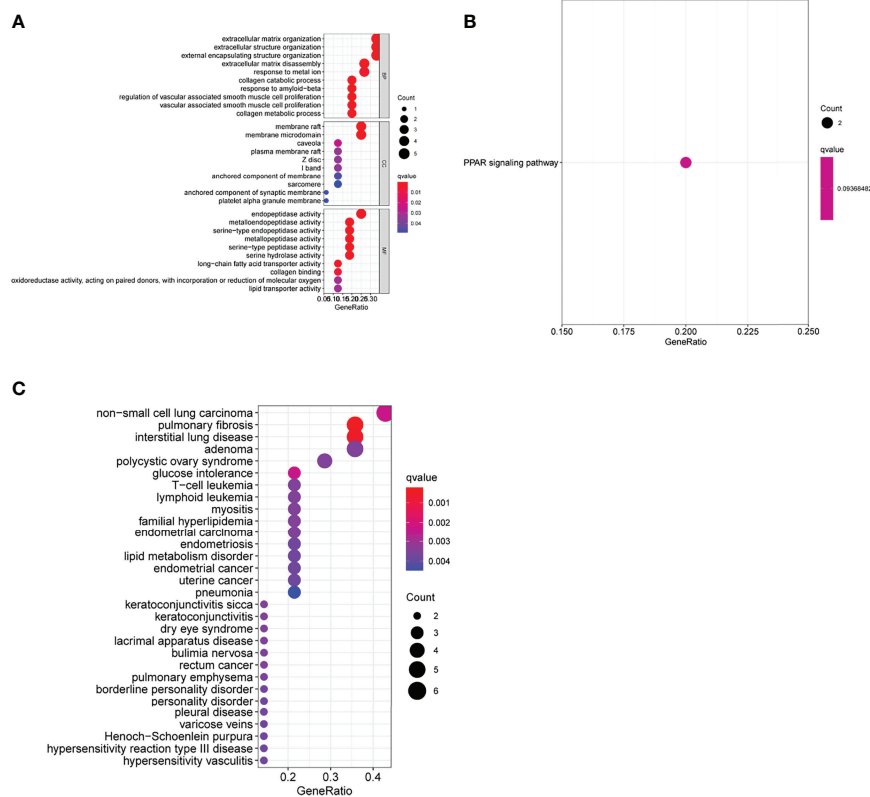


**FIGURE 2** | Function enrichment analyses of differentially expressed genes (DEGs). **(A)** Gene Ontology enrichment for DEGs. **(B)** Kyoto Encyclopedia of Genes and Genomes pathways enrichment for DEGs. **(C)** Enrichment study of genes differentially expressed between atherosclerosis and healthy samples using the disease ontology.

(**Figure 5A**), and the low FHL5 expression had an AUC result of 0.897 (95% CI: 0.821 to 0.954) in AS (**Figure 5B**). However, the high IBSP expression had an AUC result of 0.840 (95% CI: 0.746 to 0.914) in AS (**Figure 5C**). Our findings suggested that FHL5, IBSP, and SCRG1 had a high diagnostic ability.

### Correlation of FHL5, IBSP, and SCRG1 With the Proportion of Immune Cell Infiltration

To deeply identify the pertinence in FHL5, IBSP, SCRG1, and the immune microenvironment, the ratio of immune cell infiltration was studied with the CIBERSORT algorithm, and 21 types of immune cell profiling of AS persons were accomplished (**Figures 6A–C**). In addition, it has clear pertinence in FHL5 expression and the ratio in nine types of tumor-infiltrating immune cells (TICs), including CD8 T cells, regulatory T cells (Tregs), naïve B cells, excited NK cells, excited dendritic cells, memory B cells, plasma cells, activated memory CD4 T cells, and macrophage M0 (**Figure 7A** and **Supplementary Figure S1**). It has clear pertinence in IBSP expressions and the ratio in macrophage M0, activated memory CD4 T cells, neutrophils, memory B cells, monocytes, Tregs, naïve B cells, excited NK cells, and CD8 T cells (**Figure 7B** and

**Supplementary Figure S2**). In addition, SCRG1 expression was distinctly associated with excited NK cells, CD8 T cells, resting dendritic cells, naïve B cells, macrophage M2, excited memory CD4 T cells, plasma cells, and macrophage M0 (**Figure 7C** and **Supplementary Figure S3**). These results further support the effect of FHL5, IBSP, and SCRG1 on the immune activity of the immune microenvironment.

### Demonstration of the Expression of FHL5, IBSP, and SCRG1 in AS Patients

To further demonstrate the expression of FHL5, IBSP, and SCRG1 in AS patients, we performed RT-PCR in 10 serum samples from AS patients and 10 healthy samples. The results showed that SCRG1 and FHL5 decreased in AS samples compared with those in healthy samples (**Figures 8A, B**), while IBSP expression was distinctly increased in AS samples compared with that in healthy samples (**Figure 8C**).

## DISCUSSION

The number of people with atheroma plaque among 30–70-year-olds worldwide was 57.79 million in 2020, an increase of

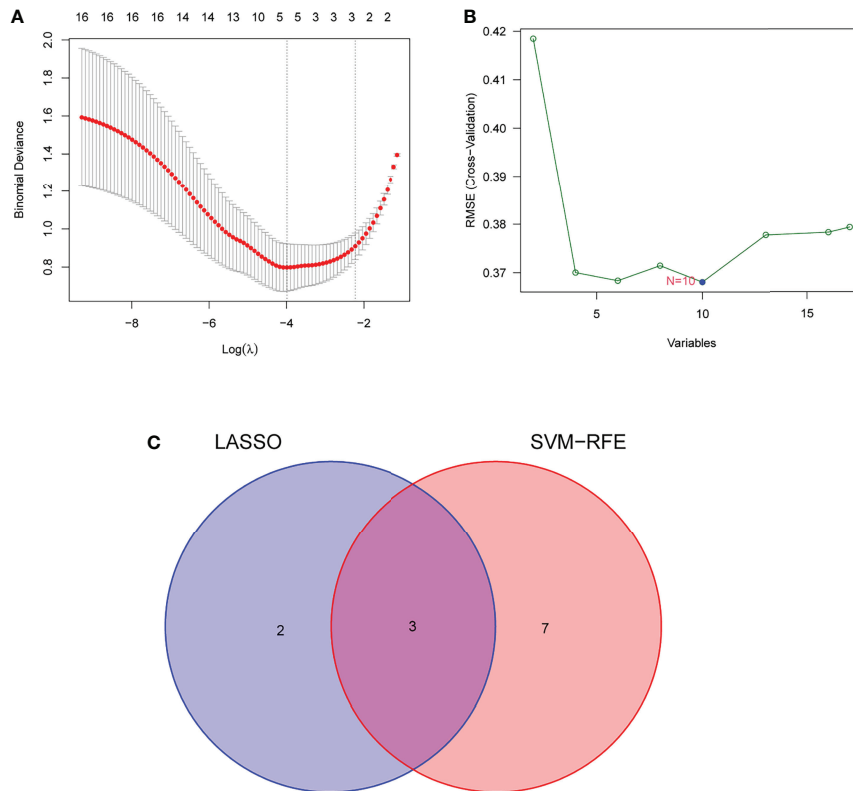


**FIGURE 3** | Filtering course in diagnostic candidates in atherosclerosis. **(A)** Tuning character option in the least unconditional shrinkage and option operator model. **(B)** A plot of biomarker option by support vector machine recursive feature elimination (SVM-RFE) algorithm. **(C)** The least unconditional shrinkage, option operator, and SVM-RFE algorithms all share a Venn diagram to provide three diagnostic indicators.

59.13% compared with that in 2000 (1, 22). Nevertheless, effective therapy was rare, so it is urgent to identify the genes that result in the development of AS and explore possible efficient treatment targets.

The potential reason for cardiovascular incidents is AS, a chronic inflammatory illness. Accurately diagnosing and treating cardiovascular illnesses necessitated research into the probable processes of AS at the cellular level (23, 24). Because

microarrays and high-throughput sequencing have supplied thousands of different gene expression data types, it has become increasingly popular to anticipate prospective treatment targets for atherosclerosis (25, 26). This study retrospectively analyzed data from 42 non-AS arterial and 41 AS arterial samples from two GEO datasets (GSE43292 and GSE57691). We identified 17 abnormally expressed genes between healthy and atherosclerotic tissues. Then, we performed KEGG assays

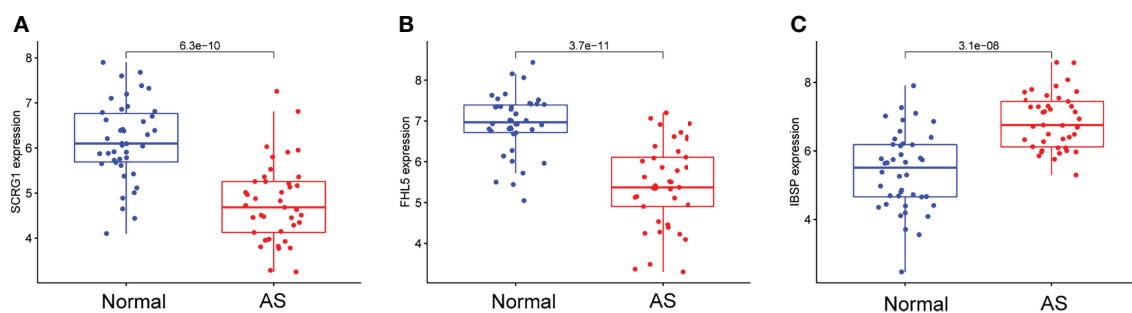
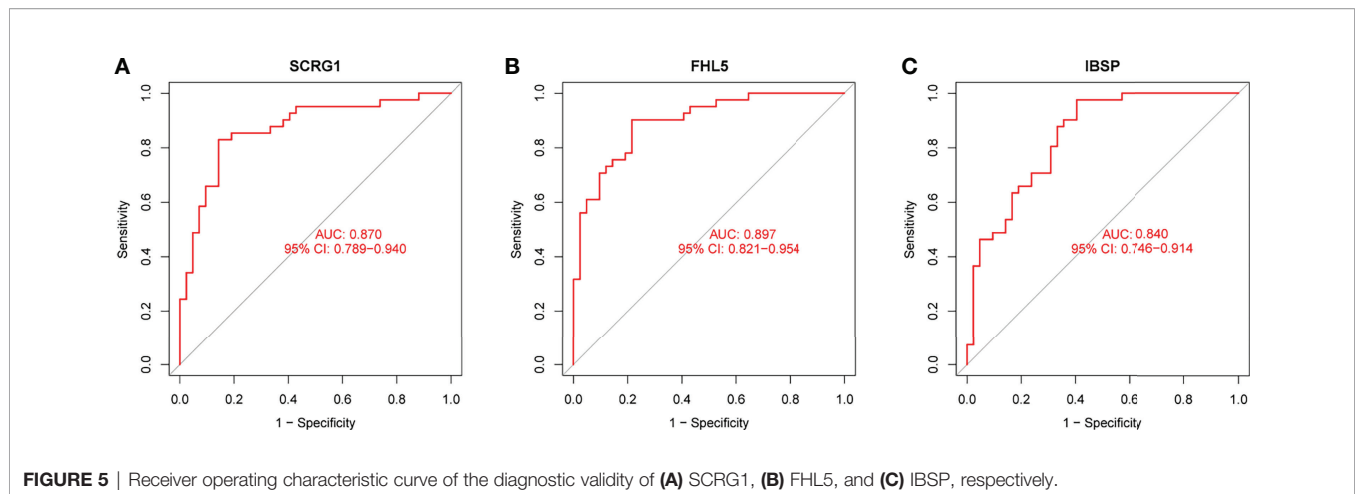


**FIGURE 4** | Expression of **(A)** SCRG1, **(B)** FHL5, and **(C)** IBSP, respectively, in atherosclerosis samples and healthy samples from GSE43292 and GSE57691 datasets.



which indicated that the above-mentioned 17 genes might be primarily enriched in the PPAR signaling pathway, which has been reported to be related to the regulation of cardiovascular illnesses (27, 28). The DO assays showed that the above-mentioned 17 genes might be primarily associated with fibrosis, familial hyperlipidemia, lipid metabolism disorder, and several cancers. Our findings suggested that the 17 abnormally expressed genes may be involved in the progression of AS.

SVM-RFE is favorable to small-specimen-size datasets. SVM-RFE also removes spare elements and keeps just the results of the involved variables (29). LASSO regression analysis is always used to screen variables to stop overfitting (30). This study used the above-mentioned two machine learning algorithms to screen possible diagnostic biomarkers for AS, and three genes were identified, including FHL5, IBSP, and SCRG1. Previously, several studies have reported that FHL5, IBSP, and SCRG1 were involved in the progression of several diseases (31–33). However, their effects on AS progression were largely indistinct. In this paper, we first put forward evidence that the expression of FHL5 and SCRG1, respectively, were distinctly decreased in AS samples compared with those in control samples, while IBSP exhibited an increased level in AS samples for the first time. The ROC assays further confirmed their diagnostic value in distinguishing AS from the healthy samples. Our findings highlighted the potential of FHL5, IBSP, and SCRG1 to be used as novel biomarkers for AS patients.

Cells of inborn and adapted immune systems consist of atherosclerotic lesions (34). Infiltrating immune cells have recently been characterized in mouse and human atherosclerosis and revealed activated, cytotoxic, and possibly dysfunctional and exhausted cell phenotypes (35, 36). The chronic accumulation of vascular occlusion plaques in the subendothelial intimal layer of large and medium arteries leads to significant stenosis that restricts blood flow and causes critical tissue hypoxia (37, 38). The autoimmune

reply is determinable in human and animal models of AS. While the typical percept is that autoimmunity can be pathogenic *per se*, the present proof indicates that ApoB-specific CD4<sup>+</sup> T-helper cells have already been determined among subjects without clinical atherosclerosis and with atheroprotective characters mostly. In the paper, it was indicated that FHL5 expression was distinctly related to nine types of TICs, including CD8 T cells, regulatory T cells (Tregs), naïve B cells, activated NK cells, excited dendritic cells, memory B cells, plasma cells, activated memory CD4 T cells, and macrophage M0. IBSP expression was distinctly associated with macrophage M0, activated memory CD4 T cells, neutrophils, memory B cells, monocytes, regulatory T cells (Tregs), naïve B cells, excited NK cells, and CD8 T cells. Moreover, SCRG1 expression was distinctly associated with excited NK cells, CD8 T cells, resting dendritic cells, naïve B cells, macrophage M2, excited memory CD4 T cells, plasma cells, and macrophage M0. Our findings suggested that FHL5, IBSP, and SCRG1 may influence AS progression *via* regulating the activity of the immune system.

Although our findings support that FHL5, IBSP, and SCRG1 have a high clinical application potential, the study faces some limitations. AS samples were limited in this study, and further demonstration by future studies is necessary. Furthermore, particular biological functions in three genes of AS progression are required to be explored experimentally. Moreover, the potential functions of FHL5, IBSP, and SCRG1 on the immune system need to be further studied.

## CONCLUSIONS

Our study identified three diagnostic genes, including FHL5, IBSP, and SCRG1. Drugs targeting FHL5, IBSP, and SCRG1 could be potential immunotherapy for AS patients in the future. Nevertheless, other independent cohorts and functional tests for FHL5, IBSP, and SCRG1 are warranted.

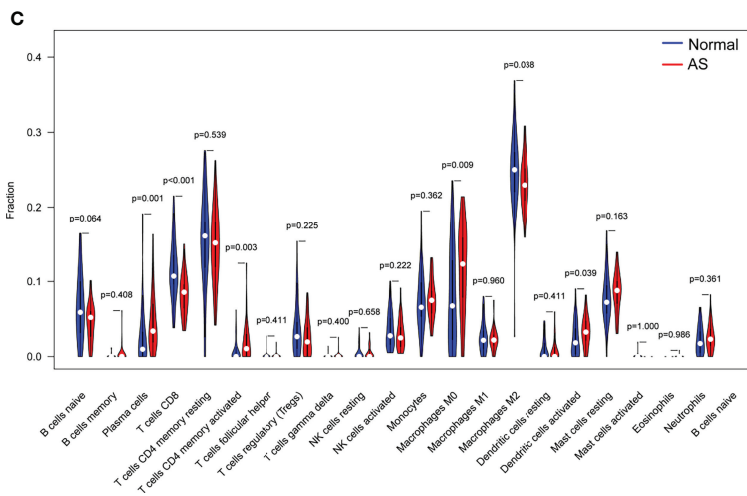
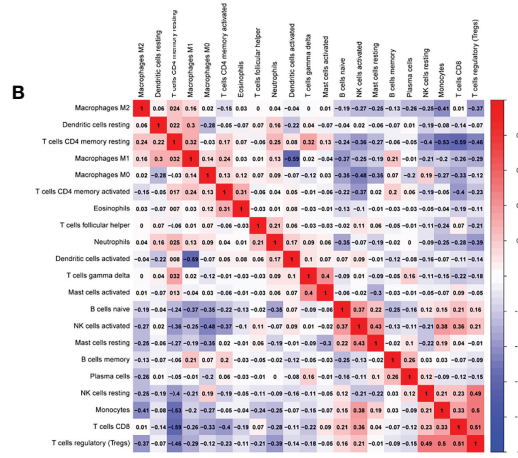
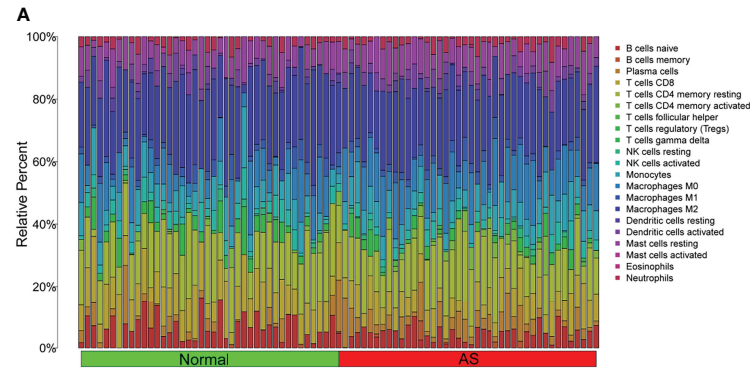


**FIGURE 6** | Profile of infiltrating immune cells. **(A)** The ratio of 22 different infiltrating immune cells in atherosclerosis (AS) samples is shown graphically in a bar plot. Column names, sample ID. **(B)** Heat map showing the relationship between 22 different types of infiltrating immune cells. **(C)** Violin plot displaying the variation among 22 types of infiltrating immune cells between AS specimens and healthy samples.

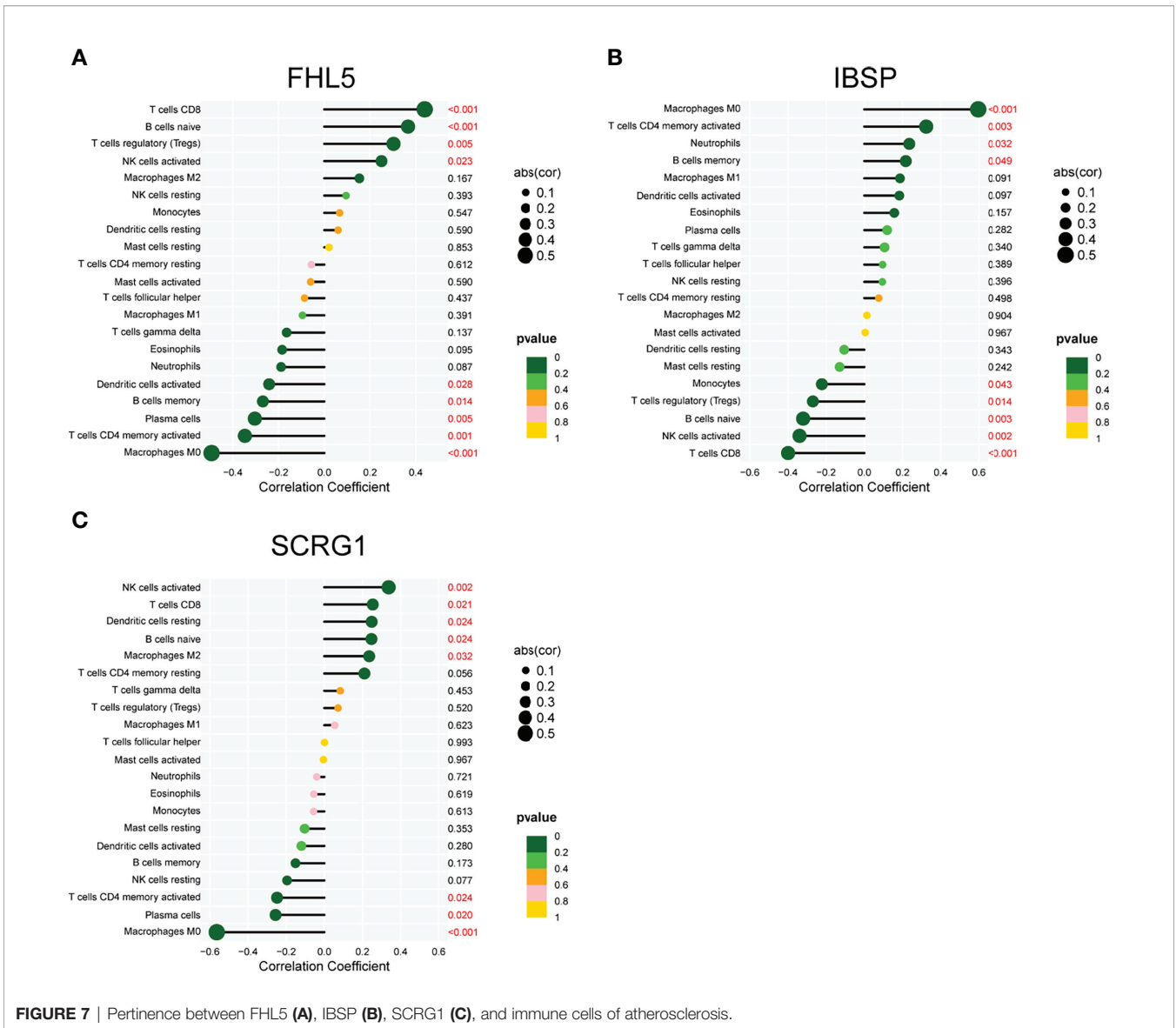


**FIGURE 7 |** Pertinence between FHL5 (A), IBSP (B), SCRG1 (C), and immune cells of atherosclerosis.

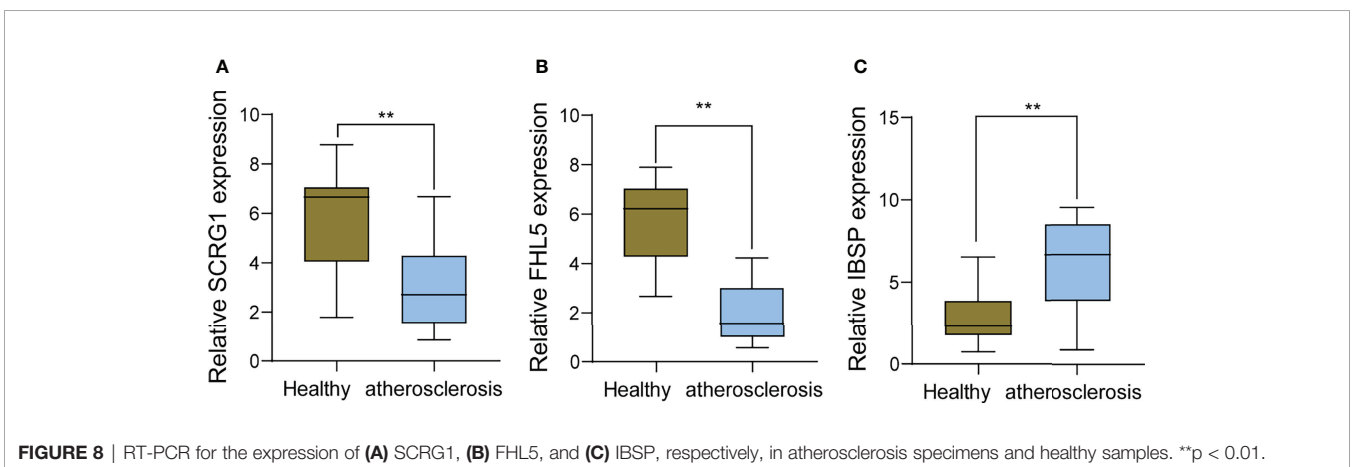


**FIGURE 8 |** RT-PCR for the expression of (A) SCRG1, (B) FHL5, and (C) IBSP, respectively, in atherosclerosis specimens and healthy samples. \*\*p < 0.01.

## DATA AVAILABILITY STATEMENT

The datasets presented in this study can be found in online repositories. The name of the repository and the accession numbers can be found below:

<https://www.ncbi.nlm.nih.gov/>, GSE43292

<https://www.ncbi.nlm.nih.gov/>, GSE57691

## ETHICS STATEMENT

The studies involving human participants were reviewed and approved by Suqian First Hospital. The patients/participants provided their written informed consent to participate in this study.

## AUTHOR CONTRIBUTIONS

YC conceived and designed the study. ZY, XW, and YL provided equal contributions to the research design, data analysis, and article writing. XW revised the manuscript. All authors contributed to the article and approved the submitted version.

## REFERENCES

- Libby P. The Changing Landscape of Atherosclerosis. *Nature* (2021) 592:524–33. doi: 10.1038/s41586-021-03392-8
- Libby P, Ridker PM, Hansson GK. Progress and Challenges in Translating the Biology of Atherosclerosis. *Nature* (2011) 473:317–25. doi: 10.1038/nature10146
- Schaftenaar F, Frodermann V, Kuiper J, Lutgens E. Atherosclerosis: The Interplay Between Lipids and Immune Cells. *Curr Opin Lipidol* (2016) 27:209–15. doi: 10.1097/MOL.0000000000000302
- Frostegård J. Immunity, Atherosclerosis and Cardiovascular Disease. *BMC Med* (2013) 11:117. doi: 10.1186/1741-7015-11-117
- Williams JW, Winkels H, Durant CP, Zaitsev K, Ghosheh Y, Ley K. Single Cell RNA Sequencing in Atherosclerosis Research. *Circ Res* (2020) 126:1112–26. doi: 10.1161/CIRCRESAHA.119.315940
- Tedgui A, Mallat Z. Cytokines in Atherosclerosis: Pathogenic and Regulatory Pathways. *Physiol Rev* (2006) 86:515–81. doi: 10.1152/physrev.00024.2005
- Lechner K, von Schacky C, McKenzie AL, Worm N, Nixdorff U, Lechner B, et al. Lifestyle Factors and High-Risk Atherosclerosis: Pathways and Mechanisms Beyond Traditional Risk Factors. *Eur J Prev Cardiol* (2020) 27:394–406. doi: 10.1177/2047487319869400
- Katsiki N, Mantzoros C, Mikhailidis DP. Adiponectin, Lipids and Atherosclerosis. *Curr Opin Lipidol* (2017) 28:347–54. doi: 10.1097/MOL.0000000000000431
- Barrington WT, Lusic AJ. Atherosclerosis: Association Between the Gut Microbiome and Atherosclerosis, *Nature Reviews. Cardiology* (2017) 14:699–700. doi: 10.1038/nrcardio.2017.169
- Sun W, Cai Z, Li Y, Liu F, Fang S, Wang G. Data Processing and Text Mining Technologies on Electronic Medical Records: A Review. *J Healthc Eng* (2018) 2018:4302425. doi: 10.1155/2018/4302425
- Alonso SG, de la Torre-Diez I, Hamrioui S, López-Coronado M, Barreno DC, Nozaleda LM, et al. Data Mining Algorithms and Techniques in Mental Health: A Systematic Review. *J Med Syst* (2018) 42:161. doi: 10.1007/s10916-018-1018-2
- Su W, Zhao Y, Wei Y, Zhang X, Ji J, Yang S. Exploring the Pathogenesis of Psoriasis Complicated With Atherosclerosis via Microarray Data Analysis. *Front Immunol* (2021) 12:667690. doi: 10.3389/fimmu.2021.667690

## FUNDING

This study was supported by the National Natural Science Foundation of China (81970387 and 81200213 to YC), Natural Science Foundation of Beijing (7172181 to YC), and Natural Science Foundation of Suqian (K201918 to ZY).

## SUPPLEMENTARY MATERIAL

The Supplementary Material for this article can be found online at: <https://www.frontiersin.org/articles/10.3389/fimmu.2022.905921/full#supplementary-material>

**Supplementary Figure 1** | Nine different types of infiltrating immune cells were linked to FHL5 expression in a scatter plot.

**Supplementary Figure 2** | Nine different types of infiltrating immune cells were linked to IBS expression in a scatter plot.

**Supplementary Figure 3** | Eight different types of infiltrating immune cells were linked to SCRG1 expression in a scatter plot.

- Zhu F, Zuo L, Hu R, Wang J, Yang Z, Qi X, et al. A Ten-Genes-Based Diagnostic Signature for Atherosclerosis. *BMC Cardiovasc Disord* (2021) 21:513. doi: 10.1186/s12872-021-02323-9
- Huang T, Wang K, Li Y, Ye Y, Chen Y, Wang J, et al. Construction of a Novel Ferroptosis-Related Gene Signature of Atherosclerosis. *Front Cell Dev Biol* (2021) 9:800833. doi: 10.3389/fcell.2021.800833
- Chen Q, Lv J, Yang W, Xu B, Wang Z, Yu Z, et al. Targeted Inhibition of STAT3 as a Potential Treatment Strategy for Atherosclerosis. *Theranostics* (2019) 9:6424–42. doi: 10.7150/thno.35528
- Preiss DJ, Sattar N. Vascular Cell Adhesion Molecule-1: A Viable Therapeutic Target for Atherosclerosis? *Int J Clin Pract* (2007) 61:697–701. doi: 10.1111/j.1742-1241.2007.01330.x
- Sasikala T, Manohar SM, Bitla ARR, Sarala S, Vaikkakara S. Intercellular Adhesion Molecule-1 is a Surrogate Biomarker for Subclinical Atherosclerosis in Type 2 Diabetes Mellitus. *Biomarkers Med* (2021) 15:121–32. doi: 10.2217/bmm-2020-0428
- Ayari H, Bricca G. Identification of Two Genes Potentially Associated in Iron-Heme Homeostasis in Human Carotid Plaque Using Microarray Analysis. *J Biosci* (2013) 38:311–5. doi: 10.1007/s12038-013-9310-2
- Biros E, Gäbel G, Moran CS, Schreurs C, Lindeman JH, Walker PJ, et al. Differential Gene Expression in Human Abdominal Aortic Aneurysm and Aortic Occlusive Disease. *Oncotarget* (2015) 6:12984–96. doi: 10.18632/oncotarget.3848
- Wu T, Hu E, Xu S, Chen M, Guo P, Dai Z, et al. Clusterprofiler 4.0: A Universal Enrichment Tool for Interpreting Omics Data. *Innovation (New York N.Y.)* (2021) 2:100141. doi: 10.1016/j.xinn.2021.100141
- Ito K, Murphy D. Application of Ggplot2 to Pharmacometric Graphics. *CPT: Pharmacometrics Syst Pharmacol* (2013) 2:e79. doi: 10.1038/psp.2013.56
- Bentzon JF, Otsuka F, Virmani R, Falk E. Mechanisms of Plaque Formation and Rupture. *Circ Res* (2014) 114:1852–66. doi: 10.1161/CIRCRESAHA.114.302721
- Schade DS, Shey L, Eaton RP. Cholesterol Review: A Metabolically Important Molecule. *Endocr Pract Off J Am Coll Endocrinol Am Assoc Clin Endocrinol* (2020) 26:1514–23. doi: 10.4158/EP-2020-0347
- Cainzos-Achirica M, Glassner K, Zawahir HS, Dey AK, Agrawal T, Quigley EMM, et al. Inflammatory Bowel Disease and Atherosclerotic Cardiovascular Disease: JACC Review Topic of the Week. *J Am Coll Cardiol* (2020) 76:2895–905. doi: 10.1016/j.jacc.2020.10.027

25. Liu Y, Liu N, Liu Q. Constructing a ceRNA-Immunoregulatory Network Associated With the Development and Prognosis of Human Atherosclerosis Through Weighted Gene Co-Expression Network Analysis. *Aging* (2021) 13:3080–100. doi: 10.18632/aging.202486
26. Chen Y, Zeng A, He S, He S, Li C, Mei W, et al. Autophagy-Related Genes in Atherosclerosis. *J Healthc Eng* (2021) 2021:6402206. doi: 10.1155/2021/6402206
27. Wang S, Dougherty EJ, Danner RL. Ppar $\gamma$  Signaling and Emerging Opportunities for Improved Therapeutics. *Pharmacol Res* (2016) 111:76–85. doi: 10.1016/j.phrs.2016.02.028
28. Wagner N, Wagner KD. The Role of PPARs in Disease. *Cells* (2020) 9:2367. (2020). doi: 10.3390/cells9112367
29. Sanz H, Valim C, Vegas E, Oller JM, Reverter F. vm-RFE: Selection and Visualization of the Most Relevant Features Through Non-Linear Kernels. *S BMC Bioinf* (2018) 19:432. doi: 10.1186/s12859-018-2451-4
30. Tibshirani R. The Lasso Method for Variable Selection in the Cox Model. *Stat Med* (1997) 16:385–95. doi: 10.1002/(SICI)1097-0258(19970228)16:4<385::AID-SIM380>3.0.CO;2-3
31. Jiang Z, Zhao L, Zhang X, Zhang W, Feng Y, Li T. Common Variants in KCNK5 and FHL5 Genes Contributed to the Susceptibility of Migraine Without Aura in Han Chinese Population. *Sci Rep* (2021) 11:6807. doi: 10.1038/s41598-021-86374-0
32. Wu K, Feng J, Lyu F, Xing F, Sharma S, Liu Y, et al. Exosomal miR-19a and IBSP Cooperate to Induce Osteolytic Bone Metastasis of Estrogen Receptor-Positive Breast Cancer. *Nat Commun* (2021) 12:5196. doi: 10.1038/s41467-021-25473-y
33. Wu JC, Luo SZ, Liu T, Lu LG, Xu MY. Linc-SCRG1 Accelerates Liver Fibrosis by Decreasing RNA-Binding Protein Tristetraprolin. *FASEB J Off Publ Fed Am Soc Exp Biol* (2019) 33:2105–15. doi: 10.1096/fj.201800098RR
34. Hansson GK, Hermansson A. The Immune System in Atherosclerosis. *Nat Immunol* (2011) 12:204–12. doi: 10.1038/ni.2001
35. Schäfer S, Zerneck A. CD8(+) T Cells in Atherosclerosis. *Cells* (2020) 10. doi: 10.3390/cells10010037
36. Guzik TJ, Skiba DS, Touyz RM, Harrison DG. The Role of Infiltrating Immune Cells in Dysfunctional Adipose Tissue. *Cardiovasc Res* (2017) 113:1009–23. doi: 10.1093/cvr/cvx108
37. Xiao Q, Li X, Li Y, Wu Z, Xu C, Chen Z, et al. Biological Drug and Drug Delivery-Mediated Immunotherapy. *Acta Pharmaceutica Sinica. B* (2021) 11:941–60. doi: 10.1016/j.apsb.2020.12.018
38. Rocha VZ, Libby P. Obesity, Inflammation, and Atherosclerosis. *Nature Reviews. Cardiology* (2009) 6:399–409. doi: 10.1038/nrcardio.2009.55

**Conflict of Interest:** The authors declare that the research was conducted in the absence of any commercial or financial relationships that could be construed as a potential conflict of interest.

**Publisher's Note:** All claims expressed in this article are solely those of the authors and do not necessarily represent those of their affiliated organizations, or those of the publisher, the editors and the reviewers. Any product that may be evaluated in this article, or claim that may be made by its manufacturer, is not guaranteed or endorsed by the publisher.

Copyright © 2022 Ye, Wang, Lv, Wang and Cui. This is an open-access article distributed under the terms of the Creative Commons Attribution License (CC BY). The use, distribution or reproduction in other forums is permitted, provided the original author(s) and the copyright owner(s) are credited and that the original publication in this journal is cited, in accordance with accepted academic practice. No use, distribution or reproduction is permitted which does not comply with these terms.





# Advances in Vaccine Development of the Emerging Novel Genotype Fowl Adenovirus 4

Aijing Liu<sup>1</sup>, Yu Zhang<sup>1</sup>, Hongyu Cui<sup>1</sup>, Xiaomei Wang<sup>1,2</sup>, Yulong Gao<sup>1\*</sup> and Qing Pan<sup>1\*</sup>

<sup>1</sup> State Key Laboratory of Veterinary Biotechnology, Harbin Veterinary Research Institute of Chinese Academy of Agricultural Sciences, Harbin, China, <sup>2</sup> Jiangsu Co-Innovation Center for Prevention and Control of Important Animal Infectious Disease and Zoonoses, Yangzhou University, Yangzhou, China

## OPEN ACCESS

### Edited by:

Chenhe Su,  
Wistar Institute, United States

### Reviewed by:

Zhenyu Zhang,  
University of Wisconsin-Madison,  
United States  
Wencheng Lin,  
South China Agricultural University,  
China

### \*Correspondence:

Qing Pan  
panqing20050101@126.com  
Yulong Gao  
gaoyulong@caas.cn

### Specialty section:

This article was submitted to  
Viral Immunology,  
a section of the journal  
Frontiers in Immunology

**Received:** 09 April 2022

**Accepted:** 27 April 2022

**Published:** 20 May 2022

### Citation:

Liu A, Zhang Y, Cui H, Wang X, Gao Y  
and Pan Q (2022) Advances in Vaccine  
Development of the Emerging Novel  
Genotype Fowl Adenovirus 4.  
*Front. Immunol.* 13:916290.  
doi: 10.3389/fimmu.2022.916290

Fowl adenovirus (FAdV) was first reported in Angara Goth, Pakistan, in 1987. For this reason, it is also known as “Angara disease.” It was later reported in China, Japan, South Korea, India, the United States, Canada, and other countries and regions, causing huge economic losses in the poultry industry worldwide. Notably, since June 2015, a natural outbreak of severe hydropericardium hepatitis syndrome (HHS), associated with a hypervirulent novel genotype FAdV-4 infection, has emerged in most provinces of China. The novel virus FAdV-4 spread rapidly and induced a 30-100% mortality rate, causing huge economic losses and threatening the green and healthy poultry breeding industry. Vaccines against FAdV-4, especially the emerging novel genotype, play a critical role and will be the most efficient tool for preventing and controlling HHS. Various types of FAdV-4 vaccines have been developed and evaluated, such as inactivated, live-attenuated, subunit, and combined vaccines. They have made great contributions to the control of HHS, but the details of cross-protection within FAdVs and the immunogenicity of different vaccines require further investigation. This review highlights the recent advances in developing the FAdV-4 vaccine and promising new vaccines for future research.

**Keywords:** HHS, vaccine advances, emerging, FAdV-4, novel genotype

## INTRODUCTION

Fowl adenovirus (FAdV) belongs to the family Adenoviridae and genus *Aviadenovirus* and is further divided into five species (FAdV-A-E) with 12 serotypes (FAdV-1-8a, 8b-11) based on the profile of restriction enzyme digestion and sera cross-neutralization assay according to the guidelines of the International Committee on Taxonomy of Viruses (1). FAdVs are capable of infecting various birds, such as chickens (2, 3), ducks (4–6), geese (7), pigeons (8), peacocks (9), and other wild birds, inducing severe clinical symptoms or potential infection. FAdVs show different tropisms for multiple organs and are associated with several high-impact poultry diseases, such as hydropericardium-hepatitis syndrome (HHS), inclusion body hepatitis (IBH), and gizzard erosion (GE). FAdV infection associated with HHS, IBH, and GE has been reported worldwide and induces huge economic losses in the poultry industry.

HHS associated with serotype 4 fowl adenovirus (FAdV-4) infection was first found and reported in Angara Goth, a region of Pakistan, in 1987, so the disease is also known as “Angara disease” (10). It was later reported in China (3, 11), Japan (12, 13), South Korea (14), India (15), the United States (16), Canada (17), and other countries and regions, causing huge economic losses in the poultry industry worldwide. Notably, since June 2015, a natural outbreak of severe HHS associated with a hypervirulent novel genotype FAdV-4 infection has emerged in most provinces of China (3, 11). The novel genotype FAdV-4 spread rapidly and induced a 30-100% mortality rate, causing huge economic losses and threatening the green and healthy poultry breeding industry. Furthermore, co-infections of FAdV-4 with other virus further aggravate the harmfulness of the disease (18–20).

Currently, various types of vaccines have been developed and evaluated to control HHS, and several inactivated combined vaccines have been licensed and produced by commercial companies, which have made important contributions to the poultry industry. Given the ability to deliver foreign adenovirus genes, natural non-pathogenic FAdV-4 (16) and artificial attenuated FAdV-4 (17) have developed efficient vaccine vectors, which protect chickens against HHS and significantly reduce the cost of the combined vaccine. This brief review summarizes vaccine development efforts using inactivated viruses, live-attenuated viruses, subunit antigens, and combined vaccines against FAdV-4, especially novel FAdV-4.

## Inactivated Monovalent Vaccines

Traditional inactivated vaccine immunization remains the main preventive method for some poultry diseases, especially emerging viruses such as SARS-CoV-2 (21, 22). Given the emergence of the hypervirulent novel genotype FAdV-4, inactivated vaccine immunization remains the main prevention method, having the advantages of safety, cost-saving, good humoral immunity effect, and low influence by maternal antibodies. For the emerging HHS, Pan et al. isolated and identified the HLJFAd15 strain as a novel hypervirulent FAdV-4 from the field layers with HHS in China in 2015 (2). Subsequently, SPF chickens were immunized with an inactivated oil-emulsion FAdV-4 vaccine formulated with the HLJFAd15 strain, and the vaccine’s protective effect was evaluated (23). The results indicated that the vaccine could provide a high-level antibody, preferential T helper 2 (Th2) response, and full protection against a lethal dose of novel hypervirulent FAdV-4. Similarly, the novel genotype SDJN0105 strain (24), HN strain (25), and CH/GZXF/1602 strain (26) developed an inactivated vaccine, and all vaccines induced high levels of antibodies and showed sufficient protection for chickens from HHS.

Du et al. attempted to develop vaccines from both embryo-adapted and cell culture-derived viruses to optimize the manufacturing technique of inactivated vaccines (25). The results showed no mortality in either of the immunized groups in the challenge experiment. However, cell-culture-derived vaccines could induce earlier and higher humoral immune responses and no lesions appeared, but IBH was observed in

the embryo-adapted derived vaccine, indicating that cell-culture-derived vaccines could be a better candidate to control emerging HHS.

For cross-protection of the FAdV-4 inactivated vaccine, Kim et al. developed an inactivated vaccine with a traditional FAdV-4 strain K531/07 and evaluated the cross-protection of the vaccine against various serotypes of FAdV causing IBH or HHS, including serotypes 5, 8a, 8b and 11 (27). They found that the inactivated FAdV-4 vaccine could provide cross-protection against various serotypes of FAdV in vaccinated chickens and progenies of vaccinated breeders, indicating that the FAdV-4 vaccine could be an effective candidate for the prevention of IBH and HHS. Furthermore, Xia et al. prepared an inactivated vaccine using a novel genotype FAdV-4 strain CH/GZXF/1602, and the immunogenicity evaluation results showed that the FAdV-4 vaccine could protect chickens against both virulent FAdV-4 and virulent FAdV-8b (26).

Notably, all inactivated vaccines were derived from wild-type virulent FAdV-4 strains. As biosafety threats of inactivated vaccines from potential pathogenic components have been presented to the poultry industry, safer vaccines are urgently needed. Zhang et al. replaced the virulent vaccine formulation with an artificial non-pathogenic FAdV-4 strain rHN20 using a reverse genetic technique and developed a novel inactivated oil-adjuvanted vaccine derived from the rHN20 strain (28). The results showed that the vaccine-induced high titers of neutralizing antibodies provided full protection from a lethal dose of virulent FAdV-4 challenge and significantly reduced potential biosafety threats. The details of inactivated vaccines are summarized in **Table 1**.

## Live-Attenuated Monovalent Vaccines

For the traditional genotype FAdV-4, Schonewille et al. developed an attenuated FAdV-4 vaccine by adapting a pathogenic virus to the QT35 cell line, and no clinical signs or mortality were observed in birds challenged with the attenuated virus (29). Although enzyme-linked immunosorbent assay (ELISA) and neutralization tests indicated a weak antibody response in some birds following immunization with the live vaccine, the vaccine provided full protection against the challenge, which is an interesting phenomenon for FAdVs.

For the novel genotype FAdV-4, Zhang et al. identified the critical gene and amino acid (aa) for virus virulence (30), subsequently, two non-pathogenic strains, rHN20 and rR188I, were rescued by the reverse genetic technique based on the fosmid system. rHN20 caused no clinical signs or mortality, indicating that hexon determines the virulence of FAdV-4. Furthermore, Zhang et al. identified aa 188R of hexon as the critical aa for virulence of the novel genotype FAdV-4, and the rR188I strain also showed no pathogenicity in SPF chickens. The immunogenicity of both rHN20 (28) and rR188I (30) was evaluated in SPF chickens when they were used as live-attenuated vaccines. Chickens inoculated with different doses and routes of rHN20 or rR188I produced high levels of neutralizing antibodies and were fully protected against a lethal dose challenge of the pathogenic novel genotype FAdV-4. Furthermore, the immunized groups showed no clinical

**TABLE 1** | List of inactivated and live-attenuated vaccines against FAdV-4.

Inactivated vaccine						Live-attenuated vaccine				
Strain	Origin	Adjuvant	Dosage (/bird)	Immune route	Survival rate (%)	Strain	Origin	Dosage (/bird)	Immune route	Survival rate (%)
HLJFAd15	CEL <sup>a</sup>	Oil	10 <sup>6</sup> TCID <sub>50</sub>	IM <sup>f</sup>	100	FAdV-4/QT35	QT35	5×10 <sup>4</sup> TCID <sub>50</sub>	IM	100
CH/GZXF/1602	CEK <sup>b</sup>	Oil	4.5×10 <sup>5</sup> TCID <sub>50</sub>	H <sup>g</sup>	100	rR188I	LMH	10 <sup>5</sup> PFU	IM	100
SDJN0105	CEF <sup>c</sup>	Oil	10 <sup>6</sup> TCID <sub>50</sub>	IM	100	rHN20	LMH	10 <sup>6</sup> PFU	IN	100
HN	LMH <sup>d</sup>	Oil	10 <sup>6</sup> TCID <sub>50</sub>	H <sup>h</sup>	100	rHN20	LMH	10 <sup>6</sup> PFU	IM	100
HN	CE <sup>e</sup>	Oil	10 <sup>6</sup> TCID <sub>50</sub>	H	100 (IBH)	rHN20	LMH	10 <sup>6</sup> PFU	H	100
K531/07	CEL	Seppic ISA 70	5×10 <sup>5</sup> TCID <sub>50</sub>	IM	80	FAdV4-RFP_F1	LMH	2×10 <sup>5</sup> TCID <sub>50</sub>	IM	100
rHN20	LMH	Oil	3×10 <sup>6</sup> PFU	IM	100	FA4-EGFP	LMH	10 <sup>6</sup> TCID <sub>50</sub>	IM	100
rHN20	LMH	Oil	3×10 <sup>6</sup> PFU	H	100	FAdV4-EGFP-rF2	LMH	2.5×10 <sup>4</sup> TCID <sub>50</sub>	IM	100

<sup>a</sup>Chicken embryo liver cells.

<sup>b</sup>Chicken embryo kidney cells.

<sup>c</sup>Chicken embryo fibroblast cells.

<sup>d</sup>Leghorn male hepatocellular cells.

<sup>e</sup>Chicken embryo.

<sup>f</sup>Intramuscular.

<sup>g</sup>Subcutaneous.

<sup>h</sup>Intranasal.

symptoms or histopathological changes, and the viral load was significantly lower after the challenge.

Not only was the hexon-edited virus significantly attenuated, but the fiber-1 and fiber-2 edited viruses were rescued and identified as non-pathogenic to SPF chickens. Mu et al. rescued the recombinant virus FAdV4-RFP\_F1 via the CRISPR/Cas9 technique, which contained a fusion protein of RFP and fiber-1 (31). The recombinant virus was efficiently attenuated and provided full protection against the lethal challenge of FAdV-4, demonstrating that fiber-1-edited FAdV4-RFP\_F1 could be a live-attenuated vaccine candidate and fiber-1 could be a potential insertion site for novel vaccine development. In addition, Xie et al. generated a recombinant virus FA4-EGFP expressing EGFP-fiber-2 fusion protein via the CRISPR/Cas9 technique (32). FA4-EGFP caused no clinical signs or mortality in chickens, indicating that the virus was significantly attenuated.

Moreover, FA4-EGFP could also provide efficient protection against a lethal dose challenge, suggesting that fiber-2 edited FA4-EGFP is a vaccine candidate and a potential insertion site for delivering foreign antigens. Furthermore, Xie et al. replaced the fiber-2 gene with *egfp* and rescued FAdV-4-EGFP-rF2, which could efficiently replicate in LMH-F2 cell lines expressing fiber-2 protein (33). FAdV-4-EGFP-rF2 was highly attenuated and provided full protection against the pathogenic FAdV-4 challenge. The FAdV-4-EGFP-rF2 vaccine-induced neutralizing antibodies are at the same level as FA4-EGFP. The details of live-attenuated monovalent vaccines are summarized in **Table 1**.

## Subunit Monovalent Vaccines

Subunit vaccines are safer than vaccines based on the whole virus in production and vaccination procedures, and researchers have made important efforts to develop subunit vaccines against FAdV-4. Different subunit antigens, expression systems, and adjuvants have been evaluated to develop FAdV-4 subunit vaccines.

Before the novel genotype FAdV-4, several studies tried to develop a subunit vaccine of the traditional genotype FAdV-4.

Shah et al. utilized a prokaryotic expressed structure protein penton base coupled with Freund's complete adjuvant (FCA) to develop a subunit vaccine that showed 90% protection for chickens (34). Aziz et al. evaluated both the prokaryotic expressed full-length and epitope-focused 1-225 aa of penton formulated with Montanide ISA 71VG adjuvant, and both vaccines showed protection rates of 50% (35). Schachner et al. compared the immunogenicity of different capsid proteins of FAdV-4, including fiber-1, fiber-2, and L1 region of hexon (L1-hexon) (36). Fiber-1, fiber-2, and L1-hexon were simultaneously expressed in the baculovirus system and composed of GERBU Adjuvant LQ no.3000, and fiber-2 (27/28) showed better protection efficacy than fiber-1 (16/26) and L1-hexon (7/26), highlighting that fiber-2 might be an ideal antigen component for subunit vaccine development. Shah et al. first tried a prokaryotic-expressed non-structural protein 100 K of FAdV-4 coupled with FCA; unfortunately, it showed only a 40% protection rate (37).

Although HHS associated with a novel genotype FAdV-4 emerged in 2015, great progress has been made in subunit vaccine development. Wang et al. tested the efficacy of FAdV-4 surface protein fiber-1, fiber-2, L1-hexon, and penton base expressed in *Escherichia coli* and formulated with FCA (38). The results indicated that fiber-2 (50 µg/bird) and fiber-1 (100 µg/bird) could induce complete protection, while protection of the L1-hexon and penton bases could induce considerable protection at high dosages but not completely. The good immunogenicity of prokaryotic expressed fiber-2 was further confirmed when fiber-2 was coupled with different adjuvants, such as FCA (39), Montanide ISA 71VG (40), and Sigma adjuvant (41), respectively. However, fiber-1 showed better protection than fiber-2 when expressed in a eukaryotic system, although the protection rates of both fiber-1 and fiber-2 were higher than those of the penton base (42). Wang et al. utilized a commercial adenovirus vector to express antigens in HEK293 cells, and the antigen was assembled into a penton-

dodecahedron (Pt-Dd), which provided 100% protection (42). Jia et al. constructed a recombinant *Lactococcus lactis* and *Enterococcus faecalis* expressing truncated hexon protein or fused with a dendritic cell-targeting peptide, which was orally immunized and induced protection rates varying from 50 to 90% (43). These studies provide a solid theoretical basis for the research and development of subunit vaccines.

In addition, several studies have been conducted to obtain many results. Yin et al. constructed a pVAX1-Fiber2 DNA vaccine, but the protection was also insufficient (60%) for the novel genotype FAdV-4, and the above studies require further optimization (41). Nevertheless, many improvements have achieved good results. Hu et al. developed a fusion subunit antigen of fiber-2 (Gly275- Pro479) and hexon (Met21-Val51) that was capable of providing full protection for chickens (44). Tufail et al. displayed several highly conserved epitopic regions of hexon on the virus-like particle (VLP) of the core protein of the hepatitis B virus (45). The VLP vaccine containing Asp348-Phe369, Ser19-Pro82, and Gly932-Phe956 confer 90%, 70%, and

40% protection. The details of subunit vaccines against FAdV-4 are summarized in **Table 2**.

## Combined Vaccines

Adenovirus, especially the commercial human adenovirus, is an efficient and stable delivery carrier widely used for gene therapy (46) and vaccines against emergent viruses, such as Ebola (47) and SARS-CoV-2 (48). With gene editing and reverse genetic technology, the emerging novel genotype, FAdV-4, has been successfully modified as a viral vector and applied to construct combined vaccines. Pan et al. firstly developed a novel genotype, FAdV-4, and identified the natural large genomic 1966bp deletion as a foreign gene insertion site (49). Mu et al. also optimized the CRISPR/Cas9 operating platform to insert a foreign gene into the fiber gene of FAdV-4 (31). Meanwhile, Yan et al. established an easy-to-use reverse genetics system based on Gibson assembly to modify the right and partial left genes (50). Pei et al. developed an infectious clone based on cosmid and found that ORF16 and 17 were important for virus

**TABLE 2** | List of subunit vaccines against FAdV-4.

Subunit vaccine						
Antigen	Strain	Expression system	Dosage (/bird)	Adjuvant	Immune route	Survival rate (%)
penton	PR-06	<i>E. coli</i> <sup>e</sup>	25 µg	FCA <sup>h</sup>	H <sup>i</sup>	90
penton	NIAB/NIBGE 01	<i>E. coli</i>	100 µg	Montanide ISA 71VG	H	50
penton (1-225 aa <sup>a</sup> )	NIAB/NIBGE 01	<i>E. coli</i>	100 µg	Montanide ISA 71VG	H	50
fiber-1	KR5	Baculovirus	50 µg	GERBU Adjuvant LQ no.3000	IM <sup>j</sup>	61.5
fiber-2	KR5	Baculovirus	50 µg	GERBU Adjuvant LQ no.3000	IM	96.4
L1-hexon <sup>b</sup>	KR5	Baculovirus	50 µg	GERBU Adjuvant LQ no.3000	IM	26.9
100K	NIAB/NIBGE 01	<i>E. coli</i>	25 µg	FCA	H	40
fiber-1	SXD15	<i>E. coli</i>	100 µg	FCA	IM	100
			50 µg	FCA	IM	75
fiber-2	SXD15	<i>E. coli</i>	50 µg	FCA	IM	100
L1-hexon	SXD15	<i>E. coli</i>	50 µg	FCA	IM	70
penton	SXD15	<i>E. coli</i>	50 µg	FCA	IM	35
fiber-2	HB1501	<i>E. coli</i>	2.5 µg	FCA	H	100
fiber-2	–	<i>E. coli</i>	10 µg	Montanide ISA 71VG	IM	100
fiber-2	GZ-QL	<i>E. coli</i>	150 µg	Sigma	IM	100
			100 µg	Sigma	IM	100
			50 µg	Sigma	IM	80
fiber-1	SXD15	Ad-HK2	0.5 µg	N/A <sup>l</sup>	IM	100
fiber-2	SXD15	Ad-HK2	0.5 µg	N/A	IM	80
penton	SXD15	Ad-HK2	0.5 µg	N/A	IM	67.7
PtDd <sup>c</sup>	SXD15	Ad-HK2	0.5 µg	N/A	IM	100
DC-hexon <sup>d</sup>	GX01	<i>L. lactis</i> <sup>f</sup>	10 <sup>10</sup> CFU	N/A	O <sup>k</sup>	60
hexon	GX01	<i>L. lactis</i>	10 <sup>10</sup> CFU	N/A	O	50
DC-Hexon	GX01	<i>E. faecalis</i> <sup>g</sup>	5×10 <sup>9</sup> CFU	N/A	O	90
hexon	GX01	<i>E. faecalis</i>	5×10 <sup>9</sup> CFU	N/A	O	80

<sup>a</sup>Amino acid.

<sup>b</sup>Loop 1 region of hexon.

<sup>c</sup>Penton-dodecahedron.

<sup>d</sup>DC-Hexon: hexon fused with dendritic cell targeting peptide.

<sup>e</sup>*Escherichia coli*.

<sup>f</sup>*Lactococcus lactis*.

<sup>g</sup>*Enterococcus faecalis*.

<sup>h</sup>Freund's complete adjuvant.

<sup>i</sup>Subcutaneous.

<sup>j</sup>Intramuscular.

<sup>k</sup>Oral.

<sup>l</sup>Not applicable.

replication and unsuitable for foreign gene insertion (51). Finally, Pan et al. built a reverse genetic technique based on the fosmid system to operate the genome of the novel genotype FAdV-4 and further identified 10 ORFs at the left end and 13 ORFs at the right end of the novel FAdV-4 as non-essential regions for virus replication, which provided a good foundation for foreign gene delivery (52).

Virulence weakening is critical for vector development because of the high pathogenicity of the novel genotype FAdV-4. Zhang et al. first identified the critical gene and key aa for the virulence of the novel FAdV-4 (30) and subsequently obtained the non-pathogenic strain rHN20, posting the basis for development and application. Subsequently, the immunogenetic VP2 gene of the very virulent infectious bursal disease virus (vvIBDV) was inserted into the natural 1966Del deletion site and induced complete protection in chickens against both the novel genotype FAdV-4 and vvIBDV challenge when used as an inactivated vaccine (53) or live vectored vaccine (52). Lu et al. inserted a FAdV-8b fiber into the fiber-2 position of FAdV-4, which simultaneously protected chickens from novel genotype FAdV-4 induced HHS and FAdV-8b induced IBH (54).

In addition to the above FAdV-4 vectored vaccines, several other combined vaccines were evaluated and showed good effects. Luca et al. constructed a chimeric fiber protein (crecFib-4/11) capable of simultaneously protecting chickens against HHS and IBH (55), highlighting a new concept: chimeric fiber vaccines can be extended across viral species. Tian et al. developed a recombinant Newcastle disease virus (NDV) LaSota vaccine strain expressing fiber-2 of FAdV-4 (rLaSota-fiber2) and live and inactivated vaccines derived from rLaSota-fiber2 (56). Both vaccines provided complete protection against virulent NDV. However, the live rLaSota-fiber2 vaccine provided better protection against the FAdV-4 challenge than the inactivated vaccine, indicating that the NDV-vectored FAdV-4 vaccine is a promising bivalent vaccine candidate to control both HHS and ND.

## REFERENCES

1. Steer PA, Kirkpatrick NC, O'Rourke D, Noormohammadi AH. Classification of Fowl Adenovirus Serotypes by Use of High-Resolution Melting-Curve Analysis of the Hexon Gene Region. *J Clin Microbiol* (2009) 47:311–21. doi: 10.1128/jcm.01567-08
2. Pan Q, Liu L, Wang Y, Zhang Y, Qi X, Liu C, et al. The First Whole Genome Sequence and Pathogenicity Characterization of a Fowl Adenovirus 4 Isolated From Ducks Associated With Inclusion Body Hepatitis and Hydropericardium Syndrome. *Avian Pathol* (2017) 46:571–78. doi: 10.1080/03079457.2017.1311006
3. Liu Y, Wan W, Gao D, Li Y, Yang X, Liu H, et al. Genetic Characterization of Novel Fowl Adenovirus 4 Isolates From Outbreaks of Hepatitis-Hydropericardium Syndrome in Broiler Chickens in China. *Emerg Microbes Infect* (2016) 5:e117. doi: 10.1038/emi.2016.115
4. Pan Q, Yang Y, Shi Z, Liu L, Gao Y, Qi X, et al. Different Dynamic Distribution in Chickens and Ducks of the Hypervirulent, Novel Genotype Fowl Adenovirus Serotype 4 Recently Emerged in China. *Front Microbiol* (2017) 8:1005. doi: 10.3389/fmicb.2017.01005
5. Chen H, Dou Y, Zheng X, Tang Y, Zhang M, Zhang Y, et al. Hydropericardium Hepatitis Syndrome Emerged in Cherry Valley Ducks in China. *Transbound Emerg Dis* (2017) 64:1262–67. doi: 10.1111/tbed.12500

## CONCLUSIONS

Although various vaccines against the novel genotype FAdV-4 have been developed, and great progress has been made in controlling emerging HHS, many studies need further investigation. Preliminary evaluation of the inactivated vaccine derived from the traditional genotype FAdV-4 has been conducted in cross-protection with other serotypes of FAdV, but cross-protection vaccines based on the novel genotype FAdV-4 need systemic analysis within different serotypes of FAdV. Furthermore, the FAdV-4 vaccine vector needs to be deeply explored as an efficient vector to deliver multiple foreign antigens to reduce vaccine costs further. Meanwhile, studies on novel vaccine adjuvants, subunit antigens, and new vaccines such as DNA or mRNA vaccines against the novel genotype FAdV-4 have been limited, and more research is needed on the control of HHS.

## AUTHOR CONTRIBUTIONS

QP and YG conceived of and designed the study. AL and YZ conducted the literature search, analysis, and draft-writing. HC and XW helped write the research questions in the first draft and the modifications. All the authors contributed to the study and approved the final manuscript for publication.

## FUNDING

This study was supported in part by the National Natural Science Foundation of China (32072879), the China Agriculture Research System (CARS-41-G15), and the Natural Science Foundation of Heilongjiang Province (TD2019C003).

6. Tang Z, Liu M, Gao Z, Li M, Cao J, Ye H, et al. Pathogenicity and Virus Shedding Ability of Fowl Adenovirus Serotype 4 to Ducks. *Vet Microbiol* (2022) 264:109302. doi: 10.1016/j.vetmic.2021.109302
7. Wei Z, Liu H, Diao Y, Li X, Zhang S, Gao B, et al. Pathogenicity of Fowl Adenovirus (FadV) Serotype 4 Strain SDJN in Taizhou Geese. *Avian Pathol* (2019) 48:477–85. doi: 10.1080/03079457.2019.1625305
8. Hess M, Prusas C, Vereecken M, And De Herdt P Isolation of Fowl Adenoviruses Serotype 4 From Pigeons With Hepatic Necrosis. *Berl Munch Tierarztl Wochenschr* (1998) 111:140–2.
9. Wang X, Li D, Deng Y, Yang X, Li Y, Wang Z, et al. Molecular Characterization and Pathogenicity of a Fowl Adenovirus Serotype 4 Isolated From Peacocks Associated With Hydropericardium Hepatitis Syndrome. *Infect Genet Evol* (2021) 90:104766. doi: 10.1016/j.meegid.2021.104766
10. Afzal M, Muneer R, And Stein G Studies on the Aetiology of Hydropericardium Syndrome (Angara Disease) in Broilers. *Vet Rec* (1991) 128:591–3. doi: 10.1136/vr.128.25.591
11. Ye J, Liang G, Zhang J, Wang W, Song N, Wang P, et al. Outbreaks of Serotype 4 Fowl Adenovirus With Novel Genotype, China. *Emerg Microbes Infect* (2016) 5:e50. doi: 10.1038/emi.2016.50
12. Del Valle FP, Camba SI, Umali DV, Sasai K, Shirota K, Katoh H, et al. Research Note: Molecular and Pathologic Characterization of Avian

- Adenovirus Isolated From the Oviducts of Laying Hens in Eastern Japan. *Poult Sci* (2020) 99:2459–68. doi: 10.1016/j.psj.2019.12.059
13. Mase M, Tanaka Y, Iseki H, And Watanabe S Genomic Characterization of a Fowl Adenovirus Serotype 4 Strain Isolated From a Chicken With Hydropericardium Syndrome in Japan. *Arch Virol* (2022) 167:1191–95. doi: 10.1007/s00705-022-05390-1
  14. Lai VD, Min K, Lai HTL, And Mo J Epidemiology of Fowl Adenovirus (FadV) Infections in South Korean Chickens During 2013–2019 Following Introduction of FAdV-4 Vaccines. *Avian Pathol* (2021) 50:182–89. doi: 10.1080/03079457.2021.1872766
  15. Chitradevi S, Sukumar K, Suresh P, Balasubramaniam GA, And Kannan D Molecular Typing and Pathogenicity Assessment of Fowl Adenovirus Associated With Inclusion Body Hepatitis in Chicken From India. *Trop Anim Health Prod* (2021) 53:412. doi: 10.1007/s11250-021-02851-8
  16. Mete A, Armien AG, Rejmanek D, Mott M, Crossley BM. Emergence of Fowl Aviadennovirus C-4 in a Backyard Chicken Flock in California. *J Vet Diagn Invest* (2021) 33:806–09. doi: 10.1177/104063872111019962
  17. Grgić H, Poljak Z, Sharif S, And Nagy É Pathogenicity and Cytokine Gene Expression Pattern of a Serotype 4 Fowl Adenovirus Isolate. *PLoS One* (2013) 8:e77601. doi: 10.1371/journal.pone.0077601
  18. Liu J, Shi X, Lv L, Wang K, Yang Z, Li Y, et al. Characterization of Co-infection With Fowl Adenovirus Serotype 4 and 8a. *Front Microbiol* (2021) 12:771805. doi: 10.3389/fmicb.2021.771805
  19. Xu AH, Sun L, Tu KH, Teng QY, Xue J, Zhang GZ. Experimental Co-Infection of Variant Infectious Bursal Disease Virus and Fowl Adenovirus Serotype 4 Increases Mortality and Reduces Immune Response in Chickens. *Vet Res* (2021) 52:61. doi: 10.1186/s13567-021-00932-y
  20. Yan T, Zhu S, Wang H, Li C, Diao Y, And Tang Y Synergistic Pathogenicity in Sequential Coinfection With Fowl Adenovirus Type 4 and Avian Orthoreovirus. *Vet Microbiol* (2020) 251:108880. doi: 10.1016/j.vetmic.2020.108880
  21. Gao Q, Bao L, Mao H, Wang L, Xu K, Yang M, et al. Development of an Inactivated Vaccine Candidate for SARS-Cov-2. *Sci* (2020) 369:77–81. doi: 10.1126/science.abc1932
  22. Wang H, Zhang Y, Huang B, Deng W, Quan Y, Wang W, et al. Development of an Inactivated Vaccine Candidate, Bbip-CorV, With Potent Protection Against SARS-Cov-2. *Cell* (2020) 182:713–21.e9. doi: 10.1016/j.cell.2020.06.008
  23. Pan Q, Yang Y, Gao Y, Qi X, Liu C, Zhang Y, et al. An Inactivated Novel Genotype Fowl Adenovirus 4 Protects Chickens Against the Hydropericardium Syndrome That Recently Emerged in China. *Viruses* (2017) 9:216. doi: 10.3390/v9080216
  24. Meng K, Yuan X, Yu J, Zhang Y, Ai W, Wang Y. Identification, Pathogenicity of Novel Fowl Adenovirus Serotype 4 SDJN0105 in Shandong, China and Immunoprotective Evaluation of the Newly Developed Inactivated Oil-Emulsion FAdV-4 Vaccine. *Viruses* (2019) 11:627. doi: 10.3390/v11070627
  25. Du D, Zhang P, Li X, Tian H, Cheng Y, Sheng D, et al. Cell-Culture Derived Fowl Adenovirus Serotype 4 Inactivated Vaccine Provides Complete Protection for Virus Infection on SPF Chickens. *Virus Disease* (2017) 28:182–88. doi: 10.1007/s13337-017-0372-x
  26. Xia J, Yao KC, Liu YY, You GJ, Li SY, Liu P, et al. Isolation and Molecular Characterization of Prevalent Fowl Adenovirus Strains in Southwestern China During 2015–2016 for the Development of a Control Strategy. *Emerg Microbes Infect* (2017) 6:e103. doi: 10.1038/emi.2017.91
  27. Kim MS, Lim TH, Lee DH, Youn HN, Yuk SS, Kim BY, et al. An Inactivated Oil-Emulsion Fowl Adenovirus Serotype 4 Vaccine Provides Broad Cross-Protection Against Various Serotypes of Fowl Adenovirus. *Vaccine* (2014) 32:3564–8. doi: 10.1016/j.vaccine.2014.03.015
  28. Zhang Y, Pan Q, Guo R, Liu A, Xu Z, Gao Y, et al. Immunogenicity of Novel Live Vaccine Based on an Artificial Rhn20 Strain Against Emerging Fowl Adenovirus 4. *Viruses* (2021) 13:2153. doi: 10.3390/v13112153
  29. Schonewille E, Jaspers R, Paul G, Hess M. Specific-pathogen-free Chickens Vaccinated With a Live FAdV-4 Vaccine are Fully Protected Against a Severe Challenge Even in the Absence of Neutralizing Antibodies. *Avian Dis* (2010) 54:905–10. doi: 10.1637/8999-072309-Reg.1
  30. Zhang Y, Liu A, Wang Y, Cui H, Gao Y, Qi X, et al. A Single Amino Acid at Residue 188 of the Hexon Protein Is Responsible for the Pathogenicity of the Emerging Novel Virus Fowl Adenovirus 4. *J Virol* (2021) 95:e0060321. doi: 10.1128/jvi.00603-21
  31. Mu Y, Xie Q, Wang W, Lu H, Lian M, Gao W, et al. A Novel Fiber-1-Edited and Highly Attenuated Recombinant Serotype 4 Fowl Adenovirus Confers Efficient Protection Against Lethal Challenge. *Front Vet Sci* (2021) 8:759418. doi: 10.3389/fvets.2021.759418
  32. Xie Q, Cao S, Zhang W, Wang W, Li L, Kan Q, et al. A Novel fiber-2-edited Live Attenuated Vaccine Candidate Against the Highly Pathogenic Serotype 4 Fowl Adenovirus. *Vet Res* (2021) 52:35. doi: 10.1186/s13567-021-00907-z
  33. Xie Q, Wang W, Kan Q, Mu Y, Zhang W, Chen J, et al. FAdV-4 Without Fiber-2 Is a Highly Attenuated and Protective Vaccine Candidate. *Microbiol Spectr* (2022) 10:e0143621. doi: 10.1128/spectrum.01436-21
  34. Shah MS, Ashraf A, Rahman M, Khan MI, Qureshi JAA. Subunit Vaccine Against Hydropericardium Syndrome Using Adenovirus Penton Capsid Protein. *Vaccine* (2012) 30:7153–6. doi: 10.1016/j.vaccine.2012.10.013
  35. Aziz F, Tufail S, Shah MA, Salahuddin Shah M, Habib M, Mirza O, et al. In Silico Epitope Prediction and Immunogenic Analysis for Penton Base Epitope-Focused Vaccine Against Hydropericardium Syndrome in Chicken. *Virus Res* (2019) 273:197750. doi: 10.1016/j.virusres.2019.197750
  36. Schachner A, Marek A, Jaskulska B, Bilic I, Hess M. Recombinant FAdV-4 Fiber-2 Protein Protects Chickens Against Hepatitis-Hydropericardium Syndrome (HHS). *Vaccine* (2014) 32:1086–92. doi: 10.1016/j.vaccine.2013.12.056
  37. Shah MS, Ashraf A, Khan MI, Rahman M, Habib M, Qureshi JA. Molecular Cloning, Expression and Characterization of 100K Gene of Fowl Adenovirus-4 for Prevention and Control of Hydropericardium Syndrome. *Biologicals* (2016) 44:19–23. doi: 10.1016/j.biologicals.2015.10.002
  38. Wang X, Tang Q, Chu Z, Wang P, Luo C, Zhang Y, et al. Immune Protection Efficacy of FAdV-4 Surface Proteins fiber-1, fiber-2, Hexon and Penton Base. *Virus Res* (2018) 245:1–6. doi: 10.1016/j.virusres.2017.12.003
  39. Ruan S, Zhao J, Yin X, He Z, Zhang GA. Subunit Vaccine Based on Fiber-2 Protein Provides Full Protection Against Fowl Adenovirus Serotype 4 and Induces Quicker and Stronger Immune Responses Than an Inactivated Oil-Emulsion Vaccine. *Infect Genet Evol* (2018) 61:145–50. doi: 10.1016/j.meegid.2018.03.031
  40. Chen L, Yin L, Zhou Q, Li Q, Luo Y, Xu Z, et al. Immunogenicity and Protective Efficacy of Recombinant Fiber-2 Protein in Protecting SPF Chickens Against Fowl Adenovirus 4. *Vaccine* (2018) 36:1203–08. doi: 10.1016/j.vaccine.2018.01.028
  41. Yin D, He L, Zhu E, Fang T, Yue J, Wen M, et al. A Fowl Adenovirus Serotype 4 (Fadv-4) Fiber2 Subunit Vaccine Candidate Provides Complete Protection Against Challenge With Virulent FAdV-4 Strain in Chickens. *Vet Microbiol* (2021) 263:109250. doi: 10.1016/j.vetmic.2021.109250
  42. Wang X, Tang Q, Qiu L, Yang Z. Penton-dodecahedron of Fowl Adenovirus Serotype 4 as a Vaccine Candidate for the Control of Related Diseases. *Vaccine* (2019) 37:839–47. doi: 10.1016/j.vaccine.2018.12.041
  43. Jia Z, Ma C, Yang X, Pan X, Li G, Ma D. Oral Immunization of Recombinant Lactococcus Lactis and Enterococcus Faecalis Expressing Dendritic Cell Targeting Peptide and Hexon Protein of Fowl Adenovirus 4 Induces Protective Immunity Against Homologous Infection. *Front Vet Sci* (2021) 8:632218. doi: 10.3389/fvets.2021.632218
  44. Hu J, Li G, Wang X, Cai L, Rong M, Li H, et al. Development of a Subunit Vaccine Based on Fiber2 and Hexon Against Fowl Adenovirus Serotype 4. *Virus Res* (2021) 305:198552. doi: 10.1016/j.virusres.2021.198552
  45. Tufail S, Shah MA, Zafar M, Asif TA, Shehzad A, Shah MS, et al. Identification of Potent Epitopes on Hexon Capsid Protein and Their Evaluation as Vaccine Candidates Against Infections Caused by Members of Adenoviridae Family. *Vaccine* (2021) 39:3560–64. doi: 10.1016/j.vaccine.2021.05.023
  46. Arnone CM, Polito VA, Mastronuzzi A, Carai A, Diomedei FC, Antonucci L, et al. Oncolytic Adenovirus and Gene Therapy With EphA2-BiTE for the Treatment of Pediatric High-Grade Gliomas. *J Immunother Cancer* (2021) 9:e001930. doi: 10.1136/jitc-2020-001930
  47. Zhu FC, Wurie AH, Hou LH, Liang Q, Li YH, Russell JB, et al. Safety and Immunogenicity of a Recombinant Adenovirus Type-5 Vector-Based Ebola Vaccine in Healthy Adults in Sierra Leone: A Single-Centre, Randomised, Double-Blind, Placebo-Controlled, Phase 2 Trial. *Lancet* (2017) 389:621–28. doi: 10.1016/s0140-6736(16)32617-4

48. Wu S, Zhong G, Zhang J, Shuai L, Zhang Z, Wen Z, et al. A Single Dose of an Adenovirus-Vectored Vaccine Provides Protection Against SARS-CoV-2 Challenge. *Nat Commun* (2020) 11:4081. doi: 10.1038/s41467-020-17972-1
49. Pan Q, Wang J, Gao Y, Cui H, Liu C, Qi X, et al. The Natural Large Genomic Deletion Is Unrelated to the Increased Virulence of the Novel Genotype Fowl Adenovirus 4 Recently Emerged in China. *Viruses* (2018) 10:494. doi: 10.3390/v10090494
50. Yan B, Zou X, Liu X, Zhao J, Zhang W, Guo X, et al. User-Friendly Reverse Genetics System for Modification of the Right End of Fowl Adenovirus 4 Genome. *Viruses* (2020) 12:301. doi: 10.3390/v12030301
51. Pei Y, Corredor JC, Griffin BD, Krell PJ, Nagy É. Fowl Adenovirus 4 (Fadv-4)-Based Infectious Clone for Vaccine Vector Development and Viral Gene Function Studies. *Viruses* (2018) 10:97. doi: 10.3390/v10020097
52. Pan Q, Zhang Y, Liu A, Cui H, Gao Y, Qi X, et al. Development of a Novel Avian Vaccine Vector Derived From the Emerging Fowl Adenovirus 4. *Front Microbiol* (2021) 12:780978. doi: 10.3389/fmicb.2021.780978
53. Zhang Y, Liu A, Jiang N, Qi X, Gao Y, Cui H, et al. A Novel Inactivated Bivalent Vaccine for Chickens Against Emerging Hepatitis-Hydropericardium Syndrome and Infectious Bursal Disease. *Vet Microbiol* (2022) 266:109375. doi: 10.1016/j.vetmic.2022.109375
54. Lu H, Xie Q, Zhang W, Zhang J, Wang W, Lian M, et al. A Novel Recombinant FAdV-4 Virus With Fiber of FAdV-8b Provides Efficient Protection Against Both FAdV-4 and Fadv-8b. *Viruses* (2022) 14:376. doi: 10.3390/v14020376
55. De Luca C, Schachner A, Heidl S, Hess M. Vaccination With a Fowl Adenovirus Chimeric Fiber Protein (crecFib-4/11) Simultaneously Protects Chickens Against Hepatitis-Hydropericardium Syndrome (HHS) and Inclusion Body Hepatitis (IBH). *Vaccine* (2022) 40:1837–45. doi: 10.1016/j.vaccine.2022.01.060
56. Tian KY, Guo HF, Li N, Zhang YH, Wang Z, Wang B, et al. Protection of Chickens Against Hepatitis-Hydropericardium Syndrome and Newcastle Disease With a Recombinant Newcastle Disease Virus Vaccine Expressing the Fowl Adenovirus Serotype 4 Fiber-2 Protein. *Vaccine* (2020) 38:1989–97. doi: 10.1016/j.vaccine.2020.01.006

**Conflict of Interest:** The authors declare that the research was conducted without potential commercial or financial relationships construed as a potential conflict of interest.

**Publisher's Note:** All claims expressed in this article are solely those of the authors and do not necessarily represent those of their affiliated organizations, or those of the publisher, the editors and the reviewers. Any product that may be evaluated in this article, or claim that may be made by its manufacturer, is not guaranteed or endorsed by the publisher.

Copyright © 2022 Liu, Zhang, Cui, Wang, Gao and Pan. This is an open-access article distributed under the terms of the Creative Commons Attribution License (CC BY). The use, distribution or reproduction in other forums is permitted, provided the original author(s) and the copyright owner(s) are credited and that the original publication in this journal is cited, in accordance with accepted academic practice. No use, distribution or reproduction is permitted which does not comply with these terms.



# Bat Employs a Conserved MDA5 Gene to Trigger Antiviral Innate Immune Responses

Jie Wang, Zhenyu Lin, Qiuju Liu, Feiyu Fu, Zhaofei Wang, Jingjiao Ma, Hengan Wang, Yaxian Yan, Yuqiang Cheng\* and Jianhe Sun\*

Shanghai Key Laboratory of Veterinary Biotechnology, Key Laboratory of Urban Agriculture (South), Ministry of Agriculture, School of Agriculture and Biology, Shanghai Jiao Tong University, Shanghai, China

## OPEN ACCESS

### Edited by:

Chenhe Su,  
Wistar Institute, United States

### Reviewed by:

Xiaoqian Gong,  
Wageningen University and Research,  
Netherlands  
Peng Xia,  
Massachusetts General Hospital and  
Harvard Medical School, United States

### \*Correspondence:

Jianhe Sun  
sunjhe@sjtu.edu.cn  
Yuqiang Cheng  
wyyqyq@sjtu.edu.cn

### Specialty section:

This article was submitted to  
Viral Immunology,  
a section of the journal  
Frontiers in Immunology

Received: 25 March 2022

Accepted: 22 April 2022

Published: 23 May 2022

### Citation:

Wang J, Lin Z, Liu Q, Fu F, Wang Z,  
Ma J, Wang H, Yan Y, Cheng Y  
and Sun J (2022) Bat Employs a  
Conserved MDA5 Gene to Trigger  
Antiviral Innate Immune Responses.  
*Front. Immunol.* 13:904481.  
doi: 10.3389/fimmu.2022.904481

Bats are important hosts for various zoonotic viral diseases. However, they rarely show signs of disease infection with such viruses. As the first line for virus control, the innate immune system of bats attracted our full attention. In this study, the *Tadarida brasiliensis* MDA5 gene (batMDA5), a major sensor for anti-RNA viral infection, was first cloned, and its biological functions in antiviral innate immunity were identified. Bioinformatics analysis shows that the amino acid sequence of batMDA5 is poorly conserved among species, and it is evolutionarily closer to humans. The mRNA of batMDA5 was significantly upregulated in Newcastle disease virus (NDV), avian influenza virus (AIV), and vesicular stomatitis virus (VSV)-infected bat TB 1 Lu cells. Overexpression of batMDA5 could activate IFN $\beta$  and inhibit vesicular stomatitis virus (VSV-GFP) replication in TB 1 Lu cells, while knockdown of batMDA5 yielded the opposite result. In addition, we found that the CARD domain was essential for MDA5 to activate IFN $\beta$  by constructing MDA5 domain mutant plasmids. These results indicated that bat employs a conserved MDA5 gene to trigger anti-RNA virus innate immune response. This study helps understand the biological role of MDA5 in innate immunity during evolution.

**Keywords:** BAT, MDA5, antiviral innate immunity, virus, IFN $\beta$

## INTRODUCTION

Bats are one of the most abundant and geographically distributed vertebrates on earth. There are more than 1,300 species of bats, and they are considered to be the second most ancient mammal species after rodents (1, 2). Bats are hosts of zoonotic viruses such as rabies, Hendra and Nipah, which are highly pathogenic to humans. In addition, bats are increasingly recognized as the reservoir host of coronaviruses, such as severe acute respiratory syndrome (SARS) and the Middle East respiratory syndrome (MERS), and the 2019 outbreak of coronaviruses (CoVID-19), which have caused deadly diseases in humans and animals (3–6). However, bats rarely display signs of disease upon viral infection.

The host immune system plays an important role in preventing viral infection and replication. Studies have found that both innate immunity and adaptive immunity exist in the immune system of bats (7). Innate immunity is the first line of defense against virus invasion. Viruses or pathogen-associated molecular patterns (PAMPS) can be recognized by the host pattern recognition receptors



(PRRs) and induce antiviral responses (8). The pattern recognition receptors in the host mainly include toll-like receptors (TLRs), retinoic acid-inducible gene I (RIG-I)-like receptors (RLRs), and nucleotide-binding oligomerization domain (NOD)-like receptors (NLRs) (9). Studying flying fox and a few other bat species have identified PRRs known in humans are conserved in bats, including TLRs and RLRs. Viruses, bacteria, fungi, and parasitic pathogens invade the host and can be recognized by TLRs and induce the host's innate immune response (10). There are 10 TLRs (TLR1-10) in humans (11). The black flying fox and the fruit bat have TLR1-10 and TLR-13, of which TLR-13 is absent in humans and most mammals (12). The RLRs family mainly recognizes and binds viral RNA nucleic acids in the cytoplasm to activate the downstream antiviral immune response (13). Transcriptome analysis revealed that RLRs family members of retinoic acid-inducible gene I (RIG-I), melanoma differentiation-associated gene 5 (MDA5), and laboratory of genetics and physiology 2 (LGP2) existed in the black flying fox and the bat RLRs were similar in structure and expression to human (2, 14).

RIG-I and MDA5 share many structural similarities, and both contain two caspase activation and recruitment domains (CARD), a central DEAD helicase domain (ATP), and a C-terminal repressor domain (CTD) (15, 16). The ATP domain can utilize ATP hydrolysis to unwind and bind viral RNA. The CTD domain has an auto-inhibitory function, which can only be released after binding to RNA virus nucleic acid. Its existence effectively prevents the continuous activation of host immune signals. The CARD domain can transmit signals to downstream adapters, the mitochondrial antiviral signaling protein (MAVS), to induce the production of type I interferons or cytokines (17, 18). The study found that stimulation of bat kidney cells with synthetic dsRNA (ploy: IC) significantly upregulated the expression of three RLRs, suggesting that bat RLRs function similarly to humans (14). RLRs can activate downstream interferon signaling pathways to exert antiviral effects after RNA virus infection. Previous studies have shown that the bat type I interferon gene *IFN $\alpha$*  is constitutively expressed in unstimulated bats cells and tissues. However, infection with virus or stimulation of ploy: IC did not affect its expression (19). Therefore, the researchers hypothesized that bats control viral replication in the early stages of the immune response through antiviral mechanisms (2).

The coronaviruses (CoVID-19) outbreak has brought serious disasters worldwide (20). However, bats have no signs of disease as the natural host of many coronaviruses, including CoVID-19 (21, 22). Therefore, bats' unique innate immune system has attracted great attention. *Tadarida brasiliensis* is one of the most widespread mammalian species in the Western Hemisphere, inhabiting a wide range of urban and wild environments. Researchers have isolated and identified a variety of viruses from the bats that are likely to transmit spontaneously the viruses to humans and other animals due to the specificity of their migration and habitat (23, 24). In this study, we cloned *Tadarida brasiliensis* MDA5 for the first time, analyzed its function, explored the differences in bats' innate immunity,

and explained the coexistence of bats with viruses. We found that the amino acid sequence of batMDA5 is poorly conserved among species, and RNA viruses such as NDV, VSV-GFP, and AIV infection *Tadarida brasiliensis* TB 1 Lu cells significantly upregulate the expression of batMDA5. Overexpression of batMDA5 noticeably activates the expression of IFN $\beta$ , MX1, and OAS1 and inhibits the VSV-GFP virus replication, while knockdown of batMDA5 yields the opposite results. At the same time, we also found that the CARD domain is essential for the activation of IFN $\beta$  by batMDA5. Therefore, we found that bat MDA5 can activate IFN $\beta$  to inhibit virus replication in this study.

## MATERIALS AND METHODS

### Cell Culture and Virus

Chicken embryonic fibroblast cell line DF1, human 293T cells, and bat TB1 Lu cells were obtained from ATCC and cultured in DMEM supplemented with 10% FBS and cells were incubated at 37°C in a 5% CO<sub>2</sub> incubator. Newcastle disease virus (NDV-GFP) was a low virulent strain LaSota named NDV-GFP. Avian influenza virus (AIV) were A/Chicken/Shanghai/010/2008 (H9N2) virus (SH010) was isolated from chicken in Shanghai, China, in 2008 and identified as H9N2 avian influenza A virus. The GFP tagged vesicular stomatitis virus (VSV) VSV-GFP were stored in our Laboratory. The viruses were purified, propagated, and stored as described in our previous study (25).

### Cloning and Bioinformatics Analysis of batMDA5

Based on the *Molossus molossus* MDA5 sequence (NW\_023425346.1) obtained from the National Center for Biotechnology Information (NCBI), the primers batMDA5-F and batMDA5-R (**Supplementary Table 1**) were designed and used to amplify batMDA5 cDNA *via* RT-PCR from TB 1 Lu cells. The PCR product was ligated into a pTOPO-Blunt vector (Aidlab, Beijing, China) for sequencing, and the positive colonies were sent to the Beijing Genomics Institute (Beijing, China) for sequencing. The amino acid sequence of batMDA5 was aligned with the other animal MDA5 proteins from mammals such as humans, mice, pigs, goats, and bats; Birds and Reptiles such as chicken, ducks, goose, and fishes such as zebrafish, common carp, and black carp using Clustal W and edited with ESPrict 3.0 (<http://http://esprict.ibcp.fr/ESPrict/cgi-bin/ESPrict.cgi>) as previously described (26). Sequence homology and phylogenetic analysis of the MDA5 amino acid sequences were conducted using DNASTAR. A phylogenetic tree was constructed based on the MDA5 from 30 different species, including mammals, birds, fish, and 10 different bat species. Different domains in the MDA5 amino acid sequences were predicted using the simple modular architecture research tool (SMART) program (<http://smart.embl-heidelberg.de/>) as previously described (27). Homology modeling for MDA5 was conducted using the online protein-modeling server SwissModel (<http://swissmodel.expasy.org/>) as previously described (28).

## Plasmid Construction

pcDNA3.1-batMDA5-FLAG plasmids were constructed by inserting full-length batMDA5 into the HindIII, and EcoRI sites pcDNA3.1-FLAG of the expression vector using a ClonExpress II one-step cloning kit (Yeasen, Shanghai, China). The primers used in the PCR are listed in **Supplementary Table 1**. The truncated plasmids of batMDA5, including CARD1 domain, CARD2 domain, DEXDc domain (ATP), HELICc domain (CTD), CARD domain, were constructed using a modified homologous recombination method and the primers listed in **Supplementary Table 1**. The  $\chi$ IFN- $\beta$  and huIFN- $\beta$  promoter-luciferase reporter plasmids (pGL-IFN- $\beta$ -Luc). The DH5 $\alpha$  Chemically Competent Cell (Tsingke Biology Technology, Beijing, China) was used for plasmid transformation. The pGL-IFN- $\beta$ -Luc plasmid was constructed in our previous study (29).

## Cells Transfection

DF1, 293T, and TB 1 Lu cells were seeded in 12-well or 24-well plates (NEST Biotechnology, Wuxi, China) at  $5 \times 10^5$ /mL or  $1 \times 10^6$ /mL. And the plasmid were transfected 500 ng/well in 12-well or 1000 ng/well in 6-well with Nulen PlusTrans<sup>TM</sup> Transfection Reagent (Nulen, Shanghai, China) according to the manufacturer's protocol.

## RNA Extraction and qPCR

Cells' total RNAs were extracted with AG RNAex Pro Reagent (Accurate Biology, Hunan, China). mRNA was reverse-transcribed to cDNA with reverse transcription kits (Vazyme, Nanjing, China), and the cDNA was analyzed using the SYBR green PCR mix (Vazyme, Nanjing, China) with the Applied Biosystems machine (ABI 7500; Thermo Fisher Scientific). Relative gene expression was analyzed using the  $2^{-\Delta\Delta Ct}$  method. The  $\beta$ -actin was the internal reference when examining the level of genes. The primer sequences for the genes are shown in **Supplementary Table 1**.

## Western Blot Analysis

The cells' total proteins were extracted by radioimmunoprecipitation assay (Beyotime, Shanghai, China) containing a protease cocktail (Yeasen, Shanghai, China) and phenylmethylsulfonyl fluoride (PMSF) (Yeasen, Shanghai, China). The lysate was centrifuged at 13,000 rpm for 10 min to obtain the supernatant, and a  $5 \times$  SDS loading buffer was added before the lysates were boiled for 10 min. The proteins isolated from the cell lysates were separated *via* SDS-PAGE and analyzed using Western blot. The antibody included anti-FLAG (Nulen, Shanghai, China) and  $\beta$ -tubulin overnight at 4°C. The membrane was washed 3 times with tris buffered saline and Tween-20 (TBST) (Sangon Biotech Co., Ltd, Shanghai, China). Then, the secondary antibody was added for 1 h incubation at 4°C shaker Images were obtained using the Tanon 5200 imaging system (Tanon, Shanghai, China).

## Luciferase Reporter Assay

The DF-1, 293T, and TB 1 Lu cells were plated in 24-well plates and were transiently transfected with the reporter plasmid pGL- $\chi$ IFN- $\beta$ -Luc or pGL-HuIFN- $\beta$ -Luc (120 ng/well) and the control Renilla luciferase (pRL-TK, 60 ng/well). According to the manufacturer's instructions, the cells were lysed 24 hours

after transfection, and luciferase activity was detected using a Dual-Luciferase Reporter Assay System kit (Promega, Madison, WI). Renilla luciferase activity was used for normalization. All reporter assays were repeated at least three times.

## Statistical Analysis

Results are expressed as the mean  $\pm$  SD. GraphPad Prism 8.0 was utilized to graph the results. Data were analyzed by using a two-tailed independent the Student's *t*-test.  $P < 0.05$  was considered statistically significant, and  $P < 0.01$  was considered highly statistically significant (\* $P < 0.05$ ; \*\* $P < 0.01$ ).

## RESULTS

### Conservation Analysis of batMDA5

To clarify the biological function of bat MDA5 in antiviral innate immunity, we amplified *Tadarida brasiliensis* MDA5 using the *Tadarida brasiliensis* 1 lung cell line (TB 1 Lu) cDNA. The ORF of batMDA5 contains 3084 bp and encodes 1027 amino acids residues (**Figure 1A**). After predicting the secondary structure of batMDA5 through the online website SMART (<http://smart.embl-heidelberg.de/>), it was found that batMDA5 has four typical domains of CARD DEXDc, HELICc, and RIG-I-CARD (**Figure 1B**). Multiple sequence analysis found that batMDA5 is poorly conserved among species, and the similarity with mammals such as humans (NC\_000002.12), mice (NC\_000068.8), pig (NC\_010457.5), and cattle (NC\_037329.1) respectively 88.0%, 77.6%, 84.3%, and 83.5%. The similarity with poultry were 59.8% (chicken NC\_052538.1), 60.7% (duck NC\_051778.1). The lowest similarity to fish was 47.0% (zebrafish NC\_007120.7) (**Figure 1C**). Also, there are multiple species of bats. After analyzing the batMDA5 sequences of NCBI, we found that the batMDA5-encoded amino acid sequences size was similar in different bats species, but the similarity is very low (**Figure S1A**). *Tadarida brasiliensis* has the highest similarity with the common vampire bat, Jamaican fruit-eating bat, pale spear-nosed bat, and Chinese rufous horseshoe bat, respectively 56.3%, 55.2%, 56.9%, 56.3% (**Figure S1B**). Next, we used SwissModel to predict the protein structure of batMDA5 (**Figure 1D**).

### Phylogenetic Tree Analyses of batMDA5

As an RNA virus sensor, MDA5 plays an important role in the process of antiviral innate immunity. In this study, we found that the batMDA5 has the highest similarity with humans, only 80%. And the similarity within species, *Tadarida brasiliensis* batMDA5 has the highest similarity with the common vampire bat, only 56.3%. This indicates that batMDA5 is less conserved among species. We performed a phylogenetic tree analysis of MDA5 in mammals, birds, reptiles, and fish to elucidate its molecular function further. As mammals, bats are more closely related to humans, pigs, dogs, and horses in evolution, and farther related to birds, fish, and reptiles (**Figure 2A**). Similarly, after analyzing the batMDA5 phylogenetic tree between bats, we found that batMDA5 also has a complex evolutionary relationship among bats, *Tadarida brasiliensis* with a common vampire bat, Jamaican fruit-eating bat, pale

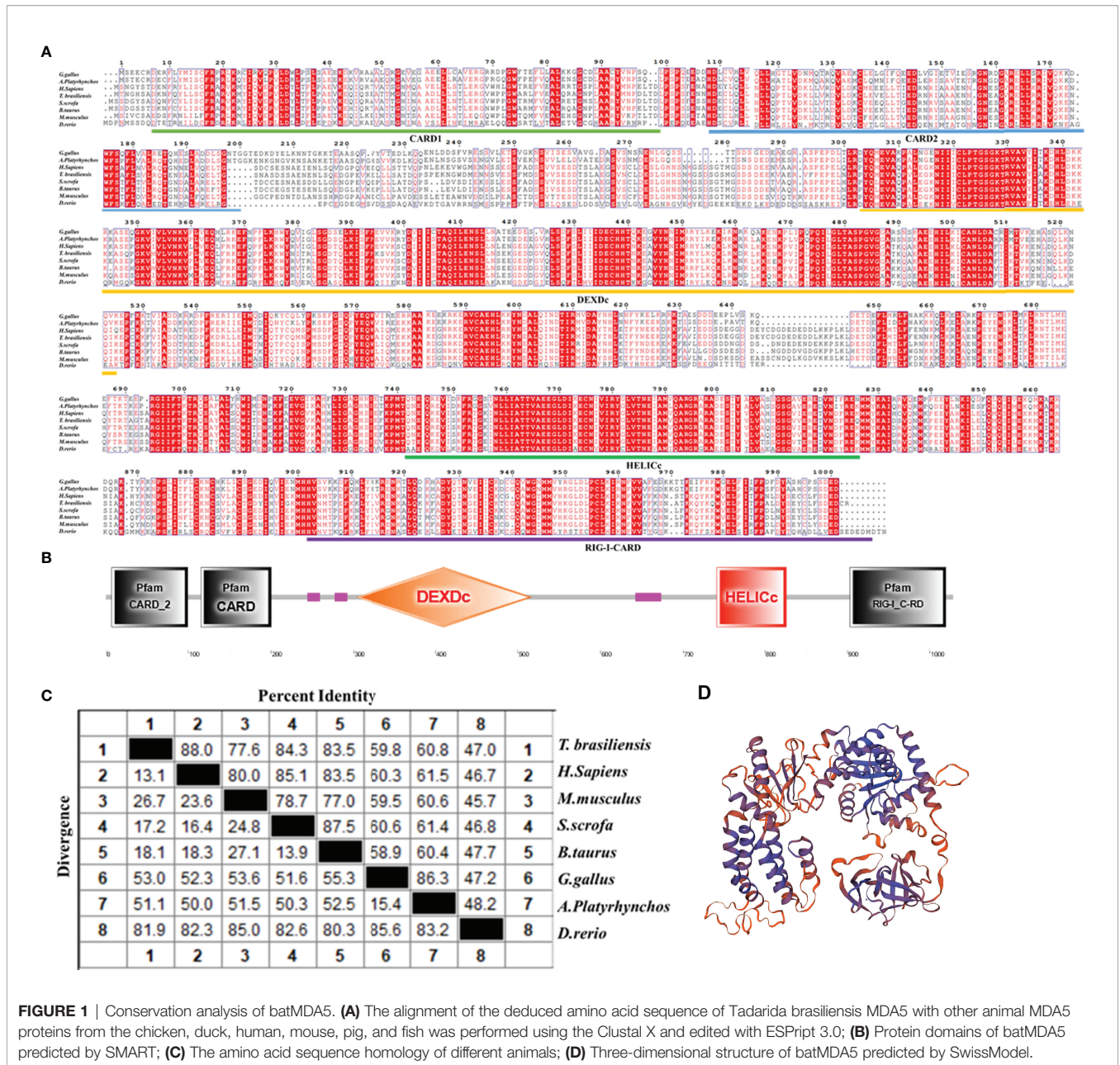


**FIGURE 1 |** Conservation analysis of batMDA5. **(A)** The alignment of the deduced amino acid sequence of *Tadarida brasiliensis* MDA5 with other animal MDA5 proteins from the chicken, duck, human, mouse, pig, and fish was performed using the Clustal X and edited with ESPrnt 3.0; **(B)** Protein domains of batMDA5 predicted by SMART; **(C)** The amino acid sequence homology of different animals; **(D)** Three-dimensional structure of batMDA5 predicted by SwissModel.

spear-nosed bat, and Chinese rufous horseshoe bat belong to the same branch in evolution (Figure 2B).

### Upregulation of batMDA5 Expression in Response to RNA Viral Infection

Bats are natural hosts of many RNA viruses. Previous studies have found that Newcastle disease virus (NDV-GFP), vesicular stomatitis virus (VSV-GFP), and avian influenza virus (AIV) can infect bats. And NDV, AIV and VSV infection significantly upregulate mammalian or avian MDA5 expression levels. However, the effect of RNA viruses on bat MDA5 expression remains unclear. Therefore, in this study, we infected the TB 1 Lu cell line with RNA viruses such as NDV-GFP, VSV-GFP, and AIV. We detected

the expression levels of batMDA5 and immune-related genes at infected with the virus for 3, 6, 12, and 24 h, respectively. The results showed that infection of TB 1 Lu cells with the above three RNA viruses could significantly upregulate the expression of batMDA5 (Figures 3A–C). Moreover, they also significantly upregulate the expression of immune-related genes such as batIFNβ, batMX1, and IL-6 mRNA (Figures 3D–F).

### Overexpression of batMDA5 Promoted Bats Antiviral Innate Immunity During VSV-GFP Infection

To further explore the role of MDA5 in innate antiviral immunity, we transfection batMDA5 plasmids in the TB 1 Lu cells, collected the

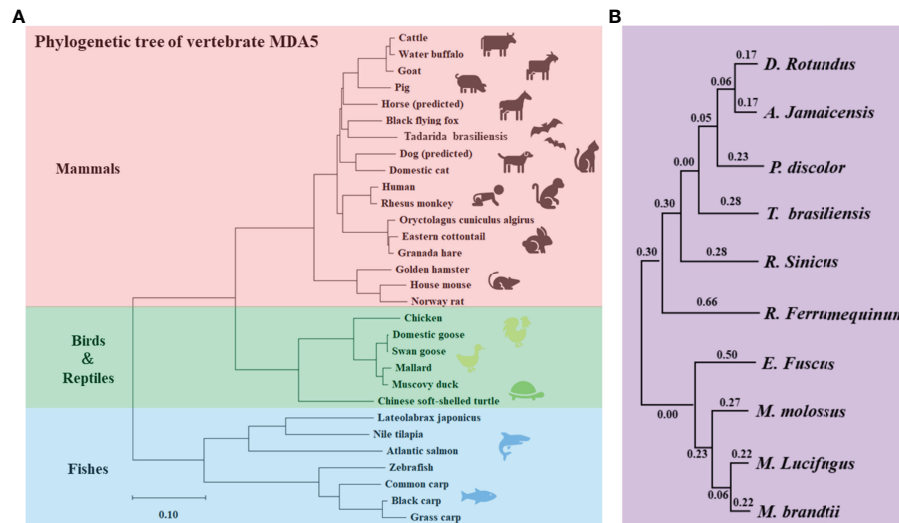


**FIGURE 2** | Phylogenetic Tree Analyses of batMDA5. **(A)** Phylogenetic tree of the deduced amino acid sequence of batMDA5 and other animal MDA5 proteins; **(B)** Phylogenetic tree of the deduced amino acid sequence of MDA5 among different bat species.

cells after infecting VSV-GFP for 24 h and detected the immune-related gene expression. It was found that overexpression of batMDA5 significantly promotes the expression of batIFN $\beta$  and interferon-stimulated related genes batMX1 and batOAS1 after infection with VSV-GFP (**Figures 4A–D**), suggesting that batMDA5 can sense RNA virus invasion and promote batIFN $\beta$  expression.

## Overexpression of batMDA5 Inhibits Vesicular Stomatitis Virus (VSV-GFP) Replication

Next, we explored the role of batMDA5 in virus replication. After overexpression of huMDA5, chMDA5, and batMDA5 in human 293T cells, chicken DF1 cells, and bat TB 1 Lu cells, VSV-GFP was infected for 12 h and detected the expression of MDA5 in the

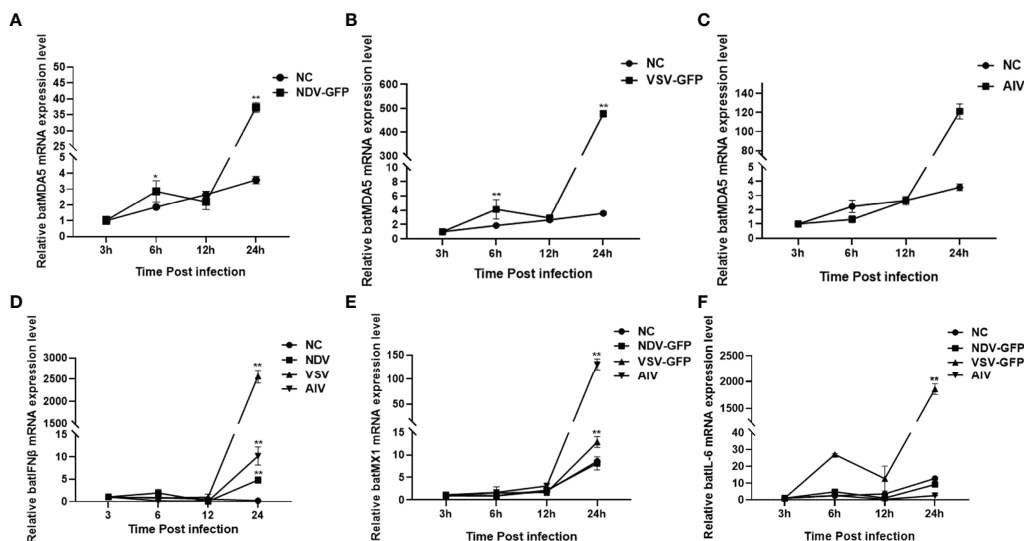


**FIGURE 3** | Upregulation of batMDA5 expression in response to RNA viral infection. **(A)** RT-qPCR was used to detect the expression level of batMDA5 in TB 1 Lu cells infection with NDV at 1.0 MOI. **(B)** RT-qPCR was used to detect the expression level of batMDA5 in TB 1 Lu cells infected with VSV at 1.0 MOI. **(C)** RT-qPCR was used to detect the expression level of batMDA5 in TB 1 Lu cells infection with AIV at 1.0 MOI. **(D)** RT-qPCR was used to detect the expression level of batIFN $\beta$  in TB 1 Lu cells infection with NDV, VSV, and AIV at 1.0 MOI. **(E)** RT-qPCR was used to detect the expression level of batMX1 in TB 1 Lu cells infection with NDV, VSV, and AIV at 1.0 MOI. **(F)** RT-qPCR was used to detect the expression level of batIL-6 in TB 1 Lu cells infection with NDV, VSV, and AIV at 1.0 MOI. Data are expressed as the means  $\pm$  SD of three independent experiments. \* $P < 0.05$ ; \*\* $P < 0.01$ .

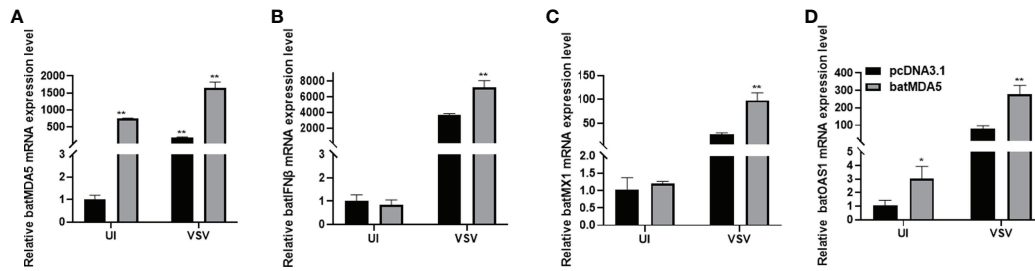


**FIGURE 4** | Overexpression of batMDA5 promoted bats' antiviral innate immunity during VSV-GFP infection. **(A)** RT-qPCR was used to detect the overexpression efficiency of batMDA5 in TB1 Lu cells transfected with 500 ng/well of pcDNA3.1 or pcDNA3.1-batMDA5 uninfected (UI) or infected with VSV-GFP at 1.0 MOI. **(B–D)** RT-qPCR was used to detect the overexpression level of IFN $\beta$ , MX1, and OAS1 in TB 1 Lu cells after overexpression of pcDNA3.1-batMDA5, uninfected (UI) or infected with VSV-GFP at 1.0 MOI. Data are expressed as the means  $\pm$  SD of three independent experiments. \* $P < 0.05$ ; \*\* $P < 0.01$ .

cells by Western blot (**Figures 5A, B**). The fluorescence intensity of VSV-GFP reflects its replication in cells. Through fluorescence microscope observation, we found that overexpression of batMDA5 in 293T and TB 1 Lu cells obviously inhibits the replication of VSV-GFP, but in DF1, only chMDA5 significantly inhibited the replication of GFP-VSV, huMDA5, and batMDA5 do not affect controlling VSV-GFP replication in DF1 cells (**Figures 5C–F**). The results above indicate that batMDA5 inhibits virus replication by activating the innate immunity of bats.

### Knockdown of batMDA5 Inhibits Bats Antiviral Innate Immunity Promotes the VSV-GFP Replication

To further prove the effectiveness of batMDA5 on bat antiviral innate immunity, we constructed RNAi plasmids of batMDA5 plasmids (shMDA5-1#, shMDA5-2#, shNC). The shRNA was transferred into TB 1 Lu cells for 24 h and infected with VSV-GFP for 12 h. The expression level of batMDA5 was detected by RT-qPCR, and it was found that both shMDA5-1# and shMDA5-2# could significantly inhibit the expression of batMDA5 (**Figure 6A**). At the same time, after the knockdown of the expression of batMDA5, infection with VSV-GFP significantly inhibits the expression of batIFN $\beta$  and interferon-stimulated related genes batMX1 and OAS1 (**Figures 6B–D**). In addition, we also found that knockdown of batMDA5 could promote the VSV-GFP virus replication (**Figures 6E–G**). The above results further demonstrate that batMDA5 can activate the innate immunity of bat and suppress viral replication.

### The batMDA5 Essential Domain for Activation of the IFN $\beta$

To further explore the essential functional domains of batMDA5 inactivation of the IFN $\beta$ , we constructed batMDA5 mutant plasmids lacking different functional domains of batMDA5 (**Figure 7A**). Their IFN $\beta$  activation abilities were assessed with the huIFN $\beta$  luciferase report assay in 293T cells. The results found that deletion of the CARD1 and CARD2 domains of batMDA5 loses the function of batMDA5 for activating the huIFN $\beta$  promoter. However, the batMDA5-CARD domain

strongly activates the huIFN $\beta$  promoter (**Figure 7B**). Next, we overexpressed batMDA5 and batMDA5-CARD domains in TB 1 Lu cells. After overexpression of batMDA5-CARD, batIFN $\beta$  and the expression of interferon-stimulated related genes batMX1 and batOAS1 could be significantly activated without virus stimulation. While batMDA5 is in a state of self-inhibition under normal circumstances, overexpression of MDA5 does not activate IFN $\beta$  in the absence of viral stimulation (**Figures 7C–E**), suggesting that the CARD domain is critical for batMDA5 to activate batIFN $\beta$ .

## DISCUSSION

The host's innate immune system plays an important antiviral role during viral infection. The host mainly detects the presence of viruses by using recognition receptors, among which MDA5 is an important RNA virus nucleic acid sensor, mainly recognizes and binds to long double-stranded RNA (dsRNA) viruses, which can sense virus invasion and transmit signals to the adapter mitochondrial antiviral Signal protein (MAVS) that promotes the secretion of type I interferon (30). Type I interferons further orchestrate the cellular immune response to viral infection (31). Bats, being mammals, carry many very pathogenic viruses to humans, but they rarely display signs of illness (1). Whether RNA viral recognition sensors such as MDA5 in bat cells can recognize viral nucleic acids and exert antiviral effects remains unknown.

In this study, we cloned *Tadarida brasiliensis* MDA5. We found that batMDA5 and huMDA5 have high homology through sequence analysis and phylogenetic tree analysis. By analyzing the MDA5 of different species of bats, we found that *Tadarida brasiliensis* MDA5 has low homology in different bats. Evolutionarily, batMDA5 is closer to mammals such as humans, pigs, and horses, indicating that MDA5 has homology in species evolution. It has been found that the amino acid sequence of *P. alecto* MDA5 is most closely related to horses in evolution (32). After high-throughput whole-genome sequencing of bats, studies have found that bat-encoding genes and many mammalian genes have a single orthologous copy (33). RIG-I and MDA5 are

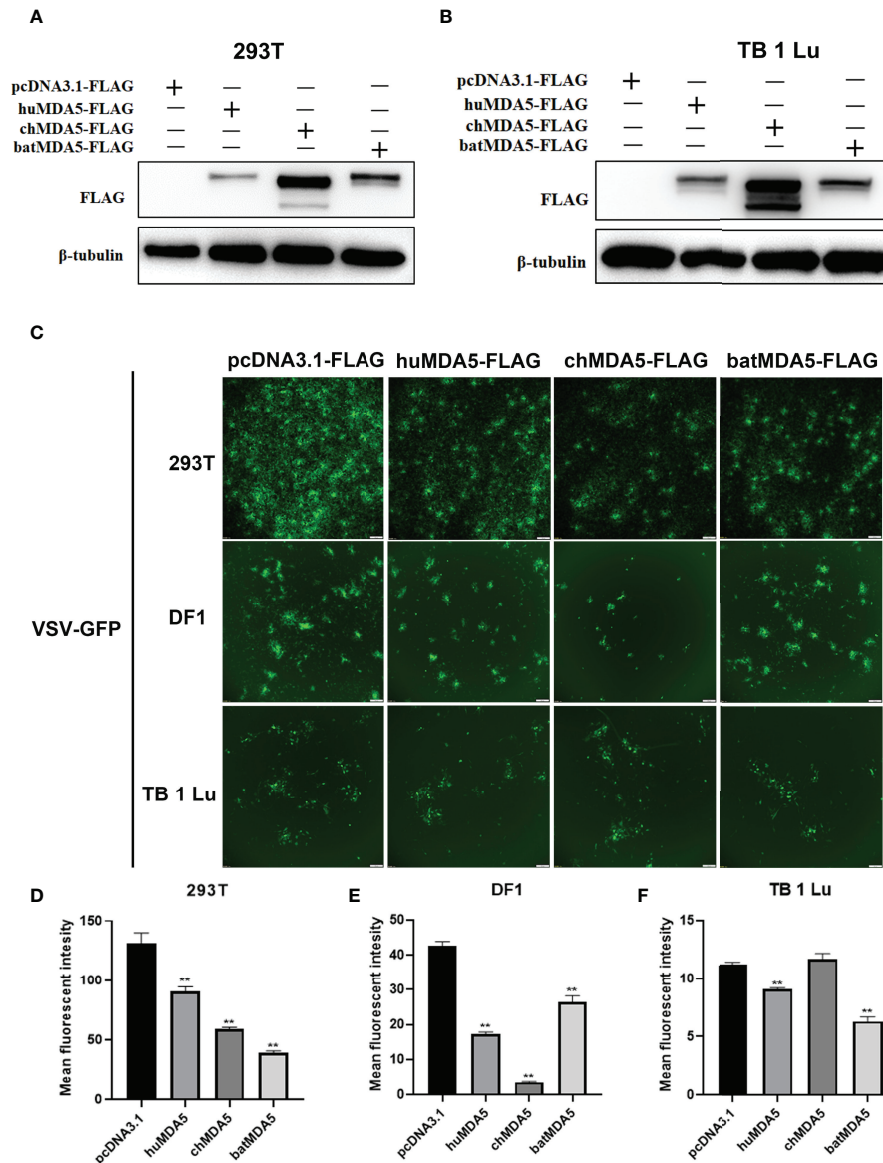


**FIGURE 5** | Overexpression of batMDA5 inhibits vesicular stomatitis virus (VSV-GFP) replication. **(A, B)** Western blotting analysis of the expression of pcDNA3.1-huMDA5-flag or pcDNA3.1-chMDA5-flag or pcDNA3.1-batMDA5-flag or pcDNA3.1-flag in 293T and TB 1 Lu cells after overexpression of pcDNA3.1-huMDA5-flag or pcDNA3.1-chMDA5-flag or pcDNA3.1-batMDA5-flag or pcDNA3.1-flag infected with VSV-GFP at 1.0 MOI for 12 h. **(C)** Viral fluorescence in 293T, DF1 and TB 1 Lu cells after overexpression of pcDNA3.1-huMDA5-flag or pcDNA3.1-chMDA5-flag or pcDNA3.1-batMDA5-flag or pcDNA3.1-flag infected with VSV-GFP at 1.0 MOI for 12 h. **(D-F)** VSV-GFP mean fluorescent intensity in 293T, DF1 and TB 1 Lu cells after overexpression of pcDNA3.1-huMDA5-flag or pcDNA3.1-chMDA5-flag or pcDNA3.1-batMDA5-flag or pcDNA3.1-flag infected with VSV-GFP at 1.0 MOI for 12 h. Data are expressed as the means  $\pm$  SD of three independent experiments. **\*\*** $P < 0.01$ .

critical for activating type I interferon expression during viral infection. Phylogenetic analysis suggests that RIG-I and MDA5 come from a common origin, with MDA5 orthologs present in most vertebrates. In contrast, RIG-I orthologs exist only in mammals, ducks, geese, and some specific fish and reptiles (34), suggesting that MDA5 plays an important role across species. So during viral infection, can batMDA5 also recognize RNA viruses to activate antiviral innate immunity?

Mammalian cells or chicken fibroblast DF1 cells infected with RNA virus significantly upregulate the expression level of MDA5 (35–37). In this study, we also found the same results in the TB 1 Lu cells after infecting RNA viruses such as NDV-GFP, AIV, or VSV-GFP upregulated the expression of batMDA5 and innate immunity-related genes batIFN $\beta$ , batMX1, and batIL-6, suggesting that the innate immune system of bats also can sense the invasion of the virus and play an antiviral role. It has

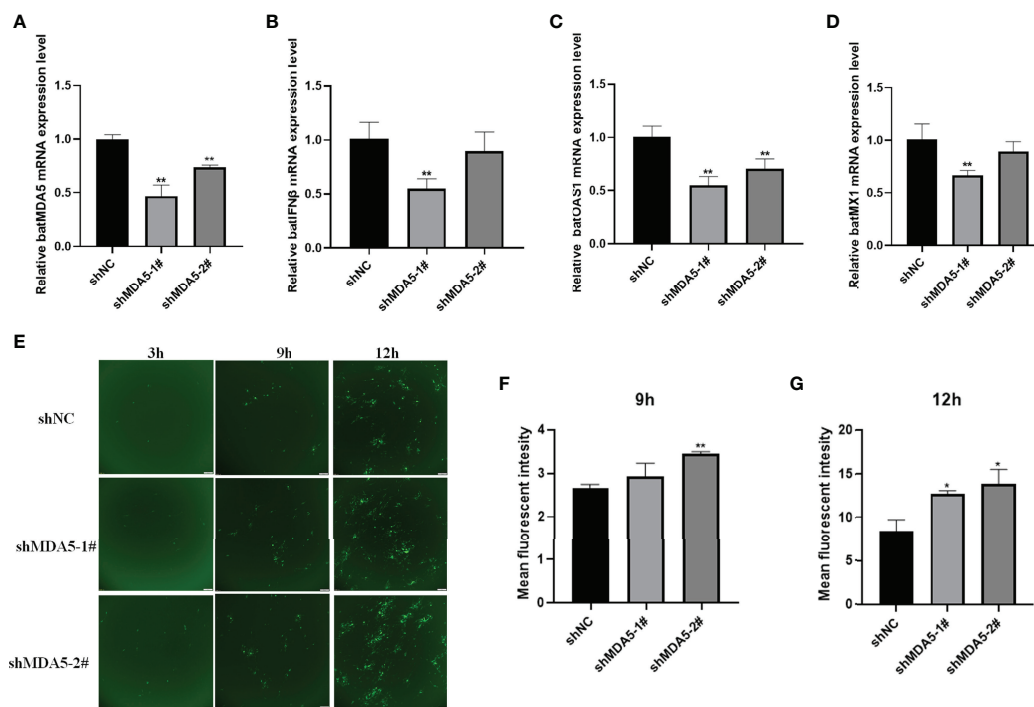


**FIGURE 6** | Knockdown of batMDA5 inhibits bats' antiviral innate immunity and promotes the VSV-GFP replication. **(A)** RT-qPCR was used to detect the Knockdown efficiency of batMDA5 in TB 1 Lu cells transfected with shNC or shMDA5-1# or shMDA5-3#, infected with VSV-GFP at 1 MOI for 12 h **(B–D)** RT-qPCR was used to detect the expression level of IFN $\beta$ , MX1 and OAS1 in TB 1 Lu cells after knockdown of batMDA5, infected with VSV-GFP at 1.0 MOI for 12 h **(E)** Viral fluorescence in TB 1 Lu cells, after knockdown of batMDA5, infected with VSV-GFP at 1 MOI for 3 h, 9 h and 12 h **(F, G)** The VSV-GFP mean fluorescent intensity in 2 TB 1 Lu cells after knockdown of batMDA5, infected with VSV-GFP at 1.0 MOI for 9 h and 12 h Data are expressed as the means  $\pm$  SD of three independent experiments. \* $P < 0.05$ ; \*\* $P < 0.01$ .

been found that kidney epithelial cell lines derived from four bat species infected with Encephalomyocarditis virus (EMCV) and Japanese encephalitis virus (JEV) can also significantly upregulate the expression of batMDA5, indicating that a variety of RNA viruses can upregulate batMDA5, and batMDA5 in different bat species appear to be functionally similar (38). Interestingly, after we infected TB 1 Lu cells with three RNA viruses for 12h, the expression levels of batMDA5, batIFN $\beta$ , batMX1, and batIL-6 were lower than those of 6h infection. This may be due to the cell cycle or the viral replication cycle. However, the specific reasons still need further research.

Next, we overexpressed batMDA5 in TB 1 Lu cells. The results showed that overexpression of MDA5 could significantly promote the expression of IFN $\beta$  and inhibit virus replication after infection with VSV-GFP, indicating that the function of batMDA5 is conserved among species, and batMDA5 can recognize RNA viruses to activate the host's innate immune response to inhibit virus replication (39). Pteropine Orthoreovirus (PRV) is a zoonotic disease for which bats are its natural host. The study found that the replication ability of PRV in BHK-21 and HEK293T cells was significantly stronger than that in various bat cells. Therefore, the researchers speculate that bats can use their powerful immune systems to suppress virus replication and reduce clinical symptoms (32).

To further explore the function of batMDA5, we knocked down its expression and found that it could significantly inhibit the expression of IFN $\beta$  and promote virus replication, indicating that batMDA5 could activate IFN $\beta$  expression and exert an antiviral effect.

Structurally, batMDA5 also contains four domains, 2CARD, ATP, and CTD (40). In general, the MDA5 CARD domain can interact with the downstream MAVS CARD domain through a series of cascade reactions that ultimately lead to the expression of IFN $\beta$  (34, 41). This study found that the amino acid sequence of the CARD region of batMDA5 was very poorly conserved among species. To further explore the structure and function of batMDA5, we constructed batMDA5 plasmids with different functional domains deleted. Deleting CARD1 or CARD2 was found that batMDA5 loses the ability to activate IFN $\beta$ . On the contrary, only retaining the CARD domain can strongly activate IFN $\beta$ , indicating that the function of batMDA5 is conserved in evolution.

Combining the above studies, we found that batMDA5 is conserved between species in structure and function, suggesting that batMDA5 can activate downstream antiviral immune responses to inhibit viral replication after bat infection with RNA viruses. Nevertheless, how do viruses settle in bats without being cleared by the host's innate immune system? Relevant

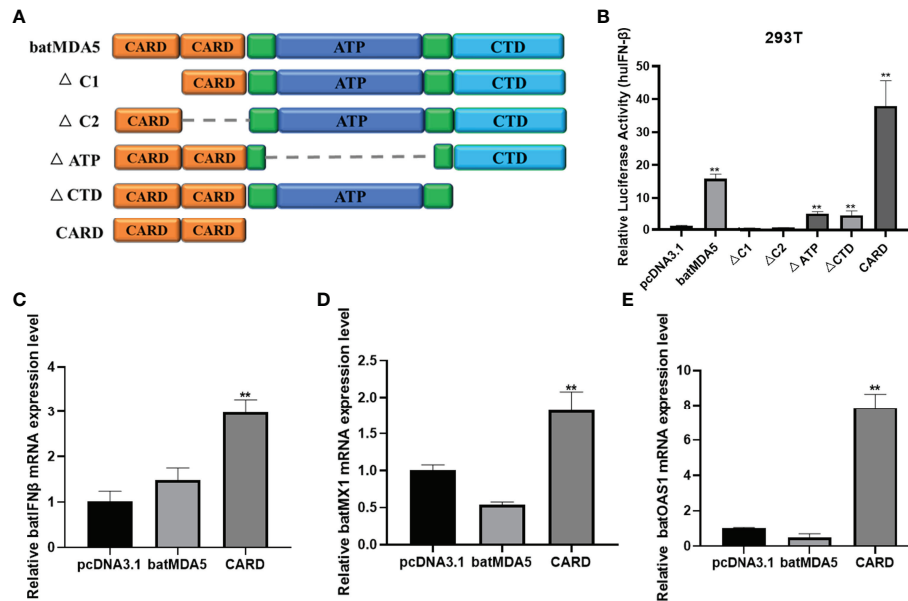


**FIGURE 7** | The batMDA5 is an essential adaptor for activation of the IFN $\beta$ . **(A)** Schematic structure of batMDA5 mutants. **(B)** 293T cells were co-transfected with luciferase reporter plasmids (pRL-TK and pGL-huIFN- $\beta$ -Luc) and pcDNA3.1-batMDA5 mutants or pcDNA3.1. After transfection 12 h infection VSV-GFP at 1 MOI, luciferase assays were performed after 24 h of co-transfection. **(C–E)** RT-qPCR was used to detect the expression level of IFN $\beta$ , MX1, and OAS1 in TB1 Lu cells after overexpression of batMDA5 or batMDA5-CARD or pcDNA3.1. Data are expressed as the means  $\pm$  SD of three independent experiments. \*\* $P$  < 0.01.

studies have shown that several immune-related genes have high expression levels in bats, including RIG-I, MDA5, IFN $\alpha$ , and IRF family, which makes viruses recognized by the immune system and quickly eliminated once they invade bats (42–44). However, a rapid and intense immune response can cause a “cytokine storm” that damages host tissues and organs and leads to death (45). To avoid this severe consequence, bats evolved to activate genes for inflammation or IFNs, which either lost or altered their function (46), which explains why bats are asymptomatic virus hosts. That is to say, the ability of batMDA5 to activate IFN $\beta$  after virus invasion is relatively mild, which was also consistent with previous studies that virus or ploy(I:C) stimulation did not induce the activate IFN $\alpha$ . Therefore, we believe that batMDA5 can sense virus invasion and activate IFN $\beta$ , but this activation is relatively mild, which is one of the reasons why bats can colonize hundreds of viruses without the disease.

## DATA AVAILABILITY STATEMENT

The original contributions presented in the study are included in the article/**Supplementary Material**. Further inquiries can be directed to the corresponding authors.

## REFERENCES

- Wang LF, Anderson DE. Viruses in Bats and Potential Spillover to Animals and Humans. *Curr Opin Virol* (2019) 34:79–89. doi: 10.1016/j.coviro.2018.12.007

## AUTHOR CONTRIBUTIONS

JW, YC, and JS designed the research and analyzed the data. JW, ZL, QL, FF, ZW, JM, HW, YY, and JS conducted the experiments and collected the data. JW and YC wrote the paper. All authors approved the final version of the manuscript.

## FUNDING

This research was supported by the National Natural Science Foundation of China (32072864 and 32072865), the Natural Science Foundation of Shanghai (20ZR1425100), Science and Technology Commission of Shanghai Municipality (21N41900100), Shanghai Agriculture Applied Technology Development Program, China (2022-02-08-00-12-F01191).

## SUPPLEMENTARY MATERIAL

The Supplementary Material for this article can be found online at: <https://www.frontiersin.org/articles/10.3389/fimmu.2022.904481/full#supplementary-material>

- Clayton E, Munir M. Fundamental Characteristics of Bat Interferon Systems. *Front Cell Infect Microbiol* (2020) 10:527921. doi: 10.3389/fcimb.2020.527921
- Swanepoel R, Smit SB, Rollin PE, Formenty P, Leman PA, Kemp A, et al. Studies of Reservoir Hosts for Marburg Virus. *Emerg Infect Dis* (2007) 13:1847–51. doi: 10.3201/eid1312.071115



4. Ge XY, Li JL, Yang XL, Chmura AA, Zhu G, Epstein JH, et al. Isolation and Characterization of a Bat SARS-Like Coronavirus That Uses the ACE2 Receptor. *Nature* (2013) 503:535–8. doi: 10.1038/nature12711
5. Forbes KM, Webala PW, Jaaskelainen AJ, Abdurahman S, Ogola J, Masika MM, et al. Bombali Virus in Mops Condylurus Bat, Kenya. *Emerg Infect Dis* (2019) 25:955–7. doi: 10.3201/eid2505.181666
6. Anthony SJ, Gilardi K, Menachery VD, Goldstein T, Ssebide B, Mbabazi R, et al. Further Evidence for Bats as the Evolutionary Source of Middle East Respiratory Syndrome Coronavirus. *mBio* (2017) 8:e00373–17. doi: 10.1128/mBio.00373-17
7. De La Cruz-Rivera PC, Kanchwala M, Liang H, Kumar A, Wang LF, Xing C, et al. The IFN Response in Bats Displays Distinctive IFN-Stimulated Gene Expression Kinetics With Atypical RNASL Induction. *J Immunol* (2018) 200:209–17. doi: 10.4049/jimmunol.1701214
8. Iwasaki A, Pillai PS. Innate Immunity to Influenza Virus Infection. *Nat Rev Immunol* (2014) 14:315–28. doi: 10.1038/nri3665
9. Campbell LK, Magor KE. Pattern Recognition Receptor Signaling and Innate Responses to Influenza A Viruses in the Mallard Duck, Compared to Humans and Chickens. *Front Cell Infect Microbiol* (2020) 10:209. doi: 10.3389/fcimb.2020.00209
10. Kawai T, Akira S. The Role of Pattern-Recognition Receptors in Innate Immunity: Update on Toll-Like Receptors. *Nat Immunol* (2010) 11:373–84. doi: 10.1038/ni.1863
11. Boyd A, Philbin VJ, Smith AL. Conserved and Distinct Aspects of the Avian Toll-Like Receptor (TLR) System: Implications for Transmission and Control of Bird-Borne Zoonoses. *Biochem Soc Trans* (2007) 35:1504–7. doi: 10.1042/BST0351504
12. Cowled C, Baker M, Tachedjian M, Zhou P, Bulach D, Wang LF. Molecular Characterisation of Toll-Like Receptors in the Black Flying Fox Pteropus Alecto. *Dev Comp Immunol* (2011) 35:7–18. doi: 10.1016/j.dci.2010.07.006
13. Loo YM, Gale M Jr. Immune Signaling by RIG-I-Like Receptors. *Immunity* (2011) 34:680–92. doi: 10.1016/j.immuni.2011.05.003
14. Cowled C, Baker ML, Zhou P, Tachedjian M, Wang LF. Molecular Characterisation of RIG-I-Like Helicases in the Black Flying Fox, Pteropus Alecto. *Dev Comp Immunol* (2012) 36:657–64. doi: 10.1016/j.dci.2011.11.008
15. Zou J, Chang M, Nie P, Secombes CJ. Origin and Evolution of the RIG-I Like RNA Helicase Gene Family. *BMC Evol Biol* (2009) 9:85. doi: 10.1186/1471-2148-9-85
16. Yoneyama M, Kikuchi M, Matsumoto K, Imaizumi T, Miyagishi M, Taira K, et al. Shared and Unique Functions of the DExD/H-Box Helicases RIG-I, MDA5, and LGP2 in Antiviral Innate Immunity. *J Immunol* (2005) 175:2851–8. doi: 10.4049/jimmunol.175.5.2851
17. Wu B, Hur S. How RIG-I Like Receptors Activate MAVS. *Curr Opin Virol* (2015) 12:91–8. doi: 10.1016/j.coviro.2015.04.004
18. Jacobs JL, Coyne CB. Mechanisms of MAVS Regulation at the Mitochondrial Membrane. *J Mol Biol* (2013) 425:5009–19. doi: 10.1016/j.jmb.2013.10.007
19. Zhou P, Tachedjian M, Wynne JW, Boyd V, Cui J, Smith I, et al. Contraction of the Type I IFN Locus and Unusual Constitutive Expression of IFN-Alpha in Bats. *Proc Natl Acad Sci USA* (2016) 113:2696–701. doi: 10.1073/pnas.1518240113
20. Pierce JD, Shen Q, Cintron SA, Hiebert JB. Post-COVID-19 Syndrome. *Nurs Res* (2022) 71:164–74. doi: 10.1097/NNR.0000000000000565
21. Woo PC, Lau SK, Huang Y, Yuen KY. Coronavirus Diversity, Phylogeny and Interspecies Jumping. *Exp Biol Med (Maywood)* (2009) 234:1117–27. doi: 10.3181/0903-MR-94
22. Zhou P, Yang XL, Wang XG, Hu B, Zhang L, Zhang W, et al. A Pneumonia Outbreak Associated With a New Coronavirus of Probable Bat Origin. *Nature* (2020) 579:270–3. doi: 10.1038/s41586-020-2012-7
23. Allen LC, Turmelle AS, Mendonca MT, Navara KJ, Kunz TH, McCracken GF. Roosting Ecology and Variation in Adaptive and Innate Immune System Function in the Brazilian Free-Tailed Bat (*Tadarida brasiliensis*). *J Comp Physiol B* (2009) 179:315–23. doi: 10.1007/s00360-008-0315-3
24. Cibulski SP, de Sales Lima FE, Teixeira TF, Varela APM, Scheffer CM, Mayer FQ, et al. Detection of Multiple Viruses in Oropharyngeal Samples From Brazilian Free-Tailed Bats (*Tadarida brasiliensis*) Using Viral Metagenomics. *Arch Virol* (2021) 166:207–12. doi: 10.1007/s00705-020-04825-x
25. Cheng Y, Liu Y, Shi S, Niu Q, Zhu W, Wang Z, et al. Functional Characterization of Duck STING in IFN-Beta Induction and Anti-H9N2 Avian Influenza Viruses Infections. *Front Immunol* (2019) 10:2224. doi: 10.3389/fimmu.2019.02224
26. Lin Z, Wang J, Zhu W, Yu X, Wang Z, Ma J, et al. Chicken DDX1 Acts as an RNA Sensor to Mediate IFN-Beta Signaling Pathway Activation in Antiviral Innate Immunity. *Front Immunol* (2021) 12:742074. doi: 10.3389/fimmu.2021.742074
27. Letunic I, Khedkar S, Bork P. SMART: Recent Updates, New Developments and Status in 2020. *Nucleic Acids Res* (2021) 49:D458–60. doi: 10.1093/nar/gkaa937
28. Waterhouse A, Bertoni M, Bienert S, Studer G, Tauriello G, Gumienny R, et al. Et Al: SWISS-MODEL: Homology Modelling of Protein Structures and Complexes. *Nucleic Acids Res* (2018) 46:W296–303. doi: 10.1093/nar/gky427
29. Cheng Y, Zhu W, Ding C, Niu Q, Wang H, Yan Y, et al. IRF7 Is Involved in Both STING and MAVS Mediating IFN-Beta Signaling in IRF3-Lacking Chickens. *J Immunol* (2019) 203:1930–42. doi: 10.4049/jimmunol.1900293
30. Dias Junior AG, Sampaio NG, Rehwinkel J. A Balancing Act: MDA5 in Antiviral Immunity and Autoinflammation. *Trends Microbiol* (2019) 27:75–85. doi: 10.1016/j.tim.2018.08.007
31. Barrat FJ, Elkon KB, Fitzgerald KA. Importance of Nucleic Acid Recognition in Inflammation and Autoimmunity. *Annu Rev Med* (2016) 67:323–36. doi: 10.1146/annurev-med-052814-023338
32. Tarigan R, Katta T, Takemae H, Shimoda H, Maeda K, Iida A, et al. Distinct Interferon Response in Bat and Other Mammalian Cell Lines Infected With Pteropine Orthoreovirus. *Virus Genes* (2021) 57:510–20. doi: 10.1007/s11262-021-01865-6
33. Zhang G, Cowled C, Shi Z, Huang Z, Bishop-Lilly KA, Fang X, et al. Et Al: Comparative Analysis of Bat Genomes Provides Insight Into the Evolution of Flight and Immunity. *Science* (2013) 339:456–60. doi: 10.1126/science.1230835
34. Brisse M, Ly H. Comparative Structure and Function Analysis of the RIG-I-Like Receptors: RIG-I and MDA5. *Front Immunol* (2019) 10:1586. doi: 10.3389/fimmu.2019.01586
35. Broquet AH, Hirata Y, McAllister CS, Kagnoff MF. RIG-I/MDA5/MAVS Are Required to Signal a Protective IFN Response in Rotavirus-Infected Intestinal Epithelium. *J Immunol* (2011) 186:1618–26. doi: 10.4049/jimmunol.1002862
36. Lee SB, Park YH, Chungu K, Woo SJ, Han ST, Choi HJ, et al. Targeted Knockout of MDA5 and TLR3 in the DF-1 Chicken Fibroblast Cell Line Impairs Innate Immune Response Against RNA Ligands. *Front Immunol* (2020) 11:678. doi: 10.3389/fimmu.2020.00678
37. Lu HL, Liao F. Melanoma Differentiation-Associated Gene 5 Senses Hepatitis B Virus and Activates Innate Immune Signaling to Suppress Virus Replication. *J Immunol* (2013) 191:3264–76. doi: 10.4049/jimmunol.1300512
38. Tarigan R, Shimoda H, Doysabas KCC, Ken M, Iida A, Hondo E. Role of Pattern Recognition Receptors and Interferon-Beta in Protecting Bat Cell Lines From Encephalomyocarditis Virus and Japanese Encephalitis Virus Infection. *Biochem Biophys Res Commun* (2020) 527:1–7. doi: 10.1016/j.bbrc.2020.04.060
39. Huang Y, Yu Y, Yang Y, Yang M, Zhou L, Huang X, et al. Antiviral Function of Grouper MDA5 Against Iridovirus and Nodavirus. *Fish Shellfish Immunol* (2016) 54:188–96. doi: 10.1016/j.fsi.2016.04.001
40. Berke IC, Modis Y. MDA5 Cooperatively Forms Dimers and ATP-Sensitive Filaments Upon Binding Double-Stranded RNA. *EMBO J* (2012) 31:1714–26. doi: 10.1038/emboj.2012.19
41. Uchikawa E, Lethier M, Malet H, Brunel J, Gerlier D, Cusack S. Structural Analysis of dsRNA Binding to Anti-Viral Pattern Recognition Receptors LGP2 and MDA5. *Mol Cell* (2016) 62:586–602. doi: 10.1016/j.molcel.2016.04.021
42. Irving AT, Zhang Q, Kong PS, Luko K, Rozario P, Wen M, et al. Interferon Regulatory Factors IRF1 and IRF7 Directly Regulate Gene Expression in Bats in Response to Viral Infection. *Cell Rep* (2020) 33:108345. doi: 10.1016/j.celrep.2020.108345
43. Lin HH, Horie M, Tomonaga K. A Comprehensive Profiling of Innate Immune Responses in *Eptesicus* Bat Cells. *Microbiol Immunol* (2022) 66:97–112. doi: 10.1111/1348-0421.12952

44. Zhou P, Cowled C, Mansell A, Monaghan P, Green D, Wu L, et al. IRF7 in the Australian Black Flying Fox, *Pteropus Alecto*: Evidence for a Unique Expression Pattern and Functional Conservation. *PLoS One* (2014) 9:e103875. doi: 10.1371/journal.pone.0103875
45. Fajgenbaum DC, June CH. Cytokine Storm. *N Engl J Med* (2020) 383:2255–73. doi: 10.1056/NEJMra2026131
46. Giotis ES, Matthews DA, Smith J. Editorial: Host Innate Immune Responses to Infection by Avian- and Bat-Borne Viruses. *Front Cell Infect Microbiol* (2021) 11:651289. doi: 10.3389/fcimb.2021.651289

**Conflict of Interest:** The authors declare that the research was conducted in the absence of any commercial or financial relationships that could be construed as a potential conflict of interest.

**Publisher's Note:** All claims expressed in this article are solely those of the authors and do not necessarily represent those of their affiliated organizations, or those of the publisher, the editors and the reviewers. Any product that may be evaluated in this article, or claim that may be made by its manufacturer, is not guaranteed or endorsed by the publisher.

Copyright © 2022 Wang, Lin, Liu, Fu, Wang, Ma, Wang, Yan, Cheng and Sun. This is an open-access article distributed under the terms of the Creative Commons Attribution License (CC BY). The use, distribution or reproduction in other forums is permitted, provided the original author(s) and the copyright owner(s) are credited and that the original publication in this journal is cited, in accordance with accepted academic practice. No use, distribution or reproduction is permitted which does not comply with these terms.



# Paeonol Interferes With Quorum-Sensing in *Pseudomonas aeruginosa* and Modulates Inflammatory Responses *In Vitro* and *In Vivo*

Huaqiao Tang<sup>†</sup>, Dan Yang<sup>†</sup>, Ling Zhu, Fei Shi, Gang Ye, Hongrui Guo, Huidan Deng, Ling Zhao, Zhiwen Xu<sup>\*</sup> and Yinglun Li<sup>\*</sup>

College of Veterinary Medicine, Sichuan Agricultural University, Chengdu, China

## OPEN ACCESS

### Edited by:

Chenhe Su,  
Wistar Institute, United States

### Reviewed by:

Yiping Wang,  
University of Florida, United States  
Lianci Peng,  
Southwest University, China

### \*Correspondence:

Zhiwen Xu  
abtcxzw@126.com  
Yinglun Li  
liyinglun02@163.com

<sup>†</sup>These authors share first authorship

### Specialty section:

This article was submitted to  
Viral Immunology,  
a section of the journal  
Frontiers in Immunology

Received: 15 March 2022

Accepted: 19 April 2022

Published: 24 May 2022

### Citation:

Tang H, Yang D, Zhu L, Shi F, Ye G,  
Guo H, Deng H, Zhao L, Xu Z and Li Y  
(2022) Paeonol Interferes With  
Quorum-Sensing in *Pseudomonas*  
*aeruginosa* and Modulates Inflammatory  
Responses *In Vitro* and *In Vivo*.  
*Front. Immunol.* 13:896874.  
doi: 10.3389/fimmu.2022.896874

Developing quorum-sensing (QS) based anti-infection drugs is one of the most powerful strategies to combat multidrug-resistant bacteria. Paeonol has been proven to attenuate the QS-controlled virulence factors of *P. aeruginosa* by down-regulating the transcription of QS signal molecules. This research aimed to assess the anti-virulence activity and mechanism of paeonol against *P. aeruginosa* infection *in vitro* and *in vivo*. In this study, paeonol was found to reduce the adhesion and invasion of *P. aeruginosa* to macrophages and resist the cytotoxicity induced by *P. aeruginosa*. Paeonol reduced the expression of virulence factors of *P. aeruginosa* by inhibiting QS, thereby reducing the LDH release and damage of *P. aeruginosa*-infected macrophages. Paeonol can inhibit bacterial virulence and enhance the ability of macrophages to clear *P. aeruginosa*. In addition, paeonol exerts anti-inflammatory activity by reducing the expression of inflammatory cytokines and increasing the production of anti-inflammatory cytokines. Paeonol treatment significantly inhibited the activation of TLR4/MyD88/NF- $\kappa$ B signaling pathway and decreased the inflammation response of *P. aeruginosa*-infected macrophages. Paeonol also significantly reduced the ability of *P. aeruginosa* to infect mice and reduced the inflammatory response. These data suggest that paeonol can inhibit the virulence of *P. aeruginosa* and decrease the inflammation response in *P. aeruginosa*-infected macrophages and mice, which can decrease the damage induced by *P. aeruginosa* infection and enhance the ability of macrophages to clear bacteria. This study supports the further development of new potential anti-infective drugs based on inhibition of QS and virulence factors.

**Keywords:** paeonol, *P. aeruginosa*, RAW264.7, quorum sensing, inflammation

## INTRODUCTION

*Pseudomonas aeruginosa* (*P. aeruginosa*) is a common gram-negative bacterial opportunistic pathogen that is related to the development of acute and chronic pulmonary infections in cystic fibrosis (CF), non-CF bronchiectasis, and chronic obstructive pulmonary disease with high morbidity and mortality (1–3). Lung infections caused by *P. aeruginosa* are exacerbated by the intracellular invasion and persistence of the pathogen, especially in CF patients. Intracellular

invasion is a favorable mechanism for pathogens to avoid host defense and antimicrobial therapy (4). The intrinsic ability for *P. aeruginosa* to invade and adhere to host cells of infection is ascribed to its impenetrable biofilm formation and an elaborate arsenal of virulence factors designed to damage the host membrane barrier and evade immune responses, coupled with its rapidly acquired antibiotic resistance (5, 6).

Quorum-sensing (QS) is a signaling mechanism by which cell-to-cell communication receives input from adjacent cells and coordinates collective behavior, enabling the bacteria to survive within the host, releasing a range of virulence factors, and developing biofilm (7, 8). *P. aeruginosa* produces an armory of factors associated with intracellular communication and extracellular virulence, regulated by the quorum-sensing system of the diffusible signaling molecule (N-acyl L-homoserine lactone, AHLs) and determines the pathogenesis of bacteria (9, 10). Early colonization and dissemination of *P. aeruginosa* infection in host tissues is initiated by proteases and elastases, while pyocyanin interferes with various cellular functions such as chelated iron absorption, respiration, and enhances virulence expression (11, 12). Rhamnolipid promotes the surface movement of *P. aeruginosa* to form biofilms and participates in the diffusion of mature biofilms (13). *P. aeruginosa* produces different secondary metabolites and multiple virulence factors to modify host defense response, and macrophages play a crucial role in infections of patients with CF (14).

The lung innate immune response plays an important role in clearing lung pathogens. During the initial stages of *P. aeruginosa* invasion, the secretion of cytokines and chemokines induces many neutrophils to migrate to the infected site. However, the overactivation of innate immune cells (alveolar macrophages or neutrophils) can produce various proinflammatory molecules, causing severe airway injury and damaged lung function (15–17). After specifically recognizing microbial ligands, Toll-like receptors (TLRs) recruit various binding molecules to activate inflammatory gene transcription, and immune responses (18, 19). *P. aeruginosa*-induced activation of macrophages is majorly based on the recognition of pathogens by molecular pattern receptors, including TLRs, such as TLR2 and TLR4, and the mannose receptor, thus activating downstream nuclear factor kappa B (NF- $\kappa$ B) and mitogen-activated protein kinase (MAPK) signaling pathway increasing macrophages release of various cytokines and chemokines from response to *P. aeruginosa* infection (20–22).

Natural products targeted specific genes that inhibit the growth or pathogenicity of bacteria and control extracellular virulence, such as EGCG, Curcumin, and Eugenol-Containing Essential Oils, which have been investigated as QS inhibitors (23–25). Paeonol is a polyphenolic compound originally extracted from *Paeonia lactiflora*, *Moutan cortex*, and *Cynanchum paniculatum*, which has been used widely due to various medicinal benefits as an analgesic, antipyretic, and anti-inflammatory agent in traditional Chinese medicine (26, 27). Previous studies have demonstrated that paeonol attenuates quorum-sensing, inhibits virulence factors, and biofilm

formation (28). Paeonol has been well-documented for revealing potential anti-inflammatory activity in macrophages (29, 30), but the possible mechanism by regulating virulence and inflammation to reduce pathological damage upon pathogenic *P. aeruginosa* infection has not yet been fully studied *in vitro* and *in vivo*.

## MATERIALS AND METHODS

### Bacterial Strains and Culture Conditions

*P. aeruginosa* PAO1 (ATCC 15692) was stored in our laboratory. For all the experiments, PAO1 was grown in LB broth at 37°C with shaking, collected by centrifugation (4,000 rpm for 5 min), and diluted in the appropriate experimental medium.

### Cell Culture

RAW264.7 cells were obtained from the Cell Bank of the Chinese Academic of Sciences (Shanghai, China) and cultured in DMEM medium (HyClone, Beijing, China) with 10% fetal bovine serum (FBS, TransGen Biotech, Beijing, China) and antibiotics (100 U/ml penicillin and 100  $\mu$ g/ml streptomycin) (Haimen, China). The cells incubated in a cell incubator at 37°C with humidified air and 5% CO<sub>2</sub>.

### Cell Viability

The viability of RAW264.7 macrophage cells was determined using the CCK8 assay. Briefly, RAW264.7 ( $1 \times 10^5$  cells/mL) were suspended in complete cell culture media, and 150  $\mu$ L of the cell suspension was cultured in 96-well plates for 24 h. After treatment with paeonol, cell viability was evaluated using the Cell Counting Kit-8 (Sangon, Biotech, Shanghai, China).

### *P. aeruginosa* Infection of Macrophages

The *P. aeruginosa*-infected macrophages model used in this study was performed as described previously (31). RAW264.7 cells were seeded into 12-well tissue culture plates at a density of  $5 \times 10^5$  cells/well and then reached 80–90% confluence. *P. aeruginosa* were collected and suspended to  $10^8$  CFUs/mL in DMEM without antibiotics. RAW264.7 cells were incubated with *P. aeruginosa* at three multiplicity of infection (MOIs, 25, 50, or 100) in DMEM without antibiotics. After 2 h or 4 h of PAO1 infection, cells were washed with phosphate-buffered saline (PBS), then lysed with 0.5% Triton-X for 15 min at 37 °C. For invasion assay, extracellular bacteria were killed with 200  $\mu$ g/mL gentamicin for 1 h. The attachment and invasion levels were assessed by bacterial plate count.

### Cell Treatment

At 80%–90% confluence, cells were washed third with PBS, then subsequently incubated with *P. aeruginosa* of 100 (MOI) in antibiotic-free DMEM for 4 h. Cells were divided into four groups: the first part involved the control group (RAW264.7 cells group) and the *P. aeruginosa* infection group (PAO1). On this basis, the second part was set up as three parallel groups, namely PAO1 (MOI = 100:1, infection for 4 h) as cells model

group, paeonol pretreatment (32  $\mu\text{g}/\text{mL}$ , 64  $\mu\text{g}/\text{mL}$  and 128  $\mu\text{g}/\text{mL}$ , pretreatment for 3 h) + PAO1 group and paeonol (32  $\mu\text{g}/\text{mL}$ , 64  $\mu\text{g}/\text{mL}$  and 128  $\mu\text{g}/\text{mL}$ , treatment for 4 h) + PAO1 treatment group. These concentrations were no bacteriostatic effect, and previous studies confirmed that the MIC of paeonol against *P.aeruginosa* was greater than 512  $\mu\text{g}/\text{ml}$ .

### Determine mRNA Expression Levels of QS-Related Virulence Genes of *P. aeruginosa* by qPCR

Total RNA was reverse-transcribed to cDNA, and qPCR was carried out by the instruction of commercial kit. **Table 1** shows the primers used to amplify *lasI/R*, *rhII/R*, *pqsA/R*, *LasA*, *LasB*, *rhIA*, *rhIC*, *phzM*, *phzM*, *phzH*, *phzS*, and *rpoD* (reference gene). qPCR data were analyzed to calculate the relative differences in mRNA expression using the  $2^{-\Delta\Delta\text{CT}}$  method.

### Lactate Dehydrogenase Assay

The macrophages infected with *P. aeruginosa* (MOI=100:1) for 4 h, then treated with Paeonol at the concentrations of 32  $\mu\text{g}/\text{mL}$ , 64  $\mu\text{g}/\text{mL}$  and 128  $\mu\text{g}/\text{mL}$ . The culture supernatants were harvested and centrifuged at 12,000 g for 5 min, and LDH activity was monitored by an LDH cytotoxicity assay kit (Jiancheng Biotech, Nanjing, China).

### Live/Dead cell Assay

The effects of paeonol on the viability or cytotoxicity of macrophages cells were assayed using the Calcein-AM/PI Double Stain Kit (Solarbio, Beijing, China). In brief, RAW264.7 cells were exposed to *P. aeruginosa* in DMEM without antibiotics and treated with paeonol. The cells washed with PBS three times and stained with a 100  $\mu\text{L}$  Calcein-AM/PI stain solution at 37°C for 15 min. Living cells with green cytoplasmic fluorescence and dead cells with red nuclei were immediately observed by the fluorescence microscope.

### Adhesion and Invasion Assay

To further reveal the role of paeonol on macrophage-mediated phagocytosis, the intracellular killing of *P. aeruginosa*.

Macrophages infected with *P. aeruginosa* (MOI=25:1 for 4 h) treated with paeonol (32, 64, and 128  $\mu\text{g}/\text{mL}$ ). Cells were washed with phosphate-buffered saline (PBS) and then lysed with 0.5% Triton-X for 15 min at 37°C. Extracellular bacteria were killed with 200  $\mu\text{g}/\text{mL}$  gentamicin for 1 h to evaluate the intracellular bacteria. Attachment and invasion levels were assessed by bacterial plate count.

### Ultrastructure Examination by Transmission Electron Microscope

The macrophages infected with *P. aeruginosa* (MOI=25:1 for 2 h) were treated with Paeonol (128  $\mu\text{g}/\text{ml}$ ). The cells were washed with PBS three times, and fixed with 2.5% glutaraldehyde at 4°C overnight. Samples were collected and treated with osmium ferrocyanide for 1 h, dehydrated in graded ethanol concentrations (50%, 70%, 80%, 90%, 95%, and 100%) and 100% acetone, infiltrated, and embedded in epoxy resin. Subsequently, ultrathin sections (60-80 nm) were cut with a diamond knife on a microtome (Leica EM UC7; Leica Corporation, Germany) and were stained with saturated aqueous uranyl acetate and counterstained with 4% lead citrate, and finally observed using HT-7700 TEM (Hitachi, Tokyo, Japan).

### Flow Cytometry Assay

Paeonol (32  $\mu\text{g}/\text{mL}$ , 64  $\mu\text{g}/\text{mL}$  and 128  $\mu\text{g}/\text{mL}$ ) treated macrophages (infected with *P. aeruginosa* (MOI=25:1) for 2 h) were washed with PBS, separated to single-cell suspension, and resuspended in staining buffer (BD Biosciences). The cells were stained with F4/80 (Elabscience, E-AB-F0995C), CD86 (Elabscience, E-AB-F0994E), and CD206 (Elabscience, E-AB-F1135D) fluorescently labeled antibody, then detected by a flow cytometer (Beckman coulter, CytoFLEX) and analyzed by the Flowjo software.

### Determination of mRNA Expression Levels of Inflammation and TLR4/MyD88/NF- $\kappa$ B Pathway of Macrophages by qPCR

The mRNA expression levels of the TLR4/MyD88/NF- $\kappa$ B pathway of Paeonol treated RAW264.7 (infected with *P.*

**TABLE 1** | qPCR primers of *P. aeruginosa* for analysis of gene expression.

Genes	Primer sequences (5, -3, )	
<i>lasI</i>	F: CGCACATCTGGGAAGCTCA	R: CGGCACGGATCATCATCT
<i>lasR</i>	F: CTGTGGATGCTCAAGGACTAC	R: AACTGGTCTTGCCGATGG
<i>rhII</i>	F: GTAGCGGGTTTTGCGGATG	R: CGGCATCAGGTCTTCATCG
<i>rhIR</i>	F: GCCAGCGTCTTGTTCGG	R: CGGTCTGCCTGAGCCATC
<i>pqsA</i>	F: GACCGGCTGTATTTCGATTC	R: GCTGAACCCAGGGAAGAAG
<i>pqsR</i>	F: CTGATCTGCCGGTAATTGG	R: ATCGACGAGGAAGTGAAGA
<i>lasA</i>	F: CTGTGGATGCTCAAGGACTAC	R: AACTGGTCTTGCCGATGG
<i>lasB</i>	F: AACCGTGCGTTCTACCTGTT	R: CGGTCCAGTAGTAGCGGTTG
<i>rhIA</i>	F: TGGCCGAACATTTCAACGT	R: GATTTCCACCTCGTCGTCCTT
<i>rhIC</i>	F: GCCATCCATCTCGACGGAC	R: CGCAGGCTGTATTTCGGTG
<i>phzM</i>	F: ACGGCTGTGGCGGTTTA	R: CCGTGACCGTCCGATT
<i>phzA</i>	F: AACGGTCAGCGGTACAGGGAAC	R: AACGGTCAGCGGTACAGGGAAC
<i>phzH</i>	F: GCTCATCGACAATGCCGAAGT	R: GCGGATCTCGCCGAACATCAG
<i>phzS</i>	F: CCGAAGGCAAGTCGCTGGTGA	R: GGTCCAGTCGGCGAAGAAGC
<i>rpoD</i>	F: GGGCGAAGAAGGAAATGGTC	R: CAGGTGGCGTAGGTGGAGAA

*aeruginosa* (MOI=100:1) for 4 h) cells were assayed by qPCR. The gene sequences of TLR4, MyD88, TRAM, NF- $\kappa$ B, I $\kappa$ B, I $\kappa$ B $\alpha$ , IKK- $\beta$ , p65, p50, TNF- $\alpha$ , IL-1 $\beta$ , IL-6, IL-8, iNOS, COX-2, IL-2, IL-4, and IL-10 were retrieved from NCBI, and the primers of these genes (Table 2) were synthesized by HuaDa Gene company (Beijing, China). GAPDH gene was selected as the reference gene. qPCR reaction was conducted on a LightCycler<sup>®</sup>II real-time fluorescent quantitative PCR instrument (Roche, USA) using the PerfectStart<sup>™</sup> Green qPCR SuperMix (TransGen Biotech, Beijing, China) following the standard steps. All data output from the qPCR experiments were analyzed using the 2<sup>- $\Delta\Delta$ CT</sup> method.

## Anti-Infection Activity of Paeonol Against *P. aeruginosa* by Quorum Sensing *In Vivo*

Fifty SPF mice (4 weeks) were obtained from Sibeifu Biotechnology Co. Ltd. (Beijing, China). The animals were housed at 22-25°C on a 12 h day-night cycle, fed standard rodent chow and sterile water ad libitum for 1 week of acclimation. All protocols for animal studies were reviewed and approved by the Animal Ethical Committee of Sichuan Agricultural University (#20210021). The mice were randomly divided into six groups (n=10): the control group, PAO 1 group, PAO 1+Pae (25 mg/kg) group, PAO 1+Pae (50 mg/kg), PAO 1+Pae (100 mg/kg), and CIP (20 mg/kg) group (positive control). The mice were administered the same dose of saline or drugs by intragastric administration for three days. In mice, infection was induced using the previously described method with modifications (32). Briefly, mice were weighed, anesthetized, and then received an intratracheal instillation of PAO 1 (2.5  $\times$  10<sup>8</sup> CFU) in 20  $\mu$ l phosphate-buffered saline (PBS) to model the acute infection of PAO 1. The mice were anesthetized and sacrificed after 24 h of infection, and lung tissue samples were harvested rapidly for subsequent analysis. Then the bacterial load, the expression of virulence, and inflammation cytokines were evaluated by PCR.

## Statistical Analysis

All values are expressed as mean  $\pm$  standard deviation (SD). All statistical analyses were performed using SPSS 20.0. Differences between all groups were analyzed using the one-way ANOVA test, and the result with  $P < 0.05$  or  $P < 0.01$  was considered statistically significant.

## RESULTS

### The Cytotoxicity Evaluation of Paeonol

The viability of RAW264.7 cells was performed in the presence of paeonol (0-512  $\mu$ g/mL) using the CCK-8 assay. The viability of cells is more than 90% at concentrations of 0-128  $\mu$ g/mL of paeonol, indicating that paeonol was not cytotoxic to RAW264.7 cells (Figure 1).

### The Model of Macrophages Infected With *P. aeruginosa*

The prolonged *P. aeruginosa* infection has been shown to cause a significant decrease in cell viability, arrest of cell growth, and morphology alternation, ultimately weakening the host's innate immune system's defense function and impaired bacterial clearance function. RAW264.7 cells were infected with *P. aeruginosa* at different MOI (25, 50, 100) to explore the effect of *P. aeruginosa* infection on bacterial adhesion and invasion. Figures 2A, B indicated that *P. aeruginosa* could adhere to and invade the cells. As the PAO1 MOI value and infection time increased, the number of *P. aeruginosa* attaching to and invading macrophages increased (Figure 2).

### Paeonol Attenuate QS Genes of *P. aeruginosa* in Macrophages Infection Model

*P. aeruginosa* secretes various virulence factors and forms biofilms regulated by the QS system. QS-related genes, including *lasI*, *lasR*, *rhlI*, *rhlR*, *pqsA*, and *pqsR* were analyzed

**TABLE 2** | List of primers of the macrophage TLR4/MyD88/NF- $\kappa$ B pathway in qPCR analysis.

Genes	Primer sequences (5, -3, )	
<i>TNF-<math>\alpha</math></i>	F: CTTCTGTCTACTGAACCTTCGGG	R: CAGGCTTGTCACTCGAATTTTG
<i>IL-1<math>\beta</math></i>	F: GAAATGCCACCTTTTGACAG	R: TGGATGCTCTCATCAGGACAG
<i>IL-6</i>	F: CTTCCATCCAGTTGCCTTCT	R: CTTCTGTGACTCCAGCTTATC
<i>IL-8</i>	F: TGTGGGAGGCTGTGTTTGTGA	R: ACGAGACCAGGAGAAACAGG
<i>IFN-<math>\beta</math></i>	F: CAGCTCCAAGAAAGGACGAAC	R: GGCAGTGTAACTCTTCTGCAT
<i>iNOS</i>	F: ACTGTGCCATCAGCAAGGTT	R: GCTCTTTGTCCATTGGGTTCTT
<i>COX-2</i>	F: TGCTGTACAAGCAGTGGCAA	R: GCAGCCATTTCTCTCTCTCC
<i>IL-2</i>	F: TGTGGAATGGCGTCTCTGTGTC	R: AGTTCAATGGGCAGGGTCTC
<i>IL-4</i>	F: GGTCTCAACCCCGAGCTAGT	R: GCCGATGATCTCTCTCAAGTGAT
<i>IL-10</i>	F: GCCGAGGAGATCGTCACC	R: CAGGCGTAGAAGATGTCGGA
<i>TLR4</i>	F: GGACTCTGATCATGGCACTG	R: CTGATCCATGCATTGGTAGGT
<i>MyD88</i>	F: ACTCGCAGTTTGTGGATG	R: CACCTGTAAGGCTTCTCG
<i>TRAM</i>	F: AGCCAGAAAGCAATAAGC	R: CAAACCCAAAGAACCAAG
<i>NF-<math>\kappa</math>B</i>	F: CTGAAACTACTGATTGCTGCTGGA	R: GCTATGTGAAGAGGGCGTTGTGC
<i>I<math>\kappa</math>B</i>	F: GCCATCCCAGGCAGTATCTA	R: TTCCAAGACCAGACCTCCAG
<i>I<math>\kappa</math>B<math>\alpha</math></i>	F: GCCCTTCTGGGATTTCTC	R: GCGGCTCCGCTTCGTTCT
<i>IKK-<math>\beta</math></i>	F: TCAGCTAATGTCCAGCCTTC	R: CCAGTCTAGAGTCTGTGAAGC
<i>P65</i>	F: CGGGATGGCTACTATGAGGCTGACC	R: GATTGCTGGCTAATGGCTTGCT
<i>P50</i>	F: GTGATTTGTGCCAGCCAGGAAGC	R: TTCTTAACCCGAAGCCCTTGATT
<i>GAPDH</i>	F: GGTGAAGGTGCGGTGTGAACG	R: CTCGCTCTGGAAGATGGTG

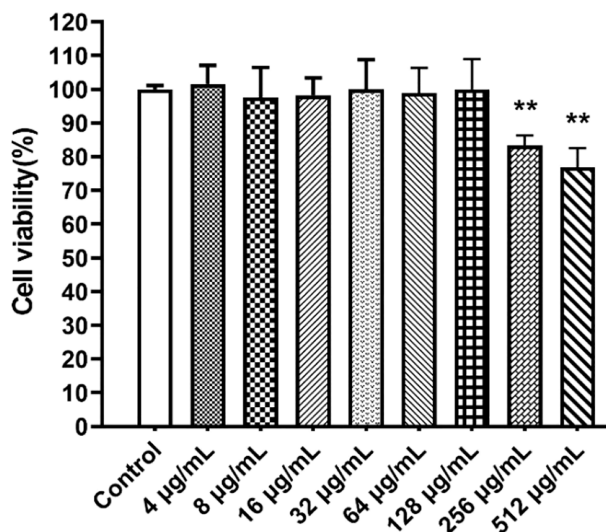


**FIGURE 1** | The CCK8 assay was used to determine the cytotoxicity of paeonol on RAW264.7 cells. All data were expressed as means  $\pm$  SD (n=3). \*\*P < 0.01 vs the control group.

following pretreatment or treatment with paeonol. The results showed that paeonol downregulated the expression of QS-related virulence genes of PAO1, and the therapeutic effect is significantly greater than the preventive effect. The inhibition rate in the presence of paeonol (128  $\mu$ g/ml) was as follows: *lasI* 58.95%, *lasR* 59.20%, *rhII* 40.19%, *rhIR* 41.20%, *pqsA* 39.33%, *pqsR* 58.26%. These results demonstrated the anti-infection activity of paeonol against *P. aeruginosa*-infected macrophages by interfering with QS-mediated related genes expression in a concentration-dependent manner (Figure 3).

### Paeonol Attenuate Virulence Genes During *P. aeruginosa* Infected Macrophages

*P. aeruginosa* secretes a variety of virulence factors and forms biofilms, the expression of QS-regulated and QS-virulence genes was detected to assess the anti-infection activity of paeonol against *P. aeruginosa*-infected macrophages. QS system was analyzed in the macrophages cell infected *P. aeruginosa*

following pretreatment and treatment at the same time with paeonol. The results showed that paeonol downregulated the expression of QS-related virulence genes in PAO1 infected RAW264.7 macrophages, and the therapeutic effect is significantly greater than the preventive effect. The inhibition rate in the presence of paeonol (128  $\mu$ g/ml) was as follows: *lasA* 56.47%, *lasB* 61.81%, *rhIA* 47.65%, *rhIC* 56.74%, *phzA* 18.28%, *phzM* 7.73%, *phzH* 45.50% and *phzS* 35.47% (Figure 4).

### Viability and Cytotoxicity of Paeonol on Macrophages Infected With *P. aeruginosa*

Bacterial infection can cause the destruction of the membrane structure of cells, resulting in the release of LDH in the cytoplasm into the culture medium. The detection of cytotoxicity can be achieved by detecting the activity of LDH in the culture medium. The LDH levels were detected by Fe<sup>2+</sup>-xylene orange-based kit. Compared with the control (RAW264.7), PAO1 significantly inhibited the proliferation of macrophages cells, but the release of

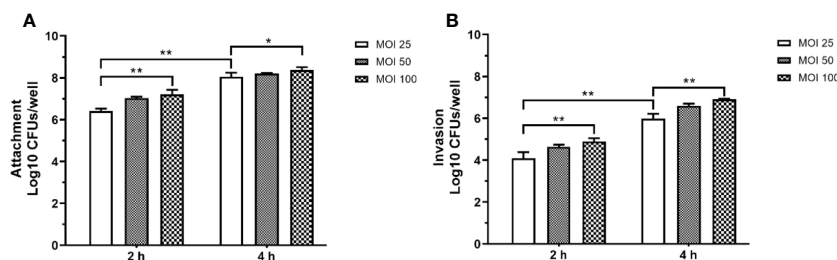


**FIGURE 2** | The adhesion (A) and invasion (B) of *P. aeruginosa* infected RAW264.7 cells with different MOI (10, 50, 100). The extracellular or intracellular bacteria were counted by plate. For the invasion assay, extracellular bacteria were killed with 200  $\mu$ g/mL gentamicin. All data were expressed as means  $\pm$  SD (n=3). \*P < 0.05, \*\*P < 0.01 vs the control group.

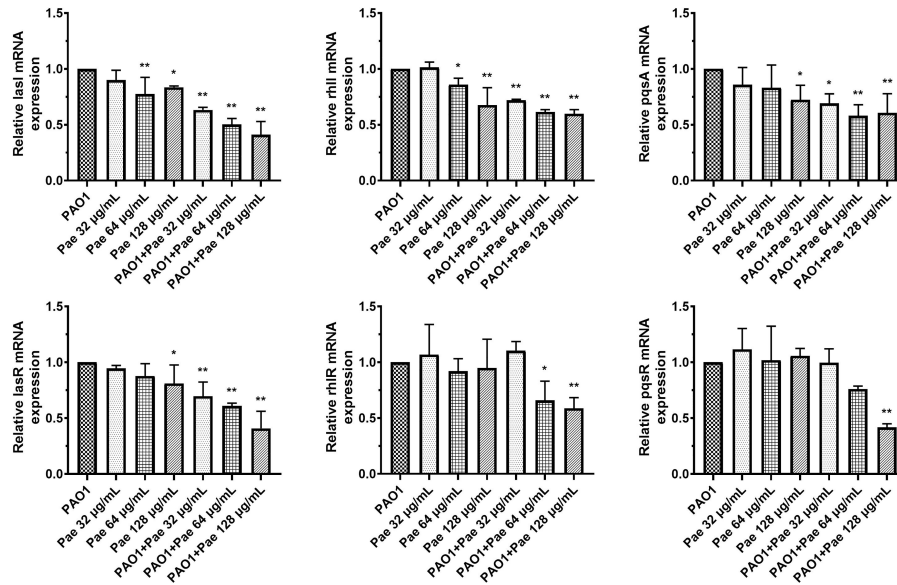


**FIGURE 3** | Transcriptional levels of the QS genes during *P. aeruginosa* infected macrophages (MOI = 100:1) following pretreatment and treatment with paeonol. lasI, rhlI, pqxA, lasR, rhlR, and pqeR. “Pae 32 µg/mL”, “Pae 64 µg/mL”, “Pae 128 µg/mL” indicate that RAW264.7 cells were pretreated with paeonol for 3 h before infection with PAO1. “PAO1+Pae 32 µg/mL”, “PAO1+Pae 64 µg/mL”, “PAO1+Pae 128 µg/mL” indicate that RAW264.7 cells were infected with PAO1 and treated with paeonol at the same time. The expression of mRNA was tested by RT-PCR. All data were expressed as means ± SD (n=3). \* $P < 0.05$  or \*\* $P < 0.01$  vs the control group.

LDH decreased in a concentration-dependent manner by paeonol treatment, and paeonol did not affect the proliferation of macrophages at the experimental concentrations (**Figure 5A**). To directly examine the cell viability or cytotoxicity, RAW264.7 cells were exposed to PAO1 treated without or with paeonol, then labeled with Calcein-AM and PI dyes and immediately

observed by fluorescence microscope. **Figure 6** illustrates that macrophages cells infected with PAO1 were mainly dead (red, propidium iodide-positive), but treated with paeonol groups were mainly viable cells (green, calcein-positive) and a few dead cells. The results indicated that paeonol within 128 µg/mL is not cytotoxic to RAW264.7 cells (**Figure 5B**).

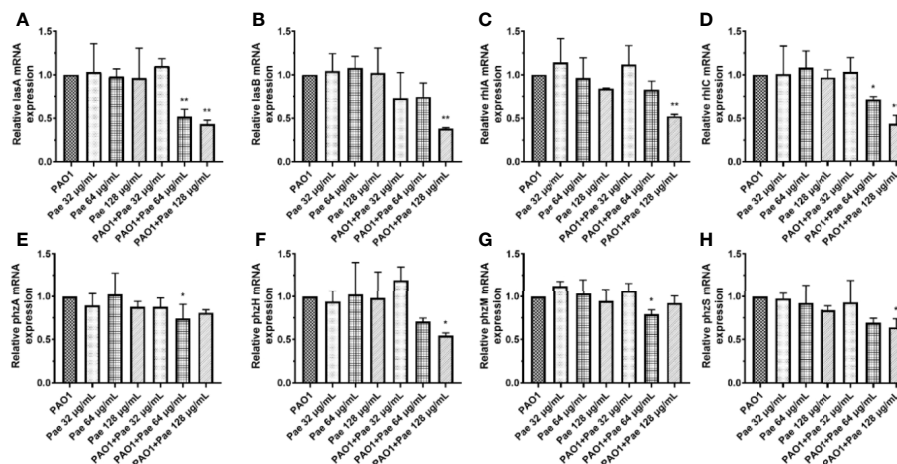


**FIGURE 4** | Transcriptional levels of the virulence genes during *P. aeruginosa* infected macrophages (MOI = 100:1) following pretreatment and treatment with paeonol. (A) lasA, (B) lasB, (C) rhlA, (D) rhlC (E) phzA, (F) phzH, (G) phzM, (H) phzS. “Pae 32 µg/mL”, “Pae 64 µg/mL”, “Pae 128 µg/mL” indicate that RAW264.7 cells were treated with paeonol for 3 h before infection with PAO1. “PAO1+Pae 32 µg/mL”, “PAO1+Pae 64 µg/mL”, “PAO1+Pae 128 µg/mL” indicate that RAW264.7 cells were infected with PAO1 and treated with paeonol at the same time. The expression of mRNA was tested by RT-PCR. All data were expressed as means ± SD (n=3). \* $P < 0.05$  or \*\* $P < 0.01$  vs the control group.



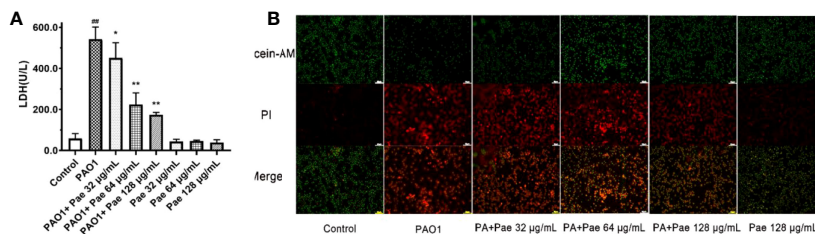


**FIGURE 5** | Cell viability were tested in PAO1 infected RAW264.7 (MOI = 25:1) without or with paeonol treatment for 4 h. The  $\text{Fe}^{2+}$ -xylenol orange-based LDH kit (A) and calcein-AM or PI dyes (B) were used in the testing. “Pae 32 µg/mL”, “Pae 64 µg/mL”, “Pae 128 µg/mL” indicate that RAW264.7 cells were pretreated with paeonol for 3 h before infection with PAO1. “PAO1+Pae 32 µg/mL”, “PAO1+Pae 64 µg/mL”, “PAO1+Pae 128 µg/mL” indicate that RAW264.7 cells were infected with PAO1 and treated with paeonol. ## $p < 0.01$  vs. Control Group, \* $P < 0.05$  or \*\* $P < 0.01$  vs the PAO1 group.

## Paeonol Decreased the Adhesion and Invasion of PAO1

RAW264.7 cells were infected with PAO1 to determine the bacterial adhesion and invasion. Compared with the PAO1 group, bacteria adhesion on macrophages significantly decreased after paeonol treatment. Further study revealed that paeonol reduced the invasion of PAO1 to RAW264.7 cells (Figure 6).

## Effects of Paeonol on the Ultrastructure of RAW264.7 Macrophages Infected by PAO1

TEM was performed to detect the ultrastructure of RAW264.7 macrophages infected by PAO1 and treated with paeonol. As shown in Figure 7, there were no significant changes in the blank control group. In the PAO1 group, *P. aeruginosa* invaded macrophages, PAO1 was encapsulated by vesicles, part of the vesicle membrane was destroyed, mitochondria were swollen and vacuolized, escaped phagosomes into the cytoplasm, causing nuclear shrinkage, and even cell damage or lysis. In the paeonol (128 µg/mL) treated group, *P. aeruginosa* invasion was reduced and encapsulated by intact vesicles, the mycelium changed from rod-like to round, the fusion between PAO1 and lysosome

increased, the mitochondria slightly swollen and more filamentous, the nucleus of the cell was intact, and the cell injury was reduced.

## Paeonol Suppressed Inflammation in RAW264.7 Cells Infected *P. aeruginosa*

Compared with the control group, the relative mRNA expression level of IL-1 $\beta$ , IL-6, IL-8, TNF- $\alpha$ , COX2, and iNOS in the PAO1 group was upregulated, respectively. Compared with the PAO1 group, paeonol can attenuate the expression of inflammatory cytokines like IL-1 $\beta$ , IL-6, IL-8, TNF- $\alpha$ , various inflammatory mediators such as COX2, iNOS, and upregulated the relative mRNA expression level of IL-2, IL-4, IL-10. Paeonol treatment significantly prevented the inflammation changes induced by *P. aeruginosa* in a dose-dependent manner (Figure 8).

## Paeonol Changed the Polarization of Macrophages

Flow cytometry was used to detect macrophage polarization. F4/80 biomarker was used to label macrophages, and CD86/CD206 anti-body was used to check the surface biomarker of macrophages, respectively. The CD86 biomarker significantly

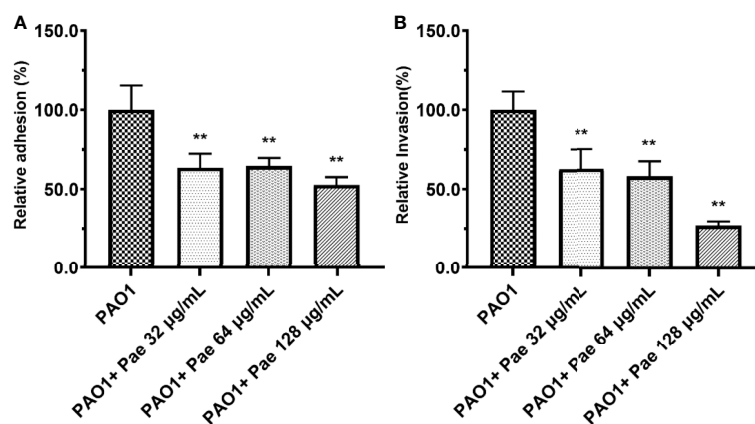


**FIGURE 6** | Adhesion (A) and invasion (B) were tested in PAO1-infected RAW264.7 (MOI = 25:1) with paeonol treatment for 4 hours. “PAO1+Pae 32 µg/mL”, “PAO1+Pae 64 µg/mL”, “PAO1+Pae 128 µg/mL” indicate that RAW264.7 cells were infected with PAO1 and treated with paeonol. The bacteria were cultivated and counted on a TSB plate. All data were expressed as means  $\pm$  SD (n=3). \*\* $P < 0.01$  vs the control group.

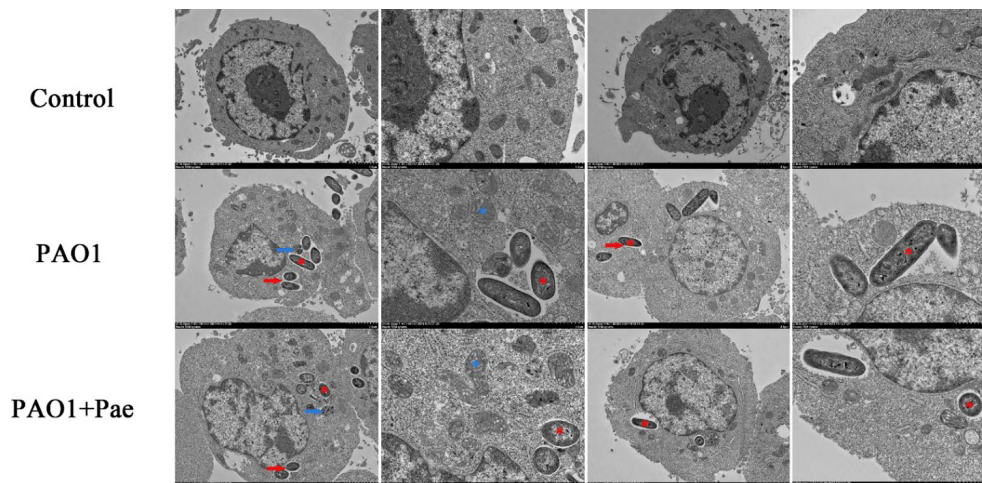


**FIGURE 7** | Transmission electron microscope observation of paeonol on the ultrastructure of RAW264.7 macrophages infected with *P. aeruginosa* PAO1 (MOI=25:1). Scale bar, 2  $\mu$ m (low magnification in columns one and three) and 1  $\mu$ m (high magnification in columns two and four); red\* indicates PAO1, blue\* indicates mitochondria; red arrows indicate vesicles, blue arrows indicate autophagosome-lysosomes.

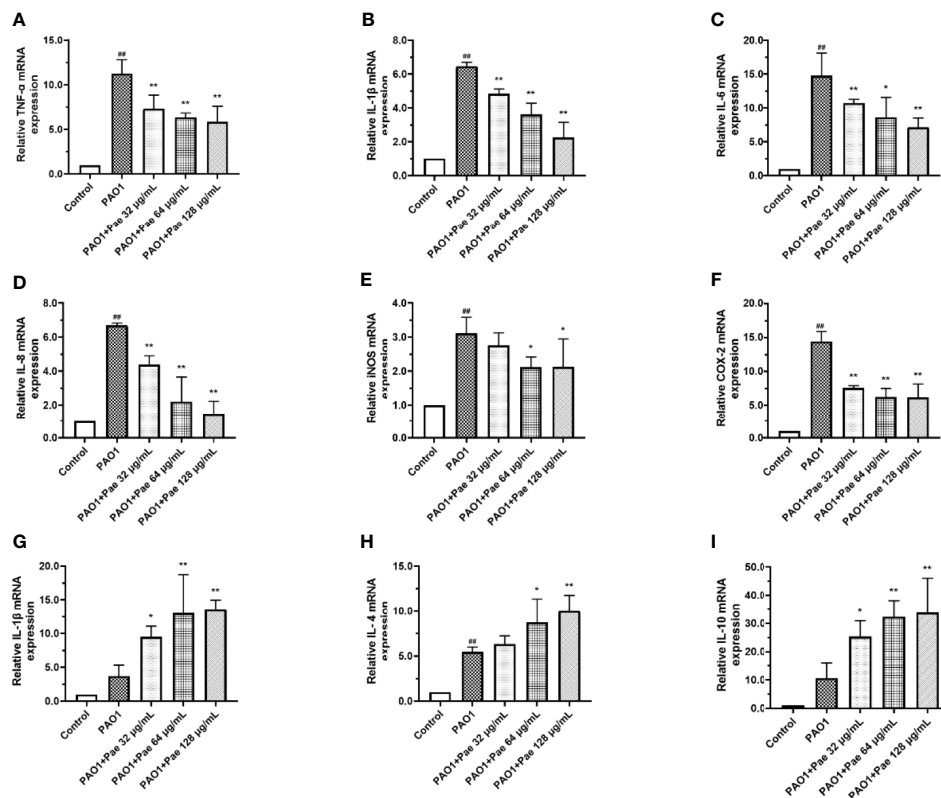


**FIGURE 8** | Cytokines mRNA expression were tested in PAO1-infected RAW264.7 (MOI = 100:1) with paeonol treatment. **(A)** TNF- $\alpha$ , **(B)** IL-1 $\beta$ , **(C)** IL-6, **(D)** IL-8, **(E)** iNOS, **(F)** COX-2, **(G)** IL-2, **(H)** IL-4, **(I)** IL-10, “PAO1+Pae 32  $\mu$ g/mL”, “PAO1+Pae 64  $\mu$ g/mL”, “PAO1+Pae 128  $\mu$ g/mL” indicate that RAW264.7 cells were infected with PAO1 and treated with paeonol. The expression of mRNA was tested by RT-PCR. All data were expressed as means  $\pm$  SD (n=3). \* $p$  < 0.05, \*\* $p$  < 0.01 vs. control Group, \* $P$  < 0.05 or \*\* $P$  < 0.01 vs the PAO1 group.

was significantly upregulated when macrophages were infected with PAO1. Paeonol significantly decreased the polarization of macrophages by decreasing the CD86 biomarker when the treatment concentrations higher than 64  $\mu\text{g}/\text{mL}$  (Figure 9).

### Effect of Paeonol on the TLR4/MyD88/NF- $\kappa\text{B}$ Pathway of Macrophages Infected With *P. aeruginosa*

TLR4/MyD88/NF- $\kappa\text{B}$  pathway is the fetal inflammation pathway for macrophages responding to the bacteria infection. To investigate the effect of paeonol on the TLR4/MyD88/NF- $\kappa\text{B}$  signaling pathway, the mRNA expression levels of TLR4, MyD88, TRAM, NF- $\kappa\text{B}$ , I $\kappa\text{B}$ , I $\kappa\text{B}\alpha$ , IKK- $\beta$ , p65, and p50 were measured by qPCR. In Paeonol treated cells, the mRNA expression levels of TLR4, MyD88, TRAM, NF- $\kappa\text{B}$ , I $\kappa\text{B}$ , I $\kappa\text{B}\alpha$ , IKK- $\beta$ , p65, and p50 were significantly downregulated, and I $\kappa\text{B}$  was markedly higher in comparison with those in the PAO1 group. These results demonstrated that paeonol attenuated *P. aeruginosa*-induced inflammation as evidenced by decreased expressions of TLR4/MyD88/NF- $\kappa\text{B}$  pathway in RAW264.7 cells, data were included in Figure 10.

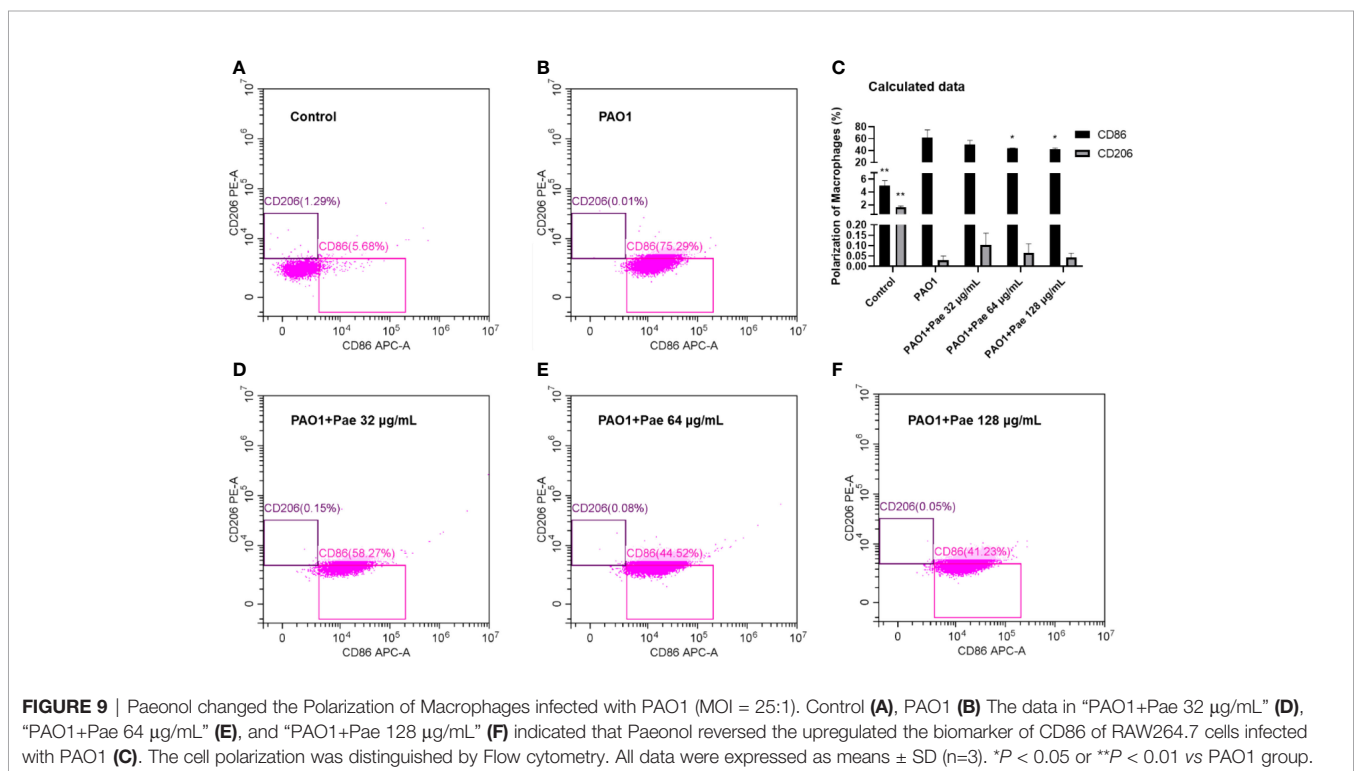
### Paeonol Showed an Effective Anti-Infection Activity *In Vivo*

Paeonol decreased the PAO1 load in the lung and inhibited the mRNA expression of inflammation cytokines, including IL-1 $\beta$ , IL-6, and TNF- $\alpha$  (Figures 11, 12). The mRNA expression of IL-4 was increased by IL-4. All three concentrations of paeonol decreased the expression of quorum sensing-related genes, *rhlR*, *LasR*, and *pqsA* (Figure 13).

## DISCUSSION

Due to the excessive and indiscriminate use of antibiotics, multidrug-resistant (MDR) bacteria are rapidly increasing and difficult to control by using conventional antibiotics (33–35). *P. aeruginosa*, a prevalent nosocomial-acquired and opportunistic pathogen, causes various acute and chronic infections, often involving the synergy of multiple virulence gene regulatory factors (36, 37). Macrophages are crucial innate immune cells that play a critical role in the host's response to bacterial infection. Macrophages pattern recognition receptors (PRRs), especially TLRs, recognize pathogen-associated molecular patterns (PAMPs) and activate intracellular various signaling pathways, such as inflammation, phagocytosis, apoptosis, and autophagy (38). Excessive inflammatory cytokines are detrimental to the host at the later stages of infection, and limiting excessive inflammatory response is crucial to controlling *P. aeruginosa* infection (39).

In the model of macrophages infected with *P. aeruginosa*, there was a significant up-regulation in the number of bacterial attachments and invasions to cells as the MOI value and infection time increased (40, 41). Therefore, the increase of co-aggregation between *P. aeruginosa* promotes the invasion of bacteria to macrophages, which may enable bacteria to evade host immune defense and cause great damage to host cells. The pathogenesis of *P. aeruginosa* is closely associated with biofilm formation, motility, and a myriad of extracellular virulence factors regulated by the QS system (42, 43). Large-scale expression of QS-related signaling molecules (AHL) or virulence factors (pyocyanin, protease, elastase, and rhamnolipids) were cytotoxic to



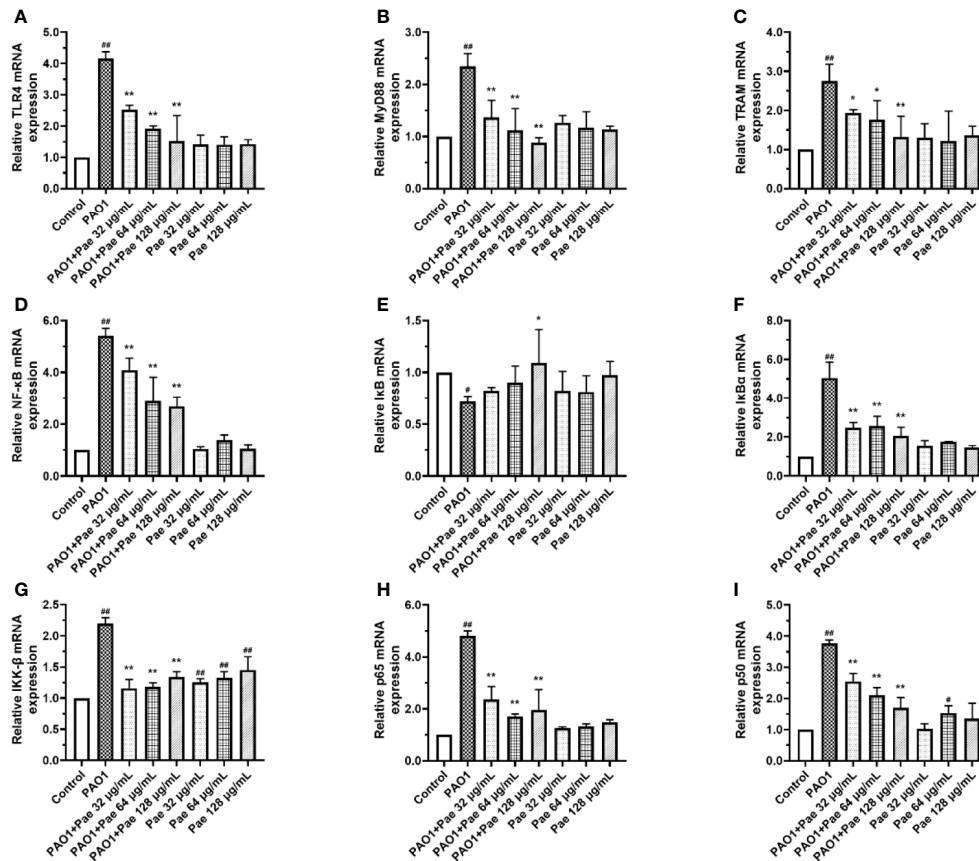


**FIGURE 10** | Paeonol inhibited the activation of TLR4/MyD88/NF-κB pathway in PAO1 infected RAW264.7 (MOI = 100:1). RAW264.7 were exposed to PAO1 treated without or with paeonol for 4 h to determine the mRNA expression levels of the TLR4/MyD88/NF-κB pathway. **(A)** TLR4, **(B)** MyD88, **(C)** TRAM, **(D)** NF-κB, **(E)** IκB, **(F)** IκBα, **(G)** IKK-β, **(H)** p65, **(I)** p50, “PAO1+Pae 32 μg/mL”, “PAO1+Pae 64 μg/mL”, “PAO1+Pae 128 μg/mL” indicate that RAW264.7 cells were infected with PAO1 and treated with paeonol. “Pae 32 μg/mL”, “Pae 64 μg/mL”, “Pae 128 μg/mL” indicate that RAW264.7 cells were treated with paeonol but without PAO1 infection. The expression of mRNA was tested by RT-PCR. All data were expressed as means ± SD (n=3). #p < 0.05, ##p < 0.01 vs. Control Group, \*P < 0.05 or \*\*P < 0.01 vs the PAO1 group.

macrophages (44). PAO1 significantly inhibited macrophages cell proliferation, induced cytotoxic responses, and led to cell membrane damage and rupture, lysis, and death. Our former studies had revealed that paeonol could attenuate quorum-sensing regulated virulence and biofilm formation in *P. aeruginosa* and show a protective effect on *C. elegans* infected with *P. aeruginosa* *in vivo* (28). Here, the potential therapeutic effect and mechanism of paeonol were investigated in a macrophage infected with a PAO1 cell model. The results revealed that paeonol inhibited *P. aeruginosa* QS-signaling pathway (*lasI/R*, *rhlI/R*, *pqsA/pqsR*) and virulence factors (*lasA*, *lasB*, *rhlA*, *rhlC*, *phzA*, *phzM*, *phzH*, and *phzS*) to alleviate the PAO1 induced cell damage (28).

The attachment and invasion of host cells is the key step in the *P. aeruginosa* infection cycle, and macrophages employ a variety of defense mechanisms to defend against invading pathogens. Phagocytosis and intracellular killing are two of the most important steps for bacterial eradication (45, 46). The motility of *P. aeruginosa* regulated by the QS system was crucial for colonization (13, 47). Studies showed that paeonol could resist the

adhesion and invasion of *P. aeruginosa* to infect macrophages, which may be related to the fact that paeonol reduced the motility ability of *P. aeruginosa*. Previous studies had shown that *P. aeruginosa* could directly induce cell death to aggravate tissue damage through its QS system or toxic factors such as pyocyanin (48, 49). TEM results showed that PAO1 co-polymerized with each other to adhere to cell junctions and invaded the interior of cells. Compared with the PAO1 group, the phagocytosis ability of macrophages was enhanced in the paeonol treatment groups. Paeonol resists the cell toxicity induced by *P. aeruginosa* and improves cell viability. This work confirmed the effect of paeonol against *P. aeruginosa* by attenuating virulence factors and its cytoprotective activity during bacterial infection either by downregulating the virulence or providing a protective effect to the host cells. Zhang et al. have reported that phagocytic macrophages undergo apoptosis 48 h after ingestion of *P. aeruginosa* (50). Moussouni et al. have reported that OprF regulates *P. aeruginosa* virulence factors and protects macrophages during acute infection by avoiding phagolysosome destruction (51).

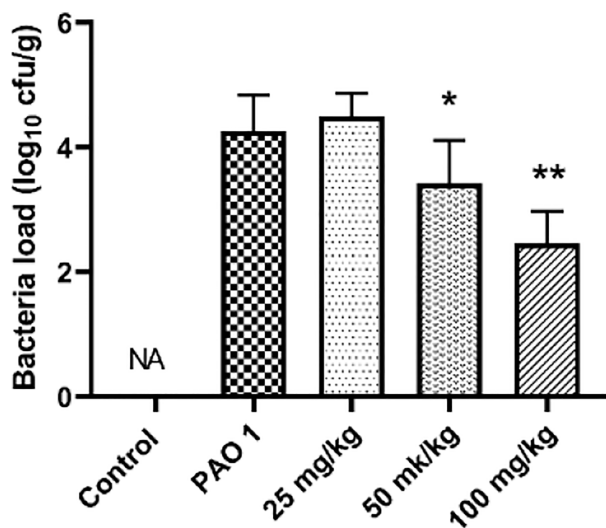


**FIGURE 11** | Paeonol decreased the bacterial load in the lung. All data were expressed as means  $\pm$  SD (n=3). \* $P$  < 0.05 or \*\* $P$  < 0.01 vs PAO1 group.

It has been reported that *P. aeruginosa* infection often exacerbates symptoms in patients, leading to organ dysfunction, followed by systemic inflammatory response syndrome and increased morbidity and mortality (52, 53). As an indispensable part of innate immunity, macrophages play an important role in inflammatory and immune responses. In this study, paeonol treatment significantly reduced *P. aeruginosa*-induced proinflammatory cytokine and improved anti-inflammatory factors produced by macrophages. The anti-inflammatory effect of paeonol was demonstrated in a PAO1-infected macrophage model and a PAO1 infected pneumonia model, and the results were consistent with LPS-induced

RAW264.7 inflammatory factors (30). Generally, activated macrophages differentiate into M1 or M2 phenotypes. M1 macrophages (the classically activated, proinflammatory) increase the level of oxidative stress-induced products, and tissue damage was noted in the acute inflammatory phase, and M2 macrophages (the alternative activated, anti-inflammatory) decrease inflammation and promote tissue repair (54, 55). Classically activated (M1) macrophages can be triggered by recognizing Gram-negative bacteria, and cascade inflammatory responses will be triggered. TLR4 recruits myeloid MyD88, leading to proinflammatory cytokine production with activation of NF- $\kappa$ B and the downstream gene targets (56, 57).

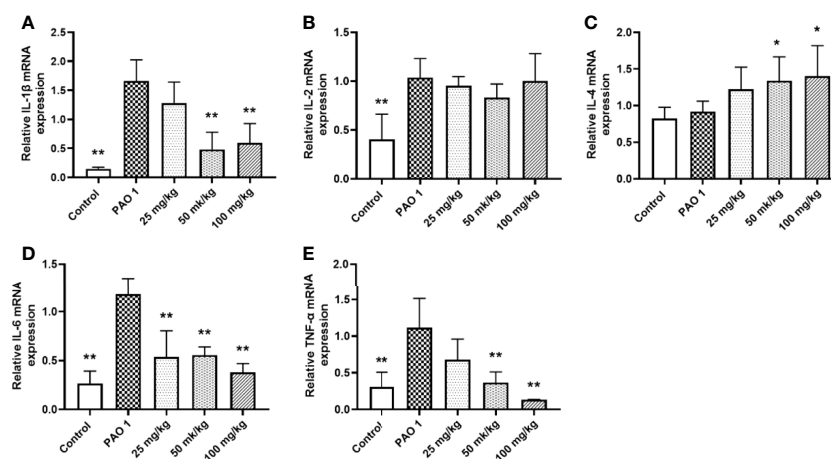


**FIGURE 12** | Paeonol inhibited the mRNA expression of inflammation cytokines in the lung. All data were expressed as means  $\pm$  SD (n=3). (A) IL-1 $\beta$ , (B) IL-2, (C) IL-4, (D) IL-6, (E) TNF- $\alpha$ . \* $P$  < 0.05 or \*\* $P$  < 0.01 vs PAO1 group.

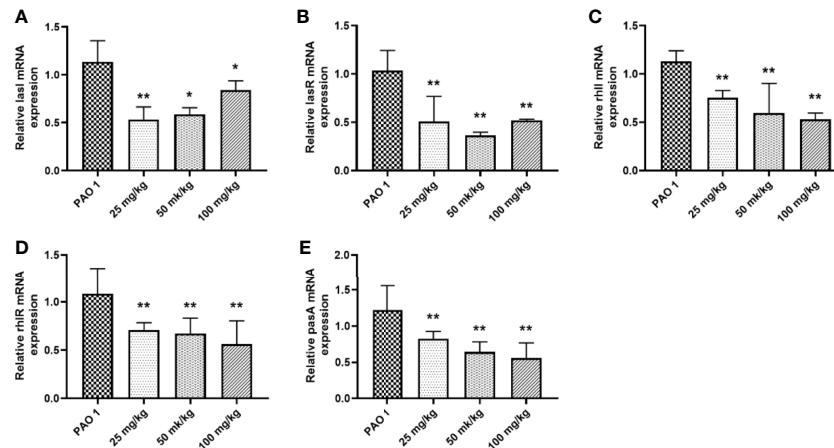


**FIGURE 13** | Paeonol inhibited the mRNA expression of QS genes in the lung. (A) *lasI*, (B) *lasR*, (C) *rhlI*, (D) *rhlR*, (E) *pqsA*. All data were expressed as means  $\pm$  SD (n=3). \* $P < 0.05$  or \*\* $P < 0.01$  vs PAO1 group.

The expression of key genes in the TLR4/MyD88/NF- $\kappa$ B signaling pathway and proinflammatory cytokines were induced by *P. aeruginosa* infection. After treatment with paeonol, the activation of inflammation pathway, expression of proinflammatory cytokines, and the M1 macrophages polarization were significantly inhibited in our results. Paeonol against PAO1 infection by inhibiting bacterial virulence and enhancing the clearance of pathogen by immune cells, which avoided severe inflammatory damage to cells and body. Collectively, this suggests that paeonol may represent a new promising anti-QS and anti-inflammatory agent that may prevent *P. aeruginosa*-mediated impairment of inflammation and infection.

## CONCLUSION

This research exhibited direct evidence that paeonol possessed the anti-QS activity against *P. aeruginosa* virulence, which decreased the adhesion, invasion, and cytotoxicity of *P. aeruginosa* to macrophages. Paeonol improved cell viability in the cell model of macrophages infected with *P. aeruginosa* by inhibiting the expression of QS-related virulence genes of *P. aeruginosa* and reducing the activation of macrophage proinflammation cytokines and inflammation pathway. Paeonol also decreased the bacterial load and alleviated the inflammation response in a *P. aeruginosa* pneumonia model.

## REFERENCES

- Zoumot Z, Wilson R. Respiratory Infection in Noncystic Fibrosis Bronchiectasis. *Curr Opin Infect Dis* (2010) 23(2):165–70. doi: 10.1097/QCO.0b013e328335af91
- Murphy TF. Pseudomonas Aeruginosa in Adults With Chronic Obstructive Pulmonary Disease. *Curr Opin Pulm Med* (2009) 15(2):138–42. doi: 10.1097/MCP.0b013e328321861a
- Hilliam Y, Moore MP, Lamont IL, Bilton D, Haworth CS, Foweraker J, et al. Pseudomonas Aeruginosa Adaptation and Diversification in the non-Cystic Fibrosis Bronchiectasis Lung. *Eur Respir J* (2017) 49(4). doi: 10.1183/13993003.02108-2016
- Moradali MF, Ghods S, Rehm BH. Pseudomonas Aeruginosa Lifestyle: A Paradigm for Adaptation, Survival, and Persistence. *Front Cell Infect Microbiol* (2017) 7:39. doi: 10.3389/fcimb.2017.00039
- Kang CI, Kim SH, Kim HB, Park SW, Choe YJ, Oh MD, et al. Pseudomonas Aeruginosa Bacteremia: Risk Factors for Mortality and Influence of Delayed

## DATA AVAILABILITY STATEMENT

The raw data supporting the conclusions of this article will be made available by the authors, without undue reservation.

## ETHICS STATEMENT

The animal study was reviewed and approved by Sichuan Agricultural University.

## AUTHOR CONTRIBUTIONS

HT and DY designed and performed the study, analyzed the data, and wrote the draft paper. LZhu, FS, GY, RG, HD, and LZhuo performed experiments, analyzed the data, and edited the manuscript. ZW and YL designed, organized, supervised research, and edited the paper. All authors contributed to the paper and approved the submitted version.

## FUNDING

This study was supported by the International Science and Technology Cooperation Program of Sichuan: 2020YFH0143.

- Receipt of Effective Antimicrobial Therapy on Clinical Outcome. *Clin Infect Dis* (2003) 37(6):745–51. doi: 10.1086/377200
6. Singh PK, Schaefer AL, Parsek MR, Moninger TO, Welsh MJ, Greenberg EP. Quorum-Sensing Signals Indicate That Cystic Fibrosis Lungs Are Infected With Bacterial Biofilms. *Nature* (2000) 407(6805):762–4. doi: 10.1038/35037627
  7. Bassler BL, Losick R. Bacterially Speaking. *Cell* (2006) 125(2):237–46. doi: 10.1016/j.cell.2006.04.001
  8. Swift S, Throup JP, Williams P, Salmond GP, Stewart GS. Quorum Sensing: A Population-Density Component in the Determination of Bacterial Phenotype. *Trends Biochem Sci* (1996) 21(6):214–9. doi: 10.1016/S0968-0004(96)80018-1
  9. Goodman AL, Lory S. Analysis of Regulatory Networks in *Pseudomonas Aeruginosa* by Genomewide Transcriptional Profiling. *Curr Opin Microbiol* (2004) 7(1):39–44. doi: 10.1016/j.mib.2003.12.009
  10. Geisenberger O, Givskov M, Riedel K, Hoiby N, Tummler B, Eberl L. Production of N-Acyl-L-Homoserine Lactones by *P. Aeruginosa* Isolates From Chronic Lung Infections Associated With Cystic Fibrosis. *FEMS Microbiol Lett* (2000) 184(2):273–8. doi: 10.1016/S0378-1097(00)00059-8
  11. Adonizio A, Kong K, Mathee K. Inhibition of Quorum Sensing-Controlled Virulence Factor Production in *Pseudomonas Aeruginosa* by South Florida Plant Extracts. *Antimicrobial Agents Chemother* (2008) 52(1):198–203. doi: 10.1128/AAC.00612-07
  12. Stehling EG, Silveira WD, Leite DS. Study of Biological Characteristics of *Pseudomonas Aeruginosa* Strains Isolated From Patients With Cystic Fibrosis and From Patients With Extra-Pulmonary Infections. *Braz J Infect Dis* (2008) 12(1):86–8. doi: 10.1590/S1413-86702008000100018
  13. O'May C, Tufenkji N. The Swarming Motility of *Pseudomonas Aeruginosa* Is Blocked by Cranberry Proanthocyanidins and Other Tannin-Containing Materials. *Appl Environ Microbiol* (2011) 77(9):3061–7. doi: 10.1128/AEM.02677-10
  14. Nieuwenhuis EE, Matsumoto T, Exley M, Schleipman RA, Glickman J, Bailey DT, et al. CD1d-Dependent Macrophage-Mediated Clearance of *Pseudomonas Aeruginosa* From Lung. *Nat Med* (2002) 8(6):588–93. doi: 10.1038/nm0602-588
  15. Cohen TS, Prince AS. Activation of Inflammasome Signaling Mediates Pathology of Acute *P. Aeruginosa* Pneumonia. *J Clin Invest* (2013) 123(4):1630–7. doi: 10.1172/JCI66142
  16. Zhang L, Wang CC. Inflammatory Response of Macrophages in Infection. *Hepatobiliary Pancreat Dis Int* (2014) 13(2):138–52. doi: 10.1016/S1499-3872(14)60024-2
  17. Pollard AJ, Currie A, Rosenberger CM, Heale JP, Finlay BB, Speert DP. Differential Post-Transcriptional Activation of Human Phagocytes by Different *Pseudomonas Aeruginosa* Isolates. *Cell Microbiol* (2004) 6(7):639–50. doi: 10.1111/j.1462-5822.2004.00388.x
  18. Romagne F. Current and Future Drugs Targeting One Class of Innate Immunity Receptors: The Toll-Like Receptors. *Drug Discovery Today* (2007) 12(1-2):80–7. doi: 10.1016/j.drudis.2006.11.007
  19. Kawai T, Akira S. The Role of Pattern-Recognition Receptors in Innate Immunity: Update on Toll-Like Receptors. *Nat Immunol* (2010) 11(5):373–84. doi: 10.1038/ni.1863
  20. Greenberg S, Grinstein S. Phagocytosis and Innate Immunity. *Curr Opin Immunol* (2002) 14(1):136–45. doi: 10.1016/S0952-7915(01)00309-0
  21. Epelman S, Stack D, Bell C, Wong E, Neely GG, Krutzik S, et al. Different Domains of *Pseudomonas Aeruginosa* Exoenzyme S Activate Distinct TLRs. *J Immunol* (2004) 173(3):2031–40. doi: 10.4049/jimmunol.173.3.2031
  22. Trinchieri G, Sher A. Cooperation of Toll-Like Receptor Signals in Innate Immune Defence. *Nat Rev Immunol* (2007) 7(3):179–90. doi: 10.1038/nri2038
  23. Hao S, Yang D, Zhao L, Shi F, Ye G, Fu H, et al. EGCG-Mediated Potential Inhibition of Biofilm Development and Quorum Sensing in *Pseudomonas Aeruginosa*. *Int J Mol Sci* (2021) 22(9). doi: 10.3390/ijms22094946
  24. Rudrappa T, Bais HP. Curcumin, a Known Phenolic From *Curcuma Longa*, Attenuates the Virulence of *Pseudomonas Aeruginosa* PAO1 in Whole Plant and Animal Pathogenicity Models. *J Agric Food Chem* (2008) 56(6):1955–62. doi: 10.1021/jf072591j
  25. Antunes JC, Tavares TD, Teixeira MA, Teixeira MO, Homem NC, Amorim M, et al. Eugenol-Containing Essential Oils Loaded Onto Chitosan/Polyvinyl Alcohol Blended Films and Their Ability to Eradicate *Staphylococcus Aureus* or *Pseudomonas Aeruginosa* From Infected Microenvironments. *Pharmaceutics* (2021) 13(2). doi: 10.3390/pharmaceutics13020195
  26. Lin HC, Ding HY, Ko FN, Teng CM, Wu YC. Aggregation Inhibitory Activity of Minor Acetophenones From *Paeonia* Species. *Planta Med* (1999) 65(7):595–9. doi: 10.1055/s-1999-14030
  27. Zhang L, Li DC, Liu LF. Paeonol: Pharmacological Effects and Mechanisms of Action. *Int Immunopharmacol* (2019) 72:413–21. doi: 10.1016/j.intimp.2019.04.033
  28. Yang D, Hao S, Zhao L, Shi F, Ye G, Zou Y, et al. Paeonol Attenuates Quorum-Sensing Regulated Virulence and Biofilm Formation in *Pseudomonas Aeruginosa*. *Front Microbiol* (2021) 12:692474. doi: 10.3389/fmicb.2021.692474
  29. Huang H, Chang EJ, Lee Y, Kim JS, Kang SS, Kim HH. A Genome-Wide Microarray Analysis Reveals Anti-Inflammatory Target Genes of Paeonol in Macrophages. *Inflammation Res* (2008) 57(4):189–98. doi: 10.1007/s00011-007-7190-3
  30. Miao J, Zhong J, Lan J, Ye S, Ye P, Li S, et al. Paeonol Attenuates Inflammation by Confining HMGB1 to the Nucleus. *J Cell Mol Med* (2021) 25(6):2885–99. doi: 10.1111/jcmm.16319
  31. Thurlow LR, Hanke ML, Fritz T, Angle A, Aldrich A, Williams SH, et al. *Staphylococcus Aureus* Biofilms Prevent Macrophage Phagocytosis and Attenuate Inflammation In Vivo. *J Immunol (Baltimore Md: 1950)* (2011) 186(11):6585–96. doi: 10.4049/jimmunol.1002794
  32. Traber KE, Dimbo EL, Symer EM, Korkmaz FT, Jones MR, Mizgerd JP, et al. Roles of Interleukin-11 During Acute Bacterial Pneumonia. *PLoS One* (2019) 14(8):e221029. doi: 10.1371/journal.pone.0221029
  33. Davies J, Davies D. Origins and Evolution of Antibiotic Resistance. *Microbiol Mol Biol Rev* (2010) 74(3):417–33. doi: 10.1128/MMBR.00016-10
  34. Levin AS, Barone AA, Penco J, Santos MV, Marinho IS, Arruda EA, et al. Intravenous Colistin as Therapy for Nosocomial Infections Caused by Multidrug-Resistant *Pseudomonas Aeruginosa* and *Acinetobacter Baumannii*. *Clin Infect Dis* (1999) 28(5):1008–11. doi: 10.1086/514732
  35. Miller LG, Perdreaux-Remington F, Rieg G, Mehdi S, Perlroth J, Bayer AS, et al. Necrotizing Fasciitis Caused by Community-Associated Methicillin-Resistant *Staphylococcus Aureus* in Los Angeles. *N Engl J Med* (2005) 352(14):1445–53. doi: 10.1056/NEJMoa042683
  36. Sadikot RT, Blackwell TS, Christman JW, Prince AS. Pathogen-Host Interactions in *Pseudomonas Aeruginosa* Pneumonia. *Am J Respir Crit Care Med* (2005) 171(11):1209–23. doi: 10.1164/rccm.200408-1044SO
  37. Mesaros N, Nordmann P, Plésiat P, Roussel-Delvallez M, Van Eldere J, Glupczynski Y, et al. *Pseudomonas Aeruginosa*: Resistance and Therapeutic Options at the Turn of the New Millennium. *Clin Microbiol Infect* (2007) 13(6):560–78. doi: 10.1111/j.1469-0691.2007.01681.x
  38. Iwasaki A, Medzhitov R. Control of Adaptive Immunity by the Innate Immune System. *Nat Immunol* (2015) 16(4):343–53. doi: 10.1038/ni.3123
  39. Aachoui Y, Sagulenko V, Miao EA, Stacey KJ. Inflammasome-Mediated Pyroptotic and Apoptotic Cell Death, and Defense Against Infection. *Curr Opin Microbiol* (2013) 16(3):319–26. doi: 10.1016/j.mib.2013.04.004
  40. Fleiszig SM, Zaidi TS, Fletcher EL, Preston MJ, Pier GB. *Pseudomonas Aeruginosa* Invades Corneal Epithelial Cells During Experimental Infection. *Infect Immun* (1994) 62(8):3485–93. doi: 10.1128/iai.62.8.3485-3493.1994
  41. Del Mar Cendra M, Torrents E. Differential Adaptability Between Reference Strains and Clinical Isolates of *Pseudomonas Aeruginosa* Into the Lung Epithelium Intracellular Lifestyle. *Virulence* (2020) 11(1):862–76. doi: 10.1080/21505594.2020.1787034
  42. Davies DG, Parsek MR, Pearson JP, Iglewski BH, Costerton JW, Greenberg EP. The Involvement of Cell-to-Cell Signals in the Development of a Bacterial Biofilm. *Science* (1998) 280(5361):295–8. doi: 10.1126/science.280.5361.295
  43. Kharazmi A. Interactions of *Pseudomonas Aeruginosa* Proteases With the Cells of the Immune System. *Antibiot Chemother* (1971) 42:42–9. doi: 10.1159/000417602
  44. Santajit S, Seesuwat W, Mahasongkram K, Sookkrung N, Pumirap P, Ampawong S, et al. Human Single-Chain Variable Fragments Neutralize *Pseudomonas Aeruginosa* Quorum Sensing Molecule, 3o-C12-HSL, and Prevent Cells From the HSL-Mediated Apoptosis. *Front Microbiol* (2020) 11:1172. doi: 10.3389/fmicb.2020.01172

45. Sun M, Zhu M, Chen K, Nie X, Deng Q, Hazlett LD, et al. TREM-2 Promotes Host Resistance Against *Pseudomonas Aeruginosa* Infection by Suppressing Corneal Inflammation via a PI3K/Akt Signaling Pathway. *Invest Ophthalmol Visual Sci* (2013) 54(5):3451–62. doi: 10.1167/iops.12-10938
46. Wang J, Yang K, Zhou L, Minhaowu, Wu Y, Zhu M, et al. MicroRNA-155 Promotes Autophagy to Eliminate Intracellular Mycobacteria by Targeting Rheb. *PLoS Pathog* (2013) 9(10):e1003697. doi: 10.1371/journal.ppat.1003697
47. Deligianni E, Pattison S, Berrar D, Ternan NG, Haylock RW, Moore JE, et al. *Pseudomonas Aeruginosa* Cystic Fibrosis Isolates of Similar RAPD Genotype Exhibit Diversity in Biofilm Forming Ability In Vitro. *BMC Microbiol* (2010) 10:38. doi: 10.1186/1471-2180-10-38
48. Rada B, Leto TL. Pyocyanin Effects on Respiratory Epithelium: Relevance in *Pseudomonas Aeruginosa* Airway Infections. *Trends Microbiol* (2013) 21(2):73–81. doi: 10.1016/j.tim.2012.10.004
49. Harshey RM. Bacterial Motility on a Surface: Many Ways to a Common Goal. *Annu Rev Microbiol* (2003) 57:249–73. doi: 10.1146/annurev.micro.57.030502.091014
50. Zhang J, Jiang R, Wang W, et al. Apoptosis are Induced in J774 Macrophages Upon Phagocytosis and Killing of *Pseudomonas Aeruginosa*. *Cell Immunol* (2013) 286(1-2):11–5. doi: 10.1016/j.cellimm.2013.10.006
51. Moussouni M, Berry L, Sipka T, et al. *Pseudomonas Aeruginosa* OprF Plays a Role in Resistance to Macrophage Clearance During Acute Infection. *Sci Rep* (2021) 11(1):359. doi: 10.1038/s41598-020-79678-0
52. Banerjee D, Khair OA, Honeybourne D. Impact of Sputum Bacteria on Airway Inflammation and Health Status in Clinical Stable COPD. *Eur Respir J* (2004) 23(5):685–91. doi: 10.1183/09031936.04.00056804
53. Hauser AR, Jain M, Bar-Meir M, et al. Clinical Significance of Microbial Infection and Adaptation in Cystic Fibrosis. *Clin Microbiol Rev* (2011) 24(1):29–70. doi: 10.1128/CMR.00036-10
54. Sica A, Mantovani A. Macrophage Plasticity and Polarization: *In Vivo* Veritas. *J Clin Invest* (2012) 122(3):787–95. doi: 10.1172/JCI59643
55. Mantovani A, Biswas SK, Galdiero MR, et al. Macrophage Plasticity and Polarization in Tissue Repair and Remodelling. *J Pathol* (2013) 229(2):176–85. doi: 10.1002/path.4133
56. Anwar MA, Basith S, Choi S. Negative Regulatory Approaches to the Attenuation of Toll-Like Receptor Signaling. *Exp Mol Med* (2013) 45:e11. doi: 10.1038/emmm.2013.28
57. Zhao G, Jiang K, Wu H, et al. Polydatin Reduces *Staphylococcus Aureus* Lipoteichoic Acid-Induced Injury by Attenuating Reactive Oxygen Species Generation and TLR2-NFkappaB Signalling. *J Cell Mol Med* (2017) 21(11):2796–808. doi: 10.1111/jcmm.13194

**Conflict of Interest:** The authors declare that the research was conducted in the absence of any commercial or financial relationships that could be construed as a potential conflict of interest.

**Publisher's Note:** All claims expressed in this article are solely those of the authors and do not necessarily represent those of their affiliated organizations, or those of the publisher, the editors and the reviewers. Any product that may be evaluated in this article, or claim that may be made by its manufacturer, is not guaranteed or endorsed by the publisher.

Copyright © 2022 Tang, Yang, Zhu, Shi, Ye, Guo, Deng, Zhao, Xu and Li. This is an open-access article distributed under the terms of the Creative Commons Attribution License (CC BY). The use, distribution or reproduction in other forums is permitted, provided the original author(s) and the copyright owner(s) are credited and that the original publication in this journal is cited, in accordance with accepted academic practice. No use, distribution or reproduction is permitted which does not comply with these terms.





# The Investigation of Hepatitis B Vaccine Immune Responses in Occult Hepatitis B Virus-Infected Patients

Jing Peng<sup>1†</sup>, Xueying Yao<sup>2†</sup>, Chunyan Yuan<sup>1†</sup>, Xiaoli Liu<sup>1†</sup>, Renxiang Xia<sup>1</sup>, Jian He<sup>1</sup>, Rui Li<sup>1</sup> and Yunqing Yao<sup>1\*</sup>

<sup>1</sup> The Department of Infectious Diseases, The First Affiliated Hospital of Chongqing Medical University, Chongqing, China,

<sup>2</sup> The Department of Radiology, The Second Affiliated Hospital of Chongqing Medical University, Chongqing, China

## OPEN ACCESS

### Edited by:

Chenhe Su,  
Wistar Institute, United States

### Reviewed by:

Junhua Huang,  
Wuhan Polytechnic University, China  
Longhuan Ma,  
University of Florida, United States

### \*Correspondence:

Yunqing Yao  
yaoyunqing@hospital.cqmu.edu.cn

<sup>†</sup>These authors have contributed  
equally to this work

### Specialty section:

This article was submitted to  
Viral Immunology,  
a section of the journal  
Frontiers in Immunology

Received: 24 March 2022

Accepted: 03 May 2022

Published: 27 May 2022

### Citation:

Peng J, Yao X, Yuan C, Liu X,  
Xia R, He J, Li R and Yao Y  
(2022) The Investigation of  
Hepatitis B Vaccine Immune  
Responses in Occult Hepatitis B  
Virus-Infected Patients.  
Front. Immunol. 13:903685.  
doi: 10.3389/fimmu.2022.903685

**Objectives:** There is no effective treatment for occult hepatitis B virus infection (OBI) patients, and immunotherapy may be one of the most promising options. We aim to investigate the underlying mechanism and therapeutic potential of hepatitis B vaccine immunotherapy for OBI patients.

**Methods:** Outpatient OBI patients were screened and randomly divided into treatment (Group A) and control (Group B) groups. At weeks 0, 4, and 24, patients in Group A received a subcutaneous/intramuscular injection of hepatitis B vaccine (Engerix-B, 20 µg/time) according to the standard vaccination schedule; patients in Group B served as blank control. The patients were followed for 36 weeks, with clinical, biochemical, virological, immunological, and imaging data collected and analyzed at weeks 0, 12, 24, and 36, respectively, and the relation between the virology and immunology results was analyzed.

**Results:** Of the 228 OBI patients, 28 were excluded, and 200 were enrolled for observation. In the end, 44 patients were included in Group A and 39 in Group B after excluding lost cases. At week 0 (baseline), some patients in two groups had liver disease symptoms, HBV-related liver function damage, and liver fibrosis. 86.36% (38/44) and 82.05% (32/39) patients were positive for serum hepatitis B surface antibodies (anti-HBs) in Group A and Group B, respectively, with the median (quartile) of 42.47 (16.85, 109.1) and 39.27 (16.06, 117.4) mIU/ml, respectively. Reduced peripheral blood CD4<sup>+</sup>T, CD8<sup>+</sup>T, and B lymphocytes were found in some patients in two groups. These results were not statistically different between Group A and Group B ( $P>0.05$ ). At week 36, all patients were serum anti-HBs (+) in Group A, with a median (quartile) of 1000 (483.9, 1000) mIU/ml, which was significantly higher than that at week 0 ( $P<0.05$ ) and that in Group B ( $P<0.05$ ). Compared to week 0, the number of CD8<sup>+</sup> T and B lymphocytes increased significantly and were significantly higher than Group B at the same point. Two patients in Group B were found to have hepatitis B virus reactivation from week 12 to week 36.

**Correlation Analysis:** Anti-HBs in Group A patients were positively correlated with B lymphocytes ( $r=0.3431$ ,  $0.3087$ , and  $0.3041$ , respectively) and positively correlated with CD8<sup>+</sup> T lymphocytes ( $r=0.4954$ ,  $0.3054$ , and  $0.3455$ , respectively) at weeks 12, 24, and 36.

**Conclusion:** Virological reactivation is a risk for OBI patients. Serum hepatitis B surface antibodies were significantly increased after hepatitis B vaccine treatment, the same as the numbers of peripheral blood B and CD8<sup>+</sup> T lymphocytes; changes in hepatitis B surface antibody levels were positively correlated with the changes in peripheral blood B and CD8<sup>+</sup> T lymphocytes.

**Keywords:** OBI, T lymphocyte, B lymphocyte, hepatitis B vaccine, anti-HBs, immunotherapy, therapeutic potential

## 1 INTRODUCTION

There is about 296 million hepatitis B surface antigen (HBsAg) positive chronic hepatitis B virus infection (CHB) patients around the world, and approximately 820,000 people die each year from HBV-related liver cirrhosis or/and HBV-related hepatocellular carcinoma (HCC) (1). OBI is defined as serum HBsAg negative, hepatitis B core antibody (anti-HBc) positive, normal ALT values, and usually, but not always, undetectable serum HBV DNA, but HBV covalently closed circular DNA (cccDNA) was detectable in the liver, according to the latest guidelines from the European Association for the Study of the Liver (EASL) (2). HBV pregenomic RNA (pgRNA) and hepatitis B core-related antigen (HBcrAg) are reliable substitutes for cccDNA (2–6). The prevalence of OBI patients with HBsAg negative is not significant and varies by region and disease. The overall prevalence of OBI in Sudan was 15.51%, with a high level of heterogeneity (7). A meta-analysis showed that the overall prevalence of OBI in Western Europe and Northern America was 34%, 28% in 329 subjects without chronic liver disease, and 35% in 2400 patients with chronic liver disease (8). The prevalence of OBI is significantly different among patients with different diseases. That is, in patients with cryptogenic cirrhosis or advanced liver fibrosis, the prevalence of OBI ranges from 4% to 38%, in the case of parenteral blood exposure, it is about 45%, in patients with chronic hepatitis C, it is estimated at 52%, in HIV-infected patients, it ranges from 0% to 45%, in blood donors from 0% to 22.7% and in hemodialysis patients, it ranges from 0% to 54% (9). In local areas of China, the prevalence of OBI was 19.48% (640/3100 cases) in the young people without the hepatitis B vaccine and 4.70% (170/3615 cases) in that vaccinated with the hepatitis B vaccine (10). Our research team estimates at least 20 million OBI patients in China (11).

Currently, major international guidelines (2, 4, 5) believe that no treatment is necessary once CHB has achieved a “functional cure” (i.e., HBsAg-negative OBI status). However, even when HBsAg is negatively converted, cccDNA remains in the liver, and HBV replicates at a low level and integrates into the host (12), resulting in “asymptomatic” chronic inflammation. OBI is a unique type of HBV infection that is currently circulating. Our research team and others have discovered that OBI can cause HBV reactivation, liver cirrhosis, and HCC (11, 13, 14).

Chronic exposure to high levels of HBsAg causes immune cell depletion and inadequate responses in CHB. OBI had a significantly better immune response than CHB, but it was still below that of healthy people (15, 16). Restoring the immune function of HBV-infected patients might eradicate the virus (6). Anti-HBs are known to be protective antibodies (17), capable of preventing reinfection and maintaining host immunosuppression against HBV (18), and our research team discovered that anti-HBs might also prevent HCC progression (11). It is proposed to treat OBI with a recombinant yeast-derived hepatitis B vaccine, observe immunological changes, and investigate its therapeutic potential.

## 2 MATERIALS AND METHODS

### 2.1 Study Objects

From November 2019 to November 2021, 228 OBI patients aged 18 to 65 admitted to the outpatient department of the Department of Infectious Diseases of the First Affiliated Hospital of Chongqing Medical University were screened, 28 cases were excluded, and 200 cases were enrolled for observation and randomly divided into treatment group (Group A) and control group (Group B). The study was conducted following the Declaration of Helsinki, and all participants signed informed consent forms.

#### (1) Criteria for Inclusion:

According to the EASL guidelines (2), the following criteria must be met: serum HBsAg negative ( $<0.05$  IU/ml), HBeAg negative ( $<1$ S/CO), anti-HBc positive ( $>1$ S/CO) for more than 6 months, with/without anti-HBe positive ( $<1$ S/CO), with/without anti-HBs positive ( $\geq 10$  mIU/ml); with/without serum HBV DNA positive ( $\geq 10$  IU/ml); HBcrAg positive ( $\geq 3$  LogU/mL); With or without imaging abnormalities.

#### (2) Criteria for Exclusion:

Co-infection with hepatitis A, B, C, D, E, HIV, Epstein-Barr virus, autoimmune hepatitis, hereditary liver disease, steatohepatitis, liver cirrhosis, HCC, and serious other system diseases, patients who received anti-HBV therapy or immunomodulatory treatment in 6 months, pregnant women, and lactating women.

## 2.2 Treatment Methods and Observation Indicators

### (1) Treatment Methods:

The patients in Group A received a 20 µg/time injection of recombinant *Saccharomyces cerevisiae*-derived hepatitis B vaccine (Engerix B) subcutaneously/intramuscularly at weeks 0, 4, and 24, according to standard vaccination procedures. Patients in Group B served as blank control.

### (2) Observation Indicators:

At weeks 0, 12, 24, and 36, the patients were observed, and the following data were collected: 1) Epidemiological and clinical information, such as a family history of hepatitis B, clinical symptoms, and signs. 2) Biochemistry, including blood tests, liver function (ALT, GGT, TBIL, Alb), renal function, and AFP. 3) Virological indicators: serum HBV DNA, HBcrAg, HBsAg, HBeAg, anti-HBs, anti-HBe, and anti-HBc; 4) Immunological indicators: total lymphocytes (tLymph), CD3<sup>+</sup>T, CD4<sup>+</sup>T, CD8<sup>+</sup>T, and B lymphocytes in peripheral blood; 5) Imaging data: color Doppler ultrasound of the upper abdomen/CT enhanced scan/MRI enhanced scan, liver transient elastography, and liver fat content detection. (Anti-HBs were expressed and calculated as 1000 mIU/ml when ≥1000 mIU/ml).

## 2.3 Statistical Analysis

GraphPad Prism 8.0.1 was used to conduct the statistical analysis. If the two groups of data have a normal distribution, the t-test was used; otherwise, the Wilcoxon test was used; when comparing multiple groups, the RM one-way ANOVA analysis was used if the data had a normal distribution. Otherwise, the Friedman analysis was used. The correlation analysis was performed with the Spearman.  $P < 0.05$  denotes a statistically significant difference.

## 3 RESULTS

In the end, 117 cases were excluded from the 200 OBI patients. 44 cases in Group A and 39 cases in Group B were included in the statistical analysis.

### 3.1 Baseline Information at Week 0

#### 3.1.1 Some Patients in the Two Groups Had Liver Disease Symptoms

There was no statistical difference between Group A and Group B ( $P > 0.05$ ), as shown in **Table 1**.

### 3.2 Results of Biochemical and Imaging Tests

#### 3.2.1 Some Patients in Two Groups Had HBV-Related Liver Function Damage and Liver Fibrosis at Week 0

From week 0 to week 36, all patients' test results for blood routine, renal function, and alpha fetal protein (AFP) were normal. There were no vaccine-related adverse events found in Group A. There was no liver cirrhosis and HCC in the two groups.

At week 0, after removing hemolysis, drug/alcoholism, steatohepatitis, and other liver damage factors, 4.55% (2/44) of patients in Group A and 7.7% (3/39) in Group B had HBV-related liver function damage (one or more of ALT/GGT/TBIL abnormal, as shown in **Table 2**), and all returned to normal after treatment with liver-protective drugs within 24 weeks. There was no statistical difference between Group A and Group B ( $P > 0.05$ ).

At week 0, liver fibrosis was found in 61.36% (27/44) and 64.1% (25/39) of Group A and B patients, respectively. There was no statistical difference between Group A and Group B ( $P > 0.05$ ), as shown in **Table 2**.

**TABLE 1** | Baseline characteristics of OBI patients at week 0.

Items	Group A (n=44)	Group B (n=39)
Mean age (± SD)	49.55 ± 9.43	46.54 ± 10.42
Male n° (%)	22 (50.00)	20 (51.28)
History of drinking n° (%)	17 (38.64)	16 (41.03)
History of smoking n° (%)	14 (31.82)	14 (35.90)
Family history of hepatitis B n° (%)	20 (45.45)	18 (46.15)
Liver disease related symptoms n° (%)	7 (15.91)	6 (15.38)

n°, number of cases.

**TABLE 2** | Results of biochemical and imaging examination in OBI patients at week 0.

Items	Group A (n=44)	Group B (n=39)
<b>Biochemical</b>		
Alb, M (Q1,Q3), g/L	49.00 (47.00,50.00)	48.00 (45.00,50.00)
ALT, M (Q1,Q3), U/L	20.50 (13.00,28.00)	22.00 (15.00,33.00)
GGT, M (Q1,Q3), U/L	20.50 (15.00,33.00)	24.00 (16.00,41.00)
TBIL, M (Q1,Q3), µmol/L	12.05 (8.15,16.68)	11.00 (7.10,14.00)
HBV related liver dysfunction n° (%)	2 (4.55)	3 (7.70)
<b>Imaging</b>		
Hepatic fibrosis n° (%)	27(61.36)	25(64.10)

M, median; Q1, first quartile; Q3, third quartile; n°, number of cases.

**TABLE 3** | Results of serum markers of hepatitis B virus in OBI patients.

Group	Time	HBcrAg(+) n° (%)	HBV DNA(+) n° (%)	HBsAg(+) n° (%)	HBeAg(+) n° (%)	anti-HBe(+) n° (%)	anti-HBc(+) n° (%)
Group A (n=44)	0 w	44 (100.00)	N	N	N	23 (52.27)	44 (100.00)
	12 w	-	N	N	N	22 (50.00)	44 (100.00)
	24 w	-	N	N	N	22 (50.00)	44 (100.00)
	36 w	-	N	N	N	22 (50.00)	44 (100.00)
Group B (n=39)	0 w	39 (100.00)	N	N	N	24 (61.54)	39 (100.00)
	12 w	-	N	1 (2.56)	N	24 (61.54)	39 (100.00)
	24 w	-	1 (2.56)	2 (5.13)	N	24 (61.54)	39 (100.00)
	36 w	-	N	2 (5.13)	N	24 (61.54)	39 (100.00)

N, none; n°, number of cases; -, without detection.

### 3.3 Virological Findings

#### 3.3.1 Serum Anti-HBs of OBI Patients in Two Groups Were Very Low at Week 0, But They Significantly Increased After HBV Vaccine Treatment in Group A; HBV Reactivation Was Observed in 2 Patients in Group B From Week 12 to Week 36

At week 0, all patients in Group A and Group B had serum anti-HBc(+) and HBcrAg(+), 52.27% (23/44) of patients in Group A and 61.54% (24/39) in Group B had anti-HBe(+). 86.36% (38/44) of patients in Group A and 82.05% (32/39) in Group B were anti-HBs(+), the median (quartile) of anti-HBs was 42.47 (16.85, 109.1) and 39.27 (16.06, 117.4) mIU/ml in all patients of Group A and Group B, respectively. There was no statistical difference between Group A and Group B ( $P>0.05$ ). Serum HBV DNA, HBsAg, and HBeAg were negative, as shown in **Table 3**.

At weeks 12, 24, and 36, 2 cases in Group B and 0 cases in Group A were tested for HBV DNA and/or HBsAg re-positive. After the treatment of the HBV vaccine, all patients in Group A were anti-HBs(+), with a median (quartile) of 1000 (483.9, 1000) mIU/ml at week 36, which was significantly higher than that at week 0 ( $P<0.05$ ), also significantly higher than that in Group B ( $P<0.05$ ). However, the rate of anti-HBs(+) in Group B had no significant changes compared with week 0, and neither did the anti-HBs titer ( $P>0.05$ ), as shown in **Table 4**.

### 3.4 Immunological Findings

#### 3.4.1 At Baseline, the Number of Immune Cells Decreased in OBI Patients But Increased After HBV Vaccine Treatment

At week 0, the numbers of tLymph, CD3<sup>+</sup> T, CD4<sup>+</sup> T, CD8<sup>+</sup> T, and B lymphocytes in peripheral blood were found lower than the Lower Limit of Normal (LLN, 1752, 1185, 561, 464, and 180 cells/ $\mu$ l, respectively) in 43.18% (19/44), 47.73% (21/44), 43.18% (19/44), 52.27% (23/44), and 38.64% (17/44) of patients in Group A and 41.03% (16/39), 46.15% (18/39), 35.90% (14/39), 58.97% (23/39), and 33.33% (13/39) of patients in Group B. There was no statistical difference between Group A and Group B ( $P>0.05$ ), as shown in **Table 5**.

Compared with week 0, the number of tLymph in Group A patients was significantly increased at week 12, 24, and 36 ( $P<0.05$ ); CD3<sup>+</sup> T lymphocyte significantly increased at week 24 ( $P<0.05$ ); CD4<sup>+</sup> T lymphocyte increased at week 12 and 24 but decreased at week 36, and the difference was not statistically significant ( $P>0.05$ ). CD8<sup>+</sup> T lymphocyte was significantly increased ( $P<0.05$ ) at week 12, 24, and 36; B lymphocyte was significantly increased at week 36 ( $P<0.05$ ). Conversely, the number of lymphocytes in Group B showed a downward trend as a whole, among which CD3<sup>+</sup> T lymphocytes decreased significantly at week 12 ( $P<0.05$ ); CD4<sup>+</sup> T lymphocytes decreased significantly at week 12 and 36 ( $P<0.05$ ); and CD8<sup>+</sup> T lymphocytes decreased significantly at week 24 and 36 ( $P<0.05$ ).

**TABLE 4** | Results of serum hepatitis B virus surface antibody test in OBI patients.

Group	Time	anti-HBs (+)				anti-HBs, (Q1, Q3), mIU/ml
		n° (%)				
		$\geq 10$ and $<100$ mIU/ml	$\geq 100$ and $<500$ mIU/ml	$\geq 500$ and $<1000$ mIU/ml	$\geq 1000$ mIU/ml	
Group A (n=44)	0 w	27 (61.36)	10 (22.73)	1 (2.27)	N	42.47 (16.85,109.10)
	12 w	6 (13.64)	9 (20.45)	2 (4.55)	27 (61.36)	1000 (230.4,1000)*
	24 w	4 (9.09)	7 (15.91)	5 (11.36)	28 (63.64)	1000 (485.1,1000)*
	36 w	4 (9.09)	7 (15.91)	4 (9.09)	29 (65.91)	1000 (483.9,1000)*
Group B (n=39)	0 w	20 (51.28)	12 (30.77)	N	N	39.27 (16.06,117.40)
	12 w	19 (48.72)	13 (33.33)	N	N	39.04 (16.09,112.60)
	24 w	20 (51.28)	12 (30.77)	N	N	40.48 (18.97,117.20)
	36 w	21 (53.85)	11 (28.21)	N	N	38.78 (16.18,115.20)

N, none; n°, number of cases; M, median; Q1, first quartile; Q3, third quartile; \*, the difference was statistically significant compared with week 0 ( $P<0.05$ ).

**TABLE 5** | Results of peripheral blood immune cell test in OBI patients.

Group	Time	tLymph ( $\bar{x} \pm SD$ )/ $\mu$ l	CD3 <sup>+</sup> T ( $\bar{x} \pm SD$ )/ $\mu$ l	CD4 <sup>+</sup> T ( $\bar{x} \pm SD$ )/ $\mu$ l	CD8 <sup>+</sup> T ( $\bar{x} \pm SD$ )/ $\mu$ l	B ( $\bar{x} \pm SD$ )/ $\mu$ l
Group A (n=44)	0 w	1801.00±445.30	1210.00±371.90	646.10±240.80	459.50±191.70	232.30±100.70
	12 w	1926.00±486.90 <sup>a</sup>	1291.00±376.90	666.70±258.90	516.60±192.70 <sup>ac</sup>	245.90±101.20
	24 w	1898.00±423.30 <sup>a</sup>	1316.00±362.00 <sup>a</sup>	661.20±240.40	494.90±188.80 <sup>a</sup>	245.50±115.80
	36 w	1853.00±446.80 <sup>a</sup>	1241.00±357.80	645.80±232.10	487.70±188.50 <sup>ac</sup>	249.30±107.90 <sup>ac</sup>
Group B (n=39)	0 w	1803.00±482.00	1211.00±373.00	634.60±231.60	445.40±201.20	222.50±106.40
	12 w	1802.00±481.20	1205.00±372.60 <sup>b</sup>	631.20±228.90 <sup>b</sup>	430.50±191.20	211.20±110.50
	24 w	1791.00±484.90	1208.00±340.90	630.60±203.30	417.00±191.40 <sup>b</sup>	210.80±84.59
	36 w	1782.00±470.40	1187.00±340.30	619.20±231.10 <sup>b</sup>	404.10±189.80 <sup>b</sup>	206.80±82.79

<sup>a</sup>The difference was statistically significant compared with week 0 in Group A ( $P < 0.05$ );

<sup>b</sup>The difference was statistically significant compared with week 0 in Group B ( $P < 0.05$ );

<sup>c</sup>The difference was statistically significant compared with Group B ( $P < 0.05$ ).

The numbers of CD8<sup>+</sup> T and B lymphocytes in Group A were significantly higher than in Group B at week 36 ( $P < 0.05$ ), as shown in Table 5.

### 3.5 Results of Correlation Analysis of Anti-HBs and Key Immune Cells:

#### 3.5.1 The Change of Anti-HBs Was Positively Correlated With the Change of CD8<sup>+</sup> T Lymphocyte and B Lymphocyte in Group A During Treatment

In Group A, at week 12, the changes of serum anti-HBs ( $\Delta$ anti-HBs) showed a moderate positive correlation with changes in

CD8<sup>+</sup> T levels ( $\Delta$ CD8<sup>+</sup>T) ( $r = 0.4954$ ,  $P < 0.05$ ), while they were weakly positively correlated with changes in peripheral blood tLymph levels ( $\Delta$ tLymph), CD3<sup>+</sup> T levels ( $\Delta$ CD3<sup>+</sup> T), and B lymphocyte levels ( $\Delta$ B lymphocyte) ( $r = 0.2978$ ,  $0.3291$ , and  $0.3431$ , respectively,  $P < 0.05$ ). The change in CD4<sup>+</sup>T level ( $\Delta$ CD4<sup>+</sup> T) did not correlate. At week 24,  $\Delta$ anti-HBs showed a moderate positive correlation with  $\Delta$ tLymph ( $r = 0.4056$ ,  $P < 0.05$ ), a weak positive correlation with  $\Delta$ CD8<sup>+</sup> T and  $\Delta$ B lymphocyte ( $r = 0.3054$  and  $0.3087$ ,  $P < 0.05$ ), but no correlation with  $\Delta$ CD3<sup>+</sup> T and  $\Delta$ CD4<sup>+</sup> T. At week 36,  $\Delta$ anti-HBs was weakly positively correlated with  $\Delta$ tLymph,  $\Delta$ CD8<sup>+</sup> T, and  $\Delta$ B

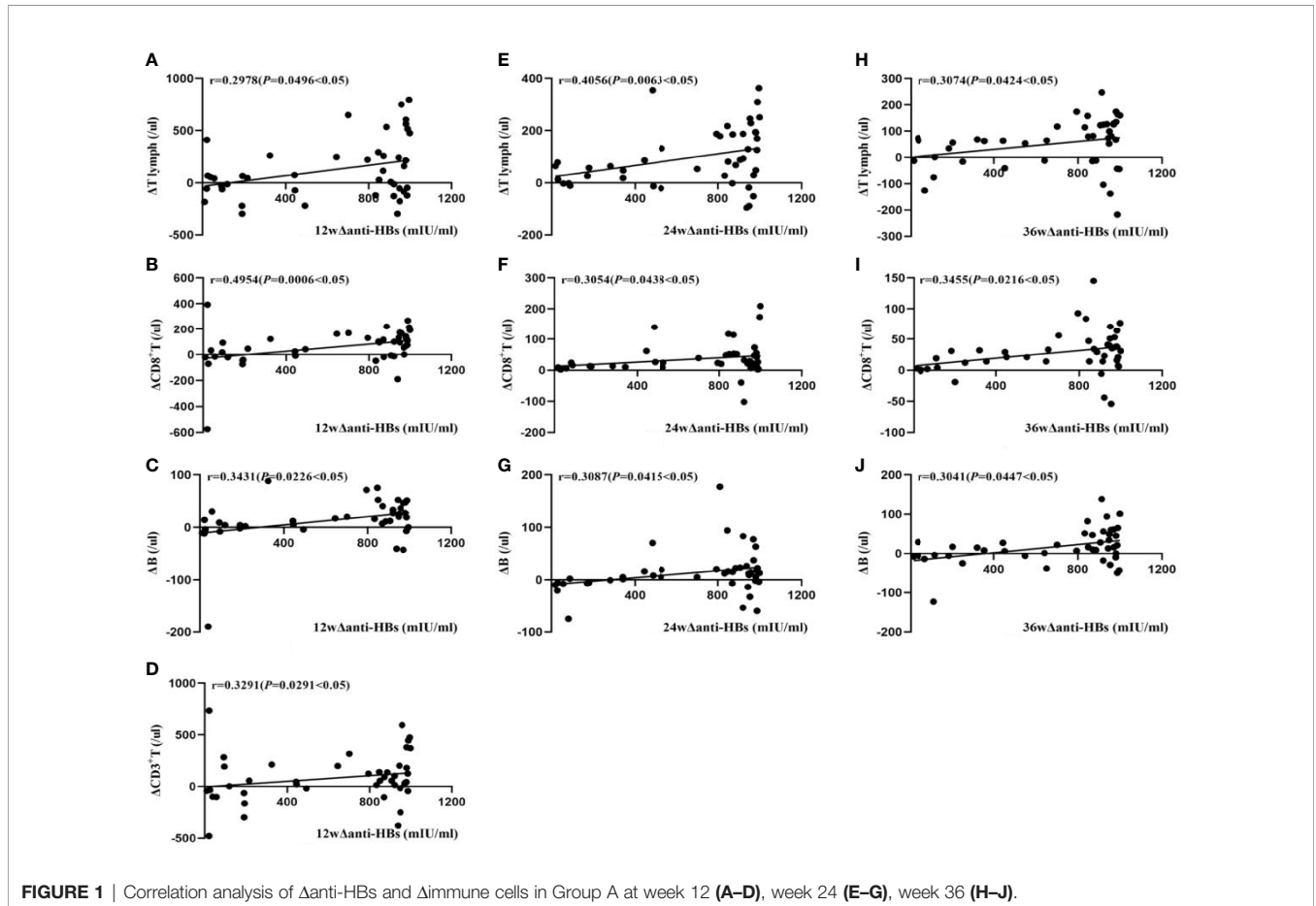


**FIGURE 1** | Correlation analysis of  $\Delta$ anti-HBs and  $\Delta$ immune cells in Group A at week 12 (A–D), week 24 (E–G), week 36 (H–J).

lymphocyte ( $r=0.3074$ ,  $0.3455$ , and  $0.3041$ , respectively,  $P<0.05$ ), but not with  $\Delta CD3^+T$  and  $\Delta CD4^+T$  cells, as shown in **Figure 1**.

In Group B, at week 12,  $\Delta$ anti-HBs was moderately positively correlated with  $\Delta B$  lymphocyte ( $r = 0.5363$ ,  $P<0.05$ ), weakly positively correlated with  $\Delta CD3^+ T$  and  $\Delta CD8^+T$  lymphocyte ( $r = 0.3908$ , and  $0.3247$ , respectively,  $P<0.05$ ); at week 24, it was weakly positively correlated with  $\Delta CD8^+ T$  and  $\Delta B$  lymphocyte ( $r = 0.3205$  and  $0.3558$ , respectively,  $P<0.05$ ); at week 36, it was weakly positively correlated with  $\Delta CD8^+ T$  and  $\Delta B$  lymphocyte ( $r = 0.3523$  and  $0.3929$ , respectively,  $P<0.05$ ), as shown in **Figure 2**.

## 4 DISCUSSION

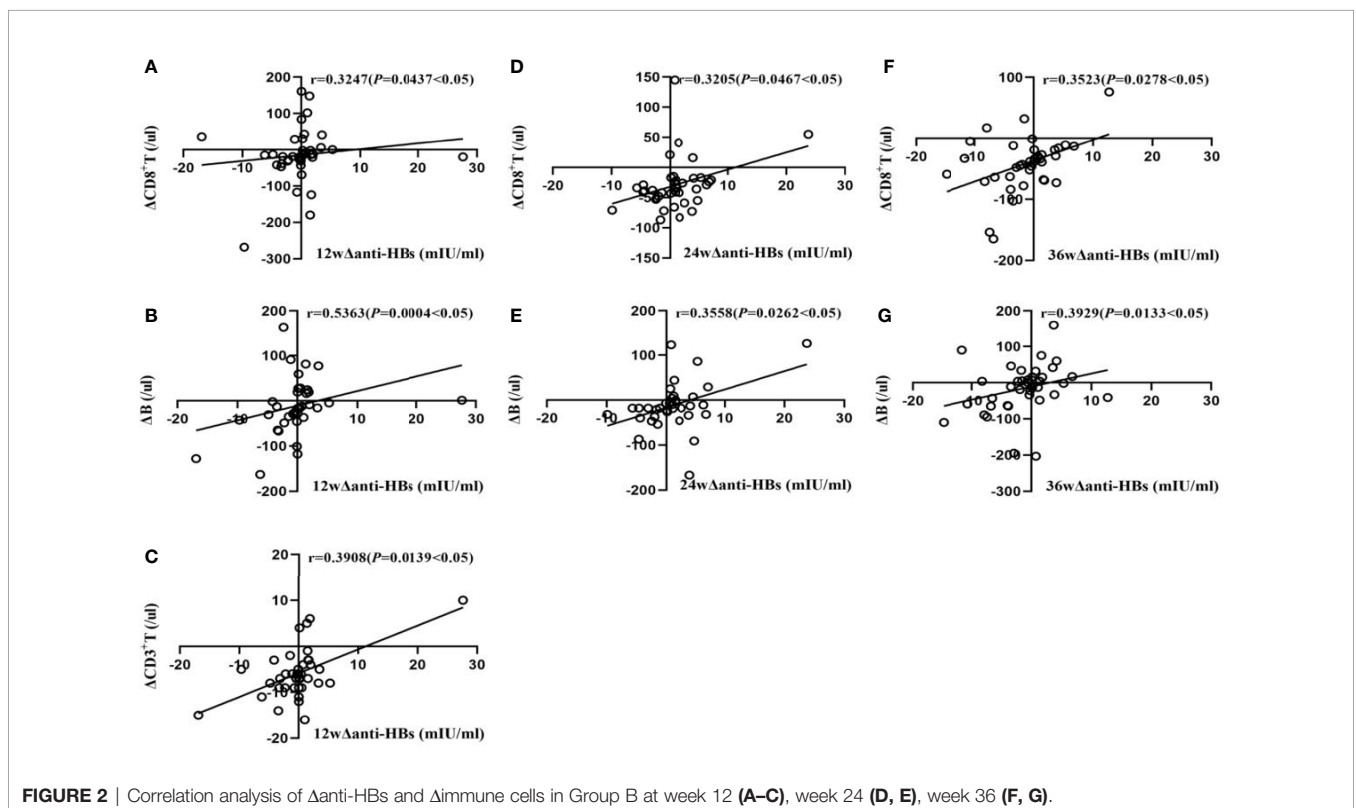
Patients with OBI are not safe, according to our findings. Nearly two-thirds of OBI patients have varying degrees of liver fibrosis. A small number of OBI patients have an abnormal liver function and liver disease-related symptoms, indicating that OBI is not in a “healthy state.” From 12 to 36 weeks of observation, serum hepatitis B surface antigen and HBV DNA reactivation were found in two patients of Group B, which meant that HBV in the OBI state is not always stable or cleared, consistent with our previous findings (11, 13).

According to our findings, the immune status of patients with OBI is subtle and complex. Before treatment, about half of patients with OBI had a lower number of  $CD8^+ T$  lymphocytes in their peripheral blood than the lower limit of normal, about

two-fifths of patients had a lower number of  $CD4^+ T$  lymphocytes in their peripheral blood, and about a third of patients had a lower number of peripheral blood B lymphocyte, all of which are linked to the clearance process and pathogenic consequences of HBV. At the same time, even though more than three-quarters of OBI patients had positive serum anti-HBs, they all had low titers, which could be linked to a reduction in B cell number and/or function.

According to our findings, the hepatitis B vaccine can be used to treat and benefit patients with OBI. After hepatitis B vaccine treatment, the serum anti-HBs titer of OBI patients were significantly higher than week 0 and that of the control group, reaching the level of medium and high titers, significantly improving patient protection. At the same time, the serum hepatitis B surface antibody in the control group without hepatitis B vaccine treatment was always low positive rate and low level. Kato M et al. reported that serum high anti-HBs titers obtained after hepatitis B vaccination could prevent non-vaccine genotype HBV infection (19). Chen et al. also found that serum anti-HBs titers were inversely proportional to the risk of HBV reactivation following re-positivity of the surface antigen (20). In a previous study of OBI patients, our team discovered that the average diameter of HCC in anti-HBs-positive patients was significantly smaller than that in anti-HBs-negative patients (11).

The number of tLymph cells,  $CD8^+ T$  lymphocytes, and B lymphocytes in the peripheral blood of OBI patients of the treatment group after 36 weeks of hepatitis B vaccine treatment were significantly increased and positively correlated with the levels of anti-HBs. We discovered that the hepatitis B



vaccine not only activates B lymphocytes to produce anti-HBs but may also promote the activation and proliferation of CD8<sup>+</sup> T lymphocytes directly or indirectly *via* anti-HBs, all of which aid the body's eventual clearance of HBV. Contrarily, the number of peripheral blood immune cells in the control group was low during the observation period. We can only perform limited analysis with the results of other scholars' studies in healthy and surface antigen-positive CHB patients because no similar studies have been reported. After hepatitis B vaccination, the number of B lymphocytes producing anti-HBs was positively correlated with the titer of anti-HBs ( $r=0.909$ ) (21). After repeated hepatitis B vaccination, however, some CHB patients are unable to produce anti-HBs (22) because the number and function of HBsAg-specific B lymphocytes that produce anti-HBs are significantly reduced (21), and only a small amount of anti-HBs can be produced, resulting in the formation of immune complexes that are undetectable. When HBsAg is cleared, the total number of B lymphocytes in the peripheral blood increases (23), and HBsAg-specific memory B lymphocytes that have recovered their function can produce effective antibodies (24), or they can break the body's immune tolerance to achieve clearance with the help of an effective therapeutic hepatitis B vaccine (25).

In conclusion, our ground-breaking research discovered that patients with OBI are not healthy, and their HBV is at risk of reactivation. The use of the hepatitis B vaccine in the treatment of OBI patients can increase serum hepatitis B surface antibody titers, reducing the risk of reinfection with other genotypes of HBV, as well as promote complete clearance of HBV by activating the body's cellular and humoral immunity and even reduce the risk of HBV-related cirrhosis and HCC.

Our research still has room for improvement: many patients were lost to follow-up during the research process, and the number of cases available for statistical analysis needs to be increased. Treatment time and duration should be extended, and immunological mechanism research, liver histological examination, intrahepatic HBV-related virology, and immunological research should all be improved.

## DATA AVAILABILITY STATEMENT

The raw data supporting the conclusions of this article will be made available by the authors, without undue reservation.

## ETHICS STATEMENT

The studies involving human participants were reviewed and approved by Ethics Committee of the First Affiliated Hospital of Chongqing Medical University. The patients/participants provided their written informed consent to participate in this study.

## AUTHOR CONTRIBUTIONS

YY designed the project, revised the manuscript, and approved the submission; JP, XY, CY, and XL collected and analyzed case data and wrote the manuscript; RX, JH, and RL participated in collecting case data. All authors contributed to the article and approved the submitted version.

## REFERENCES

1. WHO. *Global Progress Report on HIV, Viral Hepatitis and Sexually Transmitted Infections, 2021* (2021). Available at: <https://www.who.int/publications/i/item/9789240027077>.
2. European Association for the Study of the Liver (EASL) 2017 Clinical Practice Guidelines on the Management of Hepatitis B Virus Infection. *J Hepatol* (2017) 67(2):370–98. doi: 10.1016/j.jhep.2017.03.021
3. Testoni B, Lebossé F, Scholtes C, Berby F, Miaglia C, Subic M, et al. Serum Hepatitis B Core-Related Antigen (HBcrAg) Correlates With Covalently Closed Circular DNA Transcriptional Activity in Chronic Hepatitis B Patients. *J Hepatol* (2019) 70(4):615–25. doi: 10.1016/j.jhep.2018.11.030
4. Sarin SK, Kumar M, Lau GK, Abbas Z, Chan HL, Chen CJ, et al. Asian-Pacific Clinical Practice Guidelines on the Management of Hepatitis B: A 2015 Update. *Hepatol Int* (2016) 10(1):1–98. doi: 10.1007/s12072-015-9675-4
5. Terrault NA, Lok ASF, McMahon BJ, Chang KM, Hwang JP, Jonas MM, et al. Update on Prevention, Diagnosis, and Treatment of Chronic Hepatitis B: AASLD 2018 Hepatitis B Guidance. *Hepatology* (2018) 67(4):1560–99. doi: 10.1002/hep.29800
6. Raimondo G, Locarnini S, Pollicino T, Levrero M, Zoulim F, Lok AS. Update of the Statements on Biology and Clinical Impact of Occult Hepatitis B Virus Infection. *J Hepatol* (2019) 71(2):397–408. doi: 10.1016/j.jhep.2019.03.034
7. Eltom K, Albeely A, El Hussein ARM, Elkhidir IM, Enan K. Occult Hepatitis B Virus Infection in Sudan: A Systematic Review and Meta-Analysis. *JGH Open* (2020) 4(5):800–7. doi: 10.1002/jgh3.12411
8. Pisaturo M, Onorato L, Russo A, Chiodini P, Coppola N. An Estimation of the Prevalence of Occult HBV Infection in Western Europe and in Northern America: A Meta-Analysis. *J Viral Hepat* (2020) 27(4):415–27. doi: 10.1111/jvh.13248
9. Pisaturo M, Onorato L, Russo A, Coppola N. Prevalence of Occult HBV Infection in Western Countries. *J Med Virol* (2020) 92(12):2917–29. doi: 10.1002/jmv.25867
10. Wang R, Liu C, Chen T, Wang Y, Fan C, Lu L, et al. Neonatal Hepatitis B Vaccination Protects Mature Adults From Occult Virus Infection. *Hepatol Int* (2021) 15(2):328–37. doi: 10.1007/s12072-021-10156-z
11. Xia R, Peng J, He J, Jiang P, Yuan C, Liu X, et al. The Serious Challenge of Occult Hepatitis B Virus Infection-Related Hepatocellular Carcinoma in China. *Front Microbiol* (2022) 13:840825. doi: 10.3389/fmicb.2022.840825
12. Jang JW, Kim JS, Kim HS, Tak KY, Nam H, Sung PS, et al. Persistence of Intrahepatic Hepatitis B Virus DNA Integration in Patients Developing Hepatocellular Carcinoma After Hepatitis B Surface Antigen Seroclearance. *Clin Mol Hepatol* (2021) 27(1):207–18. doi: 10.3350/cmh.2020.0115
13. Yuan C, Peng J, Xia R, He J, Qiu T, Yao Y. Reactivation of Occult Hepatitis B Virus Infection During Long-Term Entecavir Antiviral Therapy. *Front Microbiol* (2022) 13:865124. doi: 10.3389/fmicb.2022.865124
14. Song A, Wang X, Lu J, Jin Y, Ma L, Hu Z, et al. Durability of Hepatitis B Surface Antigen Seroclearance and Subsequent Risk for Hepatocellular Carcinoma: A Meta-Analysis. *J Viral Hepat* (2021) 28(4):601–12. doi: 10.1111/jvh.13471
15. Sosa-Jurado F, Sánchez-Reza L, Mendoza-Torres M, Meléndez-Mena D, García V, Guzmán-Flores B, et al. Serum Th17 and TNF- $\alpha$  Distinguish Between Patients With Occult Hepatitis B Infection, Chronic Hepatitis B Infection and Healthy Individuals. *Eur Cytokine Netw* (2021) 32(2):23–30. doi: 10.1684/ecn.2021.0466

16. Le Bert N, Salimzadeh L, Gill US, Dutertre CA, Facchetti F, Tan A, et al. Comparative Characterization of B Cells Specific for HBV Nucleocapsid and Envelope Proteins in Patients With Chronic Hepatitis B. *J Hepatol* (2020) 72(1):34–44. doi: 10.1016/j.jhep.2019.07.015
17. Xu H, Locarnini S, Wong D, Hammond R, Colledge D, Soppe S, et al. Role of Anti-HBs in Functional Cure of HBeAg+ Chronic Hepatitis B Patients Infected With HBV Genotype a. *J Hepatol* (2022) 76(1):34–45. doi: 10.1016/j.jhep.2021.07.031
18. Paul S, Dickstein A, Saxena A, Terrin N, Viveiros K, Balk EM, et al. Role of Surface Antibody in Hepatitis B Reactivation in Patients With Resolved Infection and Hematologic Malignancy: A Meta-Analysis. *Hepatology* (2017) 66(2):379–88. doi: 10.1002/hep.29082
19. Kato M, Hamada-Tsutsumi S, Okuse C, Sakai A, Matsumoto N, Sato M, et al. Effects of Vaccine-Acquired Polyclonal Anti-HBs Antibodies on the Prevention of HBV Infection of Non-Vaccine Genotypes. *J Gastroenterol* (2017) 52(9):1051–63. doi: 10.1007/s00535-017-1316-3
20. Chen MH, Lee IC, Chen MH, Hou MC, Tsai CY, Huang YH. Abatacept Is Second to Rituximab at Risk of HBsAg Reverse Seroconversion in Patients With Rheumatic Disease. *Ann Rheum Dis* (2021) 80(11):1393–9. doi: 10.1136/annrheumdis-2021-220774
21. Tian C, Chen Y, Liu Y, Wang S, Li Y, Wang G, et al. Use of Elispot Assay to Study HBs-Specific B Cell Responses in Vaccinated and HBV Infected Humans. *Emerg Microbes Infect* (2018) 7(1):16. doi: 10.1038/s41426-018-0034-0
22. Yao X, Zheng B, Zhou J, Xu DZ, Zhao K, Sun SH, et al. Therapeutic Effect of Hepatitis B Surface Antigen-Antibody Complex Is Associated With Cytolytic and Non-Cytolytic Immune Responses in Hepatitis B Patients. *Vaccine* (2007) 25(10):1771–9. doi: 10.1016/j.vaccine.2006.11.019
23. Cao Z, Meng S, Zheng Y, Wang J, Wang R, Chen X. B Cells Were Related to HBsAg Seroconversion in Inactive HBsAg Carriers Following Peginterferon Therapy. *PLoS One* (2020) 15(12):e0242559. doi: 10.1371/journal.pone.0242559
24. Hehle V, Beretta M, Bourguine M, Ait-Goughoulte M, Planchais C, Morisse S, et al. Potent Human Broadly Neutralizing Antibodies to Hepatitis B Virus From Natural Controllers. *J Exp Med* (2020) 217(10):e20200840. doi: 10.1084/jem.20200840
25. Zhu D, Liu L, Yang D, Fu S, Bian Y, Sun Z, et al. Clearing Persistent Extracellular Antigen of Hepatitis B Virus: An Immunomodulatory Strategy to Reverse Tolerance for an Effective Therapeutic Vaccination. *J Immunol* (2016) 196(7):3079–87. doi: 10.4049/jimmunol.1502061

**Conflict of Interest:** The authors declare that the research was conducted in the absence of any commercial or financial relationships that could be construed as a potential conflict of interest.

**Publisher's Note:** All claims expressed in this article are solely those of the authors and do not necessarily represent those of their affiliated organizations, or those of the publisher, the editors and the reviewers. Any product that may be evaluated in this article, or claim that may be made by its manufacturer, is not guaranteed or endorsed by the publisher.

Copyright © 2022 Peng, Yao, Yuan, Liu, Xia, He, Li and Yao. This is an open-access article distributed under the terms of the Creative Commons Attribution License (CC BY). The use, distribution or reproduction in other forums is permitted, provided the original author(s) and the copyright owner(s) are credited and that the original publication in this journal is cited, in accordance with accepted academic practice. No use, distribution or reproduction is permitted which does not comply with these terms.





# The Correlation Between Immune Invasion and SARS-COV-2 Entry Protein ADAM17 in Cancer Patients by Bioinformatic Analysis

## OPEN ACCESS

### Edited by:

Chunfu Zheng,  
University of Calgary, Canada

### Reviewed by:

Ali Hafez El-Far,  
Damanhour University, Egypt  
Jun Hong,  
Vanderbilt University Medical Center,  
United States

### \*Correspondence:

Junjiang Fu  
fujunjiang@hotmail.com  
orcid.org/0000-0002-0708-2200  
Jingliang Cheng  
jingliangc@swmu.edu.cn  
Zhiqiang Mei  
xuguangyin1@163.com

†These authors have contributed  
equally to this work

### Specialty section:

This article was submitted to  
Viral Immunology,  
a section of the journal  
Frontiers in Immunology

Received: 19 April 2022

Accepted: 11 May 2022

Published: 03 June 2022

### Citation:

Wang K, Deng H, Song B, He J,  
Liu S, Fu J, Zhang L, Li D, Balaji KS,  
Mei Z, Cheng J and Fu J (2022)  
The Correlation Between Immune  
Invasion and SARS-COV-2 Entry  
Protein ADAM17 in Cancer  
Patients by Bioinformatic Analysis.  
*Front. Immunol.* 13:923516.  
doi: 10.3389/fimmu.2022.923516

Kai Wang<sup>1†</sup>, Haoyue Deng<sup>1†</sup>, Binghui Song<sup>1†</sup>, Jiayue He<sup>1†</sup>, Shuguang Liu<sup>1</sup>, Jiewen Fu<sup>1</sup>, Lianmei Zhang<sup>2</sup>, Dabing Li<sup>1,3</sup>, Kyathegowdanadoddi Srinivasa Balaji<sup>4</sup>, Zhiqiang Mei<sup>1\*</sup>, Jingliang Cheng<sup>1\*</sup> and Junjiang Fu<sup>1\*</sup>

<sup>1</sup> Key Laboratory of Epigenetics and Oncology, Research Center for Preclinical Medicine, Southwest Medical University, Luzhou, China, <sup>2</sup> Department of Pathology, The Affiliated Huaian No. 1 People's Hospital of Nanjing Medical University, Huai'an, China, <sup>3</sup> Basic Medical School, Southwest Medical University, Luzhou, China, <sup>4</sup> PG Department of Biotechnology, Teresian College, University of Mysore, Mysore, India

SARS-Cov-2 caused the COVID-19 pandemic worldwide. ADAM17 functions as a disintegrin and transmembrane metalloproteinase domain protein involved in the regulation of SARS-CoV-2 receptor ACE2. However, its impact on cancer patients infected with COVID-19 and its correlation with immune cell infiltration is unclear. This study compared ADAM17 expression between normal and tumor tissues based on GEPIA. The correlations between ADAM17 expression and immune cell infiltration and immunomodulators were investigated. Besides, treated drugs for targeting ADAM17 were searched in the TISDB database. We found that ADAM17 was highly conserved in many species and was mainly expressed in lung, brain, female tissues, bone marrow and lymphoid tissues. It was also highly expressed in respiratory epithelial cells of rhinitis and bronchus. ADAM17 expression in tumors was higher than that in several paired normal tissues and was negatively correlated with the prognosis of patients with malignant tumors. Interestingly, ADAM17 expression significantly correlated with immunomodulators and immune cell infiltration in normal and tumor tissues. Moreover, eight small molecules targeting ADAM17 only demonstrate therapeutic significance. These findings imply important implications for ADAM17 in cancer patients infected with COVID-19 and provide new clues for development strategy of anti-COVID-19.

**Keywords:** ADAM17, cancer, SARS-CoV-2, susceptibility, therapeutics, small molecule

**Abbreviations:** SARS-Cov-2, Severe acute respiratory syndrome coronavirus 2; COVID-19, Coronavirus Disease 2019; ADAM17, A disintegrin and metalloproteinase domain 17; ACE2, Angiotensin-Converting Enzyme 2; HPA, Human Protein Atlas; NX, Normalized expression; IHC, Immunohistochemistry; GEPIA, The Gene Expression Profiling Interactive Analysis; TCGA, The Cancer Genome Atlas.

## INTRODUCTION

SARS-Cov-2 has caused a worldwide pandemic of Corona Virus Disease 2019 (COVID-19) since December 2019. It is an enveloped virus belonging to the beta coronavirus family that has infected about 300 million people worldwide and killed more than 5 million. The process by which the entry of SARS-Cov-2 into host cells is mediated by transmembrane spike (S) glycoproteins (1). Envelope-anchored S protein is cleaved into functional S1 and S2 subunits in the boundary region. S1 binds to host cell receptors, and S2 fuses with coronavirus membranes and cell membranes (2). Emerging evidence suggests that both S1 protein-receptor interaction and the fusion of the viral envelope with the host cell membrane are critical two steps in driving a successful infection of SARS-Cov-2 (3).

Recently, multiple potential SARS-Cov-2-related receptors have been identified, including heparan sulfate proteoglycans (HSPGs), angiotensin-Converting Enzyme 2 (ACE2), aminopeptidase N (APN), cathepsin L (CTSL), Heat Shock Protein A5 (HSPA5), transmembrane serine protease 2 (TMPRSS2), furin, O-Acetylated Sialic Acid (O-Ac-Sia) (4–6). Among them, ACE2 serves as a functional receptor of SARS-Cov-2 spike glycoprotein that is widely expressed on the membrane of apical epithelial cells, especially on ciliated cells (7). In addition, ACE2 is also found in kidney, cardiovascular, and gastrointestinal tissues. It can bind to the B domain of COVID-19 virus S protein, enabling the virus to enter target cells and start replicating leading to infection (8). ADAM metallopeptidase domain 17 (ADAM17, Ensembl: ENSG00000151694; OMIM: 603639), also known as ADAM18, CD156B, CSVP, NISBD, NISBD1 and TACE, is another newly identified potential receptor for SARS-Cov-2 (9). As a type-I multidomain transmembrane protein, the pro-domain of ADAM17 possesses catalytic activity (10). Once the pre-domain is hydrolyzed, ADAM17 participates in the hydrolysis and abscission of various extracellular functional regions of proteins, such as ACE2 (11). Increased ACE2 shedding triggers enhanced viral infection.

Infection of SARS-Cov-2 is closely connected with regulating the body's cellular immunity and humoral immunity. Initially, the body protects against viral infection through humoral immunity, i.e., neutralizing antibody (NAb) levels (12). Within two weeks of infection, plasma cells increase and virus-specific IgM and IgG can be detected (12). In the advanced stage of the disease, lymphocytes, CD4+T cells, CD8+T cells and natural killer cells (NK) are reduced in COVID-19 patients, accompanied by cytokine storms. In addition, PD-1, T-cell immunoglobulins, and mucin domain-3 (Tim-3) have also contributed to exacerbating infection (13), indicating the occurrence of adaptive immune escape.

Increasing evidence indicates that malignant tumors can induce the transport of immature neutrophils and monocytes into the tumor microenvironment, thereby causing immunosuppression (14). Besides, after treatment with chemotherapeutic agents and immunosuppressants, the body's immunity will also decline sharply, making the immune system of cancer patients abnormally changed and patients more

susceptible to infection. Immune cell infiltration in the tumor microenvironment plays a key role in tumor development and influences cancer patients' prognosis. Studies have shown that patients with advanced cancer are more likely to infect with COVID-19 and have a worse prognosis than normal individuals (15, 16).

ADAM17 has been reported to induce local tumor invasion and metastasis *via* degrading the cell basement membrane and extracellular matrix and affecting tissue remodeling. ADAM17 is usually expressed in various malignant tumors, while rarely expressed in normal cells (17), implying its specificity in the tumor. The effect of ADAM17 on cancer patients infected with COVID-19 and its correlation with immune cell infiltration have not been fully elucidated. This study investigated ADAM17 expression in cancer patients and/or normal individuals by bioinformatics analysis.

## MATERIALS AND METHODS

### Databases and Sources

The expressions of ADAM17 (Ensembl ID: ENSG00000151694) in mRNA and protein from normal human tissues were obtained from the database of Human Protein Atlas (HPA) (<https://www.proteinatlas.org/ENSG00000151694-ADAM17>) (18, 19). Immunohistochemical or immunofluorescence images of ADAM17 in normal tissues (v20.proteinatlas.org/ENSG00000151694-ADAM17/tissue), tumor tissues (v20.proteinatlas.org/ENSG00000151694-ADAM17/pathology), and cancer cell lines (v20.proteinatlas.org/ENSG00000151694-ADAM17/cell#img) were obtained from the HPA database (20, 21). The ADAM17 expressions were verified using the project of Genotype-Tissue Expression (GTEx). The Gene Expression Profiling Interactive Analysis (GEPIA) dataset (GEPIA 2) was obtained from the website (<http://gepia2.cancer-pku.cn/#index>) (22) to compare the expressions between tumor and matched normal tissues. The ADAM17 structure with indicated residues of amino acids for each domain was gained in the Uniprot database (<https://www.uniprot.org/uniprot/P78536>) (UniProtKB/Swiss-Prot number P78536.1). The NCBI (National Center for Biotechnology Information) database was applied to perform homology analysis (<https://www.ncbi.nlm.nih.gov/homologene/2395>) (23). The correlation between ADAM17 and treated drugs targeting ADAM17 was performed in the TISDB database (<http://cis.hku.hk/TISIDB/browse.php?gene=ADAM17>) (24).

### HPA (Human Protein Atlas) Analysis for ADAM17

The mRNA and protein expressions of ADAM17 were analyzed in normal and tumor tissues from the HPA database (<https://www.proteinatlas.org/ENSG00000151694-ADAM17>) (21). ADAM17 mRNA levels in various normal tissues were gained from the consensus datasets of three sources of HPA, GTEx, and FANTOM5 (18, 25). Consensus Normalized expression levels for tissues and blood cells were acquired through the above three datasets (v20.proteinatlas.org/about/assays+annotation#normalization\_rna). For IHC staining in these

data, two antibodies for ADAM17 (cat #: CAB025906, R&D Systems; cat #: HPA010738, Sigma-Aldrich) were used for tissue and cell line IHC staining (26).

## GEPIA and Prognostic Value Analysis for ADAM17

The ADAM17 mRNA expressions in 8,587 normal samples and 9,736 tumor tissues were analyzed with GEPIA (22). The correlation between ADAM17 expression level and median overall survival (OS) was also analyzed using the GEPIA database.

## Immunohistochemistry (IHC)

ADAM17 antibody for IHC was purchased from Sigma (HPA010738, Sigma-Aldrich). The IHC protocols were described previously (27–29).  $\beta$ -actin was served as an internal control.

## Correlation Analysis for ADAM17 Expression and Immunoregulation

We downloaded the pan-cancer dataset (PANCAN, N=10535, G=60499) from the UCSC database (<http://xenabrowser.net/>) and extracted the ADAM17 gene and 60 immune checkpoint regulatory genes (30), 150 immune regulatory genes (41 chemokines, 18 receptors, 21 MHCs, 24 immunoinhibitors, 46 immunostimulators) and 64 tumor-related immune cells for immune checkpoint genetic analysis, immunomodulatory gene analysis, immune cell analysis, and immune invasion analysis, respectively. Log<sub>2</sub> (x+0.001) transformation was performed for each expressed value. For immune cell infiltration analysis, Pearson correlations of these genes were calculated using TIMER (31) and deconvol xCell (32) algorithms of the R software package IOBR (version 0.99.9) (33).

## Statistical Analysis

ADAM17 expressions of samples in survival analysis were divided into two groups (high vs. low) using a median expression with overall survival (OS). Logrank with  $P < 0.05$  was considered a significant difference.

## RESULTS

### Highly Conserved ADAM17 and Its Structure for Ectodomain Shedding

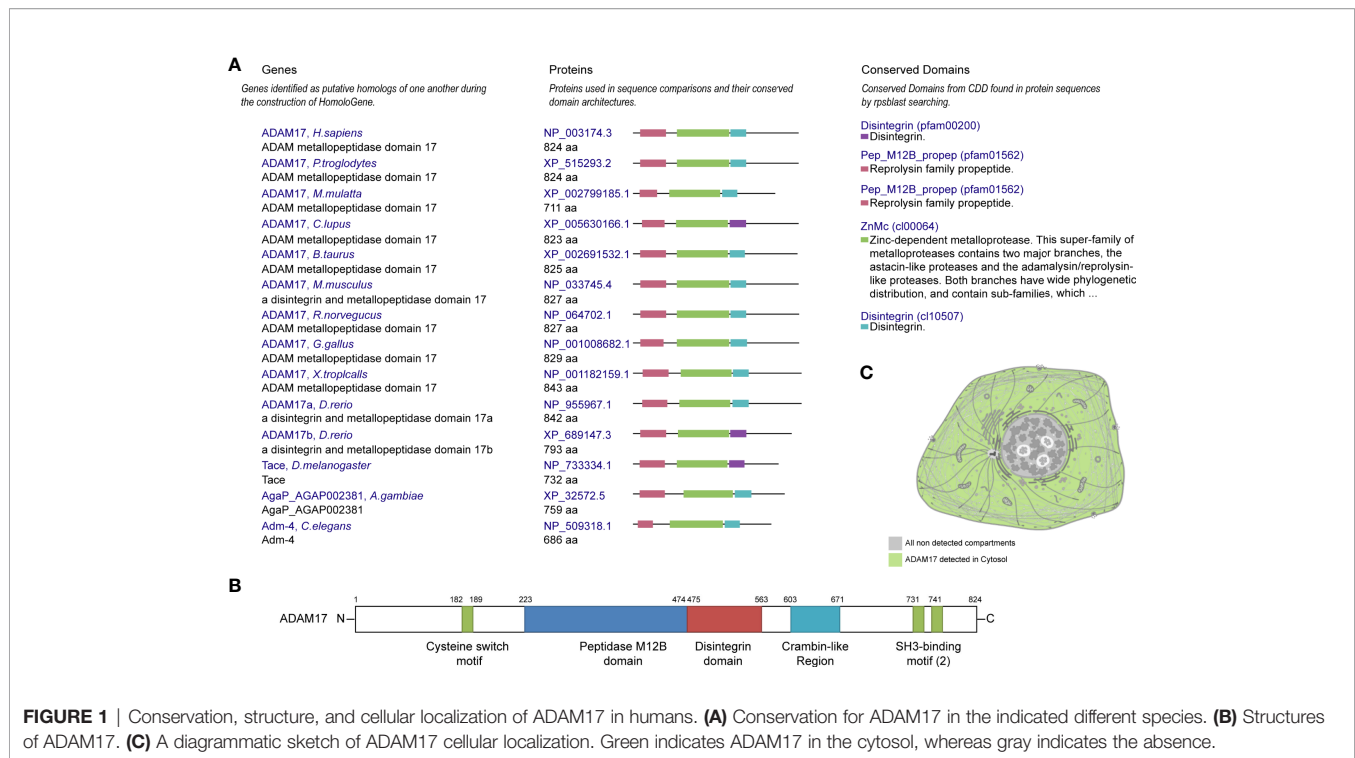
Protein homology analysis suggested that ADAM17 protein is highly conserved in various species, including *H. sapiens*, chimpanzee, rhesus monkey, dog, cow, mouse, rat, chicken, zebrafish, fruit fly, mosquito, *C. elegans*, and frog (Figure 1A), suggesting that ADAM17 has the potential to recognize SARS-CoV-2 spike proteins, which is similar to the function of ACE2 (23, 34). The UniProtKB/Swiss-Prot database analysis showed that ADAM17 has a peptidase M12B domain, a disintegrin domain, a crambin-like region, a cysteine switch motif and two SH3-binding motifs (Figure 1B). The longest domain (252 aa) of peptidase M12B (M12B proteinases, adamalysins or reprolysins) is a catalytic domain with the metal endopeptidase activity (35, 36), which is zinc ion-dependent endopeptidases. The conserved

cysteine presents in the cysteine-switch motif and binds with the catalytic zinc ion to inhibit the enzymatic activity, whereas cysteine dissociates from the zinc ion upon activation of the peptide to release the activity of the enzyme (37). Disintegrins, a family of small proteins in viper venoms, initially act as potent inhibitors of platelet aggregation and integrin-dependent cell adhesion (38), thus participating in the cellular-extracellular matrix and subcellular interactions. The SH3-binding motif originally binds to the Src homology 3 (SH3) region, the latter of which binds with target proteins and mediates the functional assembly of protein complexes. The crambin-like domain is an amphipathic region (39). In addition, the topological extracellular domain, the helical transmembrane, the topological cytoplasmic domain and signal peptide are located at 215–671, 672–692, 693–824, and 1–17 amino acid residues, respectively. ADAM17 locates in the cytoplasm of cells (Figure 1C, and Supplementary Figures 1A–D) and the cytoplasm and membrane of tissues (Supplementary Figure 1E). Collectively, these results suggest that ADAM17 may play a role in proteolysis and extracellular domain shedding of diverse proteins, including ACE2 (40).

### ADAM17 Is Mainly Expressed in Placental, Lung, Nasopharynx, Bronchus, Bone Marrow and Lymphatic Tissues

ADAM17 mRNA has low specificity in various human tissues and is highly expressed in the placenta (NX: 29.0), followed by the lung (NX: 24.7), and yet extremely low in total peripheral blood mononuclear cell (PBMC) (NX: 6), liver tissue (NX: 7.8) and NK cells (NX: 6) (Figures 2A, B). ADAM17 protein has cytoplasmic and membranous expression in various tissues, with moderate expression in 36 tissue types and low expression in the remaining 9 tissues (Figures 2A, C). Brain mRNA expression for ADAM17 showed either low tissue specificity or low region specificity (Figure 2D). Immune cell type expression for ADAM17 mRNA showed low immune cell specificity but higher in monocytes and granulocytes (Figure 2E).

Since the process by which SARS-Cov-2 entering host cells is mediated by transmembrane spike (S) glycoproteins. ACE2 serves as one of the main receptors for SARS-COV-2 that can bind to the B domain of the COVID-19 viral S protein, which in turn allows the virus to enter the target cells and begin to replicate leading to infection. However, ACE2 is found to be widely expressed on the membrane of the pulmonary ciliated epithelium (7). Besides, in an *in vivo* study using an ACE2 mutant mouse model, it was found that acute lung injury and even lung failure were aggravated by injection of coronavirus spike, while treatment with recombinant ACE2 significantly reduced acute lung failure (41). In this regard, it has been speculated that increased plasma membrane binding to ACE2 may lead to higher infections (42). Here, we investigated the role of ADAM17 in the human respiratory tract and found that its mRNA or protein levels were markedly elevated in lung tissue, rhinitis and bronchus (Figures 2B, C, F–H). In-depth analysis showed that ADAM17 is expressed in pneumocytes (31.67%), endothelial cells (28.33%), macrophages (10%) and bronchial



epithelial cells (5%) (**Table 1**). Immunohistochemical staining revealed that the expression of ADAM17 protein was detected in alveolar macrophages (blue arrows)/type I (red arrows) and type II (black arrow) alveolar epithelial cells, which are mostly located in the cytoplasm/cytoplasm (**Supplementary Figures 2A, B**). Furthermore, HPA, GTEx and FANTOM5 database analysis suggested that the mRNA level of ADAM17 in lung tissue was significantly higher than ACE2 ( $30.88 = 24.7/0.8$ , **Figure 2I**). As ADAM17 is a type I multi-domain transmembrane protein, and participates in the hydrolysis and shedding of ACE2, the latter of which further aggravates viral infection. We suggest that ADAM17 might also play a key role in entering SARS-COV-2 into the lung cells.

While attacking the new coronavirus in the lungs, many cytokines affect organs outside the lungs, such as the heart, kidney, liver, and other organs. Expression of ADAM17 in those tissues was also conducted in this study. The expression of ADAM17 in normal and tumor tissues was lower in the kidney and liver than in the heart (**Figures 2A, B**). Thus, we focused on analyzing the expression of ADAM17 in normal heart tissue because the cytokines can easily increase the severity in younger people severity and eventually lead to death. The results are shown in **Supplementary Figure 3**. The expression of ADAM17 protein in normal heart tissue was medium in both two antibodies (HPA010738, CAB025906) (**Supplementary Figures 3A, B**, <https://www.proteinatlas.org/ENSG00000151694-ADAM17/tissue/heart+muscle>), whereas the expression in normal heart tissue of ACE2 protein was low in the ACE2 antibody CAB080024, and antibody CAB080025, but there were no signals detected in the ACE2 antibody HPA000288, antibody CAB026174, and antibody

CAB026213 (data not shown, URL: [v20.proteinatlas.org/ENSG00000130234-ACE2/tissue/heart+muscle](http://v20.proteinatlas.org/ENSG00000130234-ACE2/tissue/heart+muscle)). Both proteins of ADAM17 and ACE2 were also found to be the membranous and cytoplasmic expression, mainly in the myocytes (**Supplementary Figures 3A–D**, data not shown). The mRNA expressions comparison between ADAM17 and ACE2 in heart tissues showed that the ADAM17 mRNA levels are 1.28-fold higher than ACE2 (**Figure 2J**).

## Differential Expression of ADAM17 in Tumor Tissues and Corresponding Normal Tissues

By analyzing distinct malignant tissues, we found that ADAM17 was highly expressed in lung cancer tissues (9 FPKM) and low in liver cancer tissues (1.3 FPKM) (**Figure 3A**). ADAM17 protein is located in the membrane and cytoplasm in distinct tumor tissues. Moreover, weak to moderate cytoplasmic immune responses were observed in most tumor tissues (**Figures 3B, 4A, B**, data not shown).

Next, we analyzed the expression values of ADAM17, HSPA5, TMPRSS2, FURIN, and ACE2 in different cancers and corresponding normal individuals. As shown in **Figure 4C**, compared with relative normal tissues, only ADAM17 was highly expressed in lung cancer, while the other four genes did not show any significant difference. ADAM17 mRNA levels were lower than HSPA5 and FURIN but higher than ACE2 and TMPRSS2 in most cancer types (**Figure 4D**). Furthermore, we analyzed ADAM17 mRNA and ACE2 mRNA from 994 samples through the TCGA dataset and found that ADAM17 mRNA level was 10-fold higher than ACE2 (**Figure 4D**), suggesting that

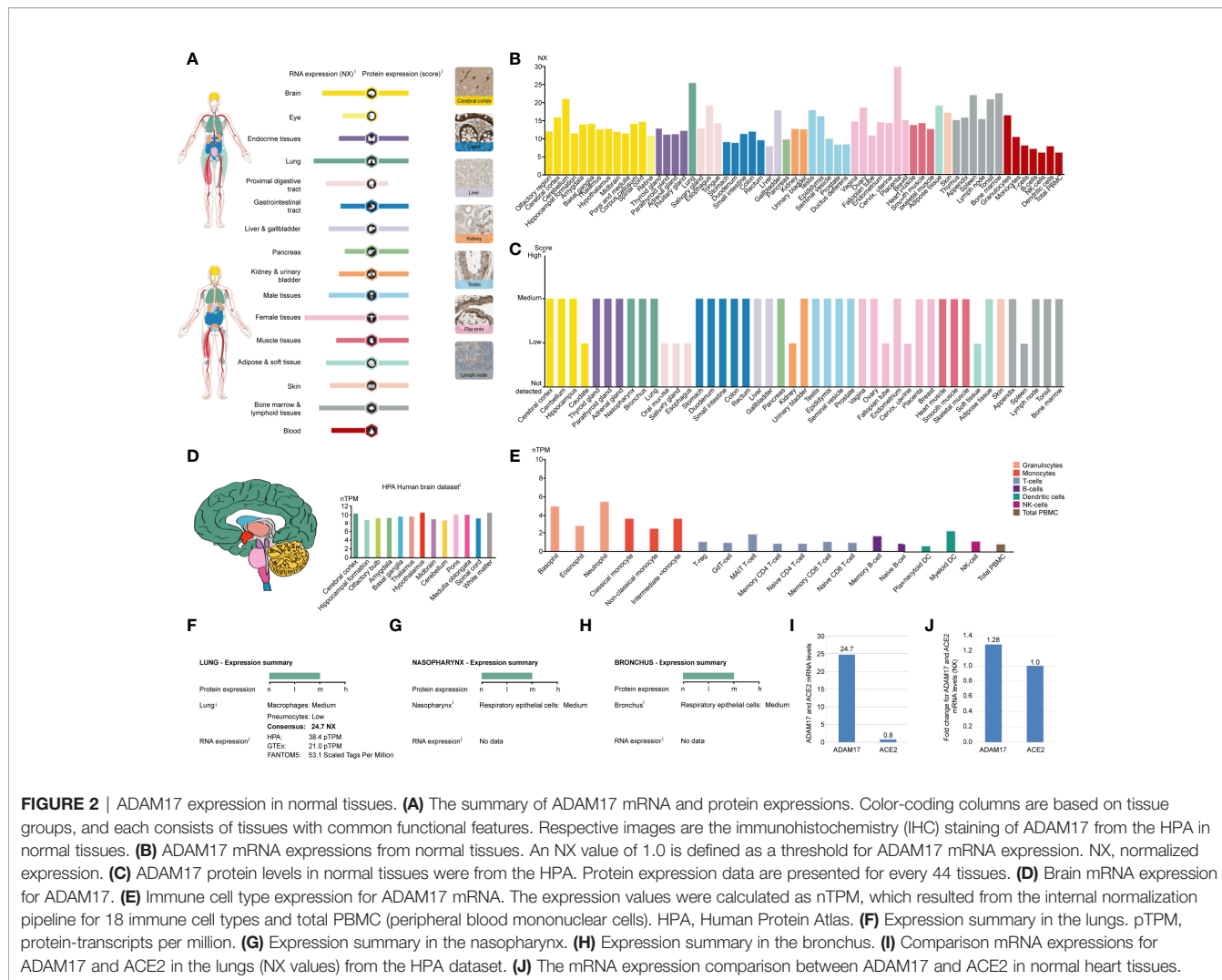


**FIGURE 2 |** ADAM17 expression in normal tissues. **(A)** The summary of ADAM17 mRNA and protein expressions. Color-coding columns are based on tissue groups, and each consists of tissues with common functional features. Respective images are the immunohistochemistry (IHC) staining of ADAM17 from the HPA in normal tissues. **(B)** ADAM17 mRNA expressions from normal tissues. An NX value of 1.0 is defined as a threshold for ADAM17 mRNA expression. NX, normalized expression. **(C)** ADAM17 protein levels in normal tissues were from the HPA. Protein expression data are presented for every 44 tissues. **(D)** Brain mRNA expression for ADAM17. **(E)** Immune cell type expression for ADAM17 mRNA. The expression values were calculated as nTPM, which resulted from the internal normalization pipeline for 18 immune cell types and total PBMC (peripheral blood mononuclear cells). HPA, Human Protein Atlas. **(F)** Expression summary in the lungs. pTPM, protein-transcripts per million. **(G)** Expression summary in the nasopharynx. **(H)** Expression summary in the bronchus. **(I)** Comparison mRNA expressions for ADAM17 and ACE2 in the lungs (NX values) from the HPA dataset. **(J)** The mRNA expression comparison between ADAM17 and ACE2 in normal heart tissues.

ADAM17 might play a critical role in SARS-Cov-2 entry in patients of the lungs, which was supported partially by a systematic review that showed the level of malignancy in lung cancer patients correlated with the likelihood of having COVID-19 (43).

Then, the ADAM17 mRNA expression profile across distinct tumors and the corresponding normal tissues in pan-cancer were assessed with the GEPIA dataset (Figures 4D, E). We found that the ADAM17 gene was expressed in nearly all tumor tissues, and was significantly upregulated in five types of tumors, including

cholangio carcinoma (CHOL), brain lower-grade glioma (LGG), glioblastoma multiforme (GBM), pancreatic adenocarcinoma (PAAD), and stomach adenocarcinoma (STAD) (Figure 4F), and these tumor tissues expressing ADAM17 at higher levels than corresponding normal tissues in the brain and digestive tract (Figure 4E). However, no significant difference in ADAM17 expression was observed in the remaining tumor tissues (Figure 4E). The gene expression of ADAM17 in human tumors and matched normal tissues were validated in the database of ONCOMINE (Data not shown). ADAM17 expressions in lung cancer were increased, but not significantly compared to normal tissues in the TCGA dataset (Data not shown).

Next, the pathological stage plots in all indicated 26 cancer types (<http://gepia2.cancer-pku.cn/#analysis>) were performed and the results showed that the ADAM17 expressions are positively correlated with advanced tumor stages of the pan-cancer [Pr(>F), 2.5e-12] (Figure 4G); specific for kidney chromophobe (KICH) [Pr(>F), 0.022], liver hepatocellular carcinoma (LIHC) [Pr(>F), 0.0106], and ovarian serous cystadenocarcinoma (OV) [Pr(>F), 0.0139]; but not for lung

**TABLE 1 |** ADAM17 RNA expression in different cells from the lung.

Cell types	Percentages
Pneumocytes	31.67
Bronchial epithelium	5
Endothelial cells	28.33
Macrophages	10
Other cell types	25

data was normalized to nine samples from HPA RNA-sequencing.

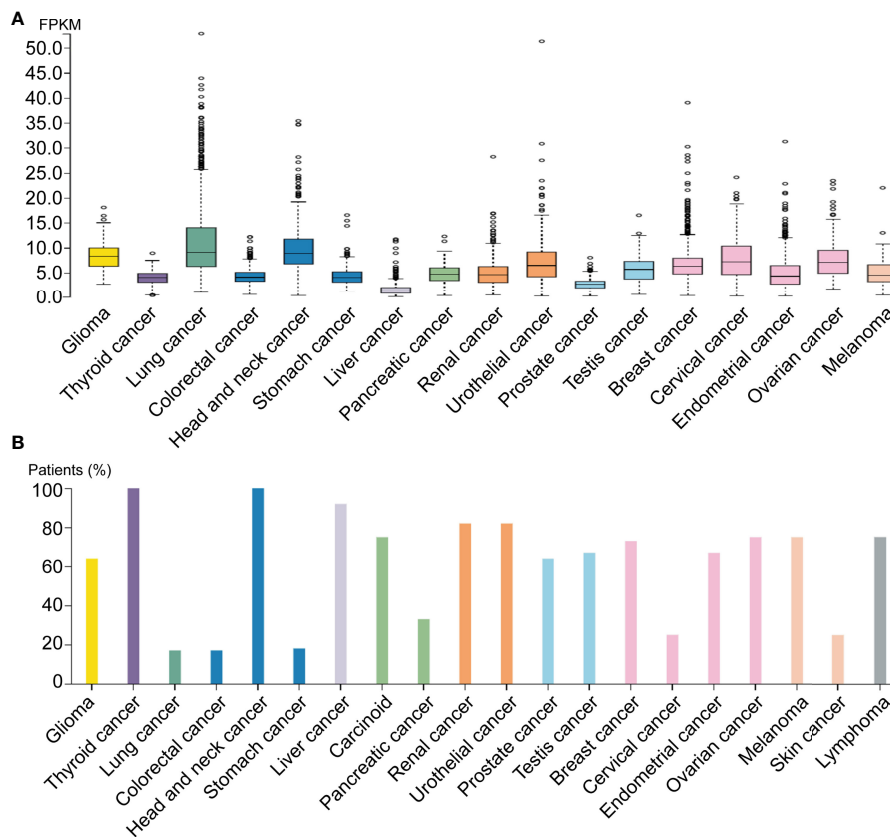


**FIGURE 3** | ADAM17 expression levels in different human cancers. **(A)** ADAM17 mRNA expression in different cancer tissues. **(B)** The protein expressions of ADAM17. In each cancer type, color-coded bars show the percentage of patients with high and medium levels of ADAM17 protein. The cancer types are color-coded according to organ type, and cancer originates.

cancers, either lung adenocarcinoma (LUAD) [ $Pr(>F)$ , 0.067] (**Figure 4H**) or Lung squamous cell carcinoma (LUSC) [ $Pr(>F)$ , 0.945] (Data not shown).

The prognostic value for ADAM17 in pan-cancer was investigated by Kaplan-Meier analysis and found that the high expression of ADAM17 significantly decreased patients' overall survival (OS) in four types of cancers, i.e., adrenocortical carcinoma (ACC), breast invasive carcinoma (BLCA), mesothelioma (MESO), and liver hepatocellular carcinoma (LIHC) (**Figures 4I–L**); whereas low expression of ADAM17 significantly decreased patient OS only in kidney renal clear cell carcinoma (KIRC) (**Figure 4M**). These results indicate that the OS of cancer patients is markedly reduced in most types of malignant tumors.

### ADAM17 Expression Is Associated With Immune Cell Infiltration in Several Tumors and Is a Potential Drug Target

Due to the indispensability of the immune system during antiviral processes, the correlations between the expression of ADAM17 and the level of immune infiltration in cancers were performed. By analyzing the correlation between the ADAM17

gene and immune invasion scores in 9,555 tumor samples from 39 cancer species, we observed a significant correlation between the expression of this gene and immune invasion in 21 cancer species, with 7 (GBMLGG, COAD, COADREAD, KIPAN, READ, PAAD, DLBC) positive and 14 (CESC, ESCA, STES, KIRP, UCEC, HNSC, LUSC, THYM, THCA, SKCM-M, SKCM, TGCT, SKCM-P, ACC) negative correlations (**Figure 5**).

Besides, we collected ADAM17 gene and 60 immune checkpoint regulatory genes, 150 immune regulatory genes (41 chemokines, 18 receptors, 21 MHCs, 24 immunoinhibitors, 46 immunostimulators) and 64 tumor-related immune cells for immune checkpoint genetic analysis, immunomodulatory gene analysis, immune cell analysis, and immune invasion analysis, respectively. Bioinformatics analysis aimed to explore the importance of the ADAM17 immune response in identifying different types of cancer that might benefit from anti-ADAM17 therapy. Results showed that the expression of ADAM17 was mutually exclusive of several tumor immune checkpoints, like CD40LG, CX3CL1, VEGFB, TNFSF9, IFNA2 in ESCA, STES, LAML, DLBC, UVM, THYM, KIRP, LGG or GBMLGG (**Figure 6A**). Furthermore, ADAM17 was negatively connected with several immunoregulatory genes (i.e., CCL25, CCL15,

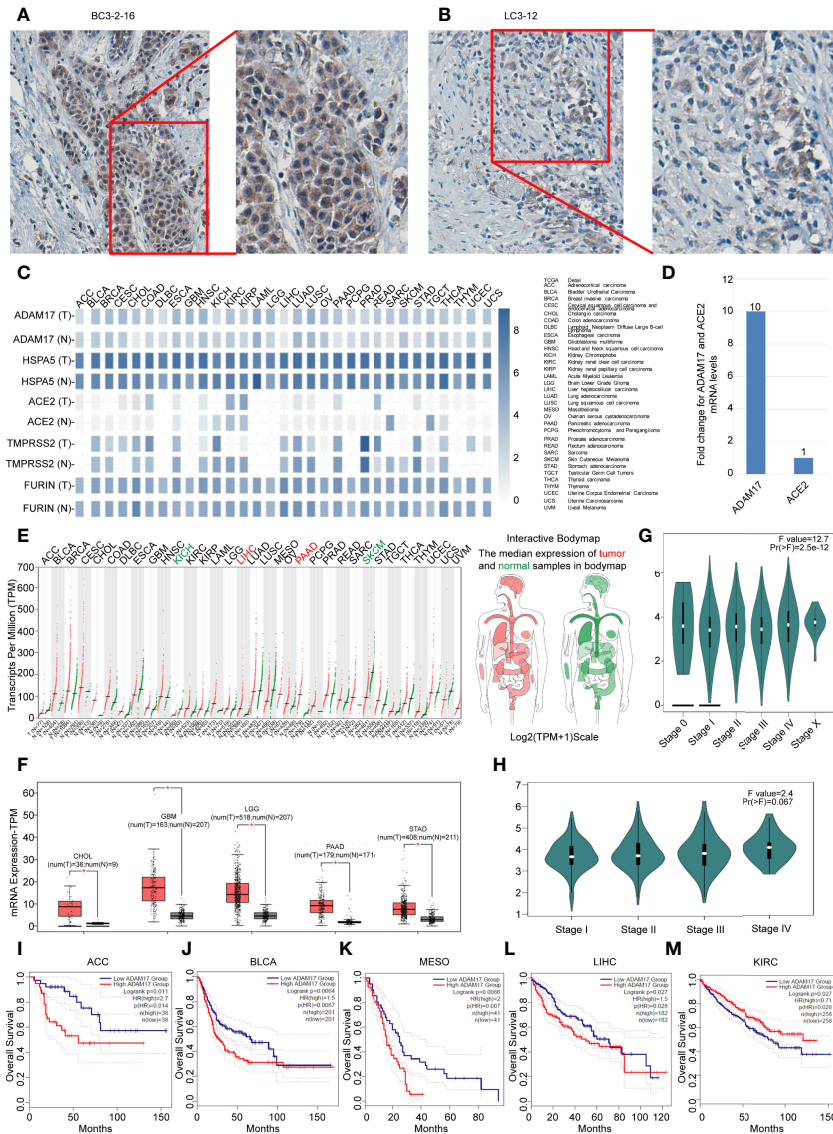


**FIGURE 4** | Differential expressions of ADAM17, HSPA5, ACE2, Furin, and TMPRSS2 in tumors and corresponding normal tissues, and prognostic values of ADAM17 expression in multiple cancer types. **(A)** The representative IHC images of tumors from Chinese breast cancer patients. **(B)** The representative IHC images of tumors from Chinese lung cancer patients. IHC was performed by ADAM17 antibody (HPA010738, Sigma-Aldrich). B&D, enlarged images from A&C respectively. **(C)** Expression comparisons of ADAM17 with HSPA5, TMPRSS2, Furin, and ACE2 in 31 types of normal and cancer tissues. “T” stands for tumors, whereas “N” denotes matched normal tissues. The cancer types of full names are shown on the right panel. **(D)** mRNA comparison between ADAM17 and ACE2 in lung cancer from the TCGA dataset. **(E)** The ADAM17 expression profiles across all cancers and paired normal individuals of tissues with dot plots. **(F)** ADAM17 was overexpressed in 5 cancer types with box plots. ADAM17 mRNA levels in cancers and matched normal individuals of tissues were obtained through the dataset of GEPIA. \**P*<0.05. **(G)** Pathological stage plots in pan-cancer. Pr(>F), 2.5e-12. **(H)** Pathological stage plots in LUAD. Pr(>F), 0.067. **(I–M)** The prognostic values for ADAM17 in five cancer types from the GEPIA dataset. I–M indicates ACC, BLCA, MESO, LIHC, and KIRC. \**P* < 0.05. HR, Hazards Ratio. GEPIA, Gene Expression Profiling Interactive Analysis.

TNFRSF18, HHLA2, CXCL12, CXCL17, TMIGD2, CXCR5, TNFRSF9, CCL25, CXCL17, IAG3, TNFRSF4) in ESCA, STES, LAML, COAD, KIPAN, PRAD, READ, THYM, LUAD, MESO, GBMLGG, THCA, UCS, or HNSC (**Figure 6B**).

Based on ADAM17 gene expression, we reassessed the invasion scores of aDC, Adipocytes, Astrocytes, B-cells, Basophils, CD4+

memory T-cells, CD4+ naive T-cells, CD4+ T-cells, CD4+ Tcm, CD4+ Tem, CD8+ naive T-cells, CD8+ T-cells, CD8+ Tcm, CD8+ Tem, cDC, Chondrocytes, Class-switched\_memory\_B-cells, CLP, CMP, DC, Endothelial\_cells, Eosinophils, Epithelial\_cells, Erythrocytes, Fibroblasts, GMP, Hepatocytes, HSC, iDC, Keratinocytes, Ly Endothelial cells, Macrophages, M1

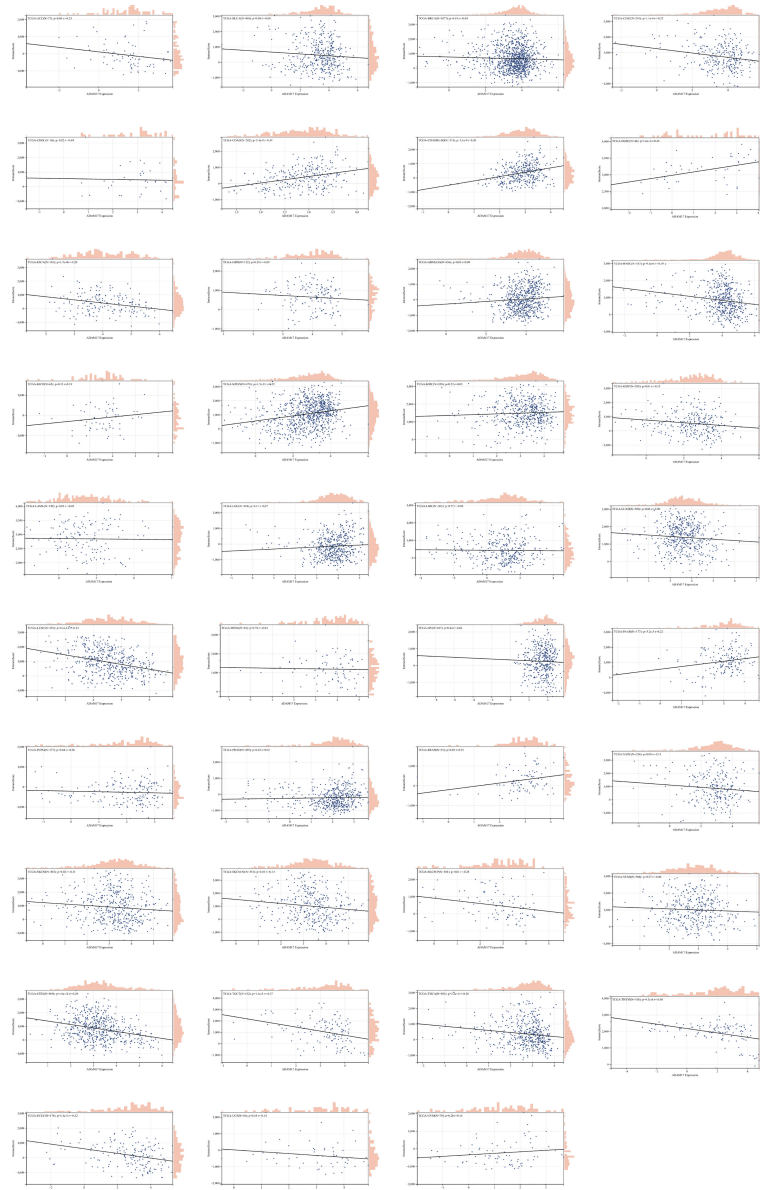


**FIGURE 5** | The correlation between ADAM17 expression and immune invasion score in multiple cancer types.

Macrophages, M2 Macrophages, Mast cells, Megakaryocytes, Melanocytes, Memory\_B-cells, MEP, Mesangial\_cells, Monocytes, MPP, MSC, mv Endothelial cells, Myocytes, naïve B-cells, Neurons, Neutrophils, NK cells, NKT, Osteoblast, pDC, Pericytes, Plasma cells, Platelets, Preadipocytes, pro B-cells, Sebocytes, Skeletal\_muscle, Smooth\_muscle, Tgd\_cells, Th1 cells, Th2 cells, Tregs, ImmuneScore, StromaScore, and MicroenvironmentScore in tumor tissues of cancer patients, and found that the expression of ADAM17 was positively related to some lymphocytes (Th2 and Men B) (Figure 7A), as well as B cells, CD4 T cells, CD8 T cells, Neutrophils, Macrophages and DC cells (Figures 7E, F). It was also positively related to regulatory T

cells (Tregs) and M2 Macrophages, which exhibited the inhibition of anti-tumor immunity and promotion of tumor development, respectively (Figure 7F). We speculate that ADAM17 is likely to be a novel target for tumor immunotherapy.

In addition, the results uncovered that the expression of ADAM17 was positively correlated with an immunostimulator (IL6R) (Figure 7B) and immunoinhibitors (CD274, KDR, TGFBR1) (Figure 7C) in most cancer types. However, there was a reverse correlation between the expression of ADAM17 and an immunoinhibitor (TNFRSF14) (Figure 7B).

Moreover, since ADAM17 correlated with immune cell infiltration in multiple cancers, drugs targeting ADAM17 from



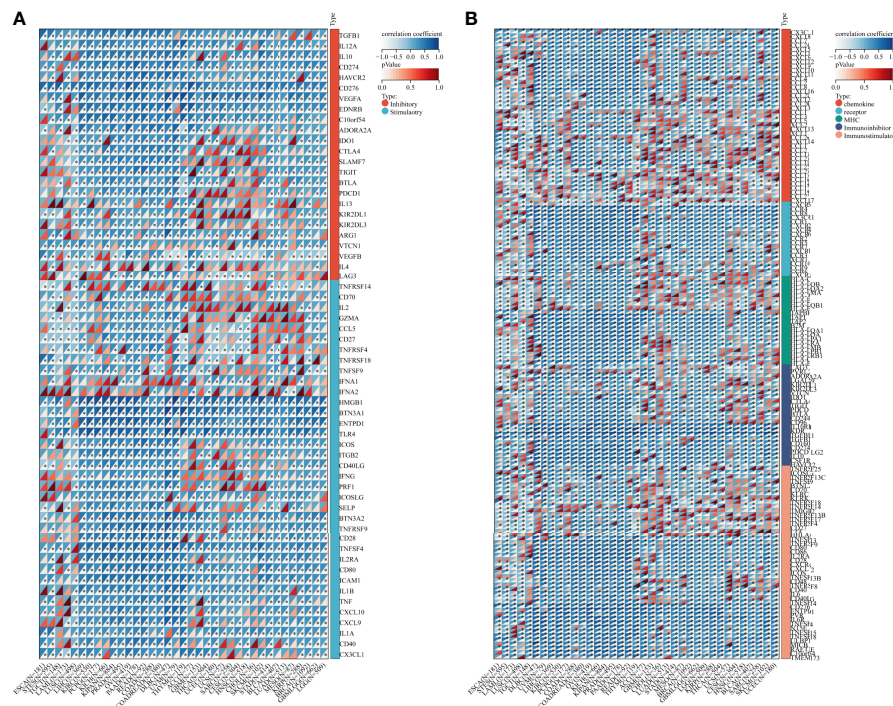


**FIGURE 6** | Bioinformatics analysis of the immunomodulatory role of ADAM17 in multiple cancer types. **(A)** Correlation between ADAM17 and 60 genes related to immune checkpoints. **(B)** Correlation between ADAM17 and 150 immunomodulators (41 chemokines, 18 receptors, 21 MHCs, 24 immunoinhibitors, and 46 immunostimulators). \* $P < 0.05$ .

DrugBank database were performed, and results showed that there are eight drugs targeted only for ADAM17 (**Figure 7D**), which all are small molecules (**Table 2**).

## DISCUSSION

As a global public health issue for COVID-19, understanding the expressions and localizations of potential SARS-CoV-2 receptors such as ACE2 and ADAM17 in host tissues may provide insights into prevention or treatments that can reduce the viral infection replication, COVID-19 spread, severity of pathology. It has been shown that ACE2 is implied in viral infection (44–46). Other host receptors like ADAM17 might also function as one of the receptors for viral recognition (47). ADAM17 would closely relate to this viral entry, and the distribution and expression levels of ADAM17 might reflect the susceptibility, viral replication and viral entry. Inhibition of ADAM17 would exert a protective effect on COVID-19 (48). However, the ADAM17 expression in different normal tissues and cancer patients, the impacts of ADAM17 on susceptibility for SARS-CoV-2, and the significance for cancer patients in the COVID-19 outbreaks are unclear.

The homological analysis showed that ADAM17 protein is highly conserved in various species in this study. Its structures and localization prediction indicated the role of ACE2 ectodomain shedding when SARS-CoV-2 attacks, particularly in human airway epithelia (49). ADAM17 is expressed in all normal tissues and

upregulated in some tumor tissues, suggesting that all the organs can be potentially infected. In normal lung tissues, ADAM17 mRNA levels increased 30.88-fold more than that in ACE2, and in lung cancer tissues, ADAM17 mRNA levels increased 10-fold more than that of ACE2, suggesting that ADAM17 might play a critical role in SARS-Cov-2 entry in cancer patients *via* lungs, which was supported partially by a systematic review in cancer patients with COVID-19 that lung cancer was more likely to have the risk of COVID-19 when studied the ACE2 expression (43). Moreover, the comparison of ADAM17 expression among normal tissues of the lungs, nasopharynx, and bronchus was also conducted and found to be low at pneumocytes and medium at macrophages. Both protein levels at the nasopharynx and bronchus are medium in respiratory epithelial cells, demonstrating that ADAM17 at respiratory airways might play a critical role in SARS-Cov-2 entry. ADAM17 has also been shown to transform TNF- $\alpha$  precursors into soluble TNF- $\alpha$ , and plays an important role in the processing of many substrates, such as cell adhesion molecule, cytokine growth factor receptor, epidermal growth factor receptor. In addition, ADAM17 can induce diabetes and cardiomyopathy and play an important role in a variety of tumors, such as gastric cancer, breast cancer, prostate cancer, cervical cancer, etc. All these are of great significance to the further study of ADAM17, especially, in cancer patients with SARS-CoV-2.

Furthermore, in cancer patients, higher expression of ADAM17 significantly decreased patient survival in overall survival (OS) in four types of cancers, which was supported by our systematic review results that 7.15% of COVID-19 patients (5,068) had cancer

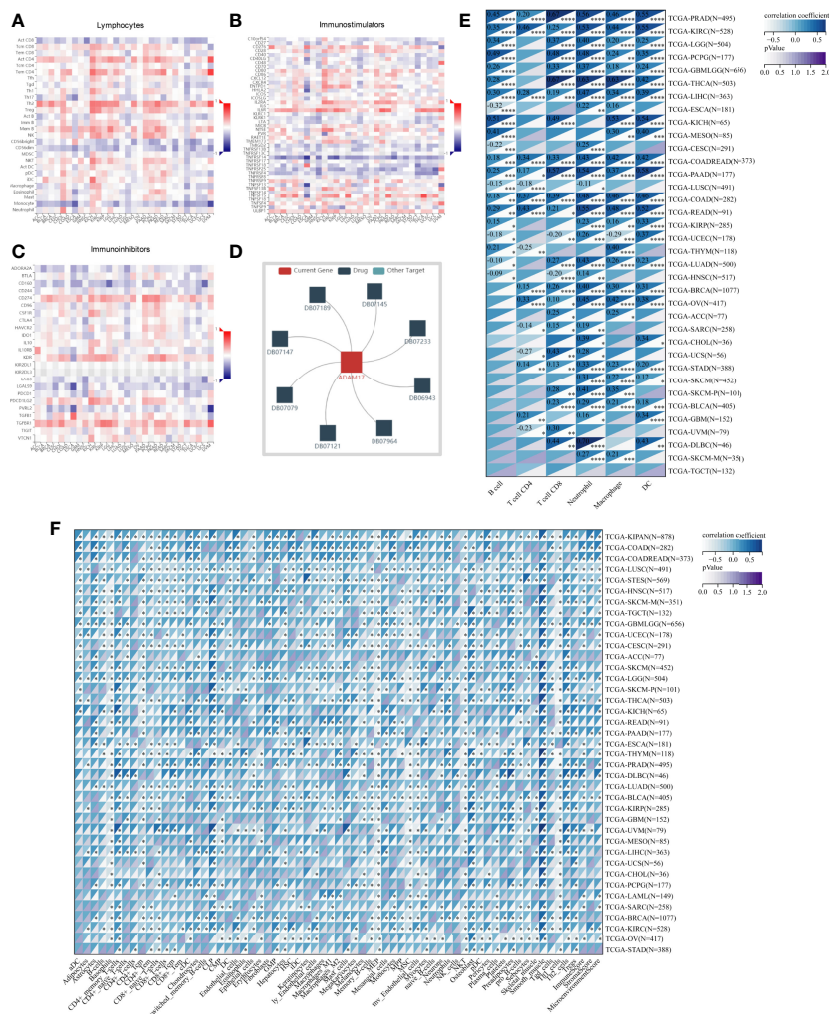


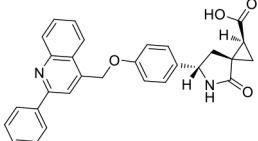
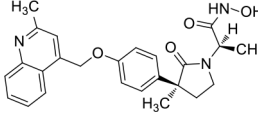
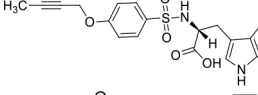
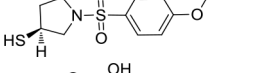
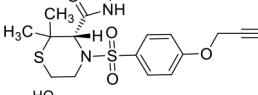
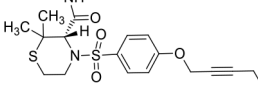
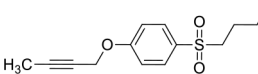
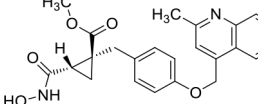
**FIGURE 7 |** Spearman correlations of the ADAM17 expression with tumor-immune systems in multiple cancer types and targeted drugs. **(A)** Lymphocytes. **(B)** Immunostimulators. **(C)** Immunoinhibitors. **(D)** targeted drugs. **(E)** Correlation between ADAM17 and 6 tumor-related immune cells calculated with TIMER. **(F)** Correlation between ADAM17 and 64 tumor-related immune cells and three Immune cell infiltration scores calculated with the deconvol xCell algorithm. \**P* < 0.05; \*\**P* < 0.005; \*\*\**P* < 0.001; \*\*\*\**P* < 0.0001.

coincidental situations, and the rate of more severe events of COVID-19 patients with malignant cancers (33.33%) presented a higher trend than that for all COVID-19 patients (16.09%) with a significant difference (50).

When the virus enters the body, it will down-regulate the ACE2 level and facilitate the expression of AngII and AT1 $\alpha$  receptor in the lung, resulting in the increase of pulmonary capillary permeability and lung injury *via* the activation of the immune system (cytokines and inflammatory factors). In addition, SARS-CoV-2 fatality is attributed to a cytokine storm triggered by excessive pro-inflammatory responses. While attacking the lungs, a large number of cytokines can cause damage to organs outside the lungs, such as the heart, kidney, liver, and other organs. A large number of plasma cytokines and chemokines (i.e., CCL2, CXCL8, TNF $\alpha$ , etc) were found to be accumulated in patients with SARS-

CoV-2 (51). In addition to acting as a viral binding receptor, ACE2 is also involved in modulating immune processes, leading to cytokine storms and exacerbation of pneumonia (52). ADAM17 may be the master molecule involved in regulating IL-6 class switching, and through this, it can control inflammatory response to viral antigenic stimuli (53). We thus focus on analyzing the expressions of ADAM17 in normal heart tissues because the cytokine can easily increase the severity in younger people and eventually lead to death (54, 55). The expressions in normal heart tissues of ADAM17 protein were medium, whereas those in normal heart tissues of ACE2 protein were under medium or lower, localizing in both membrane and cytoplasm. The mRNA levels of ADAM17 are increased 1.28-fold than that of ACE2 in heart muscles. ADAM17, as a type I multi-domain transmembrane protein, has a similar function to ACE2 and contributes to the

**TABLE 2** | Representative small molecule compounds targeting ADAM17.

DrugBank accession number	Chemical name or compound name	Chemical structure	Chemical formula
DB07189	(1S,3R,6S)-4-oxo-6-{4-[(2-phenylquinolin-4-yl)methoxy]phenyl}-5-azaspiro[2.4]heptane-1-carboxylic acid		C <sub>29</sub> H <sub>24</sub> N <sub>2</sub> O <sub>4</sub>
DB07145	(2R)-N-hydroxy-2-[(3S)-3-methyl-3-{4-[(2-methylquinolin-4-yl)methoxy]phenyl}-2-oxopyrrolidin-1-yl]propanamide		C <sub>25</sub> H <sub>27</sub> N <sub>3</sub> O <sub>4</sub>
DB07233	N-[[4-(but-2-yn-1-yloxy)phenyl]sulfonyl]-5-methyl-D-tryptophan		C <sub>22</sub> H <sub>22</sub> N <sub>2</sub> O <sub>5</sub> S
DB06943	(3S)-1-[[4-(but-2-yn-1-yloxy)phenyl]sulfonyl]pyrrolidine-3-thiol		C <sub>14</sub> H <sub>17</sub> NO <sub>3</sub> S <sub>2</sub>
DB07964	(3S)-4-[[4-(but-2-yn-1-yloxy)phenyl]sulfonyl]-N-hydroxy-2,2-dimethylthiomorpholine-3-carboxamide		C <sub>17</sub> H <sub>22</sub> N <sub>2</sub> O <sub>5</sub> S <sub>2</sub>
DB07121	4-[[4-[(4-aminobut-2-ynyl)oxy]phenyl]sulfonyl]-N-hydroxy-2,2-dimethylthiomorpholine-3-carboxamide		C <sub>17</sub> H <sub>23</sub> N <sub>3</sub> O <sub>5</sub> S <sub>2</sub>
DB07079	3-[[4-(but-2-yn-1-yloxy)phenyl]sulfonyl]propane-1-thiol		C <sub>13</sub> H <sub>16</sub> O <sub>3</sub> S <sub>2</sub>
DB07147	Methyl(1R,2S)-2-(hydroxycarbamoyl)-1-{4-[(2-methylquinolin-4-yl)methoxy]benzyl}cyclopropanecarboxylate		C <sub>24</sub> H <sub>24</sub> N <sub>2</sub> O <sub>5</sub>

hydrolysis and shedding of ACE2, while an increase in shedding of ACE2 can aggravate viral infection. Therefore, we speculate that ADAM17 might play an important role in cytokine storms. Indeed, compared to normal values, cytokine factors, including IL-6, were higher in severe patients with COVID-19 (56, 57). Thus, ADAM17 should be considered a potential target for drug discovery that regulates host reactivity to viral infection and prevents fatal outcomes (58).

Moreover, drugs targeting ADAM17 from the DrugBank database showed eight small molecule compounds targeted only for ADAM17, demonstrating the therapeutic significance of targeting ADAM17 for both the prevention of tumor progression and SARS-CoV-2 attacking in immune implications.

## CONCLUSION

In summary, our analysis uncovered that ADAM17 is expressed in both normal (especially in the lung) and tumor tissues and is highly expressed in several tumor samples. High expression of ADAM17 significantly reduces the prognosis of patients with malignant tumors. These results suggest that ADAM17 may promote coronavirus infection in patients with malignant tumors.

Lung tissue cell analysis showed that ADAM17 protein was highly expressed in respiratory epithelial cells of the nasopharynx and bronchus, suggesting that viral infection may be mainly distributed in respiratory epithelial cells. Eight drugs were targeted only for ADAM17, demonstrating the immune implications of targeting ADAM17 to prevent tumor progression and SARS-CoV-2 attack. These drugs that might be useful for targeting ADAM17 and SARS-CoV-2 in addition to enhancement of respiratory tract immune defense.

## DATA AVAILABILITY STATEMENT

The original contributions presented in the study are included in the article/**Supplementary Material**. Further inquiries can be directed to the corresponding author.

## ETHICS STATEMENT

The study was approved by the Ethical Committee of Southwest Medical University. The patients/participants provided their written informed consent to participate in this study.

## AUTHOR CONTRIBUTIONS

JF conceived and coordinated the study. JF, JH, DL, HD, ZM, BS, KW, JC, and JfF conducted experiments and analyzed and interpreted data. LZ provided pathology expertise. KW and KSB edited the manuscript. JuF wrote and edited the manuscript. All authors agreed that the manuscript should be submitted to the Journal.

## FUNDING

This work was supported in part by the National Natural Science Foundation of China (grant nos. 82073263, 81672887, and

30371493), the Research Foundation of Luzhou City (grant no. 2021-SYF-37), the Foundation of Southwest Medical University (grant nos. 2021ZKMS004, 2021ZKQN109), and the Translational Medicine Foundation of Southwest Medical University (grant no. 00031476).

## SUPPLEMENTARY MATERIAL

The Supplementary Material for this article can be found online at: <https://www.frontiersin.org/articles/10.3389/fimmu.2022.923516/full#supplementary-material>

## REFERENCES

- Khan RJ, Jha RK, Amara GM, Jain M, Singh E, Pathak A, et al. Targeting Sars-Cov-2: A Systematic Drug Repurposing Approach to Identify Promising Inhibitors Against 3c-Like Proteinase and 2'-O-Ribose Methyltransferase. *J biomol struct dynam* (2021) 39(8):2679–92. doi: 10.1080/07391102.2020.1753577
- Rossi GA, Sacco O, Mancino E, Cristiani L, Midulla F. Differences and Similarities Between Sars-Cov and Sars-Cov-2: Spike Receptor-Binding Domain Recognition and Host Cell Infection With Support of Cellular Serine Proteases. *Infection* (2020) 48(5):665–9. doi: 10.1007/s15010-020-01486-5
- V'Kovski P, Kratzel A, Steiner S, Stalder H, Thiel V. Coronavirus Biology and Replication: Implications for Sars-Cov-2. *Nat Rev Microbiol* (2021) 19(3):155–70. doi: 10.1038/s41579-020-00468-6
- Hasan A, Paray BA, Hussain A, Qadir FA, Attar F, Aziz FM, et al. A Review on the Cleavage Priming of the Spike Protein on Coronavirus by Angiotensin-Converting Enzyme-2 and Furin. *J biomol struct dynam* (2021) 39(8):3025–33. doi: 10.1080/07391102.2020.1754293
- Ibrahim IM, Abdelmalek DH, Elshahat ME, Elfiky AA. Covid-19 Spike-Host Cell Receptor Grp78 Binding Site Prediction. *J infect* (2020) 80(5):554–62. doi: 10.1016/j.jinf.2020.02.026
- Li D, Liu X, Zhang L, He J, Chen X, Liu S, et al. Covid-19 Disease and Malignant Cancers: The Impact for the Furin Gene Expression in Susceptibility to Sars-Cov-2. *Int J Biol Sci* (2021) 17(14):3954–67. doi: 10.7150/ijbs.63072
- Ziegler CGK, Allon SJ, Nyquist SK, Mbano IM, Miao VN, Tzouanas CN, et al. Sars-Cov-2 Receptor Ace2 Is an Interferon-Stimulated Gene in Human Airway Epithelial Cells and Is Detected in Specific Cell Subsets Across Tissues. *Cell* (2020) 181(5):1016–35.e19. doi: 10.1016/j.cell.2020.04.035
- Abassi Z, Higazi AAR, Kinaneh S, Armaly Z, Skorecki K, Heyman SN. Ace2, Covid-19 Infection, Inflammation, and Coagulopathy: Missing Pieces in the Puzzle. *Front Physiol* (2020) 11:574753. doi: 10.3389/fphys.2020.574753
- Mukhopadhyay D, AlSawafah N, Hussein GA. Identification of Novel Micrnas as Promising Therapeutics for Sars-Cov-2 by Regulating the Egfr-Adam17 Axis: An in Silico Analysis. *ACS Pharmacol Trans Sci* (2021) 4(1):396–9. doi: 10.1021/acspstsci.0c00199
- Dobert JP, Cabron AS, Arnold P, Pavlenko E, Rose-John S, Zunke F. Functional Characterization of Colon-Cancer-Associated Variants in Adam17 Affecting the Catalytic Domain. *Biomedicines* (2020) 8(11):463. doi: 10.3390/biomedicines8110463
- Healy EF, Lilic M. A Model for Covid-19-Induced Dysregulation of Ace2 Shedding by Adam17. *Biochem Biophys Res Commun* (2021) 573:158–63. doi: 10.1016/j.bbrc.2021.08.040
- Xu K, Dai L, Gao GF. Humoral and Cellular Immunity and the Safety of Covid-19 Vaccines: A Summary of Data Published by 21 May 2021. *Int Immunol* (2021) 33(10):529–40. doi: 10.1093/intimm/dxab061
- Alsayb MA, Alsamiri ADD, Makhdoom HQ, Alwasaidi T, Osman HM, Mahallawi WH. Prolonged Humoral and Cellular Immunity in Covid-19-Recovered Patients. *Saudi J Biol Sci* (2021) 28(7):4010–5. doi: 10.1016/j.sjbs.2021.04.008
- Hiam-Galvez KJ, Allen BM, Spitzer MH. Systemic Immunity in Cancer. *Nat Rev Cancer* (2021) 21(6):345–59. doi: 10.1038/s41568-021-00347-z
- Liang W, Guan W, Chen R, Wang W, Li J, Xu K, et al. Cancer Patients in Sars-Cov-2 Infection: A Nationwide Analysis in China. *Lancet Oncol* (2020) 21(3):335–7. doi: 10.1016/S1470-2045(20)30096-6
- Yu J, Ouyang W, Chua MLK, Xie C. Sars-Cov-2 Transmission in Patients With Cancer at a Tertiary Care Hospital in Wuhan, China. *JAMA Oncol* (2020) 6(7):1108–10. doi: 10.1001/jamaoncol.2020.0980
- Sinnathamby G, Zerfass J, Hafner J, Block P, Nickens Z, Hobeika A, et al. Adam Metallopeptidase Domain 17 (Adam17) Is Naturally Processed Through Major Histocompatibility Complex (Mhc) Class I Molecules and Is a Potential Immunotherapeutic Target in Breast, Ovarian and Prostate Cancers. *Clin Exp Immunol* (2011) 163(3):324–32. doi: 10.1111/j.1365-2249.2010.04298.x
- Uhlen M, Fagerberg L, Hallstrom BM, Lindskog C, Oksvold P, Mardinoglu A, et al. Proteomics. Tissue-Based Map of the Human Proteome. *Science* (2015) 347(6220):1260419. doi: 10.1126/science.1260419
- Uhlen M, Oksvold P, Fagerberg L, Lundberg E, Jonasson K, Forsberg M, et al. Towards a Knowledge-Based Human Protein Atlas. *Nat Biotechnol* (2010) 28(12):1248–50. doi: 10.1038/nbt1210-1248
- Thul PJ, Akesson L, Wiking M, Mahdessian D, Geladaki A, Ait Blal H, et al. A Subcellular Map of the Human Proteome. *Science* (2017) 356(6340):eaal3321. doi: 10.1126/science.aal3321
- Uhlen M, Zhang C, Lee S, Sjostedt E, Fagerberg L, Bidkhorji G, et al. A Pathology Atlas of the Human Cancer Transcriptome. *Science* (2017) 357(6352):eaan2507. doi: 10.1126/science.aan2507
- Tang Z, Li C, Kang B, Gao G, Li C, Zhang Z. Gepia: A Web Server for Cancer and Normal Gene Expression Profiling and Interactive Analyses. *Nucleic Acids Res* (2017) 45(W1):W98–W102. doi: 10.1093/nar/gkx247
- Fu J, Zhou B, Zhang L, Balaji KS, Wei C, Liu X, et al. Expressions and Significances of the Angiotensin-Converting Enzyme 2 Gene, the Receptor of Sars-Cov-2 for Covid-19. *Mol Biol Rep* (2020) 47(6):4383–92. doi: 10.1007/s11033-020-05478-4
- Ru B, Wong CN, Tong Y, Zhong JY, Zhong SSW, Wu WC, et al. Tisidb: An Integrated Repository Portal for Tumor-Immune System Interactions. *Bioinformatics* (2019) 35(20):4200–2. doi: 10.1093/bioinformatics/btz210
- Cheng J, Zhou J, Fu S, Fu J, Zhou B, Chen H, et al. Prostate Adenocarcinoma and Covid-19: The Possible Impacts of Tmprss2 Expressions in Susceptibility to Sars-Cov-2. *J Cell Mol Med* (2021) 25(8):4157–65. doi: 10.1111/jcmm.16385
- Berglund L, Bjorling E, Oksvold P, Fagerberg L, Asplund A, Szzygiarto CA, et al. A Genecentric Human Protein Atlas for Expression Profiles Based on Antibodies. *Mol Cell Proteomics MCP* (2008) 7(10):2019–27. doi: 10.1074/mcp.R800013-MCP200
- Zhang L, Yang M, Gan L, He T, Xiao X, Stewart MD, et al. Dlx4 Upregulates Twist and Enhances Tumor Migration, Invasion and Metastasis. *Int J Biol Sci* (2012) 8(8):1178–87. doi: 10.7150/ijbs.4458
- Fu J, Zhang L, He T, Xiao X, Liu X, Wang L, et al. Twist Represses Estrogen Receptor-Alpha Expression by Recruiting the Nurd Protein Complex in Breast Cancer Cells. *Int J Biol Sci* (2012) 8(4):522–32. doi: 10.7150/ijbs.4164

29. Zhang L, Wei C, Li D, He J, Liu S, Deng H, et al. Covid-19 Receptor and Malignant Cancers: Association of Ctsl Expression With Susceptibility to Sars-Cov-2. *Int J Biol Sci* (2022) 18(6):2362–71. doi: 10.7150/ijbs.70172
30. Thorsson V, Gibbs DL, Brown SD, Wolf D, Bortone DS, Ou Yang TH, et al. The Immune Landscape of Cancer. *Immunity* (2018) 48(4):812–30.e14. doi: 10.1016/j.immuni.2018.03.023
31. Li T, Fan J, Wang B, Traugh N, Chen Q, Liu JS, et al. Timer: A Web Server for Comprehensive Analysis of Tumor-Infiltrating Immune Cells. *Cancer Res* (2017) 77(21):e108–e10. doi: 10.1158/0008-5472.CAN-17-0307
32. Aran D, Hu Z, Butte AJ. Xcell: Digitally Portraying the Tissue Cellular Heterogeneity Landscape. *Genome Biol* (2017) 18(1):220. doi: 10.1186/s13059-017-1349-1
33. Zeng D, Ye Z, Shen R, Yu G, Wu J, Xiong Y, et al. Iobr: Multi-Omics Immunology Biological Research to Decode Tumor Microenvironment and Signatures. *Front Immunol* (2021) 12:687975. doi: 10.3389/fimmu.2021.687975
34. Yan R, Zhang Y, Li Y, Xia L, Guo Y, Zhou Q. Structural Basis for the Recognition of Sars-Cov-2 by Full-Length Human Ace2. *Science* (2020) 367(6485):1444–8. doi: 10.1126/science.abb2762
35. Takeda S. Adam and Adamts Family Proteins and Snake Venom Metalloproteinases: A Structural Overview. *Toxins* (2016) 8(5):155. doi: 10.3390/toxins8050155
36. Fox JW, Serrano SM. Structural Considerations of the Snake Venom Metalloproteinases, Key Members of the M12 Reprolysin Family of Metalloproteinases. *Toxicon* (2005) 45(8):969–85. doi: 10.1016/j.toxicon.2005.02.012
37. Van Wart HE, Birkedal-Hansen H. The Cysteine Switch: A Principle of Regulation of Metalloproteinase Activity With Potential Applicability to the Entire Matrix Metalloproteinase Gene Family. *Proc Natl Acad Sci USA* (1990) 87(14):5578–82. doi: 10.1073/pnas.87.14.5578
38. McLane MA, Sanchez EE, Wong A, Paquette-Straub C, Perez JC. Disintegrins. *Curr Drug Targets Cardiovasc Haematol Disord* (2004) 4(4):327–55. doi: 10.2174/1568006043335880
39. Hendrickson WA, Teeter MM. Structure of the Hydrophobic Protein Crambin Determined Directly From the Anomalous Scattering of Sulphur. *Nature* (1981) 290(5802):107–13. doi: 10.1038/290107a0
40. Heurich A, Hofmann-Winkler H, Gierer S, Liepold T, Jahn O, Pohlmann S. Tmprss2 and Adam17 Cleave Ace2 Differentially and Only Proteolysis by Tmprss2 Augments Entry Driven by the Severe Acute Respiratory Syndrome Coronavirus Spike Protein. *J Virol* (2014) 88(2):1293–307. doi: 10.1128/JVI.02202-13
41. Kuba K, Imai Y, Rao S, Gao H, Guo F, Guan B, et al. A Crucial Role of Angiotensin Converting Enzyme 2 (Ace2) in Sars Coronavirus-Induced Lung Injury. *Nat Med* (2005) 11(8):875–9. doi: 10.1038/nm1267
42. Leow MKS. Clarifying the Controversial Risk-Benefit Profile of Soluble Ace2 in Covid-19. *Crit Care* (2020) 24(1):396. doi: 10.1186/s13054-020-03097-w
43. Ren P, Gong C, Ma S. Evaluation of Covid-19 Based on Ace2 Expression in Normal and Cancer Patients. *Open Med* (2020) 15(1):613–22. doi: 10.1515/med-2020-0208
44. Hikmet F, Mear L, Edvinsson A, Micke P, Uhlen M, Lindskog C. The Protein Expression Profile of Ace2 in Human Tissues. *Mol Syst Biol* (2020) 16(7):e9610. doi: 10.15252/msb.20209610
45. Lan J, Ge J, Yu J, Shan S, Zhou H, Fan S, et al. Structure of the Sars-Cov-2 Spike Receptor-Binding Domain Bound to the Ace2 Receptor. *Nature* (2020) 581(7807):215–20. doi: 10.1038/s41586-020-2180-5
46. Shang J, Ye G, Shi K, Wan Y, Luo C, Aihara H, et al. Structural Basis of Receptor Recognition by Sars-Cov-2. *Nature* (2020) 581(7807):221–4. doi: 10.1038/s41586-020-2179-y
47. Schreiber B, Patel A, Verma A. Shedding Light on Covid-19: Adam17 the Missing Link? *Am J Ther* (2020) 28(3):e358–60. doi: 10.1097/MJT.0000000000001226
48. Palau V, Riera M, Soler MJ. Adam17 Inhibition May Exert a Protective Effect on Covid-19. *Nephrol Dialysis Transplant Off Publ Eur Dialysis Transplant Assoc - Eur Renal Assoc* (2020) 35(6):1071–2. doi: 10.1093/ndt/gfaa093
49. Jia HP, Look DC, Tan P, Shi L, Hickey M, Gakhar L, et al. Ectodomain Shedding of Angiotensin Converting Enzyme 2 in Human Airway Epithelia. *Am J Physiol Lung Cell Mol Physiol* (2009) 297(1):L84–96. doi: 10.1152/ajplung.00071.2009
50. Fu J, Wei C, He J, Zhang L, Zhou J, Balaji KS, et al. Evaluation and Characterization of Hspa5 (Grp78) Expression Profiles in Normal Individuals and Cancer Patients With Covid-19. *Int J Biol Sci* (2021) 17(3):897–910. doi: 10.7150/ijbs.54055
51. Wang J, Kaplan N, Wysocki J, Yang W, Lu K, Peng H, et al. The Ace2-Deficient Mouse: A Model for a Cytokine Storm-Driven Inflammation. *FASEB J Off Publ Fed Am Soc Exp Biol* (2020) 34(8):10505–15. doi: 10.1096/fj.202001020R
52. Chen L, Liu Y, Wu J, Deng C, Tan J, Liu H, et al. Lung Adenocarcinoma Patients Have Higher Risk of SARS-CoV-2 Infection. *Aging (Albany NY)* (2021) 13(2):1620–32. doi: 10.18632/aging.202375
53. Gomez MI, Sokol SH, Muir AB, Soong G, Bastien J, Prince AS. Bacterial Induction of Tnf-Alpha Converting Enzyme Expression and Il-6 Receptor Alpha Shedding Regulates Airway Inflammatory Signaling. *J Immunol* (2005) 175(3):1930–6. doi: 10.4049/jimmunol.175.3.1930
54. Ben Moffah M, Eswayah A. Intricate Relationship Between Sars-Cov-2-Induced Shedding and Cytokine Storm Generation: A Signaling Inflammatory Pathway Augmenting Covid-19. *Health Sci Rev* (2022) 2:100011. doi: 10.1016/j.hsr.2021.100011
55. Karki R, Sharma BR, Tuladhar S, Williams EP, Zalduondo L, Samir P, et al. Synergism of Tnf-Alpha and Ifn-Gamma Triggers Inflammatory Cell Death, Tissue Damage, and Mortality in Sars-Cov-2 Infection and Cytokine Shock Syndromes. *Cell* (2021) 184(1):149–68.e17. doi: 10.1016/j.cell.2020.11.025
56. Wan S, Yi Q, Fan S, Lv J, Zhang X, Guo L, et al. Relationships Among Lymphocyte Subsets, Cytokines, and the Pulmonary Inflammation Index in Coronavirus (Covid-19) Infected Patients. *Br J Haematol* (2020) 189(3):428–37. doi: 10.1111/bjh.16659
57. Xu B, Fan CY, Wang AL, Zou YL, Yu YH, He C, et al. Suppressed T Cell-Mediated Immunity in Patients With Covid-19: A Clinical Retrospective Study in Wuhan, China. *J Infect* (2020) 81(1):e51–60. doi: 10.1016/j.jinf.2020.04.012
58. Mahmud-Al-Rafat A, Majumder A, Taufiqur Rahman KM, Mahedi Hasan AM, Didarul Islam KM, Taylor-Robinson AW, et al. Decoding the Enigma of Antiviral Crisis: Does One Target Molecule Regulate All? *Cytokine* (2019) 115:13–23. doi: 10.1016/j.cyto.2018.12.008

**Conflict of Interest Statement:** The authors declare that the research was conducted in the absence of any commercial or financial relationships that could be construed as a potential conflict of interest.

**Publisher's Note:** All claims expressed in this article are solely those of the authors and do not necessarily represent those of their affiliated organizations, or those of the publisher, the editors and the reviewers. Any product that may be evaluated in this article, or claim that may be made by its manufacturer, is not guaranteed or endorsed by the publisher.

Copyright © 2022 Wang, Deng, Song, He, Liu, Fu, Zhang, Li, Balaji, Mei, Cheng and Fu. This is an open-access article distributed under the terms of the Creative Commons Attribution License (CC BY). The use, distribution or reproduction in other forums is permitted, provided the original author(s) and the copyright owner(s) are credited and that the original publication in this journal is cited, in accordance with accepted academic practice. No use, distribution or reproduction is permitted which does not comply with these terms.



# Duck LGP2 Downregulates RIG-I Signaling Pathway-Mediated Innate Immunity Against Tembusu Virus

Tianxu Li<sup>1</sup>, Yanyan Ren<sup>1</sup>, Tingting Zhang<sup>2</sup>, Xinyu Zhai<sup>1</sup>, Xiuyuan Wang<sup>1</sup>, Jinchao Wang<sup>1</sup>, Bin Xing<sup>1</sup>, Runchun Miao<sup>1</sup>, Ning Li<sup>1</sup> and Liangmeng Wei<sup>1,2\*</sup>

<sup>1</sup> Shandong Provincial Key Laboratory of Animal Biotechnology and Disease Control and Prevention, College of Animal Science and Veterinary Medicine, Sino-German Cooperative Research Centre for Zoonosis of Animal Origin of Shandong Province, Shandong Provincial Engineering Technology Research Center of Animal Disease Control and Prevention, Shandong Agricultural University, Tai'an City, China, <sup>2</sup> Collaborative Innovation Center for the Origin and Control of Emerging Infectious Diseases, College of Basic Medical Sciences, Shandong First Medical University, Tai'an City, China

## OPEN ACCESS

### Edited by:

Chenhe Su,  
Wistar Institute, United States

### Reviewed by:

Huibin Yu,  
Yale University, United States  
Xiaochuan Liu,  
University of California, Riverside,  
United States

### \*Correspondence:

Liangmeng Wei  
lmwei@sdau.edu.cn

### Specialty section:

This article was submitted to  
Viral Immunology,  
a section of the journal  
Frontiers in Immunology

Received: 09 April 2022

Accepted: 25 May 2022

Published: 15 June 2022

### Citation:

Li T, Ren Y, Zhang T, Zhai X,  
Wang X, Wang J, Xing B, Miao R,  
Li N and Wei L (2022) Duck LGP2  
Downregulates RIG-I Signaling  
Pathway-Mediated Innate Immunity  
Against Tembusu Virus.  
Front. Immunol. 13:916350.  
doi: 10.3389/fimmu.2022.916350

In mammals, the retinoic acid-inducible gene I (RIG-I)-like receptors (RLR) has been demonstrated to play a critical role in activating downstream signaling in response to viral RNA. However, its role in ducks' antiviral innate immunity is less well understood, and how gene-mediated signaling is regulated is unknown. The regulatory role of the duck laboratory of genetics and physiology 2 (duLGP2) in the duck RIG-I (duRIG-I)-mediated antiviral innate immune signaling system was investigated in this study. In duck embryo fibroblast (DEF) cells, overexpression of duLGP2 dramatically reduced duRIG-I-mediated IFN-promotor activity and cytokine expression. In contrast, the knockdown of duLGP2 led to an opposite effect on the duRIG-I-mediated signaling pathway. We demonstrated that duLGP2 suppressed the duRIG-I activation induced by duck Tembusu virus (DTMUV) infection. Intriguingly, when duRIG-I signaling was triggered, duLGP2 enhanced the production of inflammatory cytokines. We further showed that duLGP2 interacts with duRIG-I, and this interaction was intensified during DTMUV infection. In summary, our data suggest that duLGP2 downregulated duRIG-I mediated innate immunity against the Tembusu virus. The findings of this study will help researchers better understand the antiviral innate immune system's regulatory networks in ducks.

**Keywords:** LGP2, RIG-I, signaling pathway, Tembusu virus, innate immunity

## INTRODUCTION

The innate immune system is the first line of defense against infectious pathogens. Pattern-recognition receptors (PRRs) recognize microbial components or structures, known as pathogen-associated molecular patterns (PAMPs), that activate the immune system (1). Typically, viruses produce viral RNA and other PAMPs during the replication process and are recognized by PRRs to activate innate immune responses (2, 3). The effective innate immune response is essential for host survival during viral infection as the virus can also evade or inhibit the immune response in many ways.

PRRs include C-type lectin receptors, Toll-like receptors (TLRs), nucleotide-binding oligomerization domain (NOD)-like receptors (NLRs), and retinoic acid-inducible gene I (RIG-I)-like receptors (RLRs) (4). Among them, RLRs respond to intracellular viral double-stranded RNA (dsRNA) *via* a C-terminal RNA helicase and C-terminal domain (CTD) as a non-self-pattern and then activate downstream signaling (5). The family of RLRs contains three members: (1) RIG-I, (2) differentiation-associated gene 5 (MDA5), and (3) laboratory of genetics and physiology 2 (LGP2), among which RIG-I and MDA5 recognize the viral RNA and form a complex with the mitochondrial antiviral-signaling protein (MAVS) in the cytoplasmic. There are differential roles of RIG-I and MDA5 in RNA virus recognition that have been found. It has been demonstrated that 5'-triphosphate- or 5'-diphosphate-containing RNA structure and small RNA duplexes (influenza A, Newcastle disease, Sendai, vesicular stomatitis, measles, and Hepatitis C viruses) are recognized by RIG-I (6–10).

Duck Tembusu virus (DTMUV) is a plus-strand RNA virus belonging to the Flavivirus genus of the Flaviviridae family, which comprises other arthropod-borne viruses such as Japanese encephalitis virus (JEV) and dengue fever virus (DENV). Early in 2010, an outbreak of DTMUV was observed in Zhejiang and Shanghai in China and rapidly spread throughout the country. DTMUV infection causes nerve malfunction and disruption of the reproductive system, which account for huge losses experienced by duck breeding (11, 12). In addition to infecting ducks of various breeds, the disease can also infect other poultry such as chickens and geese (13) and can cause systemic lesions in infected mice (14), indicating the possibility of cross-host transmission of DTMUV from ducks to other non-avian animals. Importantly, the neutralizing antibodies targeting DTMUV have been isolated from humans (15). Therefore, effective prevention and treatment of the disease are also important public health security. The innate immune response mediated by PRRs plays an important role in the antiviral response, and DTMUV is no exception (16). At present, there are a lot of diagnosis methods for DTMUV, but the antiviral treatment options are few. Therefore, a systematic study of the interaction between DTMUV and the host's innate immune system will help better to understand the duck's antiviral innate immune system.

The third member of RLRs, LGP2, was identified in earlier studies and is considered to be the negative regulatory element of the RLR pathway (17). These studies indicated that LGP2 competitively associates with viral RNA to interfere with the recognition by RIG-I and MDA5; in addition, LGP2 forms a complex with MAVS independent of viral infection or dsRNA stimulation, thereby inhibiting the transduction of antiviral signals (17, 18). However, many other studies have shown that LGP2 plays a positive role in regulating the antiviral immune response. Mice with an LGP2 gene deletion cannot effectively produce type I interferon (IFN) during *Picornaviridae* infection. This process occurs because LGP2 can promote RIG-I and MDA5 recognition of viral RNAs through their ATPase domains (19). Previous studies have shown that duRIG-I and duMDA5 recognize the viral RNA of DMTUV and inhibit its

replication (20). As an important regulator in the RLRs signaling pathway, duck LGP2 (duLGP2) has been proved to regulate RLRs family members' duMDA5-dependent anti-DTMUV innate immune responses (21). However, the regulatory role of duLGP2 in duRIG-I-mediated innate immunity against DTMUV infection remains unclear. Previous studies showed that the identity of duLGP2 in humans and mice was only 52.4 and 51.9%, respectively (22). Therefore, it is reasonable to infer that the function of duck LGP2 may be different from that of mammals.

In this study, we provided more detailed experimental data to support the regulatory function of duLGP2 in the duRIG-I-mediated signaling pathway. In addition, we investigated the function of duLGP2 in duRIG-I-mediated anti-DTMUV innate immunity and illustrated that duLGP2 plays a negative role in duRIG-I-mediated limiting DTMUV viral replication and infection. Furthermore, the interaction between duLGP2 and duRIG-I was confirmed by co-immunoprecipitation experiments. This interaction was intensified during DTMUV infection, which inhibits duRIG-I-mediated antiviral innate immune signaling transduction. These results will advance our knowledge of the biological role of LGP2 in innate immunity and the relationship between LGP2 and innate immunity in ducks.

## MATERIALS AND METHODS

### Cells and Virus

Duck embryo fibroblast (DEF) cells were prepared by enzyme digestion from 10-day-old duck embryos according to the method described previously (23). The human embryonic kidney 293 (HEK293) cells were kindly provided by Dr. Cheng (Shanghai Jiaotong University). Cells were maintained in Dulbecco's modified Eagle medium (DMEM, Gibco, Grand Island, NY, USA) containing 10% fetal bovine serum (FBS) (TransGen, Beijing, China), 1% penicillin/streptomycin (Solarbio, Beijing, China), and all incubations were performed in an incubator (5% CO<sub>2</sub>, 37°C). The DTMUV-FX2010 strain used in this study was stored in our laboratory (24). The virus titers were determined by median tissue culture infective dose (TCID<sub>50</sub>) assay in DEF cells using the Reed and Muench calculation (25).

### Plasmids

The expression plasmids pduRIG-I-CARD, pduLGP2-Flag, empty vector pCAGGS, and luciferase reporter promoter plasmid pGL3-chIRF-7-Luc, pGL3-chIFN $\beta$ -Luc, pGL3-chNF- $\kappa$ B-Luc, and pTK-Renilla were previously described (21, 26, 27), the pduRIG-I-Flag and pduLGP2-HA plasmids were constructed using Hieff Clone<sup>®</sup> Plus One Step Cloning Kit (Yeasen, Shanghai, China) in this study. All plasmids were verified by sequencing.

### Cell Transfection, RNA Interference, and Dual-Luciferase Reporter Assay

DEF cells were seeded in 6-well plates incubated overnight to achieve 90%–100% confluence for further transfection. The

plasmids (2 µg/well) or siRNAs (100 nM) were transfected into cells using Nulen PlusTrans™ Transfection Reagent (Nulen, Shanghai, China). Three small interfering RNAs (siRNAs) against the duLGP2 and one scramble siRNA as negative control were designed and purchased from GenePharma Co., Ltd (Shanghai, China). The siRNA sequences used were as described in **Table 1**. Knockdown mRNA efficiency was determined for each siRNA by qRT-PCR analysis. For studies involving siRNA and plasmid transfection, cells were transfected with plasmid 24 h after transfection with siRNAs.

For the reporter gene assays, the cells (24-well plates) were transiently transfected with firefly luciferase reporter (100 ng/well) and pTK-Renilla luciferase reporter (50 ng/well) and indicated expression plasmids or empty vector. After 36 h, luciferase assays were performed as previously described (28) using the Dual-Luciferase Reporter Assay Kit (Vazyme, Nanjing, China). Firefly luciferase activity was normalized to Renilla luciferase.

## Viral Infection

For antiviral effect evaluation, DEF cells were transfected with indicated expression plasmids. After 24 h post-transfection (hpt), the transfected cells were washed twice with PBS and infected with DTMUV-FX2010 (100 TCID<sub>50</sub>) for 1 h, after which the media was changed to low-serum media (2% FBS) after infection. The infected cells were collected for RNA extraction. Viral replication was measured by qRT-PCR described previously (29).

## Co-Immunoprecipitation

For exogenous co-immunoprecipitation experiments, HEK293 cells were seeded in 100-mm dishes (7 × 10<sup>6</sup> cells/dish) overnight and co-transfected indicated plasmids (10 µg) using a PEI 40K transfection reagent (Servicebio, Wuhan, China). 24h after transfection, HEK293 cells were stimulated with DTMUV or PBS for 2 h, and cells were lysed at 24 hpi in 1 mL Western and IP lysis buffer (25 mM Tris [pH=7.4], 150 mM NaCl, 1% NP-40, 5% glycerol) (New Cell & Molecular Biotech, Suzhou, China) containing with protease inhibitor cocktail (New Cell & Molecular Biotech). Cell debris was removed by centrifugation (12,000 rpm for 15 min at 4°C), and the supernatant was taken as the total protein fraction. 50 µl of supernatant was taken as input samples, and the remaining samples were incubated with 20 µL anti-Flag M2 magnetic beads (Sigma-Aldrich, Louis, MO, USA) for 1 h at room temperature. The immunoprecipitated proteins were analyzed by Western blot assay with the antibodies as indicated.

**TABLE 1** | The sequences of siRNAs.

siRNAs	Sequences (5'-3')	Positions
si-NC (sense)	UUCUCCGAACGUGUCACGUTT	–
si-NC (antisense)	ACGUGACACGUUAGAATT	–
si-LGP2-1 (sense)	CCGUCUACAACAAGAUCAUTT	417
si-LGP2-1 (antisense)	AUGAUCUUGUUGUAGACGGTT	–
si-LGP2-2 (sense)	CGGACGAUGUUUACUUCUATT	1638
si-LGP2-2 (antisense)	UAGAAGUAAACAUCGUCCGTT	–
si-LGP2-3 (sense)	GAGAAGAGGAGGUACAAGATT	1925
si-LGP2-3 (antisense)	UCUUGUACCUCCUCUUCUCTT	–

## Western Blot

The cell lysates were eluted with SDS loading buffer (Beyotime) and boiled for 5 min. Denatured protein samples were separated by 10% SDS-PAGE (New Cell & Molecular Biotech) and transferred to polyvinylidene difluoride (PVDF) membranes (Millipore). Subsequently, the PVDF membranes were blocked in NcmBlot blocking buffer (New Cell & Molecular Biotech) for 30 min at room temperature. Membranes were incubated with mouse anti-Flag mAb (Nulen) (1: 2000), rabbit anti-HA mAb (Cell signaling pathway Danvers, MA, USA) (1: 1000), mouse anti-GAPDH mAb (ABclonal, Wuhan, China) (1: 5000) or mouse anti-β-actin mAb (Abbkine, Wuhan, China) (1: 10000) overnight at 4°C. and then incubated with HRP-conjugated goat anti-mouse or -rabbit IgG antibodies (Abbkine) (1: 10000) for 1 h at room temperature. All membrane washing steps were washed 3 times for 10 min each with 1×TBST at room temperature. Immunoblotting was visualized using the ECL Ultra kit (New Cell & Molecular Biotech).

## qRT-PCR

Total RNA was extracted using the FastPure Cell/Tissue Total RNA Isolation Kit (Vazyme). The resulting RNA was reversely transcribed to cDNA using HiScript III All-in-one RT SuperMix Perfect for qPCR (Vazyme). qRT-PCR was performed using the Hieff UNICON® Universal Blue qPCR SYBR Green Master Mix (Yeasen) on the Roche 96 Light Cycler and under the conditions described previously (23, 30). Primers were synthesized by Tsingke Biotechnology Co., Ltd (Beijing, China), and sequences are shown in **Table 2**. The relative expression of each target gene was analyzed using the 2<sup>-ΔΔCt</sup> method using duck GAPDH as the internal reference. At least three independent experiments were performed for each sample.

## Statistical Analyses

Expression levels and endogenous housekeeping gene, GAPDH, were analyzed using the 2<sup>-ΔΔCt</sup> method (31). All experimental data were presented as mean ± standard error of the mean (SEM). Student's t- and one-way analysis of variance (ANOVA) tests were used to determine the statistical significance of the differences using GraphPad Prism 8.0.1 software (GraphPad Software Inc., SanDiego, CA). *P* < 0.05 was considered to be statistically significant, *P* < 0.01 was highly significant, and *P* < 0.001 was extremely significant.

## RESULTS

### pduRIG-I-Flag and pduLGP2-Flag Expression Plasmids are Expressed in DEF Cells

To detect the expression pduRIG-I-Flag and pduLGP2-Flag, the DEF cells were co-transfected with indicated expression plasmids. The duLGP2 and duRIG-I expression levels were detected by Western blot. As shown in **Figure 1A**, Flag-tag duRIG-I and duLGP2 plasmids were coexpressed in DEF cells.



**TABLE 2** | Primer sequences used in this study.

Primer name	Primer sequence (5'-3')	Purpose
qLGP2-F	GTGGTGGAGCTGGAGAAGAG	qRT-PCR
qLGP2-R	CCCTGTTCTCCTCAAAGGTG	qRT-PCR
qMAVS-F	ACATCCTGAGGAACATGGAC	qRT-PCR
qMAVS-R	AGACCTCCTGCAGCTCTTCG	qRT-PCR
qIL-1 $\beta$ -F	TCATCTTCTACCGCTGGAC	qRT-PCR
qIL-1 $\beta$ -R	GTAGGTGGCGATGTTGACCT	qRT-PCR
qIL-2-F	GCCAAGAGCTGACCAACTTC	qRT-PCR
qIL-2-R	ATCGCCACACTAAGAGCAT	qRT-PCR
qIL-6-F	TTCGACGAGGAGAAATGCTT	qRT-PCR
qIL-6-R	CCTTATCGTGTGTCGAGAT	qRT-PCR
qIL-8-F	AAGTTCATCCACCCTAAATC	qRT-PCR
qIL-8-R	GCATCAGAATTGAGCTGAGC	qRT-PCR
qIFN- $\alpha$ -F	TCCTCCAACACTCTTCGAC	qRT-PCR
qIFN- $\alpha$ -R	GGGCTGTAGGTGTGGTTCTG	qRT-PCR
qIFN- $\beta$ -F	AGATGGCTCCAGCTCTACA	qRT-PCR
qIFN- $\beta$ -R	AGTGGTTGAGCTGGTTGAGG	qRT-PCR
qOAS-F	TCTTCTCAGCTGCTCTCC	qRT-PCR
qOAS-R	ACTTCGATGGACTCGCTGTT	qRT-PCR
qPKR-F	AATTCCTTGCCCTTTTCATTCAA	qRT-PCR
qPKR-R	TTTGTTTTGTGCCATATCTTGG	qRT-PCR
qMx-F	TGCTGTCTTCATGACTTCG	qRT-PCR
qMx-R	GCTTTGCTGAGCCGATTAAC	qRT-PCR
qMHC-I-F	GAAGGAAGAGACTTCATTGCCTTG	qRT-PCR
qMHC-I-R	CTCTCTCTCCAGTACGCTCTCC	qRT-PCR
qMHC-II-F	CCACCTTTACCAGCTTCGAG	qRT-PCR
qMHC-II-R	CCGTTCTTCATCCAGGTGAT	qRT-PCR
qGAPDH-F	ATGTTCTGATGGGTGTGAA	qRT-PCR
qGAPDH-R	CTGTCTTCGTGTGTGGCTGT	qRT-PCR
qDTMUV-F	CGCTGAGATGGAGATTATGG	qRT-PCR
qDTMUV-R	ACTGATTGTTTGGTGGCGTG	qRT-PCR

F, forward primer; R, reverse primer; q, qRT-PCR.

## siRNA Knock Down of Endogenous duLGP2 in DEF Cells

To knockdown endogenous duLGP2 in DEF cells, each siRNA was transfected into DEF cells, and knockdown efficiency was assessed by qRT-PCR in 24 hpt. The results showed that si-duLGP2-1 and si-duLGP2-3 had a pronounced effect on duLGP2 mRNA expression ( $P < 0.01$ ) (Figure 1B). However, the si-duLGP2-3 with better knockdown efficiency (68.8%,  $P < 0.01$ ) were used for the following experiments.

## DuLGP2 Involved in the Regulation of duRIG-I-Mediated IFN- $\beta$ Signaling Pathway

The structure of full-length RIG-I without RNA ligand showed that RIG-I is in a signaling-repressed in mammals (32). Therefore, we choose pduRIG-I-CARD to detect the regulation role of duLGP2 on duRIG-I signaling. LGP2 protein has been proved to inhibit RIG-I-mediated IFN- $\beta$ , IRF-3/7, and NF- $\kappa$ B promoter activities in mammalian cells (33). DEF cells were co-transfected with indicated expression plasmids, firefly luciferase reporter gene, and internal reference plasmids to investigate whether duLGP2 regulates duRIG-I-mediated IFN- $\beta$  expression. The results demonstrated that overexpression of duLGP2 derepresses the duRIG-I-mediated IFN- $\beta$  promoter activity in a dose-dependent manner (Figure 2A). Moreover,

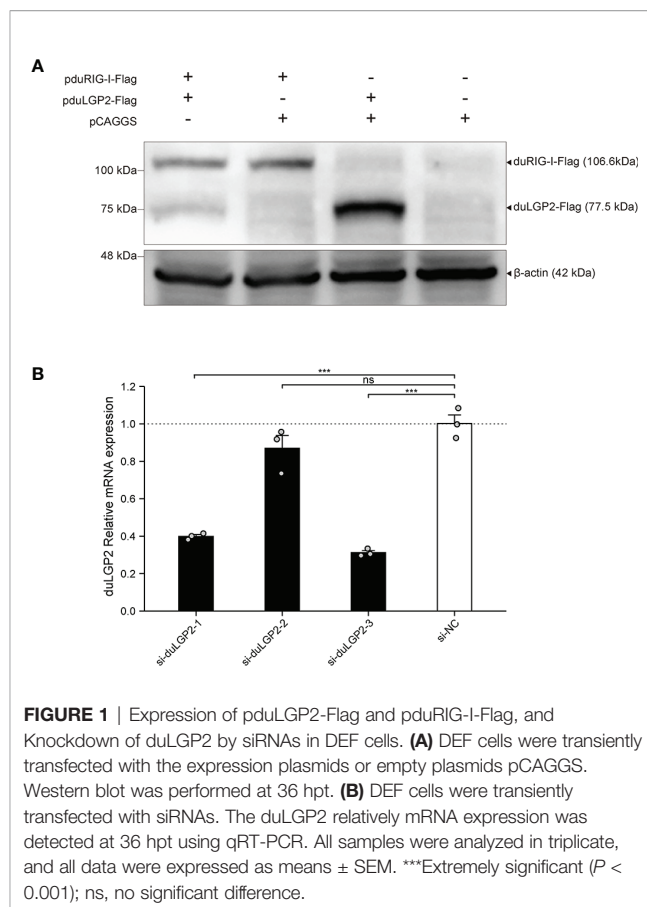
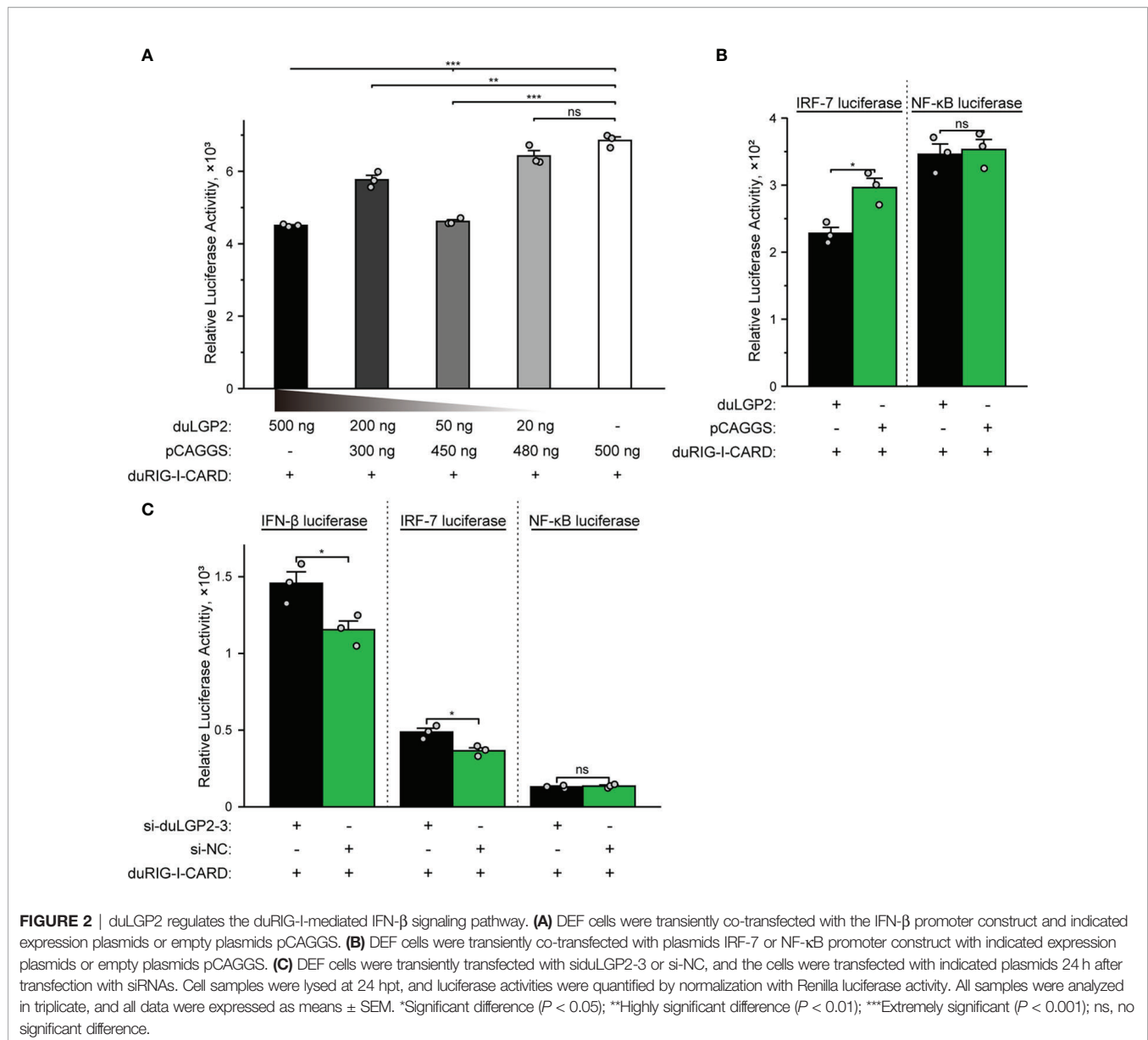


**FIGURE 1** | Expression of pduLGP2-Flag and pduRIG-I-Flag, and Knockdown of duLGP2 by siRNAs in DEF cells. (A) DEF cells were transiently transfected with the expression plasmids or empty plasmids pCAGGS. Western blot was performed at 36 hpt. (B) DEF cells were transiently transfected with siRNAs. The duLGP2 relative mRNA expression was detected at 36 hpt using qRT-PCR. All samples were analyzed in triplicate, and all data were expressed as means  $\pm$  SEM. \*\*\*Extremely significant ( $P < 0.001$ ); ns, no significant difference.

duLGP2 may inhibit duRIG-I-mediated IFN- $\beta$  transcription via IRF-7 rather than the NF- $\kappa$ B signaling pathway (Figure 2B). In contrast, knockdown of duLGP2 led to an opposite effect on the IFN- $\beta$  and IRF-7 signaling pathway, and there were still no significant changes for NF- $\kappa$ B (Figure 2C).

## DuLGP2 Regulates the Expression of duRIG-I-Mediated Cytokines

To further examine the regulatory role of duLGP2 on the duRIG-I signaling pathway, DEF cells were co-transfected with indicated expression plasmids, and the duRIG-I signaling-related cytokines mRNA expression levels were detected by qRT-PCR. The results showed that duRIG-I-mediated MAVS, type I IFNs, ISGs and MHCs were all significantly down-regulated by duLGP2 overexpression (Figures 3A, F-L), and the expression of duRIG-I-mediated proinflammatory cytokines were upregulated by duLGP2 (Figures 3B-E). In contrast, knockdown of duLGP2 led to an opposite effect on the duRIG-I-mediated type I IFNs, ISGs, and MHC-I (Figures 4F, G-K), and although the expression of duRIG-I-mediated proinflammatory cytokines (IL-1 $\beta$ , -6 and -8) was upregulated by knockdown of duLGP2 at 12-24 hpt, but down-regulated at 36 hpt (Figures 4B-E).



## DuLGP2 Promotes DTMUV Replication in DEF Cells Overexpressing duRIG-I

Previously, duRIG-I has been proved to inhibit DTMUV replication *in vitro* (34, 35). To examine whether duLGP2 can regulate RIG-I-mediated anti-DTMUV ability, the co-overexpressing duRIG-I and duLGP2 or empty vector pCAGGS DEF cells were inoculated with DTMUV-FX2010. The results showed that viral titers of duLGP2-overexpressing DEF cells were higher than those of the control cells at all the tested time points, and it was upregulated by 7.26- ( $P < 0.001$ ), 4.29- ( $P < 0.001$ ), and 3.10-fold ( $P < 0.01$ ), at 12, 24, and 36 hpi, respectively (Figure 5).

## DuLGP2 Inhibits duRIG-I Mediated IFN-β Signaling Pathway During DTMUV Infection

To investigate whether duLGP2 regulates duRIG-I-mediated IFN-β expression during DTMUV infection. DEF cells were co-transfected with indicated expression and reporter gene plasmids. The results showed that duLGP2 led to significant down-regulation of duRIG-I-mediated IFN-β promoter activity during DTMUV infection, and this regulatory effect is likely exerted *via* the IRF-7 signaling pathway. However, the duRIG-I-mediated NF-κB activity displayed a degree of up-regulation (Figure 6).

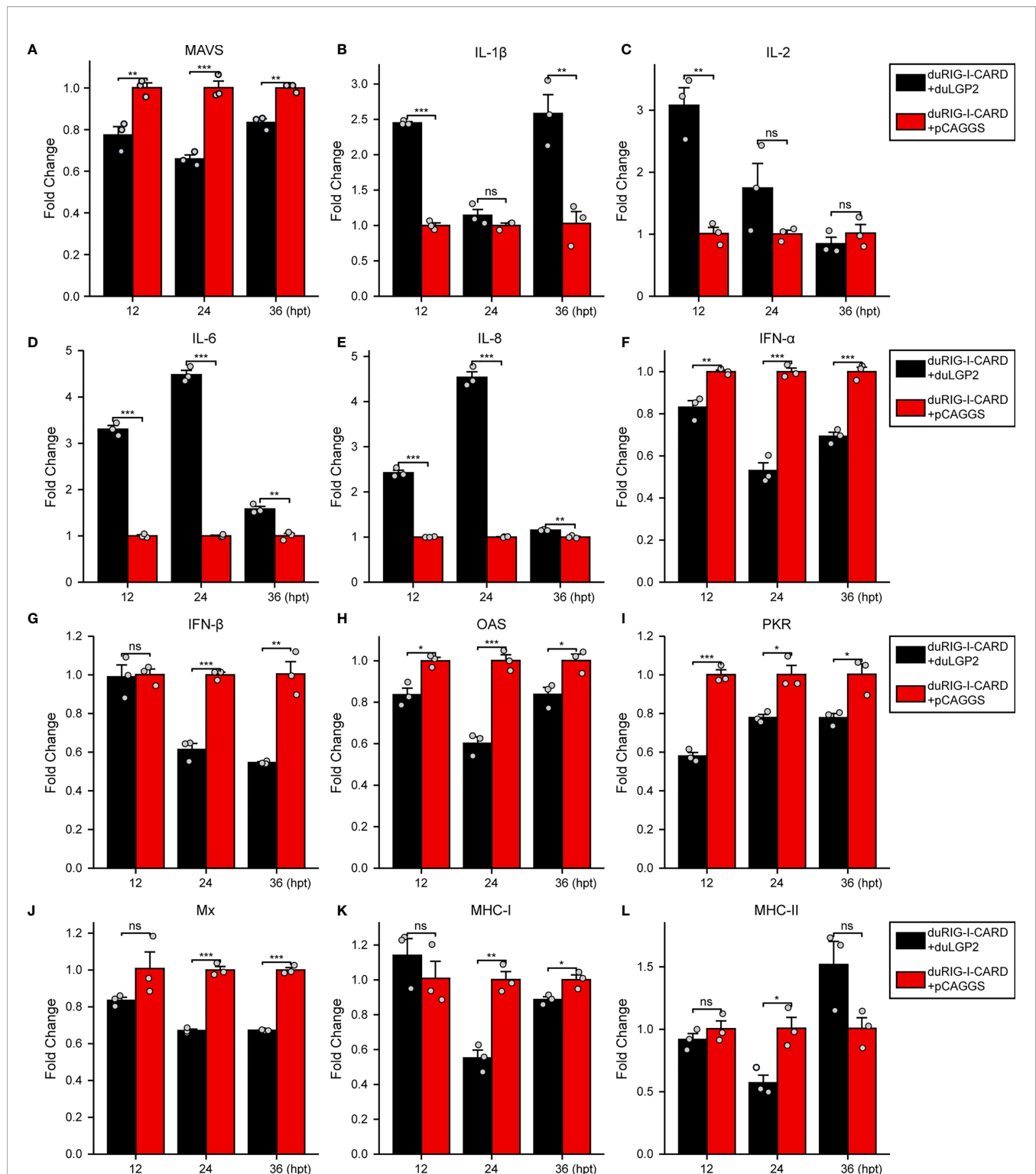


**FIGURE 3** | Overexpression of duLGP2 regulates duRIG-I-mediated cytokines expression. DEF cells were transiently co-transfected with indicated expression plasmids or empty plasmids pCAGGS. Cell samples were collected for analysis of cytokine detection at different time points. **(A)** MAVS **(B)** IL-1 $\beta$  **(C)** IL-2 **(D)** IL-6 **(E)** IL-8 **(F)** IFN- $\alpha$  **(G)** IFN- $\beta$  **(H)** OAS **(I)** PKR **(J)** Mx. **(K)** MHC-I **(L)** MHC-II. The relative expression of gene mRNA was calculated using the  $2^{-\Delta\Delta Ct}$  method with GAPDH serving as a normalization gene and mean control values as a baseline reference, and the values in the control groups (pCAGGS co-transfection) were set to 1. All samples were analyzed in triplicate, and all data were expressed as means  $\pm$  SEM. \*Significant difference ( $P < 0.05$ ); \*\*Highly significant difference ( $P < 0.01$ ); \*\*\*Extremely significant ( $P < 0.001$ ); ns, no significant difference.

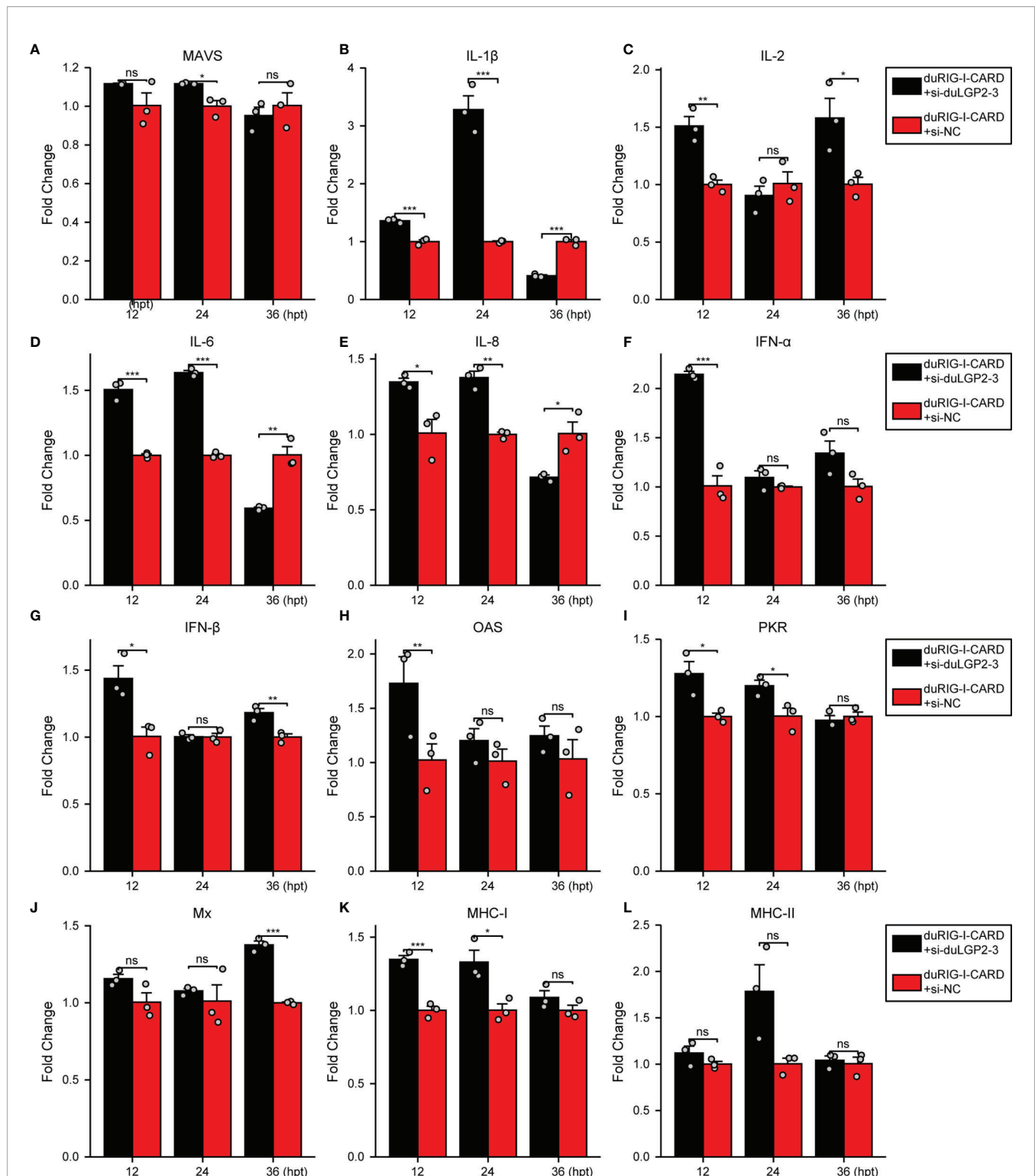
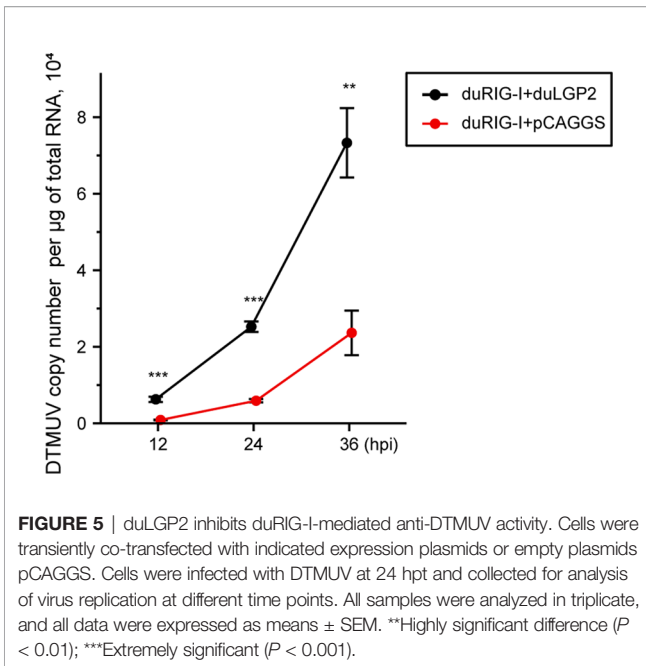
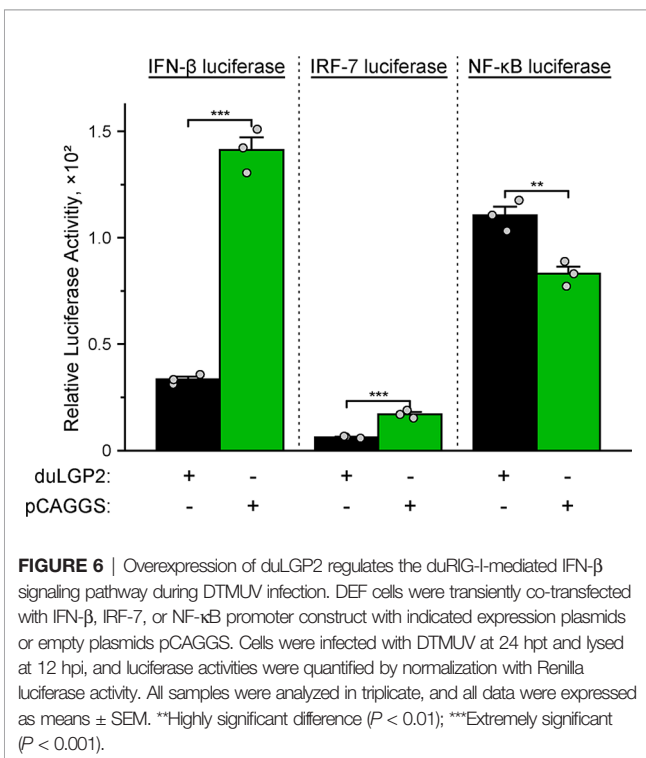


**FIGURE 4** | Knockdown of duLGP2 regulates duRIG-I-mediated cytokines expression. DEF cells were transiently transfected with si-duLGP2-3 or si-NC, and the cells were transfected with indicated plasmids or empty plasmids pCAGGS 24 h after transfection with siRNAs. Cell samples were collected for analysis of cytokine detection at different time points. **(A)** MAVS **(B)** IL-1 $\beta$  **(C)** IL-2 **(D)** IL-6 **(E)** IL-8 **(F)** IFN- $\alpha$  **(G)** IFN- $\beta$  **(H)** OAS **(I)** PKR **(J)** Mx. **(K)** MHC-I **(L)** MHC-II. The relative expression of gene mRNA was calculated using the  $2^{-\Delta\Delta Ct}$  method with GAPDH serving as a normalization gene and mean control values as a baseline reference, and the values in the control groups (pCAGGS co-transfection) were set to 1. All samples were analyzed in triplicate, and all data were expressed as means  $\pm$  SEM. \*Significant difference ( $P < 0.05$ ); \*\*Highly significant difference ( $P < 0.01$ ); \*\*\*Extremely significant ( $P < 0.001$ ); ns, no significant difference.



## DuLGP2 Regulates the Expression of duRIG-I Mediated Cytokines During DTMUV Infection

To further examine the regulatory role of duLGP2 on the duRIG-I signaling pathway during DTMUV infection. DEF cells were co-transfected with indicated expression plasmids. After 24 hpt,



the cells were infected with DTMUV-FX2010, and the duRIG-I signaling-related cytokines expression levels were detected by qRT-PCR. As expected, the results indicated that the RIG-I downstream key adaptor protein MAVS, type I IFNs (IFN- $\alpha$  and - $\beta$ ), ISGs (PKR, OAS, and Mx), and MHC-I were significantly down-regulated by duLGP2 during DTMUV infection (Figures 7A, F-K). In addition, duLGP2 upregulated the expression of duRIG-I mediated several key pro-inflammatory cytokines during DTMUV infection, including IL-1 $\beta$ , -2, -6, and -8 (Figures 7B-E).

## DuLGP2 Interacts With duRIG-I

Our study indicated that duLGP2 is a negatively regulatory molecule functioning of the duRIG-I-mediated signaling pathway. However, the mechanisms involved in this regulation are currently unknown. Reciprocal co-immunoprecipitation assays were performed to determine if duLGP2 regulates duRIG-I through interaction between the proteins. As shown in Figure 8, when the lysates were immunoprecipitated with anti-Flag-tag magnetic beads, duLGP2 could be detected *via* an immunoblotting assay using an anti-HA antibody in immunoprecipitated protein complexes. The result suggested an interaction between duRIG-I and duLGP2, and this interaction was intensified during DTMUV infection.

## DISCUSSION

RLRs have been identified as major PRRs that respond to viral RNA in the cytoplasm (5). RIG-I, a member of the RLRs family, recognizes RNA structures of multiple viruses, including DTMUV RNA, which is activated and binds to adaptor protein MAVS, leading to NF- $\kappa$ B and IRF-3/7 pathway activation (34, 36). LGP2, the third member of the RLRs family, lacks the CARD domains compared with RIG-I and MDA5 and has been proven a regulatory factor of the RIG-I and MDA5 signaling pathway (36, 37), and the regulatory function of LGP2 in RLRs-mediated signaling pathways is controversial. Previous studies have also proven that duLGP2 has high homology with mammals (22), and it is speculated that the function of duLGP2 may be similar to that in mammals. A recent study from our group demonstrated that duLGP2 plays a negative role in duMDA5-dependent anti-DTMUV innate immune responses (21). However, the regulatory effect of duLGP2 on duRIG-I-mediated anti-DTMUV infection is currently not known.

It is well established that type I IFN plays an important role in antiviral immunity. Previous studies have shown that IRF-7 and NF- $\kappa$ B are key transcriptional regulators that activate type I IFN and inflammatory cytokines ducks (27, 38). The present experiment indicates that the duRIG-I-mediated IFN- $\beta$  promoter activity was effectively down-regulated by co-transfection with duLGP2, and this effect may be the result of inhibition of IRF-7 rather than an NF- $\kappa$ B dependent signaling pathway (Figure 2). Furthermore, the qRT-PCR results showed

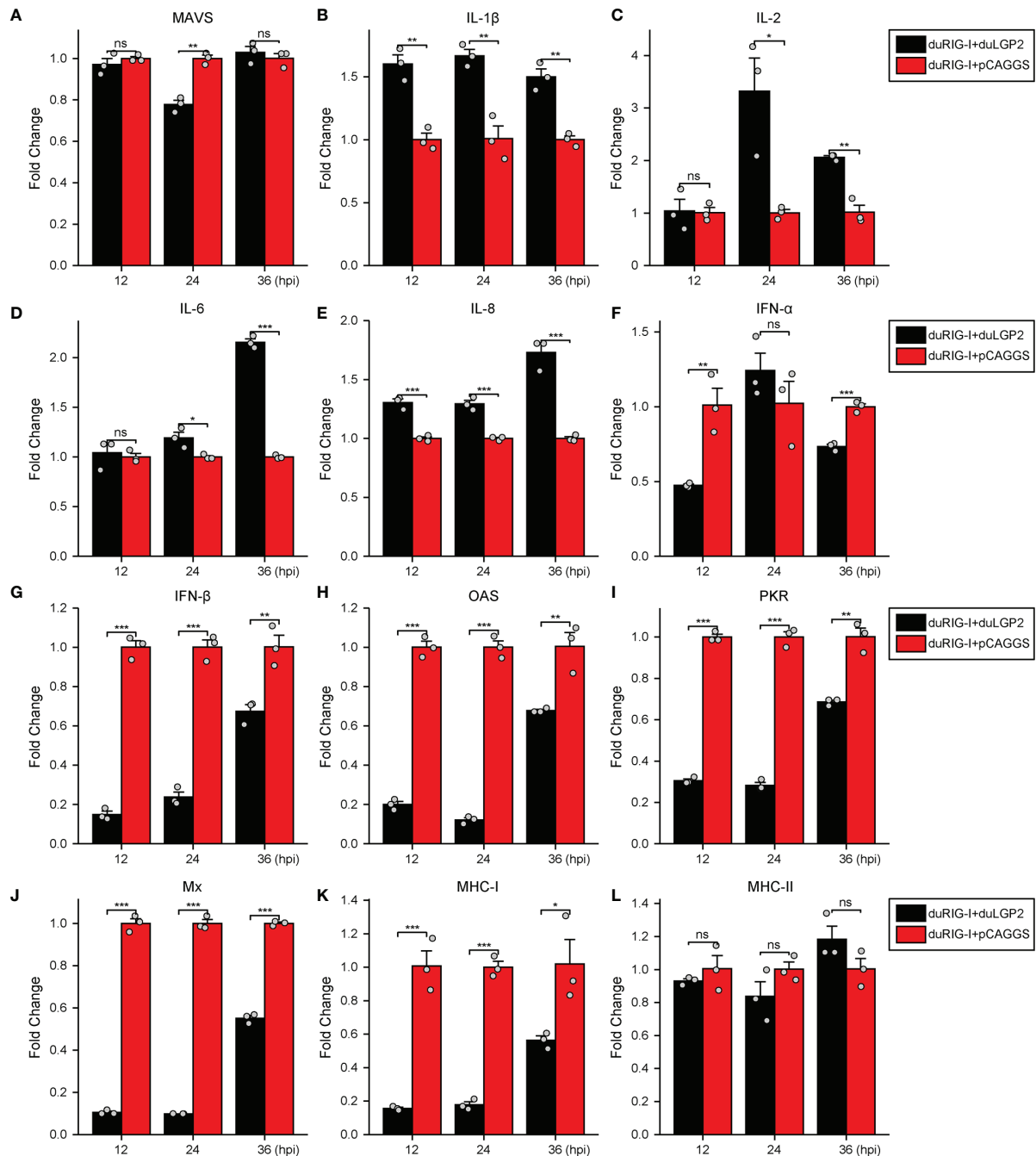
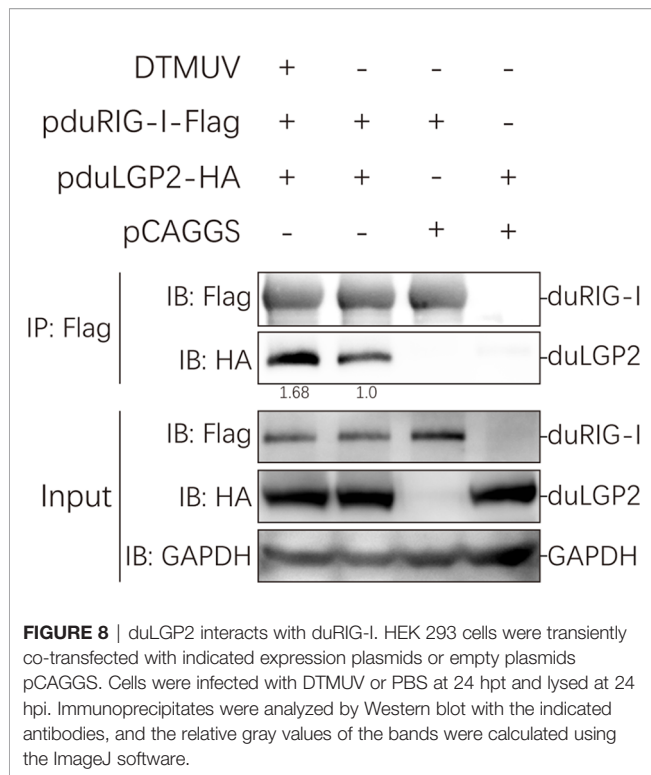


**FIGURE 7** | duLGP2 regulates duRIG-I-mediated cytokine expression during DTMUV infection. DEF cells were transiently co-transfected with indicated expression plasmids or empty plasmids pCAGGS. Cells were infected with DTMUV at 24 hpt and collected for analysis of cytokine detection at different time points. **(A)** MAVS **(B)** IL-1 $\beta$  **(C)** IL-2 **(D)** IL-6 **(E)** IL-8 **(F)** IFN- $\alpha$  **(G)** IFN- $\beta$  **(H)** OAS **(I)** PKR **(J)** Mx. **(K)** MHC-I **(L)** MHC-II. The relative expression of gene mRNA was calculated using the  $2^{-\Delta\Delta Ct}$  method with GAPDH serving as a normalization gene and mean control values as a baseline reference, and the values in the control groups (pCAGGS co-transfection) were set to 1. All samples were analyzed in triplicate, and all data were expressed as means  $\pm$  SEM. \*Significant difference ( $P < 0.05$ ); \*\*Highly significant difference ( $P < 0.01$ ); \*\*\*Extremely significant ( $P < 0.001$ ); ns, no significant difference.

that the duRIG-I-mediated expression level of adaptor protein MAVS, pro-inflammatory cytokines, Type I IFNs, and ISGs was significantly down-regulated by overexpression duLGP2 (Figure 3), and these results have been validated by

knockdown of duLGP2 endogenous expression (Figures 2, 4). It remains controversial how LGP2 regulates RIG-I function (19, 32, 37, 39–41). The present study indicated that duLGP2 might function as a negative regulator in duRIG-I signaling.



DTMUV is a viral disease that is currently very serious to the duck industry. Both duRIG-I and duMDA5 participate in the anti-virus immune response, and duRIG-I has a more pronounced anti-DTMUV effect than duMDA5 (34). RIG-I is a well-known strong inducer of the type I IFN response (3). Moreover, the expression of RIG-I is positively regulated by IFNs, IL-1 $\beta$ , and LPS (42–47). An intense inflammatory reaction is induced by DTMUV infection, which may lead to the host's death (48). Since the duRIG-I expression is strongly induced in response to DTMUV infection, it is likely to play an important role in host defense (49–53). We speculate that the duRIG-I-mediated immune response during DTMUV infection may be one of the reasons for this strong inflammatory response. Consequently, it is important to understand the duRIG-I-mediated anti-DTMUV immune function regulation.

Studies of knockout mice have shown that the loss of LGP2 is highly susceptible to encephalomyocarditis virus infection (19). Additionally, the effect of porcine RIG-I against RNA virus infection was positively regulated by LGP2. In contrast, another study showed that LGP2 binds to protein kinase activator A (PACT) to blocks of RIG-I-mediated IFN- $\beta$  promoter signaling (54). In the absence of RNA ligands, the CARDS fold back to the C-terminal portion of RIG-I, which causes it to be in an auto-inhibited state (55). Upon recognizing the viral RNA of flavivirus, the RIG-I undergoes a conformational change to trigger type I IFN signaling (56, 57). Multiple studies demonstrate that DTMUV can impair the

host's innate immune response *via* non-structural proteins resulting in viral escape (58–60). A recent study showed that duck interferon-induced protein 35 (IFI35) binds to duRIG-I to counteract its antiviral signal, the interaction enhanced by DTMUV infection (61), which indicated that the virus evades host immunity by several mechanisms. The present study suggests that duRIG-I-mediated IRF-7 signaling was down-regulated by duLGP2 during DTMUV infection, leading to the down-regulation of IFN- $\beta$  promoter activity (**Figure 6**). Additionally, the mRNA expression of cytokines was detected during DTMUV infection. As expected, the results showed that duRIG-I-mediated type I IFNs (IFN- $\alpha$  and - $\beta$ ) and downstream ISGs (OAS, PKR, and Mx) were found to be significantly down-regulated in the duLGP2 overexpression group during DTMUV infection (**Figure 7**). Type I IFNs was considered the most important cytokine involved in the antiviral immune response, which directly and/or indirectly drives antiviral effects through the induction of other mediators and induces the activation of immune cells (62). These results collectively indicate that the anti-DTMUV antiviral capability of duRIG-I was down-regulated by duLGP2, which ultimately resulted in enhanced DTMUV replication *in vitro* (**Figure 5**). Additionally, we demonstrate that regulation of the duLGP2 is achieved by direct binding of the duRIG-I, and this interaction was intensified during DTMUV infection (**Figure 8**).

Interestingly, duRIG-I-CARD- or full-length duRIG-I- (DTMUV infection) mediated pro-inflammatory cytokines (IL-1 $\beta$ , IL-2, IL-6, IL-8) expression level was significantly promoted by overexpression of duLGP2 (**Figures 2, 7**). Recently, DTMUV has been proven to cross the blood-brain barrier into the central nervous system and cause nonsuppurative encephalitis in ducklings. The blood-brain barrier will eventually be destroyed by the virus, thus triggering a subsequent “inflammatory storm”. There is no doubt that RLRs play an important role in DTMUV infection-mediated inflammatory response (49, 63). The present experiment shows that duLGP2 is involved in the expression of inflammatory factors in the duRIG-I-mediated anti-DTMUV immune response and the regulatory role of duLGP2 on the duRIG-I may *via* NF- $\kappa$ B signaling pathway and contribute to promoting inflammation and regulating inflammatory responses (**Figure 6**).

In conclusion, our study provides further evidence for the regulatory role of duLGP2 in duRIG-I-mediated anti-DTMUV. Although LGP2 per se function impacts RLRs has been controversial, we demonstrated that duLGP2 negatively affects duRIG-I-mediated anti-DTMUV immune responses.

## DATA AVAILABILITY STATEMENT

The original contributions presented in the study are included in the article/supplementary material. Further inquiries can be directed to the corresponding author.

## ETHICS STATEMENT

The animal study was reviewed and approved by Shandong Agricultural University Animal Care and Use Committee (SDAUA-2020-005).

## AUTHOR CONTRIBUTIONS

TL wrote the manuscript and performed most of the experiments. YR, TZ, XZ, XW, JW, BX, and RM experimented and wrote the discussion. NL analyzed the data. LW designed the study and reviewed the manuscript. All authors read and approved the final manuscript.

## REFERENCES

1. Yu HB, Bruneau RC, Brennan G, Rothenburg S. Battle Royale: Innate Recognition of Poxviruses and Viral Immune Evasion. *Biomedicine* (2021) 9(7):765. doi: 10.3390/biomedicine9070765
2. Tang D, Kang R, Coyne CB, Zeh HJ, Lotze MT. PAMPs and DAMPs: Signal 0s That Spur Autophagy and Immunity. *Immunol Rev* (2012) 249(1):158–75. doi: 10.1111/j.1600-065X.2012.01146.x
3. Yoneyama M, Kikuchi M, Natsukawa T, Shinobu N, Imaizumi T, Miyagishi M, et al. The RNA Helicase RIG-I Has an Essential Function in Double-Stranded RNA-Induced Innate Antiviral Responses. *Nat Immunol* (2004) 5(7):730–7. doi: 10.1038/ni1087
4. Akira S, Uematsu S, Takeuchi O. Pathogen Recognition and Innate Immunity. *Cell* (2006) 124(4):783–801. doi: 10.1016/j.cell.2006.02.015
5. Yoneyama M, Onomoto K, Jogi M, Akaboshi T, Fujita T. Viral RNA Detection by RIG-I-Like Receptors. *Curr Opin Immunol* (2015) 32:48–53. doi: 10.1016/j.coi.2014.12.012
6. Hornung V, Ellegast J, Kim S, Brzozka K, Jung A, Kato H, et al. 5'-Triphosphate RNA Is the Ligand for RIG-I. *Science* (2006) 314(5801):994–7. doi: 10.1126/science.1132505
7. Pichlmair A, Schulz O, Tan CP, Naslund TI, Liljestrom P, Weber F, et al. RIG-I-Mediated Antiviral Responses to Single-Stranded RNA Bearing 5'-Phosphates. *Science* (2006) 314(5801):997–1001. doi: 10.1126/science.1132998
8. Takahashi K, Yoneyama M, Nishihori T, Hirai R, Kumeta H, Narita R, et al. Nonself RNA-Sensing Mechanism of RIG-I Helicase and Activation of Antiviral Immune Responses. *Mol Cell* (2008) 29(4):428–40. doi: 10.1016/j.molcel.2007.11.028
9. Wang Y, Ludwig J, Schuberth C, Goldeck M, Schlee M, Li H, et al. Structural and Functional Insights Into 5'-PPP RNA Pattern Recognition by the Innate Immune Receptor RIG-I. *Nat Struct Mol Biol* (2010) 17(7):781–7. doi: 10.1038/nsmb.1863
10. Goubau D, Schlee M, Deddouch S, Puijssers AJ, Zillinger T, Goldeck M, et al. Antiviral Immunity via RIG-I-Mediated Recognition of RNA Bearing 5'-Diphosphates. *Nature* (2014) 514(7522):372–5. doi: 10.1038/nature13590
11. Cao Z, Zhang C, Liu Y, Liu Y, Ye W, Han J, et al. Tembusu Virus in Ducks, China. *Emerg Infect Dis* (2011) 17(10):1873–5. doi: 10.3201/eid1710.101890
12. Su J, Li S, Hu X, Yu X, Wang Y, Liu P, et al. Duck Egg-Drop Syndrome Caused by BYD Virus, A New Tembusu-Related Flavivirus. *PLoS One* (2011) 6(3):e18106. doi: 10.1371/journal.pone.0018106
13. Liu M, Chen SY, Chen YH, Liu CG, Chen SL, Yin XC, et al. Adapted Tembusu-Like Virus in Chickens and Geese in China. *J Clin Microbiol* (2012) 50(8):2807–9. doi: 10.1128/jcm.00655-12
14. Li S, Li XX, Zhang LJ, Wang YY, Yu XL, Tian KG, et al. Duck Tembusu Virus Exhibits Neurovirulence in BALB/c Mice. *Viral J* (2013) 10:260. doi: 10.1186/1743-422x-10-260
15. Tang Y, Gao X, Diao Y, Feng Q, Chen H, Liu X, et al. Tembusu Virus in Human, China. *Transbound Emerg Dis* (2013) 60(3):193–6. doi: 10.1111/tbed.12085

## FUNDING

This work was supported by the National Natural Science Foundation of China (31972664) and the Local Science and Technology Development Fund Project Guided by the Central Government of Shandong Province (YDZX20203700004857).

## ACKNOWLEDGMENTS

We are grateful to Dr. Cheng for providing the HEK 293 cells and guidance in experiments.

16. Li N, Jiang S, Zhao J, Yang Y, Deng K, Wei L, et al. Molecular Identification of Duck DDX3X and Its Potential Role in Response to Tembusu Virus. *Dev Comp Immunol* (2020) 106:103599. doi: 10.1016/j.dci.2019.103599
17. Yoneyama M, Kikuchi M, Matsumoto K, Imaizumi T, Miyagishi M, Taira K, et al. Shared and Unique Functions of the DExD/H-Box Helicases RIG-I, MDA5, and LGP2 in Antiviral Innate Immunity. *J Immunol (Baltimore Md 1950)* (2005) 175(5):2851–8. doi: 10.4049/jimmunol.175.5.2851
18. Komuro A, Horvath CM. RNA- and Virus-Independent Inhibition of Antiviral Signaling by RNA Helicase LGP2. *J Virol* (2006) 80(24):12332–42. doi: 10.1128/JVI.01325-06
19. Satoh T, Kato H, Kumagai Y, Yoneyama M, Sato S, Matsushita K, et al. LGP2 is a Positive Regulator of RIG-I- and MDA5-Mediated Antiviral Responses. *Proc Natl Acad Sci USA* (2010) 107(4):1512–7. doi: 10.1073/pnas.0912986107
20. Huo H, Wang Y, Wang D, Wang Y, Chen X, Zhao L, et al. Duck RIG-I Restricts Duck Enteritis Virus Infection. *Vet Microbiol* (2019) 230:78–85. doi: 10.1016/j.vetmic.2019.01.014
21. Li T, Zhai X, Wang W, Lin Y, Xing B, Wang J, et al. Regulation of MDA5-Dependent Anti-Tembusu Virus Innate Immune Responses by LGP2 in Ducks. *Vet Microbiol* (2021) 263:109281–. doi: 10.1016/j.vetmic.2021.109281
22. Jiao PR, Wei LM, Song YF, Cui J, Zhang S, Han F, et al. Molecular Cloning and Immune Responsive Expression of LGP2 Gene, A Pivotal Member of the RLR Gene Family From Muscovy Duck *Cairina Moschata*. *Poult Sci* (2015) 94(6):1170–6. doi: 10.3382/ps/pev082
23. Li T, Hu X, Zhang T, Song X, Zhang H, Dai N, et al. Cloning, Analysis, and Anti-Duck Tembusu Virus Innate Immune Response of Cherry Valley Duck Tripartite Motif-Containing 32. *Poult Sci* (2021) 100(5):101048. doi: 10.1016/j.psj.2021.101048
24. Li N, Hong T, Li R, Wang Y, Guo M, Cao Z, et al. Cherry Valley Ducks Mitochondrial Antiviral-Signaling Protein-Mediated Signaling Pathway and Antiviral Activity Research. *Front Immunol* (2016) 7:377. doi: 10.3389/fimmu.2016.00377
25. Reed LJ, Muench H. A Simple Method of Estimating Fifty Percent Endpoints. *Am J Epidemiol* (1938) 27(3):493–7. doi: 10.1093/oxfordjournals.aje.a118408
26. Cheng Y, Huang Q, Ji W, Du B, Fu Q, An H, et al. Muscovy Duck Retinoic Acid-Induced Gene I (MdrIG-I) Functions in Innate Immunity Against H9N2 Avian Influenza Viruses (AIV) Infections. *Vet Immunol Immunopathol* (2015) 163(3-4):183–93. doi: 10.1016/j.vetimm.2014.12.009
27. Wei L, Cui J, Song Y, Zhang S, Han F, Yuan R, et al. Duck MDA5 Functions in Innate Immunity Against H5N1 Highly Pathogenic Avian Influenza Virus Infections. *Vet Res* (2014) 45:66. doi: 10.1186/1297-9716-45-66
28. Hou X, Liu G, Zhang H, Hu X, Zhang X, Han F, et al. High-Mobility Group Box 1 Protein (HMGB1) From Cherry Valley Duck Mediates Signaling Pathways and Antiviral Activity. *Vet Res* (2020) 51(1):12. doi: 10.1186/s13567-020-00742-8
29. Li N, Hong T, Li R, Wang Y, Guo M, Cao Z, et al. Cherry Valley Ducks Mitochondrial Antiviral-Signaling Protein-Mediated Signaling Pathway and Antiviral Activity Research. *Front Immunol* (2016) 7:377. doi: 10.3389/fimmu.2016.00377



30. Zhang H, Song X, Li T, Wang J, Xing B, Zhai X, et al. DDX1 From Cherry Valley Duck Mediates Signaling Pathways and Anti-NDRV Activity. *Vet Res* (2021) 52(1):9. doi: 10.1186/s13567-020-00889-4
31. Pfaffl MW. A New Mathematical Model for Relative Quantification in Real-Time RT-PCR. *Nucleic Acids Res* (2001) 29(9):e45–e. doi: 10.1093/nar/29.9.e45
32. Rehwinkel J, Gack MU. RIG-I-Like Receptors: Their Regulation and Roles in RNA Sensing. *Nat Rev Immunol* (2020) 20(9):537–51. doi: 10.1038/s41577-020-0288-3
33. Quicke KM, Kim KY, Horvath CM, Suthar MS. RNA Helicase LGP2 Negatively Regulates RIG-I Signaling by Preventing TRIM25-Mediated Caspase Activation and Recruitment Domain Ubiquitination. *J Interferon Cytokine Res* (2019) 39(11):669–83. doi: 10.1089/jir.2019.0059
34. Chen S, He Y, Zhang RJ, Liu P, Yang C, Wu Z, et al. Establishment of a Reverse Genetics System for Duck Tembusu Virus to Study Virulence and Screen Antiviral Genes. *Antiviral Res* (2018) 157:120–7. doi: 10.1016/j.antiviral.2018.06.016
35. Yu GL, Lin Y, Tang Y, Diao YX. Comparative Transcriptomic Analysis of Immune-Related Gene Expression in Duck Embryo Fibroblasts Following Duck Tembusu Virus Infection. *Int J Mol Sci* (2018) 19(8):2328. doi: 10.3390/ijms19082328
36. Loo YM, Gale MJr. Immune Signaling by RIG-I-Like Receptors. *Immunity* (2011) 34(5):680–92. doi: 10.1016/j.immuni.2011.05.003
37. Reikine S, Nguyen JB, Modis Y. Pattern Recognition and Signaling Mechanisms of RIG-I and MDA5. *Front Immunol* (2014) 5:342. doi: 10.3389/fimmu.2014.00342
38. Kawai T, Takahashi K, Sato S, Coban C, Kumar H, Kato H, et al. IPS-1, an Adaptor Triggering RIG-I- and Mda5-Mediated Type I Interferon Induction. *Nat Immunol* (2005) 6(10):981–8. doi: 10.1038/ni1243
39. Moresco EM, Beutler B. LGP2: Positive About Viral Sensing. *Proc Natl Acad Sci USA* (2010) 107(4):1261–2. doi: 10.1073/pnas.0914011107
40. Esser-Nobis K, Hatfield LD, Gale MJr. Spatiotemporal Dynamics of Innate Immune Signaling via RIG-I-Like Receptors. *Proc Natl Acad Sci USA* (2020) 117(27):15778–88. doi: 10.1073/pnas.1921861117
41. Stone AEL, Green R, Wilkins C, Hemann EA, Gale MJr. RIG-I-Like Receptors Direct Inflammatory Macrophage Polarization Against West Nile Virus Infection. *Nat Commun* (2019) 10(1):3649. doi: 10.1038/s41467-019-11250-5
42. Cui X-F, Imaizumi T, Yoshida H, Borden EC, Satoh K. Retinoic Acid-Inducible Gene-I is Induced by Interferon-Gamma and Regulates the Expression of Interferon-Gamma Stimulated Gene 15 in MCF-7 Cells. *Biochem Cell Biol* (2004) 82(3):401–5. doi: 10.1139/o04-041
43. Imaizumi T, Yagihashi N, Hatakeyama M, Yamashita K, Ishikawa A, Taima K, et al. Expression of Retinoic Acid-Inducible Gene-I in Vascular Smooth Muscle Cells Stimulated With Interferon-Gamma. *Life Sci* (2004) 75(10):1171–80. doi: 10.1016/j.lfs.2004.01.030
44. Imaizumi T, Hatakeyama M, Yamashita K, Yoshida H, Ishikawa A, Taima K, et al. Interferon-Gamma Induces Retinoic Acid-Inducible Gene-I in Endothelial Cells. *Endothelium J Endothelial Cell Res* (2004) 11(3-4):169–73. doi: 10.1080/10623320490512156
45. Imaizumi T, Yagihashi N, Hatakeyama M, Yamashita K, Ishikawa A, Taima K, et al. Upregulation of Retinoic Acid-Inducible Gene-I in T24 Urinary Bladder Carcinoma Cells Stimulated With Interferon-Gamma. *Tohoku J Exp Med* (2004) 203(4):313–8. doi: 10.1620/tjem.203.313
46. Imaizumi T, Aratani S, Nakajima T, Carlson M, Matsumiya T, Tanji K, et al. Retinoic Acid-Inducible Gene-I Is Induced in Endothelial Cells by LPS and Regulates Expression of COX-2. *Biochem Biophys Res Commun* (2002) 292(1):274–9. doi: 10.1006/bbrc.2002.6650
47. Sakaki H, Imaizumi T, Matsumiya T, Kusumi A, Nakagawa H, Kubota K, et al. Retinoic Acid-Inducible Gene-I Is Induced by Interleukin-1beta in Cultured Human Gingival Fibroblasts. *Oral Microbiol Immunol* (2005) 20(1):47–50. doi: 10.1111/j.1399-302X.2005.00181.x
48. Yang S, Huang Y, Shi Y, Bai X, Yang P, Chen Q. Tembusu Virus Entering the Central Nervous System Caused Nonsuppurative Encephalitis Without Disrupting the Blood-Brain Barrier. *J Virol* (2021) 95(7):e02191-20. doi: 10.1128/JVI.02191-20
49. Li N, Wang Y, Li R, Liu JY, Zhang JZ, Cai YM, et al. Immune Responses of Ducks Infected With Duck Tembusu Virus. *Front Microbiol* (2015) 6:425. doi: 10.3389/fmicb.2015.00425
50. Fu G, Chen C, Huang Y, Cheng L, Fu Q, Wan C, et al. Comparative Analysis of Transcriptional Profiles of Retinoic-Acid-Induced Gene I-Like Receptors and Interferons in Seven Tissues From Ducks Infected With Avian Tembusu Virus. *Arch Virol* (2016) 161(1):11–8. doi: 10.1007/s00705-015-2621-x
51. Sun X, Li W, Liu E, Huang H, Wang T, Wang X, et al. *In Vivo* Cellular and Molecular Study on Duck Spleen Infected by Duck Tembusu Virus. *Vet Microbiol* (2019) 230:32–44. doi: 10.1016/j.vetmic.2018.12.003
52. Zhang J, Huang Y, Li L, Dong J, Liao M, Sun M. Transcriptome Analysis Reveals the Neuro-Immune Interactions in Duck Tembusu Virus-Infected Brain. *Int J Mol Sci* (2020) 21(7):2402. doi: 10.3390/ijms21072402
53. Han K, Zhao D, Liu Q, Liu Y, Huang X, Yang J, et al. Transcriptome Analysis Reveals New Insight of Duck Tembusu Virus (DTMUV)-Infected DF-1 Cells. *Res Veterinary Sci* (2021) 137:150–8. doi: 10.1016/j.rvsc.2021.04.028
54. David RYS, Combredet C, Najburg V, Millot GA, Beauclair G, Schwikowski B, et al. LGP2 Binds to PACT to Regulate RIG-I- and MDA5-Mediated Antiviral Responses. *Sci Signaling* (2019) 12(601):eaar3993. doi: 10.1126/scisignal.aar3993
55. Luo D, Ding SC, Vela A, Kohlway A, Lindenbach BD, Pyle AM. Structural Insights Into RNA Recognition by RIG-I. *Cell* (2011) 147(2):409–22. doi: 10.1016/j.cell.2011.09.023
56. Xian H, Xie W, Yang S, Liu Q, Xia X, Jin S, et al. Stratified Ubiquitination of RIG-I Creates Robust Immune Response and Induces Selective Gene Expression. *Sci Adv* (2017) 3(9):e1701764. doi: 10.1126/sciadv.1701764
57. Suthar MS, Diamond MS, Gale MJr. West Nile Virus Infection and Immunity. *Nat Rev Microbiol* (2013) 11(2):115–28. doi: 10.1038/nrmicro2950
58. Wang J, Lei CQ, Ji YH, Zhou HB, Ren YJ, Peng QQ, et al. Duck Tembusu Virus Nonstructural Protein 1 Antagonizes IFN-Beta Signaling Pathways by Targeting VISA. *J Immunol* (2016) 197(12):4704–13. doi: 10.4049/jimmunol.1502317
59. Wu Z, Zhang W, Wu YY, Wang T, Wu SX, Wang MS, et al. Binding of the Duck Tembusu Virus Protease to STING Is Mediated by NS2B and Is Crucial for STING Cleavage and for Impaired Induction of IFN-Beta. *J Immunol* (2019) 203(12):3374–85. doi: 10.4049/jimmunol.1900956
60. Zhang W, Jiang B, Zeng M, Duan Y, Wu Z, Wu Y, et al. Binding of Duck Tembusu Virus Nonstructural Protein 2A to Duck STING Disrupts Induction of Its Signal Transduction Cascade To Inhibit Beta Interferon Induction. *J Virol* (2020) 94(9):e01850-19. doi: 10.1128/JVI.01850-19
61. Zhou P, Ma L, Rao ZX, Li YQ, Zheng HJ, He QG, et al. Duck Tembusu Virus Infection Promotes the Expression of Duck Interferon-Induced Protein 35 to Counteract RIG-I Antiviral Signaling in Duck Embryo Fibroblasts. *Front Immunol* (2021) 12:711517. doi: 10.3389/fimmu.2021.711517
62. McNab F, Mayer-Barber K, Sher A, Wack A, O'Garra A. Type I Interferons in Infectious Disease. *Nat Rev Immunol* (2015) 15(2):87–103. doi: 10.1038/nri3787
63. Han K, Zhao D, Liu Y, Liu Q, Huang X, Yang J, et al. Quantitative Proteomic Analysis of Duck Ovarian Follicles Infected With Duck Tembusu Virus by Label-Free LC-MS. *Front Microbiol* (2016) 7:463. doi: 10.3389/fmicb.2016.00463

**Conflict of Interest:** The authors declare that the research was conducted in the absence of any commercial or financial relationships that could be construed as a potential conflict of interest.

**Publisher's Note:** All claims expressed in this article are solely those of the authors and do not necessarily represent those of their affiliated organizations, or those of the publisher, the editors and the reviewers. Any product that may be evaluated in this article, or claim that may be made by its manufacturer, is not guaranteed or endorsed by the publisher.

Copyright © 2022 Li, Ren, Zhang, Zhai, Wang, Wang, Xing, Miao, Li and Wei. This is an open-access article distributed under the terms of the Creative Commons Attribution License (CC BY). The use, distribution or reproduction in other forums is permitted, provided the original author(s) and the copyright owner(s) are credited and that the original publication in this journal is cited, in accordance with accepted academic practice. No use, distribution or reproduction is permitted which does not comply with these terms.



# Viral Circular RNAs and Their Possible Roles in Virus-Host Interaction

Xing Zhang<sup>1†</sup>, Zi Liang<sup>1†</sup>, Chonglong Wang<sup>1</sup>, Zeen Shen<sup>1</sup>, Sufei Sun<sup>1</sup>, Chengliang Gong<sup>1,2\*</sup> and Xiaolong Hu<sup>1,2\*</sup>

<sup>1</sup> School of Biology and Basic Medical Science, Soochow University, Suzhou, China, <sup>2</sup> Institute of Agricultural Biotechnology and Ecological Research, Soochow University, Suzhou, China

Circular RNAs (circRNAs) as novel regulatory molecules have been recognized in diverse species, including viruses. The virus-derived circRNAs play various roles in the host biological process and the life cycle of the viruses. This review summarized the circRNAs from the DNA and RNA viruses and discussed the biogenesis of viral and host circRNAs, the potential roles of viral circRNAs, and their future perspective. This review will elaborate on new insights gained on viruses encoded circRNAs during virus infection.

**Keywords:** circRNA, host-virus interactions, viral infection, DNA viruses, RNA viruses

## OPEN ACCESS

### Edited by:

Junji Xing,  
Houston Methodist Research Institute,  
United States

### Reviewed by:

Baolei Jia,  
Chung-Ang University, South Korea  
Ping Yuan,  
Tongji University, China

### \*Correspondence:

Xiaolong Hu  
xlhu2013@suda.edu.cn  
Chengliang Gong  
gongcl@suda.edu.cn

<sup>†</sup>These authors have contributed  
equally to this work

### Specialty section:

This article was submitted to  
Viral Immunology,  
a section of the journal  
Frontiers in Immunology

**Received:** 09 May 2022

**Accepted:** 26 May 2022

**Published:** 17 June 2022

### Citation:

Zhang X, Liang Z, Wang C, Shen Z,  
Sun S, Gong C and Hu X (2022) Viral  
Circular RNAs and Their Possible  
Roles in Virus-Host Interaction.  
*Front. Immunol.* 13:939768.  
doi: 10.3389/fimmu.2022.939768

## INTRODUCTION

Viruses are a major class of intracellular parasites that use the transcription and translation machinery of the host to produce nucleic acids and proteins for their life cycle and reproduction. Virally infected hosts suffer immunosuppression, development disorder, and loss of energy and nutrients, causing diseases. Another subset of viruses can mutually benefit the hosts that will not cause disease (1). These virus-host interactions may appear by coevolution for more than thousands of years. Hosts have evolved various antiviral immune protection mechanisms due to the selection pressure caused by viral infection. At the same time, viruses have developed a variety of evasion defenses, including innate and adaptive immunity for their reproduction (2, 3). In the interaction between viruses and hosts, a variety of regulatory molecules have evolved from multiple mechanisms, which include interferon regulatory factors (4), antisense RNAs (5), microRNAs (6), and antiviral peptides (7).

Circular RNA (circRNA) is a recently discovered functional non-coding RNA molecule, covalently closed circular single-stranded RNA molecules without a 5'-terminal cap structure and a 3'-terminal polyadenylate (8, 9). circRNA with a stable structure is resistant to degradation by exonuclease R and has spatio-temporal and tissue expression specificity (10–12). Before 2013, circRNA was always considered the byproduct of abnormal RNA splicing without regulatory function. However, increasing evidence showed that various circRNAs commonly existed in natural organisms with conservative sequences among different species. Until now, the identification of circRNAs and their possible roles have been explored in more than 20 species, including Archaea (8), plants (11, 13, 14), viruses (15–19), insects (20, 21), and mammals (12, 22, 23). A small subset of circRNAs with different activities was confirmed to play vital roles in regulating individual growth and development, environmental stress, innate immunity, and disease occurrence (13, 24–28).

Normally, circRNAs are often ignored by their low expression pattern and non-poly (A) tail in the experiment. Recently, virally encoded circRNAs were reported from more than 10 different viruses with various genome types (Figure 1).

This review will concentrate on circRNAs in viruses, focusing on classes and features of virally circRNAs, the potential functions of virally circRNAs, and possible biogenesis mechanisms, providing clues to explore better the roles in the interplay between viruses and hosts.

## VIRALLY CIRCRNAs ENCODED BY DNA VIRUSES

DNA viruses with a relatively larger and more stable DNA genome mainly include three categories according to the types of their genome: double-stranded DNA viruses, single-stranded DNA viruses, and pararetroviruses (29). Genomes of DNA viruses have a wide size range from less than 2 kb to over 375 kb. It is noted that DNA viruses can be separated into early and late phases based on the transcription of viral genes before DNA synthesis (30). Host transcription and translation systems were involved in the viral mRNAs transcription and viral proteins production. Most DNA viruses are intranuclear replicating viruses, but only a small fraction of the virus (poxviruses) is entirely replicated in the cytoplasm (31). The most widely studied DNA viruses encoded circRNAs were related to the disease pathogenesis by acting as miRNA or RNA-binding

protein sponge, oncoprotein translation, transcriptional regulators, and mRNA trap (19, 32–37).

## Human Papillomaviruses (HPVs) Encoded circRNAs

HPVs with small double-stranded DNA genomes can infect stratified epithelia. It is noted that most the HPV infections were not brought risks to the infected individuals with asymptomatic or caused benign warty, and only a small subset of 'high-risk' HPV infected individuals developed into cancers based on the infection sites (19). circRNA (circE7) encoded by Human papillomavirus type 16 (HPV16) could be identified in two HPV16-positive cervical cancer cell lines (CaSki and SiHa), and circE7 was formed *via* the pre-mRNA back-splicing of E6E7 (35). HPV16 circE7 with N6-methyladenosine (m6A) modification is predominantly distributed in the cytoplasm, translating E7 oncoprotein (19). These circRNAs derived from HPV were demonstrated to have translation activity and could be modified by the host cellular RNA methyltransferase. Viral circRNAs, viral circRNAs translated proteins, and m6A modified circRNAs play vital roles in mediating the infection, latency, and tumorigenesis.

## Hepatitis B Virus (HBV) Encoded circRNAs

HBV with partially double-stranded relaxed circular DNA genome converted into the covalently closed circular DNA following HBV infection. circRNA HBV\_circ\_1 was confirmed and generated by HBV and could be detected in HBV-positive HepG2.2.15 cells and HBV-related hepatocellular carcinoma

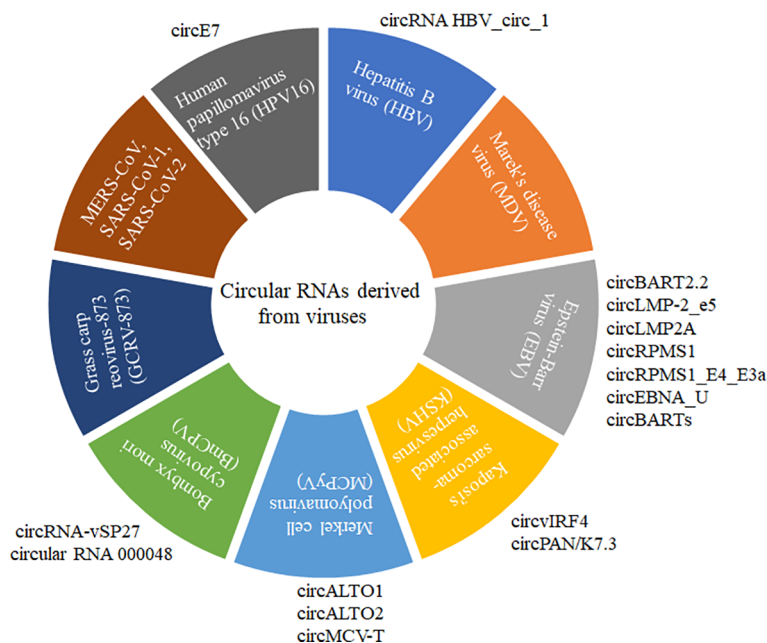


**FIGURE 1** | CircRNAs derived from different DNA and RNA viruses with various genome types. MERS-CoV, SARS-CoV-1, SARS-CoV-2, GCRV-873, and BmCPV are RNA viruses. HPV16, HBV, MDV, EBV, KSHV, and MCPyV are DNA viruses. MERS-CoV, SARS-CoV-1, and SARS-CoV-2 belong to Coronaviridae with positive sense and single-strand RNA genome. GCRV-873 and BmCPV belong to Reoviridae with a double-strand RNA genome. HPV16, HBV, MDV, EBV, KSHV, and MCPyV with double-strand DNA genomes are closely related to the occurrence of tumors or cancers.

tissue. The interaction between HBV\_circ\_1 and cyclin-dependent kinase 1 played pivotal roles in the cell proliferation, and the ectopic HBV\_circ\_1 expression in nude mice could stimulate the tumor growth (37). RNA binding factor DExH-Box helicase 9 (DHX9) bound to the inverted repeat sequences flanking the HBV pgRNA that inhibited the viral circRNA biogenesis, and this host protein DHX9 may be a novel regulator of the expression levels of viral circRNA and viral protein (38).

### **Marek's Disease Virus (MDV) Encoded circRNAs**

MDV infection cause Marek's disease (MD), which widespread induces T-cell lymphomagenesis in the domestic chicken. A large variety of MDV circRNAs was identified through RNA-sequencing, and the hot spots of circRNAs expression occurred on the major viral oncogenes in herpesviruses. Moreover, many noncanonical junction sites were observed in viral circRNAs compatible with the U2-dependent splicing machinery (39).

### **Epstein-Barr Virus (EBV) Related circRNAs**

EBV was identified as the first human tumor virus, closely related to the occurrence and development of gastric carcinoma (GC), nasopharyngeal carcinoma (NPC), and several lymphomas. CircBART2.2 derived from EBV could increase the expression level of PDL-1 in NPC and dysregulate the function of T-cells, leading to the tumor immune escape by multiple biological processes (33). EBV circLMP-2\_e5 formed from the fifth exon of the *LMP-2* gene could be universally detected in EBV-positive cell lines. The expression pattern of circLMP-2\_e5 was consistent with its linear parental transcript following EBV lytic reactivation. circLMP-2\_e5 may be generated by exon skipping because none of the cis-elements were found in the short flanking introns (40). EBV circLMP2A induced and maintained the stemness phenotypes by the competing endogenous RNA (ceRNA) mechanism of the miR-3908/TRIM59/p53 signaling pathway, and its high expression level was associated with EBV-associated GC (34). EBV-derived circRPMS1 was associated with a short survival time, and the reduced expression level suppressed NPC proliferation and metastasis (41). EBV circ\_RPMS1 localized in cytoplasm and nuclei is derived from the exons 2-4 of its *RPMS1* gene (42). CircRPMS1\_E4\_E3a and circEBNA\_U were revealed in rhesus macaque lymphocryptovirus orthologues of the latency-associated EBV. CircBARTs were expressed in EBV-positive patients' tissues and cells. Two EBV circRNAs derived from the *RPMS1* locus were detected in EBV-positive clinical stomach cancer specimens (17).

### **Kaposi's Sarcoma-Associated Herpesvirus (KSHV) Related circRNAs**

Kaposi's sarcoma-associated herpesvirus (KSHV) is an oncogenic  $\gamma 2$  herpesvirus, also called human herpesvirus-8 (HHV-8) (43). It is closely linked to primary effusion lymphoma, multicentric Castlemans' disease, and Kaposi's sarcoma (44). CircvIRF4 was constitutively expressed in virally infected patients (16). CircvIRF4 generated by KSHV viral

interferon regulatory factor 4 (vIRF4) was highly expressed in the KSHV-positive patient and cell lines (45). KSHV-derived circRNA could be incorporated into virions, while the viral circRNA produced on polyadenylated nuclear (PAN) RNA/K7.3 locus was found with its expression level paralleled with the linear transcript (46). Multiple viral circRNAs derived from the KSHV genome were revealed in KSHV-positive cells and patients (15). KSHV circvIRF4 was identified as the predominant viral circRNA (47). These viral circRNAs derived from the HSKV genome may be closely linked to the occurrence and development of related cancers. MDV, EBV, and KSHV-associated herpesvirus were related to the development of lymphoma, and the viral circRNAs encoded by these viruses were comprehensively reported by different groups.

### **Merkel Cell Polyomavirus (MCPyV) Encoded circRNAs**

Two viral circALTO1 and circALTO2 encompassing the complete gene of alternative large T antigen open reading frame (ALTO) were encoded by Merkel Cell Polyomavirus (MCPyV), and they could also be detected in the virus-positive cells and patients' tissues. In addition, the related *Trichodysplasia spinulosa* polyomavirus (TSPyV) also encoded a circALTO, which existed in the virally infected tissues and cell lines (48). MCPyV encoded four circRNAs in its early region by detecting RNase R-resistant RNA sequencing. circMCPV-T, with the most abundant expression level, was formed by back-splicing all early region exon II (49). Viral circRNAs are widespread in various DNA virus-infected individuals or cell lines, and their generation has been confirmed as key regulators in virus-induced cancers and tumorigenesis.

## **VIRALLY CIRC RNAs ENCODED BY RNA VIRUSES**

RNA viruses are normally recognized as very simple entities with small genomes, and the size of the length is from less than 2 to 32 kb. A relatively small genome of these RNA viruses has been confirmed with limited coding capacity. They are obligate intracellular parasites like DNA viruses. Host cells provide the energy, ribosome, deoxyribonucleotides, transcription and translation machinery, and other components that play important roles in assembling and releasing progeny virus (50). The genome types of RNA viruses have single-stranded (ssRNA) and double-stranded (dsRNA) nucleic acid. RNA viruses with a high mutation rate for the variation of the RNA genome that enable them to survive the varied environments during their life cycles (50, 51). Only several RNA viruses have been reported to encode viral circRNAs, including members from Reoviridae (36, 52, 53) and Coronaviridae (54, 55).

### **Reoviridae Related circRNAs**

*Bombyx mori* cytoplasmic polyhedrosis virus (BmCPV) is one of the most serious pathogens in the sericulture and bright huge economic loss to the farmers. This virus with 10 segmented

dsRNA genome can specifically infect the midgut of the silkworm. Until now, the interaction between BmCPV and silkworm are poorly understood. circRNAs was considered a novel type of regulators that can regulate multiple biological processes of viruses or host. BmCPV derived circRNA-vSP27 have translation activity, and its translation production vSP27 small peptide suppressed viral replication *via* ROS-NF- $\kappa$ B signaling pathway, and was recruited with nuclear factor Akirin for activating NF- $\kappa$ B signaling pathway (53) as well as vsp21 was translated from the BmCPV circular RNA 000048 and attenuated viral replication (36). In addition, Grass carp reovirus (GCRV) is also a member of Reoarviridae with a segmented dsRNA genome containing 11 segmented dsRNAs. Infection of GCRV leads to grass carp hemorrhagic disease, one of the most serious diseases in the grass carp aquaculture industry (52, 56). In the GCRV-873 strain infected kidney cell line CIK, 32 circRNAs were identified, and some were confirmed to mediate the viral proliferation (52).

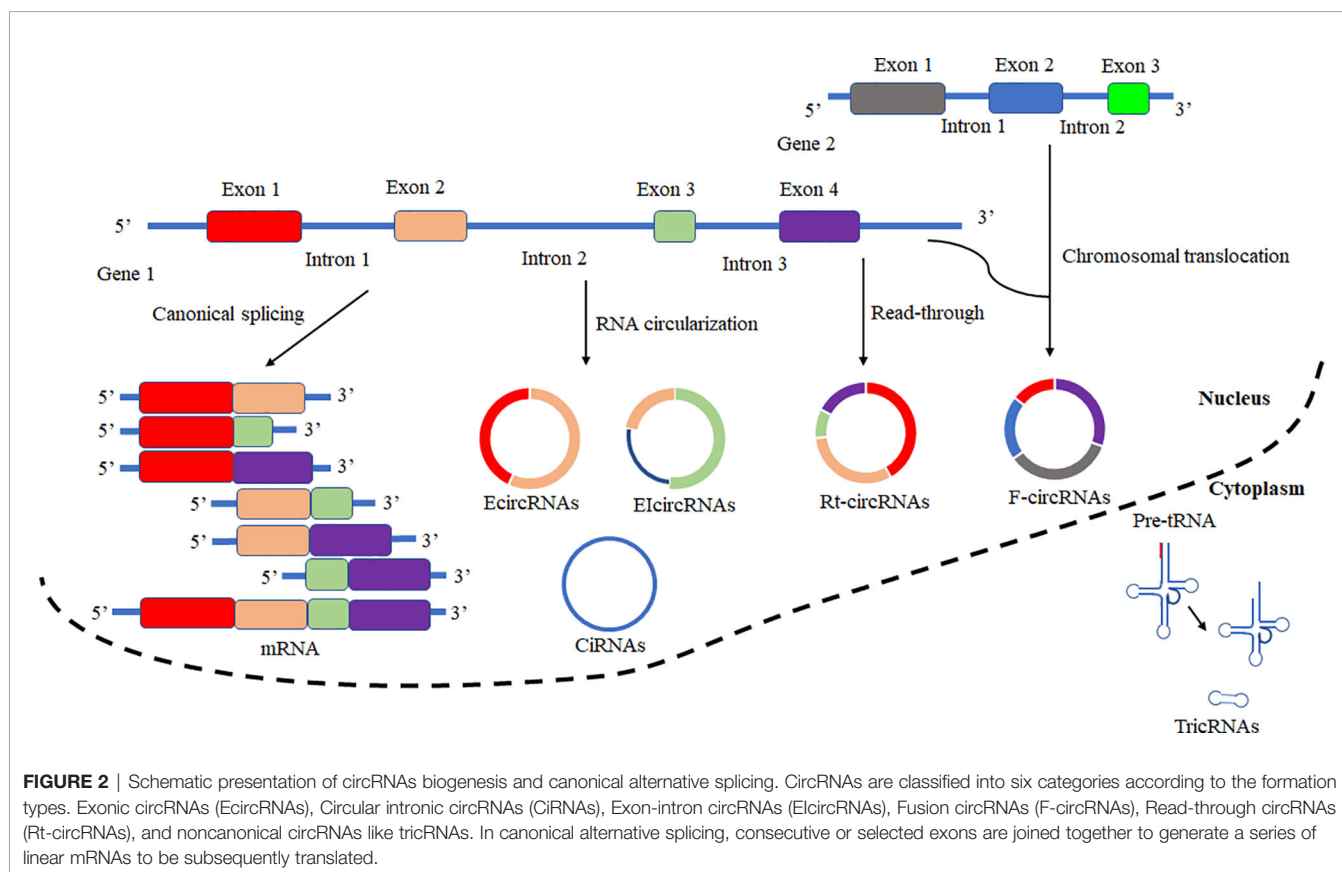
### Coronaviridae Related circRNAs

Coronaviruses MERS-CoV, SARS-CoV-1, and SARS-CoV-2 (SARS-CoV-1/2) have brought huge threatening to our life and cause enormous morbidity and mortality to humans (54). MERS-CoV, SARS-CoV-1, and SARS-CoV-2 were identified to produce multiple viral circRNAs with low expression levels, but these viral circRNAs played important roles in several biological processes (54). Two major back-splice events were found among

these viruses, and coronavirus produced more abundant and longer than their host circRNAs (55). It is noted that major dsRNA viruses have only exons and the viral circRNAs derived from these viruses have noncanonical splicing mechanisms. The viral transcripts circularization still needs more exploration by increasing groups.

### THE FEATURES OF VIRALLY CIRCRNAs

Based on the biogenesis of circRNAs in a eukaryote, the formation of circRNAs is classified into six categories: exonic circRNAs (EcircRNAs), circular intronic circRNAs (CiRNAs), exon-intron circRNAs (ElicircRNAs), fusion circRNAs (f-circRNAs), read-through circRNAs (rt-circRNAs) and noncanonical circRNAs like tricRNAs (Figure 2) (57). Most of these circRNAs were generated by RNA circularization using back-splicing, and this process is like the alternative splicing event of the pre-mRNA. The same splicing signals were utilized by back-splicing and alternative splicing of the pre-mRNA. During the back-splicing, the junction site of circRNA is formed by a 3',5' phosphodiester bond using the downstream 5' splice site and an upstream 3' splice site, whereas, in the canonical alternative splicing, a 5' splice site is joint with a downstream 3' splice site (Figure 3) (58, 59). Many DNA viruses have split genes in their viral genomes, and most of the circRNAs derived from these viruses may form on reported mechanisms



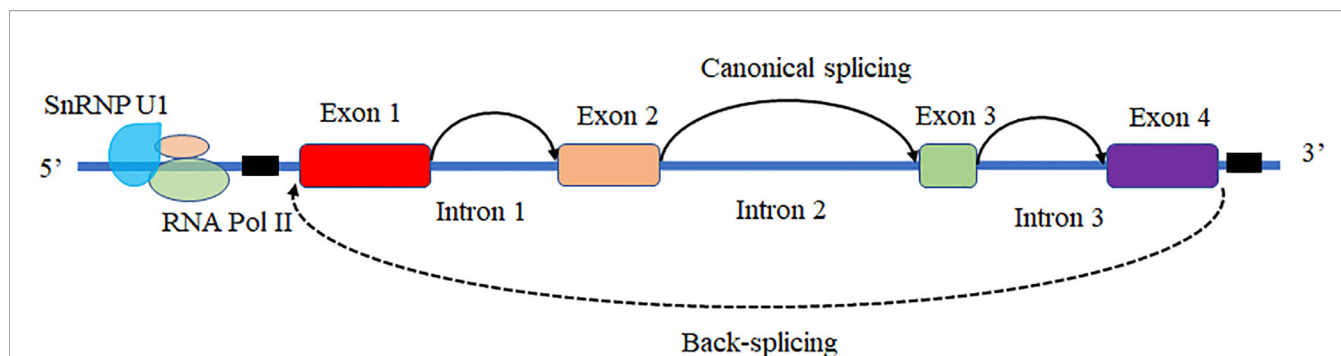


**FIGURE 3** | The mechanism of back-splicing and alternative splicing of the pre-mRNA. CircRNA is formed by a 3',5' phosphodiester bond using the downstream 5' splice site (A5SS) and an upstream 3' splice site (A3SS). Alternative splicing linear RNAs are formed by a 3',5' phosphodiester bond using an upstream 5' splice site (A5SS) and a downstream 3' splice site (A3SS).

from eukaryotes, including inverted repeat sequences, exon skipping, RNA-binding proteins, repetitive complementary sequences, or m6A modification in pre-RNA (60–67). It is noted that most of the circRNAs are formed by these strategies after 3' end processing (67). However, RNA viruses with small genomes and relatively fewer split genes in the viral genome. Therefore, the biogenesis of circRNAs from the RNA viruses may have distinct mechanisms that differ from DNA viruses.

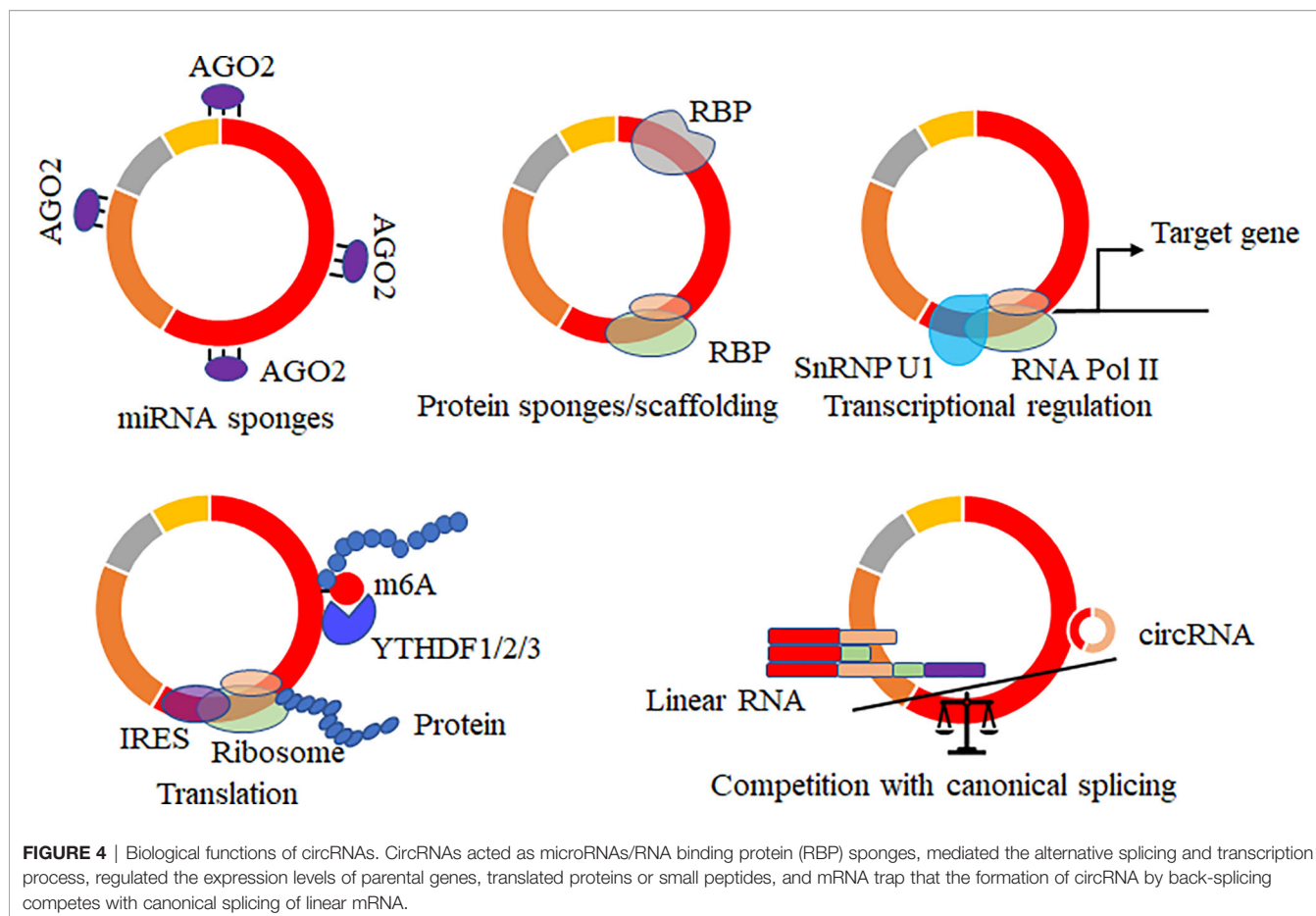
Several RNA viruses have been confirmed with the RNA circularization in the virally infected cells. Most RNA viruses derived circRNAs were produced with the noncanonical mechanism. The circularization events of viral RNAs found in the BmCPV and GCRV showed that the splicing signals flanking the junction sites of vcircRNAs differed from the reported circRNAs formation in animals and some DNA viruses (36, 52, 53). However, viral circRNAs identified from the MERS-CoV, SARS-CoV-1, and SARS-CoV-2 showed that some were generated with back-splicing of the viral RNAs (54, 55). Viral circRNAs with less conservation than those generated from host pre-mRNA may have evolved rapidly (68). Therefore, we concluded that viral circRNAs among different viral genomes might have different RNA circularization mechanisms, especially these viral circRNAs derived from the RNA viruses with segmented dsRNA genomes.

## THE POTENTIAL ROLES OF VIRALLY CIRC RNAs

Increasing potential roles of circRNAs of hosts were reported, and several data showed that virally circRNAs with similar structures might have similar regulatory roles in various biological processes. The mainly reported roles of circRNAs acted as microRNAs (69–71)/RNA binding proteins (37, 72, 73) sponges, mediated the alternative splicing and transcription process (74–76), regulated the expression levels of parental genes (77), translated proteins or small peptides (36, 53, 78–80) (Figure 4). circRNA acts on the miRNA sponge, indirectly regulating the mRNA expression level of miRNA target genes

and affecting various biological processes. circRNA generated by the parental sequence inevitably leads to a decrease in the level of linear RNA (25, 74). circRNA can also bind proteins or as the protein scaffolds to mediate the function of proteins. In addition, circRNAs containing partial internal ribosome entry sites (IRES) or m6A sites have been shown to translate proteins/small peptides in a cap-structure-independent manner (19, 36, 53).

Innate immunity acts as the first line of hosts to defend against pathogen invasion. During interactions and coevolution between the viruses and their hosts, the host's immune system evolved various antiviral mechanisms, such as RNA interference, interferon, NF- $\kappa$ B-mediated, immune deficiency, stimulator interferon gene pathways, and Janus kinase/signal transducer and activator of transcription pathway. The generation of these antiviral signaling pathways restricts the process and speed of virus infection and the degree of disease in susceptible hosts. Meanwhile, various immune evasion strategies are evolved by viruses (81–84). Recently, a novel antiviral mechanism has been found that may evolve an immune regulatory mechanism to recognize exogenous circRNA (28). It has been established that RNA recognition receptor RIG-I is a receptor molecule that recognizes exogenous circRNA and activates the autoimmune effect pathway (85, 86). CircRNA forms a double-stranded RNA stem-loop structure that binds to the double-stranded RNA-dependent protein kinase (PKR). In normal cells, the antiviral PKR molecule is bound to the stem-loop structure of circRNA, avoiding the immune response caused by overactivation. During viral infection, RNase L cleaves the interacting circRNA and then degrades it. The released PKR participates in the antiviral immune process (24). When cells are infected with viruses, NF90/NF110, an antiviral dsRNA-binding protein originally located in the nucleus, will rapidly be transported to the cytoplasm, reducing mature circRNA that cannot be produced normally in cells. NF90/NF110 binds to viral mRNA and plays an antiviral role (87). There is a question about why viruses utilize their viral RNAs to produce viral circRNAs. We have predicted that these viral circRNAs may be generated by a host of unknown factors to suppress the viral overproliferation and avoid triggering innate immunity. A similar report said Simian virus 40 encodes miRNA to control its T-antigen to evade T cell



immunity (88). Therefore, due to the similar structure and the conservation of the generation among species, we concluded that circRNAs derived from DNA or RNA viruses might have similar regulatory roles as these circRNAs encoded by the hosts.

## POSSIBLE BIOGENESIS MECHANISM OF VIRAL CIRCRNAs AND HOST CIRCRNAs

### Possible Biogenesis Mechanism of Viral circRNAs

CircRNA is a new type of RNA molecule derived from parental genes and mainly generated by a reverse splicing mechanism. This RNA molecule exists widely in nature and is highly conserved (47). Many reports on circRNA molecules encoded by natural organisms, from bacteria to mammals. A small subset of circRNA molecules with regulatory roles are associated with a verity of signaling pathways, among which the most in-depth studies are mainly focused on human cancer or tumor and other related studies. There are still some reports about circRNA produced by acellular organisms, predominantly in viruses. In the virally infected host cells, viral circRNA molecules may be widely produced in all types of viruses using various strategies. Some of these novel circRNAs could be

assembled into virions (46). There are few reports on the formation mechanism of viral circRNAs. The circRNA production mechanism of DNA viruses with a large genome containing introns may be like that of circRNA production in higher animals by the back-splicing mechanism. However, some RNA viruses' mechanism of circRNA production, which genomes have not contained introns, and the viral circRNAs derived from these viruses have not been well reported *in vitro* and *in vivo*. Several formation mechanisms for circRNAs in other species, including inverted repeat sequences, exon skipping, RNA-binding proteins, repetitive complementary sequences, or m6A modification in pre-mRNA, may be associated with the production of viral circRNAs from DNA viruses (60–67). However, the viral RNA circularization for circRNA was not comprehensively validated in some RNA viruses. In the SARS-CoV-2-infected Vero E6 cells, the homologous and reverse complementary sequences flanking the junction of sites of viral circRNAs may play vital roles in the frequency and the accuracy of viral RNA circularization (55).

### Possible Biogenesis Mechanism of Host circRNAs

The RNA circularization for circRNAs has been comprehensively reported, and too many RNA-binding proteins, cis-regulatory elements, trans-acting factors, and m6A modification were

confirmed to take part in the host circRNA formation. Heterogeneous nuclear ribonucleoprotein M (HNRNPM) suppressed aberrant exon inclusion and circularization of transcripts in cells. HNRNPM preferentially interacted with GU-rich elements in the long flanking proximal introns in the mis-spliced linear and circular transcripts (89). Heterogeneous nuclear ribonucleoprotein L (HNRNPL) facilitated the generation of a novel oncogenic circARHGAP35 originating from the back-splicing of Exon2 and Exon3 of the *ARHGAP35* gene (90). Long flanking and minimal repeats (<40 nt) in pre-mRNA-controlled circRNAs predominately after 3' end processing. Heterogeneous nuclear ribonucleoprotein and serine-arginine proteins regulated the expression of circRNAs with a common back-splicing strategy (66). Heterogeneous nuclear ribonucleoprotein C (HnRNP C) controlled the expression of MERS-CoV-derived circRNAs (91).

Neuro-oncological ventral antigen 2 (NOVA2) related to splicing event globally promoted circRNA circularization using the NOVA2 binding sites in both flanking introns of circRNA loci (92, 93). Cannabinoid receptor type-1 (CB1) and fused in sarcoma (FUS) protein were involved in circCNOT6L circularization in testis (94). Splicing factor proline/glutamine-rich and non-POU domain-containing octamer-binding protein mediated the Alu-independent circRNA production (64). Cap-binding protein 80, C2HC zinc fingers superfamily protein, and flowering locus kh domain were related to the processes of splicing and the proper order of the exons, which expression levels were negative with the circRNA production (14). Serine and Arginine Rich Splicing Factor 10 (SRSF10) promoted circ-ATXN1 production by binding to the 5'-end and 3'-end of its pre-mRNA (95). Src-associated protein (Sam68) is a member of the signal transduction activator of the RNA family favored circRNA production *in vitro* and *in vivo* via binding in the proximity of intronic Alus in the pre-mRNA of Spinal Muscular Atrophy gene (96). Long and distinct repeat-rich intronic sequences and more reverse complementary motifs favored circular RNA biogenesis (97). Nudix Hydrolase 21 (NUDT21) as an RNA splice factor was confirmed to promote circRNA production, and the UGUA sequences in the pre-mRNAs were vital for circRNA circularization (98). Trans-acting factors such as RtcB ligase and the tRNA splicing endonuclease (TSEN) complex components played important roles in tricRNA formation (99).

*Drosophila* DEXH/D-box helicase Hel25E and human homologs of Hel25E were related to the nuclear accumulation of long circRNAs. UAP56 (DDX39B) and URH49 (DDX39A) controlled the nuclear export of long and short circRNAs (100). RNA circularization was mediated by RNA binding protein Quaking (QKI) *via* binding upstream and downstream of exons (101). Several RNA binding proteins, FUS, Adenosine Deaminases Acting on RNA (ADAR), QKI, and Muscleblind (MBL), were associated with splicing regulation, RNA editing, and circRNAs production (32, 62, 94, 102). RNA-binding protein Trinucleotide repeat-containing 6A was responsible for circ0006916 formation *via* binding to the flanked intron region of the cognate linear transcript of circ0006916 (63). The RNA-

binding protein FUS controlled circRNA production by back-splicing reactions (103).

The back-splicing occurred at m6A-enriched sites in male germ cells, and these circRNAs encompassed the m6A-modified start codons in their junction sites in large ORFs (67). Increasing data showed that intronic repetitive elements, complementary sequences from different introns, and RNA-binding proteins play crucial roles in forming circRNAs based on the canonical spliceosomal machinery (102, 104–106). In addition, the functional 3' end processing signal was reported to be responsible for the RNA circularization, indicating that circRNAs were likely to form post-transcriptionally (65). The variety of circRNAs formation and the alternative circularization of RNA sequences will broaden the posttranscriptional regulation of RNAs in different species.

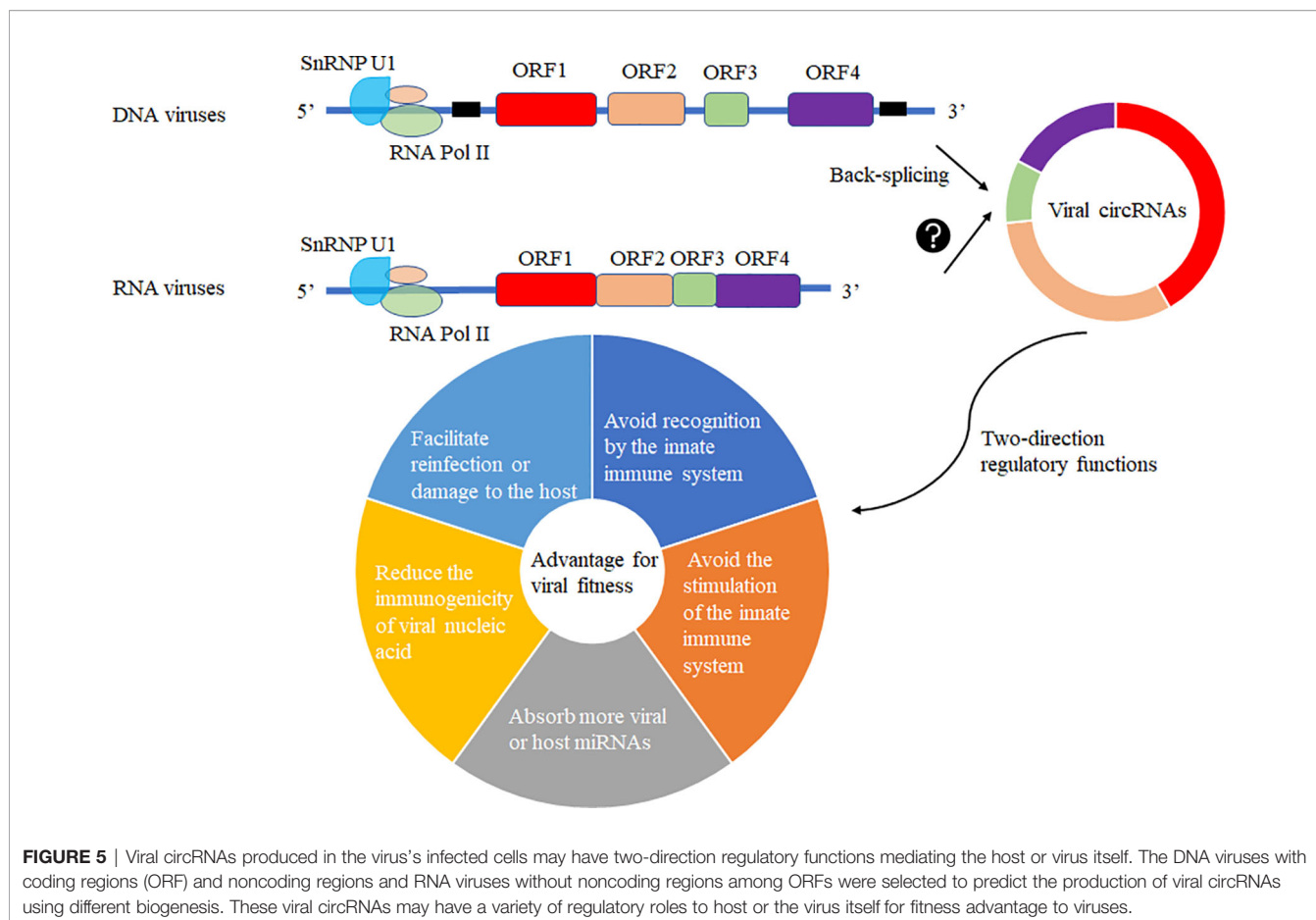
## CONCLUSIONS AND FUTURE PERSPECTIVES

The production of circRNA may be due to the fine regulation of the host cell to the genetic information of the virus so that its smaller genome carries more genetic information and regulates the immune system of the host cell or the life cycle of the virus to achieve mutual "reciprocity". In the virally infected cells, viral circRNAs may be generated by the host cell machinery for its advantage or recruitment to suppress viral replication. Various viral circRNAs produced in the virus's infected cells may have two-direction regulatory functions mediating the host or virus itself (**Figure 5**). Increasing functional viral circRNAs was confirmed, but there are still many mysteries about vcircRNA biogenesis.

Viruses invade host cells and release genetic material inside the cells. These genetic materials enter the nucleus for replication and proliferation. As the circRNA formation machinery is conservative in the cell, we can observe the existence of circRNA in lower animals to higher animals, which proves that the formation mechanism of circRNA is very conservative. The modification system may covalently modify the viral genetic material entering the nucleus in the host cell, such as m6A modification. Such modification will make the host immune system unable to distinguish whether it is its genetic material or foreign nucleic acid species, thus avoiding recognition by the innate immune system. The modified genetic species can be selectively spliced, recombined, and translated like the host genetic material. Another mechanism may be that foreign substances are circularized in host cells to reduce the levels of linear RNA and corresponding proteins, avoiding the stimulation of the innate immune system. Third, circularization may absorb more viral or host miRNAs that are not conducive to virus proliferation. Forth, the circularization of RNAs in host cells may reduce the immunogenicity of viral nucleic acid. Fifth, the circularization of RNAs may preserve the virus's genetic material to facilitate reinfection or damage to the host (**Figure 5**).

As to these novel types of RNA molecules, more questions need to be answered:





- (1) Whether multiple circRNAs are produced simultaneously or followed with cognate linear RNA transcripts?
- (2) Can these circularizations of viral RNAs be inherited vertically in virally infected cells as regulatory elements to protect the host from reinfection?
- (3) Whether viral circRNAs formation strategy will be manipulated by the host to avoid the degradation of viral RNAs?
- (4) Whether these viral circRNAs are produced under certain circumstances, such as virus infection, different developmental stages, and other stimulates or other stimuli?
- (5) Whether multiple viral circRNAs produced in the virally cells have a competitive interaction with other RNA transcripts, such as non-coding RNA, small RNAs, and genes between viruses and hosts?
- (6) Whether the translation of viral circRNAs is the novel, unknown structural, and nonstructural proteins required for the viral life cycle?
- (7) Whether these circRNAs can form a circRNA subgenome of viruses?
- (8) Whether circRNAs are recruited by RNA binding proteins to form RNA virus replication regions?
- (9) Why so small a virus genome can produce so many circRNAs?
- (10) How do we balance the roles conducted by circRNAs and other non-coding RNAs or genes?
- (11) Whether some viral circRNAs are pro-virions (immature virions)?
- (12) Can some viral circRNAs fuse with the host or other viral circRNAs?

## AUTHOR CONTRIBUTIONS

XZ and ZL wrote the draft. XH and CG reviewed and supervised the manuscript. XZ, ZL, CW, ZS and SS collected the data. All authors contributed to the article and approved the submitted version.

## FUNDING

This study was supported by the National Natural Science Foundation of China (31872424, 32072792, and 31972620) and the Priority Academic Program of Development of Jiangsu Higher Education Institutions. The funders had no role in study design, data collection, analysis, publishing decisions, or manuscript preparation.

## REFERENCES

- Más V, Melero JA. Entry of Enveloped Viruses Into Host Cells: Membrane Fusion. *Subcell Biochem* (2013) 68:467–87. doi: 10.1007/978-94-007-6552-8\_16
- Takeuchi O, Akira S. Innate Immunity to Virus Infection. *Immunol Rev* (2009) 227:75–86. doi: 10.1111/j.1600-065X.2008.00737.x
- Whitton JL, Cornell CT, Feuer R. Host and Virus Determinants of Picornavirus Pathogenesis and Tropism. *Nat Rev Microbiol* (2005) 3:765–76. doi: 10.1038/nrmicro1284
- Al Hamrashdi M, Brady G. Regulation of IRF3 Activation in Human Antiviral Signaling Pathways. *Biochem Pharmacol* (2022) 200:115026. doi: 10.1016/j.bcp.2022.115026
- Xu JZ, Zhang JL, Zhang WG. Antisense RNA: The New Favorite in Genetic Research. *J Zhejiang Univ Sci B* (2018) 19:739–49. doi: 10.1631/jzus.B1700594
- Zhang J, Li Z, Huang J, Yin H, Tian J, Qu L. miR-26a Inhibits Feline Herpesvirus 1 Replication by Targeting SOCS5 and Promoting Type I Interferon Signaling. *Viruses* (2019) 12:2. doi: 10.3390/v12010002
- Pang Y, Yao L, Jhong JH, Wang Z, Lee TY. AVPIden: A New Scheme for Identification and Functional Prediction of Antiviral Peptides Based on Machine Learning Approaches. *Brief Bioinform* (2021) 22:bbab263. doi: 10.1093/bib/bbab263
- Danan M, Schwartz S, Edelheit S, Sorek R. Transcriptome-Wide Discovery of Circular RNAs in Archaea. *Nucleic Acids Res* (2012) 40:3131–42. doi: 10.1093/nar/gkr1009
- Lasda E, Parker R. Circular RNAs: Diversity of Form and Function. *RNA* (2014) 20:1829–42. doi: 10.1261/rna.047126.114
- Holdt LM, Kohlmaier A, Teupser D. Molecular Roles and Function of Circular RNAs in Eukaryotic Cells. *Cell Mol Life Sci* (2018) 75:1071–98. doi: 10.1007/s00018-017-2688-5
- Lu T, Cui L, Zhou Y, Zhu C, Fan D, Gong H, et al. Transcriptome-Wide Investigation of Circular RNAs in Rice. *RNA* (2015) 21:2076–87. doi: 10.1261/rna.052282.115
- Veno MT, Hansen TB, Veno ST, Clausen BH, Grebing M, Finsen B, et al. Spatio-Temporal Regulation of Circular RNA Expression During Porcine Embryonic Brain Development. *Genome Biol* (2015) 16:245. doi: 10.1186/s13059-015-0801-3
- Wang X, Chang X, Jing Y, Zhao J, Fang Q, Sun M, et al. Identification and Functional Prediction of Soybean CircRNAs Involved in Low-Temperature Responses. *J Plant Physiol* (2020) 250:153188. doi: 10.1016/j.jplph.2020.153188
- Philips A, Nowis K, Stelmaszczuk M, Handschuh L, Jackowiak P, Figlerowicz M. Arabidopsis Thaliana Cbp80, C2h2, and Flk Knockout Mutants Accumulate Increased Amounts of Circular RNAs. *Cells* (2020) 9:1937. doi: 10.3390/cells9091937
- Tagawa T, Gao S, Koparde VN, Gonzalez M, Spouge JL, Serquina AP, et al. Discovery of Kaposi's Sarcoma Herpesvirus-Encoded Circular RNAs and a Human Antiviral Circular RNA. *Proc Natl Acad Sci U S A* (2018) 115:12805–10. doi: 10.1073/pnas.1816183115
- Toptan T, Abere B, Nalesnik MA, Swerdlow SH, Ranganathan S, Lee N, et al. Circular DNA Tumor Viruses Make Circular RNAs. *P Natl Acad Sci U S A* (2018) 115:E8737–45. doi: 10.1073/pnas.1811728115
- Ungerleider N, Concha M, Lin Z, Roberts C, Wang X, Cao S, et al. The Epstein Barr Virus Circrnaome. *PLoS Pathog* (2018) 14:e1007206. doi: 10.1371/journal.ppat.1007206
- Ungerleider NA, Tibbetts SA, Renne R, Flemington EK. Gammaherpesvirus RNAs Come Full Circle. *mBio* (2019) 10:e00071–00019. doi: 10.1128/mBio.00071-19
- Zhao J, Lee EE, Kim J, Yang R, Chamseddin B, Ni C, et al. Transforming Activity of an Oncoprotein-Encoding Circular RNA From Human Papillomavirus. *Nat Commun* (2019) 10:2300. doi: 10.1038/s41467-019-10246-5
- Hu X, Zhu M, Liu B, Liang Z, Huang L, Xu J, et al. Circular RNA Alterations in the Bombyx Mori Midgut Following B. Mori Nucleopolyhedrovirus Infection. *Mol Immunol* (2018) 101:461–70. doi: 10.1016/j.molimm.2018.08.008
- Hu X, Zhu M, Zhang X, Liu B, Liang Z, Huang L, et al. Identification and Characterization of Circular RNAs in the Silkworm Midgut Following Bombyx Mori Cytoplasmic Polyhedrosis Virus Infection. *RNA Biol* (2018) 15:292–301. doi: 10.1080/15476286.2017.1411461
- Wang D, Chen Z, Zhuang X, Luo J, Chen T, Xi Q, et al. Identification of circRNA-Associated-ceRNA Networks Involved in Milk Fat Metabolism Under Heat Stress. *Int J Mol Sci* (2020) 21:4162. doi: 10.3390/ijms21114162
- Zhu J, Zhou Y, Zhu S, Li F, Xu J, Zhang L, et al. circRNA Circ\_102049 Implicates in Pancreatic Ductal Adenocarcinoma Progression Through Activating CD80 by Targeting miR-455-3p. *Mediators Inflammation* (2021) 2021:8819990. doi: 10.1155/2021/8819990
- Liu CX, Li X, Nan F, Jiang S, Gao X, Guo SK, et al. Structure and Degradation of Circular RNAs Regulate PKR Activation in Innate Immunity. *Cell* (2019) 177:865–880.e821. doi: 10.1016/j.cell.2019.03.046
- Shao T, Pan YH, Xiong XD. Circular RNA: An Important Player With Multiple Facets to Regulate its Parental Gene Expression. *Mol Ther Nucleic Acids* (2021) 23:369–76. doi: 10.1016/j.omtn.2020.11.008
- Shen X, Tang J, Ru W, Zhang X, Huang Y, Lei C, et al. CircINSR Regulates Fetal Bovine Muscle and Fat Development. *Front Cell Dev Biol* (2020) 8:615638. doi: 10.3389/fcell.2020.615638
- Wang L, Yu F, Xu N, Lu L. Grass Carp Reovirus Capsid Protein Interacts With Cellular Proteasome Subunit Beta-Type 7: Evidence for the Involvement of Host Proteasome During Aquareovirus Infection. *Fish Shellfish Immunol* (2020) 98:77–86. doi: 10.1016/j.fsi.2019.12.047
- Xiao MS, Ai Y, Wilusz JE. Biogenesis and Functions of Circular RNAs Come Into Focus. *Trends Cell Biol* (2020) 30:226–40. doi: 10.1016/j.tcb.2019.12.004
- Sanjuán R, Pereira-Gómez M, Risco J. *Genome Instability in DNA Viruses*. (2016) New York: Elsevier Inc., 37–47.
- Payne S. Introduction to DNA Viruses. *Viruses* (2017) 97:231–6. doi: 10.1016/B978-0-12-803109-4.00028-3
- Dirk G. Cellular RNA Interference Mechanisms. Preface. *Prog Mol Biol Transl Sci* (2011) 102:xi–xiii. doi: 10.1016/B978-0-12-415795-8.00012-X
- Ashwal-Fluss R, Meyer M, Pamudurti NR, Ivanov A, Bartok O, Hanan M, et al. circRNA Biogenesis Competes With pre-mRNA Splicing. *Mol Cell* (2014) 56:55–66. doi: 10.1016/j.molcel.2014.08.019
- Ge J, Wang J, Xiong F, Jiang X, Zhu K, Wang Y, et al. Epstein-Barr Virus-Encoded Circular RNA CircBART2.2 Promotes Immune Escape of Nasopharyngeal Carcinoma by Regulating PD-L1. *Cancer Res* (2021) 81:5074–88. doi: 10.1158/0008-5472.CAN-20-4321
- Gong LP, Chen JN, Dong M, Xiao ZD, Feng ZY, Pan YH, et al. Epstein-Barr Virus-Derived Circular RNA LMP2A Induces Stemness in EBV-Associated Gastric Cancer. *EMBO Rep* (2020) 21:e49689. doi: 10.15252/embr.201949689
- Yu LL, Zheng ZM. Human Papillomavirus Type 16 Circular RNA Is Barely Detectable for the Claimed Biological Activity. *Mbio* (2022) 13:e0359421. doi: 10.1128/mbio.03594-21
- Zhang Y, Zhu M, Zhang X, Dai K, Liang Z, Pan J, et al. Micropeptide Vsp21 Translated by Reovirus Circular RNA 000048 Attenuates Viral Replication. *Int J Biol Macromol* (2022) 209:1179–87. doi: 10.1016/j.ijbiomac.2022.04.136
- Zhu M, Liang Z, Pan J, Zhang X, Xue R, Cao G, et al. Hepatocellular Carcinoma Progression Mediated by Hepatitis B Virus-Encoded circRNA HBV\_circ\_1 Through Interaction With CDK1. *Mol Ther Nucleic Acids* (2021) 25:668–82. doi: 10.1016/j.omtn.2021.08.011
- Sekiba K, Otsuka M, Ohno M, Kishikawa T, Yamagami M, Suzuki T, et al. DHX9 Regulates Production of Hepatitis B Virus-Derived Circular RNA and Viral Protein Levels. *Oncotarget* (2018) 9:20953–64. doi: 10.18632/oncotarget.25104
- Chasseur AS, Trozzi G, Istasse C, Petit A, Rasschaert P, Denesvre C, et al. Marek's Disease Virus Virulence Genes Encode Circular RNAs. *J Virol* (2022) 96:e0032122. doi: 10.1128/jvi.00321-22
- Tan KE, Ng WL, Marinov GK, Yu KH, Tan LP, Liao ES, et al. Identification and Characterization of a Novel Epstein-Barr Virus-Encoded Circular RNA From LMP-2 Gene. *Sci Rep* (2021) 11:14392. doi: 10.1038/s41598-021-93781-w
- Liu Q, Shuai M, Xia Y. Knockdown of EBV-Encoded circRNA Circrps1 Suppresses Nasopharyngeal Carcinoma Cell Proliferation and Metastasis Through Sponging Multiple miRNAs. *Cancer Manag Res* (2019) 11:8023–31. doi: 10.2147/CMAR.S218967

42. Huang JT, Chen JN, Gong LP, Bi YH, Liang J, Zhou L, et al. Identification of Virus-Encoded Circular RNA. *Virology* (2019) 529:144–51. doi: 10.1016/j.virol.2019.01.014
43. Ganem D. Kaposi's Sarcoma-Associated Herpesvirus. In: *Fields Virology 5th ed.* D Knipe and P Howley. Philadelphia, PA: Lippincott Williams & Wilkins (2007) 2005:2847–88.
44. Mekni-Toujani M, Mousavizadeh L, Gallo A, Ghram A. Thymus Capitatus Flavonoids Inhibit Infection of Kaposi's Sarcoma-Associated Herpesvirus. *FEBS Open Bio* (2022) 6:1166–77. doi: 10.1002/2211-5463.13407
45. Tagawa T, Oh D, Santos J, Dremel S, Mahesh G, Uldrick TS, et al. Characterizing Expression and Regulation of Gamma-Herpesviral Circular RNAs. *Front Microbiol* (2021) 12:670542. doi: 10.3389/fmicb.2021.670542
46. Abere B, Li J, Zhou H, Toptan T, Moore PS, Chang Y. Kaposi's Sarcoma-Associated Herpesvirus-Encoded circRNAs Are Expressed in Infected Tumor Tissues and Are Incorporated Into Virions. *mBio* (2020) 11:e03027–03019. doi: 10.1128/mBio.03027-19
47. Ungerleider NA, Jain V, Wang Y, Maness NJ, Blair RV, Alvarez X, et al. Comparative Analysis of Gammaherpesvirus Circular RNA Repertoires: Conserved and Unique Viral Circular RNAs. *J Virol* (2019) 93:e01952–01918. doi: 10.1128/JVI.01952-18
48. Yang R, Lee EE, Kim J, Choi JH, Kolitz E, Chen Y, et al. Characterization of ALTO-Encoding Circular RNAs Expressed by Merkel Cell Polyomavirus and Trichodysplasia Spinulosa Polyomavirus. *PLoS Pathog* (2021) 17:e1009582. doi: 10.1371/journal.ppat.1009582
49. Abere B, Zhou H, Li J, Cao S, Toptan T, Grundhoff A, et al. Merkel Cell Polyomavirus Encodes Circular RNAs (circRNAs) Enabling a Dynamic circRNA/microRNA/mRNA Regulatory Network. *mBio* (2020) 11:e03059–03020. doi: 10.1128/mBio.03059-20
50. Barr J, Fearn R. Genetic Instability of RNA Viruses. In *Genome Stability* (Elsevier) (2016) 21–35. doi: 10.1016/B978-0-12-803309-8.00002-1
51. Bujarski JJ. Recombination of Viruses. *Encyclopedia Virol* (1999), 1446–53. doi: 10.1006/rwvi.1999.0334
52. Pan J, Zhang X, Zhang YS, Yan BY, Dai K, Zhu M, et al. Grass Carp Reovirus Encoding Circular RNAs With Antiviral Activity. *Aquaculture* (2021) 533:736135. doi: 10.1016/j.aquaculture.2020.736135
53. Zhang Y, Zhang X, Dai K, Zhu M, Liang Z, Pan J, et al. Bombyx Mori Akirin Hijacks a Viral Peptide Vsp27 Encoded by BmCPV circRNA and Activates the ROS-NF-kappaB Pathway Against Viral Infection. *Int J Biol Macromol* (2022) 194:223–32. doi: 10.1016/j.ijbiomac.2021.11.201
54. Cai Z, Lu C, He J, Liu L, Zou Y, Zhang Z, et al. Identification and Characterization of circRNAs Encoded by MERS-CoV, SARS-CoV-1 and SARS-CoV-2. *Briefings Bioinf* (2020) 2:1297–308. doi: 10.1093/bib/bbaa1334
55. Yang S, Zhou H, Cruz-Cosme R, Liu M, Xu J, Niu X, et al. Circular RNA Profiling Reveals Abundant and Diverse circRNAs of SARS-CoV-2, SARS-CoV and MERS-CoV Origin. *bioRxiv* (2020) 2020.12.07.415422. doi: 10.1101/2020.11.12.1107.415422
56. Liu B, Yuan R, Liang Z, Zhang TT, Zhu M, Zhang X, et al. Comprehensive Analysis of circRNA Expression Pattern and circRNA-mRNA-miRNA Network in Ctenopharyngodon Idellus Kidney (CIK) Cells After Grass Carp Reovirus (GCRV) Infection. *Aquaculture* (2019) 512:734349. doi: 10.1016/j.aquaculture.2019.734349
57. Huang X, Zhao Y, Zhou H, Li Y. Circular RNAs in Atherosclerosis. *Clin Chim Acta* (2022) 531:71–80. doi: 10.1016/j.cca.2022.03.016
58. Zhang Y, Xue W, Li X, Zhang J, Chen S, Zhang JL, et al. The Biogenesis of Nascent Circular RNAs. *Cell Rep* (2016) 15:611–24. doi: 10.1016/j.celrep.2016.03.058
59. Welden JR, Stamm S. Pre-mRNA Structures Forming Circular RNAs. *Biochim Biophys Acta Gene Regul Mech* (2019) 1862:194410. doi: 10.1016/j.jbbagrm.2019.194410
60. Sirono A, Takeshima Y, Wibawa T, Ikezawa M, Nonaka I, Matsuo M. Circular Dystrophin RNAs Consisting of Exons That Were Skipped by Alternative Splicing. *Hum Mol Genet* (1999) 8:493–500. doi: 10.1093/hmg/8.3.493
61. Cao D. Reverse Complementary Matches Simultaneously Promote Both Back-Splicing and Exon-Skipping. *BMC Genomics* (2021) 22:586. doi: 10.1186/s12864-021-07910-w
62. Conn SJ, Pillman KA, Toubia J, Conn VM, Salmanidis M, Phillips CA, et al. The RNA Binding Protein Quaking Regulates Formation of circRNAs. *Cell* (2015) 160:1125–34. doi: 10.1016/j.cell.2015.02.014
63. Dai X, Zhang N, Cheng Y, Yang T, Chen Y, Liu Z, et al. RNA-Binding Protein Trinucleotide Repeat-Containing 6A Regulates the Formation of Circular RNA Circ006916, With Important Functions in Lung Cancer Cells. *Carcinogenesis* (2018) 39:981–92. doi: 10.1093/carcin/bgy061
64. Stagsted LVW, O'Leary ET, Ebbesen KK, Hansen TB. The RNA-Binding Protein SFPQ Preserves Long-Intron Splicing and Regulates circRNA Biogenesis in Mammals. *Elife* (2021) 10:e63088. doi: 10.7554/eLife.63088.sa2
65. Liang D, Wilusz JE. Short Intronic Repeat Sequences Facilitate Circular RNA Production. *Genes Dev* (2014) 28:2233–47. doi: 10.1101/gad.251926.114
66. Kramer MC, Liang D, Tatomer DC, Gold B, March ZM, Cherry S, et al. Combinatorial Control of Drosophila Circular RNA Expression by Intronic Repeats, hnRNPs, and SR Proteins. *Genes Dev* (2015) 29:2168–82. doi: 10.1101/gad.270421.115
67. Tang C, Xie Y, Yu T, Liu N, Wang Z, Woolsey RJ, et al. M(6)A-Dependent Biogenesis of Circular RNAs in Male Germ Cells. *Cell Res* (2020) 30:211–28. doi: 10.1038/s41422-020-0279-8
68. Niu MT, Ju Y, Lin C, Zou Q. Characterizing Viral circRNAs and Their Application in Identifying circRNAs in Viruses. *Briefings Bioinf* (2022) 23:bbab404. doi: 10.1093/bib/bbab404
69. Du N, Li K, Wang Y, Song B, Zhou X, Duan S. CircRNA Circbach1 Facilitates Hepatitis B Virus Replication and Hepatoma Development by Regulating the miR-200a-3p/MAP3K2 Axis. *Histol Histopathol* (2022), 18452. doi: 10.14670/HH-18-452
70. Huang H, Wei L, Qin T, Yang N, Li Z, Xu Z. Circular RNA ciRS-7 Triggers the Migration and Invasion of Esophageal Squamous Cell Carcinoma via miR-7/KLF4 and NF-kappaB Signals. *Cancer Biol Ther* (2019) 20:73–80. doi: 10.1080/15384047.2018.1507254
71. Piwecka M, Glazar P, Hernandez-Miranda LR, Memczak S, Wolf SA, Rybak-Wolf A, et al. Loss of a Mammalian Circular RNA Locus Causes miRNA Deregulation and Affects Brain Function. *Science* (2017) 357:eaam8526. doi: 10.1126/science.aam8526
72. Du WW, Yang W, Liu E, Yang Z, Dhaliwal P, Yang BB. Foxo3 Circular RNA Retards Cell Cycle Progression via Forming Ternary Complexes With P21 and CDK2. *Nucleic Acids Res* (2016) 44:2846–58. doi: 10.1093/nar/gkw027
73. Zeng Y, Du WW, Wu Y, Yang Z, Awan FM, Li X, et al. A Circular RNA Binds To and Activates AKT Phosphorylation and Nuclear Localization Reducing Apoptosis and Enhancing Cardiac Repair. *Theranostics* (2017) 7:3842–55. doi: 10.7150/thno.19764
74. Conn VM, Hugouvieux V, Nayak A, Conos SA, Capovilla G, Cildir G, et al. A circRNA From SEPALLATA3 Regulates Splicing of its Cognate mRNA Through R-Loop Formation. *Nat Plants* (2017) 3:17053. doi: 10.1038/nplants.2017.53
75. Patil NS, Feng B, Su ZL, Castellani CA, Chakrabarti S. Circular RNA Mediated Gene Regulation in Chronic Diabetic Complications. *Sci Rep-Uk* (2021) 11:23766. doi: 10.1038/s41598-021-02980-y
76. Yu YH, Fang L. CircRPAP2 Regulates the Alternative Splicing of PTK2 by Binding to SRSF1 in Breast Cancer. *Cell Death Discovery* (2022) 8:152. doi: 10.1038/s41420-022-00965-y
77. Eyob W, George AK, Homme RP, Stanic D, Sandhu H, Tyagi SC, et al. Regulation of the Parental Gene GRM4 by Circgrm4 RNA Transcript and Glutamate-Mediated Neurovascular Toxicity in Eyes. *Mol Cell Biochem* (2021) 476:663–73. doi: 10.1007/s11010-020-03934-0
78. Duan JL, Chen W, Xie JJ, Zhang ML, Nie RC, Liang H, et al. A Novel Peptide Encoded by N6-Methyladenosine Modified Circmap3k4 Prevents Apoptosis in Hepatocellular Carcinoma. *Mol Cancer* (2022) 21:93. doi: 10.1186/s12943-022-01537-5
79. Li Y, Wang Z, Su P, Liang Y, Li Z, Zhang H, et al. Circ-EIF6 Encodes EIF6-224aa to Promote TNBC Progression via Stabilizing MYH9 and Activating the Wnt/beta-Catenin Pathway. *Mol Ther* (2022) 30:415–30. doi: 10.1016/j.jymthe.2021.08.026
80. Wang L, Zhou J, Zhang C, Chen R, Sun Q, Yang P, et al. A Novel Tumour Suppressor Protein Encoded by Circmapk14 Inhibits Progression and Metastasis of Colorectal Cancer by Competitively Binding to MKK6. *Clin Transl Med* (2021) 11:e613. doi: 10.1002/ctm2.613

81. Zhu HF, Zheng CF. The Race Between Host Antiviral Innate Immunity and the Immune Evasion Strategies of Herpes Simplex Virus 1. *Microbiol Mol Biol R* (2020) 84:e00099–00020. doi: 10.1128/MMBR.00099-20
82. Zheng C. Evasion of Cytosolic DNA-Stimulated Innate Immune Responses by Herpes Simplex Virus 1. *J Virol* (2018) 92:e00099–00017. doi: 10.1128/JVI.00099-17
83. Lin Y, Zheng C. A Tug of War: DNA-Sensing Antiviral Innate Immunity and Herpes Simplex Virus Type 1 Infection. *Front Microbiol* (2019) 10:2627. doi: 10.3389/fmicb.2019.02627
84. Su C, Zhan G, Zheng C. Evasion of Host Antiviral Innate Immunity by HSV-1, an Update. *Virology* (2016) 13:38. doi: 10.1186/s12985-016-0495-5
85. Cadena C, Hur S. Antiviral Immunity and Circular RNA: No End in Sight. *Mol Cell* (2017) 67:163–4. doi: 10.1016/j.molcel.2017.07.005
86. Chen YG, Kim MV, Chen X, Batista PJ, Aoyama S, Wilusz JE, et al. Sensing Self and Foreign Circular RNAs by Intron Identity. *Mol Cell* (2017) 67:228–238.e225. doi: 10.1016/j.molcel.2017.05.022
87. Li X, Liu CX, Xue W, Zhang Y, Jiang S, Yin QF, et al. Coordinated circRNA Biogenesis and Function With NF90/NF110 in Viral Infection. *Mol Cell* (2017) 67:214–227.e217. doi: 10.1016/j.molcel.2017.05.023
88. Sullivan CS, Grundhoff AT, Tevethia S, Pipas JM, Ganem D. SV40-Encoded microRNAs Regulate Viral Gene Expression and Reduce Susceptibility to Cytotoxic T Cells. *Nature* (2005) 435:682–6. doi: 10.1038/nature03576
89. Ho JS, Di Tullio F, Schwarz M, Low D, Incarnato D, Gay F, et al. HNRNPM Controls circRNA Biogenesis and Splicing Fidelity to Sustain Cancer Cell Fitness. *Elife* (2021) 10:e59654. doi: 10.7554/eLife.59654
90. Li Y, Chen B, Zhao J, Li Q, Chen S, Guo T, et al. HNRNPL Circularizes ARHGAP35 to Produce an Oncogenic Protein. *Adv Sci (Weinh)* (2021) 8:2001701. doi: 10.1002/advs.202001701
91. Zhang X, Chu H, Chik KK, Wen L, Shuai H, Yang D, et al. hnRNP C Modulates MERS-CoV and SARS-CoV-2 Replication by Governing the Expression of a Subset of circRNAs and Cognitive mRNAs. *Emerg Microbes Infect* (2022) 11:519–31. doi: 10.1080/22221751.2022.2032372
92. Knupp D, Cooper DA, Saito Y, Darnell RB, Miura P. NOVA2 Regulates Neural circRNA Biogenesis. *Nucleic Acids Res* (2021) 49:6849–62. doi: 10.1093/nar/gkab523
93. Vuong CK, Black DL, Zheng S. The Neurogenetics of Alternative Splicing. *Nat Rev Neurosci* (2016) 17:265–81. doi: 10.1038/nrn.2016.27
94. Chioccarelli T, Falco G, Cappetta D, De Angelis A, Roberto L, Addeo M, et al. FUS Driven Circnot6l Biogenesis in Mouse and Human Spermatozoa Supports Zygote Development. *Cell Mol Life Sci* (2021) 79:50. doi: 10.1007/s00018-021-04054-8
95. Liu X, Shen S, Zhu L, Su R, Zheng J, Ruan X, et al. SRSF10 Inhibits Biogenesis of Circ-ATXN1 to Regulate Glioma Angiogenesis via miR-526b-3p/MMP2 Pathway. *J Exp Clin Cancer Res* (2020) 39:121. doi: 10.1186/s13046-020-01625-8
96. Pagliarini V, Jolly A, Bielli P, Di Rosa V, de la Grange P, Sette C. Sam68 Binds Alu-Rich Introns in SMN and Promotes pre-mRNA Circularization. *Nucleic Acids Res* (2020) 48:633–45. doi: 10.1093/nar/gkz1117
97. Wang M, Hou J, Muller-McNicoll M, Chen W, Schuman EM. Long and Repeat-Rich Intronic Sequences Favor Circular RNA Formation Under Conditions of Reduced Spliceosome Activity. *iScience* (2019) 20:237–47. doi: 10.1016/j.isci.2019.08.058
98. Li X, Ding J, Wang X, Cheng Z, Zhu Q. NUDT21 Regulates circRNA Cyclization and ceRNA Crosstalk in Hepatocellular Carcinoma. *Oncogene* (2020) 39:891–904. doi: 10.1038/s41388-019-1030-0
99. Schmidt CA, Giusto JD, Bao A, Hopper AK, Matera AG. Molecular Determinants of Metazoan tricRNA Biogenesis. *Nucleic Acids Res* (2019) 47:6452–65. doi: 10.1093/nar/gkz311
100. Huang C, Liang D, Tatomer DC, Wilusz JE. A Length-Dependent Evolutionarily Conserved Pathway Controls Nuclear Export of Circular RNAs. *Genes Dev* (2018) 32:639–44. doi: 10.1101/gad.314856.118
101. Li Z, Kearse MG, Huang C. The Nuclear Export of Circular RNAs is Primarily Defined by Their Length. *RNA Biol* (2019) 16:1–4. doi: 10.1080/15476286.2018.1557498
102. Ivanov A, Memczak S, Wyler E, Torti F, Porath HT, Orejuela MR, et al. Analysis of Intron Sequences Reveals Hallmarks of Circular RNA Biogenesis in Animals. *Cell Rep* (2015) 10:170–7. doi: 10.1016/j.celrep.2014.12.019
103. Errichelli L, Dini Modigliani S, Laneve P, Colantoni A, Legnini I, Caputo D, et al. FUS Affects Circular RNA Expression in Murine Embryonic Stem Cell-Derived Motor Neurons. *Nat Commun* (2017) 8:14741. doi: 10.1038/ncomms14741
104. Wilusz JE. Repetitive Elements Regulate Circular RNA Biogenesis. *Mobile Genet Elements* (2015) 5:39–45. doi: 10.1080/2159256X.2015.1045682
105. Starke S, Jost I, Rossbach O, Schneider T, Schreiner S, Hung LH, et al. Exon Circularization Requires Canonical Splice Signals. *Cell Rep* (2015) 10:103–11. doi: 10.1016/j.celrep.2014.12.002
106. Zhang XO, Wang HB, Zhang Y, Lu X, Chen LL, Yang L. Complementary Sequence-Mediated Exon Circularization. *Cell* (2014) 159:134–47. doi: 10.1016/j.cell.2014.09.001

**Conflict of Interest:** The authors declare that the research was conducted in the absence of any commercial or financial relationships that could be construed as a potential conflict of interest.

**Publisher's Note:** All claims expressed in this article are solely those of the authors and do not necessarily represent those of their affiliated organizations, or those of the publisher, the editors and the reviewers. Any product that may be evaluated in this article, or claim that may be made by its manufacturer, is not guaranteed or endorsed by the publisher.

Copyright © 2022 Zhang, Liang, Wang, Shen, Sun, Gong and Hu. This is an open-access article distributed under the terms of the Creative Commons Attribution License (CC BY). The use, distribution or reproduction in other forums is permitted, provided the original author(s) and the copyright owner(s) are credited and that the original publication in this journal is cited, in accordance with accepted academic practice. No use, distribution or reproduction is permitted which does not comply with these terms.



# Investigation of Antibody Levels During Three Doses of Sinopharm/BBIBP Vaccine Inoculation

Jing Ma<sup>1†</sup>, Zhangkai J. Cheng<sup>1†</sup>, Mingshan Xue<sup>1†</sup>, Huimin Huang<sup>1†</sup>, Shiyun Li<sup>1</sup>, Yanting Fang<sup>1</sup>, Yifeng Zeng<sup>1</sup>, Runpei Lin<sup>1</sup>, Zhiman Liang<sup>1</sup>, Huan Liang<sup>1</sup>, Yijun Deng<sup>1</sup>, Yuanyi Cheng<sup>1</sup>, Shuangshuang Huang<sup>1</sup>, Qian Wang<sup>1</sup>, Xuefeng Niu<sup>1\*</sup>, Siping Li<sup>2\*</sup>, Peiyan Zheng<sup>1\*</sup> and Baoqing Sun<sup>1\*</sup>

## OPEN ACCESS

### Edited by:

Chenhe Su,  
Wistar Institute, United States

### Reviewed by:

Huibin Yu,  
Yale University, United States  
Junlin Liu,  
Sun Yat-sen University Cancer Center  
(SYSUCC), China

### \*Correspondence:

Baoqing Sun  
sunbaoqing@vip.163.com  
Peiyan Zheng  
gdmcslx@126.com  
Siping Li  
lsp020@163.com  
Xuefeng Niu  
niuxuefeng@gird.cn

<sup>†</sup>These authors have contributed  
equally to this work

### Specialty section:

This article was submitted to  
Viral Immunology,  
a section of the journal  
Frontiers in Immunology

Received: 06 April 2022

Accepted: 18 May 2022

Published: 22 June 2022

### Citation:

Ma J, Cheng ZJ, Xue M,  
Huang H, Li S, Fang Y, Zeng Y,  
Lin R, Liang Z, Liang H, Deng Y,  
Cheng Y, Huang S, Wang Q,  
Niu X, Li S, Zheng P and Sun B (2022)  
Investigation of Antibody Levels  
During Three Doses of Sinopharm/  
BBIBP Vaccine Inoculation.  
*Front. Immunol.* 13:913732.  
doi: 10.3389/fimmu.2022.913732

<sup>1</sup> Department of Allergy and Clinical Immunology, State Key Laboratory of Respiratory Disease, Guangzhou Institute of Respiratory Health, National Clinical Research Center of Respiratory Disease, First Affiliated Hospital of Guangzhou Medical University, Guangzhou, China, <sup>2</sup> Clinical Laboratory, Dongguan Eighth People's Hospital, Dongguan, China

Levels of neutralizing antibodies (NAb) after vaccine against coronavirus disease 2019 (COVID-19) can be detected using a variety of methods. A critical challenge is how to apply simple and accurate methods to assess vaccine effect. In a population inoculated with three doses of the inactivated Sinopharm/BBIBP vaccine, we assessed the performance of chemiluminescent immunoassay (CLIA) in its implementation to detect severe acute respiratory syndrome coronavirus-2 (SARS-CoV-2) specific antibodies, as well as the antibody kinetics of healthcare workers throughout the course of vaccination. The antibody levels of NAb, the receptor-binding-domain (RBD) antibodies and IgG peaked one month after the second and remained at a relatively high level for over three months after the booster injection, while IgM and IgA levels remained consistently low throughout the course of vaccination. The production of high-level neutralizing antibodies is more likely when the inoculation interval between the first two doses is within the range of one to two months, and that between the first and booster dose is within 230 days. CLIA showed excellent consistency and correlation between NAb, RBD, and IgG antibodies with the cytopathic effect (CPE) conventional virus neutralization test (VNT). Receiver operating characteristic (ROC) analysis revealed that the optimal cut-off levels of NAb, RBD and IgG were 61.77 AU/ml, 37.86 AU/ml and 4.64 AU/ml, with sensitivity of 0.833, 0.796 and 0.944, and specificity of 0.768, 0.750 and 0.625, respectively, which can be utilized as reliable indicators of COVID-19 vaccination immunity detection.

**Keywords:** coronavirus disease 2019, vaccine, antibody persistence, booster, chemiluminescent immunoassay

## INTRODUCTION

The SARS-CoV-2 is an extremely contagious virus that emerged unexpectedly in 2019 and remains to spread globally today (1). Spike protein (S), nucleocapsid protein (N), an envelope protein (E), and membrane protein (M) are the four structural proteins of the virus. The S protein contains different functional domains at the amino (S1) and carboxyl (S2) terminals, with S1 containing the

RBD, which binds to the peptidase domain of angiotensin-converting enzyme 2 (ACE 2) to execute the first stage of infection. It is currently widely assumed that S protein, particularly S-RBD, can induce NAb (2).

Vaccination is widely acknowledged as the most effective strategy for preventing and controlling infectious diseases. Inactivated vaccinations, mRNA vaccines, and viral vaccines have all been widely utilized (3, 4). Furthermore, the inactivated vaccine has been widely used to prevent diseases caused by the influenza virus and poliovirus (5, 6), which has a high level of safety and immunogenicity. Studies have demonstrated that complete vaccination with an inactivated vaccine has been to protect against wild strains by up to 65.9% (7). Phase 1-2 clinical trials showed that the positive conversion rate of neutralizing antibodies in normal adults reached 100% 28 days after the first injection of BBIBP-CorV, and the level of neutralizing antibodies showed an upward trend within one month after the second dose (8). However, it is undeniable that its protective effect will gradually weaken over time (9), so the booster dose is essential. Prior research has indicated that neutralizing antibodies on the 14th day after the booster dose were significantly higher than those of the previous two doses (10). Meanwhile, data describing changes in antibody dynamics over time after vaccination began to emerge, but descriptions of the duration of immunity remained incomplete.

Changes in specific antibody levels (IgM, IgG, IgA) and neutralizing antibody (NAb) is not only associated with the diagnosis of the disease (11) but can also predict population immunity after vaccination (12). Currently, virus neutralization tests (VNTs) are utilized as the primary standard method for assessing neutralizing antibody levels (13), but due to their complex operations, high cost, and special facility requirements, pseudovirus neutralization tests (pVNTs) are served as substitutions for VNTs. However, neither of these two methodologies has received a widespread promotion, as the cost of performance for pVNTs is still too expensive, both in money and time, for ordinary clinics to afford (14). In contrast, CLIA provides high-throughput, rapid, and reproducible assays for neutralizing antibodies, as well as detecting trends and influencing variables in IgM, IgG, IgA, RBD, and neutralizing antibody levels after vaccination. As a result, the objective of this study is to investigate the changes in antibody levels after inactivated vaccine vaccination as well as evaluate the detection performance of CLIA, providing a valuable reference for vaccine development, drug therapy, epidemiology, and immune monitoring.

## MATERIALS AND METHODS

### Study Subjects

Blood samples were taken from healthcare workers who had received inactivated vaccinations at the First Affiliated Hospital of Guangzhou Medical University between December 27, 2020 and January 13, 2022. The study protocol was approved by the Ethics Committee of the First Affiliated Hospital of Guangzhou

Medical University (2021, No.31) and informed consent was obtained from each volunteer. The vaccine was inoculated three times, 0.5mL each, using Sinopharm/BBIBP (Beijing Bio-Institute of Biological Products Co., Ltd.) vaccine. The recommended interval between the first and second doses is 21-28 days, and the booster dose is recommended to be completed within 6 months of the first dose. Before the immunization (V1), the second dose (V2), 7 days after the second dose (V2+7), one month after the second dose (V2+30), and two months after the second dose (V2+60), 5 months after the second dose (V2+150), 14 days after the booster dose (180 V3+14), one month after the booster dose (180 V3+30) and three months after the booster dose (180 V3+90), a total of nine time points were followed up and samples were collected. After standing for two hours, all the whole blood samples were separated at 1600 rpm/s for 10min under sterile conditions and stored at -80°C. Serum samples were used for VNTs, while plasma samples were used for CLIA and pVNT. All plasma samples were mixed by freeze-thawing before detection, and the supernatant was obtained for detection after 10000 rpm/s within 10 min.

Inclusion criteria: healthy healthcare workers who signed an informed consent form, all volunteers had a negative nucleic acid test during the monitoring period and had no contact history with suspected or confirmed cases of COVID-19. Exclusion criteria: severe allergic reactions to previous vaccinations or allergic reactions to active ingredients, inactive ingredients or substances used in the preparation of vaccines contained in the new crown vaccine, and allergic reactions after the first dose; patients with severe chronic diseases or in the acute exacerbation stage of chronic diseases; patients with platelet dysfunction or bleeding disorder; patients with severe immunodeficiency diseases, liver and kidney diseases, malignant tumors, etc.; in the period of other vaccinations.

### CPE Neutralization Test Based on SARS-CoV-2 Live Virus Cells

All serum samples were labeled and inactivated at 56°C for 30 minutes before being examined. 180  $\mu$ l of maintenance solution was added to each well on a 96-well plate. 60  $\mu$ l of the heat-inactivated serum was added to the first well, then 60  $\mu$ l of the diluted serum was transferred to the next row and mixed evenly. 1:4 gradient dilution was performed 5 times, and the excess 60  $\mu$ l of liquid was discarded from the last row.

125  $\mu$ l of each dilution was transferred to a separate 96-well plate. The SARS-CoV-2 virus was diluted to 100 TCID<sub>50</sub>/50  $\mu$ l using Dulbecco's Modified Eagle's culture medium (DMEM) +2% fetal bovine serum (FBS). The diluted virus was added at a ratio of 1:1 (V/V), then the virus was placed in an incubator with 5% CO<sub>2</sub> at 36°C for 2 hours after being shaken evenly and gently once after culture for 1.5 hours. VeroE6 cells were inoculated at a density of  $1 \times 10^4 \sim 2 \times 10^4$  cells per well into 96-well plates. After neutralization, 100  $\mu$ l of VeroE6 cells were added to the cell hole and cultured in a 36°C incubator with 5% CO<sub>2</sub>. CPE in each well was recorded on days 5-8 when complete lesions formed in the 100 TCID<sub>50</sub> antigen control, with the results monitored every day. The SARS-CoV-2 neutralizing antibody titer of the serum is

the reciprocal of the maximum serum dilution that can protect 50% of cell wells from CPE.

## Neutralization Test Based on SARS-CoV-2 Pseudovirus

To manufacture SARS-CoV-2 pseudovirus, the SARS-CoV-2 spike expression plasmid was cotransfected into HEK-293t cells with an HIV-1 backbone vector containing a luciferase reporter gene. The virus was diluted to  $1-2 \times 10^4$  TCID<sub>50</sub>/ml in DMEM medium containing 10% FBS serum. The plasma after heat extinguishment was diluted 20 times with DMEM medium and filtered *via* a 0.22  $\mu$ m filter membrane. Diluted 30 times in the first well, mixed evenly, then diluted three times in six gradients, and discard the excess 50  $\mu$ l in the last row. Incubate at 37°C for one hour with 50  $\mu$ l of diluted virus in each well. Add 50  $\mu$ l 293-ACE2 with a density of  $0.4 \times 10^6$  cells/ml to each well, culture at 37°C with 5% CO<sub>2</sub> for 48 h, then take out the 96-well whiteboard, equilibrate to room temperature, suck out 100  $\mu$ l medium from the well plate, add 100  $\mu$ l Bio-Lite reporter reagent after equilibrating to room temperature. The plate was shaken for 2 min and placed at room temperature for 5 min. The relative light unit (RLU) was detected by a microplate reader.

## Chemiluminescence Immunoassay

The SARS-CoV-2 NAb testing employs CLIA (competitive method). The detection principle utilizes the idea that the NAb of SARS-CoV-2 will impede ACE2's particular binding to RBD. Magnetic particles were coated with recombinant ACE2 antigen and labeled with recombinant RBD antigen by horseradish peroxidase. The RBD antigen, which was not neutralized by antibodies, formed a complex with ACE2 on magnetic particles. These complexes catalyze the emission of photons from luminous substrates, the intensity of which is inversely proportional to the concentration of the antibody. When the concentration value of the sample is less than 30.00 AU/ml, it is regarded as positive for neutralizing antibodies of wild strain. When a sample's concentration value is less than 30.00 AU/ml, it is regarded as negative.

The capture method was used to detect SARS-CoV-2 IgM, anti-human IGM was coated with magnetic particles, and horseradish-peroxidase-labeled SARS-CoV-2 antigen to prepare enzyme conjugate. SARS-CoV-2 IgG and IgA were detected by indirect method, using SARS-CoV-2 antigen-coated with magnetic particles and horseradish-peroxidase-labeled anti-human IgG/IgA antibody to form solid-phase antigen-IgG/IgA antibody-conjugated secondary antibody complex. The sandwich method was used to detect anti-SARS-CoV-2 RBD antibody, using SARS-CoV-2 RBD antigen coated with magnetic particles, and horseradish-peroxidase-labeled SARS-CoV-2 RBD antigen to form solid-phase SARS-CoV-2 RBD antigen-specific antibody-enzyme conjugate antigen complex. These complexes catalyze the emission of photons from luminous substrates, whose intensity is proportional to antibody concentration. The manufacturer-defined positive threshold for IgM, IgG, and IgA were all 1 AU/ml, while the positive threshold for RBD was 8 AU/ml. Autolumo A2000 PLUS Automatic Chemiluminescence immunoassay

(Autobio Diagnostics Co., Ltd.) was used as a matching instrument for the above reagents.

## Statistical Analysis

SPSS 25.0 was used for analysis. The Mann-Whitney U test was used to assess the measurement data between the two groups, and median and quartile distance were used to describe them. The Spearman correlation analysis was used to analyze correlation between two groups.  $P \leq 0.05$  was considered statistically significant. Graph Pad Prism 8.0 (La Jolla, USA) was used to plot the results.

## RESULTS

### Baseline Data

187 participants were recruited from the First Affiliated Hospital of Guangzhou Medical University, with none having a prior history of COVID-19 and were negative for SARS-CoV-2 nucleic acid tests, due to the Zero-COVID strategy employed in China (15). The basic information of participants is shown in **Table 1**, which includes 39 males and 148 females, with a male to female ratio of 1:3.79. The participants ranged in age from 20 to 58 years old, with an average age of 37.1 years. Blood samples were obtained at various time intervals to monitor the dynamic changes in antibody levels in individuals, as depicted in **Figure 1** and **Supplementary Table 1**.

### Plasma Antibody Kinetics Throughout BBIBP Vaccination

CLIA was used to examine the development of IgG, IgA, IgM, RBD, and NAb antibodies during immunization (**Figure 2**). We found that NAb, RBD and IgG had a consistent trend of change, and the antibody level showed an increasing trend after the first dose, and further increased after the second dose and reached the highest level (peak) one month after the second dose, then slowly decreased. The levels of NAb, RBD and IgG antibodies were further increased after the booster dose and the antibody levels were significantly decreased but remained high three months after the booster dose, even the antibody levels of RBD were significantly higher than one month after the second dose ( $P < 0.05$ ). However, IgA and IgM also reached their peak one month after the second injection. Although IgA and IgM levels were significantly increased after the booster injection, the peak antibody level was significantly lower than that one month after the second dose ( $P < 0.05$ ). We also looked at age (20-29, 30-39,

**TABLE 1** | Baseline characteristics.

		N	Mean $\pm$ SD/%
Sex	Male	39	20.86%
	Female	148	79.14%
Age (years)	20-29	45	37.06 $\pm$ 8.76
	30-39	72	24.07%
	40-49	57	38.50%
	≥50	13	30.48%
			13

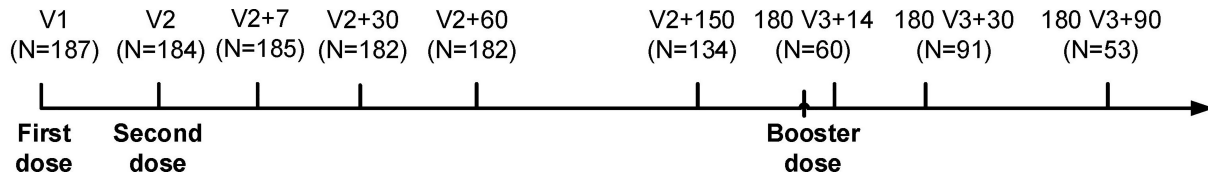


**FIGURE 1** | Group entry process and time interval. V1: first injection (before immunization). V2: second injection. V2+7: seven days after the second injection. V2+30: one month after the second injection. V2+60: two months after the second injection. V2+150: five months after the second injection. 180 V3+14: 14 days after booster injection. 180 V3+30: one month after booster injection. 180 V3+90: three months after booster injection.

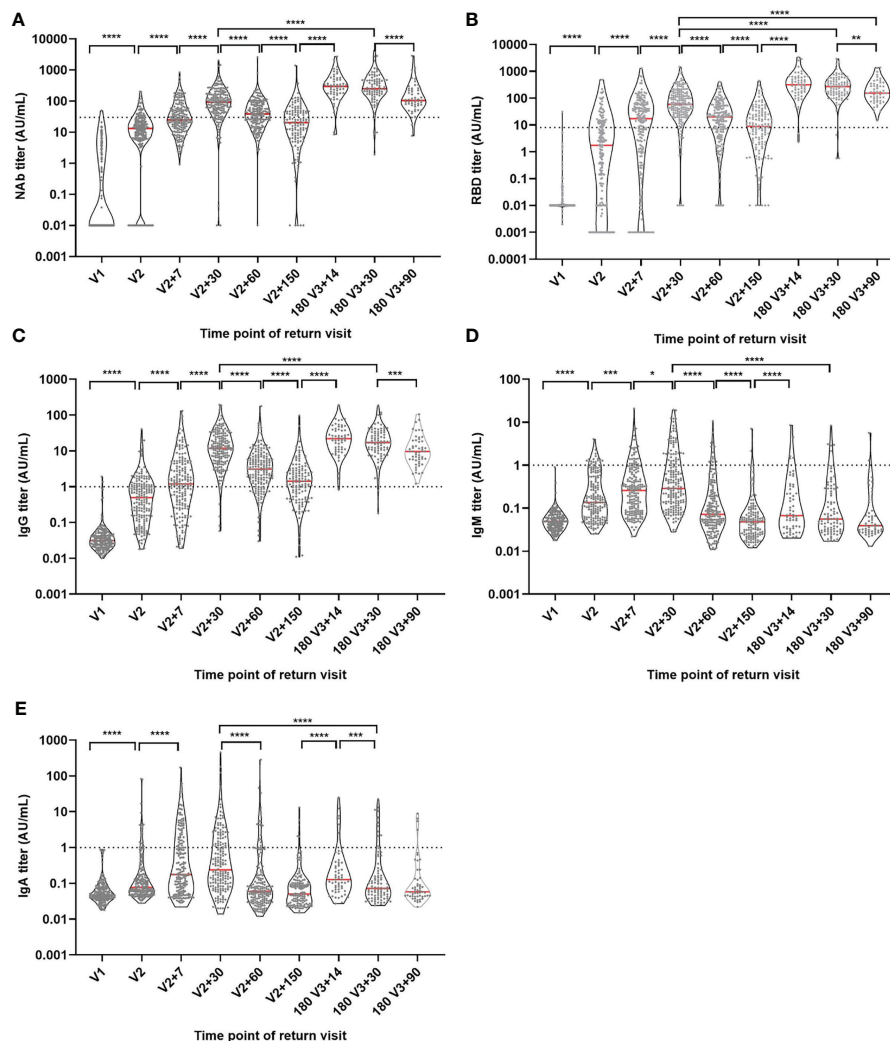


**FIGURE 2** | Antibody titer levels at different time points during vaccination. **(A)** NAb antibody level. **(B)** RBD antibody level. **(C)** IgG antibody level. **(D)** IgM antibody level. **(E)** IgA antibody level. Red lines: median titer. Dotted lines: manufacturer-defined positive threshold values. \* $P \leq 0.05$ . \*\* $P \leq 0.01$ . \*\*\* $P \leq 0.001$ . \*\*\*\* $P \leq 0.0001$  (Mann-Whitney U test).

40-49 and  $\geq 50$  years old) and gender groups, the results showed that there was no significant difference in the trend of antibody levels among different ages and genders (**Supplementary Figures 1, 2**).

A total of 37 volunteers, with a male to female ratio of 1:2.7 and an average age of  $39.08 \pm 8.44$ , were selected for continuous follow-up at six main time points: V1, V2+30, V2+60, V2+150, 180 V3+30 and 180 V3+90 and the dynamic changes of



their antibody levels were analyzed. Compared with one month after the second injection, NAb, RBD and IgG antibody titer levels were 3.8, 5 and 8.2 times lower at 5 months after the second dose (Figures 3A–C), but increased by 4.7, 7.6 and 2 times on one month after the booster dose. Compared with one month after the booster injection, the median level of NAb, RBD and IgG antibodies decreased by 2.8 times, 1.8 times and 2 times three months after the booster dose. Despite the fact that antibody levels were much lower three months after the booster dose, the median NAb and RBD antibody titer levels were still 1.6 and 4.1 times higher than they were one month after the second dose. Meanwhile, we observed that one month after the second dose, the peaks of IgM and IgA antibody titer levels were attained (Figures 3D, E) but the booster dose did not significantly increase their titer levels.

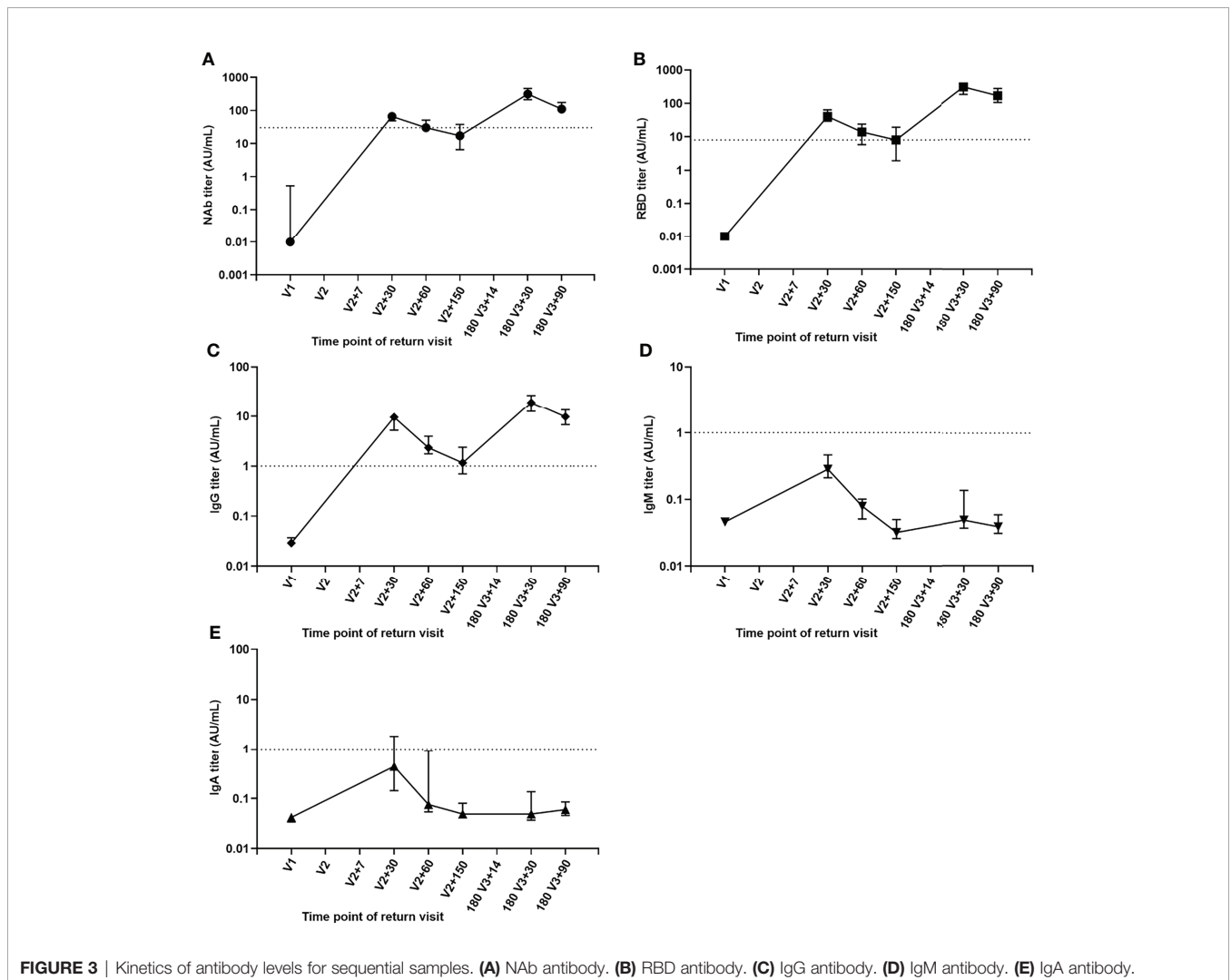
### Effects of Different Inoculation Intervals on Antibody Levels

Vaccine administration at regular intervals is difficult in the actual world. As a result, the time interval between the first dose

and the second dose is wide in actuality. The currently recommended time interval for inactivated vaccinations is one month, with 30 days serving as the dividing line. The longer the interval between the first and second doses (25–57 days in this study), the higher the NAb titer levels produced (Figure 4A). The interval between the first and booster doses in our study was 200–276 days. NAb titer levels after the booster injection were compared at the median level of 230 days as the dividing line. It was discovered that a longer time interval did not increase the antibody level after three doses, but rather had a declining tendency (Figure 4B).

### Performance Verification of Neutralizing Antibody Detection by Chemiluminescence Immunoassay

We validated neutralizing antibody levels using VNT and pVNT in addition to the CLIA. The trends of NAb, RBD and IgG antibodies were consistent with those of VNT titers, and the first peak of antibody levels appeared one month after the second injection (Figure 5A). In order to perform comparison between



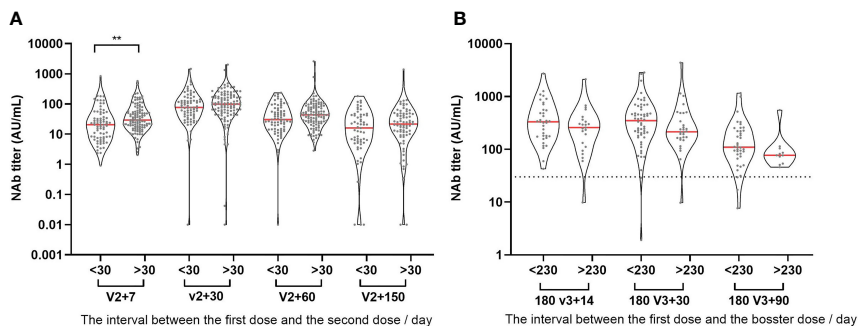


**FIGURE 4** | Effects of different inoculation intervals on antibody levels. **(A)** The relationship between NAb titer level and the time interval for the first two injections. **(B)** The relationship between NAb titer level and the time interval for the first and booster injection. >30: the interval between the first two injections is longer than or equal to 30 days. <30: the interval between the first two injections is less than 30 days. >230: the interval between the first and booster injection is longer than or equal to 230 days. <230: the interval between the first and booster injection is less than 230 days. \*\*P ≤ 0.01 (Mann-Whitney U test).

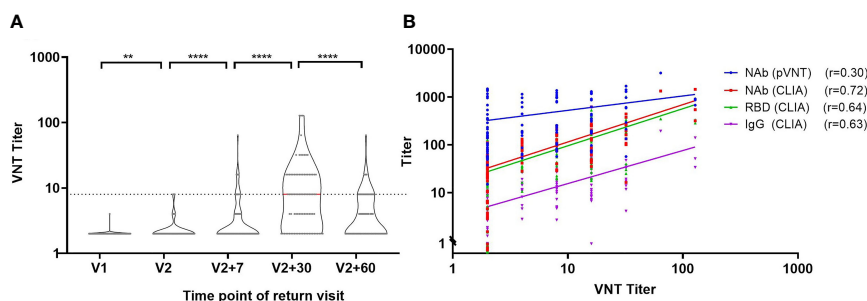


**FIGURE 5** | Correlation analysis of CLIA, VNT and pVNT antibody detection. **(A)** Trend of VNT titer over time. **(B)** Correlation between neutralizing antibodies detected by VNT and pVNT and NAb, RBD and IgG antibodies detected by CLIA. r: Spearman correlation coefficient. \*\*P ≤ 0.01. \*\*\*\*P ≤ 0.0001 (Mann-Whitney U test).

the CLIA, VNT and pVNT methods, we analyzed 111 samples during follow-up that were simultaneously detected with all three methods and found that the NAb, RBD and IgG antibodies have strong correlations with VNT titers (**Figure 5B**), with correlation coefficients of 0.72, 0.64 and 0.63, respectively. On the other hand, the correlation between pVNT and VNT results have a weak correlation, having a correlation coefficient of only 0.30.

Then, using VNT titers as the standard, the optimal cut-off values of NAb, RRD, IgG and pVNT titers by receiver operating characteristic (ROC) curve were calculated to be 61.77 AU/mL, 37.86 AU/mL, 4.64 AU/mL and 182 (ID50), respectively (**Table 2**). The area under curve (AUC) were 0.875, 0.855, 0.852, and 0.681, respectively. At this cut-off value, NAb, RBD and IgG all had good detection performance and were superior to pVNT methodology (**Figure 6** and **Table 2**).

**TABLE 2** | Optimal cut-off values.

	AUC	95%CI	Cutoff	Sensitivity	Specificity	Youden index
NAb	0.875	0.812-0.937	61.77	0.833	0.768	0.601
RBD	0.855	0.788-0.922	37.86	0.796	0.750	0.546
IgG	0.852	0.783-0.920	4.64	0.944	0.625	0.569
pVNT	0.681	0.581-0.781	182.00	0.778	0.589	0.367

## DISCUSSION

Since the prevalence of COVID-19 from early 2020 to the present, vaccines are considered the primary way to defend against the viruses. As a result, various types of vaccines swiftly enter the clinic and are widely administered, such as inactivated virus vaccines, mRNA vaccines encoding the spike protein of SARS-CoV-2, and viral vector-based vaccines (e.g. adenovirus). The inactivated vaccine is undoubtedly the earliest and most widely used vaccine in China. The two whole virus inactivated vaccines provided 72.8% and 78.1% protection in clinical studies of healthy individuals injected with domestic inactivated vaccines (16). Although the protection rate is lower than that of some RNA and adenovirus vaccines (17, 18), the advantages of inactivated vaccines in large-scale and diverse populations are determined by their superior safety and immunogenicity.

The neutralizing antibody is undoubtedly the best choice for monitoring vaccine protection, and their detection results are subject to VNT and pVNT. However, the complexity of the procedure and the length of time it takes to complete limit its widespread application (14). Relatively, CLIA is a rapid and stable method, which is widely used in the early stage of

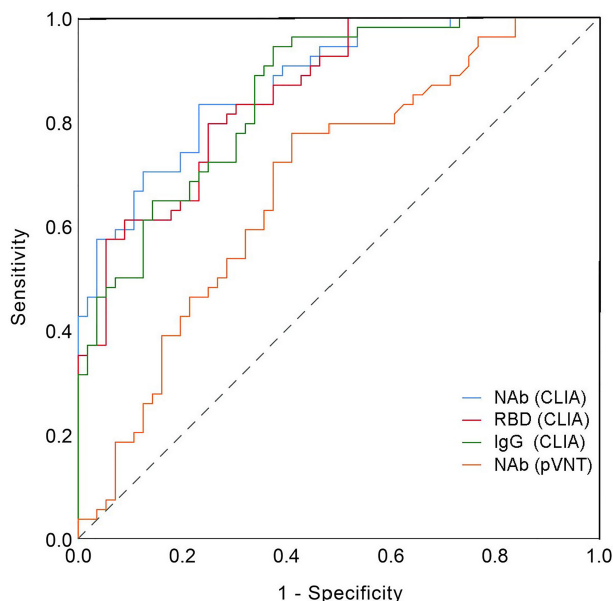


**FIGURE 6** | Receiver operating curve (ROC).

COVID-19 outbreak (19). The combination of IgG and IgM detection is crucial in the diagnosis of COVID-19. In addition, the CLIA also provides the possibility to replace the conventional standard method in the monitoring of the immune effect of vaccines (20, 21). CLIA was primarily used in our study to detect changes in various antibody levels after inactivated vaccine inoculation. According to our comparison, the variation trend of VNT and pVNT was consistent with the results of NAb, RBD and IgG detected by the CLIA, and there was a significant association between NAb, RBD and IgG and VNT results. In comparison to VNT, NAb detection has a sensitivity of up to 63%, but its specificity is low. ROC curves were used to determine the optimal thresholds for NAb, RBD, IgG and pVNT and they were 61.77 AU/ml, 37.86 AU/ml, 4.64 AU/ml and 182 (ID<sub>50</sub>). The sensitivity was 0.833, 0.796, 0.944, and 0.778 under the cutoff value, while the specificity was 0.768, 0.750, 0.625, and 0.589. According to studies, the sensitivity of NAb, RBD, and IgG antibody detection by CLIA is no less than pVNT, and the specificity is even better. In general, CLIA can be used as a reliable indicator of vaccine immunity detection.

The dynamic variations in antibody levels after vaccination are critical for monitoring population immunity and preventing viral infection. The trajectory of antibody alterations in the population revealed that the highest antibody level peaked in the first month after the second dose. Related studies have found that antibodies generated by the inactivated vaccine can still be detected in humans up to month 6 after the second dose (22). We also discovered that NAb detection could still be positive in some populations five months after the second dose. Compared to one month after the second dose, NAb, RBD, and IgG

antibody titer levels declined approximately 3.8, 5, and 8.2 times, respectively, whereas IgA and IgM antibody levels reduced around 9 times. Similar to inactivated vaccine antibody levels, BNT162b2 (Pfizer-BioNTech) vaccine antibody levels peaked one month after vaccination (23), while mRNA-1273 peaked around 2 weeks after the second dose and subsequently decreased (24). At 6 months after the second dose, antibody levels of the BNT162b2 vaccine were approximately 2-fold lower (23) and neutralizing antibody levels of mRNA-1273 were approximately 4-fold lower (24). However, due to the heterogeneity of the antibody neutralization analysis, it is difficult to directly compare these estimates with the results of this study. A month after a booster injection, the antibody levels began to decline significantly. At three months after the booster dose, median levels of NAb, RBD, and IgG antibodies were 2.8, 1.8 and 2 times lower than the first month after the booster. However, the median levels of NAb and RBD antibodies in the third month after the booster dose were still 1.6 times and 4.1 times higher than those in the first month after the second dose, while the levels of IgA and IgM antibodies were about 1/7 of those in the first month after the second dose. In conclusion, NAb, RBD and IgG antibody levels were significantly decreased by the third dose of the vaccine. It has remained at a high level for three months, which is higher than the first month after the second dose.

In our study, the levels of IgA and IgM were consistently low, and their antibody levels were not further boosted by the booster vaccination. The researchers discovered that detectable IgM levels were typically lower after vaccination and lasted for a shorter period of time, as a result, IgM may be of minor consequence in viral neutralization *in vivo* (25, 26). Mucosal immunity is a critical

aspect in preventing and resisting infection in SARS-CoV-2, which is a respiratory transmission virus (27). Plasma IgA levels not only correlate with mucosal IgA levels (28) but also exhibit a higher neutralization capacity early in infection (29, 30). Only 1.7 percent of participants remained IgA negative against S1 in the first month after the second dose in related investigations using mRNA vaccine (31), which was significantly higher than the IgA positive rate induced by inactivated vaccination. Furthermore, we discovered that IgA and IgG had identical induction kinetics and times to peak levels during the first two doses vaccinations (32). We further observed that the booster dose vaccination does not further improve the level of IgA. Moreover, relevant investigations revealed that the development of specific antibody IgA occurred earlier than IgG after inactivated vaccine immunization (33). However, we did not observe this trend due to the low levels of IgA in plasma or discrepancies in methodological detection.

Vaccine effectiveness is affected by a variety of elements, including the underlying disease of the vaccinee, age, gender, and the time interval between vaccine booster doses (22, 28, 34–36). Previous research has demonstrated that underlying illnesses can alter antibody levels before immunization (28, 35, 36). Male populations beyond the age of 65 will have significantly lower levels of antibodies (22, 36). The longer the time interval between the first and second dose, the more favorable is the production of high levels of antibodies (7). Our study found that there was no significant difference in the trend of antibody change in people under 58 years old, and gender was not related to the change in antibody level. We also discovered that a time interval of one to two months between the first and second doses, while less than 230 days between the first and booster doses were more conducive to the production of high levels of neutralizing antibodies in our study. Our research involved a group of healthcare workers, among this cohort contains a higher proportion of women, most of whom are healthy and young, therefore the study group does not represent the general public. However, this cohort is a highly exposed and high-risk population, and assessing their vaccination protection is clinically meaningful.

In conclusion, our study found that chemiluminescence NAb, RBD and IgG antibodies can be reliable indicators for vaccine immunity detection. People who received three doses of inactivated vaccine declined after peaking one month after the second dose, and antibody levels persisted at higher levels for more than three months after the booster dose. Furthermore, the optimal interval for the second dose is one to two months, while the optimal interval for the booster dose is 230 days.

## REFERENCES

1. Tang X, Wu C, Li X, Song Y, Yao X, Wu X, et al. On the Origin and Continuing Evolution of Sars-Cov-2. *Natl Sci Rev* (2020) 7(6):1012–23. doi: 10.1093/nsr/nwaa036
2. Hoffmann M, Kleine-Weber H, Schroeder S, Kruger N, Herrler T, Erichsen S, et al. Sars-Cov-2 Cell Entry Depends on Ace2 and Tmprss2 and Is Blocked by a Clinically Proven Protease Inhibitor. *Cell* (2020) 181(2):271–80.e8. doi: 10.1016/j.cell.2020.02.052
3. Awadasseid A, Wu Y, Tanaka Y, Zhang W. Current Advances in the Development of Sars-Cov-2 Vaccines. *Int J Biol Sci* (2021) 17(1):8–19. doi: 10.7150/ijbs.52569
4. Yu H, Huang L, Zhang Y, Hu L, Wang S, Li J, et al. An Attenuated Emcv-Hb10 Strain Acts as a Live Viral Vector Delivering a Foreign Gene. *J Gen Virol* (2016) 97(9):2280–90. doi: 10.1099/jgv.0.000541
5. Murdin AD, Barreto L, Plotkin S. Inactivated Poliovirus Vaccine: Past and Present Experience. *Vaccine* (1996) 14(8):735–46. doi: 10.1016/0264-410x(95)00211-i

## DATA AVAILABILITY STATEMENT

The original contributions presented in the study are included in the article material, further inquiries can be directed to the corresponding authors.

## ETHICS STATEMENT

The studies involving human participants were reviewed and approved by The First Affiliated Hospital of Guangzhou Medical University Scientific Research Project Reviews Ethics Committee, clinical research approval 2021 No.31. The patients/participants provided their written informed consent to participate in this study.

## AUTHOR CONTRIBUTIONS

All authors made a significant contribution to the work reported, whether that is in the conception, study design, execution, acquisition of data, analysis, and interpretation, or in all these areas; took part in drafting, revising, or critically reviewing the article; gave final approval of the version to be published; have agreed on the journal to which the article has been submitted; and agree to be accountable for all aspects of the work.

## FUNDING

This study was supported by the emergency key project of Guangzhou Laboratory (EKPG21-30-2), Zhongnanshan Medical Foundation of Guangdong Province (ZNSA-2021005), State Key Laboratory of Respiratory Disease, Guangdong-Hong Kong-Macao Joint Laboratory of Respiratory Infectious Disease (GHMJLRID-Z-202102). Cultivation Project of the First Affiliated Hospital of Guangzhou Medical University (ZH202105), and Guangzhou Institute of Respiratory Health Open Project (Funds provided by China Evergrande Group) (2020GIRHHMS04).

## SUPPLEMENTARY MATERIAL

The Supplementary Material for this article can be found online at: <https://www.frontiersin.org/articles/10.3389/fimmu.2022.913732/full#supplementary-material>

6. Vellozzi C, Burwen DR, Dobardzic A, Ball R, Walton K, Haber P. Safety of Trivalent Inactivated Influenza Vaccines in Adults: Background for Pandemic Influenza Vaccine Safety Monitoring. *Vaccine* (2009) 27(15):2114–20. doi: 10.1016/j.vaccine.2009.01.125
7. Jara A, Undurraga EA, Gonzalez C, Paredes F, Fontecilla T, Jara G, et al. Effectiveness of an Inactivated Sars-Cov-2 Vaccine in Chile. *N Engl J Med* (2021) 385(10):875–84. doi: 10.1056/NEJMoa2107715
8. Xia S, Zhang Y, Wang Y, Wang H, Yang Y, Gao GF, et al. Safety and Immunogenicity of an Inactivated Sars-Cov-2 Vaccine, Bbibp-Corv: A Randomised, Double-Blind, Placebo-Controlled, Phase 1/2 Trial. *Lancet Infect Dis* (2021) 21(1):39–51. doi: 10.1016/S1473-3099(20)30831-8
9. Li X, Liang C, Xiao X. Sars-Cov-2 Neutralizing Antibody Levels Post Covid-19 Vaccination Based on Elisa Method-A Small Real-World Sample Exploration. *Vaccines (Basel)* (2021) 9(10):1139. doi: 10.3390/vaccines9101139
10. Yue L, Xie T, Yang T, Zhou J, Chen H, Zhu H, et al. A Third Booster Dose May Be Necessary to Mitigate Neutralizing Antibody Fading After Inoculation With Two Doses of an Inactivated Sars-Cov-2 Vaccine. *J Med Virol* (2022) 94(1):35–8. doi: 10.1002/jmv.27334
11. Fu Y, Pan Y, Li Z, Li Y. The Utility of Specific Antibodies Against Sars-Cov-2 in Laboratory Diagnosis. *Front Microbiol* (2020) 11:603058. doi: 10.3389/fmicb.2020.603058
12. Mazzini L, Martinuzzi D, Hyseni I, Benincasa L, Molesti E, Casa E, et al. Comparative Analyses of Sars-Cov-2 Binding (Igg, Igm, Iga) and Neutralizing Antibodies From Human Serum Samples. *J Immunol Methods* (2021) 489:112937. doi: 10.1016/j.jim.2020.112937
13. Montesinos I, Dahma H, Wolff F, Dauby N, Delaunoy S, Wuyts M, et al. Neutralizing Antibody Responses Following Natural Sars-Cov-2 Infection: Dynamics and Correlation With Commercial Serologic Tests. *J Clin Virol* (2021) 144:104988. doi: 10.1016/j.jcv.2021.104988
14. Mahmoud SA, Ganesan S, Naik S, Bissar S, Zamel IA, Warren KN, et al. Serological Assays for Assessing Postvaccination Sars-Cov-2 Antibody Response. *Microbiol Spectr* (2021) 9(2):e0073321. doi: 10.1128/Spectrum.00733-21
15. Cheng ZJ, Zhan Z, Xue M, Zheng P, Lyu J, Ma J, et al. Public Health Measures and the Control of Covid-19 in China. *Clin Rev Allergy Immunol* (2021) 1-16. doi: 10.1007/s12016-021-08900-2
16. Al Kaabi N, Zhang Y, Xia S, Yang Y, Al Qahtani MM, Abdulrazzaq N, et al. Effect of 2 Inactivated Sars-Cov-2 Vaccines on Symptomatic Covid-19 Infection in Adults: A Randomized Clinical Trial. *JAMA* (2021) 326(1):35–45. doi: 10.1001/jama.2021.8565
17. Baden LR, El Sahly HM, Essink B, Kotloff K, Frey S, Novak R, et al. Efficacy and Safety of the Mrna-1273 Sars-Cov-2 Vaccine. *N Engl J Med* (2021) 384(5):403–16. doi: 10.1056/NEJMoa2035389
18. Logunov DY, Dolzhikova IV, Shcheblyakov DV, Tukhvatulin AI, Zubkova OV, Dzharullaeva AS, et al. Safety and Efficacy of an Rad26 and Rad5 Vector-Based Heterologous Prime-Boost Covid-19 Vaccine: An Interim Analysis of a Randomised Controlled Phase 3 Trial in Russia. *Lancet* (2021) 397(10275):671–81. doi: 10.1016/S0140-6736(21)00234-8
19. Rai P, Kumar BK, Deekshit VK, Karunasagar I, Karunasagar I. Detection Technologies and Recent Developments in the Diagnosis of Covid-19 Infection. *Appl Microbiol Biotechnol* (2021) 105(2):441–55. doi: 10.1007/s00253-020-11061-5
20. Padoan A, Cosma C, Bonfante F, Rocca FD, Barbaro F, Santarossa C, et al. Sars-Cov-2 Neutralizing Antibodies After One or Two Doses of Comirnaty (Bnt162b2, Biontech/Pfizer): Kinetics and Comparison With Chemiluminescent Assays. *Clin Chim Acta* (2021) 523:446–53. doi: 10.1016/j.cca.2021.10.028
21. Liu B, Su X, Yu G, Yang S, Wang F, Huang T, et al. An Automated Chemiluminescent Immunoassay (Clia) Detects Sars-Cov-2 Neutralizing Antibody Levels in Covid-19 Patients and Vaccinees. *Int J Infect Dis* (2022) 115:116–25. doi: 10.1016/j.ijid.2021.12.316
22. Levin EG, Lustig Y, Cohen C, Fluss R, Indenbaum V, Amit S, et al. Waning Immune Humoral Response to Bnt162b2 Covid-19 Vaccine Over 6 Months. *N Engl J Med* (2021) 385(24):e84. doi: 10.1056/NEJMoa2114583
23. Salvagno GL, Henry BM, Pighi L, de NS, Lippi G. Total Anti-Sars-Cov-2 Antibodies Measured 6 Months After Pfizer-Biontech Covid-19 Vaccination in Healthcare Workers. *J Med Biochem* (2022) 41(2):199–203. doi: 10.5937/jomb0-33999
24. Doria-Rose N, Suthar MS, Makowski M, O'Connell S, McDermott AB, Flach B, et al. Antibody Persistence Through 6 Months After the Second Dose of Mrna-1273 Vaccine for Covid-19. *N Engl J Med* (2021) 384(23):2259–61. doi: 10.1056/NEJMc2103916
25. Wang Z, Schmidt F, Weisblum Y, Muecksch F, Barnes CO, Finkin S, et al. Mrna Vaccine-Elicited Antibodies to Sars-Cov-2 and Circulating Variants. *Nature* (2021) 592(7855):616–22. doi: 10.1038/s41586-021-03324-6
26. Danese E, Montagnana M, Salvagno GL, Peserico D, Pighi L, De Nitto S, et al. Comprehensive Assessment of Humoral Response After Pfizer Bnt162b2 Mrna Covid-19 Vaccination: A Three-Case Series. *Clin Chem Lab Med* (2021) 59(9):1585–91. doi: 10.1515/cclm-2021-0339
27. Xiaojie S, Yu L, Lei Y, Guang Y, Min Q. Neutralizing Antibodies Targeting Sars-Cov-2 Spike Protein. *Stem Cell Res* (2020) 50:102125. doi: 10.1016/j.scr.2020.102125
28. Ali H, Alterki A, Sindhu S, Alahmad B, Hammad M, Al-Sabah S, et al. Robust Antibody Levels in Both Diabetic and Non-Diabetic Individuals After Bnt162b2 Mrna Covid-19 Vaccination. *Front Immunol* (2021) 12:752233. doi: 10.3389/fimmu.2021.752233
29. Ejemel M, Li Q, Hou S, Schiller ZA, Tree JA, Wallace A, et al. A Cross-Reactive Human Iga Monoclonal Antibody Blocks Sars-Cov-2 Spike-Ace2 Interaction. *Nat Commun* (2020) 11(1):4198. doi: 10.1038/s41467-020-18058-8
30. Sterlin D, Mathian A, Miyara M, Mohr A, Anna F, Claer L, et al. Iga Dominates the Early Neutralizing Antibody Response to Sars-Cov-2. *Sci Transl Med* (2021) 13(577):eabd2223. doi: 10.1126/scitranslmed.abd2223
31. Salvagno GL, Henry BM, di Piazza G, Pighi L, de Nitto S, Bragantini D, et al. Anti-Spike S1 Iga, Anti-Spike Trimeric Igg, and Anti-Spike Rbd Igg Response After Bnt162b2 Covid-19 Mrna Vaccination in Healthcare Workers. *J Med Biochem* (2021) 40(4):327–34. doi: 10.5937/jomb0-32373
32. Wisniewski AV, Campillo Luna J, Redlich CA. Human Igg and Iga Responses to Covid-19 Mrna Vaccines. *PLoS One* (2021) 16(6):e0249499. doi: 10.1371/journal.pone.0249499
33. Chan RWY, Liu S, Cheung JY, Tsun JGS, Chan KC, Chan KYY, et al. The Mucosal and Serological Immune Responses to the Novel Coronavirus (Sars-Cov-2) Vaccines. *Front Immunol* (2021) 12:744887. doi: 10.3389/fimmu.2021.744887
34. Xia S, Duan K, Zhang Y, Zhao D, Zhang H, Xie Z, et al. Effect of an Inactivated Vaccine Against Sars-Cov-2 on Safety and Immunogenicity Outcomes: Interim Analysis of 2 Randomized Clinical Trials. *JAMA* (2020) 324(10):951–60. doi: 10.1001/jama.2020.15543
35. Huang Y, Lu Y, Huang YM, Wang M, Ling W, Sui Y, et al. Obesity in Patients With Covid-19: A Systematic Review and Meta-Analysis. *Metabolism* (2020) 113:154378. doi: 10.1016/j.metabol.2020.154378
36. Lustig Y, Sapir E, Regev-Yochay G, Cohen C, Fluss R, Olmer L, et al. Bnt162b2 Covid-19 Vaccine and Correlates of Humoral Immune Responses and Dynamics: A Prospective, Single-Centre, Longitudinal Cohort Study in Health-Care Workers. *Lancet Respir Med* (2021) 9(9):999–1009. doi: 10.1016/S2213-2600(21)00220-4

**Conflict of Interest:** The authors declare that the research was conducted in the absence of any commercial or financial relationships that could be construed as a potential conflict of interest.

**Publisher's Note:** All claims expressed in this article are solely those of the authors and do not necessarily represent those of their affiliated organizations, or those of the publisher, the editors and the reviewers. Any product that may be evaluated in this article, or claim that may be made by its manufacturer, is not guaranteed or endorsed by the publisher.

Copyright © 2022 Ma, Cheng, Xue, Huang, Li, Fang, Zeng, Lin, Liang, Liang, Deng, Cheng, Huang, Wang, Niu, Li, Zheng and Sun. This is an open-access article distributed under the terms of the Creative Commons Attribution License (CC BY). The use, distribution or reproduction in other forums is permitted, provided the original author(s) and the copyright owner(s) are credited and that the original publication in this journal is cited, in accordance with accepted academic practice. No use, distribution or reproduction is permitted which does not comply with these terms.



# Duck Plague Virus Negatively Regulates IFN Signaling to Promote Virus Proliferation via JNK Signaling Pathway

Liping Wu<sup>1,2,3†</sup>, Bin Tian<sup>1,2,3†</sup>, Mingshu Wang<sup>1,2,3\*</sup>, Anchun Cheng<sup>1,2,3</sup>, Renyong Jia<sup>1,2,3</sup>, Dekang Zhu<sup>2,3</sup>, Mafeng Liu<sup>1,2,3</sup>, Qiao Yang<sup>1,2,3</sup>, Ying Wu<sup>1,2,3</sup>, Juan Huang<sup>1,2,3</sup>, XinXin Zhao<sup>1,2,3</sup>, Shun Chen<sup>1,2,3</sup>, Shaqiu Zhang<sup>1,2,3</sup>, Xumin Ou<sup>1,2,3</sup>, Sai Mao<sup>1,2,3</sup>, Qun Gao<sup>1,2,3</sup>, Di Sun<sup>1,2,3</sup>, Yanling Yu<sup>1,2,3</sup>, Ling Zhang<sup>1,2,3</sup> and LeiCHang Pan<sup>1,3</sup>

## OPEN ACCESS

### Edited by:

Chenhe Su,  
Wistar Institute, United States

### Reviewed by:

Hongyi Xin,  
National University of Singapore,  
Singapore  
Junhua Huang,  
Wuhan Polytechnic University, China

### \*Correspondence:

Mingshu Wang  
mshwang@163.com

<sup>†</sup>These authors have contributed  
equally to this work and share  
first authorship

### Specialty section:

This article was submitted to  
Viral Immunology,  
a section of the journal  
Frontiers in Immunology

Received: 04 May 2022

Accepted: 31 May 2022

Published: 28 June 2022

### Citation:

Wu L, Tian B, Wang M, Cheng A, Jia R,  
Zhu D, Liu M, Yang Q, Wu Y, Huang J,  
Zhao X, Chen S, Zhang S, Ou X,  
Mao S, Gao Q, Sun D, Yu Y, Zhang L  
and Pan L (2022) Duck Plague Virus  
Negatively Regulates IFN Signaling to  
Promote Virus Proliferation via  
JNK Signaling Pathway.  
Front. Immunol. 13:935454.  
doi: 10.3389/fimmu.2022.935454

<sup>1</sup> Institute of Preventive Veterinary Medicine, Sichuan Agricultural University, Chengdu City, China, <sup>2</sup> Key Laboratory of Animal Disease and Human Health of Sichuan Province, Sichuan Agricultural University, Chengdu City, China, <sup>3</sup> Avian Disease Research Center, College of Veterinary Medicine, Sichuan Agricultural University, Chengdu City, China

Duck plague virus (DPV), a member of the *alphaherpesvirus* subfamily, can cause severe damage and immunosuppression in ducks and geese in China. Since lacking an available cell model, the antiviral signal transduction pathways induction and regulation mechanisms related to DPV infection in duck cells are still enigmatic. Our previous study developed a monocyte/macrophages cell model, which has been applied to study innate immunity with DPV. In the present study, we compared and analyzed transcriptome associated with the DPV infection of CHv (virulent strain) and CHa (avirulent strain) at 48hpi based on the duck monocyte/macrophages cell model and RNA-seq technology. Differentially expressed genes (DEGs) analysis showed 2,909 and 2,438 genes altered in CHv and CHa infected cells compared with control cells. Gene Ontology (GO) and Kyoto Encyclopedia of Genes and Genomes (KEGG) pathway enrichment analysis showed that the DEGs were mainly involved in biological processes such as metabolic pathways, viral infectious diseases, immune system, and signal transduction. The CHv and CHa virus differentially regulated MAPK, NF- $\kappa$ B, and IFN signaling pathways based on transcriptome sequencing data and RT-qPCR results. The JNK inhibitor SP600125 enhanced the IFN signaling, but potentially reduced the VSV and DPV titers in the cell culture supernatant, indicating that JNK negatively regulates the IFN pathway and the inflammatory pathway to promote virus proliferation. The research results may provide promising information to understand the pathogenesis of DPV and provide a novel mechanism by which DPV modulates antiviral signaling and facilitate virus proliferation through hijacking the JNK pathway, which provides a new means for the prevention and control of DPV infection.

**Keywords:** duck plague virus, duck monocytes/macrophages, RNA-seq, signal transduction pathway, JNK signaling pathway

## INTRODUCTION

Duck plague (also known as duck viral enteritis) was initially identified in 1957 in China by Yinxian Huang and is now prevalent in many duck-raising places worldwide (1). Duck plague is an acute, contagious, septic infectious disease among waterfowl (ducks, geese, swans of all ages and species) with high morbidity and mortality, and is a major hazard to the waterfowl industry (2). The DP causative agent, duck plague virus (DPV) or duck enteritis virus (DEV), is a member of the subfamily *Alphaherpesvirinae*, whose genome consists of a linear double-stranded DNA, including a unique long region (UL), a unique short region (US), terminal short repeats (TR) and internal short repeats (IR), forming the genomic structure of UL-IRS-US-TRS (3). DPV Chinese virulent (CH virulent, CHv) strain, isolated from dead infected ducks in China, is highly pathogenic and could cause massive spotting hemorrhages in parenchymal organs, lymphoid and digestive tract, resulting in massive mortality of ducks (4–6). Immunization with DPV attenuated strain (CHa) is one of the most effective measures to control DP (7). Studies on DPV have been carried out for many years. However, the signaling pathways and antiviral mechanisms related to the infection of host cells by CHv strain and CHa strain are still unclear.

Cell signal transduction pathways regulate cell growth, cell survival, apoptosis, and immune responses. Mitogen-activated protein kinase (MAPK) cascades are crucial intracellular signaling pathways and transmit signals from the cell membrane to the nucleus, which is activated by a series of extracellular and intracellular stimuli, including growth factors, virus infection, bacterial complexes, cytokines, and various cellular stressors (8–10). MAPKs are involved in the cell survival stage, regulating intracellular metabolism, cell differentiation, gene expression, and integral activities in diverse cellular processes (11, 12). MAPK kinase kinases (MKKKs) activate MAPK kinases (MKKs) which in turn activate and phosphorylate MAPKs (13). Three major groups in the MAPKs cascades, such as p38, extracellular signal-regulated protein kinases (ERK), and c-Jun N-terminal kinases (JNK, also called stress-activated protein kinase/SAPK) (14).

Viruses can resort to modulating and hijacking the cellular signaling transduction pathways for efficient replication (15). For instance, HSV-1 infection stimulated PI3K/AKT and ERK MAPK signaling pathways that in turn contributed to KSHV reactivation (16); ERK activation mediated by KSHV virion enhances viral gene expression (17); HCV infection triggers TAB1-dependent p38 activation, which in turn phosphorylates the HCV core protein to promote HCV replication (18); FMDV infection induces the activation of MAPK signaling cascades, and inhibition of MAPK signaling pathway by MAPK pathway-specific inhibitor U1026 significantly impaired FMDV replication (19). However, little is known about the role of the MAPK signal pathway in DPV pathogenesis in duck cells.

In the present study, we applied the RNA-Seq method to analyze and compare the gene expression patterns in duck monocytes/macrophages infected by CHv strain and CHa strain at the late infection phase. The DEGs were mainly involved in biological processes such as metabolic pathways, viral infectious diseases, immune system, and signal transduction. We found that the

MAPK inflammatory signaling pathway was significantly activated by CHv strain and CHa strain. Unexpectedly, the JNK inhibitor SP600125 significantly enhanced the IFN signaling under VSV and DPV infection, but potentially inhibited the replication of VSV and DPV, indicating that JNK negatively regulates the IFN pathway and the inflammatory pathway to promote virus proliferation. Our data suggested that JNK signaling is a promising target for DPV control. These results may provide information that will increase our understanding of DPV pathogenesis and the mechanisms underlying virus-host interactions.

## MATERIALS AND METHODS

### Ethics Statement

All animal experiments were performed following approved guidelines. One-month-old Peking ducklings were conducted from a DPV-free farm, where vaccination against DPV was not implemented. All the ducks were housed in the animal facility at Sichuan Agricultural University in Chengdu, China. This study was approved by the Experimental Procedures and Animal Welfare Committee of Sichuan Agricultural University (approval permit number SYXK 2019-187).

### Cells, Virus Stains, and Reagents

Duck embryo fibroblast (DEF) cells were obtained from 9-day-old duck embryos. DEF and baby hamster kidney (BHK21) cells were cultured in Dulbecco's Modified Eagle Medium (DMEM) (Gibco Life Technologies, Shanghai, China) supplemented with 10% fetal bovine serum (FBS; Gibco, USA) and 1% penicillin-streptomycin. Duck monocytes/macrophages were isolated, cultured, and identified as described earlier (20). Briefly, duck PBMCs were isolated using the Duck Leukocyte Isolation Kit (TBD science, Tianjin, China), plated on cell culture plates for 2 h, washed three times with PBS to remove non-adherent cells, and cells were digested with trypsin for cell counting. Duck monocyte-derived macrophages were differentiated from adherent monocytes in RPMI 1640 medium supplemented with l -glutamine (2 mM), sodium pyruvate (1 mM), 10% heat-inactivated fetal bovine serum, 1% penicillin-streptomycin and 50 ng/ml human M-CSF (Novo protein, Shanghai, China). The medium was changed every two days and the duck macrophages formed a monolayer on day 7. All cells were incubated at 37°C in a 5% CO<sub>2</sub> humidified incubator.

Highly virulence DPV CHv strain, attenuated modified vaccine DPV CHa strain and the recombinant VSV strain harboring GFP (VSV-GFP) were obtained from the Key Laboratory of Animal Disease and Human Health of Sichuan Province. DPV strains were propagated and titrated on DEFs. VSV-GFP was propagated and titrated on BHK21.

SP600125 (c-Jun NH<sub>2</sub>-terminal kinase [JNK] inhibitor, purity 99.55%), LY3214996 (extracellular signal-regulated kinase [ERK] inhibitor, purity 99.85%), TAK-715 (p38 inhibitor, purity 99.89%), BAY-11-7802 (NF-κB inhibitor, purity 99.98%), and Ruxolitinib (interferon receptor inhibitor)

were purchased from MedChemExpress (Monmouth Junction, NJ). All inhibitors were diluted in dimethyl sulfoxide (DMSO).

## RNA Extraction, Library Construction and Illumina Sequencing

Total RNA was extracted from samples stored in the RNastore using TRIzol reagent (Invitrogen Corporation, Carlsbad, CA, USA) following the manufacturer's protocol. Total RNA was characterized and quantified using a Nano Drop and Agilent 2100 bioanalyzer (Thermo Fisher Scientific, MA, USA). Oligo (dT)-adhered magnetic beads were used to purify mRNA, and then fragmented with fragment buffer. cDNA was synthesized using the fragmented mRNA as a template, and the A-Tailing mix was added after repairing the end and connected with the RNA Index Adapters to construct the final library. Then the library was sequenced on the BGISEQ500 platform (BGI-Shenzhen, China) to obtain 100 base paired-end reads.

## GO and KEGG Enrichment Analysis

All DEGs were annotated with GO and KEGG analysis. Gene ontology (GO) enrichment analysis of differentially expressed genes was implemented by the Goseq R package, in which gene length bias was corrected. KEGG is a database for understanding systematic gene function analysis and genomic information. The significant levels of terms and pathways were selected with a *P*-value of less than 0.05.

## Real-Time Quantitative PCR

Isolation of total RNA from cells at different time points using Trizol reagent. All RNA samples' purity was detected by analyzing the A260/A280 ratio using a Nano drop ND-1000 spectrophotometer (Nano drop Technologies), which was expected to be 1.8~2.0. Total RNAs were reverse transcribed into cDNA with the ReverTra Ace qPCR RT Kit (Toyobo, Osaka, Japan); RT-qPCR was performed primarily according to a previous method (21). Target genes were detected using the previously described primers. All reactions were performed in triplicate and in at least three independent experiments. The relative levels of gene expression were determined with the  $2^{-\Delta\Delta Ct}$  method. All primer sequences are listed in **Table 1**.

## Virus Infection and Determination of Fluorescence Formation Units and Tissue Culture Infectious Dose 50

The required dose of virus was diluted in the medium used to culture the various cell types for viral infection. The culture

medium was removed after incubation for 1 h at 37°C in 5% CO<sub>2</sub>. The cells were washed twice with PBS and then maintained in the corresponding medium containing 1% FBS and 1% penicillin-streptomycin. The culture supernatant of virus-infected cells was collected and titrated to determine the tissue culture infectious dose 50 (TCID<sub>50</sub>) on DEFs for DPV, or FFU on BHK21 for VSV-GFP.

## Cytotoxicity Assay

DEF cells were treated with different concentrations of each inhibitor or the solvent DMSO for 24 h and the cell viability of DEF cells was determined with a Cell Titer 96 Non-Radioactive Cell Proliferation Assay kit (MTT, Promega Corp., Madison, WI).

## Antiviral Activity Assay

Cells were first treated with different concentrations of the inhibitors SP600125 (10 μmol/mL), LY3214996 (5 μmol/mL), TAK-715 (5 μmol/mL), BAY-117082 (5 μmol/mL), and Ruxolitinib (10 μmol/mL) at 37°C for 1 h, the cells were washed three times with PBS. The same doses of viruses DPV (CHv strain), DPV (CHa strain) or VSV-GFP were incubated with cells at 37°C for 1h, washed three times with PBS, and then treated with different concentrations of inhibitors SP600125, LY3214996, TAK -715, BAY-117082. Cell supernatants were collected for TCID<sub>50</sub> or FFU assay. GFP expression was detected under fluorescence microscopy to observe VSV-GFP and DPV virus plaque formation.

## Statistical Analysis

Data are expressed as the mean and standard error of the mean (SEM), and the significance of differences between groups was evaluated using the students' t-test or one-way analysis of variance followed by Tukey's *post-hoc* test. Results with \**P* < 0.05, \*\**P* < 0.01, \*\*\**P* < 0.001, and \*\*\*\**P* < 0.0001 were considered to be statistically significant.

## RESULTS

### Significantly Differentially Expressed Genes After CHv and CHa Infection

The second-generation sequencing RNA-seq has been widely used in oncology, immunology, and cell biology in recent years (22, 23). To clarify the differences in gene expression in the duck immune cells, we applied the RNA-seq transcriptome

**TABLE 1** | Primers for RT-qPCR analysis of gene expression.

Target Gene	Forward primer sequence	Reverse primer sequence	Accession no.
IL-6	TTCGACGAGGAGAAATGCTT	CCTTATCGTCGTTGCCAGAT	XM_013100522.2
IL-1β	AAAACGCTCTTCGTGCTGTC	CTCCTGCTGCTCTTCTCTCAC	DQ393268
IFN-β	TCTACAGAGCCTTGCCTGCAT	TGTCGGTGTCCAAAAGGATGT	KM035791.2
MX	TGCTGTCTTCATGACTTCG	GCTTTGCTGAGCCGATTAAC	NM_001310409.1
OASL	AGTTTGACATTGCCAGTCC	TCCTCCTCGTGATTCCATTT	KY775584
CCL21	GGAGAAGCAGAAGAACCCTC	GGGAAAGCATCCGTCCTCTC	DR764376
β-actin	GCCTCTTCCAGCCATCTTT	CTTCTGCATCCTGTCAGCGA	EF667345.1



sequencing technology to analyze the gene expression differences in the duck monocytes/macrophages cell model infected with DPV CHv strain or CHa strain at 48 hpi.

611 million read number or read counts were generated from nine samples. To ensure ideal results for subsequent genomic mapping and differential gene change analysis, raw reads were filtered to remove low-quality data, resulting in a total of 574 million (574 660 000) clean reads, achieving high-quality eukaryotic transcriptome reconstructions of the standard, an average of 53.13% of which mapped to the duck reference genome (Table 2). The raw sequencing data of the control group, CHv infected group and CHa infection group have been deposited into the Short Reads Archive (SRA) database under the accession numbers, SRR18825687, SRR18825689 and SRR18825688, respectively.

The heat map visually compares the overall level of differential expression genes (DEGs), as shown in Figure 1A, the regulation of gene expression was at a completely different level in the CHv strain infection, CHa strain infection, or control groups. By Venn analysis the DEGs were further divided into three main parts (Figure 1B). There are 1438 DE genes in the green part representing the number of genes expressed only in CHv infected cells, while the red part has 967 DEGs that are expressed only in CHa infected cells. Compared with the control group, the intersection part with 1471 DE genes was co-expressed in CHv and CHa infected groups.

To comprehensively understand the changes in gene expression between different treatment groups, we performed three pairwise comparisons (Mock vs. CHa, Mock vs. CHv, CHv vs. CHa). DEGs were identified by  $p$ -value  $< 0.05$  (Figure 1C). There were 2,438 DEGs significantly differentially expressed in Mock vs. CHa, which include 2,239 up-regulated genes and 199 down-regulated genes. Among 2,909 DEGs in Mock vs. CHv group, the up-regulated genes were 2,468 and the down-regulated genes were 441. Moreover, there were 1,399 DEGs in CHv vs. CHa group, among which 858 were up-regulated genes and 541 were downregulated genes. At 48 hpi, DEGs were associated with innate immune and inflammatory responses and may play an important role in the host's defense response to DPV infection. Furthermore, these results cluster the samples by differential processing and are visible by constructing volcano plots of DEGs.

## Analysis of GO Annotation and KEGG Pathway

To confirm which biological processes were involved in DPV infection and those that were unidentified previously, the collected DEGs were categorized into three functional groups according to Gene Ontology (GO): Cellular Composition (CC), Molecular Function (MF) and Biological Process (BP). The GO analysis and enrichment results of the transcripts from the 3 groups were similar (Supplementary Figures S1A–C). To select useful genes for further exploration, 30 significant GO terms were listed (Figures 2A–C). Functional analysis showed that the top three important GO terms for DEGs expressed in CHa strain infected at 48hpi were intrinsic component of membrane, stimulus responsiveness, and molecular function regulator; The top three important GO terms of DEGs expressed in CHv infected were membrane part, an integral component of the membrane and intrinsic component of membrane. The top three important GO terms for DEGs expressed in both the CHa infected group and the CHv infected group were stimulus responsiveness, integral membrane component, and intrinsic membrane component.

The KEGG database is used for pathway-based classification of orthologous genes, providing useful information for predicting genes' biological processes and phenotypic characteristics (24). The KEGG database was used to map DEGs to reference canonical signaling pathways in monocytes/macrophages after infection with DPV strains. The results showed that DEGs were mainly related to metabolism, viral infectious diseases, endocrine system, immune system, transcription, replication repair, and signaling transduction (Supplementary Figures S2A–C).

Next, to deeply investigate the functions of these DEGs, KEGG pathway/enrichment analysis was performed. As shown in Figures 3A–C, the top 20 enriched KEGG pathways are listed based on  $P < 0.05$ . The DEGs identified in the uninfected and DPV CHa strain-infected groups were mainly involved in cytokine-cytokine receptor interaction, Toll-like receptor signaling pathway, inflammatory bowel disease, and TNF signaling pathway. The DEGs identified in the uninfected and DPV CHv-infected groups mainly involved interactions between neuroactive ligands and receptors, protein digestion and absorption, interactions between cytokines and cytokine

**TABLE 2** | The number of reads of all bases detected using RNA-seq in DPV-infected and control cells.

Library	Number of raw reads (M)	Total Clean reads (M)	Number of uniquely mapped reads (M)	Uniquely Mapping (%)
CHa-1	67.68	63.73	36.587393	57.41
CHa-2	67.68	63.73	36.561901	57.37
CHa-3	67.68	63.66	36.496278	57.33
CHv-1	67.68	63.28	24.691856	39.02
CHv-2	67.68	63.52	25.719248	40.49
CHv-3	67.68	63.31	25.621557	40.47
Mock-1	67.56	63.85	39.49761	61.86
Mock-2	70.19	65.91	40.409421	61.31
Mock-3	67.68	63.67	39.742814	62.42
Total	611.51	574.66	305.328078	

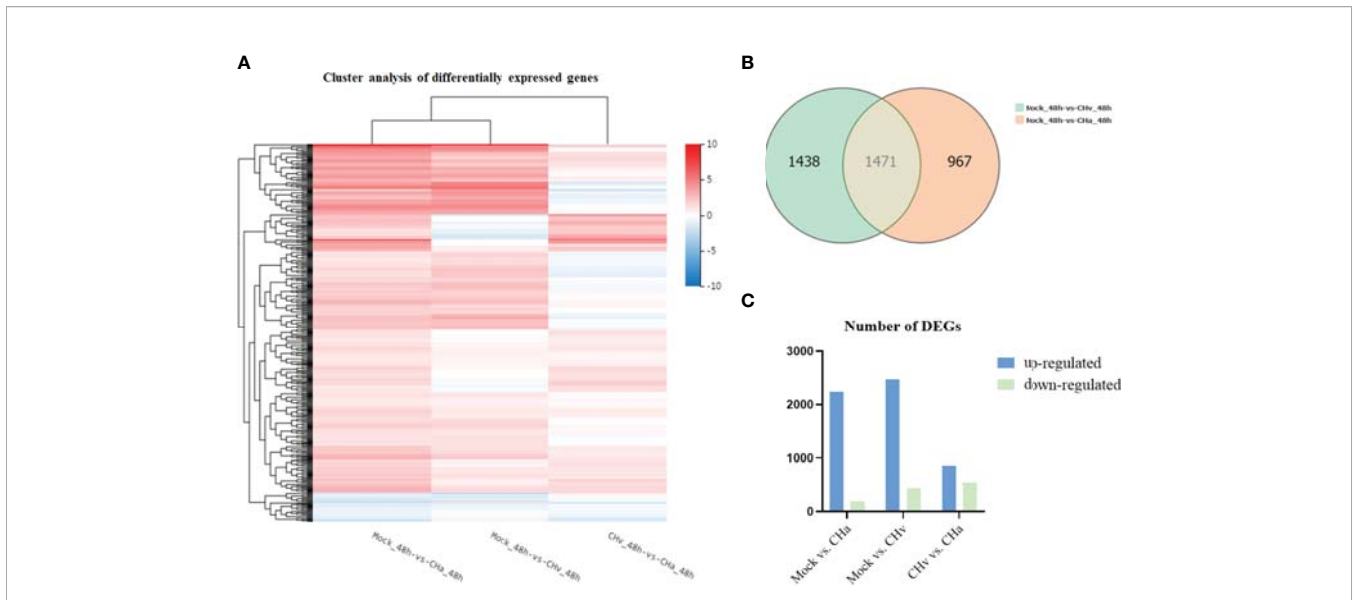


**FIGURE 1** | Transcriptome data profile generated by BGIseq-500 platform and differential expression analysis. **(A)** Heat map analysis is used to classify gene expression patterns at 48 hpi. Genes with similar expression patterns were clustered, as shown in the heat map. To intensity of the color indicates gene expression levels that were normalized according to log10 (FPKM + 1) values. Red represents high expression level genes and blue represents low expression level genes. **(B)** Venn diagram displaying a global view of the numbers of differentially expressed genes. The overlap of differentially expressed genes at 48hpi Mock vs. CHa and Mock vs. CHv. The numbers in the diagram indicate gene numbers and refer to each comparison. **(C)** Histogram showing screened differentially expressed genes.

receptors, and interactions between ECM and receptors. However, the DEGs identified in CHa and CHv infection groups mainly involved cytokine-cytokine receptor interaction, PI3K-AKT pathway, ECM-receptor interaction, and JAK-STAT signaling pathway. Here, we listed the signaling pathways associated with infection with DPV in the transcriptome of duck monocyte/macrophage cell models (**Table 3**). We found that DPV virus-infected cells significantly activated MAPK and NF-kappa B signaling pathways in host cells. This finding suggests that viruses and host cells utilize different strategies that may be involved in DPV infection-induced pathogenesis.

### Viruses Induced the Expression of Cytokine in Host Cells

It was reported that cytokines are key modulators of inflammation, participating in acute and chronic inflammation *via* a complex and sometimes seemingly contradictory network

of interactions (25). To determine whether DPV infection induces cytokine expression in host cells, we infected duck monocyte/macrophage cells with CHa virulent strain at 5 MOI and examined the mRNA expression of IL-1 $\beta$ , IL-6, CCL21, IFN- $\beta$ , MX, and OASL at 24 hpi. We found the expression of inflammatory cytokines IL-1 $\beta$ , IL-6, CCL21, type I interferon  $\beta$  (IFN- $\beta$ ), and interferon-stimulated genes (ISGs) MX and OASL were upregulated in CHa strain infected monocyte/macrophage cells (**Figure 4D**). Vesicular stomatitis virus (VSV) is a prototypical enveloped animal virus that has been widely explored as a virus model to assess the antiviral activity of IFN due to its broad host range and robust replication properties in a variety of mammalian and insect cells (26). Here, we found that the expression of IL-1 $\beta$ , IFN- $\beta$  and OASL was significantly induced in VSV infected monocytes/macrophage cells (**Figure 4B**). In addition, similar results were obtained when duck embryo fibroblasts (DEFs) were infected with CHa strain or

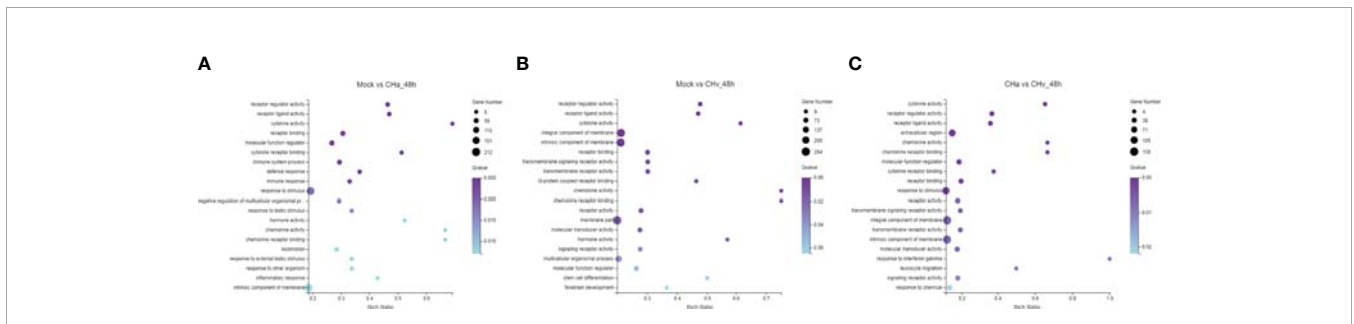


**FIGURE 2** | Top 20 Gene ontology (GO) terms of DEGs expressed in DPV CHv or CHa infected MM cells. The top 20 GO terms were selected according to *p* -value < 0.05. **(A)** Mock and CHa. **(B)** Mock and CHv. **(C)** CHa and CHv.

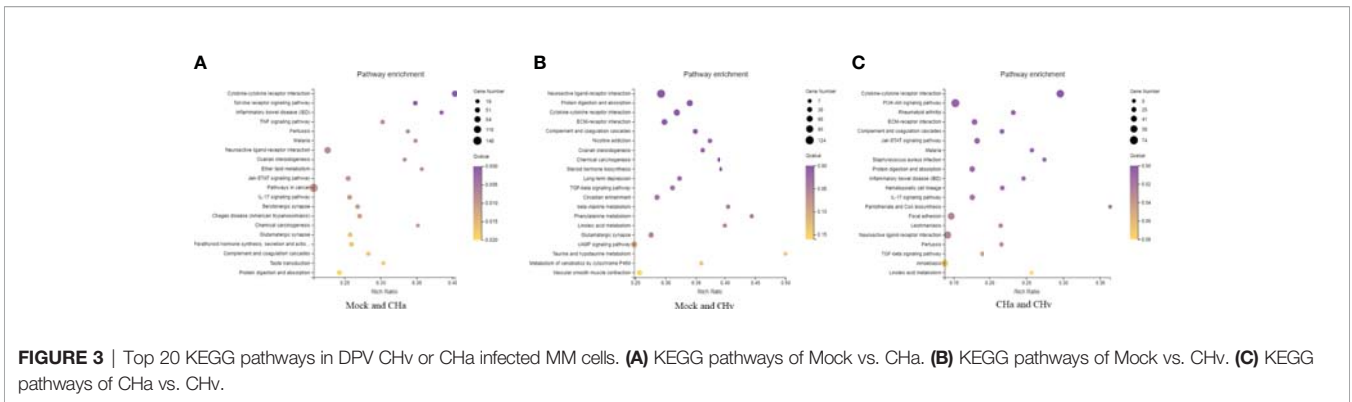


**FIGURE 3** | Top 20 KEGG pathways in DPV CHv or CHa infected MM cells. **(A)** KEGG pathways of Mock vs. CHa. **(B)** KEGG pathways of Mock vs. CHv. **(C)** KEGG pathways of CHa vs. CHv.

VSV at the 5 MOI (**Figures 4A, C**). These results demonstrated that CHa induces the production of inflammatory cytokines, type I interferons, and ISGs in duck cells.

### Inflammatory Pathways Are Involved in Viral Induction of Cytokines

Pattern recognition receptors (PRRs) that sense pathogen-associated molecular patterns, are responsible for recognizing invading viruses, and then initiating antiviral innate immune responses. Following the engagement of these PRRs, type I and III interferons (IFN), chemokines and proinflammatory cytokines are produced to activate inflammation (27). The above results indicate that DPV virus-infected cells significantly activate the MAPK and NF-kappa B signaling pathways in host cells.

To testify that MAPK and NF-kB pathways impact virus infection of duck cells, we compared cytokine transcriptional levels after blocking of JNK, ERK, p38, and NF-kB pathways with specific inhibitors. Firstly, the duck monocytes/macrophages

were pretreated with SP600125 (JNK inhibitor, 10 μmol/mL), LY3214996 (ERK inhibitor, 5 μmol/mL), TAK-715 (p38 inhibitor, 5 μmol/mL), BAY-11-7802 (NF-KB inhibitor, 5 μmol/mL), or solvent DMSO for 1 h, and then infected with 5 MOI of the CHa strain for another 1 h, after infection the cells were washed with PBS and the same concentration of each inhibitor was added. Cell samples were harvested at 24 hpi, and the transcript levels of cytokines were detected by RT-qPCR. We observed that SP600125 promoted the expression levels of IL-6, CCL21, IFN-β, MX, and OASL, but the expression level of IL-1β decreased in DEF cells in the presence of CHa strain infection (**Figures 5A–F**). In monocytes or macrophages, SP600125 treatment also promoted the expression levels of IFN-β, MX, and OASL, but not CCL21, under CHa strain infection (**Figures 6A–F**). However, the expression levels of IL-1β and IL-6 were decreased by SP600125 treatment in monocytes or macrophages in the presence of CHa strain infection.

Next, the same experiment was performed with the VSV-GFP model virus at the same MOI. We found that four pathway

**TABLE 3** | Associated with signal transduction in the transcriptome of duck monocytes or macrophages infected with DPV at 48hpi.

Description	P-value	Corrected P-value	Number of DEG
<b>DPV CHv vs. MOCK</b>			
PI3K-Akt signaling pathway	0.05175328	0.4983102	104
cAMP signaling pathway	0.004924622	0.09762339	67
MAPK signaling pathway	0.3974499	0.979198	67
Rap1 signaling pathway	0.2252467	0.8162165	65
Jak-STAT signaling pathway	0.7118586	0.9999972	35
TGF-beta signaling pathway	0.001056776	0.03237577	33
TNF signaling pathway	0.3560591	0.9523168	22
Phosphatidylinositol signaling system	0.9378876	0.9999972	19
NF-kappa B signaling pathway	0.7776547	0.9999972	18
mTOR signaling pathway	0.9999857	0.9999972	16
<b>DPV CHa vs. MOCK</b>			
PI3K-Akt signaling pathway	0.00765817	0.0647999	98
MAPK signaling pathway	0.002785986	0.03405094	76
Rap1 signaling pathway	0.01756472	0.1114684	66
Jak-STAT signaling pathway	0.000293616	0.00950868	52
cAMP signaling pathway	0.08399132	0.3079682	52
TNF signaling pathway	0.00013179	0.007467114	33
TGF-beta signaling pathway	0.007921306	0.06535077	27
NF-kappa B signaling pathway	0.01656176	0.1114684	27
mTOR signaling pathway	0.9960666	1	19
Phosphatidylinositol signaling system	0.9810913	1	14

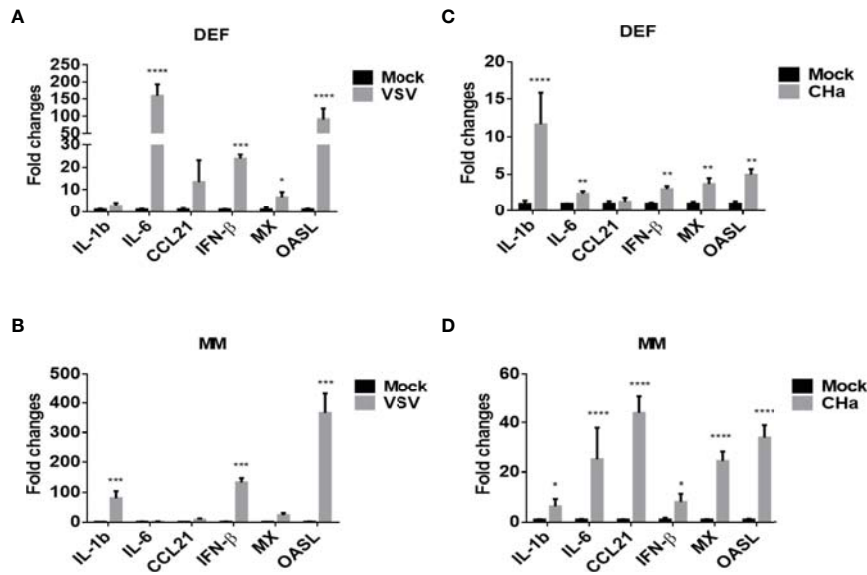


**FIGURE 4** | VSV and DPV CHa strain-induced IFN, ISGs and cytokines in duck DEF and MM cells. DEF cells were infected with VSV (A) or DPV CHa strain (C) at 5 MOI for 24 h. MM cells were infected with VSV (B) or DPV CHa strain (D) at 5 MOI for 24 h. The expression level of IL-1 $\beta$ , IL-6, CCL21, IFN- $\beta$ , MX and OASL were tested using RT-qPCR 24 h post-treatment. The relative expression was presented as fold changes compared to mock treatment. “\*” was considered significant difference ( $p < 0.05$ ); “\*\*” was considered highly significant difference ( $p < 0.01$ ); “\*\*\*” was considered highly significant difference ( $p < 0.001$ ); “\*\*\*\*” was considered highly significant difference ( $p < 0.0001$ ).

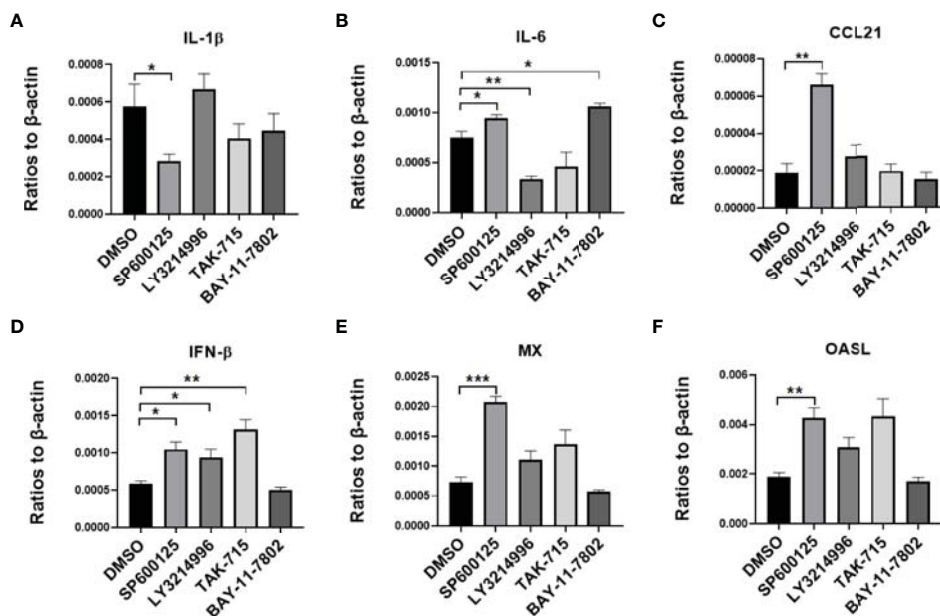


**FIGURE 5** | IFN, ISGs, and cytokines were regulated by inflammatory signaling in duck DEF cells infected with the CHa strain. DEF cells were pretreated with SP600125 (JNK inhibitor), LY3214996 (ERK inhibitor), TAK-715 (p38 inhibitor) and BAY-117802 (NF- $\kappa$ B inhibitor) for 1 h at 10, 5, 5 and 5  $\mu$ M respectively, DMSO as control, then the cells were infected with CHa strain at 5 MOI for 1 h, then the same concentration of inhibitor was added. The expression level of IL-1 $\beta$  (A), IL-6 (B), CCL21 (C), IFN- $\beta$  (D), MX (E), and OASL (F) were tested using RT-qPCR 24 h post-treatment. The relative expression was presented as ratios to  $\beta$ -actin compared to mock treatment. “\*” was considered significant difference ( $p < 0.05$ ); “\*\*” was considered highly significant difference ( $p < 0.01$ ); “\*\*\*” was considered highly significant difference ( $p < 0.001$ ).

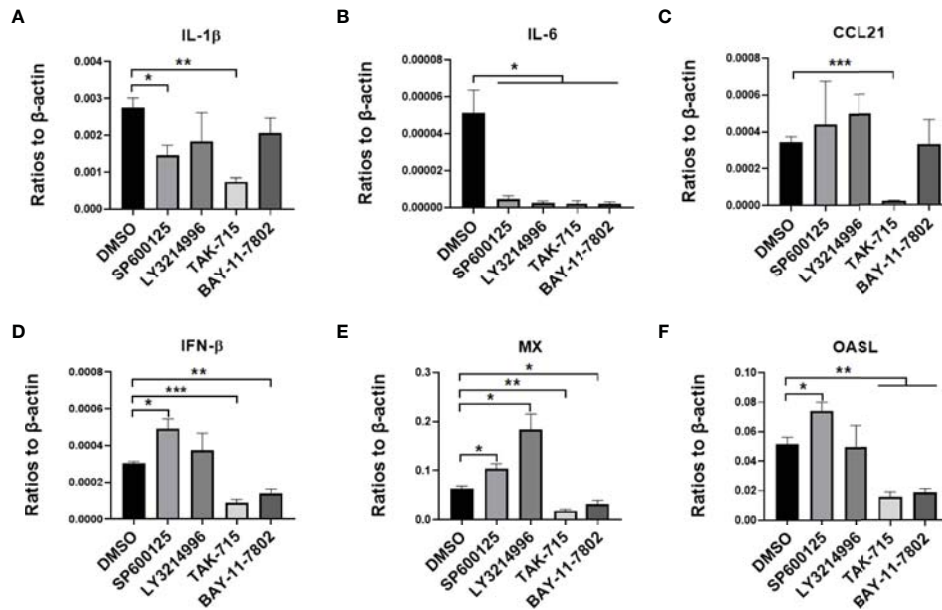


**FIGURE 6** | IFN, ISGs, and cytokines were regulated by inflammatory signaling in duck MM cells infected with the CHa strain. MM were pretreated with SP600125 (JNK inhibitor), LY3214996 (ERK inhibitor), TAK-715 (p38 inhibitor) and BAY-117082 (NF-κB inhibitor) for 1 h at 10, 5, 5 and 5 μM respectively, DMSO as control, then the cells were infected with CHa strain at 5 MOI for 1 h, then the same concentration of inhibitor was added. The expression level of IL-1β (A), IL-6 (B), CCL21 (C), IFN-β (D), MX (E), and OASL (F) were tested using RT-qPCR 24 h post-treatment. The relative expression was presented as ratios to β-actin compared to mock treatment. “\*” was considered significant difference ( $p < 0.05$ ); “\*\*” was considered highly significant difference ( $p < 0.01$ ); “\*\*\*” was considered highly significant difference ( $p < 0.001$ ).

inhibitors reduced the expression level of IL-1β, but not IL-6 or CCL21, in duck monocytes/macrophages (**Supplementary Figures S3A–C**). Besides, we observed that the expression levels of IFN-β, MX, and OASL expression levels were promoted by SP600125 treatment in duck monocytes/macrophages and VSV infection (**Supplementary Figures S3D–F**). Similar results were observed in DEF cells (**Supplementary Figures S4A–F**). Thus, we proposed that SP600125 may promote IFN signaling in cells in the context of viral infection. Altogether, these data demonstrated that the JNK, ERK, p38 and NF-κB pathways all regulate intracellular cytokines in the case of virus infection in duck cells. Interestingly, virus-induced cytokine expression was significantly enhanced in different cell types treated with SP600125. These results suggest that SP600125 strengthens the anti-viral responses of host cells.

### SP600125 Inhibits DPV CHv Infection in Different Duck Cell Types

Cytokines play an important role in the antiviral response of host cells. Firstly, the cell viability was detected with an MTT assay after the cells were treated with different doses of SP600125, LY3214996, TAK-715 or BAY117082. That data showed no obvious cell death induced by these four inhibitors (**Figure 7A**). Therefore, the antiviral ability of SP600125 is independent of cell death.

The above results showed that SP600125 treatment significantly promotes cytokine expression, which implied that SP600125 treatment may inhibit the growth of the virus in different types of cells. To clarify this hypothesis, cells were

infected with DPV at 1 MOI, with or without the addition of SP600125, LY3214996, TAK-715, BAY-11-7802, or DMSO. The viral load in the cell culture supernatants was measured at 24 hpi. As shown in **Figures 7B–D**, the viral load in the supernatant was significantly reduced after SP600125 treatment compared to the DMSO controls, indicating that SP600125 treatment restricted the growth of VSV-GFP and CHv strain in DEF cells but did not affect the growth of CHa strain. Subsequently, we observed that the viral load in the supernatant was significantly reduced after SP600125 treatment compared to the DMSO controls, indicating that SP600125 restricted the growth of CHv, but not CHa in monocytes/macrophages (**Figures 7E–F**). Altogether, these data suggest that the JNK pathway plays a role in VSV and DPV infection in duck cells.

### SP600125 Enhances IFN and IFN-Stimulated Gene (ISG) Expression, but Inhibits Inflammatory Responses in DPV-Infected DEF Cells

We focused on the antiviral mechanism of SP600125 in duck cells. We further examined the modulation of IFN signaling under CHa strain or CHv strain infection and combined with SP600125 treatment. Since SP600125 inhibited DPV infection, we infected DEF cells with 5 MOI of CHa strain or CHv strain for 1 h, and SP600125 was added to treat cells for 6 or 24 h. The transcription levels of cytokines IL-1β, IL-6, CCL21, IFN-β, MX and OASL were detected at 6h and 24h. Since DPV infection causes obvious cellular lesions and changes the expression level

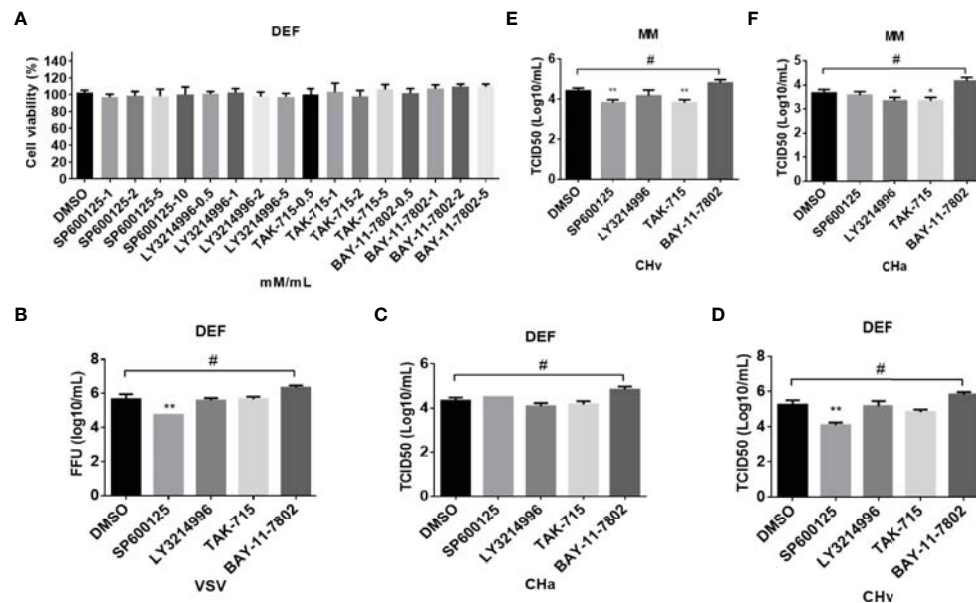


**FIGURE 7** | The inflammatory signaling affects virus replication in DEF and MM cells. **(A)** The cell toxicity of the JNK, ERK, p38, and NF- $\kappa$ B inhibitor was determined through MTT. **(B–F)** The viral titer was detected. DEF cells were pretreated with SP600125 (JNK inhibitor), LY3214996 (ERK inhibitor), TAK-715 (p38 inhibitor) and BAY-117802 (NF- $\kappa$ B inhibitor) for 1 h at 10, 5, 5, and 5 M respectively, DMSO as control, then the cells were infected with VSV **(B)**, CHv **(C, E)** and CHa strain **(D, F)** at 1 MOI for 1 h, then the same concentration of inhibitor was added. At 24 hpi, the cell culture supernatants were collected and the FFU of VSV-GFP and the TCID50 of CHa or CHv were determined on BHK21 or DEF cells. \*\*\*\* was considered significant difference ( $p < 0.05$ ); \*\*\*\*\* was considered highly significant difference ( $p < 0.01$ ). \*\*\*\* indicates significantly down-regulated group compared to DMSO group, # indicates up-regulated group compared to DMSO group.

of the housekeeping genes, so we chose the Cq value to make the map. As shown in **Figures 8A–F**, the IFN- $\beta$  level was reduced in CHv strain infection cells. However, the SP600125 treatment reversed this phenomenon of IFN- $\beta$  at the late time point of CHv infection, indicating that inhibiting the activation of the JNK pathway will be beneficial to the regulation of the IFN signaling pathway under virus infection.

Next, we explored the impact of the JNK pathway on viral replication. Here we applied the IFNR-specific inhibitor Ruxolitinib to block IFN signaling in DEF cells to examine the specificity of the effect of JNK pathway inhibitors on viral replication. Under these conditions, we found that VSV and CHv strain replication in DEF cells was inhibited in SP600125-treated cells, but virus titers were recovered in SP600125 and Ruxolitinib combination treatment cells (**Figures 8G, I**). We also found that Ruxolitinib alone promoted the replication of the CHa virus, while SP600125 alone did not affect on the replication of CHa vaccination (**Figure 8H**). In conclusion, our results suggest that SP600125 acts as an antiviral inhibitor in host cells against DPV CHv virulent strain by inhibiting the JNK MAPK signaling pathway to enhance the expression of type I interferon.

## DISCUSSION

Duck plague, caused by duck plague virus (DPV), is an acute hemorrhagic disease that causes huge economic losses to the poultry industry worldwide due to reduced egg production and

high mortality in infected ducks (28). Therefore, deepening the understanding of the molecular mechanisms of the host-pathogen interaction is of great significance in suppressing the occurrence and prevalence of DPV infection. In recent years, RNA-Seq technology has become a powerful tool that provides high-resolution expression and high-sensitivity measurements when detecting low-abundance transcripts, and has also been used to determine the mechanism of action of DPV (29–31). However, there is no assay executed in duck immune cells which is unavailable before. The previous study successfully established the duck monocyte/macrophages models for duck pathogenesis research (20). RNA-Seq was used to study molecular expression profiles in the monocytes/macrophages and further to gain insight into the immune response patterns of DPV.

Raw reads were filtered to remove low-quality data, coming with 574 million clean reads. DEGs were classified and annotated by GO and KEGG signaling pathway analysis. By comparing the transcriptome data of the libraries, the results showed that most of the DEGs were associated with cytokine-cytokine receptors, the immune system and signal transduction. At 48hpi, the regulation of the MAPK signaling pathway (CHv: 67 genes, CHa: 76 genes) and the NF- $\kappa$ B signaling pathway (CHv: 18 genes, CHa: 27 genes) were affected, implying an alteration of the inflammatory response (**Table 3**).

Excessive inflammation is becoming a critical factor in many viral infectious diseases. MAPKs are important regulators for inflammatory cytokine and chemokine expression (32, 33). Cytokines are a class of small molecular weight soluble

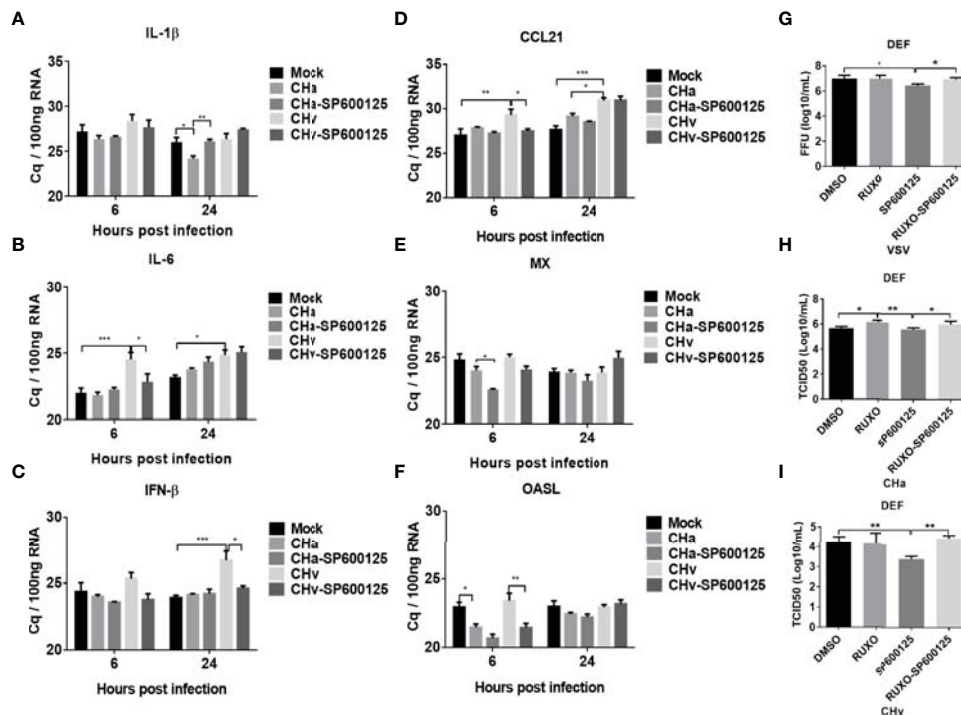


**FIGURE 8** | JNK signaling regulates IFN signaling and virus replication. The inflammatory signaling affects virus replication in DEF cells. **(A-F)** DEF cells were pretreated with SP600125 (JNK inhibitor) for 1 h at 10  $\mu$ M, DMSO as control, then the cells were infected with CHa or CHv strain at 5 MOI for 1 h, then the same concentration of inhibitor was added. The expression level of IL-1 $\beta$ , IL-6, CCL21, IFN- $\beta$ , MX, and OASL were tested using RT-qPCR at 6 and 24 h post-treatment. The relative expression was presented as Cq values compared to mock treatment. **(G-I)** The DEF cells were pretreated with SP600125 (JNK inhibitor) and (or) Ruxolitinib (IFN $\alpha$  inhibitor) for 1 h at 10  $\mu$ M, then the cells were infected with VSV, CHa or CHv strain at 1 MOI for 1 h, then the same concentration of inhibitor was added. The cell culture supernatant was collected and the viral titer was determined on DEF cells. “\*” was considered significant difference ( $p < 0.05$ ); “\*\*\*” was considered highly significant difference ( $p < 0.01$ ); “\*\*\*\*” was considered highly significant difference ( $p < 0.001$ ).

glycoproteins or protein polypeptides that are stimulated and secreted by immune cells and some non-immune cells, and play critical roles in many cellular biological processes (34). From the results of the KEGG analysis in this study, we found that the expression of many important cytokines and cytokine receptor genes, CHv-infected and CHa-infected groups. Viral infection usually induces the expression of interferons, interferon-stimulating factors, chemokines and cytokines. Excessive expression of such proteins may have irreversible effects on the host (35). For instance, this “cytokine storm” can lead to severe pathological damage and high mortality (36, 37). Our results showed that the transcript levels of IL-1 $\beta$ , IL-6, CCL21, IFN- $\beta$ , MX and OASL in DPV CHa strain-infected monocytes/macrophages were 2-40-fold higher than those in the mock-infected group, while the transcript levels of IFN- $\beta$  and OASL in VSV virus-infected monocytes/macrophages were 80-300-fold higher than those in the mock-infected group. In addition, similar results were obtained when duck embryo fibroblasts were infected with CHa strain or VSV virus at the same MOI. These results suggested that cytokines play an important role in host responses against the infection of CHa strain or VSV.

Viruses usually modulate the immune system of host cells in the early or middle stage of infection, when most of the signaling pathways are activated by the cells to fight the invading pathogen

(38). Therefore, we mainly analyzed the influence of DPV invasion on the signaling pathway in host cells at 48hpi, and we found that the signaling pathways including JAK-STAT, MAPK, and NF- $\kappa$ B, were involved in CHv strain and CHa strain infection at 48hpi (Figure 5). The JAK/STAT signaling pathway is a ubiquitously expressed intracellular signal transduction pathway involved in crucial biological processes, including cell proliferation, differentiation, apoptosis, and immune regulation (39). PRRSV nonstructural protein 1 $\beta$  induces degradation of nuclear membrane protein a1, thereby blocking nuclear translocation of STAT1 and STAT2, leading to the inhibition of the interferon-activated JAK-STAT signaling (40). In monocytes/macrophages, JNK, P38 and ERK1/2 of MAPKs are involved in TLR-induced IL-10 production and are tightly controlled by IFN- $\gamma$  (41). The nuclear factor NF- $\kappa$ B pathway has long been regarded as a typical pro-inflammatory signaling pathway, which participates in the immune regulation and inflammatory response and participates in cell cycle regulation, cell differentiation, and apoptosis (42). Human papilloma virus (HPV) down-regulated NF- $\kappa$ B to eliminate the inhibitory activity of the immune system on its replication, ultimately leading to a persistent HPV infection state (43).

Some viruses exploited MAPK signaling to sustain excessive inflammation for their replication. Our transcriptome

sequencing results found that virus infection leads to activation of the MAPK signaling pathway, but the addition of JNK pathway inhibitor SP600125 leads to up-regulation of innate immunity. In addition, similar results were obtained in the DEF cells and monocytes/macrophages infected with VSV virus. These results suggest that the JNK pathway regulates expression of cytokines under viral infection conditions. Herpes simplex virus (HSV), Epstein-Barr virus (EBV), and varicella-zoster virus (VZV) activate the JNK pathway through various mechanisms, resulting in different consequences on infected cells. For example, in neurons, sustained activation of JNK by VZV favors viral lytic infection (44), HSV-2 infection increases JNK phosphorylation, and JNK signaling is involved in HSV-2-induced TLR9 transcriptional activation (45). EBV activates NF- $\kappa$ B and JNK *via* LMP1 (latent membrane protein 1), which is essential for the oncogenic activity of LMP1 (46). JNK/AP-1 signaling pathway is involved in PRRSV N protein-induced SOCS1 production, thereby promoting PRRSV replication. We further tested the antiviral activity of JNK pathway inhibitor SP600125 and found that it inhibited DPV CHv infection in MM cells, and VSV and DPV CHv infection in DEF cells. We postulated that SP600125 has broad-spectrum antiviral activity and can inhibit RNA and DNA virus infection in different duck cell types.

Our study shed broad spectra light on the transcriptome changes of monocytes/macrophages response to DPV infection. The transcriptome analysis results showed that DEGs related to signal transduction, including the MAPK signaling pathway, NF- $\kappa$ B signaling pathway and JAK-STAT signaling pathway, were involved in DPV infection. In addition, we found that activating the JNK signaling pathway inhibits the expression of cytokines in host cells and promotes viral replication, suggesting that DPV may take over the JNK signaling pathway for its benefit and that MAPK JNK may be a new target for antiviral drugs design. Altogether, our data provide new insights into signaling pathways and the potential responses of cytokines to DPV infection, broaden the activation of signaling pathways by a viral infection and help us better understand the molecular mechanisms underlying pathogen-host interactions.

## DATA AVAILABILITY STATEMENT

The datasets presented in this study can be found in online repositories. The names of the repository/repositories and accession number(s) can be found below: Short Reads Archive (SRA) database under the accession numbers: SRR18825687, SRR18825689 and SRR18825688.

## ETHICS STATEMENT

The animal study was reviewed and approved by the Experimental Procedures and Animal Welfare Committee of

Sichuan Agricultural University (approval permit number SYXX 2019-187).

## AUTHOR CONTRIBUTIONS

LP and BT carried out the experiment. AC and MW conceived of and supervised the study. AC, RJ, DZ, QY, YW, JH, XZ, SC and SZ provided ideas contributing to the conception of this article. XO, SM, QG and DS helped to draw the pictures. MW modified the article. All authors contributed to the article and approved the submitted version.

## FUNDING

This work was supported by China Agriculture Research System of MOF and MARA, and the Sichuan Veterinary Medicine and Drug Innovation Group of China Agricultural Research System (SCCXTD-2020-18).

## SUPPLEMENTARY MATERIAL

The Supplementary Material for this article can be found online at: <https://www.frontiersin.org/articles/10.3389/fimmu.2022.935454/full#supplementary-material>

**Supplementary Figure 1** | Gene ontology (GO) terms of DEGs expressed in DPV CHv or CHa infected MM cells. GO terms were classified into 3 categories, including cellular component (CC), molecular function (MF), and biological process (BP). **(A)** GO annotation of DEGs expressed in Mock and CHa. **(B)** GO annotation of DEGs expressed in Mock and CHv. **(C)** GO annotation of DEGs expressed in CHa and CHv.

**Supplementary Figure 2** | KEGG analysis of genes identified in each group at 48 hpi. **(A)** KEGG analysis of Mock vs. CHa. **(B)** KEGG analysis of Mock vs. CHv. **(C)** KEGG analysis of CHa vs. CHv.

**Supplementary Figure 3** | IFN, ISGs, and cytokines were regulated by inflammatory signaling in duck MM cells infected with the VSV-GFP model virus. MM cells were pretreated with SP600125 (JNK inhibitor), LY3214996 (ERK inhibitor), TAK-715 (p38 inhibitor) and BAY-117082 (NF- $\kappa$ B inhibitor) for 1 h at 10, 5, 5 and 5  $\mu$ M respectively, DMSO was used as control, then the cells were infected with VSV at 5 MOI for 1 h, then the same concentration of inhibitor was added. The expression level of IL-1 $\beta$ , IL-6, CCL21, IFN- $\beta$ , MX and OASL were tested using RT-qPCR 24 h post-treatment. The relative expression was presented as ratios to  $\beta$ -actin compared to mock treatment. “\*” was considered significant difference ( $p < 0.05$ ); “\*\*\*\*” was considered highly significant difference ( $p < 0.001$ ).

**Supplementary Figure 4** | IFN, ISGs, and cytokines were regulated by inflammatory signaling in duck DEF cells infected with the VSV-GFP model virus. DEF cells were pretreated with SP600125 (JNK inhibitor), LY3214996 (ERK inhibitor), TAK-715 (p38 inhibitor) and BAY-117082 (NF- $\kappa$ B inhibitor) for 1 h at 10, 5, 5 and 5  $\mu$ M respectively, DMSO was used as control, then the cells were infected with VSV at 5 MOI for 1 h, then the same concentration of inhibitor was added. The expression level of IL-1 $\beta$ , IL-6, CCL21, IFN- $\beta$ , MX and OASL were tested using RT-qPCR 24 h post-treatment. The relative expression was presented as ratios to  $\beta$ -actin compared to mock treatment. “\*” was considered significant difference ( $p < 0.05$ ); “\*\*\*\*” was considered highly significant difference ( $p < 0.01$ ); “\*\*\*\*\*” was considered highly significant difference ( $p < 0.001$ ).



## REFERENCES

- Khan KA, Islam MA, Sabuj AAM, Bashar MA, Islam MS, Hossain MG, et al. Molecular Characterization of Duck Plague Virus From Selected Haor Areas of Bangladesh. *Open Vet J* (2021) 11(1):42–51. doi: 10.4314/ovj.v11i1.8
- Cheng A. *Duck Plague*. Beijing (2015). (Beijing:China Agriculture Press.)
- Wu Y, Cheng A, Wang M, Zhu D, Jia R, Chen S, et al. Comparative Genomic Analysis of Duck Enteritis Virus Strains. *J Virol* (2012) 86(24):13841–2. doi: 10.1128/jvi.01517-12
- Qi X, Yang X, Cheng A, Wang M, Guo Y, Jia R. Replication Kinetics of Duck Virus Enteritis Vaccine Virus in Ducklings Immunized by the Mucosal or Systemic Route Using Real-Time Quantitative PCR. *Res Vet Sci* (2009) 86(1):63–7. doi: 10.1016/j.rvsc.2008.05.001
- Qi X, Yang X, Cheng A, Wang M, Zhu D, Jia R, et al. Intestinal Mucosal Immune Response Against Virulent Duck Enteritis Virus Infection in Ducklings. *Res Vet Sci* (2009) 87(2):218–25. doi: 10.1016/j.rvsc.2009.02.009
- Dhama K, Kumar N, Saminathan M, Tiwari R, Karthik K, Kumar MA, et al. Duck Virus Enteritis (Duck Plague) - a Comprehensive Update. *Vet Q* (2017) 37(1):57–80. doi: 10.1080/01652176.2017.1298885
- Yang X, Qi X, Cheng A, Wang M, Zhu D, Jia R, et al. Intestinal Mucosal Immune Response in Ducklings Following Oral Immunisation With an Attenuated Duck Enteritis Virus Vaccine. *Vet J* (2010) 185(2):199–203. doi: 10.1016/j.tvjl.2009.04.011
- Kim EK, Choi EJ. Pathological Roles of MAPK Signaling Pathways in Human Diseases. *Biochim Biophys Acta* (2010) 1802(4):396–405. doi: 10.1016/j.bbdis.2009.12.009
- Peng H, Shi M, Zhang L, Li Y, Sun J, Zhang L, et al. Activation of JNK1/2 and P38 MAPK Signaling Pathways Promotes Enterovirus 71 Infection in Immature Dendritic Cells. *BMC Microbiol* (2014) 14:147. doi: 10.1186/1471-2180-14-147
- Hepworth EMW, Hinton SD. Pseudophosphatases as Regulators of MAPK Signaling. *Int J Mol Sci* (2021) 22(22):12595. doi: 10.3390/ijms222212595
- Yang SH, Sharrocks AD, Whitmarsh AJ. MAP Kinase Signalling Cascades and Transcriptional Regulation. *Gene* (2013) 513(1):1–13. doi: 10.1016/j.gene.2012.10.033
- Fung TS, Liao Y, Liu DX. Regulation of Stress Responses and Translational Control by Coronavirus. *Virus* (2016) 8(7):184. doi: 10.3390/v8070184
- Johnson GL, Dohman HG, Graves LM. MAPK Kinase Kinases (MKKKs) as a Target Class for Small-Molecule Inhibition to Modulate Signaling Networks and Gene Expression. *Curr Opin Chem Biol* (2005) 9(3):325–31. doi: 10.1016/j.cbpa.2005.04.004
- Dhillon AS, Hagan S, Rath O, Kolch W. MAP Kinase Signalling Pathways in Cancer. *Oncogene* (2007) 26(22):3279–90. doi: 10.1038/sj.onc.1210421
- Kumar R, Khandelwal N, Thachamvally R, Tripathi BN, Barua S, Kashyap SK, et al. Role of MAPK/MNK1 Signaling in Virus Replication. *Virus Res* (2018) 253:48–61. doi: 10.1016/j.virusres.2018.05.028
- Qin D, Feng N, Fan W, Ma X, Yan Q, Lv Z, et al. Activation of PI3K/AKT and ERK MAPK Signal Pathways is Required for the Induction of Lytic Cycle Replication of Kaposi's Sarcoma-Associated Herpesvirus by Herpes Simplex Virus Type 1. *BMC Microbiol* (2011) 11:240. doi: 10.1186/1471-2180-11-240
- Sharma-Walia N, Krishnan HH, Naranant PP, Zeng L, Smith MS, Chandran B. ERK1/2 and MEK1/2 Induced by Kaposi's Sarcoma-Associated Herpesvirus (Human Herpesvirus 8) Early During Infection of Target Cells are Essential for Expression of Viral Genes and for Establishment of Infection. *J Virol* (2005) 79(16):10308–29. doi: 10.1128/jvi.79.16.10308-10329.2005
- Cheng Y, Sun F, Wang L, Gao M, Xie Y, Sun Y, et al. Virus-Induced P38 MAPK Activation Facilitates Viral Infection. *Theranostics* (2020) 10(26):12223–40. doi: 10.7150/thno.50992
- Zhu Z, Li W, Zhang X, Wang C, Gao L, Yang F, et al. Foot-And-Mouth Disease Virus Capsid Protein Vp1 Interacts With Host Ribosomal Protein Sa to Maintain Activation of the MAPK Signal Pathway and Promote Virus Replication. *J Virol* (2020) 94(3):e01350-19. doi: 10.1128/jvi.01350-19
- Tian B, Cai D, He T, Deng L, Wu L, Wang M, et al. Isolation and Selection of Duck Primary Cells as Pathogenic and Innate Immunologic Cell Models for Duck Plague Virus. *Front Immunol* (2019) 10:3131. doi: 10.3389/fimmu.2019.03131
- Tian B, Cai D, Wang M, He T, Deng L, Wu L, et al. SC75741 Antagonizes Vesicular Stomatitis Virus, Duck Tembusu Virus, and Duck Plague Virus Infection in Duck Cells Through Promoting Innate Immune Responses. *Poult Sci* (2021) 100(5):101085. doi: 10.1016/j.psj.2021.101085
- Han K, Zhao D, Liu Q, Liu Y, Huang X, Yang J, et al. Transcriptome Analysis Reveals New Insight of Duck Tembusu Virus (DTMUV)-Infected DF-1 Cells. *Res Vet Sci* (2021) 137:150–8. doi: 10.1016/j.rvsc.2021.04.028
- Pan Y, Wu X, Cai W, Cheng A, Wang M, Chen S, et al. RNA-Seq Analysis of Duck Embryo Fibroblast Cells Gene Expression During Duck Tembusu Virus Infection. *Vet Res* (2022) 53(1):34. doi: 10.1186/s13567-022-01051-y
- Kanehisa M, Furumichi M, Sato Y, Ishiguro-Watanabe M, Tanabe M. KEGG: Integrating Viruses and Cellular Organisms. *Nucleic Acids Res* (2021) 49(D1):D545–d551. doi: 10.1093/nar/gkaa970
- Yoshimura A, Ito M, Chikuma S, Akanuma T, Nakatsukasa H. Negative Regulation of Cytokine Signaling in Immunity. *Cold Spring Harb Perspect Biol* (2018) 10(7):a028571. doi: 10.1101/cshperspect.a028571
- Liu C, Zhang L, Xu R, Zheng H. Mir-26b Inhibits Virus Replication Through Positively Regulating Interferon Signaling. *Viral Immunol* (2018) 31(10):676–82. doi: 10.1089/vim.2018.0067
- Schoggins JW. Interferon-Stimulated Genes: What do They All do? *Annu Rev Virol* (2019) 6(1):567–84. doi: 10.1146/annurev-virology-092818-015756
- Zhao C, Wang M, Cheng A, Yang Q, Wu Y, Jia R, et al. Duck Plague Virus Promotes DEF Cell Apoptosis by Activating Caspases, Increasing Intracellular ROS Levels and Inducing Cell Cycle s-Phase Arrest. *Viruses* (2019) 11(2):196. doi: 10.3390/v11020196
- Liu T, Cheng A, Wang M, Jia R, Yang Q, Wu Y, et al. RNA-Seq Comparative Analysis of Peking Ducks Spleen Gene Expression 24 H Post-Infected With Duck Plague Virulent or Attenuated Virus. *Vet Res* (2017) 48(1):47. doi: 10.1186/s13567-017-0456-z
- Menicucci AR, Versteeg K, Woolsey C, Mire CE, Geisbert JB, Cross RW, et al. Transcriptome Analysis of Circulating Immune Cell Subsets Highlight the Role of Monocytes in Zaire Ebola Virus Makona Pathogenesis. *Front Immunol* (2017) 8:1372. doi: 10.3389/fimmu.2017.01372
- Chen G, He L, Luo L, Huang R, Liao L, Li Y, et al. Transcriptomics Sequencing Provides Insights Into Understanding the Mechanism of Grass Carp Reovirus Infection. *Int J Mol Sci* (2018) 19(2):488. doi: 10.3390/ijms19020488
- Cheng SC, Huang WC, JH SP, Wu YH, Cheng CY. Quercetin Inhibits the Production of IL-1 $\beta$ -Induced Inflammatory Cytokines and Chemokines in ARPE-19 Cells via the MAPK and NF- $\kappa$ B Signaling Pathways. *Int J Mol Sci* (2019) 20(12):2957. doi: 10.3390/ijms20122957
- Soto-Díaz K, Juda MB, Blackmore S, Walsh C, Steelman AJ. TAK1 Inhibition in Mouse Astrocyte Cultures Ameliorates Cytokine-Induced Chemokine Production and Neutrophil Migration. *J Neurochem* (2020) 152(6):697–709. doi: 10.1111/jnc.14930
- Turner MD, Nedjai B, Hurst T, Pennington DJ. Cytokines and Chemokines: At the Crossroads of Cell Signalling and Inflammatory Disease. *Biochim Biophys Acta* (2014) 1843(11):2563–82. doi: 10.1016/j.bbamcr.2014.05.014
- Yuan S, Jiang SC, Zhang ZW, Fu YF, Hu J, Li ZL. Quantification of Cytokine Storms During Virus Infections. *Front Immunol* (2021) 12:659419. doi: 10.3389/fimmu.2021.659419
- Xie J, Wang M, Cheng A, Zhao XX, Liu M, Zhu D, et al. Cytokine Storms are Primarily Responsible for the Rapid Death of Ducklings Infected With Duck Hepatitis A Virus Type 1. *Sci Rep* (2018) 8(1):6596. doi: 10.1038/s41598-018-24729-w
- Morris G, Bortolasci CC, Puri BK, Marx W, O'Neil A, Athan E, et al. The Cytokine Storms of COVID-19, H1N1 Influenza, CRS and MAS Compared. Can One Sized Treatment Fit All? *Cytokine* (2021) 144:155593. doi: 10.1016/j.cyto.2021.155593
- Ludwig S, Hrinicus ER, Boergeling Y. The Two Sides of the Same Coin: Influenza Virus and Intracellular Signal Transduction. *Cold Spring Harb Perspect Med* (2021) 11(1):a038513. doi: 10.1101/cshperspect.a038513
- Ciechanowicz P, Rakowska A, Sikora M, Rudnicka L. JAK-Inhibitors in Dermatology: Current Evidence and Future Applications. *J Dermatolog. Treat* (2019) 30(7):648–58. doi: 10.1080/09546634.2018.1546043
- Xu Y, Wang H, Zhang X, Zheng X, Zhu Y, Han H, et al. Highly Pathogenic Porcine Reproductive and Respiratory Syndrome Virus (HP-PRRSV) Induces IL-6 Production Through TAK-1/JNK/Ap-1 and TAK-1/Nf- $\kappa$ B Signaling Pathways. *Vet Microbiol* (2021) 256:109061. doi: 10.1016/j.vetmic.2021.109061
- Saraiva M, O'Garra A. The Regulation of IL-10 Production by Immune Cells. *Nat Rev Immunol* (2010) 10(3):170–81. doi: 10.1038/nri2711

42. Deng L, Zeng Q, Wang M, Cheng A, Jia R, Chen S, et al. Suppression of NF- $\kappa$ B Activity: A Viral Immune Evasion Mechanism. *Viruses* (2018) 10(8):409. doi: 10.3390/v10080409
43. Tilborghs S, Corthouts J, Verhoeven Y, Arias D, Rolfo C, Trinh XB, et al. The Role of Nuclear Factor-Kappa B Signaling in Human Cervical Cancer. *Crit Rev Oncol Hematol* (2017) 120:141–50. doi: 10.1016/j.critrevonc.2017.11.001
44. Kurapati S, Sadaoka T, Rajbhandari L, Jagdish B, Shukla P, Ali MA, et al. Role of the JNK Pathway in Varicella-Zoster Virus Lytic Infection and Reactivation. *J Virol* (2017) 91(17):e00640–17. doi: 10.1128/jvi.00640-17
45. Hu K, Fu M, Wang J, Luo S, Barreto M, Singh R, et al. HSV-2 Infection of Human Genital Epithelial Cells Upregulates Tlr9 Expression Through the SP1/JNK Signaling Pathway. *Front Immunol* (2020) 11:356. doi: 10.3389/fimmu.2020.00356
46. Uemura N, Kajino T, Sanjo H, Sato S, Akira S, Matsumoto K, et al. TAK1 is a Component of the Epstein-Barr Virus LMP1 Complex and is Essential for Activation of JNK But Not of NF-Kappab. *J Biol Chem* (2006) 281(12):7863–72. doi: 10.1074/jbc.M509834200

**Conflict of Interest:** The authors declare that the research was conducted in the absence of any commercial or financial relationships that could be construed as a potential conflict of interest.

**Publisher's Note:** All claims expressed in this article are solely those of the authors and do not necessarily represent those of their affiliated organizations, or those of the publisher, the editors and the reviewers. Any product that may be evaluated in this article, or claim that may be made by its manufacturer, is not guaranteed or endorsed by the publisher.

Copyright © 2022 Wu, Tian, Wang, Cheng, Jia, Zhu, Liu, Yang, Wu, Huang, Zhao, Chen, Zhang, Ou, Mao, Gao, Sun, Yu, Zhang and Pan. This is an open-access article distributed under the terms of the Creative Commons Attribution License (CC BY). The use, distribution or reproduction in other forums is permitted, provided the original author(s) and the copyright owner(s) are credited and that the original publication in this journal is cited, in accordance with accepted academic practice. No use, distribution or reproduction is permitted which does not comply with these terms.



# Identification of Critical Biomarkers and Immune Infiltration in Rheumatoid Arthritis Based on WGCNA and LASSO Algorithm

Fan Jiang<sup>1,2</sup>, Hongyi Zhou<sup>3</sup> and Haili Shen<sup>4\*</sup>

<sup>1</sup> Second Clinical Medical College, Lanzhou University, Lanzhou, China, <sup>2</sup> Department of General Medicine, Beijing Luhe Hospital, Capital Medical University, Beijing, China, <sup>3</sup> Department of Anesthesiology, Tongzhou Maternal and Child Health Hospital of Beijing, Beijing, China, <sup>4</sup> Department of Rheumatology, Lanzhou University Second Hospital, Lanzhou, China

## OPEN ACCESS

### Edited by:

Rongtuan Lin,  
McGill University, Canada

### Reviewed by:

Jin Zhang,  
I.M. Sechenov First Moscow State  
Medical University, Russia  
Ying-Lie Shang,  
Shandong Provincial Chest Hospital,  
China

### \*Correspondence:

Haili Shen  
shenhl@lzu.edu.cn

### Specialty section:

This article was submitted to  
Viral Immunology,  
a section of the journal  
Frontiers in Immunology

**Received:** 21 April 2022

**Accepted:** 27 May 2022

**Published:** 29 June 2022

### Citation:

Jiang F, Zhou H and Shen H  
(2022) Identification of Critical  
Biomarkers and Immune Infiltration in  
Rheumatoid Arthritis Based on  
WGCNA and LASSO Algorithm.  
*Front. Immunol.* 13:925695.  
doi: 10.3389/fimmu.2022.925695

Rheumatoid arthritis (RA) is the most common inflammatory arthritis, and a significant cause of morbidity and mortality. RA patients' synovial inflammation contains a variety of genes and signalling pathways that are poorly understood. It was the goal of this research to discover the major biomarkers related to the course of RA and how they connect to immune cell infiltration. The Gene Expression Omnibus was used to download gene microarray data. Differential expression analysis, weighted gene co-expression network analysis (WGCNA), and least absolute shrinkage and selection operator (LASSO) regression were used to identify hub markers for RA. Single-sample GSEA was used to examine the infiltration levels of 28 immune cells and their connection to hub gene markers. The hub genes' expression in RA-HFLS and HFLS cells was verified by RT-PCR. The CCK-8 assay was applied to determine the roles of hub genes in RA. In this study, we identified 21 differentially expressed genes (DEGs) in RA. WGCNA yielded two co-expression modules, one of which exhibited the strongest connection with RA. Using a combination of differential genes, a total of 6 intersecting genes was discovered. Six hub genes were identified as possible biomarkers for RA after a lasso analysis was performed on the data. Three hub genes, CKS2, CSTA, and LY96, were found to have high diagnostic value using ROC curve analysis. They were shown to be closely related to the concentrations of several immune cells. RT-PCR confirmed that the expressions of CKS2, CSTA and LY96 were distinctly upregulated in RA-HFLS cells compared with HFLS cells. More importantly, knockdown of CKS2 suppressed the proliferation of RA-HFLS cells. Overall, to help diagnose and treat RA, it's expected that CKS2, CSTA, and LY96 will be available, and the aforementioned infiltration of immune cells may have a significant impact on the onset and progression of the disease.

**Keywords:** rheumatoid arthritis, diagnostic marker, machinelearning, GEO datasets, immune cells infiltration

## INTRODUCTION

Rheumatoid arthritis (RA) is a common chronic inflammatory joint disease characterized by persistent synovial hyperplasia and progressive destruction of joint cartilage and bone (1, 2). It is well recognized that RA can lead to decreased functional status, disability, and increased mortality (3). Around 1% of the population suffers from RA at any given time, and females are more likely than males to be affected (4, 5). The exact pathophysiology of RA is still not well understood. Studies have shown that it may be linked to immune system variables, environmental factors, genetics, and other factors (6, 7). Key aspects of RA's pathogenesis, including lymphocyte infiltration and development of fibroblast-like synoviocytes (FLS) in the synovial fluid, have received major study attention (8, 9). Accordingly, it is imperative to investigate the molecular pathways that underlie the disease and find diagnostic biomarkers for RA in order to improve treatment outcomes for people with RA.

As more and more publicly available high-throughput data in worldwide were developed, an unanswered question has arisen: How can we leverage these large-scale data effectively to gain a full understanding of various diseases at the molecular levels (10, 11)? Human life is enriched by machine learning (ML), which is the scientific study of algorithms and statistical models (12). ML is particularly important in the identification of the potential biomarkers for the diagnosis and prognosis of human diseases, which is why it is being studied more and more in this sector (13, 14). A number of studies have used numerous markers to develop prediction models for early diagnosis in clinical patients, with mixed results (15, 16). However, prior researches have found that the accuracy of these models, which are comprised of predictive biomarkers, as well as their application scope, are significantly limited by the sample size (17, 18). The weighted gene co-expression network analysis (WGCNA) and the least absolute shrinkage and selection operator (LASSO) algorithms are widely used in bioinformatics analysis and exhibit an important in clinical application of various fields (19, 20). However, their application in screening potential biomarkers for RA was rarely reported.

In this investigation, we aimed to discover the major biomarkers related to the course of RA and how they connect to immune cell infiltration. We used two microarray datasets of RA that were retrieved from the GEO datasets. The study of differentially expressed genes (DEGs) was carried out between the RA and the controls. To filter and discover diagnostic biomarkers of RA, machine-learning techniques were applied. As a result of this study, for the first time, the fraction of immune cells in samples of RA and normal tissues was quantified using ssGSEA (single-sample gene set enrichment analysis). Moreover, we investigated the association between the biomarkers identified and the infiltrating immune cells in order to lay the groundwork for future studies.

## MATERIALS AND METHODS

### Data Collection

The mRNA expression profile (Number: GSE17755 and GSE93272) was obtained from the GEO database (<https://www.ncbi.nlm.nih.gov/geo/>). GSE17755 contained blood samples of 99 RA patients and 45 healthy controls. GSE93272 contained blood samples of 232 RA patients and 43 healthy controls. The expression analysis of mRNA profile was detected by GPL1291 and GPL570.

### Cell Incubation and Transfection

HFLS and RA-infected HFLS (RA-HFLS) were obtained from Cell Applications, Inc. DMEM containing 10% fetal bovine serum, 1% penicillin/streptomycin, and 5% CO<sub>2</sub> was used to keep the cells at 37°C in an incubator. Lipo 3000 transfection reagent (Thermo Fisher Scientific, MA, USA) was used to deliver the CKS2 siRNA (siCKS2) and its negative control into RAHFLS.

### Quantitative Real-Time PCR (qRT-PCR)

Based on manufacturer's instructions, we extracted total RNA from cells using the TRIZOL reagent (Invitrogen, Carlsbad, CA, USA). The Reverse Transcription Kit was used to reverse-transcribe one microgram of total RNA into cDNA for use in the qRT-PCR assay (Takara, Dalian, China). With the use of the Fast Real-time PCR 7500 System (Applied Biosystems, Foster City, CA, USA), we were able to determine gene expression. After two minutes at 50°C, the PCR reaction was subjected to 40 cycles of 95°C for 15 seconds, followed by one minute at 60°C. The GAPDH gene was amplified to serve as an internal control. The relative quantification values for CKS2 were calculated by the  $2^{-\Delta\Delta C_t}$  method. The primers were as follows: CKS2 sense: 5'-TTTCGACGAACTACGAGTACC-3'; CKS2 antisense: 5'-GGACACCAAGTCTCCTCCAC-3'; GAPDH sense: 5'-AGAAGGCT-GGGCTCATTTC-3'; GAPDH antisense: 5'-AGGGGCCATCCA CAGTCTTC-3'.

### Cell Proliferation Assay

Cells were harvested and detachable with 0.25 percent trypsin during the logarithmic growth phase. In 96-well plates, the cells were planted at a density of  $2 \times 10^3$  cells per well. Each well was incubated at 37°C for an additional 2 h after incubation for 0, 24, 48, 72 and 96 hours with sterile Cell Counting Kit-8 solution (15  $\mu$ L). Finally, an optical density (OD) value measurement at 450 nm was performed using a Thermo Multiskan MK3 reader (Thermo Fisher, Schwerte, Germany).

### Identification of Differentially Expressed Genes (DEGs)

It was normalised using RMA and the DEGs were evaluated using a limma R tool for GSE17755 dataset. Raw signals from the analysis were log<sub>2</sub> transformed after quantile normalisation.  $|\log_2FC| > 1$  and a false discovery rate of 0.05 were used to identify DEGs in this study.

## Construction of Gene Co-Expression Network

WGCNA is a bioinformatics analytical method that is used frequently to explore effectively the relationships between genes and phenotypes (21). The WGCNA tool in R was used to build a weighted co-expression network for the GSE17755 dataset's expressing data before a subset of genes with absolute deviations greater than 25% from the median were selected for further investigation. The "goodSampleGenes" function was used to verify the data's integrity. PickSoftThreshold was used to select and verify an optimum soft threshold ( $\beta$ ). In order to find modules based on topological overlap, the matrix data were transformed into an adjacency matrix, and then clustered. Clustering dendrograms were generated after the computation of module eigengene (ME) and merging of related modules in the tree based on ME. Using phenotypic data and modules, the importance of genes and clinical data was assessed, and the relationship between models and modules was examined.

## Screening of the Critical Genes

Candidate hub genes were chosen from a pool of genes with the greatest degree of connection among modules. Absolute GS values tend to be greater in genes having biological importance. The criteria (absolute values of  $GS > 0.20$  and  $MM > 0.80$ ) were used to screen potential hub genes. LASSO is a regression-based methodology permitting for a large number of covariates in the model, and importantly has the unique feature penalizing the absolute value of a regression coefficient (22). In order to identify the final hub genes, we used the 'glmnet' package of R software to run LASSO analysis on the candidate hub genes and DEGs. Analysis of the levels of genes in RA samples and normal samples was carried out using box plots. The levels of hub genes that identify RA samples from healthy samples were assessed using ROC curves. In addition, a different dataset (GSE93272) was used to validate the levels of hub genes and diagnostic value.

## Immune Cells Infiltration Analysis

ssGSEA in the "GSVA" R package was used to analyse the immune infiltration of RA (23). Immune cells and hub gene expression were then correlated using Spearman's correlation.

## Functional Enrichment Analysis

R packages "clusterProfiler" and "enrichplot" were used to perform GO assays, KEGG assays, and GSEA of DEGs with a statistically significant difference of at least  $P < 0.05$  (24, 25). Gene sets with  $P < 0.05$  and a FDR  $q$ -value 0.05 were considered highly enriched in the MsigDB datasets for GSEA.

## Statistical Analysis

Statistical analyses and graphs were generated using GraphPad Prism version 5.0 (La Jolla, CA, USA) or R.4.1.1 (R Core Team, Massachusetts, USA). By using the Student  $t$ -test, we were able to determine the differences between groups. Hub genes' diagnostic accuracy was tested using ROC curves. For all tests,  $p$ -values of  $< 0.05$  were interpreted as statistically significant.

## RESULTS

### Identification of DEGs in RA

To explore the possible biomarkers for RA, data from a total of 99 RA and 48 control samples from GSE17755 were retrospectively analyzed in this study. A total of 21 DEGs were discovered, and all of them showed significant increases in expressions (Figures 1A, B).

### Functional Enrichment Analysis of DEGs

For a better understanding of the biological processes and signal pathways linked with RA DEGs, researchers used GO and KEGG analyses. The results of GO assays revealed that DEGs were mainly enriched in ATP synthesis coupled electron transport, mitochondrial ATP synthesis coupled electron transport, respiratory electron transport chain, cytochrome complex, mitochondrial respiratory chain complex IV, respiratory chain

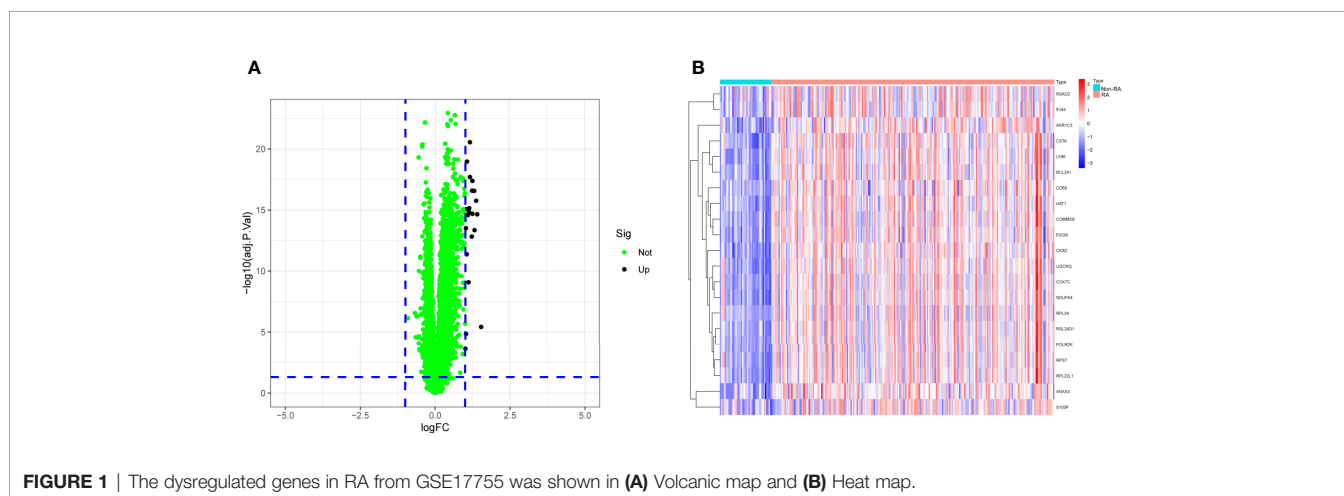


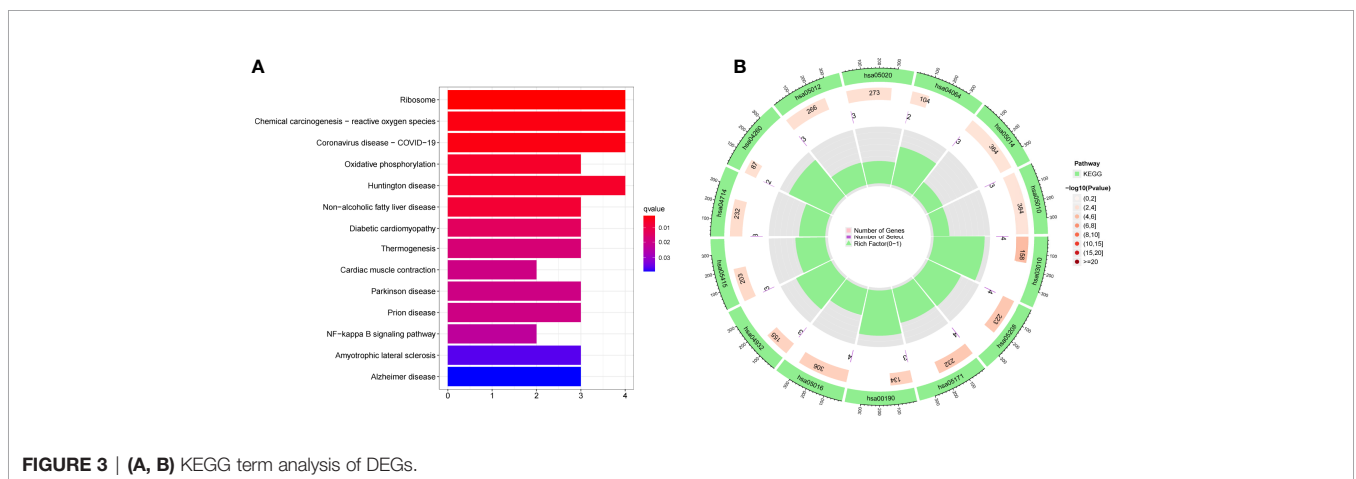
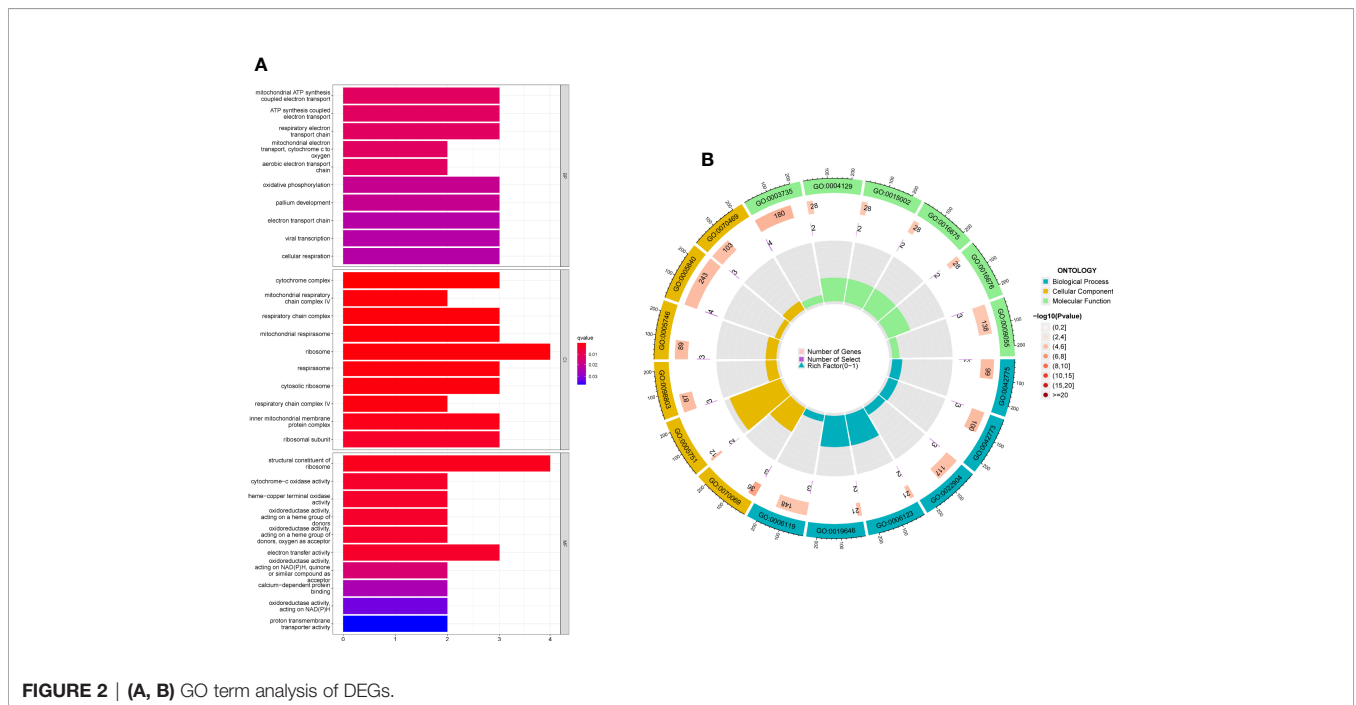
FIGURE 1 | The dysregulated genes in RA from GSE17755 was shown in (A) Volcanic map and (B) Heat map.

complex, structural constituent of ribosome, cytochrome-c oxidase activity and heme-copper terminal oxidase activity (Figures 2A, B). The outcomes of KEGG assays revealed that DEGs were mainly enriched in pathways involved in Ribosome, Chemical carcinogenesis-reactive oxygen species, Coronavirus disease- COVID-19, Oxidative phosphorylation and Huntington disease (Figures 3A, B). In addition, the results of GSEA assays were shown in Figures 4A, B.

### Screening and Verification of Diagnostic Markers

Using WGCNA analysis, we were able to construct four exceptional coexpression modules. Multiple modules were shown to be associated with RA, as evidenced by the module-trait correlation studies (Figure 5A). This data was represented as heat maps, with turquoise (six genes) showing the strongest

link to RA of all the modules studied thus far, as well as that of healthy controls (Figures 5B-D). Then, six overlapping features (CKS2, UQCRQ, NDUFA4, EVI2A, CSTA and LY96) between the group of DGEs and the group of turquoise were ultimately selected (Figure 5E). Moreover, The LASSO regression approach was used to narrow down the six overlapping features, and six variables were identified as diagnostic biomarkers for RA (Figures 6A, B). The distinct upregulation of CKS2, UQCRQ, NDUFA4, EVI2A, CSTA and LY96 were observed in RA samples compared with normal samples (Figure 7). To further confirm the expressing pattern of the above six genes in RA, we further analyzed GSE93272, and found that only CKS2, UQCRQ, EVI2A, CSTA and LY96 were highly expressed in RA compared with normal samples (Figures 8A, B). However, the expression of NDUFA4 remained unchanged between RA samples and healthy samples (Figure 8C). Analysis of the



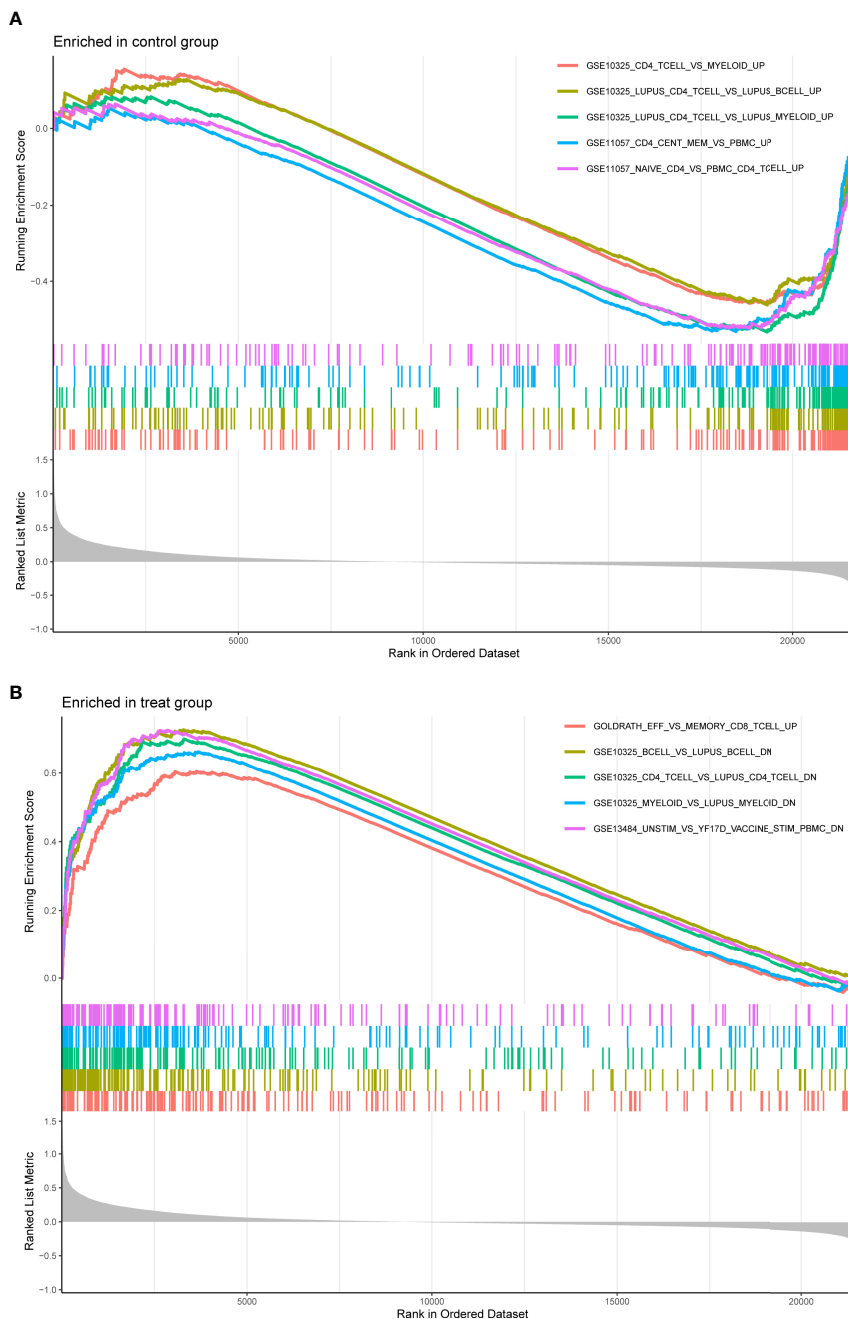


**FIGURE 4** | Enrichment analyses via gene set enrichment analysis. **(A)** Enriched in control group. **(B)** Enriched in treat group.

AUC values of the six hub genes was used to evaluate their sensitivity and specificity for RA diagnosis in ROC curve analysis. The AUC values of six genes were greater than 0.85, which suggested that these genes were highly diagnostic for RA (**Figure 9**). Using the GSE93272 dataset, the diagnostic usefulness of the six hub genes listed above was further confirmed for clinical purposes. CKS2, CSTA and LY96 had AUC values > 0.75 (**Figure 10A**), whereas the UQCRQ, NDUFA4 and EVI2A had an AUC value <0.7 (**Figure 10B**).

Our findings highlighted the potential of CKS2, CSTA and LY96 used as novel diagnostic biomarkers for RA patients.

### Immune Cell Infiltration and Its Associations With Diagnostic Genes

The ssGSEA algorithm was used to examine the association between RA and healthy controls in terms of differences in immune cell infiltration. **Figure 11A** showed the GSE17755 datasets’ distribution of 28 immune cells. We observed a distinctly higher infiltration of

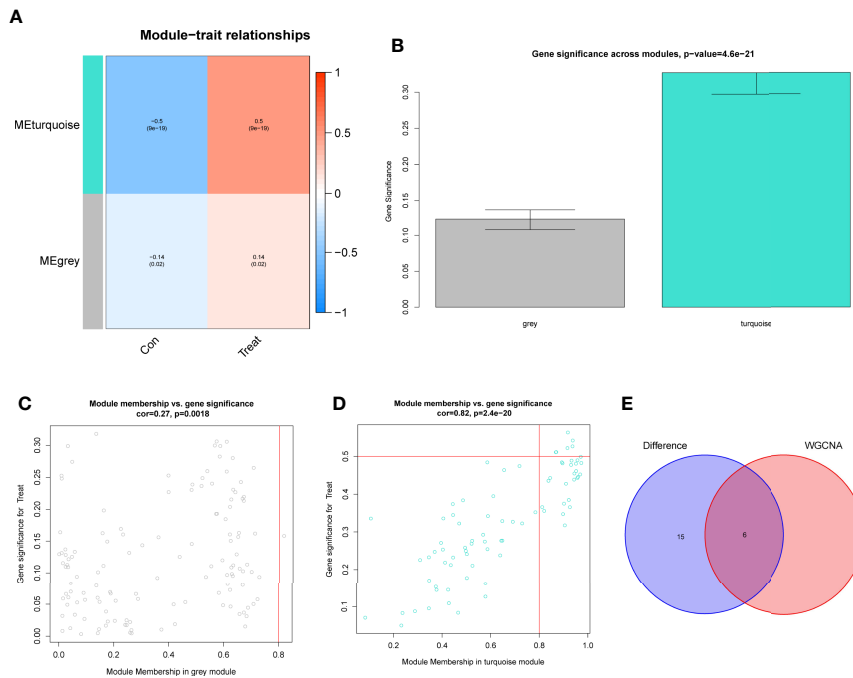


**FIGURE 5** | Construction of WGCNA modules. **(A)** The module-trait relationship heat map. RA was strongly linked to the turquoise module. **(B)** Distribution of average gene significance in the modules related to RA. **(C, D)** Associations between module membership and gene importance is depicted in a scatter plot. **(E)** The Overlapping genes between DEGs and the MEturquoise module.

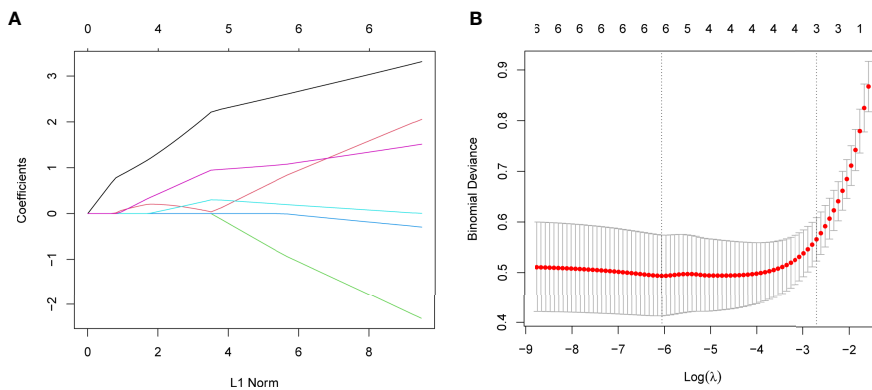


**FIGURE 6** | Establishment of diagnostic biomarkers by LASSO regression analysis. **(A)** LASSO coefficient profiles of the six genes in RA. **(B)** The log (lambda) sequence was used to construct a coefficient profile diagram. The LASSO model's optimal parameter (lambda) was chosen.

Activated.CD4.T.cell, Activated.CD8.T.cell, Activated.dendritic.cell, Eosinophil, CD56dim.natural.killer.cell, MDSC, Macrophage, Mast.cell, Neutrophil, Regulatory.T.cell, Type.17.T.helper.cell, Type.2.T.helper.cell, Memory.B.cell, Central.memory.CD4.T.cell in RA than in normal specimens, indicating that they play a critical role in developments of RA (**Figure 11B**). Furthermore, correlation analysis confirmed positive correlations of many types of immune cell infiltration with the expression of CKS2, CSTA and LY96 (**Figure 11C**).

### Impact of CKS2 on RA-HFLS Cell Proliferation

To further demonstrate whether CKS2, CSTA and LY96 exhibited a dysregulated level in RA, we performed RT-PCR and found that the expression of CKS2, CSTA and LY96 was distinctly upregulated in RA-HFLS cells compared with normal HFLS cells (**Figures 12A-C**). Next, we decreased CKS2 expression by the use of siRNA in RA-HFLS cells. RT-PCR demonstrated the distinct down-regulation of CKS2 in RA-HFLS



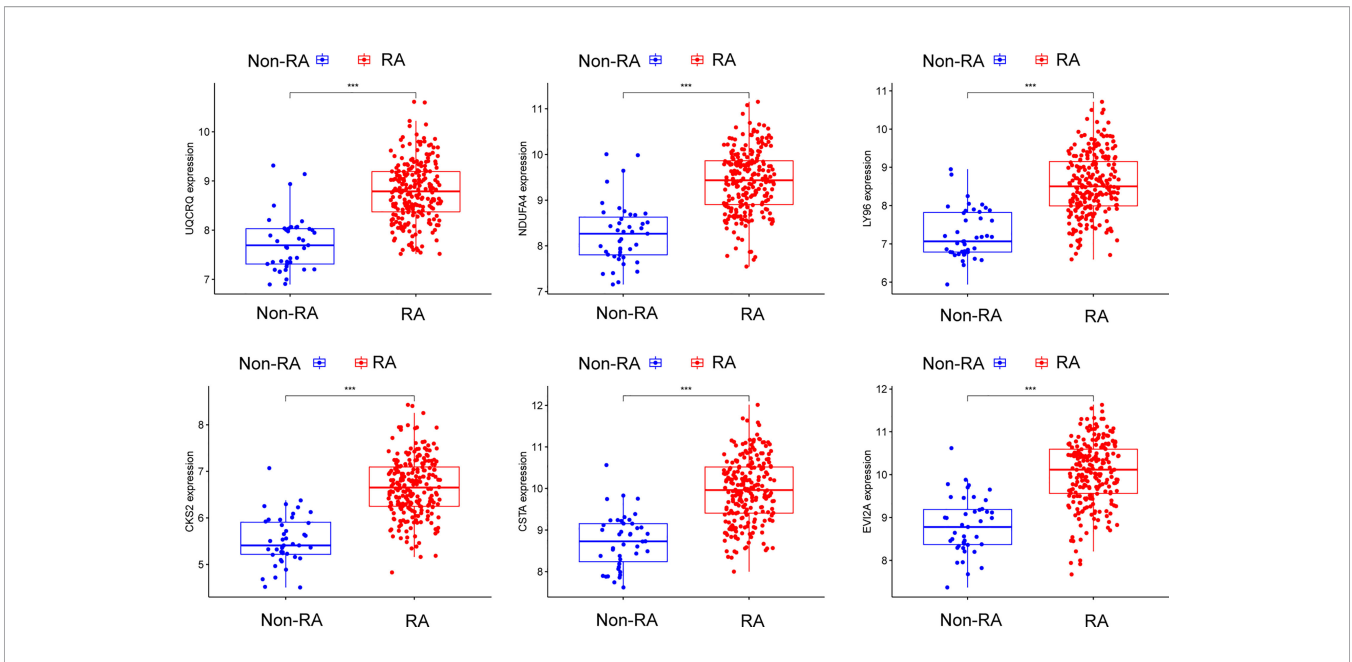


**FIGURE 7** | The expressing pattern of six genes in RA samples and normal samples from GSE17755. \*\*\* $p < 0.001$ .

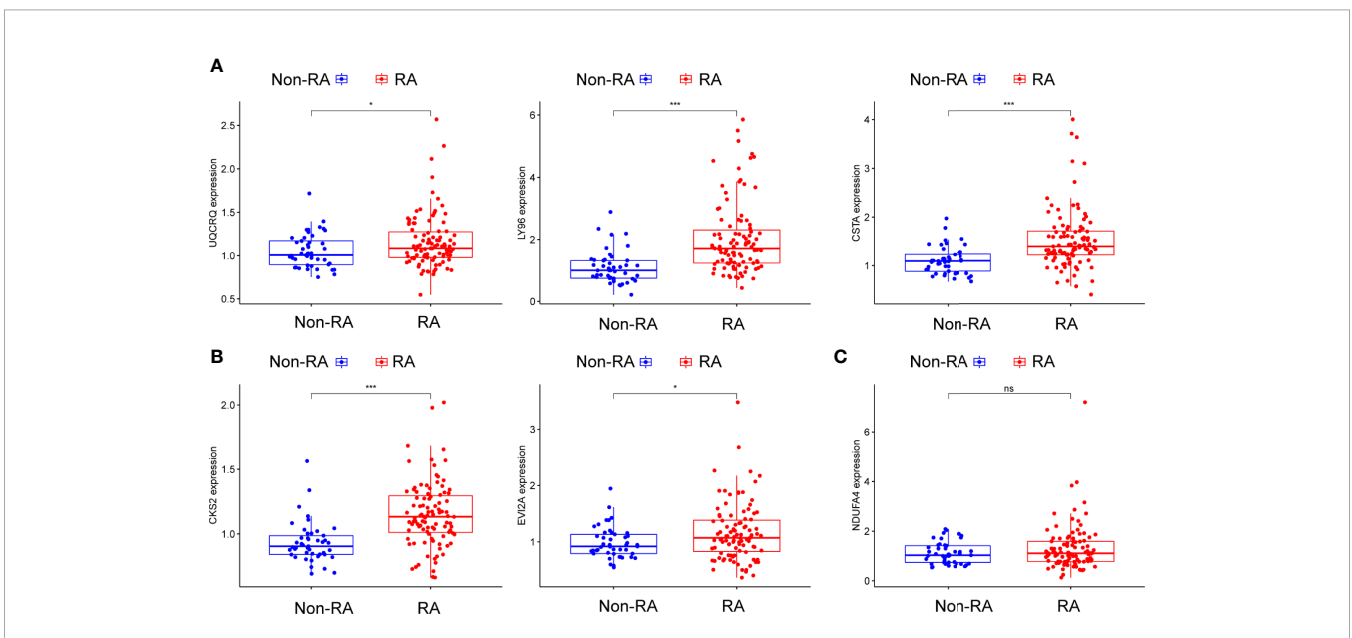


**FIGURE 8 | (A–C)** The expressing pattern of six genes in RA samples and normal samples from GSE93272. \* $p < 0.05$ , \*\*\* $p < 0.001$ . ns represents no significance.

cells (**Figure 12D**). In addition, the proliferation of RA-HFLS upon CKS2 silence were examined by CCK-8. As displayed in **Figure 12E**, knockdown of CKS2 suppressed the proliferation of RA-HFLS cells.

## DISCUSSION

RA is the most commonly diagnosed systemic inflammatory arthritis (26). An untreated RA may exhibit a distinct impact

on the quality of life of patients, potentially leading to disability (27). A better understanding of the molecular level of illness detection and treatment is inevitable. Biomarkers that are related with rheumatoid arthritis have been identified. However, the precise mechanism of gene regulation that leads to disease progression has not yet been fully understood (28, 29).

In this study, we analyzed GSE17755 datasets and identified 21 DEGs in RA. Interesting, all 21 DEGs were highly expressed in RA, suggesting them as positive

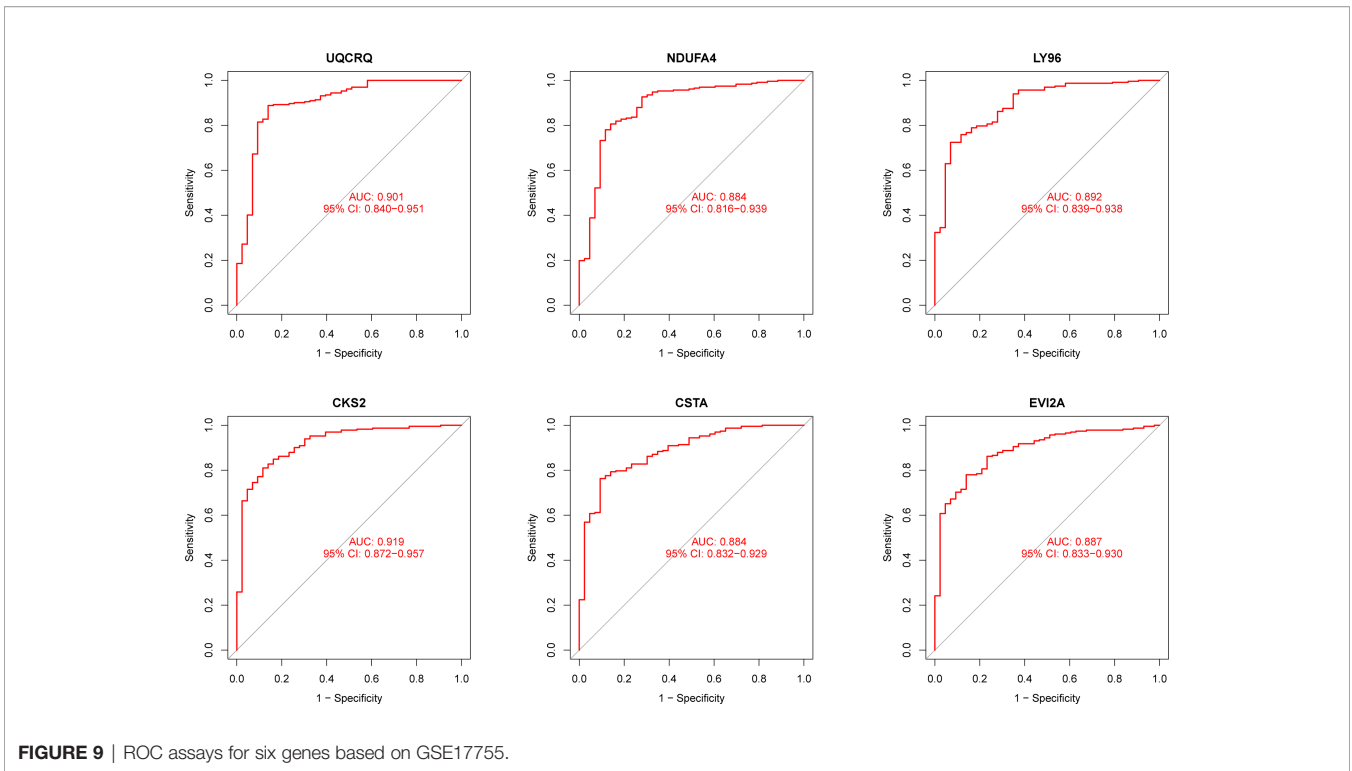


**FIGURE 9** | ROC assays for six genes based on GSE17755.

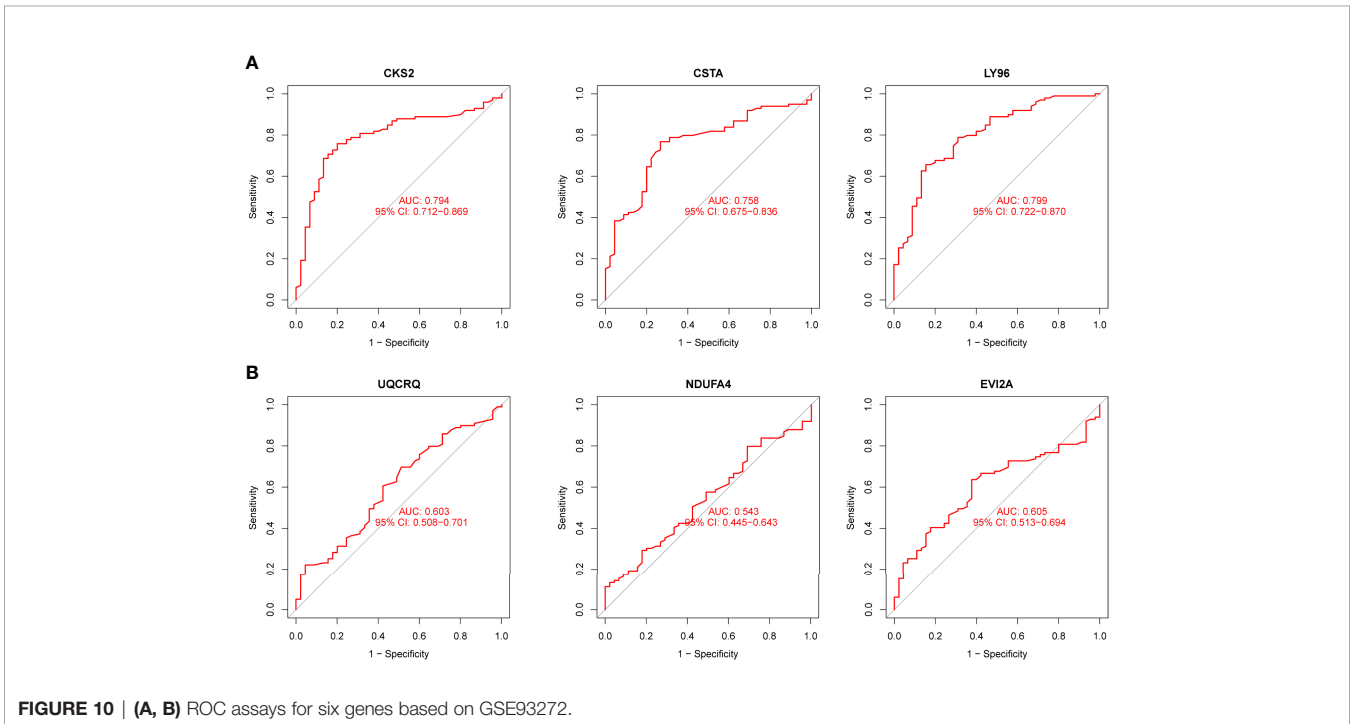
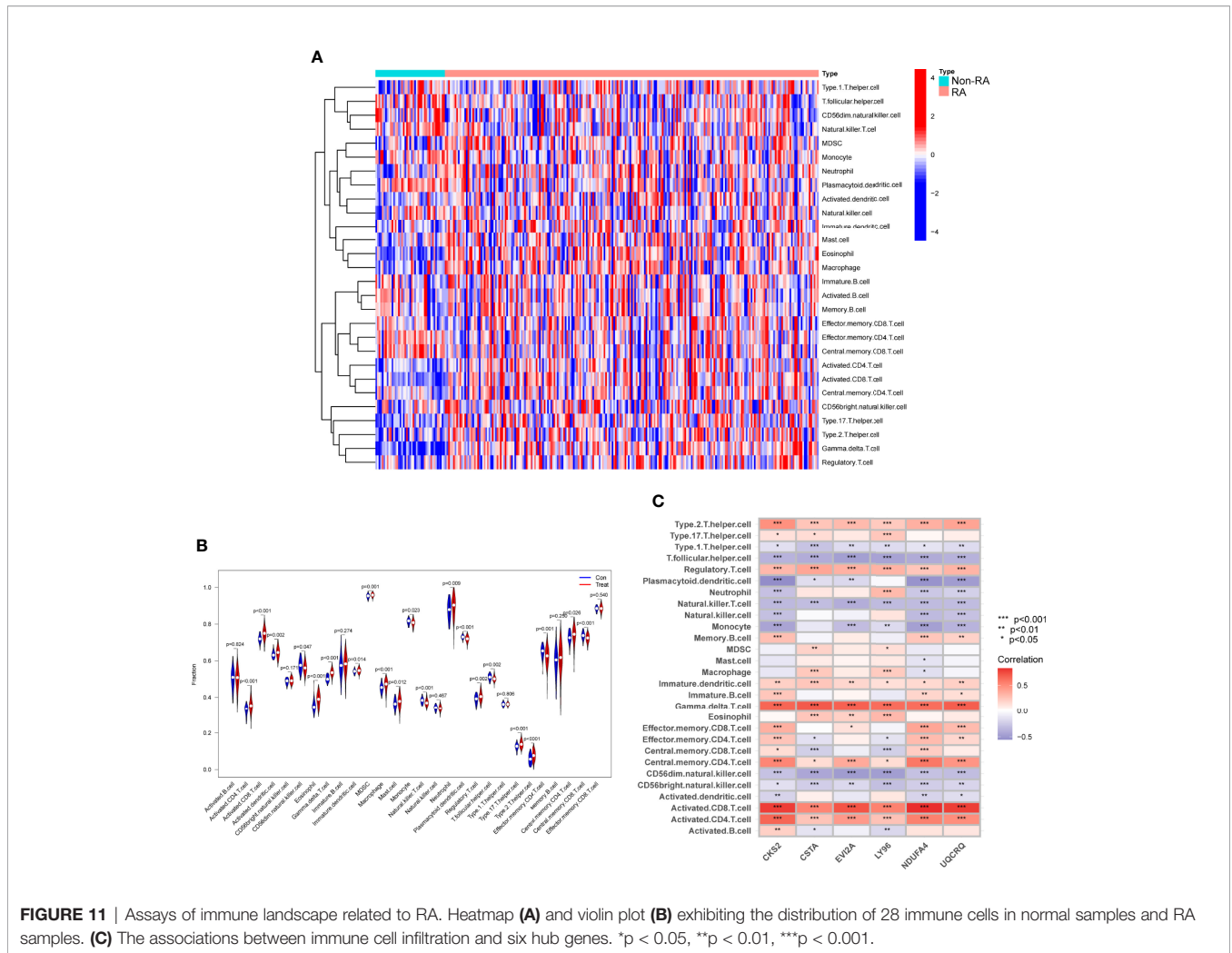


**FIGURE 10** | (A, B) ROC assays for six genes based on GSE93272.

regulator factors in progressions of RA. Then, our group carried out KEGG assays using the 21 DEGs, finding that they were mainly enriched in pathways associated with Ribosome, Chemical carcinogenesis-reactive oxygen species, Coronavirus disease – COVID-19, Oxidative phosphorylation

and Huntington disease. Then, we screened 6 possible diagnostic biomarkers for RA, based on WGCNA analysis and LASSO regression algorithm, including CKS2, UQCQRQ, NDUFA4, EVI2A, CSTA and LY96. As a data reduction method and an unsupervised classification method, the



WGCNA is a hybrid (19). Numerous synthetic gene groups (or modules) are reduced to a handful of easily interpreted gene responses. The use of machine learning-based algorithms in clinical decision-making is widespread (30, 31). Clinical efficacy has been proven for LASSO, one of the most often utilised algorithms. The diagnostic classifier constructed by the LASSO methods and WGCNA has been frequently used in many diseases, such as esophageal cancer, acute coronary syndrome and Sepsis (32–34). However, its application in RA was rarely.

After, we screened six possible biomarkers. Then, we further confirmed their diagnostic using GSE93272 datasets, and further demonstrated CKS2, CSTA and LY96 as critical biomarkers for RA based on the results of ROC assays. Cyclin-dependent kinase regulatory subunits 1 (CKS1) and 2 (CKS2) belong to a family of highly conserved small (9 KDa) cyclin-dependent kinase (CDK)-binding proteins that are involved in the modulation of the cell cycle (35, 36). CKS2 has previously been found to have a significant role in early embryonic developments and somatic cell division (37). However, its

function in RA has not been investigated. Similar, the expression and function of CSTA and LY96 in RA also remained largely unclear. In this study, we further used the ssGSEA algorithm to analyze the infiltration of 28 immune cells in RA samples. Compared with normal samples, RA samples had distinctly higher levels of Activated.CD4.T.cell, Activated.CD8.T.cell, Activated.dendritic.cell, Immature.dendritic.cell, Gamma.delta.T.cell, Eosinophil, CD56dim.natural.killer.cell, MDSC, Macrophage, Mast.cell, Neutrophil, Regulatory.T.cell, Type.17.T.helper.cell, Type.2.T.helper.cell, Memory.B.cell, Central.memory.CD4.T.cell. CD8 infiltration in synovial tissues was revealed to be a predictor of RA progression and the existence of antibodies against citrullinated peptides by one investigation (38, 39). Moreover, our group found that the expressions of CKS2, CSTA and LY96 were related to the levels of many immune cells, highlighting their potential used as therapeutic targets for RA.

Finally, we performed RT-PCR to confirm the expressions of CKS2, CSTA and LY96 in RA-HFLS cells and normal HFLS cells.

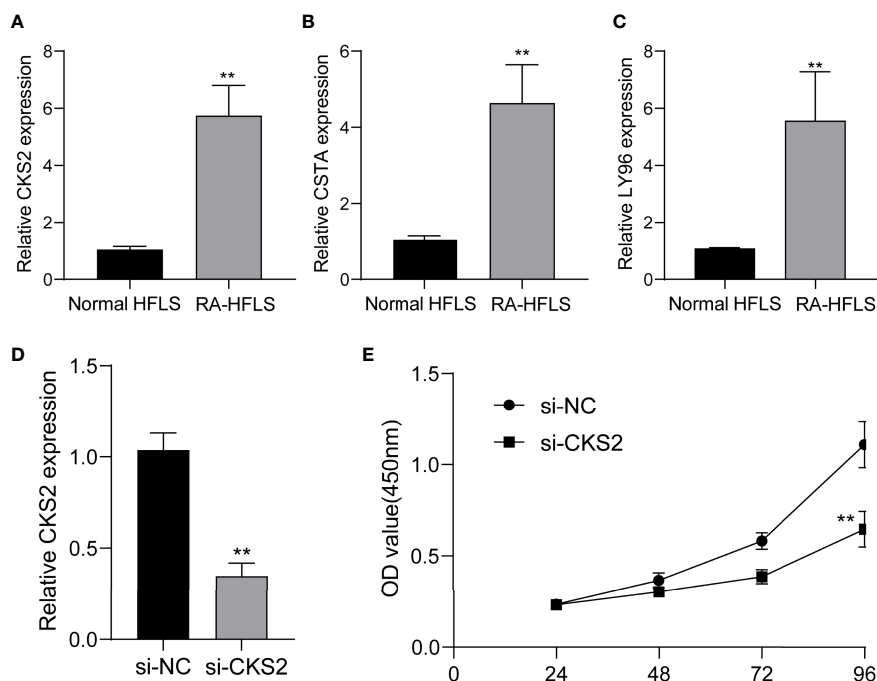


**FIGURE 12 |** The expression of CKS2, CSTA and LY96 in RA cells and the potential functions. **(A)** CKS2, **(B)** STA, and **(C)** LY96 was highly expressed in RA-HFLS cells compared with normal HFLS cells. **(D)** RT-PCR confirmed the distinct down-regulation of CKS2 in RA-HFLS cells after the transfection of si-CKS2. **(E)** CCK-8 assays revealed that knockdown of CKS2 suppressed the proliferation of RA-HFLS cells. \*\* $p < 0.01$ .

Our findings were consistent with the results from GEO datasets. The levels of CKS2, CSTA and LY96 were distinctly upregulated in RA-HFLS cells compared with normal HFLS cells. Moreover, we decreased the CKS2 expressions by introducing si-CKS2 or their NC cells into RA-HFLS. Then, the results of CCK-8 assays revealed that knockdown of CKS2 distinctly suppressed the proliferation of RA-HFLS cells. Our findings further demonstrated CKS2 as a therapeutic target for RA.

Although we integrated a number of bioinformatics approaches and statistical methodologies, and performed diverse studies to uncover the diagnostic biomarkers, significant limitations should be noted. Firstly, this was a retrospective study, and thus it lacked new clinical samples and data. Secondly, the biological activities of the identified genes and the connections between those genes and RA have not been completely researched. Finally, the analysis relies solely on GEO databases. To support our findings, we would benefit from additional data from other sources.

## CONCLUSION

Overall, we integrated multiple bioinformatics tools and identified three critical diagnostic genes in RA. In addition, three critical diagnostic genes infiltrating the immune microenvironment were identified in this research, which could function as novel markers and immune therapeutic

targets. However, Further research is needed to support our findings that they may act as therapeutic targets for RA.

## DATA AVAILABILITY STATEMENT

The datasets presented in this study can be found in online repositories. The names of the repository/repositories and accession number(s) can be found below: <https://www.ncbi.nlm.nih.gov/>, GSE17755, <https://www.ncbi.nlm.nih.gov/>, GSE93272.

## AUTHOR CONTRIBUTIONS

Conception, FJ and HS. Design and revision of the manuscript, FJ and HZ. Analysis and interpretation of data, FJ and HS. All authors contributed to the article and approved the submitted version.

## FUNDING

This work was supported by National Natural Science Foundation of China (No. 81960302), Gansu Province Clinical Research Center for Rheumatology(21JR7RA437), Cuiying Scientific and Technological Innovation Program of Lanzhou University Second Hospital (No. CY2021-BJ-A01).

## REFERENCES

- Sayah A, English JC3rd. Rheumatoid Arthritis: A Review of the Cutaneous Manifestations. *J Am Acad Dermatol* (2005) 53:191–209; quiz 210–2. doi: 10.1016/j.jaad.2004.07.023
- Smolen JS, Aletaha D, McInnes IB. Rheumatoid Arthritis. *Lancet* (2016) 388:2023–38. doi: 10.1016/S0140-6736(16)30173-8
- Lin YJ, Anzaghe M, Schülke S. Update on the Pathomechanism, Diagnosis, and Treatment Options for Rheumatoid Arthritis. *Cells* 9 (2020). doi: 10.3390/cells9040880
- McInnes IB, Schett G. The Pathogenesis of Rheumatoid Arthritis. *N Engl J Med* (2011) 365:2205–19. doi: 10.1056/NEJMra1004965
- Marsal S, Julià A. Rheumatoid Arthritis Pharmacogenomics. *Pharmacogenomics* (2010) 11:617–9. doi: 10.2217/pgs.10.53
- Burmester GR, Pope JE. Novel Treatment Strategies in Rheumatoid Arthritis. *Lancet* (2017) 389:2338–48. doi: 10.1016/S0140-6736(17)31491-5
- Deane KD, Holers VM. Rheumatoid Arthritis Pathogenesis, Prediction, and Prevention: An Emerging Paradigm Shift. *Arthritis Rheumatol* (2021) 73:181–93. doi: 10.1002/art.41417
- Sharif K, Sharif A, Jumah F, Oskouian R, Tubbs RS. Rheumatoid Arthritis in Review: Clinical, Anatomical, Cellular and Molecular Points of View. *Clin Anat* (2018) 31:216–23. doi: 10.1002/ca.22980
- van der Woude D, van der Helm-van Mil AHM. Update on the Epidemiology, Risk Factors, and Disease Outcomes of Rheumatoid Arthritis. *Best Pract Res Clin Rheumatol* (2018) 32:174–87. doi: 10.1016/j.berh.2018.10.005
- Liang S. Artificial Intelligence on High Throughput Data for Biomedical Research. *Comb Chem High Throughput Screen* (2021) 24:891–2. doi: 10.2174/138620732407210504084747
- Gao M, Ling M, Tang X, Wang S, Xiao X, Qiao Y, et al. Comparison of High-Throughput Single-Cell RNA Sequencing Data Processing Pipelines. *Brief Bioinform* 22 (2021). doi: 10.1093/bib/bbaa116
- DeGregory KW, Kuiper P, DeSilvio T, Pleuss JD, Miller R, Roginski JW, et al. A Review of Machine Learning in Obesity. *Obes Rev* (2018) 19:668–85. doi: 10.1111/obr.12667
- Sirsat MS, Fermé E, Câmara J. Machine Learning for Brain Stroke: A Review. *J Stroke Cerebrovasc Dis* (2020) 29:105162. doi: 10.1016/j.jstrokecerebrovasdis.2020.105162
- Triantafyllidis AK, Tsanas A. Applications of Machine Learning in Real-Life Digital Health Interventions: Review of the Literature. *J Med Internet Res* (2019) 21:e12286. doi: 10.2196/12286
- Rauschert S, Raubenheimer K, Melton PE, Huang RC. Machine Learning and Clinical Epigenetics: A Review of Challenges for Diagnosis and Classification. *Clin Epigenet* (2020) 12:51. doi: 10.1186/s13148-020-00842-4
- Peiffer-Smadja N, Rawson TM, Ahmad R, Buchard A, Georgiou P, Lescuré FX, et al. Machine Learning for Clinical Decision Support in Infectious Diseases: A Narrative Review of Current Applications. *Clin Microbiol Infect* (2020) 26:584–95. doi: 10.1016/j.cmi.2019.09.009
- Heo J, Yoon JG, Park H, Kim YD, Nam HS, Heo JH. Machine Learning-Based Model for Prediction of Outcomes in Acute Stroke. *Stroke* (2019) 50:1263–5. doi: 10.1161/STROKEAHA.118.024293
- Vamathevan J, Clark D, Czodrowski P, Dunham I, Ferran E, Lee G, et al. Applications of Machine Learning in Drug Discovery and Development. *Nat Rev Drug Discov* (2019) 18:463–77. doi: 10.1038/s41573-019-0024-5
- Zhao W, Langfelder P, Fuller T, Dong J, Li A, Hovarth S. Weighted Gene Coexpression Network Analysis: State of the Art. *J Biopharm Stat* (2010) 20:281–300. doi: 10.1080/10543400903572753
- Climente-González H, Azencott CA, Kaski S, Yamada M. Block HSIC Lasso: Model-Free Biomarker Detection for Ultra-High Dimensional Data. *Bioinformatics* (2019) 35:i427–35. doi: 10.1093/bioinformatics/btz333
- Langfelder P, Horvath S. WGCNA: An R Package for Weighted Correlation Network Analysis. *BMC Bioinf* (2008) 9:559. doi: 10.1186/1471-2105-9-559
- Maksimov MO, Pan SJ, James Link A. Lasso Peptides: Structure, Function, Biosynthesis, and Engineering. *Nat Prod Rep* (2012) 29:996–1006. doi: 10.1039/c2np20070h
- Subramanian A, Tamayo P, Mootha VK, Mukherjee S, Ebert BL, Gillette MA, et al. Gene Set Enrichment Analysis: A Knowledge-Based Approach for Interpreting Genome-Wide Expression Profiles. *Proc Natl Acad Sci U S A* (2005) 102:15545–50. doi: 10.1073/pnas.0506580102
- Yu G, Wang LG, Han Y, He QY. ClusterProfiler: An R Package for Comparing Biological Themes Among Gene Clusters. *Omics* (2012) 16:284–7. doi: 10.1089/omi.2011.0118
- Gaudet P, Dessimoz C. Gene Ontology: Pitfalls, Biases, and Remedies. *Methods Mol Biol* (2017) 1446:189–205. doi: 10.1007/978-1-4939-3743-1\_14
- Song X, Lin Q. Genomics, Transcriptomics and Proteomics to Elucidate the Pathogenesis of Rheumatoid Arthritis. *Rheumatol Int* (2017) 37:1257–65. doi: 10.1007/s00296-017-3732-3
- Kumar LD, Karthik R, Gayathri N, Sivasudha T. Advancement in Contemporary Diagnostic and Therapeutic Approaches for Rheumatoid Arthritis. *BioMed Pharmacother* (2016) 79:52–61. doi: 10.1016/j.biopha.2016.02.001
- Mun S, Lee J, Park M, Shin J, Lim MK, Kang HG. Serum Biomarker Panel for the Diagnosis of Rheumatoid Arthritis. *Arthritis Res Ther* (2021) 23:31. doi: 10.1186/s13075-020-02405-7
- Wang J, Yan S, Yang J, Lu H, Xu D, Wang Z. Non-Coding RNAs in Rheumatoid Arthritis: From Bench to Bedside. *Front Immunol* (2019) 10:3129. doi: 10.3389/fimmu.2019.03129
- Reel PS, Reel S, Pearson E, Trucco E, Jefferson E. Using Machine Learning Approaches for Multi-Omics Data Analysis: A Review. *Biotechnol Adv* (2021) 49:107739. doi: 10.1016/j.biotechadv.2021.107739
- Glaab E, Rauschenberger A, Banzi R, Gerardi C, Garcia P, Demotes J. Biomarker Discovery Studies for Patient Stratification Using Machine Learning Analysis of Omics Data: A Scoping Review. *BMJ Open* (2021) 11:e053674. doi: 10.1136/bmjopen-2021-053674
- Li D, Zhang L, Liu Y, Sun H, Onwuka JU, Zhao Z, et al. Specific DNA Methylation Markers in the Diagnosis and Prognosis of Esophageal Cancer. *Aging (Albany NY)* (2019) 11:11640–58. doi: 10.18632/aging.102569
- Li YM, Li ZL, Chen F, Liu Q, Peng Y, Chen M. A LASSO-Derived Risk Model for Long-Term Mortality in Chinese Patients With Acute Coronary Syndrome. *J Transl Med* (2020) 18:157. doi: 10.1186/s12967-020-02319-7
- Zhang Z, Chen L, Xu P, Xing L, Hong Y, Chen P. Gene Correlation Network Analysis to Identify Regulatory Factors in Sepsis. *J Transl Med* (2020) 18:381. doi: 10.1186/s12967-020-02561-z
- You H, Lin H, Zhang Z. CKS2 in Human Cancers: Clinical Roles and Current Perspectives (Review). *Mol Clin Oncol* (2015) 3:459–63. doi: 10.3892/mco.2015.501
- Pines J. Cell Cycle: Reaching for a Role for the Cks Proteins. *Curr Biol* (1996) 6:1399–402. doi: 10.1016/S0960-9822(96)00741-5
- Martinsson-Ahlzén HS, Liberal V, Grünenfelder B, Chaves SR, Spruck CH, Reed SI. Cyclin-Dependent Kinase-Associated Proteins Cks1 and Cks2 Are Essential During Early Embryogenesis and for Cell Cycle Progression in Somatic Cells. *Mol Cell Biol* (2008) 28:5698–709. doi: 10.1128/MCB.01833-07
- Liao L, Liang K, Lan L, Wang J, Guo J. Marker Genes Change of Synovial Fibroblasts in Rheumatoid Arthritis Patients. *BioMed Res Int* (2021) 2021:5544264. doi: 10.1155/2021/5544264
- Goronzy JJ, Weyand CM. T and B Cell-Dependent Pathways in Rheumatoid Arthritis. *Curr Opin Rheumatol* (1995) 7:214–21. doi: 10.1097/00002281-199505000-00010

**Conflict of Interest:** The authors declare that the research was conducted in the absence of any commercial or financial relationships that could be construed as a potential conflict of interest.

**Publisher's Note:** All claims expressed in this article are solely those of the authors and do not necessarily represent those of their affiliated organizations, or those of the publisher, the editors and the reviewers. Any product that may be evaluated in this article, or claim that may be made by its manufacturer, is not guaranteed or endorsed by the publisher.

Copyright © 2022 Jiang, Zhou and Shen. This is an open-access article distributed under the terms of the Creative Commons Attribution License (CC BY). The use, distribution or reproduction in other forums is permitted, provided the original author(s) and the copyright owner(s) are credited and that the original publication in this journal is cited, in accordance with accepted academic practice. No use, distribution or reproduction is permitted which does not comply with these terms.



# SARS-CoV-2 Achieves Immune Escape by Destroying Mitochondrial Quality: Comprehensive Analysis of the Cellular Landscapes of Lung and Blood Specimens From Patients With COVID-19

Chenyang Duan<sup>1\*</sup>, Ruiyan Ma<sup>2</sup>, Xue Zeng<sup>1</sup>, Bing Chen<sup>1</sup>, Dongyao Hou<sup>1</sup>, Ruixue Liu<sup>1</sup>, Xuehan Li<sup>1</sup>, Liangming Liu<sup>3</sup>, Tao Li<sup>3</sup> and He Huang<sup>1\*</sup>

## OPEN ACCESS

### Edited by:

Hongjuan You,  
Xuzhou Medical University, China

### Reviewed by:

Ming-bo Cao,  
First Affiliated Hospital of Zhengzhou  
University, China  
Xiaochuan Liu,  
University of California, Riverside,  
United States

### \*Correspondence:

Chenyang Duan  
duanchenyang1991@cqmu.edu.cn  
He Huang  
huanghe@cqmu.edu.cn

### Specialty section:

This article was submitted to  
Viral Immunology,  
a section of the journal  
Frontiers in Immunology

**Received:** 17 May 2022

**Accepted:** 13 June 2022

**Published:** 01 July 2022

### Citation:

Duan C, Ma R, Zeng X, Chen B,  
Hou D, Liu R, Li X, Liu L, Li T  
and Huang H (2022) SARS-CoV-2  
Achieves Immune Escape by  
Destroying Mitochondrial Quality:  
Comprehensive Analysis of the  
Cellular Landscapes of Lung  
and Blood Specimens From  
Patients With COVID-19.  
*Front. Immunol.* 13:946731.  
doi: 10.3389/fimmu.2022.946731

<sup>1</sup> Department of Anesthesiology, The Second Affiliated Hospital of Chongqing Medical University, Chongqing, China, <sup>2</sup> Department of Cardiovascular Surgery, Xinqiao Hospital, Army Medical University, Chongqing, China, <sup>3</sup> Department of Shock and Transfusion, State Key Laboratory of Trauma, Burns and Combined Injury, Daping Hospital, Army Medical University, Chongqing, China

Mitochondria get caught in the crossfire of coronavirus disease 2019 (COVID-19) and antiviral immunity. The mitochondria-mediated antiviral immunity represents the host's first line of defense against viral infection, and the mitochondria are important targets of COVID-19. However, the specific manifestations of mitochondrial damage in patients with COVID-19 have not been systematically clarified. This study comprehensively analyzed one single-cell RNA-sequencing dataset of lung tissue and two bulk RNA-sequencing datasets of blood from COVID-19 patients. We found significant changes in mitochondrion-related gene expression, mitochondrial functions, and related metabolic pathways in patients with COVID-19. SARS-CoV-2 first infected the host alveolar epithelial cells, which may have induced excessive mitochondrial fission, inhibited mitochondrial degradation, and destroyed the mitochondrial calcium uniporter (MCU). The type II alveolar epithelial cell count decreased and the transformation from type II to type I alveolar epithelial cells was blocked, which exacerbated viral immune escape and replication in COVID-19 patients. Subsequently, alveolar macrophages phagocytized the infected alveolar epithelial cells, which decreased mitochondrial respiratory capacity and activated the ROS-HIF1A pathway in macrophages, thereby aggravating the pro-inflammatory reaction in the lungs. Infected macrophages released large amounts of interferon into the blood, activating mitochondrial IFI27 expression and destroying energy metabolism in immune cells. The plasma differentiation of B cells and lung-blood interaction of regulatory T cells (Tregs) was exacerbated, resulting in a cytokine storm and excessive inflammation. Thus, our findings systematically explain immune escape and excessive inflammation seen during COVID-19 from the perspective of mitochondrial quality imbalance.

**Keywords:** COVID-19, mitochondrial quality, immune escape, inflammation, cytokine storm

## INTRODUCTION

Coronavirus disease 2019 (COVID-19) is an acute respiratory syndrome caused by severe acute respiratory syndrome coronavirus 2 (SARS-CoV-2) infection (1). Patients with COVID-19 manifest a range of varying severity, ranging from no symptoms (asymptomatic) to severe pneumonia, which can progress to acute respiratory distress syndrome, metabolic acidosis, septic shock, coagulopathy, organ failure, and even death (2). According to the World Health Organization, the cumulative numbers of confirmed cases and deaths reported worldwide have exceeded 433 and 5.9 million until April 2022, respectively, since its outbreak in 2019 (3, 4). The disease is still spreading with more than 5,00,000 new confirmed cases and nearly 20,000 deaths per day. Thus, the spread of SARS-CoV-2 is still a serious Public Health Emergency of International Concern. Therefore, it is essential to investigate the pathological reactions involved in and immune mechanisms underlying the effects of COVID-19.

SARS-CoV-2 is an enveloped positive-strand single-stranded RNA virus of the family Coronaviridae, which binds to human angiotensin-converting enzyme 2 or human dipeptidyl peptidase 4 with its receptor-binding domain of the S protein (5). After SARS-CoV-2 enters the cell, it efficiently replicates and produces offspring. In patients with COVID-19, the most common presentation in the chest computed tomography scan is ground glass shadows distributed in one or both peripheral lung and subpleural regions, and reticular and/or interlobular septal thickening and consolidation (6). These signs are closely related to the alveolar edema and inflammatory response caused by SARS-CoV-2 infection (7). Tissue biopsies and autopsies have revealed pathological manifestations such as alveolar edema, hyaline membrane formation, multinucleated enlarged cell deposition, and diffuse thickening of the alveolar wall in the lungs of COVID-19 patients (8).

Recent studies have suggested that COVID-19 should be considered a vascular disease (9). In addition to lung injury, patients with COVID-19 also show obvious characteristics of vascular damage, including endothelial cell inflammation in the pulmonary artery, extensive thrombosis, and microvascular lesions (2). Electron microscopic analysis has shown the presence of virus particles in lymphocytes and vascular endothelial cells, indicating that the vascular injury and blood immune response may be directly related to cytotoxic invasion by the virus (10). Cytokine storm (CS) has also been observed in the blood of patients with moderate or severe COVID-19; strong systemic symptoms have been noted in such cases. In the absence of timely and effective treatment, CS can lead to the systemic inflammatory syndrome, multiple organ dysfunction, and even death (11). Many cytokines, such as interleukin (IL)-6, IL-1, IL-10, tumor necrosis factor- $\alpha$ , and interferon (IFN)- $\gamma$  (12), and various types of cells, including macrophages, neutrophils, eosinophils, lymphocytes, and basophils, are involved in CS (13). However, the relationship between the CS in the blood and the lung injury caused by SARS-CoV-2 has not yet been clarified.

Mitochondria are organelles that constitute key components of human innate immunity and energy metabolism. Mitochondrial

quality control factors, including mitochondrion-related gene expression, mitochondrial functions, and related metabolic pathways, regulate the processing and turnover of native proteins to control protein import, signaling cascades, mitochondrial dynamics, lipid biogenesis the proper function of mitochondria. Thus, mitochondrial quality control mechanisms are important in integrating mitochondria into the cellular environment (14). Recent research has shown that SARS-CoV-2 can inhibit the innate immune response of the human body and that mitochondria comprise one of the first lines of defense against SARS-CoV-2 infection (15). Compared with other viruses, such as respiratory syncytial virus, seasonal influenza A virus, and human parainfluenza virus, SARS-CoV-2 is the only virus that can reduce mitochondrion-related protein expression (16). SARS-CoV-2 can colonize mitochondria and interact with mitochondrial protein translocation mechanisms to target its coding products to the mitochondria (17); this process enables inhibition of the degradation of viral proteins and host misfolded proteins (including mitochondrial proteins) and is, therefore, crucial for viral replication and escape from host innate immunity (16). This phenomenon partly explains why COVID-19 causes more severe effects in older people and people with mitochondrial metabolic dysfunction (17). Although studies (17, 18) have reported that mitochondria are intricately involved in COVID-19 etiopathogenesis, the specific manifestations of mitochondrial damage in patients with this disease and the relationship between this damage and COVID-19 occurrence and development have not been systematically clarified.

This study aimed to clarify the process involved in immunopathological changes, such as immune escape, and the cell fate in COVID-19 by studying the expression and translocation of mitochondrion-related genes in lung tissue and the process involved in the lung–blood interaction in COVID-19. Therefore, we performed in-depth analysis of a set of single-cell datasets of the lung tissue as well as two sets of transcriptome datasets of the peripheral blood from COVID-19 patients and systematically detected the changes in mitochondrion-related gene expression, mitochondrial functions as well as related metabolic pathways to lay the foundation on using mitochondrial quality control as the main intervention for COVID-19.

## MATERIALS AND METHODS

### Processing of Data Obtained From the Gene Expression Omnibus Dataset

Single-cell RNA-seq datasets pertaining to human lung tissue were obtained from a Gene Expression Omnibus (GEO) dataset (GSE171524), including data for frozen lung specimens obtained from 19 patients with COVID-19 and 7 control patients for whom short postmortem interval autopsies had been performed. Two RNA-seq datasets pertaining to human blood samples were obtained from two GEO datasets (GSE157103 and GSE152641). The GSE157103 dataset includes data for 126 plasma and leukocyte samples from hospitalized patients with or without

COVID-19 ( $n = 100$  and  $26$ , respectively). The GSE152641 dataset includes data for peripheral blood samples from 24 healthy controls and 62 prospectively enrolled patients with community-acquired lower respiratory tract infection by SARS-CoV-2 within the first 24 h of hospital admission.

## Single-Cell RNA-Seq Data Processing

Single-cell RNA-seq data were analyzed using a NovaSeq 6000 sequencing system (Illumina, USA). Unique molecular identifier tools were used to identify the whitelist of the cell barcodes. Single-cell gene expression matrices were generated using the Celescope software (version 1.7.2, Singleron, Germany). The transcripts were aligned to the human GRCh38 reference genome, which was appended with the entire SARS-CoV-2 genome (GenBank, MN908947.3) as an additional chromosome to the human reference genome (19). Cells with more than 200 detected genes and a mitochondrial unique molecular identifier rate of less than 30% were considered to have passed cell quality control. Subsequently, principal component analysis was performed for the scaled data to determine the top 2,000 highly variable genes and top 10 principal components, as well as for tSNE and UMAP construction (20). The main cell types were identified by manual annotation of the genes differentially expressed between the clusters. The positive markers for each cluster were identified on the basis of a previous study (19), with a minimal fraction of 25% and log-transformed fold change threshold of 0.25.

## Bulk RNA-Seq Data Processing

Raw reads were trimmed using the GeneChem cloud analysis platform. The trimmed reads were mapped to the hg19 genome using HISAT2 (version 2.0.4), thereby generating sam files, which were then converted to bam files using SAMtools (version 1.6). HTSeq (version 0.11.0) was used to calculate the read count for each gene. DEGs were identified using the R package DESeq2 (version 1.26.0), with a cutoff of adjusted  $p$ -value  $< 0.05$  and  $|\log_2FC| > 1$ .

## Annotation of Gene Functions

To investigate the potential biological functions of mitochondrial DEGs in individuals with or without COVID-19, the “clusterProfiler” package (version 3.16.1) in R was used to perform the GO analysis, KEGG analysis, and GSEA (21). We performed GSEA using the “GSEA” R package to estimate the biological function of different clusters, which estimates the variations in pathway activity over a sample population in an unsupervised manner (22). Significantly enriched pathways were filtered using an adjusted  $p$ -value of  $< 0.05$ .

## Estimation of Immune Cell Fractions

The abundance of immune cells was determined by cell type identification *via* “CIBERSORT,” an algorithm that combines support vector regression from purified leukocyte subsets. The bulk RNA-seq data were uploaded to the CIBERSORT website (<https://cibersortx.stanford.edu/>), and the LM22 signature gene matrix served as an input of the “CIBERSORT” algorithm. Correlations between gene expression and the immune infiltrate abundance were estimated using the “Gene” module.

Additionally, the “SCNA” module was used to examine the correlation between somatic copy number alterations and immune infiltrate abundance.

## Statistical Analysis

The statistical analysis was performed using R (version 3.6.1; R Foundation for Statistical Computing, Vienna, Austria), complemented by IBM SPSS Statistics 24.0 (IBM, Inc., Armonk, NY, USA). All statistical tests were two-sided, and a  $p$ -value  $< 0.05$  was considered statistically significant. Other statistical methods were described within the related results and Figure legends.

## RESULTS

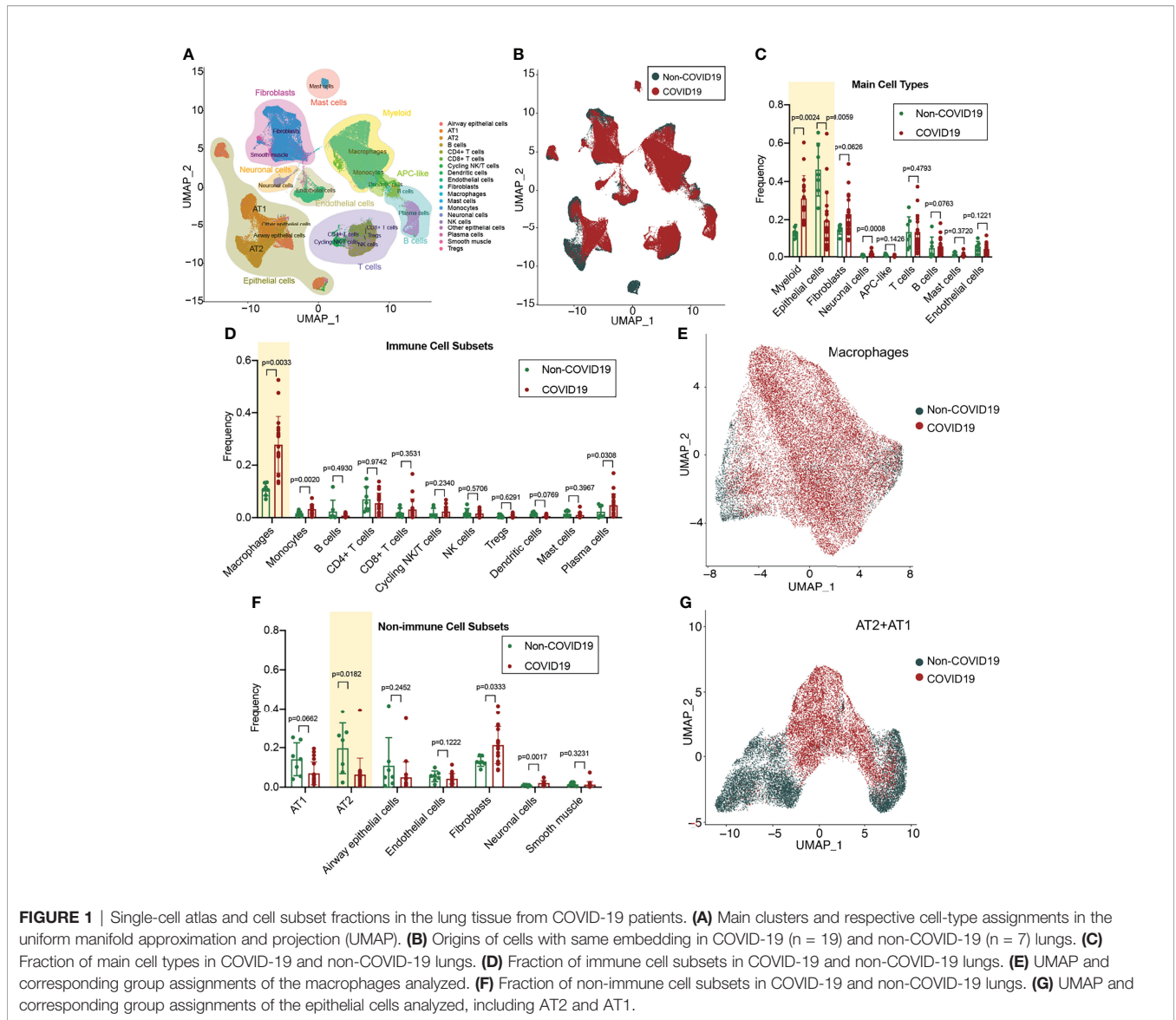
### The Cellular Landscape of Lung Tissue From Patients With COVID-19

The cell types in the lung tissue are complex. For in-depth analysis of lung tissue lesions from patients with COVID-19, we selected a single-cell RNA-sequencing (RNA-seq) dataset of lung tissue from patients with COVID-19 (GSE171524), which includes data on the frozen lung specimens obtained from 19 patients with COVID-19 and 7 control patients with short postmortem interval autopsies. We identified nine main cell types by using the uniform manifold approximation and projection (UMAP) method: epithelial cells ( $n = 30,070$  cells), myeloid cells ( $n = 29,632$  cells), fibroblasts ( $n = 22,909$  cells), endothelial cells ( $n = 5,386$  cells), T and natural killer lymphocytes ( $n = 16,751$  cells), lymphocytes and plasma cells ( $n = 7,236$  cells), neuronal cells ( $n = 2,017$  cells), mast cells ( $n = 1,464$  cells), and antigen-presenting cells (primarily dendritic cells;  $n = 849$  cells) (Figure 1A). The disease sorting results showed that the cell types and counts in the lung tissue of COVID-19 patients significantly differed from those of non-COVID-19 patients (Figure 1B). In the lung tissue of patients with severe COVID-19, the myeloid cell count significantly increased ( $p=0.0024$ ) and the epithelial cell count significantly decreased ( $p=0.0059$ ) (Figure 1C). Further analysis of immune-related cell subsets revealed that the increase in myeloid cells was mainly due to the large increase in the alveolar macrophage count ( $p=0.0033$ ) (Figure 1D) and that the macrophage functions in the COVID-19 group may also be significantly different from those in the non-COVID-19 group (Figure 1E). Assays of non-immune-related cell subsets indicated that the decrease in epithelial cells was mainly due to the considerable decrease in type II alveolar epithelial cell (AT2) count ( $p=0.0182$ ) (Figure 1F); it was found that the transformation from AT2 to type I alveolar epithelial cells (AT1) may be blocked in the lung tissue of patients with COVID-19 (Figures 1F, G).

### Aberrant Macrophage Transformation Was Influenced by Mitochondrial Dysfunction in the Lung Tissue of COVID-19 Patients

To analyze the changes in the alveolar macrophage count and functions in COVID-19 lung tissues, we performed dimensionality reduction clustering and subgroup annotation





of the macrophages. Seven subsets were identified using the t-distributed stochastic neighbor embedding (tSNE) method: monocytes, transition monocytes, infiltrating macrophages, regulatory macrophages, primary macrophages, mature macrophages, and active macrophages (**Figure 2A**). The first three subsets belonged to the macrophage infiltrating trail, whereas the last three subsets belonged to the macrophage activating trail (**Figure 2B**).

To analyze the mitochondrial damage in the alveolar macrophages of patients with COVID-19, we first searched for all mitochondrion-encoding genes and mitochondrial function-regulating genes from the Gene Set Enrichment Analysis (GSEA), Gene Cards, and UniProt databases and merged them into a complete mitochondrion-related gene cluster comprising 1,513 genes (**Table S1**). We screened mitochondrial differentially expressed genes (mito-DEGs) in at least 3 macrophage subsets and identified 31 upregulated

mito-DEGs (HIF1A, HSPA1A, HSP90AA1, TYMP, HSPD1, SQSTM1, SOD2, SLC44A1, IDH1, HSPE1, GLUL, ATP6V1C1, ANXA6, TSPO, MTUS1, MRPS6, LRRK2, IFI27, GLS, GK, ATP13A3, VAT1, SLC25A6, RPS3, RALA, MT-CO2, GPX4, GABARAP, DDTT4, CYBSA, and ATP6AP1) (**Figure 2C**) and 27 downregulated mito-DEGs (PRKN, ACSM3, WWOX, MT-ND1, MHP2, IGF1, ANK2, ACSM1, NUBPL, MTERF1, FOXO3, VRK2, TRAK1, SGK1, OPA3, MTHFD1L, MT-ND2, MT-CO1, KMO, IMMP2L, ECHDC2, DECR1, ATG7, ACSM3, ACSM6, ACACB, and RDH13) (**Figure 2D**). Gene expression analysis of macrophage subsets revealed that the mito-DEGs in the macrophage infiltrating trail were gradually upregulated, whereas those in the macrophage activating trail were gradually downregulated (**Figure 2E**). These results suggested that alveolar macrophage transformation is closely related to the expression of mitochondrion-related genes in patients with COVID-19.

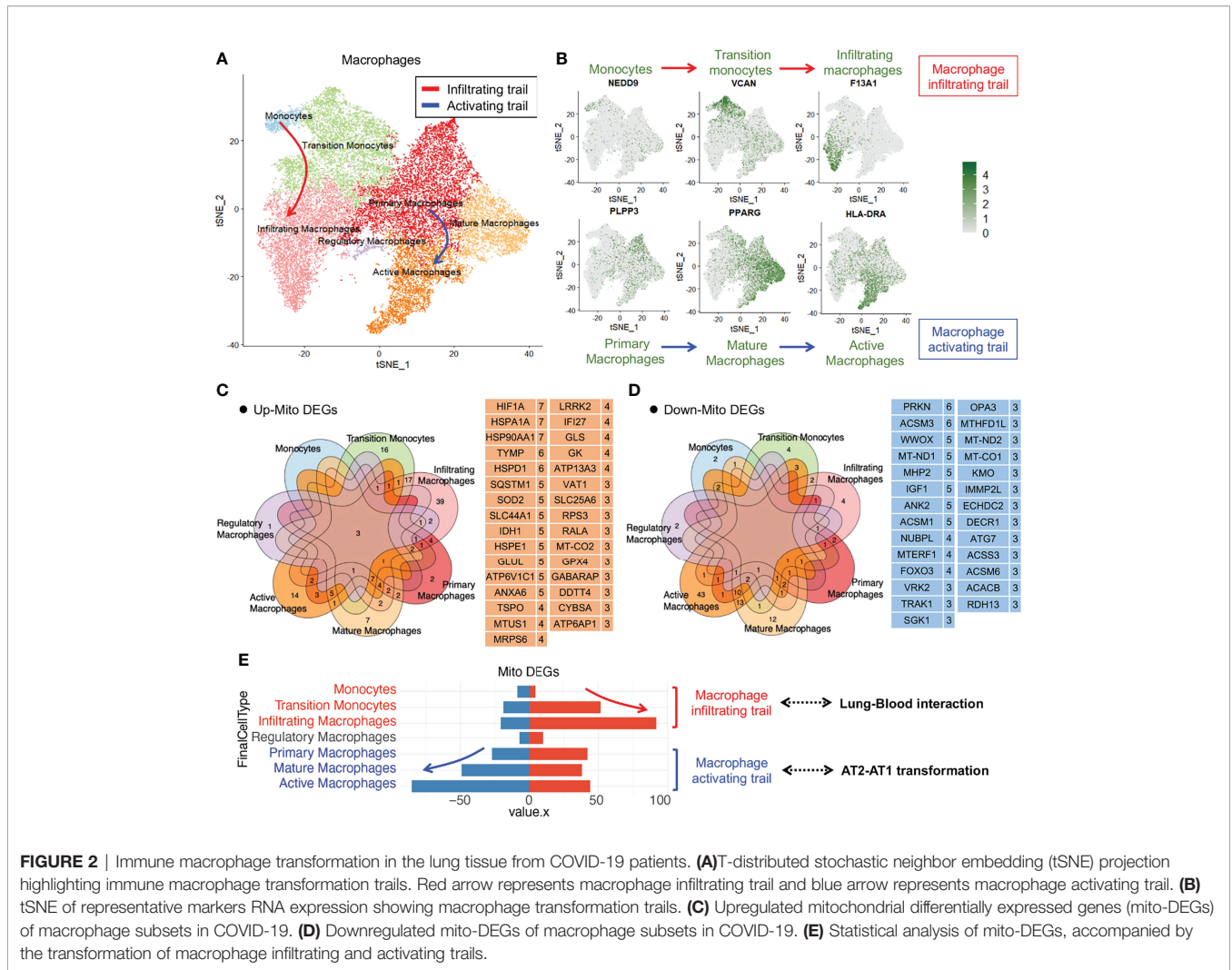


**FIGURE 2 |** Immune macrophage transformation in the lung tissue from COVID-19 patients. **(A)**T-distributed stochastic neighbor embedding (tSNE) projection highlighting immune macrophage transformation trails. Red arrow represents macrophage infiltrating trail and blue arrow represents macrophage activating trail. **(B)** tSNE of representative markers RNA expression showing macrophage transformation trails. **(C)** Upregulated mitochondrial differentially expressed genes (mito-DEGs) of macrophage subsets in COVID-19. **(D)** Downregulated mito-DEGs of macrophage subsets in COVID-19. **(E)** Statistical analysis of mito-DEGs, accompanied by the transformation of macrophage infiltrating and activating trails.

The changes in mito-DEGs in different macrophage subsets are directly reflected in the bubble chart provided in **Figure 3A**; after SARS-CoV-2 infection, *HIF1A* expression significantly increased and *PRKN* expression significantly decreased (**Figure 3B**) in all the macrophage subsets. Based on these mito-DEGs, we further analyzed the mitochondrial functions of macrophage subsets by using GSEA-based pathway enrichment analysis. The key pathways involved in mitochondrial quality regulation, such as mitochondrial oxidative phosphorylation, mitochondrial autophagy, and apoptotic mitochondrial changes, were generally enriched in most macrophage subsets in patients with COVID-19 (**Figure S1**). Gene set variation analysis (GSVA) further showed that the mitochondrial pathway activity in the macrophage activating trail was much higher in patients with COVID-19 (**Figure 3C**). Activated macrophages are a subset of innate alveolar macrophages; they have antigen-presenting characteristics and can phagocytize virus-infected alveolar epithelial cells, which may play an important role in the repair of lung tissue injury. The mitochondrial pathway activity in the macrophage infiltrating trail was lower in patients with COVID-19 (**Figure 3C**). Infiltrating

macrophages may belong to the exogenous macrophage subsets produced by the lung's damaged blood immune cells.

### Impaired Alveolar Epithelial Regeneration Was Influenced by Excessive Mitochondrial Fission and MCU Destruction in the Lung Tissue of COVID-19 Patients

To investigate alveolar epithelial regeneration in patients with COVID-19, we performed subset analysis and found that the two typical alveolar epithelial cell subsets, AT2 and AT1, were clearly distinguished in the non-COVID-19 group; by contrast, in patients with COVID-19, the cellular properties of the AT2 and AT1 subsets gradually converged, leading to their transformation to mitochondrion-damaged alveolar epithelial cells (**Figure 4A**).

To examine the link between alveolar epithelial regeneration and mitochondrial damage in patients with COVID-19, we separately analyzed the mito-DEGs of the AT2 and AT1

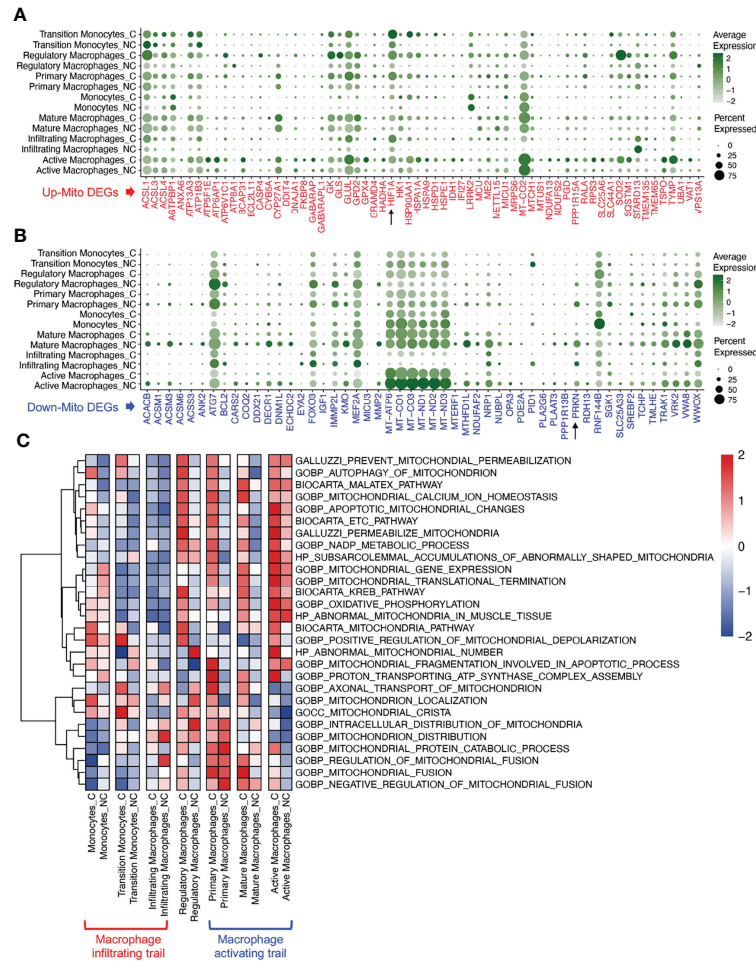


**FIGURE 3** | Mitochondrial functions of macrophage subsets in COVID-19 lung tissues. **(A)** Bubble chart of upregulated mito-DEGs of macrophage subsets in COVID-19. **(B)** Bubble chart of downregulated mito-DEGs of macrophage subsets in COVID-19. **(C)** GSEA of mitochondrion-related pathways in macrophage subsets in COVID-19.

subsets in patients with COVID-19 (Figures 4B, C). We identified 38 mito-DEGs that showed consistent changes in expression in the AT2 and AT1 subsets in patients with COVID-19. The mito-DEGs upregulated in AT2 and AT1 included the following: 13 mitochondrion-coding genes (mitochondrial COX subunits, i.e., MT-CO1, MT-CO2, and MT-CO3; mitochondrial NADH subunits, i.e., MT-ND1, MT-ND2, MT-ND3, MT-ND4, MT-ND4L, MT-ND5, and MT-ND6; and ATP synthases, i.e., MT-ATP6, MT-ATP8, and MT-CYB) and 20 mitochondrial function regulatory genes (HSPD1, HSPA1A, SQSTM1, MUC1, SFN, BIRC3, TKT, BNIP3L, RACK1, MRPS6, TNFSF10, YWHAG, CTTN, NDUFS1, MRPS25, ME1, XIAP, MRPL14, BCL2L1, and VPS13C). The mito-DEGs showing downregulation in the AT2 and AT1 subsets included MCU, TP53BP2, JUN, PRKG1, and NR4A1. In addition, some mito-DEGs were reversely altered in the AT2 and AT1 subsets (e.g., LRRK2, PID1, SOD2, CLIC4, and ERBB4) or showed altered expression in the AT2 or AT1 subset in patients with COVID-19 (Figures 4B–D). It should be noted

that the general upregulation of mitochondrion-encoding genes suggested that the alveolar epithelial cells of patients with COVID-19 would have excessive mitochondrial fission, resulting in a large increase in the number of damaged mitochondria, and the decrease in MCU expression suggested that the mitochondrial calcium transport channels of alveolar epithelial cells were disrupted in patients with COVID-19 (Figure 4D).

Functional enrichment analysis also established that several key aspects of mitochondrial quality regulation, such as mitochondrial organization, apoptotic mitochondrial changes, mitochondrial membrane permeability, mitochondrial membrane potential, mitophagy, mitochondrial calcium homeostasis, and cytoskeleton regulation, were impaired to various degrees (Figure 4E). The Kyoto Encyclopedia of Genes and Genomes (KEGG) annotation results further showed that the damaged mitochondrial clearance and degradation pathways in alveolar epithelial cells were significantly inhibited, resulting in the accumulation of large amounts of mitochondrion-damaged

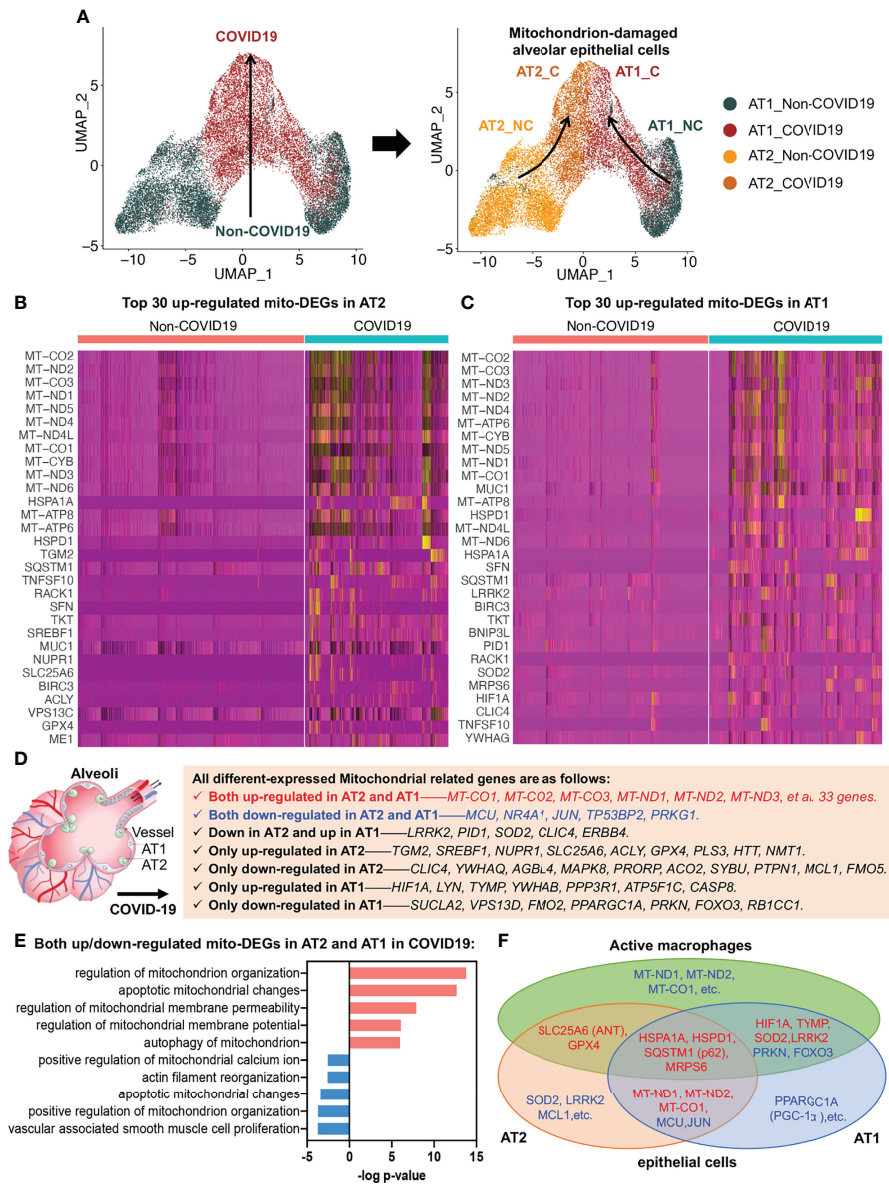


**FIGURE 4 |** Alveolar epithelial regeneration in COVID-19 lung tissues. **(A)** UMAP and corresponding group assignments of AT2 and AT1 in COVID-19. C: COVID-19 group; NC: Non-COVID-19 group. **(B)** Heat map of top 30 upregulated mito-DEGs in AT2 during COVID-19. **(C)** Heat map of top 30 upregulated mito-DEGs in AT1 during COVID-19. **(D)** Statistical analysis of mito-DEGs in AT2 and AT1 during COVID-19. **(E)** GO pathway enrichment analysis in relation to mito-DEGs in AT2 and AT1 during COVID-19. **(F)** Venn diagram showing the intersection mito-DEGs from AT2, AT1, and active macrophages during COVID-19.

alveolar epithelial cells in patients with COVID-19 (Figure S2). The accumulation of damaged mitochondria in the AT2 subset was mainly due to inhibition of apoptotic mitochondrial changes (Figure S2A), whereas the accumulation in the AT1 subset was mainly due to inhibition of the mitophagy pathway (Figure S2B).

The mito-DEGs in the AT2, AT1, and active macrophage subsets are shown in the Venn diagram in Figure 4F; the main genetic signatures of active macrophages that phagocytized virus-infected epithelial cells were found to be increased expression of HIF1A, TYMP, SOD2, LRRK2, HSPA1A, HSPD1, SQSTM1 (p62), MRPS6, SLC25A6 (ANT), GPX4 and decreased expression of

PRKN, FOXO3. In addition, the decreased expression of mitochondrion-encoding genes, such as MT-ND1, MT-ND2, and MT-CO1, were also found in active macrophages after phagocytosis of virus-infected alveolar epithelial cells (Figure 4F).

### Irregular Distribution of Immune Cells Was Affected by the Mitochondrial IFI27-Mediated IFN Immune Response in the Blood Samples of COVID-19 Patients

To analyze mitochondrial damage in the blood immune cells of patients with COVID-19, we selected two bulk RNA-seq datasets

(GSE157103 and GSE152641) of peripheral blood from patients with this disease. The GSE157103 dataset contains information on the blood leukocyte samples from 100 patients with severe COVID-19 and 26 patients without COVID-19. The GSE152641 dataset contains information on the peripheral blood samples from 62 patients with COVID-19 and whole blood samples from 24 healthy controls. The differential expression analysis of mitochondrion-related genes is shown in **Figures 5A, B**. The Venn diagram shows that the following 14 mitochondrion-related genes were upregulated in the blood of patients with COVID-19 in both datasets: IFI27, IFIH1, IFIT2, IFI6, OAS1, XAF1, IFIT3, CMPK2, RSAD2, GLDC, CCNB1, TYMS, CDK1, and OLFM4 (**Figure 5C**). KEGG annotation showed that these significantly upregulated mitochondrion-related genes were closely related to the blood immune response after viral infection. Gene Ontology (GO) functional enrichment analysis showed that these significantly upregulated mitochondrion-related genes were closely related to viral immune response pathways, such as the type I IFN signaling pathway, the

pathways involved in the response to virus and viral genome replication, and mitochondrial dysfunction pathways such as those involved in mitochondrial ATP synthesis and apoptotic mitochondrial changes (**Figure 5D**). Among the 14 mitochondrion-related genes showing upregulation in the blood samples, IFI27 showed significantly upregulated expression in the infiltrating macrophage subsets of patients with COVID-19 (**Figures 2C, 5E**), suggesting that IFI27 is involved in the blood immune response and in the lung–blood interaction process after viral infection.

To examine the blood immune response of patients with COVID-19 and its relationship with IFI27, we used CIBERSORT to analyze the landscape of immune cells in the blood of patients with COVID-19. GSE157103 dataset analysis showed that the proportions of naïve B cells and regulatory T cells (Tregs) decreased, whereas the proportions of memory B cells, plasma cells, and activated dendritic cells increased in the blood of patients with COVID-19 (**Figures 6A, B**). Furthermore, GSE157103 dataset analysis showed that the proportions of

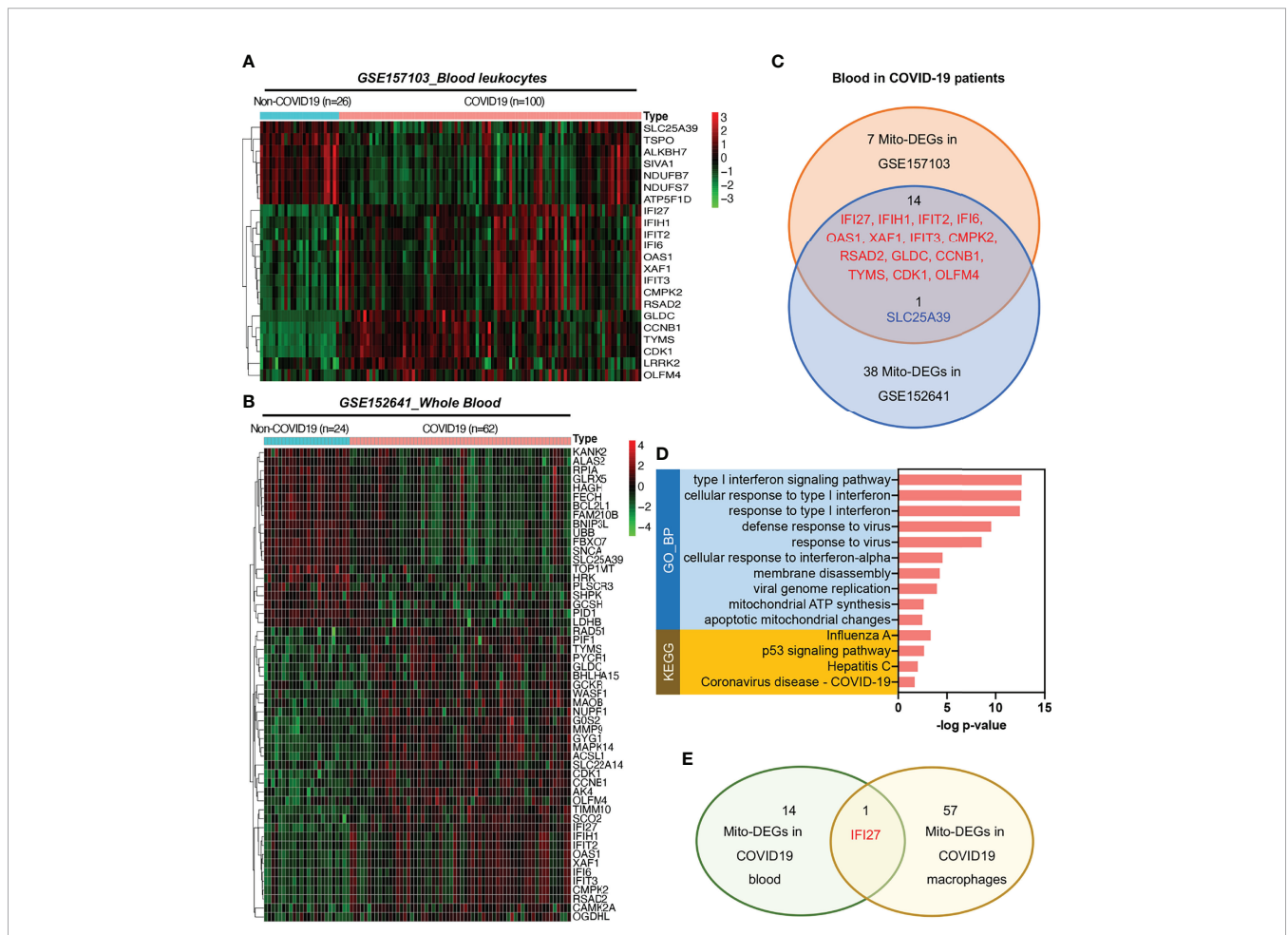


**FIGURE 5** | Expression of mitochondrion-related genes in the blood of patients with COVID-19. **(A)** Heat map of mito-DEGs in blood leukocytes from GSE157103. **(B)** Heat map of mito-DEGs in the whole blood from GSE152641. **(C)** Venn diagram showing the intersection mito-DEGs between these two GSE datasets. **(D)** Functional enrichment analysis of mito-DEGs in blood from patients with COVID-19. GO analysis and KEGG annotation are both listed. **(E)** Venn diagram showing the intersection mito-DEGs between blood and macrophages in COVID-19.

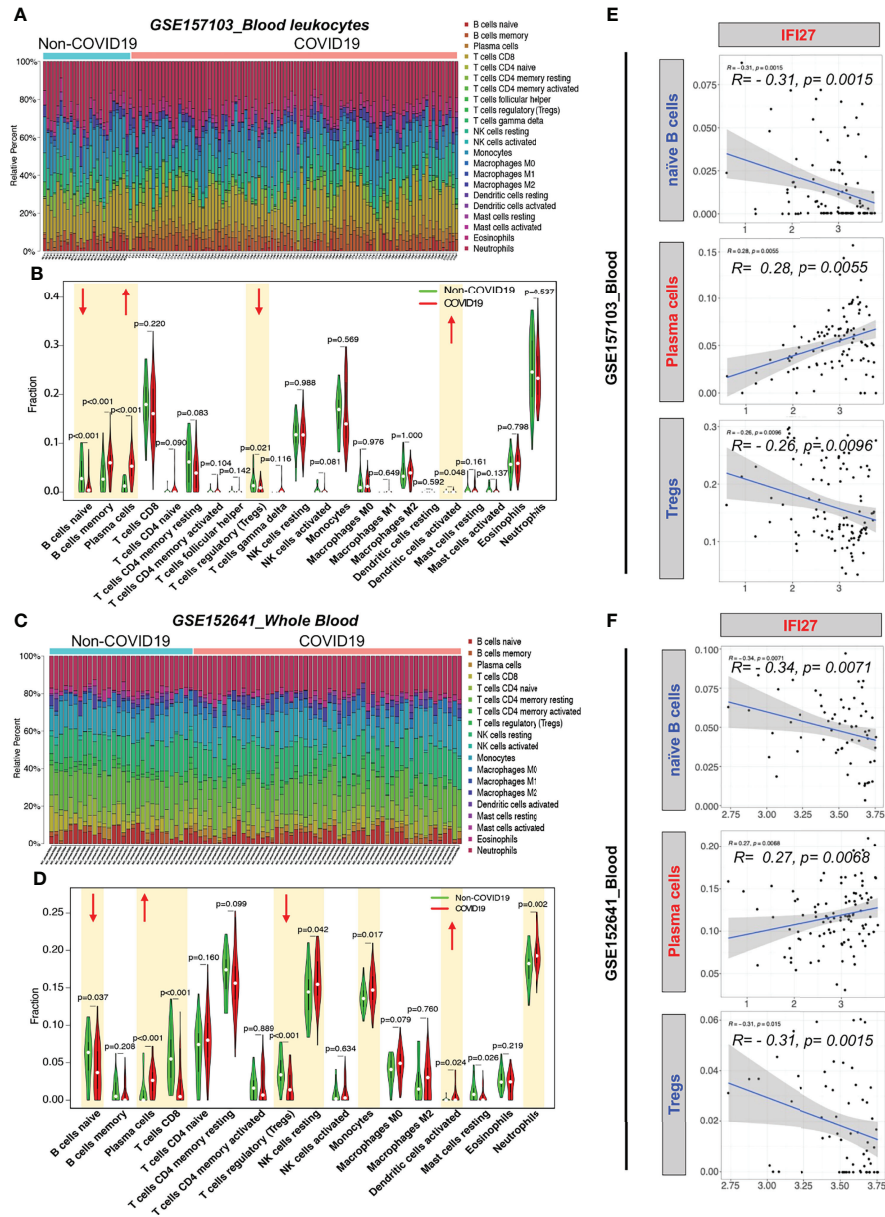


**FIGURE 6** | CIBERSORT analysis of immune cell count in the blood of patients with COVID-19. **(A)** Distribution proportion of immune cells in each sample from GSE157103. **(B)** Statistical analysis of various immune cell types in blood leukocytes from patients with COVID-19 and non-COVID-19 patients in GSE157103. **(C)** Distribution proportion of immune cells in each sample from GSE152641. **(D)** Statistical analysis of various immune cell types in whole blood from patients with COVID-19 and non-COVID-19 patients in GSE152641. **(E)** Correlation analysis between IFI expression and immune cell content in GSE157103. **(F)** Correlation analysis between IFI expression and immune cell content in GSE152641.

naïve B cells, CD8<sup>+</sup> T cells, and Tregs decreased, whereas those of plasma cells, resting natural killer cells, monocytes, activated dendritic cells, and neutrophils increased in the blood of patients with COVID-19 (**Figures 6C, D**).

To determine whether the IFI27-mediated IFN immune response affects the counts of blood immune cells in patients with COVID-19, we analyzed the correlation between IFI27 expression and the abovementioned significantly altered

immune cell counts. IFI27 expression was negatively correlated with the naïve B cell and Treg counts and positively correlated with the plasma cell counts in the blood of patients with COVID-19 (**Figures 6E, F**). The abovementioned results suggested that IFI27 expression upregulation in the blood immune cells of patients with COVID-19 accelerated the differentiation of naïve B cells into plasma cells and the infiltration of Tregs into alveoli.

## DISCUSSION

This study noted the severe mitochondrial quality imbalance in the lung tissue and blood immune cells of patients with COVID-19, which played a key role in viral immune escape and cell turnover. Our findings indicated that the mechanism underlying the damage caused by the virus was as follows: (1) In alveolar epithelial cells infected by SARS-CoV-2, there exists excessive mitochondrial fission, inhibition of mitochondrial degradation pathway and destruction of MCU calcium channel, thereby resulting in decreased AT2 counts and blocking the transformation of AT2 to AT1. The accumulation of many mitochondrion-damaged alveolar epithelial cells exhibit an impaired immune response, enhancing viral immune escape and replication. (2) In alveolar macrophages that swallow virus-infected alveolar epithelial cells or are directly infected by SARS-CoV-2, the low mitochondrial respiratory ability and the subsequently activated mitochondrial ROS-HIF1A pathway aggravate the pro-inflammatory response of lung tissue in patients with COVID-19. The infected alveolar macrophages further release high levels of IFN into the blood. (3) In blood immune cells of patients with COVID-19, the IFN release activates mitochondrial IFI27 and destroys mitochondrial energy metabolism in T and B cells, thereby promoting the plasma cell differentiation and lung–blood shuttle of Tregs, and eventually leading to cytokine storm and excessive inflammation (**Figure 7**).

Under normal circumstances, host cells rapidly respond to invading viruses by coordinating the functions of various organelles after viral infection (23). However, during highly invasive/aggressive viral infection, including that with SARS-CoV-2, the immune response function of organelles is controlled by the virus and is used to avoid the antiviral response, enhancing the ability of virus replication, and cause immune escape. Recent studies have shown that the viral structural proteins of SARS-CoV-2 can be translated and inserted into endoplasmic reticulum–mitochondrial contacts. Viral RNA synthesis is associated with endoplasmic reticulum and mitochondrial membrane modifications, and double-membrane vesicles produced by the endoplasmic reticulum and mitochondria may be central hubs for viral RNA synthesis and replication (24). Travaglini et al. detected the protein products of SARS-CoV-2 using affinity purified mass spectrometry and found that three nonstructural proteins (NSP4, NSP8, and ORF9c) were enriched in mitochondrial ribosomes, suggesting that mitochondria are one of the important target organelles of SARS-CoV-2, which disrupts host cell function (25). Miller et al. showed that SARS-CoV-2 could mask the reactive oxygen species (ROS) produced during cellular energy metabolism by inhibiting mitochondrial respiratory chain complex I, resulting in inability to activate cells to produce immune resistance (16). Ajaz et al. showed that abnormal mitochondrial pentose phosphate metabolism in host cells could enhance viral RNA replication and viral pathogenicity and help evade antiviral responses (26). In the current study, we found that multiple key factors affecting mitochondrial quality, such as mitochondrial coding and regulation of gene expression,

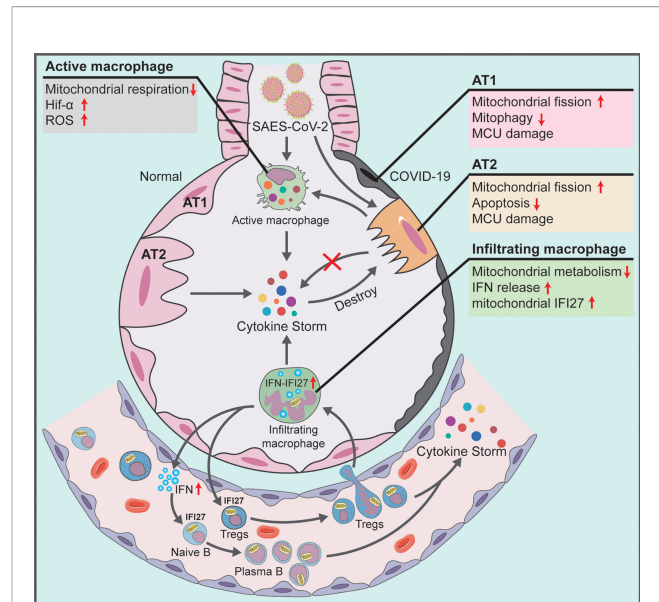


**FIGURE 7** | Schematic showing the systemic pathological changes in the lung and blood specimens of patients with COVID-19.

mitochondrial function, and related metabolic pathways, were impaired to different degrees in various types of tissue cells in patients with COVID-19, indicating that mitochondria play a critical role in the immune response of host cells to SARS-CoV-2.

We found significant changes in the expression of mitochondrion-related genes in the lung tissue and blood of patients with COVID-19. The specific alterations were as follows: In alveolar macrophages, the expression of 31 mitochondrion-related genes such as HIF1A, SQSTM1, SOD2, IDH1, TSPO, LRRK2, and GPX4 was upregulated and the expression of 27 mitochondrion-related genes such as PRKN, ATG7, FOXO3, MT-ND1, MT-ND-2, MT-CO1, and OPA3 was downregulated. In lung epithelial cells, the genes that were simultaneously upregulated in the AT2 and AT1 subtypes included 13 mitochondrion-encoding genes (e.g., genes encoding the COX subunit, NADH subunit, and ATP synthase, etc.) and 20 mitochondrial function–regulating genes (e.g., HSPD1, HSPA1A, SQSTM1 and BNIP3L, etc.); the genes that were simultaneously downregulated in the AT2 and AT1 subtypes included MCU, TP53BP2, JUN, PRKG1, and NR4A1. In blood leukocytes, 14 mitochondrion-related genes, namely, IFFI27, IFIH1, IFIT2, IFI6, OAS1, XAF1, IFIT3, CMPK2, RSAD2, GLDC, CCNB1, TYMS, CDK1, and OLFM4, were upregulated. Our study systematically describes the specific changes that occurred in mitochondrion-related genes in the lung tissue of patients with COVID-19 and during lung–blood interaction. It also provides data supporting the requirement for further analysis of the important role of and specific regulatory mechanism underlying mitochondrial quality imbalance in immune escape and cell outcome in patients with COVID-19.

SARS-CoV-2 has been reported to first invade ciliated cells in the proximal airways and AT2 cells in the gas-exchange zone of the distal lung (5, 27). AT2 cells are progenitor cells of the lung

epithelium and precursor cells of AT1 and can, therefore, regulate lung epithelial cell homeostasis *via* self-renewal and differentiation, maintain alveolar tension by secreting pulmonary surfactant, and support efficient gas exchange at the lung–blood interface (28). After mild inflammatory stimulation or viral infection, AT2 cells can present antigens to T cells to initiate T cell responses (29) and maintain alveolar function by increasing citrate synthase expression, upregulating the expression of the mitochondrial biogenesis–related gene *PPARGC1A* (*PGC-1 $\alpha$* ), and promoting mitochondrial apoptosis and other approaches for maintaining alveolar function (30). However, our current study showed that the AT2 count significantly decreased in the lung tissue of patients with COVID-19. The conversion of AT2 to AT1 was blocked, which may be an important reason for the body's failure to mount an immune response against SARS-CoV-2. In addition, mitochondrial calcium uptake plays an important role in the conversion of AT2 to AT1, and *MICU1-MCU* channels represent important mechanisms for regulating the differentiation of AT2 to AT1 cells (31). In our current study, we found that *MCU* expression was significantly downregulated in both AT2 and AT1 cells in patients with COVID-19, suggesting that the destruction/blocking of *MCU* channels in alveolar epithelial cells by SARS-CoV-2 infection may be a potential mechanism underlying the blocking of AT2 to AT1 conversion.

Our study showed that the expression of mitochondrion-encoding genes was upregulated and that of the mitochondrial biogenesis–related gene *PPARGC1A* (*PGC-1 $\alpha$* ) was downregulated in the alveolar epithelial cells of patients with COVID-19. These findings suggested that the mitochondria in alveolar epithelial cells from such patients exhibit excessive fission without additional biogenesis, resulting in a considerable increase in the number of damaged mitochondria. Moreover, our findings showed that, after SARS-CoV-2 infection, multiple key aspects of mitochondrial quality regulation, such as mitochondrial morphological features, mitochondrial apoptosis, and mitochondrial membrane potential, are affected in lung epithelial cells. In patients with COVID-19, the *JUN-MCL1*-mediated mitochondrial apoptosis pathway is inhibited in AT2 cells and the *PRKN-FOXO3*-mediated mitophagy pathway is inhibited in AT1 cells. The abovementioned results suggested that, because damaged mitochondria cannot be effectively degraded and cleared *via* apoptosis or mitophagy, many mitochondrion-damaged lung epithelial cells cannot initiate the damage repair mechanism of the host in the lung epithelial cells of patients with COVID-19, resulting in COVID-19 immune escape, which accelerates the viral replication process.

Alveolar macrophages are yolk sac–derived heterogeneous mononuclear phagocytes with complex ontogeny and reside in the alveolus pulmonis. When infection is initiated, these cells are responsible for early pathogen identification, inflammation initiation and regression, and tissue damage and repair (32). In alveolar tissue, cleaning of residual, such as virus or damaged cells, depends on macrophages to swallow and transfer to local lymph nodes, thus triggering immune protection (33). However, in the lung tissue of patients with severe COVID-19, macrophages have been found to be infected by SARS-CoV-2,

as indicated by the presence of viral nucleocapsid proteins (34), and these macrophages aggravate the damage in concert with the virus itself (35). In our current study, we found that *HIF1A* expression significantly increased in the alveolar macrophages of patients with COVID-19. Zhu et al. (36) also noted upregulation of *HIF1A* expression in the alveolar lavage fluid of patients with COVID-19, consistent with our findings. High *HIF1A* levels can promote glycolysis in alveolar macrophages, inhibit mitochondrial function, and aggravate proinflammatory responses and lung tissue damage (37). In virally infected animal and cell models, inhibiting the *HIF1A* pathway can promote the proliferation of reparative macrophages, which is conducive to tissue repair and homeostasis after infection and increase in survival rate.

Our current study also showed that the alveolar macrophages in patients with COVID-19 have two developmental trajectories. The expression level of mitochondrion-related genes was upregulated, consistent with the maturation process of infiltrating macrophages, whereas that of active macrophages was gradually downregulated. Thus, SARS-CoV-2 infection may have a greater impact on the mitochondrial pathway activity of active macrophages. This effect is probably due to the recognition and phagocytosis of virus-infected lung epithelial cells; expression of mitochondrion-encoding genes such as *MT-ND1*, *MT-ND2*, and *MT-CO1* decreased in active macrophages, whereas that of mitochondrion-regulatory genes such as *SOD2*, *SQSTM1* (*p62*), and *LRRK2* increased. The decreased expression of the mitochondrion-encoding genes suggested that mitochondrial spare respiratory capacity decreased in the alveolar macrophages of patients with COVID-19 (37). Furthermore, increased expression of the mitochondrion-regulatory genes, such as *SOD2*, *SQSTM1* (*p62*), and *LRRK2*, activated the oxidative stress pathway of macrophages and led to production of large amounts of ROS, which helped stabilize *HIF1A* (38–40). These results suggest that activation of the macrophage ROS-*HIF1A* pathway due to phagocytosis of apoptotic lung epithelial cells or directly due to viral infection may be pivotal in aggravating the pro-inflammatory response in lung tissue.

Some studies have shown that macrophages infected with SARS-CoV-2 release T cell chemokines, thereby attracting many T cells into the lungs and promoting T cell activation and proliferation (35, 41). T cells produce large amounts of IFN, which induces the release of many inflammatory factors by alveolar macrophages into the blood. However, they also induce the death of infected macrophages and spread to the microvasculature to recruit monocytes into the lungs, where the cells rapidly differentiate into alveolar macrophages, thereby leading to positive feedback regulation. In our current study, we noted decrease in the counts of naïve B cells and Tregs and increase in the counts of plasma cells and activated dendritic cells in the blood of patients with COVID-19. The differential expression of mitochondrion-related genes in these cells suggests that this process may be closely related to the type I IFN immune response to virus. A large amount of IFN is produced by infected blood immune cells; it activates effectors such as *IFI27* to fight the



virus (42). In addition, IFI27, which is located in the mitochondria, plays an important role in regulating mitochondrial energy metabolism, such as the tricarboxylic acid (TCA) cycle and respiratory chain uncoupling (43). Our study showed that IFI27 expression significantly increased in alveolar invasive macrophage subsets and blood immune cells in patients with COVID-19 and played an important role in the disproportion of peripheral blood immune cells and lung–blood interaction. These results suggest that IFI27 can be used as a mitochondrial immune marker to evaluate the degree of viral infection and cell turnover in patients with COVID-19 (44).

Mitochondrial quality is extremely important for B cell transformation. When mitochondrial quality is excellent, B cells tend to undergo type transformation; however, when the mitochondrial quality is imbalance, they undergo differentiation to plasma cells (45). We found that the proportion of naïve B cells decreased and that of plasma cells increased in patients with COVID-19, suggesting that the mitochondrial damage to blood B cells caused by SARS-CoV-2 infection accelerates the differentiation of B cells to plasma cells (effector B cells). T cell dysregulation is closely related to COVID-19 severity. Tregs are regulatory CD4<sup>+</sup> T cell subsets that maintain peripheral immune tolerance (46). Tregs play a key role in maintaining immune homeostasis and inhibiting excessive inflammatory responses by inducing other immune cell activation, proliferation, and effector functions (47). They have been found to alleviate virus-induced pneumonia and acute lung injury by inhibiting CS in respiratory virus infection (48, 49). On the basis of our findings, it can be presumed that the CS and excessive inflammatory response caused by the decrease in Tregs in the blood of patients with severe COVID-19 may be the main reasons for the poor prognosis of patients with severe COVID-19.

The limitations of this study are as follows: (1) Owing to the stringent experimental requirements of SARS-CoV-2-related research, we could not perform the relevant animal or cell experiments. (2) The current available public datasets have less accurate prognostic information and have scattered information regarding related biochemical indicators on patients with COVID-19, which are insufficient for determining the correlation between mitochondrial-related genes and organ functions or prognosis of patients with COVID-19. We plan to perform further research after identifying more detailed datasets with multiple organ indexes when available. (3) Currently, a SARS-CoV-2 mutant strain, that is, Omicron, has been identified (50). Further studies are required to determine whether the mutant viruses cause differing degrees of mitochondrial damage in the lung tissue and blood immune cells. We will continue to follow up on detailed information and related sequencing data of patients infected with the original virus or with different mutants.

In conclusion, our study emphasizes that mitochondria get caught in the crossfire of COVID-19 and immunity, and systematically explains the reasons for the immune escape and excessive inflammation noted during COVID-19 from the perspective of mitochondrial quality imbalance in lung tissue and lung–blood interaction. Further studies should be performed to develop mitochondrial quality control as the main

intervention for functional protection of critically affected organs, for example, in the lungs of patients with COVID-19.

## DATA AVAILABILITY STATEMENT

The datasets presented in this study can be found in online repositories. The names of the repository/repositories and accession number(s) can be found in the article/**Supplementary Material**.

## ETHICS STATEMENT

Ethical review and approval was not required for the study on human participants in accordance with the local legislation and institutional requirements. Written informed consent for participation was not required for this study in accordance with the national legislation and the institutional requirements.

## AUTHOR CONTRIBUTIONS

CD designed the whole project. XZ and CD performed the single-cell RNA-seq data processing in this study. BC and RN performed the bulk RNA-seq data processing in this study. DH, RL and XL were responsible for literature search. CD wrote the manuscript and LL, TL, HH were responsible for manuscript editing and revision. CD and HH provided scientific research funding support. All authors read and approved the final manuscript.

## FUNDING

This work was supported by the China Postdoctoral Science Foundation (2021MD703924), Chongqing Postdoctoral Innovative Talents Support Program (CQBX2021018) and Kuanren Talents Program of the second affiliated hospital of Chongqing Medical University.

## SUPPLEMENTARY MATERIAL

The Supplementary Material for this article can be found online at: <https://www.frontiersin.org/articles/10.3389/fimmu.2022.946731/full#supplementary-material>

**Supplementary Figure 1** | GSEA-based pathway enrichment analysis in relation to the macrophage subsets in COVID-19. **(A)** Macrophage infiltrating trails, including monocytes, transition monocytes, and infiltrating macrophages. **(B)** Macrophage activating trails, including primary macrophages, mature macrophages, and active macrophages.

**Supplementary Figure 2** | Representative KEGG annotation in relation to mito-DEGs in AT2 and AT1 during COVID-19. **(A)** Apoptosis pathway (KEGG: hsa04210) enriched by mito-DEGs in AT2. **(B)** Mitophagy pathway (KEGG: hsa04137) enriched by mito-DEGs in AT1.

**Supplementary Table 1** | Cluster lists of 1,513 mitochondrion-related genes.

## REFERENCES

1. Coronavirusidae Study Group of the International Committee on Taxonomy of Viruses. The Species Severe Acute Respiratory Syndrome-Related Coronavirus: Classifying 2019-nCoV and Naming It SARS-CoV-2. *Nat Microbiol* (2020) 5:536–44. doi: 10.1038/s41564-020-0695-z
2. Perico L, Benigni A, Casiraghi F, Ng LFP, Renia L, Remuzzi G. Immunity, Endothelial Injury and Complement-Induced Coagulopathy in COVID-19. *Nat Rev Nephrol* (2021) 17:46–64. doi: 10.1038/s41581-020-00357-4
3. Fiolet T, Kherabi Y, MacDonald CJ, Ghosn J, Peiffer-Smadja N. Comparing COVID-19 Vaccines for Their Characteristics, Efficacy and Effectiveness Against SARS-CoV-2 and Variants of Concern: A Narrative Review. *Clin Microbiol Infect Off Publ Eur Soc Clin Microbiol Infect Dis* (2022) 28:202–21. doi: 10.1016/j.cmi.2021.10.005
4. Yüce M, Filiztekin E, Özkaya KG. COVID-19 Diagnosis -A Review of Current Methods. *Biosensors bioelectronics* (2021) 172:112752. doi: 10.1016/j.bios.2020.112752
5. Hoffmann M, Kleine-Weber H, Schroeder S, Kruger N, Herrler T, Erichsen S, et al. SARS-CoV-2 Cell Entry Depends on ACE2 and TMPRSS2 and Is Blocked by a Clinically Proven Protease Inhibitor. *Cell* (2020) 181:271–280 e278. doi: 10.1016/j.cell.2020.02.052
6. Wang H, Wang L, Lee EH, Zheng J, Zhang W, Halabi S, et al. Decoding COVID-19 Pneumonia: Comparison of Deep Learning and Radiomics CT Image Signatures. *Eur J Nucl Med Mol Imaging* (2021) 48:1478–86. doi: 10.1007/s00259-020-05075-4
7. Rodda LB, Netland J, Shehata L, Pruner KB, Morawski PA, Thouvenel CD, et al. Functional SARS-CoV-2-Specific Immune Memory Persists After Mild COVID-19. *Cell* (2021) 184:169–183 e117. doi: 10.1016/j.cell.2020.11.029
8. Halpin DMG, Criner GJ, Papi A, Singh D, Anzueto A, Martinez FJ, et al. Global Initiative for the Diagnosis, Management, and Prevention of Chronic Obstructive Lung Disease. The 2020 GOLD Science Committee Report on COVID-19 and Chronic Obstructive Pulmonary Disease. *Am J Respir Crit Care Med* (2021) 203:24–36. doi: 10.1164/rccm.202009-3533SO
9. Lei Y, Zhang J, Schiavon CR, He M, Chen L, Shen H, et al. SARS-CoV-2 Spike Protein Impairs Endothelial Function via Downregulation of ACE 2. *Circ Res* (2021) 128:1323–6. doi: 10.1161/CIRCRESAHA.121.318902
10. Vasuri F, Ciavarella C, Collura S, Mascoli C, Valente S, Degiovanni A, et al. Adventitial Microcirculation Is a Major Target of SARS-CoV-2-Mediated Vascular Inflammation. *Biomolecules* (2021) 11:1063. doi: 10.3390/biom11071063
11. Mehta P, McAuley DF, Brown M, Sanchez E, Tattersall RS, Manson JJ, et al. COVID-19: Consider Cytokine Storm Syndromes and Immunosuppression. *Lancet* (2020) 395:1033–4. doi: 10.1016/S0140-6736(20)30628-0
12. Moore JB, June CH. Cytokine Release Syndrome in Severe COVID-19. *Science* (2020) 368:473–4. doi: 10.1126/science.abb8925
13. Toor SM, Saleh R, Sasidharan Nair V, Taha RZ, Elkord E. T-Cell Responses and Therapies Against SARS-CoV-2 Infection. *Immunology* (2021) 162:30–43. doi: 10.1111/imm.13262
14. Song J, Herrmann JM, Becker T. Quality Control of the Mitochondrial Proteome. *Nat Rev Mol Cell Biol* (2021) 22:54–70. doi: 10.1038/s41580-020-00300-2
15. Burtcher J, Cappellano G, Omori A, Koshiba T, Millet GP. Mitochondria: In the Cross Fire of SARS-CoV-2 and Immunity. *iScience* (2020) 23:101631. doi: 10.1016/j.isci.2020.101631
16. Miller B, Silverstein A, Flores M, Cao K, Kumagai H, Mehta HH, et al. Host Mitochondrial Transcriptome Response to SARS-CoV-2 in Multiple Cell Models and Clinical Samples. *Sci Rep* (2021) 11:3. doi: 10.1038/s41598-020-79552-z
17. Mehrzadi S, Karimi MY, Fatemi A, Reiter RJ, Hosseinzadeh A. SARS-CoV-2 and Other Coronaviruses Negatively Influence Mitochondrial Quality Control: Beneficial Effects of Melatonin. *Pharmacol Ther* (2021) 224:107825. doi: 10.1016/j.pharmthera.2021.107825
18. Peluso MJ, Deeks SG, Mustapic M, Kapogiannis D, Henrich TJ, Lu S, et al. SARS-CoV-2 and Mitochondrial Proteins in Neural-Derived Exosomes of COVID-19. *Ann Neurol* (2022) 91:772–781. doi: 10.1002/ana.26350
19. Melms JC, Biermann J, Huang H, Wang Y, Nair A, Tagore S, et al. A Molecular Single-Cell Lung Atlas of Lethal COVID-19. *Nature* (2021) 595:114–9. doi: 10.1038/s41586-021-03569-1
20. Zhang J, Hou S, You Z, Li G, Xu S, Li X, et al. Expression and Prognostic Values of ARID Family Members in Breast Cancer. *Aging* (2021) 13:5621–37. doi: 10.18632/aging.202489
21. Tan Y, Zhang W, Zhu Z, Qiao N, Ling Y, Guo M, et al. Integrating Longitudinal Clinical Laboratory Tests With Targeted Proteomic and Transcriptomic Analyses Reveal the Landscape of Host Responses in COVID-19. *Cell Discovery* (2021) 7:42. doi: 10.1038/s41421-021-00274-1
22. Qiu X, Hua X, Li Q, Zhou Q, Chen J. M(6)A Regulator-Mediated Methylation Modification Patterns and Characteristics of Immunity in Blood Leukocytes of COVID-19 Patients. *Front Immunol* (2021) 12:774776. doi: 10.3389/fimmu.2021.774776
23. Afghah Z, Chen X, Geiger JD. Role of Endolysosomes and Inter-Organelle Signaling in Brain Disease. *Neurobiol Dis* (2020) 134:104670. doi: 10.1016/j.nbd.2019.104670
24. Mandala VS, McKay MJ, Shcherbakov AA, Dregni AJ, Kolocouris A, Hong M. Structure and Drug Binding of the SARS-CoV-2 Envelope Protein Transmembrane Domain in Lipid Bilayers. *Nat Struct Mol Biol* (2020) 27:1202–8. doi: 10.1038/s41594-020-00536-8
25. Travaglini KJ, Nabhan AN, Penland L, Sinha R, Gillich A, Sit RV, et al. A Molecular Cell Atlas of the Human Lung From Single-Cell RNA Sequencing. *Nature* (2020) 587:619–25. doi: 10.1038/s41586-020-2922-4
26. Ajaz S, McPhail MJ, Singh KK, Mujib S, Trovato FM, Napoli S, et al. Mitochondrial Metabolic Manipulation by SARS-CoV-2 in Peripheral Blood Mononuclear Cells of Patients With COVID-19. *Am J Physiol Cell Physiol* (2021) 320:C57–65. doi: 10.1152/ajpcell.00426.2020
27. Hou YJ, Okuda K, Edwards CE, Martinez DR, Asakura T, Dinnon KH3rd, et al. SARS-CoV-2 Reverse Genetics Reveals a Variable Infection Gradient in the Respiratory Tract. *Cell* (2020) 182:429–446 e414. doi: 10.1016/j.cell.2020.05.042
28. Salahudeen AA, Choi SS, Rustagi A, Zhu J, van Unen V, de la OS, et al. Progenitor Identification and SARS-CoV-2 Infection in Human Distal Lung Organoids. *Nature* (2020) 588:670–5. doi: 10.1038/s41586-020-3014-1
29. Huang J, Hume AJ, Abo KM, Werder RB, Villacorta-Martin C, Alysandratos KD, et al. SARS-CoV-2 Infection of Pluripotent Stem Cell-Derived Human Lung Alveolar Type 2 Cells Elicits a Rapid Epithelial-Intrinsic Inflammatory Response. *Cell Stem Cell* (2020) 27:962–973 e967. doi: 10.1016/j.stem.2020.09.013
30. Suliman HB, Kraft B, Bartz R, Chen L, Welty-Wolf KE, Piantadosi CA. Mitochondrial Quality Control in Alveolar Epithelial Cells Damaged by S. Aureus Pneumonia in Mice. *Am J Physiol Lung Cell Mol Physiol* (2017) 313: L699–709. doi: 10.1152/ajplung.00197.2017
31. Ali M, Zhang X, LaCanna R, Tomar D, Elrod JW, Tian Y. MICU1-Dependent Mitochondrial Calcium Uptake Regulates Lung Alveolar Type 2 Cell Plasticity and Lung Regeneration. *JCI Insight* (2022) 7:e154447. doi: 10.1172/jci.insight.154447
32. Merad M, Martin JC. Pathological Inflammation in Patients With COVID-19: A Key Role for Monocytes and Macrophages. *Nat Rev Immunol* (2020) 20:355–62. doi: 10.1038/s41577-020-0331-4
33. Martinez EC, Garg R, van Drunen Littel-van den Hurk S. Innate Immune Protection From Pneumonia Virus of Mice Induced by a Novel Immunomodulator is Prolonged by Dual Treatment and Mediated by Macrophages. *Antiviral Res* (2019) 171:104594. doi: 10.1016/j.antiviral.2019.104594
34. Schaefer IM, Padera RF, Solomon IH, Kanjilal S, Hammer MM, Hornick JL, et al. *In Situ* Detection of SARS-CoV-2 in Lungs and Airways of Patients With COVID-19. *Mod Pathol* (2020) 33:2104–14. doi: 10.1038/s41379-020-0595-z
35. Grant RA, Morales-Nebreda L, Markov NS, Swaminathan S, Querrey M, Guzman ER, et al. Circuits Between Infected Macrophages and T Cells in SARS-CoV-2 Pneumonia. *Nature* (2021) 590:635–41. doi: 10.1038/s41586-020-03148-w
36. Zhu B, Wu Y, Huang S, Zhang R, Son YM, Li C, et al. Uncoupling of Macrophage Inflammation From Self-Renewal Modulates Host Recovery From Respiratory Viral Infection. *Immunity* (2021) 54:1200–1218 e1209. doi: 10.1016/j.immuni.2021.04.001
37. Codo AC, Davanzo GG, Monteiro LB, de Souza GF, Muraro SP, Virgilio-da-Silva JV, et al. Elevated Glucose Levels Favor SARS-CoV-2 Infection and Monocyte Response Through a HIF-1alpha/Glycolysis-Dependent Axis. *Cell Metab* (2020) 32:437–446.e435. doi: 10.1016/j.cmet.2020.07.007

38. Bae YH, Joo H, Bae J, Hyeon SJ, Her S, Ko E, et al. Brain Injury Induces HIF-1alpha-Dependent Transcriptional Activation of LRRK2 That Exacerbates Brain Damage. *Cell Death Dis* (2018) 9:1125. doi: 10.1038/s41419-018-1180-y
39. Katwal G, Baral D, Fan X, Weiyang H, Zhang X, Ling L, et al. SIRT3 a Major Player in Attenuation of Hepatic Ischemia-Reperfusion Injury by Reducing ROS via Its Downstream Mediators: SOD2, CYP-D, and HIF-1alpha. *Oxid Med Cell Longev* (2018) 2018:2976957. doi: 10.1155/2018/2976957
40. Lyu L, Chen Z, McCarty N. TRIM44 Links the UPS to SQSTM1/p62-Dependent Aggrephagy and Removing Misfolded Proteins. *Autophagy* (2021) 18:783–98. doi: 10.1080/15548627.2021.1956105
41. Hoang TN, Pino M, Boddapati AK, Viox EG, Starke CE, Upadhyay AA, et al. Baricitinib Treatment Resolves Lower-Airway Macrophage Inflammation and Neutrophil Recruitment in SARS-CoV-2-Infected Rhesus Macaques. *Cell* (2021) 184:460–475 e421. doi: 10.1016/j.cell.2020.11.007
42. Villani AC, Satija R, Reynolds G, Sarkizova S, Shekhar K, Fletcher J, et al. Single-Cell RNA-Seq Reveals New Types of Human Blood Dendritic Cells, Monocytes, and Progenitors. *Science* (2017) 356:eaah4573. doi: 10.1126/science.aah4573
43. Jin W, Jin W, Pan D. Ifi27 is Indispensable for Mitochondrial Function and Browning in Adipocytes. *Biochem Biophys Res Commun* (2018) 501:273–9. doi: 10.1016/j.bbrc.2018.04.234
44. Swadling L, Diniz MO, Schmidt NM, Amin OE, Chandran A, Shaw E, et al. Pre-Existing Polymerase-Specific T Cells Expand in Abortive Seronegative SARS-CoV-2. *Nature* (2022) 601:110–7. doi: 10.1038/s41586-021-04186-8
45. Waters LR, Ahsan FM, Wolf DM, Shirihai O, Teitell MA. Initial B Cell Activation Induces Metabolic Reprogramming and Mitochondrial Remodeling. *iScience* (2018) 5:99–109. doi: 10.1016/j.isci.2018.07.005
46. Ahmad S, Hatmal MM, Lambuk L, Al-Hatamleh MAI, Alshaer W, Mohamad R. The Role of TNFR2(+) Tregs in COVID-19: An Overview and a Potential Therapeutic Strategy. *Life Sci* (2021) 286:120063. doi: 10.1016/j.lfs.2021.120063
47. Wang Y, Zheng J, Islam MS, Yang Y, Hu Y, Chen X. The Role of CD4(+) FoxP3(+) Regulatory T Cells in the Immunopathogenesis of COVID-19: Implications for Treatment. *Int J Biol Sci* (2021) 17:1507–20. doi: 10.7150/ijbs.59534
48. Lin S, Wu H, Wang C, Xiao Z, Xu F. Regulatory T Cells and Acute Lung Injury: Cytokines, Uncontrolled Inflammation, and Therapeutic Implications. *Front Immunol* (2018) 9:1545. doi: 10.3389/fimmu.2018.01545
49. Shi Y, Wang Y, Shao C, Huang J, Gan J, Huang X, et al. COVID-19 Infection: The Perspectives on Immune Responses. *Cell Death Differ* (2020) 27:1451–4. doi: 10.1038/s41418-020-0530-3
50. Karim SSA, Karim QA. Omicron SARS-CoV-2 Variant: A New Chapter in the COVID-19 Pandemic. *Lancet* (2021) 398:2126–8. doi: 10.1016/S0140-6736(21)02758-6

**Conflict of Interest:** The authors declare that the research was conducted in the absence of any commercial or financial relationships that could be construed as a potential conflict of interest.

**Publisher's Note:** All claims expressed in this article are solely those of the authors and do not necessarily represent those of their affiliated organizations, or those of the publisher, the editors and the reviewers. Any product that may be evaluated in this article, or claim that may be made by its manufacturer, is not guaranteed or endorsed by the publisher.

Copyright © 2022 Duan, Ma, Zeng, Chen, Hou, Liu, Li, Liu, Li and Huang. This is an open-access article distributed under the terms of the Creative Commons Attribution License (CC BY). The use, distribution or reproduction in other forums is permitted, provided the original author(s) and the copyright owner(s) are credited and that the original publication in this journal is cited, in accordance with accepted academic practice. No use, distribution or reproduction is permitted which does not comply with these terms.



# Insights on the cGAS-STING Signaling Pathway During Herpesvirus Infections

Lishuang Deng<sup>1</sup>, Zhiwen Xu<sup>1,2</sup>, Fengqin Li<sup>1,3</sup>, Jun Zhao<sup>1</sup>, Zhijie Jian<sup>1</sup>, Huidan Deng<sup>1</sup>, Siyuan Lai<sup>1</sup>, Xiangang Sun<sup>1</sup>, Yi Geng<sup>1</sup> and Ling Zhu<sup>1,2\*</sup>

<sup>1</sup> College of Veterinary Medicine, Sichuan Agricultural University, Chengdu, China, <sup>2</sup> Key Laboratory of Animal Disease and Human Health of Sichuan Province, Sichuan Agricultural University, Chengdu, China, <sup>3</sup> College of Animal Science, Xichang University, Xichang, China

## OPEN ACCESS

### Edited by:

Rongtuan Lin,  
McGill University, Canada

### Reviewed by:

Wentao Li,  
Huazhong Agricultural University,  
China  
Jishu Shi,  
Kansas State University, United States

### \*Correspondence:

Ling Zhu  
abtcl72@126.com

### Specialty section:

This article was submitted to  
Viral Immunology,  
a section of the journal  
Frontiers in Immunology

Received: 29 April 2022

Accepted: 06 June 2022

Published: 01 July 2022

### Citation:

Deng L, Xu Z, Li F, Zhao J, Jian Z,  
Deng H, Lai S, Sun X, Geng Y and  
Zhu L (2022) Insights on the cGAS-  
STING Signaling Pathway During  
Herpesvirus Infections.  
Front. Immunol. 13:931885.  
doi: 10.3389/fimmu.2022.931885

Herpesviruses belong to large double-stranded DNA viruses. They are under a wide range of hosts and establish lifelong infection, which creates a burden on human health and animal health. Innate immunity is the host's innate defense ability. Activating the innate immune signaling pathway and producing type I interferon is the host's first line of defense against infectious pathogens. Emerging evidence indicates that the cGAS-STING signaling pathway plays an important role in the innate immunity in response to herpesvirus infections. In parallel, because of the constant selective pressure imposed by host immunity, herpesvirus also evolves to target the cGAS-STING signaling pathway to inhibit or escape the innate immune responses. In the current review, we insight on the classical cGAS-STING signaling pathway. We describe the activation of cGAS-STING signaling pathway during herpesvirus infections and strategies of herpesvirus targeting this pathway to evade host antiviral response. Furthermore, we outline the immunotherapy boosting cGAS-STING signaling pathway.

**Keywords:** cGAS-STING signaling pathway, herpesvirus, innate immune, antiviral response, viral evasion, immunotherapy

## 1 INTRODUCTION

Herpesviruses belong to double-stranded DNA viruses with virions ranging in size from 120 to as much as 260 nm (1). They are ubiquitous worldwide and under a wide range of hosts, infecting almost all vertebrates, including humans, mammals, birds, and reptiles (2). The *Herpesviridae* family comprises three subfamilies: *alphaherpesvirinae*, *betaherpesvirinae*, and *gammaherpesvirinae*, composed of 115 viruses (3). Herpesviruses included in the *alphaherpesvirinae* subfamily have a wide range of hosts, a short reproduction cycle, rapid spread, and can destroy host cells. These viruses are reported to establish latent infections in sensory ganglia. Characteristics of the *betaherpesvirinae* subfamily members are markedly different from those of members of the *alphaherpesvirinae* subfamily. These viruses tend to latently infect lymphoreticular cells, secretory glands and kidneys. The hosts for members of the *gammaherpesvirus* subfamily often span different families. These viruses usually specifically infect T or B lymphocytes (4). Herpesviruses are ancient viruses that co-evolved with their hosts, and following exposure, they establish a lifelong infection that burdens human health and animal health (5). However, only fetuses and immunocompromised hosts usually exhibit severe clinical symptoms after

herpesviruses infection (3). Notably, a few herpesviruses have certain interspecies transmission abilities: one kind of livestock and poultry may infect several types of virus, and one virus may also infect several animals, and even transmission infection between humans and animals occurs (6). The role of the innate immune system during herpesvirus infections is a worthy but grossly understudied aspect that calls for much more attention.

Innate immune system is the host's first and most rapid line of defense in recognizing pathogens. It works by activating multiple intra- and extracellular signaling pathways to defend against pathogenic infection and protect organisms (7). Host recognition of pathogens relies on the pattern recognition receptors (PRRs) and their ligands, which include the conserved pathogen structures, pathogen-associated molecular patterns (PAMPs) and the newly reported host-derived damage-associated molecular patterns (DAMPs). Nucleic acids, lipoproteins, or polysaccharides associated with pathogenic structures are common PAMPs. In contrast, DAMPs are usually associated with cellular exposure to stress, and are therefore also known as alarmins (8, 9). Among infectious agents, viruses have a wide range of ecosystem impacts as an intracellular specialized pathogen and pose a serious threat to all living organisms (10, 11). Different PRRs are present in host cells to recognize viral nucleic acids (DNA or RNA). DNA is predominantly targeted by DNA-dependent activator of interferon response factors (DAI), cyclic GMP-AMP synthase (cGAS), absent in melanoma 2 (AIM2), interferon-gamma-inducible protein 16 (IFI16), interferon-inducible protein X (IFIX), and Toll-like receptors (TLRs) (7, 9, 12). Interestingly, TLR9 exclusively recognizes unmethylated DNA with CpG-motifs (CpG DNA) (9, 13). Viral RNA is mainly sensed by RIG-I-like receptors (RLRs) and some Toll-like receptors (TLR3/7/8) (14, 15).

cGAS plays a prominent role in viral DNA sensing and is rapidly activated by cytosolic DNA. Subsequently, the activated cGAS promotes the synthesis of 2', 3'-cGAMP. Then 2', 3'-cGAMP activates a protein located on the endoplasmic reticulum (ER), stimulator of interferon genes (STING) (16, 17).

Subsequently, STING mediates several downstream signaling cascades to protect the host from pathogen invasion (18). Numerous studies have suggested that the cGAS-STING signaling pathway, mainly responsible for cytoplasmic DNA sensing, plays an important role in host innate immunity against viruses. In addition to recognizing and sensing DNA virus infection, this pathway has been reported to be involved in restricting the infection of RNA viruses (9, 19). At the same time, because of the constant selective pressure imposed by host immunity, viruses are also evolving to target the cGAS-STING signaling pathway to inhibit or evade the host immune response (7, 11). Numerous recent studies have shown that the cGAS-STING signaling pathway is an ideal target for therapeutic intervention in diseases, especially in cancer and tumors (20–23), which may provide new ideas for combating herpesvirus.

In the current review, we insight on the classical cGAS-STING signaling pathway. Then we describe the activation of cGAS-STING signaling pathway during herpesvirus infections and strategies of herpesvirus targeting this pathway to inhibit and evade the host antiviral response. Finally, we outline the immunotherapy enhancing cGAS-STING signaling pathway.

## 2 SIGNALING IN THE CLASSICAL cGAS-STING SIGNALING PATHWAY

cGAS-STING signaling pathway is one of the important pattern recognition and effector pathways in host innate immunity. The signaling of classical cGAS-STING signaling pathway is generally thought to consist of three main phases: nucleic acid-sensing, intracellular signal transduction, and immune response activation (**Figure 1**).

### 2.1 Nucleic Acid Sensing

Viral DNA is sensed by specific sensor proteins which mainly present in the cytoplasm of host cells. Sensor proteins recognize

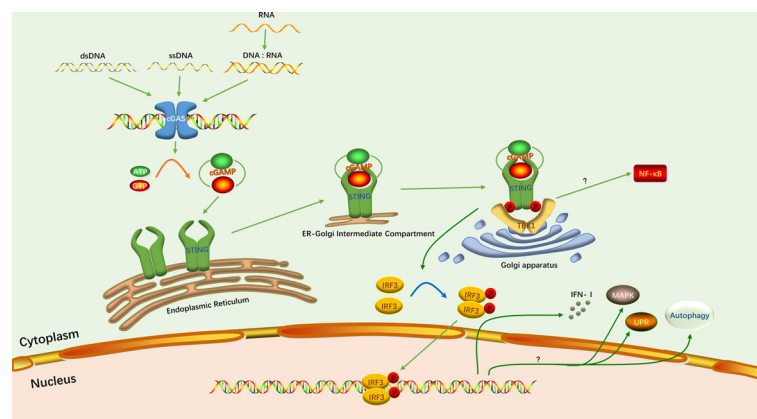


**FIGURE 1** | The classical cGAS-STING signaling pathway. The green arrows indicate the activation of this pathway and induction of the IFN-I response. The yellow arrow indicates the synthesis of cGAMP. The blue arrow indicates the phosphorylation of IRF3. Protein phosphorylation is depicted as P. The question mark indicates that the specific mechanism has not been elucidated.

viral DNA and activate an innate immune response against the virus (9). cGAS is one of the most important DNA sensors, and in particular its ability to induce type I interferon (IFN-I) responses has been well documented (24, 25). The DNA-sensing and enzymatic activity of cGAS were first described in 2013 (25, 26). cGAS belongs to the nucleotidyltransferase family, and uses purines or pyrimidines to synthesize linear or cyclic dinucleotide or trinucleotides to activate downstream signaling molecules (27). cGAS is activated by double-stranded DNA (dsDNA) and recognizes dsDNA in a length-dependent manner. cGAS binding to short dsDNA less than 20 bp results in incomplete formation of cGAS dimers, which prevent the formation of stable complexes. On the contrary, binding to large fragments of dsDNA induces high affinity of cGAS for the target nucleic acid and the formation of a network of cGAS-DNA oligomers (24, 28, 29). cGAS binds directly to dsDNA through its zinc-ribbon domain. Subsequently, its conformation changes and induces its enzymatic activity. Then, cGAS utilizes its enzymatic function to catalyze adenosine triphosphate (ATP) and guanosine triphosphate (GTP) into a second cyclic messenger, 2', 3'-cGAMP (11, 30). cGAS has been reported to bind to single-stranded DNA (ssDNA), but only induces small amounts of cGAMP (31). Hybrid DNA and RNA, as well as stem-like ssDNA, can also activate cGAS, but with lower potency (9). In addition, cGAS can bind to dsRNA, but this does not induce cGAMP production (24).

## 2.2 Intracellular Signal Transduction

STING is an important junctional protein in the cGAS-STING signaling pathway and is the downstream ligand of cGAMP. STING utilizes its amino-terminal transmembrane domain to anchor it to the ER membrane, with the carboxyl terminus projecting into the cytoplasm (32). With or without ligand, STING exists as a dimer on the ER membrane (33–36). When cGAMP is synthesized, the STING dimer binds to a molecule of cGAMP through hydrophobic interactions and hydrogen bonding (33, 34). Then STING undergoes conformational change, activation and release of the carboxy-terminal tail (CTT) domain, which resembles a TANK binding kinase 1 (TBK1) substrate and permits recruitment of the downstream TBK1 (37). The complex of cGAMP and STING will be transferred from the ER to the Golgi apparatus by the ER-Golgi intermediate compartment (ERGIC) to further recruit TBK1 (38). Subsequently, the CTT domain exposed by STING is inserted into the groove formed between the kinase domain and scaffold dimerization domain (SDD) of TBK1 dimer, which is tightly bound (39, 40). TBK1 in turn promotes the phosphorylation of the CTT domain, which causes the recruitment of the interferon regulatory factor 3 (IRF3) (41).

## 2.3 Immune Response Activation

The recruited IRF3 forms a dimer after phosphorylation by TBK1. It then enters the nucleus to induce transcription of IFN-I (42). Triggering the IFN response is the most important function of the cGAS-STING signaling pathway. However, studies have confirmed that this pathway has functions not related to IFN (10). In inflammation, the cGAS-STING

signaling pathway is associated with activation of the nuclear factor- $\kappa$ B (NF- $\kappa$ B) pathway. Although the exact mechanism is currently unknown, STING and TBK1 are indispensable for inducing NF- $\kappa$ B signaling pathway (43, 44). In addition, there are three other downstream responses of cGAS-STING signaling pathway have been reported: mitogen-activated protein kinase (MAPK) pathway, autophagy, and the unfolded protein response (UPR) (45–47).

## 3 THE cGAS-STING SIGNALING PATHWAY IN HERPESVIRUS INFECTIONS

The cGAS-STING signaling pathway is activated during herpesvirus infections (Figure 2). As herpesviruses co-evolved with hosts, some members of viruses have acquired their unique mechanisms and strategies to evade innate antiviral immunity, which mainly interferes with different factors in the cGAS-STING signaling pathway (Table 1 and Figure 2).

### 3.1 Activation of the cGAS-STING Signaling Pathway During Herpesvirus Infections

The cGAS-STING signaling pathway is critical to drive the initial IFN-I response and limit herpesvirus infection. Multiple herpesviruses have been shown to trigger this pathway, including herpes simplex virus-1 (HSV-1), oncolytic herpes simplex viruses (oHSV), pseudorabies virus (PRV), human cytomegalovirus (HCMV), mouse cytomegalovirus (MCMV), Kaposi's sarcoma-associated herpesvirus (KSHV) (63, 67–72). HSV-1 is the most widely reported member associated with cGAS-STING signaling pathway in various studies.

In addition to being directly activated by viral DNA, the cGAS-STING signaling pathway can undergo different modifications for optimal signaling of HSV-1 infection, including ubiquitination and phosphorylation. E3 ubiquitin ligases, TRAF6 and RINCK (also known as TRIM41), promotes ubiquitination and activation of cGAS in IFN-I production during HSV-1 infection. IFN- $\beta$  production is inhibited in TRAF6-knockdown cells infected with HSV-1. IFN-I production also is inhibited in the RINCK-deletion cells upon HSV-1 infection, which is associated with the phosphorylation of TBK1 and IRF3 (73, 74). TRIM9s, believed to function as E3 ubiquitin ligases, are also identified as positive IFN-I regulators. Upon cellular sensing of HSV-1 DNA, TRIM9s undergo ubiquitination, and promote the recruitment and activation of TBK1, leading to IRF3 activation and IFN-I production (75). Deubiquitinases (DUB) also play an important role in the cGAS-STING signaling pathway. The ovarian tumor deubiquitinase 5 (OTUD5) can target STING to cleave its polyubiquitin chain and promote its stability. In cells with knockdown of OTUD5, degradation of STING in the HSV-1 triggered cGAS-STING signaling pathway is accelerated, thereby inhibiting IFN-I production (76).

Other cellular proteins also contribute to activating the cGAS-STING signaling pathway during HSV-1 infection.

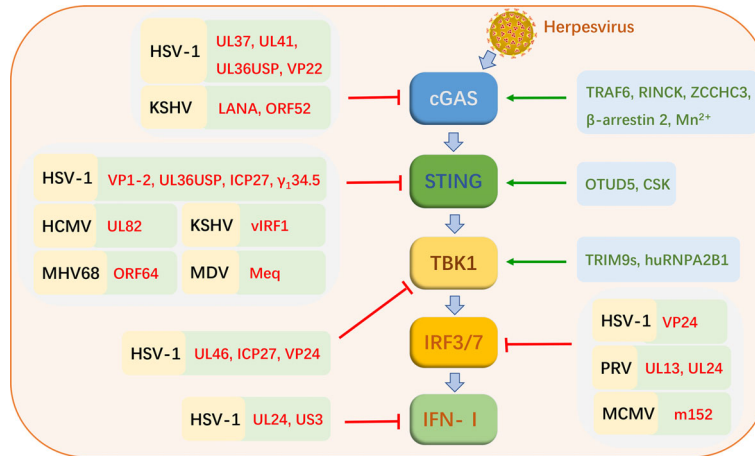


**FIGURE 2 |** Strategies of cGAS-STING signaling pathway activation and virus evasion during herpesvirus infections. Black letters represent herpesviruses. Red letters indicate the proteins of these viruses. Green letters indicate cellular proteins that favor cGAS-STING signaling pathway activation.

**TABLE 1 |** Herpesvirus evasion of innate immunity via cGAS-STING signaling pathway.

Subfamily	Virus	Proteins	Target	Mechanism	Reference	
Alphaherpesvirinae	HSV-1	UL46	TBK1	Targeting TBK1 and inhibiting TBK1 dimer formation to suppress IRF3 activation.	(48)	
		UL41	cGAS	Degrading cGAS via its RNase activity.	(49)	
		UL37	cGAS	Deamidating cGAS to catalyze cGAMP synthesis.	(50)	
		UL24	IFN-β promoter	Inhibiting the activation of the promoters of IFN-β and IL-6.	(51)	
		VP24	TBK1 and IRF3	Disrupting the interaction between TBK1 and IRF3 to impair IRF3 activation.	(52)	
		VP22	cGAS	Interacting with cGAS and inhibiting the enzymatic activity of cGAS.	(53)	
		VP1-2	STING	Directly interacting with STING and promoting the deubiquitination of STING to evade antiviral responses.	(54)	
		UL36USP	cGAS and STING	Blocking the activation of the IFN-β promoter to evade host antiviral innate immunity by targeting cGAS and STING.	(55)	
		ICP27	TBK1 and STING	Interacting with TBK1 and STING via its RGG motif.	(56)	
		γ1,34.5	STING	Directly interacting with STING to further inhibit the activation of TBK1.	(57)	
Betaherpesvirinae	HCMV	US3	β-catenin	Hyperphosphorylating β-catenin via its kinase activity.	(58)	
		PRV	UL13	IRF3	Phosphorylating IRF3 and disrupting IRF3 binding to downstream factor promoter.	(59)
		UL24	IRF7	Inhibiting the production of IFN-β by targeting IRF7.	(60)	
		UL82	STING	Interacting with STING and iRhom2, and disrupting the binding of STING to TRAPb to prevent the transfer of STING to the Golgi apparatus. Additionally inhibiting the recruitment of downstream signaling molecules.	(61)	
Gammaherpesvirinae	MCMV	m152	IRF3	Inhibiting STING-mediated IRF signaling.	(62)	
		KSHV	vIRF1	STING	Blocking the interaction of STING with TBK1, and then inhibiting the phosphorylation and activation of STING to suppress cGAS-STING-mediated antiviral immunity.	(63)
	KSHV	LANA	cGAS	Directly binding to cGAS and inhibits the downstream phosphorylation of TBK1 and IRF3.	(62)	
		ORF52	cGAS	Directly inhibiting cGAS enzymatic activity.	(64)	
	MHV68	ORF64	STING	ORF64 DUB active site mutant is associated with impaired delivery of viral DNA to the nucleus.	(65)	
		MDV	Meq	STING	Blocked the recruitment of downstream TBK1 and IRF7 to the STING.	(66)

Heterogeneous nuclear ribonucleoprotein A2B1 (hnRNPA2B1) is a newly identified intranuclear DNA sensing protein. hnRNPA2B1 binds intranuclear viral DNA and transfers it to the cytoplasm during HSV-1 infection. It then activates TBK1 to promote the expression of downstream antiviral genes (77).

ZCCHC3, a CCHC-type zinc-finger protein, positively regulates cGAS. Upon HSV-1 infection, binding of ZCCHC3 to viral DNA promotes cGAS binding to DNA, thereby facilitating cGAS activation. Conversely, ZCCHC3 deficiency leads to suppression of downstream antiviral gene expression

triggered by viral DNA, which makes it easier for the virus to proliferate in the host (78). The nonreceptor tyrosine kinase CSK is also important for sensing of DNA viruses in the cGAS-STING signaling pathways. Deletion of CSK inhibits the expression of multiple downstream antiviral genes in the cGAS-STING pathway, including *ifnb1*, *ifm4*, and *isg56*. Following HSV-1 infection, CSK phosphorylates STING at Y240 and Y245 after the phosphorylation of STING at S366 by TBK1 (79).  $\beta$ -arrestin 2, a multifunctional adaptor, promotes the clearance of HSV-1 and vesicular stomatitis virus (VSV) and virus-induced production of IFN- $\beta$  in macrophages.  $\beta$ -arrestin 2 targets cGAS and promotes dsDNA-cGAS interactions as well as cGAMP production to induce STING expression and innate immune responses (80). A recent study reported that  $Mn^{2+}$  is a positive regulator of cGAS.  $Mn^{2+}$  promotes dsDNA binding to cGAS and increases the enzymatic activity of cGAS, which is beneficial to cGAS sensing low concentration of dsDNA. Furthermore,  $Mn^{2+}$  also promotes cGAMP binding to STING and increases the activity of STING. In the Mn-deficient mouse model, the production of antiviral factors is deprived, which is more conducive to viral infection and replication (81).

### 3.2 Evasion of the cGAS-STING Signaling Pathway by Herpesvirus

Herpesviruses are remarkable pathogens, which encode at least 70 functional proteins. The member known to encode the largest number proteins is HCMV that encode about 170 proteins. They can efficiently utilize their proteins and host components to evade host immunity and achieve proliferation and egress. With the in-depth study of herpesvirus-host interactions, we have understood how herpesviruses evade the cGAS-STING signaling pathway (Table 1 and Figure 2).

#### 3.2.1 Alphaherpesviruses Evade the cGAS-STING Signaling Pathway

HSV-1 is the first virus reported triggering the cGAS-STING signaling pathway, and it encodes many proteins targeting this pathway to inhibit the host antiviral responses (82–84). HSV-1 tegument protein UL46 targets TBK1, and inhibits TBK1 dimer formation and its interaction with IRF3. Ultimately, it inhibits the activation of IRF3 and the production of IFN-I. UL46-deficient HSV-1 enhances the production of IFN-I and inhibits viral replication. Not surprisingly, the proliferation of UL46-deficient HSV-1 is stronger in TBK1-deficient cells (48). It has been proven that HSV-1-encoded UL41 inhibits host perception of the virus by targeting cGAS. The detailed mechanism is that UL41 has RNase activity to degrade cGAS. Deletion of UL41 promotes activation of the IFN- $\beta$  promoter and production of IFN- $\beta$  (49). UL37, another tegument protein of HSV-1, also targets cGAS to escape the host antiviral response. UL37 has been shown to have a deamidating effect, which disrupts the catalytic function of cGAS by deamidating it to inhibit the synthesis of cGAMP. Deamidase-deficient HSV-1 triggers a strong immune response in mice, leading to inhibition of viral replication (50). UL24 of HSV-1, an essential protein that promotes herpesvirus replication. It was demonstrated that UL24 inhibits the activation of the promoters of IFN- $\beta$  and interleukin-6 (IL-6), thus facilitating HSV-1 evasion of antiviral responses and

achieving efficient viral proliferation (51). The VP24 of HSV-1 is a newly identified protein that inhibits the production of IFN- $\beta$ . VP24 inhibits the expression of DNA-induced IFN- $\beta$  and the activation of the IFN- $\beta$  promoter in the cGAS-STING signaling pathway. The specific mechanism is that VP24 impairs IRF3 activation and IFN-I production by disrupting the interactions between TBK1 and IRF3 (52). HSV-1 tegument protein VP22 acts as an antagonist of the IFN-I pathway. VP22 interacts with cGAS and inhibits the enzymatic activity of cGAS from evading innate immune responses persistently (53). VP1-2 of HSV-1 is a protein with DUB activity that interacts directly with STING. VP1-2 promotes the deubiquitination of STING to evade antiviral responses, especially in the brain. VP1-2 DUB activity deficient HSV-1 promotes IFN-stimulated gene expression and IFN production, and inhibits the replication of this virus. This is due to promoted ubiquitination of STING and phosphorylation of TBK1 as well as IRF3 (54). Another protein with DUB activity, HSV-1 ubiquitin-specific protease (UL36USP), is thought to primarily inhibits the activation of the IFN- $\beta$  promoter to evade host antiviral responses by targeting cGAS and STING (55). HSV-1 inhibits IFN-I induction in human macrophages *via* the conserved herpesvirus protein ICP27. ICP27 targets TBK1 and STING in the cGAS-STING signaling pathway. The activity of TBK1 is important for this process (56).  $\gamma_134.5$  of HSV-1 directly interacts with STING to inhibit the activation of TBK1. During viral infection, the  $\gamma_134.5$  protein disrupts the transport of STING from the ER to the Golgi apparatus, which leads to downregulation of IRF3 and IFN responses (57).  $\beta$ -catenin is a crucial protein that promotes the expression of IFN-I. US3 encoded by HSV-1 inhibits IFN-I production by hyperphosphorylating  $\beta$ -catenin *via* its kinase activity (58).

In animal herpesviruses, research into the mechanisms of evasion of the cGAS-STING signaling pathway is just beginning. There are limited reports. PRV is a DNA virus that seriously affects the health of the pig industry worldwide. The proteins of PRV inhibit the production of IFN-I by targeting IRFs in the cGAS-STING pathway. PRV UL13 potentially inhibits IFN- $\beta$  production by phosphorylating IRF3 and disrupting IRF3 binding to downstream factor promoter (59). Another study showed that UL24 of PRV inhibits the production of IFN- $\beta$  by targeting IRF7. UL24-deleted PRV strain significantly increased the transcription levels of IFN-I in PK-15 cells (60).

#### 3.2.2 Betaherpesviruses Evade the cGAS-STING Signaling Pathway

Not only alphaherpesviruses can use their proteins to escape host innate immunity through the cGAS-STING signaling pathway, but some members of the *betaherpesvirinae* subfamily have also evolved their escape mechanisms. Tegument protein UL82 plays an important role in immune evasion of HCMV, which directly targets STING for inhibition of innate antiviral responses. UL82 facilitates the replication of HCMV. Conversely, inhibition of UL82 expression or deletion of UL82 results in high levels of intracellular antiviral genes. UL82 inhibits the STING signaling pathway by interacting with STING and iRhom2 and by disrupting the binding of STING to TRAPb to prevent the transfer of STING to the Golgi apparatus. In addition, UL82 inhibits the recruitment of downstream signaling molecules



(TBK1 and IRF3) (61). MCMV m152 protein targets the IFN-I response by inhibiting STING-mediated IRF signaling (62).

### 3.2.3 Gammaherpesviruses Evade the cGAS-STING Signaling Pathway

The proteins of several gammaherpesviruses have been reported to inhibit the cGAS-STING signaling pathway. The viral IFN regulatory factor 1 (vIRF1) of KSHV was shown to be an important negative regulator of STING. vIRF1 blocks the interactions of STING with TBK1 and then inhibits the phosphorylation and activation of STING to suppress cGAS-STING-mediated antiviral immunity (63). The latency-associated nuclear antigen (LANA) encoded by KSHV is also one of the proteins that facilitate viral escape. LANA inhibits the clearance of KSHV from host cells by directly binding to cGAS to inhibit the phosphorylation of TBK1 and IRF3 (62). KSHV tegument protein, ORF52, also directly targets cGAS to inhibit its enzymatic activity and inhibit the sensing of viral DNA (64). In the murine gammaherpesvirus 68 (MHV68) infection model, deletion of ORF64 DUB has been shown to inhibit viral replication and proliferation. And mutation of the ORF64 DUB active site also diminishes the ability of the virus to establish latent infection in mice. However, this phenomenon does not occur in mice lacking STING, which indicates that MHV68 mainly escapes the host immune responses by inhibiting the function of STING through the ORF64 DUB (65). Meq, the major oncoprotein encoded by Malik's disease virus (MDV), is also a negative regulatory protein of STING. Overexpression of Meq significantly inhibits antiviral responses. In contrast, knockdown of Meq significantly increased the expression levels of antiviral genes and IFN- $\beta$  in cells infected with MDV. The specific mechanism is that Meq blocks the recruitment of downstream TBK1 and IRF7 to the STING complex to inhibit IFN- $\beta$  production (66).

## 4 IMMUNOTHERAPY BOOSTING cGAS-STING SIGNALING PATHWAY

The cGAS-STING signaling pathway is indispensable for the sensing of herpesvirus in host innate immunity, which makes this pathway an important candidate target for the therapy of herpesvirus infections. In fact, numerous studies have explored the immunotherapy targeting cGAS-STING signaling pathway, especially in tumor and cancer treatment, showing great therapeutic potential. Immunotherapy boosting the cGAS-STING pathway mainly includes STING agonist, improved delivery system and combination therapy. We outline these therapeutic approaches below, which may provide new ideas for against herpesvirus infections.

### 4.1 STING Agonist

#### 4.1.1 Cyclic Dinucleotide

Cyclic dinucleotides (CDNs) have been verified as a class of cGAS-STING signaling pathways agonist involved in the immune system in prokaryotic cells and mammalian cells. CDNs consist of cyclic di-GMP (cdGMP), cyclic di-AMP

(cdAMP), cyclic AMP-GMP (cGAMP) (20). cGAMP is one kind of the most classical CDNs, including 2', 3'-cGAMP, 2', 5'-cGAMP, 3', 3'-cGAMP and 3', 5'-cGAMP. CDNs have various applications in antitumor immunity (20–23). For instance, intratumoral injection of 2', 3'-cGAMP significantly retards tumor growth in B16F10 mice (85).

Except for natural CDNs, synthetic CDNs with better properties are developed in recent years, such as ADU-S100 and ADU-V19. ADU-S100 (ML RR-S2 CDN), also known as MIW815, is a dithio CDN with high affinity to human STING. Therefore, it becomes the first STING agonist to enter clinical trials for advanced metastatic solid tumors or lymphomas. ADU-V19 (RR-S2 cGAMP) is similar to ADU-S100 and targets human STING (21).

#### 4.1.2 Non-CDN Agonist

Recent studies indicate that non-CDN agonists also play an important pharmacological role in immunotherapy targeting the cGAS-STING signaling pathway. 5,6-dimethylxanthenone-4-acetic acid, also named DMXAA or ASA404, is a flavonoid. DMXAA is a STING non-CDN agonist and is found to be selective for STING. In T cells of B6 mice, the IFN-I response is considerably enhanced after treatment with DMXAA (86). However, DMXAA is not effective in phase III trials in patients with non-small cell lung cancer (87). Together, DMXAA induces mice STING rather than human STING to enhance the innate immune response, which may be caused by the structural differences between the two STINGs. Amidobenzimidazole (ABZI) is another STING non-CDN agonist. After dimerization of ABZI (di-ABZI) with a 4-carbon butane linker, the binding affinity of di-ABZI to STING is significantly enhanced (22).

### 4.2 Improved Delivery System

cGAS-STING agonists are usually soluble, susceptible to enzymatic hydrolysis, and negatively charged, limiting their therapeutic efficacy (21). Therefore, efficient biomaterial delivery systems are essential to optimize the therapeutic strategy and enhance the biotherapeutic efficacy of these agonists. There are a variety of cGAS-STING agonist delivery systems, three of which have been extensively studied: nanocarrier, microparticle, and hydrogel.

Liposome is the first FDA-approved nano-biotherapeutic carrier. Liposome nano-delivery systems containing STING agonists can target specific cells for cell activation. Liposome nanoparticles encapsulating cdGMP target to draining lymph nodes. The therapeutic efficacy of the nano-delivery system is considerably improved in murine compared with cdGMP alone (88). Polymer nanoparticle is another promising nano-delivery system. Studies have demonstrated that synthetic polymeric nanocarrier, PC7A NP, induces robust immune response through the cGAS-STING pathway in mice (89).

Microparticle, a recently developed STING agonist delivery system, include tumor cell-derived microparticle (TMP) and acid-sensitive acetylated dextran (Ace-DEX) polymer microparticle (Ace-DEX MP) (21). TMPs are microparticles produced by apoptotic cancer cells that promote the production of IFN-I by activating the cGAS-STING signaling pathway. Ace-DEX MP is another MP

delivery system and is a powerful subunit vaccine delivery system. Ace-DEX MPs encapsulating 3', 3'-cGAMP in combination with a soluble TLR7/8 agonist elicit robust cytokine responses in mouse bone marrow-derived dendritic cells (90). Another study showed that in influenza vaccine, Ace-DEX MPs containing 3', 3'-cGAMP induce the strongest antibody production and immune responses *in vivo* (91).

Hydrogel is another common delivery system that forms viscoelastic gels by binding and retaining water. Cross-linked hyaluronic acid (HA) hydrogel loaded with 2', 3'-cdAM (PS)2 (Rp,Rp) significantly enhances the therapeutic effect of tumors (92). cGAMP-loaded linear HA hydrogel promotes the IFN-I production in macrophages (21, 93). Matrigel is a thermally responsive hydrogel. Matrigel combined with a STING agonist is beneficial for the treatment of localized tumors in mice with head and neck squamous cell carcinoma (94). STINGel is a peptide hydrogel for intra-tumoral CDN delivery. In mice with oral cancer, CDN-loaded STINGel activates the cGAS-STING pathway to promote immune response (95).

### 4.3 Combination Therapy

STING agonists and optimized delivery systems target and activate the cGAS-STING signaling pathway to promote immunotherapy of tumors and other diseases. However, a growing body of research has shown that combination immunotherapy targeting the cGAS-STING signaling pathway maximizes the efficacy of STING agonists in immunotherapy of disease and reduce drug negative impacts.

#### 4.3.1 STING Agonist Vaccine Adjuvant

Appropriate adjuvants play a major role in enhancing the specific immunity of vaccines. To increase the effectiveness of vaccines, various adjuvants have been developed to promote innate immunity. Among them, STING agonists have shown potential as adjuvants in vaccinology. STINGVAX (ML-RR-S2-CDA) is believed to be the first cancer vaccine to utilize a STING agonist as an adjuvant, which comprises cancer cells secreting granulocyte-macrophage colony-stimulating factor and ADU-S100 (22). STINGVAX shows strong antitumor effects in mouse models (20, 22, 23). Another study showed that using 2', 3'-cGAMP as an adjuvant of the recombinant hemagglutinin (rHA) influenza vaccine increases rHA-specific antibody titers in adult mice (96). Furthermore, influenza vaccine using 3', 3'-cGAMP as an adjuvant elicits potent immune response with protection against lethal influenza challenge (91).

#### 4.3.2 Combination With Chemotherapy

Synergistic administration reduces the required dose of each drug and narrows the side effects of drugs. STING agonists combined with other chemotherapy drugs have achieved good efficacy in anti-tumor. DMXAA synergistically promotes cell death in mouse sarcomas when treated with cyclophosphamide (20). The combination of the chemotherapy drug fluorouracil (5FU) and cGAMP was beneficial in reducing colon cancer tumor activity (97). Importantly, side effects of both cyclophosphamide and 5FU are reduced. In addition, paclitaxel and carboplatin can be combined with STING agonists to produce better therapeutic effects (98, 99).

#### 4.3.3 Combination With Immune Checkpoint Blockade and Other Therapies

Usually, immune checkpoint blockers (ICBs) target cytotoxic T lymphocyte-associated protein 4 (CTLA4) and programmed cell death 1 (PD-1) or its ligand PD-L1 (23). Combination therapy of STING agonists and ICBs has attracted considerable attention in recent years. cGAMP combined with anti-CTLA4 and anti-PD-1 mAb treatment inhibits tumor growth (100). Moreover, cdGMP combined with anti-CTLA-4/PD-1, and dithio-cdGMP combined with anti-PD-L1 have been verified to enhance the anti-tumor effect of ICB therapy (20). STING agonists are also combined with radiotherapy, chimeric antigen receptor T cell therapy and surgery to achieve better therapy outcomes (22, 23). Indeed, the combination of STING agonists with multiple immunotherapies tends to induce the strongest immune responses, which may be one of the main strategies for treating diseases in the future.

## 5 CONCLUSIONS AND FUTURE PERSPECTIVES

In the current review, we describe the cGAS-STING signaling pathway in herpesvirus infections and outline the immunotherapy boosting this pathway. The cGAS-STING signaling pathway is essential for immunological defense of the host against herpesvirus infections. In parallel, herpesviruses also evolves to target the cGAS-STING signaling pathway to inhibit or escape the host innate immune response, thereby promoting their replication. Given the importance of the cGAS-STING signaling pathway in the sensing of herpesvirus in innate immunity, it is an attractive antiviral strategy to develop and utilize immunotherapy that enhances the cGAS-STING signaling pathway. In addition, since our review is limited to the classical cGAS-STING signaling pathway in herpesvirus infections, exploring the potential crosstalk between this pathway and other pathways of the innate immune system during viral or other pathogenic infections may be a matter of great interest in the future, such as MAPK pathway and autophagy.

## AUTHOR CONTRIBUTIONS

LZ, LD, and ZX provided ideas. LD wrote the manuscript and designed the figures. ZX, FL, JZ, ZJ, HD, SL, XS, YG, and LZ reviewed and modified the manuscript. All authors contributed to the article and approved the submitted version.

## FUNDING

This article was supported by the Sichuan Province's "14th Five-Year Plan" Sichuan Pig Major Science and Technology Project (No. 2021ZDZX0010) and the Key R&D Program in Rural Areas of Sichuan Provincial Department of Science and Technology (No. 2020YFN0147).

## ACKNOWLEDGMENTS

We would like to thank the members of the Animal Biotechnology Center for assistance and helpful.

## REFERENCES

- Zarrouk K, Piret J, Boivin G. Herpesvirus DNA Polymerases: Structures, Functions and Inhibitors. *Virus Res* (2017) 234:177–92. doi: 10.1016/j.virusres.2017.01.019
- Sathiyamoorthy K, Chen J, Longnecker R, S Jaredtzky T. The COMPLEXity in Herpesvirus Entry. *Curr Opin Virol* (2017) 24:97–104. doi: 10.1016/j.coviro.2017.04.006
- Derek G, Depledge DP, Hartley CA, Szpara ML, Vaz PK, Mária B, et al. ICTV Virus Taxonomy Profile: *Herpesviridae* 2021. *J Gen Virol* (2021) 102(10):1–2. doi: 10.1099/jgv.0.001673
- Roizmann B, Desrosiers RC, Fleckenstein B, Lopez C, Minson AC, Studdert MJ. The Family *Herpesviridae*: An Update. *Arch Virol* (1992) 123(3):425–49. doi: 10.1007/bf01317276
- Lacoste V, Lavergne A, Thoisy BD, Pouliquen JF, Gessain A. Genetic Diversity and Molecular Evolution of Human and non-Human Primate Gammaherpesvirinae. *Infect Genet Evol* (2010) 10(1):1–13. doi: 10.1016/j.meegid.2009.10.009
- Ehlers B, Dural G, Yasmun N, Lembo T, Thoisy BD, Ryser-Degiorgis MP, et al. Novel Mammalian Herpesviruses and Lineages Within the *Gammaherpesvirinae*: Cospeciation and Interspecies Transfer. *J Virol* (2008) 82(7):3509–16. doi: 10.1128/JVI.02646-07
- Ma Z, Damania B. The cGAS-STING Defense Pathway and Its Counteraction by Viruses. *Cell Host Microbe* (2016) 19(2):150–8. doi: 10.1016/j.chom.2016.01.010
- Seong RJ, Hyun SD. Damage-Associated Molecular Patterns in Inflammatory Diseases. *Immune Netw* (2018) 18(4):e27–31. doi: 10.4110/in.2018.18.e27
- Anwar S, Ul Islam K, Azmi MI, Iqbal J. cGAS-STING-Mediated Sensing Pathways in DNA and RNA Virus Infections: Crosstalk With Other Sensing Pathways. *Arch Virol* (2021) 166:3255–68. doi: 10.1007/s00705-021-05211-x
- Cai H, Imler JL. cGAS-STING: Insight on the Evolution of a Primordial Antiviral Signaling Cassette. *Fac Rev* (2021) 10(54):1–12. doi: 10.12703/r/10-54
- Phelan T, Little MA, Brady G. Targeting of the cGAS-STING System by DNA Viruses. *Biochem Pharmacol* (2020) 174:113831. doi: 10.1016/j.bcp.2020.113831
- Cheng WY, He XB, Jia HJ, Chen GH, Jin QW, Long ZL, et al. The Cgas-Sting Signaling Pathway Is Required for the Innate Immune Response Against Ectromelia Virus. *Front Immunol* (2018) 9:1297. doi: 10.3389/fimmu.2018.01297
- Kumagai Y, Takeuchi O, Akira S. TLR9 as a Key Receptor for the Recognition of DNA. *Adv Drug Deliv Rev* (2008) 60(7):795–804. doi: 10.1016/j.addr.2007.12.004
- Kawai T, Akira S. Toll-Like Receptors and Their Crosstalk With Other Innate Receptors in Infection and Immunity. *Immunity* (2011) 34(5):637–50. doi: 10.1016/j.immuni.2011.05.006
- Hu MM, Liao CY, Yang Q, Xie XQ, Shu HB. Innate Immunity to RNA Virus is Regulated by Temporal and Reversible Sumoylation of RIG-I and MDA5. *J Exp Med* (2017) 214(4):973–89. doi: 10.1084/jem.20161015
- Cheng Z, Dai T, He X, Zhang Z, Xie F, Wang S, et al. The Interactions Between cGAS-STING Pathway and Pathogens. *Signal Transduct Target Ther* (2020) 5(1):1–15. doi: 10.1038/s41392-020-0198-7
- Webb LG, Fernandez-Sesma A. RNA Viruses and the cGAS-STING Pathway: Reframing Our Understanding of Innate Immune Sensing. *Curr Opin Virol* (2022) 53:101206. doi: 10.1016/j.coviro.2022.101206
- Ran Y, Shu HB, Wang YY. MITA/STING: A Central and Multifaceted Mediator in Innate Immune Response. *Cytokine Growth Factor Rev* (2014) 25(6):631–9. doi: 10.1016/j.cytogfr.2014.05.003
- Ni G, Ma Z, Damania B. cGAS and STING: At the Intersection of DNA and RNA Virus-Sensing Networks. *PLoS Pathog* (2018) 14(8):e1007148. doi: 10.1371/journal.ppat.1007148
- Yum S, Li M, Frankel AE, Chen ZJ. Roles of the cGAS-STING Pathway in Cancer Immunovigilance and Immunotherapy. *Annu Rev Cancer Biol* (2019) 3:323–44. doi: 10.1146/annurev-cancerbio-030518-055636
- Wang Y, Luo J, Alu A, Han X, Wei Y, Wei X. cGAS-STING Pathway in Cancer Biotherapy. *Mol Cancer* (2020) 19(1):1–16. doi: 10.1186/s12943-020-01247-w
- Jiang M, Chen P, Wang L, Li W, Chen B, Liu Y, et al. cGAS-STING, an Important Pathway in Cancer Immunotherapy. *J Hematol Oncol* (2020) 13(1):1–11. doi: 10.1186/s13045-020-00916-z
- Du H, Xu T, Cui M. cGAS-STING Signaling in Cancer Immunity and Immunotherapy. *Biomed Pharmacother* (2021) 133:110972. doi: 10.1016/j.biopha.2020.110972
- Civril F, Deimling T, De Oliveira Mann CC, Ablasser A, Moldt M, Witte G, et al. Structural Mechanism of Cytosolic DNA Sensing by cGAS. *Nature* (2013) 498(7454):332–7. doi: 10.1038/nature12305
- Sun L, Wu J, Du F, Chen X, Chen Z. Cyclic GMP-AMP Synthase is a Cytosolic DNA Sensor That Activates the Type I Interferon Pathway. *Science* (2013) 339(6121):786–91. doi: 10.1126/science.1232458
- Gao P, Ascano M, Wu Y, Barchet W, Gaffney BL, Zillinger T, et al. Cyclic [G (2', 5') pA (3', 5') P] is the Metazoan Second Messenger Produced by DNA-Activated Cyclic GMP-AMP Synthase. *Cell* (2013) 153(5):1094–107. doi: 10.1016/j.cell.2013.04.046
- Whiteley AT, Eaglesham JB, de Oliveira Mann CC, Morehouse BR, Lowey B, Nieminen EA, et al. Bacterial cGAS-Like Enzymes Synthesize Diverse Nucleotide Signals. *Nature* (2019) 567(7747):194–9. doi: 10.1038/s41586-019-0953-5
- Luecke S, Holleufer A, Christensen MH, Jonsson KL, Boni GA, Sorensen LK, et al. cGAS is Activated by DNA in a Length-Dependent Manner. *EMBO Rep* (2017) 18(10):1707–15. doi: 10.15252/embr.201744017
- Andreeva L, Hiller B, Kostrewa D, Lissig C, de Oliveira Mann CC, Drexler DJ, et al. cGAS Senses Long and HMGB/TFAM-Bound U-Turn DNA by Forming Protein-DNA Ladders. *Nature* (2017) 549(7672):394–8. doi: 10.1038/nature23890
- Li X, Shu C, Yi G, Chaton CT, Shelton CL, Diaio J, et al. Cyclic GMP-AMP Synthase is Activated by Double-Stranded DNA-Induced Oligomerization. *Immunity* (2013) 39(6):1019–31. doi: 10.1016/j.immuni.2013.10.019
- Mankan AK, Schmidt T, Chauhan D, Goldeck M, Honing K, Gaidt M, et al. Cytosolic RNA: DNA Hybrids Activate the cGAS-STING Axis. *EMBO J* (2014) 33(24):2937–46. doi: 10.15252/embj.201488726
- Chen Q, Sun L, Chen ZJ. Regulation and Function of the cGAS-STING Pathway of Cytosolic DNA Sensing. *Nat Immunol* (2016) 17(10):1142–9. doi: 10.1038/ni.3558
- Zhang X, Shi H, Wu J, Zhang X, Sun L, Chen C, et al. Cyclic GMP-AMP Containing Mixed Phosphodiester Linkages is an Endogenous High-Affinity Ligand for STING. *Mol Cell* (2013) 51(2):226–35. doi: 10.1016/j.molcel.2013.05.022
- Gao P, Ascano M, Zillinger T, Wang W, Dai P, Serganov AA, et al. Structure-Function Analysis of STING Activation by C [G (2', 5') pA (3', 5') P] and Targeting by Antiviral DMXAA. *Cell* (2013) 154(4):748–62. doi: 10.1016/j.cell.2013.07.023
- Shu C, Yi G, Watts T, Kao CC, Li P. Structure of STING Bound to Cyclic Di-GMP Reveals the Mechanism of Cyclic Dinucleotide Recognition by the Immune System. *Nat Struct Mol Biol* (2012) 19(7):722–4. doi: 10.1038/nsmb.2331
- Ouyang S, Song X, Wang Y, Ru H, Shaw N, Jiang Y, et al. Structural Analysis of the STING Adaptor Protein Reveals a Hydrophobic Dimer Interface and Mode of Cyclic Di-GMP Binding. *Immunity* (2012) 36(6):1073–86. doi: 10.1016/j.immuni.2012.03.019
- Tsuchiya Y, Jounai N, Takeshita F, Ishii KJ, Mizuguchi K. Ligand-Induced Ordering of the C-Terminal Tail Primes STING for Phosphorylation by TBK1. *EBioMedicine* (2016) 9:87–96. doi: 10.1016/j.ebiom.2016.05.039
- Gao M, He Y, Tang H, Chen X, Liu S, Tao Y, et al. cGAS/STING: Novel Perspectives of the Classic Pathway. *Mol Biomed* (2020) 1(1):1–16. doi: 10.1186/s43556-020-00006-z
- Zhang X, Bai X, Chen ZJ. Structures and Mechanisms in the cGAS-STING Innate Immunity Pathway. *Immunity* (2020) 53(1):43–53. doi: 10.1016/j.immuni.2020.05.013
- Zhao B, Du F, Xu P, Shu C, Sankaran B, Bell SL, et al. A Conserved PLPLRT/SD Motif of STING Mediates the Recruitment and Activation of TBK1. *Nature* (2019) 569(7758):718–22. doi: 10.1038/s41586-019-1228-x
- Margolis SR, Wilson SC, Vance RE. Evolutionary Origins of cGAS-STING Signaling. *Trends Immunol* (2017) 38(10):733–43. doi: 10.1016/j.it.2017.03.004

42. Liu S, Cai X, Wu J, Cong Q, Chen X, Li T, et al. Phosphorylation of Innate Immune Adaptor Proteins MAVS, STING, and TRIF Induces IRF3 Activation. *Science* (2015) 347(6227):aaa2630. doi: 10.1126/science.aaa2630
43. de Oliveira Mann CC, Orzalli MH, King DS, Kagan JC, Lee ASY, Kranzusch PJ, et al. Modular Architecture of the STING C-Terminal Tail Allows Interferon and NF- $\kappa$ B Signaling Adaptation. *Cell Rep* (2019) 27(4):1165–75. doi: 10.1016/j.celrep.2019.03.098
44. Abe T, Barber GN. Cytosolic-DNA-Mediated, STING-Dependent Proinflammatory Gene Induction Necessitates Canonical NF- $\kappa$ B Activation Through TBK1. *J Virol* (2014) 88(10):5328–41. doi: 10.1128/JVI.00037-14
45. Gui X, Yang H, Li T, Tan X, Shi P, Li M, et al. Autophagy Induction via STING Trafficking Is a Primordial Function of the cGAS Pathway. *Nature* (2019) 567(7747):262–6. doi: 10.1038/s41586-019-1006-9
46. Moretti J, Roy S, Bozec D, Martinez J, Chapman JR, Ueberheide B, et al. STING Senses Microbial Viability to Orchestrate Stress-Mediated Autophagy of the Endoplasmic Reticulum. *Cell* (2017) 171(4):809–23. doi: 10.1016/j.cell.2017.09.034
47. Wu J, Chen YJ, Dobbs N, Sakai T, Liou J, Miner JJ, et al. STING-Mediated Disruption of Calcium Homeostasis Chronically Activates ER Stress and Primes T Cell Death. *J Exp Med* (2019) 216(4):867–83. doi: 10.1084/jem.20182192
48. You H, Zheng S, Huang Z, Lin Y, Shen Q, Zheng C. Herpes Simplex Virus 1 Tegument Protein UL46 Inhibits TANK-Binding Kinase 1-Mediated Signaling. *MBio* (2019) 10(3):1–10. doi: 10.1128/mBio.00919-19
49. Su C, Zheng C. Herpes Simplex Virus 1 Abrogates the cGAS/STING-Mediated Cytosolic DNA-Sensing Pathway via Its Virion Host Shutoff Protein, UL41. *J Virol* (2017) 91(6):e02414–02416. doi: 10.1128/JVI.02414-16
50. Zhang J, Zhao J, Xu S, Li J, He S, Zeng Y, et al. Species-Specific Deamidation of cGAS by Herpes Simplex Virus UL37 Protein Facilitates Viral Replication. *Cell Host Microbe* (2018) 24(2):234–48. doi: 10.1016/j.chom.2018.07.004
51. Xu H, Su C, Pearson A, Mody CH, Zheng C. Herpes Simplex Virus 1 UL24 Abrogates the DNA Sensing Pathway by Inhibiting NF- $\kappa$ B Activation. *J Virol* (2017) 91(7):e00017–00025. doi: 10.1128/JVI.00025-17
52. Zhang D, Su C, Zheng C. Herpes Simplex Virus 1 Serine Protease VP24 Blocks the DNA-Sensing Signal Pathway by Abrogating Activation of Interferon Regulatory Factor 3. *J Virol* (2016) 90(12):5824–9. doi: 10.1128/JVI.00186-16
53. Huang J, You H, Su C, Li Y, Chen S, Zheng C. Herpes Simplex Virus 1 Tegument Protein VP22 Abrogates cGAS/STING-Mediated Antiviral Innate Immunity. *J Virol* (2018) 92(15):e00818–00841. doi: 10.1128/JVI.00841-18
54. Bodda C, Reinert LS, Fruhwürth S, Richardo T, Sun C, Zhang BC, et al. HSV1 VP1-2 Deubiquitinates STING to Block Type I Interferon Expression and Promote Brain Infection. *J Exp Med* (2020) 217(7):e20191422. doi: 10.1084/jem.20191422
55. Ye R, Su C, Xu H, Zheng C. Herpes Simplex Virus 1 Ubiquitin-Specific Protease UL36 Abrogates NF- $\kappa$ B Activation in DNA Sensing Signal Pathway. *J Virol* (2017) 91(5):e02416–02417. doi: 10.1128/JVI.02417-16
56. Christensen MH, Jensen SB, Miettinen JJ, Luecke S, Prabakaran T, Reinert LS, et al. HSV-1 ICP 27 Targets the TBK 1-Activated STING Signaling to Inhibit Virus-Induced Type I IFN Expression. *EMBO J* (2016) 35(13):1385–99. doi: 10.15252/embj.201593458
57. Pan S, Liu X, Ma Y, Cao Y, He B. Herpes Simplex Virus 1  $\gamma$ 134.5 Protein Inhibits STING Activation That Restricts Viral Replication. *J Virol* (2018) 92(20):e01015–01018. doi: 10.1128/JVI.01015-18
58. You H, Lin Y, Lin F, Yang M, Li J, Zhang R, et al.  $\beta$ -Catenin is Required for the cGAS/STING Signaling Pathway But Antagonized by the Herpes Simplex Virus 1 US3 Protein. *J Virol* (2020) 94(5):1–19. doi: 10.1128/JVI.01847-19
59. Bo Z, Miao Y, Xi R, Zhong Q, Bao C, Chen H, et al. PRV UL13 Inhibits cGAS-STING-Mediated IFN- $\beta$  Production by Phosphorylating IRF3. *Vet Res* (2020) 51(1):118–25. doi: 10.1186/s13567-020-00843-4
60. Liu X, Zhang M, Ye C, Ruan K, Xu A, Gao F, et al. Inhibition of the DNA-Sensing Pathway by Pseudorabies Virus UL24 Protein via Degradation of Interferon Regulatory Factor 7. *Vet Microbiol* (2021) 255:109023. doi: 10.1016/j.vetmic.2021.109023
61. Fu YZ, Su S, Gao YQ, Wang PP, Huang ZF, Hu MM, et al. Human Cytomegalovirus Tegument Protein UL82 Inhibits STING-Mediated Signaling to Evade Antiviral Immunity. *Cell Host Microbe* (2017) 21(2):231–43. doi: 10.1016/j.chom.2017.01.001
62. Zhang G, Chan B, Samarina N, Schulz TF. Cytoplasmic Isoforms of Kaposi Sarcoma Herpesvirus LANA Recruit and Antagonize the Innate Immune DNA Sensor cGAS. *Proc Natl Acad Sci* (2016) 113(8):E1034–1043. doi: 10.1073/pnas.1516812113
63. Ma Z, Jacobs SR, West JA, Stopford C, Zhang Z, Davis Z, et al. Modulation of the cGAS-STING DNA Sensing Pathway by Gammaherpesviruses. *Proc Natl Acad Sci* (2015) 112(31):E4306–4315. doi: 10.1073/pnas.1503831112
64. Wu J, Li W, Shao Y, Avey D, Fu B, Gillen J, et al. Inhibition of cGAS DNA Sensing by a Herpesvirus Virion Protein. *Cell Host Microbe* (2015) 18(3):333–44. doi: 10.1016/j.chom.2015.07.015
65. Sun C, Schattgen SA, Pisitkun P, Jorgensen JP, Hilterbrand AT, Wang LJ, et al. Evasion of Innate Cytosolic DNA Sensing by a Gammaherpesvirus Facilitates Establishment of Latent Infection. *J Immunol* (2015) 194(4):1819–31. doi: 10.4049/jimmunol.1402495
66. Li K, Liu Y, Xu Z, Zhang Y, Luo D, Gao Y, et al. Avian Oncogenic Herpesvirus Antagonizes the cGAS-STING DNA-Sensing Pathway to Mediate Immune Evasion. *PLoS Pathog* (2019) 15(9):e1007999. doi: 10.1371/journal.ppat.1007999
67. Lio CWJ, McDonald B, Takahashi M, Dhanwani R, Sharma N, Huang J, et al. cGAS-STING Signaling Regulates Initial Innate Control of Cytomegalovirus Infection. *J Virol* (2016) 90(17):7789–97. doi: 10.1128/JVI.01040-16
68. Wang J, Chu B, Du L, Han Y, Zhang X, Fan S, et al. Molecular Cloning and Functional Characterization of Porcine Cyclic GMP-AMP Synthase. *Mol Immunol* (2015) 65(2):436–45. doi: 10.1016/j.molimm.2015.02.002
69. Wang J, Wang CF, Ming SL, Li GL, Zeng L, Wang MD, et al. Porcine IFITM1 Is a Host Restriction Factor That Inhibits Pseudorabies Virus Infection. *Int J Biol Macromol* (2020) 151:1181–93. doi: 10.1016/j.ijbiomac.2019.10.162
70. Bianco C, Mohr I. Restriction of Human Cytomegalovirus Replication by ISG15, a Host Effector Regulated by cGAS-STING Double-Stranded-DNA Sensing. *J Virol* (2017) 91(9):e02483–02486. doi: 10.1128/JVI.02483-16
71. Reinert LS, Lopušná K, Winther H, Sun C, Thomsen MK, Nandakumar R, et al. Sensing of HSV-1 by the cGAS-STING Pathway in Microglia Orchestrates Antiviral Defence in the CNS. *Nat Commun* (2016) 7(1):1–12. doi: 10.1038/ncomms13348
72. Lee JM, Ghonime MG, Cassady KA. STING Restricts oHSV Replication and Spread in Resistant MPNSTs But Is Dispensable for Basal IFN- $\sigma$ -Stimulated Gene Upregulation. *Mol Ther Oncolytics* (2019) 15:91–100. doi: 10.1016/j.omto.2019.09.001
73. Chen X, Chen Y. Ubiquitination of cGAS by TRAF6 Regulates Anti-DNA Viral Innate Immune Responses. *Biochem Biophys Res Commun* (2019) 514(3):659–64. doi: 10.1016/j.bbrc.2019.05.022
74. Liu ZS, Zhang ZY, Cai H, Zhao M, Mao J, Dai J, et al. RINCK-Mediated Monoubiquitination of cGAS Promotes Antiviral Innate Immune Responses. *Cell Biosci* (2018) 8(1):1–9. doi: 10.1186/s13578-018-0233-3
75. Qin Y, Liu Q, Tian S, Xie W, Cui J, Wang RF. TRIM9 Short Isoform Preferentially Promotes DNA and RNA Virus-Induced Production of Type I Interferon by Recruiting GSK3 $\beta$  to TBK1. *Cell Res* (2016) 26(5):613–28. doi: 10.1038/cr.2016.27
76. Guo Y, Jiang F, Kong L, Wu H, Zhang H, Chen X, et al. OTUD5 Promotes Innate Antiviral and Antitumor Immunity Through Deubiquitinating and Stabilizing STING. *Cell Mol Immunol* (2021) 18(8):1945–55. doi: 10.1038/s41423-020-00531-5
77. Wang L, Wen M, Cao X. Nuclear Hnrnpa2b1 Initiates and Amplifies the Innate Immune Response to DNA Viruses. *Science* (2019) 365(6454):e0758. doi: 10.1126/science.aav0758
78. Lian H, Wei J, Zang R, Ye W, Yang Q, Zhang XN, et al. ZCCHC3 is a Co-Sensor of cGAS for dsDNA Recognition in Innate Immune Response. *Nat Commun* (2018) 9(1):1–13. doi: 10.1038/s41467-018-05559-w
79. Gao P, Hu MM, Shu HB. CSK Promotes Innate Immune Response to DNA Virus by Phosphorylating MITA. *Biochem Biophys Res Commun* (2020) 526(1):199–205. doi: 10.1016/j.bbrc.2020.03.069
80. Zhang Y, Li M, Li L, Qian G, Wang Y, Chen Z, et al.  $\beta$ -Arrestin 2 as an Activator of cGAS-STING Signaling and Target of Viral Immune Evasion. *Nat Commun* (2020) 11(1):1–15. doi: 10.1038/s41467-020-19849-9
81. Wang C, Guan Y, Lv M, Zhang R, Guo Z, Wei X, et al. Manganese Increases the Sensitivity of the cGAS-STING Pathway for Double-Stranded DNA and is Required for the Host Defense Against DNA Viruses. *Immunity* (2018) 48(4):675–87. doi: 10.1016/j.immuni.2018.03.017

82. Lin Y, Zheng C. A Tug of War: DNA-Sensing Antiviral Innate Immunity and Herpes Simplex Virus Type I Infection. *Front Microbiol* (2019) 10:2627. doi: 10.3389/fmicb.2019.02627
83. Zheng C. Evasion of Cytosolic DNA-Stimulated Innate Immune Responses by Herpes Simplex Virus 1. *J Virol* (2018) 92(6):1–6. doi: 10.1128/JVI.00099-17
84. Zhu H, Zheng C. The Race Between Host Antiviral Innate Immunity and the Immune Evasion Strategies of Herpes Simplex Virus 1. *Microbiol Mol Biol Rev* (2020) 84(4):1–27. doi: 10.1128/MMBR.00099-20
85. Demaria O, De Gassart A, Coso S, Gestermann N, Di Domizio J, Flatz L, et al. STING Activation of Tumor Endothelial Cells Initiates Spontaneous and Therapeutic Antitumor Immunity. *Proc Natl Acad Sci* (2015) 112(50):15408–13. doi: 10.1073/pnas.1512832112
86. Larkin B, Ilyukha V, Sorokin M, Buzdin A, Vannier E, Poltorak A. Cutting Edge: Activation of STING in T Cells Induces Type I IFN Responses and Cell Death. *J Immunol* (2017) 199(2):397–402. doi: 10.4049/jimmunol.1601999
87. Lara PN Jr., Douillard J-Y, Nakagawa K, Von Pawel J, McKeage MJ, Albert J, et al. Randomized Phase III Placebo-Controlled Trial of Carboplatin and Paclitaxel With or Without the Vascular Disrupting Agent Vadimezan (ASA404) in Advanced non-Small-Cell Lung Cancer. *J Clin Oncol* (2011) 29(22):2965–71. doi: 10.1200/JCO.2011.35.0660
88. Hanson MC, Crespo MP, Abraham W, Moynihan KD, Szeto GL, Chen SH, et al. Nanoparticulate STING Agonists Are Potent Lymph Node-Targeted Vaccine Adjuvants. *J Clin Invest* (2015) 125(6):2532–46. doi: 10.1172/JCI79915
89. Luo M, Wang H, Wang Z, Cai H, Lu Z, Li Y, et al. A STING-Activating Nanovaccine for Cancer Immunotherapy. *Nat Nanotechnol* (2017) 12(7):648–54. doi: 10.1038/nnano.2017.52
90. Collier MA, Junkins RD, Gallovic MD, Johnson BM, Johnson MM, Macintyre AN, et al. Acetalated Dextran Microparticles for Codelivery of STING and TLR7/8 Agonists. *Mol Pharm* (2018) 15(11):4933–46. doi: 10.1021/acs.molpharmaceut.8b00579
91. Chen N, Gallovic MD, Tiet P, Ting JP-Y, Ainslie KM, Bachelder EM. Investigation of Tunable Acetalated Dextran Microparticle Platform to Optimize M2e-Based Influenza Vaccine Efficacy. *J Controlled Release* (2018) 289:114–24. doi: 10.1016/j.jconrel.2018.09.020
92. Park CG, Hartl CA, Schmid D, Carmona EM, Kim H-J, Goldberg MS. Extended Release of Perioperative Immunotherapy Prevents Tumor Recurrence and Eliminates Metastases. *Sci Trans Med* (2018) 10(433):eaar1916. doi: 10.1126/scitranslmed.aar1916
93. Lee E, Jang H-E, Kang YY, Kim J, Ahn J-H, Mok H. Submicron-Sized Hydrogels Incorporating Cyclic Dinucleotides for Selective Delivery and Elevated Cytokine Release in Macrophages. *Acta Biomater* (2016) 29:271–81. doi: 10.1016/j.actbio.2015.10.025
94. Baird JR, Bell RB, Troesch V, Friedman D, Bambina S, Kramer G, et al. Evaluation of Explant Responses to STING Ligands: Personalized Immunosurgical Therapy for Head and Neck Squamous Cell Carcinoma. *Cancer Res* (2018) 78(21):6308–19. doi: 10.1158/0008-5472.can-18-1652
95. Leach DG, Dharmaraj N, Piotrowski SL, Lopez-Silva TL, Lei YL, Sikora AG, et al. STINGel: Controlled Release of a Cyclic Dinucleotide for Enhanced Cancer Immunotherapy. *Biomaterials* (2018) 163:67–75. doi: 10.1016/j.biomaterials.2018.01.035
96. Borriello F, Pietrasanta C, Lai JC, Walsh LM, Sharma P, O'Driscoll DN, et al. Identification and Characterization of Stimulator of Interferon Genes as a Robust Adjuvant Target for Early Life Immunization. *Front Immunol* (2017) 8:1772. doi: 10.3389/fimmu.2017.01772
97. Li T, Cheng H, Yuan H, Xu Q, Shu C, Zhang Y, et al. Antitumor Activity of cGAMP via Stimulation of cGAS-cGAMP-STING-IRF3 Mediated Innate Immune Response. *Sci Rep* (2016) 6(1):1–14. doi: 10.1038/srep19049
98. Zierhut C, Yamaguchi N, Paredes M, Luo JD, Funabiki H. The Cytoplasmic DNA Sensor cGAS Promotes Mitotic Cell Death. *Cell* (2019) 178(2):302–15. doi: 10.1016/j.cell.2019.05.035
99. Ghaffari A, Peterson N, Khalaj K, Vitkin N, Robinson A, Francis J-A, et al. STING Agonist Therapy in Combination With PD-1 Immune Checkpoint Blockade Enhances Response to Carboplatin Chemotherapy in High-Grade Serous Ovarian Cancer. *Br J Cancer* (2018) 119(4):440–9. doi: 10.1038/s41416-018-0188-5
100. Da Hoong BY, Gan YH, Liu H, Chen ES. cGAS-STING Pathway in Oncogenesis and Cancer Therapeutics. *Oncotarget* (2020) 11(30):2930. doi: 10.18632/oncotarget.27673

**Conflict of Interest:** The authors declare that the research was conducted in the absence of any commercial or financial relationships that could be construed as a potential conflict of interest.

**Publisher's Note:** All claims expressed in this article are solely those of the authors and do not necessarily represent those of their affiliated organizations, or those of the publisher, the editors and the reviewers. Any product that may be evaluated in this article, or claim that may be made by its manufacturer, is not guaranteed or endorsed by the publisher.

Copyright © 2022 Deng, Xu, Li, Zhao, Jian, Deng, Lai, Sun, Geng and Zhu. This is an open-access article distributed under the terms of the Creative Commons Attribution License (CC BY). The use, distribution or reproduction in other forums is permitted, provided the original author(s) and the copyright owner(s) are credited and that the original publication in this journal is cited, in accordance with accepted academic practice. No use, distribution or reproduction is permitted which does not comply with these terms.



# Characterization of the Immunologic Phenotype of Dendritic Cells Infected With Herpes Simplex Virus 1

Jingjing Zhang<sup>1,2</sup>, Xingli Xu<sup>1,2</sup>, Suqin Duan<sup>1,2</sup>, Yang Gao<sup>1,2</sup>, Danjing Ma<sup>1,2</sup>, Rong Yue<sup>1,2</sup>, Fengyuan Zeng<sup>1,2</sup>, Xueqi Li<sup>1,2</sup>, Ziyang Meng<sup>1,2</sup>, Xinghang Li<sup>1,2</sup>, Zhenye Niu<sup>1,2</sup>, Guorun Jiang<sup>1,2</sup>, Li Yu<sup>1,2</sup>, Yun Liao<sup>1,2</sup>, Dandan Li<sup>1,2</sup>, Lichun Wang<sup>1,2</sup>, Heng Zhao<sup>1,2</sup>, Ying Zhang<sup>1,2\*</sup> and Qihan Li<sup>1,2\*</sup>

<sup>1</sup> Institute of Medical Biology, Chinese Academy of Medical Sciences & Peking Union Medical College, Kunming, China,

<sup>2</sup> Yunnan Key Laboratory of Vaccine Research and Development on Severe Infectious Diseases, Kunming, China

## OPEN ACCESS

### Edited by:

Chenhe Su,  
Wistar Institute, United States

### Reviewed by:

Genhong Cheng,  
University of California, Los Angeles,  
United States  
Xiaolong Zhang,  
Harvard Medical School,  
United States

### \*Correspondence:

Qihan Li  
liqihan@imbcams.com.cn  
Ying Zhang  
cherryzhang629@126.com

### Specialty section:

This article was submitted to  
Viral Immunology,  
a section of the journal  
Frontiers in Immunology

Received: 29 April 2022

Accepted: 09 June 2022

Published: 05 July 2022

### Citation:

Zhang J, Xu X, Duan S, Gao Y, Ma D,  
Yue R, Zeng F, Li X, Meng Z, Li X,  
Niu Z, Jiang G, Yu L, Liao Y, Li D,  
Wang L, Zhao H, Zhang Y and Li Q  
(2022) Characterization of the  
Immunologic Phenotype of  
Dendritic Cells Infected With  
Herpes Simplex Virus 1.  
*Front. Immunol.* 13:931740.  
doi: 10.3389/fimmu.2022.931740

Due to viral envelope glycoprotein D binding to cellular membrane HVEM receptor, HSV-1 can infect certain dendritic cells, which becomes an event in the viral strategy to interfere with the host's immune system. We previously generated the HSV-1 mutant strain M6, which produced an attenuated phenotype in mice and rhesus monkeys. The attenuated M6 strain was used to investigate how HSV-1 infection of dendritic cells interferes with both innate and adaptive immunity. Our study showed that dendritic cells membrane HVEM receptors could mediate infection of the wild-type strain and attenuated M6 strain and that dendritic cells infected by both viruses in local tissues of animals exhibited changes in transcriptional profiles associated with innate immune and inflammatory responses. The infection of pDCs and cDCs by the two strains promoted cell differentiation to the CD103<sup>+</sup> phenotype, but varied transcriptional profiles were observed, implying a strategy that the HSV-1 wild-type strain interferes with antiviral immunity, probably due to viral modification of the immunological phenotype of dendritic cells during processing and presentation of antigen to T cells, leading to a series of deviations in immune responses, ultimately generating the deficient immune phenotype observed in infected individuals in the clinical.

**Keywords:** herpes simplex virus type 1, dendritic cells, wild-type strain, attenuated strain M6, HVEM

## INTRODUCTION

Herpes simplex virus 1 (HSV-1), a member of the alpha group in the herpesvirus family and the agent of oral and genital herpetic diseases (1, 2), has long been a public health concern due to its significance for clinical treatment and pandemic control (3, 4). The disease caused by this agent and its clinical outcomes has substantial effects on the quality of human life (5, 6) due to the complicated mode of viral infection in the human body, as various virus-encoded proteins enable interaction with the immune system during infection (7–9). Previous data suggested that viral proteins could have different interference effects targeting various cells involved in innate and adaptive immunity, including dendritic cells and lymphocytes, and shape the immune response and pathological

outcomes (10–13). Dendritic cells, as important innate immune cells, function not only in phagocytosis and uptake of antigens from infected epithelial tissues and presentation to T cells (14, 15) but also in regulation of the relationship between innate immunity and inflammatory reactions for further activation of adaptive immunity (16, 17). Reported data indicated that HSV is capable of infecting some dendritic cells and replicating in those cells. This event is due to the viral envelope glycoprotein D binding to the HVEM receptor in the membrane dendritic cells (18, 19). Based on these findings, a study tracing HSV-1 infection discovered that not only was viral antigen in tissues phagocytized by activated dendritic cells with infected epithelial cells and transferred to lymph nodes for antigen presentation to T cells, but that infected dendritic cells also carried the complete virion to T cells for antigen transfer during the infection process (20, 21), which raised the logical question of how and to what extent dendritic cells infected with HSV-1 could influence the differentiation process and the activation of T cells through specific antigen presentation. Our previous work showed that HSV-1 infection in HVEM<sup>-/-</sup> mice elicited a disparate immune response phenotype in comparison with that in wild-type mice (unpublished data) and suggested that viral infection of dendritic cells could interfere with innate immune cells, activating adaptive immunity, although the role of dendritic cells in this process is unknown. In the current work, we used the attenuated HSV-1 strain M6, with gene modifications, as a control (22), investigated the possible mechanism of the altered immunological phenotype induced by infected dendritic cells in mice, and explored the relationship of this alteration with the development of specific antiviral immunity during HSV-1 infection. All of the results suggested that viral infection of dendritic cells is an important factor that interferes with the immune response.

## MATERIAL AND METHODS

### Animal and Ethics

Four-to six-week-old female Balb/c mice were purchased from Vital River (Beijing, China) and housed in a specific pathogen-free facility at the Institute of Medical Biology. The room temperature was maintained at approximately 25°C during the experiments. Food and water were readily available. All animals were fully under the care of veterinarians at the Institute of Medical Biology (IMB), Chinese Academy of Medicine Science (CAMS). All animal experiments were performed according to the National Institutes of Health Guide for the Care and Use of Laboratory Animals, with approval from the Institutional Animal Care and Use Committee of the IMB, CAMS (approval number: WSP 201803014).

### Cell Culture

The Vero African green monkey kidney cell line (ATCC, Manassas, Virginia, USA) and the KMB17 cell line (IMB, CAMS, Yunnan, China) were cultured in minimum Eagle's medium (MEM; Thermo Fisher Scientific, Waltham,

Massachusetts, USA) supplemented with 10% fetal bovine serum (FBS; HyClone, GE Healthcare, Chicago, Illinois, USA), 10% 100 U/mL penicillin and 100 mg/mL streptomycin. JASWII dendritic cells (ATCC, Manassas, Virginia, USA) were cultured in MEM Alpha (Thermo Fisher Scientific, Waltham, Massachusetts, USA) supplemented with 20% fetal bovine serum (FBS; HyClone, GE Healthcare, Chicago, Illinois, USA), 10% 100 U/mL penicillin and 100 mg/mL streptomycin, and 5 ng/mL murine GM-CSF (HY-P7361, MCE, USA), and the cells were maintained at 37°C with 5% CO<sub>2</sub>. The culture medium was changed to MEM (MEM Alpha) supplemented with 2% FBS after viral infection.

### Virus

The HSV-1 wild-type (WT) strain 8F (23) and the HSV-1 mutant strain M6 (22) were used in the experiments. The mutants were verified by PCR and sequencing of PCR products.

### Animal Experiment Design

Balb/c mice were randomly divided into three groups (Figure S1).

In group A, the mice were infected with a low dose ( $2 \times 10^4$  PFU) of the wild-type (WT) or attenuated M6 strain *via* the intranasal route. The mice were observed and weighed every day. The nose, brain, spinal cord, trigeminal ganglion, and inguinal lymph nodes were obtained at 3, 7, 14, 21, and 28 days after viral infection (dpi), followed by viral load detection. At 14, 21, and 28 days post-infection, the blood was obtained for neutralizing antibody testing, and the spleen was subjected to lymphocyte separation for ELISpot assays. At 28 days post-infection, all infected mice were challenged with a lethal dose ( $1 \times 10^5$  PFU) of the WT strain *via* the intranasal route and observed and weighed every day.

In group B, the mice were infected with  $1 \times 10^5$  PFU of the WT or M6 strain *via* the intranasal (IN) route, intradermal (ID) route and intramuscular (IM) route. At 36, 48, and 72 hours post-infection (hpi), tissues (nose, muscle, and skin) from the infected site were obtained for immunofluorescence detection, viral load detection, and qRT-PCR cytokine detection.

In group C, for the transfusion experiment, CD11c<sup>+</sup> DC cells were obtained from healthy mice's skin and infected with WT or M6 (MOI=1) *in vitro*. At 24 hpi, the *in vitro*-infected CD11c<sup>+</sup> DC cells ( $1 \times 10^5$  cells per mouse), washed with PBS three times, were transfused into 100 healthy mice through the tail vein, respectively. Then, the mice were observed and weighed daily. The spleen, brain, spinal cord, trigeminal ganglion, and inguinal lymph nodes were obtained at 1, 3, 7, 14, 21, 28, and 56 days after adoptive transfer, followed by viral load detection, and at 1, 3, and 7 days inguinal lymph nodes were obtained to detect changes in cytokine levels. At 21 and 28 days after adoptive transfer, the spleen was subjected to lymphocyte separation for ELISopt assays. At 28 days post-transfused, 25 infected mice in each group were challenged with a lethal dose ( $1 \times 10^5$  PFU) of the WT strain *via* the intranasal route and observed and weighed every day. At 28 days after the challenge, blood was obtained for neutralizing antibody testing.

## Virus Infection of JASWII-Dendritic Cells

Virus-infected JASWII-dendritic cells (or HVEM-specific antibody blocked, rabbit anti-TNFSF14 antibody, BS-2462R) infected with the wild-type strain or attenuated M6 strain were tested for virus proliferation at 8 to 72 h at a MOI=0.1; after infected 12, 24, 36, and 48 h, the cells were used to detect cytokines.

## RT-PCR and qRT-PCR

The viral loads in the tissues were determined by qPCR with absolute quantification. Based on the methods performed by Ryncarz AJ et al. (24), the binding site designed by the primer was located in the HSV-1 gG gene region, and the gG gene was constructed on the p-GMT plasmid as a standard DNA sample. The primers were F: T C C T S G T T C C T M A C K G C C T C C C and R: G C A G I C A Y A C G T A A C G C A C G C T. Viral genomic DNA was extracted from tissues using an AxyPrep™ Body Fluid Viral DNA/RNA Miniprep kit (Central Avenue Union City, CA, USA). The TaqMan probe (Sangon Biotech, Shanghai, China) had the sequence 5'-6FAMCGTCTGGACCAACCGCCACACAGGTTAMRA. The reactions were performed using Premix Ex Taq™ (Probe qPCR; TaKaRa, Dalian, China) on a CFX96 Connect Real-Time System (Bio-Rad, Hercules, CA, USA).

For the relative expression of cytokines in tissues and cells, total RNA was extracted with TRIzol-A+ Reagent (Cat# DP421, Tiangen) according to the manufacturer's protocol. Gene expression was expressed as the fold-change ( $2^{-\Delta\Delta Ct}$ ) relative to the levels in samples from PBS-injected mice or virus-uninfected cells used for calibration. The reactions were performed using a One-Step SYBR Prime Script™ PLUS RT-PCR kit (TaKaRa, Dalian, China). The specific primers used are listed in **Table S1**.

## Virus Titration

The virus titer was determined following standard protocols, as described previously (25). In brief, the virus was subjected to gradient dilution and added to 96-well plates containing  $10^4$  Vero cells in each well, and the cells were cultured at 37°C with 5% CO<sub>2</sub> for 7 days.

## Neutralization Assay

A neutralization assay was performed following standard protocols. Briefly, the diluted serum (1:4, 1:8, 1:16, 1:32, and 1:64) and the virus were mixed with a titer of 100 times the 50% cell culture infectious dose (CCID<sub>50</sub>)/100 μL and incubated at 37°C for 2 hours. Vero cells were then added to 96-well plates and incubated at 37°C, and the CPE of the virus was observed after 1 week.

## IFN-γ-Specific and IL-4-Specific ELISpot ASSAY

The spleen was isolated under sterile conditions, and the splenic lymphocytes were divided into lymphocyte suspensions according to the instructions of the lymphocyte separation solution (Dakewe Biotech, Beijing, China). For the ELISpot assay, the mouse IFN-γ (or IL-4) ELISpot kit (MABTECH Inc., Cincinnati, OH, USA) was used for the manufacturer's protocol.

Briefly, a plate was conditioned and seeded with splenic lymphocytes ( $10^4$  cells per well) before adding 10 μg of stimulant (two peptides: gB498-505, SSIEFARL; and ICP6 822-829, QTFDFGRL) (Sangon Biotech, Shanghai, China). Then, the cells were incubated at 37°C for 30 h. After that, the cells and medium were removed, and the plate was developed. The colored spots were counted using an automated ELISpot reader (CTL, Cleveland, OH, USA) (22).

## Immunofluorescence and Confocal Microscopy

Skin, nose, and muscle tissue from immunized mice were collected and immediately frozen in liquid nitrogen. According to the manufacturer, the tissue sections were embedded in OCT (Tissue-Tek OCT Compound 4583, Sakura) and sliced on a cryostat at a 5 μm thickness (CM1850, Leica) protocol. The tissue sections were fixed with 4% paraformaldehyde solution for 20 min and blocked with 5% bovine serum albumin (BSA) at 37°C for 2 h. The sections were sequentially incubated with a primary rabbit anti-HSV-1 antibody (Thermo) at 4°C overnight, washed three times with TBST buffer (0.15 M NaCl, 20 mM Tris-HCl, 0.05% Tween 20, pH 7.4), and then incubated an Alexa Fluor 647-conjugated donkey anti-rabbit IgG secondary antibody (Invitrogen) at 37°C for 0.5 h to detect the viral antigen. DCs were detected with a rat anti-CD11c antibody (Abcam, Cat# ab33483) and Alexa Fluor 488-conjugated donkey anti-rat IgG secondary antibody (Invitrogen). All cell nuclei were detected with DAPI. Fluorescence was visualized and analyzed using a confocal microscope (TCS SP2, Leica).

## Isolation of Lymphocytes From Mouse Skin

Back skin tissues dissected from euthanized mice were placed into dishes and cut into 0.2mm<sup>2</sup> pieces with scissors. The pieces of tissue were transferred into 100 mm dishes and incubated with a digestion solution containing 2.5 mg/mL collagenase I (Cat # C0130, Sigma), 2.5 mg/mL trypsin (Cat # 27250018, Thermo Fisher Scientific), and 1 U/mL DNase I (D8071, Solarbio) in Roswell Park Memorial Institute (RPMI) 1640 medium for 2 h at 37°C. The digested supernatant was filtered through a 70 μm cell strainer to obtain a single-cell suspension. Skin lymphocytes were isolated by centrifugation in lymphocyte separation solution (Dakewe Biotech, Beijing, China). CD11c-positive dendritic cells were enriched with the EasySep Mouse CD11c Positive Selection Kit (Stemcell, Cat# 18780) for subtype sorting.

## Bone Marrow-Derived Dendritic Cells

Murine bone marrow (BM) cultures were initiated at  $1 \times 10^6$  cells/mL in Roswell Park Memorial Institute (RPMI) 1640 complete medium (Cat#R8758, Sigma) containing 20 ng/mL GM-CSF (HY-P7361, MCE, USA) and 10 ng/mL IL-4 (HY-P70644, MCE, USA). Cells were collected following 6-7 days of culture.

## Flow Cytometry Analysis and Cell Sorting

Skin and spleen lymphocytes were cultured in Roswell Park Memorial Institute (RPMI) 1640 medium (Cat #R8758, Sigma)



supplemented with 10% fetal bovine serum (FBS; HyClone, GE Healthcare, Chicago, Illinois, USA), 10% 100 U/mL penicillin and 100 mg/mL streptomycin, and the cells were maintained at 37°C with 5% CO<sub>2</sub>. To sort the pDCs subgroup, first use the B cell positive selection kit to isolate B cells (EasySep™ Mouse CD19 Positive Selection Kit, Catalog #18754). Then, the liquid passing through the column of B cell positive selection was performed by EasySep Mouse CD11c Positive Selection Kit (Stemcell, Cat# 18780) to enrich DCs cells. The CD11c-positive DCs were washed three times with PBS, and then added 10μL fluorophore-conjugated antibody (PerCP/Cy5.5-CD103 (Cat#121416), PE/Cy7-CD11c (Cat#117318), FITC-CD11b (Cat#101206), PE-CD45R (Cat#103208) and APC-CD8α (Cat#100712) purchased from BioLegend). The cells were stained for 30 min at 4°C and washed twice prior to flow cytometric analysis (LSR Fortessa, BD) and to sort (Influx, BD).

### Transcriptome Analysis of Dendritic Cells

The skin CD103<sup>+</sup> dendritic cells were sorted by flow cytometry and infected with WT and M6 (MOI=0.1) at 24, 48, and 72hpi. At the same time, a control group (CD103<sup>+</sup> DCs) without viral infection was established. According to the manufacturer's instructions, total RNA was extracted using TRIzol (Cat # DP421, Tiangen). RNA quantity and integrity were evaluated using the NanoDrop system and a Bioanalyzer, and the samples were prepared according to Illumina's instructions and sequenced (Gene Denovo Biotechnology Co., Guangzhou, China). Genes with 2-fold or greater changes in expression at  $P < 0.05$  in the Kyoto Encyclopedia of Genes and Genomes (KEGG) analyses were selected and grouped into functional categories. The raw sequence data were deposited in the Sequence Read Archive under BioProject number PRJNA834578.

### Statistical Analysis

All the data are expressed as the mean value with the standard error of the mean. Significant differences between groups were analyzed by two-way ANOVA (GraphPad Prism; GraphPad Software, San Diego, CA, USA), and  $P < 0.05$  was considered to indicate statistical significance.

## RESULTS

### The Attenuated HSV-1 Mutant Strain M6 Leads to an Effectual Immune Response in Comparison With the Wild-Type Strain

Our previous published work showed that this M6 strain was capable of leading to an immunoprotective effect after inoculation in mice *via* nasal spray, with indicators of neutralizing antibodies, specific T cell responses with IFN- $\gamma$  and IL-4 production 4 to 8 weeks after inoculation in the mice, and clinical protection, including a lower viral load in tissues and mild pathologic injuries observed during virus challenge

(22). Here, we further compared the characteristics of the immune responses and pathologic injuries elicited by the M6 and wild-type strains in Balb/c mice and found first that mild clinical manifestations, including weight loss and death rate, were observed in the M6 group compared to the wild-type strain group (**Figures 1A, B**); second, the viral load assay in various tissues from sacrificed animals at different times post-inoculation did not show obvious proliferative peaks in the M6 group (**Figure 1C**); and third, the neutralizing antibody assay and ELISpot detection of specific T cell responses of mice showed that the M6 strain elicited a no less strong response than by the wild-type strain (**Figures 1D, E**). Further observation of the mice inoculated with the M6 or wild-type strain in the viral challenge test suggested different clinical outcomes in the two groups (**Figures 1F, G**), with decreased body weight and a higher death rate in the group inoculated with the wild-type strain. These results identified the M6 strain as an attenuated strain that induces mild pathologic injury in mice and better immunogenicity, eliciting an immunoprotective effect. This result is significant compared to the wild-type strain for investigating the relationship between HSV-1 infection in dendritic cells and the development of antiviral immunity.

### Differences in Infection Between the Wild-Type Strain and Attenuated M6 Strain in Cultured Mouse JAWSII-Dendritic Cells

Based on the disparate immunological phenotypes observed in mice infected with the wild-type strain and attenuated M6 strain, our work using cultured JAWS II-dendritic cells investigated the dynamic infection process with the two virus strains. The results indicated that the wild-type strain or the attenuated strain replicated in these dendritic cells with different efficiencies (**Figure 2A**), while the viral proliferation of both strains was inhibited in the cells treated with a specific antibody against HVEM (**Figure 2A**). Other viral load detection in these infected JAWS II-dendritic cells confirmed this finding (**Figure 2B**). The transcriptional profile analysis of some immune regulators and effectors in these infected cells *via* q-RT-PCR found that most immune molecules, including IFN- $\alpha$ , IFN- $\beta$ , IFN- $\gamma$ , IL-4, IL-10, IL-23, IL-27, and GM-CSF, which are important for the activation of antiviral immunity, were consistently upregulated in the infected cells by the attenuated strain (**Figure 2C**), while the expression of marker molecules for the maturation of dendritic cells, such as CD83 and CD40, are less activated in WT group than in M6 group (**Figure 2E**). However, no significant variation in these molecules was found in cells infected with the wild-type strain (**Figures 2C, D**). Interestingly, some inflammatory factors, such as IL-6, IL-12, and CXCL12, were upregulated in cells infected with the wild-type strain (**Figure 2D**). These results suggested the capacity of HSV-1 to infect certain dendritic cells and that dendritic cells respond differently to viral infection depending upon the virulence of the viral strain. Theoretically, this difference might impact the phenotype of antiviral immunity.

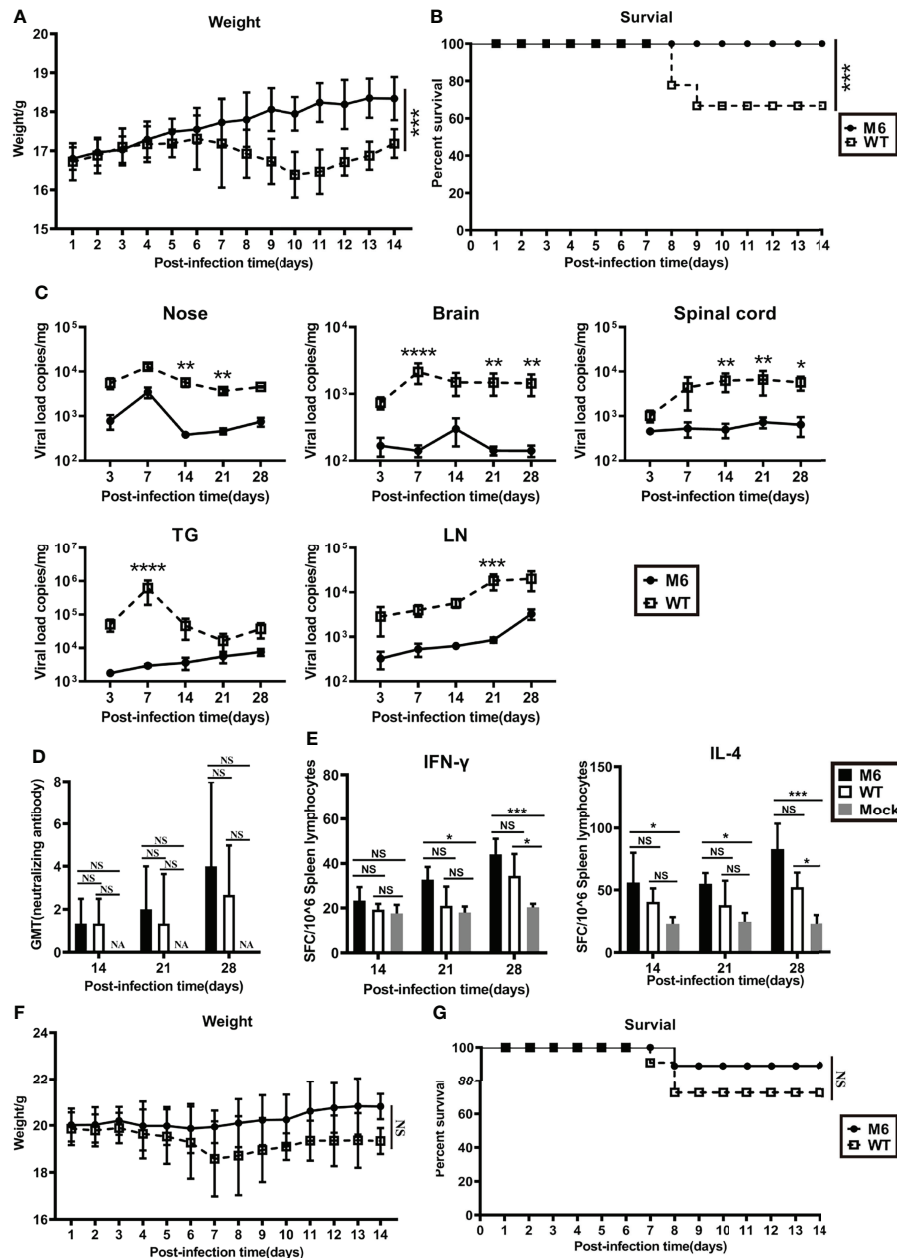


**FIGURE 1** | The mutated strain M6 produced a more effective immune response than the wild-type strain. Bodyweight (A) and survival rate (B) of mice infected with the attenuated HSV-1 mutant M6 (circle) and the wild-type strain (square) *via* nasal spray. (C) Viral loads in the nose, brain, spinal cord, trigeminal ganglion, and inguinal lymph node after infection with M6 (circle) and WT (square), as determined by RT-qPCR. (D) The HSV-1 neutralizing antibody titer in mice infected with M6 (black square), WT (white square), and Mock (gray square). (E) The ELISpot responses show IFN- $\gamma$ - and IL-4-secreting cells among splenic lymphocytes after infection with M6 (black square), WT (white square), and Mock (gray square). Bodyweight (F) and survival rate (G) of mice immunized with M6 (circle) and WT (square) after wild-type viral challenge. The data are shown as the mean  $\pm$  SEM based on data from three independent experiments. \* $P$  < 0.05, \*\* $P$  < 0.01, \*\*\* $P$  < 0.001, \*\*\*\* $P$  < 0.0001. NS, no significance.

## HSV-1 Infection in Dendritic Cells Alters the Dynamic Process of the Innate Immune Response in Local Tissue

Based upon the observed characteristics of the immune response elicited by the attenuated M6 strain and the biological process of M6 infection in cultured dendritic cells, our work investigated

the interaction of this strain or the wild-type strain and dendritic cells in infected mice and suggested interesting differences in the mouse groups inoculated with the two strains at the same infectious dose ( $10^5$  CCID<sub>50</sub>/mouse). Observation of the nasal mucosa, intradermal and muscular tissues using a fluorescence microscope indicated that the attenuated M6 strain had a higher

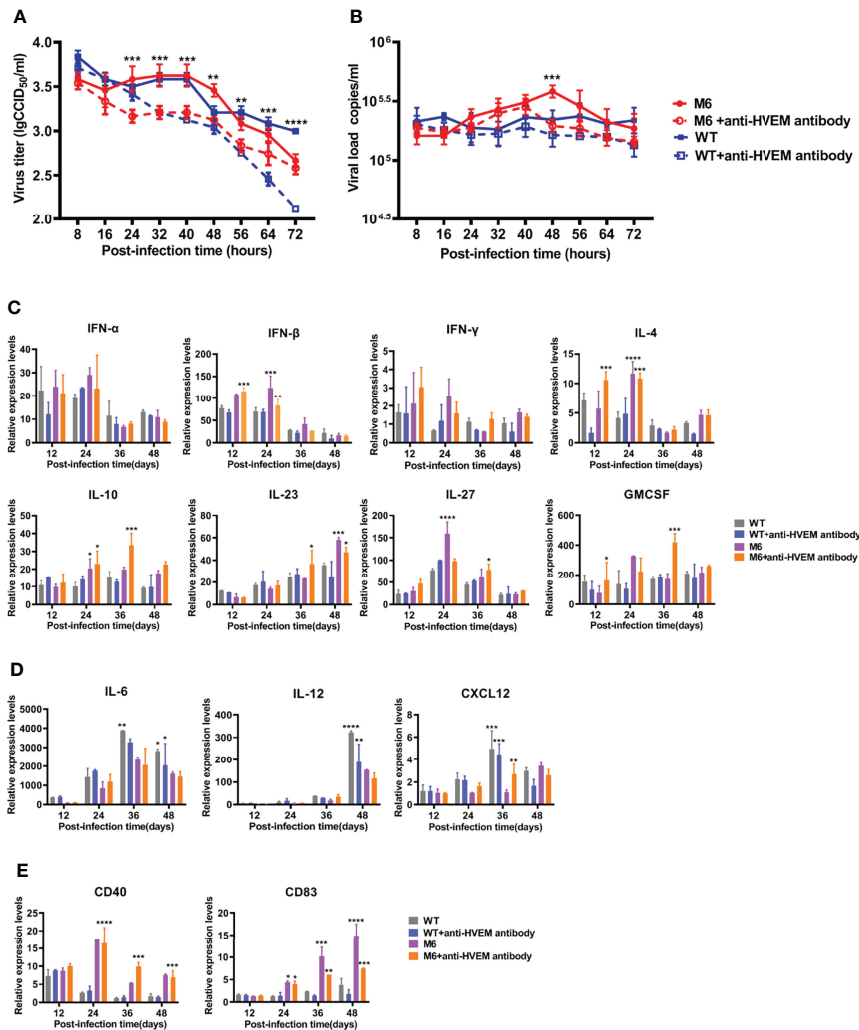


**FIGURE 2** | The dynamic processes in JAWS II-dendritic cells infected with the wild-type strain and attenuated M6 strain. The replication (A) and viral load (B) of JAWSII-dendritic cells infected with the wild-type strain (solid blue square and hollow square) and attenuated M6 strain (solid red circle and hollow circle). The M6+anti-HVEM antibody group is compared with the M6 group, and the WT+anti-HVEM antibody group is compared with the WT group. Transcriptional profile analysis of immune regulators and effectors (C, D) in JAWSII-dendritic cells infected with the wild-type strain (gray and blue) and attenuated M6 strain (purple and orange). The relative expression levels of inflammatory cytokines in JAWSII dendritic cells were normalized to their levels in the blank control group (without viral infection and antibody) using the comparative Ct ( $\Delta\Delta C_t$ ) method. The data are shown as the mean  $\pm$  SEM based on data from three independent experiments. \* $P < 0.05$ , \*\* $P < 0.01$ , \*\*\* $P < 0.001$ , \*\*\*\* $P < 0.0001$ .

rate of antigenic colocalization with dendritic cells in three tissues at 36, 48, and 72 hours post-inoculation than the wild-type strain (Figures 3A–C). The viral load of the M6 strain in these infected tissues was lower than that of the wild-type strain in these tissues (Figures 3D, F, H). These results suggest that wild-type strain infection might attenuate the phagocytosis of viral antigen by dendritic cells in epithelial tissues *via* some unknown mechanisms. mRNA transcriptional profile assays of various immune-regulating molecules in these three tissues suggested that the two strains led to different profiles (Figures 3E, G, I), with some important molecules, including type 1 interferon (including IFN- $\alpha$ , IFN- $\beta$ ), IL-6 and TNF- $\alpha$ , showing significant differences in all tissues between the two

groups (Figures 3E, G, I). The difference was significant in the nasal mucosa (Figure 3E). These results indicate that the characterized interaction of the HSV-1 wild-type strain and dendritic cells might be involved in the varied innate immune responses and inflammatory reactions in tissues, which might be relevant to specific antiviral immunity.

### Infection With a Wild-Type Strain and Attenuated Strain in Dendritic Cells Leads to the Differentiation States With Disparate Biological Characteristics

The wild-type strain and attenuated strain are capable of infecting dendritic cells, and the available information about

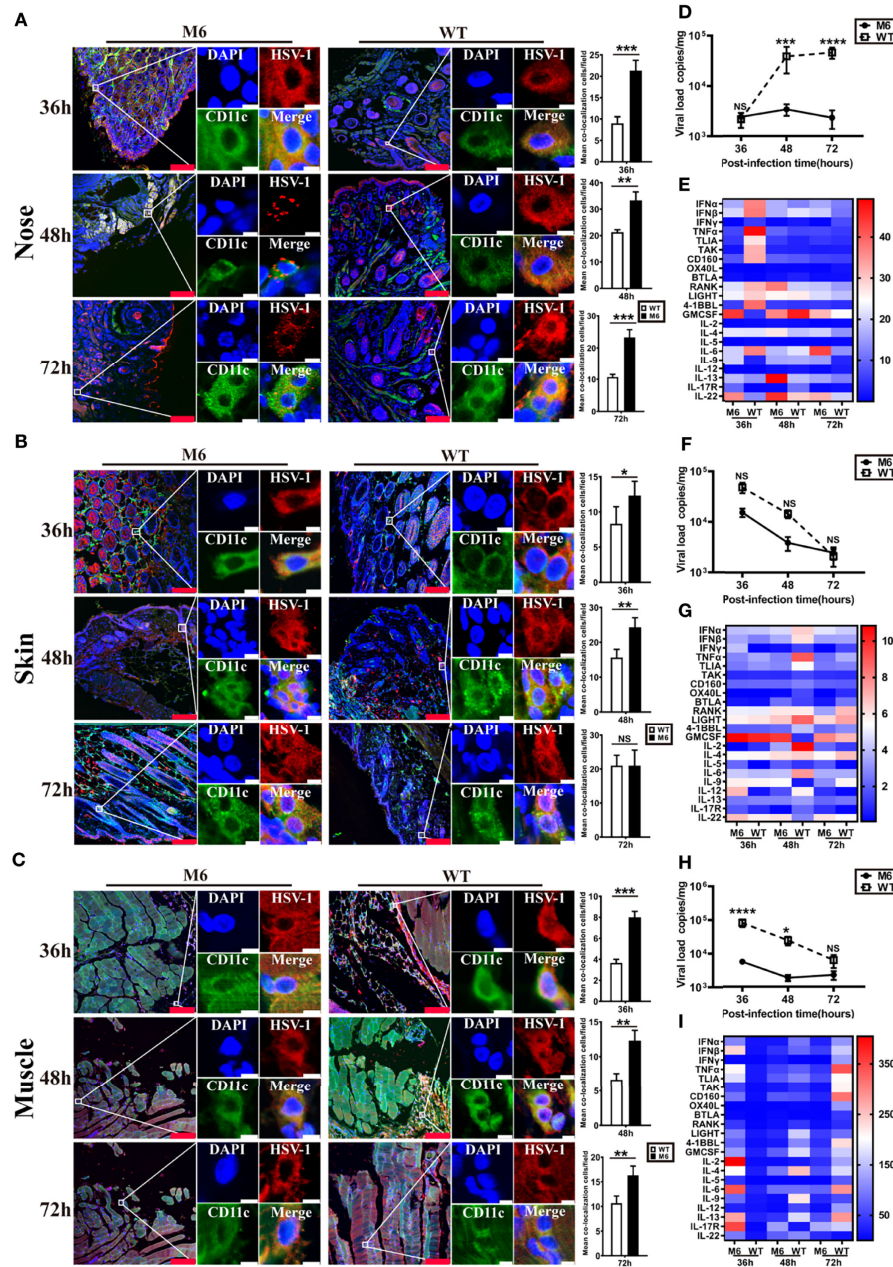


**FIGURE 3** | The innate immune responses in local tissues after HSV-1 via different infection routes. Representative confocal fluorescence images of HSV-1 expression (red) and CD11c (green) after intranasal (IN) (A), intradermal (ID) (B) and intramuscular (IM) (C) administration of HSV-1 antigen at 36 h, 48 h and 72 hpi. The image on the right represents the colocalization rates of DC cells after intranasal (IN) (A), intradermal (ID) (B), and intramuscular (IM) (C) administration. White represents M6 infection, and black represents WT infection. Representative fluorescent cells in the white rectangle are shown at 20 $\times$  magnification. The red scale bar is 100  $\mu$ m, white scale bar is 5  $\mu$ m. Statistical analysis of colocalization with both HSV-1 and DCs (marked by CD11c) compared to observations of 50 DCs randomly counted. Viral load in the nose (D), skin (F), and muscle (H) tissue of mice infected with M6 (circle) and WT (square) via different routes. Expression profiles of immune regulatory molecules in the nose (E), skin (G), and muscle (I) tissue of mice infected with M6 and WT. A heat map shows the dynamic gene expression profiles. Each column represents one dataset. The red color indicates the genes expressed at higher levels in the samples than those at 0 hpi, and the blue color indicates the genes expressed at lower levels. The darker the color, the more significant the change. The data are shown as the mean  $\pm$  SEM based on data from three independent experiments. \* $P < 0.05$ , \*\* $P < 0.01$ , \*\*\* $P < 0.001$ , \*\*\*\* $P < 0.0001$ . NS, no significance.

the immunological function of dendritic cells suggests the significance of the interaction between viral infection and various subpopulations of dendritic cells for understanding the immune response after HSV-1 infection. Dendritic cells with different surface markers were collected from normal Balb/c mice and cultured *in vitro*. Furthermore, these cells were infected with the wild-type strain or attenuated strain, and their surface marker molecules were detected at different time points of 24 and 48 hpi. The results suggested that both strains can not only infect plasmacytoid dendritic cells and conventional dendritic cells but also stimulate them to further differentiate to a state with a CD103<sup>+</sup> phenotype (Figures 4A, B). Interestingly, the transcriptional profiles of some significant immune molecules of these infected CD103<sup>+</sup> dendritic cells suggested that the cells infected with the attenuated M6 strain showed higher expression of the immune molecules than those in cells infected with the wild-type strain (Figure 4C and Figure S2), which seems to indicate that infection with the wild-type strain inhibits cellular immune activity, as these cells are involved in antigen presentation to T cells. Previous data showed that CD103<sup>+</sup> dendritic cells possess powerful antigen presentation capacity (26). All of the data from our experiment suggested different interactions between the wild-type strain and

attenuated strain, which implies a possible mechanism for the ineffective immune response in the infected population.

## Viral Infection in CD103<sup>+</sup> Dendritic Cells Leads to Alteration of the Transcription Profile Related to the Immune Response

Based upon the characterized biological features of dendritic cells infected by the HSV-1 wild-type strain or attenuated strain, we analyzed the dynamic alterations in the mRNA profile of infected CD103<sup>+</sup> cells at different time points after infection. The results suggested different alterations within the two groups and showed a consistently increasing number of upregulated differential genes in the two groups during the infectious process (Figure 5A). These data also suggested that the wild-type strain altered the transcriptional profile based upon its pathogenic effect on dendritic cells, even though its proliferation peak was lower than that of the attenuated M6 strain. The analysis suggested that these different genes were related to various cellular biological properties (Figure 5B), especially genes that play a role in immune regulation (Figure 5B). Further analysis found that the expression of genes related to cytotoxic effects mediated by NK cells, complement reactions, and the signaling pathways of Rap1, PI3K-Akt, and Hippo presented different patterns of alterations in dendritic cells

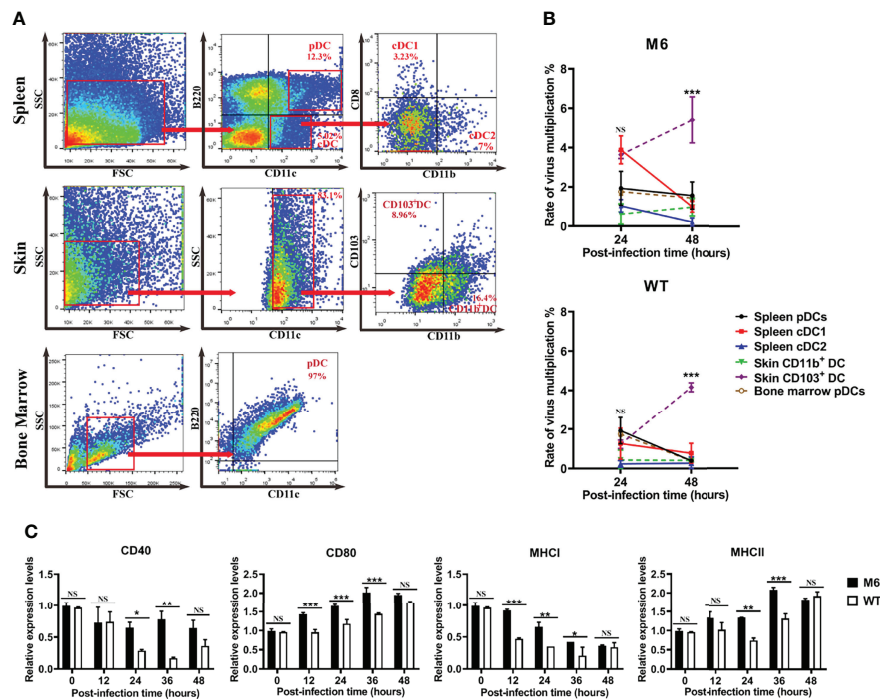


**FIGURE 4 |** M6- and WT-infected dendritic cells. **(A)** Flow cytometric sorting of dendritic cells from different tissues. **(B)** Rate of virus multiplication in dendritic cells with different surface markers after M6 and WT infection ((the viral load (24 or 48 h)-the viral load (0 h))/the viral load (0 h)). The black circle represents the data in spleen pDCs infected with the virus, the red square represents those in infected-spleen-cDC1, the blue triangle represents those in infected-spleen-cDC2, the green triangle represents those in infected-skin-CD103<sup>+</sup> DC, the purple circle represents those in infected-skin-CD11b<sup>+</sup> DC, and the brown circle represents those in infected-bone-marrow-pDCs. **(C)** mRNA expressions of key surface markers on dendritic cells infected with M6 (circle) and WT (square). The relative expression levels of key surface markers in dendritic cells were normalized to their levels in the blank control group (without viral infection) using the comparative Ct ( $\Delta\Delta C_t$ ) method. The data are shown as the mean  $\pm$  SEM based on data from three independent experiments. \* $P < 0.05$ , \*\* $P < 0.01$ , \*\*\* $P < 0.001$ , \*\*\*\* $P < 0.0001$ . NS, no significance.

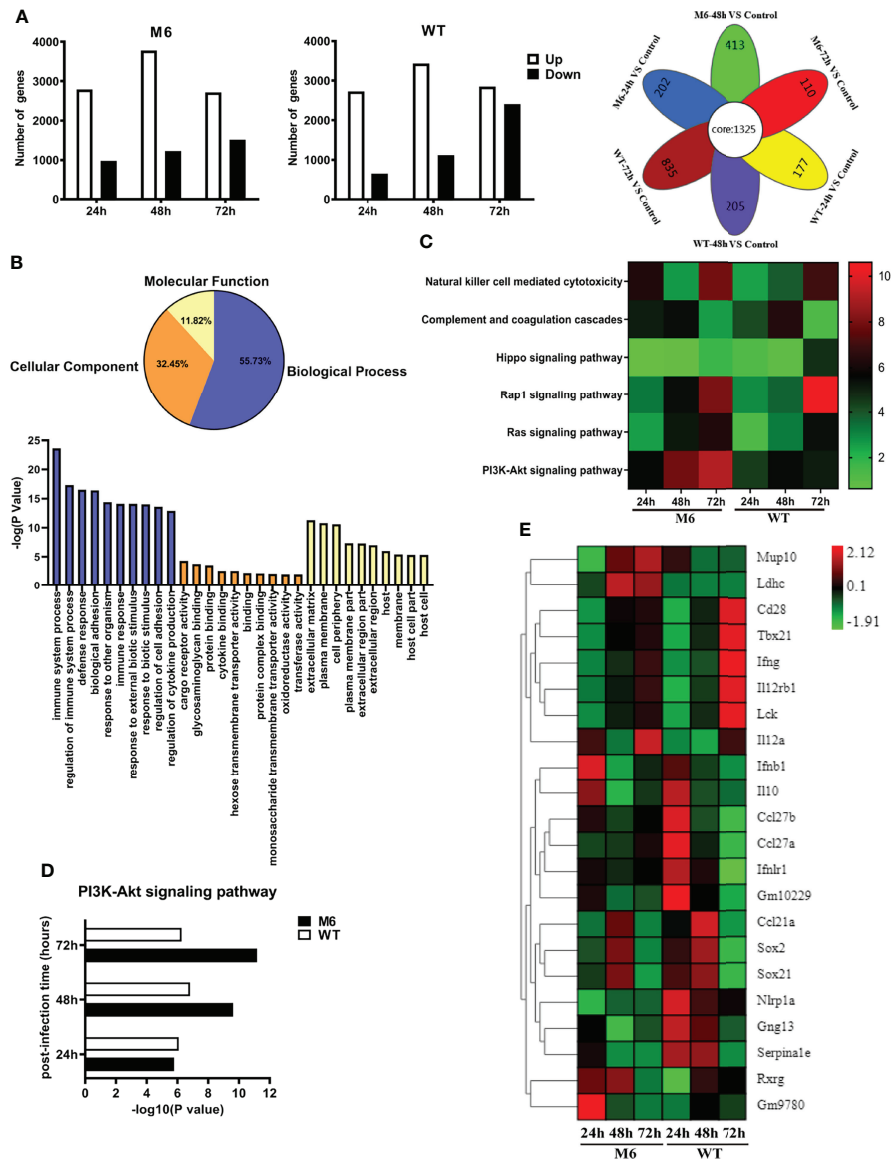


**FIGURE 5** | The change in the transcriptional profile of CD103<sup>+</sup> dendritic cells infected with the wild-type strain and attenuated M6 strain. **(A)** The number of significantly differential genes in dendritic cells infected with M6 and WT. All the data of infected samples were compared with those of the control group (blank DCs without viral infection). The white square represents upregulated genes, and the black represents downregulated genes. The image on the right shows the Venn diagram of the differential genes of M6 and WT infection DCs at different times. The overlapping differentially expressed genes are shown as “core” between the M6-infected and WT-infected groups during the entire sampling period (24, 48, and 72 hpi). **(B)** Gene Ontology enrichment terms for differential genes in dendritic cells infected with M6 and WT, compared with the control group. Blue represents the analysis of biological progress, light yellow represents the analysis of molecular function, and orange represents the cellular component analysis. The histograms represent the number of GOs annotated as unique GO terms and presented in the below panel. **(C)** The pathways involved in immune-related differential gene expression for M6 and WT compared with the control group. Each row represents a pathway, and the samples are depicted in the columns. Red indicates the numbers of the differentially expressed genes in the more pathways, and green denotes those of the differentially expressed genes in the pathways that were less than the control. **(D)** Compared with the control, the number of significant differential genes involved in PI3k-Akt pathways after M6 and WT infection of dendritic cells. **(E)** Fold changes in the expression of differential genes in infected dendritic cells at different times compared with the control. A heat map and supervised hierarchical clustering analysis revealed 22 genes associated with T and B cells activation. Each row represents a gene, and the samples are depicted in the columns. Red indicates genes expressed at higher levels, and green denotes genes expressed at lower levels. The color bars represent log<sub>2</sub> of fold change.

infected with the M6 strain and wild-type strain (Figure 5C). Among these genes with varied expression, the abundance of genes related to the PI3K-Akt signaling pathway in the cells was upregulated gradually starting at 24 hours post-infection by the M6 strain and reached the highest degree of variation (Figure 5D), while this tendency was reversed in cells infected with the wild-type strain (Figure 5D). The differences in expressed genes between the groups were principally involved in T and B cells activation (Figure 5E), including CD28, Lck, and Tbx21.

### Information Carried in Dendritic Cells Infected With HSV-1 is Insufficient to Establish Effective Antiviral Immunity

The above data revealed the immunologic features of dendritic cells infected with the HSV-1 wild-type strain and suggested the physiological role of dendritic cells, which enables their uptake of viral antigens and their transfer to lymph nodes for antigen presentation to T cells, might be modified to some extent. To investigate this possibility, we infected dendritic cells (CD11c) isolated from the skin of mice with the wild-type strain or attenuated M6 strain and transferred them to mice intravenously 24 hpi. The evaluation of these mice suggested that the viral load in some tissues of mice receiving dendritic cells infected with the wild-type strain 4 weeks after the transfer was higher than that of mice receiving cells infected with the M6 strain (Figure 6A), especially in the inguinal lymph nodes (Figure 6A). The detection of mRNA transcripts related to immune regulation in lymph node tissue revealed different expression profiles of genes related to T-cell activation in both groups (Figure 6B), and the expression of genes encoding marker molecules on the activated T-cell surface presented different trends in both groups (Figure 6C). Further IFN- $\gamma$ -specific ELISpot assays against the viral gB protein to evaluate the T cell response showed higher counts in the M6 strain group than in the wild-type strain group (Figure 6D). In a viral challenge test *via* the nasal route, the two groups of mice receiving dendritic cells infected with the wild-type strain or the M6 strain showed obvious differences in body weight and death rate (Figure 6E), suggesting different capacities of immune defense against virus infection in the two groups of mice, which was supported by the different neutralizing antibody GMT values of the two groups (Figure 6F).

## DISCUSSION

Studies of the immune response in individuals infected with HSV-1 suggested the low efficacy of immune-mediated viral clearance *in vivo* and defense against viral reinfection due to the interference of various virus-encoded proteins in innate and adaptive immunity (27–29), leading to challenges in developing antiviral drugs and vaccines and highlights the need to elucidate the detailed mechanism of viral interference with the immune system. Both HSV-1 and HSV-2 were found to be able to infect dendritic cells due to membrane glycoprotein D binding to the HVEM receptor (30–33). This receptor, as a member of the TNF

receptor family, can interact with the LIGHT molecule with the assistance of TNF- $\alpha$  from NK cells activated by IL-2 secreted from local tissues during inflammatory reactions (34, 35) and is involved in the differentiation and maturation of dendritic cells (34). During HSV-1 infection, this physiological process might be utilized to lead to not only the active phagocytosis of antigen from infected epithelial tissue by dendritic cells but also dendritic cell infection by the virus *via* gD protein binding to HVEM, which could be recognized as one viral strategy to disturb the host immune system (36). These data raised the question of what outcome could be induced by these infected dendritic cells in innate and adaptive immunity. M6, an attenuated strain, was used in our study since it could elicit significant immune protection in mice (22). We analyzed HSV-1 infection in mouse JAWS II-dendritic cells and the subsequent variations in the cellular immune phenotype. Furthermore, our study in mice investigated the variations in the innate immune response and inflammatory response induced by the wild-type strain and attenuated strain during infection of dendritic cells in local tissues and outlined some events induced by these variations during the process viral infection in detail. We aimed to elucidate the immunological mechanism occurring in individuals infected with HSV-1 who cannot eliminate the virus *in vivo* post-infection or prevent reinfection by comparing infection with wild-type and attenuated strains in dendritic cells. Our work not only identified HSV-1 infection in dendritic cells with the surface markers CD11c and CD11b *in vitro* and *in vivo* but also revealed that this infection enabled the stimulation of cellular differentiation to the CD103<sup>+</sup> phenotype, which was described as being associated with a powerful capacity for antigen presentation (26). Interestingly, CD103<sup>+</sup> cells infected with the wild-type and attenuated strains showed different transcriptional profiles of most immune regulators and effector molecules. Considering the efficiency of antiviral immunity elicited by the attenuated strain in animals, these results implied a strategy by which the HSV-1 wild-type strain interferes with the development of effective antiviral immunity, which is probably due to viral replication and associated with some viral-encoded proteins that modify the immunological phenotype of dendritic cells during antigen processing and presentation to T cells. Specific activation of T cells depends on the ability to accurately transfer antigenic information carried in dendritic cells to the T-cell population (37), and a small error in this process might lead to disruption of the immune response. The results obtained in our experiment on dendritic cells infected with the wild-type strain and attenuated strain and transferred to normal mice further suggested that the antigen information carried in infected cells by the wild-type strain did not work well in the recipient mice in comparison to that from cells infected with the attenuated strain.

All of the data support the conclusion that HSV-1 infection in dendritic cells based upon envelope glycoprotein D binding to HVEM is an important component of the viral infection strategy, with alterations in the phenotype of the active response of dendritic cells during recognition of viral antigens and transfer of antigen information to T cells from infected tissues *via*

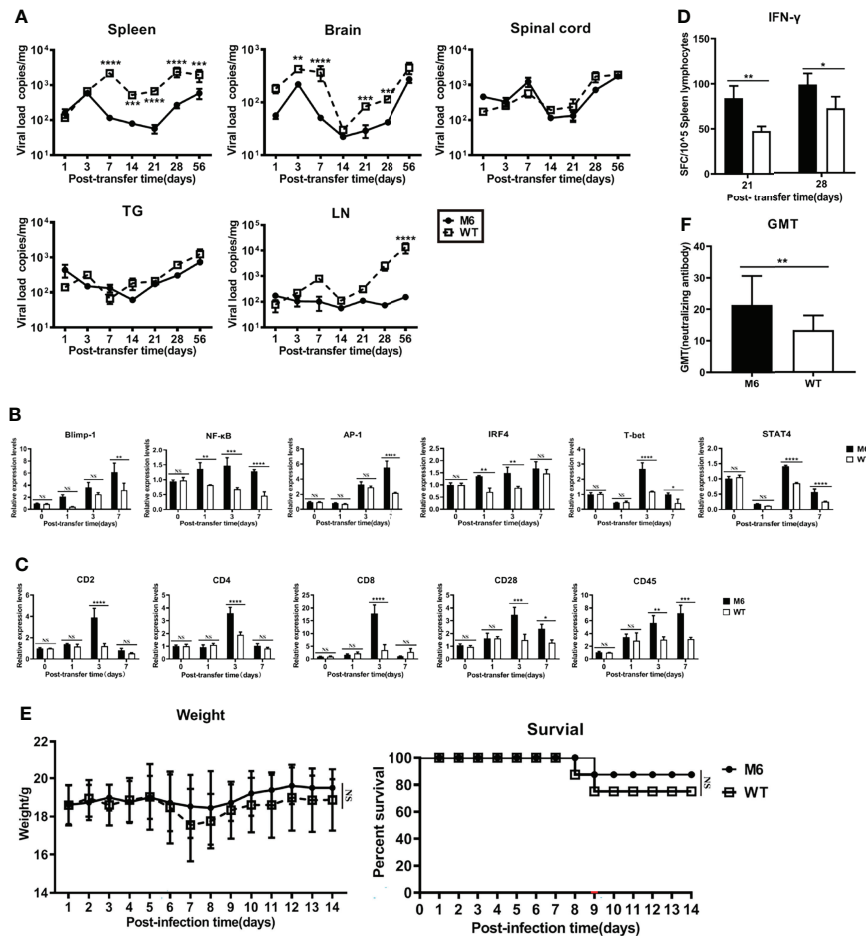


**FIGURE 6** | Dendritic cells carrying HSV-1 antigen were adoptively transferred into mice. **(A)** As determined by RT-qPCR, viral load in the spleen, brain, spinal cord, trigeminal ganglion, and inguinal lymph node after DCs carrying M6 (circle) and WT (square) antigens transferred into mice. **(B)** The expression levels of genes associated with T-cell activation in inguinal lymph node tissue after transferring dendritic cells infected with WT (white square) and M6 (black square) compared with the control group (transferring uninfected DCs). Detection of the p105 subunit to represent the level of NF- $\kappa$ B and detection of the c-Jun subunit to represent the level of AP-1. The results are normalized by the endogenous GAPDH expression level. The expression levels were calculated using the comparative Ct ( $\Delta\Delta$ Ct) method by relative quantification. **(C)** The expression levels of genes associated with surface marker molecules after T cell activation in lymph node tissue after transferring dendritic cells infected with WT (white square) and M6 (black square) compared with the control group. The results are normalized by the endogenous GAPDH expression level. The expression levels were calculated using the comparative Ct ( $\Delta\Delta$ Ct) method by relative quantification. **(D)** The ELISpot responses show IFN- $\gamma$ -secreting T cells among splenic lymphocytes after transferring dendritic cells carrying M6 (black square) and WT (white square) antigens. **(E)** Bodyweight and survival rate of mice subjected to transfer of dendritic cells carrying M6 (circle) and WT (square) antigens followed by wild-type challenge. **(F)** The titer of neutralizing antibody against HSV-1 in transferred-DCs mice after being challenged with the wild-type strain. The samples were obtained at 28 dpi. The data are shown as the mean  $\pm$  SEM based on data from three independent experiments. \* $P$  < 0.05, \*\* $P$  < 0.01, \*\*\* $P$  < 0.001, \*\*\*\* $P$  < 0.0001. NS, no significance.

interference with the cellular transcription of various genes. The outcome of this event might lead to a series of deviations in the immune response, with a deficient immune phenotype in infected individuals in the clinic. However, the details of the mechanism need further investigation in the future.

## DATA AVAILABILITY STATEMENT

The datasets presented in this study can be found in online repositories. The name of the repository and accession number

can be found below: National Center for Biotechnology Information (NCBI) BioProject, <https://www.ncbi.nlm.nih.gov/bioproject/>, PRJNA834578.

## ETHICS STATEMENT

The animal study was reviewed and approved by The Institutional Animal Care and Use Committee of the IMB, CAMS (approval number: WSP 201803014).



## AUTHOR CONTRIBUTIONS

QHL and YZ conceived and designed the study; JJZ, XLX, SQD, YG, and DJM performed the research; RY, FYZ, XQL, ZYM, XHL, ZYN, GRJ, and LCW contributed reagents; LY, YL, DDL, and HZ contributed materials; JJZ, QHL, and YZ analyzed the data; QHL wrote the first draft. All authors contributed to the article and approved the submitted version.

## FUNDING

This work was supported by the National Natural Science Foundation of China (No. 82171817 and No.81802868) and grants from the Major Science and Technology Special Projects of

Yunnan Province (No.202001AU070142, No.202002AA100009, No. H-2019060).

## ACKNOWLEDGMENTS

We would like to thank Guolan Ma for the technical help.

## SUPPLEMENTARY MATERIAL

The Supplementary Material for this article can be found online at: <https://www.frontiersin.org/articles/10.3389/fimmu.2022.931740/full#supplementary-material>

## REFERENCES

- Nicoll MP, Proença JT. The Molecular Basis of Herpes Simplex Virus Latency. *FEMS Microbiol Rev* (2012) 36:684–705. doi: 10.1111/j.1574-6976.2011.00320.x
- Steiner I, Kennedy PG, Pachner AR. The Neurotropic Herpes Viruses: Herpes Simplex and Varicella-Zoster. *Lancet Neurol* (2007) 11:1015–28. doi: 10.1016/S1474-4422(07)70267-3
- Arduino PG, Porter SR. Herpes Simplex Virus Type 1 Infection: Overview on Relevant Clinico-Pathological Features. *J Oral Pathol Med* (2010) 2:107–21. doi: 10.1111/j.1600-0714.2007.00586.x. Medicine.
- Kukhanova MK, Korovina AN, Kochetkov SN. Human Herpes Simplex Virus: Life Cycle and Development of Inhibitors. *Biochem (Mosc)* (2014) 13:1635–52. doi: 10.1134/S0006297914130124
- Crimi S, Fiorillo L, Bianchi A, D'Amico C, Viruses MC. Herpes Virus, Oral Clinical Signs and QoL: Systematic Review of Recent Data. *Viruses* (2019) 5:463. doi: 10.3390/v11050463
- Armangue T, Spatola M, Vlaga A. Frequency, Symptoms, Risk Factors, and Outcomes of Autoimmune Encephalitis After Herpes Simplex Encephalitis a Prospective Observational Study and Retrospective Analysis. *Lancet Neurology* (2018) 9:760–72. doi: 10.1016/S1474-4422(18)30244-8
- Connolly SA, Jardetzky TS, Longnecker R. The Structural Basis of Herpesvirus Entry. *Nat Rev Microbiol* (2021) 2:110–21. doi: 10.1038/s41579-020-00448-w
- Xinghong D, ZHong Z. Structure of the Herpes Simplex Virus 1 Capsid With Associated Tegument Protein Complexes. *Science* (2018) 6384. doi: 10.1126/science.aao7298
- Ma F, Li D, Ei T, Pa G. Herpes Simplex Virus Interference With Immunity: Focus on Dendritic Cells. *Virulence* (2021) 1:2583–607. doi: 10.1080/21505594.2021.1980990
- Matundan H, Ghiasi H. Herpes Simplex Virus 1 ICP22 Suppresses CD80 Expression by Murine Dendritic Cells. *J Virol* (2019) 3:e01803-18. doi: 10.1128/JVI.01803-18
- Hirose S, Wang S, Tormanen K, Wang Y, Ghiasi H. Roles of Type 1, 2 and 3 Innate Lymphoid Cells in HSV-1 Infection *In Vitro* and *In Vivo*. *J Virol* (2019) 13:e00523-19. doi: 10.1128/JVI.00523-19
- Lee AJ, Chen B, Chew MV, Barra NG, Shenouda MM, Nham T, et al. Inflammatory Monocytes Require Type I Interferon Receptor Signaling to Activate NK Cells *via* IL-18 During a Mucosal Viral Infection. *J Exp Med* (2017) 4:1153–67. doi: 10.1084/jem.20160880
- Matundan HH, Wang S, Jaggi U, Yu J, Ghiasi H. Suppression of CD80 Expression by ICP22 Affect HSV-1 Replication and CD8+IFN $\gamma$ + Infiltrates in the Eye of Infected Mice But Not Latency-Reactivation. *J Virol* (2021) 19: e0103621. doi: 10.1128/JVI.01036-21
- Novak N, Peng WM. Dancing With the Enemy: The Interplay of Herpes Simplex Virus With Dendritic Cells. *Clin Exp Immunol* (2005) 3:405–10. doi: 10.1111/j.1365-2249.2005.02927.x
- Heath WR, Carbone FR. The Skin-Resident and Migratory Immune System in Steady State and Memory: Innate Lymphocytes, Dendritic Cells and T Cells. *Nat Immunol* (2013) 10:978–85. doi: 10.1038/ni.2680
- Merad M, Sathe P, Helft J, Miller J, Mortha A. The Dendritic Cell Lineage: Ontogeny and Function of Dendritic Cells and Their Subsets in the Steady State and the Inflamed Setting. *Annu Rev Immunol* (2013) 31:563–604. doi: 10.1146/annurev-immunol-020711-074950
- Pollara G, Speidel K, Samady L, et al. Herpes Simplex Virus Infection of Dendritic Cells: Balance Among Activation, Inhibition, and Immunity. *J Infect Dis* (2003) 2:165–78. doi: 10.1086/367675
- Spear PG. Herpes Simplex Virus: Receptors and Ligands for Cell Entry. *Cell Microbiol* (2004) 5:401–10. doi: 10.1111/j.1462-5822.2004.00389.x
- Ware CF. The TNF Receptor Super Family in Immune Regulation. *Immunol Rev* (2011) 1:5–8. doi: 10.1111/j.1600-065X.2011.01065.x
- Heung K, Lee M, Zamora M, et al. Differential Roles of Migratory and Resident DCs in T Cell Priming After Mucosal or Skin HSV-1 Infection. *J Exp Med* (2009) 2:359–70. doi: 10.1084/jem.20080601
- Collins N, Hochheiser K, Carbone F, et al. Sustained Accumulation of Antigen-Presenting Cells After Infection Promotes Local T-Cell Immunity. *Immunol Cell Biol* (2017) 10:878–83. doi: 10.1038/icb.2017.60
- Xu X, Feng X, Wang L, Yi T, Li Q. A HSV1 Mutant Leads to an Attenuated Phenotype and Induces Immunity With a Protective Effect. *PLoS Pathog* (2020) 8:e1008703. doi: 10.1371/journal.ppat.1008703
- Yu X, Liu L, Wu L, Wang L, Dong C, Li W, et al. Herpes Simplex Virus Type 1 Tegument Protein VP22 is Capable of Modulating the Transcription of Viral TK and gC Genes *via* Interaction With Viral ICP0. *Biochimie* (2010) 8:1024–30. doi: 10.1016/j.biochi.2010.04.025
- Ryncarz AJ, Goddard J, Wald A, Huang ML, Roizman B, Corey L. Development of a High-Throughput Quantitative Assay for Detecting Herpes Simplex Virus DNA in Clinical Samples. *J Clin Microbiol* (1999) 6:1941–7. doi: 10.1128/JCM.37.6.1941-1947.1999
- Zhang J, Xiao H, Bi Y, Long Q, Wei C. Characteristics of the Tree Shrew Humoral Immune System. *Mol Immunol* (2020) 127:175–85. doi: 10.1016/j.molimm.2020.09.009
- Kim TS, Braciale TJ, Derya U. Respiratory Dendritic Cell Subsets Differ in Their Capacity to Support the Induction of Virus-Specific Cytotoxic CD8+ T Cell Responses. *PLoS One* (2009) 1:e4204. doi: 10.1371/journal.pone.0004204
- Sun H, Zhang Q, Jing YY, Man Z, Bo Z. USP13 Negatively Regulates Antiviral Responses by Deubiquitinating STING. *Nat Commun* (2017) 8:15534. doi: 10.1038/ncomms15534
- Uyangaa E, Patil AM, Eo SK. Prophylactic and Therapeutic Modulation of Innate and Adaptive Immunity Against Mucosal Infection of Herpes Simplex Virus. *Immune Netw* (2014) 4:187–200. doi: 10.4110/in.2014.14.4.187
- Zheng C. The Race Between Host Antiviral Innate Immunity and the Immune Evasion Strategies of Herpes Simplex Virus 1. *Microbiol Mol Biol Rev* (2020) 4: e00099-20. doi: 10.1128/MMBR.00099-20

30. Salio M, Cella M, Suter M, Lanzavecchia A. Inhibition of Dendritic Cell Maturation by Herpes Simplex Virus. *Eur J Immunol Eur J Immunol* (1999) 10:3245–53. doi: 10.1002/(SICI)1521-4141(199910)29:10<3245::AID-IMMU3245>3.0.CO;2-X
31. Eisenberg RJ, Atanasiu D, Cairns TM, et al. Herpes Virus Fusion and Entry: A Story With Many Characters. *Viruses* (2012) 5:800–32. doi: 10.3390/v4050800
32. Turner A, Bruun B, Minson T, Browne H. 1 Glycoproteins Gb, Gd, and Gh/gL of Herpes Simplex Virus Type 1 Are Necessary and Sufficient To Mediate Membrane Fusion in a Cos Cell Transfection System. *J Virol* (1998) 1:873–5. doi: 10.1128/JVI.72.1.873-875.1998
33. Atanasiu D, Whitbeck JC, Cairns TM, Reilly B, Cohen GH, Eisenberg R. Bimolecular Complementation Reveals That Glycoproteins gB and Gh/gL of Herpes Simplex Virus Interact With Each Other During Cell Fusion. *Proc Natl Acad Sci USA* (2007) 47:18718–23. doi: 10.1073/pnas.0707452104
34. Holmes TD, Wilson EB, Black E, Benest AV, Vaz C, Tan B, et al. Licensed Human Natural Killer Cells Aid Dendritic Cell Maturation via TNFSF14/LIGHT. *Proc Natl Acad Sci USA* (2014) 52:E5688–96. doi: 10.1073/pnas.1411072112
35. Fan Z, Yu P, Wang Y, Wang Y, Fu ML, Liu W, et al. NK-Cell Activation by LIGHT Triggers Tumor-Specific CD8+ T-Cell Immunity to Reject Established Tumors. *Blood* (2006) 4:1342–51. doi: 10.1182/blood-2005-08-3485
36. Suazo PA, Ibañez FJ, Retamal-Díaz A, Paz-Fiblas MV, Bueno SM, Kalergis AM, et al. Evasion of Early Antiviral Responses by Herpes Simplex Viruses. *Mediators Inflamm* (2015) 2015:593757. doi: 10.1155/2015/593757
37. Sallusto F, Lanzavecchia A. *The Role of Dendritic Cells in T-Cell Activation and Differentiation: Handbook of Dendritic Cells*. (2008).

**Conflict of Interest:** The authors declare that the research was conducted without any commercial or financial relationships construed as a potential conflict of interest.

**Publisher's Note:** All claims expressed in this article are solely those of the authors and do not necessarily represent those of their affiliated organizations, or those of the publisher, the editors and the reviewers. Any product that may be evaluated in this article, or claim that may be made by its manufacturer, is not guaranteed or endorsed by the publisher.

Copyright © 2022 Zhang, Xu, Duan, Gao, Ma, Yue, Zeng, Li, Meng, Li, Niu, Jiang, Yu, Liao, Li, Wang, Zhao, Zhang and Li. This is an open-access article distributed under the terms of the Creative Commons Attribution License (CC BY). The use, distribution or reproduction in other forums is permitted, provided the original author(s) and the copyright owner(s) are credited and that the original publication in this journal is cited, in accordance with accepted academic practice. No use, distribution or reproduction is permitted which does not comply with these terms.



# The Essential Role of Sorting Nexin 5 in Virus-Induced Autophagy

Dong-Yi Li<sup>†</sup>, Jun-Hao Wen<sup>†</sup>, Shan Liang<sup>†</sup> and Ji-Xin Tang<sup>\*</sup>

Guangdong Provincial Key Laboratory of Autophagy and Major Chronic Non-Communicable Diseases, Key Laboratory of Prevention and Management of Chronic Kidney Disease of Zhanjiang, Institute of Nephrology, Affiliated Hospital of Guangdong Medical University, Zhanjiang, China

**Keywords:** sorting nexin 5, autophagy, virus, PtdIns (3)P, endocytosis

## INTRODUCTION

Autophagy, a conserved lysosomal degradation pathway, can degrade intracellular waste, such as damaged organelles or misfolded proteins, to meet the metabolic needs of cells and maintain the homeostasis of the intracellular environment (1). In addition, autophagy also plays an essential role in immunity. First, autophagy can be induced by invading virus and provides a way for the host to limit or eliminate the intracellular virus; second, autophagy can also control inflammation by regulating interactions with natural immune signaling pathways, removing endogenous inflammasome agonists, and influencing the secretion of immune mediators; third, autophagy involves in antigen presentation and T polarization (2, 3).

The virus typically enters host cells *via* endocytosis and thus remains enclosed in the endosomes during the early stages of infection, making it difficult to identify by the host cellular autophagy. There is unknown how the virus can be specifically identified as selective autophagy cargo so as to be eliminated by host cellular autophagy and how does virus-induced autophagy occur in mammalian cells. Recently, Dong et al. found that the endosomal protein sorting nexin 5 (SNX5) is critically required for virus-induced, but not for other factor induced autophagy (4).

## SNX5: A PROTEIN INVOLVED IN ENDOSOMES

As a member of the sorting nexin family, SNX5 associates with the retromer, a complex of proteins that has been shown to be important in recycling transmembrane receptors from endosomes to the trans-Golgi network, and plays an important role in endosomal transport and protein sorting. SNX5 mainly contains two major domains: Phox homology (PX) domain and carboxy-terminal Bin, Amphiphysin, Rvs (BAR) domain, both of which are evolutionarily conserved domains. PX domain mainly recognizes the sorting motif of cargo (proteins to be sorted), and can help SNX5 to localize to the endosomal membrane of endocytosis pathway (5). SNX5-BAR domain mediates the biogenesis of cargo transport carriers and plays an essential role to sense and drive membrane bending (6, 7). SNX 5 is involved in endosomal sorting and is also related to PI signal pathway. SNX5 participates in caspase 9 mediated IGF2R retrieval mechanism (8) and forms a recycler complex with SNX4 and SNX17, which mediates the autophagosomal components recycling (ACR) process and helps the autophagosome membrane components on autophagy lysosomes to be recycled (9). In addition, SNX5 is also involved in the progression of cancers such as hepatocellular carcinoma (10) head and neck squamous cell carcinoma (11) and clear cell renal carcinoma (12).

## OPEN ACCESS

### Edited by:

Junji Xing,  
Houston Methodist Research Institute,  
United States

### Reviewed by:

Mintu Chandra,  
Vanderbilt University, United States

### \*Correspondence:

Ji-Xin Tang  
tjx986@163.com

<sup>†</sup>These authors have contributed  
equally to this work

### Specialty section:

This article was submitted to  
Viral Immunology,  
a section of the journal  
Frontiers in Immunology

**Received:** 18 May 2022

**Accepted:** 20 June 2022

**Published:** 11 July 2022

### Citation:

Li D-Y, Wen J-H, Liang S and Tang J-X  
(2022) The Essential Role of Sorting  
Nexin 5 in Virus-Induced Autophagy.  
*Front. Immunol.* 13:947384.  
doi: 10.3389/fimmu.2022.947384

Most of the virus, such as hepatitis B virus (13), SARS-COV-2 (14), influenza virus (15), and herpes virus (16) infect host cells *via* an endocytic vesicle. Only a small number of viruses infect host cells by means of genetic material injection, such as phages, and the targeted cells are generally cells with the cell wall and outer membrane (17). Recently, it has been found that SNX5 is involved in the virus-induced autophagy. SNX5 can inhibit virus replication in an autophagy-dependent manner and reduce the susceptibility and lethality of host cells (4).

## SNX5 IN VIRUS-INDUCED AUTOPHAGY

A team led by the late Beth Levine found that SNX5 is critically required for virus-induced, but not for basal or stress-induced autophagy through genome-wide short interfering RNA screens (4) (**Figure 1**). Sindbis virus (SIN) and a genetically engineered strain of herpes simplex virus type 1 (HSV-1) lacking the beclin 1-binding domain (BBD) of the HSV-1 neurovirulence protein ICP34.5 that cannot inhibit host autophagy (HSV-1 $\Delta$ BBD) failed to induce autophagy after the knockout of SNX5 *via* CRISPR-Cas9, but this defect can be rescued by expressing the recombinant wild-type SNX5. These results suggest that SNX5 may be necessary for most virus-induced autophagy. Besides,

they also found that SNX5 only had an effect on virus-induced autophagy, but had no effect on basal autophagy, starvation or mTOR-induced autophagy and bacterial heterophagy. Therefore, SNX5 is specifically required for virus-induced autophagy, and the role of SNX5 in virus-induced autophagy is unlikely to be related to its reverse transport function or other endocytosis function.

*In vivo* experiments showed that neonatal *Snx5* knockout (*Snx5*<sup>-/-</sup>) mice were more susceptible to lethal infection with SIN, Chikungunya virus (CHIKV), or West Nile virus (WNV) virus than their wild-type littermates (*Snx5*<sup>+/+</sup>) (4). Whereas, there has no difference in mortality between *Snx5*<sup>+/+</sup> and *Snx5*<sup>-/-</sup> mice when infection with autophagy-suppressive viral strains such as SIN or HSV-1 $\Delta$ BBD, suggesting that SNX5 also plays an important antiviral defense function through autophagy *in vivo* (4).

Mechanistically, SNX5 can be selectively recruited to the endosomes containing virus particles, sensing membrane curvature, driving membrane bending and increasing membrane curvature through its BAR domain (**Figure 1**). The key mediator regulating the generation of PtdIns (3)P is ATG14-containing class III phosphatidylinositol-3-kinase complex 1 (PI3KC3-C1), which contains a component molecule ATG that can sense membrane curvature. With the change of membrane

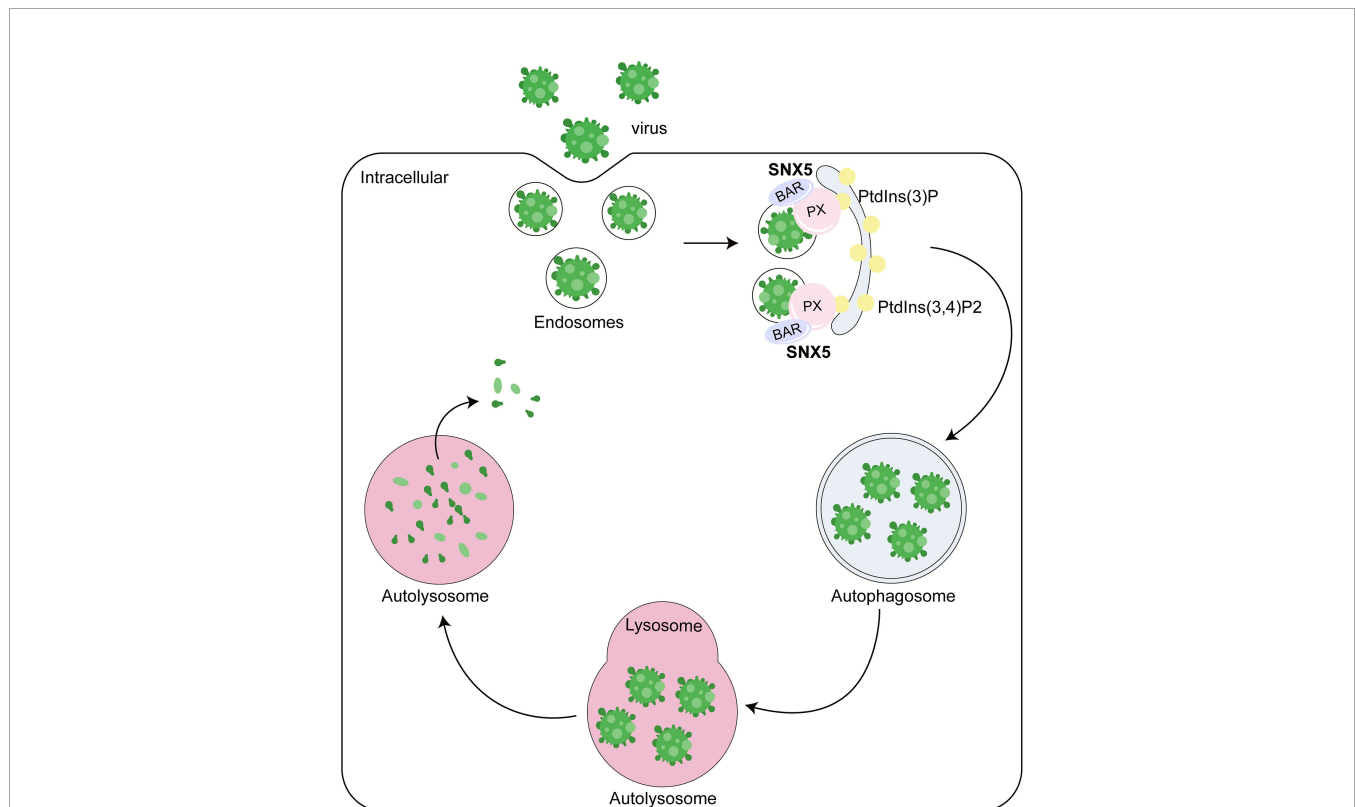


**FIGURE 1** | Role of SNX5 in the antiviral process. SNX5 mainly contains two major domains: phox (PX) domain and BAR domain. PX domain mainly recognizes the sorting motif of cargo and binds to phosphatidylinositol-3-phosphate (PtdIns (3)P) or PtdIns (3,4)P2 to regulate the localization of SNX5 to the autophagosome membrane. SNX5-BAR domain mediates the biogenesis of cargo transport carriers and plays an essential role to sense and drive membrane bending. Therefore, SNX5 can promote the virus's clearance, reduce the virus's susceptibility and lethality to host cells and inhibit virus replication in an autophagy-dependent manner.

curvature, the activity of PI3KC3-C1 kinase and the efficiency of PtdIns (3)P production changed. Generally speaking, the greater the membrane curvature, the higher the activity of PI3KC3-C1 kinase and the higher the PtdIns (3)P generation efficiency. SNX5 can directly interact with PI3K complex 1 and regulate it through modulating membrane curvature on the low-curvature membrane structures, such as endosomes. By doing this, SNX5 can further promote the biogenesis of autophagy, and autophagosome formation by improving the activity of PI3KC3-C1 kinase and increasing PtdIns (3)P production. Besides, SNX5 can initiate the clearance of virus, reduce the susceptibility and lethality of virus to host cells. And it can inhibit virus replication in an autophagy dependent manner. The ability of SNX5 to change membrane curvature and PI3KC3-C1 kinase activity plays an essential role in virus-induced autophagy (4).

## DISCUSSION

Although autophagy plays an essential role in fighting virus infections and eliminating viruses. But, in some cases, the existence of autophagy may have a negative effect on the antiviral response of cells and even enhance the replication of some viruses. Therefore, SNX5 itself, which is necessary for virus-induced autophagy, is likely to be an accomplice of the virus in some cases. Besides, the endosomal membrane wrapping virus particles is also an accomplice to help the virus to escape host cell attack.

After the viruses entered into the lumen of endosomes or the endoplasmic reticulum (ER), they will get some cues, such as exposure to low pH or proteolytic cleavage, which will trigger changes in the virus particle, and the activated viruses can penetrate the vacuolar membrane, enter the cytoplasm or nucleus to replicate their genetic material, synthesize virus protein, and so on (17). The cytoplasmic retinoic acid-inducible gene I (RIG-I) receptor is activated after recognizing viral RNA and increases the expression of antiviral genes and antiviral activities such as type I interferons and inflammatory cytokine genes through cascaded reaction with downstream molecules. However, SNX5 can negatively regulate RIG-I-like

receptor (RLR)-mediated antiviral signaling by inhibiting virus-induced RIG-I receptor expression and weakening the interaction between downstream molecule virus-induced signaling adaptor (VISA) and Tumor necrosis factor (TNF) receptor-associated factor 2/5 (TRAF2/5). Overexpression of SNX5 can inhibit the virus-induced activation of nuclear factor  $\kappa$ B (NF- $\kappa$ B) and Type-I interferons (IFN) regulatory factor 3 (IRF3), which may lead to a decrease in the cell's ability to fight viral infection (18).

Although, SNX5 is essential for virus-induced autophagy and can inhibit the transmission of the virus and reduce the harm of the virus to the host. It may be a double-edged sword for the hosts, considering that some viruses may kidnap the host's autophagy process to serve its replication and transmission. Therefore, we should take this into account when we want to target SNX5 to against the virus. Our understanding of SNX5 in virus-induced autophagy is far from enough. For example, how does SNX5 only recognize endosomes that contain virus particles rather than other substances? In the future, it will be interesting to investigate how SNX5 can specifically "recognizes" virus-infected endosomes and promote the activity of autophagy. This will be an important step towards understanding how specificity is achieved in selective autophagy and how can we use this to against and to combat the spread of the virus, thereby reducing its damage to the host.

## AUTHOR CONTRIBUTIONS

D-YL, J-HW, SL, and J-XT wrote the first draft of the manuscript. All authors contributed to the article and approved the submitted version.

## FUNDING

This work was supported by Natural Science Foundation of Guangdong Province (2019A1515110152) and Discipline construction project of Guangdong Medical University (4SG21229G).

## REFERENCES

- Klionsky DJ, Petroni G, Amaravadi RK, Baehrecke EH, Ballabio A, Boya P, et al. Autophagy in Major Human Diseases. *EMBO J* (2021) 40(19):e108863. doi: 10.15252/embj.2021108863
- Deretic V, Saitoh T, Akira S. Autophagy in Infection, Inflammation and Immunity. *Nat Rev Immunol* (2013) 13(10):722–37. doi: 10.1038/nri3532
- Liang S, Wu YS, Li DY, Tang JX, Liu HF. Autophagy in Viral Infection and Pathogenesis. *Front Cell Dev Biol* (2021) 9:766142. doi: 10.3389/fcell.2021.766142
- Dong X, Yang Y, Zou Z, Zhao Y, Ci B, Zhong L, et al. Sorting Nexin 5 Mediates Virus-Induced Autophagy and Immunity. *Nat* (2021) 589(7842):456–61. doi: 10.1038/s41586-020-03056-z
- Simonetti B, Paul B, Chaudhari K, Weeratunga S, Steinberg F, Gorla M, et al. Molecular Identification of a BAR Domain-Containing Coat Complex for Endosomal Recycling of Transmembrane Proteins. *Nat Cell Biol* (2019) 21(10):1219–33. doi: 10.1038/s41556-019-0393-3
- Mim C, Unger VM. Membrane Curvature and its Generation by BAR Proteins. *Trends Biochem Sci* (2012) 37(12):526–33. doi: 10.1016/j.tibs.2012.09.001
- Suetsugu S, Toyooka K, Senju Y. Subcellular Membrane Curvature Mediated by the BAR Domain Superfamily Proteins. *Semin Cell Dev Biol* (2010) 21(4):340–9. doi: 10.1016/j.semcdb.2009.12.002
- Han J, Goldstein LA, Hou W, Watkins SC, Rabinowich H. Involvement of CASP9 (Caspase 9) in IGF2R/CI-MPR Endosomal Transport. *Autophagy* (2021) 17(6):1393–409. doi: 10.1080/15548627.2020.1761742
- Zhou C, Wu Z, Du W, Que H, Wang Y, Ouyang Q, et al. Recycling of Autophagosomal Components From Autolysosomes by the Recycler Complex. *Nat Cell Biol* (2022) 24(4):497–512. doi: 10.1038/s41556-022-00861-8

10. Zhou Q, Huang T, Jiang Z, Ge C, Chen X, Zhang L, et al. Upregulation of SNX5 Predicts Poor Prognosis and Promotes Hepatocellular Carcinoma Progression by Modulating the EGFR-ERK1/2 Signaling Pathway. *Oncogene* (2020) 39(10):2140–55. doi: 10.1038/s41388-019-1131-9
11. Cai J, Sun M, Hu B, Windle B, Ge X, Li G, et al. Sorting Nexin 5 Controls Head and Neck Squamous Cell Carcinoma Progression by Modulating Fbw7. *J Cancer* (2019) 10(13):2942–52. doi: 10.7150/jca.31055
12. Zhou Q, Li J, Ge C, Chen J, Tian W, Tian H. SNX5 Suppresses Clear Cell Renal Cell Carcinoma Progression by Inducing CD44 Internalization and Epithelial-to-Mesenchymal Transition. *Mol Ther Oncolytics* (2021) 24:87–100. doi: 10.1016/j.omto.2021.12.002
13. Herrscher C, Pastor F, Burlaud-Gaillard J, Dumans A, Seigneuret F, Moreau A, et al. Hepatitis B Virus Entry Into HepG2-NTCP Cells Requires Clathrin-Mediated Endocytosis. *Cell Microbiol* (2020) 22(8):e13205. doi: 10.1111/cmi.13205
14. Bayati A, Kumar R, Francis V, McPherson PS. SARS-CoV-2 Infects Cells After Viral Entry via Clathrin-Mediated Endocytosis. *J Biol Chem* (2021) 296:100306. doi: 10.1016/j.jbc.2021.100306
15. Sun X, Whittaker GR. Entry of Influenza Virus. *Adv Exp Med Biol* (2013) 790:72–82. doi: 10.1007/978-1-4614-7651-1\_4
16. Nicola AV. Herpesvirus Entry Into Host Cells Mediated by Endosomal Low Ph. *Traffic* (2016) 17(9):965–75. doi: 10.1111/tra.12408
17. Mercer J, Schelhaas M, Helenius A. Virus Entry by Endocytosis. *Annu Rev Biochem* (2010) 79:803–33. doi: 10.1146/annurev-biochem-060208-104626
18. Li J, Chen T, Xie T, Yang YX, He TS, Xu LG. SNX5 Inhibits RLR-Mediated Antiviral Signaling by Targeting RIG-I-VISA Signalosome. *Biochem Biophys Res Commun* (2020) 522(4):889–96. doi: 10.1016/j.bbrc.2019.11.121

**Conflict of Interest:** The authors declare that the research was conducted in the absence of any commercial or financial relationships that could be construed as a potential conflict of interest.

**Publisher's Note:** All claims expressed in this article are solely those of the authors and do not necessarily represent those of their affiliated organizations, or those of the publisher, the editors and the reviewers. Any product that may be evaluated in this article, or claim that may be made by its manufacturer, is not guaranteed or endorsed by the publisher.

Copyright © 2022 Li, Wen, Liang and Tang. This is an open-access article distributed under the terms of the Creative Commons Attribution License (CC BY). The use, distribution or reproduction in other forums is permitted, provided the original author(s) and the copyright owner(s) are credited and that the original publication in this journal is cited, in accordance with accepted academic practice. No use, distribution or reproduction is permitted which does not comply with these terms.



# 2B and 3C Proteins of Senecavirus A Antagonize the Antiviral Activity of DDX21 via the Caspase-Dependent Degradation of DDX21

Kuan Zhao<sup>1,2†</sup>, Xiao-Ran Guo<sup>1†</sup>, Shuai-Feng Liu<sup>1</sup>, Xiao-Na Liu<sup>1</sup>, Ying Han<sup>1</sup>, Lu-Lu Wang<sup>1</sup>, Bai-Shi Lei<sup>1</sup>, Wu-Chao Zhang<sup>1,2</sup>, Li-Min Li<sup>1,2</sup> and Wan-Zhe Yuan<sup>1,2,3\*</sup>

<sup>1</sup> College of Veterinary Medicine, Hebei Agricultural University, Baoding, China, <sup>2</sup> Hebei Veterinary Biotechnology Innovation Center, Hebei Agricultural University, Baoding, China, <sup>3</sup> North China Research Center of Animal Epidemic Pathogen Biology, China Agriculture Ministry, Baoding, China

## OPEN ACCESS

### Edited by:

Rongtuan Lin,  
McGill University, Canada

### Reviewed by:

Yan-Dong Tang,  
Chinese Academy of Agricultural  
Sciences, China  
Hong Dong,  
The Ohio State University,  
United States

### \*Correspondence:

Wan-Zhe Yuan  
yuanwanzhe@126.com

<sup>†</sup>These authors have contributed  
equally to this work and share  
first authorship

### Specialty section:

This article was submitted to  
Viral Immunology,  
a section of the journal  
Frontiers in Immunology

Received: 24 May 2022

Accepted: 20 June 2022

Published: 14 July 2022

### Citation:

Zhao K, Guo X-R, Liu S-F, Liu X-N,  
Han Y, Wang L-L, Lei B-S,  
Zhang W-C, Li L-M and Yuan W-Z  
(2022) 2B and 3C Proteins of  
Senecavirus A Antagonize the Antiviral  
Activity of DDX21 via the Caspase-  
Dependent Degradation of DDX21.  
*Front. Immunol.* 13:951984.  
doi: 10.3389/fimmu.2022.951984

Senecavirus A (SVA), also known as Seneca Valley virus, is a recently discovered picornavirus that can cause swine vesicular disease, posing a great threat to the global swine industry. It can replicate efficiently in cells, but the molecular mechanism remains poorly understood. This study determined the host's differentially expressed proteins (DEPs) during SVA infection using dimethyl labeling based on quantitative proteomics. Among the DE proteins, DDX21, a member of the DEAD (Asp-Glu-Ala-Asp)-box RNA helicase (DDX) family, was downregulated and demonstrated inhibiting SVA replication by overexpression and knockdown experiment. To antagonize this antiviral effect of DDX21, SVA infection induces the degradation of DDX21 by 2B and 3C proteins. The Co-IP results showed that 2B and 3C did not interact with DDX21, suggesting that the degradation of DDX21 did not depend on their interaction. Moreover, the 3C protein protease activity was necessary for the degradation of DDX21. Furthermore, our study revealed that the degradation of DDX21 by 2B and 3C proteins of SVA was achieved through the caspase pathway. These findings suggest that DDX21 was an effective antiviral factor for suppressing SVA infection and that SVA antagonized its antiviral effect by degrading DDX21, which will be useful to guide further studies into the mechanism of mutual regulation between SVA and the host.

**Keywords:** senecavirus A (SVA), DDX21, 2B protein, 3C protein, caspase pathway

## INTRODUCTION

Senecavirus A (SVA), a nonenveloped single-strand positive-sense RNA virus, is the only member of the genus *Senecavirus* within the family *Picornaviridae*. As a serendipitous finding, it was first discovered in the cell line PER.C6 cultivating adenovirus-5-based vectors in 2002 (1). The genome of SVA is about 7.3 kb and encodes only one polyprotein, which follows the standard L-4-3-4 layout for picornavirus genomes. The polyprotein is processed into the structural and nonstructural proteins by proteases 2A and 3C, including the leader protein and three major protein regions (P1, P2, and P3) (2). Until 2014, only three complete genomic sequences of SVA were available in the National Center for Biotechnology Information databases (GenBank accession numbers

NC\_011349, DQ641257, and KC667560), and the biological properties and the pathogenicity of SVA for swine were unknown. In early 2015, numerous SVA strains were isolated and reported in vesicular disease outbreaks in Brazil, China, and Thailand (3). The diseased swine are characterized by severe vesicular and/or ulcerative lesions on the oral mucosa, snout, coronary bands, and hooves, which are indistinguishable from the clinical symptoms caused by the foot-and-mouth disease virus (FMDV) and vesicular stomatitis virus (VSV). From then, SVA was confirmed as the agent of the vesicular disease of swine and began to spread in many countries.

The hosts have developed highly efficient strategies to detect and control invading viruses to resist infection and maintain a normal physiological state. In contrast, most viruses have evolved strategies to evade host defenses and thus effectively infect and replicate in host cells. Increasing evidence suggests that SVA can escape the host's antiviral effect in several ways for better infection and replication. For example, the 2B protein of SVA, whose secondary structures are similar to those of the picornaviruses, can act like a viroporin and likely enhance membrane permeability. It interacted with mitochondrial antiviral signaling (MAVS) and induced the degradation of MAVS depending on caspase-9 and caspase-3 to suppress the activation of the RLR pathway (4). Furthermore, the 3C protein of SVA inhibited antiviral type I IFN responses by targeting different host adaptors, including MAVS, Toll/interleukin 1 (IL-1) receptor domain-containing adaptor inducing IFN- $\beta$  (TRIF), and TRAF family member-associated NF- $\kappa$ B activator (TANK).

Moreover, the SVA 3C protein reduces interferon regulatory factor 3 (IRF3) and IRF7 protein expression levels and phosphorylation and blocks the transcription of IFN- $\beta$ , IFN- $\alpha$ 1, IFN- $\alpha$ 4, and ISG54 (5). More and more evidence indicated that 3C protein plays a crucial role in modulating virus and host gene expression by cleaving and degrading various host protein factors. Furthermore, the protease activity of 3C protein is required for these reactions (6). Therefore, the relationship between virus and host should be investigated to uncover the mechanisms of SVA antagonizing the host antiviral effect.

DEAD (Asp-Glu-Ala-Asp)-box RNA helicases (DDXs) are the largest family of evolutionarily conserved RNA helicases that are involved in a broad array of host processes, especially in antiviral immunity (7–9). DDX21, a member of the DDX family, possesses all the signature motifs required for DEAD-helicase function and contains atypical FRGQR repeats in its C-terminus. Furthermore, growing evidence suggests that DDX21 plays an important role in regulating host antiviral immunity. For example, DDX21 inhibits influenza viral RNA synthesis by binding to the PB1 polymerase subunit (10). Furthermore, DDX21 regulated the replication of FMDV by increasing IFN- $\beta$  and IL-8 production in FMDV-infected cells. It also coprecipitates with FMDV IRES and restricts viral IRES-dependent translation and replication (11). Moreover, the infection process of human cytomegalovirus, human immunodeficiency virus, and dengue virus were also regulated by DDX21. However, the reciprocal regulation mechanism between DDX21 and SVA is still unclear.

Our study has determined changes in the host cell protein expression during SVA infection using dimethyl labeling-based quantitative proteomics. Among these proteins, the expression

level of DDX21 was significantly downregulated during SVA infection, and the antiviral effect of DDX21 was also verified by overexpressing and knockdown experiments. Moreover, SVA 2B and 3C proteins induce the degradation of DDX21 *via* caspase to antagonize the antiviral activity of DDX21. The results helped study the interaction between host and virus.

## MATERIALS AND METHODS

### Cells, Viruses, and Drug

Porcine kidney-15 (PK-15), human embryonic kidney (HEK293T) cells, and baby hamster kidney cells (BHK-21) cells were cultured in Dulbecco's modified Eagle's medium containing 10% fetal bovine serum (Gibco, Thermo Fisher Scientific, Waltham, MA, USA). Cells were maintained at 37°C with 5% CO<sub>2</sub>. The SVA virus (GenBank accession number: MZ375462) was used for all the experiments. The proteasome inhibitor MG-132, the lysosomal inhibitor chloroquine (CQ), and the caspase inhibitor carbobenzoxy-valyl-alanyl-aspartyl-[O-methyl]-fluoro-methyl ketone (Z-VAD-FMK) was purchased from Beijing Solarbio Science & Technology Co. Ltd.

### Construction of Plasmids

The porcine DDX21 gene (GenBank accession number: XM\_005657387.3) was amplified and cloned into pCAGEN (modified from pCAGGS) to generate pCAGEN-DDX21-HA. The other proteins of SVA were cloned into pCAGGS to generate pCAGGS-VP1-Flag, pCAGGS-VP2-Flag, pCAGGS-VP3-Flag, pCAGGS-2B-Flag, pCAGGS-2C-Flag, pCAGGS-3A-Flag, pCAGGS-3C-Flag, and pCAGGS-3D-Flag. All plasmids were constructed by homologous recombination with the NEBuilder<sup>®</sup> HiFi DNA Assembly Master Mix (New England Biolabs, Ipswich, MA, USA) according to the manufacturer's instructions. Mutagenesis of SVA 3C protein was generated using overlap PCR and cloned into vector pCAGGS-3C-Flag (H48A), pCAGGS-3C-Flag (C160A, USA), and pCAGGS-3C-Flag (double-site mutation (DM) H48A-C160A). The primers used for gene amplification are listed in **Table 1**.

### Dynamics of SVA in PK-15 Cells

PK-15 cells were infected with SVA at a multiplicity of infection (MOI) of 0.5, and normal cells were set as the control. Cytopathic effects (CPEs) were observed at 12, 24, 36, 48, 60, and 72 h postinfection (hpi) under a microscope. Subsequently, the cell culture supernatant at different time points was collected to determine 50% tissue culture infective doses (TCID<sub>50</sub>). The viral titers were determined by the Reed–Muench method and expressed as TCID<sub>50</sub>/ml. Mean values and standard deviations were calculated from the results of three independent experiments. According to the flow chart, the cells infected or uninfected with SVA at 48 hpi were chosen for the following quantitative proteomics.

### Sample Preparation, Digestion, and TMT Labeling

Mock- or SVA-infected PK-15 cells were cultured in 6-well plates for 48 hpi. The cells were then washed with cold phosphate-buffered



**TABLE 1 |** The sequence of primers and siRNAs used in the study.

Primers and siRNAs	Sequence (5'-3')
pCAGGS-VP1-F	CATCATTTTGGCAAAGATGTCCACCGACAACGCCGAGAC
pCAGGS-VP1-FLAG-R	CGAGAGATCTGAATTTCACTTATCGTCGTCATCCTTGTAACTCTTGCATCAGCATCTTCTGCT
pCAGGS-VP2-F	CATCATTTTGGCAAAGATGGATCACAATACCGAAGAAAT
pCAGGS-VP2-FLAG-R	CGAGAGATCTGAATTTCACTTATCGTCGTCATCCTTGTAACTCTTGCATCAGCATCTTCTGCT
pCAGGS-VP3-F	CATCATTTTGGCAAAGATGGGGCCCATCCACAGCACC
pCAGGS-VP3-FLAG-R	CGAGAGATCTGAATTTCACTTATCGTCGTCATCCTTGTAACTCTTGCATCAGCATCTTCTGCT
pCAGGS-2B-F	CATCATTTTGGCAAAGATGCCTGCTTCTGACAACCCAAT
pCAGGS-2B-FLAG-R	CGAGAGATCTGAATTTCACTTATCGTCGTCATCCTTGTAACTCTTGCATCTTAAACAGCTTTC
pCAGGS-2C-F	CATCATTTTGGCAAAGATGGGACCCATGGACACAGTCAAAGA
pCAGGS-2C-FLAG-R	CGAGAGATCTGAATTTCACTTATCGTCGTCATCCTTGTAACTCTTGTAGAACCAGAGTCTGCATAT
pCAGGS-3A-F	CATCATTTTGGCAAAGATGAGCCCTAACGAGAACGACGA
pCAGGS-3A-FLAG-R	CGAGAGATCTGAATTTCACTTATCGTCGTCATCCTTGTAACTCTTGCATCTTAAACAGCTTTC
pCAGGS-3C-F	CATCATTTTGGCAAAGATGCAGCCCAACGTCGACATGGG
pCAGGS-3C-FLAG-R	CGAGAGATCTGAATTTCACTTATCGTCGTCATCCTTGTAACTCTTGCATCTTAAACAGCTTTC
pCAGGS-3D-F	CATCATTTTGGCAAAGATGGGACTGATGACCGAGCTAGAGCCT
pCAGGS-3D-FLAG-R	CGAGAGATCTGAATTTCACTTATCGTCGTCATCCTTGTAACTCTTGCATCTTAAACAGCTTTC
pCAGGS-3C-H48A-F	CCTTCTAGTCAATGAGGCCACATGGTCCAACCCCTCCTG
pCAGGS-3C-H48A-R	CAGGAGGGGTTGGACCATGTGGCCCTATTGACTAGGAAGG
pCAGGS-3C-C160A-F	GTGACGACTTACAAGGGATGGGCCGGTTCGGCCCTGGTCTGTGA
pCAGGS-3C-C160A-R	TCACAGACCAGGGCCGAACCGGCCATCCCTTGTAAAGTCGTAC
pCAGEN-DDX21-HA-F	GTTCCAGATTACGCTGAAATGCCGGGGAAACTTCGTAGT
pCAGEN-DDX21-R	GGGTACCATCGATGAATTAAGTCCAAACGCTTTGTCTAA
Q-STAT1-F	CCTGTTGCGGTTTCAGTGAGAGC
Q-STAT1-R	GAAGTAAGGTTGCGCTCCGTTCTG
Q-OAS1-F	ACCTCGTCGTTCTCCTCACCAAG
Q-OAS1-R	CCTGTCGTGGAGTCTGGACCTC
Q-MX2-F	CGGCTGTTTACCAAGATGCGAAATG
Q-MX2-R	ATTACAAAACCCCTGGCAACTCTCTC
Q-ZAP-F	AGCAGACACCCCGAAATAAACC
Q-ZAP-R	CAGCAGCCGAAGCAGATGGAAG
Q-IFIT1-F	AGATGGACTGTGAGGAAGGATGGG
Q-IFIT1-R	GGTCTAGGCGATAGATGTTGATTGC
Q-ZC3H11A-F	TCCTCCATTGAAACGTAGCCTTGC
Q-ZC3H11A-R	GCTGACACACCTAATCGCTCCTTC
Q-DDX21-F	CGGACAGGAACCTGGGAAGACATTC
Q-DDX21-R	TCTGCTTACTTGACTTGCCAACTCC
Q-IL-18-F	AGACCTGGAATCGGATTACTTTGGC
Q-IL-18-R	ACGGCTTGATGTCCTGGTTAATG
Q-ZCCHC9-F	ATCAAGTGAAGGCTCAAGTAGACC
Q-ZCCHC9-R	GCAACCACCATCAGCATAGAGTCC
DDX21-1651-senece	GCAGGAUGCCCAGUCUUUATT
DDX21-1651-antisenece	UAAAGACUUGGCAUCCUGCTT
DDX21-673-senece	GGAAGCCAAUGGAGACAUUT
DDX21-673-antisenece	AAUGUCUCCAUUGGCUUCCTT
DDX21-1712-senece	GGUUUCCGAAAUGGCAGUUTT
DDX21-1712-antisenece	AACUGCCAUUUCGGAAACCTT

saline (PBS), lysed by sonication in STD lysate buffer [4% (w/v) SDS, 100 mM Tris/HCl pH 7.6, 0.1 M DTT] (12), and quantified using a BCA assay. 200 ug of protein per sample for trypsin digestion using filter-aided sample preparation (FASP) (12), after trypsin digestion, the peptides were desalted on a C18 column and 40 µl of dissolution buffer was added after the lyophilization of peptides. The peptides were quantified by OD280. According to the manufacturer’s instructions, peptides were labeled using a TMT Reagent kit.

**LC-MS/MS Analysis**

Labeled samples were analyzed using an Easy-nLC 1200 nanoflow HPLC system (Thermo Fisher Scientific, Waltham, MA, USA). Buffer: solution A is 0.1% formic acid in the water, and solution B is 0.1% formic acid in acetonitrile in water (84% in acetonitrile). The

sample was loaded by the autosampler onto the loading column (Thermo Scientific EASY column, 100 µm \* 2 cm, 5 µm, C18) and then separated by an analytical column (Thermo Scientific EASY column, 75 µm \* 10 cm, 3 µm, C18) with a flow rate of 250 nl/min. After chromatographic separation, the samples were analyzed by a Q Exactive mass spectrometer (13).

**Quantitative Real-Time PCR**

Total RNA was extracted with TRIzol (Thermo Fisher Scientific, Waltham, MA, USA). The PrimeScript™ 1st-Strand cDNA Synthesis Kit (TaKaRa, Dalian, China) was used for reverse transcription. The SYBR Premix Ex Taq™ (TaKaRa, Dalian, China) was used to quantify the mRNA levels of ZC3H11A, DDX21, IL-18, ZCCHC9, STAT1, OAS1, MX2, ZAP, and IFIT1.

Relative expression levels were analyzed using the  $2^{-\Delta\Delta Ct}$  method, with glyceraldehyde-3-phosphate dehydrogenase (GAPDH) mRNA as a control. Primers are listed in **Table 1**.

## Plasmid Transfection and Virus Challenge

To investigate the effect of DDX21 on SVA replication, BHK-21 cells cultured in 6-well plates were transfected with 2  $\mu\text{g}$  of pCAGEN-DDX21-HA using X-treme GENE HP DNA reagent (Roche Applied Science, Penzberg, Germany). Next, 36 h posttransfection (hpt), the cells were infected with SVA at a MOI of 0.1. After inoculation for 1.5 h at 37°C, the supernatants were discarded, and the cells were washed three times with PBS. The supernatant was harvested at 12, 24, 36, and 48 hpi, and the cells were lysed using RIPA lysis buffer (Thermo Fisher Scientific, Waltham, MA, USA). Viral titers in the supernatants were determined using a microtitration assay. The amount of the VP2 protein was then detected in cell lysates by Western blotting (WB) using a rabbit anti-VP2 polyclonal antibody (1:1,000).

## Western Blotting

Cell lysates were prepared by harvesting virus-infected or plasmid-transfected cells in RIPA or IP-lysate buffer at 4°C for 15 min containing 1 mM of phenylmethylsulfonyl fluoride and 1 mg/ml of protease inhibitor cocktail (Roche). After centrifuging at 12,000 rpm/min for 10 min, the supernatants of cell lysates were mixed with 5 $\times$  sodium dodecyl sulfate-polyacrylamide gel electrophoresis (SDS-PAGE) sample loading buffer (Beyotime) and placed in boiling water for 5 min. The proteins were then separated by SDS-PAGE and transferred onto a nitrocellulose membrane. The membrane was blocked in 5% skim milk for 2 h at room temperature and then incubated with the indicated primary antibody for 1 h at room temperature. After washing three times with Tris-buffered saline with 0.1% Tween 20, the membrane was incubated with horseradish peroxidase-conjugated goat anti-mouse IgG (H+L) and/or goat anti-rabbit IgG (H+L) secondary antibody (1:5,000) for 1 h at room temperature. The target proteins were visualized by treating the membrane with Pierce ECL WB substrate (Thermo Fisher Scientific, Waltham, MA, USA). To quantify target proteins, their levels were normalized to the levels of  $\beta$ -actin.

## RNA Interference

Three small interfering RNAs (siRNAs) against hamster DDX21 (GenBank No. XM\_013113937.3) were synthesized by GenePharma (Shanghai, China). The sequence of siRNA is listed in **Table 1**. BHK-21 cells were seeded in 6-well plates and transfected with 100 pM of indicated siRNA or NC using Lipofectamine<sup>TM</sup> RNAiMAX transfection reagent (cat. No. 13778075; Thermo Fisher Scientific, Waltham, MA, USA). The cells were lysed in RIPA lysis buffer after 36 h of transfection, and the effects of siRNAs were analyzed by WB using an anti-DDX21 polyclonal antibody (cat. No. 10528-1-AP; Proteintech; 1:1,000). Next, efficient siRNA and NC were selected for transfection. At 36 hpt, the cells were infected with SVA at a MOI of 0.1. The supernatant and cells were harvested at 12, 24, 36, and 48 hpi and analyzed based on virus titers and WB.

## Coimmunoprecipitation

HEK293T cells were cotransfected with 1.5  $\mu\text{g}$ /well of DDX21-HA and 1.5  $\mu\text{g}$ /well of 2B-Flag or 3C-Flag using X-tremeGENE DNA transfection reagent. At 24 hpt, cells were lysed with IP lysis buffer containing phenylmethanesulfonyl fluoride and a protease inhibitor cocktail at 4°C for 20 min. Approximately 10% of the lysate supernatant was used as an input control, and the remaining lysates were incubated with anti-Flag agarose beads for 8 h at 4°C. The beads were washed with the lysis buffer five times and then analyzed by WB with the indicated antibodies.

## Cell Viability Assay

Cells at  $10^4$  were seeded into 96-well plates and treated with the proteasome inhibitor MG132 concentrations (0–50  $\mu\text{M}$ ), the caspase inhibitor Z-VAD-FMK (0–50  $\mu\text{M}$ ), or the lysosomal inhibitor CQ (0–100  $\mu\text{M}$ ) for 24 h, at five replicate wells per dilution. Subsequently, the 3-(4,5-dimethylthiazol-2-yl)-diphenyl tetrazolium bromide (MTT) assay (14) was used to detect cytotoxicity.

## Statistical Analysis

All the experiments mentioned above were performed with three independent experiments. The GraphPad Prism software was used for statistical analysis by a two-tailed Student's *t*-test. The data shown are three independent experiments' means  $\pm$  standard variations (SD).

## RESULTS

### Virus Infection and Determination of Optimal Collection Time

PK-15 cells were infected with SVA at a MOI of 0.5, and the CPE began to appear at 36 hpi. Subsequently, the cell showed typical CPE, characterized as rounding, shrinkage, and detachment (**Figure 1A**). The virus titers of SVA almost reached the highest value at 48 hpi (**Figure 1B**). At 48 hpi, the CPE of the cells was typical, and the virus titers reached the peak, so the cells were collected and subjected to proteomics analyses by LC-MS/MS (**Figure 1C**).

### Proteomics Analysis of Host Proteins Upon SVA Infection

SVA infection affects various host cellular pathways. Knowledge of changes in host protein expression caused by SVA infection helps to understand the interaction between the virus and the host. Our study employed a dimethyl labeling-based quantitative proteomics strategy to characterize the host cell proteome changes upon SVA infection in PK-15 cells at 48 hpi. The results showed that 333 proteins were downregulated and 137 were upregulated in the cells infected with SVA. In contrast, the expression level of 5,122 proteins was not affected by SVA infection (**Figure 2A**). These results were also visualized by clustering the samples according to differential treatment (**Figure 2B**). To further verify the accuracy of the proteomics and the relationships of the differentially expressed proteins (DEPs) at the translational and transcriptional levels, the

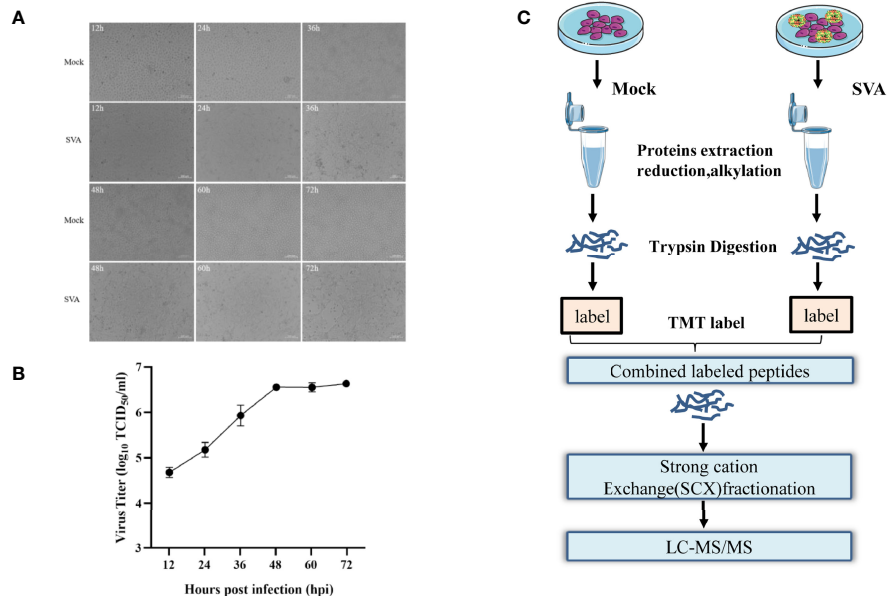


**FIGURE 1** | Experimental design for identifying candidate novel cellular factors in mock- and SVA-infected PK-15 cells. **(A)** PK-15 cells were infected with 0.5 MOI of SVA for 12, 24, 36, 48, 60, or 72 h. The virus-induced CPE was observed and recorded by the microscope. **(B)** PK-15 cells were infected with 0.5 MOI of SVA for 12, 24, 36, 48, 60, or 72 h, and the viral titers were determined by the TCID<sub>50</sub> assay. **(C)** Schematic illustration of the sample preparation. PK-15 cells mock infected or infected by SVA at an MOI of 0.5 for 48 h were subjected to TMT-based proteomic analysis.

transcriptional level of some DEPs (STAT1, IFIT1, OAS1, ZAP, MX2, DDX21, IL-18, ZCCHC9, and ZC3H11A) were verified by qPCR. The results showed that the transcriptional and translational levels are almost identical to DEPs except for DDX21 during SVA infection (**Figures 2C, D**). The translational level of DDX21 was downregulated during SVA infection (**Figure 2B**). In contrast, the transcription level of DDX21 was upregulated in the SVA-infected cells (**Figure 2C**). Thus, the SVA infection inevitably affects the protein function of DDX21.

### DDX21 Restricts the Replication of SVA

To further examine the effects of DDX21 on SVA replication, DDX21 was overexpressed in the BHK-21 cells by transfecting them with pCAGEN-DDX21-HA. As shown in **Figure 3A**, when DDX21 was overexpressed, the VP2 protein levels of SVA were lower than those in the control cells, especially at 12–36 hpi. Furthermore, there was a significant difference in virus titers between cells transfected with pCAGEN-DDX21-HA or pCAGEN, with an approximate 0.5–1.0 log decrease in virus titers from 12 to 36 hpi ( $p < 0.05$ ) (**Figure 3B**). By contrast, three specific siRNAs (siRNA-1651, siRNA-673, and siRNA1712) were synthesized to knock down the expression level of DDX21 in BHK-21 cells. The results suggested that siRNA-1651 had the best knockdown effect (**Figure 3C**). Thus, siRNA-1651 was used in the subsequent interference experiments. As shown in **Figure 3D**, the expression level of VP2 was increased upon transfection with siRNA-1651, especially 36 and 48 hpi, compared with those in NC-transfected cells. Virus titers in the culture supernatants of cells transfected with siRNA-1651

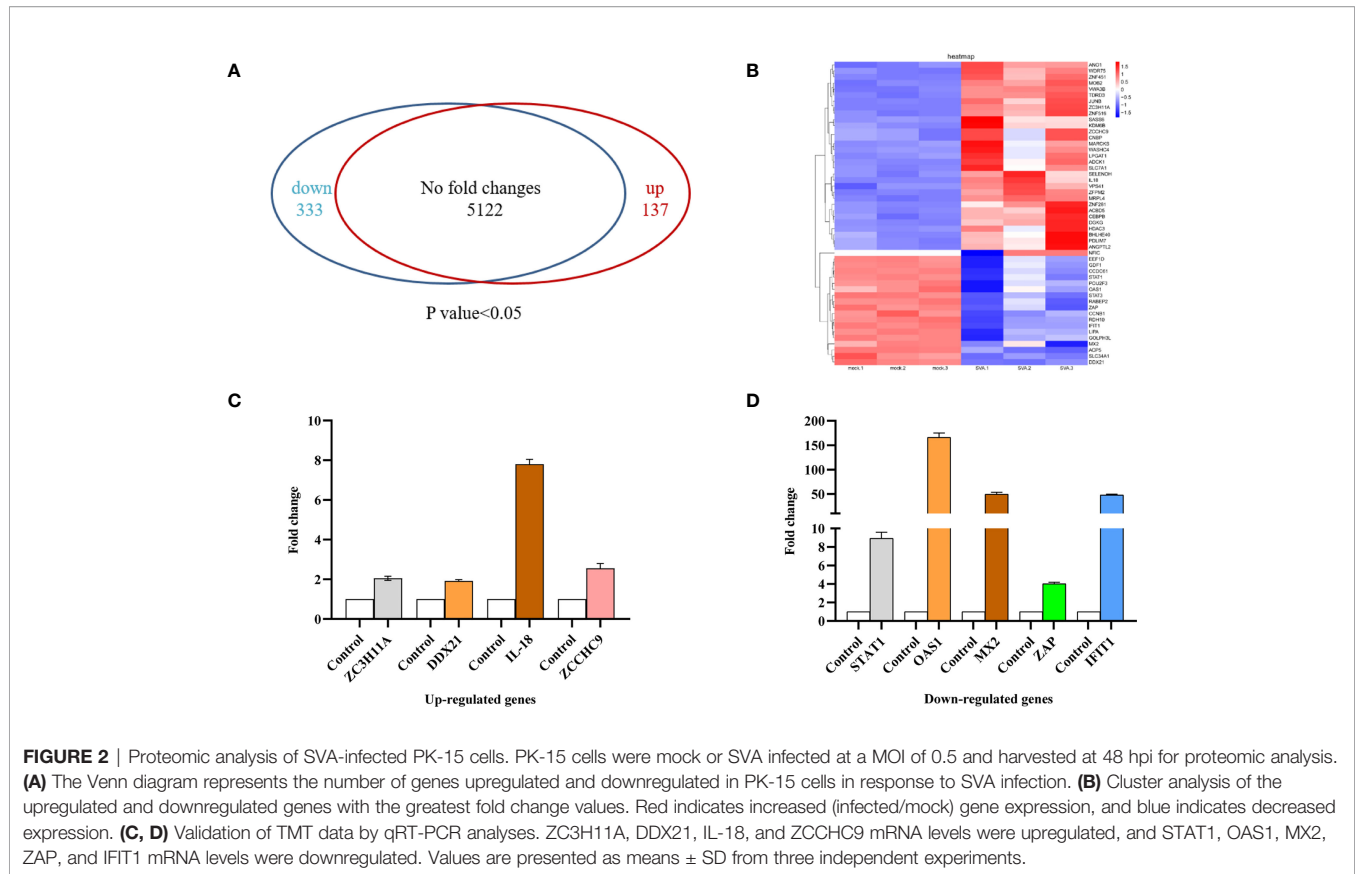
were also increased, which was consistent with the expression levels of the VP2 protein, with a significant difference at 36 and 48 hpi ( $p < 0.05$ ; **Figure 3E**). These observations suggest that DDX21 is a cellular antiviral factor that represses SVA infection.

### SVA 2B and 3C Degrade DDX21

As shown in **Figure 3A**, the expression level of DDX21-HA decreased gradually upon SVA infection, which was consistent with the proteomics results. Furthermore, the transcription level of DDX21 was upregulated during SVA infection. Therefore, we speculated that SVA infection could degrade DDX21. To verify this hypothesis, BHK-21 cells infected with SVA were lysed at 12, 24, 36, and 48 hpi, and the expression level of DDX21 was analyzed by WB. The results revealed that the expression of DDX21 decreased in SVA-infected cells with the prolongation of infection time (**Figure 4A**). Furthermore, to confirm which protein of SVA induces the degradation of DDX21, DDX21 was cotransfected with the protein of SVA. The results revealed that proteins 2B and 3C of SVA induced the degradation of DDX21 (**Figure 4B**). Furthermore, the 2B and 3C of SVA degraded DDX21 in a dose-dependent manner (**Figures 4C, D**).

### 3C Protein of SVA Degrades DDX21 Depending on Its 3C Protein Protease Activity

The SVA 3C protein contained a conserved catalytic box with histidine (His) and cysteine (Cys) residues, which was essential for its protease activity (15). Single-site mutation H48A (3C-H48A) or C160A (3C-C160A) and double-site mutation H48A-C160A (3C-DM) were catalytically inactive (16). To detect whether 3C protease



activity was involved in DDX21 degradation, HEK293T cells were cotransfected with plasmids encoding wild-type 3C protein (3C protein-WT) or its mutants, and HA-DDX21 for 30 h. The results showed that all 3C protein mutants losing protease activity failed to induce DDX21 to degrade (Figures 5A, C).

## DDX21 Does Not Interact With SVA 2B and 3C Proteins

DDX21 was degraded by SVA 2B and 3C proteins, so we speculate that the 2B and 3C may interact with DDX21. To verify this hypothesis, we performed coimmunoprecipitation (Co-IP) assays to analyze the interaction between nonstructural proteins (2B and 3C) and DDX21. HEK293T cells were cotransfected with plasmids expressing HA-tagged DDX21 and Flag-tagged 2B or 3C proteins. Co-IP assays were performed with anti-Flag monoclonal antibody at 48 hpt. Interestingly, coimmunoprecipitation assays showed that DDX21 did not precipitate 2B and 3C proteins (Figures 6A, B).

## Effect of Inhibitors on the Viability of Cells

We examined the effects of different inhibitors on the growth of BHK-21 cells at 24 h by an MTT assay. As shown in Figures 7A, C, compared with the DMSO-treated group, MG132 (0–20  $\mu$ M) and Z-VAD-FMK (0–20  $\mu$ M) did not affect the cell viability. However, a concentration of 50  $\mu$ M reduced the cell viability. In contrast, CQ (0–100  $\mu$ M) did not affect cell viability. So, we choose the proteasome inhibitor MG-132 (10–

20  $\mu$ M), the caspase inhibitor Z-VAD-FMK (10–20  $\mu$ M), and the lysosomal inhibitor CQ (50–100  $\mu$ M) for subsequent experiments.

## 2B and 3C Protein of SVA Degrade the DDX21 via the Caspase Pathway

To further confirm whether DDX21 was degraded upon virus infection, cells were treated with the proteasome inhibitor MG-132, the caspase inhibitor Z-VAD-FMK, and the lysosomal inhibitor CQ, followed by SVA for 36 h. As shown in Figures 7D–F, DDX21 degradation was inhibited after treatment with Z-VAD-FMK. Notably, CQ also seemed to inhibit the degradation of DDX21 (Figure 7F). However, viral protein expression was also inhibited after treatment with CQ, indicating that the inhibition of DDX21 degradation may be due to its severe inhibition of virus replication. Next, we investigated which pathways were involved in the degradation of DDX21 by 2B and 3C proteins. The results showed that 2B and 3C degraded DDX21 through the caspase pathway and not *via* the lysosome and proteasome pathways (Figures 7G–L). These results suggest that DDX21 was degraded through the caspase pathways.

## DISCUSSIONS

As an emerging infectious disease pathogen of swine, SVA has demonstrated its capacity to cause vesicular diseases, neonatal mortality, and persistent infection in pigs. Furthermore, it

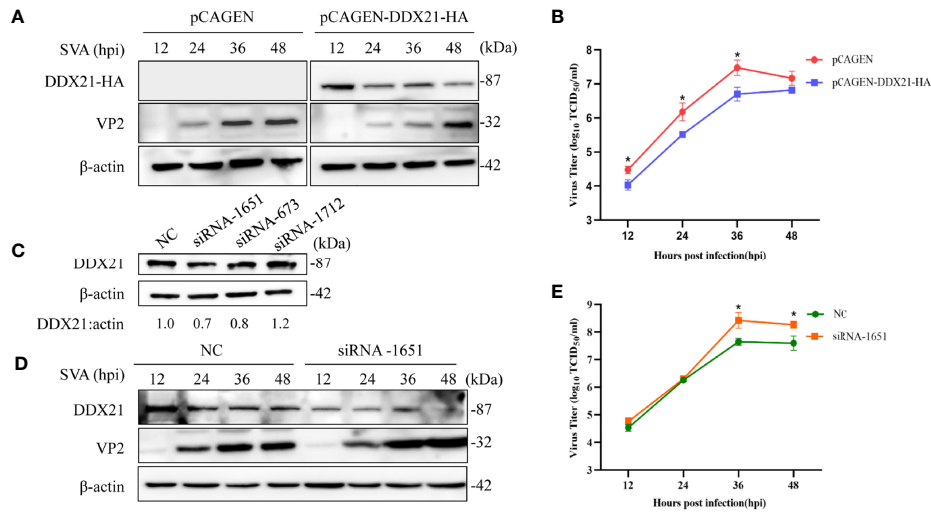


**FIGURE 3 |** DDX21 affects the replication of SVA. **(A)** BHK-21 cells were transfected with pCAGEN-DDX21-HA or pCAGEN. At 36 hpt, the cells were inoculated with SVA at an MOI of 0.1. The cells and supernatant were harvested at the indicated times, and the expression level of the VP2 protein of SVA was analyzed by WB with an anti-VP2 pAb. DDX21-HA was detected with an anti-HA mAb.  $\beta$ -Actin served as the internal reference. **(B)** Virus titers were calculated and expressed as TCID<sub>50</sub>/ml at the indicated times. **(C)** BHK-21 cells seeded in 6-well plates were transfected with siRNA-1651, siRNA-673, siRNA-1712, or negative control (NC) (50 pM/well). At 36 hpt, the cells were lysed and analyzed by Western blotting (WB) with an anti-DDX21 polyclonal antibody (mAb), and  $\beta$ -actin was probed as the internal reference. **(D)** Knocking down the expression of DDX21 promoted the replication of SVA in BHK-21 cells. BHK-21 cells were transfected with NC or siRNA-1651 at 50 pM. At 36 hpt, the cells were infected with SVA at a MOI of 0.1. The cells and the supernatant were harvested at indicated times. The cells were lysed and analyzed by WB using an anti-VP2 pAb. **(E)** The infectious virus titers in the supernatant were determined by a TCID<sub>50</sub>/ml assay. The statistical significance of differences was determined using a Student's *t*-test (NS, not significant; \**p* < 0.05).

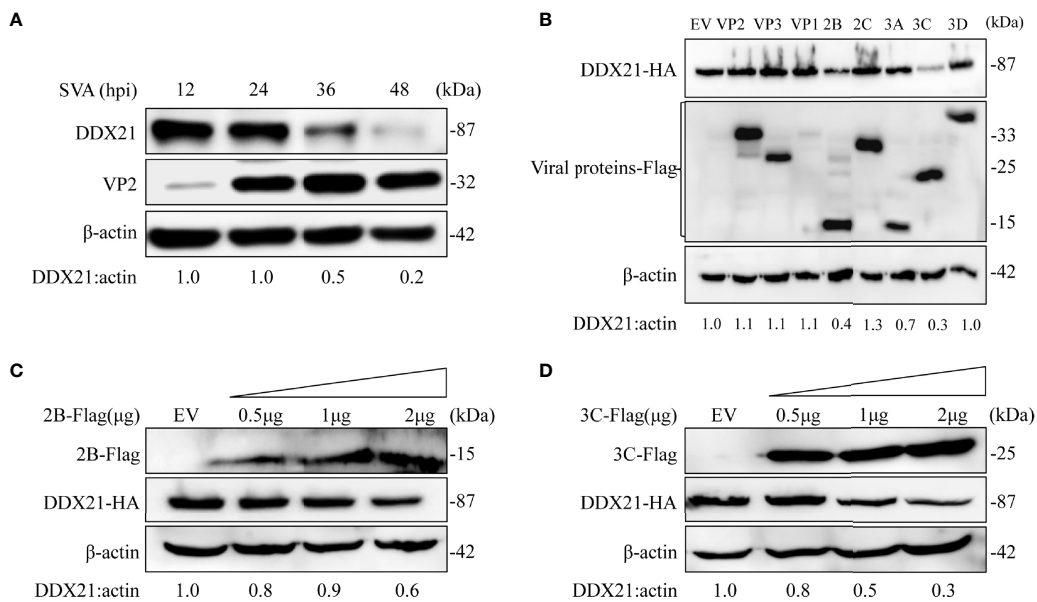


**FIGURE 4 |** SVA degrades endogenous DDX21 during viral infection, and DDX21 is degraded by SVA 2B and 3C. **(A)** BHK-21 cells in 6-well plates were infected with SVA at a MOI of 0.1, cells were harvested at indicated times, and the expression level of endogenous DDX21 protein was analyzed by WB. **(B)** HEK293T cells in six-well plates were cotransfected with HA-DDX21 and Flag-VP1, VP2, VP3, 2B, 2C, 3A, 3C, or 3D, cells were harvested at 30 h, and the samples were analyzed by WB. **(C, D)** HEK293T cells were cotransfected with HA-DDX21 and different concentrations of Flag-2B or Flag-3C for 30 h. The cell lysates were analyzed by WB.

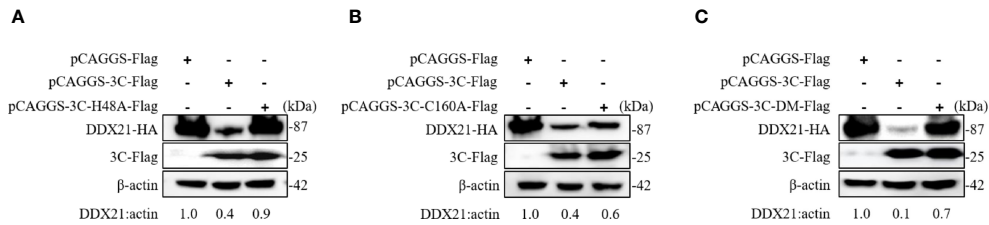


**FIGURE 5** | SVA 3C protein targets DDX21 for degradation through its protease activity. **(A)** HEK293T cells were cotransfected with HA-DDX21 and 3C protein or 3C-H48A for 30 h. The cell lysates were prepared for Western blot analysis using the indicated antibodies. **(B)** HEK293T cells were cotransfected with HA-DDX21 and 3C protein or 3C-C160A for 30 h. The cell lysates were prepared for Western blot analysis using the indicated antibodies. **(C)** HEK293T cells were cotransfected with HA-DDX21 and 3C protein or 3C-DM for 30 h. The cell lysates were prepared for Western blot analysis using the indicated antibodies.

induces immunodepression in suckling piglets and effectively replicates in piglets’ tonsils, mesenteric lymph nodes, and spleen (17, 18). With SVA disease appearing in new countries each year, the virus has become a virus with a global prevalence (19). There must be a molecular mechanism by which SVA antagonizes host antiviral immunity. Although much work has been done in SVA research, there is currently no effective vaccine to control the disease. The interaction of SVA with the host immune response and the pathogenesis remains largely unknown, resulting in the continuous spreading of the disease.

Cell lines have been used as important tools to study virus–host interactions during viral infection. It allows the investigation of the host proteins and pathways involved in viral replication. SVA can infect a variety of cells, such as swine testis (ST), human embryonic kidney-293T, swine kidney (IBRS-2 and PK-15), and human lung cancer cells (NCI-H1299) and BHK-21 (20, 21). To explore the mechanism of SVA infection, the PK-15 cell line can be used as a model for evaluating SVA-induced innate immune signaling and the involved antagonistic effects caused by viral proteins (22). In this study, we screened several candidate cellular proteins in SVA-infected PK-15 by proteomic analysis. In total, 470 DEPs were verified, of which 333 were downregulated and 137 were upregulated. Among the DE proteins, four host proteins with antiviral effects on other viruses were used for screening (10, 23–25). Only DDX21 and IL-18 can suppress the expression of VP2 of SVA (date not shown). Interestingly, unlike IL-18, DDX21 decreased during SVA infection (Figure 2B), while the transcription level of DDX21 surprisingly increased (Figure 2C). Similar phenomena were previously reported for DDX21, DDX23, and DDX1, whose mRNA levels are higher in

FMDV-infected cells than in mock-infected cells (11, 26, 27). The transcription level of DDX21 was inconsistent with the translation level, implying that SVA infection affects the function of DDX21. DDX21 is involved in a variety of cell functions, including transcription, protein translation, processing, and modification of pre-rRNA, mediating and sensing transcription during nucleotide stress, as well as regulating various innate immunity (28–31). Many studies have confirmed that DDX21 may act as an antiviral protein. It has been reported that DDX21 restricts infection and replication of several viruses, including the influenza virus, Borna disease virus (BDV), dengue virus (DENV), FMDV, and SARS-CoV-2 (10, 11, 28, 32, 33). To further verify the effect of DDX21 on the virus replication, overexpression and knockdown experiments of DDX21 were conducted. The results demonstrated that DDX21 could effectively inhibit SVA replication in BHK-21 cells (Figures 3A, E). However, many viruses have evolved general strategies to evade host defenses, such as influencing mRNA translation, protein localization, and cleaving or degrading host proteins (15, 34). In a natural infection, SVA can effectively replicate; therefore, we assumed that SVA could evade the antiviral effect by some means. During the overexpression experiments, we found that as the virus replicated, the expression of DDX21 dropped, which was consistent with the proteomics results. All of these suggest that SVA may escape the antiviral effect of DDX21 by degrading DDX21.

To investigate the mechanism of SVA degrading the DDX21, SVA and the viral proteins were used for verification. With the prolongation of virus infection, the more severe the degradation of DDX21 (Figure 4A). In addition, only the 2B and 3C proteins of SVA can induce the degradation of DDX21 (Figure 4B). With the

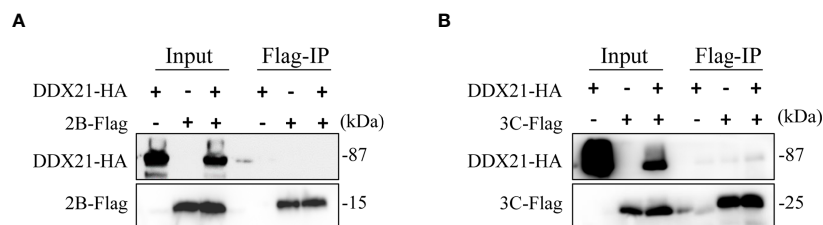


**FIGURE 6** | DDX21 does not interact with SVA 2B and 3C protein. **(A)** HEK293T cells were cotransfected with HA-DDX21 and 2B-Flag. **(B)** HEK293T cells were cotransfected with HA-DDX21 and 3C-Flag. Coimmunoprecipitation (Co-IP) was performed using agarose beads conjugated with anti-Flag mAb agarose beads. Precipitated proteins were analyzed by WB using antibodies against the Flag and HA.

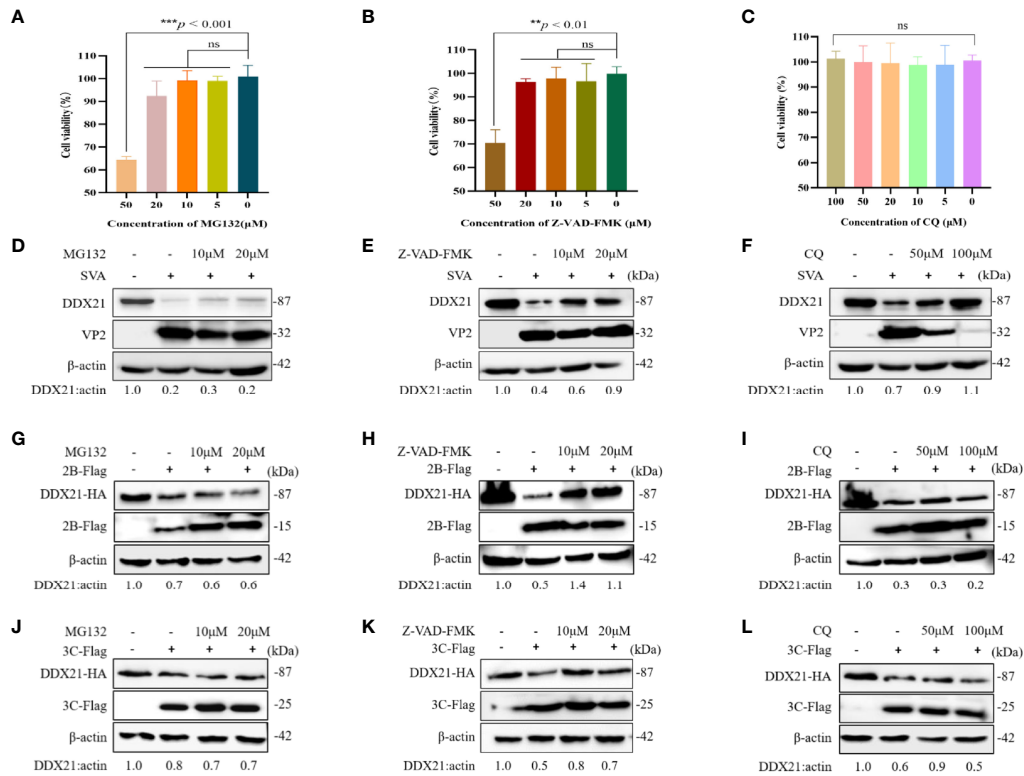


**FIGURE 7 |** DDX21 is degraded through the caspase pathway during SVA infection. Cells were treated with the indicated concentrations of inhibitors for 24 h. MTT method is used to detect BHK-21 cells cytotoxicity. **(A)** MG132. **(B)** Z-VAD-FMK. **(C)** CQ. **(D–F)** BHK-21 cells in six-well plates were incubated with different inhibitors and then infected with SVA at an MOI of 0.1. The cell lysates were analyzed by WB. MG132 was added at 10 to 20  $\mu$ M, Z-VAD-FMK was added at 10 to 20  $\mu$ M, and CQ was added at 50 to 100  $\mu$ M. **(G–I)** BHK-21 cells were cotransfected with HA-DDX21 and 2B-Flag and then treated with different inhibitors. MG132 was added at 10 to 20  $\mu$ M, Z-VAD-FMK was added at 10 to 20  $\mu$ M, and CQ was added at 50 to 100  $\mu$ M. The cell lysates were analyzed by WB. **(J–L)** BHK-21 cells were cotransfected with HA-DDX21 and 3C-Flag and then treated with different inhibitors. MG132 was added at 10 to 20  $\mu$ M, Z-VAD-FMK was added at 10 to 20  $\mu$ M, and CQ was added at 50 to 100  $\mu$ M. The cell lysates were analyzed by WB. The statistical significance of differences was determined using a Student's *t*-test (NS, not significant; \*\**p* < 0.01; \*\*\**p* < 0.001).

increase of 2B and 3C proteins, the degradation of DDX21 was more significant (**Figures 4C, D**). The 2B and 3C proteins are important nonstructural proteins of SVA with multiple roles, especially in antagonizing host innate immunity. 2B protein can suppress type I interferon production by inducing the degradation of MAVS, indicating that 2B protein has the function of degrading and antagonizing innate immunity. It likely enhances membrane permeability, acting like a viroporin (4).

Furthermore, SVA 2AB protein promoted MARCHF8 and MAVS degradation to inhibit IFN-I signaling during SVA infection (35). In contrast, the 3C protein of SVA cleaves PABPC1 to promote viral replication through 3C protease activity (36) and 3C protein-induced hnRNP A1 degradation through its protease activity to promote virus replication (37). SVA suppressed the innate immune response and mediated host cell autophagy and apoptosis to improve viral replication through 2C and 3C proteins (38). Similar to other picornaviruses, the protease activity of the SVA 3C protein depends on a conserved catalytic box with Cys and His residues (16). When the Cys and His residues of 3C protein were mutated (H48A, C160A, or H48A/C160A), it failed to induce

the degradation of DDX21, indicating that the degradation of DDX21 by 3C was dependent on protease activity. Since 2B and 3C proteins did not interact with DDX21, the degradation of DDX21 did not depend on their interaction (**Figures 6A, B**). Subsequently, we investigated the involvement of the lysosome, proteasome, and caspase pathways in SVA, 2B, and 3C protein-dependent degradation of DDX21. The results revealed that SVA, 2B, and 3C proteins use the caspase pathway to degrade DDX21 (**Figure 7**). Although infection with SVA after treatment of cells with CQ can alleviate the degradation of DDX21 (**Figure 7F**), it may be related to autophagy. As shown by Hou et al. (39), SVA infection induces autophagy in BHK-21 cells, and SVA utilizes autophagy machinery to promote its proliferation in BHK-21 cells. After treatment with CQ (a specific inhibitor of autophagosome-lysosome fusion), the VP1 protein expression and viral yields were appreciably reduced. Similarly, we obtained the same results as above after CQ treatment. Therefore, we speculated that the inhibition of DDX21 degradation might be due to inhibition of autophagy and decreased VP2 expression in SVA-infected BHK-21 cells. CQ did not alleviate the degradation effects of 2B and 3C

proteins on DDX21, so we believe that the lysosomal pathway is not the main way for SVA to degrade DDX21 (Figures 7G–L).

In summary, we confirmed that DDX21 inhibits SVA replication. Furthermore, SVA can evade the antiviral activity of DDX21 by decreasing its expression through the 2B and 3C proteins of SVA. The degradation of DDX21 by 2B and 3C proteins depends on the caspase pathway. Moreover, SVA 3C protein can degrade DDX21 through 3C protease activity. Our findings provide new insight into the development of antivirals against SVA infection.

## DATA AVAILABILITY STATEMENT

The data presented in the study are deposited in the ProteomeXchange Consortium (<http://proteomecentral.proteomexchange.org>) repository, accession number PXD034197.

## AUTHOR CONTRIBUTIONS

KZ designed the experiments. KZ, XRG, SFL, XNL, YH, LLW, BSL, WCZ, and LML performed the experiments. KZ and XRG analyzed the data and wrote the manuscript. WZY made

constructive comments on the experiments. All authors contributed to the article and approved the submitted version.

## FUNDING

This work was supported by the Key Research and Development Projects of Hebei (Grant No. 20326625D); the Talents Introduction Projects of Hebei Agricultural University (Grant No. YJ201945); the State Key Laboratory of Veterinary Etiological Biology, Lanzhou Veterinary Research Institute, Chinese Academy of Agricultural Sciences (Grant No. SKLVEB2020KFKT016); the National Natural Science Foundation of China (Grant No. 32102644); Basic Scientific Research Funds of Provincial Universities in Hebei Province (KY202017); and the Precision Animal Husbandry Discipline Group Construction Project of Hebei Agricultural University (1090064).

## ACKNOWLEDGMENTS

We thank all of the members of the Veterinary Biologics Team for their suggestions and excellent technical assistance. Thanks to Dr. Zuzhang Wei, Guangxi University, China, for the SVA antibody.

## REFERENCES

- Hales LM, Knowles NJ, Reddy PS, Xu L, Hay C, Hallenbeck PL. Complete Genome Sequence Analysis of Seneca Valley Virus-001, a Novel Oncolytic Picornavirus. *J Gen Virol* (2008) 89:1265–75. doi: 10.1099/vir.0.83570-0
- Willcocks MM, Locker N, Gomwalk Z, Royall E, Bakhshesh M, Belsham GJ, et al. Structural Features of the Seneca Valley Virus Internal Ribosome Entry Site (IRES) Element: A Picornavirus With a Pestivirus-Like IRES. *J Virol* (2011) 85:4452–61. doi: 10.1128/JVI.01107-10
- Leme RA, Alfieri AF, Alfieri AA. Update on Senecavirus Infection in Pigs. *Viruses* (2017) 9(7):170. doi: 10.3390/v9070170
- Liu H, Li K, Chen W, Yang F, Cao W, Zhang K, et al. Senecavirus A 2b Protein Suppresses Type I Interferon Production by Inducing the Degradation of MAVS. *Mol Immunol* (2022) 142:11–21. doi: 10.1016/j.molimm.2021.12.015
- Xue Q, Liu H, Zhu Z, Yang F, Ma L, Cai X, et al. Seneca Valley Virus 3cpro Abrogates the IRF3-And IRF7-Mediated Innate Immune Response by Degrading IRF3 and IRF7. *Virology* (2018) 518:1–7. doi: 10.1016/j.virol.2018.01.028
- Miles LA, Brennan WN, Rudin CM, Poirier JT. Seneca Valley Virus 3cpro Substrate Optimization Yields Efficient Substrates for Use in Peptide-Prodrug Therapy. *PLoS One* (2015) 10:e0129103. doi: 10.1371/journal.pone.0129103
- Linder P, Jankowsky E. From Unwinding to Clamping—the DEAD Box RNA Helicase Family. *Nat Rev Mol Cell Biol* (2011) 12:505–16. doi: 10.1038/nrm3154
- Su C, Tang YD, Zheng C. DExD/H-Box Helicases: Multifunctional Regulators in Antiviral Innate Immunity. *Cell Mol Life Sci* (2021) 79(1):1–12. doi: 10.1007/s00018-021-04072-6
- Ullah R, Li J, Fang P, Shaobo X, Fang L. DEAD/H-Box Helicases: Antiviral and Pro-Viral Roles During Infections. *Virus Res* (2021) 309:198658. doi: 10.1016/j.virusres.2021.198658
- Chen G, Liu CH, Zhou L, Krug RM. Cellular DDX21 RNA Helicase Inhibits Influenza A Virus Replication But Is Counteracted by the Viral NS1 Protein. *Cell Host Microbe* (2014) 15:484–93. doi: 10.1016/j.chom.2014.03.002
- Abdullah SW, Wu J, Zhang Y, Bai M, Guan J, Liu X, et al. DDX21, a Host Restriction Factor of FMDV IRES-Dependent Translation and Replication. *Viruses* (2021) 13(9):1765. doi: 10.3390/v13091765
- Wisniewski JR, Zougman A, Nagaraj N, Mann M. Universal Sample Preparation Method for Proteome Analysis. *Nat Methods* (2009) 6:359–62. doi: 10.1038/nmeth.1322
- Kuo RL, Lin YH, Wang RY, Hsu CW, Chiu YT, Huang HI, et al. Proteomics Analysis of EV71-Infected Cells Reveals the Involvement of Host Protein NEDD4L in EV71 Replication. *J Proteome Res* (2015) 14:1818–30. doi: 10.1021/pr501199h
- Takeuchi H, Baba M, Shigeta S. An Application of Tetrazolium (MTT) Colorimetric Assay for the Screening of Anti-Herpes Simplex Virus Compounds. *J Virological Methods* (1991) 33:61–71. doi: 10.1016/0166-0934(91)90008-N
- Wen W, Li X, Yin M, Wang H, Qin L, Li H, et al. Selective Autophagy Receptor SQSTM1/p62 Inhibits Seneca Valley Virus Replication by Targeting Viral VP1 and VP3. *Autophagy* (2021) 17:3763–75. doi: 10.1080/15548627.2021.1897223
- Qian S, Fan W, Liu T, Wu M, Zhang H, Cui X, et al. Seneca Valley Virus Suppresses Host Type I Interferon Production by Targeting Adaptor Proteins MAVS, TRIF, and TANK for Cleavage. *J Virol* (2017) 91(16):e00823–17. doi: 10.1128/JVI.00823-17
- Maggioli MF, Fernandes MHV, Joshi LR, Sharma B, Tweet MM, Noll JCG, et al. Persistent Infection and Transmission of Senecavirus A From Carrier Sows to Contact Piglets. *J Virol* (2019) 93(16):e00819–19. doi: 10.1128/JVI.00819-19
- Oliveira TES, Leme RA, Agnol AMD, Gerez JR, Pelaquim IF, Miyabe FM, et al. Seneca Valley Virus Induces Immunodepression in Suckling Piglets by Selective Apoptosis of B Lymphocytes. *Microbial Pathogenesis* (2021) 158:105022. doi: 10.1016/j.micpath.2021.105022
- Houston E, Temeeyasen G, Pineyro PE. Comprehensive Review on Immunopathogenesis, Diagnostic and Epidemiology of Senecavirus A. *Virus Res* (2020) 286:198038. doi: 10.1016/j.virusres.2020.198038
- Segales J, Barcellos D, Alfieri A, Burrough E, Marthaler D. Senecavirus A. *Veterinary Pathol* (2017) 54:11–21. doi: 10.1177/0300985816653990
- Yang F, Zhu Z, Cao W, Liu H, Zhang K, Tian H, et al. Immunogenicity and Protective Efficacy of an Inactivated Cell Culture-Derived Seneca Valley Virus Vaccine in Pigs. *Vaccine* (2018) 36:841–6. doi: 10.1016/j.vaccine.2017.12.055
- Zhang X, Yang F, Li K, Cao W, Ru Y, Chen S, et al. The Insufficient Activation of RIG-I-Like Signaling Pathway Contributes to Highly Efficient Replication of Porcine Picornaviruses in IBRS-2 Cells. *Mol Cell Proteomics: MCP* (2021) 20:100147. doi: 10.1016/j.mcpro.2021.100147
- Kimura T, Katoh H, Kayama H, Saiga H, Okuyama M, Okamoto T, et al. Ifit1 Inhibits Japanese Encephalitis Virus Replication Through Binding to 5' Capped 2'-O Methylated RNA. *J Virol* (2013) 87:9997–10003. doi: 10.1128/JVI.00883-13



24. Wang X, Mbondji-Wonje C, Zhao J, Hewlett I. IL-1 $\beta$  and IL-18 Inhibition of HIV-1 Replication in Jurkat Cells and PBMCs. *Biochem Biophys Res Commun* (2016) 473:926–30. doi: 10.1016/j.bbrc.2016.03.153
25. Zhao J, Feng N, Li Z, Wang P, Qi Z, Liang W, et al. 2',5'-Oligoadenylate Synthetase 1(OAS1) Inhibits PRRSV Replication in Marc-145 Cells. *Antiviral Res* (2016) 132:268–73. doi: 10.1016/j.antiviral.2016.07.001
26. Abdullah SW, Han S, Wu J, Zhang Y, Bai M, Jin Y, et al. The DDX23 Negatively Regulates Translation and Replication of Foot-And-Mouth Disease Virus and Is Degraded by 3C Proteinase. *Viruses* (2020) 12(12):1348. doi: 10.3390/v12121348
27. Zhu Z, Wang G, Yang F, Cao W, Mao R, Du X, et al. Erratum for Zhu Et Al., "Foot-And-Mouth Disease Virus Viroprotein 2b Antagonizes RIG-I-Mediated Antiviral Effects by Inhibition of Its Protein Expression". *J Virol* (2021) 95:e0054521. doi: 10.1128/JVI.00545-21
28. Dong Y, Ye W, Yang J, Han P, Wang Y, Ye C, et al. DDX21 Translocates From Nucleus to Cytoplasm and Stimulates the Innate Immune Response Due to Dengue Virus Infection. *Biochem Biophys Res Commun* (2016) 473:648–53. doi: 10.1016/j.bbrc.2016.03.120
29. McRae EKS, Booy EP, Moya-Torres A, Ezzati P, Stetefeld J, McKenna SA. Human DDX21 Binds and Unwinds RNA Guanine Quadruplexes. *Nucleic Acids Res* (2017) 45:6656–68. doi: 10.1093/nar/gkx380
30. McRae EKS, Dupas SJ, Booy EP, Piragasam RS, Fahlman RP, McKenna SA. An RNA Guanine Quadruplex Regulated Pathway to TRAIL-Sensitization by DDX21. *RNA* (2020) 26:44–57. doi: 10.1261/rna.072199.119
31. Santoriello C, Sporrij A, Yang S, Flynn RA, Henriques T, Dorjsuren B, et al. RNA Helicase DDX21 Mediates Nucleotide Stress Responses in Neural Crest and Melanoma Cells. *Nat Cell Biol* (2020) 22:372–9. doi: 10.1038/s41556-020-0493-0
32. Ariumi Y. Host Cellular RNA Helicases Regulate SARS-CoV-2 Infection. *J Virol* (2022) 96:e0000222. doi: 10.1128/jvi.00002-22
33. Watanabe Y, Ohtaki N, Hayashi Y, Ikuta K, Tomonaga K. Autogenous Translational Regulation of the Bornavirus Negative Control Factor X From Polycistronic mRNA Using Host RNA Helicases. *PLoS Pathog* (2009) 5:e1000654. doi: 10.1371/journal.ppat.1000654
34. Clementz MA, Chen Z, Banach BS, Wang Y, Sun L, Ratia K, et al. Deubiquitinating and Interferon Antagonism Activities of Coronavirus Papain-Like Proteases. *J Virol* (2010) 84:4619–29. doi: 10.1128/JVI.02406-09
35. Sun D, Kong N, Dong S, Chen X, Qin W, Wang H, et al. 2ab Protein of Senecavirus A Antagonizes Selective Autophagy and Type I Interferon Production by Degrading LC3 and MARCF8. *Autophagy* (2021) (17):1–13. doi: 10.1080/15548627.2021.2015740
36. Xue Q, Liu H, Zhu Z, Xue Z, Liu X, Zheng H. Seneca Valley Virus 3c(Pro) Cleaves PABPC1 to Promote Viral Replication. *Pathogens* (2020) 9(6):443. doi: 10.3390/pathogens9060443
37. Song J, Wang D, Quan R, Liu J. Seneca Valley Virus 3c(Pro) Degrades Heterogeneous Nuclear Ribonucleoprotein A1 to Facilitate Viral Replication. *Virulence* (2021) 12:3125–36. doi: 10.1080/21505594.2021.2014681
38. Liu T, Li X, Wu M, Qin L, Chen H, Qian P. Seneca Valley Virus 2C and 3C (Pro) Induce Apoptosis via Mitochondrion-Mediated Intrinsic Pathway. *Front Microbiol* (2019) 10:1202. doi: 10.3389/fmicb.2019.01202
39. Hou L, Dong J, Zhu S, Yuan F, Wei L, Wang J, et al. Seneca Valley Virus Activates Autophagy Through the PERK and ATF6 UPR Pathways. *Virology* (2019) 537:254–63. doi: 10.1016/j.virol.2019.08.029

**Conflict of Interest:** The authors declare that the research was conducted without any commercial or financial relationships that could be construed as a potential conflict of interest.

**Publisher's Note:** All claims expressed in this article are solely those of the authors and do not necessarily represent those of their affiliated organizations, or those of the publisher, the editors and the reviewers. Any product that may be evaluated in this article, or claim that may be made by its manufacturer, is not guaranteed or endorsed by the publisher.

Copyright © 2022 Zhao, Guo, Liu, Liu, Han, Wang, Lei, Zhang, Li and Yuan. This is an open-access article distributed under the terms of the Creative Commons Attribution License (CC BY). The use, distribution or reproduction in other forums is permitted, provided the original author(s) and the copyright owner(s) are credited and that the original publication in this journal is cited, in accordance with accepted academic practice. No use, distribution or reproduction is permitted which does not comply with these terms.



## OPEN ACCESS

EDITED BY  
Chenhe Su,  
Wistar Institute, United States

REVIEWED BY  
Shen Yang,  
University of California, San Diego,  
United States  
Xiangdong Li,  
Yangzhou University, China

\*CORRESPONDENCE  
Guangzhi Tong  
gztong@shvri.ac.cn  
Yanjun Zhou  
yjzhou@shvri.ac.cn

<sup>†</sup>These authors have contributed  
equally to this work

SPECIALTY SECTION  
This article was submitted to  
Viral Immunology,  
a section of the journal  
Frontiers in Immunology

RECEIVED 02 July 2022

ACCEPTED 06 July 2022

PUBLISHED 25 July 2022

## CITATION

Chen P, Zhu J, Yu J, Liu R, Lao M,  
Yu L, Gao F, Jiang Y, Liu C, Tong W,  
Liu H, Tong G and Zhou Y (2022)  
Porcine epidemic diarrhea virus strain  
FJzz1 infection induces type I/III IFNs  
production through RLRs and TLRs-  
mediated signaling.  
*Front. Immunol.* 13:984448.  
doi: 10.3389/fimmu.2022.984448

## COPYRIGHT

© 2022 Chen, Zhu, Yu, Liu, Lao, Yu,  
Gao, Jiang, Liu, Tong, Liu, Tong and  
Zhou. This is an open-access article  
distributed under the terms of the  
[Creative Commons Attribution License  
\(CC BY\)](https://creativecommons.org/licenses/by/4.0/). The use, distribution or  
reproduction in other forums is  
permitted, provided the original  
author(s) and the copyright owner(s)  
are credited and that the original  
publication in this journal is cited, in  
accordance with accepted academic  
practice. No use, distribution or  
reproduction is permitted which does  
not comply with these terms.

# Porcine epidemic diarrhea virus strain FJzz1 infection induces type I/III IFNs production through RLRs and TLRs-mediated signaling

Pengfei Chen<sup>1,2†</sup>, Junrui Zhu<sup>1†</sup>, Jiarong Yu<sup>1</sup>, Ruilin Liu<sup>1</sup>,  
Mengqin Lao<sup>1</sup>, Lingxue Yu<sup>1</sup>, Fei Gao<sup>1</sup>, Yifeng Jiang<sup>1</sup>,  
Changlong Liu<sup>1</sup>, Wu Tong<sup>1</sup>, Huili Liu<sup>2</sup>,  
Guangzhi Tong<sup>1,3\*</sup> and Yanjun Zhou<sup>1\*</sup>

<sup>1</sup>Department of Swine Infectious Diseases, Shanghai Veterinary Research Institute, Chinese Academy of Agricultural Sciences, Shanghai, China, <sup>2</sup>Institute of Animal Husbandry and Veterinary, Shanghai Academy of Agricultural Science, Shanghai, China, <sup>3</sup>Jiangsu Co-innovation Center for Prevention and Control of Important Animal Infectious Diseases and Zoonoses, Yangzhou University, Yangzhou, China

Interferons (IFNs) including type I/III IFNs are the major components of the host innate immune response against porcine epidemic diarrhea virus (PEDV) infection, and several viral proteins have been identified to antagonize type I/III IFNs productions through diverse strategies. However, the modulation of PEDV infection upon the activation of the host's innate immune response has not been fully characterized. In this study, we observed that various IFN-stimulated genes (ISGs) were upregulated significantly in a time- and dose-dependent manner in LLC-PK1 cells infected with the PEDV G2 strain FJzz1. The transcriptions of IRF9 and STAT1 were increased markedly in the late stage of FJzz1 infection and the promotion of the phosphorylation and nuclear translocation of STAT1, implicating the activation of the JAK-STAT signaling pathway during FJzz1 infection. In addition, abundant type I/III IFNs were produced after FJzz1 infection. However, type I/III IFNs and ISGs decreased greatly in FJzz1-infected LLC-PK1 cells following the silencing of the RIG-I-like receptors (RLRs), including RIG-I and MDA5, and the Toll-like receptors (TLRs) adaptors, MyD88 and TRIF. Altogether, FJzz1 infection induces the production of type-I/III IFNs in LLC-PK1 cells, in which RLRs and TLRs signaling pathways are involved, followed by the activation of the JAK-STAT signaling cascade, triggering the production of numerous ISGs to exert antiviral effects of innate immunity.

## KEYWORDS

porcine epidemic diarrhea virus, ISG, JAK-STAT pathway, IFN-I/III, innate immunity

## Introduction

Porcine epidemic diarrhea (PED) is an acute and highly contagious enteric viral disease of swine caused by the porcine epidemic diarrhea virus (PEDV). Neonatal piglets are most susceptible to PEDV, characterized by severe acute watery diarrhea, vomiting, dehydration, high morbidity and high mortality (1–3). Since PED was first reported in England in 1971, the outbreak has occurred frequently in many pig-producing countries (4–10). Despite the availability of CV777-derived vaccines, outbreaks continued to increase, especially the highly virulent G2 PEDV re-emerged in China in 2010, followed by the first introduction into the United States in 2013, resulting in substantial economic losses to the pork industry worldwide (11–17). PEDV is an enveloped, positive single-stranded, plus-sense RNA virus that belongs to the genus Alphacoronavirus of the family Coronaviridae in the order Nidovirales (18). PEDV consists of about 28 Kb PEDV genome including a capped 5'-untranslated region (5'-UTR), a tailed 3'-UTR, and seven open reading frames (ORF), which encodes polymerase peptides pp1a, pp1ab, S glycoprotein, accessory protein ORF3, envelope (E), membrane (M) and nucleocapsid (N) (19, 20).

Antiviral innate immunity is regarded as the first line of defense against viral infection, and typical antiviral responses in host cells are mediated by type I interferons (IFNs), such as IFN- $\beta$  (21). During viral infection and replication, RNA virus genomes replication produces double-stranded (ds) RNA, which can be recognized as a pathogen-associated molecular pattern by host pattern recognition receptors including RIG-I-like receptors (RLRs) in the cytoplasm or Toll-like receptors (TLRs) in endosomes (22, 23), leading to the synthesis and secretion of type I IFNs. Subsequently, the secretion of IFNs induces hundreds of IFN-stimulated genes (ISGs) through the Janus kinase (JAK)-signal transducer and activator of transcription (STAT) signaling pathway to act the antiviral effects (24, 25). In recent years type III IFNs have been identified as novel viral factors that target the downstream signaling pathways needed to amplify ISGs to establish a host antiviral state (26–28). Although type III IFNs bind to a receptor complex distinct from the type I IFNs receptor, type I and III IFNs have been reported to share a common downstream signaling pathway *via* JAK-STAT, leading to the induction of ISGs (29, 30).

Virus interactions with host innate immune responses drive mutual evolutionary changes, which result in the remarkable diversification of viruses and host antiviral responses (31). In the competition between virus and host cells, many viruses including coronavirus have evolved various strategies to evade or disrupt the antiviral immunity such as the type I and III IFNs (32, 33). Several viral proteins have been identified as IFN- I/III antagonists in members of the family *Coronaviridae*, including Middle East respiratory syndrome coronavirus (34, 35), mouse hepatitis virus (36, 37), severe acute respiratory syndrome coronavirus (SARS-CoV) (38) and SARS-CoV-2 (39–41), a

novel emerging  $\beta$ -coronavirus that causes the coronavirus disease 2019 (COVID-19). PEDV belongs to  $\alpha$ -coronavirus together with transmissible gastroenteritis virus (TGEV). Accumulating evidence showed that several PEDV proteins such as nsp1, nsp3, nsp5, nsp15, nsp16, and N could antagonize type I and/or type III productions through diverse molecular mechanisms (30, 42–45). Additionally, limited reports showed that PEDV could suppress IFNs production (43, 44, 46), but the detailed mechanism regarding IFNs inhibition remained elusive. More interestingly, some studies reported that ISGs were upregulated significantly during PEDV infection (47, 48), which were consistent with our previous results based on proteomics analysis. Therefore, further investigations are needed to elucidate the modulations of ISGs and IFNs responses in PEDV-infected cells. In the present study, we demonstrated that PEDV-infection induced IFN-I/III productions through RLRs and TLRs-mediated pathways to produce a large number of ISGs by activating the JAK-STAT signaling pathway to exert antiviral effects. This study provides new insight into understanding the modulation of host natural immune responses to PEDV infection.

## Materials and methods

### Cells and antibodies

Porcine kidney epithelial cells (LLC-PK1) used in this study were cultured in modified Eagle's medium (MEM, Life Technologies, 11095098) with 10% fetal bovine serum (FBS, Gibco, 10,099,141) at 37°C in a humidified atmosphere of 5% CO<sub>2</sub>. Swine testis epithelial cells (ST) and African green monkey kidney epithelial cells (MARC-145) were grown in Dulbecco' Modified Eagle's Medium nutrient (DMEM, Sigma-Aldrich, D6429) with 10% FBS at 37°C with 5% CO<sub>2</sub>. Anti-STAT1 antibody (14994) and anti-Phospho-STAT1 antibody (9167) were purchased from Cell Signaling Technology (CST). Anti-ISG15 antibody (ab285367) was purchased from Abcam. Anti- $\beta$ -actin antibody (60,008-1), Horseradish peroxidase (HRP)-conjugated anti-mouse IgG antibody (SA00001-1), and HRP-conjugated anti-rabbit IgG antibody (SA00001-2) were obtained from Proteintech Group. The monoclonal antibody (Mab) against PEDV N protein was made in our laboratory (49). 4' 6-diamidino-2-phenylindole (DAPI, C1002) was purchased from Beyotime. poly(I:C) LMW (low molecular weight) was obtained from *In vivo*Gen.

### PEDV propagations and infections

PEDV G2 strain FJzz1 (GenBank accession no. MK288006) was previously isolated in Vero E6 cells in our laboratory (50,

51), and virus titers were determined by 50% tissue culture infective doses (TCID<sub>50</sub>). LLC-PK1 cells grown to approximately 90% confluence in 6-well plates were mock-infected with FBS-free MEM containing 10 µg/mL trypsin or infected with PEDV at the indicated multiplicity of infection (MOI). After incubation for 1 hour (h) at 37°C, LLC-PK1 cells were washed with phosphate-buffered saline (PBS) 3 times to remove the unattached viruses and maintained in MEM supplemented with 5 µg/ml trypsin at 37°C. ST and MARC-145 cells were mocked infected with FBS-free DMEM containing 10 µg/ml trypsin or infected with PEDV at an MOI of 0.01. After incubation for 1 h at 37°C, ST and MARC-145 cells were washed by PBS 3 times and maintained in DMEM supplemented with 10 µg/ml trypsin at 37°C. Then the cells were collected at the indicated time points for further analyses.

## Quantitative Real-time PCR

According to the manufacturer's instructions, total RNA was extracted from PEDV-infected LLC-PK1, ST and MARC-145 cells using the RNeasy Mini kit (QIAGEN, 74104) For reverse transcription (RT)-qPCR analysis, one microgram of total RNA was transcribed to cDNA using the Revert Aid First Stranded cDNA Synthesis Kit (Thermo Fisher Scientific, K1622). The synthesized cDNA was then used as the template for quantitative PCR using SYBR Green PCR mix according to the manufacturer's instructions with a LightCycler system (Roche, Switzerland). The RT-qPCR-specific primers are listed in

**Table 1.** The glyceraldehyde-3-phosphate dehydrogenase (GAPDH) gene was used for each experiment's internal control. Relative transcription levels of target genes were presented as fold changes relative to the respective controls using the 2<sup>-ΔΔCt</sup> threshold method.

## Western blotting analysis

LLC-PK1 cells infected with PEDV or mock-infected at the indicated time points were harvested and lysed on ice in RIPA Lysis and Extraction Buffer (Thermo Fisher Scientific, 89,901) supplemented with Protease Inhibitor Cocktail (Bimake, B14001) and Phosphatase Inhibitor Cocktail (Bimake, B15001) for 30 min. The cell lysates were then centrifuged at 4°C at 10,000 rpm for 10 min to remove insoluble components. Equal amounts of protein were resolved by 10% SDS-PAGE and electrophoretically transferred onto 0.2-µm nitrocellulose Western blotting membranes (GE Healthcare, 10,600,001). After blocking with 5% nonfat dry milk in tris-buffered saline-Tween (TBST) for 2 h at room temperature, the membranes were incubated with the anti-STAT1 antibody, anti-Phospho-STAT1 antibody, anti-ISG15 antibody, anti-N antibody or anti-β-actin antibody at 4°C overnight. After washing with TBST for 30 min, the membranes were incubated with the HRP-conjugated anti-rabbit IgG antibodies or HRP-conjugated anti-mouse IgG antibodies for 1 h at room temperature, followed by washing with TBST for 30 min. Signals were detected with chemiluminescence (Thermo Fisher Scientific, 34,580).

TABLE 1 Primer sequences in this study.

Gene name	Forward primer (5'-3')	Reverse primer (5'-3')
Porcine-RSAD2	ATCTGCCACCACCCCACTA	ACGGCTCTCCGCTGAAAAGT
Porcine-OAS1	GAGTTTTCCACCTGCTTCACG	AAATCTGTTTTCCCGCTTCCT
Porcine-Mx1	GGAGGCGGAAGAAGAAAAGAA	CAGAGGGATGTGGCTGGAGAT
Porcine-Mx2	AGAGGCAGCGGAATCATCAC	CTCCACTTTGCGGTAGCTGA
Porcine-IFIT1	AAGAAGATGAAGGAGAAAAGT	CAGGAGAGAAGAGAAGGGTGT
Porcine-ISG15	AATGTGCTTCAGGATGGGGTG	CCAGGATGCTCAGTGGGTCTC
Porcine-IRF9	ATCCTCCAGGACCCCTTCAA	AACCCTACCTCCGGAGACT
Porcine-STAT1	TCCGTTTTTCATGACCTTCTGT	CTGAATATTCCCTGACTGAGT
Porcine-IFN-β	GCTAACAAGTGCATCCTCCAAA	CCAGGAGCTTCTGACATGCCA
Monkey-IFN-β	CTAGCACTGGCTGGAATGAGACT	GGCCTTCAGGTAATGCAGAATC
Monkey-GAPDH	CCTCCGTGTCCCTACTGCCAAC	GACGCCGTCTTACCACCTTCT
Porcine-IFN-λ1	GGTGTGGCGACTGTGATG	GATTGGAAGTGGCCCATGTG
Porcine-IFN-λ3	ACTTGGCCAGTTCAAGTCT	CATCCTTGGCCCTCTTGA
Porcine-IFN-λ4	GCTATGGGACTGTGGGTCTT	AGGGAGCGGTAGTGAGAGAG
Porcine-RIG-I	GTGTGCGGTGTTTCAGATGC	AGCCTGTGCTCGGATATTT
Porcine-MDA5	CACITGCCCGCAATTAACA	GTCCGAGACGTCCAGACTTG
Porcine-MAVS	CCTCTGGGACCTCTTCGACA	GCTGTTTGAATCCGCAGCA
Porcine-MyD88	CCATTCGAGATGACCCCTG	TAGCAATGGACCAGACGCAG
Porcine-TRIF	GCTCCCGAGCTGGAGTTATC	GGTACCTGGAAATCCTCGCA
Porcine-GAPDH	ATGGTGAAGTCCGGAGTGAAC	CGTGGGTGGAATCATACTGG

## Immunofluorescence assay

LLC-PK1 cells seeded in 6-well plates were mock-infected or infected with PEDV at an MOI of 0.01 for 18 h, as described above. Then cells were fixed with 4% paraformaldehyde for 10 min at room temperature and permeabilized using 0.1% Triton X-100 for 10 min at 4°C. After three washes with PBS, the cells were sealed with 3% bovine serum albumin (BSA) in PBS for 1 h and then incubated with anti-STAT1 antibody and anti-N antibody, followed by secondary AF488-conjugated goat anti-rabbit IgG antibody and AF594-conjugated goat anti-mouse IgG antibody in the dark for 1 h. The cell nuclei were stained with 0.1% DAPI in the dark for 15 min at room temperature. Immunofluorescence images were captured with inverted fluorescence microscopy in the dark.

## SiRNA-mediated interference

Small interfering RNA (siRNA) against pig RIG-I, MDA5, MAVS, MyD88, TRIF, and negative control (NC) siRNA referred to in the previous report were synthesized by GenePharma (Shanghai, China) (52). LLC-PK1 cells were seeded in 12-well plates, and transient transfections of siRNAs were performed using Lipofectamine<sup>TM</sup> RNAiMAX transfection reagent (13,778,075; Thermo Fisher Scientific) according to the manufacturer's instructions. The interfering efficiency of siRNA was analyzed by RT-qPCR due to the lack of specific antibodies against pig RIG-I, MDA5, MAVS, MyD88 or TRIF. LLC-PK1 cells were transfected with specific siRNAs or NC siRNA, followed by PEDV infection, and the transcriptions of I/III IFNs and ISGs were analyzed by RT-qPCR. The siRNA sequences are listed in Table 2.

## Statistical analysis

GraphPad Prism 6 (GraphPad, La Jolla, CA, USA) was used for statistical analyses. Statistical significance was assessed with the Student's *t*-test, and data are presented as mean ± SD for at least two independent experiments. Differences were considered statistically significant (Asterisks) when the *P*-value was less than 0.05.

TABLE 2 Short interfering RNA target sequences.

Gene name	The target sequence (5'-3')
RIG-I	CUCUUGGAGGCUUAUUUCA
MDA5	GAGAAACCAGUGAUUCCCU
MAVS	CUGCUGCGGAAUCAAACA
MyD88	CGGCUGAAGUUAUGUGUGU
TRIF	CCACCUUUCAGAAGAAGAU

## Results

### Proliferation characteristics of FJzz1 in LLC-PK1 cells

Vero cells are widely used as suitable cell models for PEDV isolation and propagation *in vitro*. However, Vero cells lost the capacity to produce type I IFNs due to a chromosomal deletion. Thus, Vero cells are considered less suitable for studies of PEDV-cell interactions, especially innate immunity, during PEDV infection. PEDV mainly infects the intestinal tract of piglets, where villous epithelial cells are regarded as the primary target cells *in vivo* for PEDV. Although IPEC-J2 is a line of porcine intestinal epithelial cells, its susceptibility to PEDV is controversial. LLC-PK1, as a kind of porcine kidney epithelial cell, is reported to be permissive to PEDV infection (30, 53, 54). To determine the proliferative kinetics of PEDV in LLC-PK1 cells, cytopathic effect (CPE), immunofluorescence assay (IFA) identification, viral protein expression, and multi-step growth curve were performed. As shown in Figure 1A, LLC-PK1 cells inoculated with FJzz1 developed visible CPEs at 18 h post-infection (hpi), while no CPEs were found in the mock-infected cells. In addition, LLC-PK1 cells infected with FJzz1 displayed specific green fluorescence when treated with a Mab directed against PEDV N protein, but no green fluorescence was observed in the mock-infected cells. Western blotting analysis further confirmed the productive and efficient infection of LLC-PK1 cells by FJzz1 (Figure 1B). Moreover, a multi-step growth curve of FJzz1 based on the TCID<sub>50</sub> at different hpi was visualized. It showed that the titers of FJzz1 increased steadily during infection and reached a peak at 24 hpi (Figure 1C). Our results showed that FJzz1 could infect LLC-PK1 cells and have good proliferation, demonstrating that LLC-PK1 is an alternative cell line for studying innate immunity modulated by PEDV infection *in vitro*.

### FJzz1 infection induces the production of ISGs in LLC-PK1 cells

The interactions between PEDV and host cells have been studied previously in our laboratory using TMT relative quantitative proteomics method. The results showed that

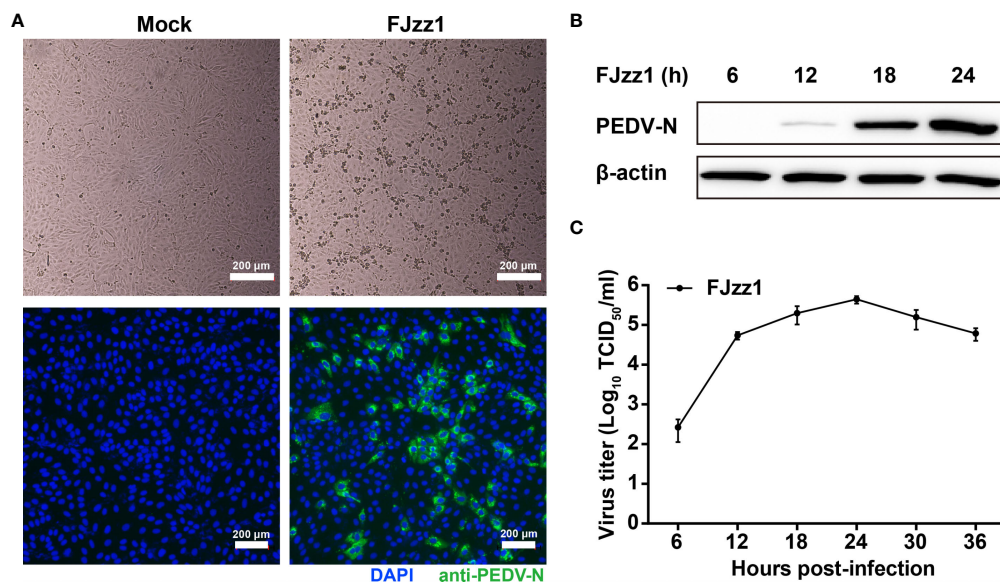


FIGURE 1

Efficient replication of FJzz1 in LLC-PK1 cells. (A) CPE and immunofluorescence identification of PEDV replication in LLC-PK1 cells. LLC-PK1 cells were infected with FJzz1 at an MOI of 0.01, and a CPE was observed at 18 hpi. Then cells were fixed with 4% paraformaldehyde and stained with mouse anti-N MAb. Scale bar = 200 μm. (B) Expression of the N protein in FJzz1-infected LLC-PK1 cells was detected by Western blotting. LLC-PK1 cells were infected with PEDV at an MOI of 0.01, and Western blotting was conducted using anti-N MAb at 6, 12, 18, and 24 hpi, respectively. (C) Multi-step growth kinetics of FJzz1 in LLC-PK1 cells. LLC-PK1 cells were infected with FJzz1 at an MOI of 0.01. The cell lysates were collected at the designated times and titrated with a TCID<sub>50</sub> infectivity assay.

compared with mock-infected LLC-PK1 cells, ISGs including radical S-adenosylmethionine domain containing 2 (RSAD2; also known as viperin), 2',5'-Oligoadenylate synthetase 1 (OAS1), the GTPase Mx proteins (Mx1 and Mx2), interferon-induced protein with tetratricopeptide repeats 1 (IFIT1), and ISG15 were upregulated significantly in FJzz1 infected LLC-PK1 cells (Supplementary Figure 1). To confirm the relative quantitative proteomics results, the transcriptional levels of ISGs were examined by RT-qPCR. As shown in Figure 2, after infection with FJzz1 at MOI of 0.01, the mRNA of ISGs climbed at 12 hpi and continued to upregulated for hundred times at 18 hpi and 24 hpi. By contrast, the mRNA of ISGs in mock-infected LLC-PK1 cells remained relatively stable at different time points. Furthermore, the mRNA expressions of ISGs induced by FJzz1 infection were upregulated in dose-dependent manners (Supplementary Figure 2). Together, these results suggest that FJzz1 infection induces the production of ISGs, and we speculate that FJzz1 infection may activate the IFNs signaling cascade.

## JAK-STAT signaling pathway is activated during FJzz1 infection

In general, IFNs recognition of IFN receptors on the surface of host cells activates the JAK-STAT signaling pathway to induce the production of numerous ISGs, which elicit antiviral and

immune-regulatory activities. To investigate the effect of PEDV infection on the JAK-STAT signaling pathway, total RNA of FJzz1-infected LLC-PK1 cells was extracted at different time points, and RT-qPCR was conducted to explore the transcriptional levels of IRF9 and STAT1, the key molecules in the JAK-STAT signaling pathway. The results showed that the transcriptional levels of IRF9 and STAT1 were upregulated significantly at 12-24 hpi in time-dependent manners (Figures 3A, B). Western blotting analysis showed that compared with the mock-infected cells, both phosphorylated and non-phosphorylated forms of STAT1 as well as the expression of ISG15, were upregulated markedly in PEDV-infected cells, especially in the late stage of infection (18-24 hpi) (Figure 3C). STAT1 mediates the production of ISGs only when its nuclear translocation occurs from the cytoplasm to the nucleus. To understand the regulation of PEDV to the JAK-STAT1 signaling pathway, we then examined whether PEDV infection induced the STAT1 nuclear translocation. LLC-PK1 cells were mock-infected or infected with FJzz1, and another group of cells was treated with hIFN-α as a positive control, followed by co-staining with anti-STAT1 mAb and anti-PEDV N mAb. As shown in Figure 3D, STAT1 was mainly observed in the cytoplasm of mock-infected cells without hIFN-α treatment. After hIFN-α stimulation, STAT1 was mainly observed in the nuclei of mock-infected cells as anticipated. It is noteworthy that STAT1 could also be observed in the nuclei of FJzz1-infected

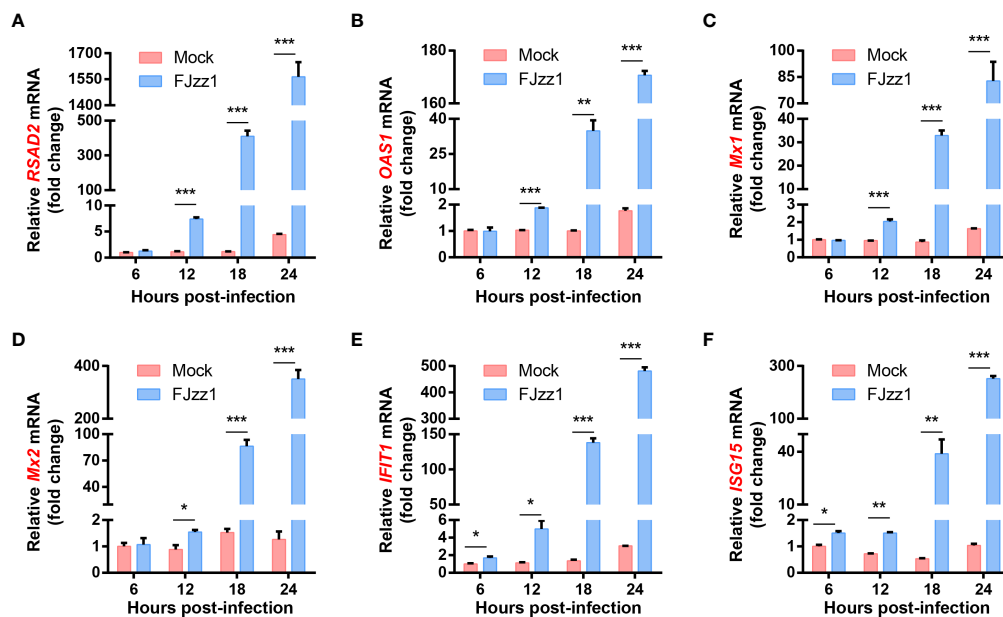


FIGURE 2

FJzz1 infection induced the production of ISGs in LLC-PK1 cells. LLC-PK1 cells were seeded in 12-well plates, followed by mock-infection or FJzz1 infection at an MOI of 0.01. Total cellular RNA was prepared at indicated times post-PEDV infection, and the mRNA levels of RSAD2 (A), OAS1 (B), Mx1 (C), Mx2 (D), IFIT1 (E), and ISG15 (F) were determined by RT-qPCR and normalized to that of porcine GAPDH. These data are representative of the results of at least two independent experiments and error bars represent standard deviations. Asterisks indicate statistical significance. \*,  $P < 0.05$ ; \*\*,  $P < 0.01$ ; \*\*\*,  $P < 0.001$ .

cells, implicating the induction of STAT1 nuclear translocation by FJzz1 infection. Altogether, the JAK-STAT signaling pathway is activated during FJzz1 infection.

## FJzz1 infection induces the production of type I/III IFNs

To further explore the regulation of PEDV infection on the production of type I IFN, total RNA of FJzz1-infected LLC-PK1 cells was extracted at 6, 12, 18 and 24 hpi, and RT-qPCR was performed to examine the IFN- $\beta$  transcription. As shown in Figure 4A, after infection with FJzz1 at MOI of 0.01, the mRNA of IFN- $\beta$  climbed at 12 hpi and culminated at 24 hpi, indicating time-dependent induction of IFN- $\beta$ . Meanwhile, the up-regulation of FJzz1 infection on the production of IFN- $\beta$  was dose-dependent (Figure 4B), demonstrating that FJzz1 infection induces the IFN- $\beta$  production, which was contrary to previous reports (43, 44, 46). To further determine the induction of IFN- $\beta$  by PEDV infection, IFN- $\beta$  responses were evaluated in FJzz1-infected cells including LLC-PK1, ST and Marc-145 simultaneously. The results showed that FJzz1 could induce IFN- $\beta$  production in various cell lines. Meanwhile, FJzz1 infection could also enhance the poly(I:C) induced IFN- $\beta$  production (Figures 4C–E), which was in line with our

conclusion that FJzz1 infection induces the IFN- $\beta$  expression. Type III IFNs play a crucial role in innate antiviral immunity, especially in mucosal immunity induced by intestinal viruses (55–57). Therefore, we also examined the type III IFNs responses in FJzz1-infected LLC-PK1 cells. Interestingly, the mRNA of type III IFNs including IFN- $\lambda$ 1, IFN- $\lambda$ 3 and IFN- $\lambda$ 4 in FJzz1-infected LLC-PK1 cells were upregulated significantly in time-dependent manners with those in mock-infected LLC-PK1 cells (Figures 4F–H). Altogether, FJzz1 infection induces the production of type I/III IFNs in LLC-PK1 cells.

## Both RLRs and TLRs signaling pathways mediated in the production of type I/III IFNs during FJzz1 infection

Antiviral responses in mammals are mediated by type I/III IFNs, which trigger hundreds of ISGs production through the JAK-STAT signaling pathway to establish the antiviral state. Upon virus infection, TLRs and RLRs signaling pathways may be activated. To determine whether TLRs and/or RLRs signaling pathways mediated in the production of I/III IFNs, transcriptional levels of the five key molecules including RIG-I, MDA5, MAVS, MyD88 and TRIF were detected. As shown in Figures 5A–E, transcriptional levels of RIG-I, MDA5, MyD88

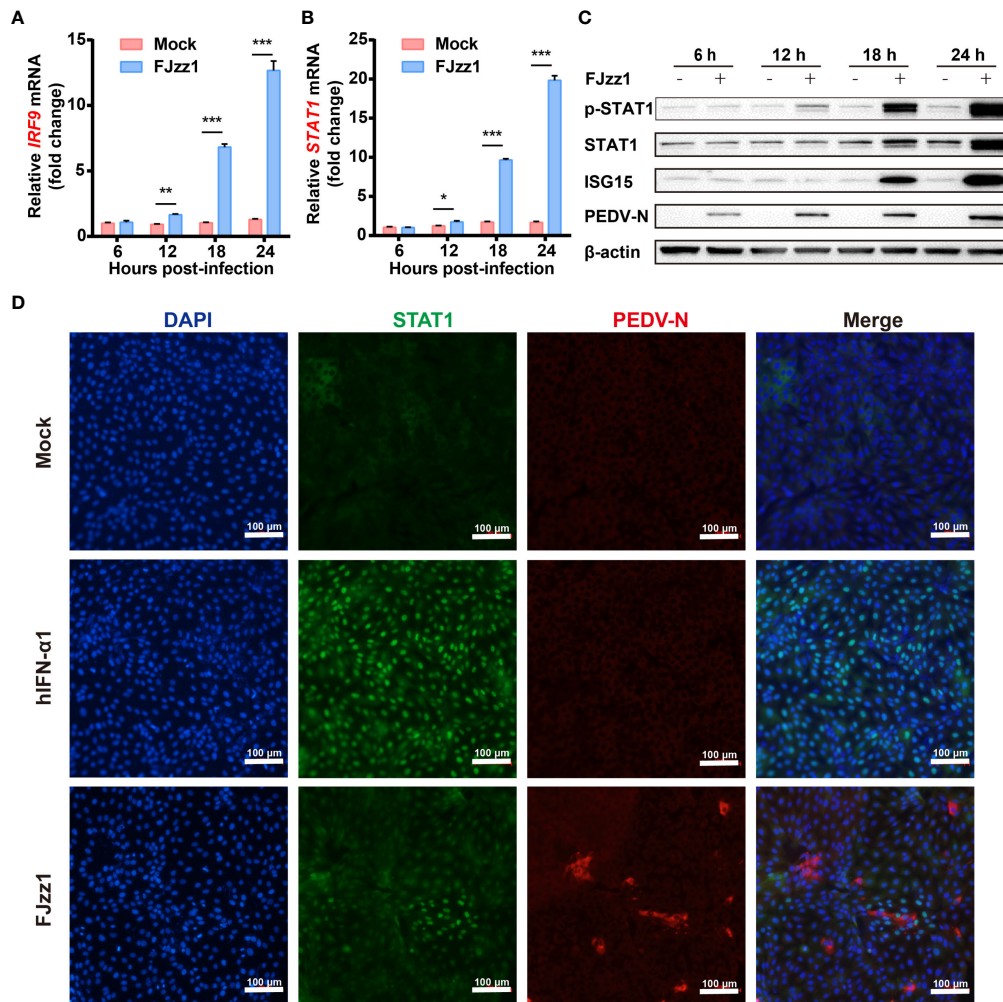


FIGURE 3

JAK-STAT signaling pathway was activated during FJzz1 infection. (A, B) Transcriptional levels of IRF9 and STAT1 in PEDV-infected cells. LLC-PK1 cells were infected with FJzz1 at an MOI of 0.01, and total cellular RNA was prepared at the indicated times post-infection to determine the IRF9 (A) and STAT1 (B) mRNA levels by RT-qPCR. (C) Expression of the phosphorylated and non-phosphorylated forms of STAT1 and the downstream ISG15 in FJzz1-infected LLC-PK1 cells. LLC-PK1 cells were infected with FJzz1 at an MOI of 0.01, and Western blotting was conducted at the indicated times post-infection using an anti-STAT1 antibody, anti-Phospho-STAT1 antibody, and anti-ISG15 antibody, respectively. (D) FJzz1 infection-induced STAT1 nuclear translocation. LLC-PK1 cells were infected with FJzz1 at an MOI of 0.01 for 18 h. Cells were then fixed and stained with anti-STAT1 and anti-N antibodies for 1 h. Alexa Fluor 488-conjugated goat anti-mouse secondary antibody and Alexa Fluor 594-conjugated goat anti-rabbit antibody was used to visualize STAT1, and N. Nuclei were stained with DAPI. Scale bar = 100  $\mu$ m. \*,  $P < 0.05$ ; \*\*,  $P < 0.01$ ; \*\*\*,  $P < 0.001$ .

and TRIF in FJzz1-infected LLC-PK1 cells were upregulated significantly at 12–24 hpi in a time-dependent manner, while the mRNA of MAVS did not change remarkably compared with that of the mock-infected LLC-PK1 cells. We speculated that both RIG-I/MDA5-mediated RLRs signaling pathway and MyD88/TRIF-mediated TLRs signaling pathway might be triggered by FJzz1 infection to produce type I/III IFNs. Specific siRNAs targeting RIG-I, MDA5, MAVS, MyD88, and TRIF, adaptor molecules in the RLRs and TLRs signaling pathways, were synthesized to verify this hypothesis. Transient transfection and RT-qPCR assays were conducted to assess the knockdown

efficiency of each siRNA (Supplementary Figure 3). LLC-PK1 cells were transfected with each siRNA followed by PEDV infection to examine the transcriptional levels of type I/III IFNs under RLRs/TLRs signaling pathways interruption. The results showed that siRNAs targeting RIG-I, MDA5, and TRIF but not MAVS or MyD88 significantly reduced the mRNA of IFN- $\beta$  (Figure 5F), demonstrating that RIG-I/MDA5-mediated RLRs signaling pathway and TRIF-mediated TLRs signaling pathway involved in the production of IFN- $\beta$  during FJzz1 infection. Moreover, the transcriptional levels of IFN- $\lambda$  including IFN- $\lambda$ 1, IFN- $\lambda$ 3 and IFN- $\lambda$ 4 were diminished



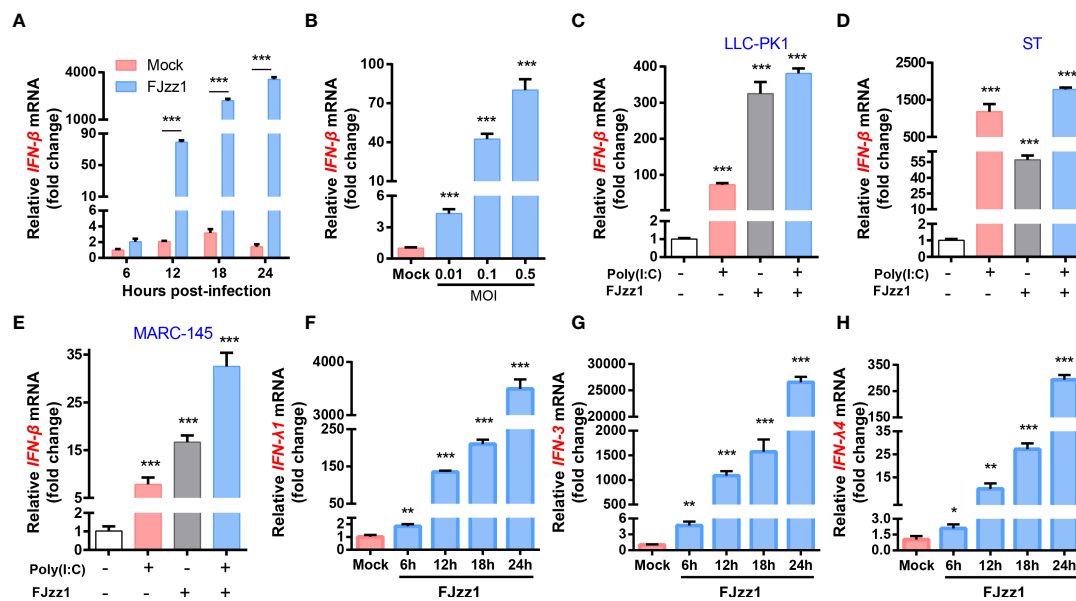


FIGURE 4

FJzz1 infection induced the production of type I and type III IFNs. (A) Transcriptional levels of IFN- $\beta$  in PEDV-infected cells. LLC-PK1 cells were infected with FJzz1 at an MOI of 0.01, and total cellular RNA was prepared at the indicated times post-infection to determine the IFN- $\beta$  mRNA level by RT-qPCR. (B) PEDV infection induced IFN- $\beta$  production in a dose-dependent manner. LLC-PK1 cells were infected with different MOI (0.01, 0.1, 0.5) of FJzz1 for 18 h, and total mRNA was extracted to detect the IFN- $\beta$  mRNA level by RT-qPCR. (C–E) PEDV infection induced IFN- $\beta$  production in different cell lines. LLC-PK1 cells (C), ST cells (E), and MARC-145 cells (E) were infected with FJzz1 at an MOI of 0.01 for 12 h, followed by stimulation with poly(I:C) for 12 h, and total cellular RNA was extracted to detect the IFN- $\beta$  mRNA level by RT-qPCR. (F–H) PEDV infection induced type III IFNs production. LLC-PK1 cells were infected with FJzz1 at an MOI of 0.01, and total cellular RNA was prepared at the indicated times post-infection to determine the mRNA level of IFN- $\lambda$ 1 (F), IFN- $\lambda$ 3 (G), and IFN- $\lambda$ 4 (H) by RT-qPCR. These data are representative of the results of at least two independent experiments and error bars represent standard deviations. Asterisks indicate statistical significance. \*,  $P < 0.05$ ; \*\*,  $P < 0.01$ ; \*\*\*,  $P < 0.001$ .

markedly in cells transfected with siRIG-I, siMDA5, siMyD88 or siTRIF but not MAVS, compared with the siNC following FJzz1 infection (Figures 5G–I), demonstrating that RIG-I/MDA5-mediated RLRs signaling pathway and MyD88/TRIF-mediated TLRs signaling pathway involved in the production of type III IFNs during FJzz1 infection. Altogether, both RLRs and TLRs signaling pathways mediated in the production of type I/III IFNs during FJzz1 infection.

## The expression of ISGs induced by FJzz1 infection depends on the production of type I/III IFNs

To further determine the effect of RLRs/TLRs signaling on PEDV-induced ISGs production, LLC-PK1 cells were transfected with specific siRNAs targeting adaptor molecules in the RLRs and TLRs signaling pathways such as RIG-I, MDA5, MAVS, MyD88 and TRIF, followed by FJzz1 infection, and the expression of various ISGs was analyzed by RT-qPCR. The results showed that knockdown of RIG-I, MDA5, MyD88, or TRIF significantly decreased FJzz1-induced ISGs mRNA expression, including RSAD2, OAS1, Mx1, Mx2, IFIT1, and ISG15 (Figures 6A–F).

Interestingly, we noticed that the transcriptional levels of these ISGs did not decrease or even increase in cells transfected with siRNA targeting MAVS compared with cells transfected with siNC, which was consistent with the appreciable trends of the production of type I/III IFNs. These results further demonstrate that the RIG-I/MDA5-mediated RLRs signaling pathway and MyD88/TRIF-mediated TLRs signaling pathway are involved in the production of ISGs during FJzz1 infection. Considering the consistent production trends between ISGs and type I/III IFNs, we think the expression of ISGs induced by FJzz1 infection depends on the production of type I/III IFNs.

## Discussion

The first line of defense against viral infection and replication is the innate immune system, in which ISGs are the major components for the establishment of a host antiviral state (58). Many ISGs have been reported to suppress viral replication through diverse mechanisms (59–63). In the present study, we found that the mRNA expressions of ISGs including RSAD2, OAS1, Mx1, Mx2, IFIT1, and ISG15 in FJzz1-infected LLC-PK1 cells were upregulated significantly in dose-dependent manners,

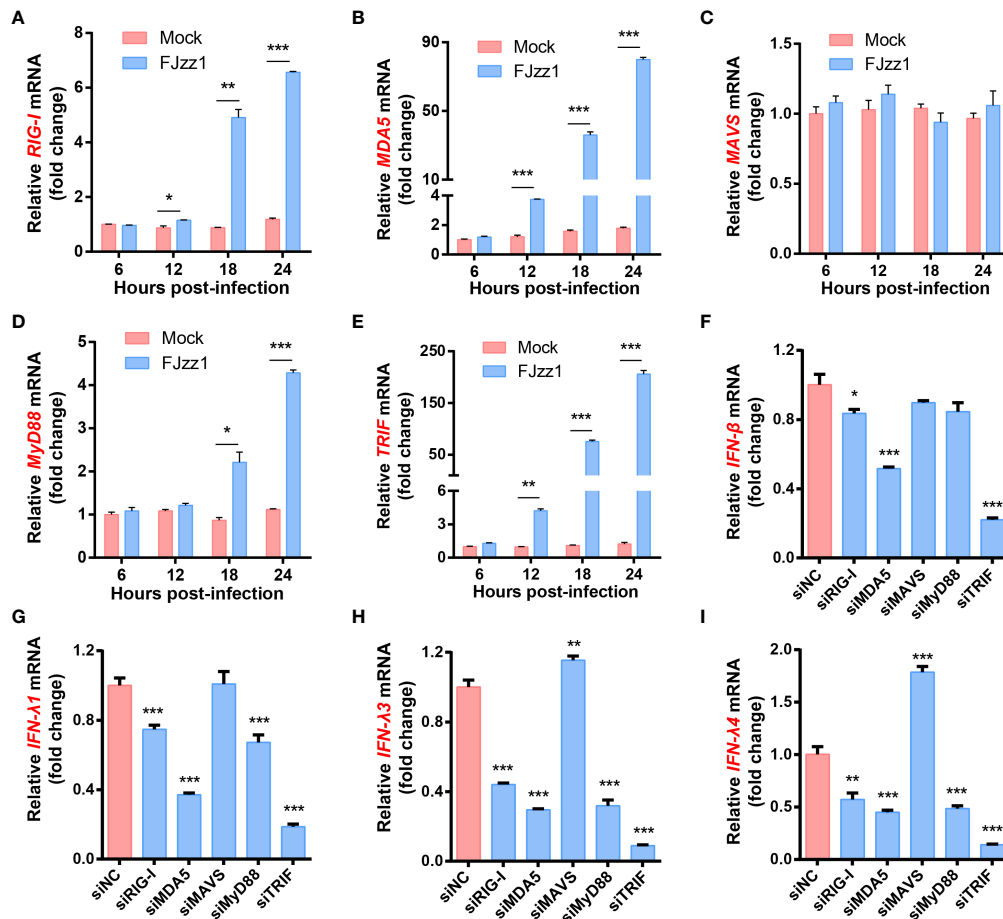


FIGURE 5

FJzz1 infection induced the production of type I/III IFNs through RLRs and TLRs signaling pathways. (A–E) FJzz1 infection increased the production of RIG-I, MDA5, MAVS, MyD88, and TRIF. LLC-PK1 cells were infected with FJzz1 at an MOI of 0.01, and total cellular RNA was prepared at the indicated times post-infection to determine the mRNA level of RIG-I (A), MDA5 (B), MAVS (C), MyD88 (D), and TRIF (E) by RT-qPCR. (F–I) RLRs and TLRs signaling pathways mediated in the production of type I/III IFNs. LLC-PK1 cells were transfected with 80 nM specific siRNA targeting RIG-I, MDA5, MAVS, MyD88, TRIF, or an NC siRNA for 24 h, and then cells were mocked or PEDV-infected (MOI=0.01). At 18 hpi, total cellular RNA was extracted to determine the mRNA level of IFN-β (F), IFN-λ1 (G), IFN-λ3 (H), and IFN-λ4 (I) by RT-qPCR. These data are representative of the results of at least two independent experiments and error bars represent standard deviations. Asterisks indicate statistical significance. \*,  $P < 0.05$ ; \*\*,  $P < 0.01$ ; \*\*\*,  $P < 0.001$ .

indicating that the innate immune responses mediated by ISGs were induced and activated by FJzz1 infection. Remarkably, RSAD2 and ISG15 were confirmed to inhibit CV777 replication in Vero E6 cells through functional analysis (64). Therefore, we speculated that the abundant ISGs induced by PEDV infection might display excellent antiviral activities. Although the invasion of PEDV could not induce efficient ISGs transcription in the early stage of infection (6 hpi), the mRNA of ISGs increased for hundred times in the late stage of FJzz1 infection (18–24 hpi) (Figure 2). Coincidentally, the up-regulation induced by PEDV infection could also be found in other studies. For example, the mRNA expression of the Mx1 gene in PEDV-infected IPEC-J2 cells was significantly increased after 48 h of CV777 infection as measured by RT-qPCR, and the

transcription trend of the Mx1 gene was parallel with the increase of viral RNA (65). In addition, several ISGs were identified to increase significantly in porcine jejunum tissues in response to a virulent strain of PEDV and its attenuated strain through comparative proteome analysis (47). Moreover, both endoribonuclease-deficient PEDV and wild-type PEDV infections induce robust expression of ISGs and proinflammatory cytokines in PK1 cells (30). However, PEDV proliferation was too fast that the adequate ISGs produced by host cells failed to inhibit PEDV replication in the late stage of infection. The interplay between PEDV infection and the host's innate immune responses is so complicated that further investigations are needed to elucidate the modulation of ISGs during PEDV infection.

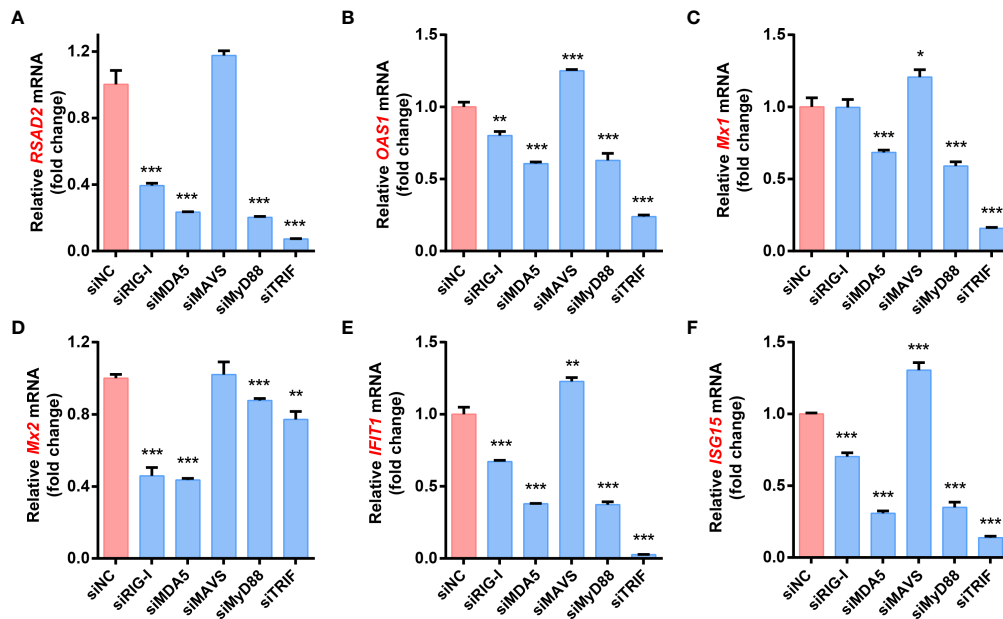


FIGURE 6

RLRs and TLRs signaling pathways are involved in the production of ISGs during FJzz1 infection. LLC-PK1 cells were infected with FJzz1 at an MOI of 0.01 for 18 h, and total cellular RNA was extracted to determine the mRNA level of RSAD2 (A), OAS1 (B), Mx1 (C), Mx2 (D), IFIT1 (E), and ISG15 (F) by RT-qPCR. These data are representative of the results of three independent experiments and error bars represent standard deviations. Asterisks indicate statistical significance. \*,  $P < 0.05$ ; \*\*,  $P < 0.01$ ; \*\*\*,  $P < 0.001$ .

The production of ISGs mainly depends on the activation of the JAK-STAT signaling pathway, in which the recruited upstream signals activate JAK1 and Tyk2, leading to the phosphorylation of the STAT proteins, such as STAT1 and STAT2. Subsequently, phosphorylated STAT1 and STAT2 form heterodimers and then combine with IRF9 to form IFN-stimulated gene factor 3 (ISGF-3), a transcriptional complex that could translocate into the nucleus and bind to the IFN-stimulated response elements, resulting in the production of abundant ISGs (66, 67). In this study, we observed that the transcriptional level of STAT1 was increased in FJzz1-infected LLC-PK1 cells, and the consistent conclusion could also be reported in PEDV-infected Vero and IPEC-J2 cells in other studies (65, 68). Moreover, compared with the mock-infected group, both phosphorylated and non-phosphorylated forms of STAT1 were upregulated significantly in FJzz1-infected LLC-PK1 cells in time-dependent manners. Conversely, Guo et al. demonstrated that STAT1 expression was markedly reduced in a proteasome-dependent manner without inhibiting STAT1 transcription in PEDV-infected Vero and IPEC-J2 cells (68). In our perspective, these conflicting results are most likely due to the different cell lines or the different PEDV strains. With these in mind, more integrated and detailed studies of strain-resolved or even single-cell-resolved responses to the JAK-STAT signaling pathway are needed to aid in understanding the modulations of host innate immune response to PEDV infection.

In terms of different cell lines involved in the interaction between host and PEDV infection, Vero cells are widely used as a suitable cell model for PEDV isolation and propagation *in vitro* (8, 69). However, they are not suitable for studies of PEDV-cell interactions, especially innate immunity during PEDV infection, because of the chromosomal defectiveness of type I IFNs (70, 71). Zhang et al. demonstrated that MARC-145, a subline of African green monkey kidney cells, was an alternative cell line that supports PEDV replication with typical CPE characterized by syncytium formation (43), which was similar to that in Vero cells. PEDV mainly infects the intestinal tract of piglets, where villous epithelial cells are regarded as the primary target cells *in vivo* for PEDV. IPEC-J2, a nonhomogeneous porcine intestinal epithelial cell line, was isolated from the jejunum of neonatal piglets. Although several studies reported the susceptibility of IPEC-J2 cells to PEDV (46, 68, 72), we found that IPEC-J2 cells possessed very low efficiencies of infection by PEDV through IFA and Western blotting experiments. Coincidentally, the controversial susceptibility of IPEC-J2 cells to PEDV was also reported in other studies (44, 73). Considering the species specificity and efficiency of infection, we determined to use LLC-PK1, a kind of porcine kidney epithelial cells, to study the innate immune responses upon PEDV infection. In this study, our results showed that FJzz1 could infect LLC-PK1 cells and have good proliferation, which was in line with other studies (30, 53, 54). Moreover, LLC-PK1 cells have been identified to

have the ability to express a high level of ISGs and type I/III IFNs in this and other studies (30, 53), demonstrating that LLC-PK1 cells are a suitable cell model for the study of the interactions between innate immunity and PEDV infection *in vitro*. Recently, the nonhomogeneous IPEC-J2 cells were subcloned by limited serial dilutions to obtain a homogeneous cell population, named IPEC-DQ, which were susceptible to PEDV infection with high efficiency and expressed high levels of ISGs and type I/III IFNs (44, 45, 74). Therefore, IPEC-DQ cells may be the optimal cell model for the study of innate immunity possibly modulated by enteric coronavirus including PEDV and TGEV in the future.

To establish persistent infection, viruses have developed diverse molecular mechanisms to evade or disrupt the host's innate immune response, particularly by inhibition or disruption of IFN signaling cascades (38, 75, 76). PEDV, as a member of the Coronaviridae, also encodes some proteins that serve as IFNs antagonists. PEDV papain-like protease 2 was reported firstly as a type I IFN antagonist, which negatively regulated RIG-I and STING mediated IFN- $\beta$  expression (77). PEDV N protein antagonizes IFN- $\beta$  production by sequestering the interaction between IRF3 and TBK1 (42), and PEDV-encoded 3C-like protease, nsp5 regulates its IFN antagonism by cleaving NEMO (78). It is worth noting that nsp1 can inhibit type I and III IFNs production by different molecular mechanisms (43, 44), indicating the important role of nsp1 in suppressing innate immunity upon PEDV infection. Moreover, PEDV nsp15 can directly degrade the RNA levels of TBK1 and IRF3 dependent on its endoribonuclease activity to suppress IFN production and constrain the ISGs, by which PEDV antagonizes the host innate response to facilitate its replication (79). Recently, a study reported that PEDV nsp7 antagonized IFN- $\alpha$ -induced IFN signaling by competing with KPNA1 for binding to STAT1, thereby revealing a new mechanism developed by PEDV to inhibit the type I IFN signaling pathway (80). These identified IFN antagonists may contribute to the delay of type I/III IFNs transcriptions in the early stage of PEDV infection. However, the present study showed that the mRNA of type I/III IFNs was upregulated significantly in a time-depend manner, suggesting that these antagonists could not limit the production of type I/III IFNs, especially in the late stage of infection. Further studies demonstrated that RLRs and TLRs-mediated pathways were involved in the high levels of type-I/III IFNs productions, which triggered abundant ISGs by activating the JAK-STAT signaling pathway. It is confusing that the adequate type-I/III IFNs and ISGs transcription failed to suppress PEDV replication in the late stage, although many type-I/III IFNs antagonists were highly expressed at the same time. Interestingly, this surprising phenomenon could also be found in TGEV infection (25). In this study, we proposed for the first time that FJzz1 did not suppress type-I/III IFNs induction at the early stage of infection and induced abundant type-I/III IFNs production in the peak of FJzz1 replication, which was contrary to several reports that PEDV infection inhibited type-I/III IFNs production (43, 44,

46). In our opinion, these differences may result from the different PEDV strains. So far, most of the strains used to study the interaction between PEDV and host innate immune responses have been concentrated in CV777, AJ1102, USA/Colorado/2013, and PC22A strains, which had 97.1%, 99.1%, 98.9%, and 98.9% nucleotide homology with FJzz1, respectively (Supplementary Table 1). Moreover, compared with the identified type I/III IFNs antagonists including nsp3, nsp15, and nsp16 of CV777 (77, 79, 81), nsp5, nsp7, and N of AJ1102 (42, 78, 80), nsp1, nsp14 and nsp15 of USA/Colorado/2013 (30, 43–45), as well as nsp16 of PC22A (82), many amino acid mutations occurred in those of FJzz1. We speculate that these mutations between FJzz1 and other PEDV strains may lead to the difference in modulations of host innate immune responses to PEDV infection, which should be confirmed by further experiments, including reverse genetic analyses. Meanwhile, we observed the induction of type-I/III IFNs in LLC-PK1 cells infected by FJzz1-F200 (Supplementary Figure 3), an attenuated FJzz1 strain that was obtained *via* serially passaging *in vitro* (51), suggesting that the attenuated FJzz1-F200 may have the potential for developing PEDV live-attenuated vaccines.

In summary, our data demonstrate for the first time that FJzz1 infection induces the production of type-I/III IFNs in LLC-PK1 cells, which depends on the mediation of RLRs and TLRs signaling pathways. Subsequently, the downstream JAK-STAT signaling cascade is activated, triggering the production of a large number of ISGs to exert antiviral effects. This study provides new insight into the interaction between PEDV and host's natural immune responses.

## Data availability statement

The original contributions presented in the study are included in the article/Supplementary Material. Further inquiries can be directed to the corresponding authors.

## Author contributions

PC and YZ conceived and designed the experiments. PC, JZ, and JY performed the experiments. PC, RL, and ML analyzed the data. LY, FG, YJ, CL, and WT contributed reagents/materials/analysis tools. HL, GT, and YZ participated in analysis and discussion. PC wrote the paper. YZ and GT checked and finalized the manuscript. All authors contributed to the article and approved the submitted version.

## Funding

The study was supported by the National Natural Science Foundation of China (32102657, 31472207), the Shanghai Youth

Scientific and Technological Yang Fan Program Grant (20YF1457800), the China Postdoctoral Science Foundation (2020M670555), Shanghai Municipal Agriculture Science and Technology Project (2020-02-08-00-08-F01465), and China Agriculture Research System of MOF and MARA (NYCYTX-009).

## Conflict of interest

The authors declare that the research was conducted in the absence of any commercial or financial relationships that could be construed as a potential conflict of interest.

## Publisher's note

All claims expressed in this article are solely those of the authors and do not necessarily represent those of their affiliated organizations, or those of the publisher, the editors and the reviewers. Any product that may be evaluated in this article, or claim that may be made by its manufacturer, is not guaranteed or endorsed by the publisher.

## Supplementary material

The Supplementary Material for this article can be found online at: <https://www.frontiersin.org/articles/10.3389/fimmu.2022.984448/full#supplementary-material>

## References

- Wood EN. An apparently new syndrome of porcine epidemic diarrhoea. *Vet Rec* (1977) 100:243–4. doi: 10.1136/vr.100.12.243
- Coussemont W, Ducatelle R, Debouck P, Hoorens J. Pathology of experimental CV777 coronavirus enteritis in piglets. i. histological and histochemical study. *Vet Pathol* (1982) 19:46–56. doi: 10.1177/030098588201900108
- Shibata I, Tsuda T, Mori M, Ono M, Sueyoshi M, Uruno K. Isolation of porcine epidemic diarrhoea virus in porcine cell cultures and experimental infection of pigs of different ages. *Vet Microbiol* (2000) 72:173–82. doi: 10.1016/S0378-1135(99)00199-6
- Pensaert MB, de Bouck P. A new coronavirus-like particle associated with diarrhoea in swine. *Arch Virol* (1978) 58:243–7. doi: 10.1007/BF01317606
- Horvath I, Mocsari E. Ultrastructural changes in the small intestinal epithelium of suckling pigs affected with a transmissible gastroenteritis (TGE)-like disease. *Arch Virol* (1981) 68:103–13. doi: 10.1007/BF01314440
- Pospischil A, Hess RG, Bachmann PA. Light microscopy and ultrahistology of intestinal changes in pigs infected with epizootic diarrhoea virus (EVD): comparison with transmissible gastroenteritis (TGE) virus and porcine rotavirus infections. *Zentralbl Veterinarmed B* (1981) 28:564–77. doi: 10.1111/j.1439-0450.1981.tb01774.x
- Takahashi K, Okada K, Ohshima K. An outbreak of swine diarrhoea of a new-type associated with coronavirus-like particles in Japan. *Nihon Juigaku Zasshi* (1983) 45:829–32. doi: 10.1292/jvms1939.45.829
- Kusanagi K, Kuwahara H, Katoh T, Nunoya T, Ishikawa Y, Samejima T, et al. Isolation and serial propagation of porcine epidemic diarrhoea virus in cell cultures

### SUPPLEMENTARY FIGURE 1

The comparison of the dysregulated proteins in FJzz1-infected LLC-PK1 cells. LLC-PK1 cells were mock-infected or infected with FJzz1 at an MOI of 0.01 for 18 h, and all cells were collected to perform the TMT labeled comparative proteomic analysis. The heatmap shows the relative expression level of the dysregulated proteins in both Mock- and FJzz1-infected LLC-PK1 cells (Log<sub>2</sub> fold-change).

### SUPPLEMENTARY FIGURE 2

FJzz1 infection induced the production of ISGs in LLC-PK1 cells in a dose-dependent manner. LLC-PK1 cells were infected with different MOI (0.01, 0.1, 0.5) of FJzz1 for 18 h, and total cellular RNA was extracted to determine the mRNA level of RSAD2 (A), OAS1 (B), Mx1 (C), Mx2 (D), IFIT1 (E), and ISG15 (F) by RT-qPCR. These data are representative of the results of three independent experiments, and error bars represent standard deviations. Asterisks indicate statistical significance. \*\*\*,  $P < 0.001$ .

### SUPPLEMENTARY FIGURE 3

siRNA interference. LLC-PK1 cells were transfected with 80 nM specific siRNA targeting RIG-I, MDA5, MAVS, MyD88, TRIF, or an NC siRNA for 24 h, and then cellular RNA was extracted for analysis of RIG-I (A), MDA5 (B), MAVS (C), MyD88 (D), and TRIF (E) mRNA levels by RT-qPCR. These data are representative of the results of three independent experiments, and error bars represent standard deviations. Asterisks indicate statistical significance. \*\*\*,  $P < 0.001$ .

### SUPPLEMENTARY FIGURE 4

The attenuated strain FJzz1-F200 infection induced the production of type I and type III IFNs. (A–D) Transcriptional levels of IFN- $\beta$ , IFN- $\lambda$ 1, IFN- $\lambda$ 3, and IFN- $\lambda$ 4 in PEDV-infected cells. LLC-PK1 cells were infected with FJzz1-F200 at an MOI of 0.01, and total cellular RNA was prepared at 18 hpi to determine the mRNA level of IFN- $\beta$  (A), IFN- $\lambda$ 1 (B), IFN- $\lambda$ 3 (C) and IFN- $\lambda$ 4 (D) by RT-qPCR. These data are representative of the results of three independent experiments and error bars represent standard deviations. Asterisks indicate statistical significance. \*\*\*,  $P < 0.001$ .

### SUPPLEMENTARY TABLE 1

Nucleotide and amino acid homology analysis of the FJzz1 strain.

and partial characterization of the isolate. *J Vet Med Sci* (1992) 54:313–8. doi: 10.1292/jvms.54.313

9. Smid B, Valicek L, Rodak L, Kudrna J, Musilova J. [Detection of porcine epidemic diarrhoea virus using electron microscopy in the Czech republic]. *Vet Med (Praha)* (1993) 38:333–41.

10. Ben Salem AN, Chupin Sergei A, Bjadovskaya Olga P, Andreeva Olga G, Mahjoub A, Prokhvatilova Larissa B. Multiplex nested RT-PCR for the detection of porcine enteric viruses. *J Virol Methods* (2010) 165:283–93. doi: 10.1016/j.jviromet.2010.02.010

11. Li W, Li H, Liu Y, Pan Y, Deng F, Song Y, et al. New variants of porcine epidemic diarrhoea virus, China 2011. *Emerg Infect Dis* (2012) 18:1350–3. doi: 10.3201/eid1803.120002

12. Sun RQ, Cai RJ, Chen YQ, Liang PS, Chen DK, Song CX. Outbreak of porcine epidemic diarrhoea in suckling piglets, China. *Emerg Infect Dis* (2012) 18:161–3. doi: 10.3201/eid1801.111259

13. Zhou YJ, Wu YL, Zhu JP, Tong W, Yu H, Jiang YF, et al. Complete genome sequence of a virulent porcine epidemic diarrhoea virus strain. *J Virol* (2012) 86:13862. doi: 10.1128/JVI.02635-12

14. Lee S, Lee C. Outbreak-related porcine epidemic diarrhoea virus strains similar to US strains, south korea. *Emerg Infect Dis* (2014) 20:1223–6. doi: 10.3201/eid2007.140294

15. Vlasova AN, Marthaler D, Wang Q, Culhane MR, Rossow KD, Rovira A, et al. Distinct characteristics and complex evolution of pedv strains, north america, may 2013–february 2014. *Emerg Infect Dis* (2014) 20:1620–8. doi: 10.3201/eid2010.140491

16. Song D, Huang D, Peng Q, Huang T, Chen Y, Zhang T, et al. Molecular characterization and phylogenetic analysis of porcine epidemic diarrhoea viruses associated with outbreaks of severe diarrhoea in piglets in Jiangxi, China 2013. *PLoS One* (2015) 10:e0120310. doi: 10.1371/journal.pone.0120310

17. Zhang Y, Chen Y, Yuan W, Peng Q, Zhang F, Ye Y, et al. Evaluation of cross-protection between g1a- and g2a-genotype porcine epidemic diarrhea viruses in suckling piglets. *Anim (Basel)* (2020) 10:1674. doi: 10.3390/ani10091674
18. Song D, Park B. Porcine epidemic diarrhoea virus: a comprehensive review of molecular epidemiology, diagnosis, and vaccines. *Virus Genes* (2012) 44:167–75. doi: 10.1007/s11262-012-0713-1
19. Kocherhans R, Bridgen A, Ackermann M, Tobler K. Completion of the porcine epidemic diarrhoea coronavirus (PEDV) genome sequence. *Virus Genes* (2001) 23:137–44. doi: 10.1023/A:1011831902219
20. Hou Y, Wang Q. Emerging highly virulent porcine epidemic diarrhea virus: Molecular mechanisms of attenuation and rational design of live attenuated vaccines. *Int J Mol Sci* (2019) 20:5478. doi: 10.3390/ijms20215478
21. O'Neill LA, Bowie AG. Sensing and signaling in antiviral innate immunity. *Curr Biol* (2010) 20:R328–333. doi: 10.1016/j.cub.2010.01.044
22. Arpaia N, Barton GM. Toll-like receptors: key players in antiviral immunity. *Curr Opin Virol* (2011) 1:447–54. doi: 10.1016/j.coviro.2011.10.006
23. Loo YM, Gale MJr. Immune signaling by RIG-I-like receptors. *Immunity* (2011) 34:680–92. doi: 10.1016/j.immuni.2011.05.003
24. Wong MT, Chen SS. Emerging roles of interferon-stimulated genes in the innate immune response to hepatitis C virus infection. *Cell Mol Immunol* (2016) 13:11–35. doi: 10.1038/cmi.2014.127
25. Zhu L, Yang X, Mou C, Yang Q. Transmissible gastroenteritis virus does not suppress IFN-beta induction but is sensitive to IFN in IPEC-J2 cells. *Vet Microbiol* (2017) 199:128–34. doi: 10.1016/j.vetmic.2016.12.031
26. Lazear HM, Nice TJ, Diamond MS. Interferon-lambda: immune functions at barrier surfaces and beyond. *Immunity* (2015) 43:15–28. doi: 10.1016/j.immuni.2015.07.001
27. Wack A, Terczynska-Dyla E, Hartmann R. Guarding the frontiers: the biology of type III interferons. *Nat Immunol* (2015) 16:802–9. doi: 10.1038/ni.3212
28. Lee S, Baldrige MT. Interferon-lambda: a potent regulator of intestinal viral infections. *Front Immunol* (2017) 8:749. doi: 10.3389/fimmu.2017.00749
29. Zhang L, Jilg N, Shao RX, Lin W, Fusco DN, Zhao H, et al. IL28B inhibits hepatitis C virus replication through the JAK-STAT pathway. *J Hepatol* (2011) 55:289–98. doi: 10.1016/j.jhep.2010.11.019
30. Deng X, van Geelen A, Buckley AC, O'Brien A, Pillatzki A, Lager KM, et al. Coronavirus endoribonuclease activity in porcine epidemic diarrhea virus suppresses type I and type III interferon responses. *J Virol* (2019) 93:e02000–18. doi: 10.1128/JVI.02000-18
31. Duggal NK, Emerman M. Evolutionary conflicts between viruses and restriction factors shape immunity. *Nat Rev Immunol* (2012) 12:687–95. doi: 10.1038/nri3295
32. Perlman S, Netland J. Coronaviruses post-SARS: update on replication and pathogenesis. *Nat Rev Microbiol* (2009) 7:439–50. doi: 10.1038/nrmicro2147
33. Fehr AR, Perlman S. Coronaviruses: an overview of their replication and pathogenesis. *Methods Mol Biol* (2015) 1282:1–23. doi: 10.1007/978-1-4939-2438-7\_1
34. Niemeyer D, Zillinger T, Muth D, Zieleski F, Horvath G, Suliman T, et al. Middle East respiratory syndrome coronavirus accessory protein 4a is a type I interferon antagonist. *J Virol* (2013) 87:12489–95. doi: 10.1128/JVI.01845-13
35. Yang Y, Zhang L, Geng H, Deng Y, Huang B, Guo Y, et al. The structural and accessory proteins m, ORF 4a, ORF 4b, and ORF 5 of middle East respiratory syndrome coronavirus (MERS-CoV) are potent interferon antagonists. *Protein Cell* (2013) 4:951–61. doi: 10.1007/s13238-013-3096-8
36. Ye Y, Hauns K, Langland JO, Jacobs BL, Hogue BG. Mouse hepatitis coronavirus A59 nucleocapsid protein is a type I interferon antagonist. *J Virol* (2007) 81:2554–63. doi: 10.1128/JVI.01634-06
37. Koetzner CA, Kuo L, Goebel SJ, Dean AB, Parker MM, Masters PS. Accessory protein 5a is a major antagonist of the antiviral action of interferon against murine coronavirus. *J Virol* (2010) 84:8262–74. doi: 10.1128/JVI.00385-10
38. Totura AL, Baric RS. SARS coronavirus pathogenesis: host innate immune responses and viral antagonism of interferon. *Curr Opin Virol* (2012) 2:264–75. doi: 10.1016/j.coviro.2012.04.004
39. Li JY, Liao CH, Wang Q, Tan YJ, Luo R, Qiu Y, et al. The ORF6, ORF8 and nucleocapsid proteins of SARS-CoV-2 inhibit type I interferon signaling pathway. *Virus Res* (2020) 286:198074. doi: 10.1016/j.virusres.2020.198074
40. Yuen CK, Lam JY, Wong WM, Mak LF, Wang X, Chu H, et al. SARS-CoV-2 nsp13, nsp14, nsp15 and orf6 function as potent interferon antagonists. *Emerg Microbes Infect* (2020) 9:1418–28. doi: 10.1080/22221751.2020.1780953
41. Zheng Y, Zhuang MW, Han L, Zhang J, Nan ML, Zhan P, et al. Severe acute respiratory syndrome coronavirus 2 (SARS-CoV-2) membrane (M) protein inhibits type I and III interferon production by targeting RIG-I/MDA-5 signaling. *Signal Transduct Target Ther* (2020) 5:299. doi: 10.1038/s41392-020-00438-7
42. Ding Z, Fang L, Jing H, Zeng S, Wang D, Liu L, et al. Porcine epidemic diarrhea virus nucleocapsid protein antagonizes beta interferon production by sequestering the interaction between IRF3 and TBK1. *J Virol* (2014) 88:8936–45. doi: 10.1128/JVI.00700-14
43. Zhang Q, Shi K, Yoo D. Suppression of type I interferon production by porcine epidemic diarrhea virus and degradation of CREB-binding protein by nsp1. *Virology* (2016) 489:252–68. doi: 10.1016/j.virol.2015.12.010
44. Zhang Q, Ke H, Blikslager A, Fujita T, Yoo D. Type III interferon restriction by porcine epidemic diarrhea virus and the role of viral protein nsp1 in IRF1 signaling. *J Virol* (2018) 92:e10677–17. doi: 10.1128/JVI.01677-17
45. Lu Y, Cai H, Lu M, Ma Y, Li A, Gao Y, et al. Porcine epidemic diarrhea virus deficient in rna cap guanine-n-7 methylation is attenuated and induces higher type i and iii interferon responses. *J Virol* (2020) 94:e00447–20. doi: 10.1128/JVI.00447-20
46. Cao L, Ge X, Gao Y, Herrler G, Ren Y, Ren X, et al. Porcine epidemic diarrhea virus inhibits dsRNA-induced interferon-beta production in porcine intestinal epithelial cells by blockade of the RIG-I-mediated pathway. *Virol J* (2015) 12:127. doi: 10.1186/s12985-015-0345-x
47. Li Z, Chen F, Ye S, Guo X, Muhammmad Memon A, Wu M, et al. Comparative proteome analysis of porcine epidemic diarrhea virus strains in response to a virulent strain of porcine epidemic diarrhea virus and its attenuated strain. *Viruses* (2016) 8:323. doi: 10.3390/v8120323
48. Wu M, Zhang Q, Yi D, Wu T, Chen H, Guo S, et al. Quantitative proteomic analysis reveals antiviral and anti-inflammatory effects of puerarin in piglets infected with porcine epidemic diarrhea virus. *Front Immunol* (2020) 11:169. doi: 10.3389/fimmu.2020.00169
49. Wang K, Xie C, Zhang J, Zhang W, Yang D, Yu L, et al. The identification and characterization of two novel epitopes on the nucleocapsid protein of the porcine epidemic diarrhea virus. *Sci Rep* (2016) 6:39010. doi: 10.1038/srep39010
50. Chen P, Wang K, Hou Y, Li H, Li X, Yu L, et al. Genetic evolution analysis and pathogenicity assessment of porcine epidemic diarrhea virus strains circulating in part of China during 2011–2017. *Infect Genet Evol* (2019) 69:153–65. doi: 10.1016/j.meegid.2019.01.022
51. Chen P, Zhao X, Zhou S, Zhou T, Tan X, Wu X, et al. A virulent pedv strain fjz1 with genomic mutations and deletions at the high passage level was attenuated in piglets via serial passage *in vitro*. *Virol Sin* (2021) 36:1052–65. doi: 10.1007/s12250-021-00368-w
52. Ding Z, An K, Xie L, Wu W, Zhang R, Wang D, et al. Transmissible gastroenteritis virus infection induces NF-kappaB activation through RLR-mediated signaling. *Virology* (2017) 507:170–8. doi: 10.1016/j.virol.2017.04.024
53. Zhang Q, Ma J, Yoo D. Inhibition of NF-kappaB activity by the porcine epidemic diarrhea virus nonstructural protein 1 for innate immune evasion. *Virology* (2017) 510:111–26. doi: 10.1016/j.virol.2017.07.009
54. Kong N, Shan T, Wang H, Jiao Y, Zuo Y, Li L, et al. BST2 suppresses porcine epidemic diarrhea virus replication by targeting and degrading virus nucleocapsid protein with selective autophagy. *Autophagy* (2020) 16:1737–52. doi: 10.1080/15458627.2019.1707487
55. Mordstein M, Neugebauer E, Ditt V, Jessen B, Rieger T, Falcone V, et al. Lambda interferon renders epithelial cells of the respiratory and gastrointestinal tracts resistant to viral infections. *J Virol* (2010) 84:5670–7. doi: 10.1128/JVI.00272-10
56. Pott J, Mahlakoiv T, Mordstein M, Duerr CU, Michiels T, Stockinger S, et al. IFN-lambda determines the intestinal epithelial antiviral host defense. *Proc Natl Acad Sci U S A* (2011) 108:7944–9. doi: 10.1073/pnas.1100552108
57. Hernandez PP, Mahlakoiv T, Yang I, Schwierzeck V, Nguyen N, Guendel F, et al. Interferon-lambda and interleukin 22 act synergistically for the induction of interferon-stimulated genes and control of rotavirus infection. *Nat Immunol* (2015) 16:698–707. doi: 10.1038/ni.3180
58. Stark GR, Darnell JE Jr. The JAK-STAT pathway at twenty. *Immunity* (2012) 36:503–14. doi: 10.1016/j.immuni.2012.03.013
59. Reynaud JM, Kim DY, Atasheva S, Rasaloukaya A, White JP, Diamond MS, et al. IFIT1 differentially interferes with translation and replication of alphavirus genomes and promotes induction of type I interferon. *PLoS Pathog* (2015) 11: e1004863. doi: 10.1371/journal.ppat.1004863
60. Zhao J, Feng N, Li Z, Wang P, Qi Z, Liang W, et al. 2',5'-oligoadenylate synthetase 1(OAS1) inhibits PRRSV replication in Marc-145 cells. *Antiviral Res* (2016) 132:268–73. doi: 10.1016/j.antiviral.2016.07.001
61. Scholte FEM, Zivcec M, Dzimiński JV, Deaton MK, Spengler JR, Welch SR, et al. Crimean-Congo hemorrhagic fever virus suppresses innate immune responses via a ubiquitin and isg15 specific protease. *Cell Rep* (2017) 20:2396–407. doi: 10.1016/j.celrep.2017.08.040
62. Yogarajah T, Ong KC, Perera D, Wong KT. RSAD2 and AIM2 modulate coxsackievirus A16 and enterovirus A71 replication in neuronal cells in different ways that may be associated with their 5' nontranslated regions. *J Virol* (2018) 92: e01914-17. doi: 10.1128/JVI.01914-17

63. Zhou J, Chen J, Zhang XM, Gao ZC, Liu CC, Zhang YN, et al. Porcine mx1 protein inhibits classical swine fever virus replication by targeting nonstructural protein ns5b. *J Virol* (2018) 92:e02147-17. doi: 10.1128/JVI.02147-17
64. Zhao M, Li L, Zhai L, Yue Q, Liu H, Ren S, et al. Comparative transcriptomic and proteomic analyses prove that ifn-lambda1 is a more potent inducer of isgs than ifn-alpha against porcine epidemic diarrhea virus in porcine intestinal epithelial cells. *J Proteome Res* (2020) 19:3697-707. doi: 10.1021/acs.jproteome.0c00164
65. Hu Z, Li Y, Du H, Ren J, Zheng X, Wei K, et al. Transcriptome analysis reveals modulation of the STAT family in PEDV-infected IPEC-J2 cells. *BMC Genomics* (2020) 21:891. doi: 10.1186/s12864-020-07306-2
66. Kessler DS, Levy DE, Darnell JE Jr. Two interferon-induced nuclear factors bind a single promoter element in interferon-stimulated genes. *Proc Natl Acad Sci USA* (1988) 85:8521-5. doi: 10.1073/pnas.85.22.8521
67. Fu XY, Kessler DS, Veals SA, Levy DE, Darnell JE Jr. ISGF3, the transcriptional activator induced by interferon alpha, consists of multiple interacting polypeptide chains. *Proc Natl Acad Sci USA* (1990) 87:8555-9. doi: 10.1073/pnas.87.21.8555
68. Guo L, Luo X, Li R, Xu Y, Zhang J, Ge J, et al. Porcine epidemic diarrhea virus infection inhibits interferon signaling by targeted degradation of stat1. *J Virol* (2016) 90:8281-92. doi: 10.1128/JVI.01091-16
69. Hofmann M, Wyler R. Propagation of the virus of porcine epidemic diarrhea in cell culture. *J Clin Microbiol* (1988) 26:2235-9. doi: 10.1128/jcm.26.11.2235-2239.1988
70. Emeny JM, Morgan MJ. Regulation of the interferon system: evidence that vero cells have a genetic defect in interferon production. *J Gen Virol* (1979) 43:247-52. doi: 10.1099/0022-1317-43-1-247
71. Suspene R, Renard M, Henry M, Guetard D, Puyraimond-Zemmour D, Billecocq A, et al. Inverting the natural hydrogen bonding rule to selectively amplify GC-rich ADAR-edited RNAs. *Nucleic Acids Res* (2008) 36:e72. doi: 10.1093/nar/gkn295
72. Zhao S, Gao J, Zhu L, Yang Q. Transmissible gastroenteritis virus and porcine epidemic diarrhoea virus infection induces dramatic changes in the tight junctions and microfilaments of polarized IPEC-J2 cells. *Virus Res* (2014) 192:34-45. doi: 10.1016/j.virusres.2014.08.014
73. Zhang Q, Yoo D. Immune evasion of porcine enteric coronaviruses and viral modulation of antiviral innate signaling. *Virus Res* (2016) 226:128-41. doi: 10.1016/j.virusres.2016.05.015
74. Su Y, Hou Y, Wang Q. The enhanced replication of an s-intact PEDV during coinfection with an S1 NTD-del PEDV in piglets. *Vet Microbiol* (2019) 228:202-12. doi: 10.1016/j.vetmic.2018.11.025
75. Li S, Yang J, Zhu Z, Zheng H. Porcine epidemic diarrhea virus and the host innate immune response. *Pathogens* (2020) 9:367. doi: 10.3390/pathogens9050367
76. Park A, Iwasaki A. Type i and type iii interferons - induction, signaling, evasion, and application to combat covid-19. *Cell Host Microbe* (2020) 27:870-8. doi: 10.1016/j.chom.2020.05.008
77. Xing Y, Chen J, Tu J, Zhang B, Chen X, Shi H, et al. The papain-like protease of porcine epidemic diarrhea virus negatively regulates type i interferon pathway by acting as a viral deubiquitinase. *J Gen Virol* (2013) 94:1554-67. doi: 10.1099/vir.0.051169-0
78. Wang D, Fang L, Shi Y, Zhang H, Gao L, Peng G, et al. Porcine epidemic diarrhea virus 3c-like protease regulates its interferon antagonism by cleaving nemo. *J Virol* (2016) 90:2090-101. doi: 10.1128/JVI.02514-15
79. Wu Y, Zhang H, Shi Z, Chen J, Li M, Shi H, et al. Porcine epidemic diarrhea virus nsp15 antagonizes interferon signaling by RNA degradation of TBK1 and IRF3. *Viruses* (2020) 12:599. doi: 10.3390/v12060599
80. Zhang J, Yuan S, Peng Q, Ding Z, Hao W, Peng G, et al. Porcine epidemic diarrhea virus nsp7 inhibits interferon-induced JAK-STAT signaling through sequestering the interaction between KPNA1 and STAT1. *J Virol* (2022). doi: 10.1128/jvi.00400-22:e0040022
81. Shi P, Su Y, Li R, Liang Z, Dong S, Huang J. PEDV nsp16 negatively regulates innate immunity to promote viral proliferation. *Virus Res* (2019) 265:57-66. doi: 10.1016/j.virusres.2019.03.005
82. Hou Y, Ke H, Kim J, Yoo D, Su Y, Boley P, et al. Engineering a live attenuated porcine epidemic diarrhea virus vaccine candidate *via* inactivation of the viral 2'-O-Methyltransferase and the endocytosis signal of the spike protein. *J Virol* (2019) 93(96):e0040022. doi: 10.1128/JVI.00406-19



## OPEN ACCESS

EDITED BY  
Chenhe Su,  
Wistar Institute, United States

REVIEWED BY  
Wenting Li,  
The First Affiliated Hospital of  
University of Science and Technology  
of China Anhui Provincial Hospital,  
China  
Keshan Zhang,  
Chinese Academy of Agricultural  
Sciences, China

\*CORRESPONDENCE  
Liang Peng Ge  
geliangpeng1982@163.com  
ZhiWen Xu  
abtcxzw@126.com

†These authors have contributed  
equally to this work

SPECIALTY SECTION  
This article was submitted to  
Viral Immunology,  
a section of the journal  
Frontiers in Immunology

RECEIVED 29 May 2022  
ACCEPTED 27 June 2022  
PUBLISHED 25 July 2022

CITATION  
Deng HD, Zhu S, Zhu L, Sun J,  
Ding YC, Li FQ, Jian ZJ, Zhao J,  
Deng LS, Deng JL, Deng YT, Guo HR,  
Sun XG, Lai SY, Tang HQ, Cui HM,  
Ge LP and Xu ZW (2022) Mfn2 is  
responsible for inhibition of the  
RIG-I/IRF7 pathway and activation of  
NLRP3 inflammasome in Seneca Valley  
virus-infected PK-15 cells to promote  
viral replication.  
*Front. Immunol.* 13:955671.  
doi: 10.3389/fimmu.2022.955671

# Mfn2 is responsible for inhibition of the RIG-I/IRF7 pathway and activation of NLRP3 inflammasome in Seneca Valley virus-infected PK-15 cells to promote viral replication

HuiDan Deng<sup>1†</sup>, Song Zhu<sup>1†</sup>, Ling Zhu<sup>1,2</sup>, Jing Sun<sup>3</sup>,  
YuChun Ding<sup>3</sup>, FengQin Li<sup>4</sup>, ZhiJie Jian<sup>1</sup>, Jun Zhao<sup>1</sup>,  
LiShuang Deng<sup>1</sup>, JunLiang Deng<sup>1</sup>, YouTian Deng<sup>1</sup>,  
HongRui Guo<sup>1</sup>, XianGang Sun<sup>1</sup>, Si Yuan Lai<sup>1</sup>, HuaQiao Tang<sup>1</sup>,  
HengMin Cui<sup>1</sup>, Liang Peng Ge<sup>3\*</sup> and ZhiWen Xu<sup>1,2,3\*</sup>

<sup>1</sup>College of Veterinary Medicine, Sichuan Agricultural University, Chengdu, China, <sup>2</sup>Key Laboratory of Animal Disease and Human Health of Sichuan Province, Sichuan Agricultural University, Chengdu, China, <sup>3</sup>National Center of Technology Innovation for Pigs, Chongqing, China, <sup>4</sup>College of Animal Science, Xichang University, Xichang, China

Seneca Valley virus (SVV), a non-enveloped positive single-stranded virus can cause vesicular disease in swine. However, the mechanisms by which SVV activates an innate immune response remain unknown. Mitofusin-2 (MFN2), a mitochondria-shaping protein regulating mitochondrial fusion and fission, plays a crucial role in innate immune responses. But, the roles of Mfn2 in SVV infection have not been elucidated. Here, we show that SVV inhibited Mfn2 expression and NLRP3 inflammasome, activating RIG-I/IRF7 signaling pathway to increase IFN- $\lambda$ 3 expression. Overexpression of Mfn2 inhibited RIG-I/IRF7 signaling pathway, thus decreasing IFN- $\lambda$ 3 expression and promoting SVV replication. Interestingly, overexpression of Mfn2 also activated NLRP3 inflammasome but did not inhibit SVV proliferation. That may mean the RIG-I/IRF7 signaling pathway plays a more important role in SVV proliferation in PK-15 cells. This study could provide important insights into the modulation of host metabolism during SVV infection and provide a strong theoretical basis for a better understanding of the pathogenic mechanism and immune activation mechanism of SVV.

## KEYWORDS

SVV, Mfn2, NLRP3 inflammasome, RIG-I signaling pathway, innate immune response



## Introduction

Seneca Valley virus (SVV) is a positive single-stranded RNA virus belonging to the picornavirus family. The virus was discovered by accident in 2002 in a culture of adenovirus type 5 vectors in PER cell lines. C6, named Seneca Valley Virus 001 (SVV-001) (1). It is speculated that the agent may be introduced into cell culture through fetal bovine serum or porcine trypsin. The latter is considered more likely because abundant viruses serologically associated with SVV-001 have been isolated from pigs in the United States over the past 20 years (2). Studies on SVV-001 focused on its oncolytic activity in tumor therapy at first. In recent years, SVV infection in swine has been reported in the United States, Canada, Brazil, China and other countries (3–5). SVV infection can increase the mortality of newborn piglets and cause fluid-filled/ruptured vesicles and ulcerative lesions at the snout, coronary band, and hooves, as well as anorexia and lameness in adult pigs (6, 7). In 2015, the first Chinese SVV strain was isolated from pigs in Guangdong Province. Since then, more and more cases of SVV infection have been reported in other provinces of China and led to serious economic losses, indicating that SVV has spread rapidly and widely in China (8, 9).

An innate immune response such as retinoic acid-inducible gene I (RIG-I) like receptors (RLRs) signaling and inflammasomes is the first line of host defense in response to pathogens. According to the traditional paradigm, after the virus gets across the mucus, the virus can be sensed by the pattern recognition receptors (PRRs), triggering the production of interferons (IFNs) which induce the expression of hundreds of IFN-stimulated genes (ISGs) that block viral replication and further virus spread (10). Some PRRs, such as NACHT, LRR, PYD domains-containing protein 1 (NLRP1), NLRP3, NLR family CARD domain-containing protein 4 (NLRC4) and absent in melanoma 2 (AIM2), recruit apoptosis-associated speck-like proteins (ASC) and caspase-1 to form inflammasomes to initiate inflammation and some forms of cell death. Thus, participation in antiviral response (11). Numerous studies indicate that SVV disrupts the host defense system in virus-infected cells. Qian et al. (12) and Wen et al. (13) found that in human embryonic kidney 293T cells, SVV 2C and 3C protein induces cleavage of MAVS, TRIF, TANK and degradation of RIG-I, blocks activation of the RLR pathway and inhibits the production of type I interferon, meanwhile, SVV infection can induce host cell apoptosis to promote virus replication. In PK-15 cells, SVV 3Cpro reduces IRF3 and IRF7 protein expression to block the transcription of interferons (IFNs) such as IFN- $\beta$ , IFN- $\alpha$ 1, IFN- $\alpha$ 4 and ISG54 to escape the host's intrinsic innate immune system (14). In macrophages and pigs, SVV 3D binds with NLRP3 to activate the NLRP3 inflammasome, on the other hand, SVV 3D protein interacts with IKK $\alpha$  and IKK $\beta$  to induce NF- $\kappa$ B activation. Thus promoting IL-1  $\beta$  transcription and secretion (15). Our previous studies have proved that SVV can activate innate immune response *via* RIG-I signaling pathway

(16). However, the details on how SVV activates innate immunity are still not clear.

Mitofusin2 (Mfn2), a mitochondrial outer membrane that participates in the initial step of mitochondrial fusion and promotes the maintenance of cellular homeostasis (17, 18), regulates various other biological processes such as cell proliferation and cell death (19–21). Numerous studies have shown that Mfn2 is a key regulator of innate immune responses during viral infections. Earlier study reported that Mfn2 inhibited antiviral immune responses in hepatitis B virus related hepatocellular carcinoma (22). However, in HIV-1 Vpr infected HEK293 cells, Mfn2 overexpression can alleviating cell death *via* mediating ER-Mitochondria Interaction (23). Nonetheless the role of Mfn2 in SVV infecting PK-15 cells has not been studied yet.

Therefore, our studies were carried out to investigate the possible mechanisms of how Mfn2 affects immune response in PK-15 cells infection with SVV and find out the relationship between Mfn2, inflammasome and RIG-I signaling pathway. Our study provides a foundation and a new insight for future systematic exploring of SVV infection mechanism.

## Materials and methods

### Virus and cells

PK-15 cells (kept at Key Laboratory of Animal Disease and Human Health of Sichuan Province, Sichuan Agricultural University, Chengdu) were maintained in Dulbecco's Modified Eagle's Medium Nutrient Mixture (DMEM) (Gibco, USA), supplemented with antibiotics (100 units/ml penicillin and 100 $\mu$ g/ml streptomycin), and 10% fetal bovine serum (FBS) (Gibco, USA). The SVV was maintained at Key Laboratory of Animal Disease and Human Health of Sichuan Province, Sichuan Agricultural University, Chengdu. The virus was propagated in PK-15 cell with 2% FBS (Gibco, USA) added in the DMEM.

### Transfection

The Mfn2 was cloned into vector pcDNA3.1 (kept at Key Laboratory of Animal Disease and Human Health of Sichuan Province, Sichuan Agricultural University, Chengdu). For transfection, the cells were transiently transfected with vector pcDNA3.1 or plasmids encoding Mfn2 using Lipofectamine 3000 (Invitrogen, 2185325) following the manufacturer's protocols. Cell lysates were collected after 24 h to verify overexpression efficiency by western blot.

### Western blot assay

After PK-15 cells were lysed, total proteins were extracted with RIPA buffer (Thermo Fisher Scientific) and Thermo Scientific Halt

protease inhibitor cocktail. Protein concentration was measured by BCA protein assay kit (Thermo Fisher Scientific). Equal amounts of protein sample were loaded into 12% SDS-PAGE and transferred to nitrocellulose filter membranes. Then, the membrane was blocked in nonfat dry milk (5%) for 1 h at RT. Membranes were incubated with the primary antibodies overnight at 4°C followed by one hour of incubation using proper secondary HRP-conjugated antibodies (Bio-Rad) and development with ECL detection kit (GE Healthcare, Piscataway, NJ, USA). Then, the membranes were detected with Bio-Rad ChemiDoc XRS+System (Bio-Rad Laboratories, Inc., Hercules, CA, USA). The primary antibodies were RIG-I polyclonal antibody (CST, United States), anti-Phospho-IRF7 (Bioss, China), GAPDH (Abcam, United States), Rabbit Anti-ASC antibody (Proteintech, United States), cleaved Rabbit Anti-IL-1 $\beta$  antibody (CST, United States), Rabbit Anti-IL-18 antibody (CST, United States), Rabbit Caspase 1/p20/p10 Polyclonal antibody (proteintech, United States); Mfn2 polyclonal antibody (proteintech, United States) and NLRP3 polyclonal antibody (proteintech, United States). The second antibody was anti-Rabbit or mouse IgG-HRP (Sangon, China). At least three biological replicates were analyzed for each experiment.

## RNA extraction and quantitative real-time PCR

RNAiso Plus (9109; Takara, China) was used for extracting the PK-15 cells total RNA following protocols provided by the manufacturer. RNA (1 $\mu$ g) was used to synthesize cDNA through Prim-Script<sup>TM</sup> RT reagent Kit (RR047A, Takara, China) following specific instructions. Primers were designed and synthesized by Sangon (Shanghai, China). The mRNA expression was measured with SYBR<sup>®</sup> Premix Ex Taq<sup>TM</sup> II (RR820A, Takara, China). The reactions protocol was 95°C for 10 min, followed by under 95°C for 10 min, under 60°C for 20 s, and under 72°C for 20 s. The qRT-PCR data were analyzed using the 2- $\Delta\Delta$ CT method (21). At least three biological replicates were analyzed for each experiment. The qRT-PCR primers were shown in Table 1.

## ELISA assay

After treated with SVV for 24 h, the culture supernate was collected for IFN- $\lambda$ 1 and IFN- $\lambda$ 3 detection. Test was carried out according to the kit brochures operation (Enzyme Industrial Co.,

Ltd, China) and the spectrophotometric absorbance was assessed at 450 nm for IFN- $\lambda$ 1 and IFN- $\lambda$ 3.

## Immunocytochemistry

Immunocytochemistry was performed to detect SVV proliferation *in vitro*. PK-15 cells were cultured in 24-well plates and treated with SVV for 24 h. After that, cells were washed with PBS and fixed with 4% PFA at RT for 10 min. Then, cells were incubated with 0.1% Triton X-100 at RT for 10 min followed by blocking with 1% BSA at RT for 1 h. Next, cells were incubated with rabbit anti-VP1 antibody (saved in our lab) overnight at 4°C. After washing with PBS, cells were incubated with secondary antibodies rabbit IgG (Thermo Scientific) at RT for 1 h. Cells were analyzed using fluorescence microscopy (PhotoFluor LM-75, 89 North, Burlington, VT, USA). At least three biological replicates for each experiment were performed and representative images are shown.

## Statistical analysis

Data are expressed as mean  $\pm$  standard deviation. All statistical analyses were analyzed by GraphPad Prism (GraphPad Software, Inc). Unpaired T-test and One-way analysis of variance (ANOVA) were used to investigate the significance of differences between the experimental groups and the control group.  $p < 0.05$  indicates statistical significance of the difference. Each experiment was repeated at least three times.

## Results

### SVV decreased Mfn2 expression and inhibited NLRP3 inflammasome activation

PK-15 cells were infected with SVV strain SVV-SC-01 at the multiplicity of infection (MOI) of 2 for 24 h. As shown in Figure 1, SVV decreased Mfn2 protein expression level ( $P < 0.05$ ) in comparison with control group. At the same time, the NLRP3, ASC, caspase1/p10/p20, cleaved-IL-1 $\beta$  and IL-18 protein expression also decreased ( $P < 0.005$ ) in SVV infection group when compared to control group. That means the NLRP3 inflammasome activation was inhibited by SVV infection.

### The inhibition of RIG-I/IRF7 signaling pathway promote SVV proliferation in PK-15 cells

Our previous results also showed that SVV infection activated RIG-I/IRF7 signaling pathway shown as increased RIG-I and p-IRF7 protein expression level, 0.5  $\mu$ mol/L IRF7 inhibitor (BX795) decreased IFN- $\lambda$ 1 and IFN- $\lambda$ 3 mRNA expression levels (16). But how the content of IFN- $\lambda$ 1 and IFN- $\lambda$ 3 in the supernatant changed

TABLE 1 Primer sequences of genes selected for analysis SVV replication.

Target gene	Primer	Primer Sequence (5'->3')	Tm (°C)
SVV-VP1	Forward	AGGTACTGGAGAAGGACGCT	57
	Reverse	GGTTGACGTACAGGCCGAAA	

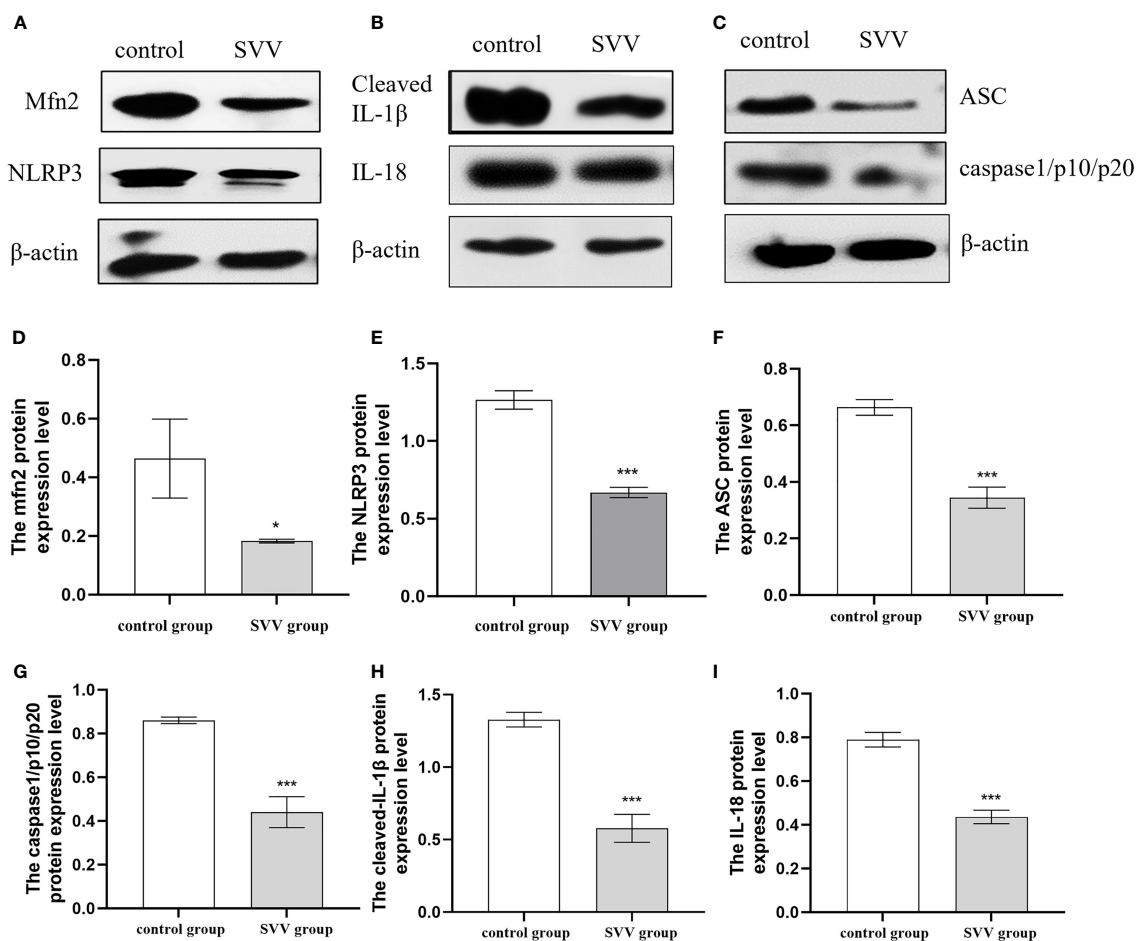


FIGURE 1

SVV decreased Mfn2 expression, inhibited NLRP3 inflammasome activation. (A–C) The western blot assay for Mfn2, NLRP3, ASC, caspase1/p10/p20, cleaved-IL-1 $\beta$  and IL-18. (D–I) The relative protein expression level of Mfn2, NLRP3, ASC, caspase1/p10/p20, cleaved-IL-1 $\beta$  and IL-18. Unpaired T-test were used to investigate the significance of differences between the experimental groups and the control group; \*;  $P < 0.05$ , \*\*\*;  $P < 0.005$ .

after SVV and BX795 treated still unknown. To further investigated the role of RIG-I/IRF7 signaling in IFN- $\lambda$ s secretion and SVV proliferation. We use 0.5  $\mu\text{mol/L}$  IRF7 inhibitor to treated cells 1 h before treated with SVV. The results showed that SVV only increased IFN- $\lambda$ 3 content ( $P < 0.005$ ). After inhibited IRF7 phosphorylation, only IFN- $\lambda$ 3 secretion was inhibited ( $P < 0.01$ ). The qRT-PCR results showed SVV proliferation was enhanced ( $P < 0.001$ ) after BX795 treatment in PK-15 cells. That means the IFN- $\lambda$ 3 may be the key factor in RIG-I/IRF7 mediated SVV proliferation. The results were shown in Figure 2.

## The activation of NLRP3 inflammasome inhibited SVV proliferation in PK-15 cells

In order to further understand the role of NLRP3 inflammasome in SVV proliferation. We use NLRP3 inflammasome activator

Nigeration to treated cells with SVV for 24 h. As shown in Figure 3. 10  $\mu\text{mol/L}$  Nigeration relieved SVV inhibited NLRP3 inflammasome activation. The NLRP3, ASC, caspase1/p10/p20, cleaved-IL-1 $\beta$  and IL-18 protein expression level all increased ( $P < 0.01$  or  $P < 0.05$ ) when compared with SVV infection group. In addition, the qRT-PCR results showed that 10  $\mu\text{mol/L}$  Nigeration inhibited the SVV proliferation in PK-15 cells. These results demonstrated that activation of NLRP3 inflammasome protect PK-15 cells from SVV infection.

## The Mfn2 overexpression enhanced SVV proliferation and promoted cell damage in PK-15 cells

To explore the function of Mfn2 in SVV infection in BHK-21. The Mfn2 was cloned into vector pcDNA3.1. The the cells were

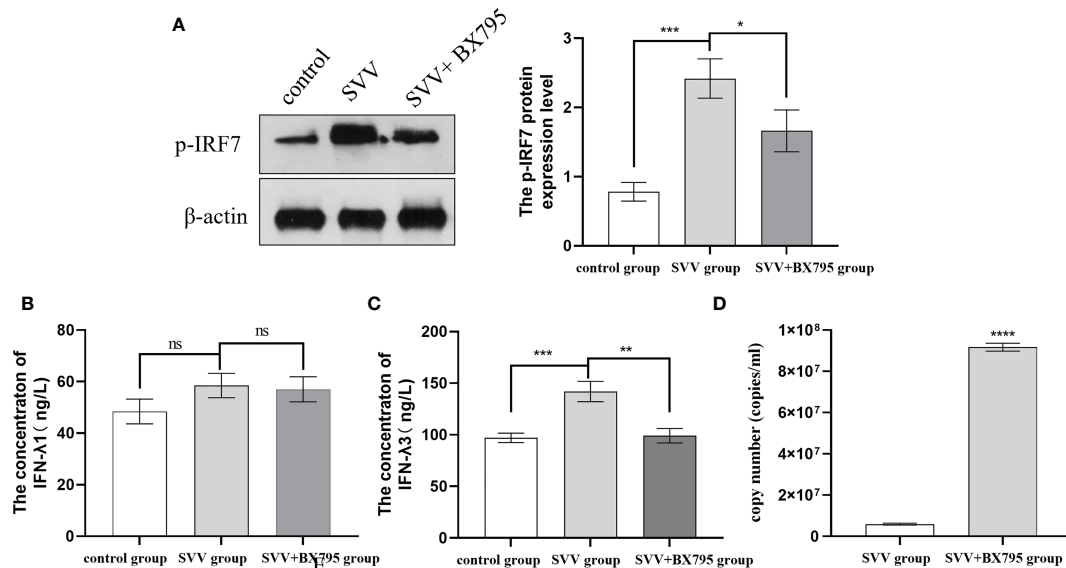


FIGURE 2

IRF7 inhibitor (BX795) inhibited IRF7 phosphorylation and IFN-λ3 secretion thus promote SVV proliferation. (A) The western blot assay for p-IRF7. (B) The relative protein expression level of IRF3. (C, D) The Elisa assay for IFN-λ1 and IFN-λ3. (E) The qRT-PCR assay for SVV copy number. One-way analysis of variance (ANOVA) were used to investigate the significance of differences between the SVV groups and the SVV+BX795 group or between the control group and SVV group \*;  $P < 0.05$ , \*\*;  $P < 0.01$ , \*\*\*;  $P < 0.005$ , \*\*\*\*;  $P < 0.001$ , ns means no significance.

transiently transfected with vector pcDNA3.1 (vector group) or plasmids encoding Mfn2 (Ad-Mfn2 group) using Lipofectamine 3000 for 24 h. Then, cells were infected with SVV for 24 h. Figures 1A, B showed that Mfn2 protein was successfully transfected into PK-15 cells. qRT-PCR and Immunocytochemistry results showed that Mfn2 overexpression increased SVV proliferation ( $P < 0.001$ ). And the cellular damage was increased in Ad-Mfn2 group when compared with WT group under microscopy (Figure 4).

### The Mfn2 overexpression inhibit RIG-I/IRF7 signaling pathway and decreased IFN-λ3 content

As shown in Figure 5, Mfn2 overexpression (Ad-Mfn2) decreased ( $P < 0.001$  or  $P < 0.005$ ) the RIG-I and p-IRF7 protein expression when compared with WT group after SVV infection. And the Elisa assay results also showed that the IFN-λ3 content in the supernatant in Ad-Mfn2 group was also decreased ( $P < 0.01$ ) compared to WT group after SVV infection.

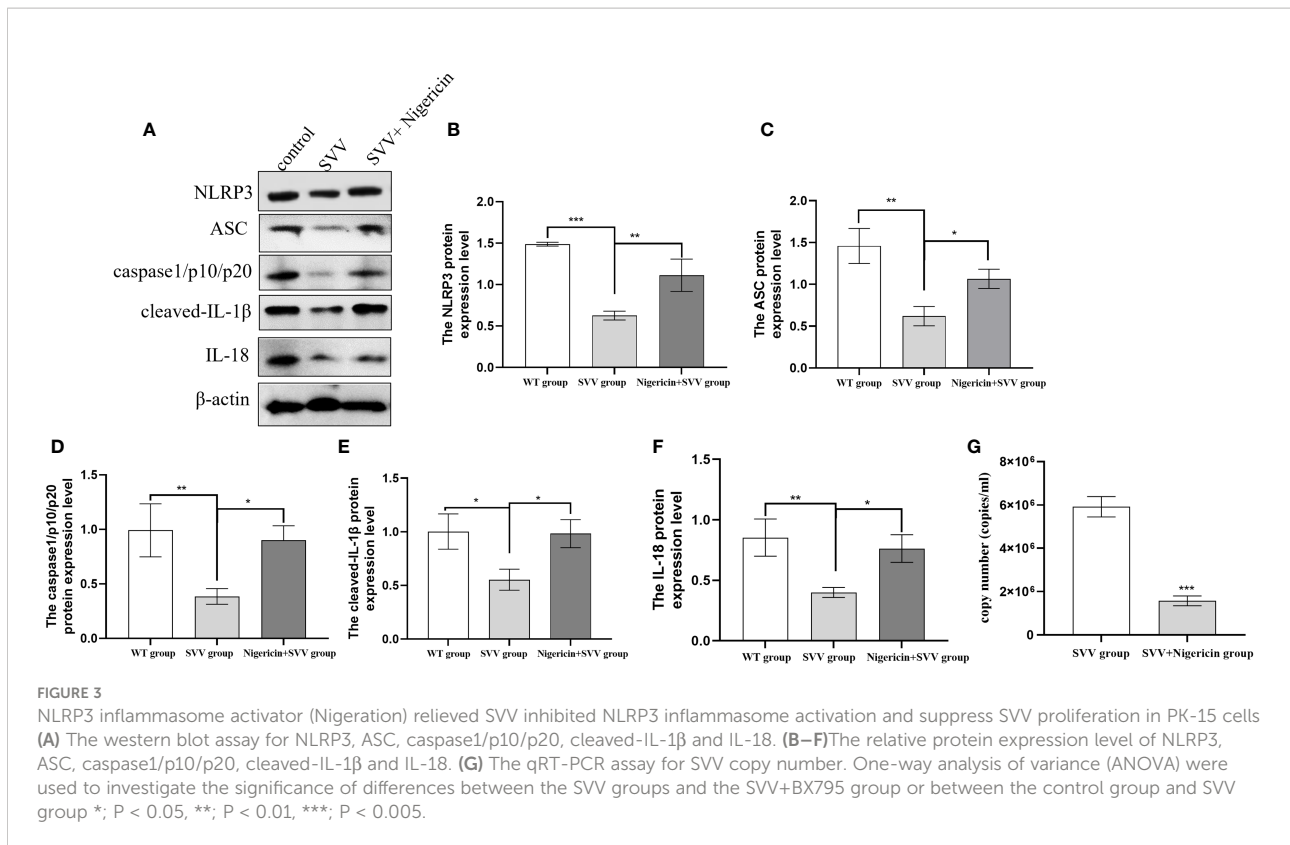
### The Mfn2 overexpression activated NLRP3 inflammasome

As illustrated in Figure 6, after SVV infection in PK-15 cells, the NLRP3 inflammasome signaling pathway was up-regulated

in Ad-Mfn2 group compared to WT group. Concretely reflected in the increased protein expression levels of NLRP3, ASC, caspase1/p10/p20, cleaved-IL-1β and IL-18 in Ad-Mfn2 group when compare with WT group during SVV infection ( $P < 0.0001$  or  $P < 0.005$  or  $P < 0.01$ ).

## Discussion

Seneca Valley virus (SVV) is a newly type of virus in pig industry in China, the first outbreak of SVV occurred in Guangdong Province in March 2015 and then spread into other province (24). SVV can cause vesicular disease and epidemic transient neonatal death in swine. The typical clinical symptoms include vesicular, ulcerative lesions on the snout, oral mucosa, coronary bands and hooves (25). Since the outbreak of SVV in China, Numerous studies have focused on innate immune response. The results proved that SVV inhibits the production of type I interferon through a variety of pathways. The SVV infection does not trigger the host's early innate immune response and the production of type I interferon in human embryonic kidney 293T cells, and its 3C protein induces the cleavage of receptor molecules of type I interferon pathways MAVS, TRIF and TANK through protease activity, blocking the activation of RLR pathway and inhibiting the production of type I interferon (12). Meanwhile, SVV 3C protease inhibits the expression of RIG-1, TBK1 and TRAF3 by degrading IRF3



and IRF7 or acting as a de-ubiquitination enzyme, and inhibits the type I interferon pathway (14), thus evading the innate immunity of the host against virus. The host protein RIG-I is responsible for activating type I interferon pathway to inhibit viral replication in SVV-infected porcine cells (26). Our previous study demonstrated that SVV induced RIG-I/IRF7 signaling pathway activation. In this study, we found that SVV inhibits Mfn2 protein expression and NLRP3 inflammasome activation. To further explore the role of Mfn2, NLRP3 inflammasome and RIG-I in SVV infection in PK-15 cells, we have conducted a series of studies shown as below.

The innate immune response mediated by RNA virus involves the RLRs signaling pathway (27). The RNA virus can be recognized by RIG-I, and then activates downstream related signal pathways to exert innate antiviral immunity such as phosphorylates IRF3 and IRF7. Phosphorylated IRF3 and IRF7 form homologous and/or heterologous dimers that are transported to the nucleus and bind to IFN-stimulated response elements (ISREs) to induce IFNs and ISGs (28–30). In HEK-293T, SW620 and SK6 cells, SVV inhibit type I interferon production by degrading RIG-I (12, 13) and IRF-7 (14). Li Pengfei (26) has proved that knock out RIG-I in PK-15 cells reduced type I interferon production. Our previous study was first carried out to investigate the relationship between RIG-I/IRF7 pathway and type III interferon. We found that inhibition of IRF7 inhibitor inhibits IFN- $\lambda$ 1 and IFN- $\lambda$ 3

mRNA expression in PK-15 cells (16). In this study, we found that inhibition of IRF7 phosphorylation promote SVV replication but only reduced IFN- $\lambda$ 3 content in supernatant. These results illustrated that RIG-I/IRF7 mediated IFN- $\lambda$ 3 production not IFN- $\lambda$ 1 play an important role in antiviral immunity.

The NLRP3 is one of the member of PRRs activate innate immune system in response to harmful stimuli (31–33). NLRP3 inflammasome is essential for host immune defense against viral infections (34). The NLRP3 interacts with the ASC to initiate inflammasome assembly. Promotes pro-caspase-1 recruitment to the inflammasome complex and activates caspase-1. Activated caspase-1 cleaves the cytokines interleukin-1 $\beta$  (pro-IL-1 $\beta$ ) and IL-18 into mature and biologically active forms. Thus, promoting immune response. Wen wei (25) demonstrated that in SK6 cells, SVV could induce pyroptosis. However, in late infection, SVV may reduced caspase-1 expression because 3C<sup>PRO</sup> cleave NLRP3. In pig bone marrow-derived macrophages (BMDMs), SVV infection activate NLRP3 to induces IL-1 $\beta$  secretion and production (15). On the contrary, our data illustrated that SVV infection inhibits the activation of NLRP3 inflammasome shown as down-regulation of NLRP3, ASC, caspase-1/p10/p20, cleaved-IL-1 $\beta$  and IL-18. The difference of the results between our study and others may because of the different cells and the different in the origin of viral strain. To further investigate the role of NLRP3 inflammasome in SVV

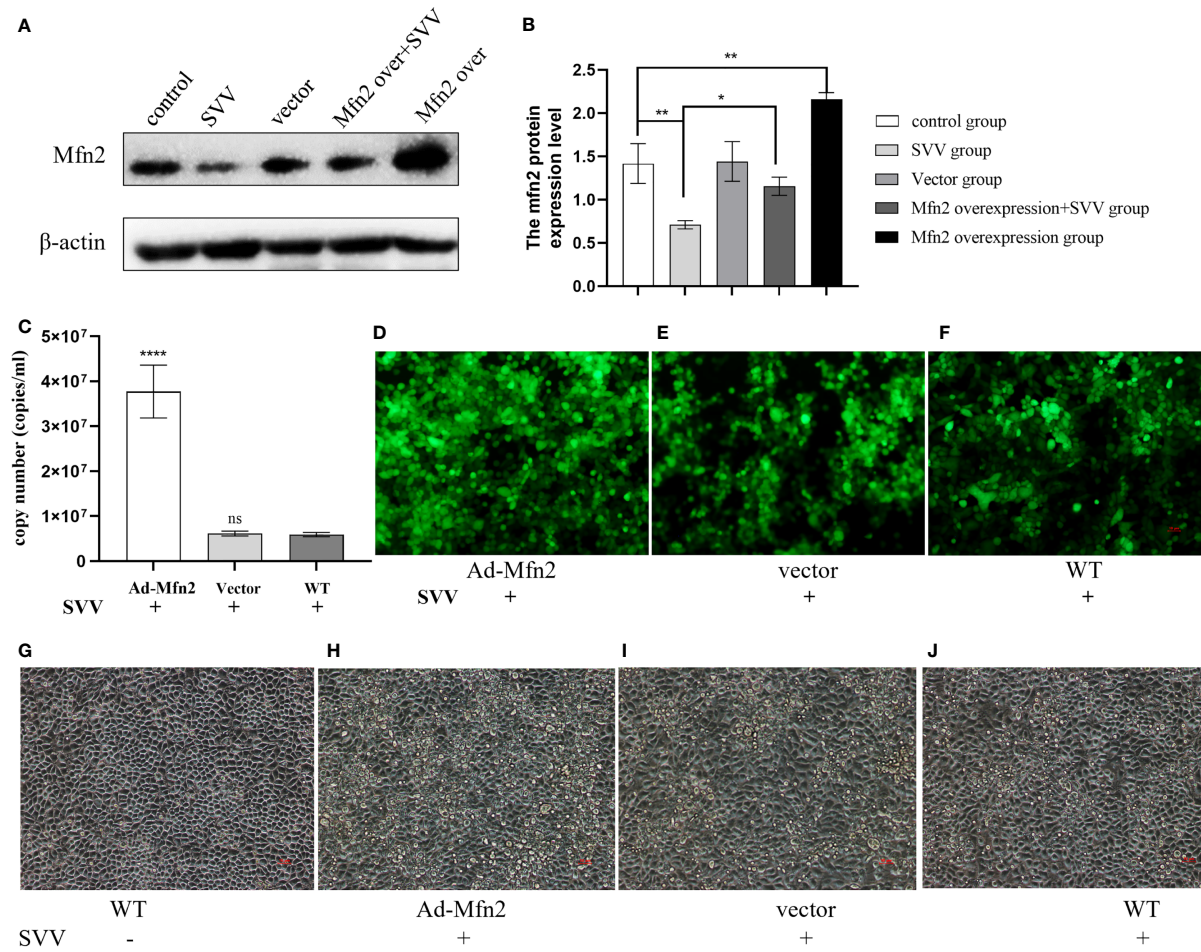


FIGURE 4

Mfn2 overexpression accelerate SVV proliferation and promote cell damage in PK-15 cells (A) The western blot assay for Mfn2. (B) The relative protein expression level of Mfn2. (C) The qRT-PCR assay for SVV copy number. (D–F) The immunocytochemistry assay for SVV detection. (G–J) The change of PK-15 cells morphology after Mfn2 overexpression. One-way analysis of variance (ANOVA) were used to investigate the significance of differences between the WT and other groups. \*,  $P < 0.05$ , \*\*,  $P < 0.01$ , \*\*\*\*,  $P < 0.001$ , ns means no significance.

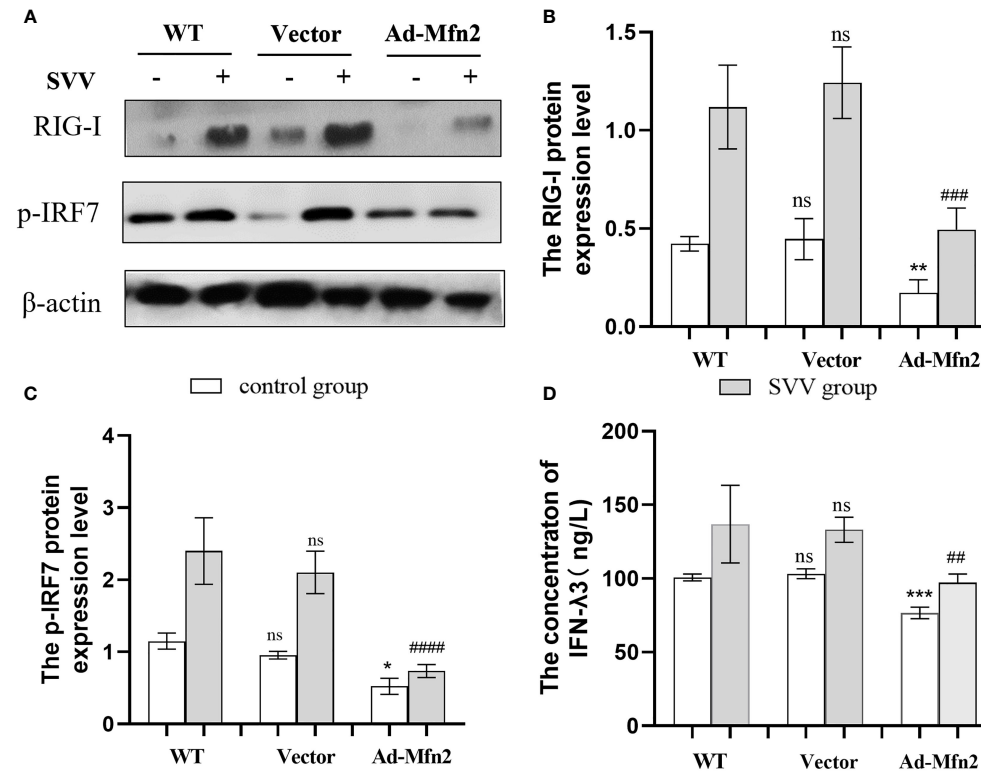


FIGURE 5

Mfn2 overexpression restrains SVV-induced RIG-I/IRF7 protein expression level and IFN- $\lambda$ 3 content in supernatant in PK-15 cells (A) The western blot assay for RIG-I and p-IRF7. (B, C) The relative protein expression level of RIG-I and p-IRF7. (D) The Elisa assay for IFN- $\lambda$ 3 detection. Unpaired T-test and One-way analysis of variance (ANOVA) were used to investigate the significance of differences. \* means the difference between the WT and Ad-Mfn2 in control group; # means the difference between the WT and Ad-Mfn2 in SVV group. \*,  $P < 0.05$ , \*\*.,  $P < 0.01$ , \*\*.,  $P < 0.005$ , \*\*.,  $P < 0.001$ , ns means no significance.

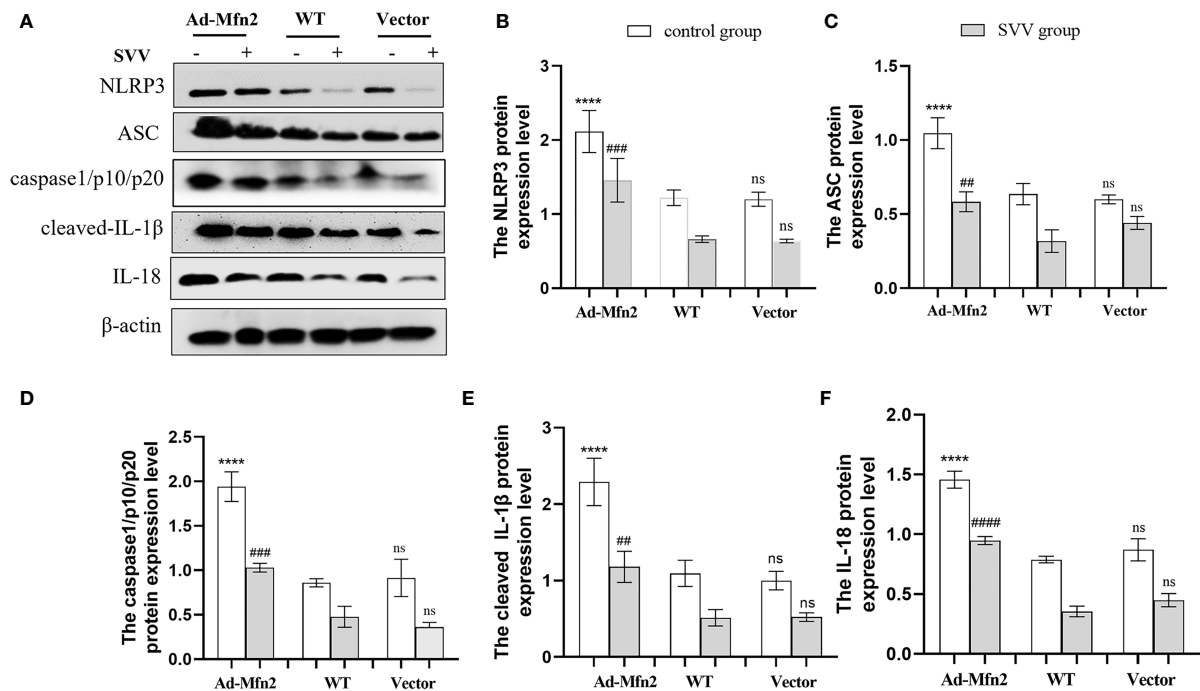


FIGURE 6

Mfn2 overexpression induced SVV-inhibited NLRP3 inflammasome activation in PK-15 cells. (A) The western blot assay for NLRP3, ASC, caspase1/p10/p20, cleaved-IL-1 $\beta$  and IL-18. (B–F) The relative protein expression level of NLRP3, ASC, caspase1/p10/p20, cleaved-IL-1 $\beta$  and IL-18. One-way analysis of variance (ANOVA) were used to investigate the significance of differences. \* means the difference between the WT and Ad-Mfn2 in control group; # means the difference between the WT and Ad-Mfn2 in SVV group; and other groups. ##; P < 0.01, ###; P < 0.005, \*\*\*\*,####; P < 0.001, ns means no significance.

replication. We use activator of NLRP3 inflammasome Nigericin to treat cells with SVV. The results showed after NLRP3 inflammasome activation, the SVV proliferation was inhibited. Declared that NLRP3 inflammasome play an antiviral function in SVV infection PK-15 cells.

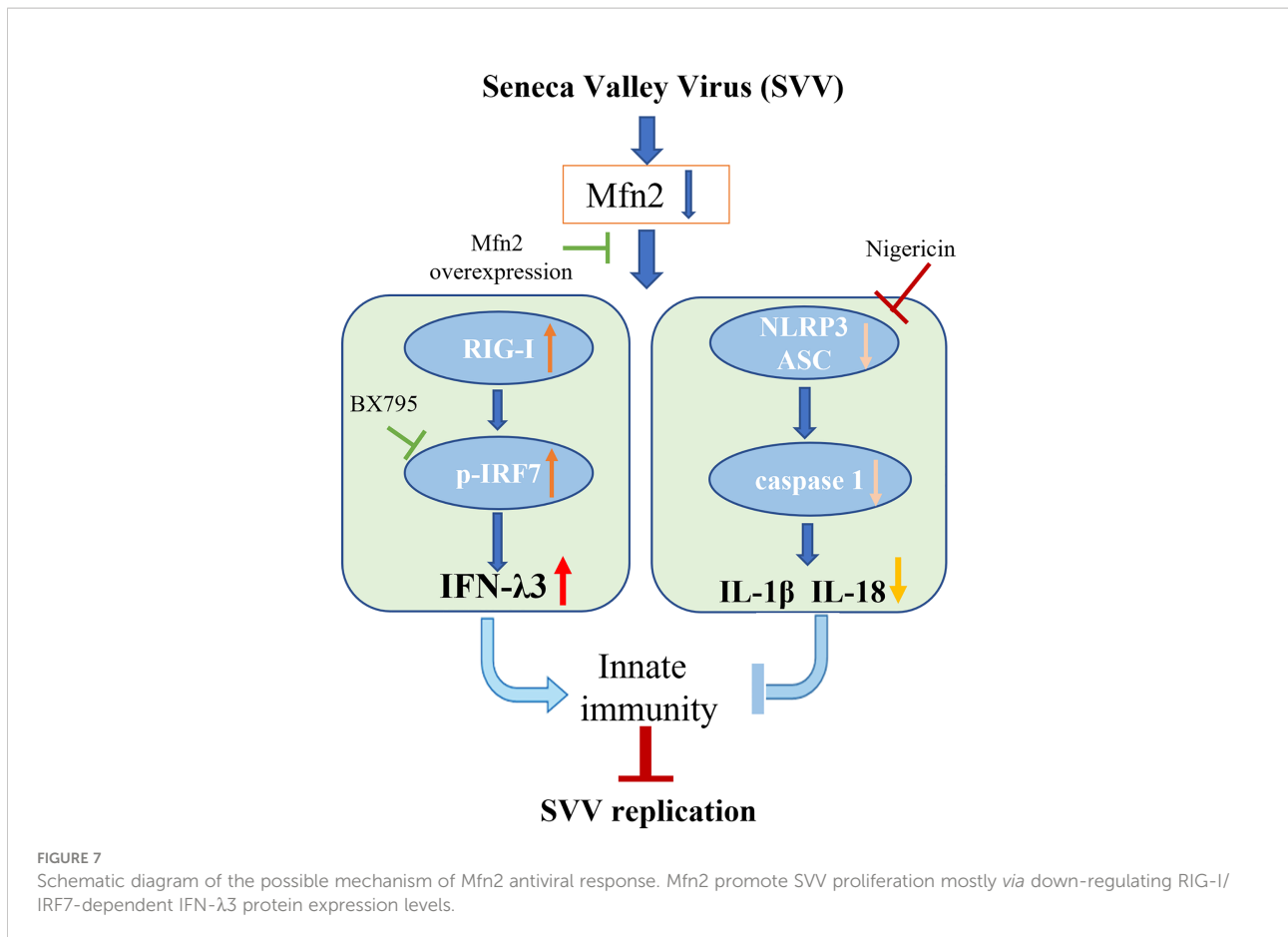
Mfn2 is a master regulator of immune responses during viral infections (35). Studies have proved that on one hand, Mfn2 inhibited antiviral immune responses by interacting with MAVs or mediating RLR signaling and IRF3 expression during encephalomyocarditis virus (EMCV), Measles, VSV, H1N1 infection (36, 37). During infection with human immunodeficiency type 1 (HIV-1) in macrophages, Mfn2 was up-regulated by TREM1. And the TREM1-dependent MFN2 upregulation contribute to the ability of HIV-1 survival in host cells (38). Interestingly, Mfn2 also have anti-viral functions. After dengue virus infection, Mfn2 are cleaved by dengue virus protease NS2B3, and the Mfn2 keeps MMP to inhibit cell death from dengue virus infection (39). In addition, Mfn2 binds to NLRP3 to promote IL-1 $\beta$  secretion after infection with RNA viruses, including influenza, measles, or EMCV (40). In this study, we found that SVV infection decreased Mfn2 protein expression. Overexpression of Mfn2 inhibited RIG-I/IRF7 signaling pathway and restrain IFN- $\lambda$ 3 secretion, thus

promoting SVV replication. Mfn2 overexpression also activate NLRP3 inflammasome. Based on aboved mentioned results, activation of NLRP3 inflammasome inhibited SVV replication. However, Mfn2 overexpression promote SVV proliferation. These results may demonstrate that RIG-I/IRF7 signaling pathway is more important than NLRP3 inflammasome in anti-SVV response. And the reason may because IFN- $\lambda$  plays the most important role in mucosal antiviral immune response (41, 42). After all, IFN- $\lambda$  is produced earlier and more frequently, has strong antiviral activity and does not mediate inflammation. Therefore, many side effects are avoided (43).

## Conclusion

Our study demonstrated that Mfn2 inhibited antiviral activity against SVV infection in PK-15 cells. Mfn2 promote SVV proliferation *via* down-regulating RIG-I/IRF7-dependent IFN- $\lambda$ 3 protein expression levels. Also, the activation of NLRP3 inflammasome alone play an antiviral function in SVV infection. However, Mfn2-dependent NLRP3 inflammasome did not inhibit SVV replication (Figure 7). That may be because of the inhibition of IFN- $\lambda$ 3 secretion during Mfn2 overexpression. Our





findings suggest that deficiency of Mfn2 may represent a promising therapeutic target for SVV prevention in the future, and the IFN-λ3 may be the most important therapeutic agent for SVV prevention and treatment.

## Data availability statement

The original contributions presented in the study are included in the article/supplementary material. Further inquiries can be directed to the corresponding author/s.

## Author contributions

HD, LZ and ZX conceived and designed the experiments. HS, SZ, ZJ performed the experiments. LD, FL, XS, SL and JZ performed the analysis. HD drafted the manuscript. ZX, JD, YDeng, HT, HC and HG substantively revised this manuscript. JS, YDing and LG helped to revised manuscript according to reviewer comments and polish the article. All authors read and approved the final manuscript.

## Funding

This work was supported by the Science and Technology Department of Sichuan Province, China [grant number 2021ZDZX0010] and [grant number 2020YFN0147], Science and Technology Department of Chongqing, China [grant number cstc2021jscx-dxwtBX0007]. The funders had no role in study design, data collection and analysis, decision to publish, or preparation of the manuscript.

## Acknowledgments

We thank Prof. Zhu for her helpful discussions.

## Conflict of interest

The research was conducted in the absence of any commercial or financial relationships that could be construed as a potential conflict of interest.

## Publisher's note

All claims expressed in this article are solely those of the authors and do not necessarily represent those of their affiliated

organizations, or those of the publisher, the editors and the reviewers. Any product that may be evaluated in this article, or claim that may be made by its manufacturer, is not guaranteed or endorsed by the publisher.

## References

- Hales LM, Knowles NJ, Reddy PS, Xu L, Hay C, Hallenbeck PL. Complete genome sequence analysis of seneca valley virus-001, a novel oncolytic picornavirus. *J Gen Virol* (2008) 89(Pt 5):1265–75. doi: 10.1099/vir.0.835700
- Segalés J, Barcellos D, Alfieri A, Burrough E, Marthaler D. Senecavirus a. *Vet Pathol* (2017) 54(1):11–21. doi: 10.1177/0300985816653990
- Canning P, Canon A, Bates JL, Gerardy K, Linhares DC, Piñeyro PE, et al. Neonatal mortality, vesicular lesions and lameness associated with senecavirus a in a U.S. sow farm. *Transbound Emerg Dis* (2016) 63(4):373–8. doi: 10.1111/tbed.12516
- Pasma T, Davidson S, Shaw SL. Idiopathic vesicular disease in swine in Manitoba. *Can Vet J = La Rev Vet Can* (2008) 49(1):84–5.
- Vannucci FA, Linhares DC, Barcellos DE, Lam HC, Collins J, Marthaler D. Identification and complete genome of seneca valley virus in vesicular fluid and sera of pigs affected with idiopathic vesicular disease, Brazil. *Transbound Emerg Dis* (2015) 62(6):589–93. doi: 10.1111/tbed.12410
- Baker KL, Mowrer C, Canon A, Linhares DC, Rademacher C, Karriker LA, et al. Systematic epidemiological investigations of cases of senecavirus a in us swine breeding herds. *Transbound Emerg Dis* (2017) 64(1):11–8. doi: 10.1111/tbed.12598
- Leme RA, Oliveira TE, Alcântara BK, Headley SA, Alfieri AF, Yang M, et al. Clinical manifestations of senecavirus a infection in neonatal pigs, Brazil, 2015. *Emerg Infect Dis* (2016) 22(7):1238–41. doi: 10.3201/eid2207.151583
- Qian S, Fan W, Qian P, Chen H, Li X. Isolation and full-genome sequencing of seneca valley virus in piglets from China, 2016. *Virology* (2016) 13(1):173. doi: 10.1186/s12985-016-0631-2
- Zhu Z, Yang F, Chen P, Liu H, Cao W, Zhang K, et al. Emergence of novel seneca valley virus strains in China, 2017. *Transbound Emerg Dis* (2017) 64(4):1024–9. doi: 10.1111/tbed.12662
- Sun Y, Jiang J, Tien P, Liu W, Li J. Ifn- $\alpha$ : a new spotlight in innate immunity against influenza virus infection. *Protein Cell* (2018) 9(10):832–7. doi: 10.1007/s13238-017-0503-6
- Man SM, Kanneganti TD. Converging roles of caspases in inflammasome activation, cell death and innate immunity. *Nat Rev Immunol* (2016) 16(1):7–21. doi: 10.1038/nri.2015.7
- Qian S, Fan W, Liu T, Wu M, Zhang H, Cui X, et al. Seneca Valley virus suppresses host type i interferon production by targeting adaptor proteins mavs, trif, and tank for cleavage. *J Virol* (2017) 91(16):e00823–17. doi: 10.1128/jvi.00823-17
- Wen W, Yin M, Zhang H, Liu T, Chen H, Qian P, et al. Seneca Valley virus 2c and 3c inhibit type i interferon production by inducing the degradation of rig-i. *Virology* (2019) 535:122–9. doi: 10.1016/j.virol.2019.06.017
- Xue Q, Liu H, Zhu Z, Yang F, Ma L, Cai X, et al. Seneca Valley virus 3c(pro) abrogates the irf3- and irf7-mediated innate immune response by degrading irf3 and irf7. *Virology* (2018) 518:1–7. doi: 10.1016/j.virol.2018.01.028
- Choudhury SM, Ma X, Zeng Z, Luo Z, Li Y, Nian X, et al. Senecavirus a 3d interacts with nlrp3 to induce il-1 $\beta$  production by activating nf- $\kappa$ b and ion channel signals. *Microbiol Spectr* (2022) 10(2):e0209721. doi: 10.1128/spectrum.02097-21
- Peng K, Deng L, Wei J, Zhao J, Deng H, Tao Q, et al. Transcriptome analyses of senecavirus a-infected pk-15 cells: rig-i and irf7 are the important factors in inducing type iii interferons. *Front Microbiol* (2022) 13:846343. doi: 10.3389/fmicb.2022.846343
- Eura Y, Ishihara N, Yokota S, Mihara K. Two mitofusin proteins, mammalian homologues of fzo, with distinct functions are both required for mitochondrial fusion. *J Biochem* (2003) 134(3):333–44. doi: 10.1093/jb/mvg150
- Filadi R, Pendin D, Pizzo P. Mitofusin 2: from functions to disease. *Cell Death Dis* (2018) 9(3):330. doi: 10.1038/s41419-017-0023-6
- Xin Y, Li J, Wu W, Liu X. Mitofusin-2: a new mediator of pathological cell proliferation. *Front Cell Dev Biol* (2021) 9:647631. doi: 10.3389/fcell.2021.647631
- Wang W, Cheng X, Lu J, Wei J, Fu G, Zhu F, et al. Mitofusin-2 is a novel direct target of p53. *Biochem Biophys Res Commun* (2010) 400(4):587–92. doi: 10.1016/j.bbrc.2010.08.108
- Zhang GE, Jin HL, Lin XK, Chen C, Liu XS, Zhang Q, et al. Anti-tumor effects of mfn2 in gastric cancer. *Int J Mol Sci* (2013) 14(7):13005–21. doi: 10.3390/ijms140713005
- Wang X, Liu Y, Sun J, Gong W, Sun P, Kong X, et al. Mitofusin-2 acts as biomarker for predicting poor prognosis in hepatitis b virus related hepatocellular carcinoma. *Infect Agents Cancer* (2018) 13:36. doi: 10.1186/s13027-018-0212-7
- Huang CY, Chiang SF, Lin TY, Chiou SH, Chow KC. Hiv-1 vpr triggers mitochondrial destruction by impairing mfn2-mediated er-mitochondria interaction. *PLoS One* (2012) 7(3):e33657. doi: 10.1371/journal.pone.0033657
- Liu F, Wang Q, Huang Y, Wang N, Shan H. A 5-year review of senecavirus a in china since its emergence in 2015. *Front Vet Sci* (2020) 7:567792. doi: 10.3389/fvets.2020.567792
- Wen W, Li X, Wang H, Zhao Q, Yin M, Liu W, et al. Seneca Valley virus 3c protease induces pyroptosis by directly cleaving porcine gasdermin d. *J Immunol (Baltimore Md 1950)* (2021) 207(1):189–99. doi: 10.4049/jimmunol.2001030
- Li P, Zhang X, Cao W, Yang F, Du X, Shi Z, et al. Rig-I is responsible for activation of type i interferon pathway in seneca valley virus-infected porcine cells to suppress viral replication. *Virology* (2018) 15(1):162. doi: 10.1186/s12985-018-1080-x
- Eisenächer K, Krug A. Regulation of rlr-mediated innate immune signaling—it is all about keeping the balance. *Eur J Cell Biol* (2012) 91(1):36–47. doi: 10.1016/j.ejcb.2011.01.011
- Saha SK, Pietras EM, He JQ, Kang JR, Liu SY, Oganessian G, et al. Regulation of antiviral responses by a direct and specific interaction between traf3 and cardif. *EMBO J* (2006) 25(14):3257–63. doi: 10.1038/sj.emboj.7601220
- Honda K, Taniguchi T. Irf5: master regulators of signalling by toll-like receptors and cytosolic pattern-recognition receptors. *Nat Rev Immunol* (2006) 6(9):644–58. doi: 10.1038/nri1900
- Chang MX. The negative regulation of retinoic acid-inducible gene i (rig-i)-like receptors (rlrs) signaling pathway in fish. *Dev Comp Immunol* (2021) 119:104038. doi: 10.1016/j.dci.2021.104038
- Takeuchi O, Akira S. Pattern recognition receptors and inflammation. *Cell* (2010) 140(6):805–20. doi: 10.1016/j.cell.2010.01.022
- Sharma D, Kanneganti TD. The cell biology of inflammasomes: mechanisms of inflammasome activation and regulation. *J Cell Biol* (2016) 213(6):617–29. doi: 10.1083/jcb.201602089
- Lamkanfi M, Dixit VM. Mechanisms and functions of inflammasomes. *Cell* (2014) 157(5):1013–22. doi: 10.1016/j.cell.2014.04.007
- Allen IC, Scull MA, Moore CB, Holl EK, McElvania-TeKippe E, Taxman DJ, et al. The nlrp3 inflammasome mediates *in vivo* innate immunity to influenza a virus through recognition of viral rna. *Immunity* (2009) 30(4):556–65. doi: 10.1016/j.immuni.2009.02.005
- Tur J, Pereira-Lopes S, Vico T, Marín EA, Muñoz JP, Hernández-Alvarez M, et al. Mitofusin 2 in macrophages links mitochondrial ros production, cytokine release, phagocytosis, autophagy, and bactericidal activity. *Cell Rep* (2020) 32(8):108079. doi: 10.1016/j.celrep.2020.108079
- Yasukawa K, Oshiumi H, Takeda M, Ishihara N, Yanagi Y, Seya T, et al. Mitofusin 2 inhibits mitochondrial antiviral signaling. *Sci Signaling* (2009) 2(84):ra47. doi: 10.1126/scisignal.2000287
- Luo Z, Liu LF, Jiang YN, Tang LP, Li W, Ouyang SH, et al. Novel insights into stress-induced susceptibility to influenza: corticosterone impacts interferon- $\beta$  responses by mfn2-mediated ubiquitin degradation of mavs. *Signal Transduct Targeted Ther* (2020) 5(1):202. doi: 10.1038/s41392-020-00238-z
- Campbell GR, To RK, Spector SA. Trem-1 protects hiv-1-infected macrophages from apoptosis through maintenance of mitochondrial function. *mBio* (2019) 10(6):e02638–19. doi: 10.1128/mBio.02638-19
- Yu CY, Liang JJ, Li JK, Lee YL, Chang BL, Su CI, et al. Dengue virus impairs mitochondrial fusion by cleaving mitofusins. *PLoS Pathog* (2015) 11(12):e1005350. doi: 10.1371/journal.ppat.1005350
- Ichinohe T, Yamazaki T, Koshiba T, Yanagi Y. Mitochondrial protein mitofusin 2 is required for Nlrp3 inflammasome activation after rna virus infection. *Proc Natl Acad Sci USA* (2013) 110(44):17963–8. doi: 10.1073/pnas.1312571110

41. Mordstein M, Neugebauer E, Ditt V, Jessen B, Rieger T, Falcone V, et al. Lambda interferon renders epithelial cells of the respiratory and gastrointestinal tracts resistant to viral infections. *J Virol* (2010) 84(11):5670–7. doi: 10.1128/jvi.00272-10
42. Pott J, Mahlaköiv T, Mordstein M, Duerr CU, Michiels T, Stockinger S, et al. Ifn-lambda determines the intestinal epithelial antiviral host defense. *Proc Natl Acad Sci USA* (2011) 108(19):7944–9. doi: 10.1073/pnas.1100552108
43. Phillips S, Mistry S, Riva A, Cooksley H, Hadzhiolova-Lebeau T, Plavova S, et al. Peg-interferon lambda treatment induces robust innate and adaptive immunity in chronic hepatitis b patients. *Front Immunol* (2017) 8:621. doi: 10.3389/fimmu.2017.00621

#### Copyright

© 2022 Deng, Zhu, Sun, Ding, Li, Jian, Zhao, Deng, Deng, Guo, Sun, Lai, Tang, Cui, Ge and Xu. This is an open-access article distributed under the terms of the Creative Commons Attribution License (CC BY). The use, distribution or reproduction in other forums is permitted, provided the original author(s) and the copyright owner(s) are credited and that the original publication in this journal is cited, in accordance with accepted academic practice. No use, distribution or reproduction is permitted which does not comply with these terms.



## OPEN ACCESS

## EDITED BY

Rongtuan Lin,  
McGill University, Canada

## REVIEWED BY

Shaopo Zu,  
Henan Agricultural University, China  
Huibin Yu,  
Yale University, United States

## \*CORRESPONDENCE

Yuqiang Cheng  
wyycyq@sjtu.edu.cn  
Jianhe Sun  
sunjhe@sjtu.edu.cn

## SPECIALTY SECTION

This article was submitted to  
Viral Immunology,  
a section of the journal  
Frontiers in Immunology

RECEIVED 16 April 2022

ACCEPTED 28 June 2022

PUBLISHED 26 July 2022

## CITATION

Fu F, Lin Z, Li Y, Wang J, Li Y, Liu P,  
Wang Z, Ma J, Yan Y, Sun J and  
Cheng Y (2022) Goose STING  
mediates IFN signaling activation  
against RNA viruses.  
*Front. Immunol.* 13:921800.  
doi: 10.3389/fimmu.2022.921800

## COPYRIGHT

© 2022 Fu, Lin, Li, Wang, Li, Liu, Wang,  
Ma, Yan, Sun and Cheng. This is an  
open-access article distributed under  
the terms of the [Creative Commons  
Attribution License \(CC BY\)](https://creativecommons.org/licenses/by/4.0/). The use,  
distribution or reproduction in other  
forums is permitted, provided the  
original author(s) and the copyright  
owner(s) are credited and that the  
original publication in this journal is  
cited, in accordance with accepted  
academic practice. No use,  
distribution or reproduction is  
permitted which does not comply with  
these terms.

# Goose STING mediates IFN signaling activation against RNA viruses

Feiyu Fu, Zhenyu Lin, Yanlin Li, Jie Wang, Yawen Li,  
Pengcheng Liu, Zhaofei Wang, Jingjiao Ma, Yaxian Yan,  
Jianhe Sun\* and Yuqiang Cheng\*

Shanghai Key Laboratory of Veterinary Biotechnology, Key Laboratory of Urban Agriculture (South), Ministry of Agriculture, School of Agriculture and Biology, Shanghai Jiao Tong University, Shanghai, China

Stimulator of the interferon gene (STING) is involved in mammalian antiviral innate immunity as an interferon (IFN) activator. However, there is still a lack of clarity regarding the molecular characterization of goose STING (GoSTING) and its role in the innate immune response. In the present study, we cloned GoSTING and performed a series of bioinformatics analyses. GoSTING was grouped into avian clades and showed the highest sequence similarity to duck STING. The *in vitro* experiments showed that the mRNA levels of GoSTING, IFNs, IFN-stimulated genes (ISGs), and proinflammatory cytokines were significantly upregulated in goose embryo fibroblast cells (GEFs) infected with Newcastle disease virus (NDV). Overexpression of GoSTING in DF-1 cells and GEFs strongly activated the IFN- $\beta$  promoter as detected by a dual-luciferase reporter assay. Furthermore, overexpression of GoSTING induced the expression of other types of IFN, ISGs, and proinflammatory cytokines and inhibited green fluorescent protein (GFP)-tagged NDV (NDV-GFP) and GFP-tagged vesicular stomatitis virus (VSV) (VSV-GFP) replication *in vitro*. In conclusion, these data suggest that GoSTING is an important regulator of the type I IFN pathway and is critical in geese's innate immune host defense against RNA viruses.

## KEYWORDS

goose, STING, IFN, innate immunity, RNA virus

## Introduction

The innate immune system is the host's first line of defense against foreign pathogen invasion and endogenous damage, which initiates appropriate host defense mechanisms by detecting a series of pathogen-associated molecular patterns (PAMPs) and endogenous danger-associated molecular patterns (DAMPs) through pattern recognition receptors (PRRs) (1, 2). After PRRs are activated, downstream signaling

pathways are triggered, resulting in the expression of chemokines, proinflammatory cytokines, and the synthesis of type I interferon (IFN) and type III IFN, which induces the expression of IFN-stimulated genes (ISGs) through IFN receptor and Janus kinase (JAK) - signal transducer and activator of transcription (STAT) signaling, to effectively inhibit the replication of pathogens, remove aliens, maintain the physiological balance of the body, and act as a driving force to influence subsequent adaptive immunity (3–6). Currently, the major families of PRRs include the Toll-like receptors (TLRs), the retinoic acid-inducible gene (RIG)-I-like receptors (RLRs), and the nucleotide oligomerization domain-like receptors (NLRs, also called NACHT, LRR and PYD domain proteins) and cytosolic DNA sensors (7).

In addition to PRRs, several junction adaptor proteins are also critical for the induction of IFN, thereby ensuring the normal function of the innate immune system (8, 9). For example, all TLRs family members associate with corresponding adaptor proteins after sensing PAMPs or DAMPs, such as myeloid differentiation major response gene 88 (MyD88), MyD88-adaptor-like protein (MAL), TIR domain-containing adaptor inducing IFN- $\beta$  (TRIF/TICAM1), TRIF-related adaptor molecule (TRAM/TICAM2), and ultimately activate downstream nuclear factor- $\kappa$ B (NF- $\kappa$ B), IFN regulatory factors (IRFs) and mitogen-activated protein kinase (MAPK) (10–12). Like MyD88, stimulator of the IFN gene (STING; also known as MITA, MYPS, ERIS, and TMEM173), a molecule in the endoplasmic reticulum (ER), is also a key adapter protein with a potent ability to induce type I IFNs, interleukins and other proinflammatory factors (9, 13, 14).

A large number of recent studies have confirmed that STING is the core molecule of innate immune response from pathogen cytosolic DNA and RNA (15). In the RNA-triggered pathway, STING is mainly involved in RIG-I rather than melanoma differentiation-associated gene 5 (MDA5) signaling and functions downstream of RIG-I and mitochondrial antiviral signaling protein (MAVS) and upstream of TANK-binding kinase 1 (TBK1) (9). Following the recognition of RNA ligands, RIG-I is activated by the virus and transmits the signal to MAVS located downstream of the mitochondria, where it interacts with STING. STING is then transported to the vesicle structure around the nucleus and acts as a reaction platform to recruit TBK1 to activate IFN regulator factor (IRF) 3, which forms a dimer and enters the nucleus to induce the synthesis of IFN (16). During the recognition of DNA viruses, the DNA sensors, such as DAI (17), IFI16 (18), DDX41 (19), and cGAS (20, 21), transmit the signal to STING after recognizing DNA, which then activates the IFN *via* the STING-TBK1-IRF3 pathway (8). IFI16 is mainly located in the nucleus and can recognize single-stranded DNA (ssDNA) or double-stranded DNA (dsDNA) ligands in a length-dependent manner through its HIN domain (22). After binding to the ligand, IFI16 induces the expression of IFN- $\beta$  through the activation of IRF3, and this

expression is STING-dependent (23). DDX41 was identified as a cytoplasmic sensor capable of recognizing viral dsDNA. After sensing dsDNA through its DEADc domain, DDX41 binds to STING and initiates activation of the IFN pathway (19, 22). It can be seen that although the localization of various DNA sensors in cells, the nucleic acid forms recognized, and the site that binds to viral nucleic acids are different, the process involves STING as a key mediator. Overall, STING plays an important role in antiviral innate immunity as a key signaling molecule that regulates type I IFNs, which is essential for establishing antiviral status.

Most of the studies mentioned above on STING have focused on mammals, whereas STING signaling events in geese have not been studied. Geese, like ducks, belong to waterfowl and play a critical role in the transmission and dissemination of many important pathogens (14). In particular, Newcastle disease virus (NDV) and avian influenza virus (AIV) cause serious and economically significant diseases in almost all birds (24, 25). Chickens are susceptible to NDV and AIV due to a lack of RIG-I naturally. Instead, chickens express MDA5 or other as yet unidentified receptors which functionally compensate for the absence of RIG-I in the chicken genome (26–28). In addition, preliminary research in our laboratory demonstrated that chicken STING (chSTING) inhibited the replication of NDV and AIV and activated IRF-7 and NF- $\kappa$ B to induce the production of type I IFNs, possibly by participating in the MDA5-STING-IFN- $\beta$  signaling pathway in chicken cells (29). Compared to chickens lacking RIG-I, ducks and geese encode RIG-I with a similar domain organization to mammals and are generally resistant to NDV and AIV (30). Overexpression of duck STING (DuSTING) has been shown to activate the type I IFN pathway and limit the replication of H9N2 AIV in our previous studies (31).

Interestingly, compared with duck RIG-I, goose RIG-I (GoRIG-I) exhibited a higher IFN-activating ability in DF-1 cells infected with or not infected with the influenza virus (30). Ding et al. have identified the key role of GoRIG-I in innate immunity against NDV infection, and goose MAVS was identified as a GoRIG-I interactive protein involved in the activation of type I IFN pathways goose cells (26, 32). However, whether goose STING (GoSTING), like its mammalian counterpart, also induces type I IFN signaling and exerts antiviral effects remains unclear.

In the present study, we cloned GoSTING and explored the function of GoSTING in innate immunity in geese. We investigated the function of GoSTING in RNA virus infection, and the effects of GoSTING on the inhibition of viral genomic RNA replication based on NDV infection were characterized *in vitro*. Furthermore, our results suggest that GoSTING is an important regulator of IFNs, proinflammatory cytokines, and ISGs in geese. These findings contribute to a more systematic understanding of the bird's biological role of STING in the innate immune system and provide new insight into general and

individual characteristics of the innate immune system in birds and mammals.

## Materials and methods

### Cells and viruses

DF-1 is a chicken embryonic fibroblast cell line from East Lansing strain eggs (33). Goose embryo fibroblast cells (GEFs) were prepared from 15-day-old goose embryos. The DF-1 cells and GEFs were maintained in high-glucose complete Dulbecco's Modified Eagle's Medium (DMEM; Corning, USA) supplemented with 10% fetal bovine serum (FBS; Nulen, Shanghai, China) and 1% penicillin-streptomycin (Gibco, USA). All cells were incubated at 37°C in a 5% CO<sub>2</sub> incubator. The NDV strain NSD14 was isolated from chickens at a farm in Shandong Province, China. Green fluorescent protein (GFP) tagged NDV low virulent strain LaSota named NDV-GFP, and GFP tagged vesicular stomatitis virus (VSV) VSV-GFP were stored in our laboratory. These viruses were purified, propagated, and stored as described in our previous study (29).

### Cloning and bioinformatics analysis of GoSTING

Based on the predicted GoSTING sequence from the National Center for Biotechnology Information (NCBI), the primers GoSTING-F and GoSTING-R (Table 1), which were located outside of the GoSTING open reading frame (ORF), were designed to amplify potential GoSTING cDNA *via* RT-PCR on total RNA extracted from the GEF cells. The PCR product was ligated into a pTOPO-Blunt vector (Aidlab Biotech, Beijing, China) for sequencing, and the positive colonies were sent to the Beijing Genomics Institute (Beijing, China) for sequencing. The deduced amino acid sequence of GoSTING was analyzed using the SMART program. The amino acid sequence of GoSTING was aligned with the other animal STING proteins from ducks, chickens, humans, and pigs using Clustal W and edited with ESPript 3.0 (<http://http://espript.ibcp.fr/ESPript/cgi-bin/ESPript.cgi>). Sequence homology and phylogenetic analysis of amino acid sequences was constructed using DNASTAR software. A phylogenetic tree was constructed based on the STING from 13 different species, including mammals, birds, and fish. Homology modeling for GoSTING was conducted using the online protein-modeling server SWISS-MODEL (<http://swissmodel.expasy.org/>).

### Construction of plasmids

The PCR primers are shown in Table 1. The expression construct pcDNA3.1-GoSTING-Flag was constructed by

inserting full-length GoSTING into the *Xho* I and *Eco*R I sites of the pcDNA3.1-Flag expression vector *via* homologous recombination. The chicken IFN- $\beta$  (ch-IFN- $\beta$ ) promoter-luciferase reporter plasmids pGL-IFN- $\beta$ -Luc was constructed from chick embryo fibroblast genomic DNA using primers with *Nhe* I and *Bgl* II sites (IFN- $\beta$ -P F and IFN- $\beta$ -P R) to amplify -158 to +14 of the chicken IFN- $\beta$  promoter motif, as described previously (29). The promoter fragment was inserted between *Nhe* I and *Bgl* II sites of the pGL3-basic luciferase reporter vector. The truncated plasmids of GoSTING, including d1-50 aa, d1-150 aa, d50-340 aa, d181-382 aa, d251-382 aa, d251-382 aa, d351-382 aa, d365-371 aa, d374-382 aa, d379-382 aa, and S369A were constructed using a modified homologous recombination method and the primers listed in Table 1.

### Luciferase reporter assays

The DF-1 or GEF cells were plated in 24-well plates (NEST Biotechnology, Wuxi, China) and transiently transfected with the reporter plasmid pGL-IFN- $\beta$ -Luc (0.12  $\mu$ g/well) and internal control Renilla luciferase (PRL-TK, 0.06  $\mu$ g/well) along with the indicated plasmids using Nulen PlusTrans<sup>TM</sup> Transfection Reagent (Nulen, Shanghai, China). According to the manufacturer's instructions, the cells were lysed 24 hours after transfection, and luciferase activity was measured using a Dual-Luciferase Reporter Assay System kit (Promega, USA). Renilla luciferase activity was employed for normalization. All reporter assays were repeated at least three times.

### Reverse transcription-quantitative real-time PCR

RNA was extracted from GEFs using an HP Total RNA kit (Omega, USA), and then the RNA was reverse-transcribed to cDNA using a cDNA synthesis kit (Vazyme). Reverse transcription-quantitative real-time PCR (qRT-PCR) tests were conducted according to the manufacturer's instructions using a ChamQ<sup>TM</sup> SYBR<sup>®</sup> qPCR Master Mix (Vazyme). The conditions and data processing method for the qRT-PCR test were previously described (29).

### Virus infection and qRT-PCR analysis

For antiviral effect evaluation, GEF cells were transfected with pcDNA3.1-GoSTING-Flag plasmid or empty plasmid. After 24 hours, the GEF cells were washed twice with PBS (Gibco) and infected at 0.05 multiplicity of infection (MOI) with NSD14. The RNA from the cells, which were infected

TABLE 1 PCR primers used in this study.

Target Gene	Purpose	Name	Sequence of Oligonucleotide (5'-3')
GoIFN- $\alpha$	qRT-PCR	qGoIFN- $\alpha$ F	CTCCAGCACCTCTTCGACAC
		qGoIFN- $\alpha$ R	GTTGATGCCGAGGTGAAGGT
GoIFN- $\gamma$	qRT-PCR	qGoIFN- $\gamma$ F	ACATCAAAAACCTGTCTGAGCAGC
		qGoIFN- $\gamma$ R	AGGTTTGACAGGTCCACGAGG
GoIFN- $\kappa$	qRT-PCR	qGoIFN- $\kappa$ F	ACAGCAAAGAAAAGTGATTG
		qGoIFN- $\kappa$ R	GTTGGAAGATCTCTCAATGG
GoIFN- $\lambda$	qRT-PCR	qGoIFN- $\lambda$ F	GAGCTCTCGGTGCCCGACC
		qGoIFN- $\lambda$ R	CTCAGCGGCCACGCAGCCT
GoIL-6	qRT-PCR	qGoIL-6 F	AGCAAAAAGTTGAGTCGCTGTGC
		qGoIL-6 R	TAGCGAACAGCCCTCACGGT
GoIL-8	qRT-PCR	qGoIL-8 F	GCTGTCCTGGCTCTTCTCCTGATT
		qGoIL-8 R	GGGTCCAAGCACACCTCTCTGTG
GoPKR	qRT-PCR	qGoPKR F	GCAACAGCAAAGACTGACGA
		qGoPKR R	TGTTTGTGACCTCTGCCTTG
GoOASL	qRT-PCR	qGoOASL F	CAGCGTGTGGTGGTTCTC
		qGoOASL R	AACCAGACGATGACATACAC
GoMx-1	qRT-PCR	qGoMx-1 F	TTCACAGCAATGGAAAGGGA
		qGoMx-1 R	ATTAGTGTGCGGTCTGGGA
GoSTING	qRT-PCR	qGoSTING F	CCATGTCTCAGGACGAGTGC
		qGoSTING R	TCCTCGTATGCAATGAGCCG
	To obtain sequence	GoSTING F	ATGTCTCAGGAACCGCAGCGC
		GoSTING R	CTGCGGAGCGACCACCCCTGA
	Construction of GoSTING	pcDNA3.1-Flag EcoR I	TAGTCCAGTGTGGTGAATTTCATGTCTCAGGAACCGCAGCGC
		pcDNA3.1-Flag Xho I	GTCGTCCTTGTAGTCTCGAGCTGCGGAGCGACCACCCCTGA
	Construct truncated forms of GoSTING	GoSTING d1-50 aa F	GTGTGGTGAATTCATG CACCGCCTCACCGCC
		GoSTING d1-50 aa R	CATGAATTCACCACAC
		GoSTING d1-150 aa F	GTGTGGTGAATTCATG ACTGAGAGGTCCAAG
		GoSTING d1-150 aa R	CATGAATTCACCACAC
		GoSTING d50-340 aa F	AGCCCCTGTACCCGCT CAGGAGGAGTTCACG
		GoSTING d50-340 aa R	AGCGGGTGACAGGGGCT
		GoSTING d181-382 aa F	TGCCACGCATAAAGGAG CTCGAGGACTACAAG
		GoSTING d181-382 aa R	CTCCTTTATGCGTGGA
		GoSTING d251-382 aa F	ACAGCTTCTACGCAATC CTCGAGGACTACAAG
		GoSTING d251-382 aa R	GATTGCGTAGAAGCTGT
		GoSTING d351-382 aa F	CGGTGTACGAGGGGACC CTCGAGGACTACAAG
		GoSTING d351-382 aa R	GGTCCCCTCGTACACCG
		GoSTING d365-371 aa F	TGGGCTCAACAGACCTC GACCTGCCCCAGCCC
		GoSTING d374-382 aa F	TCAGTGCCTCCGACCTG CTCGAGGACTACAAG
GoSTING d379-382 aa R		CCGCAGGGGCTGGGGCA	
GoSTING S369A F		CTCAGCCTCCAGATCGCTGCCCTCCGACCT	
GoSTING S369A R	GCGATCTGGAGGCTGAGGTCT		

with the viruses at different times, was then collected for qRT-PCR to measure the mRNA level of GoSTING. The GoSTING-overexpressing and normal DF-1 cells were infected at 0.01 MOI with NDV-GFP or VSV-GFP, and fluorescence was measured 24h after infection using a fluorescence microscope.

## Western blot analysis

The DF-1 cells were plated in 12-well plates at  $1 \times 10^6$ /mL and then transfected with a total of empty plasmid or GoSTING expression plasmid. At thirty-six hours post-transfection, cells were washed twice with phosphate buffer

saline (PBS) (Gibco) and then lysed with a cell lysis buffer (Beyotime, Shanghai, China) containing an InStab™ protease cocktail (Yeasen, Shanghai, China) and phenylmethylsulfonyl fluoride (PMSF) (Yeasen). Lysates were centrifuged at 13,000 rpm for 15 minutes to obtain the supernatant and were eluted with a 5×SDS-PAGE loading buffer (Yeasen) and boiled for 10 min. Then the cell lysates were separated *via* SDS-PAGE and analyzed by Western blotting. Images were collected with the Tanon 5200 imaging system (Tanon, Shanghai, China), as described in our previous study (34).

## Statistical analysis

Data were expressed as means ± standard deviations, with three biological replicates for each experiment. The two-tailed independent Student's *t*-test was used to determine the significance. (\**P* < 0.05, \*\**P* < 0.01, \*\*\**P* < 0.001, \*\*\*\**P* < 0.0001).

## Ethics statements

The studies involving goose embryos were conducted in the laboratory of Shanghai Veterinary Research Institute. The studies were reviewed and approved by the Animal Ethics Committee of Shanghai Veterinary Research Institute (20210521).

## Results

### Cloning and sequence analysis of GoSTING

Based on a predicted goose sequence (XM\_013202032.1) from NCBI, primers GoSTING-F and GoSTING-R (Table 1), located outside of GoSTING ORF, were designed and used to amplify potential GoSTING cDNA using RT-PCR on total RNA extracted from the GEF cells.

Based on cDNA, the full-length GoSTING gene contains 1149 bp and encodes 382 amino acid (aa) residues (Figure 1A). Multiple sequence alignment showed that the amino acid sequences of GoSTING are 93.5, 44.0, and 61.8% identical to the STING gene in ducks (XP\_027311055.1), humans (NP\_938023.1), zebra finches (NP\_001232785.1), respectively. The protein domains of GoSTING were predicted using the SMART program. The results show that GoSTING consists of a low compositional complexity region (31-42aa) and the TMEM173 (50-340aa) domain (Figure 1B).

### Phylogenetic tree analyses and the three-dimensional structure of GoSTING

The amino acid sequence homologies of different animals were conducted using MegAlign, and the results are shown in

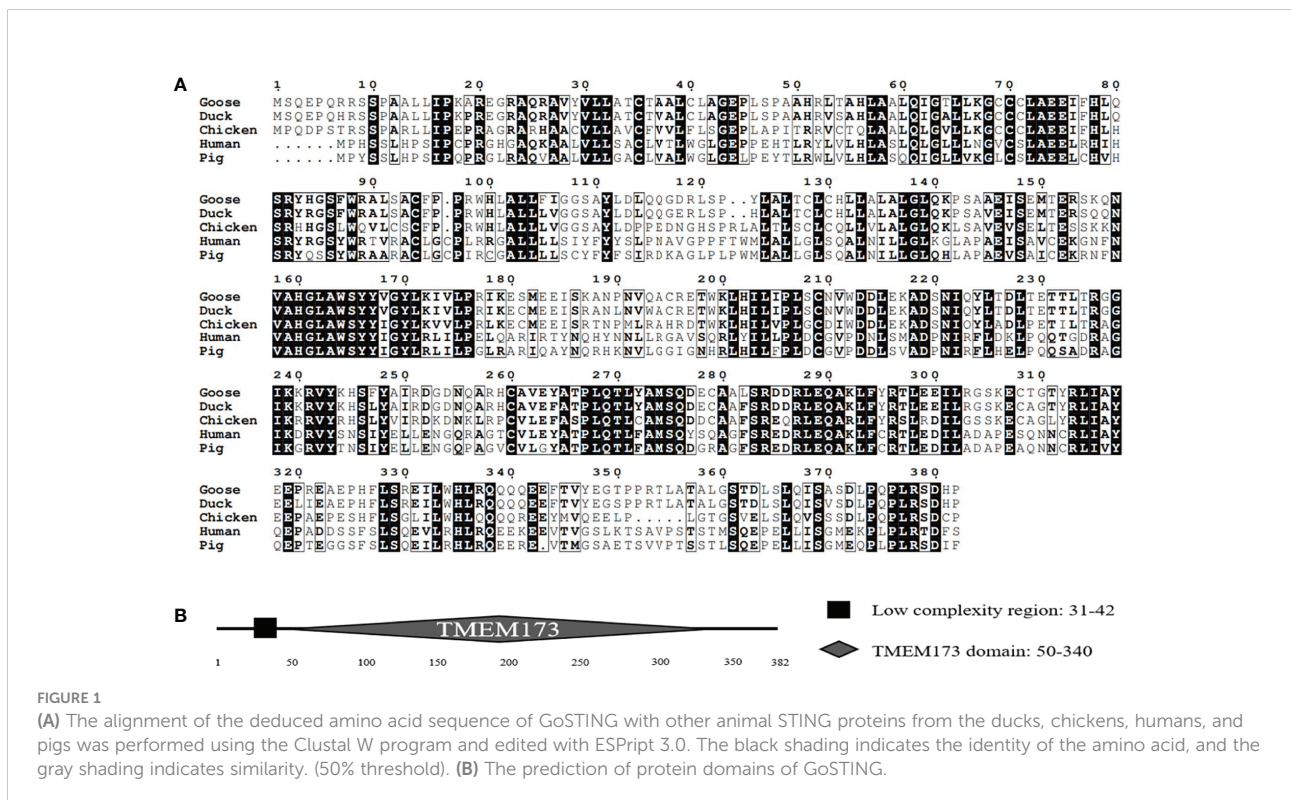


FIGURE 1

(A) The alignment of the deduced amino acid sequence of GoSTING with other animal STING proteins from the ducks, chickens, humans, and pigs was performed using the Clustal W program and edited with ESPrict 3.0. The black shading indicates the identity of the amino acid, and the gray shading indicates similarity. (50% threshold). (B) The prediction of protein domains of GoSTING.



**Figure 2A.** A phylogenetic tree was developed based on multiple alignments of STING from various species, including fish, birds, and mammals. Phylogenetic analysis showed that the goose, duck, zebra finch, and chicken STING protein sequences were in the same subgroup. STING from mammals, including goats, cattle, pigs, cats, chimpanzees, humans, monkeys, and mice, was in another subgroup, and fish STING was in a third subgroup (Figure 2B). The predicted three-dimensional structures of GoSTING are shown in Figure 2C.

## Upregulation of GoSTING expression during viral infection

In mammals, STING is involved in the type I IFN-mediated antiviral innate immune response. However, the role of GoSTING in the antiviral response remains unclear. Upregulation of some immune-related genes is an important strategy for the host to fight infection. To determine whether GoSTING could respond to the RNA virus NDV, we analyzed the expression of GoSTING, some cytokines, and the ISGs in GEFs following infection with NDV using qRT-PCR. The results illustrated that the mRNA levels of GoSTING in the NDV-infected GEF cells were significantly upregulated during the early stages of infection (Figure 3A). The mRNA levels of IFNs (IFN- $\alpha$ , IFN- $\gamma$ ) (Figures 3B, C), IL-6 (Figure 3D), and ISGs (Mx-1 and PKR) (Figures 3E, F) were significantly upregulated as well. Cells resist the invasion of foreign viruses by upregulating the expression of these genes.

## GoSTING involved in the regulation of IFNs

STING has been a critical mediator of virus-triggered type I IFN signaling in chicken and duck cells through different pathways (14, 29, 31). To investigate whether GoSTING is also involved in the type I IFN signaling pathway, we transfected DF-1 cells with constructs expressing GoSTING and the empty vector, respectively, and examined the IFN- $\beta$  activation with a luciferase reporter assay. The results showed that the overexpression of GoSTING resulted in a remarkable activation of the  $\chi$ IFN- $\beta$  promoter in DF-1 cells (Figure 4A), and the activation of IFN- $\beta$  exhibited a positive correlation with a dosage of the GoSTING plasmid (Figure 4B). To further confirm the ability of IFN activation of GoSTING, we prepared primary GEFs. Furthermore, luciferase assays were conducted with GEFs. Similarly, the overexpression of GoSTING in GEFs activated the IFN- $\beta$  promoter (Figure 4C).

## The essential domains of GoSTING in IFN activation

Based on the structural domains of GoSTING predicted by the SMART program, a series of truncated mutants lacking different function domains were constructed (Figure 5A). Their ability to activate the IFN- $\beta$  promoter was assessed with dual-luciferase reporter assays. As shown in Figure 5B, the deletion of 50 (d1-50 aa) amino acids showed a significant decrease in the

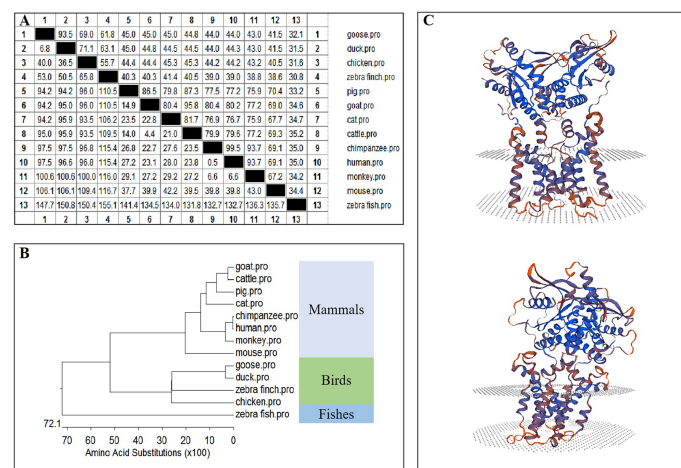


FIGURE 2

(A) The amino acid sequence homology of different animals. (B) Phylogenetic tree of the deduced amino acid sequence of GoSTING and other animal STING proteins. (C) Three-dimensional structure of GoSTING predicted by SWISS-MODEL.

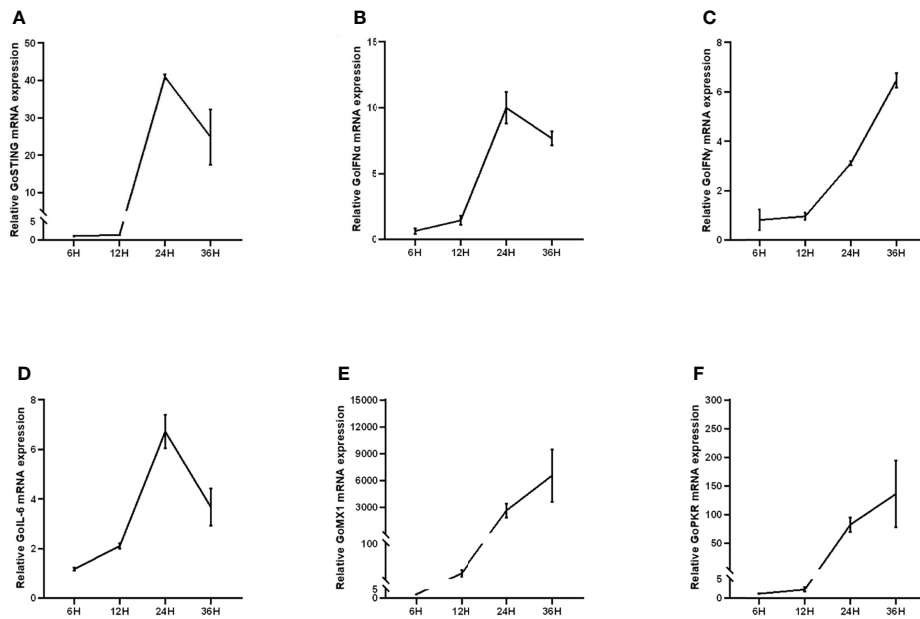


FIGURE 3

(A) Upregulation of GoSTING in GEF cells infected with NDV at 0.05 MOI. (B, C) Upregulation of IFNs (IFN- $\alpha$  and IFN- $\gamma$ ) in GEFs infected with NDV at 0.05 MOI. (D) Upregulation of IL-6 in GEFs infected with NDV at 0.05 MOI. (E, F) Upregulation of ISGs (Mx-1, PKR) in GEFs infected with NDV at 0.05 MOI. Error bars represent standard deviations.

ability to activate IFN- $\beta$  compared with the wild-type GoSTING. The further deletion of 290 residues in the GoSTING (d50-340aa) resulted in a remarkable decrease in promoter activity. In contrast, for the deletion mutant, GoSTING-d379-382aa, even with a deletion of only 4 aa at the C-terminal, led to such a strong decrease in IFN- $\beta$  induction. The N-terminal deletion mutant (d1-150aa), the C-terminal deletion mutant (d181-382aa, d251-382aa, d351-382 aa, and d374-382aa) and the mutant deleted 365-371 amino acids (d365-371aa) failed to activate the IFN- $\beta$  promoter. Moreover, the S369 (corresponds to the S366 in

human STING) seems to play a decisive role in IFN activation since the S369A mutant failed to activate IFN- $\beta$  completely.

## GoSTING plays an important role in anti-RNA viruses infection *in vitro*

To test the antiviral effects of GoSTING, the GoSTING-overexpressing and normal DF-1 cells were infected with NDV-GFP and VSV-GFP, respectively, and fluorescence was

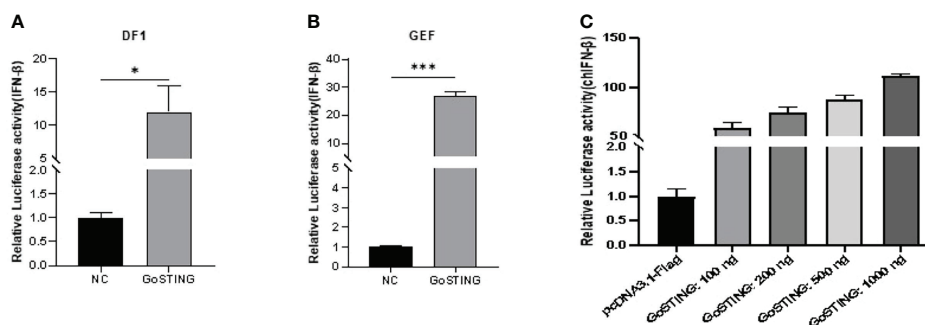


FIGURE 4

GoSTING is involved in regulating IFN- $\beta$ . (A) DF-1 cells were cotransfected with luciferase reporter plasmids (pRL-TK and pGL-IFN- $\beta$ -Luc) and pcDNA3.1-GoSTING-Flag or empty plasmid. Luciferase assays were performed after 24 hours of cotransfection. (B) GEFs were cotransfected with IFN- $\beta$  luciferase reporter plasmids and with pcDNA3.1-GoSTING-Flag or pcDNA3.1-Flag. Luciferase assays were performed 24 hours after transfection. (C) GoSTING dose-independently induced IFN- $\beta$  induction. The difference between the experimental and control groups was \* $p < 0.05$  or \*\*\* $p < 0.001$ .

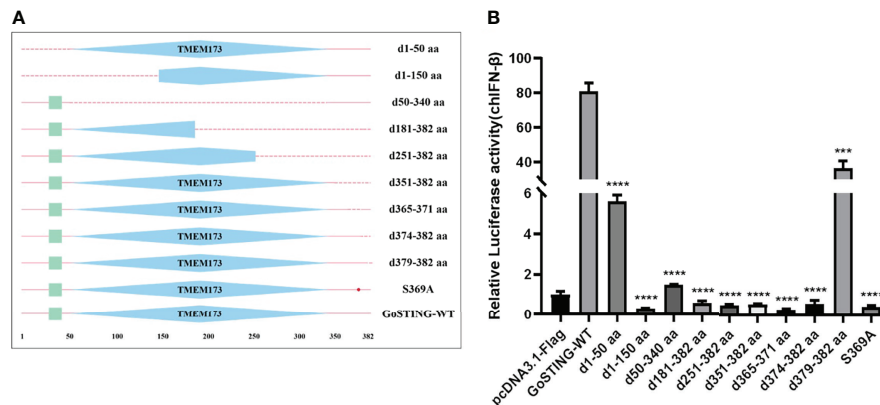


FIGURE 5

The Essential Domains of GoSTING in IFN Activation. **(A)** Schematic structure of GoSTING mutants. **(B)** The effects of GoSTING truncated mutants on IFN-β promoter activity. Cells were transfected with different expression plasmids of GoSTING and the reporter plasmids pGL-IFN-β-Luc and internal control Renilla luciferase (pRL-TK). Luciferase assays were performed 24h after transfection. All luciferase assays were repeated at least three times, and the difference between the experimental and control groups was \*\*\* $p < 0.001$  or \*\*\*\* $p < 0.0001$ .

measured with a fluorescence microscope. The fluorescence intensities of both NDV-GFP and VSV-GFP in GoSTING overexpression cells were significantly lower than those in the control DF-1 cells at 14 and 24 h after viral infection (Figures 6A, B). To further investigate the GoSTING's role during viral infection, the virus-infected cells were then lysed to detect the expression of NDV-GFP and VSV-GFP using Western blot. The protein band results showed that GoSTING could substantially reduce the expression of both NDV-GFP and VSV-GFP (Figures 6A, B). These results indicate that the overexpression of the GoSTING in DF-1 cells could inhibit NDV-GFP and VSV-GFP viral replication.

## Discussion

STING is a key signaling molecule that regulates innate immune signaling processes. Previous studies in our laboratory found that overexpression of chSTING and DuSTING in their respective cells could activate the IFN-β promoter and exert antiviral effects. Compared with chickens and ducks, the ability of geese to resist NDV and AIV showed a more significant advantage (35, 36). STING as a key IFN regulator may be one of the reasons for the difference in antiviral ability. A better understanding of the functions of GoSTING may help explain these differences. Currently, the functional characterization of

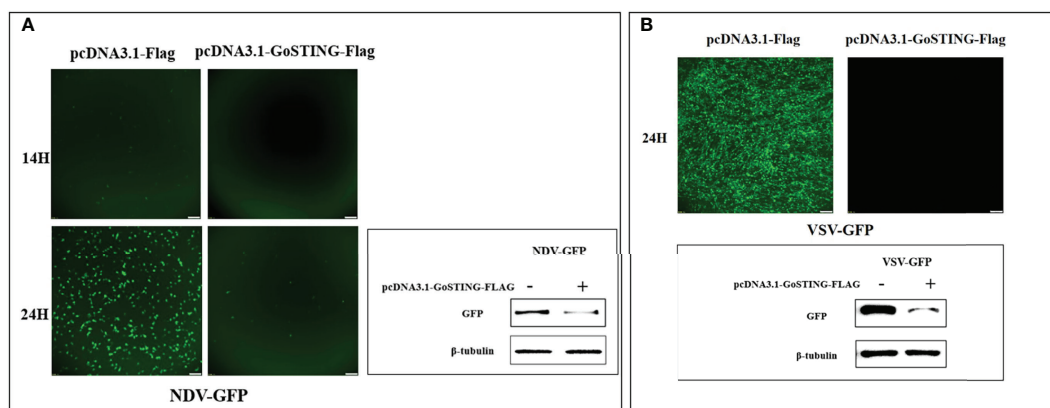


FIGURE 6

GoSTING inhibits viral yield. **(A)** Viral fluorescence in DF-1 cells transfected with pcDNA3.1-Flag or pcDNA3.1-GoSTING-Flag and infected with NDV-GFP at 0.01 MOI. Error bars represent standard deviations and Western blots for the expression of the NDV-GFP. **(B)** Viral fluorescence in DF-1 cells transfected with pcDNA3.1-Flag or pcDNA3.1-GoSTING-Flag and infected with VSV-GFP at 0.01 MOI. Error bars represent standard deviations and Western blots for the expression of the VSV-GFP.

GoSTING is pending and controversial. Therefore, it is necessary to carry out functional research on GoSTING.

In this study, GoSTING was identified with an open reading frame of 1149 bp, encoding 382 amino acid residues (Figure 1A). According to the prediction of the SMART website, GoSTING contains a TMEM173 (50–340 aa) domain (Figure 1B), which is highly conserved in GoSTING and other mammalian STINGs, indicating its important function in the host. Using MegAlign software alignment, the amino acid sequence of GoSTING was 93.5% similar to that of DuSTING, far exceeding that of other species (range from 32.1% to 69%), even to its closest relative birds, chickens, and zebra finches, the amino acid similarities were only 69% and 61.8% (Figure 2A). Similar results can be obtained by phylogenetic tree analysis (Figure 2B). The STING protein sequences of geese, ducks, zebra finches and chickens belong to one subgroup. The STING of mammals, including goats, cattle, pigs, cats, chimpanzees, humans, monkeys, and mice, belong to another subgroup. STING sequences from zebrafish belong to a third subgroup. The above results reflect that GoSTING has a closer genetic relationship with poultry, especially ducks. The predicted three-dimensional structures of GoSTING are shown in Figure 2C.

For the host, the production of IFN to induce the expression of ISGs, which is a powerful viral restriction factor in establishing an antiviral state, is a common strategy to resist viral infection (3). GEF cells were transfected with GoSTING or empty vector and then infected with NDV. As expected, the qRT-PCR test showed that the virus could significantly upregulate the mRNA levels of IFNs (IFN- $\alpha$  and IFN- $\gamma$ ) (Figures 3B, C) and downstream ISGs, including Mx-1 and PKR (Figures 3E, F), which have been shown to play an important role in the antiviral innate immune defense of IFN (37, 38). The proinflammatory factor IL-6 showed the same expression trend (Figure 3C). Many studies have shown that mammalian STING can act as an IFN-activated gene. To elucidate whether GoSTING has the same function, we overexpressed GoSTING in GEF or DF-1 cells and examined the activity of the IFN- $\beta$  promoter by a dual-luciferase reporter assay. The results showed that overexpression of GoSTING could strongly activate the IFN- $\beta$  promoter, and this induction was positively correlated with the dose of transfected GoSTING (Figures 4A–C). Based on the above findings, we infer that GoSTING inhibits NDV replication and exerts immunomodulatory effects by activating IFN pathway disorders and inducing some ISGs in the early stage of viral infection.

To identify the GoSTING domains important for IFN induction, a series of truncated forms of GoSTING mutants were generated, and their relative induction of IFN- $\beta$  promoter activity was measured (Figure 5). The results showed that GoSTING mutants' ability to miss the entire TMEM173 domain to activate the IFN- $\beta$  promoter was significantly reduced, indicating that the TMEM173 domain was necessary

for GoSTING to activate IFN- $\beta$ , which was consistent with the previous TMEM173 domain of mammalian STING. Subtle changes in the amino acid sequence of TMEM173 affect STING-dependent innate immune signaling by reducing the ability to activate type I IFNs (13). Chen et al. determined that the carboxy-terminal region of STING is required and sufficient for activation of TBK1 and stimulation of IRF3 phosphorylation (39). Deletion of GoSTING C-terminal amino acid fragments of different sizes (d181-382aa, d251-382aa, d351-382aa, d374-382aa, and d379-382aa) resulted in a marked reduction in their ability to activate the IFN- $\beta$  promoter. GoSTING-d1-50aa and GoSTING-d1-150aa, lacking 50 and 150 amino acids at the N-terminus of GoSTING, respectively, also had significantly reduced activation ability compared with wild-type GoSTING, which we speculate may be due to a barrier in its localization to the organelle. The underlying mechanism of STING regulation is phosphorylation at some sites in response to stimulation of cytoplasmic DNA (39). Our results show that the S369A point mutant abolished its IFN- $\beta$  activation, suggesting that serine 369 may be an important serine site for STING activation.

Recently, the role of STING in inhibiting RNA viruses has attracted increasing research interest. RNA virus can activate STING and upregulate its expression after invading the host (40, 41). Deletion of STING renders murine embryonic fibroblasts (STING<sup>-/-</sup>MEFs) highly susceptible to infection by minus-strand viruses, including vesicular stomatitis virus (VSV) (42). ChSTING exhibits antiviral function against RNA viruses NDV and VSV (29, 43). We performed a series of experiments to clarify whether GoSTING also has antiviral activity. By monitoring the GoSTING mRNA level, we found that NDV can regulate GoSTING at the transcriptional level and upregulate the expression of GoSTING, and this phenomenon is particularly evident in the early and middle stages of virus infection, which indicates that GoSTING may play an important role in NDV infection. We thus explored the effect of GoSTING on viral replication. The results showed that GoSTING overexpression in DF-1 cells significantly inhibited the viral replication of NDV-GFP and VSV-GFP (Figure 6). In fact, research on STING for confinement of DNA viruses has already started (44). STING has been reported to be involved in innate immune defenses triggered by adenovirus, herpes simplex virus, and papilloma virus (45–47). Studies on chickens and ducks have also shown that in addition to RNA viruses, both chSTING and DuSTING show resistance to DNA viruses (14, 48, 49). Based on the conservation of amino acids in the STING protein that are critical for the recognition of various exogenous nucleic acid moieties (30) and the close kinship of geese to two other avian species, we speculate that GoSTING is required for host responses to both DNA and RNA viruses. This paper demonstrates that GoSTING plays an important role in RNA virus infection, but the role of GoSTING in DNA virus needs further study.

Nowadays some progress has been made in the research of STING in the innate immunity of birds. In this study, the amino acid sequence alignment showed that the homology of GoSTING to DuSTING and chSTING was 93.5% and 69.0%, respectively (Figure 2A). It can be concluded that GoSTING has high homology with STING of birds, especially ducks. In addition, the results of protein domain prediction showed that the TMEM173 domain is conserved in birds, suggesting that birds may be similar in the activation of STING and the recognition of PAMPs. Previous studies have shown that overexpression of chSTING in DF-1 cells can significantly inhibit the replication of AIV and NDV, accompanied by an increase in pro-inflammatory cytokines such as IFN- $\beta$ , IL-1 $\beta$ , and IL-2 (29). The effect of DuSTING on IFN activation and anti-RNA virus has also been elucidated by multiple investigators (31, 50). This study determined the functional characterization of GoSTING and found that GoSTING also has similar functions. We therefore conclude that STING is an essential IFN mediator that plays a role in avian innate immunity against RNA viruses. It is worth mentioning that both chSTING and DuSTING show resistance to DNA viruses, but whether GoSTING has the ability to resist DNA viruses remains to be studied.

However, the IFN signaling mechanisms of STING in chickens, ducks, and geese may be different, although they belong to the same bird species. At present, a relatively comprehensive study of the innate immune signaling pathway in chickens has been carried out. The biggest difference between the RLR pathway of chickens, ducks and geese is that chickens lack RIG-I (51), a key receptor for sensing many RNA viruses in birds, including AIV and NDV (32), making chickens more susceptible to some viruses, especially RNA viruses that require RIG-I for recognition. Previous studies in our laboratory showed that chSTING senses AIV virus by using MDA5 to compensate for RIG-I, and conducts signal transduction through MDA5-STING-IFN pathway (29). Nonetheless, chicken MDA5 is not sufficient against AIV, and AIV often causes lethal death in chickens (30). In contrast, ducks and geese tend to be natural hosts for many asymptomatic AIV subtypes (30), which are related to the molecular basis of their RIG-I. DuSTING was identified as an important receptor that responds to AIV infection and induces IFN- $\beta$  production, but how RIG-I works for the function of DuSTING in RIG-I present ducks is unclear (31). Our results suggest that GoSTING is an important regulator of IFN, pro inflammatory cytokines and ISGs, and plays a role in antiviral innate immunity in geese. However, the current research on the RLR pathway of waterfowl, especially geese, is still relatively fragmented. Although both GoRIG-I (32) and GoMDA5 (52) have been shown to play a role in the anti-RNA virus innate immunity of geese, whether pathogen-associated RNA triggers STING signaling through RIG-I or MDA5 or whether RIG-I and MDA5 share the downstream STING signaling pathway is unclear. Future experiments based

on RIG-I or MDA5 knockout duck cell lines may be required for further validation.

To sum up, our findings suggest that GoSTING is an important innate immune modulatory molecule involved in antiviral innate immunity in geese through its involvement in the type I IFN signaling pathway. The overexpression of GoSTING can upregulate several important pivotal ISGs and proinflammatory factors and combat NDV infection. Our study complements the functional characteristics of GoSTING, enriches the overall understanding of avian STING, and contributes to a more comprehensive and systematic understanding of the anti-RNA virus innate immune signaling pathway of avian STING.

## Data availability statement

The original contributions presented in the study are included in the article/supplementary material. Further inquiries can be directed to the corresponding authors.

## Ethics statement

The studies involving goose embryos were conducted in the laboratory of Shanghai Veterinary Research Institute. The studies were reviewed and approved by the Animal Ethics Committee of Shanghai Veterinary Research Institute (20210521). The animal study was reviewed and approved by the Animal Ethics Committee of Shanghai Veterinary Research Institute.

## Author contributions

YC and JS designed the experiment. FF and ZL performed the majority of the experiments. JW, PL, YanL and YawL helped with the experiments. FF, ZL and YC wrote the paper. ZW, JM, and YY helped analyze the experimental results. All authors contributed to the article and approved the submitted version. All authors contributed to the article and approved the submitted version.

## Funding

This research was supported by the Natural Science foundation of Shanghai (20ZR1425100), the National Natural Science Foundation of China (32072865, and 32072864), Science and Technology Commission of Shanghai Municipality (21N41900100), the Interdisciplinary Program of Shanghai Jiao Tong University (YG2021QN108), and State Key

Laboratory of Veterinary Biotechnology Foundation Grant (SKLVBF202107).

## Conflict of interest

The authors declare that the research was conducted in the absence of any commercial or financial relationships that could be construed as a potential conflict of interest.

## References

- Aoshi T, Koyama S, Kobiyama K, Akira S, Ishii KJ. Innate and adaptive immune responses to viral infection and vaccination. *Curr Opin Virol* (2011) 1:226–32. doi: 10.1016/j.coviro.2011.07.002
- Fischer S. Pattern recognition receptors and control of innate immunity: Role of nucleic acids. *Curr Pharm Biotechnol* (2018) 19:1203–9. doi: 10.2174/138920112804583087
- Carty M, Guy C, Bowie AG. Detection of viral infections by innate immunity. *Biochem Pharmacol* (2021) 183:114316. doi: 10.1016/j.bcp.2020.114316
- Damanian B, Blackburn DJ. Innate barriers to viral infection. *Future Microbiol* (2012) 7:815–22. doi: 10.2217/fmb.12.52
- Iwasaki A, Medzhitov R. Regulation of adaptive immunity by the innate immune system. *Science* (2010) 327:291–5. doi: 10.1126/science.1183021
- Lin R, Xing J, Zheng C. Editorial: Sensing DNA in antiviral innate immunity. *Front Immunol* (2021) 12. doi: 10.3389/fimmu.2021.644310
- Thompson MR, Kaminski JJ, Kurt-Jones EA, Fitzgerald KA. Pattern recognition receptors and the innate immune response to viral infection. *Viruses* (2011) 3:920–40. doi: 10.3390/v3060920
- Cheng Y, Ma J, Liu Y, Gao Q, Yan Y, Wang H, et al. Chicken TBK1 interacts with STING and is involved in IFN- $\beta$  signaling regulation. *Dev Comp Immunol* (2017) 77:200–9. doi: 10.1016/j.dci.2017.08.011
- Chen H, Jiang Z. The essential adaptors of innate immune signaling. *Protein Cell* (2013) 4:27–39. doi: 10.1007/s13238-012-2063-0
- Gupta S, Tsoporis JN, Jia SH, Dos Santos CC, Parker TG, Marshall JC. Toll-like receptors, associated biochemical signaling networks, and S100 ligands. *Shock* (2021) 56:167–77. doi: 10.1097/SHK.0000000000001704
- Fitzgerald KA, Kagan JC. Toll-like receptors and the control of immunity. *Cell* (2020) 180:1044–66. doi: 10.1016/j.cell.2020.02.041
- Asami J, Shimizu T. Structural and functional understanding of the toll-like receptors. *Protein Sci* (2021) 30:761–72. doi: 10.1002/pro.4043
- Barber GN. STING: infection, inflammation and cancer. *Nat Rev Immunol* (2015) 15:760–70. doi: 10.1038/nri3921
- Chen S, Wu Z, Zhang J, Wang M, Jia R, Zhu D, et al. Duck stimulator of interferon genes plays an important role in host anti-duck plague virus infection through an IFN-dependent signalling pathway. *Cytokine* (2018) 102:191–9. doi: 10.1016/j.cyto.2017.09.008
- Liu Y, Goulet M-L, Sze A, Hadj SB, Belgnaoui SM, Lababidi RR, et al. RIG-I-Mediated STING upregulation restricts herpes simplex virus 1 infection. *J Virol* (2016) 90:9406–19. doi: 10.1128/JVI.00748-16
- Ran JS, Jin J, Zhang XX, Wang Y, Ren P, Li JJ, et al. Molecular characterization, expression and functional analysis of chicken STING. *Int J Mol Sci* (2018) 19(12):3706. doi: 10.3390/ijms19123706
- Takaoka A, Wang Z, Choi MK, Yanai H, Negishi H, Ban T, et al. DAI (DLM-1/ZBP1) is a cytosolic DNA sensor and an activator of innate immune response. *Nature* (2007) 448:501–5. doi: 10.1038/nature06013
- Orzalli MH, DeLuca NA, Knipe DM. Nuclear IFI16 induction of IRF-3 signaling during herpesviral infection and degradation of IFI16 by the viral ICP0 protein. *Proc Natl Acad Sci USA* (2012) 109:E3008–17. doi: 10.1073/pnas.1211302109
- Zhang Z, Yuan B, Bao M, Lu N, Kim T, Liu YJ. The helicase DDX41 senses intracellular DNA mediated by the adaptor STING in dendritic cells. *Nat Immunol* (2011) 12:959–65. doi: 10.1038/ni.2091
- Lee JH, Chiang C, Gack MU. Endogenous nucleic acid recognition by RIG-I-Like receptors and cGAS. *J Interferon Cytokine Res* (2019) 39:450–8. doi: 10.1089/jir.2019.0015
- Wang J, Ba G, Han YQ, Ming SL, Wang MD, Fu PF, et al. Cyclic GMP-AMP synthase is essential for cytosolic double-stranded DNA and fowl adenovirus serotype 4 triggered innate immune responses in chickens. *Int J Biol Macromol* (2020) 146:497–507. doi: 10.1016/j.ijbiomac.2020.01.015
- Yu H, Bruneau RC, Brennan G, Rothenburg S. Battle royale: Innate recognition of poxviruses and viral immune evasion. *Biomedicine* (2021) 9:765. doi: 10.3390/biomedicine9070765
- Li D, Wu R, Guo W, Xie L, Qiao Z, Chen S, et al. STING-mediated IFI16 degradation negatively controls type I interferon production. *Cell Rep* (2019) 29:1249–1260.e4. doi: 10.1016/j.celrep.2019.09.069
- Ganar K, Das M, Sinha S, Kumar S. Newcastle Disease virus: current status and our understanding. *Virus Res* (2014) 184:71–81. doi: 10.1016/j.virusres.2014.02.016
- Mishra A, Vijayakumar P, Raut AA. Emerging avian influenza infections: Current understanding of innate immune response and molecular pathogenesis. *Int Rev Immunol* (2017) 36:89–107. doi: 10.1080/08830185.2017.1291640
- Sun Y, Mao X, Zheng H, Wu W, Rehman ZU, Liao Y, et al. Goose MAVS functions in RIG-I-mediated IFN- $\beta$  signaling activation. *Dev Comp Immunol* (2019) 93:58–65. doi: 10.1016/j.dci.2018.12.006
- Karpala AJ, Stewart C, McKay J, Lowenthal JW, Bean AG. Characterization of chicken Mda5 activity: regulation of IFN- $\beta$  in the absence of RIG-I functionality. *J Immunol* (2011) 186:5397–405. doi: 10.4049/jimmunol.1003712
- Chen S, Cheng A, Wang M. Innate sensing of viruses by pattern recognition receptors in birds. *Vet Res* (2013) 44:82. doi: 10.1186/1297-9716-44-82
- Cheng Y, Sun Y, Wang H, Yan Y, Ding C, Sun J. Chicken STING mediates activation of the IFN gene independently of the RIG-I gene. *J Immunol* (2015) 195:3922–36. doi: 10.4049/jimmunol.1500638
- Neerukonda SN, Katneni U. Avian pattern recognition receptor sensing and signaling. *Vet Sci* (2020) 7(1):14. doi: 10.3390/vetsci7010014
- Cheng Y, Liu Y, Shi S, Niu Q, Zhu W, Wang Z, et al. Functional characterization of duck STING in IFN- $\beta$  induction and anti-H9N2 avian influenza viruses infections. *Front Immunol* (2019) 10:2224. doi: 10.3389/fimmu.2019.02224
- Sun Y, Ding N, Ding SS, Yu S, Meng C, Chen H, et al. Goose RIG-I functions in innate immunity against Newcastle disease virus infections. *Mol Immunol* (2013) 53:321–7. doi: 10.1016/j.molimm.2012.08.022
- Vaheri A, Ruoslahti E, Hovi T, Nordling S. Stimulation of density-inhibited cell cultures by insulin. *J Cell Physiol* (1973) 81:355–63. doi: 10.1002/jcp.1040810308
- Niu Q, Cheng Y, Wang H, Yan Y, Sun J. Chicken DDX3X activates IFN- $\beta$  via the chSTING-chIRF7-IFN- $\beta$  signaling axis. *Front Immunol* (2019) 10:822. doi: 10.3389/fimmu.2019.00822
- Li ZJ, Li Y, Chang S, Ding Z, Mu LZ, Cong YL. Antigenic variation between Newcastle disease viruses of goose and chicken origin. *Arch Virol* (2010) 155:499–505. doi: 10.1007/s00705-010-0610-7
- Pantin-Jackwood MJ, Swayne DE. Pathogenesis and pathobiology of avian influenza virus infection in birds. *Rev Sci Tech* (2009) 28:113–36. doi: 10.20506/rst.28.1.1869
- Chen S, Zhang W, Wu Z, Zhang J, Wang M, Jia R, et al. Goose mx and OASL play vital roles in the antiviral effects of type I, II, and III interferon against newly emerging avian flavivirus. *Front Immunol* (2017) 8:1006. doi: 10.3389/fimmu.2017.01006
- Liu WJ, Yang YT, Huang YM, Zhou DR, Xu DN, Cao N, et al. Identification of goose PKR gene: Structure, expression profiling, and antiviral activity against Newcastle disease virus. *J Interferon Cytokine Res* (2018) 38:333–40. doi: 10.1089/jir.2018.0025
- Tanaka Y, Chen ZJ. STING specifies IRF3 phosphorylation by TBK1 in the cytosolic DNA signaling pathway. *Sci Signal* (2012) 5:ra20. doi: 10.1126/scisignal.2002521

## Publisher's note

All claims expressed in this article are solely those of the authors and do not necessarily represent those of their affiliated organizations, or those of the publisher, the editors and the reviewers. Any product that may be evaluated in this article, or claim that may be made by its manufacturer, is not guaranteed or endorsed by the publisher.

40. Zhong B, Yang Y, Li S, Wang YY, Li Y, Diao F, et al. The adaptor protein MITA links virus-sensing receptors to IRF3 transcription factor activation. *Immunity* (2008) 29:538–50. doi: 10.1016/j.immuni.2008.09.003
41. Sun W, Li Y, Chen L, Chen H, You F, Zhou X, et al. ERIS, an endoplasmic reticulum IFN stimulator, activates innate immune signaling through dimerization. *Proc Natl Acad Sci USA* (2009) 106:8653–8. doi: 10.1073/pnas.0900850106
42. Ishikawa H, Barber GN. STING is an endoplasmic reticulum adaptor that facilitates innate immune signalling. *Nature* (2008) 455:674–8. doi: 10.1038/nature07317
43. Li S, Yang J, Zhu Y, Ji X, Wang K, Jiang S, et al. Chicken DNA sensing cGAS-STING signal pathway mediates broad spectrum antiviral functions. *Vaccines (Basel)* (2020) 8(3):369. doi: 10.3390/vaccines8030369
44. Ni G, Ma Z, Damania B. cGAS and STING: At the intersection of DNA and RNA virus-sensing networks. *PLoS Pathog* (2018) 14:e1007148. doi: 10.1371/journal.ppat.1007148
45. Lam E, Stein S, Falck-Pedersen E. Adenovirus detection by the cGAS/STING/TBK1 DNA sensing cascade. *J Virol* (2014) 88:974–81. doi: 10.1128/JVI.02702-13
46. Lau L, Gray EE, Brunette RL, Stetson DB. DNA Tumor virus oncogenes antagonize the cGAS-STING DNA-sensing pathway. *Science* (2015) 350:568–71. doi: 10.1126/science.aab3291
47. Ge R, Zhou Y, Peng R, Wang R, Li M, Zhang Y, et al. Conservation of the STING-mediated cytosolic DNA sensing pathway in zebrafish. *J Virol* (2015) 89:7696–706. doi: 10.1128/JVI.01049-15
48. Oliveira M, Rodrigues DR, Guillory V, Kut E, Giotis ES, Skinner MA, et al. Chicken cGAS senses fowlpox virus infection and regulates macrophage effector functions. *Front Immunol* (2021) 11:613079–9. doi: 10.3389/fimmu.2020.613079
49. Liu Y, Lin R, Olgarnier D. Regulation of STING expression: at the crossroads of viral RNA and DNA sensing pathways. *Inflammation Cell Signal* (2017) 4:e1491. doi: 10.14800/ics.1491
50. Zhang W, Jiang B, Zeng M, Duan Y, Wu Z, Wu Y, et al. Binding of duck tembusu virus nonstructural protein 2A to duck STING disrupts induction of its signal transduction cascade to inhibit beta interferon induction. *J Virol* (2020) 94(9):e01850–19. doi: 10.1128/JVI.01850-19
51. Magor KE, Miranzo Navarro D, Barber MRW, Petkau K, Fleming-Canepa X, Blyth GAD, et al. Defense genes missing from the flight division. *Dev Comp Immunol* (2013) 41:377–88. doi: 10.1016/j.dci.2013.04.010
52. Wei LM, Jiao PR, Song YF, Han F, Cao L, Yang F, et al. Identification and expression profiling analysis of goose melanoma differentiation associated gene 5 (MDA5) gene. *Poultry Sci* (2013) 92:2618–24. doi: 10.3382/ps.2013-03064



## OPEN ACCESS

## EDITED BY

Rongtuan Lin,  
McGill University, Montreal, Canada

## REVIEWED BY

Sun Zhaoyang,  
Fudan University, China  
Weizheng Liang,  
First Affiliated Hospital of Hebei North  
University, China

## \*CORRESPONDENCE

Zhongjun Wu  
wjzjtcy@126.com

## SPECIALTY SECTION

This article was submitted to  
Viral Immunology,  
a section of the journal  
Frontiers in Immunology

RECEIVED 29 April 2022

ACCEPTED 30 June 2022

PUBLISHED 28 July 2022

## CITATION

Li J, Yu J, Zhang T, Pu X, Li Y and  
Wu Z (2022) Genomic analysis  
quantifies pyroptosis in the immune  
microenvironment of HBV-related  
hepatocellular carcinoma.  
*Front. Immunol.* 13:932303.  
doi: 10.3389/fimmu.2022.932303

## COPYRIGHT

© 2022 Li, Yu, Zhang, Pu, Li and Wu.  
This is an open-access article  
distributed under the terms of the  
[Creative Commons Attribution License  
\(CC BY\)](https://creativecommons.org/licenses/by/4.0/). The use, distribution or  
reproduction in other forums is  
permitted, provided the original  
author(s) and the copyright owner(s)  
are credited and that the original  
publication in this journal is cited, in  
accordance with accepted academic  
practice. No use, distribution or  
reproduction is permitted which does  
not comply with these terms.

# Genomic analysis quantifies pyroptosis in the immune microenvironment of HBV-related hepatocellular carcinoma

Jiarui Li<sup>1</sup>, Jinghui Yu<sup>2</sup>, Ting Zhang<sup>3</sup>, Xingyu Pu<sup>4</sup>, Yilan Li<sup>1</sup>  
and Zhongjun Wu<sup>1\*</sup>

<sup>1</sup>Department of Hepatobiliary Surgery, The First Affiliated Hospital of Chongqing Medical University, Chongqing, China, <sup>2</sup>Department of International Business, College of economics, Fudan University, Shanghai, China, <sup>3</sup>Department of Phase I Clinical Trial Ward, The First Affiliated Hospital of Chongqing Medical University, Chongqing, China, <sup>4</sup>Department of Liver Surgery and Liver Transplantation Center, West China Hospital of Sichuan University, Chengdu, China

Pyroptosis, a way of pro-inflammatory death, plays a significant part in the tumor microenvironment (TME). A recent study has shown that the hepatitis C virus changes the TME by inducing pyroptosis against hepatocellular carcinoma (HCC). However, compared to TME in hepatitis C virus-infected HCC, the exploration of immune characteristics and response to immunotherapy associated with the pyroptosis phenotype is still insufficient in hepatitis B virus-related HCC (HBV-HCC). Our study constructed pyroptosis-score (PYS) *via* principal-component analysis (PCA) to unveil the link between pyroptosis and tumor immunity in 369 HBV-HCC patients. Compared with the low-PYS group, subjects with higher PYS were associated with poor prognosis but were more susceptible to anti-PD-L1 treatment. In addition, we found that PYS can serve independently as a prognostic factor for HBV-HCC, making it possible for us to identify specific small molecule drugs with a potential value in inhibiting tumors *via* targeting pyroptosis. Also, the target genes predicted by the Weighted gene co-expression network analysis (WGCNA) and pharmacophore model were enriched in the HIF-1 signaling pathway and NF- $\kappa$ B transcription factor activity, which were related to the mechanism of inflammation-driven cancer. The PYS is extremely important in predicting prognosis and responses to immunotherapy. New treatment strategies for inflammation-driven cancers may be found by targeting pyroptosis.

## KEYWORDS

hepatitis B virus, hepatocellular carcinoma, pyroptosis score, fisetin, tumor immune microenvironment, anti-PD-L1 treatment



## Introduction

Chronic hepatitis B virus (HBV) infection is one of the leading causes of liver cancer, accounting for 50–80% of all cases globally (1). Most viruses, such as HBV DNA, RNA, and similar viral proteins, have become less dangerous due to widespread immunization and antiviral medication. However, the persistence of cccDNA makes it challenging to cure HBV with current procedures. There is a chance that some viral risk factors existed or occurred before the antiviral medication. Despite undetectable HBV DNA, viral risk factors such as HBV integration and HBV mutation may persist and contribute to the advancement of HCC.

Pyroptosis is a type of programmed cell death that relates to inflammatory cells death. Pyroptosis promotes the activation of several caspase family members, including caspase-1, through inflammasomes, causing a variety of gasdermin family members, including gasdermin-D, to shear and multimerize to generate 12–14 nm membrane holes, which is the basis of antitumor action. After cell rupture, pro-inflammatory cytokines and immunogenic chemicals are released, causing the cells to expand and eventually melt, promoting immune cell activation and infiltration (2–4). Since one of the characteristics of tumors is to avoid apoptosis, the induction of pyroptosis is of paramount significance in treating anti-apoptotic tumors. In earlier studies, Wei et al. found that the deletion of NLRP3 inflammasome is closely related to the development of hepatocellular carcinoma, while 17 $\beta$ -estradiol inhibits hepatocellular carcinoma *via* activating NLRP3 (5, 6). In addition, Wei et al. also found that inhibiting autophagy can accelerate the pyroptosis of hepatoma cells (7).

On the other hand, aberrant pyroptosis may have a role in fostering the establishment of the tumor immune microenvironment (TIME) due to its inflammatory character. Like many other cancers, HCC is highly heterogeneous. Although more and more immune checkpoint inhibitors have been approved to improve chemotherapy sensitivity in HCC, the outcome can still be inaccurate. Patients who have similar disease phenotypes do not mean that they have the same molecular etiology, so they are very likely to have different immunotherapy responses. In this case, stratifying patients at the molecular level will help formulate the most effective treatment options. Therefore, it is clinically significant to determine what patients benefit from immunotherapy.

Hepatitis B infection is the main cause of HCC, but it is unknown whether pyroptosis could be a potential phenotype for prognosis in HBV-HCC. Our study has constructed two subtypes of pyroptosis, closely related to different prognosis and tumor microenvironment characteristics. Unlike prior studies, we propose using the PYS to measure each HBV-HCC patient's pyroptosis phenotype. The mRNA expression profile of pyroptosis-related genes (PRGs) is used in this technique. We

are convinced that this system will help medical workers make more effective decisions in the comprehensive management of patients.

## Materials and methods

### Hepatocellular carcinoma dataset acquisition

Open access gene-expression data and complete clinical information were retrieved from Gene-Expression Omnibus (GEO; <https://www.ncbi.nlm.nih.gov/gds/>) and the Cancer Genome Atlas (TCGA; <https://portal.gdc.cancer.gov/>) database on January 6, 2022. Based on clinical data and previous literature reports, our study collected 6 eligible HBV-HCC cohorts (GSE14520, GSE141198, GSE141200, GSE10141, GSE140901, and TCGA-HBV-LIHC) with survival information for further comprehensive analysis (8–10). Fragments per kilobase million (FPKM) values of TCGA-HBV-LIHC datasets (containing 95 HBV-HCC patients) were converted into transcripts per kilobase million (TPMs). All the genes expression analysis was generated by using R with the log (2) (TPM + 1). The “ComBat” algorithm was executed when merging different datasets to reduce the likelihood of batch effects from non-biological technical biases. The complete clinical information of 369 HBV-HCC patients is shown in [Table S1](#).

### Consensus clustering analysis based on PRGs

To identify unique pyroptosis clusters, we employed an unsupervised clustering algorithm to classify patients based on the expression profiles of 32 PRGs ([Table S2](#)) retrieved from previous reviews (11–14). The “ConsensusClusterPlus” package was performed to ensure the stability of the classification (method=“ConsensusClusterPlus”, clusterAlg=“pam”, distance=“euclidean”) (15). The subtypes, according to PRGs, were validated using principal component analysis (PCA).

### Single sample gene-set enrichment analysis

To observe the intrinsic link between different subtypes and the immune microenvironment, the degree of enrichment for 23 immune cells and 13 immunological activities in each HBV-HCC sample using the gene set variation analysis (GSVA) program (method=“gsva” and kcdf = “Gaussian”) was measured (16). A Kruskal-Wallis test was also used to assess subtypes' immune infiltration and functions.

## Prognostic differential expression genes associated with the pyroptosis subtypes

The eligible 369 HBV-HCC patients were classified into different pyroptosis subtypes, and DEGs were identified by employing the “limma” package. We used the “clusterProfiler” package to implement Gene Ontology (GO) and Kyoto Encyclopedia of Genes and Genomes (KEGG) analysis for DEGs (17). The Cox regression analysis was then conducted to discriminate prognosis-related genes among the DEGs, in which  $P < 0.05$  was considered eligible.

## Dimension reduction and calculation of PYS

Based on the expression profiles of prognostic DEGs, we classified the subjects into different gene clusters using unsupervised clustering analysis, which was verified by PCA. After that, the dimension reduction of the prognostic pyroptosis-related gene clusters was carried out by the Boruta algorithm. Principal component 1, as the gene cluster score, was obtained through the application of PCA. A formula akin to gene expression grade (18) was used to estimate PYS for each sample as follows:

$$\text{PYS} = \sum \text{PC}_{1\text{I}} - \sum \text{PC}_{1\text{II}}$$

In this formula,  $\text{PC}_{1\text{I}}$  means the first component of gene cluster I, while  $\text{PC}_{1\text{II}}$  represents the first component of gene cluster II.

## Evaluation of the PYS model

By applying the “timeROC” package, the accuracy of our model was evaluated. In contrast to the PYS model, we established nomograms that could predict patients’ 1-, 3- and 5-year overall survival using the “rms” package.

## Immune landscape of PYS model

To assess the abundances of immune cell subpopulations and immune functions of the tumor microenvironment between the low- and high-PYS groups, functional enrichment was conducted *via* ssGSEA. Besides, we compared the stromal cells and immune cells scores of HBV-HCC patients by applying the “ESTIMATE” algorithm (19).

## Assessment of tumor mutation burden of PYS model

To identify the driver genes linked to TMB, we used the “maftools” program to calculate the sum of non-synonymous

mutations in TCGA-HBV-LIHC data and compare somatic changes across high and low PYS groups.

## Drug and immune checkpoint blockade sensitivity

The sensitivity to chemotherapy was evaluated utilizing the Genomics of Drug Sensitivity in Cancer (GDSC; <https://www.cancerrxgene.org/>) database (20). Then, the half-maximal inhibitory concentration (IC50) was quantified using the “pRRophetic” package (21). We also used the Cancer Imaging Archive (TCIA; <https://tcia.at/>) website to forecast the therapeutic benefits of immune checkpoint blockade therapy between the low and high PYS groups (22).

## External validation of the immunotherapy based on PYS

The same protocols as the previous analysis to get the PYS of GSE140901 and the Kaplan-Meier survival curves were displayed by the “SurvMiner” package to compare the overall survival between low- and high-PYS groups after anti-PDL1 Immunotherapy of HBV-HCC patients.

## Detection of key co-expression modules applying WGCNA

We constructed the co-expression networks of the TCGA-HBV-LIHC and GSE14520 cohort, respectively, using the “WGCNA” package (minModuleSize = 50) (23). Function *pickSoftThreshold* was used to build a scale-free network where soft powers  $\beta = 2$  and 3 were selected for TCGA-HBV-LIHC and GSE14520. The remaining steps are consistent with those described by Langfelder and Horvath (23).

## The excavation of compounds for small molecules based on PYS

The “limma” software was used to detect DEGs between low- and high-PYS groups for further analysis, with significant differential expression set at  $|\log_2\text{FC}| \geq 1$  and  $\text{FDR} < 0.05$ . Following that, using the “VennDiagram” program, the intersection of DEGs and co-expression genes retrieved from the co-expression network was used to evaluate prospective prognostic targets (24). After that, we uploaded the overlapping parts of genes into the Connectivity map (CMap; <http://portals.broadinstitute.org/cmap/>) website (25), and the parts of the gene expression changes caused by drugs that whether are similar or opposite to these differential gene

expression profiles are identified, to screen for drugs that potentially regulate PYS. Candidate small molecular compounds whose mean is greater than 0.7 were eligible. Furthermore, we downloaded the 3D structures of compounds from PubChem (<https://pubchem.ncbi.nlm.nih.gov>) database (26) and obtained the molecule and pharmacophore model from PharmMapper (<http://www.lilab-ecust.cn/pharmmapper/>) (27). Enrichment analyses for GO and KEGG based on the specific compound's potential target genes were performed using the "clusterProfiler" package.

## Cell culture

The human HepG2 hepatoma cell line was purchased from the Cell Bank of the Chinese Academy of Sciences (Shanghai, China). HepG2 cells were incubated in DMEM medium (VivaCell, Shanghai, China), supplemented with 10% fetal bovine serum (VivaCell, Shanghai, China). Cells were cultured in a 37°C incubator containing 5% carbon dioxide.

## CCK-8, caspase-1 activity and cytokine level assay

According to the manufacturer's protocol, cell viability was measured with a CCK-8 assay (Absin Bioscience, Shanghai, China). Succinctly, mix with 10 µl of CCK-8 solution per 90ul complete medium, add to each well of the 96-well plate, and incubate at 37°C for 1 h. The optical density is then measured at an absorption wavelength of 450 nm. The enzymatic activity of Caspase-1 in HepG2 was detected by the Caspase 1 Activity Detection Kit (Beyotime Institute of Biotechnology, Beijing, China) according to the manufacturer's protocol based on the ability of Caspase-1 to change acetyl-TyrVal-Ala-Asp p-nitroanilide (Ac-YVAD-pNA) into the yellow formazan product p-nitroaniline (pNA). According to the manufacturer's instructions, cytokine levels of human IL-1β in the cell culture supernatant were determined by an ELISA kit from Neobioscience Technology (Shenzhen, China).

## Inflammasome stimulation and determination of pyroptosis

For NLRP3 inflammasome stimulation, HCC cells were stimulated by 1 µg/ml lipopolysaccharide (LPS) (Sigma-Aldrich; St. Louis, MO, USA) for 24 h to pyroptosis detection mixed with or without fisetin (MedChemExpress, New Jersey, USA). The morphology of pyroptosis was examined under light microscopy.

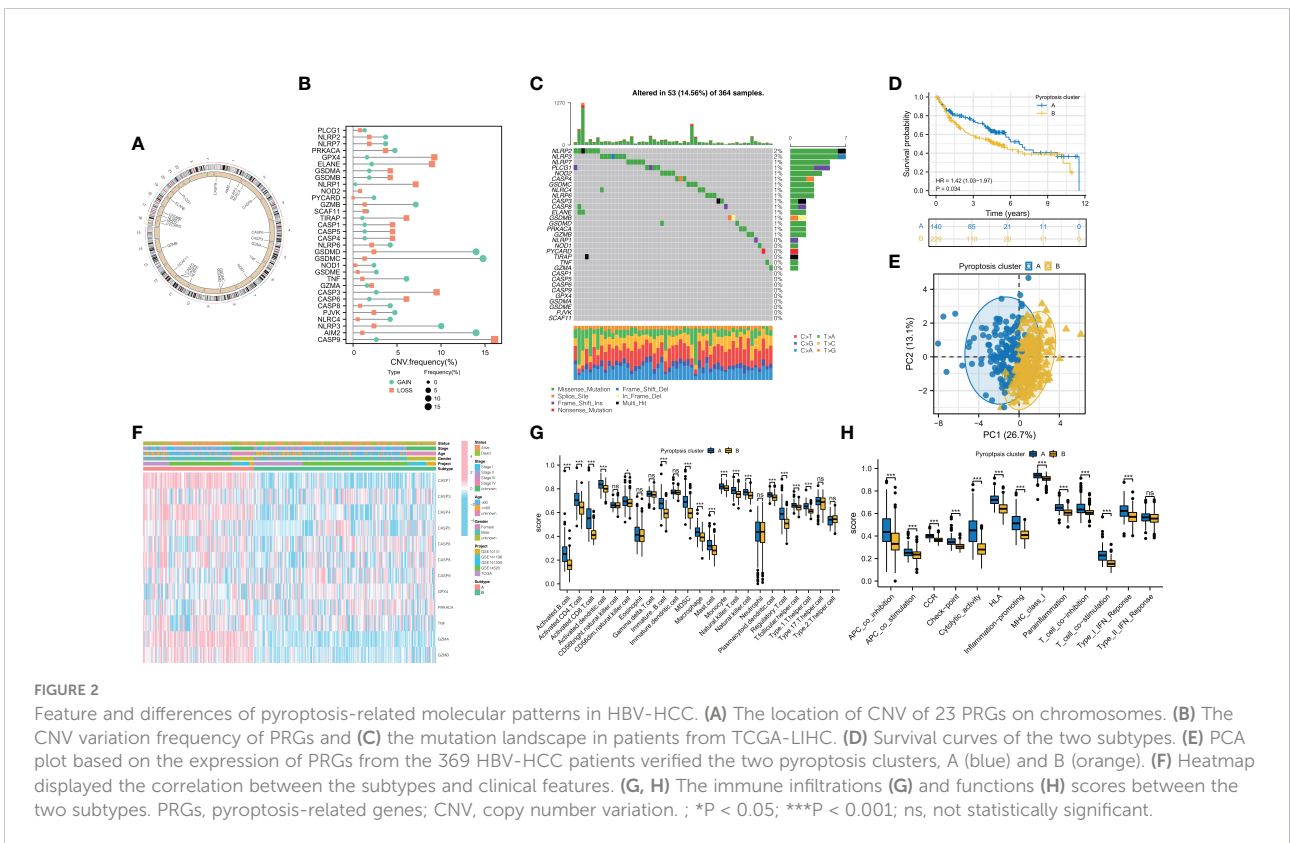
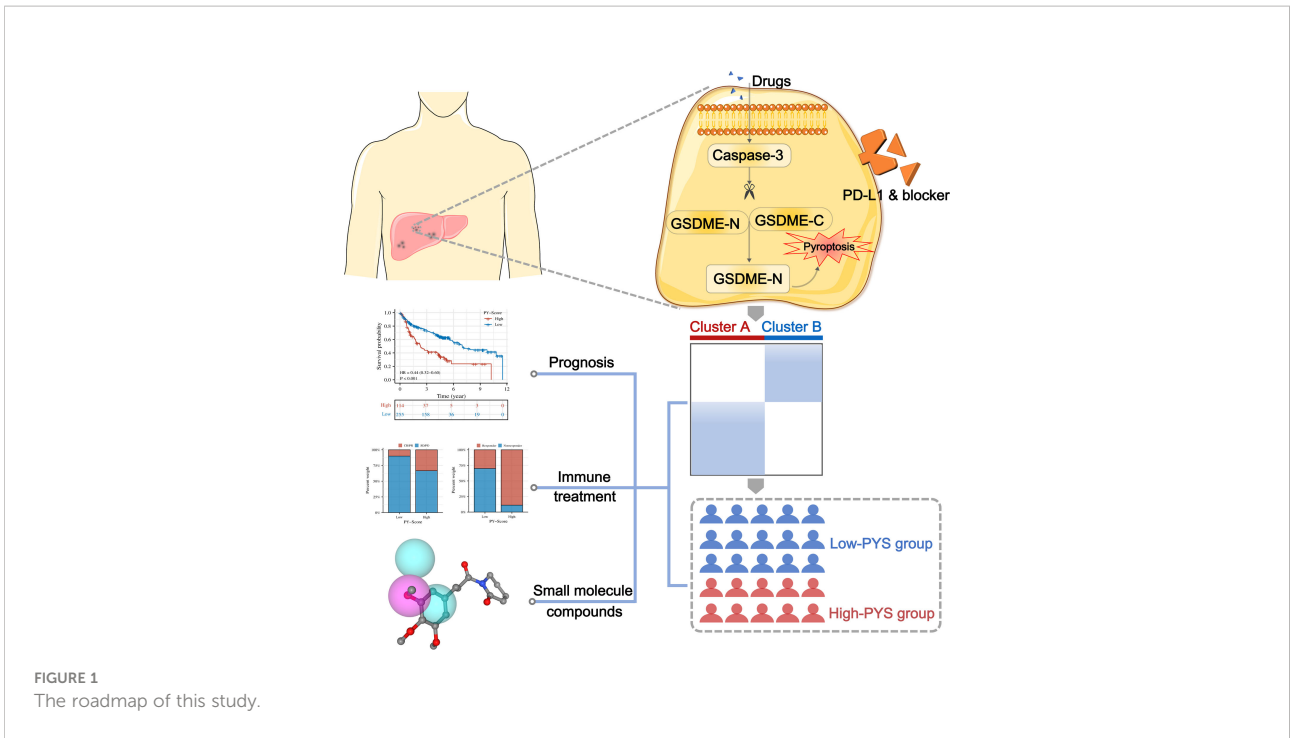
## Statistical analysis

Statistical analysis was executed by R (version 4.0.5). The "ComBat" algorithm was conducted to diminish the batch effects. The Wilcoxon rank-sum test was used to compare two groups, and multiple comparisons were presented by the Kruskal–Wallis test. Patients' overall survival (OS) in different groups was compared using the Kaplan-Meier analysis and the log-rank test. The connection between OS, clinicopathological features, and pyroptosis scores was investigated using univariate and multivariate Cox regression models. The Student's t-test was used to analyze differences between two groups, and one-way ANOVA was used when more than two groups were compared. To fix the *P*-value, we performed Bonferroni's test. Statistical significance was defined as a two-sided *P* < 0.05. The graphic abstract of this study is shown in Figure 1.

## Results

### Characteristics of TIME and survival outcomes between pyroptosis phenotypes

CNVs and TMB are not only closely linked to the occurrence and development of tumors, but also serve as an emerging biomarker for immunotherapy in diverse cancers (28–30). We found copy number variations (CNVs) in 23 of the 32 PRGs in TCGA-LIHC. The locations of CNV on chromosomes according to PRGs were shown in Figure 2A and mostly focused on copy number amplification (Figure 2B). Regarding genetic performance, 53 of the 364 samples (around 14.56%) displayed pyroptosis-related regulator mutations, among which NLRP2 had the highest frequency of mutations (Figure 2C). PRGs represent a set of genes that play an important role in the occurrence and development of pyroptosis. To investigate whether the degree of pyroptosis is related to the occurrence and development of HBV-HCC, we established two molecular patterns *via* unsupervised clustering analysis according to the mRNA expression profiles of 32 PRGs in 369 HBV-HCC patients (Figures S1A–C). As is illustrated in Figure 2D, the survival time of subjects in cluster A was significantly prolonged. Also, we have substantiated that these two subtypes can be discriminated by using PCA (Figure 2E). Figure 2F exhibited a heatmap of clinicopathological characteristics. Besides, we have evaluated the correlation between the subtypes and the characteristics of the tumor immune microenvironment. The results show differences in immune cell infiltration (Figure 2G) and immune function (Figure 2H) between the two subtypes. Compared with pyroptosis cluster B, activated B cells, CD8<sup>+</sup> T lymphocytes, and natural killer T lymphocytes were more enriched in cluster A. Meanwhile, cytolytic activity and type I IFN response in pyroptosis cluster A have a higher score.



## Clinical and TIME features between prognostic gene clusters based on pyroptosis phenotypes

To better understand the biological behaviors of these subtypes and figure out the specific score of each patient, we first performed a screen to identify the prognostic DEGs between the two subtypes. The outcomes of GO and KEGG have demonstrated that DEGs were particularly enriched in Viral protein interaction with cytokine and cytokine receptor, T cell activation, cytokine activity, and rheumatoid arthritis (Figure 3A). Next, we screened 229 prognostic DEGs *via* univariate Cox regression analysis ( $P < 0.05$ , Table S3). Based on these prognostic DEGs, the consensus cluster analysis was performed, and thus the subjects were divided into the two gene clusters (Figures S2A–C). Subsequently, the prognostic significance of the gene clusters was further analyzed. As shown in Figure 3B, subjects within gene cluster II performed better and survived much more time.

In contrast, the ones in gene cluster I had a shorter OS time. The division of subjects based on gene clusters was validated *via* PCA (Figure 3C). The clinical characteristics of prognostic DEGs between the genomic clusters were visualized through a heatmap of the transcriptomic profile (Figure 3D). Then, we investigated whether these two gene clusters have different TIME characteristics. As shown in Figure 3E, the Th17 cell in gene cluster II has a higher score, while the Treg cells, Th2 cells, and dendritic cells in gene cluster I are more prominent. Intriguingly, the activated CD8<sup>+</sup> T lymphocytes in gene cluster I infiltrate

significantly. As tumor killer cells, CD8<sup>+</sup> T lymphocytes are essential for antitumor immunity, contradicting its poor prognosis. So we looked at the expression of immune evasion-related indicators in distinct gene clusters. The results showed that T cell exhaustion-related biomarkers were up-regulated in gene cluster I, indicating that the activated CD8<sup>+</sup> T cells enriched in gene cluster I and exhibited immunosuppressive effects (Figures S3A–C). Compared with gene cluster II, gene cluster I has higher pro-inflammatory and type II interferon response scores (Figure 3F).

## Establishment and assessment of the pyroptosis scoring system for HBV-HCC

We next calculated the PYS for each subject by implementing PCA to provide useful guidance for the clinical treatment of HBV-HCC. Figure 4A illustrates subjects' PYS distribution and survival status in different subtypes and gene clusters. Subjects in pyroptosis cluster B had a higher PYS ( $P < 0.001$ ; Figure 4B). At the same time, there was a higher PYS in gene cluster II ( $P < 0.001$ ; Figure 4C). As is shown in Figures 4D–F, subjects with higher PYS usually had a worse prognosis ( $P < 0.001$ ).

In an independent prognostic analysis, *via* univariate (Figure 5A) and multivariate (Figure 5B) Cox analysis, we found that PYS (HR: 1.022, 95CI: 1.014–1.030,  $P < 0.001$ ) and tumor stage (HR: 2.418, 95CI: 1.824–3.205,  $P < 0.001$ ) can serve as independent prognostic indicators of patients. Figure 5C showed that the predicted area under the curves (AUC) of the 1, 3, and 5-

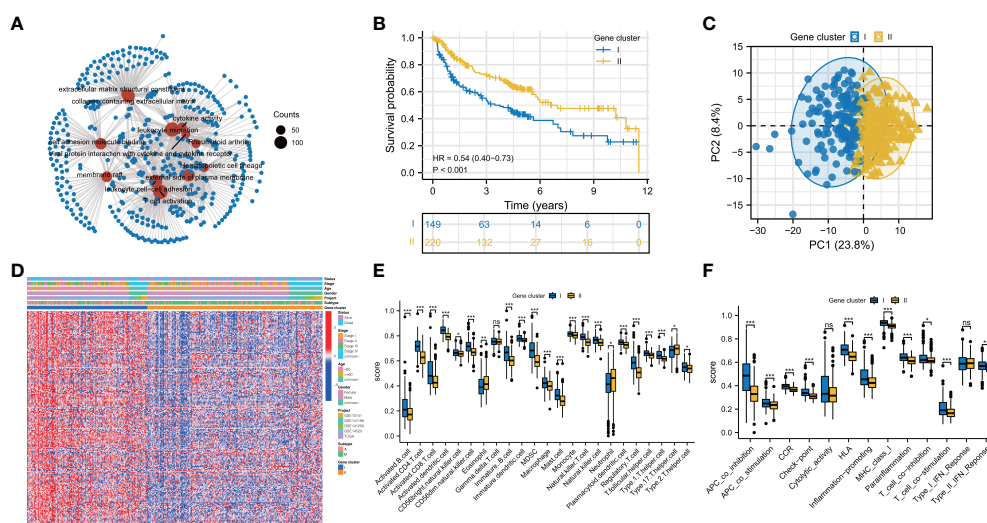


**FIGURE 3** Prognosis and immune landscape between pyroptosis gene clusters for HBV-HCC patients. **(A)** GO and KEGG enrichment analysis for DEGs between two subtypes. **(B)** Survival curves of the two gene clusters. **(C)** PCA plot based on the expression of prognostic prognosis-related DEGs from pyroptosis clusters verified the two gene clusters, I (blue) and II (orange). **(D)** Clinical characteristics of gene clusters were shown by heatmaps. **(E, F)** The immune infiltrations **(E)** and functions **(F)** scores between the two gene clusters. DEGs: differentially expressed genes; \* $P < 0.05$ ; \*\* $P < 0.01$ ; \*\*\* $P < 0.001$ ; ns, not statistically significant.

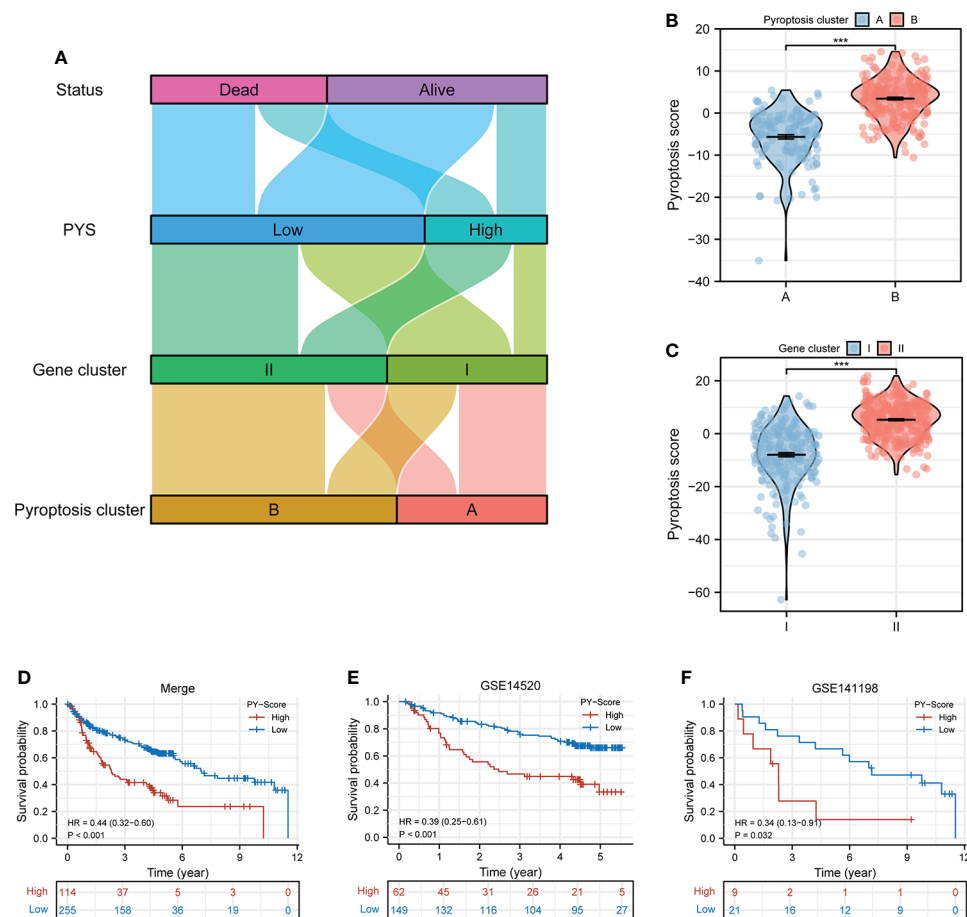


FIGURE 4

Construction of the PYS model for HBV-HCC patients. (A) Crosstalk between pyroptosis clusters, gene clusters, pyroptosis score, and survival status. (B, C) The differences in pyroptosis score in the pyroptosis clusters (B) and the gene clusters (C). (D–F) Kaplan-Meier curves of patients within PYS groups in merge cohort (D), GSE14520 (E), and GSE141198 (F). PY, pyroptosis score. \*\*\*P < 0.001

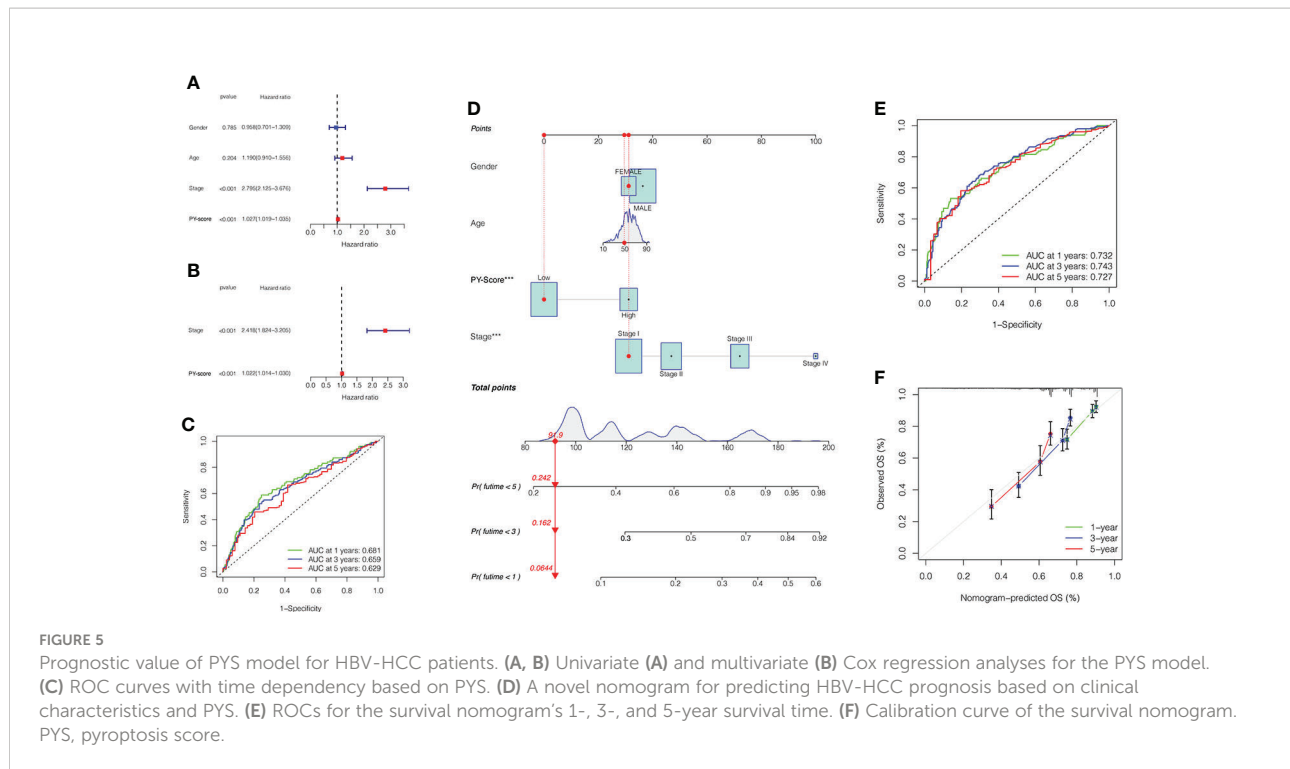
year OS are 0.681, 0.659, and 0.629, respectively, suggesting that the PYS offers an important reference value in predicting the prognosis of HBV-HCC. Meanwhile, we also constructed a survival nomogram with clinical-pathological characteristics and PYS as a “blueprint” for managing patients with HBV-HCC (Figure 5D). Compared with the PYS model, the survival nomogram can predict the HBV-HCC patients’ prognosis with higher validity and reliability (Figure 5E, F).

## The intrinsic relationship between the PYS and TMB

Many studies have concluded that TMB is not only closely related to the occurrence and development of tumors but also can predict the efficacy of immunotherapy. For example, tumors with higher mutational burdens tend to be accompanied by higher CD8<sup>+</sup> T cell infiltration and improve response to PD-1

blockades, which means that TMB may determine how patients respond to immunotherapy. However, TMB alone is insufficient to predict the prognosis of patients. Therefore, we investigated the internal relationship between TMB and PYS. First, we analyzed and compared the situation of TMB in the high-PYS and low-PYS group. Figure 6A suggested that there was a significant correlation between TMB and PYS. Then we discovered that HBV-HCC patients with a high TMB have a worse prognosis (Figure 6B). To determine whether PYS can act as a predictor independent of TMB, we evaluated the synergy of PYS and TMB in the prognostic stratification of HBV-HCC. As shown in Figure 6C, PYS differs significantly in the high-TMB and low-TMB groups ( $P=0.042$ ). The results indicate that PYS may serve as a biological indicator independent of TMB for predicting the efficacy of immunotherapy in HBV-HCC patients.

Subsequently, we researched the driver genes of somatic mutation in HBV-HCC, and the top 20 genes with the highest



mutation frequency in the low and high PYS groups were shown in **Figures 6D, E**, respectively. These gene mutations prompt new ideas for the immunotherapy of HBV-HCC patients in different PYS groups.

## PYS is related to TIME features and immune checkpoint blockade therapy of HBV-HCC

The role of pyroptosis seems to be a double-edged sword in cancer. In addition to rapidly leading to tumor regression, it can promote the development of the TIME. For further exploration of the relevance between the PYS and TIME features, the ridge plot of TIME based on PYS was shown in **Figure 7A**. Meanwhile, the immune ( $P < 0.001$ ) and stromal score ( $P < 0.001$ ) scores of patients from the low-PYS group outnumbered those of the other group (**Figure 7B**). Cellular characterization of immune infiltration suggests that tumor genotype determines immunophenotype and tumor escape mechanisms. We further worked on the expression of immune checkpoints in the high- and low-PYS groups. We found in the low-PYS group that the expression of immune escape-related biomarkers such as PD-1 and CTLA-4 were significantly up-regulated in TCGA-HBV-LIHC, GSE14520, GSE141198, and GSE141200 cohort (**Figures 7C–F**). The immunophenoscore (IPS) based on the expression of important components of tumor immunity between low- and high-PYS groups was assessed using the

TCIA database (**Figure 7G**). Herein, we found that whether the use of CTLA-4 blocker alone (**Figure 7H**), PD-1 blocker alone (**Figure 7I**), or PD-1 combined with CTLA-4 blockers (**Figure 7J**), IPS was higher in the low-PYS group.

## Sensitivity of chemotherapy and benefits of anti-PD-L1 immunotherapy in HBV-HCC patients based on the PYS model

Studies have shown that chemotherapy and some non-chemotherapeutic drugs can trigger pyroptosis in most cancers (**31–33**). Compared with monotherapy, combining chemotherapy and other methods is way more effective in promoting the pyroptosis of cancer cells, stimulating a stronger immune response to prevent the worsening of tumors. We then compared and analyzed the IC<sub>50</sub> levels among 5 chemotherapy drugs, Sorafenib, Doxorubicin, Mitomycin C, Vinblastine, and Cisplatin (**Figures 8A–E**). Our data showed that the high-PYS group possessed a lower IC<sub>50</sub> level of sorafenib ( $P < 0.001$ ) than the other group, while the IC<sub>50</sub> of Doxorubicin ( $P < 0.01$ ) was exactly the opposite, whereas the high-PYS group had a higher level. A recent study has shown that sorafenib changes the tumor immune microenvironment by inducing pyroptosis against hepatocellular carcinoma. Our results further evaluated the utility of the PYS in predicting the benefit of anti-PD-L1 immunotherapy in HBV-HCC patients. First, HBV-HCC patients in the GSE140901 cohort

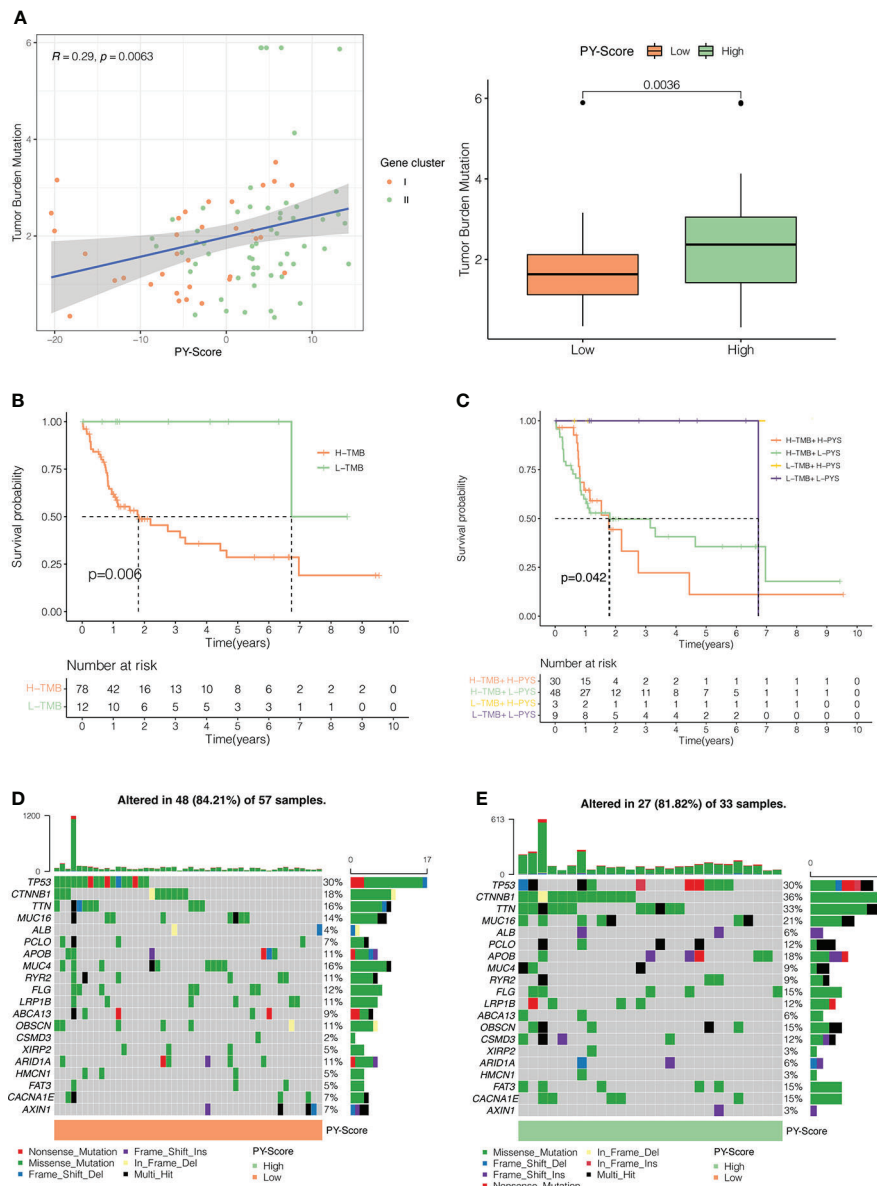


FIGURE 6

The Inner link between the PYS and TMB. (A) The correlation between the PYS and TMB.  $P < 0.01$ . (B) Survival curves for high and low TMB groups in the TCGA-HBV-LIHC cohort.  $P = 0.006$ . (C) Survival curves for HBV-HCC patients classified by TMB and PYS. The oncoPrint was constructed via the low-PYS group (D) and high-PYS group (E).

( $n=19$ ) who received anti-PD-L1 immunotherapy were assigned to low- or high-PYS groups. It is noteworthy that high-PYS subjects performed better and lived longer than the low-PYS ones for overall survival ( $P=0.011$ , Figure 8F) and progression-free survival ( $P=0.05$ , Figure 8G). Besides, high-PYS subjects showed a higher objective response rate of anti-PD-L1 treatment than the other group in the GSE140901 cohort (Figures 8H). Collectively, these data indicated that anti-PD-L1 immunotherapy was likely to provide better efficacy for high-PYS subjects.

## Prospective small molecule compounds based on PYS

We further analyzed the two groups to screen potential small molecule drugs. WGCNA package was utilized to establish a gene co-expression network from the TCGA-HBV-LIHC and GSE14520 cohorts. With colors assigned to each module, this study identified 12 modules in TCGA-HBV-LIHC (Figure 9A) and 14 modules in GSE14520 (Figure 9B). Then, we created a module-feature relationship heatmap to examine the correlation



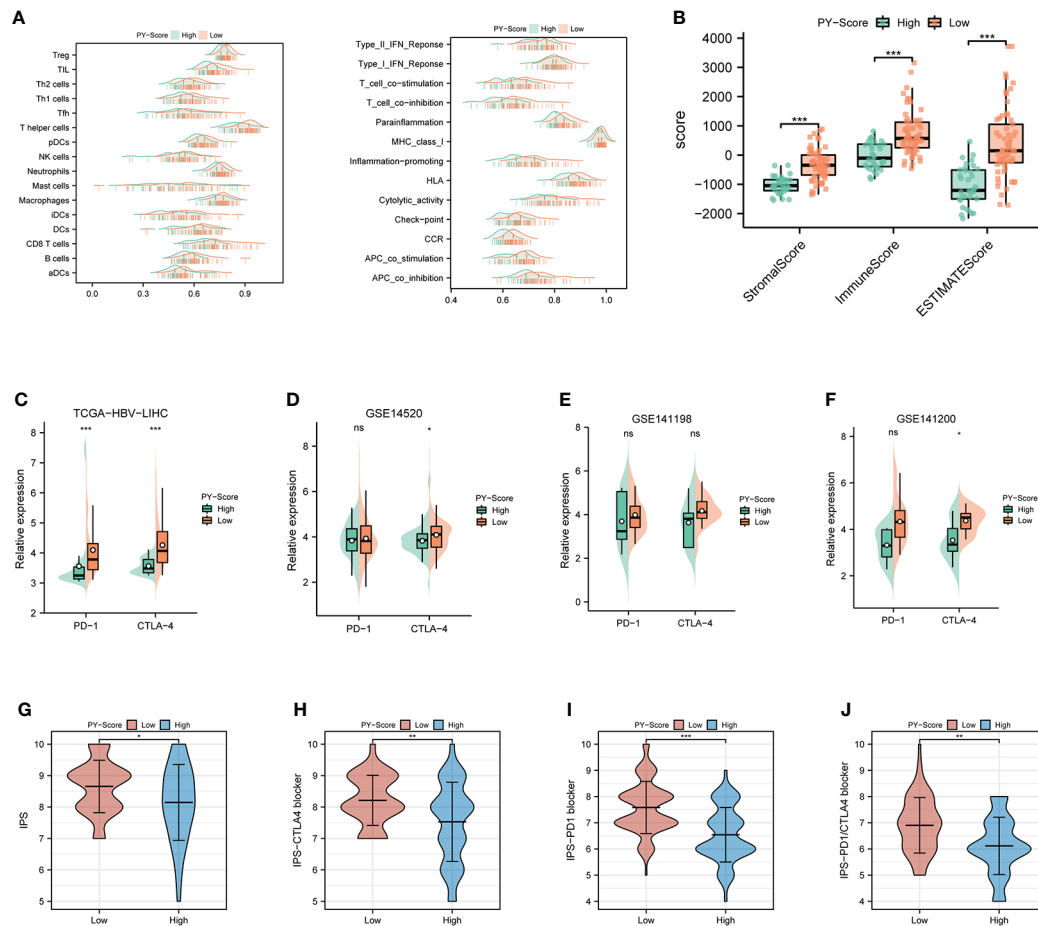


FIGURE 7

Immune landscape and immune checkpoint blockers sensitivity based on PYS. **(A)** Ridge plot of TIME-based on PYS. **(B)** tumor microenvironment scores between high- and low-PYS groups. **(C–E)** The relative expression of PD-1 and CTLA-4 between low- and high-PYS groups in TCGA-HBV-LIHC **(C)**, GSE14520 **(D)**, GSE141198 **(E)**, and GSE141200 **(F)** cohort. **(G–J)** The IPS of baseline **(G)**, CTLA-4 blocker **(H)**, PD-1 blocker **(I)**, and PD1/CTLA4 blocker **(J)**. TIME, tumor immune microenvironment; IPS, immunophenoscore; PYS, pyroptosis score. \* $P < 0.05$ ; \*\* $P < 0.01$ ; \*\*\* $P < 0.001$ ; ns, not statistically significant.

between each module and PYS, (Figures 9C, D). The turquoise module in both the TCGA-HBV-LIHC ( $r = 0.77$ ,  $P = 4e-74$ ) and GSE14520 ( $r = 0.81$ ,  $P = 6e-53$ ) were found to have the highest positive association with low PYS. On the contrary, the black module in the TCGA-HBV-LIHC ( $r = -0.53$ ,  $P = 9e-28$ ) and the brown module in GSE14520 ( $r = -0.4$ ,  $P = 8e-10$ ) were found to have the highest negative association with low PYS. According to the cut-off standard of  $|\log_2FC| \geq 1.0$  and  $adj. P < 0.05$ , 446 DEGs in the TCGA-HBV-LIHC cohort (Figure 10A) and 414 DEGs in the GSE14520 cohort (Figure 10B) were dysregulated between high- and low-PYS groups. Overlapping genes expressing was up-regulated (Figure 10C) and down-regulated (Figure 10D) in the low-PYS group were extracted for subsequent analysis. Then, we uploaded these DEGs into the CMap database. We also worked on analyzing of the underlying drug mechanisms and identified 13 potential small molecule drugs whose mean is greater than 0.7

(Table S4). The 3D structure diagrams of the pharmacophore for piperlongumine (Figure 10E) and fisetin (Figure 10G) were shown, respectively. After GO/KEGG enrichment analysis of target genes of piperlongumine (Figure 10F) and fisetin (Figure 10H), we observed that piperlongumine is related to lyase activity, HIF-1 signaling pathway, and phenylalanine metabolism, while fisetin is enriched in ubiquitin-mediated proteolysis, NF-kappaB transcription factor activity and MyD88 dependent TLR signaling pathway.

## Fisetin alleviated NLRP3 inflammasome activation inhibits HCC cell death

Caspase 1 activity, and IL-1 $\beta$  expression, were examined in this study to confirm our predicted results. In the LPS-induced

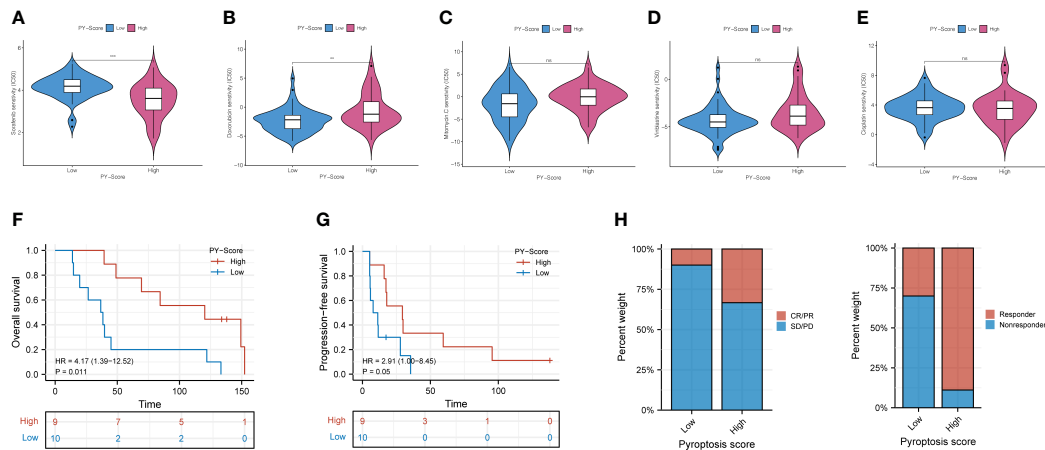


**FIGURE 8**  
The role of PYS in assessing chemotherapy and the benefit of anti-PD-L1 immunotherapy. (A–E) HBV-HCC patients in the high-PYS group were associated with a lower IC50 for chemotherapy, such as Sorafenib (A), while a higher IC 50 was associated with Doxorubicin (B). Mitomycin C (C), Vinblastine (D), and Cisplatin (E) did not show a meaningful difference. (F, G) Overall survival (F) and progression-free survival (G) curves of patients within high- and low-PYS groups in the GSE140901 cohort. (H) Clinical response to anti-PD-L1 immunotherapy between PYS groups. CR, complete response; PR, partial response; SD, stable disease; PD, progressive disease; PFS, progression-free survival; PYS, pyroptosis score. \*\*P < 0.01; \*\*\*P < 0.001; ns, not statistically significant.

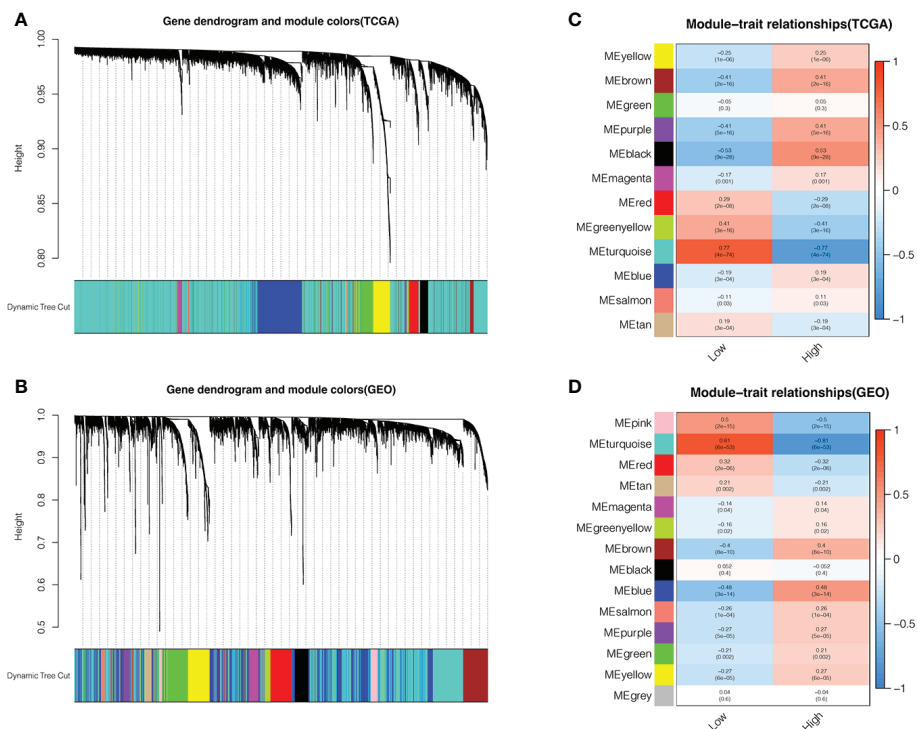


**FIGURE 9**  
Identifying modules associated with the PYS. (A–D) Co-expression network module cluster dendrogram in TCGA-HBV-LIHC (A) and GSE14520 (B) cohorts. Module-trait relationships in TCGA-HBV-LIHC (C) and GSE14520 (D) cohort, respectively.

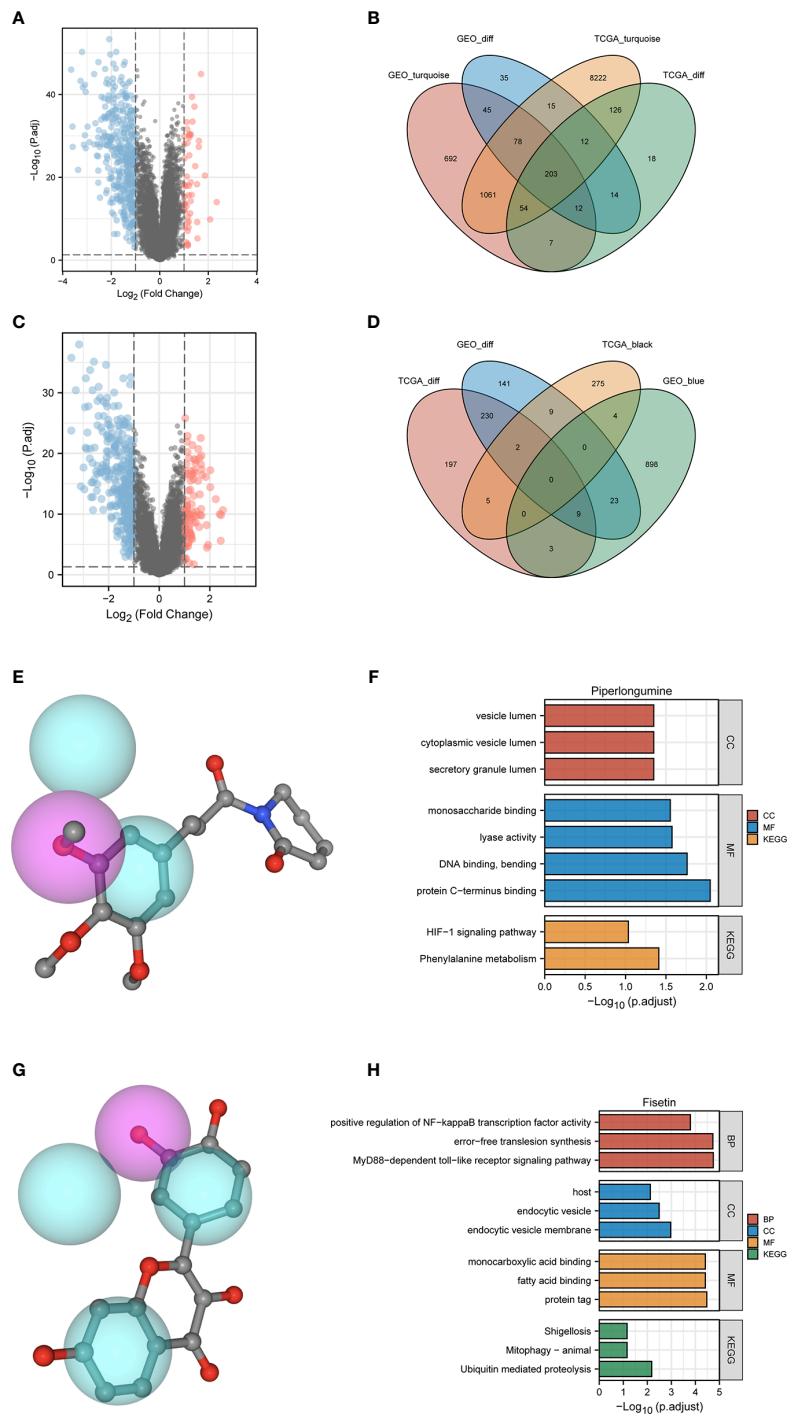


**FIGURE 10**

Potential small molecule compounds and function prediction. (A–D). Differentially expressed genes were identified between low- and high-PYS groups in TCGA-HBV-LIHC (A) and GSE14520 (B) cohort, respectively. The Venn diagram for positive correlation (C) or negative correlation (D) with the low-PYS group. (E) The 3D structure diagrams of the pharmacophore for piperlongumine. (F) GO and KEGG for target genes of piperlongumine (G) The 3D structure diagrams of the pharmacophore for fisetin. (H) GO and KEGG for target genes of fisetin. DEGs: differentially expressed genes.

pyroptosis model, the activity of Caspase 1 and the secretion of IL-1 $\beta$  were significantly downregulated in a dose-dependent manner in fisetin-treated HCC cells, suggesting that fisetin inhibits the activation of the NLRP3 inflammasome (Figure 11A, B). Besides, cell viability was detected using CCK-8 assay, as is shown in Figure 11C. The viability of HepG2 was gradually increased under the treatment of fisetin in a dose-dependent manner. Furthermore, we observed the morphology of the HepG2 by a light microscope. Under the induction of LPS, the cells swelled and enlarged with many bubble-like protrusions, and fisetin could alleviate the occurrence of pyroptosis to a certain extent. (Figure 11D).

## Discussion

In the past few years, the multi-omics analysis has finally progressed in molecular classification, which is highly related to the characteristics of genes, metabolism, immunity, and chromosome. However, the real motive for setting up a classification system is for clinical application. Therefore, stratifying patients at the molecular level will help formulate a

better treatment plan and determine how effective the immunotherapy is when faced with a certain patient. Our study comprehensively analyzed the clinical value of the pyroptosis pattern in HBV-HCC. At the same time, we have compared and contrasted the prognosis, tumor immune microenvironment, and immunotherapy of patients with HBV-HCC *via* the PYS system. As a “blueprint” for managing HBV-HCC, the PYS system will provide patients with a more robust and comprehensive plan for targeted therapy.

First, we observed the CNV and TMB of PRGs in the TCGA-HBV-LIHC cohort. Unlike the staging of HBV-HCC, the classification system mainly depends on a molecular level. Certain subtypes can be targeted, and a proven method will develop specific treatment plans for liver cancer (34). Next, we derived two molecular subtypes from the mRNA expression profile of PRGs for HBV-HCC patients. The results show that subjects in pyroptosis cluster A have a better prognosis, consistent with their active immune function. To identify the prognosis-related DEGs, we then analyzed the mRNA expression profiles of different subtypes of pyrolysis and established a classification system of HBV-HCC based on genetic features. In pursuit of higher clinical value and

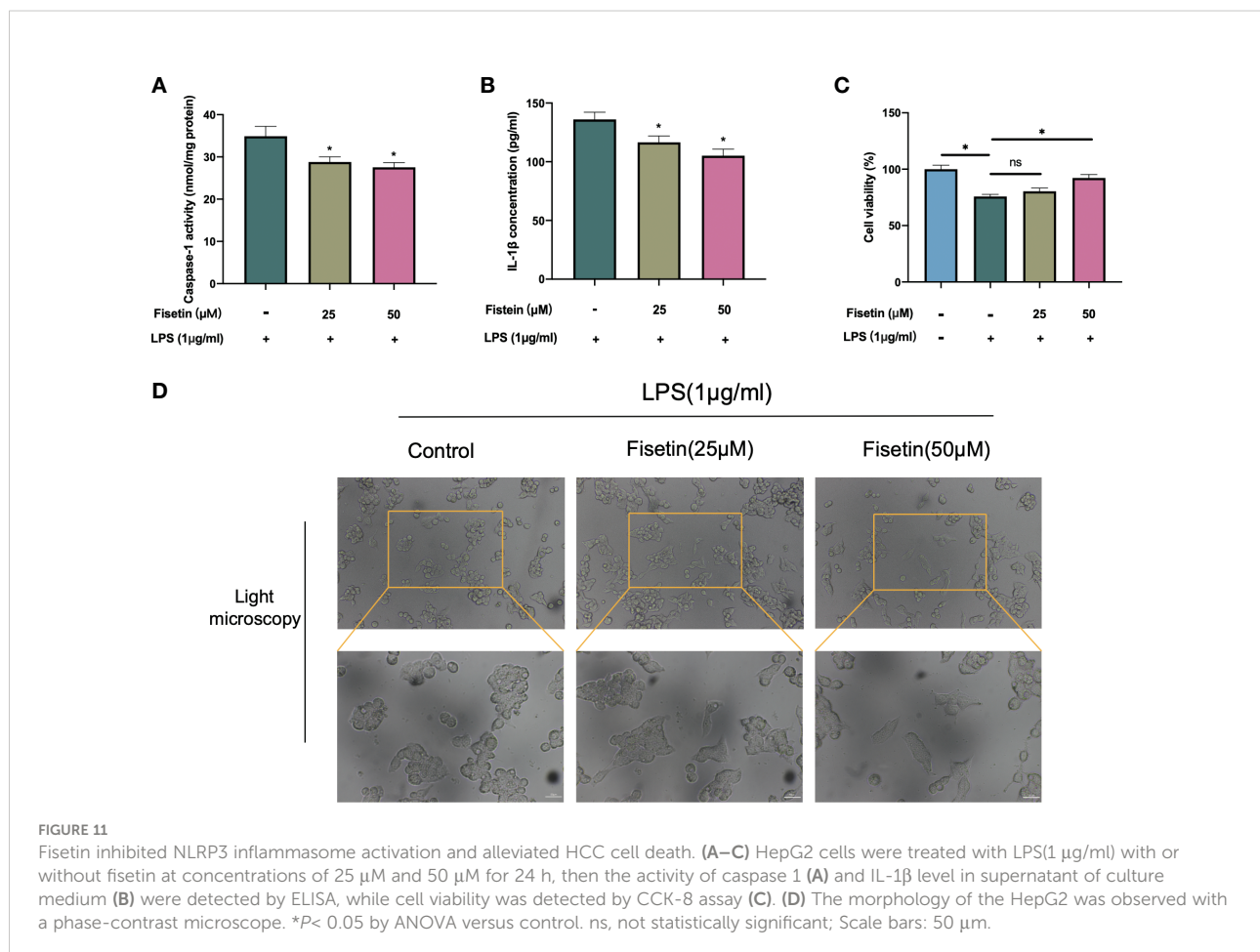


FIGURE 11

Fisetin inhibited NLRP3 inflammasome activation and alleviated HCC cell death. (A–C) HepG2 cells were treated with LPS(1  $\mu$ g/ml) with or without fisetin at concentrations of 25  $\mu$ M and 50  $\mu$ M for 24 h, then the activity of caspase 1 (A) and IL-1 $\beta$  level in supernatant of culture medium (B) were detected by ELISA, while cell viability was detected by CCK-8 assay (C). (D) The morphology of the HepG2 was observed with a phase-contrast microscope. \* $P$  < 0.05 by ANOVA versus control. ns, not statistically significant; Scale bars: 50  $\mu$ m.

potential application, we developed the PYS model based on these two clusters to quantify the prognostic risk and response to chemotherapy and immunotherapy, thereby providing strong evidence for clinical treatment. Above all, the PYS acted independently as a prognostic factor among clinical characteristics of HBV-HCC. The ROC curve shows its high efficiency in predicting survival rates, which provides strong support for predicting clinical outcomes.

Pyroptosis can create a milieu conducive to tumor growth as a form of pro-inflammatory death. Exploring the characteristics of the TIME between different PYS groups and improving clinical management through personalized prescription is of practical importance, according to the theory of inflammation-cancer transformation and chronic inflammation-induced carcinogenesis. As is shown in the results, patients with higher PYS had more restricted immune infiltration, especially the tumor killer CD8<sup>+</sup> T cells, which was consistent with their poor prognosis. A recent study has shown that sorafenib changes the TIME by inducing pyroptosis against HCC (35). We found that patients with high- PYS were more susceptible to sorafenib. As we know, multidrug resistance is the main obstacle to cancer treatment. Thus, combined with PD-L1 blockers, sorafenib may be a potentially effective treatment for the high-PYS group. In addition, for the first time, we verified that PD-L1 blockers could improve the prognosis and clinical benefit of the high-PYS group by using an external data set.

The occurrence of pyroptosis *in vivo* indicates the prospective value of pyroptosis in regulating tumorigenesis and inducing pyroptosis has been designed to eliminate tumors. Small molecule drugs like BMS-8 and BMS-202 are crucial in tumor immunotherapy by inhibiting PD-1 and PD-L1 interaction (36, 37). Recently, Yuan et al. (38) found that Cucurbitacin B inhibits non-small cell lung cancer *via* TLR4/NLRP3/GSDMD signaling pathway. Besides, Dihydroartemisinin inducing pyroptosis *via* AIM2/caspase-3/DFNA5 axis was also reported in breast cancer (39). The above studies have shown that small-molecule drugs can potentially induce pyroptosis and regulate the TIME. Using the WGCNA and limma packages, we have obtained modules with significant differences and identified DEGs significantly related to PYS. To improve the prognosis of HBV-HCC patients, we screened 13 small molecule compounds using the CMap database. Piperlongumine can reduce colitis-associated colorectal cancer (40) and relieve sepsis by attenuating the activation of inflammasomes (41). From the enrichment results, piperlongumine acts on the HIF-1 signaling pathway and lyase activity, while fisetin regulates NF- $\kappa$ B transcription factor activity. The crosstalk between oncogene and tumor suppressor transcription factors such as NF- $\kappa$ B, STAT3, HIF-1 $\alpha$ , and NRF2, is the mechanism of inflammation-driven cancer (42). Fisetin has been suggested to have a protective role in attenuating inflammation and HCC development for a few decades. Our previous study unveiled that fisetin relieves hepatic ischemia-reperfusion injury by inhibiting the NLRP3 inflammasome

activation (43), which indicates its potential value in regulating pyroptosis. In our present experiments, the inhibition of pyroptosis by fisetin was verified. Here we have demonstrated that fisetin can inhibit the activity of caspase 1 and release IL-1 $\beta$ , which indicates the occurrence of pyroptosis. Overall, the above studies have shown that small molecule compounds affect the occurrence and development of tumors *via* pyroptosis and inflammatory signaling pathways, which brings new options to clinical treatment.

Pyroptosis is a two-edged sword that can promote and inhibit cancer depending on the situation (14). Although we conducted our research from different angles and used several databases to confirm our conclusions, there are still some limitations. Due to the heterogeneity of HCC, targeted improvements of the PYS model may be needed for different tumor subtypes. At the same time, more data on immunotherapy related to HBV-HCC need to be established. Furthermore, the changes in the tumor immune milieu associated with the PYS model may necessitate additional explanations, such as single-cell sequencing. The small molecule compounds we screened should be tested further to understand better their link with pyroptosis, which is also the path we must strive for in the future.

## Data availability statement

The original contributions presented in the study are included in the article/[Supplementary Material](#). Further inquiries can be directed to the corresponding author.

## Author contributions

ZW conceived and designed the study. JL contributed to research design, data analysis, and writing. JY revised the manuscript. TZ, XP, and YL supervise the study. All authors have read and approved the submitted version.

## Funding

This study was supported by the National Natural Science Foundation of China (No. 82170666 and 81873592), and Chongqing Technology Innovation and Application Development Special Project, Key Project, cstc2021jscx-gksbX0060.

## Conflict of interest

The authors declare that the research was conducted in the absence of any commercial or financial relationships that could be construed as a potential conflict of interest.

The reviewer SZ declared a shared parent affiliation with the author JY to the handling editor at the time of review.

## Publisher's note

All claims expressed in this article are solely those of the authors and do not necessarily represent those of their affiliated organizations, or those of the publisher, the editors and the reviewers. Any product that may

be evaluated in this article, or claim that may be made by its manufacturer, is not guaranteed or endorsed by the publisher.

## Supplementary material

The Supplementary Material for this article can be found online at: <https://www.frontiersin.org/articles/10.3389/fimmu.2022.932303/full#supplementary-material>

## References

- Liu Z, Jiang Y, Yuan H, Fang Q, Cai N, Suo C, et al. The trends in incidence of primary liver cancer caused by specific etiologies: Results from the global burden of disease study 2016 and implications for liver cancer prevention. *J Hepatol* (2019) 70(4):674–83. doi: 10.1016/j.jhep.2018.12.001
- Kovacs SB, Miao EA. Gasdermins: Effectors of pyroptosis. *Trends Cell Biol* (2017) 27(9):673–84. doi: 10.1016/j.tcb.2017.05.005
- Zhang Y, Chen X, Gueydan C, Han J. Plasma membrane changes during programmed cell deaths. *Cell Res* (2018) 28(1):9–21. doi: 10.1038/cr.2017.133
- Feng S, Fox D, Man SM. Mechanisms of gasdermin family members in inflammasome signaling and cell death. *J Mol Biol* (2018) 430(18 Pt B):3068–80. doi: 10.1016/j.jmb.2018.07.002
- Wei Q, Mu K, Li T, Zhang Y, Yang ZW, Jia XQ, et al. Deregulation of the NLRP3 inflammasome in hepatic parenchymal cells during liver cancer progression. *Lab Invest* (2014) 94(1):52–62. doi: 10.1038/labinvest.2013.126
- Wei Q, Guo PB, Mu K, Zhang Y, Zhao W, Huai WW, et al. Estrogen suppresses hepatocellular carcinoma cells through ER beta-mediated upregulation of the NLRP3 inflammasome. *Lab Invest* (2015) 95(7):804–16. doi: 10.1038/labinvest.2015.63
- Wei Q, Zhu R, Zhu JY, Zhao RP, Li M. E2-induced activation of the NLRP3 inflammasome triggers pyroptosis and inhibits autophagy in HCC cells. *Oncol Res* (2019) 27(7):827–34. doi: 10.3727/096504018x15462920753012
- Zhao N, Dang H, Ma L, Martin SP, Forgues M, Ylaja K, et al. Intratumoral gammadelta T-cell infiltrates, chemokine (C-c motif) ligand 4/Chemokine (C-c motif) ligand 5 protein expression and survival in patients with hepatocellular carcinoma. *Hepatology* (2021) 73(3):1045–60. doi: 10.1002/hep.31412
- Hsu CL, Ou DL, Bai LY, Chen CW, Lin L, Huang SF, et al. Exploring markers of exhausted CD8 T cells to predict response to immune checkpoint inhibitor therapy for hepatocellular carcinoma. *Liver Cancer* (2021) 10(4):346–59. doi: 10.1159/000515305
- Moeini A, Torrecilla S, Tovar V, Montironi C, Andreu-Oller C, Peix J, et al. An immune gene expression signature associated with development of human hepatocellular carcinoma identifies mice that respond to chemopreventive agents. *Gastroenterology* (2019) 157(5):1383–1397.e1311. doi: 10.1053/j.gastro.2019.07.028
- Karki R, Kanneganti TD. Diverging inflammasome signals in tumorigenesis and potential targeting. *Nat Rev Cancer* (2019) 19(4):197–214. doi: 10.1038/s41568-019-0123-y
- Man SM, Kanneganti TD. Regulation of inflammasome activation. *Immunol Rev* (2015) 265(1):6–21. doi: 10.1111/immr.12296
- Wang B, Yin Q. AIM2 inflammasome activation and regulation: A structural perspective. *J Struct Biol* (2017) 200(3):279–82. doi: 10.1016/j.jsb.2017.08.001
- Xia XJ, Wang X, Cheng Z, Qin WH, Lei LC, Jiang JQ, et al. The role of pyroptosis in cancer: Pro-cancer or pro-“Host”? *Cell Death Dis* (2019) 10:650. doi: 10.1038/s41419-019-1883-8
- Wilkerson MD, Hayes DN. ConsensusClusterPlus: A class discovery tool with confidence assessments and item tracking. *Bioinformatics* (2010) 26(12):1572–3. doi: 10.1093/bioinformatics/btq170
- Hanzelmann S, Castelo R, Guinney J. GSEA: Gene set variation analysis for microarray and RNA-seq data. *BMC Bioinf* (2013) 14:7. doi: 10.1186/1471-2105-14-7
- Yu GC, Wang LG, Han YY, He QY. ClusterProfiler: An R package for comparing biological themes among gene clusters. *Omic-a J Integr Biol* (2012) 16(5):284–7. doi: 10.1089/omi.2011.0118
- Sotiriou C, Wirapati P, Loi S, Harris A, Fox S, Smeds J, et al. Gene expression profiling in breast cancer: Understanding the molecular basis of histologic grade to improve prognosis. *Jnci-Journal Natl Cancer Institute* (2006) 98(4):262–72. doi: 10.1093/jnci/djj052
- Yoshihara K, Shahmoradgoli M, Martinez E, Vegesna R, Kim H, Torres-Garcia W, et al. Inferring tumour purity and stromal and immune cell admixture from expression data. *Nat Commun* (2013) 4:2612. doi: 10.1038/ncomms3612
- Yang W, Soares J, Greninger P, Edelman EJ, Lightfoot H, Forbes S, et al. Genomics of drug sensitivity in cancer (GDSC): A resource for therapeutic biomarker discovery in cancer cells. *Nucleic Acids Res* (2013) 41(Database issue):D955–961. doi: 10.1093/nar/gks1111
- Geeleher P, Cox N, Huang RS. Prorophetic: An R package for prediction of clinical chemotherapeutic response from tumor gene expression levels. *PLoS One* (2014) 9(9):e107468. doi: 10.1371/journal.pone.0107468
- Clark K, Vendt B, Smith K, Freymann J, Kirby J, Koppel P, et al. The cancer imaging archive (TCIA): Maintaining and operating a public information repository. *J Digit Imaging* (2013) 26(6):1045–57. doi: 10.1007/s10278-013-9622-7
- Langfelder P, Horvath S. WGCNA: An R package for weighted correlation network analysis. *BMC Bioinf* (2008) 9:559. doi: 10.1186/1471-2105-9-559
- Chen H, Boutros PC. VennDiagram: A package for the generation of highly-customizable Venn and Euler diagrams in R. *BMC Bioinf* (2011) 12:35. doi: 10.1186/1471-2105-12-35
- Lamb J, Crawford ED, Peck D, Modell JW, Blat IC, Wrobel MJ, et al. The connectivity map: Using gene-expression signatures to connect small molecules, genes, and disease. *Science* (2006) 313(5795):1929–35. doi: 10.1126/science.1132939
- Kim S, Thiessen PA, Bolton EE, Chen J, Fu G, Gindulyte A, et al. PubChem substance and compound databases. *Nucleic Acids Res* (2016) 44(D1):D1202–13. doi: 10.1093/nar/gkv951
- Wang X, Shen YH, Wang SW, Li SL, Zhang WL, Liu XF, et al. PharmMapper 2017 update: A web server for potential drug target identification with a comprehensive target pharmacophore database. *Nucleic Acids Res* (2017) 45(W1):W356–60. doi: 10.1093/nar/gkx374
- Cao PB, Yang AQ, Wang R, Xia X, Zhai Y, Li YF, et al. Germline duplication of SNORA18L5 increases risk for HBV-related hepatocellular carcinoma by altering localization of ribosomal proteins and decreasing levels of P53. *Gastroenterology* (2018) 155(2):542–56. doi: 10.1053/j.gastro.2018.04.020
- Diskin SJ, Hou CP, Glessner JT, Attiyeh EF, Laudenslager M, Bosse K, et al. Copy number variation at 1q21.1 associated with neuroblastoma. *Nature* (2009) 459(7249):987–U112. doi: 10.1038/nature08035
- Goodman AM, Kato S, Bazhenova L, Patel SP, Frampton GM, Miller V, et al. Tumor mutational burden as an independent predictor of response to immunotherapy in diverse cancers. *Mol Cancer Ther* (2017) 16(11):2598–608. doi: 10.1158/1535-7163.Mct-17-0386
- Wu M, Wang Y, Yang D, Gong Y, Rao F, Liu R, et al. A PLK1 kinase inhibitor enhances the chemosensitivity of cisplatin by inducing pyroptosis in oesophageal squamous cell carcinoma. *EBioMedicine* (2019) 41:244–55. doi: 10.1016/j.ebiom.2019.02.012
- Wang L, Li K, Lin X, Yao Z, Wang S, Xiong X, et al. Metformin induces human esophageal carcinoma cell pyroptosis by targeting the miR-497/PELP1 axis. *Cancer Lett* (2019) 450:22–31. doi: 10.1016/j.canlet.2019.02.014
- Chen L, Weng B, Li H, Wang H, Li Q, Wei X, et al. A thiopyran derivative with low murine toxicity with therapeutic potential on lung cancer acting through a NF-kappaB mediated apoptosis-to-Pyroptosis switch. *Apoptosis* (2019) 24(1-2):74–82. doi: 10.1007/s10495-018-1499-y

34. Cristescu R, Lee J, Nebozhyn M, Kim KM, Ting JC, Wong SS, et al. Molecular analysis of gastric cancer identifies subtypes associated with distinct clinical outcomes. *Nat Med* (2015) 21(5):449–56. doi: 10.1038/nm.3850
35. Hage C, Hoves S, Strauss L, Bissinger S, Prinz Y, Poschinger T, et al. Sorafenib induces pyroptosis in macrophages and triggers natural killer cell-mediated cytotoxicity against hepatocellular carcinoma. *Hepatology* (2019) 70(4):1280–97. doi: 10.1002/hep.30666
36. Kim EH, Kawamoto M, Dharmatti R, Kobatake E, Ito Y, Miyatake H. Preparation of biphenyl-conjugated bromotyrosine for inhibition of PD-1/PD-L1 immune checkpoint interactions. *Int J Mol Sci* (2020), 21(10):3639. doi: 10.3390/ijms21103639
37. Verdura S, Cuyas E, Cortada E, Brunet J, Lopez-Bonet E, Martin-Castillo B, et al. Resveratrol targets PD-L1 glycosylation and dimerization to enhance antitumor T-cell immunity. *Aging (Albany NY)* (2020) 12(1):8–34. doi: 10.18632/aging.102646
38. Yuan R, Zhao W, Wang QQ, He J, Han S, Gao H, et al. Cucurbitacin b inhibits non-small cell lung cancer *in vivo* and *In vitro* by triggering TLR4/NLRP3/GSDMD-dependent pyroptosis. *Pharmacol Res* (2021) 170:105–748. doi: 10.1016/j.phrs.2021.105748
39. Li Y, Wang W, Li A, Huang W, Chen S, Han F, et al. Dihydroartemisinin induces pyroptosis by promoting the AIM2/caspase-3/DFNA5 axis in breast cancer cells. *Chem Biol Interact* (2021) 340:109–434. doi: 10.1016/j.cbi.2021.109434
40. Huang JR, Wang ST, Wei MN, Liu K, Fu JW, Xing ZH, et al. Piperlongumine alleviates mouse colitis and colitis-associated colorectal cancer. *Front Pharmacol* (2020) 11:586885. doi: 10.3389/fphar.2020.586885
41. Huang CH, Wang SC, Chen IC, Chen YT, Liu PL, Fang SH, et al. Protective effect of piplartine against LPS-induced sepsis through attenuating the MAPKs/NF-kappaB signaling pathway and NLRP3 inflammasome activation. *Pharm (Basel)* (2021) 14:6. doi: 10.3390/ph14060588
42. Rajagopal C, Lankadasari MB, Aranjani JM, Harikumar KB. Targeting oncogenic transcription factors by polyphenols: A novel approach for cancer therapy. *Pharmacol Res* (2018) 130:273–91. doi: 10.1016/j.phrs.2017.12.034
43. Pu JL, Huang ZT, Luo YH, Mou T, Li TT, Li ZT, et al. Fisetin mitigates hepatic ischemia-reperfusion injury by regulating GSK3beta/AMPK/NLRP3 inflammasome pathway. *Hepatobiliary Pancreat Dis Int* (2021) 20(4):352–60. doi: 10.1016/j.hbpd.2021.04.013



## OPEN ACCESS

## EDITED BY

Daxing Gao,  
University of Science and Technology  
of China, China

## REVIEWED BY

Huibin Yu,  
Yale University, United States  
Biao Qiu,  
NewYork-Presbyterian, United States

## \*CORRESPONDENCE

Chunfu Zheng  
zheng.alan@hotmail.com  
Fusheng Si  
mr.fusheng@163.com

<sup>†</sup>These authors have contributed  
equally to this work

## SPECIALTY SECTION

This article was submitted to  
Viral Immunology,  
a section of the journal  
Frontiers in Immunology

RECEIVED 04 July 2022

ACCEPTED 20 July 2022

PUBLISHED 09 August 2022

## CITATION

Wei W, Bai L, Yan B, Meng W, Wang H,  
Zhai J, Si F and Zheng C (2022) When  
liquid-liquid phase separation meets  
viral infections.  
*Front. Immunol.* 13:985622.  
doi: 10.3389/fimmu.2022.985622

## COPYRIGHT

© 2022 Wei, Bai, Yan, Meng, Wang,  
Zhai, Si and Zheng. This is an open-  
access article distributed under the  
terms of the [Creative Commons  
Attribution License \(CC BY\)](#). The use,  
distribution or reproduction in other  
forums is permitted, provided the  
original author(s) and the copyright  
owner(s) are credited and that the  
original publication in this journal is  
cited, in accordance with accepted  
academic practice. No use,  
distribution or reproduction is  
permitted which does not comply with  
these terms.

# When liquid-liquid phase separation meets viral infections

Wenqiang Wei<sup>1†</sup>, Lu Bai<sup>1,2†</sup>, Bing Yan<sup>1</sup>, Weiquan Meng<sup>1</sup>,  
Hongju Wang<sup>1</sup>, Jingbo Zhai<sup>3,4</sup>, Fusheng Si<sup>5\*</sup>  
and Chunfu Zheng<sup>2,6\*</sup>

<sup>1</sup>Kaifeng Key Laboratory of Infection and Biological Safety, School of Basic Medical Sciences, Henan University, Kaifeng, China, <sup>2</sup>Department of Immunology, School of Basic Medical Sciences, Fujian Medical University, Fuzhou, China, <sup>3</sup>Medical College, Inner Mongolia Minzu University, Tongliao, China, <sup>4</sup>Key Laboratory of Zoonose Prevention and Control at Universities of Inner Mongolia Autonomous Region, Tongliao, China, <sup>5</sup>Institute of Animal Science and Veterinary Medicine, Shanghai Key Laboratory of Agricultural Genetics and Breeding, Shanghai Engineering Research Center of Breeding Pig, Shanghai Academy of Agricultural Sciences, Shanghai, China, <sup>6</sup>Department of Microbiology, Immunology and Infectious Diseases, University of Calgary, Calgary, AB, Canada

Eukaryotic cells have both membranous and membraneless organelles. While the formation mechanism of membranous organelles is well understood, the formation mechanism of membraneless organelles remains unknown. Many biomolecules in the cytoplasm transition from the liquid phase to the agglutinated phase are known as liquid-liquid phase separation (LLPS). The biomolecular agglomerates' physical properties enable them to function as dynamic compartments that respond to external pressures and stimuli. Scientists have gradually recognized the importance of phase separation during viral infections. LLPS provides a powerful new framework for understanding the viral life cycle from viral replication to evasion of host immune surveillance. As a result, this review focuses on the progress of LLPS research in viral infection and immune regulation to provide clues for antiviral therapeutic strategies.

## KEYWORDS

liquid-liquid phase separation, membraneless organelle, inclusion, viral infection, immune regulation

## Background

The regulation, coordination, and networking of different cellular compartments underlie the function of biological systems. Among these compartments are membrane and non-membrane organelles. The membrane-bound organelles carry out functions in a selective and specific manner without any external disturbance. The exchanging information between membrane organelles is endorsed by mechanisms such as fusion and fission and vesicles trafficking in the endomembrane system (1). However, large gaps



remain in our understanding of the collaboration and regulation of membraneless organelles (MLOs) in biochemical functions.

Recent studies have shown that macromolecules' liquid-liquid phase separation (LLPS) may be the physicochemical basis for forming non-membrane organelles inside the cells (2–4). In the compartments formed by LLPS, specific molecules are concentrated in fluid-like liquid droplets that coexist stably with the surrounding fluid environment. Some examples of these biomolecular condensates include processing bodies (P-bodies), stress granules (SGs), Cajal bodies, Nucleosomes, nuclear speckles, membrane clusters, signaling puncta, Germ granules, Balbiani bodies, paraspeckles, DNA damage foci, histone locus, viral replication compartments (RCs) and inclusion bodies (IBs) (3, 5–11). After the formation of LLPS, the biomolecule exists in two forms, one at low concentration in bulk dilute phase and one at higher concentration in the formed “droplets”. The polymer molecules usually move within the dense phase or between the dense and bulk dilute phases (12, 13). The interconversion of these two phases depends upon the change in the surrounding cellular environment.

The occurrence of LLPS is highly dependent on the concentration of biomolecules (proteins, DNA, and RNA) in the solution, their physicochemical properties, and the solution environment (temperature, pH, salt concentration, and salt ion type) (14, 15). The threshold concentration of biomolecules is the major factor contributing to the phase separation of homogeneous solutions. When the concentration of biomolecules exceeds the threshold concentration, they begin to aggregate, leading to the appearance of LLPS (4). The other influencing factors include chaperones, ATP, post-transcriptional modification, pH, ionic strength, and temperature (10). Furthermore, various intermolecular interactions, including ionic bonds, van der Waals forces, hydrogen bonds,  $\pi$ - $\pi$ , and  $\pi$ -cation of aromatic residue and cation amino acid residue, are also involved in the occurrence of phase separation (16–19).

Viruses are obligate intracellular parasites that rely on the host machinery for viral replication. The concept of phase separation provides new insights into understanding the mechanisms of viral infection. Several studies revealed that viral infection is associated with membraneless condensates (9). Some viruses have been shown to assemble biomolecular condensates with liquid properties, such as rabies virus (RABV), vesicular stomatitis virus (VSV), and severe acute respiratory syndrome coronavirus 2 (SARS-COV-2) (20–22). Moreover, these condensates are also associated with SGs, suggesting the condensate's potential roles in the innate immune responses (23). A growing body of studies reveals the important role of LLPS in the viral life cycle, including viral entry, genome replication, assembly, and viral packaging, as well as antiviral innate immune signaling (20, 23). In this review, we will focus on the role of LLPS in viral infection and immune regulation to provide a novel insight into antiviral therapeutic strategies.

## Cellular factors that drive phase separation

Studies have revealed that several factors, including multivalency of proteins, temperature, ionic strength, RNA elements, and metal ions, contribute to forming liquid droplets (17). Here, we introduced these factors' roles in forming LLPS.

### Intrinsically disordered regions

Intrinsically disordered regions (IDRs) of a protein have no specific three-dimensional structure and can weakly and multivalently interact with other proteins, resulting in liquid condensates (11, 15, 24). Numerous studies have shown that weak and multivalent RNA-protein or IDR-IDR interactions are critical for the high-order assembly of biomolecules (25, 26). For example, IDRs in transcriptional coactivators BRD4 and MED1 are integral for driving phase separation (27, 28). Besides this, prion-like domains (PLDs), similar to low-complexity sequence domains (LCDs), can also drive LLPS *in vivo* (29). The valence of aromatic residues in PLDs plays a major role in LLPS, and a specific sequence of aromatic residues helps form liquid droplets. Moreover, intrinsically disordered proteins (IDPs) are also subject to phase separation resulting in the formation of membraneless organelles with various cellular functions (30). IDPs exhibit a high conformational heterogeneity due to lacking a stable and precise secondary or tertiary structure (31). Polar charged residues promote the formation of disordered proteins; therefore, IDPs are also considered polyelectrolytes (32). The protein IDRs are indispensable for forming membraneless organelles through LLPS.

### Protein multivalency

The multivalency of protein contributes to phase separation. For example, mixing an engineered protein containing multiple SRC homology 3 (SH3) repeats and another containing multiple proline-rich motifs (PRM) repeats resulted in phase separation *in vitro* (12). Another example is the nephrin-Nck-N-WASP system, in which phosphorylated nephrin binds to the SH2 domains of Nck while three SH3 domains of Nck can further bind to N-WASP six PRMs. The multivalency of these proteins results in phase separation (33). Besides SH3, other multidomain modules are also involved in phase separation. For instance, a coiled-coil trimer formed by SynGAP can bind to multiple copies of PSD-95, leading to the formation of LLPS (34). Altogether, the formation of multimers mediated by multivalent interactions can drive the formation of LLPS.

## Genomic RNA elements

Like specific multivalent protein-binding sites, Genomic RNA elements are indispensable for phase separation. It has been found that the phase separation mediated by IDP and RNA is RNA concentration-dependent. A low amount of RNA promotes phase separation, while a high amount can inhibit it (35). A recent study showed that distinct regions of viral genomic RNA have distinct roles in mediating phase separation (36). For instance, the nucleocapsid encoding region located at the 3' end of severe acute respiratory syndrome coronavirus (SARS-CoV) genomic RNA (gRNA) can promote phase separation while its frameshifting and packaging signal region can dissolve the liquid phase (37). Another study found that the viral gRNAs bind to the IDRs and RNA-binding domains of the N protein to mediate phase separation, promoting the assembly of virus particles (38).

## Zn<sup>2+</sup> ions

The metal ions regulate phase separation and are related to developing some diseases (39–41). It has been found that Zn<sup>2+</sup>, but not other ions (Mn<sup>2+</sup>, Cu<sup>2+</sup>, and Fe<sup>2+</sup>), plays a significant role in the phase separation of tau protein (42). The multiple zinc-binding sites of tau are required for the formation of LLPS. Metal ions can react with prion-like disordered protein domains (PrLDs), providing us with a doctrine to further understand phase separation (43). Further study about the mechanism of tau-mediated phase separation may improve the treatment of tau-associated degenerative diseases (44). Moreover, Zn<sup>2+</sup> is also involved in the virus-mediated phase separation. For instance, human immunodeficiency virus type 1 (HIV-1) nucleocapsid proteins are required for zinc finger (ZnF) protein-dependent LLPS, regulating genomic RNA positioning and trafficking (45). The ZnF NC mutant and Zn<sup>2+</sup> chelation inhibited NC colocalization with vRNA and suppressed NC-mediated LLPS (45–47). RABV and VSV can employ Zn<sup>2+</sup> to regulate the formation of liquid condensate mediated by N-protein and nucleic acid, promoting virus assembly (48). It is interesting to study whether the inhibition of ZnF protein can suppress viral replication.

## Roles of virus-driven phase separation during virus infection

Because the viral replication cycle is highly dependent on the infected host cell, viruses have evolved to utilize and remodel cellular structures to facilitate viral replication and counteract host cell resistance to viral infections.

Many viruses have been shown to produce biomolecular condensates with liquid properties. The formation of biomolecular agglutinates substantially leads to a significant

increase in local molecular concentration and intermolecular contacts, thus enhancing the rate of biochemical reactions. Further study showed that biomolecular condensates play a role in viral genome replication, transcriptional translation, nucleocapsid assembly, and egress. For example, DNA viruses form nuclear viral replication compartments through phase separation, and many negative RNA viruses induce the formation of viral IBs (49, 50). Besides, by sequestering antiviral sensors into viral IBs, biomolecular condensates can also prevent the activation of innate immune pathways (51–54). Here, we will cover recent progress on the roles of biomolecular condensates in the viral infection process and immune response (Figure 1).

## Phase separation regulates virus replication

### The roles of phase separation in DNA virus replication and transcription

The action of phase separation in virus replication and transcription has been reported in some members of the Herpesviridae family. It is generally accepted that the DNA replication, gene transcription, and nucleocapsid assembly of herpes simplex virus type 1 (HSV-1), a member of the alpha-Herpesviridae family, occur in the nucleus of host cells (55). When the viral genome enters the nucleus, HSV-1 sequentially expresses immediate-early, early, and late proteins. The immediate-early proteins activate the transcription and translation of early genes, which participate in the viral genome replication and replication compartments (49, 56, 57). Recent studies have shown that the immediate-early protein ICP4 is an intrinsically disordered protein that can drive the formation of condensates in the nucleus *via* LLPS (58). Since ICP4 is required for viral replication and is localized to RCs, RCs may be the product of LLPS (59).

It should be noted that not all the proteins in RC are recruited through LLPS. For example, the recruitment and retention of RNA polymerase II (Pol II) in the RC is achieved *via* the non-specific binding of Pol II to HSV-1 DNA (60). Therefore, the formation mechanisms of RCs might be complex, and the roles of LLPS in RC compartmentalization need further investigation. After completing capsid assembly and genome packaging in the nucleus, HSV-1 nucleocapsid undergoes primary envelopment and de-envelopment at the nuclear envelope, followed by secondary envelopment in the cytoplasm (55, 61). Tegument protein acts as a link between the capsid and the viral envelope, promoting secondary encapsulation. A recent study found that HSV-1 tegument protein UL11 possesses the IDR and can form LLPS *in vitro* (62). Interestingly, it is also found that several HSV-1 tegument proteins have IDRs and might have the potential to undergo LLPS, suggesting that the tegument proteins might play a role in tegument assembly through LLPS.

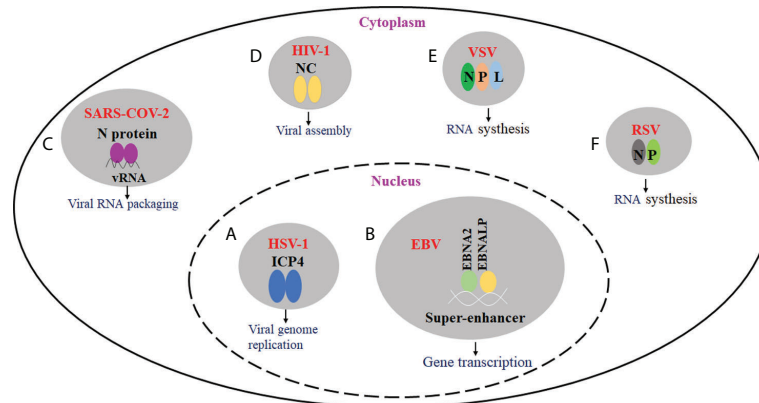


FIGURE 1

The effect of virus-driven phase separation on the viral infection. (A) HSV-1 ICP4 can drive the formation of condensates in the nucleus via LLPS. ICP4 is localized to RCs and required for viral replication. (B) EBV EBNA2, EBNA1P, and other transcription factors could form condensate at super-enhancers via LLPS. They may be involved in the epigenetic regulation of chromatin activation. (C) SARS-CoV-2 N protein can undergo LLPS in the presence of viral RNA, and LLPS may be implicated in the assembly of progeny virions. (D) For HIV-1, nucleocapsid (NC)-mediated LLPS induces translational silencing and drives viral assembly. (E) IBs are proved to be membraneless organelles. For VSV, viral IBs were formed in the presence of N, P, and L proteins, and viral RNA synthesis occurs in IBs. (F) For RSV, viral IBs were formed in the presence of N and P proteins, which play an important role in viral RNA synthesis.

The first identified human oncovirus is Epstein Barr virus (EBV), belonging to the gamma subfamily of the Herpesviridae family. EBV is closely related to multiple malignant tumors, including nasopharyngeal carcinoma and gastric cancer (63, 64). EBNA2 and EBNA1P are two EBV-encoded transcription factors expressed early after EBV infection in the B cells (65). Co-expression of both proteins can drive quiescent B cells into the cell cycle and promote B cell transformation (66). Importantly, EBNA2 binding sites are positioned near the promoter and enhancer elements in viral and cellular genomes. Recent studies found that EBNA2 can be enriched in super-enhancer regions formed by many transcriptional enhancers (67–69).

Moreover, EBNA2, EBNA1P, and other transcription factors could form condensate at super-enhancers via LLPS (70). Furthermore, EBNA2 can remodel chromatin topology through phase separation, resulting in the formation of accessible chromatin domains (ACDs) in the host genome. The N-terminal of EBNA2 is required for ACD induction and phase separation formation, whereas the C-terminal can recruit histone acetyltransferase p300 to ACDs for acetylation of ACDs (71). As a result, phase segregation theoretically supports further epigenetic regulation of chromatin activation and genomic transcription.

### Phase separation regulates RNA virus replication

The effects of phase separation on virus replication were well explored in the N protein of SARS-CoV-2. The genomes of SARS-CoV-2 are encapsulated by N protein. The presence of several RNA binding domains in this nucleocapsid protein,

including low-complexity areas and oligomerization domains, suggests that N protein can create biomolecular condensates (72). It has been demonstrated that N proteins can undergo LLPS *in vitro*. The turbidity experiments revealed that increased RNA concentration would enhance the turbidity of droplets (23). However, the turbidity decreases when RNA concentration exceeds a certain threshold due to the classical reentrant behavior (73). By measuring turbidity and spherical droplet size at different NaCl concentrations, it is found that electrostatic interactions inhibit the formation of LLPS mediated by N proteins and RNA (38). The LINK region of N protein contains a serine- and arginine-rich SR region. The phosphorylation of the SR region leads to the formation of salt bridges between the phosphate groups and arginine side chains, inhibiting N-protein and RNA-induced LLPS (23).

The N protein-mediated LLPS is a multifunctional protein involved in multiple infection processes. The SARS-CoV-2 requires RNA-dependent RNA polymerase (RdRp) and a series of cofactors during replication and transcription (74). Fluorescence co-localization experiments demonstrate that N proteins recruit RdRp/RNA complexes and promote virus replication. LLPS may promote ribonucleoprotein condensate formation while packaging viral RNA genomes into nascent virions (72). It is speculated that newly synthesized N proteins form pre-capsids with viral genomes via LLPS. Then the pre-capsids are released upon maturation and interact with structural proteins in the ER-Golgi intermediate compartment (ERGIC) for subsequent packaging (74–77).

In addition, various experiments have shown that N proteins can regulate the formation and function of SGs. SG formation

can inhibit protein synthesis, limit energy consumption, repair stress-induced damage, and promote cell survival (78). However, SARS-CoV-2 can phosphorylate eIF<sup>2+</sup> by activating the kinases PKR and PERK, which induce SG formation (79). However, SG formation does not inhibit viral proliferation, indicating that SARS-CoV-2 can counteract host cell responses (80). It has been shown that the stress granule assembly factors 1 and 2 (G3BP1/2) can interact with N proteins (81). Perdikari et al. further found that N proteins can partition into liquid phases formed by hnRNP2, FUS, and TDP-43, demonstrating that N proteins can interact with many particle-associated heterogeneous nuclear ribonucleoproteins (hnRNPs) (38). Therefore, it is speculated that N proteins, once recruited to SG, may selectively sequester the key components in SG to convert SG into a site for promoting viral replication.

### Phase separation regulates virus assembly

Here, we take HIV-1 as an example to demonstrate the role of phase separation in regulating virus assembly. HIV-1 has a complex viral life cycle as a retrovirus, including fusion, decapsulation, reverse transcription, and integration into the host cell to form a provirus, transcription of a large amount of positive-stranded RNA before exiting the nucleus. These positive-stranded RNAs can act as mRNAs directing the synthesis of viral proteins and as vRNAs assembled with the viral core proteins to form immature viral particles before budding and becoming mature viral particles (82–84). The balance between mRNA translation and RNA and core protein packaging is regulated by nucleocapsids-mediated LLPS.

HIV-1 Gag polyprotein precursor (also known as Pr55Gag) regulates viral assembly. The Gag is proteolytically sheared into multiple monomeric protein matrices (MA), capsid (CA), nucleocapsid (NC), p6 structural domain, and two spacer peptides SP1 and SP2 (85, 86). NC plays an important role in key cycle processes such as vRNA capsulization and Gag multimerization (87). The typical structural features of NC are two highly conserved CCHC-type zinc finger structures. NC also has a low-complexity, intrinsically disordered prion-like domain (43, 88). Anne Monette et al. showed that HIV-1 NC could form droplets through LLPS. NC-mediated LLPS induces translational silencing and drives viral assembly by affecting the balance between viral RNP and NC-mediated SG, resulting in the formation of infectious viral particles. To avoid viral RNP overgrowth leading to the production of dysfunctional viral particles, the formation of RNP is therefore also limited by NC-mediated SG. It has been shown that overexpression of NC protein leads to the induction of SG assembly (89).

### Phase separation is involved in the formation of IBs

IBs are proved to be membraneless organelles (90). They play an important role in virus genomic replication and transcription. Like other membraneless organelles, RSV IBs are formed in the presence of N and P through LLPS. In the N-P complex, the C-

terminus of P protein interacts with N<sub>NTD</sub>, and its N-terminus interacts with N<sub>CTD</sub>. Furthermore, the oligomerization domain and the C-terminal IDR of P are indispensable for forming IBs (91). VSV can form cytoplasmic inclusions with classical fluidic properties. When the inclusions are formed, RNA synthesis machinery is redistributed to inclusions, where RNA synthesis occurs (90). The cytoplasmic inclusions are membraneless structures. The live-cell fluorescence microscopy found that they are dynamic organelles capable of fission and fusion. In addition, cytoplasmic inclusions can maintain roundness induced by intrinsic surface tension. Moreover, the proteins in the inclusions can reversibly exchange with the cytoplasmic pool (21). Although belonging to the same Rhabdoviridae, VSV partially differs from RABV that formed the classical liquid compartments, Negri bodies (NBs), through LLPS (20, 91). In the case of RABV, the presence of N and P proteins can drive the formation of a very small NB, but for VSV, viral IBs were formed in the presence of N, P, and L proteins (21).

### Impact of virus-driven phase separation on host antiviral innate immunity

Since the phase-separated region can specifically enrich a protein and its interacting proteins while excluding others, the virus might use this strategy to evade the host's innate immune responses.

Recent studies have shown that LLPS plays an important regulatory role in the cGAS- stimulator of interferon genes (STING) immune pathway. cGAS is activated by cytoplasmic viral DNA and synthesizes the unique second messenger cyclic GMP- AMP (cGAMP) (92–94). cGAMP binds to the ER-localized junction protein STING and drives the conformational change of STING (95). STING can activate the TBK1-IRF3 pathway, promoting the production of type I IFN (96). The cGAS-STING pathway is regulated by LLPS in two ways.

On the one hand, cGAS can form a membrane-free cellular compartment through phase separation. cGAS has two structural domains: the C-terminal nucleotidyltransferase (NTase) domain and the non-fixed, positively charged N-terminal. These domains can induce LLPS by promoting the binding of cGAS to dsDNA through multivalent interactions (97). High concentrations of cGAS-DNA complexes can increase the activity of cGAS, promoting the synthesis of cGAMP.

On the other hand, viruses can also induce the formation of STING phase-separators through LLPS. Excess 2'3'-cGAMP was discovered to enable STING to form biomolecular agglutination in DNA virus-infected cells (98). It recruits excess intracellular STING and TBK1, but not IRF3, thereby inhibiting the phosphorylation of IRF3 and preventing overactivation of the cGAS-STING pathway (Figure 2) (99).

In addition, antiviral sensors isolated in IBs can suppress the activation of downstream pathways (50). Take the example of IBs formed by RSV. Initially, MAVS can activate cytosolic kinase IKK and TBK1 to activate transcription factors NF-κB and IRF3

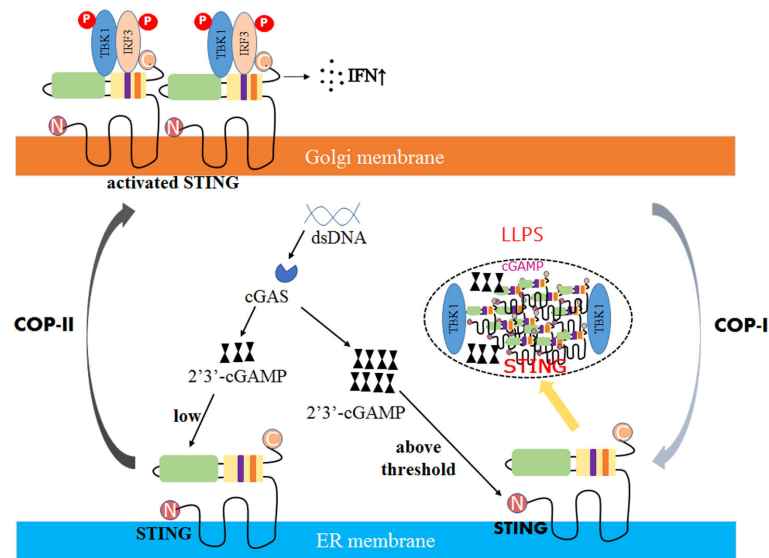


FIGURE 2

The mechanism of STING phase separators interferes with innate immune signaling. In DNA virus-infected cells, the recognition of double-stranded DNA (dsDNA) by STING on the ER membrane is followed by activating the second messenger 2'3'-cGAMP generated by the DNA sensor cGAS. Due to low levels of 2'3'-cGAMP, STING is transferred to the Golgi apparatus, polymerized, and recruited to activate TBK1 and IRF3, promoting the production of cytokines such as type I interferon (IFN). However, when the concentration of 2'3'-cGAMP reaches a threshold, the STING phase separator forms, recruiting cGAMP and unphosphorylated TBK1 into liquid droplets, separating STING and TBK1 from its downstream signaling and preventing the overactivation of the innate immune response.

(100). Lifland et al. found that MAVS and MDA5 are localized in IBs. Importantly, the proximity ligation assay showed that RSV N proteins co-localize with MAVS and MDA5 in IBs (101). Consequently, sequestering MAVS and MDA5 into IBs leads to the strong inhibition of type I interferon production. Furthermore, Fatoumatta et al. observed that p65 recruited into IBs can block the NF- $\kappa$ B signaling pathway (53).

## Conclusion

The role of phase separation in viral adsorption, replication, assembly, and release is a hot topic. Biomolecular condensates formed through LLPS can concentrate replication machinery, facilitate viral gene transcription and expression, and regulate innate immune responses by constraining the host sensors in IBs. As a result, phase separation offers a new perspective on viral replication, assembly, and egress within the host cell and a promising treatment strategy for viral infections.

However, the underlying mechanisms of LLPS's formation and action during viral replication, capsid assembly, progeny egress, and antiviral immune regulation remain unknown. All macromolecules can form a network through multivalent interaction, resulting in phase separation. The intracellular environment, on the other hand, is harsh. How do viral proteins recognize and interact before aggregating at a certain concentration? How do viruses maintain the right balance of

LLPS assembly and disassembly to meet the needs of viral replication during the infection? The phase separation phenomenon has only been observed in RNA viruses; however, it is unknown whether phase separation occurs during most other DNA viral infections and HSV-1 and EBV.

Moreover, the proteins' multivalency is indispensable for forming phase separation. Proteins containing intrinsically disordered regions (IDRs) or SRC homology 3 (SH3) repeats can interact, forming condensates. Viral proteins, like HSV-1 UL11 and ICP4, have IDRs, which can drive the formation of condensates. In addition to IDRs, other modules, like SH3 repeats, and multiple proline-rich motifs (PRM) repeats, are also involved in the multivalent interactions between proteins, leading to the formation of multimers. The formation of multimers can drive the formation of LLPS. Additionally, SH3 repeats and PRM repeats can usually be found in eukaryotic protein. So, it can be presumed that viral proteins may not have these modules and cannot mediate the formation of LLPS through these modules.

Furthermore, the investigation of LLPS's roles in antiviral immune regulation, such as the cGAS-STING signaling pathway, is still early. It is unclear whether LLPS is involved in other immune response processes like the oligomerization of the cytosolic viral RNA sensors RIG-I and MDA5 and the formation of the inflammasome. More exciting findings on the roles of LLPS in immune regulation are expected to emerge. Overall, LLPS provides a solid theoretical foundation for understanding viral infection. Further investigations into the underlying

mechanism of LLPS formation and its roles during viral infections will aid in developing novel antiviral therapies.

## Author contributions

WW designed and supervised the manuscript. LB and WW wrote the preliminary draft manuscript. WW, BY, WM, and HW reviewed the preliminary draft manuscript. JZ did the analyses. CZ, FS, and WW edited, revised, and finalized the manuscript. All the authors read and approved the manuscript.

## Funding

This study was supported by the Natural Science Foundation of China (32072838).

## References

- Abrisch RG, Gumbin SC, Wisniewski BT, Lackner LL, Voeltz GK. Fission and fusion machineries converge at ER contact sites to regulate mitochondrial morphology. *J Cell Biol* (2020) 219(4):e201911122. doi: 10.1083/jcb.201911122
- Hyman AA, Weber CA, Julicher F. Liquid-liquid phase separation in biology. *Annu Rev Cell Dev Biol* (2014) 30:39–58. doi: 10.1146/annurev-cellbio-100913-013325
- Brangwynne CP, Eckmann CR, Courson DS, Rybarska A, Hoeghe C, Gharakhani J, et al. Germline p granules are liquid droplets that localize by controlled dissolution/condensation. *Science* (2009) 324(5935):1729–32. doi: 10.1126/science.1172046
- Boeynaems S, Alberti S, Fawzi NL, Mittag T, Polymenidou M, Rousseau F, et al. Protein phase separation: a new phase in cell biology. *Trends Cell Biol* (2018) 28(6):420–35. doi: 10.1016/j.tcb.2018.02.004
- Buchan JR, Parker R. Eukaryotic stress granules: the ins and outs of translation. *Mol Cell* (2009) 36(6):932–41. doi: 10.1016/j.molcel.2009.11.020
- Decker CJ, Parker R. P-bodies and stress granules: possible roles in the control of translation and mRNA degradation. *Cold Spring Harb Perspect Biol* (2012) 4(9):a012286. doi: 10.1101/cshperspect.a012286
- Gall JG. The centennial of the cajal body. *Nat Rev Mol Cell Biol* (2003) 4(12):975–80. doi: 10.1038/nrm1262
- Feric M, Vaidya N, Harmon TS, Mitrea DM, Zhu L, Richardson TM, et al. Coexisting liquid phases underlie nucleolar subcompartments. *Cell* (2016) 165(7):1686–97. doi: 10.1016/j.cell.2016.04.047
- Banani SF, Lee HO, Hyman AA, Rosen MK. Biomolecular condensates: organizers of cellular biochemistry. *Nat Rev Mol Cell Biol* (2017) 18(5):285–98. doi: 10.1038/nrm.2017.7
- Mitrea DM, Kriwacki RW. Phase separation in biology; functional organization of a higher order. *Cell Commun Signal* (2016) 14(1):1. doi: 10.1186/s12964-015-0125-7
- Uversky VN. Intrinsically disordered proteins in overcrowded milieu: Membrane-less organelles, phase separation, and intrinsic disorder. *Curr Opin Struct Biol* (2017) 44:18–30. doi: 10.1016/j.sbi.2016.10.015
- Li P, Banjade S, Cheng HC, Kim S, Chen B, Guo L, et al. Phase transitions in the assembly of multivalent signalling proteins. *Nature* (2012) 483(7389):336–40. doi: 10.1038/nature10879
- Dolgin E. What lava lamps and vinaigrette can teach us about cell biology. *Nature* (2018) 555(7696):300–2. doi: 10.1038/d41586-018-03070-2
- Alberti S, Gladfelter A, Mittag T. Considerations and challenges in studying liquid-liquid phase separation and biomolecular condensates. *Cell* (2019) 176(3):419–34. doi: 10.1016/j.cell.2018.12.035
- Posey AE, Holehouse AS, Pappu RV. Phase separation of intrinsically disordered proteins. *Methods enzymology* (2018) 611:1–30. doi: 10.1016/bs.mie.2018.09.035
- Vernon RM, Chong PA, Tsang B, Kim TH, Bah A, Farber P, et al. Pi-pi contacts are an overlooked protein feature relevant to phase separation. *eLife* (2018) 7:e31486. doi: 10.7554/eLife.31486
- Nott TJ, Petsalaki E, Farber P, Jervis D, Fussner E, Plochowietz A, et al. Phase transition of a disordered nuage protein generates environmentally responsive membraneless organelles. *Mol Cell* (2015) 57(5):936–47. doi: 10.1016/j.molcel.2015.01.013
- Riback JA, Katanski CD, Kear-Scott JL, Pilipenko EV, Rojek AE, Sosnick TR, et al. Stress-triggered phase separation is an adaptive, evolutionarily tuned response. *Cell* (2017) 168(6):1028–1040 e1019. doi: 10.1016/j.cell.2017.02.027
- Chiu YP, Sun YC, Qiu DC, Lin YH, Chen YQ, Kuo JC, et al. Liquid-liquid phase separation and extracellular multivalent interactions in the tale of galectin-3. *Nat Commun* (2020) 11(1):1229. doi: 10.1038/s41467-020-15007-3
- Nikolic J, Le Bars R, Lama Z, Scrima N, Lagaudrière-Gesbert C, Gaudin Y, et al. Negri bodies are viral factories with properties of liquid organelles. *Nat Commun* (2017) 8(1):58. doi: 10.1038/s41467-017-00102-9
- Heinrich BS, Maliga Z, Stein DA, Hyman AA, Whelan SPJ. Phase transitions drive the formation of vesicular stomatitis virus replication compartments. *mBio* (2018) 9(5):e02290–02217. doi: 10.1128/mBio.02290-17
- Chen H, Cui Y, Han X, Hu W, Sun M, Zhang Y, et al. Liquid-liquid phase separation by SARS-CoV-2 nucleocapsid protein and RNA. *Cell Res* (2020) 30(12):1143–5. doi: 10.1038/s41422-020-00408-2
- Savastano A, Ibáñez de Opakua A, Rankovic M, Zweckstetter M. Nucleocapsid protein of SARS-CoV-2 phase separates into RNA-rich polymerase-containing condensates. *Nat Commun* (2020) 11(1):6041. doi: 10.1038/s41467-020-19843-1
- Wu H, Fuxreiter M. The structure and dynamics of higher-order assemblies: amyloids, signalosomes, and granules. *Cell* (2016) 165(5):1055–66. doi: 10.1016/j.cell.2016.05.004
- Brocca S, Grandori R, Longhi S, Uversky V. Liquid-liquid phase separation by intrinsically disordered protein regions of viruses: roles in viral life cycle and control of virus-host interactions. *Int J Mol Sci* (2020) 21(23):9045. doi: 10.3390/ijms21239045
- Etibor TA, Yamauchi Y, Amorim MJ. Liquid biomolecular condensates and viral lifecycles: review and perspectives. *Viruses* (2021) 13(3):366. doi: 10.3390/v13030366
- Kim TH, Tsang B, Vernon RM, Sonenberg N, Kay LE, Forman-Kay JD. Phospho-dependent phase separation of FMRP and CAPRIN1 recapitulates regulation of translation and deadenylation. *Science* (2019) 365(6455):825–9. doi: 10.1126/science.aax4240
- Sabari BR, Dall'Agnese A, Bojia A, Klein IA, Coffey EL, Shrinivas K, et al. Coactivator condensation at super-enhancers links phase separation and gene control. *Science* (2018) 361(6400):eaar3958. doi: 10.1126/science.aar3958
- Martin EW, Holehouse AS, Peran I, Farag M, Incicco JJ, Bremer A, et al. Valence and patterning of aromatic residues determine the phase behavior of prion-like domains. *Science* (2020) 367(6478):694–9. doi: 10.1126/science.aaw8653
- Bari KJ, Prakashchand DD. Fundamental challenges and outlook in simulating liquid-liquid phase separation of intrinsically disordered proteins. *J Phys Chem letters* (2021) 12(6):1644–56. doi: 10.1021/acs.jpcclett.0c03404

## Conflict of interest

The authors declare that the research was conducted in the absence of any commercial or financial relationships that could be construed as a potential conflict of interest.

## Publisher's note

All claims expressed in this article are solely those of the authors and do not necessarily represent those of their affiliated organizations, or those of the publisher, the editors and the reviewers. Any product that may be evaluated in this article, or claim that may be made by its manufacturer, is not guaranteed or endorsed by the publisher.

31. Forman-Kay JD, Mittag T. From sequence and forces to structure, function, and evolution of intrinsically disordered proteins. *Structure (London England: 1993)* (2013) 21(9):1492–9. doi: 10.1016/j.str.2013.08.001
32. Bianchi G, Longhi S, Grandori R, Brocca S. Relevance of electrostatic charges in compactness, aggregation, and phase separation of intrinsically disordered proteins. *Int J Mol Sci* (2020) 21(17):6208. doi: 10.3390/ijms21176208
33. Banjade S, Wu Q, Mittal A, Peebles WB, Pappu RV, Rosen MK. Conserved interdomain linker promotes phase separation of the multivalent adaptor protein nck. *Proc Natl Acad Sci United States America* (2015) 112(47):E6426–6435. doi: 10.1073/pnas.1508778112
34. Zeng M, Shang Y, Araki Y, Guo T, Hugarir RL, Zhang M. Phase transition in postsynaptic densities underlies formation of synaptic complexes and synaptic plasticity. *Cell* (2016) 166(5):1163–1175 e1112. doi: 10.1016/j.cell.2016.07.008
35. Maharana S, Wang J, Papadopoulos DK, Richter D, Pozniakovskiy A, Poser I, et al. RNA Buffers the phase separation behavior of prion-like RNA binding proteins. *Science* (2018) 360(6391):918–21. doi: 10.1126/science.aar7366
36. Iserman C, Roden CA, Boerneke MA, Sealton RSG, McLaughlin GA, Jungreis I, et al. Genomic RNA elements drive phase separation of the sars-cov-2 nucleocapsid. *Mol Cell* (2020) 80(6):1078–1091 e1076. doi: 10.1016/j.molcel.2020.11.041
37. Hsieh PK, Chang SC, Huang CC, Lee TT, Hsiao CW, Kou YH, et al. Assembly of severe acute respiratory syndrome coronavirus RNA packaging signal into virus-like particles is nucleocapsid dependent. *J virology* (2005) 79(22):13848–55. doi: 10.1128/JVI.79.22.13848-13855.2005
38. Perdikari TM, Murthy AC, Ryan VH, Watters S, Naik MT, Fawzi NL. SARS-CoV-2 nucleocapsid protein undergoes liquid-liquid phase separation stimulated by RNA and partitions into phases of human ribonucleoproteins. *bioRxiv: preprint server Biol* (2020) 141101. doi: 10.1101/2020.06.09.141101
39. Roberts TK, Eugenin EA, Morgello S, Clements JE, Zink MC, Berman JW. PrP<sup>C</sup>, the cellular isoform of the human prion protein, is a novel biomarker of HIV-associated neurocognitive impairment and mediates neuroinflammation. *Am J Pathol* (2010) 177(4):1848–60. doi: 10.2353/ajpath.2010.091006
40. Voigtlander T, Kloppel S, Birner P, Jarius C, Flicker H, Verghese-Nikolaki S, et al. Marked increase of neuronal prion protein immunoreactivity in alzheimer's disease and human prion diseases. *Acta Neuropathol* (2001) 101(5):417–23. doi: 10.1007/s004010100405
41. Wadsworth JD, Hill AF, Joiner S, Jackson GS, Clarke AR, Collinge J. Strain-specific prion-protein conformation determined by metal ions. *Nat Cell Biol* (1999) 1(1):55–9. doi: 10.1038/9030
42. Singh V, Xu L, Boyko S, Surewicz K, Surewicz WK. Zinc promotes liquid-liquid phase separation of tau protein. *J Biol Chem* (2020) 295(18):5850–6. doi: 10.1074/jbc.AC120.013166
43. Muriaux D, Darlix JL. Properties and functions of the nucleocapsid protein in virus assembly. *RNA Biol* (2010) 7(6):744–53. doi: 10.4161/rna.7.6.14065
44. Rai SK, Savastano A, Singh P, Mukhopadhyay S, Zweckstetter M. Liquid-liquid phase separation of tau: From molecular biophysics to physiology and disease. *Protein science: Publ Protein Society* (2021) 30(7):1294–314. doi: 10.1002/pro.4093
45. Monette A, Niu M, Chen L, Rao S, Gorelick RJ, Moulant AJ. Pan-retroviral nucleocapsid-mediated phase separation regulates genomic RNA positioning and trafficking. *Cell Rep* (2020) 31(3):107520. doi: 10.1016/j.celrep.2020.03.084
46. Wu H, Mitra M, Nauffer MN, McCauley MJ, Gorelick RJ, Rouzina J, et al. Differential contribution of basic residues to HIV-1 nucleocapsid protein's nucleic acid chaperone function and retroviral replication. *Nucleic Acids Res* (2014) 42(4):2525–37. doi: 10.1093/nar/gkt1227
47. Rayman JB, Karl KA, Kandel ER. TIA-1 self-multimerization, phase separation, and recruitment into stress granules are dynamically regulated by Zn<sup>2+</sup>. *Cell Rep* (2018) 22(1):59–71. doi: 10.1016/j.celrep.2017.12.036
48. Monette A, Moulant AJ. Zinc and copper ions differentially regulate prion-like phase separation dynamics of pan-virus nucleocapsid biomolecular condensates. *Viruses* (2020) 12(10):1179. doi: 10.3390/v12101179
49. Charman M, Weitzman MD. Replication compartments of dna viruses in the nucleus: location, location, location. *Viruses* (2020) 12(2):151. doi: 10.3390/v12020151
50. Dolnik O, Gerresheim GK, Biedenkopf N. New perspectives on the biogenesis of viral inclusion bodies in negative-sense rna virus infections. *Cells* (2021) 10(6):1460. doi: 10.3390/cells10061460
51. Dinh PX, Beura LK, Das PB, Panda D, Das A, Pattnaik AK. Induction of stress granule-like structures in vesicular stomatitis virus-infected cells. *J virology* (2013) 87(1):372–83. doi: 10.1128/JVI.02305-12
52. Hong Y, Bai M, Qi X, Li C, Liang M, Li D, et al. Suppression of the IFN- $\alpha$  and - $\beta$  induction through sequestering IRF7 into viral inclusion bodies by nonstructural protein NSs in severe fever with thrombocytopenia syndrome bunyavirus infection. *J Immunol (Baltimore Md: 1950)* (2019) 202(3):841–56. doi: 10.4049/jimmunol.1800576
53. Jobe F, Simpson J, Hawes P, Guzman E, Bailey D. Respiratory syncytial virus sequesters nf- $\kappa$ b subunit p65 to cytoplasmic inclusion bodies to inhibit innate immune signaling. *J virology* (2020) 94(22):e01380–01320. doi: 10.1128/jvi.01380-20
54. Fricke J, Koo LY, Brown CR, Collins PL. p38 and OGT sequestration into viral inclusion bodies in cells infected with human respiratory syncytial virus suppresses MK2 activities and stress granule assembly. *J virology* (2013) 87(3):1333–47. doi: 10.1128/JVI.02263-12
55. Johnson DC, Baines JD. Herpesviruses remodel host membranes for virus egress. *Nat Rev Microbiol* (2011) 9(5):382–94. doi: 10.1038/nrmicro2559
56. Honess RW, Roizman B. Regulation of herpesvirus macromolecular synthesis. i. cascade regulation of the synthesis of three groups of viral proteins. *J virology* (1974) 14(1):8–19. doi: 10.1128/jvi.14.1.8-19.1974
57. Honess RW, Roizman B. Regulation of herpesvirus macromolecular synthesis: sequential transition of polypeptide synthesis requires functional viral polypeptides. *Proc Natl Acad Sci United States America* (1975) 72(4):1276–80. doi: 10.1073/pnas.72.4.1276
58. Seyffert M, Georgi F, Tobler K, Bourqui L, Anfossi M, Michaelsen K, et al. The HSV-1 transcription factor icp4 confers liquid-like properties to viral replication compartments. *Int J Mol Sci* (2021) 22(9):4447. doi: 10.3390/ijms22094447
59. Everett RD, Sourvinos G, Orr A. Recruitment of herpes simplex virus type 1 transcriptional regulatory protein ICP4 into foci juxtaposed to ND10 in live, infected cells. *J virology* (2003) 77(6):3680–9. doi: 10.1128/JVI.77.6.3680-3689.2003
60. McSwiggen DT, Hansen AS, Teves SS, Marie-Nelly H, Hao Y, Heckert AB, et al. Evidence for DNA-mediated nuclear compartmentalization distinct from phase separation. *eLife* (2019) 8:e47098. doi: 10.7554/eLife.47098
61. Owen DJ, Crump CM, Graham SC. Tegument assembly and secondary envelopment of alphaherpesviruses. *Viruses* (2015) 7(9):5084–114. doi: 10.3390/v7092861
62. Metrick CM, Koenigsberg AL, Heldwein EE. Conserved outer tegument component ul11 from herpes simplex virus 1 is an intrinsically disordered, rna-binding protein. *mBio* (2020) 11(3):e00810–00820. doi: 10.1128/mBio.00810-20
63. Cao Y. EBV based cancer prevention and therapy in nasopharyngeal carcinoma. *NPJ Precis Oncol* (2017) 1(1):10. doi: 10.1038/s41698-017-0018-x
64. Network CGAR. Comprehensive molecular characterization of gastric adenocarcinoma. *Nature* (2014) 513(7517):202–9. doi: 10.1038/nature13480
65. Alferi C, Birkenbach M, Kieff E. Early events in Epstein-Barr virus infection of human b lymphocytes. *Virology* (1991) 181(2):595–608. doi: 10.1016/0042-6822(91)90893-G
66. Sinclair AJ, Palmero I, Peters G, Farrell PJ. EBNA-2 and EBNA-LP cooperate to cause G0 to G1 transition during immortalization of resting human b lymphocytes by Epstein-Barr virus. *EMBO J* (1994) 13(14):3321–8. doi: 10.1002/j.1460-2075.1994.tb06634.x
67. Zhao B, Zou J, Wang H, Johanssen E, Peng CW, Quackenbush J, et al. Epstein-Barr Virus exploits intrinsic b-lymphocyte transcription programs to achieve immortal cell growth. *Proc Natl Acad Sci United States America* (2011) 108(36):14902–7. doi: 10.1073/pnas.1108892108
68. Liang J, Zhou H, Gerdt C, Tan M, Colson T, Kaye KM, et al. Epstein-Barr Virus super-enhancer eRNAs are essential for MYC oncogene expression and lymphoblast proliferation. *Proc Natl Acad Sci United States America* (2016) 113(49):14121–6. doi: 10.1073/pnas.1616697113
69. Gunnell A, Webb HM, Wood CD, McClellan MJ, Wichaidit B, Kempkes B, et al. RUNX super-enhancer control through the notch pathway by Epstein-Barr virus transcription factors regulates b cell growth. *Nucleic Acids Res* (2016) 44(10):4636–50. doi: 10.1093/nar/gkw085
70. Peng Q, Wang L, Qin Z, Wang J, Zheng X, Wei L, et al. Phase separation of Epstein-Barr virus EBNA2 and its coactivator EBNA1 controls gene expression. *J virology* (2020) 94(7):e01771–01719. doi: 10.1128/JVI.01771-19
71. Yang Y, Ye X, Dai R, Li Z, Zhang Y, Xue W, et al. Phase separation of Epstein-Barr virus EBNA2 protein reorganizes chromatin topology for epigenetic regulation. *Commun Biol* (2021) 4(1):967. doi: 10.1038/s42003-021-02501-7
72. McBride R, van Zyl M, Fielding BC. The coronavirus nucleocapsid is a multifunctional protein. *Viruses* (2014) 6(8):2991–3018. doi: 10.3390/v6082991
73. Milin AN, Deniz AA. Reentrant phase transitions and non-equilibrium dynamics in membraneless organelles. *Biochemistry* (2018) 57(17):2470–7. doi: 10.1021/acs.biochem.8b00001
74. V'Kovski P, Kratzel A, Steiner S, Stalder H, Thiel V. Coronavirus biology and replication: implications for SARS-CoV-2. *Nat Rev Microbiol* (2021) 19(3):155–70. doi: 10.1038/s41579-020-00468-6
75. Knoops K, Kikkert M, Worm SH, Zevenhoven-Dobbe JC, van der Meer Y, Koster AJ, et al. SARS-coronavirus replication is supported by a reticulovesicular network of modified endoplasmic reticulum. *PLoS Biol* (2008) 6(9):e226. doi: 10.1371/journal.pbio.0060226

76. Snijder EJ, Limpens R, de Wilde AH, de Jong AWM, Zevenhoven-Dobbe JC, Maier HJ, et al. A unifying structural and functional model of the coronavirus replication organelle: Tracking down RNA synthesis. *PLoS Biol* (2020) 18(6): e3000715. doi: 10.1371/journal.pbio.3000715
77. de Haan CA, Kuo L, Masters PS, Vennema H, Rottier PJ. Coronavirus particle assembly: primary structure requirements of the membrane protein. *J virology* (1998) 72(8):6838–50. doi: 10.1128/JVI.72.8.6838-6850.1998
78. Eiermann N, Haneke K, Sun Z, Stoecklin G, Ruggieri A. Dance with the devil: stress granules and signaling in antiviral responses. *Viruses* (2020) 12(9):984. doi: 10.3390/v12090984
79. Kasuga Y, Zhu B, Jang KJ, Yoo JS. Innate immune sensing of coronavirus and viral evasion strategies. *Exp Mol Med* (2021) 53(5):723–36. doi: 10.1038/s12276-021-00602-1
80. Cascarina SM, Ross ED. A proposed role for the SARS-CoV-2 nucleocapsid protein in the formation and regulation of biomolecular condensates. *FASEB J* (2020) 34(8):9832–42. doi: 10.1096/fj.202001351
81. Yang P, Mathieu C, Kolaitis RM, Zhang P, Messing J, Yurtsever U, et al. G3BP1 is a tunable switch that triggers phase separation to assemble stress granules. *Cell* (2020) 181(2):325–345.e328. doi: 10.1016/j.cell.2020.03.046
82. Barajas BC, Tanaka M, Robinson BA, Phuong DJ, Chutiraka K, Reed JC, et al. Identifying the assembly intermediate in which gag first associates with unspliced HIV-1 RNA suggests a novel model for HIV-1 RNA packaging. *PLoS pathogens* (2018) 14(4):e1006977. doi: 10.1371/journal.ppat.1006977
83. Anderson EC, Lever AM. Human immunodeficiency virus type 1 gag polyprotein modulates its own translation. *J virology* (2006) 80(21):10478–86. doi: 10.1128/JVI.02596-05
84. Poon DT, Chertova EN, Ott DE. Human immunodeficiency virus type 1 preferentially encapsidates genomic RNAs that encode Pr55(Gag): functional linkage between translation and RNA packaging. *Virology* (2002) 293(2):368–78. doi: 10.1006/viro.2001.1283
85. Darlix JL, Godet J, Ivanyi-Nagy R, Fossé P, Mauffret O, Mély Y. Flexible nature and specific functions of the HIV-1 nucleocapsid protein. *J Mol Biol* (2011) 410(4):565–81. doi: 10.1016/j.jmb.2011.03.037
86. Dick RA, Vogt VM. Membrane interaction of retroviral gag proteins. *Front Microbiol* (2014) 5:187. doi: 10.3389/fmicb.2014.00187
87. Darlix JL, Lapadat-Tapolsky M, de Rocquigny H, Roques BP. First glimpses at structure-function relationships of the nucleocapsid protein of retroviruses. *J Mol Biol* (1995) 254(4):523–37. doi: 10.1006/jmbi.1995.0635
88. Gorelick RJ, Nigida SM Jr., Bess JW Jr., Arthur LO, Henderson LE, Rein A. Noninfectious human immunodeficiency virus type 1 mutants deficient in genomic RNA. *J virology* (1990) 64(7):3207–11. doi: 10.1128/jvi.64.7.3207-3211.1990
89. Rao S, Cinti A, Temzi A, Amorim R, You JC, Mouland AJ. HIV-1 NC-induced stress granule assembly and translation arrest are inhibited by the dsRNA binding protein Staufen1. *RNA (New York NY)* (2018) 24(2):219–36. doi: 10.1261/rna.064618.117
90. Rincheval V, Lelek M, Gault E, Bouillier C, Sitterlin D, Blouquit-Laye S, et al. Functional organization of cytoplasmic inclusion bodies in cells infected by respiratory syncytial virus. *Nat Commun* (2017) 8(1):563. doi: 10.1038/s41467-017-00655-9
91. Galloux M, Risso-Ballester J, Richard CA, Fix J, Rameix-Welti MA, Eléouët JF. Minimal elements required for the formation of respiratory syncytial virus cytoplasmic inclusion bodies *In vivo* and *in vitro*. *mBio* (2020) 11(5):e01202–01220. doi: 10.1128/mBio.01202-20
92. Chen Q, Sun L, Chen ZJ. Regulation and function of the cGAS-STING pathway of cytosolic DNA sensing. *Nat Immunol* (2016) 17(10):1142–9. doi: 10.1038/ni.3558
93. Ishii KJ, Coban C, Kato H, Takahashi K, Torii Y, Takeshita F, et al. A toll-like receptor-independent antiviral response induced by double-stranded b-form DNA. *Nat Immunol* (2006) 7(1):40–8. doi: 10.1038/ni1282
94. Stetson DB, Medzhitov R. Recognition of cytosolic DNA activates an IRF3-dependent innate immune response. *Immunity* (2006) 24(1):93–103. doi: 10.1016/j.immuni.2005.12.003
95. Gao P, Ascano M, Wu Y, Barchet W, Gaffney BL, Zillinger T, et al. Cyclic [G(2',5')pA(3',5')p] is the metazoan second messenger produced by DNA-activated cyclic GMP-AMP synthase. *Cell* (2013) 153(5):1094–107. doi: 10.1016/j.cell.2013.04.046
96. Ishikawa H, Ma Z, Barber GN. STING regulates intracellular DNA-mediated, type I interferon-dependent innate immunity. *Nature* (2009) 461(7265):788–92. doi: 10.1038/nature08476
97. Du M, Chen ZJ. DNA-Induced liquid phase condensation of cGAS activates innate immune signaling. *Science* (2018) 361(6403):704–9. doi: 10.1126/science.aat1022
98. Hopfner KP, Hornung V. Molecular mechanisms and cellular functions of cGAS-STING signalling. *Nat Rev Mol Cell Biol* (2020) 21(9):501–21. doi: 10.1038/s41580-020-0244-x
99. Yu X, Zhang L, Shen J, Zhai Y, Jiang Q, Yi M, et al. The STING phase-separator suppresses innate immune signalling. *Nat Cell Biol* (2021) 23(4):330–40. doi: 10.1038/s41556-021-00659-0
100. Mogensen TH. Pathogen recognition and inflammatory signaling in innate immune defenses. *Clin Microbiol Rev* (2009) 22(2):240–73. doi: 10.1128/CMR.00046-08
101. Lifland AW, Jung J, Alonas E, Zurla C, Crowe JE Jr., Santangelo PJ. Human respiratory syncytial virus nucleoprotein and inclusion bodies antagonize the innate immune response mediated by MDA5 and MAVS. *J Virol* (2012) 86(15):8245–58. doi: 10.1128/JVI.00215-12



## Glossary

LLPS	liquid-liquid phase separation
MLO	membraneless organelle
SG	stress granule
RC	replication compartment
IB	inclusion of body
SARS-COV-2	severe acute respiratory syndrome coronavirus
2RABV	rabies virus
vRNA	viral RNA
IDRs	intrinsically disordered regions
PLDs	prion-like domains
LCDs	low-complexity sequence domains
IDPs	intrinsically disordered proteins
SH3	SRC homology 3
PRM	proline-rich motif
gRNA	genomic RNA
PrLD	prion-like disordered protein domain
HIV-1	human immunodeficiency virus type 1
ZnF	zinc finger
HSV-1	herpes simplex virus type
1EBV	Epstein Barr virus
RdRp	RNA-dependent RNA polymerase
ERGIC	ER-Golgi intermediate
Compartment	
MA	matrix
CA	capsid
NC	nucleocapsid
STING	stimulator of interferon gene
cGAMP	cyclic GMP- AMP



## OPEN ACCESS

EDITED BY  
Chenhe Su,  
Wistar Institute, United States

REVIEWED BY  
Xiaochuan Liu,  
University of California, Riverside,  
United States  
Ruoxi Zhang,  
University of Texas Southwestern  
Medical Center, United States  
Bibo Zhu,  
University of Virginia, United States

\*CORRESPONDENCE  
Shaobo Xiao  
vet@mail.hzau.edu.cn

SPECIALTY SECTION  
This article was submitted to  
Viral Immunology,  
a section of the journal  
Frontiers in Immunology

RECEIVED 30 May 2022  
ACCEPTED 21 July 2022  
PUBLISHED 10 August 2022

CITATION  
Li J, Fang P, Zhou Y, Wang D, Fang L  
and Xiao S (2022) DEAD-box RNA  
helicase 21 negatively regulates  
cytosolic RNA-mediated innate  
immune signaling.  
*Front. Immunol.* 13:956794.  
doi: 10.3389/fimmu.2022.956794

COPYRIGHT  
© 2022 Li, Fang, Zhou, Wang, Fang and  
Xiao. This is an open-access article  
distributed under the terms of the  
[Creative Commons Attribution License  
\(CC BY\)](https://creativecommons.org/licenses/by/4.0/). The use, distribution or  
reproduction in other forums is  
permitted, provided the original  
author(s) and the copyright owner(s)  
are credited and that the original  
publication in this journal is cited, in  
accordance with accepted academic  
practice. No use, distribution or  
reproduction is permitted which does  
not comply with these terms.

# DEAD-box RNA helicase 21 negatively regulates cytosolic RNA-mediated innate immune signaling

Jia Li<sup>1,2</sup>, Puxian Fang<sup>1,2</sup>, Yanrong Zhou<sup>1,2</sup>, Dang Wang<sup>1,2</sup>,  
Liurong Fang<sup>1,2</sup> and Shaobo Xiao<sup>1,2\*</sup>

<sup>1</sup>State Key Laboratory of Agricultural Microbiology, College of Veterinary Medicine, Huazhong Agricultural University, Wuhan, China, <sup>2</sup>Key Laboratory of Preventive Veterinary Medicine in Hubei Province, The Cooperative Innovation Center for Sustainable Pig Production, Wuhan, China

DEAD-box RNA helicase 21 (DDX21), also known as RHII/Gu, is an ATP-dependent RNA helicase. In addition to playing a vital role in regulating cellular RNA splicing, transcription, and translation, accumulated evidence has suggested that DDX21 is also involved in the regulation of innate immunity. However, whether DDX21 induces or antagonizes type I interferon (IFN-I) production has not been clear and most studies have been performed through ectopic overexpression or RNA interference-mediated knockdown. In this study, we generated DDX21 knockout cell lines and found that knockout of DDX21 enhanced Sendai virus (SeV)-induced IFN- $\beta$  production and IFN-stimulated gene (ISG) expression, suggesting that DDX21 is a negative regulator of IFN- $\beta$ . Mechanistically, DDX21 competes with retinoic acid-inducible gene I (RIG-I) for binding to double-stranded RNA (dsRNA), thereby attenuating RIG-I-mediated IFN- $\beta$  production. We also identified that the 217–784 amino acid region of DDX21 is essential for binding dsRNA and associated with its ability to antagonize IFN production. Taken together, our results clearly demonstrated that DDX21 negatively regulates IFN- $\beta$  production and functions to maintain immune homeostasis.

## KEYWORDS

DEAD-box helicase 21 (DDX21), innate immunity, type I interferon (IFN-I), retinoic acid-inducible gene I (RIG-I), double-stranded RNA (dsRNA)

## Introduction

Innate immunity is the first line of host defense against viral infections and is triggered by pattern recognition receptors (PRRs). Several PRRs are mobilized to sense viral nucleic acids, ultimately leading to the induction of interferons (IFNs). Toll-like receptors (TLRs), retinoic acid-inducible gene I-like (RIG-I) receptors (RLRs), and

cytoplasmic DNA receptors are the three main PRRs involved in the recognition of viral pathogen-associated molecular patterns (PAMPs). DEAD-box helicases (DDXs), which contain at least 12 conserved motifs, belong to helicase superfamily 2 and are a class of enzymes that are essential to all living organisms. DDXs are involved in various cellular processes (1, 2), including binding and unwinding nucleic acid strands (DNA, RNA, or RNA-DNA hybrids) (3). Additionally, growing evidence shows that DDXs are involved in innate immunity by sensing viral nucleic acids or regulating downstream signaling pathways (4, 5). RIG-I, also known as DDX58, is a member of the RLR as well as DDX family and responsible for the recognition of cytoplasmic double-stranded RNA (dsRNA); DDX41 recognizes intracellular DNA and bacterial cyclic dinucleotides (6); and DDX3 promotes downstream antiviral signaling by binding to the TANK-binding kinase 1 (TBK1) and inhibitor of kappa B kinase  $\epsilon$  (IKK $\epsilon$ ) (7), all of which lead to IFN expression. Conversely, overproduction of IFN-I is detrimental and potentially lethal to the host, so preventing its harmful overproduction is essential to maintain the balance of innate and adaptive immunity. Several DEAD-box helicases have been identified that negatively regulate the production of IFN-I to maintain immune homeostasis. For example, DDX24 negatively regulates cytosolic RNA-mediated IFN-I signaling by competing with RIG-I for RNA (8), DDX19 inhibits IFN-I production by disrupting TBK1-IKK $\epsilon$ -interferon regulatory factor 3 (IRF3) interactions (9), and DDX46 inhibits IFN production by entrapping m6A-demethylated antiviral transcripts, preventing their translation (10, 11).

DDX21, a well-known member of the DDX family, possesses all the characteristic motifs required for DEAD-box helicase function. DDX21 also contains an atypical FRGQR repeat at its C-terminus that contributes to its RNA binding and RNA folding activities (12), allowing it to directly bind rRNA and snoRNA and facilitate rRNA transcription, processing, and modification (13–16). Furthermore, DDX21 is responsible for the unwinding of RNA or RNA/DNA hybrid strands, such as dsRNA, R-loops, and G-quadruplex, depending on its ATPase activity, RNA helicase activity (17), and RNA folding enzyme activity (12, 18). Notably, DDX21 completes cellular processes through enzymatic, but it also exhibits non-enzymatic functions. The role of DDX21 in innate immunity has also been reported. A previous study showed that DDX21, together with DDX1 and DHX36, binds to the adaptor protein TRIF and senses dsRNA to activate the IFN signaling pathway, which is independent of RLRs. Briefly, DDX1 binds to dsRNA *via* the helicase A structural domain and then recruits DDX21 to mediate the interaction of DDX1 with DHX36. DDX21 and DHX36 bind to the TIR domain of TRIF *via* their PRK and HA2-DUF domains, respectively, and activate the IFN-I and NF- $\kappa$ B pathways. Knockdown of DDX21 negatively regulates poly (I: C), influenza A virus, or reovirus-induced IFN-I production (19). A recent study showed that DDX21 may balance viral/

ligand-induced innate immune signaling by downregulating IFN- $\beta$  expression. Vesicular stomatitis virus (VSV) infection and poly (I: C) treatment resulted in caspase-dependent cleavage of DDX21 at D126, facilitating its nuclear to cytoplasmic translocation. Cleaved DDX21 inhibits IFN- $\beta$  production by preventing the assembly of the DDX1-DDX21-DHX36 complex, and knockdown of DDX21 inhibited IFN- $\beta$  production, whereas overexpression of DDX21 did not affect IFN- $\beta$  production. Interestingly, knockdown of DDX21 inhibits VSV replication and overexpression of DDX21 promotes VSV replication (20). In addition, overexpression of DDX21 has been reported to promote the activation of IFN- $\beta$  promoters induced by dengue virus infection or background (21). Obviously, DDX21 antagonism or induction of IFN-I production remains controversial. Previous results on DDX21 regulation of the innate immune response were achieved by overexpression or small RNA interference assays. Moreover, the effect of DDX21 knockout on the innate immune response and whether DDX21 is involved in RLR-mediated innate immunity remains unclear.

In this study, a DDX21-knockout HEK-293T cell line was constructed by CRISPR/cas9 technology. DDX21 was shown to negatively regulate the production of IFN- $\beta$ . Further analysis revealed that DDX21 inhibits dsRNA-mediated activation of Interferon regulatory factor 3 (IRF3) and NF- $\kappa$ B. Furthermore, we demonstrated that DDX21 is a dsRNA binding protein that antagonizes RIG-I recognition of viral dsRNA and attenuates dsRNA-mediated RIG-I signaling, leading to inhibition of IFN- $\beta$  production.

## Material and methods

### Viruses and cells

Sendai Virus (SeV) was obtained from the Centre of Virus Resource and Information, Wuhan Institute of Virology, Chinese Academy of Sciences. VSV-GFP was gifted by Zhigao Bu at the Harbin Veterinary Research Institute of the Chinese Academy of Agricultural Sciences. HEK-293T cells were obtained from the China Center for Type Culture Collection (CCTCC) and cultured at 37°C in 5% CO<sub>2</sub> in Dulbecco's modified Eagle's medium (DMEM/High glucose; HyClone, USA) supplemented with 10% heat-inactivated fetal bovine serum (FBS; PAN, USA) and 1% antibiotics (penicillin and streptomycin).

### Plasmid construction

The DNA fragment encoding DDX21 was amplified from cDNAs of HeLa cells and cloned into the pCAGGS vector with an N-terminal Flag or hemagglutinin (HA) tag to generate the expression plasmids pCAGGS-Flag-DDX21 and pCAGGS-HA-

DDX21. The mutants of DDX21 (DDX21-K236E, DDX21-S375L, and DDX21-M4) were constructed by site-directed mutagenesis and named pCAGGS-Flag-DDX21-K236E, pCAGGS-Flag-DDX21-S375L and pCAGGS-Flag-DDX21-M4, respectively. A series of wild-type DDX21 truncation mutants were amplified by overlapping extension PCR using pCAGGS-Flag-DDX21 as a template and then cloned into the pCAGGS vector with an N-terminal Flag. IFN- $\beta$ -Luc, NF- $\kappa$ B-Luc, and IRF3-Luc vectors have been described previously (22). The expression plasmids for Flag-tagged RIG-I, melanoma differentiation associated gene 5 (MDA5), Mitochondrial antiviral-signaling protein (MAVS/IPS1), TBK1, IKKe, and IRF3 have also been described previously (23).

## Dual-luciferase reporter assays

HEK-293T cells cultured in 24-well plates were co-transfected with 1  $\mu$ g of the indicated expression plasmids or empty plasmids, 0.1  $\mu$ g reporter plasmids (IFN- $\beta$ /IRF3/NF- $\kappa$ B), and 0.02  $\mu$ g pRL-TK reference plasmid (Promega, Madison, Wisconsin, USA) using jetPRIME (Polyplus, Illkirch, France) following the manufacturer's instructions. At 24 h post-transfection (hpt), the cells were infected with SeV (10 hemagglutinating activity units/well) or transfected with poly (I: C) (*In vivo* Gen, Carlsbad, CA, USA) for 12 h. Firefly and Renilla luciferase activities from lysed cells were evaluated using the dual-luciferase reporter assay system following the instructions described by the manufacturer (Promega). Representative data from three independently conducted experiments were examined and data are expressed as the relative firefly luciferase activities with normalization to the Renilla luciferase activity.

## siRNA knockdown

The small interfering RNA (siRNA) targeting DDX21 (siDDX21) and negative control siRNA (NC) were designed and synthesized by Genepharma (Suzhou, China). The sequences used in our study are as follows: siDDX21, 5'-GCAUGAGGAAUGGGAUUGATATT-3', and NC 5'-UUCUCCGAACGUGUCACGUTT-3'. HEK-293T cells with 60% confluency were transfected with 50 pmol of siRNA using jetPRIME (Polyplus) following the manufacturer's instructions.

## RNA extraction and quantitative real-time PCR

Total cellular RNA was extracted using TRIzol reagent (Invitrogen) and 1  $\mu$ g RNA of each sample was subsequently reverse transcribed to cDNA with the First Strand cDNA synthesis kit (Roche, Mannheim, Germany). The resulting

cDNA was then used as the template for SYBR Green qPCR assay (Applied Biosystems, Foster City, CA, USA). The individual mRNA transcripts were assayed three times and relative mRNA expression levels were normalized to the expression of  $\beta$ -actin mRNA. All real-time PCR reactions were performed in an ABI 7500 real-time PCR system (Applied Biosystems). The qRT-PCR primers used in this study are shown in Table S1.

## Western blot analysis

Cells were lysed in lysis buffer (4% SDS, 3% dithiothreitol [DTT], 0.065 mM Tris-HCl [pH 6.8], 30% glycerin) supplemented with a protease inhibitor cocktail and a phosphatase inhibitor cocktail (Sigma, Shanghai, China). Equal amounts of proteins were separated by 10% SDS-PAGE and then transferred to a polyvinylidene difluoride (PVDF) membrane. The membrane was blocked with 5% nonfat milk in TBST with 0.1% polysorbate-20 followed by incubation with the indicated primary antibodies at 37°C for 3 h: rabbit anti-IRF3, p-IRF3, IKKe, p-IKKe, p65, p-p65, and RIG-I polyclonal antibodies (ABclonal, Wuhan, China); rabbit anti-STAT1, p-STAT1, STAT2, and p-STAT2 polyclonal antibodies (Cell Signaling Technology, Boston, USA); rabbit anti-DDX21 polyclonal antibodies (NOVUS, St. Louis, Missouri, USA); and mouse anti- $\beta$ -actin, anti-Flag, and anti-HA antibodies (MBL, Beijing, China). After three washes in TBST, the membranes were incubated with horseradish peroxidase (HRP)-conjugated secondary antibodies (Beyotime, Shanghai, China) for 1 h at room temperature. Following washing, the membrane was visualized using enhanced chemiluminescence (ECL) reagents (BIO-RAD, USA). Expression of  $\beta$ -actin was used as a loading control.

## Co-immunoprecipitation assay

HEK-293T cells were co-transfected with expression plasmids encoding HA-DDX21 and Flag-RIG-I for 30 h. Cells were harvested and lysed on ice with lysis buffer (50 mM Tris-HCl, 150 mM NaCl, 1% NP-40, 10% glycerin, 0.1% SDS, and 2 mM Na<sub>2</sub>EDTA) for 30 min at 4°C. A portion of each supernatant from the lysed cells was used as whole-cell lysate (WCL). The remaining supernatants from the lysed cells were precipitated with mouse anti-HA monoclonal antibody (MBL) for 8 h at 4°C, followed by the addition of protein A+G agarose beads (Beyotime) for 4 h. The beads were collected by centrifugation at 3000 rpm for 5 min and washed three times with cell lysis buffer. The beads were resuspended in SDS-PAGE loading buffer and boiled at 95°C for 5 min. The samples and WCL samples were separated by SDS-PAGE and transferred to PVDF membranes, followed by western blotting analyses with the indicated antibodies.

## Poly (I: C) pulldown assay

HEK-293T cells cultured in a 60-mm plate were transfected with 3  $\mu$ g of pCAGGS-Flag-RIG-I, pCAGGS-Flag-DDX21, or empty vector for 24 h. The cells were collected and lysed in 400  $\mu$ l lysis buffer supplemented with a cocktail of protease inhibitors (Beyotime). The cellular lysates were mixed with the prepared poly (I: C)-coated agarose bead suspension and incubated at 4°C for 4 h. The beads were centrifuged and washed three times with 1 mL of lysis buffer, followed by western blot assay using mouse anti-Flag antibody as the primary antibody.

## Generation of DDX21 knockout cells

The CRISPR/Cas9 system was used to generate DDX21 knockout cells. DDX21-specific guide RNA (gRNA) was designed using the online CRISPR design tool (<https://zlab.bio/>). RNA oligonucleotides were annealed and cloned into the PX458 vector. The plasmid was transfected into HEK-293T cells for 36 h. Cells were digested with trypsin, and individual cells with green fluorescence were sorted by flow cytometry and inoculated into 96-well plates, ensuring one cell per well. Cell clones were sequenced to ensure that both alleles of the cell line contained frameshift mutations. In addition to PCR validation, western blot was also performed using the DDX21 antibody. The selected clones demonstrating unaltered DDX21 expression were used as wild-type (*DDX21*<sup>+/+</sup>) clones, while the clones deficient in DDX21 were used as *DDX21*<sup>-/-</sup> clones. The target sequences for guide RNA were as follows: DDX21 guide RNA 1: 5'-TTACAGTCCGGTTCAGGATG-3', DDX21 guide RNA 2: 5'-AGTGAAGCTGCCAGTGAAGA-3'.

## Statistical analysis

Statistical analysis was performed using GraphPad Prism 8. Two-tailed unpaired t-tests were used to determine the significance of differences between groups. A *p*-value less than 0.05 was considered to be statistically significant.

## Results

### Knockout of DDX21 enhances cytoplasmic RNA-induced IFN- $\beta$ production

To ascertain the role of DDX21 in the IFN-I production pathway, we constructed DDX21 knockout HEK-293T cells using CRISPR/Cas9 technology with DDX21 guide RNA 1 editing. The knockout cell line HEK-293T *DDX21*<sup>-/-</sup> was confirmed at the DNA and protein levels (Figures 1A, B). Next, SeV-induced IFN- $\beta$  production was analyzed by qRT-

PCR in both *DDX21*<sup>-/-</sup> and *DDX21*<sup>+/+</sup> cells. As shown in Figure 1C, IFN- $\beta$  mRNA expression was significantly upregulated in *DDX21*<sup>-/-</sup> cells compared with *DDX21*<sup>+/+</sup> cells. In addition, overexpression of DDX21 in *DDX21*<sup>-/-</sup> cells (a rescue experiment) also confirmed that DDX21 negatively regulates SeV-induced IFN- $\beta$  production (Figure 1D). To exclude the off-target effect of CRISPR/Cas9, a DDX21 knockout cell line with DDX21 guide RNA 2 editing was used to assess IFN- $\beta$  production. The qRT-PCR results showed that the deletion of DDX21 upregulated SeV-induced IFN- $\beta$  mRNA expression, which was consistent with the results of Figure 1C (Figures S1A, B). These data suggest that DDX21 negatively regulates IFN- $\beta$  production.

Given that DDX21 inhibits SeV-induced IFN- $\beta$  production and that SeV as an RNA virus is a potent activator of the RLR pathway (24), we speculated that the inhibition of IFN- $\beta$  is triggered by RNA. Poly (I: C) was used to assess the inhibition of IFN- $\beta$  by DDX21 in the RNA-induced IFN signaling pathway. As shown in Figure S2, knockout of DDX21 significantly upregulated poly (I: C)-induced IFN- $\beta$  mRNA expression. These data further demonstrate that DDX21 exerts a negative regulatory effect on cytoplasmic RNA signaling events in cells.

### DDX21 attenuates SeV-induced IRF3 and NF- $\kappa$ B activation

IRF3 and nuclear factor kappa B (NF- $\kappa$ B) are key transcription factors that mediate IFN production in the RLR pathway, and phosphorylated IRF3 and NF- $\kappa$ B subunit p65 (p-IRF3 and p-p65) are their activated forms (24). To analyze whether DDX21 affects the activation of IRF3 and NF- $\kappa$ B, *DDX21*<sup>-/-</sup> or *DDX21*<sup>+/+</sup> cells were stimulated by SeV, followed by western blot analysis. As shown in Figure 2A, DDX21 deficiency enhanced SeV-induced phosphorylation of IRF3 and p65. The same results were observed in DDX21 knockout cells edited by DDX21 guide RNA 2, excluding off-target effects (Figure S1C). HEK-293T cells were transfected with pCAGGS-Flag-DDX21 together with the luciferase reporter plasmids IRF3-Luc or NF- $\kappa$ B-Luc and pRL-TK, followed by dual-luciferase reporter assay. The results showed that SeV-induced IRF3 (Figure 2B) and NF- $\kappa$ B (Figure 2C) activation were compromised by overexpression of DDX21. These results strongly support a role for DDX21 as an IFN antagonist, blocking the activation of IRF3 and NF- $\kappa$ B in the SeV-induced RLR signaling pathway.

### DDX21 deficiency enhances anti-RNA viral responses

Several signal transduction pathways are involved in IFN production. Generated IFN- $\beta$  binds to the interferon receptor and activates the JAK-STAT pathway, inducing the expression

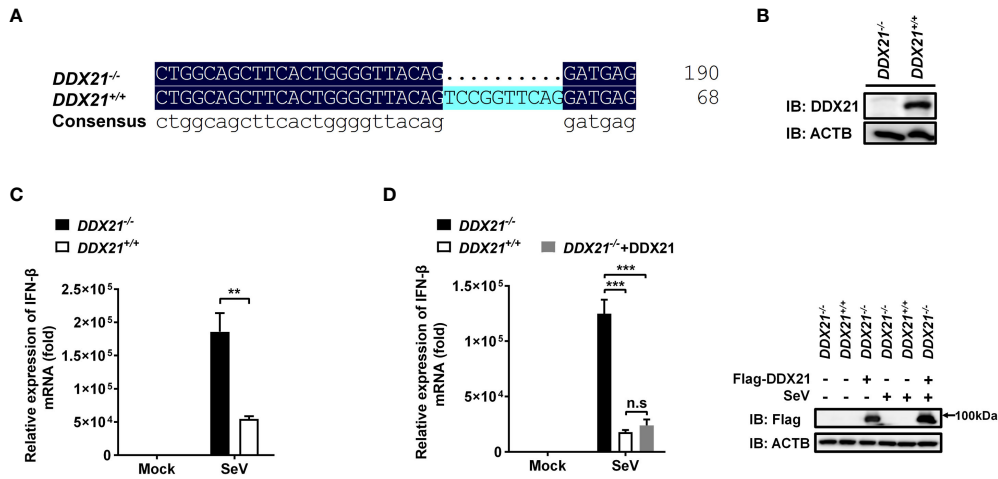


**FIGURE 1** Knockout of DDX21 enhances cytoplasmic RNA-induced IFN- $\beta$  production. (A, B) Genomic DNA and cellular lysates from *DDX21*<sup>+/+</sup> and *DDX21*<sup>-/-</sup> cells were subjected to sequencing PCR (A) and western blot assay with anti-DDX21 polyclonal antibody (B). (C) *DDX21*<sup>+/+</sup> and *DDX21*<sup>-/-</sup> cells were seeded in 24-well plates, followed by infection with SeV (10 hemagglutination units/well). At 12 h post-infection (hpi), the cells were collected for qRT-PCR analysis for detection of IFN- $\beta$  mRNA expression. (D) qRT-PCR analysis of IFN- $\beta$  mRNA expression in *DDX21*<sup>-/-</sup> cells transfected with pCAGGS-Flag-DDX21 or empty vector followed by infection with SeV for 12 h. Protein expression was evaluated by western blot assay (right blots). The experiment was repeated at least three times and the data shown are the means  $\pm$  SD (n=3) of single representative experiments (\*\**P* < 0.01; \*\*\**P* < 0.001). ns, not significant.

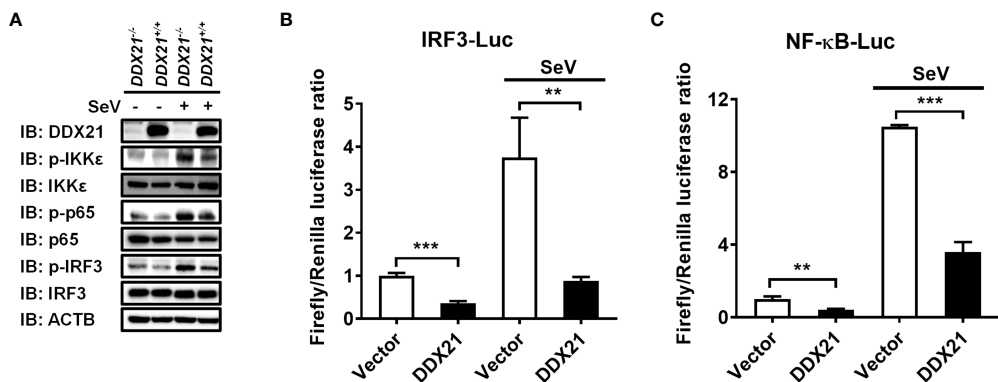


**FIGURE 2** DDX21 attenuates SeV-induced IRF3 and NF- $\kappa$ B activation. (A) *DDX21*<sup>+/+</sup> and *DDX21*<sup>-/-</sup> cells cultured in 6-well plates were infected with SeV or left untreated for 12 h, followed by western blot analysis with primary antibodies against DDX21, total IKK $\epsilon$ , total p65, total IRF3, phosphorylated IKK $\epsilon$ , phosphorylated p65, phosphorylated IRF3, and  $\beta$ -actin. (B, C) HEK-293T cells were transfected with pCAGGS-Flag-DDX21 or empty vectors, together with IRF3-Luc (B) or NF- $\kappa$ B-Luc (C), and pRL-TK receptor plasmids, followed by SeV stimulation for 12 h and dual-luciferase reporter assays. IRF3-Luc (B) and NF- $\kappa$ B-Luc (C) contain four copies of the IRF3- or NF- $\kappa$ B-binding motif in front of a luciferase reporter gene, respectively. The experiment was repeated at least three times and the data shown are the means  $\pm$  SD (n = 3) of single representative experiments (\*\**P* < 0.01; \*\*\**P* < 0.001).

of interferon-stimulated genes (ISGs) to establish a cellular antiviral state (25, 26). To further investigate whether the deletion of DDX21 affects the expression of ISGs, we examined total and phosphorylated levels of key signaling molecules in the IFN signal transduction pathway. *DDX21*<sup>-/-</sup> and *DDX21*<sup>+/+</sup> cells were stimulated by SeV, followed by western

blot analysis. As shown in Figure 3A, the phosphorylation levels of the above-mentioned signaling molecules were significantly up-regulated in SeV-infected cells compared with mock-infected cells. The expression levels of phosphorylated STAT1 (p-STAT1) and p-STAT2 were significantly up-regulated in *DDX21*<sup>-/-</sup> cells compared with *DDX21*<sup>+/+</sup> cells, but there was

no difference in the total protein levels, confirming that knockout of DDX21 promotes SeV-induced RLR signaling. The effect of DDX21 knockout on SeV-induced mRNA expression of ISGs was further examined by qRT-PCR. As shown in Figures 3B–D, the mRNA levels of *ISG15*, *Mx1*, and *OAS1* were significantly upregulated in *DDX21*<sup>-/-</sup> cells compared with *DDX21*<sup>+/+</sup> cells. To further confirm the above results, we performed IFN bioassays using IFN-sensitive vesicular stomatitis virus expressing green fluorescent protein (VSV-GFP). Replication levels of VSV-GFP were inversely correlated with IFN- $\alpha/\beta$  levels secreted in *DDX21*<sup>-/-</sup> and *DDX21*<sup>+/+</sup> cells. IFA and western blot results showed that the supernatant of SeV-infected cells significantly inhibited the replication of VSV-GFP compared with the mock-infected cells, as demonstrated by the reduced green fluorescent signal and GFP expression. However, SeV-infected *DDX21*<sup>-/-</sup> cells supernatants inhibited VSV-GFP replication more strongly compared with *DDX21*<sup>+/+</sup> cells, as evidenced by the lower level of green fluorescent signal and GFP expression in the *DDX21*<sup>-/-</sup> cell group (Figures 3E, F). Taken together, these results demonstrate that DDX21 deficiency enhances anti-RNA viral responses.

## DDX21 fails to disrupt IFN- $\beta$ promoter activation driven by RIG-I, MDA5, MAVS, TBK1, IKK $\epsilon$ , or IRF3

SeV is a strong inducer of the RLR-mediated IFN- $\beta$  signaling pathway (24). Thus, the finding that DDX21 inhibits SeV-mediated activation of IRF3 and NF- $\kappa$ B suggests that DDX21 blocks the SeV-induced RLR-mediated IFN signaling pathway. To determine at which step of the RLR pathway DDX21 exerts its activity, we examined the effect of DDX21 on the production of IFN- $\beta$  induced by a series of key signaling molecules in the RLR signaling pathway, including RIG-I (Figure 4A), MDA5 (Figure 4B), IPS1 (Figure 4C), TBK1 (Figure 4D), IKK $\epsilon$  (Figure 4E), and IRF3 (Figure 4F). The results showed that in comparison with results in the corresponding empty vector-transfected cells, these key signaling molecules significantly induced IFN- $\beta$  promoter activation, but the enhanced activation was not inhibited by DDX21 expression. These results suggest that DDX21 may act as a negative regulator of IFN- $\beta$  either upstream of RIG-I or RIG-I level during SeV infection.

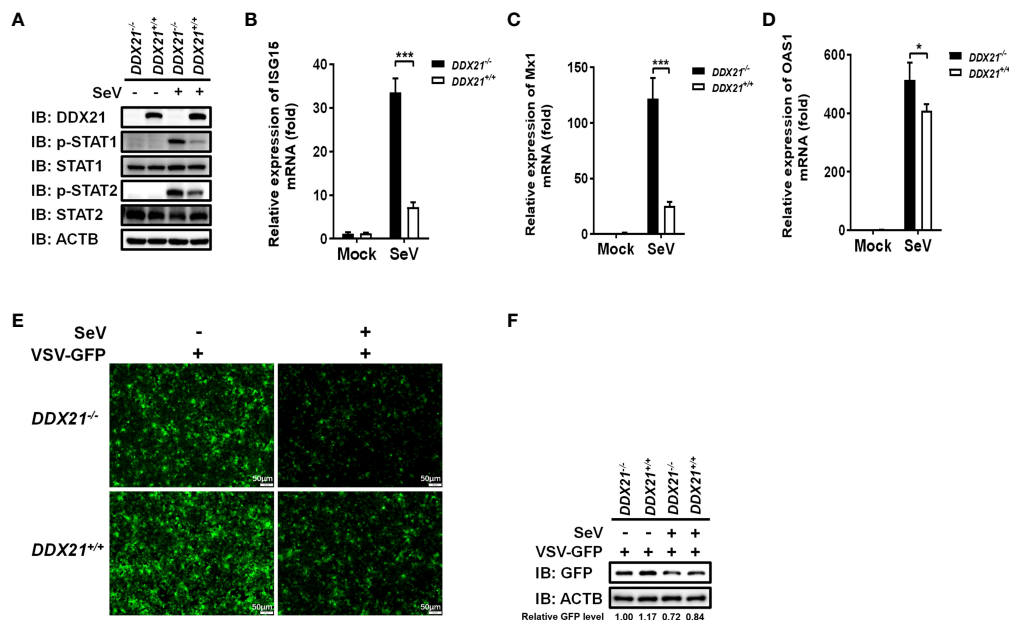


FIGURE 3

DDX21 deficiency enhances anti-RNA viral responses. (A–D) *DDX21*<sup>+/+</sup> and *DDX21*<sup>-/-</sup> cells cultured in 6-well plates were infected with SeV or left untreated. The cells were harvested at 12 hpi for western blot analysis with primary antibodies against DDX21,  $\beta$ -actin, total STAT1, total STAT2, phosphorylated STAT1, and phosphorylated STAT2 (A) or qRT-PCR for detecting the mRNA levels of *ISG15* (B), *Mx1* (C), and *OAS1* (D). (E, F) *DDX21*<sup>+/+</sup> and *DDX21*<sup>-/-</sup> cells cultured in 24-well plates were infected with SeV or left untreated for 12 h. The supernatant was harvested, treated by UV irradiation, and then overlaid onto fresh HEK-293T cells in 24-well plates. At 24 hpi, cells were infected with VSV-GFP. At 12 hpi, VSV-GFP replication was detected by fluorescence microscopy (E) or western blot with primary antibodies against GFP and  $\beta$ -actin (F). Bar, 50  $\mu$ m. The numbers below the images represent the rate of GFP to  $\beta$ -actin via ImageJ software analysis. The experiment was repeated at least three times and the data shown are the means  $\pm$  SD (n=3) of single representative experiments (\* $P$  < 0.05; \*\*\* $P$  < 0.001).

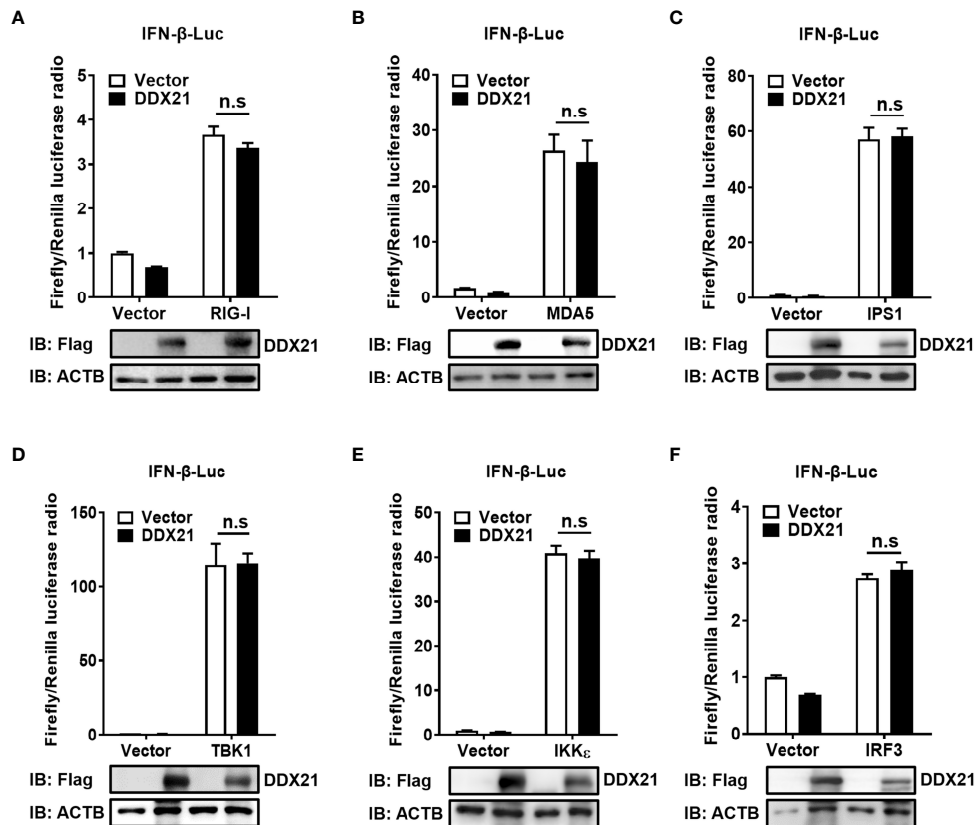


FIGURE 4

DDX21 fails to disrupt IFN- $\beta$  promoter activation driven by RIG-I, MDA5, IPS1, TBK1, IKK $\epsilon$ , or IRF3. (A–F) HEK-293T cells were co-transfected with IFN- $\beta$ -Luc, pRL-TK, and pCAGGS-Flag-DDX21 along with constructs expressing RIG-I (A), MDA5 (B), IPS1 (C), TBK1 (D), IKK $\epsilon$  (E), and IRF3 (F), respectively. Dual-luciferase reporter assay was performed 24 h after transfection. The relative firefly luciferase activity was relative to that of untreated empty vector control, with normalization of the Renilla reniformis luciferase activity. The expression of DDX21 protein was verified by western blotting with an anti-Flag antibody.  $\beta$ -actin served as a protein loading control. The results were repeated at least three times and the data shown are the means  $\pm$  SD ( $n=3$ ) of single representative experiments (n.s., no significant).

## DDX21 neither interacts with RIG-I nor affects its expression

Both RIG-I (DDX58) and DDX21 belong to the DEAD-box helicase family and have a similar functional domain. To further determine whether DDX21 targets RIG-I level to affect its function, *DDX21*<sup>-/-</sup> or *DDX21*<sup>+/+</sup> cells in monolayer culture were treated with poly (I: C) or SeV for 12 h, followed by qRT-PCR and western blot assay for evaluation of the mRNA and protein levels of RIG-I. As shown in Figure 5A and Figure 5B, DDX21 knockout did not affect the mRNA and protein levels of RIG-I. Similar results were observed in cells transfected with various concentrations of DDX21 plasmid (Figure 5C). Moreover, co-immunoprecipitation results confirmed that DDX21 does not interact with RIG-I (Figure 5D). These results suggest that the inhibition of IFN- $\beta$  production by DDX21 may occur at the RIG-I-dsRNA recognition step.

## DDX21 competes with RIG-I to bind dsRNA

RIG-I activates the IFN signaling pathway by recognizing and binding dsRNA (27). DDX21 is an RNA binding protein that directly binds various RNAs (12, 13). Therefore, it is reasonable to speculate that DDX21 competes with RIG-I to bind dsRNA for inhibition of IFN- $\beta$  production. To verify this hypothesis, we first examined the ability of DDX21 to directly associate with RNA species. An RNA pulldown assay was performed by poly (I: C)-coated agarose beads, which have been widely used to identify RNA-binding proteins such as MERS-CoV 4a and Ebola VP35 (28, 29). RIG-I served as a positive control because it has been proven to interact directly with poly (I: C) (30). As seen in Figure 6A, RIG-I bound to poly (I: C)-coated agarose beads but not bound to poly (C)-coated agarose beads, while DDX21 bound both poly (I: C)-coated agarose beads and poly (C)-coated agarose beads, indicating that



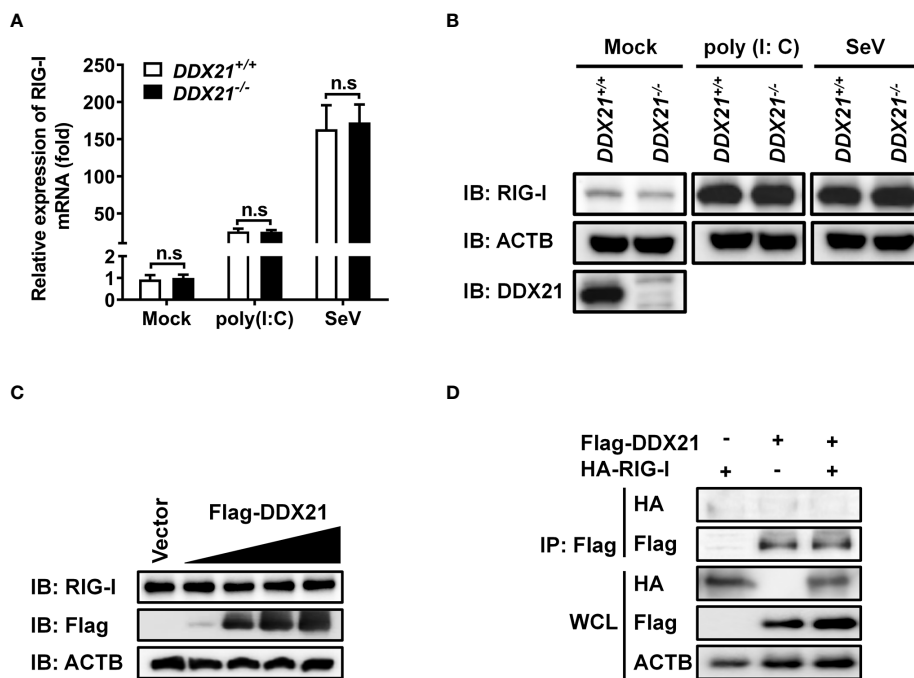


FIGURE 5

DDX21 neither interacts with RIG-I nor affects its expression. (A, B) *DDX21*<sup>+/+</sup> and *DDX21*<sup>-/-</sup> cells cultured in 6-well plates were stimulated with SeV or transfected with poly (I: C) for 12 h, followed by qRT-PCR and western blot assay for detecting the relative mRNA level (A) and protein expression (B) of RIG-I. (C) HEK-293T cells cultured in 6-well plates were transfected with increasing amounts (0.375, 0.75, 1.5, or 3  $\mu$ g) of plasmids encoding Flag-DDX21. At 24 hpt, the cells were collected for western blot analysis with primary antibodies against RIG-I, Flag, and  $\beta$ -actin. (D) HEK-293T cells cultured in 60-mm dishes were co-transfected with expression plasmids encoding HA-DDX21 and Flag-RIG-I. At 24 hpt, the cells were lysed and subjected to immunoprecipitation analysis with an anti-Flag antibody. The whole-cell lysates (WCL) and immunoprecipitation (IP) complexes were analyzed by western blot using anti-Flag, anti-HA, or anti- $\beta$ -actin antibodies. The experiment was repeated at least three times and the data shown are the means  $\pm$  SD (n=3) of single representative experiments (n.s., not significant).

DDX21 is both a dsRNA and single-strand RNA (ssRNA) binding protein.

To investigate whether DDX21 disrupts the binding of RIG-I to dsRNA, a competition assay was performed using poly (I: C) pull-down assays. HEK-293T cells were transfected with RIG-I plasmid or various concentrations of DDX21 expression plasmids for 24 h, and then the cells were collected for poly (I: C) pull-down analysis. The lysates from cells transfected with RIG-I expression plasmids were incubated with lysates from cells transfected with increasing concentrations of the DDX21 expression plasmid, followed by supplementation with prepared poly (I: C)-coated agarose beads for 4 h at 4°C. Bound RIG-I was then detected by western blotting. As shown in Figure 6B, the expression levels of RIG-I and DDX21 proteins were detected in WCL; however, significantly smaller amounts of RIG-I coimmunoprecipitated with poly (I: C)-coated agarose beads were detected with increasing concentrations of DDX21 protein. These results indicate that DDX21 at least partially functions to block the recognition or binding of dsRNA by RIG-I, leading to the antagonism of IFN- $\beta$  production.

## The amino acids 217–784 of DDX21 are essential for binding dsRNA to inhibit IFN- $\beta$ production

To determine the region of DDX21 responsible for binding dsRNA, a series of truncation mutants with N-terminal Flag tags were constructed on the basis of the reported functional domains of DDX21, which contains an N-terminal domain [amino acids (aa) 1 to 396], a Helicase ATP binding domain (aa 217 to 396), a Helicase c-terminal domain (aa 397 to 573), and a C-terminal domain (aa 574 to 784) that has been reported previously to be responsible for RNA binding (31, 32) (Figure 7A). HEK-293T cells were transfected with plasmids expressing Flag-tagged DDX21 or truncation mutants, followed by a poly (I: C) pull-down assay. As shown in Figure 7B, all truncation mutants were expressed at roughly equivalent levels in HEK-293T cells, and the pull-down assay demonstrated that the full-length DDX21, DDX21 1–396 (aa 1–396), DDX21 1–573 (aa 1–573), DDX21 217–784 (aa 217–784), DDX21 397–784 (aa 397–784), and DDX21 574–784 (aa 574–784) had the ability to bind

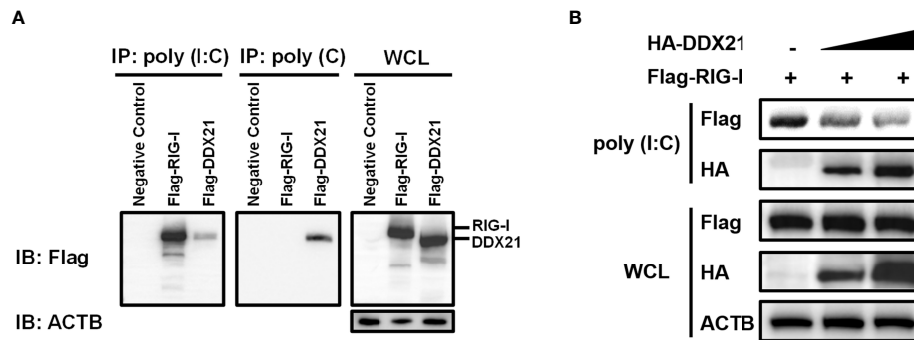


**FIGURE 6** DDX21 competes with RIG-I for binding dsRNA. **(A)** HEK-293T cells were transfected with expression plasmids encoding Flag-RIG-I, Flag-DDX21, or empty vector. Cells were lysed at 24 hpt and supernatant was incubated with poly (C)- or poly (I: C)-coated agarose beads for 4 h at 4°C. The beads were washed three times with lysis buffer by centrifugation, followed by western blot with an antibody against Flag. Poly (I: C)-coated agarose beads were prepared from poly (C)-coated beads (Sigma), which were incubated with 2 mg/ml of poly (I) (Sigma) for 1 h at 56°C. **(B)** HEK-293T cells were transfected separately with expression plasmids encoding Flag-RIG-I or HA-DDX21 for 24 h Cell lysates overexpressing DDX21 were incubated with an equal volume of cell lysates overexpressing RIG-I and then treated with poly (I: C)-coated agarose beads for 4 h at 4°C. The beads were washed three times with lysis buffer and then subjected to western blot analysis.

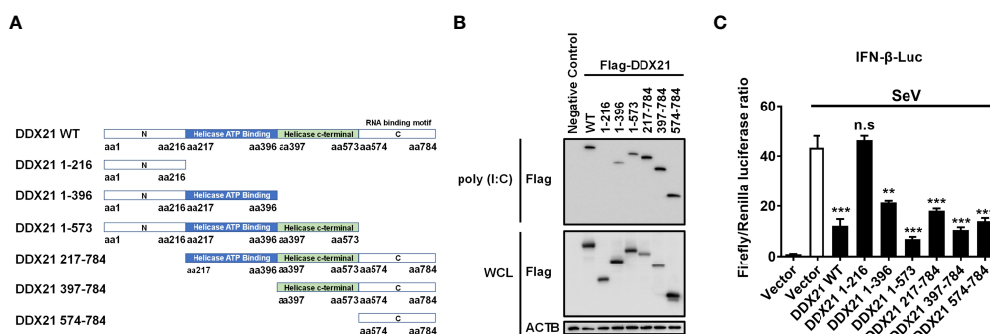


**FIGURE 7** The aa 217–784 region of DDX21 is essential for binding dsRNA to inhibit IFN-β production. **(A)** Schematic representation of DDX21 WT and the truncation mutants. **(B, C)** HEK-293T cells were co-transfected with expression plasmids encoding Flag-tagged DDX21-WT or the truncation mutants. Cells were lysed at 24 hpt, and supernatants were examined in poly (I: C) pull-down assay **(B)** or dual-luciferase reporter assay **(C)**. The experiment was repeated at least three times and the data shown are the means ± SD (n=3) of single representative experiments (\*\**P* < 0.01; \*\*\**P* < 0.001; n.s., not significant).

dsRNA, but DDX21 1–216 (aa 1–216) lacked this ability. These results suggest that aa 217–784 of DDX21 are pivotal for dsRNA binding.

To further analyze whether the inhibition of IFN-β production by DDX21 is dependent on aa 217–784, HEK-293T cells were transfected with truncation mutants of DDX21, together with IFN-β-Luc and pRL-TK reporter plasmids, followed by stimulation with SeV, and subjected to dual-luciferase reporter analysis. As shown in **Figure 7C**, SeV stimulation notably induced the activation of the IFN-β promoter, but the increased activation was significantly lower in the presence of the full-length DDX21, DDX21 1–396, DDX21 1–573, DDX21 217–784, DDX21 397–784, and

DDX21 574–784, suggesting that aa 217–784 of DDX21 are critical for suppressing SeV-induced activation of the IFN-β promoter. We conclude that DDX21 blocks IFN-β signaling by competing with RIG-I to bind dsRNA through the aa 217–784 structural domain.

### DDX21 antagonizes IFN-β independently of its ATPase, RNA helicase, and foldase activities

DDX21 belongs to the DEAD-box RNA helicase family, and lysine 236 (Lys 236) and serine 375 (Ser 375) are highly

conserved among DDX proteins and play key roles in its ATPase activity and RNA helicase activity, respectively. Mutating Lys 236 to glutamate (Glu) or Ser 375 to leucine (Leu) eliminates its ATPase activity or RNA helicase activity, respectively (33). In addition, DDX21 has an ATP-independent RNA foldase activity motif within the C-terminus, consisting of three repeating FRGQR sequences and one PRGQR sequence, and mutation of the PRGQR residues to YEGIQ has been previously shown to eliminate the foldase activity of DDX21 (17). To investigate whether DDX21 antagonization of IFN- $\beta$  depends on its enzymatic activities, we constructed three enzyme activity-deficient mutants of DDX21: DDX21-K236E (only lacking ATPase activity), DDX21-S375L (only lacking RNA helicase activity), and DDX21-M4 (only lacking RNA foldase activity) (Figure 8A). HEK-293T cells were transfected with increasing doses of expression plasmids of these mutants, respectively. Dual-luciferase reporter assays showed that overexpression of the DDX21 mutants K236E, S375L, or M4 significantly inhibited IFN- $\beta$  promoter activation in a dose-dependent manner with or without SeV stimulation, demonstrating that DDX21 inhibited IFN- $\beta$  promoter activation independently of its ATPase, RNA helicase, and RNA foldase activities (Figures 8B–G).

## Discussion

DEAD-box RNA helicases are a class of ATP-dependent RNA helicases that are widely involved in various cellular RNA metabolism processes (34). They also play a crucial role in activating/inhibiting innate immune responses. Most DDXs are positive regulators of innate immunity (19, 35–38). However, increasing evidence suggests that DDXs also function as negative regulators involved in regulating excessive immune responses to maintain immune homeostasis (9–11, 20, 39). Here, we confirmed that DDX21 negatively regulates RLR-induced IFN- $\beta$  production by knocking out DDX21 in HEK-293T cells using CRISPR/Cas9 technology. We found that DDX21 is a dsRNA/ssRNA binding protein that competes with RIG-I to bind dsRNA for inhibiting IFN- $\beta$  production. The further study identified the key functional domain of DDX21 (aa 217–784) as essential for its ability to inhibit IFN- $\beta$  production.

DDX21 has been implicated in viral RNA sensing as part of the innate immune response. However, previous reports on the effect of knockdown or overexpression of DDX21 on IFN production remain controversial. In one study, knockdown of

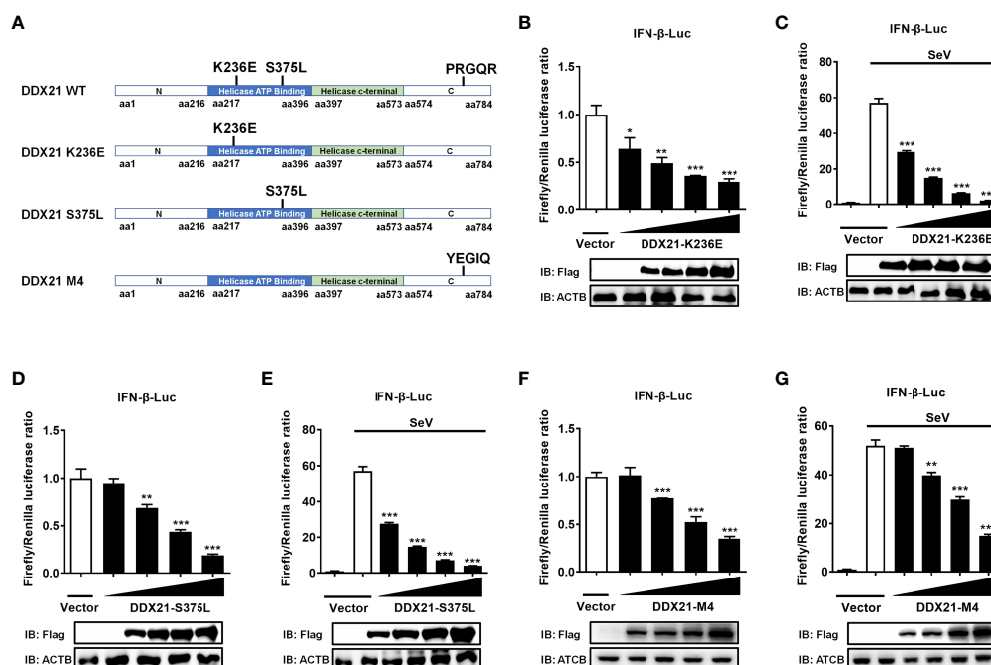


FIGURE 8

DDX21 antagonizes IFN- $\beta$  independently of ATPase, RNA helicase, and foldase activities. (A) Schematic representation of DDX21 WT and mutants (K236E, S375L, M4). (B–G) HEK-293T cells cultured in 24-well plates were transfected with increasing amounts (0.1, 0.2, 0.4, or 0.8 g) of expression plasmids encoding Flag-DDX21-K236E, Flag-DDX21-S375L, or Flag-DDX21-M4, together with IFN- $\beta$ -Luc and pRL-TK reporter plasmids for 24 h and then left untreated (B, D, F) or infected with SeV (C, E, G). At 12 hpi, cells were lysed and the cell supernatant was collected for dual-luciferase reporter assay. DDX21 expression was examined by western blot with an anti-Flag antibody.  $\beta$ -actin served as a protein loading control. The results were repeated at least three times and the data shown are the means  $\pm$  SD (n=3) of single representative experiments (\* $P$  < 0.05; \*\* $P$  < 0.01; \*\*\* $P$  < 0.001).

DDX21 in dendritic cells inhibited poly (I: C), influenza A virus, and reovirus-induced activation of IFN-I and NF- $\kappa$ B pathways (19). Overexpression of DDX21 in HEK-293T cells promoted dengue virus-induced or background level activation of the IFN- $\beta$  and ISRE promoters (21). Interestingly, a recent report showed that overexpression of DDX21 had no effect on IFN- $\beta$  production but promoted VSV replication and that knockdown of DDX21 inhibited poly (I: C) and VSV-induced IFN- $\beta$  production, as well as VSV replication (20). Notably, VSV has been reported to be an IFN-sensitive strain with a replication level that is inversely correlated with IFN expression (40, 41). In the present study, to exclude endogenous disruption, we knocked out DDX21 using CRISPR/Cas9 technology and investigated its effect on the IFN- $\beta$  production. Our work confirmed that DDX21 negatively regulates IFN- $\beta$  production; our findings using CRISPR/Cas9 technology provide more convincing results compared with previous reports using DDX21 knockdown or overexpression assays. In addition, we demonstrated that DDX21 knockout inhibited VSV-GFP replication, and IFN bioassay experiments confirmed that DDX21 knockout promoted IFN- $\beta$  expression, which is consistent with previous reports. We speculate that the reason for the controversial findings may be due to the endogenous DDX21 expression and differences among various cell lines. Thus, further confirmation is needed by constructing DDX21 knockout cell lines in other cell types.

Previous studies reported that DDX21 induced the production of IFN-I mainly through the adaptor molecule TRIF (20, 42). However, how DDX21 affects the RLR pathway to regulate IFN-I production remains unclear. Viral RNA interacts with the helicase structural domain of RIG-I, inducing their conformational changes and allowing the CARD structural domain to interact with and activate MAVS, which drives the signaling cascade by activating the cytoplasmic kinases IKK $\epsilon$  and TBK1, followed by the activation of NF- $\kappa$ B and IRF3. NF- $\kappa$ B and IRF3 act synergistically to induce IFN-I and other antiviral molecules (37, 43–45). Increasing evidence suggests that RIG-I is a target of immune regulation by various viral and host proteins. For example, murine hepatitis virus and SARS-CoV N proteins directly interact with the protein activator of protein kinase R (PACT), and the N-PACT interaction dissociates the association of PACT and RIG-I/MDA5, thereby inhibiting IFN- $\beta$  production (46). Porcine reproductive and respiratory syndrome (PRRSV) N protein competes with TRIM25 for binding to RIG-I, inhibits the expression of TRIM25 and TRIM25-mediated ubiquitination of RIG-I, and antagonizes the production of IFN- $\beta$  (47). Porcine deltacoronavirus (PDCoV) NS6 protein interacts with RIG-I/MDA5, which attenuates RIG-I/MDA5 binding to dsRNA, resulting in reduced RLR-mediated IFN- $\beta$  production (48). DDX24 specifically binds to dsRNA to inhibit RIG-I-mediated signaling and negatively regulates IFN-I production. In this study, we confirmed that DDX21 can inhibit SeV-induced activation of IRF3 and NF- $\kappa$ B and negatively regulate SeV/poly (I: C)-mediated IFN-I signaling,

Interestingly, DDX21 neither inhibited RIG-I-induced activation of the IFN- $\beta$  promoter nor affected RIG-I expression but was able to bind dsRNA. A previous study demonstrated that the RIG-I CTD domain is responsible for selectively binding dsRNA (49) and that the expression of CTD inhibits RIG-I signaling and antagonizes SeV-induced IFN production (50). It is therefore plausible that DDX21 inhibits the SeV-induced RLR signaling pathway by competing with RIG-I for binding dsRNA. Competitive binding experiments with poly (I: C) pulldown also proved our speculation (Figure 7B).

The DDXs family of RNA helicases are a class of RNA-binding proteins. Previous reports have demonstrated that DDX21 can bind small nucleolar RNA (snoRNA), ribosomal (rRNA), and specific long non-coding RNA (lncRNA) (13, 14, 51). A recent report indicated that DDX21 interacts with G4 RNA and further confirmed that its C-terminal structural domain is necessary and sufficient for binding to G4 RNA (12). Our results indicate that DDX21 is a dsRNA- and ssRNA-binding protein with an RNA-binding region located at aa 217–784. Interestingly, gray values analysis of western blot shows that the C-terminus of DDX21 is the major dsRNA binding region, which is consistent with previous findings. In addition, previous studies have shown that RIG-I, MDA5, and Toll-like receptors 3 (TLR3) are the major PRRs that recognize dsRNA in the cytoplasm (52–57), while TLR7 and TLR8 are the major PRRs that recognize ssRNA in the cytoplasm (58, 59). Therefore, it is possible that DDX21 may function as a cytoplasmic RNA sensor, competing with other cytoplasmic PRRs to bind dsRNA/ssRNA independently of the DDX1-DDX21-DHX36 complex, thereby impairing signaling and negatively regulating immune responses. However, this possibility needs to be confirmed by further studies.

DDX21 has been shown to be a multifunctional enzyme with RNA helicase activity, ATPase activity, and RNA folding enzyme activity and is involved in almost all RNA-related processes (12, 16, 60). Moreover, we found that DDX21 interrupts RIG-I signaling by binding to dsRNA. Therefore, we explored the relationship between the enzymatic activity and dsRNA binding activity of DDX21 by constructing a series of function-deficient mutants of DDX21 to determine whether their effects on the IFN are related to its enzymatic activities. Unexpectedly, our results showed that the effects of DDX21 on inhibiting IFN- $\beta$  production are independent of its ATPase, RNA unwinding, and RNA foldase activity.

In summary, we confirmed the inhibitory effect of DDX21 on dsRNA-induced IFN- $\beta$  production using a DDX21 knockout HEK-293T cell line. Our results reveal a novel mechanism by which DDX21 negatively regulates IFN- $\beta$  production by competing with RIG-I for binding to dsRNA through the aa 217–784 region. This study provides new insights into the function of the cytoplasmic dsRNA-binding protein DDX21 that negatively regulates the RLR pathway and maintains cellular homeostasis.

## Data availability statement

The original contributions presented in the study are included in the article/[Supplementary Material](#). Further inquiries can be directed to the corresponding author.

## Author contributions

LF and SX conceived the study and designed the experiments. JL performed the experiments. JL performed the analysis. JL generated HEK-293T DDX21 KO cells and contributed to data interpretation. SX and JL wrote the manuscript. PF, YZ, and DW helped analyze the data. All authors contributed to the article and approved the submitted version.

## Funding

This study was supported by grants from the National Natural Science Foundation of China (no. 32130103, 31730095).

## References

- Umate P, Tuteja N, Tuteja R. Genome-wide comprehensive analysis of human helicases. *Commun Integr Biol* (2011) 4:118–37. doi: 10.4161/cib.4.1.13844
- Singleton MR, Dillingham MS, Wigley DB. Structure and mechanism of helicases and nucleic acid translocases. *Annu Rev Biochem* (2007) 76:23–50. doi: 10.1146/annurev.biochem.76.052305.115300
- Patel SS, Donmez I. Mechanisms of helicases. *J Biol Chem* (2006) 281:18265–8. doi: 10.1074/jbc.R600008200
- Cordin O, Banroques J, Tanner NK, Linder P. The dead-box protein family of rna helicases. *Gene* (2006) 367:17–37. doi: 10.1016/j.gene.2005.10.019
- Ullah R, Li J, Fang P, Shaobo X, Fang L. Dead/H-box helicases: Anti-viral and pro-viral roles during infections. *Virus Res* (2021) 309:198658. doi: 10.1016/j.virusres.2021.198658
- Zhang Z, Yuan B, Bao M, Lu N, Kim T, Liu YJ. The helicase Ddx41 senses intracellular DNA mediated by the adaptor sting in dendritic cells. *Nat Immunol* (2011) 12:959–65. doi: 10.1038/ni.2091
- Schröder M, Baran M, Bowie AG. Viral targeting of dead box protein 3 reveals its role in Tbk1/Ikkespilon-mediated irf activation. *EMBO J* (2008) 27:2147–57. doi: 10.1038/emboj.2008.143
- Ma Z, Moore R, Xu X, Barber GN. Ddx24 negatively regulates cytosolic rna-mediated innate immune signaling. *PLoS Pathog* (2013) 9:e1003721. doi: 10.1371/journal.ppat.1003721
- Zhang K, Zhang Y, Xue J, Meng Q, Liu H, Bi C, et al. Ddx19 inhibits type I interferon production by disrupting Tbk1-Ikkes-Irf3 interactions and promoting Tbk1 and ikke degradation. *Cell Rep* (2019) 26:1258–72.e4. doi: 10.1016/j.celrep.2019.01.029
- Zheng Q, Hou J, Zhou Y, Li Z, Cao X. The rna helicase Ddx46 inhibits innate immunity by entrapping m (6)a-demethylated antiviral transcripts in the nucleus. *Nat Immunol* (2017) 18:1094–103. doi: 10.1038/ni.3830
- Li D, Fu S, Wu Z, Yang W, Ru Y, Shu H, et al. Ddx56 inhibits type I interferon by disrupting assembly of Irf3-Ipo5 to inhibit Irf3 nucleus import. *J Cell Sci* (2019) 133:jcs230409. doi: 10.1242/jcs.230409
- Mcrae E, Booy EP, Moya-Torres A, Ezzati P, McKenna SA. Human Ddx21 binds and unwinds rna guanine quadruplexes. *Nucleic Acids Res* (2017) 45:6656–68. doi: 10.1093/nar/gkx380
- Calo E, Flynn RA, Martin L, Spitale RC, Chang HY, Wysocka J. Rna helicase Ddx21 coordinates transcription and ribosomal rna processing. *Nature* (2015) 518:249–53. doi: 10.1038/nature13923
- Holmström TH, Mialon A, Kallio M, Nymalm Y, Mannermaa L, Holm T, et al. C-jun supports ribosomal rna processing and nucleolar localization of rna helicase Ddx21. *J Biol Chem* (2008) 283:7046–53. doi: 10.1074/jbc.M709613200
- Henning D, So RB, Jin R, Lau LF, Valdez BC. Silencing of rna helicase Ii/Gualpha inhibits mammalian ribosomal rna production. *J Biol Chem* (2003) 278:52307–14. doi: 10.1074/jbc.M310846200
- Flores-Rozas H, Hurwitz J. Characterization of a new rna helicase from nuclear extracts of hela cells which translocates in the 5' to 3' direction. *J Biol Chem* (1993) 268:21372–83. doi: 10.1016/S0021-9258(19)36933-9
- Valdez BC. Structural domains involved in the rna folding activity of rna helicase Ii/Gu protein. *Eur J Biochem* (2000) 267:6395–402. doi: 10.1046/j.1432-1327.2000.01727.x
- McRae EKS, Dupas SJ, Booy EP, Piragasam RS, Fahlman RP, McKenna SA. An rna guanine quadruplex regulated pathway to trail-sensitization by Ddx21. *Rna* (2020) 26:44–57. doi: 10.1261/rna.072199.119
- Zhang Z, Kim T, Bao M, Facchinetti V, Jung SY, Ghaffari AA, et al. Ddx1, Ddx21, and Dhx36 helicases form a complex with the adaptor molecule trif to sense dsrna in dendritic cells. *Immunity* (2011) 34:866–78. doi: 10.1016/j.immuni.2011.03.027
- Wu W, Qu Y, Yu S, Wang S, Yin Y, Liu Q, et al. Caspase-dependent cleavage of Ddx21 suppresses host innate immunity. *mBio* (2021) 12:e0100521. doi: 10.1128/mBio.01005-21
- Dong Y, Ye W, Yang J, Han P, Wang Y, Ye C, et al. Ddx21 translocates from nucleus to cytoplasm and stimulates the innate immune response due to dengue virus infection. *Biochem Biophys Res Commun* (2016) 473:648–53. doi: 10.1016/j.bbrc.2016.03.120
- Wang D, Fang L, Shi Y, Zhang H, Gao L, Peng G, et al. Porcine epidemic diarrhea virus 3c-like protease regulates its interferon antagonism by cleaving nemo. *J Virol* (2016) 90:2090–101. doi: 10.1128/jvi.02514-15
- Ding Z, Fang L, Jing H, Zeng S, Wang D, Liu L, et al. Porcine epidemic diarrhea virus nucleocapsid protein antagonizes beta interferon production by sequestering the interaction between Irf3 and Tbk1. *J Virol* (2014) 88:8936–45. doi: 10.1128/jvi.00700-14

## Conflict of interest

The authors declare that the research was conducted in the absence of any commercial or financial relationships that could be construed as a potential conflict of interest.

## Publisher's note

All claims expressed in this article are solely those of the authors and do not necessarily represent those of their affiliated organizations, or those of the publisher, the editors and the reviewers. Any product that may be evaluated in this article, or claim that may be made by its manufacturer, is not guaranteed or endorsed by the publisher.

## Supplementary material

The Supplementary Material for this article can be found online at: <https://www.frontiersin.org/articles/10.3389/fimmu.2022.956794/full#supplementary-material>

24. Mibayashi M, Martínez-Sobrido L, Loo YM, Cárdenas WB, Gale M Jr., García-Sastre A. Inhibition of retinoic acid-inducible gene I-mediated induction of beta interferon by the Nsl protein of influenza A virus. *J Virol* (2007) 81:514–24. doi: 10.1128/jvi.01265-06
25. Takahashi K, Horiuchi M, Fujii K, Nakamura S, Noda NN, Yoneyama M, et al. Ser386 phosphorylation of transcription factor irf-3 induces dimerization and association with Cbp/P300 without overall conformational change. *Genes Cells* (2010) 15:901–10. doi: 10.1111/j.1365-2443.2010.01427.x
26. Schoggins JW. Interferon-stimulated genes: Roles in viral pathogenesis. *Curr Opin Virol* (2014) 6:40–6. doi: 10.1016/j.coviro.2014.03.006
27. Baum A, Sachidanandam R, García-Sastre A. Preference of rig-I for short viral rna molecules in infected cells revealed by next-generation sequencing. *Proc Natl Acad Sci U.S.A.* (2010) 107:16303–8. doi: 10.1073/pnas.1005077107
28. Niemeyer D, Zillinger T, Muth D, Zieclek F, Horvath G, Suliman T, et al. Middle East respiratory syndrome coronavirus accessory protein 4a is a type I interferon antagonist. *J Virol* (2013) 87:12489–95. doi: 10.1128/jvi.01845-13
29. Cárdenas WB, Loo YM, Gale M Jr., Hartman AL, Kimberlin CR, Martínez-Sobrido L, et al. Ebola Virus Vp35 protein binds double-stranded rna and inhibits Alpha/Beta interferon production induced by rig-I signaling. *J Virol* (2006) 80:5168–78. doi: 10.1128/jvi.02199-05
30. Yoneyama M, Kikuchi M, Natsukawa T, Shinobu N, Imaizumi T, Miyagishi M, et al. The rna helicase rig-I has an essential function in double-stranded rna-induced innate antiviral responses. *Nat Immunol* (2004) 5:730–7. doi: 10.1038/ni1087
31. Daubner GM, Cléry A, Allain FH. Rrm-rna recognition: Nmr or crystallograph and new findings. *Curr Opin Struct Biol* (2013) 23:100–8. doi: 10.1016/j.sbi.2012.11.006
32. Chen Z, Li Z, Hu X, Xie F, Kuang S, Zhan B, et al. Structural basis of human helicase Ddx21 in rna binding, unwinding, and antiviral signal activation. *Adv Sci (Weinh)* (2020) 7:2000532. doi: 10.1002/advs.202000532
33. Li C, Ge LL, Li PP, Wang Y, Sun MX, Huang L, et al. The dead-box rna helicase Ddx5 acts as a positive regulator of Japanese encephalitis virus replication by binding to viral 3' utr. *Antiviral Res* (2013) 100:487–99. doi: 10.1016/j.antiviral.2013.09.002
34. Rocak S, Linder P. Dead-box proteins: The driving forces behind rna metabolism. *Nat Rev Mol Cell Biol* (2004) 5:232–41. doi: 10.1038/nrm1335
35. Liu L, Tian J, Nan H, Tian M, Li Y, Xu X, et al. Porcine reproductive and respiratory syndrome virus nucleocapsid protein interacts with Nsp9 and cellular Ddx9 to regulate viral rna synthesis. *J Virol* (2016) 90:5384–98. doi: 10.1128/jvi.03216-15
36. Lee KG, Kim SS, Kui L, Voon DC, Mauduit M, Bist P, et al. Bruton's tyrosine kinase phosphorylates Ddx41 and activates its binding of dsdna and sting to initiate type I interferon response. *Cell Rep* (2015) 10:1055–65. doi: 10.1016/j.celrep.2015.01.039
37. Seth RB, Sun L, Ea CK, Chen ZJ. Identification and characterization of MAVS, a mitochondrial antiviral signaling protein that activates NF- $\kappa$ B and IRF3. *Cell* (2005) 122:669–82. doi: 10.1016/j.cell.2005.08.012
38. Li G, Feng T, Pan W, Shi X, Dai J. Dead-box rna helicase Ddx3x inhibits dengue replication via regulating type one interferon pathway. *Biochem Biophys Res Commun* (2015) 456:327–32. doi: 10.1016/j.bbrc.2014.11.080
39. Zan J, Xu R, Tang X, Lu M, Xie S, Cai J, et al. Rna helicase Ddx5 suppresses IFN-I antiviral innate immune response by interacting with Pp2a-c $\beta$  to deactivate Irf3. *Exp Cell Res* (2020) 396:112332. doi: 10.1016/j.yexcr.2020.112332
40. Vogel SN, Fertsch D. Macrophages from endotoxin-hyporesponsive (Lpsd) C3H/HeJ mice are permissive for vesicular stomatitis virus because of reduced levels of endogenous interferon: Possible mechanism for natural resistance to virus infection. *J Virol* (1987) 61:812–8. doi: 10.1128/jvi.61.3.812-818.1987
41. Kramer MJ, Dennin R, Kramer C, Jones G, Connell E, Rolon N, et al. Cell and virus sensitivity studies with recombinant human alpha interferons. *J Interferon Res* (1983) 3:425–35. doi: 10.1089/jir.1983.3.425
42. Tsai SY, Segovia JA, Chang TH, Morris IR, Berton MT, Tessier PA, et al. Damp molecule S100a9 acts as a molecular pattern to enhance inflammation during influenza A virus infection: Role of Ddx21-Trif-Tlr4-Myd88 pathway. *PLoS Pathog* (2014) 10:e1003848. doi: 10.1371/journal.ppat.1003848
43. Loo YM, Gale M Jr. Immune signaling by rig-I-like receptors. *Immunity* (2011) 34:680–92. doi: 10.1016/j.immuni.2011.05.003
44. Kisseleva T, Bhattacharya S, Braunstein J, Schindler CW. Signaling through the Jak/Stat pathway, recent advances and future challenges. *Gene* (2002) 285:1–24. doi: 10.1016/s0378-1119(02)00398-0
45. Kawai T, Takahashi K, Sato S, Coban C, Kumar H, Kato H, et al. I $\beta$ s-1, an adaptor triggering rig-I- and Mda5-mediated type I interferon induction. *Nat Immunol* (2005) 6:981–8. doi: 10.1038/ni1243
46. Ding Z, Fang L, Yuan S, Zhao L, Wang X, Long S, et al. The nucleocapsid proteins of mouse hepatitis virus and severe acute respiratory syndrome coronavirus share the same IFN- $\beta$  antagonizing mechanism: Attenuation of pACT-mediated rig-I/Mda5 activation. *Oncotarget* (2017) 8:49655–70. doi: 10.18632/oncotarget.17912
47. Zhao K, Li LW, Jiang YF, Gao F, Zhang YJ, Zhao WY, et al. Nucleocapsid protein of porcine reproductive and respiratory syndrome virus antagonizes the antiviral activity of Trim25 by interfering with Trim25-mediated rig-I ubiquitination. *Vet Microbiol* (2019) 233:140–6. doi: 10.1016/j.vetmic.2019.05.003
48. Fang P, Fang L, Ren J, Hong Y, Liu X, Zhao Y, et al. Porcine deltacoronavirus accessory protein Ns6 antagonizes interferon beta production by interfering with the binding of rig-I/Mda5 to double-stranded rna. *J Virol* (2018) 92:e00712–18. doi: 10.1128/jvi.00712-18
49. Luo D, Ding Steve C, Vela A, Kohlway A, Lindenbach Brett D, Pyle Anna M. Structural insights into rna recognition by rig-I. *Cell* (2011) 147:409–22. doi: 10.1016/j.cell.2011.09.023
50. Saito T, Hirai R, Loo YM, Owen D, Johnson CL, Sinha SC, et al. Regulation of innate antiviral defenses through a shared repressor domain in rig-I and Lgp2. *Proc Natl Acad Sci U.S.A.* (2007) 104:582–7. doi: 10.1073/pnas.0606699104
51. Xing YH, Yao RW, Zhang Y, Guo CJ, Jiang S, Xu G, et al. Slert regulates Ddx21 rings associated with pol I transcription. *Cell* (2017) 169:664–78. doi: 10.1016/j.cell.2017.04.011
52. Sumpter RJr., Loo YM, Foy E, Li K, Yoneyama M, Fujita T, et al. Regulating intracellular antiviral defense and permissiveness to hepatitis C virus rna replication through a cellular rna helicase, rig-I. *J Virol* (2005) 79:2689–99. doi: 10.1128/jvi.79.5.2689-2699.2005
53. Foy E, Li K, Sumpter RJr., Loo YM, Johnson CL, Wang C, et al. Control of antiviral defenses through hepatitis C virus disruption of retinoic acid-inducible gene-I signaling. *Proc Natl Acad Sci U.S.A.* (2005) 102:2986–91. doi: 10.1073/pnas.0408707102
54. Kato H, Sato S, Yoneyama M, Yamamoto M, Uematsu S, Matsui K, et al. Cell type-specific involvement of rig-I in antiviral response. *Immunity* (2005) 23:19–28. doi: 10.1016/j.immuni.2005.04.010
55. Xu LG, Wang YY, Han KJ, Li LY, Zhai Z, Shu HB. VISA is an adapter protein required for virus-triggered IFN- $\beta$  signaling. *Mol Cell* (2005) 19:727–40. doi: 10.1016/j.molcel.2005.08.014
56. Matsumoto M, Funami K, Tanabe M, Oshiumi H, Shingai M, Seto Y, et al. Subcellular localization of toll-like receptor 3 in human dendritic cells. *J Immunol* (2003) 171:3154–62. doi: 10.4049/jimmunol.171.6.3154
57. Su C, Tang YD, Zheng C. Ddx/H-box helicases: Multifunctional regulators in antiviral innate immunity. *Cell Mol Life Sci* (2021) 79:2. doi: 10.1007/s00018-021-04072-6
58. Schlee M, Hornung V, Hartmann G, Sirna and isrna: Two edges of one sword. *Mol Ther* (2006) 14:463–70. doi: 10.1016/j.yth.2006.06.001
59. Heil F, Hemmi H, Hochrein H, Ampenberger F, Kirschning C, Akira S, et al. Species-specific recognition of single-stranded rna via toll-like receptor 7 and 8. *Science* (2004) 303:1526–9. doi: 10.1126/science.1093620
60. Valdez BC, Henning D, Busch RK, Woods K, Flores-Rozas H, Hurwitz J, et al. A nucleolar rna helicase recognized by autoimmunity antibodies from a patient with watermelon stomach disease. *Nucleic Acids Res* (1996) 24:1220–4. doi: 10.1093/nar/24.7.1220



## OPEN ACCESS

## EDITED BY

Junji Xing,  
Houston Methodist Research Institute,  
United States

## REVIEWED BY

Jun Zhang,  
Peking University, China  
Min Wu,  
Wuhan University, China

## \*CORRESPONDENCE

Liang-Guo Xu  
xul@jxnu.edu.cn

## SPECIALTY SECTION

This article was submitted to  
Viral Immunology,  
a section of the journal  
Frontiers in Immunology

RECEIVED 17 June 2022

ACCEPTED 25 July 2022

PUBLISHED 15 August 2022

## CITATION

Huang J-P, Li J, Xiao Y-P and  
Xu L-G (2022) BAG6 negatively  
regulates the RLR signaling  
pathway by targeting VISA/MAVS.  
*Front. Immunol.* 13:972184.  
doi: 10.3389/fimmu.2022.972184

## COPYRIGHT

© 2022 Huang, Li, Xiao and Xu. This is  
an open-access article distributed under  
the terms of the [Creative Commons  
Attribution License \(CC BY\)](https://creativecommons.org/licenses/by/4.0/). The use,  
distribution or reproduction in other  
forums is permitted, provided the  
original author(s) and the copyright  
owner(s) are credited and that the  
original publication in this journal is  
cited, in accordance with accepted  
academic practice. No use,  
distribution or reproduction is  
permitted which does not comply with  
these terms.

# BAG6 negatively regulates the RLR signaling pathway by targeting VISA/MAVS

Jing-Ping Huang, Jing Li, Yan-Ping Xiao and Liang-Guo Xu\*

College of Life Science, Jiangxi Normal University, Nanchang, China

The virus-induced signaling adaptor protein VISA (also known as MAVS, ISP-1, Cardif) is a critical adaptor protein in the innate immune response to RNA virus infection. Upon viral infection, VISA self-aggregates to form a sizeable prion-like complex and recruits downstream signal components for signal transduction. Here, we discover that BAG6 (BCL2-associated athanogene 6, formerly BAT3 or Scythe) is an essential negative regulator in the RIG-I-like receptor signaling pathway. BAG6 inhibits the aggregation of VISA by promoting the K48-linked ubiquitination and specifically attenuates the recruitment of TRAF2 by VISA to inhibit RLR signaling. The aggregation of VISA and the interaction of VISA and TRAF2 are enhanced in BAG6-deficient cell lines after viral infection, resulting in the enhanced transcription level of downstream antiviral genes. Our research shows that BAG6 is a critical regulating factor in RIG-I/VISA-mediated innate immune response by targeting VISA.

## KEYWORDS

VISA/MAVS, BAG6, TRAF2, interferon, innate immunity

## Introduction

The immune system is composed of innate and adaptive immunity. Innate immune is the first line of defense, which resists the invasion of microbial pathogens. Pathogen-associated molecular patterns (PAMPs) are recognized by pattern recognition receptors (PRRs) to initiate signal cascades resulting in the activation of antiviral genes such as type I interferon and proinflammatory cytokines for clearance of invading pathogens (1, 2).

The PRRs include Toll-like receptors (TLRs), RIG-I-like receptors (RLRs), DNA sensors and NOD-like receptors (3, 4). RLRs include RIG-I, MDA5, and LGP2, sensing cytoplasmic RNA viruses (3). Both RIG-I and MDA5 contain a C-terminal domain that

recognizes RNA ligand, two N-terminal caspase activation and recruitment domains, which are used to transfer signals, and a central DExD/H RNA helicase domain for RNA binding and facilitating ATP hydrolysis (5, 6). RIG-I and MDA5 have a common adaptor protein VISA (also termed MAVS, IPS-1, and Cardif) (7–10) located at mitochondria. Upon RNA virus infection, the RLRs mediated antiviral signaling is activated, VISA aggregates, and forms a large prion-like polymer, which recruits downstream molecules TRAFs, TBK1, IKK complex, and cIAP1/2 for signaling (11), resulting in the activation of IRF3 and NF- $\kappa$ B to initiate the transcription of antiviral genes.

Previous studies have shown that RIG-I, K63-Ub4, and SNX8 induce VISA aggregation and activate VISA signaling function (11, 12). TRIM31 promotes the aggregation of VISA by K63-linked ubiquitination (13). RNF125, RNF153, AIP4, A20, SMURF2, and MARCH5 are negative regulators that inhibit VISA signaling by K48-ubiquitinating and promoting proteasome degradation of VISA except for A20 (14–18). Besides, PINK1 inhibits the aggregation and signaling of VISA (19). Whether other molecules negatively regulate VISA aggregation is unclear after viral infection.

BAG6 (BCL2-associated athanogene 6, also known as BAT3 or Scythe) is a nucleocytoplasmic shuttling protein involved in protein quality control (20, 21), identified as a ligand for NKp30 involved in antitumor immunity of NK cells (22, 23). Moreover, BAG6 forms a complex with p300 and promotes subsequent p53 acetylation, which is essential in controlling the p53 acetylation required for DNA damage responses (24, 25). In addition, BAG6 promotes the PINK1 signaling pathway and is essential for mitophagy (26). However, whether BAG6 is involved in the innate immune response is unclear. This paper discovered that BAG6 is a negative regulator in the innate immune by targeting VISA. BAG6 interacts with VISA and inhibits VISA aggregation, reducing TRAF2 recruitment. Besides, BAG6 negatively regulates RNA virus-mediated innate immune *via* promoting K48 poly-ubiquitination of VISA/TRAF2. BAG6 knockout studies suggest that BAG6 deficiency enhances the innate immune response to RNA viruses. Upon Sendai virus infection, downstream antiviral genes' transcription level is significantly enhanced in BAG6-deficient mouse primary BMDMs cells.

## Materials and methods

### Antibodies and reagents

Anti-Flag (Sigma, F3165-0.2 MG), anti-Myc (Santa Cruz, sc-40), anti-HA (Sigma, H3663), anti-IRF3 (Santa Cruz, sc-33641; CST #4302S), anti-p-IRF3 (CST #29047, S396), anti-TBK1 (CST #3504S), anti-p-TBK1 (CST #5483S, S172), anti-P65 (CST #8242P, #12629P), anti-p-P65 (CST #3033P, S536), anti-VISA

(Santa Cruz, sc-166583, sc-68881; Proteintech, 14341-1-AP), anti-TRAF2 (Santa Cruz, sc-136999), anti-Ub (Santa Cruz, sc-8017), anti-BAG6 (Santa Cruz, sc-365928; Proteintech, 26417-1-AP), anti-actin (Santa Cruz, sc-1616), anti-mouse IgG, HRP-linked (CST #7076), Alexa Fluor 555-labeled Donkey anti-Rabbit/Mouse IgG (H+L) (Beyotime Biotechnology, cat: A0453/A0460), DAPI (Solarbio, cat: C0065), Mito-Tracker Red CMXRos (Beyotime, cat: C1035). Sendai virus, VSV and VSV-GFP were donated by Dr. Hong-Bing Shu (Medical Research Institute, Wuhan University, Wuhan, China).

### Cell culture

HEK 293, HeLa, A549, NIH3T3, Vero (provided by Dr. Hong-Bing Shu, Wuhan University, China), and mouse primary BMDMs cells were cultivated in DMEM, containing 10% (vol/vol) Fetal Bovine Serum with 1% penicillin-streptomycin, with 5% CO<sub>2</sub> at 37°C. All these cells were tested for no mycoplasma contamination.

### Transfection and dual-luciferase reporter assay

HEK 293 cells were cultured in a 100 mm dish, 6 or 24-wells plates, and the indicated plasmids were transferred into the cells with calcium phosphate. Sendai viruses were used to infect cells for the indicated time after 12 h, cells were harvested for analysis after virus infection, and the reporter gene experiments were performed as previously described (27, 28).

### Immunoprecipitation, native PAGE, and western blot

These experiments were performed as previously described (27, 29).

### Semi-denaturing detergent agarose gel electrophoresis (SDD-AGE)

Cells were harvested by native lysate buffer. Then, the lysates were diluted with 2 × sample buffer (1 × TBE, 20% glycerol, 4% SDS, and 0.005% bromophenol blue) and loaded with a vertical 1% agarose gel (SDD-AGE, 0.5 × TBE, 1% SDS and 1% agarose). Electrophoresis in running buffer (0.5 × TBE, 0.1% SDS) for 60 min with a constant voltage of 100 V at 4°C, the proteins were transferred to PVDF membranes with transfer buffer (0.5 × TBE) and a constant current of 0.3 A at 4°C for Western blot analysis.



## Mice and preparation of BMDMs

Wild-type mice (C57BL/6J) were purchased from Hunan Silaikejingda Experimental Animal Co., Ltd. The method of separating bone marrow cells as previously described (30). All mouse experiments were permitted by the Animal Care Committee of Jiangxi Normal University College of Life Sciences.

## Quantitative RT-PCR

The total RNA was extracted by RNA extraction Kit from Promega, then reverse transcription was performed with 1  $\mu$ g of total RNA by Eastep RT Master Mix Kit from Promega. The primers for qPCR were as follows:

*$\beta$ -actin* forward: GTCGTCGACAACGGCTCCGGCATG  
 *$\beta$ -actin* reverse: ATTGTAGAAGGTGTGGTGCCAGAT  
*IFN- $\beta$*  forward: CTAACGTCAACCTTTTCGAAGC  
*IFN- $\beta$*  reverse: GGAAAGAGCTGTAGTGGAGAAG  
*ISG56* forward: TCATCAGGTCAAGGATAGTC  
*ISG56* reverse: CCACACTGTATTTGGTGCTAGG  
*CXCL10* forward: TGACTCTAAGTGGCATTCAAGG  
*CXCL10* reverse: GATTGAGACATCTCTTCTCACCC  
*mGapdh* forward: TTCACCACCATGGAGAAGGC  
*mGapdh* reverse: GGCATCGACTGTGGTCATGA  
*mIfn- $\beta$*  forward: CTGCGTTCCTGCTGTGCTTCTCCA  
*mIfn- $\beta$*  reverse: TTCTCCGTCATCTCCATAGGGATC  
*mIsig56* forward: ACAGCAACCATGGGAGAGAATGCTG  
*mIsig56* reverse: ACGTAGGCCAGGAGGTTGTGCAT  
*mCxcl10* forward: CCAAGTGCTGCCGTCATTTTC  
*mCxcl10* reverse: TCCCTAAGGCCCTCATTCTCA

## Plasmids

Mammalian expression plasmids, including VISA, RIG-I, RIG-I-N (1-284aa), TBK1, IKK $\epsilon$ , TRAF2, TRAF5, IRF3-5D, IFN- $\beta$  promoter, ISRE luciferase, ubiquitin, and its mutants K48, K63 were described previously (27, 31). pRK5-Flag/HA/MyC-hBAG6 plasmids were constructed using the following primers:

hBAG6-F-SalI (Forward): AAAAGTCGACCATGGAGCC  
 TAATGATAGTACCAG;  
 hBAG6-R-NotI (Reverse): AAAAGCGGCCGCCTAAGG  
 ATCATCAGCAAAGG.

## CRISPR-Cas9 knockout.

The double-stranded oligonucleotides of human or mouse BAG6 were cloned into a lenti-CRISPR-V2 vector and transfected into HEK 293 cells with psPAX2 and pMD2G. The supernatants were harvested after 48 h and centrifuged at 3000 rpm for 15 min. The viruses were used to infect HEK 293, HeLa, NIH3T3, or BMDMs cells. The infected cells were screened with puromycin (1  $\mu$ g/mL) for 7 days to obtain BAG6 deficiency monoclonal cells, except for mouse primary BMDMs. BMDMs were infected with the above viruses for 48 h and subsequently replaced with a fresh medium for viral infection.

hBAG6 gRNA: 5'-CTGTCAGGCTCCTCCACAG3'  
 5'-GCAAGATGATAAGAAGCTTC-3';  
 mBAG6 gRNA: 5'-GCGGTACTGGCATTACTACT-3'  
 5'-GCCTGACAGCCTGGAGGTAC-3'.

## Plaque assays, VSV-GFP fluorescence imaging experiment, and viral infection

For plaque assays and VSV-GFP fluorescence imaging experiment, HEK 293-BAG6, HeLa-BAG6 wild, and knockout cells were infected with SeV, VSV or VSV-GFP (MOI = 0.1). After 1 h, the viruses were removed, pre-warmed PBS was used to wash the cell for twice, and cells were cultured in a fresh medium. The supernatants were harvested for the VSV-GFP fluorescence imaging experiment, and Vero cells were observed and imaged directly by fluorescence microscopy. For plaque assays, the supernatants were used to infect Vero cells for 48 h. The following steps and viral infection were performed as previously described (32).

## Fluorescent confocal microscopy

A549, HeLa cells were incubated with Mito-Tracker Red CMXRos (Beyotime, C1035) following protocols provided by the manufacturer. A549, HeLa cells were fixed with pre-warmed 4% paraformaldehyde for 15 min, permeabilized with 0.1% Triton X-100 (in PBS) for 10 min, and blocked with 1% BSA (in PBS) for 30 min. Then, cells were stained with anti-mouse VISA (Santa Cruz sc-166583, 1/250) and anti-BAG6 antibody (rabbit polyclonal, Proteintech, 26417-1-AP, 1/200) at RT for 60 min. Alexa Fluor 488-labeled Goat Anti-Mouse (green) (Beyotime Biotechnology, A0428) and Alexa Fluor 555-labeled Donkey Anti-Rabbit (red) (Beyotime Biotechnology, A0453) (diluted in 1% BSA) was added for 60 min to detect VISA and BAG6. Nuclei were stained with 10  $\mu$ g/mL DAPI at RT for 15 min. Finally,

images were acquired with a Leica DMI8 confocal microscopy under a  $\times 40$  objective and analyzed with Leica LAS X software.

## Result

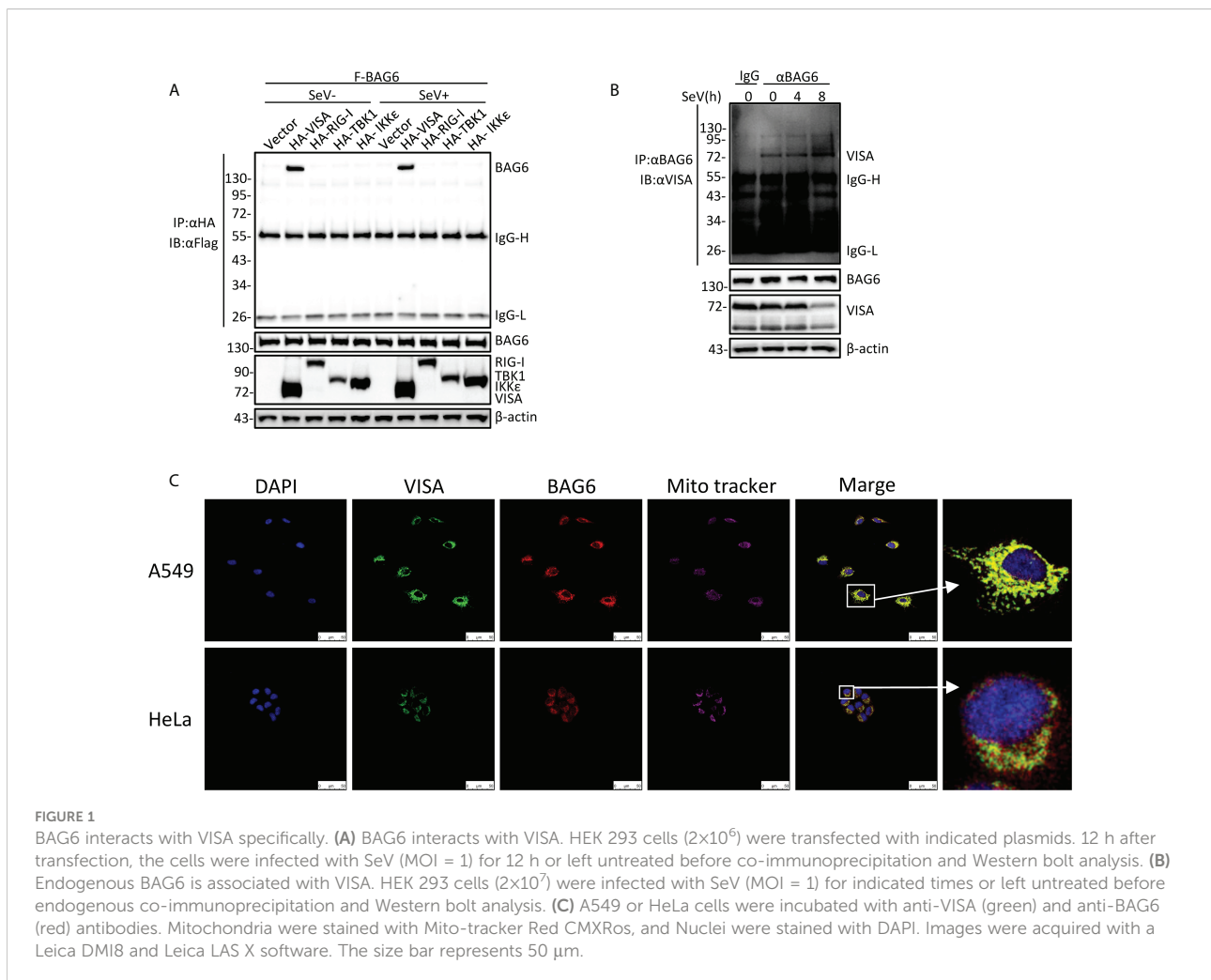
### BAG6 interacts with VISA specifically

To further investigate the regulatory mechanism of VISA in the RLRs-mediated antiviral signaling pathway, the yeast-two hybrid screening was performed by using VISA as the bait to screen the 293 cell cDNA expression library, trying to discover the novel partner of VISA. Multiple VISA-interacting candidate genes, including BAG6, were obtained. A further co-immunoprecipitation assay was performed in 293 cells, and the results showed that BAG6 interacts specifically with VISA (Figure 1A). The endogenous co-immunoprecipitation assay in HEK 293 cells consistently showed that the interaction between BAG6 and VISA was enhanced upon Sendai virus (SeV) infection (Figure 1B). Further immunofluorescence

experiments in A549 and HeLa cells showed that BAG6 was co-localized with VISA on the outer membrane of mitochondria (Figure 1C), suggesting that BAG6 interacts with VISA specifically and may play a role in VISA-mediated antiviral signaling pathways.

### BAG6 negatively regulates RLR-mediated antiviral response

To further investigate the role of BAG6 in RNA virus-triggered innate immunity, reporter assays were performed, and the results showed that overexpression of BAG6 in HEK 293 cells inhibited SeV-induced the activation of IFN- $\beta$  promoter, ISRE, and NF- $\kappa$ B in a dose-dependent manner (Figure 2A). The results of qPCR experiments indicated that overexpression of BAG6 in HEK 293 cells reduced the transcription level of *IFN $\beta$* , *ISG56*, and *CXCL10* induced by RNA virus (Figure 2B). Furthermore, overexpression of BAG6 in HEK 293 cells weakened the dimerization of IRF3 significantly



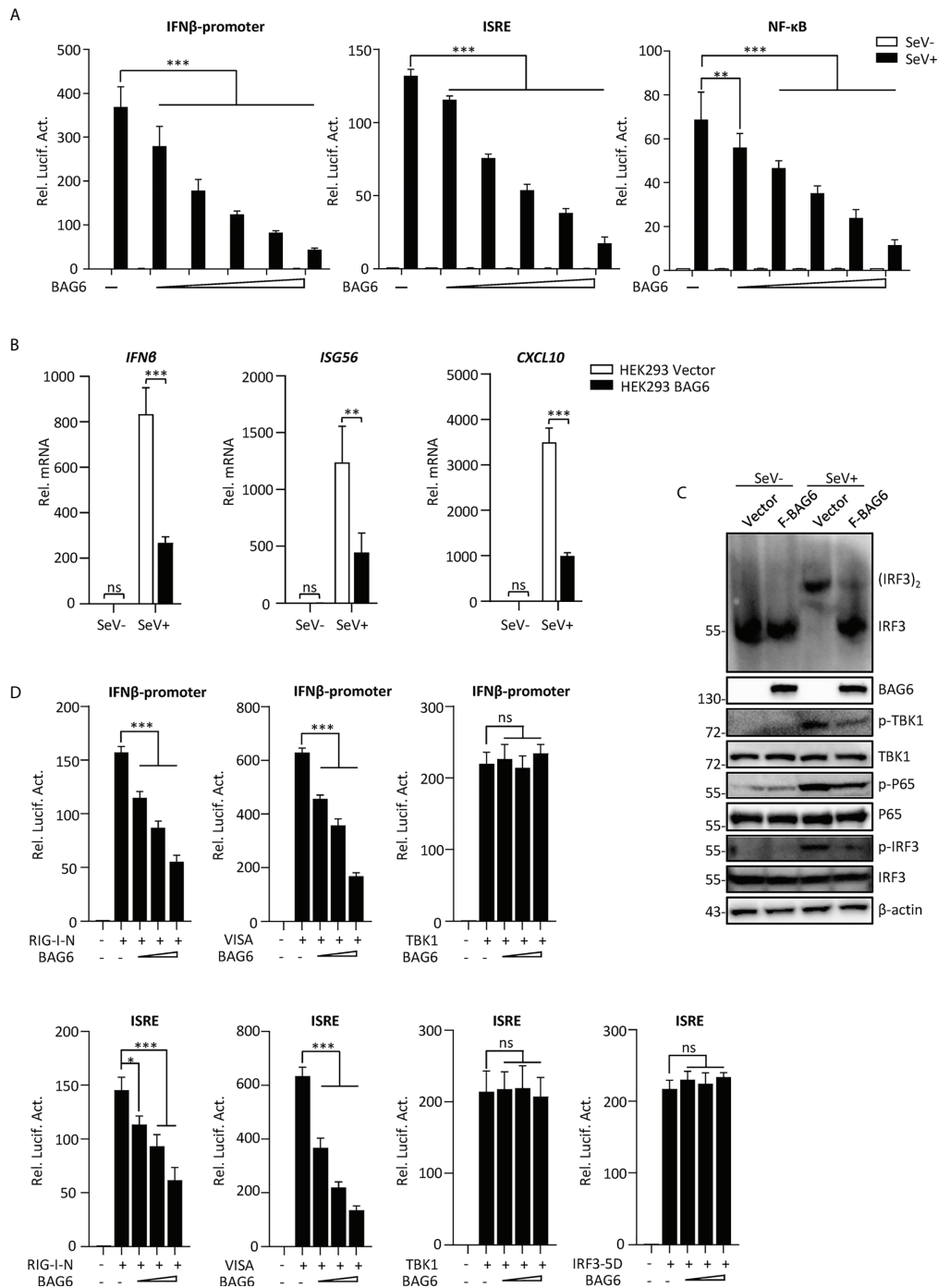


FIGURE 2

Identification of BAG6 as a negative regulator of RIG-I-mediated signaling. (A) BAG6 inhibits the IFN- $\beta$  promoter, ISRE, and NF- $\kappa$ B in a dose-dependent manner. HEK 293 cells ( $1 \times 10^5$ ) were transfected with IFN- $\beta$  promoter (0.025  $\mu$ g), ISRE (0.025  $\mu$ g) and NF- $\kappa$ B (0.05  $\mu$ g) reporter plasmids and BAG6 plasmids (0, 0.05, 0.1, 0.2, 0.4, 0.8  $\mu$ g). Twelve hours after transfection, cells were infected with SeV (MOI = 1) for 12 h or untreated before luciferase analysis. (B) Overexpression of BAG6 reduces the transcription of downstream antiviral genes. HEK 293 cells were transfected with control or BAG6 plasmid for 24 h. The cells were infected with SeV (MOI = 1) for 12 h or left untreated, followed by qPCR analysis. (C) Overexpression of BAG6 inhibits RNA virus-induced dimerization of IRF3 and phosphorylation of TBK1, P65, and IRF3. HEK 293 cells ( $2 \times 10^5$ ) were transfected with control and BAG6 plasmid for 24 h, and cells were left uninfected or infected with SeV (MOI = 1) for 12 h, followed by immunoblotting analysis. (D) BAG6 inhibits RNA virus-triggered innate immunity by targeting VISA. HEK 293 cells ( $3 \times 10^5$ ) were transfected with IFN- $\beta$  promoter (0.025  $\mu$ g), ISRE (0.025  $\mu$ g), BAG6 plasmids (0, 0.1, 0.2, 0.4  $\mu$ g) and RIG-I-N, VISA, TBK1 or IRF3-5D (0.5  $\mu$ g) for twenty h before luciferase analysis. (\* $p < 0.05$ ; \*\* $p < 0.01$ ; \*\*\* $p < 0.001$ ; ns, no significant difference).

and inhibited the phosphorylation of TBK1, P65, and IRF3 induced by SeV (Figure 2C). We then investigated BAG6's molecular target responsible for its role in innate antiviral signaling. Reporter assay results demonstrated that BAG6 inhibited RIG-I-N and VISA-mediated activation of the IFN- $\beta$  promoter and ISRE, but not the downstream TBK1 and IRF3-5D (Figure 2D), suggesting that BAG6 negatively regulated RNA virus-triggered innate immune cells by targeting VISA.

## The deficiency of BAG6 enhances SeV-mediated antiviral immune responses in human cell lines

To investigate the effect of endogenous BAG6 on antiviral innate immune signaling, we generated BAG6-deficient monoclonal HeLa and HEK 293 cell lines by using the CRISPR Cas9-mediated gene knockout method. As shown in Figures 3A, B, we successfully knocked out the expression of BAG6 in HeLa and HEK 293 cells, and the qPCR analysis indicated the transcription level of *IFN $\beta$* , *ISG56*, and *CXCL10* induced by SeV infection were significantly increased in BAG6-deficient HeLa and HEK 293 cells. Plaque assay showed that BAG6-deficiency in HeLa and HEK 293 cells inhibited the replication of SeV and VSV (Figures 3C, D). Furthermore, we found that the replication of GFP-tagged VSV was inhibited in BAG6-deficient HeLa cells compared with its wild-type cells (Figure 3E). The knockout of BAG6 in HeLa and HEK 293 cells dramatically promoted the IRF3 dimerization and the phosphorylation of TBK1, P65, and IRF3 after SeV infection (Figures 3F, G). However, the reconstitution of BAG6 in BAG6-deficient HeLa cells could turn its transcription of *IFN $\beta$* , *ISG56*, and *CXCL10* genes induced by SeV back to a level similar to those in wild-type cells (Figure 3H). The reconstitution of BAG6 in BAG6-deficient HeLa cells could also turn the replication of GFP-tagged VSV back to a level similar to those in wild-type cells (Figure 3I). Further experiments found that the reconstitution of BAG6 in BAG6-deficient HeLa turned its potentiated phosphorylation of TBK1, P65, and IRF3 induced by SeV infection back to a level similar to those in wild-type cells (Figure 3J). These data suggest that BAG6 is a negative regulator of RNA virus-triggered signaling.

## The deficiency of BAG6 enhances SeV-mediated antiviral immune responses in primary mouse cells

To further confirm the function of BAG6 in RLR-mediated signaling, we generated BAG6-deficient mixed primary mouse BMDMs cells by CRISPR Cas9-mediated gene knockout technology to assess the role of BAG6 in SeV-triggered signaling in primary mouse cells. We first verified that BAG6

was successfully knocked out in mouse NIH3T3 using the CRISPR-Cas9 method. Then, we performed a transient transfection using the CRISPR-Cas9 system to produce the BAG6-deficient primary mouse BMDMs cells. As shown in Figures 4A, B, the qPCR analysis showed that the SeV-induced transcription of *Ifn $\beta$* , *Isg56*, and *Cxcl10* was significantly increased in BAG6-deficient NIH3T3 cells and primary mouse BMDMs. The knockout of BAG6 in NIH3T3 cells and mouse primary BMDMs cells dramatically promoted the phosphorylation of TBK1, P65, and IRF3 after SeV infection (Figures 4C, D). Furthermore, plaque assay showed that BAG6-deficient inhibited the replication of SeV in mouse primary BMDMs cells (Figure 4E). These experimental data suggest that BAG6 negatively regulates the RLR-mediated signaling in primary immune cells.

## BAG6 regulates the aggregation and recruitment of downstream signaling molecules of VISA

The aggregation of VISA is essential for its activation. Upon virus infection, VISA translocates to the outer membrane of mitochondria from cytoplasm and aggregates to form a giant prion-like aggregation complex which provides a platform for recruitment of downstream signaling molecules (11). We speculate whether BAG6 has an impact on the aggregation of VISA. The semi-denaturing detergent agarose gel electrophoresis (SDD-AGE) analysis indicated that overexpression of BAG6 extremely inhibited the aggregation of VISA in HEK 293 cells (Figure 5A), whereas BAG6-deficiency increased the SeV-triggered aggregation of VISA in NIH3T3 and primary mouse BMDMs cells (Figures 5B, C). These results indicate that BAG6 reduces antiviral response by inhibiting the aggregation of VISA. The activated VISA recruits downstream signaling molecules TRAFs, TBK1 and IKK complex. The results of the overexpression experiment in HEK 293 cells indicated that BAG6 inhibited the association of VISA with TRAF2 but not other TRAFs (Figures 5D–G). Endogenous co-immunoprecipitation results confirmed that the association between VISA and TRAF2 was hindered upon SeV infection (Figure 5H). Furthermore, BAG6-deficient significantly strengthened the association of VISA with TRAF2 in HeLa cells (Figure 5I). These results suggest that BAG6 inhibits innate immune signaling by attenuating the recruitment of TRAF2 to VISA.

## BAG6 potentiates the K48-linked ubiquitination of VISA/TRAF2

It has been reported that the polyubiquitination of VISA is essential for its activation (33, 34). To further investigate

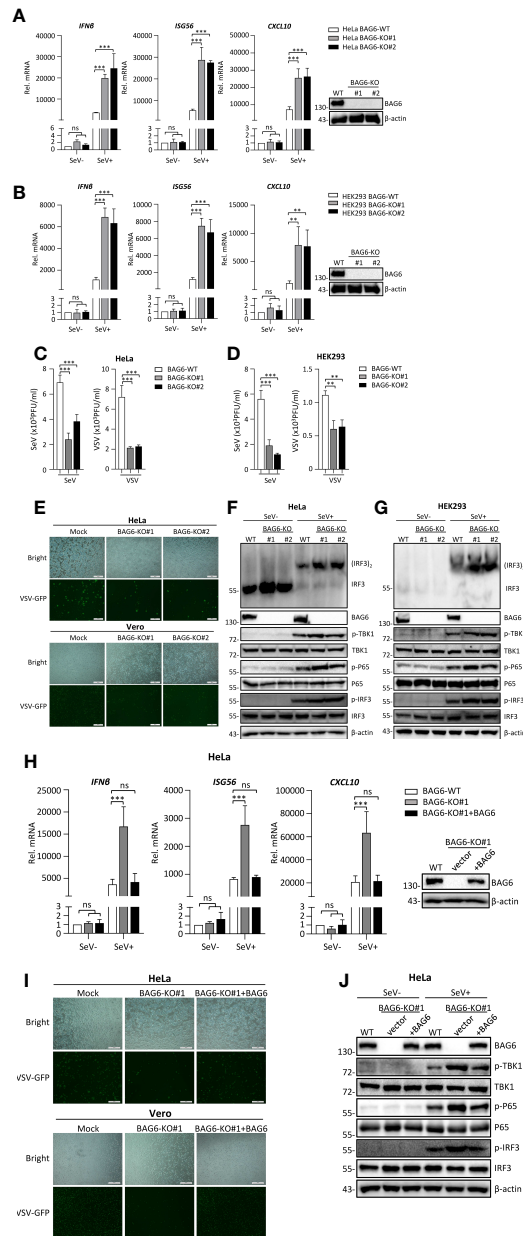


**FIGURE 3**

BAG6-deficiency significantly increases the transcription and activation of antiviral genes in HeLa and HEK 293 cells. **(A)** BAG6-deficiency enhances the transcription of downstream antiviral genes in HeLa cells. BAG6-deficient HeLa cells were left uninfected or infected with SeV (MOI = 1) for 8 h before qPCR analysis. **(B)** BAG6-deficiency enhances the transcription of downstream antiviral genes in HEK 293 cells. BAG6-deficient HEK 293 cells were left uninfected or infected with SeV (MOI = 1) for 8 h before qPCR analysis. **(C)** BAG6-deficiency inhibits the replication of SeV and VSV in HeLa cells. BAG6-deficiency HeLa cells were infected with SeV or VSV (MOI = 0.1) for twenty hours. The supernatants were collected for plaque assays to determine the viral titer. **(D)** BAG6-deficiency inhibits the replication of SeV and VSV in HEK 293 cells. BAG6-deficiency HEK 293 cells were infected with SeV or VSV (MOI = 0.1) for twenty hours. The supernatants were collected for plaque assays to determine the viral titer. **(E)** Effects of BAG6 deficiency on VSV-GFP replication. BAG6-deficient HeLa and control cells were infected with VSV-GFP (MOI = 0.1). The cells were viewed with Fluorescence Microscope after 16 h, and the supernatants were collected to infect Vero cells to determine the VSV-GFP replication. **(F, G)** BAG6 deficiency enhances RNA virus-induced dimerization of IRF3 and phosphorylation of TBK1, P65, and IRF3. BAG6-deficient HeLa and HEK 293 cells were uninfected or infected with SeV (MOI = 1) for 8 h before immunoblotting. **(H)** Reconstitution of BAG6 in BAG6-deficient HeLa cells suppresses virus-mediated innate immune responses. HeLa-BAG6-KO cells were transfected with control or BAG6 plasmids for 36 h. Cells then were left uninfected or infected with SeV (MOI = 1) for 8 h before qPCR analysis. **(I)** Reconstitution of BAG6 in BAG6-deficient HeLa cells enhances the replication of the virus. Similar to **(E)**, HeLa-BAG6-KO cells were transfected with control or BAG6 plasmids for 36 h, and cells then were infected with VSV-GFP (MOI = 0.1). **(J)** The experimental treatment was the same as **(H)** before immunoblotting. (\*\* $p < 0.01$ , \*\*\* $p < 0.001$ ; ns, no significant difference). The size bar represents 500  $\mu\text{m}$ .

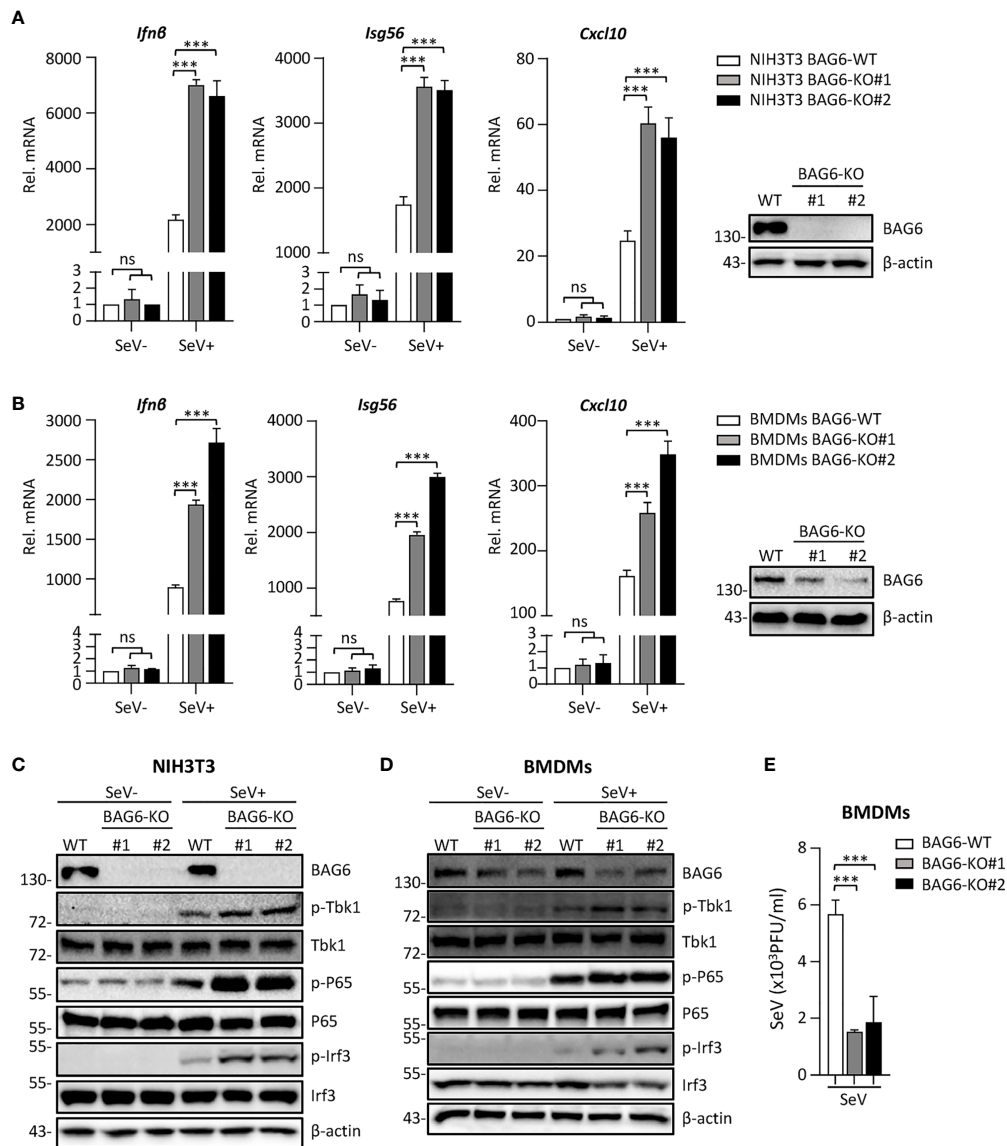


**FIGURE 4** BAG6-deficiency significantly increases the RLR signaling in primary immune cells. **(A)** BAG6-deficiency enhances the transcription of downstream antiviral genes in NIH3T3 cells. BAG6-deficient NIH3T3 cells were left uninfected or infected with SeV (MOI = 1) for 8 h before qPCR analysis. **(B)** BAG6-deficiency enhances the transcription of downstream antiviral genes in mouse BMDMs. Mouse wild-type BMDMs ( $4 \times 10^6$ ) were infected with lentivirus containing BAG6-CRISPR CAS9 sgRNA, the supernatants were replaced with fresh medium after 48 h, and the cells were infected with SeV (MOI = 1) for 8 h before qPCR analysis. **(C, D)** BAG6-deficiency enhances RNA virus-induced phosphorylation of TBK1, P65, and IRF3. BAG6-deficient NIH3T3 and BMDMs were untreated or treated with SeV for 8 h before immunoblotting. **(E)** Effects of BAG6-deficiency on virus replication. BAG6-deficient and wild-type BMDMs cells were infected with SeV (MOI = 0.1) for twenty hours. The supernatants were collected for plaque assays. (\*\* $p < 0.001$ ; ns, no significant difference).

whether BAG6 affects the ubiquitination of VISA and TRAF2, co-immunoprecipitation experiments were performed, and the results showed that the overexpression of BAG6 in HEK 293 cells enhanced K48 but not K63-linked ubiquitination of VISA (Figure 6A), and the opposite results were obtained using the endogenous co-immunoprecipitation experiments in HEK 293-BAG6-deficient cells (Figure 6B). Further experiments showed

that overexpression of BAG6 in HEK 293 cells enhanced K48-linked ubiquitination and inhibited K63-linked ubiquitination of TRAF2, ultimately leading to an increase in total ubiquitination (Figure 6C), and the consistent results were obtained using the endogenous co-immunoprecipitation experiments (Figure 6D). These data indicate that BAG6 may promote the K48-linked ubiquitination of VISA and TRAF2, reducing VISA aggregation

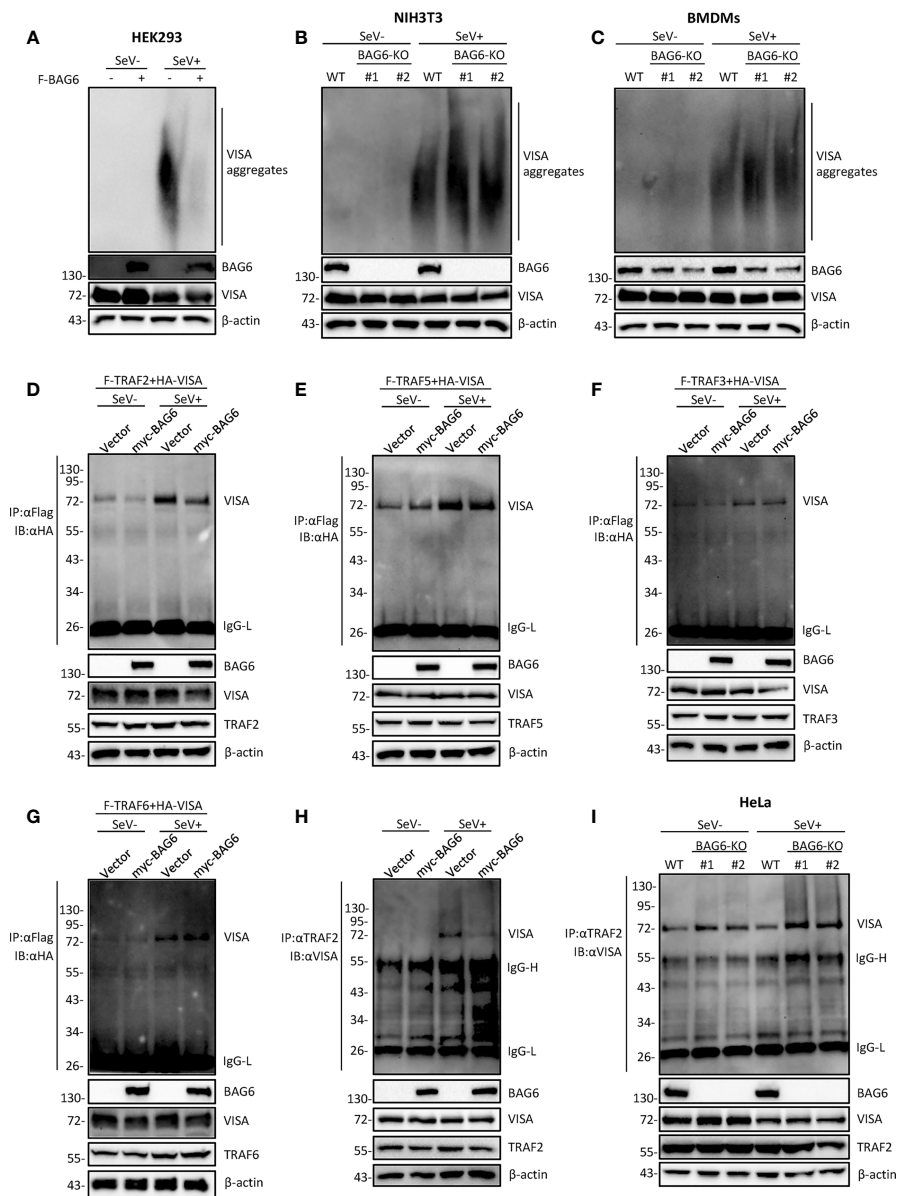
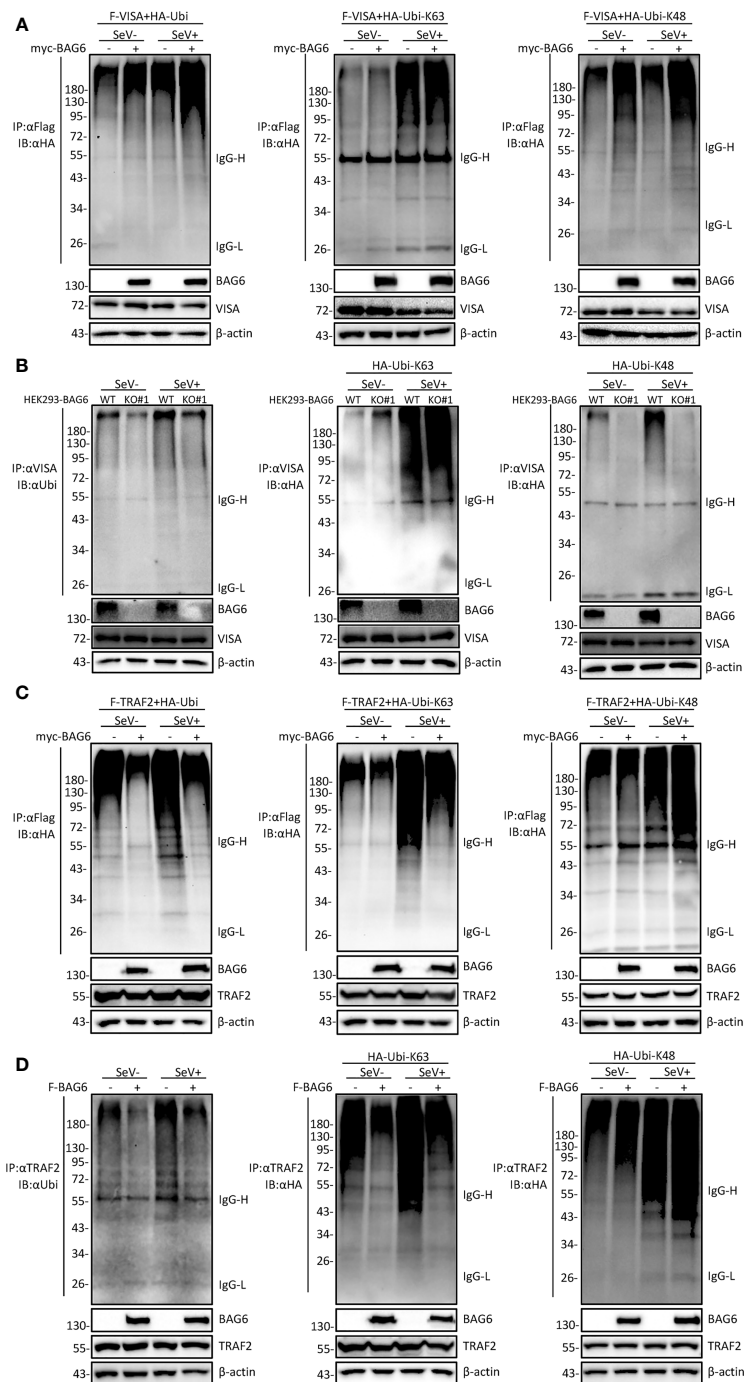


FIGURE 5

BAG6 regulates the aggregation and recruitment of downstream signaling molecules of VISA. (A) Overexpression of BAG6 inhibits SeV-induced aggregation of VISA. HEK 293 cells ( $2 \times 10^5$ ) were transfected with vector or Flag-BAG6 for 20 h, and cells were infected with SeV (MOI = 1) for 8 h before harvest. Then, the lysates were fractionated by SDD-AGE and SDS-PAGE before immunoblotting analysis. (B) BAG6-deficiency increases SeV-induced aggregation of VISA in NIH3T3 cells. Wild type and BAG6-deficient NIH3T3 cells were untreated or treated with SeV (MOI = 1) for 8 h before harvest. Then, the lysates were fractionated by SDD-AGE and SDS-PAGE before immunoblotting analysis. (C) BAG6-deficiency increases SeV-induced aggregation of VISA in BMDMs. Wild-type BMDMs were infected with lentivirus containing BAG6-CRISPR Cas9 sgRNA for 48 h before viral infection. Wild type and BAG6-deficient BMDMs cells were untreated or treated with SeV (MOI = 1) for 8 h before harvest. Then, the lysates were fractionated by SDD-AGE and SDS-PAGE before immunoblotting analysis. (D–G) BAG6 inhibits the interaction of VISA and TRAF2 specifically. HEK 293 cells ( $2 \times 10^5$ ) were transfected with the indicated plasmids for 22 h, and cells were untreated or treated with SeV (MOI = 1) for 10 h following co-immunoprecipitation and Western blotting analysis. (H) Overexpression of BAG6 impairs the endogenous interaction of VISA and TRAF2. HEK 293 cells ( $4 \times 10^6$ ) were transfected with the indicated plasmids for 22 h, and cells were untreated or treated with SeV (MOI = 1) for 10 h following co-immunoprecipitation and Western blotting analysis. (I) BAG6-deficiency increases the endogenous interaction of VISA and TRAF2. Wild type and BAG6-deficient HeLa cells ( $1 \times 10^7$ ) were untreated or treated with SeV (MOI = 1) for 10 h before co-immunoprecipitation and Western blotting analysis.



**FIGURE 6**  
 BAG6 promotes the K48-linked ubiquitination of VISA/TRAF2. **(A)** Overexpression of BAG6 increases the K48-linked polyubiquitin of VISA. HEK 293 cells ( $4 \times 10^6$ ) were transfected with Flag-VISA, HA-ubiquitin (WT, K63R, or K48R), and Myc-BAG6 plasmids for 22 h, and cells were untreated or treated with SeV (MOI = 1) for 10 h before co-immunoprecipitation and Western blotting analysis. **(B)** BAG6-deficiency inhibits the K48-linked polyubiquitin of VISA. HEK 293 wild type and BAG6-deficient cells ( $4 \times 10^6$ ) were transfected with HA-ubiquitin (K63R or K48R) for 22 h, and cells were untreated or treated with SeV (MOI = 1) for 10 h before co-immunoprecipitation and Western blotting analysis. **(C)** Overexpression of BAG6 increases the K48-linked polyubiquitin and impairs the K63-linked polyubiquitin of TRAF2. HEK 293 cells ( $4 \times 10^6$ ) were transfected with Flag-TRAF2, HA-ubiquitin (WT, K63R, or K48R), and Myc-BAG6 plasmids for 22 h. Cells were untreated or treated with SeV (MOI = 1) for 10 h before co-immunoprecipitation and Western blotting analysis. **(D)** Overexpression of BAG6 increases the K48-linked polyubiquitin and impairs the K63-linked polyubiquitin of endogenous TRAF2. HEK 293 cells ( $4 \times 10^6$ ) were transfected with HA-ubiquitin (WT, K63R, or K48R) and Flag-BAG6 plasmids for 22 h, and cells were untreated or treated with SeV (MOI = 1) for 10 h before co-immunoprecipitation and Western blotting analysis.



and further reducing the recruitment of TRAF2 to regulate RLR-mediated antiviral signal transduction negatively.

## Discussion

The RLRs (RIG-I-like receptors) in the cytoplasm, including RIG-I and MDA5, recognize viral RNA. This viral RNA binding leads to a conformational change of the RLRs, triggering their oligomerization and activation. The activated oligomerization of RLRs provides a template of the oligomer to initiate the assembly of adaptor protein VISA on the outer membrane of mitochondria, leading to VISA's activation. Once VISA is aggregated and activated, the downstream signaling molecules, including the kinase IKKs, and TBK1, are recruited to the aggregation platform, leading to the activation of IRF3/IRF7 and NF- $\kappa$ B to turn on the production of interferons and proinflammatory cytokines. A few E3 ubiquitin ligases, including TRAF2, TRAF3, TRAF5, and TRAF6, are recruited by VISA through their specific binding motif. The K63 and K48-linked polyubiquitination modification in these signaling cascades are essential for VISA downstream signaling (35). Our study demonstrates the critical role of BAG6 in the innate immune response by promoting the K48-linked ubiquitination of VISA, resulting in a weakened aggregation of VISA.

BAG6 is a ubiquitin-like protein shuttling between nuclear and cytoplasm involved in apoptosis, T-cell response, and antigen presentation (20). It interacts with HSC70 protein and recognizes the misfolded protein, allowing their proteasomal degradation (20). BAG6 is critical for regulating autophagy by modulating EP300/p300 intracellular location (36). It was reported that BAG6 associates with mitofusin1 and 2, localizing on mitochondria, and has a physiological function in mitochondrial fission (37).

Previously, we identified several regulatory proteins (including TARBP2 (31), RACK1 (38), HSPBP1 (39), SNX5 (40), DUT (41) and N4BP3 (42)) involved in the RIG-I/VISA signaling pathway. Recently, our experiments suggest that BAG6 is crucial in negatively regulating RLRs-VISA-mediated antiviral signaling. Overexpression of BAG6 hampered SeV-triggered activation of IFN- $\beta$  promoter, ISRE, and NF- $\kappa$ B. BAG6-deficiency greatly enhanced the transcription of *IFN $\beta$* , *ISG56*, and *CXCL10* induced by SeV infection. Further experimental results showed that overexpression of BAG6 inhibited SeV-induced phosphorylation of TBK1, P65, and IRF3. In contrast, the opposite results were obtained in BAG6-deficiency cells (HEK 293, HeLa, NIH3T3, and primary mouse BMDMs).

Our experimental results also showed that overexpression of BAG6 inhibited RIG-I-N and VISA-mediated, but not TBK1 or IRF3-5D-mediated activation of IFN- $\beta$  promoter and ISRE,

indicating that BAG6 inhibits RLRs-VISA-mediated signaling by targeting VISA. Consistently, BAG6 interacted with VISA specifically, and the interaction between BAG6 and VISA was enhanced upon SeV infection.

Virus infection-induced VISA aggregation is critical for downstream antiviral signaling activation (11, 13). Our experimental results demonstrated that BAG6 inhibited the aggregation of VISA induced by SeV infection. The further co-immunoprecipitation experiment showed that recruitment of TRAF2 to VISA is hindered. Previous studies have shown that the aggregation of VISA could be robustly induced *in vitro* by incubating mitochondria with RIG-I and K63 ubiquitin chains (11, 13), which suggests that K63 ubiquitination of VISA is important for its activation. The analysis of the results of ubiquitination experiments indicated that BAG6 enhanced K48-linked ubiquitination of VISA but had no effect on K63-linked ubiquitination. It has been confirmed that PINK1 inhibits aggregation and signaling of VISA (19), and BAG6 promotes the PINK1 signaling pathway (26). Perhaps BAG6 and PINK1 have a synergistic effect on inhibiting the aggregation of VISA. BAG6 facilitated the K48-linked ubiquitination of VISA may lead to inhibition of signal transduction by a failure of VISA to aggregate normally after virus infection. However, BAG6 is not an E3 ubiquitin ligase; according to current reports, E3 ubiquitin ligases-mediated (RNF5, RNF125, MARCH5, TRIM25, AIP4) K48-linked ubiquitination initiates proteasomal degradation of VISA (43, 44). Moreover, it's reported that TRIM29 induced ubiquitination of Lys371, Lys420 and Lys500 sites on VISA and degradation of VISA through K11-linked polyubiquitination (45). TRIM29 was also found to promote K48 ubiquitination and degradation of NEMO to suppress the innate immune response (46). These evidences suggest that TRIM29 is an important E3 ligase in the negative regulation of VISA-mediated signaling pathways. BAG6 correlates well with E3 ubiquitin ligases RNF126 and FBXO7-SCF. Whether BAG6 is involved in regulating the ubiquitination of VISA through them or the reported E3 ubiquitin ligases remains to be investigated. Besides, BAG6 inhibited K63-linked and promoted K48-linked ubiquitination of TRAF2. Previous studies have shown that phosphorylation and K63-linked ubiquitination of TRAF2 is important for signaling (47–50).

TRAFs, critical proteins involved in VISA-mediated signaling, are essential for RNA virus-induced IRF3 activation and IFN $\beta$  production. The current studies have shown that VISA-mediated innate immune activation is dependent on TRAFs and partially on NEMO, but not on TBK1 binding proteins (51). When TRAF2/3/5/6 were compounded *via* CRISPR Cas9 knockout, cells absolutely lost the RNA virus response, suggesting that TRAFs are essential in VISA-mediated signal transduction (51, 52). When a single TRAF was knockout, type I interferon levels in TRAF2<sup>-/-</sup> and TRAF6<sup>-/-</sup> cells were decreased substantially, while type I interferon levels in TRAF3<sup>-/-</sup> and TRAF5<sup>-/-</sup> cells remained normally induced

(51). TRAF2, TRAF3, TRAF5, and TRAF6 were reconstituted in cells with TRAF2/3/5/6 compound knockout, respectively, and cells with reintroduced TRAF6 had the strongest type I interferon production, while TRAF5 had the lowest activity, these results suggest that TRAF6 is essential, while TRAF5 is dispensable (51). Another study showed that IRF3 phosphorylation was extensively lost when TRAF2 and TRAF5 were double knockout, and IRF3 phosphorylation could be induced normally when TRAF2 or TRAF5 were knockout alone (52). Furthermore, after reconstitution of TRAF2 or TRAF5 in TRAF2 and TRAF5 double knockout cells, TRAF2 reintroduction led to a basic restoration of IRF3 phosphorylation levels. In contrast, TRAF5-induced IRF3 phosphorylation level was low, suggesting that TRAF2 is a lot greater essential than TRAF5 in the signaling process and that TRAF5 may play a partly regulatory role in VISA-mediated signaling but is not required (52). Our experimental results show that BAG6 hinders the signal transduction of VISA and downstream TRAF2 but not TRAF5 by interacting with VISA, which is consistent with the above findings.

In conclusion, our results indicate that BAG6 suppresses RNA virus-mediated innate immunity by promoting K48-linked ubiquitination of VISA/TRAF2 and inhibiting VISA aggregation, further inhibiting the recruitment of downstream components reduced the transcript levels of downstream antiviral genes.

## Data availability statement

The original contributions presented in the study are included in the article/supplementary material. Further inquiries can be directed to the corresponding author.

## Ethics statement

The animal study was reviewed and approved by the Animal Care Committee of Jiangxi Normal University College of Life Sciences.

## References

1. Takeuchi O, Akira S. Pattern recognition receptors and inflammation. *Cell* (2010) 140(6):805–20. doi: 10.1016/j.cell.2010.01.022
2. Kumar H, Kawai T, Akira S. Pathogen recognition by the innate immune system. *Int Rev Immunol* (2011) 30(1):16–34. doi: 10.3109/08830185.2010.529976
3. Kawai T, Akira S. Toll-like receptor and RIG-I-like receptor signaling. *Ann N Y Acad Sci* (2008) 1143:1–20. doi: 10.1196/annals.1443.020
4. Kawai T, Akira S. The roles of TLRs, RLRs and NLRs in pathogen recognition. *Int Immunol* (2009) 21(4):317–37. doi: 10.1093/intimm/dxp017
5. Yoneyama M, Kikuchi M, Natsukawa T, Shinobu N, Imaizumi T, Miyagishi M, et al. The RNA helicase RIG-I has an essential function in double-stranded

## Author contributions

J-PH: Investigation, formal analysis, writing-original draft. JL: Validation, formal analysis. Y-PX: Validation. L-GX: Supervision, writing-original draft, writing-review and editing, funding acquisition, conceptualization, methodology. All authors read, and approved the submitted version. All authors contributed to the article and approved the submitted version.

## Funding

This work was supported by the National Natural Science Foundation of China (Grant Nos. 81971502, 82060298).

## Acknowledgments

We sincerely thank Dr. Hong-Bing Shu (Medical Research Institute, Wuhan University) for providing plasmids and other reagents. We thank Jiangxi Normal University, College of Chemistry and Chemical Engineering for help with the Laser Confocal Microscope analysis.

## Conflict of interest

The authors declare that the research was conducted in the absence of any commercial or financial relationships that could be construed as a potential conflict of interest.

## Publisher's note

All claims expressed in this article are solely those of the authors and do not necessarily represent those of their affiliated organizations, or those of the publisher, the editors and the reviewers. Any product that may be evaluated in this article, or claim that may be made by its manufacturer, is not guaranteed or endorsed by the publisher.

RNA-induced innate antiviral responses. *Nat Immunol* (2004) 5(7):730–7. doi: 10.1038/ni1087

6. Kato H, Takeuchi O, Sato S, Yoneyama M, Yamamoto M, Matsui K, et al. Differential roles of MDA5 and RIG-I helicases in the recognition of RNA viruses. *Nature* (2006) 441(7089):101–5. doi: 10.1038/nature04734

7. Kawai T, Takahashi K, Sato S, Coban C, Kumar H, Kato H, et al. IPS-1, an adaptor triggering RIG-I- and Mda5-mediated type I interferon induction. *Nat Immunol* (2005) 6(10):981–8. doi: 10.1038/ni1243

8. Meylan E, Curran J, Hofmann K, Moradpour D, Binder M, Bartschlag R, et al. Cardif is an adaptor protein in the RIG-I antiviral pathway and is

- targeted by hepatitis c virus. *Nature* (2005) 437(7062):1167–72. doi: 10.1038/nature04193
9. Seth RB, Sun LJ, Ea CK, Chen ZJ. Identification and characterization of MAVS, a mitochondrial antiviral signaling protein that activates NF- $\kappa$ B and IRF3. *Cell* (2005) 122(5):669–82. doi: 10.1016/j.cell.2005.08.012
  10. Xu LG, Wang YY, Han KJ, Li LY, Zhai ZH, Shu HB. VISA is an adapter protein required for virus-triggered IFN- $\beta$  signaling. *Mol Cell* (2005) 19(6):727–40. doi: 10.1016/j.molcel.2005.08.014
  11. Hou F, Sun L, Zheng H, Skaug B, Jiang QX, Chen ZJ. MAVS forms functional prion-like aggregates to activate and propagate antiviral innate immune response. *Cell* (2011) 146(3):448–61. doi: 10.1016/j.cell.2011.06.041
  12. Guo W, Wei J, Zhong X, Zang R, Lian H, Hu MM, et al. SNX8 modulates the innate immune response to RNA viruses by regulating the aggregation of VISA. *Cell Mol Immunol* (2020) 17(11):1126–35. doi: 10.1038/s41423-019-0285-2
  13. Liu B, Zhang M, Chu H, Zhang H, Wu H, Song G, et al. The ubiquitin E3 ligase TRIM31 promotes aggregation and activation of the signaling adaptor MAVS through Lys63-linked polyubiquitination. *Nat Immunol* (2017) 18(2):214–24. doi: 10.1038/ni.3641
  14. Lin R, Yang L, Nakhaei P, Sun Q, Sharif-Askari E, Julkunen I, et al. Negative regulation of the retinoic acid-inducible gene 1-induced antiviral state by the ubiquitinating protein A20. *J Biol Chem* (2006) 281(4):2095–103. doi: 10.1074/jbc.M510326200
  15. Arimoto K-i, Takahashi H, Hishiki T, Konishi H, Fujita T, Shimotohno K. Negative regulation of the RIG-I signaling by the ubiquitin ligase RNF125. *Proc Natl Acad Sci USA* (2007) 104:7500–5. doi: 10.1073/pnas.0611551104
  16. You F, Sun H, Zhou X, Sun W, Liang S, Zhai Z, et al. PCBP2 mediates degradation of the adaptor MAVS via the HECT ubiquitin ligase AIP4. *Nat Immunol* (2009) 10(12):1300–8. doi: 10.1038/ni.1815
  17. Pan Y, Li R, Meng JL, Mao HT, Zhang Y, Zhang J. Smurf2 negatively modulates RIG-I-dependent antiviral response by targeting VISA/MAVS for ubiquitination and degradation. *J Immunol* (2014) 192(10):4758–64. doi: 10.4049/jimmunol.1302632
  18. Yoo YS, Park YY, Kim JH, Cho H, Kim SH, Lee HS, et al. The mitochondrial ubiquitin ligase MARCH5 resolves MAVS aggregates during antiviral signalling. *Nat Commun* (2015) 6:7910. doi: 10.1038/ncomms8910
  19. Kim SH, Shin HJ, Yoon CM, Lee SW, Sharma L, Dela Cruz CS, et al. PINK1 inhibits multimeric aggregation and signaling of MAVS and MAVS-dependent lung pathology. *Am J Respir Cell Mol Biol* (2021) 64(5):592–603. doi: 10.1165/rmb.2020-0490OC
  20. Kawahara H, Minami R, Yokota N. BAG6/BAT3: emerging roles in quality control for nascent polypeptides. *J Biochem* (2013) 153(2):147–60. doi: 10.1093/jb/mvs149
  21. Lee JG, Ye Y. Bag6/Bat3/Scythe: a novel chaperone activity with diverse regulatory functions in protein biogenesis and degradation. *Bioessays* (2013) 35(4):377–85. doi: 10.1002/bies.201200159
  22. Reiners KS, Topolar D, Henke A, Simhadri VR, Kessler J, Sauer M, et al. Soluble ligands for NK cell receptors promote evasion of chronic lymphocytic leukemia cells from NK cell anti-tumor activity. *Blood* (2013) 121(18):3658–65. doi: 10.1182/blood-2013-01-476606
  23. Dassler-Plenker J, Reiners KS, van den Boorn JG, Hansen HP, Putschli B, Barnert S, et al. RIG-I activation induces the release of extracellular vesicles with antitumor activity. *Oncotarget* (2016) 5(10):e1219827. doi: 10.1080/2162402X.2016.1219827
  24. Sasaki T, Gan EC, Wakeham A, Kornbluth S, Mak TW, Okada H. HLA-b-associated transcript 3 (Bat3)/Scythe is essential for p300-mediated acetylation of p53. *Genes Dev* (2007) 21(7):848–61. doi: 10.1101/gad.1534107
  25. Sebti S, Prebois C, Perez-Gracia E, Bauvy C, Desmots F, Pirot N, et al. BAT3 modulates p300-dependent acetylation of p53 and autophagy-related protein 7 (ATG7) during autophagy. *Proc Natl Acad Sci USA* (2014) 111(11):4115–20. doi: 10.1073/pnas.1313618111
  26. Ragimbeau R, El Kebriti L, Sebti S, Fourgous E, Boulahtouf A, Arena G, et al. BAG6 promotes PINK1 signaling pathway and is essential for mitophagy. *FASEB J* (2021) 35(2):e21361. doi: 10.1096/fj.20200930R
  27. He TS, Chen T, Wang DD, Xu LG. HAU88 regulates RLRVISA antiviral signaling positively by targeting VISA. *Mol Med Rep* (2018) 18(2):2458–66. doi: 10.3892/mmr.2018.9171
  28. He TS, Huang J, Chen T, Zhang Z, Cai K, Yu J, et al. The kinase MAP4K1 inhibits cytosolic rna-induced antiviral signaling by promoting proteasomal degradation of TBK1/IKKepsilon. *Microbiol Spectr* (2021) 9(3):e0145821. doi: 10.1128/Spectrum.01458-21
  29. Chen T, Wang D, Xie T, Xu LG. Sec13 is a positive regulator of VISA-mediated antiviral signaling. *Virus Genes* (2018) 54(4):514–26. doi: 10.1007/s11262-018-1581-0
  30. Zhou Q, Lin H, Wang S, Wang S, Ran Y, Liu Y, et al. The ER-associated protein ZDHHC1 is a positive regulator of DNA virus-triggered, MITA/STING-dependent innate immune signaling. *Cell Host Microbe* (2014) 16(4):450–61. doi: 10.1016/j.chom.2014.09.006
  31. Ling T, Li SN, Weng GX, Wang W, Li C, Cao L, et al. TARBP2 negatively regulates IFN- $\beta$  production and innate antiviral response by targeting MAVS. *Mol Immunol* (2018) 104:1–10. doi: 10.1016/j.molimm.2018.10.017
  32. Zhang M, Zhang MX, Zhang Q, Zhu GF, Yuan L, Zhang DE, et al. USP18 recruits USP20 to promote innate antiviral response through deubiquitinating STING/MITA. *Cell Res* (2016) 26(12):1302–19. doi: 10.1038/cr.2016.125
  33. Zeng W, Sun L, Jiang X, Chen X, Hou F, Adhikari A, et al. Reconstitution of the RIG-I pathway reveals a signaling role of unanchored polyubiquitin chains in innate immunity. *Cell* (2010) 141(2):315–30. doi: 10.1016/j.cell.2010.03.029
  34. Quicke KM, Diamond MS, Suthar MS. Negative regulators of the RIG-I-like receptor signaling pathway. *Eur J Immunol* (2017) 47(4):615–28. doi: 10.1002/eji.201646484
  35. Liu S, Cai X, Wu J, Cong Q, Chen X, Li T, et al. Phosphorylation of innate immune adaptor proteins MAVS, STING, and TRIF induces IRF3 activation. *Science* (2015) 347(6227):aaa2630. doi: 10.1126/science.aaa2630
  36. Sebti S, Prebois C, Perez-Gracia E, Bauvy C, Desmots F, Pirot N, et al. BAG6/BAT3 modulates autophagy by affecting EP300/p300 intracellular localization. *Autophagy* (2014) 10(7):1341–2. doi: 10.4161/aut.28979
  37. Saita S, Ishihara T, Maeda M, Iemura S, Natsume T, Mihara K, et al. Distinct types of protease systems are involved in homeostasis regulation of mitochondrial morphology via balanced fusion and fission. *Genes Cells* (2016) 21(5):408–24. doi: 10.1111/gtc.12351
  38. Xie T, Chen T, Li C, Wang W, Cao L, Rao H, et al. RACK1 attenuates RLR antiviral signaling by targeting VISA-TRAF complexes. *Biochem Biophys Res Commun* (2019) 508(3):667–74. doi: 10.1016/j.bbrc.2018.11.203
  39. Yang YX, Huang JP, Li SN, Li J, Ling T, Xie T, et al. HSPBP1 facilitates cellular RLR-mediated antiviral response by inhibiting the K48-linked ubiquitination of RIG-I. *Mol Immunol* (2021) 134:62–71. doi: 10.1016/j.molimm.2021.03.002
  40. Li J, Chen T, Xie T, Yang YX, He TS, Xu LG. SNX5 inhibits RLR-mediated antiviral signaling by targeting RIG-I-VISA signalosome. *Biochem Biophys Res Commun* (2020) 522(4):889–96. doi: 10.1016/j.bbrc.2019.11.121
  41. Weng GX, Ling T, Hou W, Li SN, Chen T, Zhang Z, et al. Mitochondrial DUT-m potentiates RLR-mediated antiviral signaling by enhancing VISA and TRAF2 association. *Mol Immunol* (2021) 132:117–25. doi: 10.1016/j.molimm.2021.01.023
  42. Wang C, Ling T, Zhong N, Xu LG. N4BP3 regulates rig-i-like receptor antiviral signaling positively by targeting mitochondrial antiviral signaling protein. *Front Microbiol* (2021) 12:770600. doi: 10.3389/fmicb.2021.770600
  43. Ren Z, Ding T, Zuo Z, Xu Z, Deng J, Wei Z. Regulation of MAVS expression and signaling function in the antiviral innate immune response. *Front Immunol* (2020) 11:1030. doi: 10.3389/fimmu.2020.01030
  44. Chen Y, Shi Y, Wu J, Qi N. MAVS: A two-sided card mediating antiviral innate immune signaling and regulating immune homeostasis. *Front Microbiol* (2021) 12:744348. doi: 10.3389/fmicb.2021.744348
  45. Xing J, Zhang A, Minze LJ, Li XC, Zhang Z. TRIM29 negatively regulates the type i ifn production in response to rna virus. *J Immunol* (2018) 201(1):183–92. doi: 10.4049/jimmunol.1701569
  46. Xing J, Weng L, Yuan B, Wang Z, Jia L, Jin R, et al. Identification of a role for TRIM29 in the control of innate immunity in the respiratory tract. *Nat Immunol* (2016) 17(12):1373–80. doi: 10.1038/ni.3580
  47. Shi CS, Kehrl JH. Tumor necrosis factor (TNF)-induced germinal center kinase-related (GCKR) and stress-activated protein kinase (SAPK) activation depends upon the E2/E3 complex Ubc13-Uev1A/TNF receptor-associated factor 2 (TRAF2). *J Biol Chem* (2003) 278(17):15429–34. doi: 10.1074/jbc.M211796200
  48. Habelhah H, Takahashi S, Cho SG, Kadoya T, Watanabe T, Ronai Z. Ubiquitination and translocation of TRAF2 is required for activation of JNK but not of p38 or NF- $\kappa$ B. *EMBO J* (2004) 23(2):322–32. doi: 10.1038/sj.emboj.7600044
  49. Wu CJ, Conze DB, Li X, Ying SX, Hanover JA, Ashwell JD. TNF- $\alpha$  induced c-IAP1/TRAF2 complex translocation to a Ubc6-containing compartment and TRAF2 ubiquitination. *EMBO J* (2005) 24(10):1886–98. doi: 10.1038/sj.emboj.7600649
  50. Li S, Wang L, Dorf ME. PKC phosphorylation of TRAF2 mediates IKK $\alpha$ /IKK $\beta$  recruitment and K63-linked polyubiquitination. *Mol Cell* (2009) 33(1):30–42. doi: 10.1016/j.molcel.2008.11.023
  51. Fang R, Jiang Q, Zhou X, Wang C, Guan Y, Tao J, et al. MAVS activates TBK1 and IKKepsilon through TRAFs in NEMO dependent and independent manner. *PLoS Pathog* (2017) 13(11):e1006720. doi: 10.1371/journal.ppat.1006720
  52. Liu S, Chen J, Cai X, Wu J, Chen X, Wu YT, et al. MAVS recruits multiple ubiquitin E3 ligases to activate antiviral signaling cascades. *Elife* (2013) 2:e00785. doi: 10.7554/eLife.00785



## OPEN ACCESS

## EDITED BY

Junji Xing,  
Houston Methodist Research Institute,  
United States

## REVIEWED BY

Yaling Dou,  
Texas A&M Health Science Center,  
United States  
Natalie A Borg,  
Monash University, Australia

## \*CORRESPONDENCE

Takayuki Komatsu  
koma@aicchi-med-u.ac.jp

## SPECIALTY SECTION

This article was submitted to  
Viral Immunology,  
a section of the journal  
Frontiers in Immunology

RECEIVED 16 June 2022

ACCEPTED 21 July 2022

PUBLISHED 15 August 2022

## CITATION

Tanaka Y, Morita N, Kitagawa Y,  
Gotoh B and Komatsu T (2022)  
Human metapneumovirus M2-2  
protein inhibits RIG-I signaling by  
preventing TRIM25-mediated  
RIG-I ubiquitination.  
*Front. Immunol.* 13:970750.  
doi: 10.3389/fimmu.2022.970750

## COPYRIGHT

© 2022 Tanaka, Morita, Kitagawa, Gotoh  
and Komatsu. This is an open-access  
article distributed under the terms of  
the [Creative Commons Attribution  
License \(CC BY\)](#). The use, distribution  
or reproduction in other forums is  
permitted, provided the original  
author(s) and the copyright owner(s)  
are credited and that the original  
publication in this journal is cited, in  
accordance with accepted academic  
practice. No use, distribution or  
reproduction is permitted which does  
not comply with these terms.

# Human metapneumovirus M2-2 protein inhibits RIG-I signaling by preventing TRIM25-mediated RIG-I ubiquitination

Yukie Tanaka<sup>1</sup>, Naoko Morita<sup>2</sup>, Yoshinori Kitagawa<sup>3</sup>,  
Bin Gotoh<sup>3</sup> and Takayuki Komatsu<sup>2\*</sup>

<sup>1</sup>Department of Integrative Vascular Biology, Faculty of Medical Sciences, University of Fukui, Fukui, Japan, <sup>2</sup>Department of Microbiology and Immunology, Aichi Medical University School of Medicine, Aichi, Japan, <sup>3</sup>Division of Microbiology and Infectious Diseases, Department of Pathology, Shiga University of Medical Science, Shiga, Japan

Retinoic acid-inducible gene I (RIG-I) is a receptor that senses viral RNA and interacts with mitochondrial antiviral signaling (MAVS) protein, leading to the production of type I interferons and inflammatory cytokines to establish an antiviral state. This signaling axis is initiated by the K63-linked RIG-I ubiquitination, mediated by E3 ubiquitin ligases such as TRIM25. However, many viruses, including several members of the family *Paramyxoviridae* and human respiratory syncytial virus (HRSV), a member of the family *Pneumoviridae*, escape the immune system by targeting RIG-I/TRIM25 signaling. In this study, we screened human metapneumovirus (HMPV) open reading frames (ORFs) for their ability to block RIG-I signaling reconstituted in HEK293T cells by transfection with TRIM25 and RIG-I CARD (an N-terminal CARD domain that is constitutively active in RIG-I signaling). HMPV M2-2 was the most potent inhibitor of RIG-I/TRIM25-mediated interferon (IFN)- $\beta$  activation. M2-2 silencing induced the activation of transcription factors (IRF and NF- $\kappa$ B) downstream of RIG-I signaling in A549 cells. Moreover, M2-2 inhibited RIG-I ubiquitination and CARD-dependent interactions with MAVS. Immunoprecipitation revealed that M2-2 forms a stable complex with RIG-I CARD/TRIM25 *via* direct interaction with the SPRY domain of TRIM25. Similarly, HRSV NS1 also formed a stable complex with RIG-I CARD/TRIM25 and inhibited RIG-I ubiquitination. Notably, the inhibitory actions of HMPV M2-2 and HRSV NS1 are similar to those of V proteins of several members of the *Paramyxoviridae* family. In this study, we have identified a novel mechanism of immune escape by HMPV, similar to that of *Pneumoviridae* and *Paramyxoviridae* family members.

## KEYWORDS

M2-2 protein, rig-i, trim25, mavs, interferon, human metapneumovirus, human respiratory syncytial virus, paramyxoviridae

## Introduction

Human metapneumovirus (HMPV) is a leading cause of upper and lower respiratory tract infections in humans, particularly in infants, young children, the elderly, and immunocompromised individuals. HMPV belongs to the family *Pneumoviridae* in the order *Mononegavirales* and was first isolated in 2001 from children with respiratory ailments (1). This virus is the second most detected human respiratory pathogen after human respiratory syncytial virus (HRSV)—a member of the same family—and is responsible for a significant percentage of bronchiolitis-related hospitalizations in infants and young children (2–4). Additionally, HMPV induces poor innate immune responses, thereby affecting adaptive immunity and interferon (IFN) production (5). However, despite the similarities between HMPV and several other viruses, such as HRSV and parainfluenza viruses—members of the family *Paramyxoviridae*, in the same order—the mechanisms by which HMPV evades the host immune system remain largely unclear.

Upon detecting viral RNA in the cytoplasm, retinoic acid-inducible gene I (RIG-I)-like receptors (RLRs), including RIG-I and melanoma differentiation-associated gene 5 (MDA5), establish an antiviral state by triggering signaling cascades that induce the expression of type I IFNs and inflammatory cytokines (6–9). Members of the families *Paramyxoviridae* and *Pneumoviridae* harbor a 5'-triphosphate moiety, which is a non-self-RNA signature specific for RIG-I; therefore, they are speculated to be recognized primarily by RIG-I (10). RIG-I comprises two N-terminal caspase domains (CARDs), a helicase domain, and a C-terminal regulatory domain (CTD). The helicase and CTD domains of RIG-I recognize viral RNAs, exposing the two N-terminal CARDs, which interact with TRIM25, an E3-ubiquitin ligase (11, 12). TRIM25 deposits the K63-linked polyubiquitin chain on RIG-I CARDs, a phenomenon that induces RIG-I oligomerization and subsequent interaction with mitochondrial antiviral signaling (MAVS) protein (13, 14). As TRIM25 is one of the E3 ubiquitin ligases that play a crucial role in the RIG-I pathway, many viral proteins target TRIM25 to evade the RIG-I-mediated antiviral responses (15, 16). In particular, the V proteins of several members of the family *Paramyxoviridae* suppress RIG-I signaling by preventing TRIM25-mediated ligation of ubiquitin to RIG-I by forming complexes with both RIG-I and TRIM25 (17). Moreover, the NS1 protein of HRSV—a member of the family *Pneumoviridae*—interacts with TRIM25 and inhibits RIG-I ubiquitination (18). The ability to inhibit RIG-I signaling appears to be a common feature in the families *Paramyxoviridae* and *Pneumoviridae*. Therefore, we hypothesized that similar innate immune escape mechanisms might exist in HMPV as it is very similar to HRSV.

HMPV has a negative-sense single-stranded RNA genome, approximately 13 kb in length, comprising eight genes (3'-N-P-

M-F-M2-SH-G-L-5') that encode nine structural proteins (19), with M2 encoding two overlapping proteins, M2-1 and M2-2. However, unlike HRSV and members of the family *Paramyxoviridae*, HMPV does not encode non-structural proteins that are able to inhibit the innate immune cascade. Previous reports have suggested that some proteins, such as G, SH, and M2-2, modulate innate host immunity to favor HMPV infection *via* different mechanisms (5, 20). The attachment G protein, one of the two proteins responsible for viral entry, has been widely studied, as it plays a role in immune response evasion by inhibiting the IFN pathways. HMPV G protein can block RIG-I signaling by interacting with RIG-I (21, 22). Moreover, HMPV M2-2 protein interacts with MAVS protein and inhibits the production of MAVS-induced type I IFN, ultimately inhibiting the innate immune responses (23). However, the mechanisms underlying this HMPV-mediated immune inhibition have not been elucidated yet.

In this study, we sought to determine the mechanisms by which HMPV escapes the immune system. We identified an HMPV protein that inhibits the RIG-I/TRIM25 axis and elucidated the mechanism underlying the immune escape of HMPV. Notably, the mechanism was similar to that for previously reported V proteins of the family *Paramyxoviridae* and was also shared by the NS1 protein of HRSV. Our data provide mechanistic insights that would aid the development of therapeutic agents against infections attributed to members of the families *Paramyxoviridae* and *Pneumoviridae*.

## Materials and methods

### Cells and viruses

HEK293T, VeroE6/TMPRSS2 (JCRB, Osaka, Japan), and HEP-2 cells were cultured in Dulbecco's modified Eagle's medium supplemented with 10% heat-inactivated fetal bovine serum (FBS). The IRF and NF- $\kappa$ B-dual reporter A549 (A549-dual) cells (*In vivo* Gen, San Diego, CA, USA) were used to monitor the activities of the IRF and NF- $\kappa$ B pathways. rHPMV-GFP derived from the HMPV strain Jpn03-1 (GenBank accession number AB503857) has been previously described (24). Wild-type rHMPV-GFP (WT) and rHMPV-GFP $\Delta$ M2-2 ( $\Delta$ M2-2), in which M2-2 had been silenced (25), were propagated in VeroE6/TMPRSS2 cells. HRSV A2 strain was propagated in HEP-2 cells.

### Plasmids

To express cellular or viral proteins with or without FLAG, V5, HA, or Myc tags, mammalian expression plasmids were created by inserting a cDNA fragment carrying the respective

gene into the multicloning site downstream of the cytomegalovirus enhancer chicken  $\beta$ -actin hybrid promoter of pCA7. cDNAs encoding human RIG-I and TRIM25 were purchased from OriGene (Rockville, MD, USA). Further, cDNA fragments encoding the RIG-I ORF [1–925 amino acid (aa)], RIG-I CARD [1–283 aa], TRIM25 [1–630 aa], and TRIM25 truncation mutants were synthesized using polymerase chain reaction (PCR). The cDNA encoding MAVS (derived from HeLa cells), NS1, and NS2 (derived from HRSV strain A2) were synthesized *via* reverse transcription (RT)-PCR. cDNA fragments encoding HMPV M2-2 deletion mutants were synthesized using PCR. pCA7, encoding P, M, F, M2-1, M2-2, SH, G, or L (derived from HMPV strain Jpn03-1) with or without the FLAG tag, were synthesized as described previously (25).

## Luciferase reporter assay

HEK293T cells ( $\sim 1 \times 10^5$ ) were seeded in a 24-well plate and transfected with the following plasmids in triplicate: IFN- $\beta$  promoter-driven firefly luciferase (Fluc) reporter [90 ng/well] (26, 27) or NF- $\kappa$ B-dependent Fluc reporter (TaKaRa Bio, Shiga, Japan) [90 ng/well] plasmid, Renilla luciferase (Rluc) pRL-TK control vector (Promega, Madison, WI, USA) [10 ng/well], plasmids encoding RIG-I signaling molecules (RIG-I CARD [10 ng/well] and/or TRIM25 [10 ng/well]) or MAVS protein (10 ng/well), and the plasmids encoding the viral proteins (NiV-V, MeV-V, HRSV-NS1, NS2, HMPV-N, P, M, F, M2-1, M2-2, SH, G, L, or M2-2 deletion mutants [280 ng/well]), using polyethyleneimine hydrochloride (MW 40,000) (PEI MAX) (#24765; Polysciences Inc., Warrington, PA, UK). An equal amount of DNA was used for transfection by adjusting the amount of the pCA7 empty plasmid. Cells were lysed 24 h post-transfection, and relative luciferase (Luc) activity was determined using the dual-Luc reporter assay system (Promega, Madison, WI, USA).

## Activities of IRF and NF- $\kappa$ B pathways

A549-dual cells were stably transfected with two inducible reporter constructs, and activation of the IRF and NF- $\kappa$ B pathways was monitored by evaluating luciferase (Luc) and secreted embryonic alkaline phosphatase (SEAP) activities, respectively, according to the manufacturer's instructions (*In vivoGen*).

## Immunoprecipitation

HEK293T cells ( $\sim 5.0 \times 10^5$ ) seeded in 6-well plates were transfected with various combinations of plasmids (2 mg/well each) using PEI MAX. After incubation for an appropriate duration, the cells were lysed in 400  $\mu$ L lysis buffer (50 mM

Tris-HCl [pH 7.4], 150 mM NaCl, and 1% Triton X-100) supplemented with a protease inhibitor cocktail (Nacalai Tesque Inc., Kyoto, Japan). Cell lysates were then incubated with anti-FLAG, anti-V5, anti-Myc, or anti-HA mouse monoclonal antibody (MAb)-coated magnetic beads (MBL, Nagoya, Japan) at 4°C for 2 h. Beads were washed five times with lysis buffer and denatured in Laemmli sample buffer (50 mM Tris-HCl [pH 6.8], 2% sodium dodecyl sulfate (SDS), 0.1% bromophenol blue, 10% glycerol, and 5% 2-mercaptoethanol). The eluted proteins were subjected to immunoblot (IB) analysis. A portion of the cell lysate was also subjected to IB analysis.

## IB analysis

Samples were separated by SDS-polyacrylamide (10–16.5%) gel electrophoresis and electroblotted onto a membrane filter (Immobilon-P; MilliporeSigma, Burlington, MA, USA). Membranes were blocked with Blocking One (Nacalai Tesque) for 30 min, followed by incubation at 20–25°C with rabbit polyclonal antibodies against FLAG (MBL), V5 (MBL), Myc (MBL), HA (MBL), MAVS (D5A9E) (#24930, Cell Signaling Technology, Danvers, MA, USA), TRIM25 (#13773, Cell Signaling Technology) or a mouse monoclonal antibody against RIG-I (D-12) (sc-376845, Santa Cruz Biotechnology, Inc., Dallas, TX, USA) for 1 h. Membranes were then incubated at 20–25°C for 30 min with horseradish peroxidase-conjugated anti-mouse or anti-rabbit IgG antibodies (GE Healthcare, Chicago, IL, USA). Protein bands were visualized using enhanced chemiluminescence Western Lightning Ultra Substrate (PerkinElmer, Waltham, MA, USA) and FUSION-Solo S Imaging System (Vilber Lourmat Sté, Collégien, France).

## Statistical analysis

Data are presented as mean  $\pm$  standard deviation (SD). Differences between two groups were analyzed using the Student's *t*-test, whereas those between three or more groups were evaluated using Tukey's test or Dunnett's test. A *p* < 0.05 was considered statistically significant. All statistical analyses were performed using Microsoft Excel 2019 for Windows, version 10.

## Results

### HMPV M2-2 inhibits TRIM25-mediated RIG-I signaling preventing the activation of the IFN- $\beta$ promoter

To identify the HMPV proteins responsible for inhibiting RIG-I/TRIM25 signaling, we screened HMPV ORFs for their

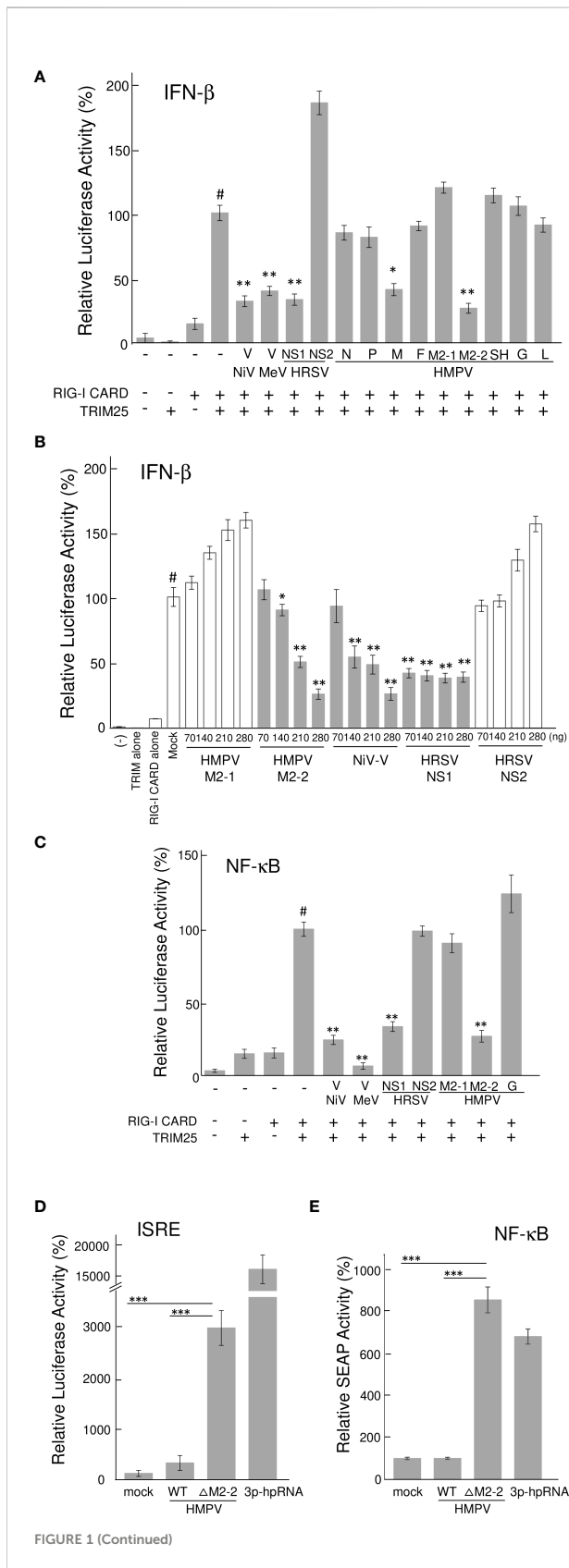


**FIGURE 1 |** Effect of HMPV proteins on RIG-I CARD/TRIM25 signaling. (A–C) An IFN-β promoter-driven (A, B) or NF-κB-dependent (C) Fluc reporter plasmids were transfected into HEK293T cells with the internal control, pRL-TK, and indicated plasmids as described in the Reporter Assay section of the Materials and Methods. Fluc and RLuc activities were evaluated 24 h post-transfection. Relative luciferase activity was calculated as the ratio of Fluc activity to RLuc activity, \**p* < 0.05, \*\**p* < 0.01 vs. transfection with an empty vector instead of a plasmid encoding viral protein (#), Dunnett’s test. (D, E) A549-dual cells were infected with wild-type rHMPV-GFP (WT) or rHMPV-GFPΔM2-2 (ΔM2-2) at a multiplicity of infection (MOI) of 1 or transfected with 5 triphosphate hairpin RNA (3p-hpRNA) (100 ng/mL) as a positive control, and culture media were collected 36 h after infection or treatment. Activation of the IRF and NF-κB pathways in the culture media was evaluated by measuring the luciferase and SEAP activities, respectively, \*\*\**p* < 0.001, Tukey’s test. Data are presented as mean ± SD of three independent experiments. HMPV, Human metapneumovirus, IFN-β, interferon-β, NF-κB, Nuclear factor-kappa B, IRF, interferon-regulatory factor, pRL-TK, Renilla luciferase plasmid, NiV, Nipah virus, MeV, measles virus. ISRE, interferon-stimulated response element.

ability to block RIG-I/TRIM25 signaling reconstituted in HEK293T cells. In this reconstitution system, TRIM25 and RIG-I CARD were co-transfected into HEK293T cells along with an IFN-β promoter-driven firefly luciferase (Fluc) reporter plasmid and internal control (pRL-TK), in accordance with previously described procedures (17, 28). The effect of HMPV proteins on RIG-I CARD/TRIM25-mediated signaling was compared to that of Nipah virus (NiV) V, measles virus (MeV) V, and HRSV NS1 and NS2 proteins, which are well-known viral antagonists of RIG-I/TRIM25 signaling (17, 18, 29). As shown in Figure 1A, co-transfection with RIG-I CARD and TRIM25 resulted in a striking increase in IFN-β promoter activity (compared to transfection with RIG-I CARD or TRIM25 alone). This increase was suppressed upon co-transfection with M2-2 but not upon co-transfection with G, which is reportedly suppressed in other strains (21, 22). The most potent suppression was by M2-2, which exhibited dose-dependent inhibition, similar to that by NiV V (Figure 1B). HRSV NS1 exerted maximum inhibition at the lowest dose tested. A similar experiment was performed using the NF-κB-Fluc reporter plasmid. HMPV M2-2 suppressed RIG-I CARD/TRIM25-mediated NF-κB activation, similar to NiV V, MeV V, and HRSV NS1, whereas the HMPV-G protein did not (Figure 1C). To ascertain the effect of the M2-2 on the IRF and NF-κB pathways in infected A549 cells, luciferase and SEAP activities were evaluated in A549-dual cells infected with rHMPV-GFPΔM2-2 (ΔM2-2), in which the M2-2 ORF was silenced (24, 25). rHMPV-GFPΔM2-2 increased the luciferase and SEAP activities in cells by 9.3- and 8.4-fold, respectively (compared to wild-type rHMPV-GFP (WT)) (Figures 1D, E). 3p-hpRNA is a well-known activator of the RIG-I pathway. These results indicated that M2-2 inhibits RIG-I/TRIM25 signaling and suppresses the activation of the IFN-β and NF-κB pathways.

### M2-2 inhibits TRIM25-mediated RIG-I ubiquitination and the downstream RIG-I-MAVS protein interaction

We investigated the role of HMPV M2-2 in TRIM25-mediated K63-linked polyubiquitination of RIG-I and the downstream RIG-I-MAVS protein interaction. FLAG-tagged RIG-I CARD (FLAG-RIG-I CARD) and HA-tagged TRIM25 (HA-TRIM25) were co-transfected into HEK293T cells along with Myc-tagged K63-linked ubiquitin (Myc-Ubk63) and subjected to IB analysis with RIG-I antibodies. As previously

reported (17, 28), ectopically expressed FLAG-RIG-I CARD was ubiquitinated, and further, the ubiquitination was enhanced by co-expressing Myc-Ubk63 or Myc-Ubk63 and HA-TRIM25 (Figure 2A). Thus, the minimal ubiquitination by RIG-I CARD alone was catalyzed by endogenous TRIM25. However, co-expression of HMPV M2-2 markedly suppressed the ubiquitination of FLAG-RIG-I CARD (this was similar to the results obtained upon NiV V co-expression). Conversely, HMPV G slightly suppressed FLAG-RIG-I CARD ubiquitination. Next, to detect the interaction between FLAG-RIG-I CARD and endogenous MAVS protein, cell lysates were

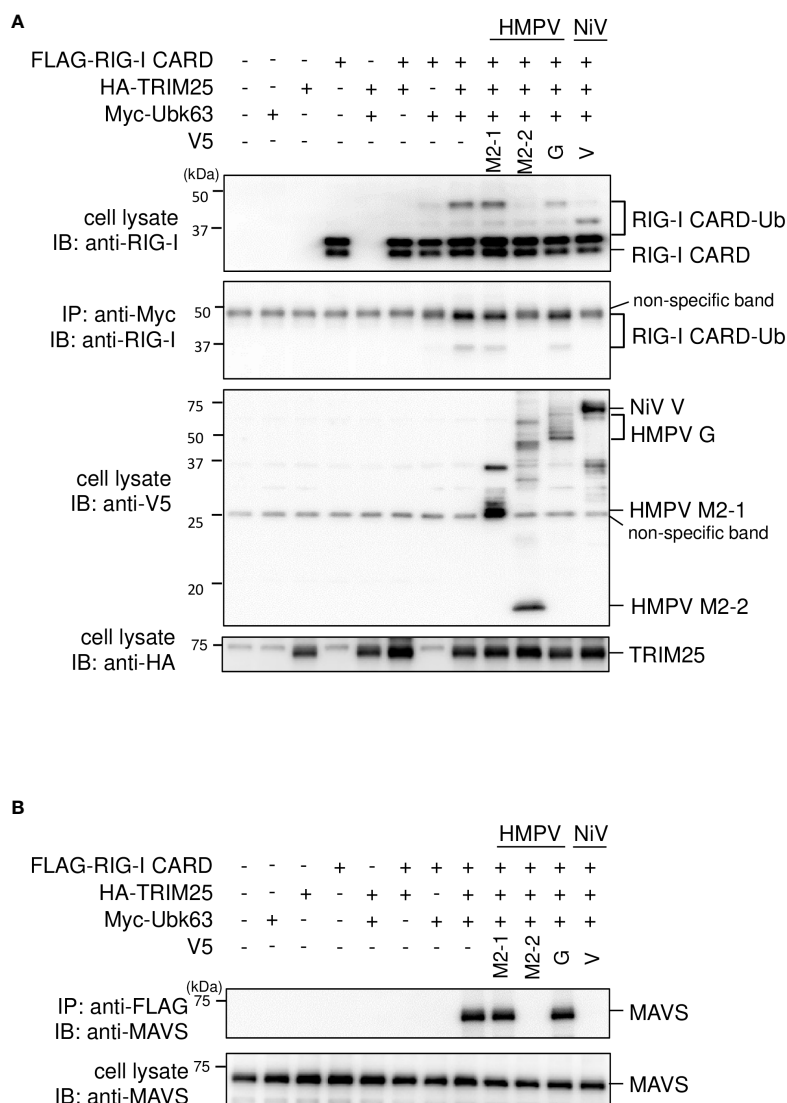


**FIGURE 2** Effect of the HMPV M2-2 protein on RIG-I ubiquitination and subsequent RIG-I-MAVS protein interaction. (A, B) HEK293T cells were transfected with indicated plasmids. Cells were lysed using lysis buffer 24 h post-transfection. Cell lysates were subjected to immunoblot (IB) analysis with anti-RIG-I, anti-V5, or anti-HA antibodies, and immunoprecipitation (IP) analysis with anti-Myc, followed by IB with an anti-RIG-I antibody (A). Cell lysates were subjected to IP with anti-FLAG, followed by IB with anti-MAVS protein antibody. A portion of the cell lysates was also subjected to IB (B). HMPV, Human metapneumovirus, NiV, Nipah virus, MeV, measles virus.



subjected to IP with an anti-FLAG antibody, followed by IB analysis with an antibody against MAVS protein. Co-expression of HA-TRIM25 and Myc-Ubk63 resulted in induced RIG-I CARD polyubiquitination, indicating an interaction between FLAG-RIG-I CARD and the MAVS protein (Figure 2B). However, this interaction was disrupted upon co-transfection with HMPV M2-2 or NiV V. In contrast, HMPV M2-1 and HMPV G did not suppress the interaction between the RIG-I CARD and MAVS protein. These results were also in alignment with those presented in Figure 2A. Thus, we can infer that M2-2 interfered with the RIG-I CARD-MAVS protein interaction, possibly by regulating the ubiquitination status of RIG-I CARD.

## TRIM25 is a potential target of M2-2 protein

To investigate the interactions among M2-2, RIG-I CARD, TRIM25, FLAG-tagged M2-2 (FLAG-M2-2) was transfected into HEK293T cells with V5-tagged RIG-I CARD (V5-RIG-I CARD) or V5-tagged TRIM25 (V5-TRIM25). Transfected cells were subjected to IP. As shown in Figure 3A, FLAG-M2-2 co-immunoprecipitated with anti-V5 antibodies in cells transfected with either V5-RIG-I CARD or V5-TRIM25. Conversely, both V5-RIG-I CARD and V5-TRIM25 co-immunoprecipitated with anti-FLAG antibodies (Figure 3B). Further IP experiments on cells transfected with V5-RIG-I CARD or Myc-tagged TRIM25 (Myc-TRIM25) and various FLAG-tagged HMPV proteins showed that only M2-2 protein interacted with both RIG-I CARD and TRIM25 (Figures 3C, D), suggesting that M2-2 specifically interacts with RIG-I CARD and TRIM25. To determine whether these interactions were direct, similar experiments were performed for mixtures of either FLAG-M2-2 and V5-RIG-I CARD or FLAG-M2-2 and V5-TRIM25, which were synthesized using a wheat germ cell-free expression system. Figure 3E shows, only V5-TRIM25 was immunoprecipitated upon using an anti-FLAG antibody, indicating that M2-2 interacted directly with TRIM25 but not RIG-I CARD.

## M2-2 binds to the SPRY domain of TRIM25

TRIM25 comprises five domains, i.e., RING (RING-finger domain), BB (B box) 1, BB (B box) 2, CCD (coiled-coil domain), and SPRY (SPRY) (30) (Figure 4A). To identify the domains that interact with M2-2, we created TRIM25 deletion mutants and performed IP experiments. V5-tagged TRIM25 deletion mutants, RING and BB1, were transfected into HEK293T cells, together with FLAG-M2-2. FLAG-M2-2 was immunoprecipitated upon using the anti-V5 antibody in cells

transfected with FLAG-SPRY but not with RING, BB1, BB2, or CCD, suggesting that the SPRY domain of TRIM25 interacts with M2-2 (Figure 4B). Furthermore, to determine whether this interaction was direct, similar experiments were performed for mixtures of either FLAG-M2-2 and V5-TRIM25 SPRY or FLAG-M2-2 and V5-TRIM25ΔSPRY (lacking SPRY), which were synthesized using a wheat germ cell-free expression system (Figure 4C). Expectedly, V5-SPRY was immunoprecipitated upon using the anti-FLAG antibody, whereas V5-TRIM25ΔSPRY was not, indicating that the interaction between M2-2 and TRIM25 SPRY is direct.

## M2-2 inhibits MAVS-mediated IFN-β activation

Ren et al. reported that the M2-2 protein of the HMPV strain CAN97-83 suppresses MAVS—which acts downstream of the RIG-I pathway—by targeting the MAVS protein (23) and that M2-2 suppresses RIG-I-mediated signaling. Thus, we tested the ability of the M2-2 protein of the JPN03-1 HMPV strain to block MAVS in HEK293T cells. Transfection with a plasmid expressing MAVS protein alone markedly enhanced the IFN-β promoter activity even in the absence of transfection of the upstream components (Figure 5A). This activation was suppressed upon co-transfection with N or M2-2 proteins. IP experiments on cells transfected with HA-tagged MAVS (HA-MAVS) and various FLAG-tagged HMPV proteins showed that N and M2-2 proteins interact with MAVS proteins (Figure 5B), suggesting the specificity of the interactions between M2-2 and MAVS proteins. Furthermore, to determine whether these interactions are direct, similar experiments were performed for mixtures of FLAG-M2-2 and V5-MAVS, which were synthesized using a wheat germ cell-free expression system (Figure 5C). V5-MAVS was not immunoprecipitated upon using the anti-FLAG antibody, indicating that the interactions between M2-2 and MAVS proteins were indirect. These results suggest that the M2-2 protein of the JPN03-1 strain also inhibits MAVS by indirectly interacting with MAVS proteins.

## M2-2 functional domains inhibit RIG-I CARD/TRIM25-mediated signaling

To examine whether the ability of M2-2 to inhibit MAVS is important for the inhibition of RIG-I CARD/TRIM25 signaling, we determined the functional domain(s) of M2-2 that inhibit RIG-I CARD/TRIM25 and MAVS-mediated signaling. Thus, we created four M2-2 deletion mutants (Δ1-4, Figure 6A) and examined their inhibitory effects on RIG-I CARD/TRIM25- and MAVS-induced IFN-β promoter activation compared to WT, M2-1, and NiV V, which was previously reported to inhibit

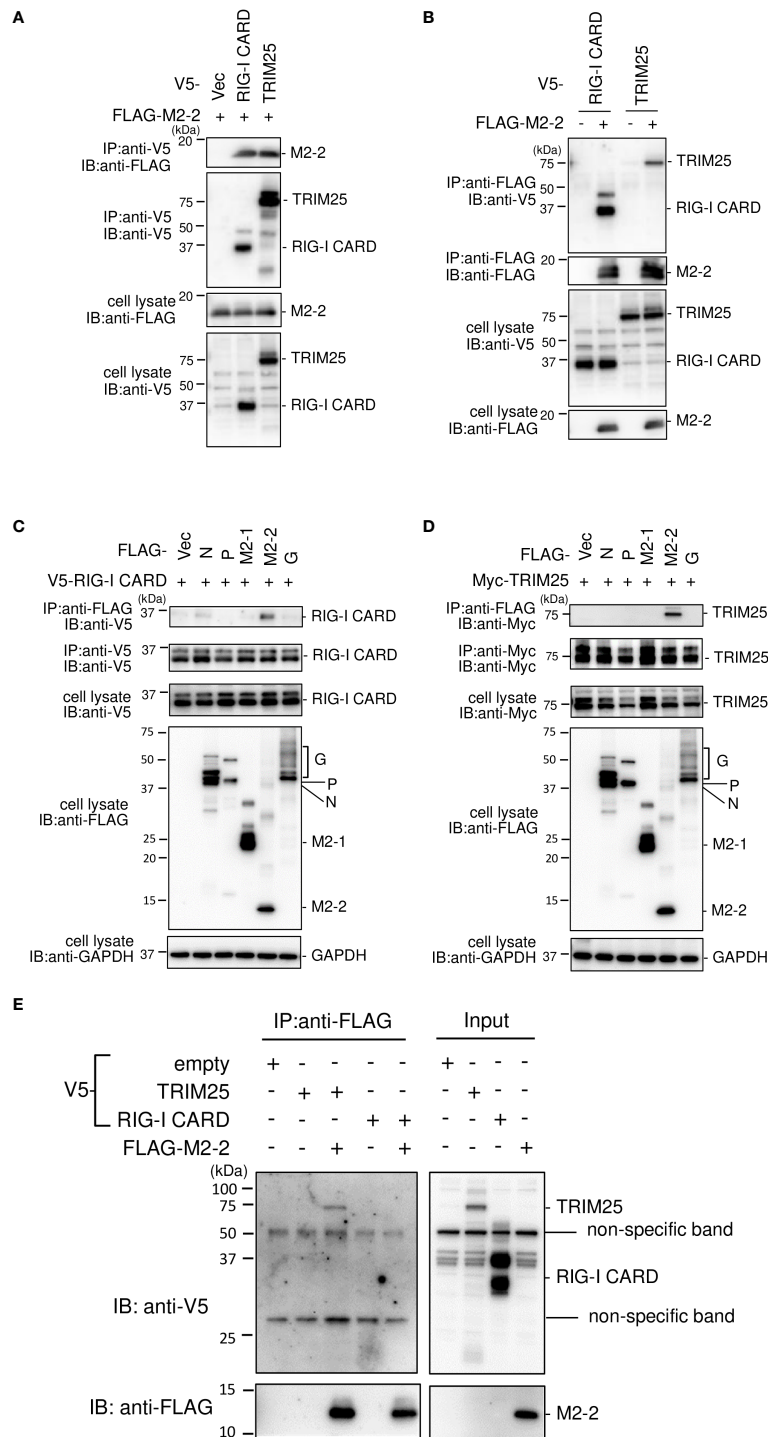


FIGURE 3

Interactions among the HMPV M2-2, RIG-I, and TRIM25 proteins. (A–D) HEK293T cells were transfected with the indicated plasmids. Cells were lysed in lysis buffer 24 h post-transfection and subjected to IP with anti-V5 (A), anti-FLAG (B), anti-FLAG, anti-V5 (C), anti-FLAG, or anti-Myc antibodies (D), followed by immunoblotting (IB) with anti-FLAG, anti-V5, or anti-Myc antibodies. (E) V5-TRIM25, V5-RIG-I CARD, and FLAG-M2-2 were synthesized using a wheat germ cell-free expression system. Then, the *in vitro* transcription/translation products were mixed in various combinations and subjected to immunoprecipitation (IP) analysis with an anti-FLAG antibody, followed by IB with an anti-V5 antibody. A portion of the cell lysates (A–D) or the *in vitro* transcription/translation products (Input) (E) was also subjected to IB.

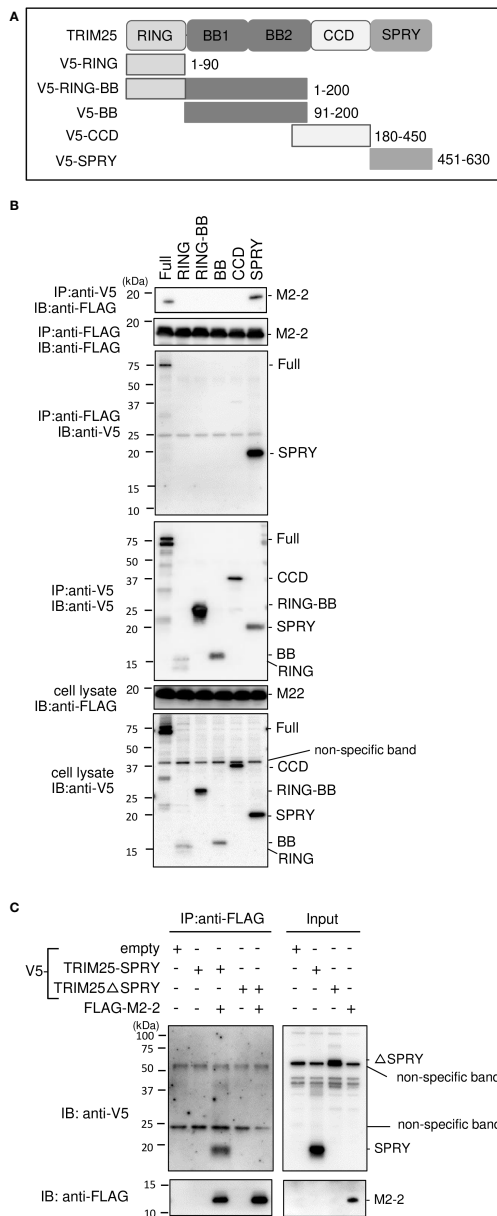


FIGURE 4

Interactions between HMPV M2-2 protein and TRIM25 truncation mutants. (A) Schematic diagram of V5-tagged truncation mutants of TRIM25. (B) HEK293T cells were transfected with the indicated plasmids and lysed 24 h post-transfection. Cell lysates were subjected to IP with anti-V5 or anti-FLAG antibodies, followed by immunoblotting (IB) with an anti-V5 antibody. (C) V5-TRIM25, V5-RIG-I CARD, and FLAG-M2-2 were synthesized using a wheat germ cell-free expression system. Then, the *in vitro* transcription/translation products were mixed in various combinations and subjected to immunoprecipitation (IP) analysis with an anti-FLAG antibody, followed by IB with an anti-V5 antibody. A portion of the total cell lysates (B) or the *in vitro* transcription/translation products (Input) (C) was also subjected to IB.

MAVS (31). As shown in Figure 6B,  $\Delta 3$  exhibited an inhibitory effect on the RIG-I CARD/TRIM25-induced IFN- $\beta$  promoter activity, similar to that induced by WT M2-2 and NiV, whereas  $\Delta 1$ ,  $\Delta 2$ , and  $\Delta 4$  did not. Additionally, we evaluated their interactions with RIG-I CARD, TRIM25, and MAVS. IP experiments showed that  $\Delta 3$  strongly binds to RIG-I CARD and TRIM25, whereas  $\Delta 1$ ,  $\Delta 2$ , and  $\Delta 4$  exhibited only a small or negligible ability to bind to RIG-I CARD and TRIM25 (Figures 6C, D), which is consistent with the results shown in Figure 6B. This suggests that the 1–48 aa region is critical for inhibiting RIG-I CARD/TRIM25 signaling. In contrast—in a manner similar to WT M2-2 and NiV V- $\Delta 2$  inhibited MAVS-induced IFN- $\beta$  promoter activity (Figure 6E). IP experiments showed that  $\Delta 2$  binds to MAVS proteins (Figure 6F). However, it should be noted that  $\Delta 2$ , which retained its inhibitory effect on MAVS and the ability to bind to MAVS proteins, did not exhibit an inhibitory effect on RIG-I CARD/TRIM25 signaling and the ability to bind to RIG-I CARD and TRIM25. Collectively, these results suggest that the inhibition of RIG-I CARD/TRIM25-mediated signaling is possibly independent of the ability of M2-2 to inhibit MAVS.

To confirm this, we performed similar experiments using finer  $\Delta 3$  deletion mutants (Figure 6G). Similar to WT M2-2,  $\Delta 3-1$ ,  $\Delta 3-2$ ,  $\Delta 3-3$ ,  $\Delta 3-4$ ,  $\Delta 3-6$ ,  $\Delta 3-7$ , and  $\Delta 3-8$  exhibited an inhibitory effect on RIG-I CARD/TRIM25-induced IFN- $\beta$  promoter activity and ability to bind to RIG-I CARD and TRIM25, whereas  $\Delta 3-5$ ,  $\Delta 3-9$ , and  $\Delta 3-10$  did not, suggesting that the 13–32 aa region is important for the inhibition of RIG-I CARD/TRIM25 signaling (Figures 6H–J). Although  $\Delta 3-8$  retained the ability to bind to the MAVS protein, it did not inhibit MAVS (Figures 6K, L). Notably,  $\Delta 3-8$ , which did not retain its inhibitory effect on MAVS, exhibited an inhibitory effect on RIG-I CARD/TRIM25 signaling. Collectively, these results suggest that the inhibition of RIG-I CARD/TRIM25 signaling by M2-2 is not due to MAVS inhibition. Furthermore, TRIM25-mediated RIG-I CARD ubiquitination was substantially and dose-dependently suppressed in response to increased M2-2 protein expression (Figure 6M). Ubiquitination was also suppressed in  $\Delta 3$ -transfected cells as efficiently as in WT M2-2-transfected cells, whereas it was not suppressed in cells transfected with  $\Delta 2$ . Therefore, these results suggest that the inhibition of RIG-I CARD/TRIM25 signaling by M2-2 is not due to MAVS inhibition.

## HMPV M2-2 is incorporated into the RIG-I CARD/TRIM25 complex

The SPRY domain of TRIM25 is necessary for TRIM25-RIG-I interactions (30). Therefore, the binding between M2-2 and SPRY may affect the interaction between RIG-I and TRIM25. To

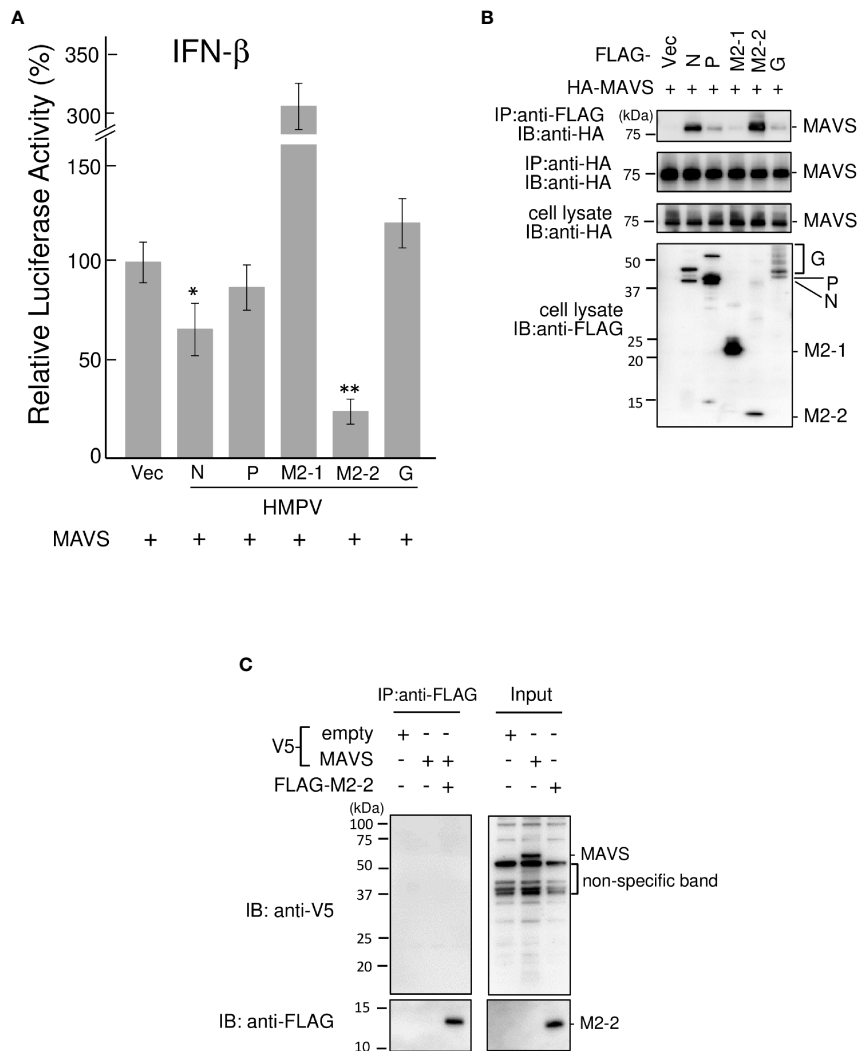
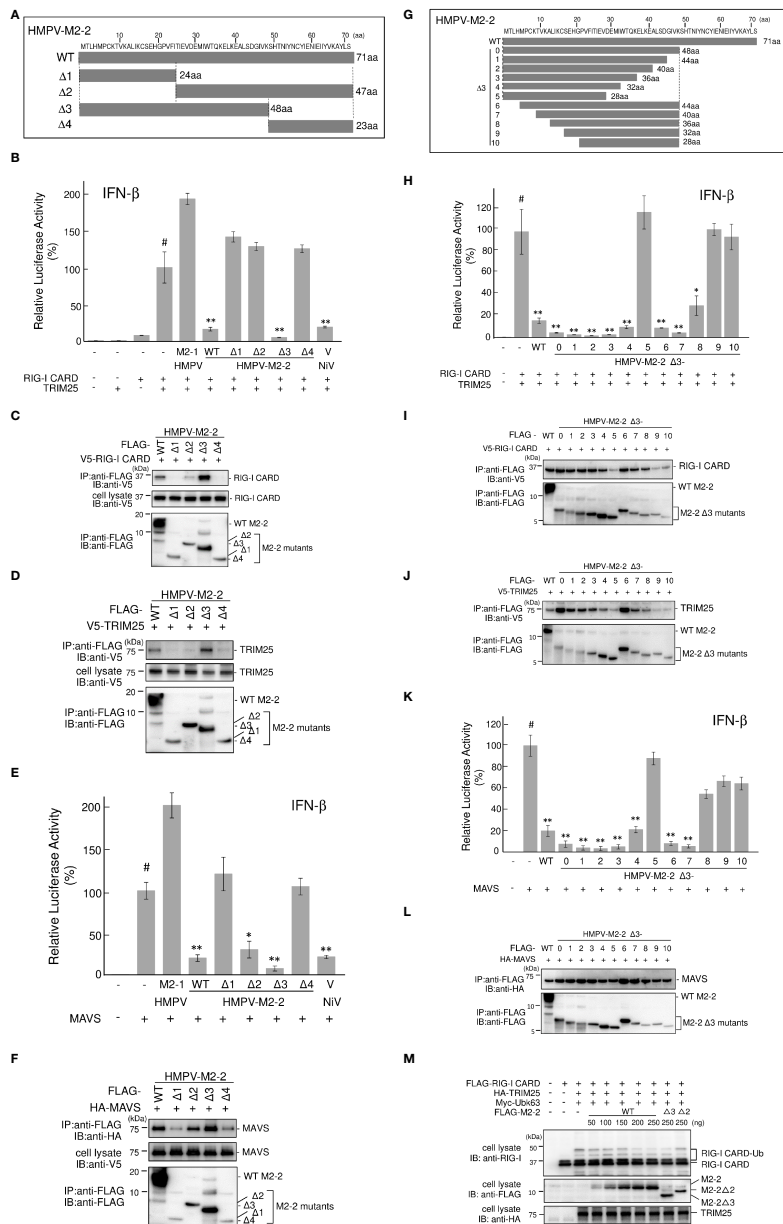


FIGURE 5

Effect of the HMPV M2-2 protein on MAVS-mediated signaling. (A) An IFN- $\beta$  promoter-driven Fluc reporter plasmid was transfected into HEK293T cells with the internal control, pRL-TK, and the indicated plasmids. Fluc and Rluc activities were evaluated 24 h post-transfection. Relative luciferase activity was calculated as the ratio of Fluc activity to Rluc activity. \* $p < 0.05$ , \*\* $p < 0.01$  vs. transfection with empty vector, Dunnett's test. (B) HEK293T cells were transfected with the indicated plasmids. Cells were lysed in lysis buffer 24 h post-transfection and subjected to immunoprecipitation (IP) with anti-FLAG or anti-HA antibodies (A), followed by immunoblotting (IB) with an anti-HA antibody. (C) V5-MAVS and FLAG-M2-2 were synthesized using a wheat germ cell-free expression system. Then, the *in vitro* transcription/translation products were mixed in various combinations and subjected to IP with an anti-FLAG antibody, followed by IB with anti-V5 or anti-FLAG antibodies. A portion of cell lysates (A, B) or the *in vitro* transcription/translation products (Input) (C) was also subjected to IB. HMPV, Human metapneumovirus, MAVS, mitochondrial antiviral signaling proteins.

evaluate this possibility, FLAG-M2-2 was transfected into HEK293T cells with various plasmid combinations, including either V5-TRIM25 and FLAG-RIG-I CARD or V5-RIG-I CARD and FLAG-TRIM25, and the transfected cells were subjected to IP analysis. FLAG-RIG-I CARD was immunoprecipitated along with V5-TRIM25 (Figure 7A). The amount of co-immunoprecipitated FLAG-RIG-I CARD was increased upon co-transfection with FLAG-M2-2. In addition, FLAG-TRIM25 was immunoprecipitated along with V5-RIG-I

CARD (Figure 7B), and the amount of co-immunoprecipitated FLAG-TRIM25 also increased upon co-transfection with FLAG-M2-2. Conversely, both V5-RIG-I CARD and V5-TRIM25 were immunoprecipitated along with FLAG-M2-2 when FLAG-M2-2 was transfected into HEK293T cells together with V5-RIG-I CARD and V5-TRIM25 (Figure 7C). These results were similar to those obtained for NiV V-transfected cells, suggesting that M2-2 is incorporated inside the RIG-I CARD/TRIM25 complex and may stabilize the complex.



**FIGURE 6**

HMPV M2-2 domains that inhibit RIG-I CARD/TRIM25-mediated IFN-β activation. **(A, G)** Schematic diagram of FLAG-tagged deletion mutants of M2-2. **(B, E, H, K)** An IFN-β promoter-driven Fluc reporter plasmid was transfected into HEK293T cells with the internal control, pRL-TK, and the indicated plasmids. Fluc and Rluc activities were evaluated 24 h post-transfection. Relative luciferase activity was calculated as the ratio of Fluc activity to Rluc activity, \**p* < 0.05, \*\**p* < 0.01 vs. transfection with empty vector (#). Dunnett's test. Data are presented as the mean ± SD of three independent experiments. **(C, D, F, I, J, L)** HEK293T cells were transfected with the indicated plasmids and lysed 24 h post-transfection. Cell lysates were subjected to immunoprecipitation (IP) with an anti-FLAG antibody, followed by immunoblotting (IB) with anti-V5, anti-HA, or anti-FLAG antibodies. A portion of the cell lysates was also subjected to IB. **(M)** HEK293T cells were transfected with the indicated plasmids and lysed 24 h post-transfection. Cell lysates were subjected to IB with anti-RIG-I, anti-FLAG, or anti-HA antibodies. HMPV, Human metapneumovirus, IFN-β, interferon-β, MAVS, mitochondrial antiviral signaling proteins.

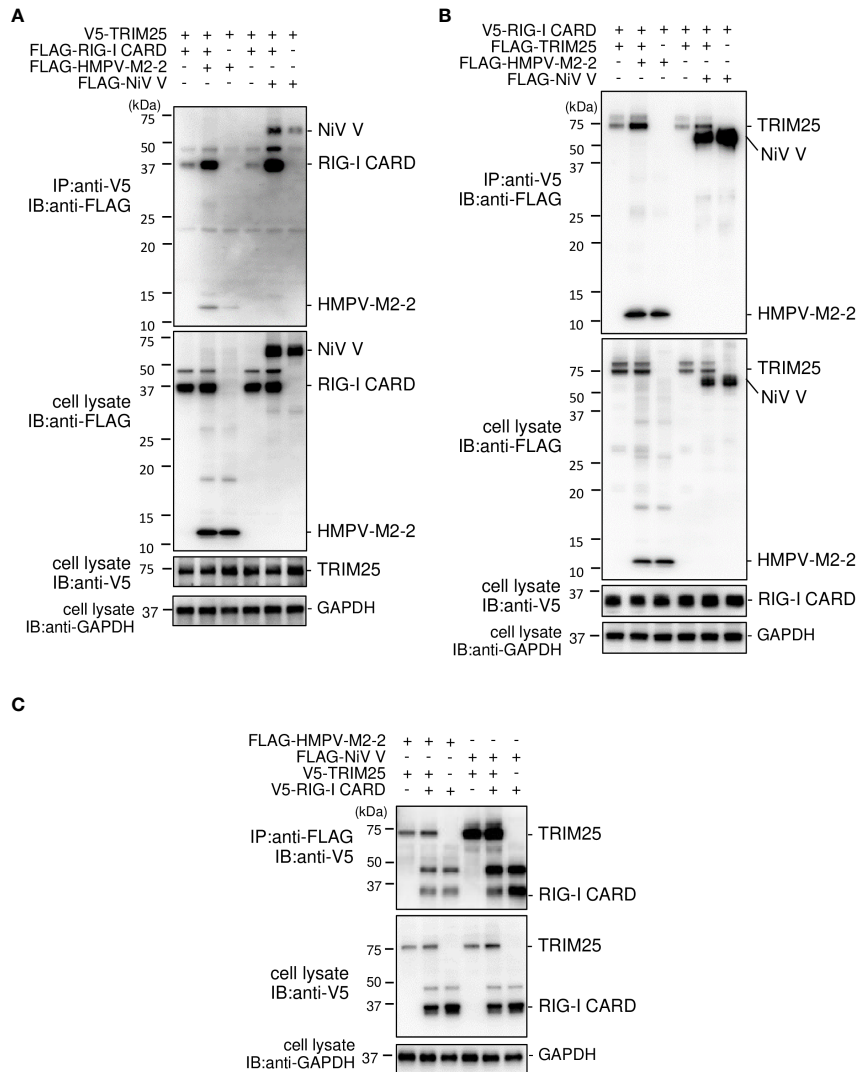


**FIGURE 7** Interaction between the HMPV M2-2 protein and the RIG-I CARD/TRIM25 complex. (A–C) HEK293T cells were transfected with the indicated plasmids. Cells were lysed in lysis buffer 24 h post-transfection and subjected to immunoprecipitation (IP) with anti-V5 (A, B) or anti-FLAG (C), followed by immunoblotting (IB) with anti-FLAG or anti-V5 antibodies. A portion of the cell lysates was also subjected to IB. HMPV, Human metapneumovirus, IFN-β, interferon-β, NiV, Nipah virus.

### HRSV NS1 is incorporated into the RIG-I CARD/TRIM25 complex

HRSV NS1 protein has been reported to target TRIM25 to inhibit RIG-I ubiquitination and the subsequent RIG-I-mediated antiviral signaling (18). To confirm this, we performed IB analysis using the same procedure as in Figure 2A. HRSV NS1 suppressed the ubiquitination of FLAG-RIG-I CARD—similar to the results obtained upon the HMPV M2-2 or NiV V co-expression, whereas HRSV NS2 did not (Figure 8A). This result suggests that NS1 may also affect RIG-I/TRIM25-mediated signaling via a mechanism similar to that

employed by HMPV M2-2 and NiV V. Next, to examine the effect of NS1 on the interaction between RIG-I and TRIM25, FLAG-HRSV NS1 or -HRSV NS2 was transfected into HEK293T cells with either V5-TRIM25 and FLAG-RIG-I CARD or V5-RIG-I CARD and FLAG-TRIM25. Transfected cells were subjected to IP with an anti-V5 antibody. FLAG-RIG-I CARD was immunoprecipitated along with V5-TRIM25 (Figure 8B). The amount of immunoprecipitated FLAG-RIG-I CARD increased upon co-transfection with FLAG-NS1. In addition, FLAG-TRIM25 was immunoprecipitated along with V5-RIG-I CARD, and the amount of co-immunoprecipitated FLAG-RIG-I CARD was also increased upon co-transfection

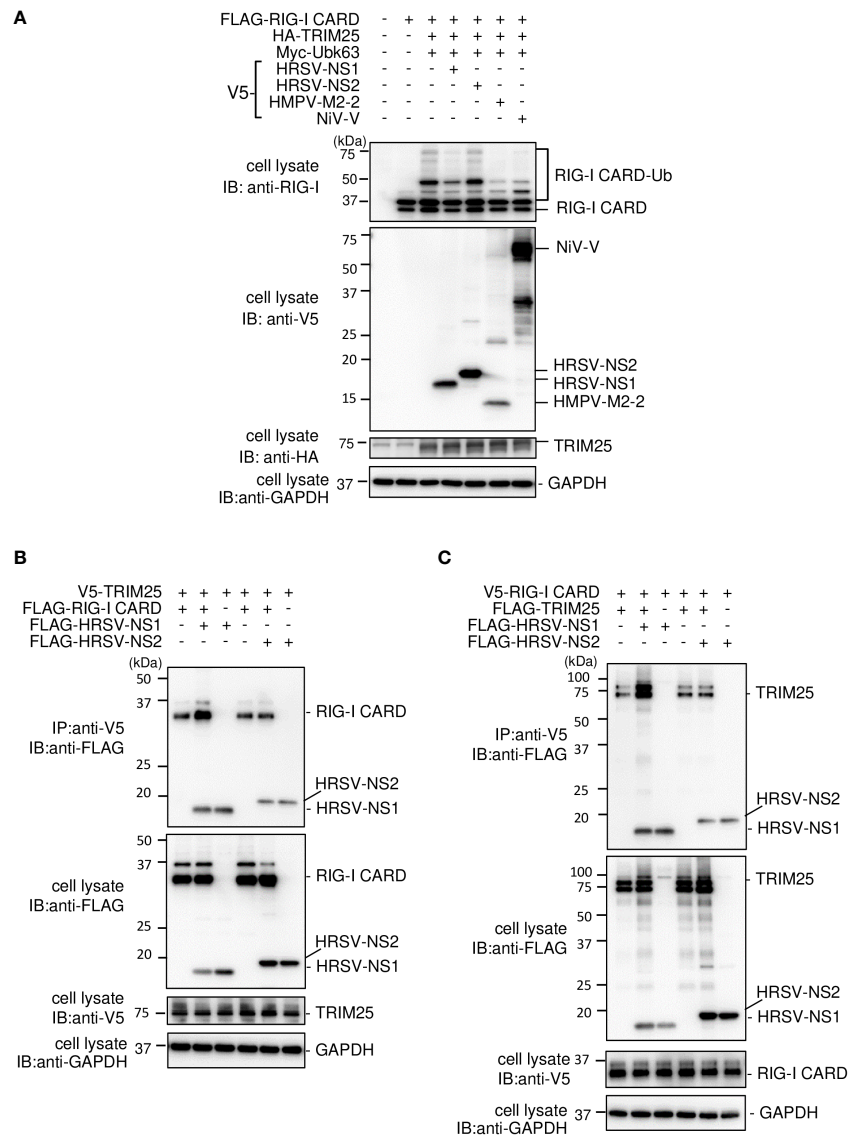


**FIGURE 8** Interaction between the HRSV NS1 protein and the RIG-I CARD/TRIM25 complex. **(A)** HEK293T cells were transfected with the indicated plasmids. Cells were lysed in lysis buffer 24 h post-transfection and subjected to immunoblotting (IB) analysis with anti-RIG-I, anti-V5, or anti-HA antibodies. **(B, C)** HEK293T cells were transfected with the indicated plasmids. Cells were lysed in lysis buffer 24 h post-transfection and subjected to immunoprecipitation (IP) with an anti-V5 antibody, followed by IB with an anti-FLAG antibody. A portion of the cell lysates was also subjected to IB. HRSV, human respiratory syncytial virus.

with NS1 (Figure 8C). Co-immunoprecipitated FLAG-HRSV-NS2 was detected in cells co-transfected with V5-RIG-I CARD and V5-TRIM25, however, the amount of precipitated proteins was small. Additionally, NS2 did not affect the RIG-I CARD/TRIM25 complex formation. This result is consistent with those in Figure 1A, where NS2 did not inhibit RIG-I CARD/TRIM25-induced IFN-β promoter activity, which has previously been reported to be suppressed in other strains (29). These results suggest that NS1, but not NS2, is also incorporated into the RIG-I CARD/TRIM25 complex and that it may stabilize this complex.

## Discussion

Innate immunity functions as the first line of host defense against invading pathogens, as well as a critical component in regulating adaptive immunity. The effectiveness of the innate immune response against viral infection depends on the interactive nature of virus components with the host innate antiviral immune systems, including the type I IFN production system (32). Although HMPV induces poor innate immune responses (5), the role of individual HMPV proteins in

modulating host innate immune responses remains largely unclear. RIG-I establishes an antiviral state by triggering signaling cascades that induce the expression of type I IFNs and inflammatory cytokines (6–9). The ability to inhibit RIG-I signaling is seemingly a common feature in the families *Paramyxoviridae* and *Pneumoviridae* in the order *Mononegavirales*. Therefore, we hypothesized that similar innate immune escape mechanisms are at play in HMPV as it is remarkably similar to HRSV and parainfluenza viruses, members of the *Pneumoviridae* and *Paramyxoviridae* families, respectively. In this study, we screened HMPV ORFs to identify HMPV proteins that inhibit the RIG-I/TRIM25 signaling axis and identified the M2-2 protein as a negative regulator of RIG-I/TRIM25 signaling. Compared to WT HMPV, recombinant  $\Delta$ M2-2 HMPV, in which M2-2 expression was abrogated, activated transcription factors downstream of the RIG-I signaling pathway in A549 cells. In this study, we focused on the mechanism(s) underlying RIG-I inhibition by M2-2.

To reveal the molecular mechanism(s) by which the M2-2 protein inhibits RIG-I/TRIM25-mediated signaling leading to IFN- $\beta$  activation, we first examined the effect of M2-2 on RIG-I activation and the downstream protein MAVS, according to a previously described procedure (17,28). M2-2 overexpression inhibited K63-linked polyubiquitination of RIG-I-CARD and CARD-dependent interactions with MAVS. Additionally, we assessed the interaction between M2-2 and RIG-I or TRIM25 by IP using extracts from cells transfected with M2-2 together with RIG-I CARD, TRIM25, or TRIM25 truncation mutants. These experiments showed that M2-2 interacts with RIG-I CARD and TRIM25 SPRY and that M2-2-TRIM25 SPRY interactions were direct, whereas M2-2-RIG-I CARD interactions were not. The TRIM25 SPRY domain is responsible for interactions with RIG-I CARD (30), therefore, the M2-2 protein may bind to the interface between RIG-I CARD and TRIM25. In this study, M2-2 enhanced the stabilization of the RIG-I CARD-TRIM25 complex. Therefore, HMPV M2-2 likely inhibits the K63-linked polyubiquitination of RIG-I by interacting with RIG-I and TRIM25 to form a complex.

This study has revealed that the mechanism underlying HMPV-M2-2 protein-mediated innate immune inhibition is similar to that by V proteins of several members of the family *Paramyxoviridae* (17). However, the previous study did not examine whether V directly binds to RIG-I and TRIM25. In addition, V proteins also reportedly inhibit MAVS-mediated signaling, leading to the production of type I IFNs (31), however, the impact of MAVS inhibition on RIG-I signaling inhibition has not been investigated. In this study, we characterized the detailed mechanisms underlying the inhibition of RIG-I signaling/MAVS by HMPV M2-2. Additionally, we also revealed that the HRSV NS1 protein also interacts with TRIM25, inhibiting RIG-I ubiquitination, which is consistent with the findings of a previous report (18). Furthermore, we revealed that the HRSV NS1 protein is incorporated into the

RIG-I CARD/TRIM25 complex and may stabilize these complexes in a manner similar to the HMPV M2-2 protein.

In addition to viruses of the families *Paramyxoviridae* and *Pneumoviridae*, several RNA viruses have evolved strategies that favor their proliferation by targeting molecules such as RIG-I, TRIM25, and MAVS proteins. The NS1 protein of the influenza A virus (IAV), belonging to the *Orthomyxoviridae* family, interacts with TRIM25 and Riplet, repressing K63-linked ubiquitination of RIG-I (33, 34). NS1 also promotes TRIM25-mediated ubiquitination *via* strain-specific direct interaction with the second CARD of RIG-I (35). The SPRY domain is also a target of the severe acute respiratory syndrome (SARS) N protein, however, in contrast to that of the M2-2 protein, the interaction between SARS-N and TRIM25 prevents the association of TRIM25 with RIG-I (36). Despite these differences, the effects of IAV NS1, SARS N, paramyxovirus V, HRSV NS1, and HMPV M2-2 proteins are similar, i.e., inhibition of RIG-I signaling/MAVS by preventing TRIM25-mediated ubiquitination of RIG-I CARDS. Several disease-causing viruses in humans target TRIM25-mediated ubiquitination in the innate immune response. Therefore, targeting this inhibitory mechanism may aid the development of novel broad-spectrum antivirals. RIG-I may be a promising target because arenavirus Z protein and herpesvirus U11 are also pathogenic viral proteins that interact with RIG-I and suppress RIG-I signaling (37, 38). The mechanism by which the M2-2 protein inhibits the type I IFN signaling cascade, i.e., by antagonizing TLR7/9 signaling, has been reported (25, 37). However, our findings present a novel mechanism for M2-2-mediated inhibition of RIG-I signaling that is MAVS-independent and specific to the TRIM25-mediated regulatory step in the RIG-I activation pathway. HMPV may evade the innate immune system by leveraging both of these mechanisms.

Ren et al. showed that the M2-2 protein interacts with the MAVS protein, but not RIG-I, to inhibit RIG-I- and MAVS-mediated IFN- $\beta$  promoter and NF- $\kappa$ B activity (23). We also confirmed an inhibitory effect on MAVS-induced IFN- $\beta$  promoter activity and a significant, albeit indirect, interaction between M2-2 and the MAVS protein. Thus, we examined the role of M2-2-mediated MAVS inhibition in RIG-I CARD/TRIM25 signaling inhibition using M2-2 deletion mutants. Our results suggested that the ability of M2-2 to inhibit MAVS is not necessary for the negative regulation of the RIG-I CARD/TRIM25 axis. Additionally, previous studies have reported that the C-terminal half of HMPV M2-2 is responsible for the inhibitory effect on MAVS-induced activation of the IFN- $\beta$  promoter (23). However, our data indicate that the N-terminal half of HMPV M2-2 is responsible for the inhibitory effect on RIG-I CARD/TRIM25 signaling and MAVS. We speculate that these results may be due to the different HMPV strains used in other studies. In comparison with the CN97/83 strain used in other studies, the Jpn03-1 strain used in our study is identical to the CAN97-83



strain in M2-1 ORF and the region of overlap between the M1 and M2 proteins but has a single amino acid difference at position 58 in M2-2 (I and L at this position in Jpn03-1 and CAN97-83, respectively), which is located in the C-terminal half of the M2-2 protein (71 aa). Thus, the reasons for these conflicting results remain unclear.

Nevertheless, the current study has limitations. M2-2 silencing induced the activation of transcription factors (IRF and NF- $\kappa$ B) downstream of RIG-I signaling in A549 cells. This activation may occur through two M2-2 activities, partly explaining why M2-2 deletion attenuates the virus (20). The first is through the inhibition of the RIG-I/TRIM25 signaling axis, in our study, M2-2 was the most potent inhibitor among all the proteins encoded by the HMPV genome in HEK293T cells. The second is through the inhibition of viral RNA synthesis. A previous study has shown that the  $\Delta$ M2-2 virus produces higher levels of viral mRNAs in Vero cells than the WT virus (39). Additionally, the inhibitory effect of M2-2 on viral RNA synthesis was also confirmed by experiments with an HMPV minigenome construct carrying a luciferase reporter gene (40). In our study, A549 cells infected with the  $\Delta$ M2-2 virus showed increased viral RNA synthesis. This may increase pathogen-associated molecular patterns (PAMP) levels, thereby inducing IFN- $\beta$  activation. However, it is difficult to determine the exact contribution of each activity to the inhibition of IFN- $\beta$  activation. Furthermore, knockout of the M2-2 gene results in the attenuation of virus pathogenicity. Therefore, the recombinant virus, whose M2-2 gene is silenced, is a candidate for attenuated virus vaccine. However, the M2-2-knockout recombinant HMPV show too poor growth in cell culture and cannot be prepared as a vaccine (5, 20, 23). The M2-2 protein is a multifunctional protein that exerts an anti-IFN effect, regulating viral RNA synthesis (39, 41). Such various functions collectively contribute to virus pathogenicity, resulting in the overattenuation of recombinant viruses. Thus moderately attenuated recombinant viruses, which could be created by silencing only a single function with other functions remaining, might be suitable for vaccine development. For this purpose, it would be necessary to determine domains or amino acid residues important for maintaining each function of the M2-2 protein.

In conclusion, we revealed that the HMPV M2-2 protein acts as an IFN antagonist that inhibits RIG-I CARD-dependent interactions with the MAVS protein by blocking TRIM25-mediated RIG-I ubiquitination, possibly by forming a stable complex with both RIG-I and TRIM25. Similarly, HRSV NS1 also formed a stable complex with RIG-I CARD/TRIM25 and inhibited RIG-I ubiquitination. Notably, the inhibitory actions of HMPV M2-2 and HRSV NS1 proteins are shared among several members of the *Paramyxoviridae* family. We identified that HMPV, similar to HRSV and parainfluenza viruses, has an innate immune escape mechanism similar to theirs. Several disease-causing human viruses target TRIM25 ubiquitination

in the innate immune response, therefore, targeting this inhibitory mechanism may aid the development of novel broad-spectrum antivirals.

Furthermore, moderately attenuated recombinant viruses, which could be created by silencing only a single function while preserving other functions, might be suitable for vaccine development.

## Data availability statement

The datasets presented in this study can be found in online repositories. The names of the repository/repositories and accession number(s) can be found in the article.

## Author contributions

YT and TK designed the study and prepared and revised the manuscript. YT, NM, YK, BG, and TK analyzed the data. YT, NM, YK, and TK performed the experiments. All authors contributed to the article and approved the submitted version.

## Funding

This work was supported by JSPS KAKENHI Grant Number 20K17463.

## Acknowledgments

We thank the Division of Bioresearch in Life Science Laboratory (Fukui University) and the Division of Advanced Research Promotion (Aichi Medical University) for technical instructions and assistance.

## Conflict of interest

The authors declare that the research was conducted in the absence of any commercial or financial relationships that could be construed as a potential conflict of interest.

## Publisher's note

All claims expressed in this article are solely those of the authors and do not necessarily represent those of their affiliated organizations, or those of the publisher, the editors and the reviewers. Any product that may be evaluated in this article, or claim that may be made by its manufacturer, is not guaranteed or endorsed by the publisher.

## References

- Van Den Hoogen BG, De Jong JC, Groen J, Kuiken T, De Groot R, Fouchier RAM, et al. A newly discovered human pneumovirus isolated from young children with respiratory tract disease. *Nat Med* (2001) 7:719–24. doi: 10.1038/89098
- Esper F, Boucher D, Weibel C, Martinello RA, Kahn JS. Human metapneumovirus infection in the united states: Clinical manifestations associated with a newly emerging respiratory infection in children. *Pediatrics* (2003) 111:1407–10. doi: 10.1542/peds.111.6.1407
- Mullins JA, Erdman DD, Weinberg GA, Edwards K, Hall CB, Walker FJ, et al. Human metapneumovirus infection among children hospitalized with acute respiratory illness. *Emerg Infect Dis* (2004) 10:700–5. doi: 10.3201/eid1004.030555
- Caracciolo S, Minini C, Colombrita D, Rossi D, Miglietti N, Vettore E, et al. Human metapneumovirus infection in young children hospitalized with acute respiratory tract disease: Virologic and clinical features. *Pediatr Infect Dis J* (2008) 27:406–12. doi: 10.1097/INF.0b013e318162a164
- Soto JA, Gálvez NMS, Benavente FM, Pizarro-Ortega MS, Lay MK, Riedel C, et al. Shared and unique functions of the DExD/H-box helicases RIG-I, MDA5, and LGP2 in antiviral innate immunity. *J Immunol* (2005) 175:2851–8. doi: 10.4049/jimmunol.175.5.2851
- Yoneyama M, Kikuchi M, Matsumoto K, Imaizumi T, Miyagishi M, Taira K, et al. The RNA helicase RIG-I has an essential function in double-stranded RNA-induced innate antiviral responses. *Nat Immunol* (2004) 5:730–7. doi: 10.1038/ni1087
- Weber M, Gawanbacht A, Habjan M, Rang A, Borner C, Schmidt AM, et al. Incoming RNA virus nucleocapsids containing a 5'-triphosphorylated genome activate RIG-I and antiviral signaling. *Cell Host Microbe* (2013) 13:336–46. doi: 10.1016/j.chom.2013.01.012
- Rehwinkel J, Tan CP, Goubau D, Schulz O, Pichlmair A, Bier K, et al. RIG-I detects viral genomic RNA during negative-strand RNA virus infection. *Cell* (2010) 140:397–408. doi: 10.1016/j.cell.2010.01.020
- Onomoto K, Onoguchi K, Yoneyama M. Regulation of RIG-I-like receptor-mediated signaling: Interaction between host and viral factors. *Cell Mol Immunol* (2021) 18:539–55. doi: 10.1038/s41423-020-00602-7
- Chan YK, Gack MU. RIG-I-like receptor regulation in virus infection and immunity. *Curr Opin Virol* (2015) 12:7–14. doi: 10.1016/j.coviro.2015.01.004
- Rehwinkel J, Gack MU. RIG-I-like receptors: Their regulation and roles in RNA sensing. *Nat Rev Immunol* (2020) 20:537–51. doi: 10.1038/s41577-020-0288-3
- Gack MU, Kirchhofer A, Shin YC, Inn KS, Liang C, Cui S, et al. Roles of RIG-I n-terminal tandem CARD and splice variant in TRIM25-mediated antiviral signal transduction. *Proc Natl Acad Sci U S A*. (2008) 105:16743–8. doi: 10.1073/pnas.0804947105
- Yoneyama M, Fujita T. RNA Recognition and signal transduction by RIG-I-like receptors. *Immunol Rev* (2009) 227:54–65. doi: 10.1111/j.1600-065X.2008.00727.x
- Martin-Vicente M, Medrano LM, Resino S, García-Sastre A, Martínez I. TRIM25 in the regulation of the antiviral innate immunity. *Front Immunol* (2017) 8:1187. doi: 10.3389/fimmu.2017.01187
- Hayman TJ, Hsu AC, Kolesnik TB, Dagley LF, Willemsen J, Tate MD, et al. RIPLET, and not TRIM25, is required for endogenous RIG-I-dependent antiviral responses. *Immunol Cell Biol* (2019) 97(9):840–52. doi: 10.1111/imcb.12284
- Sánchez-Aparicio MT, Feinman LJ, García-Sastre A, Shaw ML. Paramyxovirus V proteins interact with the RIG-I / TRIM25. *J Virol* (2018) 92:1–21. doi: 10.1128/JVI.01960-17
- Ban J, Lee NR, Lee NJ, Lee JK, Quan FS, Inn KS. Human respiratory syncytial virus NS 1 targets TRIM25 to suppress RIG-I ubiquitination and subsequent RIG-I-mediated antiviral signaling. *Viruses* (2018):716 10. doi: 10.3390/v10120716
- Van Den Hoogen BG, Bestebroer TM, Osterhaus ADME, Fouchier RAM. Analysis of the genomic sequence of a human metapneumovirus. *Virology* (2002) 295:119–32. doi: 10.1006/viro.2001.1355
- Biacchesi S, Pham QN, Skiadopoulos MH, Murphy BR, Collins PL, Buchholz UJ. Infection of nonhuman primates with recombinant human metapneumovirus lacking the SH, G, or M2-2 protein categorizes each as a nonessential accessory protein and identifies vaccine candidates. *J Virol* (2005) 79:12608–13. doi: 10.1128/JVI.79.19.12608-12613.2005
- Bao X, Kolli D, Ren J, Liu T, Garofalo RP, Casola A. Human metapneumovirus glycoprotein G disrupts mitochondrial signaling in airway epithelial cells. *PLoS One* (2013) 8:e62568. doi: 10.1371/journal.pone.0062568
- Bao X, Liu T, Shan Y, Li K, Garofalo RP, Casola A. Human metapneumovirus glycoprotein G inhibits innate immune responses. *PLoS Pathog* (2008) 4:e1000077. doi: 10.1371/journal.ppat.1000077
- Ren J, Wang Q, Kolli D, Prusak DJ, Tseng CT, Chen ZJ, et al. Human metapneumovirus M2-2 protein inhibits innate cellular signaling by targeting MAVS. *J Virol* (2012) 86:13049–61. doi: 10.1128/JVI.01248-12
- Zhou M, Kitagawa Y, Yamaguchi M, Uchiyama C, Itoh M, Gotoh B. Expeditious neutralization assay for human metapneumovirus based on a recombinant virus expressing renilla luciferase. *J Clin Virol* (2013) 56:31–6. doi: 10.1016/j.jcv.2012.09.014
- Kitagawa Y, Sakai M, Funayama M, Itoh M, Gotoh B. Human metapneumovirus M2-2 protein acts as a negative regulator of alpha interferon production by plasmacytoid dendritic cells. *J Virol* (2017) 91:e00579-17. doi: 10.1128/JVI.00579-17
- Takahashi K, Sugiyama T, Tokoro S, Neri P, Mori H. Inhibition of interferon- $\gamma$ -induced nitric oxide production by 10-hydroxy-trans-2-decenoic acid through inhibition of interferon regulatory factor-8 induction. *Cell Immunol* (2012) 273:73–8. doi: 10.1016/j.cellimm.2011.11.004
- Odkhuu E, Komatsu T, Koide N, Naiki Y, Takeuchi K, Tanaka Y, et al. Sendai Virus c protein limits NO production in infected RAW264.7 macrophages. *Innate Immun* (2018) 24:430–8. doi: 10.1177/1753425918796619
- Morita N, Tanaka Y, Odkhuu E, Naiki Y, Komatsu T, Koide N. Sendai Virus V protein decreases nitric oxide production by inhibiting RIG-I signaling in infected RAW264.7 macrophages. *Microbes Infect* (2020) 22:322–30. doi: 10.1016/j.micinf.2020.01.005
- Ling Z, Tran KC, Teng MN. Human respiratory syncytial virus nonstructural protein NS2 antagonizes the activation of beta interferon transcription by interacting with RIG-I. *J Virol* (2009) 83:3734–42. doi: 10.1128/JVI.02434-08
- Gack MU, Shin YC, Joo CH, Urano T, Liang C, Sun L, et al. TRIM25 RING-finger E3 ubiquitin ligase is essential for RIG-I-mediated antiviral activity. *Nature* (2007) 446:916–20. doi: 10.1038/nature.05732
- Sun Y, Zheng H, Yu S, Ding Y, Wu W, Mao X, et al. Newcastle Disease virus V protein degrades mitochondrial antiviral signaling protein to inhibit host type interferon production via E3 ubiquitin ligase RNF5. *J Virol* (2019) 93:1–19. doi: 10.1128/JVI.00322-19
- Akira S, Uematsu S, Takeuchi O. Pathogen recognition and innate immunity. *Cell* (2006) 124:783–801. doi: 10.1016/j.cell.2006.02.015
- Gack MU, Albrecht RA, Urano T, Inn KS, Huang IC, Carnero E, et al. Influenza A virus NS1 targets the ubiquitin ligase TRIM25 to evade recognition by the host viral RNA sensor RIG-I. *Cell Host Microbe* (2009) 5:439–49. doi: 10.1016/j.chom.2009.04.006
- Rajsbaum R, Albrecht RA, Wang MK, Maharaj NP, Versteeg GA, Nistal-Villán E, et al. Species-specific inhibition of RIG-I ubiquitination and IFN induction by the influenza A virus NS1 protein. *PLoS Pathog* (2012) 8:e1003059. doi: 10.1371/journal.ppat.1003059
- Jureka AS, Kleinpeter AB, Tipper JL, Harrod KS, Petit CM. The influenza NS1 protein modulates RIG-I activation via a strain-specific direct interaction with the second CARD of RIG-I. *J Biol Chem* (2020) 295:1153–64. doi: 10.1074/jbc.RA119.011410
- Hu Y, Li W, Gao T, Cui Y, Jin Y, Li P, et al. The severe acute respiratory syndrome coronavirus nucleocapsid inhibits type I interferon production by interfering with TRIM25-mediated RIG-I ubiquitination. *J Virol* (2017) 91:e02143-16. doi: 10.1128/JVI.02143-16
- Xing J, Ly H, Liang Y. The z proteins of pathogenic but not nonpathogenic arenaviruses inhibit RIG-I-Like receptor-dependent interferon production. *J Virol* (2015) 89:2944–55. doi: 10.1128/JVI.03349-14
- Xing J, Wang S, Lin R, Mossman KL, Zheng C. Herpes simplex virus 1 tegument protein US11 downmodulates the RLR signaling pathway via direct interaction with RIG-I and MDA-5. *J Virol* (2012) 86:3528–40. doi: 10.1128/JVI.06929-11
- Buchholz UJ, Biacchesi S, Pham QN, Tran KC, Yang L, Luongo CL, et al. Deletion of M2 gene open reading frames 1 and 2 of human metapneumovirus: Effects on RNA synthesis, attenuation, and immunogenicity. *J Virol* (2005) 79:6588–97. doi: 10.1128/JVI.79.11.6588-6597.2005
- Kitagawa Y, Zhou M, Yamaguchi M, Komatsu T, Takeuchi K, Itoh M, et al. Human metapneumovirus M2-2 protein inhibits viral transcription and replication. *Microbes Infect* (2010) 12:135–45. doi: 10.1016/j.micinf.2009.11.002
- Ren J, Liu G, Go J, Kolli D, Zhang G, Bao X, et al. Human metapneumovirus M2-2 protein inhibits innate immune response in monocyte-derived dendritic cells. *PLoS One* (2014) 9:e91865. doi: 10.1371/journal.pone.0091865

# Frontiers in Immunology

Explores novel approaches and diagnoses to treat immune disorders.

The official journal of the International Union of Immunological Societies (IUIS) and the most cited in its field, leading the way for research across basic, translational and clinical immunology.

## Discover the latest Research Topics

[See more →](#)

### Frontiers

Avenue du Tribunal-Fédéral 34  
1005 Lausanne, Switzerland  
[frontiersin.org](http://frontiersin.org)

### Contact us

+41 (0)21 510 17 00  
[frontiersin.org/about/contact](http://frontiersin.org/about/contact)

